



*medicines*

# Research Topics in Medicines and How Our Board Members Are Engaged in Them

---

Edited by

Hiroshi Sakagami

Printed Edition of the Special Issue Published in *Medicines*

# **Research Topics in Medicines and How Our Board Members Are Engaged in Them**



# Research Topics in Medicines and How Our Board Members Are Engaged in Them

Editor

**Hiroshi Sakagami**

MDPI • Basel • Beijing • Wuhan • Barcelona • Belgrade • Manchester • Tokyo • Cluj • Tianjin



*Editor*

Hiroshi Sakagami  
Meikai University Research  
Institute of Odontology  
(M-RIO)  
Japan

*Editorial Office*

MDPI  
St. Alban-Anlage 66  
4052 Basel, Switzerland

This is a reprint of articles from the Special Issue published online in the open access journal *Medicines* (ISSN 2305-6320) (available at: <http://www.mdpi.com>).

For citation purposes, cite each article independently as indicated on the article page online and as indicated below:

LastName, A.A.; LastName, B.B.; LastName, C.C. Article Title. <i>Journal Name</i> <b>Year</b> , <i>Volume Number</i> , Page Range.
--

**ISBN 978-3-0365-3685-9 (Hbk)**

**ISBN 978-3-0365-3686-6 (PDF)**

Cover image courtesy of Hiroshi Sakagami

© 2022 by the authors. Articles in this book are Open Access and distributed under the Creative Commons Attribution (CC BY) license, which allows users to download, copy and build upon published articles, as long as the author and publisher are properly credited, which ensures maximum dissemination and a wider impact of our publications.

The book as a whole is distributed by MDPI under the terms and conditions of the Creative Commons license CC BY-NC-ND.



# Contents

<b>About the Editor</b> . . . . .	<b>ix</b>
<b>Preface to "Research Topics in Medicines and How Our Board Members Are Engaged in Them"</b> xi	
<b>Akito Tomomura, Kenjiro Bandow and Mineko Tomomura</b> Purification and Biological Function of Caldecrin Reprinted from: <i>Medicines</i> <b>2021</b> , <i>8</i> , 41, doi:10.3390/medicines8080041 . . . . .	<b>1</b>
<b>Valentina Razmovski-Naumovski, Xian Zhou, Ho Yee Wong, Antony Kam, Jarryd Pearson and Kelvin Chan</b> Chromatographic, Chemometric and Antioxidant Assessment of the Equivalence of Granules and Herbal Materials of <i>Angelicae Sinensis Radix</i> Reprinted from: <i>Medicines</i> <b>2020</b> , <i>7</i> , 35, doi:10.3390/medicines7060035 . . . . .	<b>19</b>
<b>Wilson R. Tavares, Maria do Carmo Barreto and Ana M. L. Seca</b> Uncharted Source of Medicinal Products: The Case of the <i>Hedychium</i> Genus Reprinted from: <i>Medicines</i> <b>2020</b> , <i>7</i> , 23, doi:10.3390/medicines7050023 . . . . .	<b>33</b>
<b>Diana C. G. A. Pinto, Mark A. M. Simões and Artur M. S. Silva</b> <i>Genista tridentata</i> L.: A Rich Source of Flavonoids with Anti-Inflammatory Activity Reprinted from: <i>Medicines</i> <b>2020</b> , <i>7</i> , 31, doi:10.3390/medicines7060031 . . . . .	<b>57</b>
<b>Ekaterina-Michaela Tomou, Christina Barda and Helen Skaltsa</b> Genus <i>Stachys</i> : A Review of Traditional Uses, Phytochemistry and Bioactivity Reprinted from: <i>Medicines</i> <b>2020</b> , <i>7</i> , 63, doi:10.3390/medicines7100063 . . . . .	<b>77</b>
<b>Kunihiko Fukuchi, Hiroshi Sakagami, Yoshiaki Sugita, Koichi Takao, Daisuke Asai, Shigemi Terakubo, Hiromu Takemura, Hirokazu Ohno, Misaki Horiuchi, Madoka Suguro, Tomohiro Fujisawa, Kazuki Toeda, Hiroshi Oizumi, Toshikazu Yasui and Takaaki Oizumi</b> Quantification of the Ability of Natural Products to Prevent Herpes Virus Infection Reprinted from: <i>Medicines</i> <b>2020</b> , <i>7</i> , 64, doi:10.3390/medicines7100064 . . . . .	<b>151</b>
<b>Yoshiaki Sugita, Koichi Takao, Yoshihiro Uesawa, Junko Nagai, Yosuke Iijima, Motohiko Sano and Hiroshi Sakagami</b> Development of Newly Synthesized Chromone Derivatives with High Tumor Specificity against Human Oral Squamous Cell Carcinoma Reprinted from: <i>Medicines</i> <b>2020</b> , <i>7</i> , 50, doi:10.3390/medicines7090050 . . . . .	<b>171</b>
<b>Yoshihito Tanaka, Atsuko Furuta, Kazuhito Asano and Hitome Kobayashi</b> Modulation of Th1/Th2 Cytokine Balance by Quercetin In Vitro Reprinted from: <i>Medicines</i> <b>2020</b> , <i>7</i> , 46, doi:10.3390/medicines7080046 . . . . .	<b>189</b>
<b>Jun Oike, Takayuki Okumo, Hideshi Ikemoto, Yusuke Kunieda, Shingo Nakai, Haruka Takemura, Hiroshi Takagi, Koji Kanzaki and Masataka Sunagawa</b> Preventive Effect of the Japanese Traditional Herbal Medicine Boiogito on Posttraumatic Osteoarthritis in Rats Reprinted from: <i>Medicines</i> <b>2020</b> , <i>7</i> , 74, doi:10.3390/medicines7120074 . . . . .	<b>199</b>
<b>Yuko Akanuma, Mami Kato, Yasunori Takayama, Hideshi Ikemoto, Naoki Adachi, Yusuke Ohashi, Wakako Yogi, Takayuki Okumo, Mana Tsukada and Masataka Sunagawa</b> Analgesic Efficacy of a Combination of Fentanyl and a Japanese Herbal Medicine "Yokukansan" in Rats with Acute Inflammatory Pain Reprinted from: <i>Medicines</i> <b>2020</b> , <i>7</i> , 75, doi:10.3390/medicines7120075 . . . . .	<b>209</b>

<b>Angela Dalia Ricci, Alessandro Rizzo, Chiara Bonucci, Nastassja Tober, Andrea Palloni, Veronica Mollica, Ilaria Maggio, Marzia Deserti, Simona Tavolari and Giovanni Brandi</b> PARP Inhibitors in Biliary Tract Cancer: A New Kid on the Block? Reprinted from: <i>Medicines</i> 2020, 7, 54, doi:10.3390/medicines7090054 . . . . .	221
<b>Charnete Casimero, Todd Ruddock, Catherine Hegarty, Robert Barber, Amy Devine and James Davis</b> Minimising Blood Stream Infection: Developing New Materials for Intravascular Catheters Reprinted from: <i>Medicines</i> 2020, 7, 49, doi:10.3390/medicines7090049 . . . . .	235
<b>Ugo Testa, Elvira Pelosi and Germana Castelli</b> Genetic Alterations in Renal Cancers: Identification of The Mechanisms Underlying Cancer Initiation and Progression and of Therapeutic Targets Reprinted from: <i>Medicines</i> 2020, 7, 44, doi:10.3390/medicines7080044 . . . . .	259
<b>Ganesh Shenoy, Yunsung Kim, Kyra Newmaster, Kathryn L. McGillen, Francesca Ruggiero and Nelson S. Yee</b> Recurrent Superior Vena Cava Syndrome in a Patient with Sarcoidosis and Pancreatic Adenocarcinoma: A Case Report and Literature Review Reprinted from: <i>Medicines</i> 2020, 7, 56, doi:10.3390/medicines7090056 . . . . .	301
<b>Davide Giuseppe Ribaldone, Selvaggia Brigo, Michela Mangia, Giorgio Maria Saracco, Marco Astegiano and Rinaldo Pellicano</b> Oral Manifestations of Inflammatory Bowel Disease and the Role of Non-Invasive Surrogate Markers of Disease Activity Reprinted from: <i>Medicines</i> 2020, 7, 33, doi:10.3390/medicines7060033 . . . . .	313
<b>Kathryn L. McGillen, Syeda Zaidi, Amer Ahmed, Shantell Harter and Nelson S. Yee</b> Contrast-Enhanced Ultrasonography for Screening and Diagnosis of Hepatocellular Carcinoma: A Case Series and Review of the Literature Reprinted from: <i>Medicines</i> 2020, 7, 51, doi:10.3390/medicines7090051 . . . . .	325
<b>Rolf Teschke and Gaby Danan</b> Worldwide Use of RUCAM for Causality Assessment in 81,856 Idiosyncratic DILI and 14,029 HILI Cases Published 1993–Mid 2020: A Comprehensive Analysis Reprinted from: <i>Medicines</i> 2020, 7, 62, doi:10.3390/medicines7100062 . . . . .	343
<b>Erik Almazan, Youkyung S. Roh, Micah Belzberg, Caroline X. Qin, Kyle Williams, Justin Choi, Nishadh Sutaria, Benjamin Kaffenberger, Yevgeniy R. Semenov, Jihad Alhariri and Shawn G. Kwatra</b> Comorbidities Associated with Granuloma Annulare: A Cross-Sectional, Case-Control Study Reprinted from: <i>Medicines</i> 2020, 7, 53, doi:10.3390/medicines7090053 . . . . .	383
<b>Hidetaka Hamasaki</b> Effects of Diaphragmatic Breathing on Health: A Narrative Review Reprinted from: <i>Medicines</i> 2020, 7, 65, doi:10.3390/medicines7100065 . . . . .	391
<b>Byeongsang Oh, Kyeore Bae, Gillian Lamoury, Thomas Eade, Frances Boyle, Brian Corless, Stephen Clarke, Albert Yeung, David Rosenthal, Lidia Schapira and Michael Back</b> The Effects of Tai Chi and Qigong on Immune Responses: A Systematic Review and Meta-Analysis Reprinted from: <i>Medicines</i> 2020, 7, 39, doi:10.3390/medicines7070039 . . . . .	411



<b>Joanna Dietzel, Mike Cummings, Kevin Hua, Klaus Hahnenkamp, Benno Brinkhaus and Taras I. Usichenko</b> Auricular Acupuncture for Preoperative Anxiety—Protocol of Systematic Review and Meta-Analysis of Randomized Controlled Trials Reprinted from: <i>Medicines</i> 2020, 7, 73, doi:10.3390/medicines7120073 . . . . .	433
<b>Abrar-Ahmad Zulfiqar, Noël Lorenzo-Villalba, Oumair-Ahmad Zulfiqar, Mohamed Hajjam, Quentin Courbon, Lucie Esteouille, Bernard Geny, Samy Talha, Dominique Letourneau, Jawad Hajjam, Sylvie Erve, Amir Hajjam El Hassani and Emmanuel Andres</b> e-Health: A Future Solution for Optimized Management of Elderly Patients. GER-e-TEC™ Project Reprinted from: <i>Medicines</i> 2020, 7, 41, doi:10.3390/medicines7080041 . . . . .	443

## About the Editor

**Hiroshi Sakagami** was born in Tokyo (1952), and got his Ph.D. from Faculty of Pharmaceutical Sciences, University of Tokyo (1980). He worked for 17 years in Department of Biochemistry, School of Medicine, Showa University, Tokyo, with a 3 year stay as visiting researcher in Roswell Park Memorial Institute, Buffalo, NY (under the direction of Dr. Bloch). He became the professor of Division of Pharmacology, Meikai University School of Dentistry (1997) and the director of industry-supported Meikai Pharmaco-Medical Laboratory (MPL) (1999). He became the professor of Meikai University Research Institute of Odontology (M-RIO) (2017). His research interest includes the biological function of lignin-carbohydrate complex, application of plant extracts to oral diseases, exploration of anticancer drugs that has least keratinocyte toxicity and neurotoxicity, and creation of new field of research by international collaboration, resulting in the discovery of new anticancer drug candidates, such as chromone derivatives and  $\alpha,\beta$ -unsaturated ketones (with Drs. Sugita, Takao, Gul and Dimmock). He was the principal investigator for 8 Grant-in-Aids from the Ministry of Education, Science, Sports and Culture of Japan. He is also the directors of board of the trustees for both Meikai and Asahi University. He is an editor of *Medicines*, and board member of *New Food Industry* and *In Vivo*.



## **Preface to “Research Topics in Medicines and How Our Board Members Are Engaged in Them”**

The field of medicine is diverse and developing rapidly. Knowing the whole picture is necessary for future intellectuals. *Medicines* is a key journal that publishes information on drug development, mechanisms of action, and therapeutic effects. There are many competing journals of similar titles, however, *Medicines* covers a much broader range of sciences, such as traditional medicines, molecular targeted drugs, structure–activity relationship, pathway analysis, multi-omics analysis, diagnosis, therapy, and action mechanism. In this Special Issue, the editorial committee will introduce the latest trends of “Research Topics in Medicines and How Our Board Members Are Engaged in Them”. Our board members are very much delighted if this Special Issue could help the readers to understand the progress of various fields of medicine. Special thanks go to their contribution of completing each chapter.

**Hiroshi Sakagami**

*Editor*





# Purification and Biological Function of Caldecrin

Akito Tomomura <sup>1,\*</sup>, Kenjiro Bandow <sup>1</sup> and Mineko Tomomura <sup>2</sup>

<sup>1</sup> Division of Biochemistry, Department of Oral Biology & Tissue Engineering, Meikai University School of Dentistry, 1-1 Keyakidai, Sakado, Saitama 350-0283, Japan; kbando@dent.meikai.ac.jp

<sup>2</sup> Department of Oral Health Sciences, Meikai University School of Health Sciences, 1-1 Akemi, Urayasu, Chiba 279-8550, Japan; mineko-t@dent.meikai.ac.jp

\* Correspondence: atomomu@dent.meikai.ac.jp; Tel.: +81-492-79-2767

**Abstract:** Blood calcium homeostasis is critical for biological function. Caldecrin, or chymotrypsin-like elastase, was originally identified in the pancreas as a serum calcium-decreasing factor. The serum calcium-decreasing activity of caldecrin requires the trypsin-mediated activation of the protein. Protease activity-deficient mature caldecrin can also reduce serum calcium concentration, indicating that structural processing is necessary for serum calcium-decreasing activity. Caldecrin suppresses the differentiation of bone-resorbing osteoclasts from bone marrow macrophages (BMMs) by inhibiting receptor activator of NF- $\kappa$ B ligand (RANKL)-induced nuclear factor of activated T-cell cytoplasmic 1 expression via the Syk-PLC $\gamma$ -Ca<sup>2+</sup> oscillation-calcineurin signaling pathway. It also suppresses mature osteoclastic bone resorption by RANKL-stimulated TRAF6-c-Src-Syk-calcium entry and actin ring formation. Caldecrin inhibits lipopolysaccharide (LPS)-induced osteoclast formation in RANKL-primed BMMs by inducing the NF- $\kappa$ B negative regulator A20. In addition, caldecrin suppresses LPS-mediated M1 macrophage polarization through the immunoreceptor triggering receptor expressed on myeloid cells (TREM) 2, suggesting that caldecrin may function as an anti-osteoclastogenic and anti-inflammatory factor via TREM2. The ectopic intramuscular expression of caldecrin cDNA prevents bone resorption in ovariectomized mice, and the administration of caldecrin protein also prevents skeletal muscle destruction in dystrophic mice. In vivo and in vitro studies have indicated that caldecrin is a unique multifunctional protease and a possible therapeutic target for skeletal and inflammatory diseases.

**Keywords:** calcium metabolism; bone metabolism; protease; osteoclast; macrophage; RANKL; LPS; TLR4; TREM2

**Citation:** Tomomura, A.; Bandow, K.; Tomomura, M. Purification and Biological Function of Caldecrin.

*Medicines* **2021**, *8*, 41. <https://doi.org/10.3390/medicines8080041>

Academic Editor: Basil D. Roufogalis

Received: 29 May 2021

Accepted: 19 July 2021

Published: 23 July 2021

**Publisher's Note:** MDPI stays neutral with regard to jurisdictional claims in published maps and institutional affiliations.



**Copyright:** © 2021 by the authors. Licensee MDPI, Basel, Switzerland. This article is an open access article distributed under the terms and conditions of the Creative Commons Attribution (CC BY) license (<https://creativecommons.org/licenses/by/4.0/>).

## 1. Introduction

Calcium homeostasis is controlled by calcium absorption in the intestine and reabsorption along the renal tubules, as well as by bone formation and resorption. Calcium homeostasis is regulated by parathyroid hormone (PTH) and thyroid gland-derived calcitonin, and activated vitamin D<sub>3</sub> produced in the kidney. In addition, the pancreas is involved in calcium metabolism. Hypocalcemia is frequently observed in acute pancreatitis [1]. Glucagon [2,3], amylin [4,5], and calcitonin gene-related peptides [6,7] secreted from the pancreas may be responsible for hypocalcemia. While the exact pathological mechanisms of hypocalcemia are unknown, the pancreas may secrete hypocalcemic factors. We previously purified and cloned the hypocalcemic factor, caldecrin, from the pancreas [8–10]. In this review article, we discuss the roles of the multifunctional protease, caldecrin, in the pancreas.

## 2. Purification and Cloning of Caldecrin

In the 1960s, Takaoka et al. first demonstrated that a pancreatic extract of porcine had hypocalcemic activity [11,12]. In 1992, Tomomura et al. purified a hypocalcemic factor, calcium-decreasing factor (caldecrin), from a porcine pancreatic extract [8]. Caldecrin was

purified from acetone powder of porcine pancreas via fractionation with acetone (30–60%) and saturated ammonium sulfate (45–60%), followed by ion-exchange chromatography on Q Sepharose Fast-Flow (pH 5.5), gel filtration on Superdex 75 fast protein liquid chromatography (FPLC), and ion-exchange chromatography on Mono Q FPLC (pH 5.5). The isolated caldecrin was confirmed as a single peak by high-performance liquid chromatography. To identify caldecrin, each fraction of the purification steps was injected into the tail vein of fasted mice, and serum calcium concentrations were measured 4 h post-injection. The serum calcium concentration decreased in a dose-dependent manner as the products of subsequent purification steps were administered, and the hypocalcemic activity increased as a result of the purification process (Figure 1). In addition to this *in vivo* experiment, the ability of caldecrin to inhibit PTH-stimulated calcium release was assessed using  $\text{Ca}^{45}$ -prelabeled fetal mouse long bone organ cultures. Caldecrin inhibited PTH-stimulated  $\text{Ca}^{45}$  release from the bone to the culture medium at concentrations as low as 10 ng/mL. These experiments showed that caldecrin is an anionic protein (pI: 4.5) with a molecular weight of approximately 28 kDa. In addition, we showed that caldecrin is a serine protease with chymotryptic activity [8]. The immature form of caldecrin (procaldecrin), which is purified in the presence of the serine protease inhibitor diisopropyl fluorophosphate (DFP) from porcine pancreas, is activated by trypsin treatment in a dose- and time-dependent manner, giving rise to the activated caldecrin that exerts chymotryptic activity [9].

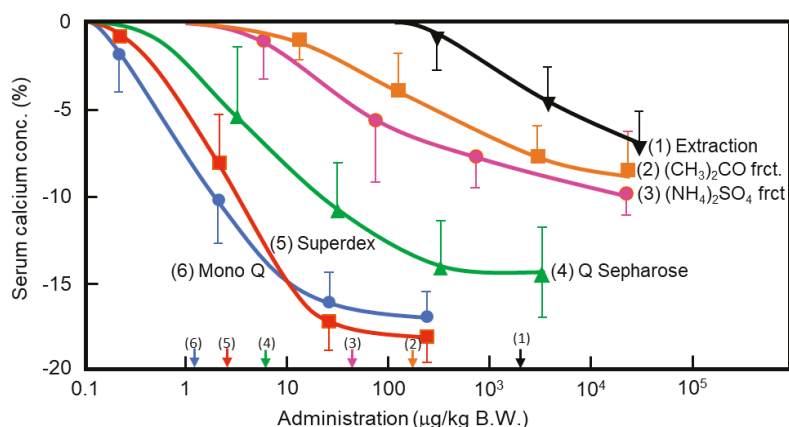


**Figure 1.** Purification of porcine caldecrin and its serum calcium-decreasing activity. The caldecrin was isolated from porcine pancreas following the following purification steps: porcine acetone powder was extracted (1), and active fraction was separated with acetone ( $\text{CH}_3$ )<sub>2</sub>CO precipitation (2), saturated ammonium sulfate ( $\text{NH}_4$ )<sub>2</sub>SO<sub>4</sub> precipitation (3), and then Q Sepharose Fast-Flow ion-exchange chromatography (4), Superdex 75 size-exclusion fast protein liquid chromatography (FPLC) (5), and Mono Q ion-exchange FPLC (6). Dose-dependent curves of serum calcium decreased activity and its half maximal effective concentration ( $\text{EC}_{50}$ ) values, as shown by arrows on the x-axis, were prepared from the representative preparation.

In 1995, we first isolated rat caldecrin cDNA by immunoscreening with an anti-caldecrin antibody [10]. The nucleotide sequence was almost identical to that of a PCR clone named rat elastase IV (ELA4) [13]. A frame shift caused by a minor nucleotide change in both genes resulted in the difference of the amino acid sequences of the central region of caldecrin from that of ELA4. Thus, the lysine-X bond of purified rat caldecrin was digested with a metal endopeptidase in the presence of the chymotrypsin inhibitor phenylmethylsulfonyl fluoride (PMSF). The partial amino acid sequence of caldecrin fragments purified from rat pancreas completely matched that encoded by cDNA. Furthermore, the partial amino acid sequence of purified porcine caldecrin was closely related to that of the corresponding fragments of purified rat caldecrin. However, the amino acid sequence

of rat and porcine caldecrin differed from the deduced amino acid sequence of rat ELA4 cDNA. Amino acid sequences of caldecrin showed higher homology with elastase than chymotrypsinogen A and B, although the N-terminal amino acid sequence of caldecrin revealed that the mature form has a disulfide-linked activation peptide, which is characteristic of chymotrypsin. In 1995, Gomis-Rüth et al. reported the crystalline structure of bovine chymotrypsinogen C [14]. The amino acid sequence of chymotrypsinogen C was very close to that of rat caldecrin, suggesting a high degree of similarity between caldecrin and chymotrypsin C (CTRC).

In 1996, human caldecrin genes were cloned [15]. We transfected the insect cell line Sf9 with a recombinant baculovirus harboring human caldecrin cDNA. Recombinant human caldecrin was purified from the culture medium by using hydroxyapatite column chromatography. Subsequently, the purified recombinant human caldecrin showed hypocalcemic activity. To address whether ELA4 is transcribed and translated *in vivo* and has proteolytic activity, we constructed rat ELA4 cDNA by combinational PCR and compared the recombinant rat ELA4 with the recombinant rat caldecrin synthesized in a baculovirus expression system [16]. We detected recombinant caldecrin protein in the medium. However, in the case of ELA4, we could not detect ELA4 protein in the cells and the medium. Furthermore, we detected caldecrin mRNA expression in rat pancreas but no ELA4, suggesting that ELA4 might be a single nucleotide polymorphism of the caldecrin gene. It is now known that chymotrypsin C, caldecrin, and ELA4 are the same protein encoded by the CTRC gene. The CTRC gene is located on chromosome 1p36.21 of the human genome [17]. The rat and mouse CTRC genes are located on 5q36 and 4E1 of each genome, respectively [18].

### 3. Protein Structure and Protease Activity of Caldecrin

#### 3.1. Structure of Chymotrypsin C (Caldecrin)

Chymotrypsin C, also termed caldecrin, is a 268-amino acid-long protein. Its sequence comprises a signal peptide (16 amino acids long, from residues 1 to 16), pro-peptide (13 amino acids, residues 17–29), and mature protein (239 amino acids, residues 30–268). The crystal structure of bovine Ctrc [14] revealed that rat and human caldecrin have five disulfide bridges: Cys17–Cys141, Cys59–Cys75, Cys155–Cys222, Cys186–Cys202, and Cys212–Cys243 [10,15] (Figure 2).

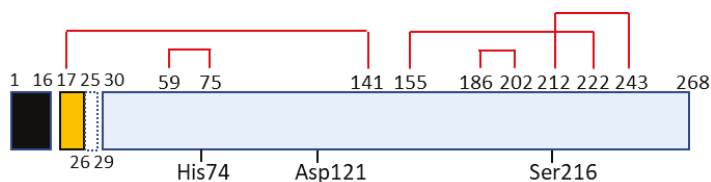


**Figure 2.** Schematic for domain structure of caldecrin. Black box (signal peptide: amino acid residue number 1–16); yellow box (pro-peptide:17–29 including 26–29 or 27–29 peptide removed by autoactivation); blue box (mature protein: 30–268); red lines (disulfide bridges with cysteine number); His74, Asp121, and Ser216 (charge relay system for serine protease activity).

Chymotrypsin C possesses two barrel structures, between which the charge-relayed catalytic triad (His74, Asp121, and Ser216) is located. The activation peptide is first cleaved at the Arg29–Ile30 peptide bond by trypsin, and further cleaved at Asp25–Leu26 [10] or Leu26–Ser27 [19] by the autoactivation of chymotrypsin C. The cleaved Cys17–Asp25 or Cys17–Leu26 long peptide remains attached to the mature protein by a disulfide bridge such as Cys17–Cys141, a structure that resembles chymotrypsin [10,14,15,19,20].

#### 3.2. Proteolytic Activity and Specificity of Chymotrypsin C (Caldecrin)

The enzyme classification of chymotrypsin C (caldecrin) is EC 3.4.21.2. It shows hydrolytic activity that can cleave leucyl, tyrosyl, phenylalanyl, methionyl, tryptophanyl,



glutamine, and asparagine bonds. Chymotrypsin C preferentially hydrolyzes leucyl bonds compared to chymotrypsin A [21]. Humans have five other chymotrypsin-like elastase genes that encode the structurally similar proteins chymotrypsin-like elastase family, member 1 (CELA1, EC3.4.21.36), pancreatic CELA2A and 2B (EC3.4.21.71), and pancreatic CELA3A and 3B (EC3.4.21.70). The protease activity of CELA2 preferentially cleaves leucine, methionyl, and phenylalanyl residues and hydrolyzes elastin [22]. CELA3B preferentially cleaves alanyl residues, but has little elastolytic activity [23]. Human caldecrin was more similar to CELA2A (63.4%), 2B (59.6%), 3A (52.2%), and 3B (53.0%) than with chymotrypsin B (42.5%) [15]. The altered protease activity of chymotrypsin C revealed that it can be a risk factor for chronic pancreatitis, a role that is described in detail in Section 3.3.

### 3.3. Chymotrypsin C (Caldecrin) and Pancreatitis

Chronic pancreatitis is a progressive inflammatory disease of the pancreas. It is characterized by acinar cell atrophy, fibrotic tissue replacement, and duct irregularities with calcifications [24]. The pathological mechanism of pancreatitis is uncontrolled trypsin activity [25]. Cationic trypsinogen (PRSS1) mutations are gain-of-function mutations that stimulate the autoactivation of the proform to trypsin, which are associated with autosomal dominant hereditary pancreatitis [26]. Loss-of-function mutations in serine protease inhibitor Kazal-type 1 (SPINK1), which can inactivate intrapancreatic trypsin activity, are associated with pancreatitis risk [27]. Therefore, the inactivation of irregularly produced intrapancreatic PRSS1 by SPINK1 or by an unidentified serine protease (Rinderknecht's enzyme Y) has been proposed to protect against pancreatitis [28–30]. In 2006, Nemoda and Sahin-Tóth reported that chymotrypsin C (caldecrin) stimulates the autoactivation of human cationic trypsinogen [31]. In 2007, Szmola and Sahin-Tóth reported that the unidentified enzyme Y was identified as chymotrypsin C (caldecrin), in which the main role of chymotrypsin C is trypsinogen activation and trypsin degradation [32]. In 2008, Rosendahl et al. reported that loss-of-function variants in the CTRC gene were risk factors for chronic pancreatitis [33]. Masson et al. also identified a CTRC mutation in patients with idiopathic chronic pancreatitis [34]. Thus, loss-of-function mutations in CTRC can cause a decrease in the catalytic activity of CTRC and impaired trypsinogen degradation, which are causative risk factors for chronic pancreatitis [35]. CTRC is also a susceptibility gene for tropical calcific pancreatitis associated with calcium deposition in the pancreas [36,37]. For genetic risk factors in chronic pancreatitis, see the [www.pancreasgenetics.org](http://www.pancreasgenetics.org) (accessed on 28 May 2021) website [38].

## 4. Non-Proteolytic Functions of Caldecrin

### 4.1. Caldecrin and Calcium Metabolism

As described above, purified porcine and rat caldecrin from the pancreas and produced recombinant rat and human caldecrin protein decreased serum calcium concentration in mice. Caldecrin dose-dependently decreased the serum calcium concentration. The effect resulted in a maximum decrease of 15–20% with 20–100 µg (about 0.7–3.5 nmol)/kg mice body weight. Procaldecrin did not exhibit serum calcium-decreasing activity, but acquired serum calcium-decreasing and protease activity after trypsin treatment. PMSF treatment after the trypsin activation of procaldecrin abolished its protease activity but did not affect the serum calcium-decreasing activity [8] (Figure 3a). The calcium-decreasing activity of porcine caldecrin was almost the same as that of porcine calcitonin (1 nmol/kg body weight) (Figure 3b). Pretreatment with PMSF or recombinant caldecrin with point mutations at positions coding for activity-related amino acids (Hm: His74Ala or Sm: Ser216Ala substitution) decreased serum calcium concentration in vivo and bone destruction activity in vitro and abolished the protease activity of caldecrin. Caldecrin not only decreased calcium concentration but also hydroxyproline serum concentration, which is a marker of bone resorption, suggesting that caldecrin inhibits bone destruction by osteoclasts [10]. Therefore, the mechanism by which caldecrin inhibits osteoclast formation and/or function remains to be investigated.

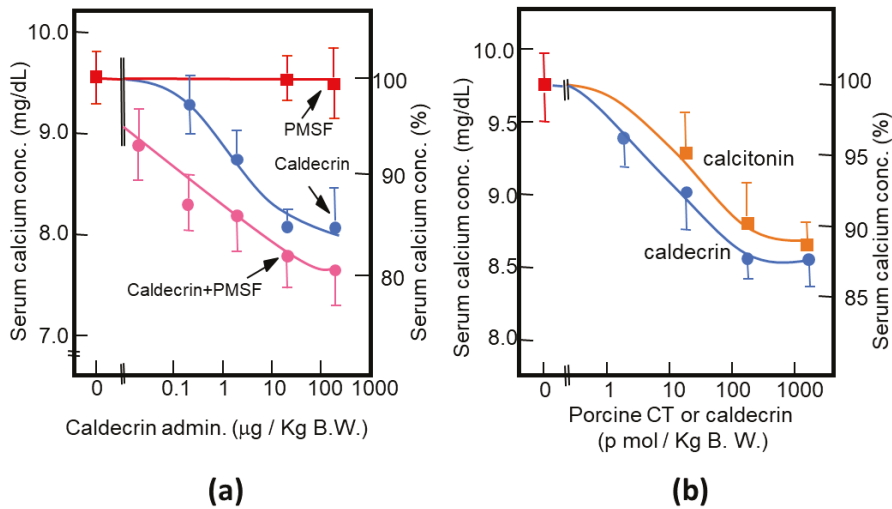


**Figure 3.** Characterization of the serum calcium-decreasing activity of caldecrin. (a) PMSF treatment does not inhibit the serum calcium-decreasing activity of activated caldecrin; (b) comparison of the serum calcium decreasing activities of porcine caldecrin and calcitonin.

In 1996, Izbicka et al. independently purified a calcium metabolism-regulating factor from a porcine pancreas by determining the inhibitory effect of the proliferation of human osteosarcoma MG-63 cells and bone resorption in organ culture stimulated by PTH [39]. The factor had a molecular weight of 28 kDa, and it showed 92% homology with human elastase IIIB (CELA3B) in the N-terminus. Recombinant human elastase IIIB inhibited bone resorption in organ cultures stimulated with 1,25-dihydroxyvitamin D<sub>3</sub>. This anti-resorptive activity was abolished by PMSF treatment, highlighting the importance of the proteolytic activity of elastase IIIB in the inhibition of bone resorption. The differences between the hypocalcemic mechanisms of caldecrin and elastase IIIB have not yet been elucidated.

#### 4.2. Caldecrin and Osteoclast

##### 4.2.1. Caldecrin and RANK Signaling

The serum calcium concentration is affected by osteoclast activity. Osteoclasts execute bone resorption, which is differentiated from bone marrow by key molecules such as macrophage colony-stimulating factor (M-CSF) and receptor activator of nuclear factor-kappa B (NF-κB) ligand (RANKL) [40–44]. Osteoclast differentiation and maturation occur in the following stages: (i) osteoclast precursor cells are produced from bone marrow cells in response to M-CSF and begin to differentiate following stimulation by RANKL; and (ii) osteoclasts fuse with each other to form multinucleated giant cells. Multinucleated cells secrete protons and cathepsin K, which are required for bone resorption. Osteoclast differentiation is tightly regulated by many molecules to maintain bone homeostasis [45–47]. (Figure 4). During the initial stage, RANKL binds to its receptor RANK, which induces the recruitment of the adaptor protein, tumor necrosis factor receptor-associated factor 6 (TRAF6) [48]. Activated TRAF6 stimulates NF-κB by activating IκB kinase (IKK) [49]. TRAF adaptor proteins also activate mitogen-activated protein kinases (MAPKs) such as extracellular signal-regulated kinase (ERK), C-Jun N-terminal kinase (JNK), and p38 [50–53]. NF-κB and MAPK signaling activates activator protein-1 (AP-1) including c-Fos, which in turn activates the master transcription factor in osteoclastogenesis, nuclear factor of activated T-cell cytoplasmic 1 (NFATc1) [54–56].

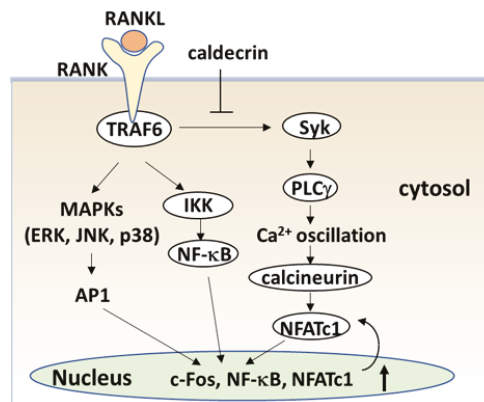


**Figure 4.** Calcecin inhibits RANKL signaling in the initial stage of osteoclast differentiation. RANKL binding to RANK activates both NF- $\kappa$ B and MAPKs, such as ERK, JNK, and p38. Activation of NF- $\kappa$ B and MAPK signals is then transmitted to c-Fos and NFATc1 induction. Calcecin inhibits RANK-stimulated phosphorylation of Syk and PLC $\gamma$ , abolishing Ca<sup>2+</sup> oscillation and activation of calcineurin, and amplification of NFATc1 in the initial stage of osteoclast differentiation. AP-1: activator protein-1; ERK: extracellular signal-regulated kinase; IKK: I $\kappa$ B kinase; JNK: C-Jun N-terminal kinase; MAPK: mitogen-activated protein kinase; NFATc1, nuclear factor of activated T-cells cytoplasmic 1; NF- $\kappa$ B: nuclear factor- $\kappa$ B; PLC $\gamma$ : phospholipase C $\gamma$ ; RANK: receptor activator of NF- $\kappa$ B; RANKL: RANK ligand; Syk: spleen tyrosine kinase; TRAF6: tumor necrosis factor receptor-associated factor 6.

RANK signaling also activates phospholipase C $\gamma$  (PLC $\gamma$ )-dependent Ca<sup>2+</sup> signaling through splenic tyrosine kinase (Syk) [57–59]. Finally, calcineurin, a calcium/calmodulin-dependent serine/threonine phosphatase activated by intracellular Ca<sup>2+</sup> concentration, causes the dephosphorylation of NFATc1 and induces translocation from the cytoplasm into the nucleus [60]. Thus, TRAF6, NF- $\kappa$ B, c-Fos and NFATc1 are required for the initiation stage of RANKL-induced osteoclast differentiation (Figure 4).

To understand the serum calcium-decreasing effects of calcecin on osteoclast-mediated bone resorption, we investigated whether calcecin inhibits the initial stage of osteoclast differentiation following RANKL exposure. In murine bone marrow macrophages and macrophage-derived RAW264.7, protease-deficient calcecin inhibited RANKL-stimulated osteoclast differentiation [61]. The macrophage-type colonies formed from BMCs in the absence or presence of calcecin were not different, suggesting that calcecin does not affect macrophage formation. The frequency of osteoclast progenitor formation in the presence of M-CSF alone was not different from that in the presence of M-CSF and calcecin. Thus, calcecin did not affect macrophage colony formation or osteoclast progenitors from BMCs. However, calcecin suppressed RANKL-stimulated mononuclear osteoclast differentiation, assessed by tartrate-resistant acid phosphatase (TRAP) staining and enzymatic activity, a specific osteoclast enzyme commonly used as a marker. Calcecin inhibited the RANKL-induced phosphorylation of Syk and PLC $\gamma$  and abolished Ca<sup>2+</sup> oscillations within 5–10 min of calcecin exposure. Calcecin inhibited the activation of calcineurin, a protein that enhances NFATc1 activity. Finally, calcecin inhibited the RANKL-stimulated nuclear translocation of NFATc1 and its mRNA accumulation, whereas other RANKL-stimulated transcription factors such as NF- $\kappa$ B  $\kappa$  and c-Fos were unaffected. Thus, we found that calcecin inhibits osteoclast differentiation by suppressing NFATc1 activity via the RANKL-mediated calcium signaling pathway at the initial stage of osteoclastogenesis (Figure 4).

In the late stage of osteoclastogenesis, amplified NFATc1 induces the expression of osteoclast-specific genes, leading to osteoclast differentiation (Figure 5). Mature osteo-

clasts create a unique cytoskeletal structure, termed the sealing zone, which consists of an actin ring attached to the bone surface [62,63]. The integrin vitronectin receptor  $\alpha\beta 3$  binds to vitronectin present in the bone matrix, inducing the recruitment of c-Src tyrosine kinase to the integrin receptor. Activated c-Src phosphorylates Syk, which phosphorylates the DNAX-activating protein of 12 kDa (DAP12) [64], and SLP-76, which induces cytoskeletal organization and bone resorption [65]. Calcium-dependent proline-rich tyrosine kinase (PYK2) is an adhesion kinase localized in the sealing zone, which is activated by binding to  $\alpha\beta 3$  integrin and subsequent phosphorylation by Src kinase [66]. TRAF6-induced cytoskeletal changes are mediated by interactions with cytoplasmic c-Src [67]. Thus, RANKL–RANK signaling enhances the TRAF6–c-Src interaction, which activates the formation of the Src–Syk and Src–Pyk2 complexes that induce the cytoskeletal organization of mature osteoclasts.

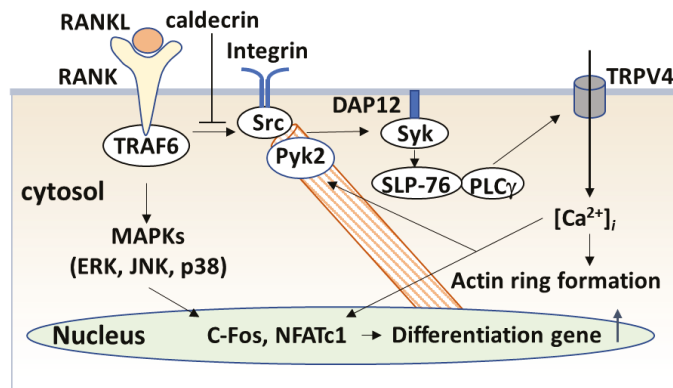


**Figure 5.** Calcestrin inhibits RANKL signaling in mature osteoclasts. RANKL–RANK binding activates c-Fos and NFATc1. RANK also activates c-Src and the c-Src–Syk complex. Activated Syk phosphorylates PLC $\gamma$  via SLP-76, which leads to the activation of TRPV4 channels and evokes Ca<sup>2+</sup> influx. Increased Ca<sup>2+</sup> levels activate Pyk2 and are associated with Src, leading to cytoskeletal organization. Calcestrin inhibits RANKL-induced phosphorylation of c-Src, Syk, PLC $\gamma$ , SLP-76, and Pyk2 in mature osteoclasts. Calcestrin also abolishes Ca<sup>2+</sup> entry into the cytoplasm through the TRPV4 channel and TRAF6–c-Src interaction. Akt: AKR mouse thymoma kinase; Src, sarcoma; SLP-76:SH2 domain containing leukocyte protein of 76kDa; TRPV4: Transient Receptor Potential Vanilloid 4.

Calcium signaling pathways have been shown to play a role in bone resorption, exerting effects on actin metabolism, cytoskeletal organization, and cell–matrix interactions. RANKL signaling activates PLC $\gamma$  and enhances the production of inositol trisphosphate (IP<sub>3</sub>), which results in the release of Ca<sup>2+</sup> from the ER through transient receptor potential vanilloid channel 2 (TRPV2), which subsequently causes oscillations in Ca<sup>2+</sup> concentration [68]. Ca<sup>2+</sup> oscillations disappear during differentiations and are replaced by RANKL-evoked Ca<sup>2+</sup> influx via TRPV4 and 5 [69,70]. Thus, RANKL-triggered Ca<sup>2+</sup> influx in multinucleated osteoclasts through TRPV channels maintains NFATc1 activity and activates Pyk2, which is essential for actin filament organization (Figure 5).

Next, we investigated whether calcestrin inhibits RANKL-induced mature osteoclast function. Calcestrin inhibited RANKL-stimulated osteoclastic bone resorption *in vitro*, but did not induce apoptosis [71]. In addition, calcestrin inhibited the RANKL-induced phosphorylation of c-Src, Syk, PLC $\gamma$ , SLP-76, and Pyk2 in mature osteoclasts but not the phosphorylation of ERK, JNK, and Akt. Furthermore, calcestrin inhibited RANKL-induced Ca<sup>2+</sup> entry through TRPV4 and actin ring formation in mature osteoclasts, RANKL-stimulated c-Src kinase activity, and integrin–c-Src–Syk association and RANKL-mediated TRAF6–c-Src association. Thus, we found that calcestrin suppresses RANKL-mediated Ca<sup>2+</sup>

signaling and actin ring formation in mature osteoclasts via suppression of the TRAF6–c-Src—Syk signaling pathway, resulting in the suppression of bone resorption (Figure 5).

In this section, we conclude that protease activity-deficient caldecrin inhibits both RANKL-stimulated osteoclast formation from bone marrow progenitors and pre-existing mature osteoclastic bone resorption, resulting in the serum calcium-decreasing activity of caldecrin *in vivo*. Next, we investigated the role of caldecrin in inflammation-induced bone loss.

#### 4.2.2. Caldecrin and TLR4 Signaling

Inflammation is known to cause bone loss. Bacterial lipopolysaccharide (LPS), a major constituent of the outer membrane of Gram-negative bacteria, is a potent inducer of bone loss in inflammatory diseases, including periodontal disease, bacterial arthritis, and dental implant infections [72,73]. Toll-like receptor (TLR) family members, which are proteins homologous to the *Drosophila* Toll protein, play a critical role in the innate immune system. TLR (TLR1–9) is expressed in osteoclast progenitors, of which TLR2 and 4 are also expressed in osteoclasts [74]. LPS has been shown to stimulate osteoclast formation and bone resorption *in vivo* through TLR4 [75,76].

The signaling cascade of TLR4 has been extensively studied in macrophages [77–79]. LPS induces inflammation upon the production of pro-inflammatory cytokines, such as interleukin-1 (IL-1)  $\beta$ , TNF- $\alpha$ , and IL-6 in macrophages and lymphocytes. Activated TLRs, except for TLR3, induce pro-inflammatory cytokine production through the canonical myeloid differentiation factor 88 (MyD88), which recruits TRAF6 downstream and activates IKK and the NF- $\kappa$ B pathway [80], leading to osteoclast formation *in vitro*. Although LPS is known to induce bone loss *in vivo*, LPS can both inhibit and stimulate osteoclastogenesis *in vitro*. The simultaneous activation of TLR4 and RANK signaling by LPS and RANKL, respectively, inhibits osteoclast formation in BMMs [74,81]. In this context, LPS/TLR4 activates NF- $\kappa$ B, p38, ERK1/2, and JNK, but inhibits RANKL-induced Nfatc1 expression. In contrast, LPS treatment enhanced the osteoclast differentiation of BMMs primed with M-CSF and RANKL [81,82]. The expression of Nfatc1 in RANKL-committed preosteoclasts is no longer affected by subsequent LPS treatment [82]. Therefore, RANKL-primed NFATc1 expression is a prerequisite for LPS-stimulated osteoclast formation.

RANKL/RANK and LPS/TLR4 signaling pathways in osteoclast formation share TRAF6, a ubiquitin E3 ligase, and downstream signaling pathways such as NF- $\kappa$ B activation. The LPS response is regulated by negative feedback with an NF- $\kappa$ B-inducible A20, which is a deubiquitinating protease encoding tumor necrosis factor alpha-induced protein 3 (TNEAIP3) [83]. A20 removes lysine 63 (K63)-linked polyubiquitin chains from TRAF6 and promotes K48-polyubiquitination for proteasomal degradation; thus, NF- $\kappa$ B-stimulated A20 plays an anti-inflammatory role by inhibiting I $\kappa$ B phosphorylation and NF- $\kappa$ B activation [84]. LPS induces osteoclast formation from RANKL-pretreated macrophages and the expression of A20, which is associated with TRAF6 degradation and NF- $\kappa$ B inhibition [85]. The overexpression of A20 inhibits osteoclastogenesis in a TRAF6-dependent manner, whereas the silencing of A20 restores TRAF6 expression and NF- $\kappa$ B activation, resulting in LPS-enhanced bone resorption [86]. Thus, the induction of NFATc1 by RANKL–TRAF6 is necessary before the increase in the levels of A20 by LPS. Therefore, the anti-inflammatory molecule A20 acts as a barrier to uncontrolled activation during osteoclast differentiation.

We investigated whether caldecrin inhibited LPS-induced osteoclastogenesis. Osteoclast progenitors from mouse BMMs and RAW264.7 cells were primed with a low dose of RANKL for 40 h and subsequently exposed to LPS in the absence of RANKL, which caused osteoclast formation [87]. LPS stimulated the phosphorylation of ERK, JNK, p38, and I $\kappa$ B. Furthermore, LPS stimulated the expression of osteoclast differentiation markers, such as ACP5 (tartrate-resistant acid phosphatase 5), CTSK (cathepsin K), and DCSTAMP (dendrocyte expressed seven transmembrane protein) in RANKL-primed RAW264.7 cells and osteoclast progenitors. When RANKL priming was combined with protease-deficient caldecrin treatment, caldecrin inhibited the LPS-stimulated phosphorylation of I $\kappa$ B and

that of JNKs, MAPKs, ERKs, and p38 to a lesser extent, leading to the inhibition of the marker gene expression.

Interestingly, pretreatment with RANKL and caldecrin increased A20 mRNA and protein levels. Furthermore, a reduction in the levels of A20 by means of RNA interference (RNAi) in RAW264.7 cells pretreated with caldecrin and RANKL resulted in enhanced osteoclast formation in response to LPS stimulation. These results indicate that caldecrin enhances A20 expression at the RANKL priming stage, which interferes with LPS-evoked NF- $\kappa$ B activation. Caldecrin alone did not activate the I $\kappa$ B, ERKs, JNKs, and p38 signaling pathways, unlike LPS, suggesting that A20-induced caldecrin may be an anti-inflammatory protein. The mechanism of A20 induction by caldecrin was further elucidated.

#### 4.2.3. Caldecrin and TREM2 Signaling

Recent studies revealed that tissue macrophages, including osteoclasts, express DAP12 and its pairing triggering receptor on myeloid cell 2 (TREM-2), and participates in diverse cell processes, including osteoclastogenesis, inflammation [88–90]. TREM-2 in mouse macrophages and RAW264.7 cells stimulated by anti-TREM-2 antibody cross-linking enhanced RANKL-stimulated osteoclast formation, whereas silencing TREM-2 resulted in the inhibition of bone differentiation, indicating that TREM-2 is a positive regulator of osteoclast differentiation and function [91]. DAP12-deficient mice also show impaired osteoclastogenesis in vitro [92]. In contrast, TREM2-deficient mice show accelerated osteoclastogenesis in vitro [93,94]. There are conflicting results regarding the relationship between TREM-2, DAP12, and osteoclastogenesis in humans and mice, suggesting that TREM-2's contribution to osteoclasts' biology may vary depending on the influence of other receptors such as TREM-1 and/or on the presence of TREM-2 ligands with variable avidity/affinity; for example, complete or partial DAP12 phosphorylation by TREM-2 ligand binding may induce either activating or inhibitory signaling through TREM-2/DAP12 [93].

TREM2/DAP12 signaling contributes to macrophage activation. Tissue macrophages have two key functions: (1) to interact with pathogens such as LPS and modulate the adaptive immune responses, and (2) to facilitate tissue repair and tissue regeneration. These macrophage polarizations, categorized as M1 and M2, are modulated by the chemokine system [95–97]. Macrophages activated by LPS or interferon- $\gamma$  alone or in combination are differentiated as classical M1 activation, which produces pro-inflammatory cytokines, whereas Th2-related cytokines IL-4 or IL-13, and anti-inflammatory molecules such as IL-10 and TGF- $\beta$ , promote alternative M2 activation, which shows an anti-inflammatory and pro-healing phenotype [97,98]. TREM-2/DAP12 signaling contributes to the negative regulation of LPS/TLR4-mediated M1 macrophage polarization [99]. TREM-2-deficient macrophages enhanced the expression of pro-inflammatory cytokines and suppressed phagocytosis following TLR4 stimulation with LPS, demonstrating that TREM-2 suppresses inflammation and promotes bacterial clearance.

To address whether caldecrin inhibits osteoclast formation via TREM-2, we prepared TREM-2 gene knockout (KO) RAW264.7 cells. Based on the study showing that TREM-2/DAP12 signaling is essential for RANKL-induced osteoclastogenesis, TREM-2-KO RAW264.7 cells were impaired to differentiate them into osteoclasts following RANKL stimulation. Therefore, to elucidate the effect of caldecrin on LPS-induced M1 macrophage polarization through TREM-2, BMMs and TREM-2-KO RAW 264.7 cells were incubated with LPS and IFN- $\gamma$  [100]. LPS induced the phosphorylation of p38, JNKs, and ERKs, the degradation of I $\kappa$ B and the expression of pro-inflammatory cytokines such as IL-1 $\beta$ , IL-6, and TNF- $\alpha$  in mouse BMMs, whereas caldecrin suppressed LPS-induced I $\kappa$ B degradation and pro-inflammatory cytokine production but did not affect p38, JNKs, and ERKs signaling pathways. Caldecrin also inhibited M1 macrophage polarization in BMMs stimulated with LPS and IFN- $\gamma$ . In RAW264.7 cells, caldecrin also inhibited LPS-induced I $\kappa$ B degradation, pro-inflammatory cytokine expression, and M1 macrophage polarization, while in Trem2-KO RAW264.7, caldecrin-mediated suppression was not observed. These results suggest that caldecrin is a negative regulator of LPS-induced inflammatory responses via

TREM2. Taken together, our findings suggest that the inhibitory mechanism of caldecrin in RANKL/RANK-mediated osteoclast formation and LPS/TLR4-mediated inflammation in macrophages relies, at least in part, on TREM2. However, this is a mere hypothesis and requires further testing (Figure 6).

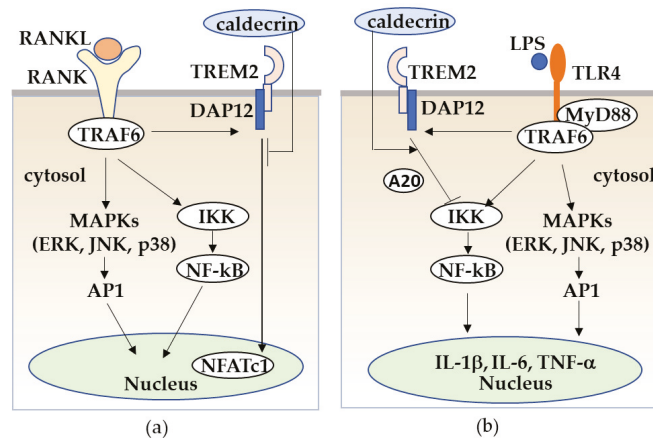


**Figure 6.** Caldecrin inhibits RANKL/RANK stimulated osteoclastogenesis from macrophages (a) and LPS/TLR4-stimulated macrophage activation through TREM-2 (b). (a) RANKL/RANK-stimulated osteoclast differentiation from macrophages is promoted with the activation of MAPKs, NF- $\kappa$ B, and the TREM-2/DAP12 axis. Caldecrin inhibits the RANKL/RANK/TRAF6 co-stimulatory TREM-2/DAP12 signal which is critical for NFATc1 activation. (b) LPS/TLR4 stimulates the TRAF6/NF- $\kappa$ B and MAPK pathways in macrophages, resulting in the activation of macrophages to M1 polarization with increased production of pro-inflammatory cytokines such as TNF- $\alpha$ , IL-1, and IL-6. Caldecrin inhibits LPS-induced M1 macrophage polarization through TREM-2/DAP12 signaling with the induction of A20.

#### 4.3. Caldecrin and Inflammation-Related Diseases

Rheumatoid arthritis (RA) is an autoimmune disease characterized by osteoclast-mediated bone and cartilage destruction resulting from inflammation in the synovium [101–103]. Osteoclast precursor cells are identified in areas of pannus invasion into the bone in RA. RANKL is expressed by both synovial fibroblasts and activated T lymphocytes derived from synovial tissues from patients with RA [104–106]. Pro-inflammatory cytokine levels, including TNF- $\alpha$ , IL1 $\alpha$ , IL-1 $\beta$ , and IL-6, induce RANKL expression in synovial fibroblasts in RA, resulting in the enhancement of osteoclastogenesis in RA [107–110]. The A20 is decreased in monocytes and synovium from RA patients, suggesting that A20 may have a protective role in RA [111–113].

We investigated whether caldecrin could improve inflammation-related bone diseases. Therefore, we investigated whether caldecrin suppresses RANKL expression in synovium derived from patients with RA. TNF- $\alpha$  treatment increased RANKL expression in synovial fibroblasts from patients with RA but not in those from healthy individuals [114]. Caldecrin inhibited TNF- $\alpha$ -stimulated RANKL overexpression in RA fibroblasts, suggesting that caldecrin inhibits inflammatory cytokine-induced RANKL expression in RA.

Osteoporosis is associated with estrogen deficiency and bone loss in postmenopausal women. The decrease in bone mass is due to enhanced or imbalanced bone resorption by osteoclasts vs. osteoblastic bone formation in osteoporosis [115,116]. While basal levels of RANKL and M-CSF are essential for physiological osteoclast formation, T-cell-derived pro-inflammatory cytokines, such as TNF- $\alpha$ , are responsible for the upregulation of osteoclast formation in estrogen deficiency [117,118]. The ovariectomy fails to induce bone loss in TNF- $\alpha$ -deficient mice and in p55 TNF receptor KO mice [119]. Ovariectomized mice are

an animal model commonly used to study postmenopausal osteoporosis, as they exhibit increased serum calcium levels due to elevated bone resorption.

To address whether caldecrin improves OVX-induced osteoporosis, we transfected plasmids encoding wild-type caldecrin or the protease-deficient mutant caldecrin in the femoral muscle of OVX model mice [120]. Caldecrin abolished changes in calcium serum concentration and collagen degradation in OVX mice, and restored bone resorption parameters to normal levels by micro-CT analysis, which decreased the bone surface to bone volume ratio, trabecular separation, increased bone volume density, and trabecular thickness and number, indicating that caldecrin suppresses estrogen deficiency-induced osteoporosis.

These findings, taken together with our *in vitro* experiments, suggest caldecrin as a possible therapeutic target in arthritis and osteoporosis.

#### 4.4. Caldecrin and Muscular Dystrophy

Takaoka et al. [11,12] administered pancreatic extract to patients diagnosed with myasthenia gravis and muscular dystrophy, including patients with fascio-scapulo-humeral muscular dystrophy (FSHD). FSHD is an autosomal dominant disease, and it is the third most common muscular dystrophy (1:15,000 to 1:20,000). It is characterized by weakness of the skeletal muscles of the face, shoulders, and upper arms. The symptoms often progress towards the lower body, and in the latest stages of the disease, the humeral, truncal, and leg muscles are also affected [121]. Takaoka et al. reported that extract administration improved the symptoms of FSHD, suggesting that the hypocalcemic effect of the pancreatic extract could contribute to slowing down the progression of muscular dystrophy [12]. In 2005, Lefkowitz D.L. and Lefkowitz S.S. reported that  $\text{Ca}^{2+}$ -triggered TNF- $\alpha$  induction, and the overexpression of adenine nucleotide translocator-1 protein, which is a component of the mitochondrial permeability transition pore, was observed in FSHD [122]. They used the  $\text{Ca}^{2+}$  channel blocker, diltiazem, for the treatment of FSHD, resulting in the prevention of the progression of muscle wasting, and proposed the use of diltiazem and a TNF- $\alpha$  inhibitor for the treatment of FSHD. In 2011, we investigated the effect of caldecrin in a naturally occurring mutant model of human congenital muscular dystrophy, a *dy/dy* mouse model. These mice lacked the laminin gene and exhibited defective muscle basement membranes. The peritoneal administration of caldecrin protein or the muscular ectopic expression of caldecrin improved the muscular destruction seen in *dy/dy* mice [123]. In 2012, Lefkowitz et al. reported that the administration of anti-RANKL reagent, denosumab, in FSHD patients improved muscle strength and dystrophic symptoms [124]. Recently, RANKL was reported to reduce muscular function when expressed in muscle cells. Anti-RANKL antibody treatment inhibits the NF- $\kappa$ B pathway and reduces muscle inflammation and damage in dystrophic mice [125]. Osteoprotegerin KO mice, which lack a secreted decoy receptor for RANKL, displayed reduced locomotor activity and signs of muscle weakness. Inhibiting RANKL improved the selective weakness and atrophy of fast-twitch IIb myofibers [126]. In addition, RANKL inhibition improved muscle strength and insulin sensitivity in osteoporotic mice and humans [127]. Therefore, caldecrin, by virtue of its anti-RANKL and anti-inflammatory activities, could be a suitable therapeutic approach for skeletal muscle dysfunction.

#### 5. Concluding Remarks

We have highlighted the serum calcium-decreasing factor caldecrin, which was first discovered in the pancreas, and its structure and protease activity were identical to those of chymotrypsin C (CTRC). Protease-deficient caldecrin inhibits RANKL-stimulated osteoclast differentiation of BMMs and bone resorption mediated by mature osteoclasts. Additionally, caldecrin inhibits osteoclast differentiation stimulated by LPS and inflammatory M1 macrophage polarization stimulated by LPS and IFN $\gamma$  through the TREM-2 pathway. Furthermore, caldecrin ameliorates the symptoms of several diseases, including osteoporosis, RA, and muscular dystrophy. Thus, caldecrin is a protease with chymotryp-



tic hydrolysis activity and non-proteolytic functions, which modulate physiological and pathological bone metabolism and inflammation via the TREM2 pathway.

**Author Contributions:** A.T. and M.T. contributed to the original draft and ideas for this review article. K.B. contributed to the research results and draft of Section 4.2.2. All authors have read and agreed to the published version of the manuscript.

**Funding:** This study was supported by KAKENHI Grant-in-Aid for Scientific Research C (A.T.: 09671904, 11671852, 14571773, 16591864, 24592811; K.B.:19K10075) from the Japan Society for the Promotion of Science, Japan.

**Institutional Review Board Statement:** The study was conducted according to the guidelines of the Declaration of Helsinki, and approved by the Institutional Review Board of Kagoshima University and Meikai University (A0703: 17 June 2008; A1006: 30 March 2010; A1107: 10 February 2011; A1207: 14 March 2012; A1733: 21 March 2017; A1814: 13 March 2018; A1942: 12 March 2019).

**Informed Consent Statement:** Not applicable.

**Data Availability Statement:** Not applicable.

**Acknowledgments:** We would like to thank Kawaguchi, S.; Tamura, N.; Hasegawa, H.; Oi, M.; Kido, S.; Fujimoto, K.; Inaba A. (Meikai University School of Dentistry), Fukushige, T.; Noda, T.; Yoshino-Yasuda, I. and Saheki T. (Kagoshima University Faculty of Medicine) for their technical support.

**Conflicts of Interest:** The authors declare no conflict of interest.

## References

- Stewart, A.F.; Longo, W.; Kreutter, D.; Jacob, R.; Burtis, W.J. Hypocalcemia associated with calcium-soap formation in a patient with a pancreatic fistula. *N. Engl. J. Med.* **1986**, *315*, 496–498. [[CrossRef](#)]
- Williams, G.A.; Bowser, E.N.; Henderson, W.J. Mode of hypocalcemic action of glucagon in the rat. *Endocrinology* **1969**, *85*, 537–541. [[CrossRef](#)]
- Stern, P.H.; Bell, N.H. Effects of glucagon on serum calcium in the rat and on bone resorption in tissue culture. *Endocrinology* **1970**, *87*, 111–117. [[CrossRef](#)]
- Zaidi, M.; Datta, H.K.; Bevis, P.J.; Wimalawansa, S.J.; MacIntyre, I. Amylin-amide: A new bone-conserving peptide from the pancreas. *Exp. Physiol.* **1990**, *75*, 529–536. [[CrossRef](#)] [[PubMed](#)]
- Alam, A.S.; Moonga, B.S.; Bevis, P.J.; Huang, C.L.; Zaidi, M. Amylin inhibits bone resorption by a direct effect on the motility of rat osteoclasts. *Exp. Physiol.* **1993**, *78*, 183–196. [[CrossRef](#)] [[PubMed](#)]
- Pettersson, M.; Ahren, B.; Böttcher, G.; Sundler, F. Calcitonin gene-related peptide: Occurrence in pancreatic islets in the mouse and the rat and inhibition of insulin secretion in the mouse. *Endocrinology* **1986**, *119*, 865–869. [[CrossRef](#)]
- D’Souza, S.M.; MacIntyre, I.; Girgis, S.I.; Mundy, G.R. Human synthetic calcitonin gene-related peptide inhibits bone resorption in vitro. *Endocrinology* **1986**, *119*, 58–61. [[CrossRef](#)]
- Tomomura, A.; Fukushige, T.; Noda, T.; Noikura, T.; Saheki, T. Serum calcium-decreasing factor (caldecrin) from porcine pancreas has proteolytic activity which has no clear connection with the calcium decrease. *FEBS Lett.* **1992**, *301*, 277–281. [[CrossRef](#)]
- Tomomura, A.; Fukushige, T.; Tomomura, M.; Noikura, T.; Nishii, Y.; Saheki, T. Caldecrin proform requires trypsin activation for the acquisition of serum calcium-decreasing activity. *FEBS Lett.* **1993**, *335*, 213–216. [[CrossRef](#)]
- Tomomura, A.; Tomomura, M.; Fukushige, T.; Akiyama, M.; Kubota, N.; Kumaki, K.; Nishii, Y.; Noikura, T.; Saheki, T. Molecular cloning and expression of serum calcium-decreasing factor (caldecrin). *J. Biol. Chem.* **1995**, *270*, 30315–30321. [[CrossRef](#)] [[PubMed](#)]
- Takaoka, Y.; Hiwaki, C.; Ozawa, H.; Ichinose, M.; Otsubo, Y.; Shikaya, T. A pancreatic protein anabolic extract. Proposal of a protein anabolic extract from pancreas. I. Preliminary report. *Acta Med. Nagasaki* **1966**, *10*, 51–57.
- Takaoka, Y.; Takamori, M.; Ichinose, M.; Shikaya, T.; Igawa, N. Hypocalcemic action of a pancreatic factor and its clinical significance on the myasthenic patients. *Acta Med. Nagasaki* **1969**, *14*, 28–35.
- Kang, J.; Wiegand, U.; Müller-Hill, B. Identification of cDNAs encoding two novel rat pancreatic serine proteases. *Gene* **1992**, *110*, 181–187. [[CrossRef](#)]
- Gomis-Rüth, F.X.; Gómez, M.; Bode, W.; Huber, R.; Avilés, F.X. The three-dimensional structure of the native ternary complex of bovine pancreatic procarboxypeptidase A with proproteinase E and chymotrypsinogen C. *EMBO J.* **1995**, *14*, 4387–4394. [[CrossRef](#)] [[PubMed](#)]
- Tomomura, A.; Akiyama, M.; Itoh, H.; Yoshino, I.; Tomomura, M.; Nishii, Y.; Noikura, T.; Saheki, T. Molecular cloning and expression of human caldecrin. *FEBS Lett.* **1996**, *386*, 26–28. [[CrossRef](#)]
- Yoshino-Yasuda, I.; Kobayashi, K.; Akiyama, M.; Itoh, H.; Tomomura, A.; Saheki, T. Caldecrin is a novel-type serine protease expressed in pancreas, but its homologue, elastase IV, is an artifact during cloning derived from caldecrin gene. *J. Biochem.* **1998**, *123*, 546–554. [[CrossRef](#)] [[PubMed](#)]

17. CTRC Chymotrypsin C. Homo Sapiens (Human). Available online: <https://www.ncbi.nlm.nih.gov/gene/11330> (accessed on 28 May 2021).
18. Chymotrypsin C | S1: Chymotrypsin | IUPHAR/BPS Guide to PHARMACOLOGY. Available online: <http://www.guidetopharmacology.org/GRAC/ObjectDisplayForward?objectId=2341> (accessed on 28 May 2021).
19. Batra, J.; Szabó, A.; Caulfield, T.R.; Soares, A.S.; Sahin-Tóth, M.; Radisky, E.S. Long-range electrostatic complementarity governs substrate recognition by human chymotrypsin C, a key regulator of digestive enzyme activation. *J. Biol. Chem.* **2013**, *288*, 9848–9859. [[CrossRef](#)] [[PubMed](#)]
20. Wang, H.; Yuan, D.; Xu, R.; Chi, C.-H. Purification, cDNA cloning, and recombinant expression of chymotrypsin C from porcine pancreas. *Acta Biochim. Biophys. Sin.* **2011**, *43*, 568–575. [[CrossRef](#)]
21. Chymotrypsin, C. Available online: <https://enzyme.expasy.org/EC/3.4.21.2> (accessed on 28 May 2021).
22. Pancreatic Elastase II. Available online: <https://enzyme.expasy.org/EC/3.4.21.71> (accessed on 28 May 2021).
23. Pancreatic Endopeptidase E. Available online: <https://enzyme.expasy.org/EC/3.4.21.70> (accessed on 28 May 2021).
24. Steer, M.L.; Waxman, I. Chronic pancreatitis. *N. Engl. J. Med.* **1995**, *332*, 1482–1490. [[CrossRef](#)] [[PubMed](#)]
25. Sahin-Tóth, M. Biochemical models of hereditary pancreatitis. *Endocrinol. Metab. Clin. North. Am.* **2006**, *35*, 303–312. [[CrossRef](#)]
26. Teich, N.; Rosendahl, J.; Tóth, M.; Mössner, J.; Sahin-Tóth, M. Mutations of human cationic trypsinogen (PRSS1) and chronic pancreatitis. *Hum. Mutat.* **2006**, *27*, 721–730. [[CrossRef](#)]
27. Drenth, J.P.; te Morsche, R.; Jansen, J.B. Mutations in serine protease inhibitor Kazal type 1 are strongly associated with chronic pancreatitis. *Gut* **2002**, *50*, 687–692. [[CrossRef](#)]
28. Whitcomb, D.C.; Gorry, M.C.; Preston, R.A.; Furey, W.; Sossenheimer, M.J.; Ulrich, C.D.; Martin, S.P.; Gates, L.K., Jr.; Amann, S.T.; Toskes, P.P.; et al. Hereditary pancreatitis is caused by a mutation in the cationic trypsinogen gene. *Nat. Genet.* **1996**, *14*, 141–145. [[CrossRef](#)] [[PubMed](#)]
29. Várallyay, E.; Pál, G.; Patthy, A.; Szilágyi, L.; Gráf, L. Two mutations in rat trypsin confer resistance against autolysis. *Biochem. Biophys. Res. Commun.* **1998**, *243*, 56–60. [[CrossRef](#)] [[PubMed](#)]
30. Rinderknecht, H.; Adham, N.F.; Renner, I.G.; Carmack, C. A possible zymogen self-destruct mechanism preventing pancreatic autodigestion. *Int. J. Pancreatol.* **1988**, *3*, 33–44. [[CrossRef](#)]
31. Nemoda, Z.; Sahin-Tóth, M. Chymotrypsin C (caldecrin) stimulates autoactivation of human cationic trypsinogen. *J. Biol. Chem.* **2006**, *281*, 11879–11886. [[CrossRef](#)]
32. Szmola, R.; Sahin-Tóth, M. Chymotrypsin C (caldecrin) promotes degradation of human cationic trypsin: Identity with Rinderknecht's enzyme. *Proc. Natl. Acad. Sci. USA* **2007**, *104*, 11227–11232. [[CrossRef](#)] [[PubMed](#)]
33. Rosendahl, J.; Witt, H.; Szmola, R.; Bhatia, E.; Ozsvári, B.; Landt, O.; Schulz, H.U.; Gress, T.M.; Pfützer, R.; Löhr, M.; et al. Chymotrypsin C (CTRC) variants that diminish activity or secretion are associated with chronic pancreatitis. *Nat. Genet.* **2008**, *40*, 78–82. [[CrossRef](#)] [[PubMed](#)]
34. Masson, E.; Chen, J.M.; Scotet, V.; Le Maréchal, C.; Férec, C. Association of rare chymotrypsinogen C (CTRC) gene variations in patients with idiopathic chronic pancreatitis. *Hum. Genet.* **2008**, *123*, 83–91. [[CrossRef](#)]
35. Hegyi, E.; Sahin-Tóth, M. Genetic Risk in Chronic Pancreatitis: The Trypsin-Dependent Pathway. *Dig. Dis. Sci.* **2017**, *62*, 1692–1701. [[CrossRef](#)] [[PubMed](#)]
36. Derix, M.H.; Szmola, R.; Morsche, R.H.; Sunderasan, S.; Chacko, A.; Drenth, J.P. Tropical calcific pancreatitis and its association with CTRC and SPINK1 (p.N34S) variants. *Eur. J. Gastroenterol. Hepatol.* **2009**, *21*, 889–894. [[CrossRef](#)] [[PubMed](#)]
37. Paliwal, S.; Bhaskar, S.; Mani, K.R.; Reddy, D.N.; Rao, G.V.; Singh, S.P.; Thomas, V.; Chandak, G.R. Comprehensive screening of chymotrypsin C (CTRC) gene in tropical calcific pancreatitis identifies novel variants. *Gut* **2013**, *62*, 1602–1606. [[CrossRef](#)]
38. Nemeth, B.C.; Sahin-Toth, M. Human cationic trypsinogen (PRSS1) variants and chronic pancreatitis. *Am. J. Physiol. Gastrointest Liver Physiol.* **2014**, *306*, G466–G473. [[CrossRef](#)] [[PubMed](#)]
39. Izbicka, E.; Yoneda, T.; Takaoka, Y.; Horn, D.; Williams, P.; Mundy, G.R. Identification of a novel bone/calcium metabolism-regulating factor in porcine pancreas. *J. Biol. Chem.* **1996**, *271*, 23230–23234. [[CrossRef](#)] [[PubMed](#)]
40. Wong, B.R.; Rho, J.; Arron, J.; Robinson, E.; Orlicki, J.; Chao, M.; Kalachikov, S.; Cayani, E.; Bartlett, F.S., III; Frankel, W.N.; et al. TRANCE is a novel ligand of the tumor necrosis factor receptor family that activates c-Jun N-terminal kinase in T cells. *J. Biol. Chem.* **1997**, *272*, 25190–25194. [[CrossRef](#)]
41. Yasuda, H.; Shima, N.; Nakagawa, N.; Yamaguchi, K.; Kinosaki, M.; Mochizuki, S.; Tomoyasu, A.; Yano, K.; Goto, M.; Murakami, A.; et al. Osteoclast differentiation factor is a ligand for osteoprotegerin/osteoclastogenesis-inhibitory factor and is identical to TRANCE/RANKL. *Proc. Natl. Acad. Sci. USA* **1998**, *95*, 3597–3602. [[CrossRef](#)] [[PubMed](#)]
42. Lacey, D.L.; Timms, E.; Tan, H.L.; Kelley, M.J.; Dunstan, C.R.; Burgess, T.; Elliott, R.; Colombero, A.; Elliott, G.; Scully, S.; et al. Osteoprotegerin ligand is a cytokine that regulates osteoclast differentiation and activation. *Cell* **1998**, *93*, 165–176. [[CrossRef](#)]
43. Fuller, K.; Wong, B.; Fox, S.; Choi, Y.; Chambers, T.J. TRANCE is necessary and sufficient for osteoblast-mediated activation of bone resorption in osteoclasts. *J. Exp. Med.* **1998**, *188*, 997–1001. [[CrossRef](#)]
44. Nakashima, T.; Hayashi, M.; Fukunaga, T.; Kurata, K.; Oh-Hora, M.; Feng, J.Q.; Bonewald, L.F.; Kodama, T.; Wutz, A.; Wagner, E.F.; et al. Evidence for osteocyte regulation of bone homeostasis through RANKL expression. *Nat. Med.* **2011**, *17*, 1231–1234. [[CrossRef](#)]
45. Suda, T.; Takahashi, N.; Martin, T.J. Modulation of osteoclast differentiation. *Endocr. Rev.* **1992**, *13*, 66–80. [[CrossRef](#)]
46. Teitelbaum, S.L. Bone resorption by osteoclasts. *Science* **2000**, *289*, 1504–1508. [[CrossRef](#)] [[PubMed](#)]

47. Asagiri, M.; Takayanagi, H. The molecular understanding of osteoclast differentiation. *Bone* **2007**, *40*, 251–264. [[CrossRef](#)] [[PubMed](#)]
48. Wong, B.R.; Josien, R.; Lee, S.Y.; Vologodskaja, M.; Steinman, R.M.; Choi, Y. The TRAF family of signal transducers mediate NF- $\kappa$ B activation by the TRANCE receptor. *J. Biol. Chem.* **1998**, *273*, 28355–28359. [[CrossRef](#)]
49. Mizukami, J.; Takaesu, G.; Akatsuka, H.; Sakurai, H.; Ninomiya-Tsuji, J.; Matsumoto, K.; Sakurai, N. Receptor activator of NF- $\kappa$ B ligand (RANKL) activates TAK1 mitogen-activated protein kinase kinase through a signaling complex containing RANK, TAB2, and TRAF6. *Mol. Cell Biol.* **2002**, *22*, 992–1000. [[CrossRef](#)] [[PubMed](#)]
50. Darnay, B.G.; Haridas, V.; Ni, J.; Moore, P.A.; Aggarwal, B.B. Characterization of the intracellular domain of receptor activator of NF- $\kappa$ B (RANK). Interaction with tumor necrosis factor receptor-associated factors and activation of NF- $\kappa$ B and c-Jun N-terminal kinase. *J. Biol. Chem.* **1998**, *273*, 20551–20555. [[CrossRef](#)]
51. Lee, S.E.; Woo, K.M.; Kim, S.Y.; Kim, H.M.; Kwack, K.; Lee, Z.H.; Kim, H.H. The phosphatidylinositol 3-kinase, p38, and extracellular signal-regulated kinase pathways are involved in osteoclast differentiation. *Bone* **2002**, *30*, 71–77. [[CrossRef](#)]
52. Li, X.; Udagawa, N.; Itoh, K.; Suda, K.; Murase, Y.; Nishihara, T.; Suda, T.; Takahashi, N. p38 MAPK-mediated signals are required for inducing osteoclast differentiation but not for osteoclast function. *Endocrinology* **2002**, *43*, 3105–3113. [[CrossRef](#)]
53. David, J.P.; Sabapathy, K.; Hoffmann, O.; Idarraga, M.H.; Wagner, E.F. JNK1 modulates osteoclastogenesis through both c-Jun phosphorylation-dependent and -independent mechanisms. *J. Cell Sci.* **2002**, *115*, 4317–4325. [[CrossRef](#)]
54. Wang, Z.Q.; Ovitt, C.; Grigoriadis, A.E.; Mohle-Steinlein, U.; Ruther, U.; Wagner, E.F. Bone and haematopoietic defects in mice lacking c-fos. *Nature* **1992**, *360*, 741–745. [[CrossRef](#)]
55. Takayanagi, H.; Kim, S.; Koga, T.; Nishina, H.; Isshiki, M.; Yoshida, H.; Saiura, A.; Isobe, M.; Yokochi, T.; Inoue, J.; et al. Induction and activation of the transcription factor NFATc1 (NFAT2) integrate RANKL signaling in terminal differentiation of osteoclasts. *Dev. Cell* **2002**, *3*, 889–901. [[CrossRef](#)]
56. Ishida, N.; Hayashi, K.; Hoshijima, M.; Ogawa, T.; Koga, S.; Miyatake, Y.; Kumegawa, M.; Kimura, T.; Takeya, T. Large scale gene expression analysis of osteoclastogenesis in vitro and elucidation of NFAT2 as a key regulator. *J. Biol. Chem.* **2002**, *277*, 41147–41156. [[CrossRef](#)] [[PubMed](#)]
57. Koga, T.; Inui, M.; Inoue, K.; Kim, S.; Suematsu, A.; Kobayashi, E.; Iwata, T.; Ohnishi, H.; Matozaki, T.; Kodama, T.; et al. Costimulatory signals mediated by the ITAM motif cooperate with RANKL for bone homeostasis. *Nature* **2004**, *428*, 758–763. [[CrossRef](#)] [[PubMed](#)]
58. Mócsai, A.; Humphrey, M.B.; van Ziffle, J.A.G.; Hu, Y.; Burghardt, A.; Spusta, S.C.; Majumdar, S.; Lanier, L.L.; Lowell, C.A.; Nakamura, M.C. The immunomodulatory adapter proteins DAP12 and Fc receptor gamma-chain (FcRgamma) regulate development of functional osteoclasts through the Syk tyrosine kinase. *Proc. Natl. Acad. Sci. USA* **2004**, *101*, 6158–6163. [[CrossRef](#)] [[PubMed](#)]
59. Asagiri, M.; Sato, K.; Usami, T.; Ochi, S.; Nishina, H.; Yoshida, H.; Morita, I.; Wagner, E.F.; Mak, T.W.; Serfling, E.; et al. Autoamplification of NFATc1 expression determines its essential role in bone homeostasis. *J. Exp. Med.* **2005**, *202*, 1261–1269. [[CrossRef](#)]
60. Hirotani, H.; Tuohy, N.A.; Woo, J.T.; Stern, P.H.; Clipstone, N.A. The calcineurin/nuclear factor of activated T cells signaling pathway regulates osteoclastogenesis in RAW264.7 cells. *J. Biol. Chem.* **2004**, *279*, 13984–13992. [[CrossRef](#)]
61. Hasegawa, H.; Kido, S.; Tomomura, M.; Fujimoto, K.; Ohi, M.; Kiyomura, M.; Kanegae, H.; Inaba, A.; Sakagami, H.; Tomomura, A. Serum calcium-decreasing factor, caldecrin, inhibits osteoclast differentiation by suppression of NFATc1 activity. *J. Biol. Chem.* **2010**, *285*, 25448–25457. [[CrossRef](#)] [[PubMed](#)]
62. Teti, A.; Marchisio, P.C.; Zallone, A.Z. Clear zone in osteoclast function: Role of podosomes in regulation of bone-resorbing activity. *Am. J. Physiol.* **1991**, *261*, C1–C7. [[CrossRef](#)]
63. Zou, W.; Teitelbaum, S.L. Integrins, growth factors, and the osteoclast cytoskeleton. *Ann. N. Y. Acad. Sci.* **2010**, *1192*, 27–31. [[CrossRef](#)]
64. Zou, W.; Kitaura, H.; Reeve, J.; Long, F.; Tybulewicz, V.L.; Shattil, S.J.; Ginsberg, M.H.; Ross, F.P.; Teitelbaum, S.L. Syk, c-Src, the avb3 integrin, and ITAM immunoreceptors, in concert, regulate osteoclastic bone resorption. *J. Cell Biol.* **2007**, *176*, 877–888. [[CrossRef](#)]
65. Reeve, J.L.; Zou, W.; Liu, Y.; Maltzman, J.S.; Ross, F.P.; Teitelbaum, S.L. SLP-76 couples Syk to the osteoclast cytoskeleton. *J. Immunol.* **2009**, *183*, 1804–1812. [[CrossRef](#)]
66. Duong, L.T.; Lakkakorpi, P.T.; Nakamura, I.; Machwate, M.; Nagy, R.M.; Rodan, G.A. PYK2 in osteoclasts is an adhesion kinase, localized in the sealing zone, activated by ligation of  $\alpha$ (v) $\beta$ 3 integrin, and phosphorylated by src kinase. *J. Clin. Investig.* **1998**, *102*, 881–892. [[CrossRef](#)]
67. Wang, K.Z.; Wara-Aswapati, N.; Boch, J.A.; Yoshida, Y.; Hu, C.D.; Galson, D.L.; Auron, P.E. TRAF6 activation of PI 3-kinase-dependent cytoskeletal changes is cooperative with Ras and is mediated by an interaction with cytoplasmic Src. *J. Cell Sci.* **2006**, *119*, 1579–1591. [[CrossRef](#)] [[PubMed](#)]
68. Kajjya, H.; Okamoto, F.; Nemoto, T.; Kimachi, K.; Toh-Goto, K.; Nakayama, S.; Okabe, K. RANKL-induced TRPV2 expression regulates osteoclastogenesis via calcium oscillations. *Cell Calcium* **2010**, *48*, 260–269. [[CrossRef](#)] [[PubMed](#)]
69. Masuyama, R.; Vriens, J.; Voets, T.; Karashima, Y.; Owsianik, G.; Vennekens, R.; Lieben, L.; Torrekens, S.; Moermans, K.; Vanden Bosch, A.; et al. TRPV4-mediated calcium influx regulates terminal differentiation of osteoclasts. *Cell Metab.* **2008**, *8*, 257–265. [[CrossRef](#)]

70. Chamoux, E.; Bisson, M.; Payet, M.D.; Roux, S. TRPV-5 mediates a receptor activator of NF- $\kappa$ B (RANK) ligand-induced increase in cytosolic Ca<sup>2+</sup> in human osteoclasts and down-regulates bone resorption. *J. Biol. Chem.* **2010**, *285*, 25354–25362. [[CrossRef](#)] [[PubMed](#)]
71. Tomomura, M.; Hasegawa, H.; Suda, N.; Sakagami, H.; Tomomura, A. Serum calcium-decreasing factor, caldecrin, inhibits receptor activator of NF- $\kappa$ B ligand (RANKL)-mediated Ca<sup>2+</sup> signaling and actin ring formation in mature osteoclasts via suppression of Src signaling pathway. *J. Biol. Chem.* **2012**, *287*, 17963–17974. [[CrossRef](#)]
72. Nair, S.P.; Meghji, S.; Wilson, M.; Reddi, K.; White, P.; Henderson, B. Bacterially induced bone destruction: Mechanisms and misconceptions. *Infect. Immun.* **1996**, *64*, 2371–2380. [[CrossRef](#)]
73. Tobias, P.S.; Gegner, J.; Tapping, R.; Orr, S.; Mathison, J.; Lee, J.D.; Kravchenko, V.; Han, J.; Ulevitch, R.J. Lipopolysaccharide dependent cellular activation. *J. Periodontal Res.* **1997**, *32*, 99–103. [[CrossRef](#)]
74. Takami, M.; Kim, N.; Rho, J.; Choi, Y. Stimulation by toll-like receptors inhibits osteoclast differentiation. *J. Immunol.* **2002**, *169*, 1516–1523. [[CrossRef](#)] [[PubMed](#)]
75. Qureshi, S.T.; Larivière, L.; Leveque, G.; Clermont, S.; Moore, K.J.; Gros, P.; Malo, D. Endotoxin-tolerant mice have mutations in Toll-like receptor 4 (Tlr4). *J. Exp. Med.* **1999**, *189*, 615–625. [[CrossRef](#)]
76. Hou, L.; Sasaki, H.; Stashenko, P. Toll-like receptor 4-deficient mice have reduced bone destruction following mixed anaerobic infection. *Infect. Immun.* **2000**, *68*, 4681–4687. [[CrossRef](#)] [[PubMed](#)]
77. Satoh, T.; Akira, S. Toll-Like receptor signaling and its inducible proteins. *Microbiol. Spectr.* **2016**, *4*. [[CrossRef](#)]
78. Takeda, K.; Akira, S. TLR signaling pathways. *Semin Immunol.* **2004**, *16*, 3–9. [[CrossRef](#)]
79. Akira, S.; Takeda, K. Toll-like receptor signaling. *Nat. Rev. Immunol.* **2004**, *4*, 499–511. [[CrossRef](#)] [[PubMed](#)]
80. Medzhitov, R.; Preston-Hurlburt, P.; Kopp, E.; Stadlen, A.; Chen, C.; Ghosh, S.; Janeway, C.A., Jr. MyD88 is an adaptor protein in the hToll/IL-1 receptor family signaling pathways. *Mol. Cell* **1998**, *2*, 253–258. [[CrossRef](#)]
81. Zou, W.; Bar-Shavit, Z. Dual modulation of osteoclast differentiation by lipopolysaccharide. *J. Bone Miner. Res.* **2002**, *17*, 1211–1218. [[CrossRef](#)]
82. Liu, J.; Wang, S.; Zhang, P.; Said-Al-Naief, N.; Michalek, S.M.; Feng, X. Molecular mechanism of the bifunctional role of lipopolysaccharide in osteoclastogenesis. *J. Biol. Chem.* **2009**, *284*, 12512–12523. [[CrossRef](#)] [[PubMed](#)]
83. O'Reilly, S.M.; Moynagh, P.N. Regulation of Toll-like receptor 4 signaling by A20 zinc finger protein. *Biochem. Biophys. Res. Commun.* **2003**, *303*, 586–593. [[CrossRef](#)]
84. Ingrid, E.; Wertz, I.E.; O'Rourke, K.M.; Zhou, H.; Eby, M.; Aravind, L.; Seshagiri, S.; Wu, P.; Wiesmann, C.; Baker, R.; et al. De-ubiquitination and ubiquitin ligase domains of A20 downregulate NF- $\kappa$ B signalling. *Nature* **2004**, *430*, 694–699. [[CrossRef](#)]
85. Mabileau, G.; Chappard, D.; Sabokbar, A. Role of the A20-TRAF6 axis in lipopolysaccharide-mediated osteoclastogenesis. *J. Biol. Chem.* **2011**, *286*, 3242–3249. [[CrossRef](#)]
86. Hong, J.-Y.; Bae, W.-J.; Yi, J.-K.; Kim, G.-T.; Kim, E.-C. Anti-inflammatory and anti-osteoclastogenic effects of zinc finger protein A20 overexpression in human periodontal ligament cells. *J. Periodontal Res.* **2016**, *51*, 529–539. [[CrossRef](#)] [[PubMed](#)]
87. Kawaguchi, S.; Bandow, K.; Tamura, N.; Tomomura, M.; Shimada, J.; Tomomura, A. Effect of caldecrin on the lipopolysaccharide-induced osteoclast differentiation. *J. Meikai Dent. Med.* **2018**, *47*, 126–138.
88. Sharif, O.; Knapp, S. From expression to signaling: Roles of TREM-1 and TREM-2 in innate immunity and bacterial infection. *Immunobiology* **2008**, *213*, 701–713. [[CrossRef](#)] [[PubMed](#)]
89. Ford, J.W.; McVicar, D.W. TREM and TREM-like receptors in inflammation and disease. *Curr. Opin. Immunol.* **2009**, *21*, 38–46. [[CrossRef](#)] [[PubMed](#)]
90. Klesney-Tait, J.; Turnbull, I.R.; Colonna, M. The TREM receptor family and signal integration. *Nat. Immunol.* **2006**, *7*, 1266–1273. [[CrossRef](#)]
91. Humphrey, M.B.; Daws, M.R.; Spusta, S.C.; Niemi, E.C.; Torchia, J.A.; Lanier, L.L.; Seaman, W.E.; Nakamura, M.C. TREM2, a DAP12-associated receptor, regulates osteoclast differentiation and function. *J. Bone Min. Res.* **2006**, *21*, 237–245. [[CrossRef](#)]
92. Kaifu, T.; Nakahara, J.; Inui, M.; Mishima, K.; Momiyama, T.; Kaji, M.; Sugahara, A.; Koito, H.; Ujike-Asai, A.; Nakamura, A.; et al. Osteopetrosis and thalamic hypomyelination with synaptic degeneration in DAP12-deficient mice. *J. Clin. Investig.* **2003**, *111*, 323–332. [[CrossRef](#)]
93. Marco Colonna, M.; Turnbull, I.; Klesney-Tait, J. The enigmatic function of TREM-2 in osteoclastogenesis. *Adv. Exp. Med. Biol.* **2007**, *602*, 97–105. [[CrossRef](#)]
94. Otero, K.; Shinohara, M.; Zhao, H.; Cella, M.; Gilfillan, S.; Colucci, A.; Faccio, R.; Ross, F.P.; Teitelbaum, S.L.; Takayanagi, H.; et al. TREM2 and beta-catenin regulate bone homeostasis by controlling the rate of osteoclastogenesis. *J. Immunol.* **2012**, *188*, 2612–2621. [[CrossRef](#)]
95. Mantovani, A.; Sica, A.; Sozzani, S.; Allavena, P.; Vecchi, A.; Locati, M. The chemokine system in diverse forms of macrophage activation and polarization. *Trends Immunol.* **2004**, *25*, 677–686. [[CrossRef](#)]
96. Gordon, S.; Taylor, P.R. Monocyte and macrophage heterogeneity. *Nat. Rev. Immunol.* **2005**, *5*, 953–964. [[CrossRef](#)]
97. Mills, C.D.; Kincaid, K.; Alt, J.M.; Heilman, M.J.; Hill, A.M. M-1/M-2 macrophages and the Th1/Th2 paradigm. *J. Immunol.* **2000**, *164*, 6166–6173. [[CrossRef](#)] [[PubMed](#)]
98. Italiani, P.; Boraschi, D. From monocytes to M1/M2 macrophages: Phenotypical vs. functional differentiation. *Front. Immunol.* **2014**, *5*, 514. [[CrossRef](#)]

99. Turnbull, I.R.; Gilfillan, S.; Cella, M.; Aoshi, T.; Miller, M.; Piccio, L.; Hernandez, M.; Colonna, M. Cutting Edge: TREM-2 Attenuates Macrophage Activation. *J. Immunol.* **2006**, *177*, 3520–3524. [\[CrossRef\]](#)
100. Bandow, K.; Hasegawa, H.; Tomomura, M.; Tomomura, A. Caldecrin inhibits lipopolysaccharide-induced pro-inflammatory cytokines and M1 macrophage polarization through the immunoreceptor triggering receptor expressed in myeloid cells-2. *Biochem. Biophys. Res. Commun.* **2020**, *523*, 1027–1033. [\[CrossRef\]](#)
101. Guo, Q.; Wang, Y.; Xu, D.; Nossent, J.; Pavlos, N.J.; Xu, J. Rheumatoid arthritis: Pathological mechanisms and modern pharmacologic therapies. *Bone Res.* **2018**, *6*, 15. [\[CrossRef\]](#) [\[PubMed\]](#)
102. Auréal, M.; Machuca-Gayet, I.; Coury, F. Rheumatoid arthritis in the view of osteoimmunology. *Biomolecules* **2020**, *11*, 48. [\[CrossRef\]](#) [\[PubMed\]](#)
103. Sweeney, S.E.; Firestein, G.S. Rheumatoid arthritis: Regulation of synovial inflammation. *Int. J. Biochem. Cell Biol.* **2004**, *36*, 372–378. [\[CrossRef\]](#)
104. Gravallesse, E.M.; Manning, C.; Tsay, A.; Naito, A.; Pan, C.; Amento, E.; Goldring, S.R. Synovial tissue in rheumatoid arthritis is a source of osteoclast differentiation factor. *Arthritis Rheum.* **2000**, *43*, 250–258. [\[CrossRef\]](#)
105. Takayanagi, H.; Iizuka, H.; Juji, T.; Nakagawa, T.; Yamamoto, A.; Miyazaki, T.; Koshihara, Y.; Oda, H.; Nakamura, K.; Tanaka, S. Involvement of receptor activator of nuclear factor kappaB ligand/osteoclast differentiation factor in osteoclastogenesis from synoviocytes in rheumatoid arthritis. *Arthritis Rheum.* **2000**, *43*, 259–269. [\[CrossRef\]](#)
106. Crotti, T.N.; Smith, M.D.; Weedon, H.; Ahern, M.J.; Findlay, D.M.; Kraan, M.; Tak, P.P.; Haynes, D.R. Receptor activator NF-kappaB ligand (RANKL) expression in synovial tissue from patients with rheumatoid arthritis, spondyloarthropathy, osteoarthritis, and from normal patients: Semiquantitative and quantitative analysis. *Ann. Rheum. Dis.* **2002**, *61*, 1047–1054. [\[CrossRef\]](#)
107. Wei, S.; Kitaura, H.; Zhou, P.; Ross, F.P.; Teitelbaum, S.L. IL-1 mediates TNF-induced osteoclastogenesis. *J. Clin. Investig.* **2005**, *115*, 282–290. [\[CrossRef\]](#) [\[PubMed\]](#)
108. Wang, T.; He, C. TNF-alpha and IL-6: The Link between Immune and Bone System. *Curr. Drug Targets.* **2020**, *21*, 213–227. [\[CrossRef\]](#)
109. Lam, J.; Takeshita, S.; Barker, J.E.; Kanagawa, O.; Ross, E.P.; Teitelbaum, S.L. TNF-alpha induces osteoclastogenesis by direct stimulation of macrophages exposed to permissive levels of RANK ligand. *J. Clin. Investig.* **2000**, *106*, 1481–1488. [\[CrossRef\]](#)
110. Hashizume, M.; Mihara, M. The roles of interleukin-6 in the pathogenesis of rheumatoid arthritis. *Arthritis* **2011**. [\[CrossRef\]](#) [\[PubMed\]](#)
111. Elsby, L.M.; Orozco, G.; Denton, J.; Worthington, J.; Ray, D.W.; Donn, R.P. Functional evaluation of TNFAIP3 (A20) in rheumatoid arthritis. *Clin. Exp. Rheumatol.* **2010**, *28*, 708–714. [\[PubMed\]](#)
112. Hah, Y.S.; Lee, Y.R.; Jun, J.S.; Lim, H.S.; Kim, H.O.; Jeong, Y.G.; Hur, G.M.; Lee, S.Y.; Chung, M.J.; Park, J.W.; et al. A20 suppresses inflammatory responses and bone destruction in human fibroblast-like synoviocytes and in mice with collagen-induced arthritis. *Arthritis Rheum.* **2010**, *62*, 2313–2321. [\[CrossRef\]](#)
113. Zhang, L.; Yao, Y.; Tian, J.; Jiang, W.; Zhou, S.; Chen, J.; Xu, T.; Wu, M. Alterations and abnormal expression of A20 in peripheral monocyte subtypes in patients with rheumatoid arthritis. *Clin. Rheumatol.* **2021**, *40*, 341–348. [\[CrossRef\]](#) [\[PubMed\]](#)
114. Fujimoto, K.; Oi, M.; Hasegawa, K.; Kanegae, H.; Inaba, A.; Tomomura, M.; Tomomura, A. Inhibition of RANKL Expression in Synovial Fibroblasts of Rheumatoid Arthritis by Serum Calcium-decreasing Factor (Caldecrin). *J. Meikai Dent. Med.* **2010**, *39*, 42–51.
115. Manolagas, S.C. Birth and death of bone cells: Basic regulatory mechanisms and implications for the pathogenesis and treatment of osteoporosis. *Endocr. Rev.* **2000**, *21*, 115–137.
116. Weitzmann, M.N.; Pacifici, R. Estrogen deficiency and bone loss: An inflammatory tale. *J. Clin. Investig.* **2006**, *116*, 1186–1194. [\[CrossRef\]](#) [\[PubMed\]](#)
117. Cenci, S.; Weitzmann, M.N.; Roggia, C.; Namba, N.; Novack, D.; Woodring, J.; Pacifici, R. Estrogen deficiency induces bone loss by enhancing T-cell production of TNF-alpha. *J. Clin. Investig.* **2000**, *106*, 1229–1237. [\[CrossRef\]](#)
118. Zhao, R. Immune regulation of osteoclast function in postmenopausal osteoporosis: A critical interdisciplinary perspective. *Int. J. Med. Sci.* **2012**, *9*, 825–832. [\[CrossRef\]](#) [\[PubMed\]](#)
119. Roggia, C.; Gao, Y.; Cenci, S.; Weitzmann, M.N.; Toraldo, G.; Isaia, G.; Pacifici, R. Up-regulation of TNF-producing T cells in the bone marrow: A key mechanism by which estrogen deficiency induces bone loss in vivo. *Proc. Natl. Acad. Sci. USA* **2001**, *98*, 13960–13965. [\[CrossRef\]](#)
120. Oi, M.; Kido, S.; Hasegawa, H.; Fujimoto, K.; Tomomura, M.; Kanegae, H.; Suda, N.; Tomomura, A. Inhibitory effects on bone resorption in postmenopausal osteoporosis model mice by delivery of serum calcium decreasing factor (Caldecrin) gene. *J. Meikai Dent. Med.* **2011**, *40*, 146–154.
121. Hamel, J.; Tawil, R. Facioscapulohumeral Muscular Dystrophy: Update on Pathogenesis and Future Treatments. *Neurotherapeutics* **2018**, *15*, 863–871. [\[CrossRef\]](#) [\[PubMed\]](#)
122. Lefkowitz, D.L.; Lefkowitz, S.S. Facioscapulohumeral muscular dystrophy: A progressive degenerative disease that responds to diltiazem. *Med. Hypotheses* **2005**, *65*, 716–721. [\[CrossRef\]](#)
123. Tomomura, M.; Fujii, T.; Sakagami, H.; Tomomura, A. Serum calcium-decreasing factor, caldecrin, ameliorates muscular dystrophy in dy/dy mice. *In Vivo* **2011**, *25*, 157–163.
124. Lefkowitz, S.S.; Lefkowitz, D.L.; Kethley, J. Treatment of facioscapulohumeral muscular dystrophy with Denosumab. *Am. J. Case Rep.* **2012**, *13*, 66–68. [\[CrossRef\]](#) [\[PubMed\]](#)

125. Hamoudi, D.; Marcadet, L.; Piette Boulanger, A.; Yagita, H.; Bouredji, Z.; Argaw, A.; Frenette, J. An anti-RANKL treatment reduces muscle inflammation and dysfunction and strengthens bone in dystrophic mice. *Hum. Mol. Genet.* **2019**, *28*, 3101–3112. [[CrossRef](#)] [[PubMed](#)]
126. Hamoudi, D.; Bouredji, Z.; Marcadet, L.; Yagita, H.; Landry, L.B.; Argaw, A.; Frenette, J. Muscle weakness and selective muscle atrophy in osteoprotegerin-deficient mice. *Hum. Mol. Genet.* **2020**, *29*, 483–494. [[CrossRef](#)] [[PubMed](#)]
127. Bonnet, N.; Bourgoin, L.; Biver, E.; Douni, E.; Ferrari, S. RANKL inhibition improves muscle strength and insulin sensitivity and restores bone mass. *J. Clin. Investig.* **2020**, *130*, 3329. [[CrossRef](#)] [[PubMed](#)]





Article

# Chromatographic, Chemometric and Antioxidant Assessment of the Equivalence of Granules and Herbal Materials of *Angelicae Sinensis Radix*

Valentina Razmovski-Naumovski <sup>1,2,3</sup>, Xian Zhou <sup>2</sup>, Ho Yee Wong <sup>3</sup>, Antony Kam <sup>3,4</sup>, Jarryd Pearson <sup>2</sup> and Kelvin Chan <sup>2,3,5,\*</sup>

<sup>1</sup> South Western Sydney Clinical School, School of Medicine, University of New South Wales, Sydney, NSW 2052, Australia; v.naumovski@unsw.edu.au

<sup>2</sup> NICM Health Research Institute, Western Sydney University, Penrith, NSW 2751, Australia; p.zhou@westernsydney.edu.au (X.Z.); j.pearson@westernsydney.edu.au (J.P.)

<sup>3</sup> School of Pharmacy, The University of Sydney, A15, Science Rd, Camperdown, NSW 2006, Australia; ellewong613@gmail.com (H.Y.W.); k.antony@ntu.edu.sg (A.K.)

<sup>4</sup> School of Biological Sciences, Nanyang Technological University, 60 Nanyang Drive, Singapore 63755, Singapore

<sup>5</sup> School of Pharmacy and Biomolecular Sciences, Liverpool John Moores University, Liverpool L3 3AF, UK

\* Correspondence: k.k.chan@ljmu.ac.uk or k.chan@westernsydney.edu.au; Tel.: +85-295-563-695

Received: 30 May 2020; Accepted: 19 June 2020; Published: 23 June 2020

**Abstract:** **Background:** Granules are a popular way of administering herbal decoctions. However, there are no standardised quality control methods for granules, with few studies comparing the granules to traditional herbal decoctions. This study developed a multi-analytical platform to compare the quality of granule products to herb/decoction pieces of *Angelicae Sinensis Radix* (Danggui). **Methods:** A validated ultra-performance liquid chromatography coupled with photodiode array detector (UPLC-PDA) method quantitatively compared the aqueous extracts. Hierarchical agglomerative clustering analysis (HCA) and principal component analysis (PCA) clustered the samples according to three chemical compounds: ferulic acid, caffeic acid and Z-ligustilide. Ferric ion-reducing antioxidant power (FRAP) and 2,2-Diphenyl-1-picrylhydrazyl radical scavenging capacity (DPPH) assessed the antioxidant activity of the samples. **Results:** HCA and PCA allocated the samples into two main groups: granule products and herb/decoction pieces. Greater differentiation between the samples was obtained with three chemical markers compared to using one marker. The herb/decoction pieces group showed comparatively higher extraction yields and significantly higher DPPH and FRAP ( $p < 0.05$ ), which was positively correlated to caffeic acid and ferulic acid, respectively. **Conclusions:** The results confirm the need for the quality assessment of granule products using more than one chemical marker for widespread practitioner and consumer use.

**Keywords:** *Angelicae Sinensis Radix*; antioxidant; Danggui; granules; herb; multivariate analysis; ultra-performance liquid chromatography

## 1. Introduction

Granule formulations have become the most popular delivery form for Chinese medicinal herbs and are used as an alternative to herb and decoction pieces in herbal prescriptions worldwide including China, Japan, USA and Europe [1]. For practitioners and consumers, granules are convenient in terms of easier administration (granules are added to water instead of boiling herbs in water which are then strained), transport (less bulky than herbs) and storage (protected from microbes and moisture). There is potential for better quality control of granules using good manufacturing practice (GMP) processes which would assure the reproducibility of products. This would promote clinical consistency as solvent



ratios to herbs and boiling times of herbs/decoction pieces are not patient-dependent [2,3]. However, standardised quality control procedures for granules are limited. In recent times, ultra-performance liquid chromatography (UPLC) has analysed the granule formulations of popular herbs such as *Panax ginseng* (Araliaceae), *Salvia miltiorrhiza* (Lamiaceae), *Panax notoginseng* (Araliaceae) and other common composite formulae [2,4–7]. However, there are few comparative studies regarding the actual quality and efficacy of granules compared to the traditional herbal decoction, and the variations between granule formulations from different manufacturers [2–4]. This calls for a simple and rapid multi-method approach to guarantee the reliability and bioequivalence of herbal products to ensure their clinical efficacy [8].

In this study, the herb/decoction pieces and granule products of *Angelicae Sinensis Radix*, also known as Danggui in Chinese, are evaluated [9]. Danggui, the dried root of *Angelica* (*A.*) *sinensis* (Oliv.) Diels (Umbelliferae), is one of the most popular Chinese materia medica and is used in dietary supplements and cosmetics globally [10]. Originally listed as top grade in the Shennong's Classic of Herbology and nowadays described as 'female ginseng', Danggui is used in gynaecological disorders such as painful dysmenorrhea, postpartum weakness and treating menopause [11]. The herb is known to regulate blood circulation, have antioxidant activity, and is widely used in cardiovascular diseases such as atherosclerosis and hypertension [12]. Danggui is present in over 80 composite formulae of traditional Chinese medicine (TCM).

Despite the popularity of Danggui, there is no quality assessment of Danggui granules [13]. With the general consensus of using a multi-method approach in assessing the quality of herbal products, the present study evaluated the differences between the Danggui samples using chromatography, chemometrics and antioxidant activity. Three chemical markers (ferulic acid, caffeic acid and Z-ligustilide) were quantified using the developed UPLC method. Hierarchical agglomerative clustering analysis (HCA) and principal component analysis (PCA) grouped the samples according to the content of the three markers. The results were compared to using either ferulic acid or Z-ligustilide as the single chemical marker as specified by the Pharmacopoeia of the People's Republic of China (PPRC) [9] and World Health Organisation (WHO) guidelines, respectively [14]. Coupled with the statistical clustering analysis, correlating the chemical markers to antioxidant activity provided a comprehensive study of the differences between the products. Any variations between the products may imply possible pharmacological differences which need to be addressed in terms of correct dosages to patients.

## 2. Materials and Methods

### 2.1. Plant Materials and Reagents

Ten commercial Danggui granule products (coded as G1–G10) were produced by companies in mainland China, Hong Kong and Taiwan, and were either purchased from their distributors in Australia or directly from the manufacturers. Product names have been omitted as consent for disclosure was not sort. One herb (coded as R2) and four decoction piece samples (coded as R1, R3, R4, R5) were sourced from Min Xian, Gansu Province in China [9]. The region where the herbal material was sourced from is well known for Danggui and considered the best quality according to TCM. They were purchased from Australia, mainland China and Hong Kong. The samples were authenticated by Dr George Li from the Faculty of Pharmacy, The University of Sydney, Australia. The taxonomic identification was carried out macroscopically and microscopically according to the descriptions in the Pharmacopoeia of People's Republic of China (PPRC) [9]. Voucher specimens were deposited at NICM Health Research Institute, Western Sydney University, Australia. They were labelled as for granules: G(number)(company)(date)AS and raw materials: R(number)(date)AS.

The three reference chemical markers (caffeic acid, ferulic acid and Z-ligustilide) were purchased from Chengdu Biopurify Phytochemicals Ltd. (Sichuan, China) and were graded > 98% HPLC purity. The compounds were verified with liquid chromatography–mass spectrometry (LC–MS).

Chloroform, formic acid and acetonitrile were obtained from Ajax Finechem (Taren Point, Australia). Methanol was purchased from Fisher Scientific (Loughborough, UK) and ethyl acetate was purchased from Biolab Ltd. (Scoresby, Australia). Water was obtained from a Milli-Q Reagent Water System (Millipore, Burlington, MA, USA). All the solvents mentioned were HPLC-grade. For the antioxidant assays, DPPH, Trolox, sodium acetate trihydrate, glacial acetic acid, TPTZ (2, 4, 6-tripyridyl-s-triazine), hydrochloric (HCl) acid and ferric chloride hexahydrate were purchased from Sigma-Aldrich Corp (St. Louis, MO, USA).

## 2.2. Preparation of the Extracts and Standards

In this study, it was anticipated that the granule manufacturing process involved the large-scale extraction of herbs with boiling water to reflect the traditional decoction, followed by spray-drying or fluidised bed drying and formulation with excipients [5]. Thus, to remove most of the water-soluble excipients, 1 g of the Danggui granule sample was suspended in methanol (10 mL) and sonicated for 30 min at 40 °C. The sonicated mixture was centrifuged at 4000 rpm for 10 min and the supernatant removed. The extraction was repeated two more times. The combined supernatants were concentrated by a rotary evaporator to dryness at 50 °C. Here, the residue obtained from the granules after the methanol extraction was assumed to be equivalent to the raw herb water extract without excipients.

The herb and decoction pieces of Danggui were ground by an electric blender and passed through a 500 µm aperture sieve. The powder (1 g) was refluxed with boiling water (30 mL) for 30 min and the extraction repeated two more times. The sample was then centrifuged at 4000 rpm for 10 min. The supernatant was transferred and evaporated to dryness at 50 °C. This was followed by the same extraction procedure as described for the granule samples to allow comparison of the samples as methanol extracts. The solutions were prepared by re-dissolving the dry extract residues with methanol followed by filtrating into the final testing samples through the filter syringes (0.2 µm).

The individual standard stock solutions of the chemical markers caffeic acid, ferulic acid and Z-ligustilide were prepared at the concentration of 2 mg/mL in methanol. To minimise the impact of the stability, the standards and samples were freshly prepared each day and protected from heat, moisture and light.

## 2.3. Determination of Chemical Marker Content

UPLC analyses were performed using a Waters Acquity ultra performance liquid chromatography (UPLC)<sup>®</sup> H series consisting of a H class quaternary solvent manager, an Acquity sample manager-FTN, an Acquity column oven and an Acquity Photodiode Array Detector (PDA) detector. The chromatographic separation was achieved using an Acquity UPLC BEH C18 column (50 mm × 2.1 mm, 1.7 µm) maintained at 40 °C [15].

The UPLC condition was based on our in-house HPLC method with modifications to the gradient condition [16–18]. The mobile phase consisted of 1% formic acid in water (A) and acetonitrile (B) (95:5, v/v), with a gradient elution as follows: 0–10 min, 5–12% B; 10–15 min, 12–20% B; 15–20 min, 20–100% B, 100% B for 5 min and reconditioning the column isocratically with 5% B for 4.5 min. The flow rate was 0.3 mL/min. The injection volume was 2 µL and the detection wavelength was set at 325 nm, which was similar to previous studies which monitored for ferulic acid and Z-ligustilide [15,17,19].

The UPLC method was validated in terms of linearity, repeatability and accuracy according to ICH guidelines [20]. Linearity testing was carried out by running six different concentrations of each chemical marker (caffeic acid (0.005–2 mg/mL), ferulic acid (0.005–2 mg/mL) and Z-ligustilide (0.01–0.3 mg/mL) in triplicate. Partial least square regression method was used to obtain the regression equations in the form of  $y = ax + b$ , where  $x$  is the concentration of the reference chemical marker and  $y$  was the peak area [21]. The limit of detection (LOD) and the limit of quantification (LOQ) were determined by standard deviation (SD) approach, where  $LOD = 3.33 \times (SD \text{ of } y\text{-intercept}/\text{mean of slope})$  and  $LOQ = 10 \times (SD \text{ of } y\text{-intercept}/\text{mean of slope})$ . For repeatability, the intra-day precision was evaluated by running six concentrations of each marker three times within a day, whilst inter-day

precision was examined on three separate consecutive days. To determine the accuracy of the method, a recovery assay was performed in triplicate by spiking two known concentrations (100 and 150 µg/mL) of the mixed standards (caffeic acid, ferulic acid) to one representative decoction piece and granule sample [22]. Percentage recovery (%) ± RSD was calculated by the equation: % = ((mean detected content – mean original content)/mean of spike content) × 100%.

#### 2.4. Antioxidant Activity Assays

The 2,2-diphenyl-1-picrylhydrazyl (DPPH) assay was performed as previously described [23]. The test samples were mixed with DPPH radical solution (0.24 mg/mL DPPH in methanol) and incubated for 30 min in the dark. The absorbance was determined at 515 nm. (±)-6-Hydroxy-2,5,7,8-tetramethylchromane-2-carboxylic acid (Trolox) was used for the calibration curve. All values were expressed as milligrams Trolox equivalents (TE) per gram of dried weight (DW) (mg TE/g DW).

The ferric ion reducing antioxidant power (FRAP) assay was performed as previously described [24]. The FRAP working solution was prepared by mixing 10 volumes of 300 mM acetate buffer (pH 3.6), 1 volume of 10 mM 2,4,6-tris(2-pyridyl)-s-triazine (TPTZ) in 40 mM HCl and 1 volume of 20 mM ferric chloride (FeCl<sub>3</sub>·6H<sub>2</sub>O). The test samples were mixed with pre-warmed FRAP reagent (37 °C) and incubated for 30 min at 37 °C. The absorbance was measured at 595 nm. The standard curve and the results of TE were obtained by the same approach as described above.

#### 2.5. Statistical Analyses

The yields (reported as percentage of the dry weight of the herb) is the mean of three extractions. One of the extracts from the same sample was analysed three times by UPLC, with the final quantitative results from UPLC analyses expressed as the mean ± standard deviation (SD). Quantitative results were reported as milligrams per grams of the DW of the raw herb (mg/g) equivalent. Non-parametric test (SPSS 20.0 software, IBM, Chicago, IL, USA) was conducted to determine whether the content of each chemical marker analysed by UPLC was significantly different between individual samples.

The chosen markers were considered as variables in the following HCA and PCA statistical analysis. HCA grouped the individual Danggui samples into clusters based on the degree of the similarity of the variables. The HCA results were expressed as a dendrogram using Ward's linkage algorithm and squared Euclidean distances (SPSS 20.0 software, IBM, Chicago, IL, USA). The different linkage criteria applied in the dendrogram revealed the degree of similarity between each sample. The length of the linkage between each sample/group represents the degree of similarity. Thus, the shorter the linkage, the more similarity there is between each group. PCA was performed using XLSTAT 2019.1 by Addinsoft (New York, USA) which reduced the original variables into two major principal components (PCs). These two PCs maintained the greatest possible variance of the original variables (three chemical markers) [7]. The PCA results were represented in a biplot (score plot and loading plot), where the score plot showed the clusters and outliers of the samples, and the loading plot demonstrated the correlation of the PC to the original variables. In the biplot, a point represented each individual sample, and the distance allocated between samples revealed the degree of their similarity in terms of the content of the chemical markers.

For the antioxidant assays, the data were expressed as the mean ± standard deviation (SD) of three repeat measurements and was analysed using independent-samples t-test and non-parametric analysis by SPSS. For this study,  $p < 0.05$  was considered as statistically significant. Pearson correlation coefficient ( $r$ ) by SPSS (20.0 software, IBM, Chicago, IL, USA) evaluated the strength of the correlation of the chemical markers to the antioxidant activities.

### 3. Results

#### 3.1. Extraction Yields

The mean yield of each sample is shown in Table 1. The yield results of the granule products were converted according to their concentrated ratio (as listed on the package) so that comparison to the original herbal material could be made. The yields of the herb/decoction pieces (33.2–44.8%) as a group were comparatively higher than that of the granules (2.7–12.9%).

**Table 1.** Average contents (mg/g, means  $\pm$  SD, n = 3) of the chemical markers in the ten Danggui granule samples (G1–G10) and the five herb/decoction piece samples (R1–R5) analysed by UPLC-PDA.

Sample	Origin	Granule to Herb Ratio <sup>c</sup>	Yield <sup>d</sup> % (with Ratio)	Caffeic Acid (mg/g)	Ferulic Acid (mg/g)	Z-Ligustilide (mg/g)
G1 <sup>a</sup>	Guangxi	1:3	12.7 (4.2)	0.0153 $\pm$ 0.001	0.111 $\pm$ 0.008	0.0105 $\pm$ 0.001
G2 <sup>b</sup>	Guangdong	1:5	31.7 (6.3)	0.0155 $\pm$ 0.000	0.0631 $\pm$ 0.002	0.0359 $\pm$ 0.001
G3 <sup>b</sup>	China	1:5	28.5 (5.7)	0.0142 $\pm$ 0.000	0.0772 $\pm$ 0.002	0.0284 $\pm$ 0.001
G4 <sup>b</sup>	Sichuan	1:10	27.3 (2.7)	0.00491 $\pm$ 0.000	0.0300 $\pm$ 0.001	0.00460 $\pm$ 0.000
G5 <sup>b</sup>	Taichung	1:6	31.3 (5.2)	0.00598 $\pm$ 0.000	0.145 $\pm$ 0.008	0.526 $\pm$ 0.032 ***
G6 <sup>a</sup>	Beijing	1:5	27.1 (5.4)	0.0179 $\pm$ 0.000	0.0764 $\pm$ 0.003	0.0367 $\pm$ 0.001
G7 <sup>a</sup>	Jiangsu	2:5	32.3 (12.9)	0.0394 $\pm$ 0.002 **	0.299 $\pm$ 0.014 **	0.0810 $\pm$ 0.004
G8 <sup>a</sup>	Guangdong	3:10	28.2 (8.5)	0.0122 $\pm$ 0.001	0.0688 $\pm$ 0.004	0.00923 $\pm$ 0.001
G9 <sup>a</sup>	Sichuan	1:5	35.4 (7.1)	0.0113 $\pm$ 0.001	0.0808 $\pm$ 0.009	0.0129 $\pm$ 0.001
G10 <sup>a</sup>	Guangdong	1:3.3	29.5 (8.9)	0.0312 $\pm$ 0.002 **	0.206 $\pm$ 0.015 **	0.183 $\pm$ 0.012 ***
R1			44.8	ND	0.274 $\pm$ 0.008	0.0262 $\pm$ 0.003
R2			42.1	0.0407 $\pm$ 0.008 *	0.503 $\pm$ 0.074 *	0.0245 $\pm$ 0.003
R3			42.3	ND	0.284 $\pm$ 0.013	0.0215 $\pm$ 0.003
R4			41.8	0.00455 $\pm$ 0.000	0.361 $\pm$ 0.006	0.0168 $\pm$ 0.001
R5			33.2	0.00396 $\pm$ 0.001	0.299 $\pm$ 0.013	0.0177 $\pm$ 0.002

G = granule; SD = standard deviation; ND = not detected. <sup>a</sup> Hospital-grade, use as directed by doctor. <sup>b</sup> Available in Australia; <sup>c</sup> Granule to raw herb ratio as specified by the manufacturer, thus 1 g granule is produced by 3 g herb etc.; <sup>d</sup> Average yield converted by granule ratio; \* Significantly different within the raw samples ( $p < 0.05$ ); \*\* Significantly different within the granule samples ( $p < 0.05$ ); \*\*\* Significantly different within the granule samples ( $p < 0.05$ ).

#### 3.2. UPLC-PDA Quantification of the Chemical Markers

The representative chromatograms of the mixed chemical markers, the granule (G1) and herb (R2) extracts are shown in Figure 1, with a total run time of 30 min. In this study, the three chemical markers, caffeic acid, ferulic acid and Z-ligustilide and their calibration curves produced good correlations between the peak area and concentration as shown in Table 2, with the correlation coefficients  $r^2 > 0.997$  for all analytes. The LODs and LOQs were in the range of 0.701–3.268  $\mu\text{g/mL}$  and 2.106–9.813  $\mu\text{g/mL}$ , respectively. The intra-day and inter-day RSD were 1.5–2.77% and 2.6–4.11%, respectively (Table 2). This suggests that the method had reasonable instrumental and method precision [22].

The addition of known amounts of the compounds to the samples is recommended for recovery testing of herbal compounds [22]. Granule sample 2 (G2) and decoction piece sample 3 (R3) were randomly chosen as representative Danggui samples from each group. The average recoveries (%)

were for G2:  $89.3 \pm 1.1\%$  (caffeic acid) and  $99.7 \pm 1.2\%$  (ferulic acid); R3:  $94.1 \pm 2.1\%$  (caffeic acid) and  $99.6 \pm 2.1\%$  (ferulic acid).

The developed UPLC-PDA method simultaneously quantified the three marker compounds in the Danggui water extract herb and granule samples, and the results are shown in Table 1. In this study, the amount of caffeic acid, ferulic acid and Z-ligustilide in all the samples ranged from 0.004–0.041, 0.030–0.503 and 0.005–0.526 mg/g DW, respectively. In the granule samples, G5 and G10 had a relatively higher amount of Z-ligustilide (0.526 mg/g DW and 0.183 mg/g DW, respectively) compared to the rest of the samples.

Nonparametric independent-samples t-testing of the raw herb samples revealed that R2 had significantly higher ferulic acid ( $p < 0.05$ ) and caffeic acid ( $p < 0.05$ ), and there was no significant difference in Z-ligustilide content ( $p > 0.05$ ).

Both caffeic acid and Z-ligustilide were not significantly different between the granule and decoction piece/raw herb groups ( $p > 0.05$ ). However, the amount of ferulic acid was found to be significantly different ( $p < 0.05$ ) between the two groups. In terms of ferulic acid and caffeic acid, G7 (higher content) and G10 were significantly different ( $p < 0.05$ ). In terms of Z-ligustilide, G5 (higher content) ( $p < 0.05$ ) and G10 ( $p < 0.05$ ) were significantly different.

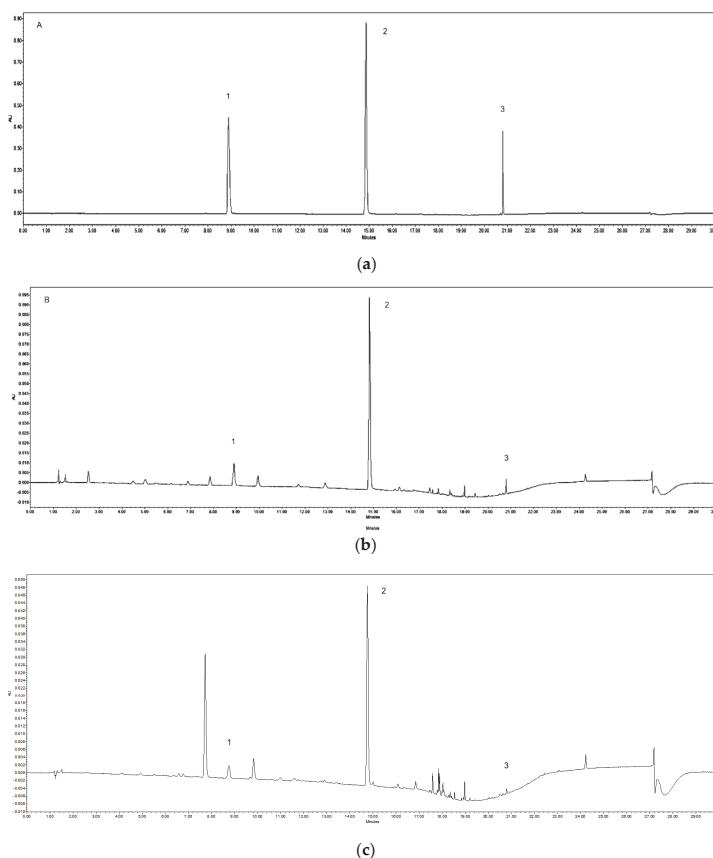


**Figure 1.** UPLC chromatograms detected under the developed mobile phase system at 325 nm. These chromatograms show: (a) three marker compounds: 1 = caffeic acid (0.1 mg/mL), 2 = ferulic acid (0.2 mg/mL), 3 = Z-ligustilide (0.1 mg/mL); (b) granule 1 (G1) sample (10 mg/mL); (c) raw herb 2 (R2) sample (10 mg/mL). AU = absorbance units.

**Table 2.** Calibration curves, detection limits and quantification limits ( $n = 6$ ) of the three chemical markers in Danggui by UPLC-PDA.

Compound	Regression Equation	R <sup>2</sup>	LOD ( $\mu\text{g/mL}$ )	LOQ ( $\mu\text{g/mL}$ )	Intra-Day RSD (%) ( $n = 6$ )	Inter-Day RSD (%) ( $n = 3$ )
Caffeic acid	$y = 1.9561x + 0.0108$	0.998	1.496	4.492	2.770	2.598
Ferulic acid	$y = 1.9915x - 3.1394$	0.999	0.701	2.106	1.496	2.790
Z-Ligustilide	$y = 0.6409x - 0.0103$	0.997	3.268	9.813	2.725	4.108

Relative standard deviation RSD (%) =  $100 \times \text{standard deviation (SD)}/\text{mean}$ ;  $y$ , peak area;  $x$ , the concentration of each reference chemical marker (mg/mL); R<sup>2</sup>, coefficient of determination; LOD, limit of detection ( $3.33 \times (\text{SD of } y\text{-intercept}/\text{mean of slope})$ ); LOQ, limit of quantification ( $10 \times (\text{SD of } y\text{-intercept}/\text{mean of slope})$ ).

### 3.3. Multivariate Analysis Using HCA and PCA

According to the dendrogram generated from HCA, the majority of the samples were divided into two main clusters. Specifically, R1, R3, R4, R5, G7 and G10 (relatively higher amounts of caffeic acid and ferulic acid) were classified into one cluster (Group 1), whereas G1–G4, G6, G8 and G9 were grouped into another cluster (Group 2) representing relatively lower amount of the marker acids. G5 (highest amount of Z-ligustilide) and R2 (highest amount of ferulic acid) were different to these two main groups (Figure 2).

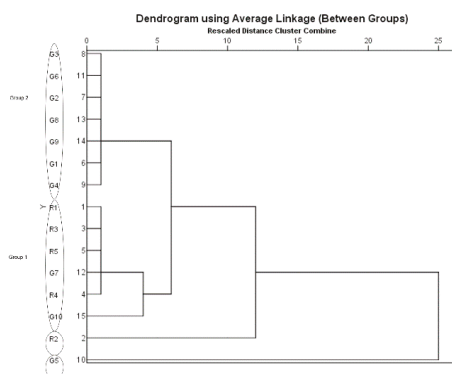


**Figure 2.** Hierarchical agglomerative clustering analysis (HCA) dendrogram of Danggui samples using SPSS 20.0 software (Chicago, USA). Ward's method as amalgamation rule and the squared Euclidean distance as metric were employed to set up the clusters. The length of the linkage between each sample/group represents the degree of similarity. G: granule samples; R: raw herbs/decoction piece samples. Group 1: R1, R3, R5, G7, R4, G10; Group 2: G1, G2, G3, G4, G6, G8, G9. R2 and G5 are outliers.

PCA was also performed to determine the main chemical markers influencing the equivalence of Danggui raw materials and granules. Based on eigenvalues  $> 1$ , the first two principal components (PC), PC1 and PC2, were used to differentiate the samples according to the input data. From the result, the first two PCs could explain 53% and 47% of the variance of the three chemical markers, respectively. According to the loading matrices from the PCA biplot, the test samples were separated in PC1 by the differences in the chemical content of ferulic acid and caffeic acid, whilst PC2 was mainly due to the chemical content of Z-ligustilide. Similar to the results of hierarchical clustering, two major groups are set up in the PCA biplot (Figure 3). The decoction pieces and G7 (Group 1) were in close proximity and showed a higher content of caffeic acid and ferulic acid, with R2 demonstrating the highest amount of caffeic acid and ferulic acid. G5 was considered as an outlier of the samples due to its excessively high amount of Z-ligustilide. The PCA loading plot indicates that the Z-ligustilide content may have more

influence on the discrimination of G5 and G10. The rest of the granules (Group 2) were near each other and represented generally lower amounts of the three chemical markers.

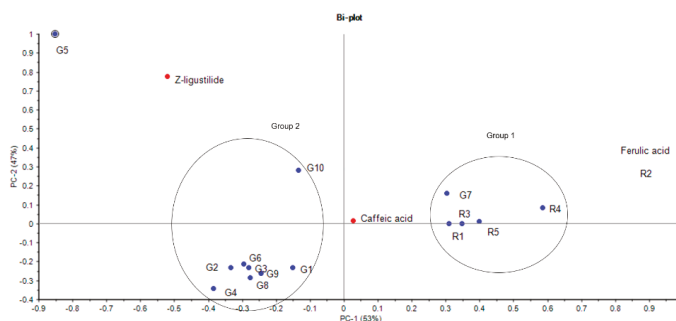


**Figure 3.** Biplot from principal component analysis (PCA) of Danggui samples (PC1 vs. PC2) based on the three components Z-ligustilide, caffeic acid and ferulic acid using Unscrambler 10.3 from Camo AS software (Trondheim, Norway). In the biplot, a point represented each individual sample, and the distance allocated between samples, revealed the degree of their similarity in terms of the content of the chemical markers. PC: principal component. G: granule samples; R: raw herbs/decoction piece samples. Group 1: R1, R3, R5, G7, R4; Group 2: G1, G2, G3, G4, G6, G8, G9.

The HCA plot of the three markers was compared to using a single marker and the combination of the markers (Supplementary Material). Ferulic acid as the sole marker grouped G5 with the granules, showing no distinct difference (Figure S1). The HCA of the two markers (ferulic acid and Z-ligustilide) showed similar results to the original three marker HCA, with R2 showing more similarity to the decoction pieces (Figure S2). Using Z-ligustilide, all samples were grouped together, with G5 on its own (Figure S3). Using caffeic acid, there were three groups: G7 and G10 grouped with R2; G4 and G5 was with the rest of the herb/decoction pieces, with G5 showing some similarity with the granules (Figure S4).

### 3.4. Antioxidant Activity

In the DPPH and FRAP assays (Table 3), all the samples showed antioxidant activity, with R2 (highest amount of ferulic acid) showing significantly higher activity in both assays using independent-samples t-test ( $p = 0.017$  and  $0.002$ , respectively), whereas G5 (highest amount of z-ligustilide) was comparable ( $p = 0.421$  and  $0.483$ , respectively). A significant difference in antioxidant activity was shown between the herb/decoction piece samples as a group and the granules as a group ( $p < 0.05$ ) in the FRAP assay. For the two major groups established by HCA and PCA, DPPH and FRAP antioxidant activities were compared by independent-samples t-test and found a significant difference ( $p = 0.027$ ) between Group 1 and 2 in the FRAP assay.

Pearson correlation coefficient analysis investigated the correlation between antioxidant activity and the chemical markers of all the Danggui samples (Table 4). Positive and significant correlations were observed between the amount of ferulic acid and the antioxidant activities of the FRAP assay ( $0.791$ ,  $p < 0.01$ ). Caffeic acid showed significant correlation with the antioxidant activities of Danggui as measured by the DPPH assay ( $0.582$ ,  $p < 0.05$ ). In contrast, the amount of Z-ligustilide and samples' antioxidant activity was negatively and not significantly correlated to either DPPH and FRAP assay ( $-0.202$  and  $-0.229$ ,  $p > 0.05$ ).

**Table 3.** Trolox equivalent (TE) of the granule and herb/decoction piece samples of dried weight (DW) using DPPH and FRAP assays, respectively.

Sample	DPPH Assay <sup>a</sup>	FRAP Assay <sup>a</sup>
	mg TE/g of DW ± SD	mg TE/g of DW ± SD
G1	1.79 ± 0.27	9.96 ± 4.90
G2	3.32 ± 0.29	13.60 ± 0.41
G3	2.83 ± 0.20	9.29 ± 0.27
G4	1.76 ± 0.04	6.21 ± 0.62
G5	2.29 ± 0.45	10.75 ± 0.30
G6	3.02 ± 0.44	10.28 ± 0.45
G7	6.33 ± 0.54	26.30 ± 0.36
G8	7.33 ± 0.32	30.82 ± 1.71
G9	4.02 ± 0.92	16.03 ± 0.05
G10	3.34 ± 0.66	13.09 ± 0.19
R1	3.26 ± 0.81	50.34 ± 10.21
R2	8.10 ± 0.59	69.38 ± 1.82
R3	3.05 ± 0.36	23.04 ± 5.21
R4	4.76 ± 0.42	25.73 ± 4.48
R5	2.76 ± 0.09	32.06 ± 4.07

<sup>a</sup> Values were the average of triplicate tests; SD = standard deviation.

**Table 4.** Pearson correlation between the three chemical markers and antioxidant activities of the samples in the DPPH and FRAP assays.

Markers	Assay	DPPH	FRAP
	Caffeic acid		0.582 *
Ferulic acid		0.507	0.791 **
Z-ligustilide		−0.202	−0.229

\* Correlation is significant at the 0.05 level (two-tailed). \*\* Correlation is significant at the 0.01 level (two-tailed).

#### 4. Discussion

As demand grows for traditional Chinese medicines, so does the need for efficient ways of administrating herbal medicines. Thus, it is important to compare new formulations such as granules to the original herb. This is the first study that compares Danggui granules to the raw products. The yield (reported as percentage of the dry weight of the herb) is indicative of the herb dosage a patient is consuming. The yields were higher for the herb/decoction pieces and were lower than the 48% water-soluble extractives in the Hong Kong Chinese Materia Medica Standards (HKCMMS) [25]. In comparison, the yield of the granule products was lower. Granule size was nonuniform in the samples, and this will affect the extraction process above. Smaller particles may be extracted more efficiently or be missed as they make their way to the bottom of the bottle. To minimise this variability, each granule bottle was shaken before sampling to redistribute the particles [26,27].

The quality control of traditional Chinese medicines and their products is a challenge for industry due to the complexity of the formulations (using a holistic approach to treat disease), as well as high outlay costs for analytical instrumentation. Danggui has a complex chromatogram because of the number of individual constituents, the possible degradation and isomerisation of the organic acids and phthalides present [28,29]. Qualitative approaches such as thin layer chromatography (TLC) are highly recommended by pharmacopoeias and monographs to compare fingerprints of samples; however, it does not usually allow for the quantification of compounds which will confirm their quality [25,30]. For this quality study on Danggui, the visual analysis of the TLC result failed to accurately determine the quantitative difference between the compounds of the samples as the LOD and concentrations of



the compounds were low and close to signal noise, and calibration curves could not be constructed (data not shown).

Other studies have used UPLC coupled with MS to investigate the chemical profile of *A. sinensis* [15,31]. This analysis would have expensive set up costs for examining herbal material. To separate the polar and non-polar constituents within a reasonably short running time, a UPLC condition was determined and optimised in this study. By adding 1% formic acid to water, the solvent system showed good separation of the constituents simultaneously, with a run time of 30 min (compared to 60 min for high-performance liquid chromatography methods) and good separation [32]. The optimised UPLC method and resulting chromatograms were able to quantify caffeic acid, ferulic acid and Z-ligustilide.

The disparity of the ferulic acid, caffeic acid and Z-ligustilide content between the granule samples indicates differences in the manufacturing processing of Danggui which may not mimic traditional water decoctions of TCM. It is interesting to note that R2 was a raw herb sample rather than a decoction piece (which has gone through a processing procedure such as smoke-drying). Its extraction in water favoured the polar compounds such as the organic acids. However, it has been reported that techniques such as steam distillation and other solvents such as ethanol may be used to enhance the extraction of the less polar components in the herb for granule production at the expense of the polar acids such as ferulic acid. Spray or vacuum drying may be used for heat sensitive compounds and for compounds in trace amounts [33]. For water insoluble compounds such as Z-ligustilide, one company mentions the use of carbon dioxide extraction [34]. Studies have established pharmaceutical approaches using methanol and hexane extraction to obtain a high content of Z-ligustilide as a lead compound for pharmacological studies [17,28,35]. Another issue could be adulteration, in which the extracts may be spiked with the known marker compound to reach the regulatory amount [14].

As differences in the chemical content of Danggui products could affect their efficacy, the identification and quantification of chemical markers is necessary to determine the quality of Danggui granules. In the study, the amount of ferulic acid in the samples (0.003–0.05%) was less than the 0.05% minimum requirement as stated in the PPRC for the quality assessment of Danggui [9]. In the PPRC, 70% ethanol is the nominated solvent, with no less than 45% ethanol-soluble extractives. This solvent will give a different chemical profile compared to water as a solvent which is used in home decoctions. However, no information is given in the PPRC regarding the standard amount of caffeic acid and Z-ligustilide for Danggui. The monograph for *Radix Angelicae Sinensis* states that a “sample contains not less than 0.6% (of Z-ligustilide) calculated with reference to the dried substance” [25]. In this study, Z-ligustilide in most of the samples were lower than the monograph and the standard range of 0.5–5% as reported by the WHO which is based on 100% methanol as the solvent [14,28]. In addition, the amount of Z-ligustilide detected in the extracts (0.005–0.526 mg/g DW) was lower due to the extraction in water (traditional decoction) than the content (1.26–37.7 mg/g from non-water solvents) found in previous studies [17,29,36].

HCA and PCA differentiated the Danggui samples based on the contents of caffeic acid, ferulic acid and Z-ligustilide on their own and in combination. In this study, a minimum of two chemical marker compounds (ferulic acid and Z-ligustilide) was required to differentiate Danggui products. This agrees with our previous findings where five rather than the nominated three chemical markers were required to differentiate raw and granule products of *Panax notoginseng* [7]. Thus, it is recommended that the WHO, the PPRC and other pharmacopoeias/monographs incorporate a minimum percentage value of at least two chemical standards, which will reflect traditional water extracts.

DPPH, along with FRAP, are commonly used to measure antioxidant activity and the methods with other herbal products have been widely published. Unlike biological cell assays, these assays have stable reaction responses and are cheap and quick for industry use. The contribution of caffeic acid and ferulic acid to antioxidant activity of Danggui was confirmed in a previous study [37]. Our findings indicated that phenolic acids such as ferulic acid are the key determinants influencing the antioxidant activities of Danggui as found in a previous study [38]. Thus, the chemical content of ferulic acid is

an important chemical marker to ensure the correlation of the antioxidant activities to the different Danggui samples. One study revealed that Danggui extracts prepared with either water or 20% ethanol with an extraction time of 15 min yielded the best antioxidant activity [39]. As expected, Z-ligustilide did not correlate to antioxidant activity.

A limitation of the present study is that the Danggui was sourced from one region which is the region recommended for quality Danggui. As expected, the results showed that the decoction pieces were consistent in composition. Future studies could include comparing granules to raw decoctions in clinical trials to gauge clinical efficacy.

## 5. Conclusions

In the present study, UPLC coupled with multivariate analysis and antioxidant activity provided a rapid method for assessing differences in Danggui products. Comprehensive quality standardisation processes in pharmacopoeias and monograph publications are required to guide the regulation and standardisation of the production of commercial herbal granules. With the increased use of herbal medicinal granules around the world, this study will provide important information for standardisation committees, industry, practitioners and consumers on the quality control of herbs and its medicinal products. It is vital that patients are better informed about their health and treatment choices and are aware of what they are consuming. More importantly, practitioners will need to determine the correct dosages for their patients so that they do not undermine the efficacy of the herb and the patient's care. Thus, granule dosages would need to equate to the decocted raw product.

**Supplementary Materials:** The following are available online at <http://www.mdpi.com/2305-6320/7/6/35/s1>, Hierarchical agglomerative clustering analysis (HCA) dendrograms of Danggui samples using SPSS 20.0 software (IBM, Chicago, IL, USA). Dendrograms show different combinations of the markers. Ward's method as amalgamation rule and the squared Euclidean distance as metric were employed to set up the clusters. G: granule samples; R: raw herbs/decoction piece samples. Figure S1: Ferulic acid as the single marker, Figure S2: Ferulic acid and Z-ligustilide as the two markers, Figure S3: Z-ligustilide as the single marker, Figure S4: Caffeic acid as the single marker.

**Author Contributions:** Conceptualisation and supervision, K.C. and V.R.-N.; methodology, all authors; validation, H.Y.W., X.Z. and V.R.-N.; formal analysis, H.Y.W. and X.Z.; investigation, H.Y.W.; resources, V.R.-N., X.Z., J.P., A.K., K.C.; writing—original draft preparation, H.Y.W., V.R.-N. and K.C.; writing—review and editing, V.R.-N., X.Z. and K.C.; project administration, V.R.-N. and K.C. All authors have read and agreed to the published version of the manuscript.

**Funding:** The project was supported by The Joint Chair in Traditional Chinese Medicine (JCTCM) Program, funded by the Office of Science and Research in NSW, the University of Sydney and Western Sydney University, Australia.

**Acknowledgments:** The authors would like to thank from the University of Sydney: Ka Ho Wong (analytical assistance), and from Western Sydney University: Leila Hejazi (LC/MS unit manager), Paul Fahey (statistical support), Samiuela Lee (general laboratory support) and Alan Bensoussan (Director of NICM) for his never-ending support and acquirer of the original program funding.

**Conflicts of Interest:** The funders had no role in the design of the study; in the collection, analyses, or interpretation of data; in the writing of the manuscript, or in the decision to publish the results. As a medical research institute, NICM Health Research Institute receives research grants and donations from foundations, universities, government agencies, individuals and industry. Sponsors and donors also provide untied funding for work to advance the vision and mission of the Institute. The authors declare no competing financial interests.

## References

1. Klein, S.D.; van der Zypen, D.; Becker, S. Prescription patterns of Chinese medicinal herbs in Switzerland. *Swiss J. Integr. Med.* **2010**, *22*, 226–231. [[CrossRef](#)]
2. Li, S.L.; Song, J.Z.; Qiao, C.F.; Zhou, Y.; Xu, H.X. UPLC–PDA–TOFMS based chemical profiling approach to rapidly evaluate chemical consistency between traditional and dispensing granule decoctions of traditional medicine combinatorial formulae. *J. Pharm. Biomed. Anal.* **2010**, *52*, 468–478. [[CrossRef](#)] [[PubMed](#)]
3. Luo, H.; Li, Q.; Flower, A.; Lewith, G.; Liu, J. Comparison of effectiveness and safety between granules and decoction of Chinese herbal medicine: A systematic review of randomized clinical trials. *J. Ethnopharmacol.* **2012**, *140*, 555–567. [[CrossRef](#)] [[PubMed](#)]

4. Chen, L.; Tang, Y.; Chen, M.; Deng, H.; Yan, X.; Wu, D. Chemical correlation between Gegen Qinlian dispensing granule and its four raw herbs by LC fingerprint. *Phytomedicine* **2010**, *17*, 100–107. [CrossRef]
5. Song, J.Z.; Li, S.L.; Zhou, Y.; Qiao, C.F.; Chen, S.L.; Xu, H.X. A novel approach to rapidly explore analytical markers for quality control of Radix Salviae Miltiorrhizae extract granules by robust principal component analysis with ultra-high performance liquid chromatography–ultraviolet–quadrupole time-of-flight mass spectrometry. *J. Pharm. Biomed. Anal.* **2010**, *53*, 279–286. [CrossRef]
6. Yang, G.L.; Yang, L.W.; Li, Y.X.; Cao, H.; Zhou, W.L.; Fang, Z.J.; Zhou, H.B.; Mo, J.L.; Xiao, S.X.; Lin, H.R. Applications of ultra-performance liquid chromatography to traditional Chinese medicines. *J. Chromatogr. Sci.* **2010**, *48*, 18–21. [CrossRef]
7. Zhou, X.; Razmovski-Naumovski, V.; Chan, K. A multivariate analysis on the comparison of raw notoginseng (Sanqi) and its granule products by thin-layer chromatography and ultra-performance liquid chromatography. *Chin. Med.* **2015**, *10*, 13. [CrossRef]
8. Razmovski-Naumovski, V.; Tongkao-on, W.; Kimble, B.; Qiao, V.L.; Beilun, L.; Li, K.M.; Roufogalis, B.; Depo, Y.; Meicun, Y.; Li, G.Q. Multiple chromatographic and chemometric methods for quality standardisation of Chinese herbal medicines. *World Sci. Technol.* **2010**, *12*, 99–106. [CrossRef]
9. State Pharmacopoeia Committee. *Pharmacopoeia of the People's Republic of China*; People's Medical Publishing House: Beijing, China, 2010.
10. Hook, I.L. Danggui to Angelica sinensis root: Are potential benefits to European women lost in translation? A review. *J. Ethnopharmacol.* **2014**, *152*, 1–13. [CrossRef]
11. Circosta, C.; Pasquale, R.D.; Palumbo, D.R.; Samperi, S.; Occhiuto, F. Estrogenic activity of standardized extract of Angelica sinensis. *Phytother. Res.* **2006**, *20*, 665–669. [CrossRef]
12. Wei, W.-L.; Zeng, R.; Gu, C.-M.; Qu, Y.; Huang, L.-F. Angelica sinensis in China—A review of botanical profile, ethnopharmacology, phytochemistry and chemical analysis. *J. Ethnopharmacol.* **2016**, *190*, 116–141. [CrossRef] [PubMed]
13. Lu, G.-H.; Chan, K.; Leung, K.; Chan, C.-L.; Zhao, Z.-Z.; Jiang, Z.-H. Assay of free ferulic acid and total ferulic acid for quality assessment of Angelica sinensis. *J. Chromatogr. A* **2005**, *1068*, 209–219. [CrossRef] [PubMed]
14. World Health Organization. WHO Monographs on Selected Medicinal Plants. Available online: <http://apps.who.int/medicinedocs/en/d/Js4927e/5.html#Js4927e.5> (accessed on 24 May 2020).
15. Wei, W.-L.; Huang, L.-F. Simultaneous determination of ferulic acid and phthalides of Angelica sinensis based on UPLC-Q-TOF/MS. *Molecules* **2015**, *20*, 4681–4694. [CrossRef] [PubMed]
16. Zschocke, S.; Liu, J.H.; Stuppner, H.; Bauer, R. Comparative study of roots of Angelica sinensis and related umbelliferous drugs by thin layer chromatography, high-performance liquid chromatography, and liquid chromatography–mass spectrometry. *Phytochem. Anal.* **1998**, *9*, 283–290. [CrossRef]
17. Lu, G.H.; Chan, K.; Chan, C.L.; Leung, K.; Jiang, Z.H.; Zhao, Z.Z. Quantification of ligustilides in the roots of Angelica sinensis and related umbelliferous medicinal plants by high-performance liquid chromatography and liquid chromatography–mass spectrometry. *J. Chromatogr. A* **2004**, *1046*, 101–107. [CrossRef]
18. Zhao, K.J.; Dong, T.T.; Tu, P.F.; Song, Z.H.; Lo, C.K.; Tsim, K.W. Molecular genetic and chemical assessment of radix Angelica (Danggui) in China. *J. Agric. Food Chem.* **2003**, *51*, 2576–2583. [CrossRef]
19. Gui, Q.; Zheng, J. Simultaneous determination of eight components in Angelica sinensis based on UHPLC-ESI-MS/MS method for quality evaluation. *Biomed. Chromatogr.* **2019**, *33*, e4326. [CrossRef]
20. Guideline, I.H.T. Validation of Analytical Procedures: Text and Methodology, Q2 (R1), Current Step 4 Version, Parent Guidelines on Methodology Dated November 6 1996, Incorporated in November 2005. In International Conference on Harmonisation, Geneva, Switzerland. Available online: <https://www.ich.org/page/quality-guidelines> (accessed on 23 June 2020).
21. Chan, C.C.; Lee, Y.; Lam, H.; Zhang, X.-M. *Analytical Method Validation and Instrument Performance Verification*; John Wiley & Sons: Hoboken, NJ, USA, 2004.
22. Chen, D.; Zhao, S.S.; Leung, K.S.Y. Improved quality assessment of proprietary Chinese medicines based on multi-chemical class fingerprinting. *J. Sep. Sci.* **2009**, *32*, 2892–2902. [CrossRef]
23. Yang, S.A.; Jeon, S.K.; Lee, E.J.; Shim, C.H.; Lee, I.S. Comparative study of the chemical composition and antioxidant activity of six essential oils and their components. *Nat. Prod. Res.* **2010**, *24*, 140–151. [CrossRef]
24. Thaipong, K.; Boonprakob, U.; Crosby, K.; Cisneros-Zevallos, L.; Hawkins Byrne, D. Comparison of ABTS, DPPH, FRAP, and ORAC assays for estimating antioxidant activity from guava fruit extracts. *J. Food Compos. Anal.* **2006**, *19*, 669–675. [CrossRef]

25. Chinese Medicine Division. *Hong Kong Chinese Materia Medica Standards*; Department of Health, Government of Hong Kong Special Administrative Region: Hong Kong, China, 2005; Volume I, pp. 42–51.
26. Loh, Z.H.; Er, D.Z.; Chan, L.W.; Liew, C.V.; Heng, P.W. Spray granulation for drug formulation. *Expert Opin. Drug Deliv.* **2011**, *8*, 1645–1661. [[CrossRef](#)] [[PubMed](#)]
27. Hu, X.; Cunningham, J.; Winstead, D. Understanding and predicting bed humidity in fluidized bed granulation. *J. Pharm. Sci.* **2008**, *97*, 1564–1577. [[CrossRef](#)] [[PubMed](#)]
28. Lin, L.-Z.; He, X.-G.; Lian, L.-Z.; King, W.; Elliott, J. Liquid chromatographic–electrospray mass spectrometric study of the phthalides of *Angelica sinensis* and chemical changes of Z-ligustilide. *J. Chromatogr. A* **1998**, *810*, 71–79. [[CrossRef](#)]
29. Yi, L.; Liang, Y.; Wu, H.; Yuan, D. The analysis of *Radix Angelicae Sinensis* (Danggui). *J. Chromatogr. A* **2009**, *1216*, 1991–2001. [[CrossRef](#)]
30. Commission, C.P. *TLC Atlas of Chinese Crude Drugs in Pharmacopoeia of the People's Republic of China*; People's Medical Publishing House: Beijing, China, 2009.
31. Qian, Y.; Wang, Y.; Sa, R.; Yan, H.; Pan, X.; Yang, Y.; Sun, Y. Metabolic fingerprinting of *Angelica sinensis* during growth using UPLC-TOFMS and chemometrics data analysis. *Chem. Cent. J.* **2013**, *7*, 42. [[CrossRef](#)]
32. Jeong, S.Y.; Kim, H.M.; Lee, K.H.; Kim, K.Y.; Huang, D.S.; Kim, J.H.; Seong, R.S. Quantitative analysis of marker compounds in *Angelica gigas*, *Angelica sinensis*, and *Angelica acutiloba* by HPLC/DAD. *Chem. Pharm. Bull.* **2015**, *63*, c15-00081. [[CrossRef](#)]
33. China Resource Sanjiu Medical & Pharmaceutical Co., Ltd. Manufacturing Technique. Available online: <https://www.999.com.cn/index.html> (accessed on 24 May 2020).
34. Guangdong Yifang Pharmaceutical Co., Ltd. Producing Process of E-Fong. Available online: <http://www.e-fong.com/en/> (accessed on 24 May 2020).
35. Yeh, J.-C.; Garrard, I.J.; Cho, C.-W.C.; Bligh, S.A.; Lu, G.-H.; Fan, T.-P.; Fisher, D. Bioactivity-guided fractionation of the volatile oil of *Angelica sinensis* radix designed to preserve the synergistic effects of the mixture followed by identification of the active principles. *J. Chromatogr. A* **2012**, *1236*, 132–138. [[CrossRef](#)]
36. Lao, S.; Li, S.; Kan, K.K.; Li, P.; Wan, J.; Wang, Y.; Dong, T.T.; Tsim, K.W. Identification and quantification of 13 components in *Angelica sinensis* (Danggui) by gas chromatography–mass spectrometry coupled with pressurized liquid extraction. *Anal. Chim. Acta* **2004**, *526*, 131–137. [[CrossRef](#)]
37. Li, X.; Wu, X.; Huang, L. Correlation between antioxidant activities and phenolic contents of *radix Angelicae sinensis* (Danggui). *Molecules* **2009**, *14*, 5349–5361. [[CrossRef](#)]
38. Wang, L.-Y.; Tang, Y.-P.; Liu, X.; Zhu, M.; Tao, W.-W.; Li, W.-X.; Duan, J.-A. Effects of ferulic acid on antioxidant activity in *Angelicae Sinensis Radix*, *Chuanxiong Rhizoma*, and their combination. *Chin. J. Nat. Med.* **2015**, *13*, 401–408. [[CrossRef](#)]
39. Huang, S.H.; Chen, C.C.; Lin, C.M.; Chiang, B.H. Antioxidant and flavor properties of *Angelica sinensis* extracts as affected by processing. *J. Food Compos. Anal.* **2008**, *21*, 402–409. [[CrossRef](#)]



© 2020 by the authors. Licensee MDPI, Basel, Switzerland. This article is an open access article distributed under the terms and conditions of the Creative Commons Attribution (CC BY) license (<http://creativecommons.org/licenses/by/4.0/>).





Review

# Uncharted Source of Medicinal Products: The Case of the *Hedychium* Genus

Wilson R. Tavares <sup>1</sup>, Maria do Carmo Barreto <sup>1</sup> and Ana M. L. Seca <sup>1,2,\*</sup>

<sup>1</sup> cE3c—Centre for Ecology, Evolution and Environmental Changes/Azorean Biodiversity Group & Faculty of Sciences and Technology, University of Azores, Rua Mãe de Deus, 9501-321 Ponta Delgada, Portugal; wrt-94@hotmail.com (W.R.T.); maria.cr.barreto@uac.pt (M.d.C.B.)

<sup>2</sup> LAQV-REQUIMTE, Department of Chemistry, University of Aveiro, 3810-193 Aveiro, Portugal

\* Correspondence: ana.ml.seca@uac.pt; Tel.: +351-296-650-172

Received: 10 April 2020; Accepted: 27 April 2020; Published: 28 April 2020

**Abstract:** A current research topic of great interest is the study of the therapeutic properties of plants and of their bioactive secondary metabolites. Plants have been used to treat all types of health problems from allergies to cancer, in addition to their use in the perfumery industry and as food. *Hedychium* species are among those plants used in folk medicine in several countries and several works have been reported to verify if and how effectively these plants exert the effects reported in folk medicine, studying their essential oils, extracts and pure secondary metabolites. *Hedychium coronarium* and *Hedychium spicatum* are the most studied species. Interesting compounds have been identified like coronarin D, which possesses antibacterial, antifungal and antitumor activities, as well as isocoronarin D, linalool and villosin that exhibit better cytotoxicity towards tumor cell lines than the reference compounds used, with villosin not affecting the non-tumor cell line. Linalool and  $\alpha$ -pinene are the most active compounds found in *Hedychium* essential oils, while  $\beta$ -pinene is identified as the most widespread compound, being reported in 12 different *Hedychium* species. Since only some *Hedychium* species have been investigated, this review hopes to shed some light on the uncharted territory that is the *Hedychium* genus.

**Keywords:** *Hedychium*; traditional medicine; coronarin D; villosin; anti-acetylcholinesterase; antidiabetic; anti-inflammatory; antimicrobial; antioxidant; antitumor

## 1. Introduction

Since the beginning of the history of mankind there was always a connection between plants and human health, as they were used as food and medicines [1]. The traditional herbal medicine outlined the foundations from which modern medicine developed and is still largely practiced around the world [2], particularly in Asian and developing countries [3,4]. This popular knowledge, also known as folk medicine, gives a good indication to scientists looking for sources of new compounds with pharmaceutical potential. Thus, medicinal plants and their derived natural compounds have become an increasing topic of investigation and interest [5,6].

According to “The Plant List” database [7], the genus *Hedychium* (Zingiberaceae family) comprises 93 species with accepted scientific plant names that, with the exception of *Hedychium peregrinum* N.E.Br. that is endemic to Madagascar [8], are native to wooded habitats in tropical and temperate Asia (i.e., China, Indian subcontinent and Southeast Asia) [8–10]. Members of this genus are well distributed worldwide, being easily found particularly throughout tropical Asia, Australia, Fiji, New Caledonia, New Guinea, New Hebrides, Samoa and the Solomon Islands [8,10,11], with some species being considered invasive in some places: e.g., *Hedychium coronarium* J. Koenig in Brazil [12] and *Hedychium gardnerianum* Sheppard ex Ker-Gawl. in Azores Archipelago [13] and Hawaii [14].

*Hedychium* species are medium-size rhizomatous perennial monocotyledonous plants that can be easily recognized by their characteristic striking foliage and terminal spikes that produce diversified numerous short-lived flamboyant flowers with several hues and fragrances varying depending on the species [15]. These features give them a high ornamental value, being cultivated worldwide mostly for this purpose and for its use in the perfumery industry, since, besides the aromatic flowers, *Hedychium* species rhizomes also originate strongly scented oils [16,17].

The use of *Hedychium* species in folk medicine is common in several countries since they are easily harvested directly from nature or obtained at local markets [18]. These plants are reported to possess analgesic, antimicrobial, antidiabetic, anti-inflammatory, antitumor, anti-allergic, anthelmintic and antioxidant properties [19–22]. In Table 1, it is summarized the different *Hedychium* species with reported traditional medicinal use in literature over different geographic areas.

**Table 1.** *Hedychium* species with reported traditional medicinal use.

<i>Hedychium</i> Species	Geographical Origin of the Reported Traditional Use	Traditional Medicinal Use	Preparation and/or Administration	
<i>Hedychium</i> sp. [23]	Myanmar [23]	Cuts and wounds [23]	Cataplasms of crushed leaves and rhizomes [23]	
		Weak blood circulation and to accelerate postpartum recovery [23]	Decoction of rhizomes is drunk [23]	
<i>Hedychium coccineum</i> Buch.-Ham. ex Sm.	India [24]	Jaundice [24]	Decoction of rhizomes [24]	
	Brazil [25,26]	Anti-inflammatory and sedative [25]	Leaves infusion [25,26]	
		Headache and fever [26]		
	China [27]	Diabetes, headache, inflammation, rheumatism and skin diseases [27]	Rhizomes [27]	
	Colombia [28]	Snake bites [28]	Decoction of rhizomes [28]	
	India [16,29–31]	Stimulant tonic, carminative, headache, fever, diphtheria and diabetes [16,29,30]	Grinded rhizomes [16,29,30]	
		Abdominal pain [31]	10 g of sun-dried rhizome powder mixed with cooked vegetables [31]	
	Malaysia [32]	Indigestion and abdominal pain [32]	Boiled leaves with betel nut are eaten [32]	
	<i>H. coronarium</i>	Mauritius [33]	Carminative, cordial, emmenagogue, diuretic and toothache [33]	Decoction of rhizomes [33]
			Rubefacient [33]	Cataplasm of fresh rhizomes [33]
			Rheumatism [33]	Rub affected areas with paste from crushed rhizomes cooked in mustard oil with garlic and crushed camphor bark [33]
		Nicaragua [34]	Snake bites [34]	Decoction of rhizomes [34]
		Peru [35]	Soothing and rheumatism [35]	Bath is prepared with the aerial part [35]
Thailand [16,36]	Sore and stiff joints [16]	Application of boiled leaves in affect areas [16]		
	Tonsillitis [16]	Decoction of the stem is gargled [16]		
	Mosquito repellent [36]	Oil from the plant [36]		
Vietnam [37]	Diabetes, headache, inflammation, rheumatism and skin diseases [37]	Rhizomes [37]		

Table 1. Cont.

<i>Hedychium</i> Species	Geographical Origin of the Reported Traditional Use	Traditional Medicinal Use	Preparation and/or Administration
<i>Hedychium cylindricum</i> Ridl.	Malaysia [38]	Antirheumatic, febrifuge, tonic, treatment of skin diseases and wounds [38]	Rhizomes [38]
<i>Hedychium ellipticum</i> Buch.-Ham. ex Sm.	Nepal [39]	Fever [39]	Five teaspoons twice a day of rhizome juice [39]
<i>Hedychium flavescens</i> Carey ex Roscoe	Madagascar [40]	Caries [40]	Squeezed leaves liquid is applied in cotton and then placed in the affected cavity [40]
	Mauritius [33]	Rheumatism [33]	Rub affected areas with paste from crushed rhizomes cooked in mustard oil [33]
<i>Hedychium longicornutum</i> Griff. ex Baker	Malaysia [41]	Intestinal worms and earache [41]	Macerated roots or the whole plant [41]
<i>Hedychium spicatum</i> Sm.	India [21,42–44]	Bad breath, bronchitis, blood diseases, hiccough and vomiting [42]	3 to 4 g of rhizome powder two times a day [42]
		Asthma, body pain, inflammation and laxative [43]	1 g dried rhizome powder twice a day [43]
		Diarrhea, fever, liver problems and pain [21]	Spoonful of dried rhizome powder thrice a day [21]
		Expectorant, stimulant, stomachic, tonic and vasodilator [21]	Cup of the rhizome decoction twice a day [21]
	Nepal [39]	Snake bites [44]	
	Nepal [39]	Indigestion and high fever [39]	Decoction of rhizome three to five teaspoons twice a day [39]

In addition to the traditional medicinal uses stated in Table 1, *Hedychium* species are also included in the diet of some populations, like in Thailand where the flowers of *Hedychium forrestii* Diels can be boiled to become a beverage [45] or in India where the fruit of *H. spicatum* may be cooked and eaten with lentils in savory dishes [42]. Moreover, the rhizome of *H. coronarium* is also included in the diet of some populations of South East Asia, being consumed as a vegetable or as a food flavoring spice [46].

The traditional uses mentioned above show that several *Hedychium* species are used to treat a wide spectrum of diseases. These uses also show that *Hedychium* species should be considered as promising sources of new bioactive natural compounds and that is why these species have been the target of research by the scientific community. In recent years, several studies have been published on the phytochemical characterization of *Hedychium* species, as well as on the evaluation of the biological activities exhibited by their organic extracts, essential oils and pure compounds, with some of them showing very interesting results. Recently, literature reviews have been published focusing only on specific species, i.e., *H. coronarium* [20,47] and *H. spicatum* [21,48]. This work aims to update the available information that were not mentioned in the previous reviews, as well as involving all the other *Hedychium* species, their bioactivities and their bioactive isolated compounds. The research for this review was made combining the terms *Hedychium*, phytochemical and biological activities in the databases Web of Science, PubMed and Scopus and were considered only the published works involving *Hedychium* species whose binominal Latin name is an accepted name on the The Plant List database [7].

## 2. In Vitro and In Vivo Activities of *Hedychium* Extracts and Essential Oils

Taking into account the traditional uses of *Hedychium* species, several works have been carried out to elucidate how effectively plants can exert the reported biological effects. The following is a



compilation and discussion of the most current works on this subject, in which essential oils and extracts of *Hedychium* species are studied and their biological activities are ascertained.

### 2.1. Anti-Acetylcholinesterase

The inhibition of the enzyme acetylcholinesterase (AChE) is one of the pathways to countering the cholinergic deficit associated with cognitive dysfunction diseases like in Alzheimer's disease [49]. Arruda and colleagues [50] showed that the leaf essential oil of *H. gardnerianum* collected from four different locations could inhibit AChE action, mainly mixed inhibition, presenting IC<sub>50</sub> values ranging from 1.03 ± 0.14 mg/mL to 1.37 ± 0.27 mg/mL, a value not statistically different from the value displayed by the AChE inhibitor standard compound α-pinene that presented an IC<sub>50</sub> value of 1.43 ± 0.07 mg/mL. This work showed no statistically significant difference between the activity of samples taken in different geographical areas [50].

### 2.2. Antidiabetic

Deficiency in insulin secretion, insulin action or both, results in chronic hyperglycemia, the main characteristic of diabetes mellitus [51], the main treatment to this condition being the use of anti-diabetic drugs that can control glucose levels in the blood [52].

An in vivo study [53] was carried out to assess the effect of *H. coronarium* aqueous extract to lower blood glucose level in induced-type 2 diabetes mellitus (T2DM) animal models (streptozotocin (STZ)-induced T2DM Wistar rats and C57BKS<sup>db/db</sup> mice, a mice model with a mutation that results in chronic hyperglycemia, pancreatic beta cell atrophy, low insulin level and obesity). After 28 days, the daily dose of *H. coronarium* aqueous extract (8.928 mg/kg for the STZ-induced T2DM rats and 17.71 mg/kg for the C57BKS<sup>db/db</sup> mice) significantly increased glucose tolerance in both diabetic models, when compared with the group treated with distilled water (control group). In addition, the treatment also helped to maintain optimal β-cell structure, moderately increased insulin, improved the lipid profile and decreased aldosterone level in STZ-induced T2DM model.

In another in vivo assay [54], after 14 days of treatment, using an oral dose of 0.3 mL of essential oil from rhizomes of *H. spicatum*, was observed the reduction of blood glucose and urea levels in rats with diabetes induced by intraperitoneal injection of a solution of alloxan monohydrate (150 mg/kg). This result is similar to those obtained in the group of rats treated with the reference drug glibenclamide. Furthermore, it was noticed that the Islets of Langerhans regained their normal shape after the treatment period [54].

### 2.3. Anti-Inflammatory

Inflammation is a vital defense mechanism that works to ensure good health [55], but uncontrolled inflammation may lead to serious repercussions [56] and so it is important to continue research into products that can help in its control.

An in vivo study [57] with rats demonstrated the anti-inflammatory effect of a single oral dose (200 mg/kg) of aqueous and ethanolic extracts of *H. spicatum* rhizome against carrageenan-induced paw edema. Measurements of the edema volume were taken in a successive interval of 1 h, 2 h and 3 h and significant decrease in paw edema volume was detected since the beginning, with the aqueous extract reporting a 28.10% decrease in inflammation and the ethanolic extract a 25.62% decrease in inflammation. Although none of the extracts performed as well as the positive control compound indomethacin (41.32% decrease in inflammation), they both proved to present no acute toxicity in a concentration as high as 2000 mg/kg, with the rats never showing secondary toxic effects like coma, convulsion, salivation, increased motor activity or death. This dose of 2000 mg/kg was previously utilized in a similar work [58] where the ethanolic extract of *H. spicatum* reported a 55.54% of anti-inflammatory activity inhibition against carrageenan-induced edema in rats.

#### 2.4. Antimicrobial

A healthy human body is a symbiosis between human and microbial components [59]. However, sometimes that symbiotic balance can be disturbed, and human health can be impaired by pathogenic microorganisms (i.e., bacteria, fungi, parasites or viruses), the use of effective antimicrobial drugs being needed to restore health normality [60,61].

Noriega et al. [62] showed that, among five different plants, the essential oil of *H. coronarium* rhizome exhibited the most relevant antibacterial activity against *Listeria grayi* (MIC value = 0.45 mg/mL) and *Streptococcus mutans* (MIC value = 0.18 mg/mL) and even against the Gram-negative bacteria *Klebsiell oxytoca* (MIC value = 0.90 mg/mL). The authors point out the compounds 1,8-cineole and terpinen-4-ol as responsible for the reported activity [62]. In another work [63], *H. coronarium* leaves essential oil was also pointed out to have antibacterial activity against different bacterial strains, i.e., *Escherichia coli* (MIC value = 3.90 µL/mL), *Staphylococcus aureus* (MIC value = 7.81 µL/mL) and *Pseudomonas aeruginosa* (MIC value = 15.62 µL/mL). These two works are presented here also as examples of two constraints which are common in a variety of scientific papers. First, no work reports, as a comparative term, the activity exhibited by a standard antibacterial compound, determined under the same experimental conditions as the essential oil samples. Without these data it is very difficult to assess the true potential of the samples tested. Second, the MIC values are expressed in non-comparable units. Fortunately, one of the works [62] presents the density of the essential oil, making it possible to convert one of the sets of results [against *Listeria grayi* (MIC value = 0.50 µL/mL), *Streptococcus mutans* (MIC value = 0.20 µL/mL), *Klebsiell oxytoca* (MIC value = 1.0 µL/mL)], allowing to conclude that the essential oil from rhizome is more active as antibacterial agent than leaves essential oil. Regrettably, some papers do not present enough experimental data to allow a unit conversion. Additionally, Ray et al. [64] reported that the essential oil extracted from the rhizome of *H. coronarium* is an effective antifungal agent since it exhibited activity against *Candida albicans* (MIC = 3.12 µg/mL), *Aspergillus flavus* and *Fusarium oxysporum* (MIC value of 6.25 µg/mL for both species), these MIC values being much lower than those reported for antibacterial activity by Noriega et al. [62].

Another work [65] found that 20 µL of *Hedychium matthewii* S. Thomas, B. Mani & S. J. Britto rhizome essential oil could be as effective as 30 µg of the standard antibiotic amoxicillin, since it exerted nearly the same growth inhibition effect against several strains of Gram- positive and Gram-negative bacteria (viz. *Bacillus cereus*, *Staphylococcus aureus*, *Enterobacter aerogens*, *Salmonella paratyphi*, *Salmonella typhi*, *Escherichia coli*, *Vibrio parahaemolyticus*, *Proteus vulgaris*, *Klebsiella pneumoniae* and *Pseudomonas aeruginosa*). Furthermore, it could be pointed out that *Streptococcus haemolyticus* and *Vibrio cholerae* were more susceptible towards the essential oil (20 µL) than towards amoxicillin (30 µg).

The activity of *H. spicatum* flowers essential oil was evaluated against the Gram-negative bacteria *Borrelia burgdorferi* in stationary phase cycle and it was found out that a 0.1% (v/v) essential oil concentration could eradicate *B. burgdorferi* (100 µL) with no regrowth [66]. This is one of the few published works that evaluates the antibacterial activity in the stationary-phase of growth.

A different work [67] found that a combination treatment using essential oil of *H. spicatum* rhizomes and  $\gamma$ -radiation was effective against *Fusarium graminearum*, inhibiting both the fungal growth in maize grains and the production of the toxic mycotoxins deoxynivalenol and zearalenone in a dose-dependent way, with a complete inhibition at the concentration of essential oil 1.89 mg/g and 4.1 kGy of  $\gamma$ -radiation. Combinational treatment proved to be better than individual treatment, since complete inhibition of *F. graminearum* required the essential oil concentration of 3.15 mg/g or 6 kGy of  $\gamma$ -radiation.

It is not just the essential oils of *Hedychium* species that have been evaluated concerning antimicrobial activity. Arora and Mazumder [68] evaluated the activity of *H. spicatum* rhizomes methanolic extract and the antibiotic ciprofloxacin against different bacterial strains (viz. *Shigella boydii*, *Shigella sonnei*, *Shigella flexneri*, *B. cereus*, *V. cholerae*, *E. coli*, *S. aureus*, *Ps. aeruginosa* and *K. pneumoniae*) at the concentrations of 200 to 1200 µg/mL. The results showed a similar inhibition effect for both antibiotic and extract, *B. subtilis* being the bacteria with greater susceptibility to the extract and antibiotic.

Another work [69] evaluated the anthelmintic activity of methanolic, ethanolic, hydromethanolic, hydroethanolic and aqueous rhizome extracts of *H. spicatum* against *Hemonchus contortus*, with the results showing that the methanolic extract were as effective as the positive control compound thiabendazole on time taken for paralysis and time taken for death (tested concentrations 20, 40 and 60 mg/mL).

## 2.5. Antioxidant

Oxygen metabolism is fundamental for human life but its reaction products, like reactive oxygen species (ROS), can increase oxidative stress, causing damage to cells and tissues [70] that, with time, leads to the development or aggravation of several chronic diseases [71]. Thus, therapeutic antioxidant agents are key to mitigate the oxidative stress impact in human health, with natural plant-derived products being the main investigation focus of search [72].

Noriega et al. [62] evaluated the antioxidant activity of the essential oil extracted from the rhizome of *H. coronarium*, reporting IC<sub>50</sub> values of 9.04 ± 0.55 mg/mL and 2.87 ± 0.17 mg/mL for 1,1-Diphenyl-2-picrylhydrazyl (DPPH) and 2,2'-azino-bis(3-ethylbenzothiazoline-6-sulphonic acid (ABTS) assays, respectively. In a similar work, Ray and colleagues [64] also evaluated the antioxidant activity of the essential oil from *H. coronarium* rhizome, but from ten distinct regions of India, obtaining activity values higher than those indicated in the work of Noriega et al. [62] (IC<sub>50</sub> values range from 0.57 to 2.19 mg/mL for the DPPH assay; and 0.12 to 0.67 mg/mL for the ABTS assay), but lower than the positive control 2,6-di-tert-butyl-4-methylphenol (BHT) (IC<sub>50</sub> = 0.12 ± 0.01 mg/mL on the DPPH assay, and 0.08 ± 0.01 mg/mL on the ABTS assay). It could be pointed out that Ray et al. [64] also demonstrate, very clearly, that the geographical origin of the samples is a relevant variable for the level of activity displayed. The same conclusion can be drawn from the results obtained by Arruda et al. [50], where the DPPH antioxidant activity of *H. gardnerianum* leaf essential oil collected from four different locations ranged from EC<sub>50</sub> = 8.46 ± 0.90 µg/mL to 31.14 ± 2.70 µg/mL (EC<sub>50</sub> = 31.00 ± 0.19 µg/mL for BHT). In a more recent work, Ray et al., [73] studied the antioxidant activity of *Hedychium greenii* W. W. Smith, and *Hedychium gracile* Roxb. rhizomes essential oils by the same methodology (DPPH and ABTS assays), with *H. greenii* showing higher antioxidant activity (IC<sub>50</sub> values of 16.73 ± 0.19 µg/mL for DPPH and 12.18 ± 0.16 µg/mL for ABTS assays) than *H. gracile* sample (IC<sub>50</sub> values of 46.94 ± 0.6 µg/mL for DPPH and 31.13 ± 0.29 µg/mL for ABTS assays), and slightly higher than the positive control BHT (IC<sub>50</sub> = 18.94 ± 0.3 µg/mL and IC<sub>50</sub> = 14.21 ± 0.27 µg/mL for DPPH and ABTS assays, respectively). These results [73], when compared with those obtained in the works mentioned above [50,64], show that the level of antioxidant activity of essential oils exhibits variability between different *Hedychium* species (IC<sub>50</sub> values range from 8.46 to 2190 µg/mL) higher than geographical variability (IC<sub>50</sub> values range from 0.57 to 2.19 mg/mL for the DPPH assay).

Zhao et al. [74] compared essential oils and ethanolic extracts from rhizomes of different species from the Zingiberaceae family in terms of its antioxidant capacity by DPPH assay. The ethanol extracts of *H. coronarium* and *H. gardnerianum* proved to be the best antioxidant samples presenting IC<sub>50</sub> values of 0.94 µg/mL and 1.59 µg/mL, respectively, even better than the reference compounds trolox (IC<sub>50</sub> = 10.19 µg/mL) or ascorbic acid (IC<sub>50</sub> = 8.37 µg/mL). Essential oils of these plants were also tested but unfortunately the authors presented the results as a graphic which does not allow the reading of numerical values of antioxidant activity.

Usha et al. [75] compared the hydromethanolic rhizome extract of different species also from Zingiberaceae family in terms of its antioxidant capacity and found out that *Hedychium* sp. reported the best results, with the lowest IC<sub>50</sub> value on DPPH assay (36.4 µg/mL). This activity was correlated with its high phenol and flavonoid content. Unfortunately, the authors do not specify neither the *Hedychium* species that was used nor the IC<sub>50</sub> value of the ascorbic acid used as positive control, which makes impossible to compare with other published works.

Another work [69] evaluated, through ABTS, DPPH and nitric oxide (NO) free radical scavenging assays, the antioxidant activity of methanolic, ethanolic, hydromethanolic, hydroethanolic and aqueous

rhizome extracts of *H. spicatum*. The results showed the methanolic extract as the most antioxidant extract, presenting the lowest EC<sub>50</sub> values for all the assays (EC<sub>50</sub> ABTS value = 24.93 mg/mL, EC<sub>50</sub> DPPH value = 8.31 mg/mL and EC<sub>50</sub> NO value = 3.57 mg/mL). However, this extract is much less active than the positive control ascorbic acid (EC<sub>50</sub> = 1.63 mg/mL to ABTS assay, EC<sub>50</sub> = 0.049 mg/mL to DPPH assay and EC<sub>50</sub> = 0.10 mg/mL to NO assay) and since the extract EC<sub>50</sub> values are very high, it should be considered an inactive extract.

In an in vivo study, Choudhary and Singh [76] demonstrated the antioxidant potential of *H. spicatum* rhizome, since an improvement in the oxidative stress state of white leghorn cockerels (*Gallus gallus domesticus*) was observed after the rhizome powder was added to the animal diet, following chronic exposure to indoxacarb.

## 2.6. Antitumor

Cancer is a complex disease that is a major cause of death worldwide [77], with several treatments but no cure [78]. In the light of the aggressive and not always effective treatments in current medicine, the demand for safer and better anticancer compounds have turned the search to natural products as another therapeutic approach to cancer [79].

Ray and colleagues [80] demonstrated the antiproliferative time-dependent effect of *H. coronarium* rhizome ethanol extract against human cervical carcinoma HeLa cells, without affecting the viability of non-tumor human umbilical vein endothelial cells (HUVEC). After 24, 48 and 72 h of incubation, the observed IC<sub>50</sub> values were 17.18 ± 0.46, 15.32 ± 0.68 and 12.57 ± 0.32 µg/mL, respectively. Although the positive control drug camphothecin presented a far greater inhibitory effect against HeLa cells (IC<sub>50</sub> values of 0.82 to 0.98 µg/mL), it is also more toxic to the HUVEC cells (IC<sub>50</sub> value for 24 h = 10.13 ± 0.62 µg/mL) than the *H. coronarium* ethanol extract (IC<sub>50</sub> value for 24 h > 320 µg/mL), which means that the extract presents a higher selective cytotoxicity. In addition, the same study shed some light on the mechanism whereby the extract exerts its antitumor activity. It denotes the modulation of the expression of proapoptotic and antiapoptotic protein levels together with an increase of ROS generation and consequent oxidative stress induction in HeLa cells that led to an apoptosis-mediated G1 phase cell arrest as the main cause of HeLa cells migratory capacity inhibition.

In another study [81], the methanolic extract of *H. spicatum* rhizomes was described as possessing a dose-dependent cytotoxicity activity against human liver hepatocellular carcinoma cell line HepG2, testing concentrations in the range of 25 to 3000 µg/mL. The concentrations tested and the IC<sub>50</sub> value (281.917 µg/mL) are very high, and the authors do not provide the cytotoxicity of a positive control nor do they evaluate the effects of such concentrations on non-tumor cells. The results obtained in the studies performed in these conditions, should be considered with many reservations as the effects observed using such high concentrations are non-specific. On the other hand, the researchers should take into account that 20 µg/mL is the limit established by the National Cancer Institute to consider an extract active enough to justify continuing its study [82], so the tested extract should be considered inactive against HepG2 cells line.

The in vitro cytotoxicity, by 3-(4,5-dimethylthiazol-2-yl)-2,5-diphenyltetrazolium bromide (MTT) assay, of *H. spicatum* rhizome chloroform extract was assessed against colorectal adenocarcinoma (Colo-205) cell line, human epidermoid carcinoma (A-431) cell line, human breast adenocarcinoma (MCF-7) cell line, human lung adenocarcinoma (A549) and Chinese hamster ovary (CHO) cell lines [83]. The results show that the extract presented cytotoxicity against all cell lines exhibiting IC<sub>50</sub> values ranging from 37.45 ± 0.90 µg/mL to 63.21 ± 1.19 µg/mL, including against non-tumor cell line CHO (39.52 ± 0.06 µg/mL), indicating that the *H. spicatum* rhizome chloroform extract have small potential as a good anticancer drug since it affected in a similar way both tumor and non-tumor cell lines. Results like these shows how difficult it is to find an ideal anti-tumor drug that affect only the tumor cells, leaving the non-tumor cells undamaged. In addition, it would have been interesting if the authors had also tested a reference compound, since it would have enriched their work.

## 2.7. Hepatoprotective

The liver is a vital organ, capable of detoxifying the body from endogenous and/or exogenous substances detrimental to the organism, and which is responsible for the regulation of diverse functions and physiological processes, such as the metabolism of carbohydrates and fats and the secretion of bile [84]. Exposure to drugs and chemicals can cause liver injury which, taking into account all the functions inherent to the liver, is a major health problem [85]. Thus, compounds that can protect the liver, stimulate hepatic function or help to regenerate hepatic cells, while simultaneously being less toxic and more effective are of great interest, with natural sources being identified as good search option [86].

A study [87] indicated that *H. spicatum* possess hepatoprotective properties since its three rhizome extracts (methanolic, ethanolic and aqueous) exerted protection on HepG2 cells against paracetamol-induced toxicity. The IC<sub>50</sub> values were 282, 356 and 515 µg/mL for the methanolic, ethanolic and aqueous extracts, respectively, which translates in a cytoprotection percentage of 16%, 13% and 9%, respectively. Compared to the 19% cytoprotection provided by the control substance silymarin (IC<sub>50</sub> = 110 µg/mL), the hepatoprotective effect of the extracts is not huge but it is worth mentioning at least the methanolic extract.

A study which was also carried out to evaluate the potential hepatoprotective effect was the in vivo study [88]. where cockerels were fed for 16 weeks with rhizome powder of *H. spicatum*, while simultaneously receiving a dose of indoxacarb intended to cause chronic toxicity. The results of the liver analysis show that, when compared with the control group (indoxacarb administration without the added *H. spicatum* rhizome powder to the cockerels diet), *H. spicatum* rhizome ameliorated the damages caused in cockerels by indoxacarb in the duration of the experiment. Apparently, the treatment with *H. spicatum* modulated the expression levels of several different hepatic genes, such as those involved in metabolism of indoxacarb (cytochrome P450 1A1), in the immune system (interleukin 6 (IL-6)) and in antioxidant function (catalase (CAT), superoxide dismutase (SOD) and glutathione peroxidase (GPx)).

## 2.8. Insecticide

Control of mosquito population is crucial, particularly in developing countries, since they act as vectors of several pathogens and parasites responsible for various worrisome diseases, e.g., dengue, filariasis, malaria, West Nile or yellow fever [89,90]. In order to reduce or eliminate the human contact with the vector, a wide range of methods exists with insecticides being a top choice in case of mosquitoes [91]. However, with insecticide resistance being a problem in recent years [92], the search for better substances with insecticide potential is imperative.

Kalimuthu and colleagues [93] carried out an interesting work where *H. coronarium*-synthesized silver nanoparticles (AgNPs) were produced and their toxicity towards larvae and pupae of the dengue vector *Aedes aegypti* was assessed, as well as their synergy with *Mesocyclops formosanus* predation over *A. aegypti* larvae. The toxicity of aqueous *H. coronarium* rhizome extract was also assessed. The results indicate that both *H. coronarium* formulations tested, aqueous rhizome extract and AgNPs, were toxic against *A. aegypti* in a dose-dependent manner. Aqueous *H. coronarium* rhizome extract caused toxicity with LC<sub>50</sub> values from 0.688% against larval instar I to 1.882% dose against pupae stage of *A. aegypti*, while AgNPs demonstrated its toxicity with LC<sub>50</sub> values varying from 24.264 ppm for larval instar I till 348.68 ppm for pupae of *A. aegypti*. Once again, we are faced with a work whose authors express results in non-comparable units and do not provide the necessary data for their conversion, significantly reducing the impact of this work. Nevertheless, AgNPs were found to be stable over time in aquatic environment and since a positive synergy was reported with *M. formosanus* predation on young *A. aegypti* larvae, its combined use could lead to a higher efficacy in removing the larval population of dengue mosquitoes from aquatic areas.

In another work [94], *Hedychium larsenii* M. Dan and C. Sathish Kumar rhizomes essential oil was evaluated regarding its toxicity against larvae of mosquito vectors of diseases, namely *Anopheles*

*stephensi* (malaria), *A. aegypti* (dengue) and *Culex quinquefasciatus* (St. Louis encephalitis). The results demonstrate that the essential oil exerted larvicidal activity over the different larvae with the LC<sub>50</sub> values of 82.02, 88.60 and 96.40 µg/mL for *A. stephensi*, *A. aegypti* and *C. quinquefasciatus*, respectively. Again, the lack of a tested reference compound impairs any conclusion taken from these results.

### 3. Secondary Metabolites from *Hedychium* Species and Its Activities

The diverse bioactivities observed on different *Hedychium* species/extracts are intrinsically linked to the compounds present in each one, so the need and interest in the phytochemical study of these extracts/species becomes clear. Several relevant works managed to isolate compounds from *Hedychium* extracts and carried out different assays to ascertain the bioactive potentials of those compounds. In Table 2 the compounds isolated from *Hedychium* extracts are gathered, as well as their bioactivities and the *Hedychium* species where they have already been identified. A figure with the chemical structures of the compounds (Figure 1) listed in this table is present after Table 2. It should be clarified that, for each compound in Table 2, only the highest activity value for each activity from each reference is presented, with some values converted from µg/mL to µM to facilitate comprehension and comparison of the different activities.

**Table 2.** Secondary metabolites isolated from *Hedychium* extracts with proven activities.

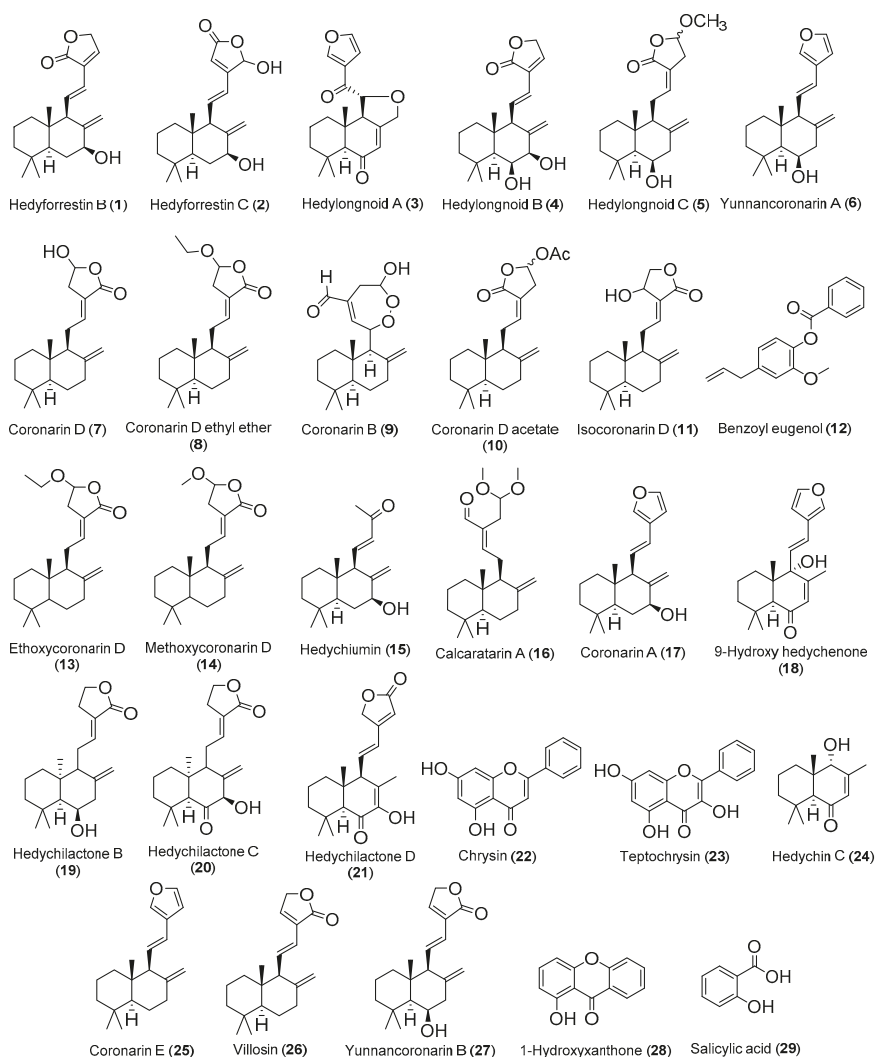
Compound	Extract	<i>Hedychium</i> Source	Activity *
Hedyforrestin B (1)	Hexane [95]	<i>H. gardnerianum</i> rhizome [95]; <i>Hedychium longipetalum</i> X.Hu and N.Liu rhizome [96]	Antitumor against NCI-H187 cell line (IC <sub>50</sub> = 3.10 µM; Vero cell line IC <sub>50</sub> = 45.07 µM with SI of 14.5; Ellipticine IC <sub>50</sub> = 1.79 µM) [95]; Anti-inflammatory by NO inhibition (IC <sub>50</sub> = 20.60 µM **; MG132 # IC <sub>50</sub> = 0.17 µM **) [96]
Hedyforrestin C (2)	Dichloromethane [95]; Methanol [37]	<i>H. gardnerianum</i> rhizome [95]; <i>H. coronarium</i> rhizome [37]; <i>H. longipetalum</i> rhizome [96]	Antitumor against NCI-H187 cell line (IC <sub>50</sub> = 2.46 µM; Vero cell line IC <sub>50</sub> = 11.88 µM with SI of 4.8; Ellipticine IC <sub>50</sub> = 1.79 µM) [95]; Anti-inflammatory by NO inhibition (IC <sub>50</sub> = 8.33 µM **; MG132 # IC <sub>50</sub> = 0.17 µM **) [96]
Hedylongnoid A (3)	+	<i>H. longipetalum</i> rhizome [96]	Anti-inflammatory by NO inhibition (IC <sub>50</sub> = 22.84 µM **; MG132 # IC <sub>50</sub> = 0.17 µM **) [96]
Hedylongnoid B (4)	+	<i>H. longipetalum</i> rhizome [96]	Anti-inflammatory by NO inhibition (IC <sub>50</sub> = 16.79 µM **; MG132 # IC <sub>50</sub> = 0.17 µM **) [96]
Hedylongnoid C (5)	+	<i>H. longipetalum</i> rhizome [96]	Anti-inflammatory by NO inhibition (IC <sub>50</sub> = 17.50 µM **; MG132 # IC <sub>50</sub> = 0.17 µM **) [96]
Yunnancoronarin A (6)	Chloroform [83]; Hexane [95]	<i>H. gardnerianum</i> rhizome [95]; <i>H. spicatum</i> rhizome [83]; <i>H. longipetalum</i> rhizome [96]	Antitumor against NCI-H187 cell line (IC <sub>50</sub> = 36.78 µM; Vero cell line IC <sub>50</sub> = 108.61 µM with SI of 2.9; ellipticine IC <sub>50</sub> = 1.79 µM) [95]; Antitumor against Colo-205 cell line (IC <sub>50</sub> = 90.35 ± 0.10 µM **) [83]; Antitumor against CHO cell line (IC <sub>50</sub> = 59.55 ± 3.93 µM **) [83]; Anti-inflammatory by NO inhibition (IC <sub>50</sub> = 1.86 µM **; MG132 # IC <sub>50</sub> = 0.17 µM **) [96]
Coronarin D (7)	Dichloromethane [97]; Ethanol [80]; Hexane [98]; Methanol [99]	<i>H. coronarium</i> rhizome [80,97-99]	Antitumor against S102 cell line (IC <sub>50</sub> = 25.13 µM **) [98]; Antitumor against P388 cell line (IC <sub>50</sub> = 4.40 µM **; Etoposide IC <sub>50</sub> = 0.12 µM **) [97]; Antibacterial against <i>B. cereus</i> (MIC = 19.63 µM **; oxacillin MIC = 62.28 µM **) [100]; Antifungal against <i>Cryptococcus albidus</i> (MIC = 78.52 µM **; Amphotericin B MIC = 0.84 µM **) [100]
Coronarin D ethyl ether (8)	Hexane [98]	<i>H. coronarium</i> rhizome [98]	Antitumor against HepG2 cell line (IC <sub>50</sub> = 46.18 µM **) [98]
Coronarin B (9)	Dichloromethane [97]; Hexane [98]	<i>H. coronarium</i> rhizome [97,98]	Antitumor against MOLT-3 cell line (IC <sub>50</sub> = 1.32 µM **; Etoposide IC <sub>50</sub> = 0.03 µM **) [97]
Coronarin D acetate (10)	Dichloromethane [97]	<i>H. coronarium</i> rhizome [97]	Antitumor against P388 cell line (IC <sub>50</sub> = 4.72 µM **; etoposide IC <sub>50</sub> = 0.12 µM **) [97]

Table 2. Cont.

Compound	Extract	Hedychium Source	Activity *
Isocoronarin D (11)	Dichloromethane [97]; Ethanol [101]; Hexane [98]	<i>H. coronarium</i> rhizome [97,98,101]	Antitumor against P388 cell line (IC <sub>50</sub> = 2.14 μM **; etoposide IC <sub>50</sub> = 0.12 μM **) [97]; Antitumor against HepG2 cell line (IC <sub>50</sub> = 54.7 ± 0.3 μM) [101]
Benzoyl eugenol (12)	Ethanol [101]	<i>H. coronarium</i> rhizome [101]	Antitumor against HEK293 by NF-κB inhibition (IC <sub>50</sub> = 32.5 ± 4.9 μM) [101]
Ethoxycoronarin D (13)	Ethanol [101]	<i>H. coronarium</i> rhizome [101]	Cancer chemo preventive by COX-1 inhibition (IC <sub>50</sub> = 3.8 ± 0.1 μM) [101] Antitumor against HEK293 by NF-κB inhibition (IC <sub>50</sub> = 3.2 ± 0.3 μM) [101]
Methoxy-coronarin D (14)	Ethanol [101]	<i>H. coronarium</i> rhizome [101]	Cancer chemo preventive by COX-1 inhibition (IC <sub>50</sub> = 0.9 ± 0.0 μM) [101] Antitumor against HEK293 by NF-κB inhibition (IC <sub>50</sub> = 7.2 ± 0.3 μM) [101]
Hedychiumin (15)	Methanol [102]	<i>H. coronarium</i> aerial part [102]	Antitumor against P388D1 cell line (IC <sub>50</sub> = 17.15 ± 1.92 μM **; doxorubicin IC <sub>50</sub> = 0.74 ± 0.11 μM **) [102]
Calcaratarin A (16)	Methanol [102]	<i>H. coronarium</i> aerial part [102]	Antitumor against P388D1 cell line (IC <sub>50</sub> = 24.56 ± 1.92 μM **; doxorubicin IC <sub>50</sub> = 0.74 ± 0.11 μM **) [102]
Coronarin A (17)	Hexane [95]; Methanol [102]	<i>H. gardnerianum</i> rhizome [95]; <i>H. coronarium</i> aerial part [102]	Antitumor against NCI-H187 cell line (IC <sub>50</sub> = 40.77 μM; Vero cell line IC <sub>50</sub> = 150.45 μM with SI of 3.7; ellipticine IC <sub>50</sub> = 1.79 μM) [95]; Antitumor against DLD-1 cell line (IC <sub>50</sub> = 41.61 ± 6.32 μM **; doxorubicin IC <sub>50</sub> = 0.39 ± 0.07 μM **) [102]
9-Hydroxy hedychenone (18)	Chloroform [83]	<i>H. spicatum</i> rhizome [83]	Antitumor against Colo-205 cell line (IC <sub>50</sub> = 76.40 ± 0.03 μM **) [83]; Antitumor against CHO cell line (IC <sub>50</sub> = 49.87 ± 0.29 μM **) [83]
Hedychilactone B (19)	Chloroform [83]	<i>H. spicatum</i> rhizome [83]	Antitumor against Colo-205 cell line (IC <sub>50</sub> = 86.55 ± 0.06 μM **) [83]; Antitumor against CHO cell line (IC <sub>50</sub> = 60.94 ± 0.25 μM **) [83]
Hedychilactone C (20)	Chloroform [83]	<i>H. spicatum</i> rhizome [83]	Antitumor against Colo-205 cell line (IC <sub>50</sub> = 111.73 ± 0.09 μM **) [83]; Antitumor against CHO cell line (IC <sub>50</sub> = 70.82 ± 0.24 μM **) [83]
Hedychilactone D (21)	Chloroform [83]	<i>H. spicatum</i> rhizome [83]	Antitumor against Colo-205 cell line (IC <sub>50</sub> = 36.41 ± 0.09 μM **) [83]; Antitumor against CHO cell line (IC <sub>50</sub> = 23.27 ± 3.39 μM **) [83]
Chrysin (22)	Chloroform [83]	<i>H. spicatum</i> rhizome [83]	Antitumor against Colo-205 cell line (IC <sub>50</sub> = 117.25 ± 0.24 μM **) [83]; Antitumor against CHO cell line (IC <sub>50</sub> = 83.94 ± 4.37 μM **) [83]
Teptochrysin (23)	Chloroform [83]	<i>H. spicatum</i> rhizome [83]	Antitumor against Colo-205 cell line (IC <sub>50</sub> = 122.63 ± 0.11 μM **) [83]; Antitumor against CHO cell line (IC <sub>50</sub> = 110.86 ± 0.15 μM **) [83]
Hedychin C (24)	Ethanol [103]	<i>H. forrestii</i> rhizome [103]	Antitumor against XWLC-05 cell line (IC <sub>50</sub> = 53.6 μM) [103]
Coronarin E (25)	Hexane [95]	<i>H. gardnerianum</i> rhizome [95]	Antitumor against NCI-H187 cell line (IC <sub>50</sub> = 49.73 μM; Vero cell line IC <sub>50</sub> = 164.19 μM with SI of 3.3; ellipticine IC <sub>50</sub> = 1.79 μM) [95]
Villosin (26)	Dichloromethane [95]	<i>H. gardnerianum</i> rhizome [95]	Antitumor against NCI-H187 cell line (IC <sub>50</sub> = 0.40 μM; Vero cell line IC <sub>50</sub> > 166.42 μM with SI > 416; ellipticine IC <sub>50</sub> = 1.79 μM) [95]
Yunnanoronarin B (27)	Hexane [95]	<i>H. gardnerianum</i> rhizome [95]	Antitumor against NCI-H187 cell line (IC <sub>50</sub> = 44.57 μM; Vero cell line IC <sub>50</sub> = 106.21 μM with SI of 2.4; ellipticine IC <sub>50</sub> = 1.79 μM) [95]
1-Hydroxyxanthone (28)	Acetone [104]	<i>H. gardnerianum</i> rhizome [104]	Anti-depressant by MAO-A inhibition (IC <sub>50</sub> = 0.31 ± 0.05 μM) [105]
Salicylic acid (29)	Acetone [104]	<i>H. gardnerianum</i> rhizome [104]	Anti-hemorrhagic (IC <sub>50</sub> = 0.20 μM) [106]

\* Only the highest activity value; \*\* Value after unit conversion from μg/mL to μM;

# MG132-carbobenzoxy-Leu-Leu-leucinal positive control; † The authors do not indicate the extract prepared.



**Figure 1.** Chemical structure of the compounds referred on Table 2.

Taking the information of Table 2 into account, it is possible to identify that *H. coronarium* provided the highest number of isolated compounds and that the antitumor activity is the most reported bioactivity in the above-mentioned studies. On the other hand, the labdane-type diterpene is the most frequent family of compounds in the genus *Hedychium*, and some flavonoids and simple phenolic compounds are also identified.

Villosin (26) can be pointed out as the most promising antitumor compound, since it presented a highest and selective cytotoxicity against NCI-H187 cell line with an  $IC_{50}$  value of 0.40  $\mu$ M, without toxicity against the non-tumor Vero cell line at 166.42  $\mu$ M and presenting better results than the positive control compound ellipticine (i.e.,  $IC_{50}$  value against NCI-H187 of 1.79  $\mu$ M and  $IC_{50}$  value against Vero of 7.47  $\mu$ M). Coronarin D (7) appears also as one interesting compound, since recent works report its antibacterial activity against *B. cereus* to be better than the positive control oxacillin.



In addition to these compounds, hedyforrestin B (1) and hedyforrestin C (2) should also be noted, since their antitumor activities against the NCI-H187 cell line are slightly lower (less than 1.7 times) than that shown by the reference compound ellipticine and with selectivity indices of 14.5 and 4.8, respectively.

On the other hand, compound isocoronarin D (11) should be highlighted since it exhibits activity against a broad spectrum of tumor cell lines (i.e., A549, human cervical carcinoma (HeLa), human hepatocellular carcinoma (HepG2), human acute promyelocytic leukemia (HL-60), human cholangiocarcinoma (HuCCA-1), human epidermoid carcinoma (KB), human breast adenocarcinoma (MDA-MB-231), human acute lymphoblastic leukemia T-lymphoblasts (MOLT-3), mouse lymphoma neoplasm (P388), human hepatocellular carcinoma (S102) and human hormone-dependent breast cancer (T-47D)), with  $IC_{50}$  values between 2.14 to 36.1  $\mu$ M, better than etoposide or doxorubicin which are toxic only to some of these cell lines, and being more active against HepG2 ( $IC_{50}$  = 16.6  $\mu$ M) than the reference compound etoposide ( $IC_{50}$  = 23.8  $\mu$ M) [98].

Bearing in mind that all these compounds have hydroxyl groups and double bonds in their chemical structure, it is suggested that these compounds could be lead compounds, and researchers in the field of medicinal chemistry should use these labile functional groups to carry out structural modifications, in order to obtain more active derivatives and to determine the structure/activity relationships.

In addition, there are some works which require a critical analysis. Zhao and colleagues [96] isolated six labdanes from *H. longipetalum* rhizome that exhibited NO production inhibitory effects in lipopolysaccharides (LPS) and interferon gamma (IFN- $\gamma$ )-induced murine macrophages RAW 264.7 cell line. The most active compound is yunnancoronarin A (6) ( $IC_{50}$  = 1.86  $\mu$ M), but less active than the positive control carbobenzoxy-Leu-Leu-leucinal (MG132) ( $IC_{50}$  = 0.17  $\mu$ M). Unfortunately, the authors do not mention the extraction and chromatographic procedures they carried out to isolate these compounds, which would have been a valuable information.

Another study that looks promising, but which actually shows very questionable results, is the one carried out by Kiem and colleagues [37]. They isolated compounds from rhizomes of *H. coronarium* methanol extract and investigated their anti-inflammatory potential through inhibition of pro-inflammatory cytokines production in LPS-stimulated bone marrow-derived dendritic cells (BMDC). The results are not acceptable and do not allow to infer conclusions since they are presented with associated standard errors greater than 20% (e.g.,  $IC_{50}$  IL-6 inhibition value =  $7.57 \pm 2.02$   $\mu$ M) and in some cases close to 100% (e.g.,  $IC_{50}$  IL-12p40 inhibition value =  $0.19 \pm 0.11$   $\mu$ M). This work [37] was only mentioned here to point out to all authors the need to present reliable data in their works, aiming always to show results with standard error less than 10%.

In other lines of work, several studies (e.g., Reddy et al. [83], Chimnoi et al. [98] and Endringer et al. [101]) assessed the antitumor potential of isolated compounds from *Hedychium* extracts without following the best guidelines for evaluating the cytotoxic potential of compounds. In fact, the authors did not test a reference compound in the same experimental conditions, and did not test the isolated compounds against a non-tumor cell line, which makes it difficult to draw conclusions. Regrettably, without these results, it is not possible to conclude about the efficacy and selectivity of the isolated compound compared to the drugs already available on the market.

In addition to compounds 28 and 29 (Figure 1), Carvalho and colleagues [104] also isolated the compounds 3-(2-hydroxyethoxy)xanthone (30) and oplopanone (31) from *H. gardenerianum* rhizome acetone extract, but the two compounds (Figure 2) do not present any reported activity and, therefore, were not included in Table 2. Since they belong to families of organic compounds well-known for their broad spectrum of activities (flavonoids and terpenes) [107], it would be worth investigating the biological activity of these compounds.

It is a fact that the availability of a specific compound in a plant can depend on several factors, like the geographic location where the plant developed [108] and/or the season when it was harvested [109]. Thus, different studies can present different percentages of the total content of the same compound which makes it difficult sometimes to make comparisons between the same

plants. This fact is particularly relevant with regard to essential oils, where the majority of published studies refers to quantitative chemical analysis. These studies reveal a complex composition and a huge variability in the content of each compound, depending on geographic, seasonal and species factors, which is reflected in the variability of the biological activity level of the respective essential oils, already highlighted in point 2.

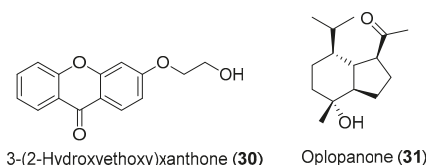


**Figure 2.** Chemical structure of the compounds 30 and 31.

*Hedychium* species are not different, with several compounds being identified with distinct percentages on its essential oils. However, a deeper analysis of the published works allows to identify some compounds that, with some slight differences, appear repeatedly as the most abundant compounds in their essential oils. In Table 3 are gathered the five most abundant compounds identified in essential oils from *Hedychium* species as well as their activities and the species where they have already been identified. The respective structures are presented on Figure 3.

**Table 3.** The five most frequent and abundant chemical compounds identified in essential oils from *Hedychium* species.

Compound	Activity *	<i>Hedychium</i> Source
1,8-Cineole (32)	Antifungal against <i>C. albicans</i> (MIC = 203 $\mu$ M **; nystatin MIC = 135 $\mu$ M **) [110]; Insecticide against <i>Rhodnius prolixus</i> (KT <sub>50</sub> = 117.2 min for 100 $\mu$ L dose) [111]	<i>H. coronarium</i> rhizome [16,112]; <i>Hedychium flavescens</i> Carey ex Rosc. rhizome [112]; <i>Hedychium flavum</i> Roxb rhizome [112]; <i>H. gardnerianum</i> rhizome [74]; <i>H. gracile</i> rhizome [73,112]; <i>H. greenii</i> rhizome [73]; <i>H. larsenii</i> rhizome [94]; <i>H. spicatum</i> rhizome [67,109,112]
$\alpha$ -Pinene (33)	Anti-acetylcholinesterase (IC <sub>50</sub> = 10.50 $\pm$ 0.51 $\mu$ M **; ursolic acid IC <sub>50</sub> = 0.416 $\pm$ 0.003 $\mu$ M **) [50]; Anti-allergic (dose of 10 mg/kg on mouse) [113]; Antidiabetic (dose of 0.25 mL/kg on mouse) [114]; Anti-inflammatory (mouse ED <sub>50</sub> = 0.039 mL/kg) [114]; Antimicrobial against <i>Streptococcus pneumoniae</i> (MIC = 5 $\mu$ L/mL; gentamicin MIC = 21 $\mu$ M **) [115]; Antitumor against A549 cell line (IC <sub>50</sub> = 161.56 $\pm$ 12.85 $\mu$ M **) [116]	<i>H. coccineum</i> (syn. <i>Hedychium aurantiacum</i> Roscoe) rhizome [112]; <i>H. coronarium</i> flower [117] and rhizome [16,112]; <i>H. flavescens</i> rhizome [112]; <i>H. flavum</i> rhizome [112]; <i>H. gardnerianum</i> flower [118], leaf [118] and rhizome [112]; <i>H. greenii</i> rhizome [73,112]; <i>H. matthewii</i> rhizome [65]; <i>H. spicatum</i> rhizome [109]
$\beta$ -Pinene (34)	Antimicrobial against <i>S. pneumoniae</i> (MIC = 20 $\mu$ L/mL; gentamicin MIC = 21 $\mu$ M **) [115]; Antitumor against HCT-8 cell line (IC <sub>50</sub> = 176.9 $\pm$ 2.9 $\mu$ M **) [119]	<i>H. coccineum</i> (syn. <i>H. aurantiacum</i> ) rhizome [112]; <i>H. coronarium</i> flower [117] and rhizome [16,108,112]; <i>H. ellipticum</i> rhizome [112]; <i>H. flavescens</i> rhizome [112]; <i>H. flavum</i> rhizome [112]; <i>H. gardnerianum</i> flower [118], leaf [118] and rhizome [112]; <i>H. gracile</i> rhizome [73,112]; <i>H. greenii</i> rhizome [73]; <i>H. larsenii</i> rhizome [94]; <i>H. matthewii</i> rhizome [65]; <i>H. spicatum</i> rhizome [67,109]; <i>Hedychium thyrisiforme</i> Smith. rhizome [112]
Linalool (35)	Antibacterial against <i>Bacillus mycoides</i> (10 $\mu$ L cause 11 mm inhibition zone; 10 $\mu$ L of penicillin = 12 mm inhibition zone) [120]; Antidepressive (dose of 100 mg/kg on mouse) [121]; Anti-inflammatory	<i>H. coronarium</i> flower [117] and rhizome [108]; <i>H. flavum</i> rhizome [112]; <i>H. larsenii</i> rhizome [94]; <i>H. matthewii</i> rhizome [65]; <i>H. spicatum</i> rhizome [67,109]
	(dose of 30 mg/kg on mouse) [122]; Antitumor against U937 cell line (IC <sub>50</sub> = 2.59 $\mu$ M; 5-FU IC <sub>50</sub> = 4.86 $\mu$ M) [123]; Fumigant against <i>Tribolium confusum</i> larvae (LC <sub>50</sub> = 14.198 $\mu$ L/L of air) [124]; Neuroprotective (100 $\mu$ M reduced 30% OHSC cell death) [125]	

Table 3. Cont.

Compound	Activity *	Hedychium Source
Terpinen-4-ol (36)	Antibacterial against <i>Burkholderia pyriocinia</i> (10 $\mu$ L cause 8 mm inhibition zone; 10 $\mu$ L of penicillin cause 9 mm inhibition zone) [120]; Antifungal against <i>Histoplasma capsulatum</i> (MIC = 129.70 $\mu$ M **; AMB MIC = 0.54 $\mu$ M **) [126]; Antitumor against MCF-7 cell line (IC <sub>50</sub> = 18.02 $\mu$ M **; doxorubicin IC <sub>50</sub> = 1.29 $\mu$ M **) [127]	<i>H. ellipticum</i> rhizome [112]; <i>H. gracile</i> rhizome [73,112]; <i>H. larsenii</i> rhizome [94]; <i>H. matthewii</i> rhizome [65]; <i>H. thyriforme</i> rhizome [112]

\* only the highest activity value; \*\* Value after unit conversion from  $\mu$ g/mL to  $\mu$ M.

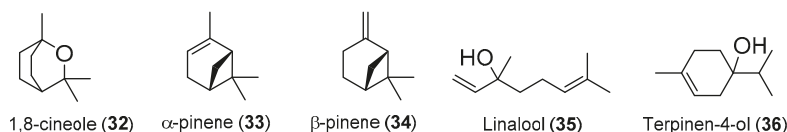


Figure 3. Chemical structure of the compounds referred on Table 3.

As it is possible to see on Table 3, linalool (35) proved to have promising antitumor potential since it presented cytotoxicity against U937 cell line (i.e., IC<sub>50</sub> = 2.59  $\mu$ M), better than the positive control 5-FU against the same cell line (i.e., IC<sub>50</sub> = 4.86  $\mu$ M). It would have been interesting if the authors had tested the compounds cytotoxicity against a non-tumor cell line, but unfortunately that was not the case.

From the five most abundant and most frequent present compounds in essential oils of *Hedychium* species,  $\beta$ -pinene (34) is the most widespread compound among species being identified in 12 *Hedychium* species, mainly rhizomes but also in some cases from flower and leaf essential oil. The compounds  $\alpha$ -pinene (33) and linalool (35), exhibit a broad range of bioactivities, being anti-acetylcholinesterase, anti-allergic, antidepressive, antidiabetic, anti-inflammatory, antimicrobial, antitumor, fumigant and neuroprotective agents.

The antimicrobial activity of  $\alpha$ -pinene (33),  $\beta$ -pinene (34) reported by Leite et al. [115] presented in Table 3 should be noted, which appears as  $\mu$ L/mL and the authors do not provide the necessary data to convert it to  $\mu$ M or  $\mu$ g/mL. Thus, it is impossible to compare the exhibited activity with other published results and even to compare with the positive control used in this study.

Despite not being so abundant as the compounds referred in Table 3, the isolation of two compounds from *H. larsenii* rhizomes essential oil could be mentioned, i.e., *ar*-curcumene (37) and *epi*- $\beta$ -bisabolol (38) (Figure 4), that presented insecticide properties against diseases mosquito vectors larvae *A. stephensi*, *A. aegypti* and *C. quinquefasciatus* [94]. The results show that the most affected vector was *A. stephensi* with compounds 37 and 38 presenting a LC<sub>50</sub> values of 51.65 and 66.02  $\mu$ M, respectively. Unfortunately, the lack of a tested reference compound is a handicap in this work.

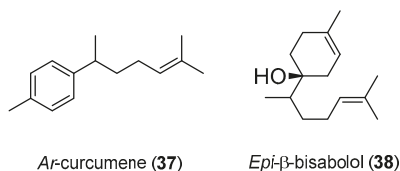


Figure 4. Chemical structure of the compounds 37 and 38.

Taking together, Tables 2 and 3 offer a summary view point of the works carried out in recent years that permitted the isolation of some compounds from *Hedychium* genus, being ascertained their bioactivities. This allows to easily identify where there is work already successfully developed and which paths have not yet been explored.

#### 4. Conclusions

*Hedychium* genus is undoubtedly proven to be a valuable group of medicinal plants, being present in several folk medicines around the world where it is known to treat allergies, cancer, diabetes, inflammation, rheumatism and skin problems, as well as being also used as an analgesic, antimicrobial, anti-helminthic, antioxidant and insect repellent. In addition, some *Hedychium* species are part of human diet, being cooked as a vegetable, used as a spice or drunk as a beverage.

Several works explored *Hedychium* species in order to confirm if and how effectively these plants exert the reported biological effects on folk medicine, studying their essential oils, extracts and their isolated compounds. Taking into account the results of the literature in recent years, *Hedychium* species have been proven to possess interesting pharmaceutical activities, i.e., anti-acetylcholinesterase, antidiabetic, anti-inflammatory, antimicrobial, antioxidant, antitumor and hepatoprotective, as well as having potential to develop insecticides.

Phytochemical works have been carried out in *Hedychium*, mainly on *H. coronarium* and *H. spicatum*, but also on other less known species, leading to the isolation of interesting compounds that, in some cases, proved to be better than reference compounds. An example is coronarin D (7), possessing antifungal, antitumor and antibacterial properties, being more effective than the positive control oxacillin against *B. cereus* in antibacterial assays. Isocoronarin D (11), villosin (26) and linalool (35) can be pointed out as very promising antitumor compounds since they exhibited better cytotoxicity towards tumor cell lines than the reference compounds used, and in case of villosin (26) without toxicity on non-tumor cell line. Furthermore, the most bioactive compounds found in *Hedychium* essential oils can be highlighted as  $\alpha$ -pinene (33) and linalool (35), since they are reported as presenting a wide spectrum of bioactivities. In addition, being identified in 12 different *Hedychium* species to this date,  $\beta$ -pinene (34) is the most widespread compound in *Hedychium* essential oils.

*Hedychium* species as proved to be a very rich genus that can still have a lot to offer to the scientific community. Moreover, the discovery in recent years of four new *Hedychium* species (i.e., *Hedychium chingmeianum* N.Odyuo and D.K.Roy [128], *Hedychium putaense* Y.H.Tan and H.B.Ding [129], *Hedychium viridibracteatum* X.Hu [130] and *Hedychium ziroense* V.Gowda and Ashokan [131]), may bring new compounds with pharmaceutical potential to the equation.

**Author Contributions:** M.d.C.B. and A.M.L.S. conceptualized and revised the paper; W.R.T. conducted the research and wrote the first draft. All authors have read and agreed to the published version of the manuscript.

**Funding:** This research was funded by project MACBIOPEST (MAC2/1.1a/289), program Interreg MAC 2014–2020 co-financed by DRCT (Azores Regional Government), supporting W.R. Tavares's grant, as well as by FCT—Fundação para a Ciência e Tecnologia, the European Union, QREN, FEDER, and COMPETE, through funding the cE3c center (UIDB/00329/2020) and the LAQV-REQUIMTE (UIDB/50006/2020).

**Acknowledgments:** Thanks are due to the University of Azores and University of Aveiro.

**Conflicts of Interest:** The authors declare no conflict of interest.

#### Abbreviations

A-431	Human epidermoid carcinoma
A549	Human lung adenocarcinoma
ABTS	2,2'-azino-bis(3-ethylbenzothiazoline-6-sulphonic acid)
AChE	Acetylcholinesterase
AgNPs	<i>H. coronarium</i> -synthesized silver nanoparticles
BHT	2,6-di-tert-butyl-4-methylphenol
BMDC	Bone marrow-derived dendritic cells
C57BKSc <sup>db/db</sup>	Strain of laboratory mouse with a mutation that results in chronic hyperglycemia, pancreatic beta cell atrophy, low insulin level and obesity
CAT	Catalase
CHO	Chinese hamster ovary cells
Colo-205	Colorectal adenocarcinoma

COX-1	Cyclooxygenase 1
DLD-1	Human colorectal carcinoma
DPPH	1,1-Diphenyl-2-picrylhydrazyl
EC <sub>50</sub>	Half maximal effective concentration
ED <sub>50</sub>	Half maximal effective dose
GPx	Glutathione peroxidase
HeLa	Human cervical carcinoma
HepG2	Human hepatocellular carcinoma
HL-60	Human acute promyelocytic leukemia
HuCCA-1	Human cholangiocarcinoma
HUVEC	Human umbilical vascular endothelial cells
IC <sub>50</sub>	Half maximal inhibitory concentration
IFN-γ	Interferon gamma
IL-6	Interleukin 6
Il-12p40	Interleukin-12 subunit p40
KB	Human epidermoid carcinoma
KT <sub>50</sub>	Knockdown time 50%
LC <sub>50</sub>	Lethal concentration that kills 50% of exposed organisms
LNCaP	Human prostate adenocarcinoma
LPS	Lipopolysaccharide
MAO-A	Monoamine oxidase A
MCF-7	Human breast adenocarcinoma
MDA-MB-231	Human breast adenocarcinoma
MG132	Carbobenzoxy-Leu-Leu-leucinal
MIC	Minimum inhibitory concentration
MOLT-3	Human acute lymphoblastic leukemia T-lymphoblasts
MTT	3-(4,5-Dimethylthiazol-2-yl)-2,5-diphenyltetrazolium bromide
NCI-H187	Human classic small cell lung carcinoma
NF-κB	Nuclear factor kappa-B
NO	Nitric oxide
OHSC	Organotypic hippocampal slice cultures
P388	Mouse lymphoma neoplasm
P388D1	Murine macrophage-like lymphoma
RAW 264.7	Murine macrophage
ROS	Reactive oxygen species
S102	Human hepatocellular carcinoma
SI	Selectivity index
SOD	Superoxide dismutase
STZ	Streptozotocin
T2DM	Type 2 <i>diabetes mellitus</i>
T-47D	Human hormone-dependent breast cancer
TNF-α	Tumor necrosis factor α
U937	Human histiocytic lymphoma
Vero	African green monkey kidney epithelial cells
XWLC-05	Human lung adenocarcinoma

## References

1. Schaal, B. Plants and people: Our shared history and future. *Plants People Planet* **2019**, *1*, 14–19. [[CrossRef](#)]
2. Lemonnier, N.; Zhou, G.-B.; Prasher, B.; Mukerji, M.; Chen, Z.; Brahmachari, S.K.; Noble, D.; Auffray, C.; Sagner, M. Traditional knowledge-based medicine: A review of history, principles, and relevance in the present context of P4 systems medicine. *Prog. Prev. Med.* **2017**, *2*, e0011. [[CrossRef](#)]
3. Kumar, A.; Aswal, S.; Chauhan, A.; Semwal, R.B.; Kumar, A.; Semwal, D.K. Ethnomedicinal investigation of medicinal plants of Chakrata region (Uttarakhand) used in the traditional medicine for diabetes by Jaunsari tribe. *Nat. Prod. Bioprospecting* **2019**, *9*, 175–200. [[CrossRef](#)] [[PubMed](#)]

4. Wyk, B.-E.V. A family-level floristic inventory and analysis of medicinal plants used in Traditional African Medicine. *J. Ethnopharmacol.* **2020**, *249*, 112351. [CrossRef] [PubMed]
5. Belokurov, S.S.; Narkevich, I.A.; Flisyuk, E.V.; Kaukhova, I.E.; Aroyan, M.V. Modern extraction methods for medicinal plant raw material (Review). *Pharm. Chem. J.* **2019**, *53*, 559–563. [CrossRef]
6. Kharbach, M.; Marmouzi, I.; Jemli, M.E.; Bouklouze, A.; Heyden, Y.V. Recent advances in untargeted and targeted approaches applied in herbal-extracts and essential-oils fingerprinting—A review. *J. Pharm. Biomed. Anal.* **2020**, *177*, 112849. [CrossRef] [PubMed]
7. The Plant List. Available online: <http://www.theplantlist.org/browse/A/Zingiberaceae/Hedychium/> (accessed on 20 February 2020).
8. Branney, T.M.E. *Hardy Gingers: Including Hedychium, Roscocea, and Zingiber*, Royal Horticultural Society Plant Collector Guide; Timber Press: Portland, OR, USA, 2005; p. 267, ISBN 0881926779.
9. Basak, S.; Ramesh, A.M.; Kesari, V.; Parida, A.; Mitra, S.; Rangan, L. Genetic diversity and relationship of *Hedychium* from Northeast India as dissected using PCA analysis and hierarchical clustering. *Meta Gene* **2014**, *2*, 459–468. [CrossRef]
10. Tanaka, N.; Ohi-Toma, T.; Aung, M.M.; Murata, J. Systematic notes on the genus *Hedychium* (Zingiberaceae) in Myanmar. *Bull. Natl. Mus. Nat. Sci. Ser. B* **2016**, *42*, 57–66.
11. Vanchhawng, L.; Lalramnghinglova, H. Notes on the genus *Hedychium* J. Koen. (Zingiberaceae) in Mizoram, north east India. *Int. J. Waste Resour.* **2016**, *6*, 1000234. [CrossRef]
12. Costa, R.O.; Batisteli, A.F.; Espindola, E.L.G.; Matos, D.M.S. Invasive *Hedychium coronarium* inhibits native seedling growth through belowground competition. *Flora* **2019**, *261*, 151479. [CrossRef]
13. Costa, H.; Bettencourt, M.J.; Silva, C.M.N.; Teodósio, J.; Gil, A.; Silva, L. Invasive alien plants in the azorean protected areas: Invasion status and mitigation actions. In *Plant Invasions in Protected Areas Patterns, Problems and Challenges*; Foxcroft, L.C., Pyšek, P., Richardson, D.M., Genovesi, P., Eds.; Invading Nature-Springer Series in Invasion Ecology; Springer Science + Business Media: Dordrecht, The Netherlands, 2013; Volume 7, Chapter 17; pp. 375–394, ISBN 978-94-007-7750-7.
14. Minden, V.; Hennenberg, K.J.; Porembski, S.; Boehmer, H.J. Invasion and management of alien *Hedychium gardnerianum* (kahili ginger, Zingiberaceae) alter plant species composition of a montane rainforest on the island of Hawai'i. *Plant Ecol.* **2010**, *206*, 321–333. [CrossRef]
15. Ashokan, A.; Gowda, V. Describing terminologies and discussing records: More discoveries of facultative vivipary in the genus *Hedychium* J. Koenig (Zingiberaceae) from Northeast India. *PhytoKeys* **2018**, *96*, 21–34. [CrossRef] [PubMed]
16. Chan, E.W.; Wong, S.K. Phytochemistry and pharmacology of ornamental gingers, *Hedychium coronarium* and *Alpinia purpurata*: A review. *J. Integr. Med.* **2015**, *13*, 368–379. [CrossRef]
17. Yue, Y.; Yu, R.; Fan, Y. Transcriptome profiling provides new insights into the formation of floral scent in *Hedychium coronarium*. *BMC Genom.* **2015**, *16*, 470. [CrossRef]
18. Badola, H.K. *Hedychium spicatum*—A commercial Himalayan herb needs entrepreneurship at local level. *Non-Wood News* **2009**, *19*, 26–27.
19. Hartati, R.; Suganda, A.G.; Fidrianny, I. Botanical, phytochemical and pharmacological properties of *Hedychium* (Zingiberaceae)—A review. *Procedia Chem.* **2014**, *13*, 150–163. [CrossRef]
20. Pachurekar, P.; Dixit, A.K. A review on pharmacognostical phytochemical and ethnomedicinal properties of *Hedychium coronarium* J. Koenig an Endangered Medicine. *IJCM* **2017**, *1*, 49–61. [CrossRef]
21. Rawat, S.; Jugran, A.K.; Bhatt, I.D.; Ranbeer, S.; Rawal, R.S. *Hedychium spicatum*: A systematic review on traditional uses, phytochemistry, pharmacology and future prospectus. *J. Pharm. Pharmacol.* **2018**, *70*, 687–712. [CrossRef]
22. Kamble, K.G.; Dale, A.V. A review on pharmacognostic and pharmacological approach of different species of *Hedychium*. *Indo Am. J. Pharmacol. Sci.* **2018**, *5*, 6030–6036.
23. Ong, H.G.; Ling, S.M.; Win, T.T.M.; Kang, D.-H.; Lee, J.-H.; Kim, Y.-D. Ethnomedicinal plants and traditional knowledge among three Chin indigenous groups in Natma Taung National Park (Myanmar). *J. Ethnopharmacol.* **2018**, *225*, 136–158. [CrossRef]
24. Panmei, R.; Gajurel, P.R.; Singh, B. Ethnobotany of medicinal plants used by the Zeliangrong ethnic group of Manipur, northeast India. *J. Ethnopharmacol.* **2019**, *235*, 164–182. [CrossRef] [PubMed]

25. Tribess, B.; Pintarelli, G.M.; Bini, L.A.; Camargo, A.; Funez, L.A.; Gasper, A.L.; Zeni, A.L.B. Ethnobotanical study of plants used for therapeutic purposes in the Atlantic Forest region, Southern Brazil. *J. Ethnopharmacol.* **2015**, *164*, 136–146. [[CrossRef](#)] [[PubMed](#)]
26. Yazbek, P.B.; Matta, P.; Passero, L.F.; Santos, G.; Braga, S.; Assunção, L.; Sauini, T.; Cassas, F.; Garcia, R.J.F.; Honda, S.; et al. Plants utilized as medicines by residents of Quilombo da Fazenda, Núcleo Picinguaba, Ubatuba, São Paulo, Brazil: A participatory survey. *J. Ethnopharmacol.* **2019**, *244*, 112123. [[CrossRef](#)] [[PubMed](#)]
27. Jain, S.K.; Fernandes, V.F.; Lata, S.; Ayub, A. Indo-Amazonian ethnobotanic connections-Similar uses of some common plants. *Ethnobotany* **1995**, *7*, 29–37.
28. Vásquez, J.; Alarcón, J.C.; Jiménez, S.L.; Jaramillo, G.I.; Gómez-Betancur, I.C.; Rey-Suárez, J.P.; Jaramillo, K.M.; Muñoz, D.C.; Marín, D.M.; Romero, J.O. Main plants used in traditional medicine for the treatment of snake bites in the regions of the department of Antioquia, Colombia. *J. Ethnopharmacol.* **2015**, *170*, 158–166. [[CrossRef](#)] [[PubMed](#)]
29. Parida, R.; Mohanty, S.; Nayak, S. Chemical composition of essential oil from leaf and rhizome of micropropagated and conventionally grown *Hedychium coronarium* Koen from Eastern India. *J. Essent. Oil Bear. Plants* **2015**, *18*, 161–167. [[CrossRef](#)]
30. Ray, A.; Dash, B.; Sahoo, S.; Sahoo, A.; Jena, S.; Kar, B.; Chatterjee, T.; Ghosh, B.; Nayak, S. Development and validation of an HPTLC method for estimation of coronarin D in *Hedychium coronarium* rhizome. *Acta Chromatogr.* **2017**, *29*, 1–12. [[CrossRef](#)]
31. Shah, A.; Bharati, K.A.; Ahmad, J.; Sharma, M.P. New ethnomedicinal claims from Gujjar and Bakerwals tribes of Rajouri and Poonch districts of Jammu and Kashmir, India. *J. Ethnopharmacol.* **2015**, *166*, 119–128. [[CrossRef](#)]
32. Chan, E.W.C.; Lim, Y.Y.; Wong, L.F.; Lianto, F.S.; Wong, S.K.; Lim, K.K.; Joe, C.E.; Lim, T.Y. Antioxidant and tyrosinase inhibition properties of leaves and rhizomes of ginger species. *Food Chem.* **2008**, *109*, 477–483. [[CrossRef](#)]
33. Suroowan, S.; Pynee, K.B.; Mahomoodally, M.F. A comprehensive review of ethnopharmacologically important medicinal plant species from Mauritius. *S. Afr. J. Bot.* **2019**, *122*, 189–213. [[CrossRef](#)]
34. Coe, F.G.; Anderson, G.J. Snakebite ethnopharmacopoeia of eastern Nicaragua. *J. Ethnopharmacol.* **2005**, *96*, 303–323. [[CrossRef](#)] [[PubMed](#)]
35. Valadeau, C.; Castillo, J.A.; Sauvain, M.; Lores, A.F.; Bourdy, G. The rainbow hurts my skin: Medicinal concepts and plants uses among the Yanesha (Amuesha), an Amazonian Peruvian ethnic group. *J. Ethnopharmacol.* **2010**, *127*, 175–192. [[CrossRef](#)] [[PubMed](#)]
36. Tawatsin, A.; Asavadachanukorn, P.; Thavara, U.; Wongsinkongman, P.; Bansidhi, J.; Boonruad, T.; Chavalittumrong, P.; Soonthornchareonnon, N.; Komalamisra, N.; Mulla, M.S. Repellency of essential oils extracted from plants in Thailand against four mosquito vectors (Diptera: Culicidae) and oviposition deterrent effects against *Aedes aegypti* (Diptera: Culicidae). *Southeast Asian J. Trop. Med. Public Health* **2006**, *37*, 915–931. [[PubMed](#)]
37. Kiem, P.V.; Thuy, N.T.K.; Anh, H.L.T.; Nhiem, N.X.; Minh, C.V.; Yen, P.H.; Ban, N.K.; Hang, D.T.; Tai, B.H.; Tuyen, N.V.; et al. Chemical constituents of the rhizomes of *Hedychium coronarium* and their inhibitory effect on the pro-inflammatory cytokines production LPS-stimulated in bone marrow-derived dendritic cells. *Bioorganic Med. Chem. Lett.* **2011**, *21*, 7460–7465. [[CrossRef](#)] [[PubMed](#)]
38. Ahmad, F.; Jantan, I.; Jalil, J. Constituents of the rhizome oil of *Hedychium cylindricum* Ridl. *J. Essent. Oil Res.* **2004**, *16*, 299–301. [[CrossRef](#)]
39. Malla, B.; Gauchan, D.P.; Chhetri, R.B. An ethnobotanical study of medicinal plants used by ethnic people in Parbat district of western Nepal. *J. Ethnopharmacol.* **2015**, *165*, 103–117. [[CrossRef](#)]
40. Ranjarisoa, L.N.; Razanamihaja, N.; Rafatro, H. Use of plants in oral health care by the population of Mahajanga, Madagascar. *J. Ethnopharmacol.* **2016**, *193*, 179–194. [[CrossRef](#)]
41. Sirirugsa, P. Thai Zingiberaceae: Species diversity and their uses. The International Conference on Biodiversity and Bioresource: Conservation and Utilization. Phuket, Thailand, 1998. Available online: <http://old.iupac.org/symposia/proceedings/phuket97/sirirugsa.html> (accessed on 27 April 2020).
42. Bhatt, V.P.; Negi, V.; Purohit, V.K. *Hedychium spicatum* Buch.-Ham.: A high valued skin glowing and curing medicinal herb needs future attention on its conservation. *N. Y. Sci. J.* **2010**, *3*, 86–88.

43. Savithamma, N.; Sulochana, C.; Rao, K.N. Ethnobotanical survey of plants used to treat asthma in Andhra Pradesh, India. *J. Ethnopharmacol.* **2007**, *113*, 54–61. [[CrossRef](#)]
44. Upasani, M.S.; Upasani, S.V.; Beldar, V.G.; Beldar, C.G.; Gujarathi, P.P. Infrequent use of medicinal plants from India in snakebite treatment. *Integr. Med. Res.* **2018**, *7*, 9–26. [[CrossRef](#)]
45. Rachkeeree, A.; Kantadoung, K.; Suksathan, R.; Puangpradab, R.; Page, P.A.; Sommano, S.R. Nutritional compositions and phytochemical properties of the edible flowers from selected Zingiberaceae found in Thailand. *Front. Nutr.* **2018**, *5*, 1–10. [[CrossRef](#)] [[PubMed](#)]
46. Prakash, O.; Rajput, M.; Kumar, M.; Pant, A.K. Chemical composition and antibacterial activity of rhizome oils from *Hedychium coronarium* Koenig and *Hedychium spicatum* Buch-Ham. *J. Essent. Oil Bear. Plants* **2010**, *13*, 250–259. [[CrossRef](#)]
47. Chaithra, B.; Satish, S.; Hegde, K.; Shabaraya, A.R. Pharmacological review on *Hedychium coronarium* Koenig: The white ginger lily. *Int. J. Pharm. Chem. Res.* **2017**, *3*, 831–836.
48. Rasool, S.; Maqbool, M. An overview about *Hedychium spicatum*: A review. *J. Drug Deliv. Ther.* **2019**, *9*, 476–480. [[CrossRef](#)]
49. Hampel, H.; Mesulam, M.M.; Cuello, A.C.; Farlow, M.R.; Giacobini, E.; Grossberg, G.T.; Khachaturian, A.S.; Vergallo, A.; Cavedo, E.; Snyder, P.J.; et al. The cholinergic system in the pathophysiology and treatment of Alzheimer's disease. *Brain* **2018**, *141*, 1917–1933. [[CrossRef](#)] [[PubMed](#)]
50. Arruda, M.; Viana, H.; Rainha, N.; Neng, N.R.; Rosa, J.S.; Nogueira, J.M.F.; Barreto, M.C. Anti-acetylcholinesterase and antioxidant activity of essential oils from *Hedychium gardnerianum* Sheppard ex Ker-Gawl. *Molecules* **2012**, *17*, 3082–3092. [[CrossRef](#)]
51. Kharroubi, A.T.; Darwish, H.M. *Diabetes mellitus*: The epidemic of the century. *World J. Diabetes* **2015**, *6*, 850–867. [[CrossRef](#)]
52. Dowarah, J.; Singh, V.P. Anti-diabetic drugs recent approaches and advancements. *Bioorganic Med. Chem.* **2020**, *28*, 115263. [[CrossRef](#)]
53. Tse, L.-S.; Liao, P.-L.; Tsai, C.-H.; Li, C.-H.; Liao, J.-W.; Kang, J.-J.; Cheng, Y.-W. Glycemia lowering effect of an aqueous extract of *Hedychium coronarium* leaves in diabetic rodent models. *Nutrients* **2019**, *11*, 629. [[CrossRef](#)]
54. Kaur, H.; Richa, R. Antidiabetic activity of essential oil of *Hedychium spicatum*. *Int. J. Pharmacogn. Phytochem. Res.* **2017**, *9*, 853–857. [[CrossRef](#)]
55. Medzhitov, R. Inflammation 2010: New adventures of an old flame. *Cell* **2010**, *140*, 771–776. [[CrossRef](#)] [[PubMed](#)]
56. Straub, R.H.; Schradin, C. Chronic inflammatory systemic diseases: An evolutionary trade-off between acutely beneficial but chronically harmful programs. *Evol. Med. Public Health* **2016**, *2016*, 37–51. [[CrossRef](#)] [[PubMed](#)]
57. Ghildiyal, S.; Gautam, M.K.; Joshi, V.K.; Goel, R.K. Pharmacological evaluation of extracts of *Hedychium spicatum* (Ham-ex-Smith) rhizome. *Anc. Sci. Life* **2012**, *31*, 117–122. [[CrossRef](#)] [[PubMed](#)]
58. Chachad, D.; Shimpi, S. Anti-inflammatory activity of “Kapurkachari”. *Electron. J. Pharmacol. Ther.* **2008**, *1*, 25–27.
59. Turnbaugh, P.J.; Ley, R.E.; Hamady, M.; Fraser-Liggett, C.; Knight, R.; Gordon, J.I. The human microbiome project: Exploring the microbial part of ourselves in a changing world. *Nature* **2007**, *449*, 804–810. [[CrossRef](#)]
60. Khezerlou, A.; Alizadeh-Sani, M.; Azizi-Lalabadi, M.; Ehsani, A. Nanoparticles and their antimicrobial properties against pathogens including bacteria, fungi, parasites and viruses. *Microb. Pathog.* **2018**, *123*, 505–526. [[CrossRef](#)]
61. Watkins, K. Emerging infectious diseases: A review. *Curr. Emerg. Hosp. Med. Rep.* **2018**, *6*, 86–93. [[CrossRef](#)]
62. Noriega, P.; Guerrini, A.; Sacchetti, G.; Grandini, A.; Ankuash, E.; Manfredini, S. Chemical composition and biological activity of five essential oils from the ecuadorian Amazon rain forest. *Molecules* **2019**, *24*, 1637. [[CrossRef](#)]
63. Rath, C.C.; Priyadarshane, M. Evaluation of in-vitro antibacterial activity of selected essential oils. *J. Essent. Oil Bear. Plants* **2017**, *20*, 359–367. [[CrossRef](#)]
64. Ray, A.; Jena, S.; Dash, B.; Kar, B.; Halder, T.; Chatterjee, T.; Ghosh, B.; Panda, P.C.; Nayak, S.; Mahapatra, N. Chemical diversity, antioxidant and antimicrobial activities of the essential oils from Indian populations of *Hedychium coronarium* Koenig. *Ind. Crops Prod.* **2018**, *112*, 353–362. [[CrossRef](#)]
65. Thomas, S.; Mani, B. Composition, antibacterial and anti-oxidant potentials of the essential oil of *Hedychium mathewii*. *Bangladesh J. Pharmacol.* **2017**, *12*, 173–179. [[CrossRef](#)]



66. Feng, J.; Shi, W.; Miklossy, J.; Tauxe, G.M.; McMeniman, C.J.; Zhang, Y. Identification of essential oils with strong activity against stationary phase *Borrelia burgdorferi*. *Antibiotics* **2018**, *7*, 89. [[CrossRef](#)] [[PubMed](#)]
67. Kalagatur, N.K.; Kamasani, J.R.; Siddaiah, C.; Gupta, V.K.; Krishna, K.; Mudili, V. Combinational inhibitory action of *Hedychium spicatum* L. essential oil and  $\gamma$ -radiation on growth rate and mycotoxins content of *Fusarium graminearum* in maize: Response surface methodology. *Front. Microbiol.* **2018**, *9*, 1511. [[CrossRef](#)] [[PubMed](#)]
68. Arora, R.; Mazumder, A. Phytochemical screening and antimicrobial activity of rhizomes of *Hedychium spicatum*. *Pharmacog. J.* **2017**, *9*, s64–s68. [[CrossRef](#)]
69. Choudhary, G.K.; Singh, S.P.; Kumar, R.R. In vitro antioxidant and anthelmintic properties of rhizome extracts of *Hedychium spicatum*. *Indian J. Anim. Sci.* **2018**, *88*, 300–303.
70. Chandel, N.S.; Budinger, G.R.S. The cellular basis for diverse responses to oxygen. *Free Radic. Biol. Med.* **2007**, *42*, 165–174. [[CrossRef](#)]
71. Tavares, W.R.; Seca, A.M.L. *Inula* L. Secondary metabolites against oxidative stress-related human diseases. *Antioxidants* **2019**, *8*, 122. [[CrossRef](#)]
72. Wright, G.D. Unlocking the potential of natural products in drug discovery. *Microb. Biotechnol.* **2019**, *12*, 55–57. [[CrossRef](#)]
73. Ray, A.; Jena, S.; Kar, B.; Patnaik, J.; Panda, P.C.; Nayak, S. Chemical composition and antioxidant activities of essential oil of *Hedychium greenii* and *Hedychium gracile* from India. *Nat. Prod. Res.* **2019**, *33*, 1482–1485. [[CrossRef](#)]
74. Zhao, M.; Zhang, L.; Yang, Z.; Wei, J.; Zhang, K.; Zheng, X.; Fang, Y.; Lin, L.; Tang, J.; Wu, F.; et al. Antioxidative activities of essential oils and ethanol extractions from ornamental Zingiberaceae species. *J. Essent. Oil Bear. Plants* **2017**, *20*, 215–222. [[CrossRef](#)]
75. Usha, T.; Pradhan, S.; Goyal, A.K.; Dhivya, S.; Kumar, H.P.P.; Singh, M.K.; Joshi, N.; Basistha, B.C.; Murthy, K.R.S.; Selvaraj, S.; et al. Molecular simulation-based combinatorial modeling and antioxidant activities of Zingiberaceae family rhizomes. *Pharmacogn. Mag.* **2017**, *13*, S715–S722. [[CrossRef](#)] [[PubMed](#)]
76. Choudhary, G.K.; Singh, S.P. Ameliorating potential of *Hedychium spictum* on oxidative stress following chronic exposure to indoxacarb in WLH cockerels. *Indian J. Anim. Res.* **2017**, *51*, 832–836. [[CrossRef](#)]
77. Bray, F.; Ferlay, J.; Soerjomataram, I.; Siegel, R.L.; Torre, L.A.; Jemal, A. Global cancer statistics 2018: GLOBOCAN estimates of incidence and mortality worldwide for 36 cancers in 185 countries. *CA Cancer J. Clin.* **2018**, *68*, 394–424. [[CrossRef](#)] [[PubMed](#)]
78. Bidram, E.; Esmaeili, Y.; Ranji-Burachaloo, H.; Al-Zaubai, N.; Zarrabi, A.; Stewart, A.; Dunstan, D.E. A concise review on cancer treatment methods and delivery systems. *J. Drug Deliv. Sci. Technol.* **2019**, *54*, 101350. [[CrossRef](#)]
79. Dutta, S.; Mahalanobish, S.; Saha, S.; Ghosh, S.; Sil, P.C. Natural products: An upcoming therapeutic approach to cancer. *Food Chem. Toxicol.* **2019**, *128*, 240–255. [[CrossRef](#)]
80. Ray, A.; Jena, S.; Dash, B.; Sahoo, A.; Kar, B.; Patnaik, J.; Panda, P.C.; Nayak, S.; Mahapatra, N. *Hedychium coronarium* extract arrests cell cycle progression, induces apoptosis, and impairs migration and invasion in HeLa cervical cancer cells. *Cancer Manag. Res.* **2019**, *11*, 483–500. [[CrossRef](#)]
81. Choudhary, G.K.; Singh, S.P. Cytotoxic potential of rhizome extracts of *Hedychium spicatum* L. in HepG2 cell line using MTT. *Indian J. Anim. Sci.* **2017**, *87*, 313–315.
82. Geran, R.I.; Greenberg, N.H.; McDonald, M.M.; Schumacher, A.M.; Abbott, B.J. Protocols for screening chemical agents and natural products against animal tumour and other biological systems. *Cancer Chemother. Rep.* **1972**, *3*, 1–103.
83. Reddy, P.P.; Rao, R.R.; Rekha, K.; Babu, K.S.; Shashidhar, J.; Shashikiran, G.; Lakshmi, V.V.; Rao, J.M. Two new cytotoxic diterpenes from the rhizomes of *Hedychium spicatum*. *Bioorganic Med. Chem. Lett.* **2009**, *19*, 192–195. [[CrossRef](#)]
84. Cornu, R.; Béduneau, A.; Martin, H. Influence of nanoparticles on liver tissue and hepatic functions: A review. *Toxicology* **2020**, *430*, 152344. [[CrossRef](#)]
85. Chen, S.; Melchior, W.B., Jr.; Wu, Y.; Guo, L. Autophagy in drug-induced liver toxicity. *J. Food Drug Anal.* **2014**, *22*, 161–168. [[CrossRef](#)] [[PubMed](#)]
86. Madrigal-Santillán, E.; Madrigal-Bujaidar, E.; Álvarez-González, I.; Sumaya-Martínez, M.T.; Gutiérrez-Salinas, J.; Bautista, M.; Morales-González, Á.; González-Rubio, M.G.-L.; Aguilar-Faisal, J.L.; Morales-González, J.A. Review of natural products with hepatoprotective effects. *World J. Gastroenterol.* **2014**, *20*, 14787–14804. [[CrossRef](#)] [[PubMed](#)]

87. Choudhary, G.K.; Singh, S.P. In vitro hepatoprotective efficacy of extract of *Hedychium spicatum* rhizome in paracetamol induced toxicity in HepG2 cell line. *Indian J. Anim. Sci.* **2018**, *88*, 546–549.
88. Choudhary, G.K.; Singh, S.P.; Kumar, A. Effects of GandhPaalashi (*Hedychium spicatum*) on the expression of hepatic genes associated with biotransformation, antioxidant and immune systems in WLH cockerels fed indoxacarb. *Indian J. Anim. Sci.* **2018**, *88*, 786–790.
89. Jamison, A.; Tuttle, E.; Jensen, R.; Bierly, G.; Gonsler, R. Spatial ecology, landscapes, and the geography of vector-borne disease: A multi-disciplinary review. *Appl. Geogr.* **2015**, *63*, 418–426. [[CrossRef](#)]
90. Flores, H.A.; O'Neill, S.L. Controlling vector-borne diseases by releasing modified mosquitoes. *Nat. Rev. Microbiol.* **2018**, *16*, 508–518. [[CrossRef](#)]
91. Wilson, A.L.; Courtenay, O.; Kelly-Hope, L.A.; Scott, T.W.; Takken, W.; Torr, S.J.; Lindsay, S.W. The importance of vector control for the control and elimination of vector-borne diseases. *PLoS Negl. Trop. Dis.* **2020**, *14*, e0007831. [[CrossRef](#)]
92. Dusfour, I.; Vontas, J.; David, J.-P.; Weetman, D.; Fonseca, D.M.; Corbel, V.; Raghavendra, K.; Coulibaly, M.B.; Martins, A.J.; Kasai, S.; et al. Management of insecticide resistance in the major *Aedes* vectors of arboviruses: Advances and challenges. *PLoS Negl. Trop. Dis.* **2019**, *13*, e0007615. [[CrossRef](#)]
93. Kalimuthu, K.; Panneerselvam, C.; Chou, C.; Tseng, L.-C.; Murugan, K.; Tsai, K.-H.; Alarfaj, A.A.; Higuchi, A.; Canale, A.; Hwang, J.-S.; et al. Control of dengue and Zika virus vector *Aedes aegypti* using the predatory copepod *Megacyclops formosanus*: Synergy with *Hedychium coronarium*-synthesized silver nanoparticles and related histological changes in targeted mosquitoes. *Proces Saf. Environ. Prot.* **2017**, *109*, 82–96. [[CrossRef](#)]
94. AlShebly, M.M.; AlQahtani, F.S.; Govindarajan, M.; Gopinath, K.; Vijayan, P.; Benelli, G. Toxicity of ar-curcumene and epi- $\beta$ -bisabolol from *Hedychium larsenii* (Zingiberaceae) essential oil on malaria, chikungunya and St. Louis encephalitis mosquito vectors. *Ecotoxicol. Environ. Saf.* **2017**, *137*, 149–157. [[CrossRef](#)]
95. Kumrit, I.; Suksamran, A.; Meepawpan, P.; Songsri, S.; Nuntawong, N. Labdane-type diterpenes from *Hedychium gardnerianum* with potent cytotoxicity against human small cell lung cancer cells. *Phytother. Res.* **2010**, *24*, 1009–1013. [[CrossRef](#)] [[PubMed](#)]
96. Zhao, H.; Zeng, G.; Zhao, S.; Xu, J.; Kong, L.; Li, Y.; Tan, N.; Yang, S. Cytotoxic labdane-type diterpenes from *Hedychium longipetalum* inhibiting production of nitric oxide. *Bioorganic Med. Chem. Lett.* **2015**, *25*, 4572–4575. [[CrossRef](#)] [[PubMed](#)]
97. Chimnoi, N.; Sarasuk, C.; Khunnawutmanotham, N.; Intachote, P.; Seangsai, S.; Saimanee, B.; Pisutjaroenpong, S.; Mahidol, C.; Techasakul, S. Phytochemical reinvestigation of labdane-type diterpenes and their cytotoxicity from the rhizomes of *Hedychium coronarium*. *Phytochem. Lett.* **2009**, *2*, 184–187. [[CrossRef](#)]
98. Chimnoi, N.; Pisutjaroenpong, S.; Ngiwsara, L.; Dechtrirut, D.; Chokchaichamnankit, D.; Khunnawutmanotham, N.; Mahidol, C.; Techasakul, S. Labdane diterpenes from the rhizomes of *Hedychium coronarium*. *Nat. Prod. Res.* **2008**, *22*, 1249–1256. [[CrossRef](#)]
99. Ray, A.; Halder, T.; Jena, S.; Sahoo, A.; Ghosh, B.; Mohanty, S.; Mahapatra, N.; Nayak, S. Application of artificial neural network (ANN) model for prediction and optimization of coronarin D content in *Hedychium coronarium*. *Ind. Crops Prod.* **2020**, *146*, 112186. [[CrossRef](#)]
100. Reuk-ngam, N.; Chimnoi, N.; Khunnawutmanotham, N.; Techasakul, S. Antimicrobial activity of coronarin D and its synergistic potential with antibiotics. *Biomed Res. Int.* **2014**, *2014*, 581985. [[CrossRef](#)]
101. Endringer, D.C.; Taveira, F.S.N.; Kondratyuk, T.P.; Pezzuto, J.M.; Braga, F.C. Cancer chemoprevention activity of labdane diterpenes from rhizomes of *Hedychium coronarium*. *Rev. Bras. Farmacogn.* **2014**, *24*, 408–412. [[CrossRef](#)]
102. Chen, L.-C.; Wen, Z.-H.; Sung, P.-J.; Shu, C.-W.; Kuo, W.-L.; Chen, P.-Y.; Jih-Jung Chen, J.-J. New labdane-type diterpenoid and cytotoxic constituents of *Hedychium coronarium*. *Chem. Nat. Compd.* **2017**, *53*, 72–76. [[CrossRef](#)]
103. Wang, W.-H.; Gao, J.-J.; Zuo, X.-F.; Qin, X.-J.; Liu, H.-Y.; Zhao, Q. New diterpenoids from the rhizomes of *Hedychium forrestii*. *Nat. Prod. Res.* **2019**, 1–7. [[CrossRef](#)]
104. Carvalho, M.J.; Carvalho, L.M.; Ferreira, A.M.; Silva, A.M.S. A new xanthone from *Hedychium gardnerianum*. *Nat. Prod. Res.* **2003**, *17*, 445–449. [[CrossRef](#)]
105. Gnerre, C.; Thull, U.; Gaillard, P.; Carrupt, P.-A.; Testa, B.; Fernandes, E.; Silva, F.; Pinto, M.; Pinto, M.M.M.; Wolfender, J.-L.; et al. Natural and synthetic xanthenes as monoamine oxidase inhibitors: Biological assay and 3D-QSAR. *Helv. Chim. Acta* **2001**, *84*, 552–570. [[CrossRef](#)]

106. Aung, H.T.; Nikai, T.; Niwa, M.; Takaya, Y. Benzenepolycarboxylic acids with potential anti-hemorrhagic properties and structure-activity relationships. *Bioorganic Med. Chem.* **2011**, *19*, 7000–7002. [[CrossRef](#)]
107. Sülsen, V.P.; Lizarraga, E.; Mamadalieva, N.Z.; Lago, J.H.G. Potential of terpenoids and flavonoids from Asteraceae as anti-inflammatory, antitumor, and antiparasitic agents. *Evid. Based. Complement. Altern. Med.* **2017**, *2017*, 6196198. [[CrossRef](#)]
108. Ray, A.; Jena, S.; Haldar, T.; Sahoo, A.; Kar, B.; Patnaik, J.; Ghosh, B.; Panda, P.C.; Mahapatra, N.; Nayak, S. Population genetic structure and diversity analysis in *Hedychium coronarium* populations using morphological, phytochemical and molecular markers. *Ind. Crops Prod.* **2019**, *132*, 118–133. [[CrossRef](#)]
109. Bhardwaj, S.; Rashmi; Parcha, V. Effect of seasonal variation on chemical composition and physicochemical properties of *Hedychium spicatum* rhizomes essential oil. *J. Essent. Oil Bear. Plants* **2019**, *22*, 1593–1600. [[CrossRef](#)]
110. Safaei-Ghomi, J.; Ahd, A.A. Antimicrobial and antifungal properties of the essential oil and methanol extracts of *Eucalyptus largiflorens* and *Eucalyptus intertexta*. *Pharmacogn. Mag.* **2010**, *6*, 172–175. [[CrossRef](#)] [[PubMed](#)]
111. Sfara, V.; Zerba, E.N.; Alzogaray, R.A. Fumigant insecticidal activity and repellent effect of five essential oils and seven monoterpenes on first-instar nymphs of *Rhodnius prolixus*. *J. Med. Entomol.* **2009**, *46*, 511–515. [[CrossRef](#)] [[PubMed](#)]
112. Ray, A.; Jena, S.; Kar, B.; Sahoo, A.; Pratap Chandra Panda, P.C.; Nayak, S.; Mahapatra, N. Volatile metabolite profiling of ten *Hedychium* species by gas chromatography mass spectrometry coupled to chemometrics. *Ind. Crops Prod.* **2018**, *126*, 135–142. [[CrossRef](#)]
113. Nam, S.-Y.; Chung, C.-K.; Seo, J.-H.; Rah, S.-Y.; Kim, H.-M.; Jeong, H.-J. The therapeutic efficacy of  $\alpha$ -pinene in an experimental mouse model of allergic rhinitis. *Int. Immunopharmacol.* **2014**, *23*, 273–282. [[CrossRef](#)]
114. Özbek, H.; Yilmaz, B.S. Anti-inflammatory and hypoglycemic activities of alpha-pinene. *Acta Pharm. Sci.* **2017**, *55*, 7–14. [[CrossRef](#)]
115. Leite, A.M.; Lima, E.O.; Souza, E.L.; Diniz, M.F.F.M.; Trajano, V.N.; Medeiros, I.A. Inhibitory effect of  $\beta$ -pinene,  $\alpha$ -pinene and eugenol on the growth of potential infectious endocarditis causing Gram-positive bacteria. *Braz. J. Pharm. Sci.* **2007**, *43*, 121–126. [[CrossRef](#)]
116. Yang, C.; Chen, H.; Chen, H.; Zhong, B.; Luo, X.; Chun, J. Antioxidant and anticancer activities of essential oil from Gannan navel orange peel. *Molecules* **2017**, *22*, 1391. [[CrossRef](#)] [[PubMed](#)]
117. Parida, R.; Nayak, S. Chemical composition of *Hedychium coronarium* Koen. flowers from eastern India. *Plant Sci. Today* **2019**, *6*, 259–263. [[CrossRef](#)]
118. Medeiros, J.R.; Campos, L.B.; Mendonça, S.C.; Davin, L.B.; Lewis, N.G. Composition and antimicrobial activity of the essential oils from invasive species of the Azores, *Hedychium gardnerianum* and *Pittosporum undulatum*. *Phytochemistry* **2003**, *64*, 561–565. [[CrossRef](#)]
119. Ribeiro, S.S.; de Jesus, A.M.; dos Anjos, C.S.; da Silva, T.B.; Santos, A.D.C.; de Jesus, J.R.; Andrade, M.S.; Sampaio, T.S.; Gomes, W.F.; Alves, P.B.; et al. Evaluation of the cytotoxic activity of some Brazilian medicinal plants. *Planta Med.* **2012**, *78*, 1601–1606. [[CrossRef](#)]
120. Kotan, R.; Kordali, S.; Cakir, A. Screening of antibacterial activities of twenty-one oxygenated monoterpenes. *Z. Naturforsch. C. J. Biosci.* **2007**, *62*, 507–513. [[CrossRef](#)]
121. Coelho, V.; Mazzardo-Martins, L.; Martins, D.F.; Santos, A.R.S.; Brum, L.F.S.; Picada, J.N.; Pereira, P. Neurobehavioral and genotoxic evaluation of (-)-linalool in mice. *J. Nat. Med.* **2013**, *67*, 876–880. [[CrossRef](#)]
122. Kim, M.-G.; Kim, S.-M.; Min, J.-H.; Kwon, O.-K.; Park, M.-H.; Park, J.-W.; Ahn, H.I.; Hwang, J.-Y.; Oh, S.-R.; Lee, J.-W.; et al. Anti-inflammatory effects of linalool on ovalbumin-induced pulmonary inflammation. *Int. Immunopharmacol.* **2019**, *74*, 105706. [[CrossRef](#)]
123. Chang, M.-Y.; Shieh, D.-E.; Chen, C.-C.; Yeh, C.-S.; Dong, H.-P. Linalool induces cell cycle arrest and apoptosis in leukemia cells and cervical cancer cells through CDKIs. *Int. J. Mol. Sci.* **2015**, *16*, 28169–28179. [[CrossRef](#)]
124. Kheloul, L.; Anton, S.; Gadenne, C.; Kellouche, A. Fumigant toxicity of *Lavandula spica* essential oil and linalool on different life stages of *Tribolium confusum* (Coleoptera: Tenebrionidae). *J. Asia Pac. Entomol.* **2020**, *23*, 320–326. [[CrossRef](#)]
125. Sabogal-Guáqueta, A.M.; Hobbie, F.; Keerthi, A.; Oun, A.; Kortholt, A.; Boddeke, E.; Dolga, A. Linalool attenuates oxidative stress and mitochondrial dysfunction mediated by glutamate and NMDA toxicity. *Biomed. Pharmacother.* **2019**, *118*, 109295. [[CrossRef](#)] [[PubMed](#)]

126. Brillhante, R.S.N.; Caetano, E.P.; Lima, R.A.C.; Marques, F.J.F.; Castelo-Branco, D.S.C.M.; Melo, C.V.S.; Guedes, G.M.M.; Oliveira, J.S.; Camargo, Z.P.; Moreira, J.L.B.; et al. Terpinen-4-ol, tyrosol, and  $\beta$ -lapachone as potential antifungals against dimorphic fungi. *Braz. J. Microbiol.* **2016**, *47*, 917–924. [[CrossRef](#)] [[PubMed](#)]
127. Abdallah, H.M.; Ezzat, S.M. Effect of the method of preparation on the composition and cytotoxic activity of the essential oil of *Pituranthos tortuosus*. *Z. Naturforsch. C. J. Biosci.* **2011**, *66*, 143–148. [[CrossRef](#)] [[PubMed](#)]
128. Odyuo, N.; Roy, D.K. *Hedychium chingmeianum* (Zingiberaceae), a new species from Nagaland, India. *Telopea* **2017**, *20*, 193–199. [[CrossRef](#)]
129. Ding, H.-B.; Bin, Y.; Zhou, S.-S.; Li, R.; Maw, M.B.; Kyaw, W.M.; Tan, Y.-H. *Hedychium putaoense* (Zingiberaceae), a new species from Putao, Kachin State, Northern Myanmar. *PhytoKeys* **2018**, *94*, 51–57. [[CrossRef](#)] [[PubMed](#)]
130. Hu, X.; Huang, J.-Q.; Tan, J.-C.; Wu, Y.-Q.; Chen, J. *Hedychium viridibracteatum* X.Hu, a new species from Guangxi Autonomous Region, South China. *PhytoKeys* **2018**, *110*, 69–79. [[CrossRef](#)]
131. Ashokan, A.; Gowda, V. *Hedychium ziroense* (Zingiberaceae), a new species of ginger lily from Northeast India. *PhytoKeys* **2019**, *117*, 73–84. [[CrossRef](#)]



© 2020 by the authors. Licensee MDPI, Basel, Switzerland. This article is an open access article distributed under the terms and conditions of the Creative Commons Attribution (CC BY) license (<http://creativecommons.org/licenses/by/4.0/>).





Review

# *Genista tridentata* L.: A Rich Source of Flavonoids with Anti-Inflammatory Activity

Diana C. G. A. Pinto \*, Mark A. M. Simões and Artur M. S. Silva

LAQV-REQUIMTE &amp; Department of Chemistry, University of Aveiro, Campus de Santiago, 3810-193 Aveiro, Portugal; mark.simoes@outlook.com (M.A.M.S.); artur.silva@ua.pt (A.M.S.S.)

\* Correspondence: diana@ua.pt

Received: 18 May 2020; Accepted: 29 May 2020; Published: 30 May 2020

**Abstract:** **Background:** *Genista tridentata* L. is an endemic species from the Iberian Peninsula used in Portuguese traditional medicine to treat inflammation-related diseases; this and other health-promoting effects are usually associated with the flavonoids produced by this species. In fact, anti-inflammatory properties were established for several of these flavonoid derivatives. **Methods:** A careful survey of the reported data, using mainly the Scopus database and *Genista tridentata* and *Pterospartum tridentatum* as keywords, was done. We have examined the papers involving the plant and those about the most relevant flavonoids anti-inflammatory activity. **Results:** The literature survey demonstrates that species are used to treat several health problems such as antihyperglycemia, hypertension, and inflammatory episodes. It was also possible to establish its richness in flavonoid derivatives, from which several are potential anti-inflammatory agents. **Conclusions:** From our described and discussed analysis, it can be concluded that *Genista tridentata* is an excellent source of bioactive flavonoids. Moreover, its traditional use to treat inflammation episodes may be due to its flavonoid content, from which genistein, biochanin A, rutin, and daidzein can be emphasized.

**Keywords:** *Genista tridentata*; *Pterospartum tridentatum*; isoflavones; flavonols; anti-inflammatory; genistein; biochanin A; rutin; daidzein

## 1. Introduction

Inflammation is a natural defense mechanism involved in the body's healing process, in which the body is protected from pathogens or abnormal cells [1]. However, if the inflammation is prolonged in time or serious, it can damage the healthy tissues and cause several diseases, such as cancer [2], Alzheimer's and Parkinson's diseases [3]. Therefore, the development of new anti-inflammatory drugs is still a demand, and plant secondary metabolites are considered a priority—in particular, those found in medicinal plants [4].

Among the plants used in Portuguese traditional medicine, *Genista tridentata* L. can be highlighted due to the important applications reported [5]; in fact, the plant, locally named carqueja, is in several regions called the “plant that heals everything” [5], and among its applications is the use to treat inflammatory diseases [6].

Flavonoids, a large family of natural compounds, are usually associated with anti-inflammatory activity [7], and most recently, we demonstrated that *G. tridentata* is rich in flavonoid derivatives [8], including some for which anti-inflammatory activities have been described. As examples, genistein, daidzein [9,10], and biochanin A [11,12] can be highlighted.

The most promising anti-inflammatory flavonoids that can be isolated from *G. tridentata* will be discussed in this review, emphasizing their mode of action and in vivo studies. Hopefully, this will help the scientific community to understand their involvement in inflammatory processes and consequently endorse the design for novel derivatives. Furthermore, the traditional medicine applications of

*G. tridentata* will also be addressed and discussed. To accomplish this survey, we used mainly the Scopus database (69 articles), but also Web of Science (61 articles) and PubMed, mostly for the anti-inflammatory activity. The keywords used were the accepted name (*Genista tridentata*), the most common synonym (*Pterospartum tridentatum*), and also the less common one (*Chamaespartium tridentatum*). Naturally, in the survey there were also the flavonoid names combined with anti-inflammatory activity. Relevance was given to the most recent biological evaluations and the *in vivo* studies and the clinical trials. In all cases, the papers involving both the plant and the most relevant flavonoids anti-inflammatory activities.

## 2. *Genista tridentata*: Traditional Applications and Biological Activities

*Genista tridentata* L. is a bush endemic to the Iberian Peninsula where it grows wild. Unfortunately, its taxonomy is a little controversial, and consequently, the literature survey is more complicated. The most found scientific name is *Pterospartum tridentatum* (L.) Willk., which is considered by some taxonomists [13] as the correct name, but other authors used *Chamaespartium tridentatum* (L.) P.E. Gibbs [14]. However, according to the Plant List database [15], these are synonyms of *Genista tridentata* L. and there are eleven other synonyms and three infraspecific *taxa* [15]. However, in our survey, only the abovementioned synonyms were found—it seems that the other synonyms and infraspecific *taxa* are not used in articles involving chemical profile and/or anti-inflammatory evaluations. Although we used all names in the literature survey, herein, we will refer the species by the accepted name reported in the Plant Lista database [15].

*Genista tridentata* is an Angiosperm belonging to the Leguminosae family [15], which grows spontaneously under Mediterranean thermal conditions, where it is known as carqueja [16]. *G. tridentata* is a perennial shrub that can reach up to one meter in height, with stems of woody and rigid consistency. The roots are well-liked and quite long and sometimes intertwine in the roots of other companion species. The stems are woody, erect or prostrate with laterally winged branches, forming false leaves of dark green color, cut out and of coriaceous consistency. Thus the branches have a flattened shape with two or three wing-shaped expansions, with an articulated appearance, ending with two or three teeth. The leaves, persistent, alternating, unifoliolate and triangular, appear to be tridentate, by the leaflets being united to the stipulations. The flowers are of an intense yellow and are arranged in corymbiform inflorescences, in groups of 3 to 10, gathered in small and tight bouquets. They have an induction in the sepals that line them. The fruit is an oblong-linear pod 10 to 12 mm long [17].

Despite the abovementioned disagreement in the *G. tridentata* taxonomy, the vernacular designation, carqueja, is referred to in the ethnopharmacological surveys. Consequently, it is possible to mention here that *G. tridentata* is used in the Iberian Peninsula, particularly in Portugal, in traditional medicine, mainly to treat influenza, cold, cough, stomach troubles, and nervousness, and is also used as a tonic, hepatic protector, sedative, cicatrizant, and diuretic [6,14,18,19]. In these applications, the population mainly uses extracts of the plant flowers, leaves, or the aerial parts. Consequently, it is suggested that the plant presents several therapeutic properties, from which antispasmodic, antihypertensive, and anti-inflammatory properties can be emphasized [6,14].

The flowers are used in folk medicine for the treatment of various disorders, including those relating to the respiratory system, digestive tract, nervous system, urinary system and dermatology; it has also been indicated for diabetes control [16,20] and is sometimes used in mixtures with other plants for this purpose [20]. Some authors referred to the use of *P. tridentatum* for the treatment of colds, stomach pains, intestinal problems, kidney disease, liver and gallbladder problems and also for rheumatism [21]. It was also indicated for pneumonia, bronchitis and tracheitis, headaches, cough, for low blood pressure levels and high levels of cholesterol, diabetes and even in weight loss programs. This species is known for its diuretic, purgative, laxative, hypotensive, hypoglycemic effects, and for its digestive properties [14,22]. The infusion of dried flowers is considered an excellent emollient [21].

One vital point that should be herein mentioned is the obligation to have scientific validations of the claimed properties, an aspect that it is not at all strange to the scientific community [23]. In this regard, several evaluation studies involving *G. tridentata* extracts were reported and will be herein

presented and discussed. Most of the studies were performed using the flowers or the aerial parts extracted with polar solvents and in vitro antioxidant evaluations (Table 1).

**Table 1.** Biological assays of *Genista tridentata* extracts.

Plant Part	Solvent	Activity Tested	Method	Ref.
Aerial parts	Ethanol and water	Antioxidant (ethanol, IC <sub>50</sub> = 60.39 ± 1.79 µg/mL; water, IC <sub>50</sub> = 42.97 ± 1.69 µg/mL)	DPPH scavenging β-Carotene bleaching test	[24]
Flowers, stems and leaves	Methanol	Antioxidant (flowers, IC <sub>50</sub> = 26.1 ± 1.3 mg/L; stems and leaves, IC <sub>50</sub> = 69.7 ± 11.9 mg/L)	DPPH scavenging β-Carotene bleaching test	[25]
Flowers	Methanol	Antioxidant	DPPH scavenging (IC <sub>50</sub> = 0.15 ± 0.01 mg/mL) β-Carotene bleaching test (IC <sub>50</sub> = 0.14 ± 0.02 mg/mL) Reducing power (IC <sub>50</sub> = 0.13 ± 0.00 mg/mL) TBARS inhibition (IC <sub>50</sub> = 0.12 ± 0.02 mg/mL)	[26]
Flowers and leaves	Hydroethanolic	Antioxidant (flowers, IC <sub>50</sub> = 1016 mg/L; leaves, IC <sub>50</sub> = 704 mg/L)	β-Carotene bleaching test Reducing power ABTS scavenging	[27]
Purchased plant material	Water	Antioxidant (%AA = 169.5 ± 17.2)	β-Carotene bleaching test ABTS scavenging DPPH scavenging (IC <sub>50</sub> = 0.18 ± 0.01 mg/mL)	[28]
Purchased plant material	Methanol	Antioxidant	β-Carotene bleaching test (IC <sub>50</sub> = 0.48 ± 0.09 mg/mL) Reducing power (IC <sub>50</sub> = 0.11 ± 0.00 mg/mL) TBARS inhibition (IC <sub>50</sub> = 1.18 ± 0.06 mg/mL) DPPH scavenging (IC <sub>50</sub> = 50 ± 1 µg/mL)	[29]
Purchased plant material	Hot water	Antioxidant	β-Carotene bleaching test (IC <sub>50</sub> = 266 ± 25 µg/mL) Reducing power (IC <sub>50</sub> = 105 ± 2 µg/mL) TBARS inhibition (IC <sub>50</sub> = 93 ± 4 µg/mL) TBARS inhibition	[30]
Flowers	Hot water	Antioxidant (TABARS, IC <sub>50</sub> = 8.4 ± 0.2 µg/mL; OxHLLA, IC <sub>50</sub> = 37.7 ± 0.9 µg/mL)	Oxidative haemolysis inhibition	[31]
Flowers	Hydromethanolic	Antifungal ( <i>Candida albicans</i> , 10 mm inhibition zone; <i>Candida glabrata</i> , 11 mm inhibition zone)	Disc diffusion test	[32]
Aerial parts	Hydromethanolic	Antibacterial ( <i>Staphylococcus aureus</i> , MIC = 39.1 µg/mL) Antimicrobial ( <i>Escherichia coli</i> , MIC = 0.5 mg/mL; <i>Salmonella typhimurium</i> , MIC = 1 mg/mL; <i>Bacillus cereus</i> , MIC = 1 mg/mL; <i>Listeria monocytogenes</i> , MIC = 1 mg/mL; <i>Aspergillus niger</i> , MIC = 8 mg/mL; <i>Aspergillus versicolor</i> , MIC = 0.5 mg/mL; <i>Penicillium funiculosum</i> , MIC = 0.5 mg/mL; <i>Penicillium verrucosum</i> , MIC = 0.5 mg/mL)	Microplate bioassay	[33]
Flowers	Hot water	Antimicrobial ( <i>Escherichia coli</i> , MIC = 0.5 mg/mL; <i>Salmonella typhimurium</i> , MIC = 1 mg/mL; <i>Bacillus cereus</i> , MIC = 1 mg/mL; <i>Listeria monocytogenes</i> , MIC = 1 mg/mL; <i>Aspergillus niger</i> , MIC = 8 mg/mL; <i>Aspergillus versicolor</i> , MIC = 0.5 mg/mL; <i>Penicillium funiculosum</i> , MIC = 0.5 mg/mL; <i>Penicillium verrucosum</i> , MIC = 0.5 mg/mL)	Disc diffusion test	[31]
Flowers	Hot water	Cytotoxicity (HeLa, GI <sub>50</sub> = 242 ± 10 µg/mL; HepG2, GI <sub>50</sub> = 262 ± 11 µg/mL)	Against tumor cells HeLa, HepG2, MCF-7 and NCI-H460 and non-tumor cells PLP2	[31]



Table 1. Cont.

Plant Part	Solvent	Activity Tested	Method	Ref.
Inflorescences	Hot water	Immunostimulatory (significant activity for 200 µg/mL)	Macrophage cell viability and NO production	[34]
Purchased plant material	Water	Toxicity (non toxic at 375 mg/L)	MTT assay; mitochondrial swelling,	[28]
Flowers, leaves, stems and roots	Ethanol	Toxicity (non toxic at 100 µg/mL)	Resazurin assay	[8]
Flowers	Hot water	Anti-inflammatory (>400 µg/mL)	Determination of LPS-induced NO production by Murine macrophage (RAW 264.7) cell lines	[31]
Flowers, leaves, stems and roots	Ethanol	Anti-inflammatory (significant at 100 µg/mL)	LPS-induced transcription of pro-inflammatory genes <i>IL-1β</i> , <i>Nos2</i> , <i>Ptgs2</i> , <i>IL-6</i> , and <i>TNF-α</i> ; Western blot analysis	[8,35]

AA, antioxidant activity; GI<sub>50</sub>, values correspond to the concentration that causes 50% inhibition of cell proliferation; IC<sub>50</sub>, values corresponded to the extract concentration that inhibits in 50% the oxidation and inflammatory process; MIC, minimum inhibitory concentration.

The authors achieved the extract antioxidant activity index or antioxidant potential through several assays, from which DPPH• (2,2-diphenyl-1-picrylhydrazyl radical) scavenging assay and β-carotene bleaching test are the most common. However, it is interesting to note that some authors used other less common tests, such as lipid peroxidation inhibition, through the decrease in TBARS (thiobarbituric acid reactive substances) [26,29–31], and, more recently, the oxidative hemolysis inhibition assay [31]. These diversifications in the assays are, in our opinion, very good because they can establish in more detail the *G. tridentata* health-promoting potential. Altogether, the reported results show that this species presents moderate to strong antioxidant activity, and apparently, the flower extracts and the water extracts are more active [25,27].

Another interesting feature in these reports is the fact that all authors obtained the total phenolic content and/or the total flavonoid content, and some established the polyphenolic profile or identified some of the phenolic compounds present [25,28–31]. In doing so, they associated the antioxidant activity to the polyphenolic content. On the other hand, some aspects of these reports are less enthusiastic, since the reported values are in different units; the positive controls used are different, making it impossible to perform comparisons.

Other evaluations, such as antifungal [32], antibacterial [31,33] agents, cytotoxicity activity in tumor and non-tumor cells [31], and even the immunostimulatory activity of the *G. tridentata* polysaccharides [34] were also performed. Additionally, Ferreira et al. also performed in vivo and in vitro toxicological assays and concluded that short-term use is safe [8,28].

The anti-inflammatory evaluation of the *G. tridentata* extracts and mainly those reports which were recently achieved [8,31,35] will be the focus of this review. In the most recent evaluations, the authors tested parts of the plant separately and established that the anti-inflammatory effects of plant extracts could occur through different mechanisms. Moreover, the roots, which are not used in traditional medicine, also presented strong anti-inflammatory activity [8]. Likewise, the antioxidant and anti-inflammatory activity is associated with the species richness in polyphenolic compounds, particularly flavonoids.

### 3. Structural Pattern of the Flavonoids Isolated from *Genista tridentata*

Several authors demonstrated that *G. tridentata* produces several flavonoids; these metabolites are those that most contribute to the plant anti-inflammatory activity. Therefore, herein the flavonoids that were isolated from *G. tridentata* extracts or identified in will be discussed.

From the several established profiles, it is evident that the only classes of flavonoids detected were isoflavones 1, flavones 2, flavonols 3, flavanones 4 and flavanonols 5 (Figure 1), and the major ones are isoflavones and flavonols (Tables 2 and 3).

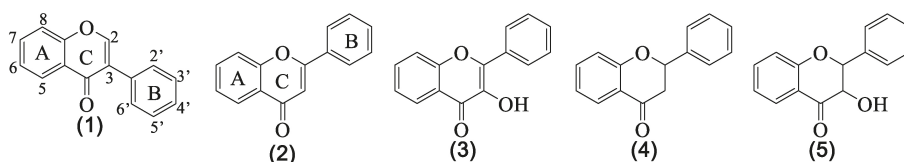


Figure 1. Structure of the classes of flavonoid derivatives found in *G. tridentata*.

Table 2. Isoflavones and flavones produced by *G. tridentata*.

N <sup>o</sup>	Name	R <sup>1</sup>	R <sup>2</sup>	R <sup>3</sup>	R <sup>4</sup>	R <sup>5</sup>	R <sup>6</sup>	R <sup>7</sup>	Ref.
1a	Sissotrin	H	OGlc	H	OH	H	OMe	H	[8,20,29,30,36]
1b	Genistin	H	OGlc	H	OH	H	OH	H	[20,29,30,33,36]
1c	5,5'-Dihydroxy-3'-methoxy-isoflavone-7-O-β-glucoside	H	OGlc	H	OH	OMe	H	OH	[8,20,29–31,36]
1d	Prunetin	H	OMe	H	OH	H	OH	H	[8,20,29,30,36]
1e	Genistein	H	OH	H	OH	H	OH	H	[8,27,29–31,33,36]
1f	7-Methylroborol	H	OMe	H	H	OH	OH	H	[29,30,36]
1g	Genistein-8-C-glucoside	Glc	OH	H	OH	H	OH	H	[29–31]
1h	Biochanin A	H	OH	H	OH	H	OMe	H	[8,29,30]
1i	5-Hydroxy-4',7-dimethoxy-isoflavone	H	OMe	H	OH	H	OMe	H	[8]
1j	Daidzein	H	OH	H	H	H	OH	H	[8]
2a	Luteolin-O-glucuronide	H	OGlc	H	OH	OH	OH	H	[28]
2b	Luteolin-O-(O-acetyl)glucuronide	H	OGlcA-Ac	H	OH	OH	OH	H	[28]
2c	Apigenin	H	OH	H	OH	H	OH	H	[33]

Glc = glucoside unit; GlcA = glucuronide unit; Ac = acetyl.

Table 3. Flavonols produced by *G. tridentata*.

N <sup>o</sup>	Name	R <sup>1</sup>	R <sup>2</sup>	R <sup>3</sup>	R <sup>4</sup>	R <sup>5</sup>	R <sup>6</sup>	R <sup>7</sup>	R <sup>8</sup>	Ref.
3a	Isoquercitrin	Glc	H	OH	H	OH	OH	OH	H	[20,29–31,33,36]
3b	Myricetin-6-C-glucoside	H	H	OH	Glc	OH	H	OH	OH	[8,29,30,36]
3c	Rutin	Rha-Glc	H	OH	H	OH	OH	OH	H	[29–31,33,36]
3d	Isorhamnetin-O-glucoside	Glc	H	OH	H	OH	OMe	OH	H	[28]
3e	Myricetin-3,4'-di-O-glucoside	Glc	H	OH	H	OH	OH	OGlc	OH	[28]
3f	Astragalol	Glc	H	OH	H	OH	H	OH	H	[8]
3g	Isorhamnetin-3-O-glucoside	Glc	H	OH	H	OH	OMe	OH	H	[8]
3h	Kaempferol	H	H	OH	H	OH	H	OH	H	[8]

Glc = glucoside unit; Rha = rhamnoside unit.

As far as we could find, the first report on the *G. tridentata* flavonoids allowed the isolation of four isoflavone derivatives **1a** to **1d**, and one flavonol **3a** (Tables 2 and 3) [20]. Four years later, the same research group found two other isoflavones **1e** and **1f**, and flavonols **3b** and **3c**, (Tables 2 and 3) [36]. The first flavone derivatives were just reported in 2012 and were luteolin derivatives **2a** and **2b**

(Table 2) [28]. Flavanonols were just uncovered, for the first time, in 2014 and are taxifolin derivatives, whereas flavanone derivatives were only reported in 2020 (Figure 2) [8,29].

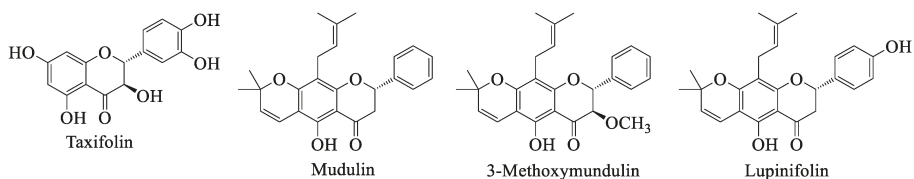


Figure 2. Structure of some flavanoid derivatives found in *G. tridentata*.

Our literature survey showed that the compounds indicated in Table 2 were found by several authors, with the exception of isoflavones **1i** and **1j**, and all the flavone derivatives that were just reported once [8,28,33]. Furthermore, through the analysis of Table 2, it is possible to detect that most of the flavonoids present one or more hydroxy groups and almost all are linked to saccharide units. Usually, this substitution pattern is associated with the anti-inflammatory property of a flavonoid [37].

It is important to complement the information listed in Table 2 with the information that other isoflavone glycosides were described, namely biochanin A hexoside [8,29,31,33] and genistein hexoside [8,31], but the authors did not identify the hexose nor its position in the isoflavone ring. There are also references describing the presence of a methylbiochanin A or a methylprunetin [8,29–31] derivative. In all of these cases, although this is important information about the *G. tridentata* profile, it was not included in Table 2 because its structure is not fully established. This suggests that some investment in phytochemical studies involving *G. tridentata* extracts is still needed.

The substitution pattern of flavanone derivatives includes several hydroxy groups and glucosides, as well as a disaccharide unit. The most referred derivatives were isoquercitrin **3a** and rutin **3c** (Table 3), and again we are in the presence of compounds having the required substitution pattern for being promising anti-inflammatory agents [37]. Additionally, quercetin hexoside derivatives were also found, but the authors were again unable to identify the hexose or its position [29–31].

Finally, we can find the identification and isolation of flavanonols and flavanones (Figure 2). Some authors have reported the presence of taxifolin [33] or its glucosides [8], whereas others just mention hexoside derivatives [29–31]. One fact is consistent—*G. tridentata* produces taxifolin derivatives. The last examples were recently reported and apart from being slightly different, they were isolated from the plant roots [8], which is also uncommon due to the fact that most of the works were performed using flowers or aerial parts. This highlights that some parts of the plant should still be studied.

#### 4. Flavonoids with Anti-Inflammatory Activity

In the previous section, we showed the richness of at *G. tridentata* in flavonoids; additionally, the major class, that is isoflavones, is commonly associated with beneficial anti-inflammatory properties [10]. Yu et al. discussed, in their excellent review [10], the possible isoflavones anti-inflammatory mechanisms, of which herein we highlight the main points (Table 4). Still, we suggest that our readers consult the original review for details. According to the authors, isoflavones may be involved in the scavenging of reactive oxygen species and, in doing so, they prevent the production of peroxynitrite, species that can oxidize low-density lipoproteins. With this effect, isoflavones can prevent cell membrane damage. However, they can also act by inhibiting the production of pro-inflammatory cytokines and chemokine species such as *IL-1 $\beta$* , *IL-6*, *IL-12* and *TNF- $\alpha$* , or by inhibiting pro-inflammatory enzymes, such as cyclooxygenase, nitric oxide synthases, lipoxygenase and phospholipase A2, enzymes involved in the production of inflammatory mediators. Finally, there is also evidence that isoflavones can be involved in the regulation of *NF- $\kappa$ B* factor signaling and, through that regulation, decrease the production of pro-inflammatory cytokines (Table 4) [10,38,39].

Spagnuolo et al. discussed the flavonoids neuroprotective potential, in particular flavonols, another family well represented in *G. tridentata* [40]. There is some evidence, at least in vitro studies, that these flavonoids reduce neuroinflammation also by regulating important signaling pathways such as *NF-κB* and MAPKs (Table 4) [40].

**Table 4.** Anti-inflammatory effects of the selected flavonoids.

Flavonoid	Model	Mechanisms
Biochanin A	In vitro: cytokine release from keratinocytes and HMEC-1 endothelial cells in serum from patients with Behçet’s disease [41]	↓IL-8
	In vitro: LPS-induced inflammation in HUVED cells [42]	↓IL-8, TNF-α, VCAM-1, ICAM-1, E-selection ↑PPAR-γ
	In vivo: focal cerebral ischemia–reperfusion model [43]	↓IL-8, TNF-α, P38 expression
	In vitro: LPS-induced pro-inflammatory responses in murine BV2 microglial cells [44]	↓IL-1β, TNF-α, NO, phosphorylation of JNK, ERK and p38
	In vitro: LPS-induced inflammatory cytokines and mediators production in murine BV2 microglial cells [45]	↓IL-1β, TNF-α, NO, PGE <sub>2</sub> , NF-κB
	In vivo: LPS/GalN-induced liver injury [46]	↑PPAR-γ
	Ex vivo: interleukin-1β-induced catabolic inflammation through the modulation of NFκB cellular signaling in primary rat chondrocytes [47]	IL-1β, TNF-α, ALT, AST, MDA, TXNIP, NLRP3 inflammasome ↑SOD, GPx, catalase, HO-1, Nrf2
	In vitro and in vivo: LPS-induced damage of dopaminergic neurons [48]	↓IL-1β, TNF-α, IL-6, IL-1α, INFγ, IL-2, GM-CSF, fractalkine, MCP-1, MIP-3α, LIX
	In vivo: cisplatin induced acute kidney injury in mice [49]	↓IL-1β, TNF-α, IL-6, phosphorylation of JNK, ERK and p38,
	In vivo: ritonavir induced hepatotoxicity [50]	↓IL-1β, TNF-α, caspase-3, p53 protein
Prunetin	In vivo: transient coronary ligation in Sprague-Dawley rats [51]	↓IL-1β, IL-6 ↑IL-10
	In vivo: LPS-induced acute lung injury in mice [52]	↓IL-1β, IL-18, IL-6, TNF-α
	In vitro: LPS-induced NO production, LPS-induced IKK activity, LPS-induced phosphorylation of IκBα and p38 MAPK [53]	IL-1β, IL-6, TNF-α, TLR4/NF-κB ↑PPAR-γ
	In vitro: CCl <sub>4</sub> -induced hepatotoxicity in rats [54]	IL-6, TNF-α PPAR-γ, PPAR-α iNOS, COX2, TNF-α
	In vivo: Sprague-Dawley rat subarachnoid hemorrhage [55]	sTNFR1, TNF-α, NF-κB, ERK, tyrosine phosphorylation ↑SOD, GSH-Px, HO-1, Nrf2
	In vitro: barrier function of intestinal epithelial CaCo-2/TC-7 cells via TEER measurements [56]	↓iNOS, phosphorylation of IκBα and p38 MAPK ↓TLR/NF-κB
	In vitro: LPS-stimulated macrophages [57]	↓sTNFR1, TNF-α, NF-κB, ERK, tyrosine phosphorylation
	In vitro: LPS-induced septic shock [59]	↓iNOS, PGE <sub>2</sub> , COX2, NF-κB, p38, IL-1β, TNF-α
	In vitro: LPS-induced in- flammatory response and MUC5AC expression [60]	IL-1β, TNF-α IL-8, IL-6, MUC5AC, TLR4/MyD88
	Daidzein	In vitro: LPS-stimulated macrophages [57]
In vivo: angiotensin II-induced AAA [61]		↓IL-1β, TNF-α, NF-κB, iNOS, COX-2, p38MAPK, TGF-β1
In vivo: 5-fluorouracil-induced intestinal mucositis [62]		↓IL-1β, IL-6, TNF-α, NO, COX-2
In vivo: cisplatin-induced kidney injury [63]		↓IL-6, TNF-α, MDA, NO, COX-2, MAPK ↑SOD, GSH
	In vivo: ischemia/reperfusion injury-induced neurological function deficits in Sprague-Dawley [64]	↓TNF-α, NF-κB subunit p65

Table 4. Cont.

Flavonoid	Model	Mechanisms	
Genistein	In vitro: LPS-stimulated macrophages [57]	↓IL-6, TNF- $\alpha$	
	In vitro: homocysteine-induced endothelial cell inflammation [65]	PPAR- $\gamma$ , PPAR- $\alpha$ NF- $\kappa$ B subunit p65, IL-6, ICAM-1	
	In vivo: cyclophosphamide - induced hepatotoxicity [66]		
	In vivo: LPS-induced microglial activation in murine BV2 microglial cell line and primary microglial culture [67]	↓IL-1 $\beta$ , COX-2, MPO	
	In vivo: imiquimod- induced psoriasis-like lesions in mice [68]	↓IL-1 $\beta$ , IL-6, IL-8, TNF- $\alpha$ , IL-17, IL-23, CCL2, NF- $\kappa$ B, VEGFA	
	In vivo: DSS-induced murine colitis [69]	↓IL-1 $\beta$ , IL-18, TNF- $\alpha$ , MPO, NLRP3 inflammasome	
	In vivo: NASH mouse model [70]	↓IL-6, TNF- $\alpha$ , ↓IL-1 $\beta$ , IL-6, COX-2, iNOS, TNF- $\alpha$ , NF- $\kappa$ B p65 ↑HO-1, Nrf2	
	In vivo: chronic sleep deprivation [71]	↓sTNFR1, tyrosine phosphorylation	
	In vitro: barrier function of intestinal epithelial CaCo-2/TC-7 cells via TEER measurements [56]	↓TNF- $\alpha$ , COX-2, Nos2, ICAM-1, MMP-2, MMP-9 ↓TNF- $\alpha$ , NF- $\kappa$ B	
	In vivo: mouse model of periodontitis [72]		
Rutin	In vivo: high-fat high-fructose diet-induced NASH rats [73]	↓p-ERK1/2, p-p38, NF- $\kappa$ B ↑PPAR- $\gamma$ ,	
	In vitro: angiotensin II-stimulated CRP and MMP-9 expression in VSMC [74]		
	In vivo: HMGB1-induced inflammation and CLP-induced sepsis model [75]	↓TLR 4, RAGE, p38 MAPK, VCAM-1, ICAM-1, ERK1/2, NF- $\kappa$ B	
	In vivo: LPS-induced acute endotoxemic kidney injury in C57BL/6 mice [76]	↓TLR 4, COX-2, TNF- $\alpha$ , IL-6, SIRT1, NF- $\kappa$ B	
	In vivo: NaF-induced neurotoxicity [77]	↓IL-1 $\beta$ , IL-6, TNF- $\alpha$	
	In vivo: HgCl <sub>2</sub> -induced nephrotoxicity [78]	↓IL-1 $\beta$ , IL-33, TNF- $\alpha$ , NF- $\kappa$ B, Bcl-3	
	In vivo: HgCl <sub>2</sub> -induced hepatotoxicity [79]	↓IL-1 $\beta$ , TNF- $\alpha$ , NF- $\kappa$ B, Bcl-3, Bax, p53, p38 MAPK, caspase-3	
	In vitro: PMA-induced neutrophil stimulation [80]	↓NO, TNF- $\alpha$ , MPO	
	Taxifolin	In vitro: osteoclastogenesis [81]	↓AKT, RANKL
		In vivo: and ovariectomy-induced osteoporosis [81]	↓TNF- $\alpha$ , IL-1 $\beta$ , NF- $\kappa$ B, MAPK, NFATc1, MMP-9, cathepsin K, TRAP
In vitro: osteolysis model [82]		↓MAPK, p38, ERK, JNK; RANKL, NF- $\kappa$ B	
In vitro: on IgE/Ag-stimulated mast cells including BMDCs [83]		↓LTC <sub>4</sub> , IL-6, COX-2, TNF- $\alpha$ , NF- $\kappa$ B	
In vivo: acetaminophen-induced liver injury [84]		↓ inhibiting metabolic activation mediated by CYP450 enzymes	

Considering all these pieces of evidence and the fact that several flavonoids were found in *G. tridentata*, we selected some significative examples to discuss their anti-inflammatory potential, and Table 4 summarizes the effect and mechanism of action of the selected flavonoids.

#### 4.1. Biochanin A and Prunetin

Biochanin A **1h** and prunetin **1d** are isomeric natural isoflavones (Figure 3) produced by *G. tridentata* not as the major components, but in small amounts, 4.8% ( $\mu$ g/g) for biochanin A **1h** and 4.1% ( $\mu$ g/g) for prunetin **1d** [29]. Some derivatives are also reported, and in particular, the methyl derivative that was not fully identified [29]; in fact, if there is no evidence of mass spectra fragments containing the characteristic A ring fragment [8] or the compound was isolated [20], it is possible to confuse these isomers. One fact is consistent—*G. tridentata* produced one or both.

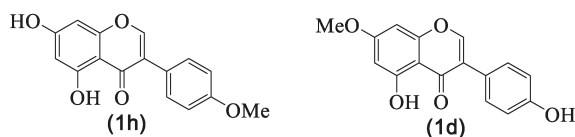


Figure 3. Biochanin A **1h** and prunetin **1d** structures.

As far as we could find, prunetin **1d** was isolated for the first time in 1952 from *Pterocarpus angolensis* DC. [85] and biochanin A **1h** was isolated from *Cicer arietinum* L. in 1945 [86]. Although these isoflavones' natural occurrence seems to be similar, from the biological evaluation point of view, biochanin A **1h** has been extensively studied, and several health benefits were attributed to its consumption as well as its possible use to develop new drugs [87,88], and anti-inflammatory activity is among those biological properties.

In this century, several evaluations regarding the biochanin A **1h** anti-inflammatory activity have been performed (Table 4), and the first example is the study of Kalayciyan et al. [41], in which the compound potential to treat the Behçet's disease was established. The main anti-inflammatory effect of the compound is to decrease the secretion of interleukin-8 (*IL-8*), a potent leukocyte chemotactic factor known to induce inflammation [41]. More recently, it was also proved that biochanin A **1h** inhibits the *IL-8* expression in lipopolysaccharides (LPS)-stimulated human vascular endothelial cells in a dose-dependent manner [42], as well as in focal cerebral ischemia/reperfusion in rats [43]. The biochanin A **1h** effects on other interleukins levels, such as *IL-1 $\beta$* , *IL-6*, *IL-10*, and *IL-18*, were evaluated in the last few years, with *IL-1 $\beta$*  being the most studied one [44–54]. All these studies proved the inhibitory effect that biochanin A **1h** has on these inflammatory cytokines. However, the most important aspect is the fact that some of the studies were performed in vivo [43,46,49–52], which is a forward step to establish this compound pharmacological potential.

The inhibition of another important pro-inflammatory species, such as TNF- $\alpha$ , was also evaluated by several authors [42–49,52–56], as well as the inhibiting pro-inflammatory enzymes [49,55] and key phosphorylation steps [44,48,56,57]. All of these studies suggested that biochanin A **1h**'s anti-inflammatory effect occurs by suppressing the pathways NF- $\kappa$ B and MAPK [53,56–58], but is also associated with the up-regulation of PPAR expression [43,45,53,54]. Prunetin **1d**, a much less studied compound, also presents potent in vitro [56,59,60] and in vivo [59] anti-inflammatory activity, and apparently, its mechanism of action is also associated with the inhibition of the NF- $\kappa$ B pathway [59].

It should be highlighted that several of the studies mentioned above included the evaluation of cytotoxic effects, and all demonstrated that both isoflavones do not affect the viability of the cells, and in the subsequent tests the authors used noncytotoxic concentrations. From these studies, essential facts arose—prunetin **1d** should be subjected to more evaluations. Moreover, pharmacodynamic and pharmacokinetic parameters of both isoflavones should be evaluated in order to implement some clinical trials in the future.

#### 4.2. Daidzein

Daidzein **1j** (Figure 4) is a natural isoflavone with a significant occurrence, mainly in fruits and nuts [89], which is the reason why humans are exposed to it and also to its health benefits [90]. In fact, several pharmacological properties are attributed to this isoflavone [91], including anti-inflammatory potential [10,91]. Although daidzein **1j** occurrence in *G. tridentata* is rare, only one report on its identification was reported (Table 2), we decided to include here the most recent works on its anti-inflammatory activity, since its occurrence seems to be exclusively in the plant roots [8]. This fact gives importance to that part of the plant, while importance usually is only given to the flowers and aerial parts, which are the ones used traditionally.

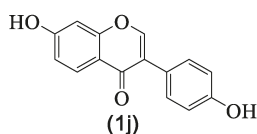


Figure 4. Daidzein **1j** structure.

The most recent studies involved in vivo studies with daidzein **1j**—the reasons why are herein highlighted. Due to its occurrence in common fruits [89], daidzein **1j** is present in mankind's diet, and it

is a nontoxic compound [52]. These recent studies confirmed daidzein **1j**'s strong anti-inflammatory activity as well as settling on its mechanism of action (Table 4). Mainly, daidzein **1j** strongly affects various pathways, including NF- $\kappa$ B, p38MAPK, and TGF- $\beta$ 1. Regardless of this potential as an anti-inflammatory drug, as far as we could find, daidzein **1j** is not involved in clinical trials.

#### 4.3. Genistein

Genistein **1e** (Figure 5), like daidzein **1j**, occurs naturally in everyday food, such as fruits and nuts [89], and as far as we could find, it is non-toxic for humans [92], which was also recently reinforced by Kumar et al. [93]. The pharmacological potential of genistein **1e** is well documented [94]; more recently, an overview regarding their mechanism of action in cancer models was published [95], and in some aspects, the anticancer and the anti-inflammatory activities are associated.

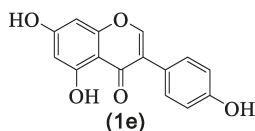


Figure 5. Genistein **1e** structure.

Regarding the anti-inflammatory activity studies, it should be emphasized that, recently, there are more in vivo studies, meaning that scientists are interested in giving this natural isoflavone new medicinal applications. From the reported results, we select a few (Table 4) that demonstrate genistein **1e**'s potential to become an anti-inflammatory drug.

It can be seen that like the isoflavones mentioned above, genistein **1e** targets the same pathways, with an emphasis on the upregulation of the PPAR $\gamma$  signaling pathway and downregulation of the NF- $\kappa$ B signaling pathway, as well as the decrease in several inflammatory mediators (Table 4). In light of the referred studies, genistein **1e** is a candidate to be used in the prevention or treatment of inflammation-related diseases. For example, it could be used to target microRNAs, which is considered a therapeutic target for liver disease. In fact, the results show that the anti-inflammatory activity of genistein **1e** downregulated microRNA expression of liver inflammation [70] but also pro-inflammatory cytokines species such as *IL-1 $\beta$*  and *TNF- $\alpha$*  [70,73]. Another interesting example is its ability to attenuate NF- $\kappa$ B inflammatory signaling in the brain with consequent inhibition of pro-inflammatory cytokines release, which gives genistein **1e** the possibility to become a new drug able to relieve chronic sleep deprivation's adverse effects [71]. Furthermore, there is some evidence supporting that genistein **1e** can, through its anti-inflammatory activity, prevent cardiovascular diseases [74]. Altogether, these findings suggest that genistein is a good candidate for future clinical trials.

#### 4.4. Rutin

Rutin **3c** (Figure 6) is amongst the most found flavonoids in *G. tridentata* (Table 3), for which several biological and pharmacological properties have been established and reviewed through the years [96–100]. Some more specific activities, such as antidiabetic effects [101], reestablishment of the immune homeostasis [96,102], neuroprotective effects [98,103,104] and anticancer effects [98,99,105] were also addressed. Furthermore, some toxicological studies were also performed [98,106] as well as pharmacokinetic [98], bioavailability [99] and formulation development [100]. It should be emphasized that the mentioned properties prompted some clinical trials using rutin **3c** [107,108] and although the results are not remarkable, they at least confirm that it is safe to use rutin **3c**.

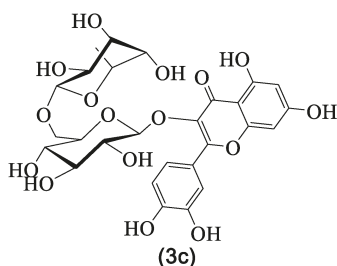


Figure 6. Rutin 3c structure.

Obviously, rutin 3c's anti-inflammatory activity was also evaluated and several interesting results were reported (Table 4). It is known that in general, flavonoids decrease the production of pro-inflammatory interleukins, mainly IL-1 $\beta$ , IL-6, and IL-8, but also tumor necrosis factor  $\alpha$  (TNF- $\alpha$ ). There is evidence that rutin 3c anti-inflammatory mechanism also involves the downregulation of these pro-inflammatory species [76–80]. The results show that rutin 3c can also exert its anti-inflammatory activity through other mechanisms (Table 4), from which can be highlighted the inhibition of the HMGB1 signaling pathway through the downregulation of TLR4 and RAGE expressions [75] and also the inhibition of the MPO activity [80]. The last one is an important example because it provides evidence that rutin 3c can be a possible therapeutic agent for autoimmune diseases [80].

Collectively, the results demonstrate that rutin 3c attenuates inflammation through several mechanisms and is a nontoxic compound, so clinical trials more focused on its anti-inflammatory potential should be implemented. In this regard, Kalita and Das [109] studied the efficiency of a rutin 3c formulation to be used in the treatment of inflammations through the long-term delivery via the skin. Their results, although preliminary, are sufficiently good to encourage future investigations.

#### 4.5. Taxifolin

Our last example is taxifolin (Figure 2), which, as shown in the previous section, occurs in *G. tridentata*, mainly linked to sugar moieties. Nevertheless, we specify here some interesting studies due to the fact that in a living organism, it is possible to obtain the aglycone. The taxifolin anti-inflammatory potential has been known, at least, since 1971 [110] and recently Sunil and Xu published an interesting review on taxifolin's health benefits [111]. Some important aspects arose from this review: the first is the broad biological potential of taxifolin, mainly using in vitro evaluations, but also that the anti-inflammatory and toxicological evaluations are still scarce. The few examples (Table 4) suggest that its mechanism of action is similar to the one reported for the other flavonoids, that is also mainly targets the NF- $\kappa$ B and MAPK pathways. Although, the anti-inflammatory assessments are scarce, they suggest taxifolin's potential to be a drug candidate for the treatment of inflammations, suggesting that it should be further investigated.

## 5. Conclusions

This survey demonstrates beyond any doubt that *G. tridentata* is a source of bioactive metabolites, some of which present interesting anti-inflammatory activities which, in turn, contribute to the extracts' anti-inflammatory activity. Amongst our findings, the toxicological evaluations of both extracts and pure compounds are important and contribute to establishing *G. tridentata*'s medicinal value as well as the secondary metabolites' pharmacological value. However, in our opinion, some efforts on the plant taxonomy should be made to prevent confusion in the data reported. Moreover, we think that an extra effort on clinical trials, mainly concerning the pure compounds used as drugs, should be performed.



**Author Contributions:** D.C.G.A.P. and M.A.M.S. performed the literature survey; D.C.G.A.P. and A.M.S.S. conceived and wrote the paper. All authors have read and agreed to the published version of the manuscript.

**Funding:** This research received no external funding.

**Acknowledgments:** Thanks are due to the University of Aveiro and FCT/MCT for the financial support for the LAQV-REQUIMTE (UIDB/50006/2020) through national funds and, where applicable, co-financed by the FEDER, within the PT2020 Partnership Agreement.

**Conflicts of Interest:** The authors declare no conflict of interest.

## Abbreviations

AAA	abdominal aortic aneurysm
ABTS	2,2'-azino-bis(3-ethylbenzothiazoline-6-sulfonic acid
Ag	antigen
AKT	serine/threonine kinase
Bax	Bcl-2 associated X protein
Bcl-2	B-cell lymphoma-2
Bcl-3	B-cell lymphoma-3
BMMCs	bone marrow derived mast cells
caspase-3	cysteine aspartate specific protease-3
CCL2	chemokine ligand 2
CLP	cecal ligation and puncture
CRP	C-reactive protein
CXC	$\alpha$ -chemokines
CYP450	Cytochrome P450
DPPH <sup>•</sup>	2,2-diphenyl-1-picrylhydrazyl radical
DSS	dextran sulfate sodium
E-selection	endothelial cells
ERK	extracellular signal-regulated protein kinase
G.	<i>Genista</i>
GalN	D-galactosamine
GM-CSF	granulocyte-macrophage colony-stimulating factor
GPx	glutathione peroxidase
HMEC-1	human dermal microvascular endothelial cell-1
HMGB1	high mobility group box 1
HO-1	heme oxygenase-1
HUVEC	human umbilical vein endothelial
ICAM-1	intercellular adhesion molecule-1
IFN $\gamma$	interferon gamma
IgE	immunoglobulin E
IKK	I $\kappa$ B kinase
IL-10	interleukin-10
IL-12	interleukin-12
IL-18	interleukin-18
IL-1 $\alpha$	interleukin-1 $\alpha$
IL-1 $\beta$	interleukin-1 $\beta$
IL-2	interleukin-2
IL-6	interleukin-6
IL-8	interleukin-8
iNOS	inducible nitric oxide synthase
JNK	c-jun N-terminal kinase
LIX	lipopolysaccharide-induced CXC chemokine
LPS	lipopolysaccharides
LTC <sub>4</sub>	cysteinyl leukotriene 4
MAPK	mitogen-activated protein kinases

MCP-1	monocyte chemoattractant protein-1
MDA	malondialdehyde
MIP-3 $\alpha$	macrophage inflammatory protein 3 $\alpha$
MMP	matrix metalloproteinases
MPO	myeloperoxidase
MTT	3-(4,5-dimethylthiazol-2-yl)-2,5-diphenyltetrazolium bromide
MUC5AC	mucin 5AC glycoprotein
MyD88	myeloid differentiation primary response 88
NASH	nonalcoholic steatohepatitis
NF- $\kappa$ B	nuclear factor kappa-light-chain-enhancer of activated B cells
NFATc1	nuclear factor-activated T cells c1
NLRP3	NRL pyrin domain containing 3
Nos2	nitric oxide synthase 2
Nrf2	nuclear factor erythroid 2
NRL	nucleotide-binding, leucine-rich repeat containing proteins
PGE <sub>2</sub>	prostaglandin E2
PMA	phorbol 12-myristate 13-acetate
PPAR- $\gamma$	peroxisome proliferator-activated receptor gamma
Ptgs2	prostaglandin-endoperoxide synthase 2
RAGE	receptor for advanced glycation end-products
RANKL	receptor activator of nuclear factor- $\kappa$ B ligand
SIRT1	sirtuin 1
SOD	superoxide dismutase
sTNFR1	soluble tumor necrosis factor receptor-1
TBARS	thiobarbituric acid reactive substances
TEER	transepithelial electrical resistance
TGF- $\beta$ 1	transforming growth factor $\beta$ 1
TLR 4	toll-like receptors 4
TNF- $\alpha$	tumor necrosis factor alpha
TRAP	tartrate-resistant acid phosphatase
TXNIP	thioredoxin-interacting protein
VCAM-1	vascular cytoadhesion molecule-1
VEGF	vascular endothelial growth factor
VEGFA	vascular endothelial growth factor A
VSMC	vascular smooth muscle cells

## References

1. Ahmed, A.U. An overview of inflammation: Mechanism and consequences. *Front. Biol.* **2011**, *6*, 274–281. [[CrossRef](#)]
2. Mantovani, A.; Allavena, P.; Sica, A.; Balkwill, F. Cancer-related inflammation. *Nature* **2008**, *454*, 436–444. [[CrossRef](#)] [[PubMed](#)]
3. Glass, C.K.; Saijo, K.; Winner, B.; Marchetto, M.C.; Gage, F.H. Mechanisms underlying inflammation in neurodegeneration. *Cell* **2010**, *140*, 918–934. [[CrossRef](#)] [[PubMed](#)]
4. Veeresham, C. Natural products derived from plants as a source of drugs. *J. Adv. Pharm. Tech. Res.* **2012**, *3*, 200–201. [[CrossRef](#)]
5. Neves, J.M.; Matos, C.M.; Moutinho, C.G.; Gomes, L.R. *Usos Populares de Plantas Mediciniais da Flora Transmontana*; Edições Universidade Fernando Pessoa: Porto, Portugal, 2008; pp. 226–235.
6. Novais, M.H.; Santos, I.; Mendes, S.; Pinto-Gomes, C. Studies on pharmaceutical ethnobotany in Arrabida Natural Park (Portugal). *J. Ethnopharm.* **2004**, *93*, 183–195. [[CrossRef](#)]
7. Ferrándiz, M.L.; Alcaraz, M.J. Anti-inflammatory activity and inhibition of arachidonic acid metabolism by flavonoids. *Agents Actions* **1991**, *32*, 283–288. [[CrossRef](#)]
8. Simões, M.A.M.; Pinto, D.C.G.A.; Neves, B.M.R.; Silva, A.M.S. Flavonoid profile of the *Genista tridentata* L., a species used traditionally to treat inflammatory processes. *Molecules* **2020**, *25*, 812. [[CrossRef](#)]

9. Hämäläinen, M.; Nieminen, R.; Vuorela, M.; Moilanen, E. Anti-inflammatory effects of flavonoids: Genistein, kaempferol, quercetin, and daidzein inhibit STAT-1 and NF- $\kappa$ B activations, whereas flavone, isorhamnetin, naringenin, and pelargonidin inhibit only NF- $\kappa$ B activation along with their inhibitory effect on iNOS expression and NO production in activated macrophages. *Mediat. Inflamm.* **2007**. [[CrossRef](#)]
10. Yu, J.; Bi, X.; Yu, B.; Chen, D. Isoflavones: Anti-inflammatory benefit and possible caveats. *Nutrients* **2016**, *8*, 361. [[CrossRef](#)]
11. Chen, H.Q.; Jin, Z.Y.; Li, G.H. Biochanin A protects dopaminergic neurons against lipopolysaccharide-induced damage through inhibition of microglia activation and proinflammatory factors generation. *Neurosci. Lett.* **2007**, *417*, 112–117. [[CrossRef](#)]
12. Tan, J.W.; Kim, M.K. Neuroprotective effects of biochanin A against b-amyloid-induced neurotoxicity in PC12 cells via a mitochondrial-dependent apoptosis pathway. *Molecules* **2016**, *21*, 548. [[CrossRef](#)] [[PubMed](#)]
13. Teixeira, G.; Pereira, A.L. Winged stems in *Pterospartum tridentatum*: Morphoanatomical study. *Acta Bot. Gall.* **2004**, *151*, 103–109. [[CrossRef](#)]
14. Neves, J.M.; Matos, C.; Moutinho, C.; Queiroz, G.; Gomes, L.R. Ethnopharmacological notes about ancient uses of medicinal plants in Trás-os-Montes (northern of Portugal). *J. Ethnopharmacol.* **2009**, *124*, 270–283. [[CrossRef](#)] [[PubMed](#)]
15. The Plant List Database. Available online: <http://www.theplantlist.org/> (accessed on 26 May 2020).
16. Carvalho, A.M. Plantas y sabiduría popular del Parque Natural de Montesinho: Un estudio etnobotánico en Portugal. In *Biblioteca de Ciencias No 35*; Consejo Superior de Investigaciones Científicas: Madrid, Spain, 2010; p. 496.
17. Flora-On. Available online: <https://flora-on.pt/index.php#/0BJwn> (accessed on 26 May 2020).
18. Camejo-Rodrigues, J.; Ascensão, L.; Bonet, M.Á.; Vallès, J. An ethnobotanical study of medicinal and aromatic plants in the natural park of “Serra de São Mamede”(Portugal). *J. Ethnopharmacol.* **2003**, *89*, 199–209. [[CrossRef](#)]
19. Rivera, D.; Verde, J.; Fajardo, J.; Obón, C.; Consuegra, V.; García-Botía, J.; Ríos, S.; Alcaraz, F.; Valdés, A.; del Moral, A.; et al. Ethnopharmacology in the upper Guadiana river área (Castile-La Mancha, Spain). *J. Ethnopharmacol.* **2019**, *241*, 111968. [[CrossRef](#)]
20. Vitor, R.F.; Mota-Filipe, H.; Teixeira, G.; Borges, C.; Rodrigues, A.I.; Teixeira, A.; Paulo, A. Flavonoids of na extract of *Pterospartum tridentatum* showing endothelial protection against oxidative injury. *J. Ethnopharmacol.* **2004**, *93*, 363–370. [[CrossRef](#)]
21. Grosso, A.C.; Costa, M.M.; Ganço, L.; Pereira, A.L.; Teixeira, G.; Lavado, J.M.G.; Figueireido, A.C.; Pedro, L.G. Essential oil composition of *Pterospartum tridentatum* grown in Portugal. *Food Chem.* **2007**, *102*, 1083–1088. [[CrossRef](#)]
22. Coelho, M.T.; Gonçalves, J.C.; Alves, V.; Martins, M.M. Antioxidant activity and phenolic content of extracts from different *Pterospartum tridentatum* populations growing in Portugal. *Procedia Food Sci.* **2011**, *1*, 1454–1458. [[CrossRef](#)]
23. Taylor, J.L.S.; Rabe, T.; McGaw, L.J.; Jäger, A.K.; van Staden, J. Towards the scientific validation of traditional medicinal plants. *Plant. Growth Reg.* **2001**, *34*, 23–37. [[CrossRef](#)]
24. Luís, Â.; Domingues, F.; Gil, C.; Duarte, A.P. Antioxidant activity of extracts of Portuguese shrubs: *Pterospartum tridentatum*, *Cytisus scoparius* and *Erica* spp. *J. Med. Plant. Res.* **2009**, *3*, 886–893.
25. Luís, Â.; Domingues, F.; Duarte, A.P. Bioactive compounds, RP-HPLC analysis of phenolics, and antioxidant activity of some Portuguese shrub species extracts. *Nat. Prod. Commun.* **2011**, *6*, 1863–1872. [[CrossRef](#)] [[PubMed](#)]
26. Pinela, J.; Barros, L.; Carvalho, A.M.; Ferreira, I.C.F.R. Influence of the drying method in the antioxidant potential and chemical composition of four shrubby flowering plants from the tribe Genisteeae (Fabaceae). *Food Chem. Toxicol.* **2011**, *48*, 2983–2989. [[CrossRef](#)] [[PubMed](#)]
27. Martínez, A.; Estévez, J.C.; Silva-Pando, F.J. Antioxidant activity, total phenolic content and skin care properties of 35 selected plants from Galicia (NW Spain). *Front. Life Sci.* **2012**, *6*, 77–86. [[CrossRef](#)]
28. Ferreira, F.M.; Dinis, L.T.; Azedo, P.; Galhano, C.I.C.; Simões, A.; Cardoso, S.M.; Domingues, M.R.M.; Pereira, O.R.; Palmeira, C.M.; Peixoto, F.P. Antioxidant capacity and toxicological evaluation of *Pterospartum tridentatum* flower extracts. *CyTA J. Food* **2012**, *10*, 92–102. [[CrossRef](#)]

29. Roriz, C.L.; Barros, L.; Carvalho, A.M.; Santos-Buelga, C.; Ferreira, I.C.F.R. Pterospartum tridentatum, Gomphrena globosa and Cymbopogon citratus: A phytochemical study focused on antioxidant compounds. *Food Res. Int.* **2014**, *62*, 684–693. [[CrossRef](#)]
30. Roriz, C.L.; Barros, L.; Carvalho, A.M.; Santos-Buelga, C.; Ferreira, I.C.F.R. Scientific validation of synergistic antioxidant effects in commercialized mixtures of Cymbopogon citratus and Pterospartum tridentatum or Gomphrena globosa for infusions preparation. *Food Chem.* **2015**, *185*, 16–24. [[CrossRef](#)]
31. Caleja, C.; Finimundy, T.C.; Pereira, C.; Barros, L.; Calheta, R.C.; Sokovic, M.; Ivanov, M.; Carvalho, A.M.; Rosa, E.; Ferreira, I.C.F.R. Challenges of traditional herbal teas: Plant infusions and their mixtures with bioactive properties. *Food Funct.* **2019**, *10*, 5939–5951. [[CrossRef](#)]
32. Martins, N.; Ferreira, I.C.F.R.; Barros, L.; Carvalho, A.M.; Henriques, M.; Silva, S. Plants used in folk medicine: The potential of their hydromethanolic extracts against Candida species. *Ind. Crops Prod.* **2015**, *66*, 62–67. [[CrossRef](#)]
33. Aires, A.; Marrinhas, E.; Carvalho, R.; Dias, C.; Saavedra, M.J. Phytochemical composition and antibacterial activity of hydroalcoholic extracts of Pterospartum tridentatum and Mentha pulegium against Staphylococcus aureus isolates. *BioMed Res. Int.* **2016**, *2016*. [[CrossRef](#)]
34. Martins, V.M.R.; Simões, J.; Ferreira, I.; Cruz, M.T.; Domingues, M.R.; Coimbra, M.A. In vitro macrophage nitric oxide production by Pterospartum tridentatum (L.) Willk. inflorescence polysaccharides. *Carbohydr. Polym.* **2017**, *157*, 176–184. [[CrossRef](#)]
35. Pinto, D.C.G.A.; Silva, A.M.S. Valorisation of Portuguese natural resources. *Phytochem. Rev.* **2020**. [[CrossRef](#)]
36. Paulo, A.; Martins, S.; Branco, P.; Dias, T.; Borges, C.; Rodrigues, A.I.; Costa, M.C.; Teixeira, A.; Mota-Filipe, H. The opposing effects of the flavonoids isoquercitrin and sissotrin, isolated from Pterospartum tridentatum, on oral glucose tolerance in rats. *Phytother. Res.* **2008**, *22*, 539–543. [[CrossRef](#)] [[PubMed](#)]
37. Silva, C.F.M.; Pinto, D.C.G.A.; Silva, A.M.S. Chromones: A promising ring-system for new anti-inflammatory drugs. *ChemMedChem* **2016**, *11*, 2252–2260. [[CrossRef](#)]
38. Fernández-Rojas, B.; Gutiérrez-Venegas, G. Flavonoids exert multiple periodontic benefits including anti-inflammatory, periodontal ligament-supporting, and alveolar bone-preserving effects. *Life Sci.* **2018**, *209*, 435–454. [[CrossRef](#)] [[PubMed](#)]
39. Choy, K.W.; Murugain, D.; Leong, X.-F.; Abas, R.; Alias, A.; Mustafa, M.R. Flavonoids as natural anti-inflammatory agents targeting nuclear factor-kappa B (NFκB) signaling in cardiovascular diseases: A mini review. *Front. Pharmacol.* **2019**, *10*, 1295. [[CrossRef](#)]
40. Spagnuolo, C.; Moccia, S.; Russo, G.L. Anti-inflammatory effects of flavonoids in neurodegenerative disorders. *Eur. J. Med. Chem.* **2018**, *153*, 105–115. [[CrossRef](#)]
41. Klayciyan, A.; Orawa, H.; Fimmel, S.; Perschel, F.H.; González, J.-B.; Fitzner, R.G.; Orfanos, C.E.; Zouboulis, C.C. Nicotine and biochanin A, but not cigarette smoke, induce anti-inflammatory effects on keratinocytes and endothelial cells in patients with Behçet’s disease. *J. Investig. Dermatol.* **2007**, *127*, 81–89. [[CrossRef](#)]
42. Ming, X.; Ding, M.; Zhai, B.; Xiao, L.; Piao, T.; Liu, M. Biochanin A inhibits lipopolysaccharide-induced inflammation in human umbilical vein endothelial cells. *Life Sci.* **2015**, *136*, 36–41. [[CrossRef](#)]
43. Wang, W.; Tang, L.; Li, Y.; Wang, Y. Biochanin A protects against focal cerebral ischemia/reperfusion in rats via inhibition of p38-mediated inflammatory responses. *J. Neurol. Sci.* **2015**, *348*, 121–125. [[CrossRef](#)]
44. Wu, W.-Y.; Wu, Y.-Y.; Huang, H.; He, C.; Li, W.-Z.; Wang, H.-L.; Chen, H.-Q.; Yin, Y.-Y. Biochanin A attenuates LPS-induced pro-inflammatory responses and inhibits the activation of the MAPK pathway in BV2 microglial cells. *Int. J. Mol. Med.* **2015**, *35*, 391–398. [[CrossRef](#)]
45. Zhang, Y.; Chen, W. Biochanin A inhibits lipopolysaccharide-induced inflammatory cytokines and mediators production in BV2 microglia. *Neurochem. Res.* **2015**, *40*, 165–171. [[CrossRef](#)] [[PubMed](#)]
46. Liu, X.; Wang, T.; Liu, X.; Cai, L.; Qi, J.; Zhang, P.; Li, Y. Biochanin A protects lipopolysaccharide/D-galactosamine-induced acute liver injury in mice by activating the Nrf2 pathway and inhibiting NLRP3 inflammasome activation. *Int. Immunopharmacol.* **2016**, *38*, 324–331. [[CrossRef](#)] [[PubMed](#)]
47. Oh, J.-S.; Cho, I.-A.; Kang, K.-R.; You, J.-S.; Yu, S.-J.; Lee, G.-J.; Seo, Y.-S.; Kim, C.S.; Kim, D.K.; Kim, S.-G.; et al. Biochanin-A antagonizes the interleukin-1β-induced catabolic inflammation through the modulation of NFκB cellular signaling in primary rat chondrocytes. *Biochem. Biophys. Res. Commun.* **2016**, *477*, 723–730. [[CrossRef](#)] [[PubMed](#)]

48. Wang, J.; Wu, W.-Y.; Huang, H.; Li, W.-Z.; Chen, H.-Q.; Yin, Y.-Y. Biochanin A protects against lipopolysaccharide-induced damage of dopaminergic neurons both in vivo and in vitro via inhibition of microglial activation. *Neurotox. Res.* **2016**, *30*, 486–498. [[CrossRef](#)]
49. Suliman, F.A.; Khodeer, D.M.; Ibrahim, A.; Mehanna, E.T.; El-Kherbetawy, M.K.; Mohmmad, H.M.F.; Zaitone, S.A.; Moustafa, Y.M. Renoprotective effect of the isoflavonoid biochanin A against cisplatin induced acute kidney injury in mice: Effect on inflammatory burden and p53 apoptosis. *Int. Immunopharmacol.* **2018**, *61*, 8–19. [[CrossRef](#)]
50. Alauddin; Chaturvedi, S.; Malik, M.Y.; Azmi, L.; Shukla, I.; Naseem, Z.; Rao, C.V.; Agarwal, N.K. Formononetin and biochanin A protects against ritonavir induced hepatotoxicity via modulation of NfκB/pAkt signaling molecules. *Life Sci.* **2018**, *213*, 174–182. [[CrossRef](#)]
51. Bai, Y.; Li, Z.; Liu, W.; Gao, D.; Liu, M.; Zhang, P. Biochanin A attenuates myocardial ischemia/reperfusion injury through the TLR4/NF-κB/NLRP3 signaling pathway. *Acta Cir. Bras.* **2019**, *34*, e201901104. [[CrossRef](#)]
52. Hu, X.; Qin, H.; Li, Y.; Li, J.; Fu, L.; Li, M.; Jiang, C.; Yun, J.; Liu, Z.; Feng, Y.; et al. Biochanin A protect against lipopolysaccharide-induced acute injury in mice by regulating TLR4//NF-κB and PPAR-γ pathway. *Microb. Pathogen.* **2020**, *138*, 103846. [[CrossRef](#)]
53. Kole, L.; Giri, B.; Manna, S.K.; Pal, B.; Ghosh, S. Biochanin A, an isoflavone, showed anti-proliferative and anti-inflammatory activities through the inhibition of iNOS expression, p38-MAPK and ATF-2 phosphorylation and blocking NFκB nuclear translocation. *Eur. J. Pharmacol.* **2011**, *653*, 8–15. [[CrossRef](#)]
54. Breikaa, R.M.; Algandaby, M.M.; El-Demerdas, E.; Abdel-Naim, A.B. Biochanin A protects against acute carbon tetrachloride-induced hepatotoxicity in rats. *Biosci. Biotechnol. Biochem.* **2013**, *77*, 909–916. [[CrossRef](#)]
55. Wu, L.; Ye, Z.; Zhuang, Z.; Gao, Y.; Tang, C.; Zhou, C.; Wang, C.; Zhang, X.; Xie, G.; Liu, J.; et al. Biochanin A reduces inflammatory injury and neuronal apoptosis following subarachnoid hemorrhage via suppression of the TLRs/TIRAP/MyD88/NF-κB pathway. *Behav. Neurol.* **2018**. [[CrossRef](#)] [[PubMed](#)]
56. Piegholdt, S.; Pallauf, K.; Esatbeyoglu, T.; Speck, N.; Reiss, K.; Ruddigkeit, L.; Stocker, A.; Huebbe, P.; Rimbach, G. Biochanin A and prunetin improve epithelial barrier function in intestinal CaCo-2 cells via downregulation of ERK, NF-κB, and tyrosine phosphorylation. *Free Radic. Biol. Med.* **2014**, *70*, 255–264. [[CrossRef](#)] [[PubMed](#)]
57. Qiu, L.; Lin, B.; Lin, Z.; Lin, Y.; Lin, M.; Yang, X. Biochanin A ameliorates the cytokine secretion profile of lipopolysaccharide-stimulated macrophages by a PPARγ-dependent pathway. *Mol. Med. Repor.* **2012**, *5*, 217–222.
58. Guo, M.; Lu, H.; Qin, J.; Qu, S.; Wang, W.; Guo, Y.; Liao, W.; Song, M.; Chen, J.; Wang, Y. Biochanin A provides neuroprotection against cerebral ischemia/reperfusion injury by Nrf2-mediated inhibition of oxidative stress and inflammation signaling pathway in rats. *Med. Sci. Monit.* **2019**, *25*, 8975–8983. [[CrossRef](#)]
59. Yang, G.; Ham, I.; Choi, H.-Y. Anti-inflammatory effect of prunetin via suppression of NF-κB pathway. *Food Chem. Toxicol.* **2013**, *58*, 124–132. [[CrossRef](#)]
60. Hu, H.; Li, H. Prunetin inhibits lipopolysaccharide -induced inflammatory cytokine production and MUC5AC expression by inactivating the TLR4/MyD88 pathway in human nasal epithelial cells. *Biomed. Pharmacother.* **2018**, *106*, 1469–1477. [[CrossRef](#)]
61. Liu, Y.-F.; Bai, Y.-Q.; Qi, M. Daidzein attenuates abdominal aortic aneurysm through NF-κB, p38MAPK and TGF-β1 pathways. *Mol. Med. Rep.* **2016**, *14*, 955–962. [[CrossRef](#)]
62. Atiq, A.; Shal, B.; Naveed, M.; Khan, A.; Ali, J.; Zeeshan, S.; Al-Sharari, S.D.; Kim, Y.S.; Khan, S. Diadzein ameliorates 5-fluorouracil-induced intestinal mucositis by suppressing oxidative stress and inflammatory mediators in rodents. *Eur. J. Pharmacol.* **2019**, *843*, 292–306. [[CrossRef](#)]
63. Tomar, A.; Kaushik, S.; Khan, S.I.; Bisht, K.; Nag, C.N.; Arya, D.S.; Bhatia, J. The dietary isoflavone daidzein mitigates oxidative stress, apoptosis, and inflammation in CDDP-induced kidney injury in rats: Impact on the MAPK signaling pathway. *J. Biochem. Mol. Toxicol.* **2020**, *34*, e22431. [[CrossRef](#)]
64. Zhang, F.; Ru, N.; Shang, X.-H.; Chen, J.-F.; Yan, C.; Li, Y.; Liang, J. Daidzein ameliorates spinal cord ischemia/reperfusion injury-induced neurological function deficits in Sprague-Dawley rats through PI3K/Akt signaling pathway. *Exp. Ther. Med.* **2017**, *14*, 4878–4886. [[CrossRef](#)]
65. Han, S.; Wu, H.; Li, W.; Gao, P. Protective effects of genistein in homocysteine-induced endothelial cell inflammatory injury. *Mol. Cell Biochem.* **2015**, *403*, 43–49. [[CrossRef](#)] [[PubMed](#)]

66. Mansour, D.F.; Saleh, D.O.; Mostafa, R.E. Genistein ameliorates cyclophosphamide-induced hepatotoxicity by modulation of oxidative stress and inflammatory mediators. *Open Access Maced. J. Med. Sci.* **2017**, *5*, 836–843. [[CrossRef](#)] [[PubMed](#)]
67. Du, Z.-R.; Feng, X.-Q.; Li, N.; Qu, J.-X.; Feng, L.; Chen, L.; Chen, W.-F. G protein-coupled estrogen receptor is involved in the anti-inflammatory effects of genistein in microglia. *Phytomedicine* **2018**, *43*, 11–20. [[CrossRef](#)] [[PubMed](#)]
68. Wang, A.; Wei, J.; Lu, C.; Chen, H.; Zhong, X.; Lu, Y.; Li, L.; Huang, H.; Dai, Z.; Han, L. Genistein suppresses psoriasis-related inflammation through a STAT3-NF- $\kappa$ B-dependent mechanism in keratinocytes. *Int. Immunopharmacol.* **2019**, *69*, 270–278. [[CrossRef](#)]
69. Chen, Y.; Le, T.H.; Du, Q.; Zhao, Z.; Liu, Y.; Zou, J.; Hua, W.; Liu, C.; Zhu, Y. Genistein protects against DSS-induced colitis by inhibiting NLRP3 inflammasome via TGR5-cAMP signaling. *Int. Immunopharmacol.* **2019**, *71*, 144–154. [[CrossRef](#)]
70. Gan, M.; Shen, L.; Fan, Y.; Tan, Y.; Zheng, T.; Tang, G.; Niu, L.; Zhao, Y.; Chen, L.; Jiang, D.; et al. MicroRNA-451 and genistein ameliorate nonalcoholic steatohepatitis in mice. *Int. J. Mol. Sci.* **2019**, *20*, 6084. [[CrossRef](#)]
71. Lu, C.; Lv, J.; Jiang, N.; Wang, H.; Huang, H.; Zhang, L.; Li, S.; Zhang, N.; Fan, B.; Liu, X.; et al. Protective effects of genistein on the cognitive deficits induced by chronic sleep deprivation. *Phytother. Res.* **2020**, *34*, 846–858. [[CrossRef](#)]
72. Bhattarai, G.; Poudel, S.B.; Kook, S.-H.; Lee, J.-C. Anti-inflammatory, anti-osteoclastic, and antioxidant activities of genistein protect against alveolar bone loss and periodontal tissue degradation in a mouse model of periodontitis. *J. Biomed. Mat. Res.* **2017**, *195A*, 2510–2521. [[CrossRef](#)]
73. Pummoung, S.; Werawatganon, D.; Klaikeaw, N.; Siriviriyakul, P. Genistein-attenuated hepatic steatosis and inflammation in nonalcoholic steatohepatitis with bilateral ovariectomized rats. *Pharmacogn. Mag.* **2018**, *14*, S20–S24.
74. Xu, L.; Liu, J.; Li, K.; Wang, S.; Xu, S. Genistein inhibits ang II- induced CRP and MMP-9 generations via Er-p38/ERK1/2-PPAR $\gamma$ -NF- $\kappa$ B signaling pathway in rat vascular smooth muscle cells. *Life Sci.* **2019**, *216*, 140–146. [[CrossRef](#)]
75. Yoo, H.; Ku, S.-K.; Baek, Y.-D.; Bae, J.-S. Anti-inflammatory effects of rutin on HMGB1-induced inflammatory responses in vitro and in vivo. *Inflamm. Res.* **2014**, *63*, 197–206. [[CrossRef](#)] [[PubMed](#)]
76. Khajevand-Khazaei, M.-R.; Mohseni-Moghaddam, P.; Hosseini, M.; Gholami, L.; Baluchnejadmojarad, T.; Roghani, M. Rutin, a quercetin glycoside, alleviates acute endotoxemic kidney injury in C57Bl/6 mice via suppression of inflammation and up-regulation of antioxidants and SIRT1. *Eur. J. Pharmacol.* **2018**, *833*, 307–313. [[CrossRef](#)] [[PubMed](#)]
77. Nkpa, K.W.; Onyeso, G.I. Rutin attenuates neurobehavioral deficits, oxidative stress, neuroinflammation and apoptosis in fluoride treated rats. *Neurosci. Lett.* **2018**, *682*, 92–99. [[CrossRef](#)] [[PubMed](#)]
78. Caglayan, C.; Kandemir, F.M.; Yildirim, S.; Kucukler, S.; Eser, G. Rutin protects mercuric chloride-induced nephrotoxicity via targeting of aquaporin 1 level, oxidative stress, apoptosis and inflammation in rats. *J. Trace Elem. Med. Biol.* **2019**, *54*, 69–78. [[CrossRef](#)] [[PubMed](#)]
79. Caglayan, C.; Kandemir, F.M.; Darendelioglu, E.; Yildirim, S.; Kucukler, S.; Dortbudak, M.B. Rutin ameliorates mercuric chloride-induced hepatotoxicity in rats via interfering with oxidative stress, inflammation and apoptosis. *J. Trace Elem. Med. Biol.* **2019**, *56*, 60–68. [[CrossRef](#)] [[PubMed](#)]
80. Nikfarjam, B.A.; Adineh, M.; Hajiali, F.; Nassiri-Asl, M. Treatment with rutin—A therapeutic strategy for neutrophil-mediated inflammation and autoimmune diseases. *J. Pharmacopunct.* **2017**, *20*, 52–56.
81. Cai, C.; Liu, C.; Zhao, L.; Liu, H.; Li, W.; Guan, H.; Zhao, L.; Xiao, J. Effects of taxifolin on osteoclastogenesis in vitro and in vivo. *Front. Pharmacol.* **2018**, *9*, 1286. [[CrossRef](#)]
82. Zhang, H.-Q.; Wang, Y.-J.; Yang, G.-T.; Gao, Q.-L.; Tang, M.-X. Taxifolin inhibits receptor activator of NF- $\kappa$ B ligand-induced osteoclastogenesis of Human bone marrow-derived macrophages in vitro and prevents lipopolysaccharide-induced bone loss in vivo. *Pharmacology* **2019**, *103*, 101–109. [[CrossRef](#)]
83. Pan, S.; Zhao, X.; Ji, N.; Shao, C.; Fu, B.; Zhang, Z.; Wang, R.; Qiu, Y.; Jin, M.; Kong, D. Inhibitory effect of taxifolin on mast cell activation and mast cell-mediated allergic inflammatory response. *Int. Immunopharmacol.* **2019**, *71*, 205–214. [[CrossRef](#)]
84. Hu, C.; Ye, J.; Zhao, L.; Li, X.; Wang, Y.; Liu, X.; Pan, L.; You, L.; Chen, L.; Jia, Y.; et al. 5,7,3',4'-Flavan-on-ol (taxifolin) protects against acetaminophen-induced liver injury by regulating the glutathione pathway. *Life Sci.* **2019**, *236*, 116939. [[CrossRef](#)] [[PubMed](#)]

85. King, F.E.; Jurd, L. The chemistry of extractives from hardwoods. Part VIII. \*the isolation of 5,4'-dihydroxy-7-methoxyisoflavone (prunetin) from the heartwood of *Pterocarpus angolensis* and a synthesis of 7,4' dihydroxy-5-methoxyisoflavone hitherto known as prunetsetin. *J. Chem. Soc.* **1952**, *1952*, 3190–3195.
86. Siddiqui, M.T.; Siddiqui, M. Hypolipidemic principles of *Cicer arietinum*: Biochanin-A and formononetin. *Lipids* **1976**, *11*, 243–246. [[CrossRef](#)] [[PubMed](#)]
87. Raheja, S.; Girdhar, A.; Lather, V.; Pandita, D. Biochanin A: A phytoestrogen with therapeutic potential. *Trends Food Sci. Technol.* **2018**, *79*, 55–66. [[CrossRef](#)]
88. Sarfraz, A.; Javeed, M.; Shah, M.A.; Hussain, G.; Shafiq, N.; Sarfraz, I.; Riaz, A.; Sadiqa, A.; Zara, S.; Kanwal, L.; et al. Biochanin A: A novel bioactive multifunctional compound from nature. *Sci. Total Environ.* **2020**, *722*, 137907. [[CrossRef](#)] [[PubMed](#)]
89. Liggins, J.; Bluck, L.J.C.; Runswick, S.; Atkinson, C.; Coward, W.A.; Bingham, S.A. Daidzein and genistein content of fruits and nuts. *J. Nutr. Biochem.* **2000**, *11*, 326–331. [[CrossRef](#)]
90. Barlow, J.; Johnson, J.A.P.; Scofield, L. *Fact Sheet on the Phytoestrogen Daidzein*; BCERC COTC Fact. Sheet; 2007. Available online: [https://www.zerobreastcancer.org/research/bcerc\\_factsheets\\_phytoestrogen\\_daidzein.pdf](https://www.zerobreastcancer.org/research/bcerc_factsheets_phytoestrogen_daidzein.pdf) (accessed on 29 May 2020).
91. Sun, M.-Y.; Ye, Y.; Xiao, L.; Rahman, K.; Xia, W.; Zhang, H. Daidzein: A review of pharmacological effects. *Afr. J. Tradit. Complement. Altern. Med.* **2016**, *13*, 117–132. [[CrossRef](#)]
92. Barlow, J.; Johnson, J.A.P.; Scofield, L. *Fact Sheet on the Phytoestrogen Genistein*; BCERC COTC Fact. Sheet; 2007. Available online: [https://www.zerobreastcancer.org/research/bcerc\\_factsheets\\_phytoestrogen\\_genistein.pdf](https://www.zerobreastcancer.org/research/bcerc_factsheets_phytoestrogen_genistein.pdf) (accessed on 29 May 2020).
93. Kumar, M.; Singh, K.; Duraisamy, K.; Allam, A.A.; Ajarem, J.; Chow, B.K.C. Protective effect of genistein against compound 48/80 induced anaphylactoid shock via inhibiting MAS related G protein-coupled receptor X2 (MRGPRX2). *Molecules* **2020**, *25*, 1028. [[CrossRef](#)]
94. Polkowski, K.; Mazurek, A.P. Biological properties of genistein. A review of in vitro and in vivo data. *Acta Poloniae Pharm. Drug Res.* **2000**, *57*, 135–155.
95. Tuli, H.S.; Tuorkey, M.J.; Thakral, F.; Sak, K.; Kumar, M.; Sharma, A.K.; Sharma, U.; Jain, A.; Aggarwal, V.; Bishayee, A. Molecular mechanisms of action of genistein in cancer: Recent advances. *Front. Pharmacol.* **2019**, *10*, 1336. [[CrossRef](#)]
96. Al-Dhabi, N.A.; Arasu, M.V.; Park, C.H.; Park, S.U. An up-to-date review of rutin and its biological and pharmacological activities. *EXCLI J.* **2015**, *14*, 59–63.
97. Rauf, A.; Imran, M.; Patel, S.; Muzaffar, R.; Bawazeer, S.S. Rutin: Exploitation of the flavonol for health and homeostasis. *Biomed. Pharmacother.* **2017**, *96*, 1559–1561. [[CrossRef](#)] [[PubMed](#)]
98. Ganeshpurkar, A.; Saluja, A.K. The pharmacological potential of rutin. *Saudi Pharm. J.* **2017**, *25*, 149–164. [[CrossRef](#)] [[PubMed](#)]
99. Gullón, B.; Lú-Chau, T.A.; Moreira, M.T.; Lema, J.M.; Eibes, G. Rutin: A review on extraction, identification and purification methods, biological activities and approaches to enhance its bioavailability. *Trends Food Sci. Technol.* **2017**, *67*, 220–235.
100. Riaz, H.; Raza, S.A.; Aslam, M.M.; Ahmad, M.S.; Ahmad, M.A.; Maria, P. An updated review of pharmacological, standardization methods and formulation development of rutin. *J. Pure App. Microbiol.* **2018**, *12*, 127–132. [[CrossRef](#)]
101. Ghorbani, A. Mechanisms of antidiabetic effects of flavonoid rutin. *Biomed. Pharmacother.* **2017**, *96*, 305–312. [[CrossRef](#)]
102. Manzoni, A.G.; Passos, D.F.; Leitemperger, J.W.; Storck, T.R.; Doleski, P.H.; Jantsch, M.H.; Loro, V.L.; Leal, D.B.R. Hyperlipidemia-induced lipotoxicity and immune activation in rats are prevented by curcumin and rutin. *Int. Immunopharmacol.* **2020**, *81*, 106217. [[CrossRef](#)]
103. Enogieru, A.B.; Haylett, W.; Hiss, D.C.; Bardien, S.; Ekpo, O.E. Rutin as a potent antioxidant: Implications for neurodegenerative disorders. *Oxid. Med. Cell. Long.* **2018**, *2018*. [[CrossRef](#)]
104. Mazumder, M.K.; Borah, A.; Choudhury, S. Inhibitory potential of plant secondary metabolites on anti-Parkinsonian drug targets: Relevance to pathophysiology, and motor and non-motor behavioural abnormalities. *Med. Hypotheses* **2020**, *137*, 109544. [[CrossRef](#)]
105. Harikrishnan, H.; Jantan, I.; Alagan, A.; Haque, M.A. Modulation of cell signaling pathways by *Phyllanthus amarus* and its major constituents: Potential role in the prevention and treatment of inflammation and cancer. *Inflammopharmacology* **2020**, *28*, 1–18. [[CrossRef](#)]

106. Hasumura, M.; Yasuhara, K.; Tamura, T.; Imai, T.; Mitsumori, K.; Hirose, M. Evaluation of the toxicity of enzymatically decomposed rutin with 13-weeks dietary administration to Wistar rats. *Food Chem. Toxicol.* **2004**, *42*, 439–444. [[CrossRef](#)]
107. Boyle, S.P.; Dobson, V.L.; Duthie, S.J.; Hinselwood, D.C.; Kyle, J.A.M.; Collins, A.R. Bioavailability and efficiency of rutin as an antioxidant: A human supplementation study. *Eur. J. Clin. Nutr.* **2000**, *54*, 774–782. [[CrossRef](#)] [[PubMed](#)]
108. Ragheb, S.R.; El Wakeel, L.M.; Nasr, M.S.; Sabri, N.A. Impact of rutin and vitamin C combination on oxidative stress and glycemic control in patients with type 2 diabetes. *Clin. Nutr. ESPEN* **2020**, *35*, 128–135. [[CrossRef](#)] [[PubMed](#)]
109. Kalita, B.; Das, M.K. Rutin-phospholipid complex in polymer matrix for long-term delivery of rutin via skin for treatment of inflammatory diseases. *Artif. Cells NanoMed. Biotechnol.* **2018**, *46*, 541–556. [[CrossRef](#)] [[PubMed](#)]
110. Gupta, M.B.; Bhalla, T.N.; Gupta, G.P.; Mitra, C.R.; Bhargava, K.P. Anti-inflammatory activity of taxifolin. *Jpn. J. Pharmacol.* **1971**, *21*, 377–382. [[CrossRef](#)] [[PubMed](#)]
111. Sunil, C.; Xu, B. An insight into the health-promoting effects of taxifolin (dihydroquercetin). *Phytochemistry* **2019**, *166*, 112066. [[CrossRef](#)] [[PubMed](#)]



© 2020 by the authors. Licensee MDPI, Basel, Switzerland. This article is an open access article distributed under the terms and conditions of the Creative Commons Attribution (CC BY) license (<http://creativecommons.org/licenses/by/4.0/>).







Review

# Genus *Stachys*: A Review of Traditional Uses, Phytochemistry and Bioactivity

Ekaterina-Michaela Tomou, Christina Barda and Helen Skaltsa \*

Department of Pharmacognosy and Chemistry of Natural Products, Faculty of Pharmacy, School of Health Sciences, National & Kapodistrian University of Athens, Panepistimiopolis, Zografou, 15771 Athens, Greece; ktomou@pharm.uoa.gr (E.-M.T.); cbarada@pharm.uoa.gr (C.B.)

\* Correspondence: skaltsa@pharm.uoa.gr; Tel.: +30-2107274593

Received: 11 August 2020; Accepted: 25 September 2020; Published: 29 September 2020

**Abstract: Background:** The genus *Stachys* L. (Lamiaceae) includes about 300 species as annual or perennial herbs or small shrubs, spread in temperate regions of Mediterranean, Asia, America and southern Africa. Several species of this genus are extensively used in various traditional medicines. They are consumed as herbal preparations for the treatment of stress, skin inflammations, gastrointestinal disorders, asthma and genital tumors. Previous studies have investigated the chemical constituents and the biological activities of these species. Thus, the present review compiles literature data on ethnomedicine, phytochemistry, pharmacological activities, clinical studies and the toxicity of genus *Stachys*. **Methods:** Comprehensive research of previously published literature was performed for studies on the traditional uses, bioactive compounds and pharmacological properties of the genus *Stachys*, using databases with different key search words. **Results:** This survey documented 60 *Stachys* species and 10 subspecies for their phytochemical profiles, including 254 chemical compounds and reported 19 species and 4 subspecies for their pharmacological properties. Furthermore, 25 species and 6 subspecies were found for their traditional uses. **Conclusions:** The present review highlights that *Stachys* spp. consist an important source of bioactive phytochemicals and exemplifies the uncharted territory of this genus for new research studies.

**Keywords:** *Stachys* L.; traditional uses; pharmacological activities; phytochemicals; bioactive compounds

## 1. Introduction

The genus *Stachys* L., a large member of the Lamiaceae family, comprises more than 300 species, dispersing in temperate and tropical regions of Mediterranean, Asia, America and southern Africa [1–3]. Up to now, the most established and comprehensive classification of the genus is introduced by Bhattacharjee (1980), categorizing into two subgenera *Betonica* L. and *Stachys* L. [2,3]. The subgenus *Stachys* includes 19 sections, while the subgenus *Betonica* comprises 2 sections [1]. However, the two subgenera present important botanical and phytochemical differences which differentiate them [1,4,5].

*Stachys* species grow as annual or perennial herbs or small shrubs with simple petiolate or sessile leaves. The number of verticillate ranges from four to many-flowered, usually forming a terminal spike-like inflorescence. Calyx tubes are tubular-campanulate, 5 or 10 veined, regular or weakly bilabiate with five subequal teeth. Corolla has a narrow tube, 2-lipped; upper lip flat or hooded and generally hairy, while the lower lip is 3-lobed and glabrous to hairy. The nutlets are oblong to ovoid, rounded at apex [6].

The genus name derived from the Greek word «stachys (=στάχυς)», referring to the type of the inflorescence which is characterized as “spike of corn” and resembles to the inflorescences of the species of genus *Triticum* L. (Gramineae). In ancient times, the name “stachys” referred mainly to the species *Stachys germanica* L. whose inflorescence is like an ear and is covered with off-white trichome [7]. The Latin name of the genus is trifarium (=tomentose) [8].

Historically, Dioscorides mentioned the species *S. germanica* L. with the name “stachys” [9]. However, in late Byzantine era, ‘Nikolaos Myrepsos’ included some species of the genus *Stachys* (*S. germanica* L., *S. officinalis* (L.) Travis, *S. alopecuros* (L.) Benth.) in his medical manuscript “Dynameron”. Precisely, *S. officinalis* and *S. alopecuros* were probably included in 11 recipes, under the names vetoniki, drosiovotanon, lauriolē, kakambri, while *S. germanica* was added in 1 recipe referred as stachys [10].

Many species of the genus are extensively used in traditional medicine of several countries, having various names. For instance, the species *S. recta*, known as yellow woundwort, is called as “erba della paura” (=“herb that keeps away fear”) in Italy, attributing to the anxiolytic properties of its herbal tea, while *S. lavandulifolia* Vahl is called as “Chaaye Koochi” in Iran [11–13]. In addition, herbal preparations of *Stachys* spp. are widely consumed in folk medicine to treat a broad array of disorders and diseases, including stress, skin inflammations, stomach disorders and genital tumors [3,14,15]. Specially, the herbal teas of these plants, known as “mountain tea”, are used for skin and stomach disorders [12,16]. The latter common name could lead to a misinterpretation since the herbal remedies of any *Sideritis* species are globally known with the same name.

In the international literature, *Stachys* species have been broadly studied through several phytochemical and pharmacological investigations, justifying their ethnopharmacological uses. Of special pharmacological interest are considered the anti-inflammatory, antioxidant, analgesic, renoprotective, anxiolytic and antidepressant activity [3,17–19]. The range of the therapeutic properties attributed to these species have been associated to their phytochemical content. Therefore, genus *Stachys* has received much attention for the screening of its bioactive secondary metabolites from different plant parts. In general, more than 200 compounds have been isolated from this genus, belonging to the following important chemical groups; terpenes (e.g., triterpenes, diterpenes, iridoids), polyphenols (e.g., flavone derivatives, phenylethanoid glycosides, lignans), phenolic acids and essential oils [3,5,14,20–22].

Consequently, plants of genus *Stachys* are considered a great source of phytochemicals with therapeutic and economic applications. Given the increasing demand for natural products, many *Stachys* species have been cultivated for uses in traditional medicine, in food market, in cosmetic industry and for ornamental reasons [21,22]. Despite the widely uses of the specific species and the large amount of research studies, there has been no recent comprehensive review including all the latest data of the specific genus and its contribution in medicine. Up to now, the available reviews are centered to the phytochemical profile and biological activities of *Stachys* spp. in correlation to chemotaxonomy approach [3,21–23]. Thus, this review summarizes the current state of knowledge on the traditional uses, phytochemistry, pharmacological activities, clinical studies and toxicity of the genus *Stachys* L.

## 2. Materials and Methods

A comprehensive search on previous studies was conducted on scientific databases such as PubMed, Scopus, Google scholar and Reaxys, including the years 1969–2020. The search terms “Stachys”, “Stachys compounds”, “Stachys phytochemicals”, “Stachys pharmacological” and “Stachys traditional uses” were used for data collection. Searches were performed for other potential studies by manual screening references in the identified studies. In total, 161 publications describing the traditional uses, bioactive compounds, pharmacological properties and the toxicity of the genus *Stachys* were included, excluding articles focuses on taxonomy, botany and agronomy. The traditional medicinal uses of *Stachys* species were reported in Table 1, while the isolated specialized products were categorized by species in Tables 2–15, with the attempt of the discrimination between publications describing metabolites’ isolation (including NMR data) or identification/screening (by means of HPLC, LC-MS, etc.). The chemical structures of the bioactive compounds were showed in Tables 16–29. The reported biological activities of extracts/compounds of the last five years were mentioned by *Stachys* species in Table 30. The general characteristics of the analyzed studies in the current review are showed in Table 31. According to recent publications which support the division of the genus *Stachys* based on Bhattacharjee (1980), the classification in the present review is formed on this latter

study. The species name and their synonyms are quoted as reporting in databases “Plant list” or “Euro + Med” or “IPNI” [24–26].

### 3. Traditional Medicinal Uses of Genus *Stachys*

Several *Stachys* spp. have been used in various ethnomedicines for thousands of years. A plethora studies mentioned their diverse traditional medicinal uses. In the current review, a detailed description of the available data of the traditional uses of *Stachys* spp. is shown in Table 1, reporting 25 species and 6 subspecies of this genus. A careful overview of the specific table reveals that the ethnomedicinal use of *Stachys* spp. is particularly in the area covering of Mediterranean to Iran. Most of the species are consumed as herbal teas for the treatment of infections, common cold, gastrointestinal disorders, inflammation, skin disorders/wounds, asthma and anxiety.

The species *S. affinis* is widely used in Chinese traditional medicine for several uses such as common cold, heart disease, pain relief, antioxidant activity, ischemic brain injury, dementia and gastrointestinal related diseases [27–30]. Another species applied in Chinese folk medicine is *S. geobombycis*, known as DongChongXiaCao, which is recommended as tonic and interestingly, this species is also used in Europe and Japan [22].

In Iran, several species are applied as traditional therapeutic agents in various conditions, including *S. acerosa* [31], *S. fruticulosa* [32], *S. byzantina* (known in Farsi as “lamb’s ear” or “lamb’s tongue” or “sonbolehe noghrehi” or “zabanehe bare”) [33–35], *S. inflata* (local names; “poulk” or “Ghol-e-Argavan”) [31,36,37], *S. lavandulifolia* (known as “Chaaye Koohi”) [12,13,31,38–44], *S. pilifera* [31,45], *S. schtschegleevii* [32,34,46], *S. sylvatica* [47] and *S. turcomanica* [34]. Of considerable interest, *S. sylvatica* (common name “hedge woundwort”) is recommended for the treatment of women with polycystic ovary syndrome (PCOS) [47].

Furthermore, in Turkish folk medicine, the species *S. cretica* subsp. *anatolica*, *S. cretica* subsp. *mersinaea*, *S. iberica* subsp. *georgica*, *S. iberica* subsp. *stenostachya*, *S. kurdica*, *S. lavandulifolia* and *S. obliqua* are used mainly to treat colds, cough, stomach ache and as antipyretic agents, while *S. sylvatica* is applied in cardiac disorders [22,48–50].

In Italy, the infusions of the leaves of *S. annua* and *S. recta* are used to wash the face to reveal headache [51], whereas the aerial parts of the subspecies *S. annua* subsp. *annua*, known as “stregona annual” or “erba strega”, are consumed as anti-catarrhal, febrifuge, tonic and vulnerary [52]. The decoction of the aerial parts of *S. recta* is also consumed as purative and for bad luck/spirit [53,54]. Interestingly, *S. annua* and *S. arvensis*, as well as the subspecies *S. recta* subsp. *recta* are applied against evil eye [11,51,52,55]. Moreover, in an area of central Italy, the species *S. officinalis* is used as oily extract to treat wounds and to dye wood yellow [29,54]. To be mentioned that *S. recta* is listed in the European Pharmacopeia, as well as *S. officinalis* is mentioned in Anthroposophic Pharmaceutical Codex (APC) [22]. However, Gören (2011) reported that some species (e.g., *S. annua*, *S. recta* and *S. sylvatica*) have been mentioned to be poisonous [22].

In North Greece, the infusion and decoction of *S. iva* are consumed against common cold and gastrointestinal disorders [56]. In addition, Fazio et al. (1994) reported different formulations of the Greek species *S. mucronata* applied in Greek traditional medicine. Precisely, the decoction of this species is consumed as an antirheumatic and antineuralgic agent, as well as the juice of fresh leaves is applied in wounds and ulcers. Moreover, the infusion of fresh leaves has antidiarrhoic effect, while the infusion of roots is purgative [57].

In addition to traditional medicinal uses, some species of genus *Stachys* are also consumed as edible plants, vegetables and food additives like the tubers of *S. affinis* (known as Chinese artichoke/chorogi; China/Japan) in China and Japan [22,27], the aerial parts of *S. lavandulifolia* in Iran [31], or the *S. palustris* in Poland [22,58]. The latter species is also included in the diet in Sweden, Ukraine and Great Britain [22]. Moreover, the dried powder of *S. palustris* is used as an additive for bread in Europe, thus it is known as “mayday flour” [22].

The infusion of the aerial parts of *Stachys* sp. LAM is used as traditional remedy for colic, gases and swollen stomach in Peru [22,59]. It is noteworthy to mention that a few species have been used in veterinary such as *S. germanica* and *S. officinalis* [30,54].

Table 1. *Stachys* species with reported traditional medicinal uses.

Species	Geographical Origin of the Reported Traditional Use	Traditional Medicinal Use	Preparation and/or Administration/ Parts of the Plant	Ref.
<i>S. acerosa</i> Boiss.	Iran	Common cold	Decoction	[31]
<i>S. affinis</i> Bunge (= <i>S. sieboldii</i> Miq.)	China	Infections, colds, heart diseases, tuberculosis, pneumonia	Edible food (tubers)	[27,28]
	China	Common cold, heart diseases, for pain relief, as antioxidant, to treat ischemic brain injury, dementia, various gastrointestinal related diseases	-	[29]
<i>S. annua</i> (L.) L	Italy	Headache	Infusion of leaves; also, external use to wash face	[51]
<i>S. annua</i> (L.) L subsp. <i>annua</i>	Italy	Anti-catarhal, febrifuge, tonic, vulnerary, against evil eye	Aerial parts	[52]
<i>S. arvensis</i> (L.) L.	-	Against evil eye	-	[55]
<i>S. balansae</i> Boiss. & Kotschy	-	Hypotonic diseases, cardiac neuroses Anti-inflammatory, antitumor, anticancer, antispasmodic, sedative and diuretic agent, and in the treatment of digestive disorders, wounds, infections, asthma, rheumatic and inflammatory disorders, dysentery, epilepsy, common cold and neuropathy	Liquid and alcoholic extracts	[23]
<i>S. byzantina</i> K. Koch.	-	-	-	[33]
<i>S. cretica</i> subsp. <i>anatolica</i> Rech. f.	Iran	Infected wounds, cutting	Decoction, Demulcent (Leaves)	[34,35]
	Brazil	Antiinflammatory	Infusion of leaves	[60]
<i>S. cretica</i> L. subsp. <i>mersinana</i> (Boiss.) Rech. f.	Turkey	Colds, stomach ailments	Infusion, decoction, internal	[49]
	Turkey	Colds, stomach ailments	Infusion, decoction, internal	[49]
<i>S. fruticulosa</i> M. Bieb.	Iran	Anti- inflammatory	Aerial parts	[32]
<i>S. geobombycis</i> C.Y.Wu	China, Japan and Europe	Tonic	-	[22]
	Iran	Gastrodynia, for painful menstruation	Infusion of flowers	[34]
<i>S. germanica</i> L.	-	Skin disorders (Veterinary use)	-	[55]

Table 1. *Cont.*

Species	Geographical Origin of the Reported Traditional Use	Traditional Medicinal Use	Preparation and/or Administration/ Parts of the Plant	Ref.
<i>S. glutinosa</i> L.	-	As antispasmodic and against chicken louse	-	[55]
<i>S. ibérica</i> subsp. <i>georgica</i> Rech. f.	Turkey	Colds, antipyretic	Decoction, internal	[49]
<i>S. ibérica</i> subsp. <i>stenotachya</i> (Boiss.) Rech. f.	Turkey	Colds, antipyretic, stomach ache	Decoction, internal	[49]
<i>S. inflata</i> Benth.	Iran	Infections, asthmatic, rheumatic, inflammatory disorders	Extracts of aerial parts (non flowering stems)	[36,37]
	Iran	Common cold, Analgesic, high blood pressure	Decoction of aerial parts	[31]
<i>S. ira</i> Griseb.	Greece	Common cold and gastrointestinal disorders	Decoction, infusion	[56]
<i>S. kurdica</i> Boiss & Hohen var. <i>kurdica</i>	Turkey	Cold, stomach-ache	Decoction of branches/flowers Drink one glass of the plant on an empty stomach in the morning	[50]
	Iran	Treat pain and inflammation	Boiled extracts of the aerial parts	[12]
	Iran	Sedative, gastrotonic and spasmolytic properties, treatment of some gastrointestinal disorders, colds and flu	Herbal tea of flowering aerial parts	[13]
<i>S. laurandulifolia</i> Vahl.	Iran	Headache, renal calculus common cold, sedative flavoring agent, abdominal pain	Decoction of aerial parts, Food additive (aerial parts)	[31]
	Turkey	Antipyretic, cough	Decoction, internal	[49]
	Iran	Painful and inflammatory disorders	Boiled extracts of aerial parts	[41]
	Iran	Anxiolytic influence	Herbal tea	[38–44]

Table 1. *Cont.*

Species	Geographical Origin of the Reported Traditional Use	Traditional Medicinal Use	Preparation and/or Administration/ Parts of the Plant	Ref.
<i>S. mucronata</i> Sieb.	Greece	Antirheumatic and antineuralgic remedy	Decoction for massage	[57]
		For wounds and ulcers	Washed with the decoction and covered with a poultice of fresh leaves for cicatrization	
		Antidiarrhoic agent	Infusion of fresh leaves	
<i>S. obliqua</i> Waldst. & Kit.	Turkey	Pugative	Infusion of roots	[22]
		Cold, stomach ailments, fever and cough	Herb, infusion, decoction	
<i>S. officinalis</i> (L.) Trevisan (= <i>S. betonica</i> Benth.; <i>Betonica officinalis</i> L.)	Serbia, Egypt, Montenegro	Skin disorders, antibacterial purposes, against headache, nervous tension, anxiety, menopausal problems, as a tobacco snuff	Tea of dried leaves	[22]
	Italy	Dye wool yellow	Plant	[51]
	Italy	Wounds, in the sores of pack animals	Oily extract of flowers	[54]
	-	Disinfectant, anti-spasmodic and for treatment of wounds	-	[17,61]
<i>S. palustris</i> L.	Poland	Wounds, additive in food	-	[58]
	-	Antiseptic, to relieve gout, to stop haemorrhage	-	[62]
<i>S. parviflora</i> Benth. (= <i>Phlomisioschiema parviflorum</i> (Benth.) Vved.)	-	Cramps, arthralgia, epilepsy, falling sickness, dracunculiasis	-	[63,64]
	Iran	Toothache, edible, tonic, analgesic, edema, expectorant, tussive	Decoction of aerial parts	[31]
<i>S. pilifera</i> Benth.	Iran	Asthma, rheumatoid arthritis and infections	-	[45]
	Anatolia	Antibacterial and healing effects	Tea of the whole part	[21]
<i>S. pumila</i> Banks & Sol.	Anatolia	Sedative, antispasmodic, diuretic and emmenagogic properties	Tea of the leaves	[21]
	-	Bronchitis, asthma, stomach pain and gall and liver disorders	-	[65]



Table 1. *Cont.*

Species	Geographical Origin of the Reported Traditional Use	Traditional Medicinal Use	Preparation and/or Administration/ Parts of the Plant	Ref.
<i>S. recta</i> L.	Europe	Anxiolytic properties	Herbal tea, Oral administration	[11]
	Italy	Headache	Infusion of leaves to wash face	[51]
	Italy	Bad influence/spirit	Decoction	[53]
	Italy	Depurative	Decoction of the aerial parts	[54]
<i>S. recta</i> L. subsp. <i>recta</i>	Italy	Tootache and other pain	Aerial parts applied in body parts	[53]
		against anxiety, pain and toothache	Decoction of flowering tops for bath or to wash face, hands and wrists for 3 days	
<i>S. schtschegleevii</i> Sosn. ex Grossh.	Iran	Antiinflammatory	Aerial parts	[32,34]
	Iran	Infectious diseases of the respiratory tract (for colds and sinusitis), for asthma, rheumatism and other inflammatory disorders	-	[46]
<i>S. sieboldii</i> Miq. (= <i>S. affinis</i> Bunge)	China	Cold and against infections, promoting blood circulation	Dried whole plant	[30]
	-	Disinfectant, anti-spasmodic and for treatment of wounds	-	[17]
<i>S. sylvatica</i> L.	Iran	Diuretic, digestive, emmenagogue, antispasmodic, anti-inflammatory, sedative, tonic properties and for the treatment of women with PCOS	-	[47]
	Turkey	Cardiac disorders	Infusion of aerial parts	[48]
<i>S. tibetica</i> Vatke	India	For fever, cough, phobias and various mental disorder	Whole plant is boiled and made into a decoction. Drink one teacup decoction twice a day to treat fever for 5–7 days	[66]
<i>S. turcomanica</i> Trautv.	Iran	Foot inflammation, toothache, bronchitis and common cold	Infusion, Demulcent, Vapor (Whole plant)	[34]

#### 4. Chemical Composition

Various non-volatile chemical constituents have been reported from different species of genus *Stachys*, categorizing into important chemical groups including fatty acids, alkaloids (e.g., stachydrine, turiaine), triterpenes, phytosterols, phytoecdysteroids, diterpenes, iridoids, flavonoids, phenylpropanoid glucosides, acetophenones, phenylethanoid glycosides, lignans, phenolic acids, megastigmanes and polysaccharides [3,20,21,23,67]. The present survey was focused on all the above groups, excluded fatty acids and alkaloids due to the limited available studies. This section summarizes the phytochemicals from the genus *Stachys* which are mainly responsible for its pharmacological benefits, presented in Tables 2–15. To be mentioned that large number of phytochemicals were mainly discovered from the aerial parts, leaves and a few were found in stems and roots.

Table 2. Flavones isolated from *Stachys* spp.

Species	Plant Parts	Compound	Ref		
<b>Subgenus <i>Stachys</i></b>					
Section <i>Ambleia</i>					
<i>S. aegyptiaca</i> Pers.	Aerial parts	Apigenin (1), Apigenin 7-O-β-D-glucoside (cosmoside) (2), Apigenin 7-O-[6'''-O-acetyl]-allosyl-(1→2)-β-D-glucoside (3), Apigenin 6,8-di-C-glucoside (Vicenin-2) (10), Isoscutellarein 7-O-allosyl-(1→2)-β-D-glucoside (13), Isoscutellarein-7-O-[6'''-O-acetyl]-β-D-allopyranosyl-(1→2)-β-D-glucoside (15), Luteolin (34), Luteolin-7-O-[6'''-O-acetyl]-allosyl-(1→2)-β-D-glucoside (39), 6,8 Di-C-β-D-glucopyranosyl luteolin (Lucenin-2) (40), Chrysoeriol (42)	[68]		
		Hypolaetin 7-O-[6'''-O-acetyl]-allosyl-(1→2)-[3''-O-acetyl]-β-D-glucoside (54), Apigenin 7-O-diglucoside (not determined), Luteolin 7-O-diglucoside (not determined)			
		Apigenin-7-(3'-E-p-coumaroyl)-β-D-glucoside (4), Apigenin 7-(6''-p-coumaroyl)-β-D-glucoside (6)	[69]		
		Isoscutellarein (11), 3',4'-Dimethyl-luteolin-7-O-β-D-glucoside (41)	[70]		
		Isoscutellarein 8-O-(6''-trans-p-coumaroyl)-β-D-glucoside (18)	[71]		
		Scutellarein 7-O-β-D-mannopyranosyl-(1→2)-β-D-glucoside (stachyflaside) (31)	[72]		
		Isoscutellarein (11), 4'-Methyl-isoscutellarein (12), Scutellarein (29)	[73]		
		Apigenin 7-O-β-D-glucoside (2), Apigenin 7-(6''-E-p-coumaroyl)-β-D-glucopyranoside (6), 3'-Hydroxy-isoscutellarein-7-O-[6'''-O-acetyl]-β-D-glucopyranoside (14), Chrysoeriol 7-(6''-E-p-coumaroyl)-β-D-glucopyranoside (47)	[74]		
		Section <i>Campanistrum</i>			
		<i>S. arvensis</i> (L.) L.	Aerial parts #	8-Hydroxyflavone-allosylglucosides (not determined)	[75]

Table 2. *Cont.*

Species	Plant Parts	Compound	Ref
<b>Subgenus <i>Stachrys</i></b>			
Section Campanistrum			
<i>S. ocymastrum</i> (L.) Briq. (= <i>S. hirta</i> L.)	Aerial parts #	8-Hydroxyflavone-allosylglucosides (not determined)	[75]
	Aerial parts	Apigenin (1), Apigenin 7-(6''-E-p-coumaroyl)-β-D-glucopyranoside (6), Isoscutellarein 7-O-allosyl-(1→2)-glucopyranoside (13), Luteolin (34)	[76]
Section Candida			
<i>S. cantida</i> Bory & Chaubard	Aerial parts	Chrysoeriol 7-(3''-E-p-coumaroyl)-β-D-glucopyranoside (46)	[77]
	Aerial parts	Apigenin 7-O-β-D-glucopyranoside (2), Isoscutellarein 7-O-[6'''-O-acetyl]-β-D-allopyranosyl-(1→2)-β-D-glucopyranoside (15), Isoscutellarein 7-O-[6'''-O-acetyl]-allosyl-(1→2)-[6''-O-acetyl]-glucopyranoside (17), 4'-Methyl-isoscutellarein 7-O-β-D-[6''-O-acetyl]-allopyranosyl-(1→2)-β-D-glucopyranoside (21), Chrysoeriol 7-O-β-D-glucopyranoside (43), Chrysoeriol 7-(3''-E-p-coumaroyl)-β-D-glucopyranoside (46), 4'-Methyl-hypolaetin-7-O-[6'''-O-acetyl]-β-D-allopyranosyl-(1→2)-β-D-glucopyranoside (56)	[78]
<i>S. chrysanthia</i> Boiss. and Heldr.	Aerial parts	Isoscutellarein 7-O-[6''-O-acetyl]-allosyl-(1→2)-[6''-O-acetyl]-glucoside (17), Luteolin 7-O-β-D-glucoside (37), Chrysoeriol (42), Chrysoeriol 7-O-β-D-glucopyranoside (43), Chrysoeriol 7-(3''-E-p-coumaroyl)-β-D-glucopyranoside (46)	[77]
<i>S. ita</i> Griseb.	Flowering aerial parts	Apigenin (1), Isoscutellarein 7-O-[6'''-O-acetyl]-β-D-allopyranosyl-(1→2)-β-D-glucopyranoside (15), Isoscutellarein 7-O-[6''-O-acetyl]-β-D-allopyranosyl-(1→2)-[6''-O-acetyl]-β-D-glucopyranoside (17), 4'-Methyl-isoscutellarein 7-O-β-D-[6''-O-acetyl]-allopyranosyl-(1→2)-β-D-glucopyranoside (21), 4'-Methyl-hypolaetin-7-O-[6'''-O-acetyl]-β-D-allopyranosyl-(1→2)-β-D-glucopyranoside (56)	[56]

Table 2. *Cont.*

Species	Plant Parts	Compound	Ref
<b>Subgenus <i>Stachys</i></b>			
Section <i>Corsica</i>			
<i>S. corsica</i> Pers.		Isoscutellarein 7-O-[6'''-O-acetyl]- $\beta$ -D-allopyranosyl-(1 $\rightarrow$ 2)- $\beta$ -D-glucopyranoside (15), 4'-Methyl-isoscutellarein 7-O- $\beta$ -D-[6'''-O-acetyl]-allopyranosyl-(1 $\rightarrow$ 2)- $\beta$ -D-glucopyranoside (21)	[79]
Section <i>Eriostomum</i>			
<i>S. alpina</i> L.	Aerial parts #	8-Hydroxyflavone-allosylglucosides (not determined)	[75]
	Leaves #	Hypolaetin 7-O-acetyl-allosyl-(1 $\rightarrow$ 2)-glucoside (not determined), Isoscutellarein-7-O-acetyl-allosyl-glucoside (not determined), Hypolaetin-4'-methyl-7-O-acetyl-allosyl-glucoside (not determined)	[5]
<i>S. byzantina</i> K. Koch.	Aerial parts	Apigenin (1), Apigenin 7-O- $\beta$ -glucoside (2), Apigenin 7-(6'''-E- <i>p</i> -coumaroyl)- $\beta$ -D-glucopyranoside (6)	[33]
	Aerial parts	Apigenin 7-(6'''-E- <i>p</i> -coumaroyl)- $\beta$ -D-glucopyranoside (6), Isoscutellarein 7-O- $\beta$ -D-allopyranosyl-(1 $\rightarrow$ 2)-[6'''-O-acetyl]- $\beta$ -D-glucopyranoside (16), 4'-Methyl-isoscutellarein-7-O- $\beta$ -D-allopyranosyl-(1 $\rightarrow$ 2)-[6'''-O-acetyl]- $\beta$ -D-glucopyranoside (20)	[80]
<i>S. cretica</i> subsp. <i>smyrnaea</i> Rech. f.	Aerial parts #	Apigenin (1)	[81]
<i>S. germanica</i> L.	Aerial parts #	Hypolaetin 7-allosyl-(1 $\rightarrow$ 2)-glucoside monoacetyl, Isoscutellarein 7-allosyl-(1 $\rightarrow$ 2)-glucoside monoacetyl, Hypolaetin 7-allosyl-(1 $\rightarrow$ 2)-glucoside diacetyl, Isoscutellarein-7-allosyl-(1 $\rightarrow$ 2)-glucoside diacetyl (not determined)	[75]
	Leaves #	Apigenin 7-O-glucoside (2), Chrysoeriol 7-O-acetyl-allosyl-glucoside (not determined), 4'-Methyl-hypolaetin 7-O-acetyl-allosyl-(1 $\rightarrow$ 2)-glucoside (not determined), Apigenin 7-O- <i>p</i> -coumaroyl-glucoside (not determined)	[5]
<i>S. heraclea</i> All.	Aerial parts #	8-Hydroxyflavone-allosylglucosides (not determined)	[75]
<i>S. lanata</i> Crantz. (= <i>S. germanica</i> L. subsp. <i>germanica</i> )	Aerial parts	Apigenin 7-O- $\beta$ -D-glucopyranoside (2), Apigenin 7-(3'''-Z- <i>p</i> -coumaroyl)- $\beta$ -D-glucopyranoside (5), Apigenin 7-(6'''-Z- <i>p</i> -coumaroyl)- $\beta$ -D-glucopyranoside (7), Apigenin 7-O-(3'''-6'''-di-O-E- <i>p</i> -coumaroyl)- $\beta$ -D-glucopyranoside (Anisofolin A) (8), Isoscutellarein 7-O-[6'''-O-acetyl]- $\beta$ -D-allopyranosyl-(1 $\rightarrow$ 2)- $\beta$ -D-glucopyranoside (15), Isoscutellarein 4'-methyl ether 7-O- $\beta$ -D-[6'''-O-acetyl]-allopyranosyl-(1 $\rightarrow$ 2)- $\beta$ -D-glucopyranoside (21), 4'-Methyl-hypolaetin-7-O-[6'''-O-acetyl]- $\beta$ -D-allopyranosyl-(1 $\rightarrow$ 2)- $\beta$ -D-glucopyranoside (56)	[82]

Table 2. *Conti.*

Species	Plant Parts	Compound	Ref
<b>Subgenus <i>Stachyis</i></b>			
Section <i>Eriostomum</i>			
<i>S. spectabilis</i> Choisy ex DC.	Epigeal parts	Isostachyflaside (25), Spectabiflaside (28), Scutellarein 7-O-β-D-mannopyranosyl-(1→2)-β-D-glucopyranoside (stachyflaside) (31)	[83]
<i>S. thirkai</i> K. Koch.	Whole plant <sup>#</sup>	Apigenin (1)	[84]
<i>S. inolea</i> Boiss.	Aerial parts <sup>#</sup>	Apigenin (1), Apigenin-7-O-glucoside (2)	[85]
<i>S. tymphaea</i> Hausskn. (= <i>S. germanica</i> subsp. <i>tymphaea</i> (Hausskn.) R. Bhattacharjee)	Flowering aerial parts	Isoscutellarein 7-O-[6'''-O-acetyl]-β-D-allopyranosyl-(1→2)-β-D-glucopyranoside (15), 4'-Methyl-isoscutellarein 7-O-β-D-[6'''-O-acetyl]-allopyranosyl-(1→2)-β-D-glucopyranoside (21), 4'-Methyl-hypolaetin-7-O-[6'''-O-acetyl]-allopyranosyl-(1→2)-[6''-O-acetyl]-glucopyranoside (58)	[86]
Section <i>Fragilicaulis</i>			
<i>S. submuda</i> Montbret & Aucher ex Benth	Aerial parts	Isoscutellarein 7-O-alloosyl-(1→2)-glucoside <sup>#</sup> (13), Isoscutellarein 7-O-[6'''-O-acetyl]-alloosyl-(1→2)-glucoside (15), 4'-Methyl-isoscutellarein-7-O-β-D-allopyranosyl-(1→2)-β-D-glucoside <sup>#</sup> (19), 4'-Methyl-isoscutellarein 7-O-β-D-[6'''-O-acetyl]-allopyranosyl-(1→2)-β-D-glucoside (21), 4'-Methyl-isoscutellarein-7-O-[6'''-O-acetyl]-alloosyl-(1→2)-[6''-O-acetyl]-glucoside <sup>#</sup> (24)	[87]
Section <i>Olisia</i>			
<i>S. atherocalyx</i> C. Koch		Stachyflaside (31)	[72]
		Diacylstachyflaside (not determined), Diacylspectabiflaside (not determined), Spectabiflaside (28)	[88]
		5,8,4'-Trihydroxy-3'-methoxy-7-O-(β-D-glucopyranosyl-2''-O-β-D-mannopyranosyl)-flavone (Spectabiflaside) (28), Acetyl-sectabiflaside (not determined), Acetyl-isostachyflaside (26), Di-acetyl-isostachyflaside (27), Spectabiflaside (28)	[89]
	Leaves <sup>#</sup>	Isoscutellarein 7-O-[6'''-O-acetyl]-β-D-allopyranosyl-(1→2)-β-D-glucopyranoside (15), 4'-Methyl-isoscutellarein-7-O-β-D-[6'''-O-acetyl]-allopyranosyl-(1→2)-β-D-glucopyranoside (21), 4'-Methyl-hypolaetin-7-O-[6'''-O-acetyl]-β-D-allopyranosyl-(1→2)-β-D-glucopyranoside (56)	[91]
<i>S. angustifolia</i> M. Bieb.		Isoscutellarein 7-O-[6'''-O-acetyl]-β-D-allopyranosyl-(1→2)-β-D-glucopyranoside (15), 4'-Methyl-isoscutellarein 7-O-β-D-[6'''-O-acetyl]-allopyranosyl-(1→2)-β-D-glucopyranoside (21)	[92]

Table 2. *Conti.*

Species	Plant Parts	Compound	Ref
<b>Subgenus <i>Stachyis</i></b>			
Section <i>Olisia</i>			
	Epigeal parts	4'-Methyl-isoscutellarein (12), 7-O-β-D-glucopyranosyl-5,6-dihydroxy-4'-methoxyflavone (Stachamin A) (32), 4'-Methoxy-scutellarein-7-[O-β-D-mannopyranosyl-(1→2)-β-D-glucopyranoside] (Stachannoside B) (33)	[93]
<i>S. annua</i> (L.) L.	Leaves #	Isoscutellarein 7-O-[6'''-O-acetyl]-β-D-allopyranosyl-(1→2)-β-D-glucopyranoside (15), 4'-Methyl-isoscutellarein-7-O-β-D-[6'''-O-acetyl]-allopyranosyl-(1→2)-β-D-glucopyranoside (21), 4'-Methyl-hypolaetin-7-O-[6'''-O-acetyl]-β-D-allopyranosyl-(1→2)-β-D-glucopyranoside (56)	[92]
	Aerial parts	4'-Methyl-isoscutellarein 7-O-β-D-[6'''-O-acetyl]-allopyranosyl-(1→2)-β-D-glucopyranoside (21)	[94]
	Aerial parts	4'-O-Methyl-isoscutellarein-7-O-[4'''-O-acetyl]allopyranosyl-(1→2)-glucopyranoside (Annuoside) (23)	[95]
	Subterranean organs	4'-O-Methyl-isoscutellarein (12), 4'-O-Methyl-isoscutellarein 7-O-(6'''-O-acetyl)allopyranosyl-(1→2)-glucopyranoside (21)	[95]
<i>S. annua</i> (L.) L. subsp. <i>annua</i>	Flowering aerial parts	4'-Methyl-isoscutellarein 7-O-β-D-[6'''-O-acetyl]-allopyranosyl-(1→2)-β-D-glucopyranoside (21), Hypolaetin 7-O-[6'''-O-acetyl]-allosyl-(1→2)-[6'''-O-acetyl]-glucopyranoside (53), 4'-Methyl-hypolaetin-7-O-[6'''-O-acetyl]-β-D-allopyranosyl-(1→2)-β-D-glucopyranoside (56)	[52]
	Leaves #	Isoscutellarein 7-O-[6'''-O-acetyl]-β-D-allopyranosyl-(1→2)-β-D-glucopyranoside (21), 4'-Methyl-hypolaetin-7-O-[6'''-O-acetyl]-β-D-allopyranosyl-(1→2)-β-D-glucopyranoside (56)	[92]
<i>S. bombyicina</i> Boiss.	Aerial parts	Apigenin 7-(6''-E-p-coumaroyl)-β-D-glucopyranoside (6), Stachyspinoside (44)	[96]
<i>S. parolinii</i> Vis.	Leaves #	Isoscutellarein 7-O-[6'''-O-acetyl]-β-D-allopyranosyl-(1→2)-β-D-glucopyranoside (15), 4'-Methyl-hypolaetin-7-O-[6'''-O-acetyl]-β-D-allopyranosyl-(1→2)-β-D-glucopyranoside (56)	[92]
	Leaves #	Isoscutellarein 7-O-[6'''-O-acetyl]-allosyl-(1→2)-[6'''-O-acetyl]-glucoside (17), 4'-Methyl-isoscutellarein 7-O-β-D-[6'''-O-acetyl]-allopyranosyl-(1→2)-β-D-glucopyranoside (21), 4'-Methyl-hypolaetin-7-O-[6'''-O-acetyl]-β-D-allopyranosyl-(1→2)-β-D-glucopyranoside (56)	[92]

Table 2. *Cont.*

Species	Plant Parts	Compound	Ref
<b>Subgenus <i>Sfachrys</i></b>			
Section <i>Olisia</i>			
<i>S. neglecta</i> Klook. ex Kossko (= <i>S. annua</i> (L.) L.)		Apigenin (1), Apigenin 7-O-β-D-glucoside (2), Luteolin (34), Luteolin 7-O-β-D-glucoside (37)	[97]
	Leaves	Isoscutellarein 7-O-[6'''-O-acetyl]-allosyl-(1→2)-[6''-O-acetyl]-glucoside (17), 4'-Methyl-isoscutellarein 7-O-β-D-[6'''-O-acetyl]-allosyl-(1→2)-β-D-glucoside (21), 4'-Methyl-hypolaetin 7-O-[6'''-O-acetyl]-β-D-allosyl-(1→2)-β-D-glucoside (56)	[91,92]
<i>S. recta</i> L.	Aerial parts	4'-Methylisoscuteallarein 7-O-[allosyl-(1→2)]-glucopyranoside (19), 4'-Methyl-isoscuteallarein 7-O-β-D-[6''-O-acetyl]-allopyranosyl-(1→2)-β-D-glucopyranoside (20), 4'-Methyl-isoscuteallarein 7-O-β-D-[6''-O-acetyl]-allosyl-(1→2)-β-D-glucopyranoside (21), 4'-Methyl-isoscuteallarein 7-O-[6''-O-acetyl]-allosyl-(1→2)-[6''-O-acetyl]-glucoside (24), Hypolaetin 7-O-allosyl-(1→2)-glucopyranoside # (50), 4'-Methyl-hypolaetin 7-O-allosyl-(1→2)-glucoside # (55), 4'-Methyl-hypolaetin-7-O-[6''-O-acetyl]-allosyl-(1→2)-glucopyranoside (57), 4'-Methyl-hypolaetin 7-O-[6'''-O-acetyl]-allosyl-(1→2)-[6''-O-acetyl]-glucopyranoside (58)	[14]
	Leaves	Isoscutellarein 7-O-β-D-[6'''-O-acetyl]-allopyranosyl-(1→2)-β-D-glucopyranoside (15), 4'-Methyl-isoscuteallarein-7-O-β-D-[6'''-O-acetyl]-allopyranosyl-(1→2)-β-D-glucopyranoside (21), 4'-Methyl-hypolaetin-7-O-β-D-[6'''-O-acetyl]-allopyranosyl-(1→2)-β-D-glucopyranoside (56)	[92]
	Leaves	Isoscutellarein 7-O-β-D-[6'''-O-acetyl]-allopyranosyl-(1→2)-β-D-glucopyranoside (15), 4'-Methyl-isoscuteallarein-7-O-β-D-[6'''-O-acetyl]-allopyranosyl-(1→2)-β-D-glucopyranoside (21), 4'-Methyl-hypolaetin-7-O-β-D-[6'''-O-acetyl]-allopyranosyl-(1→2)-β-D-glucopyranoside (56)	[92]
	Leaves #	Isoscutellarein 7-O-β-D-[6'''-O-acetyl]-allopyranosyl-(1→2)-β-D-glucopyranoside (15), 4'-Methyl-isoscuteallarein-7-O-β-D-[6'''-O-acetyl]-allopyranosyl-(1→2)-β-D-glucopyranoside (21)	[92]
<i>S. baldaccii</i> (Maly) Hand.—Mazz. (= <i>S. recta</i> L. subsp. <i>baldaccii</i> (K. Maly) Hayek)	Leaves #	Isoscutellarein 7-O-β-D-[6'''-O-acetyl]-allopyranosyl-(1→2)-β-D-glucopyranoside (15), 4'-Methyl-isoscuteallarein-7-O-β-D-[6'''-O-acetyl]-allopyranosyl-(1→2)-β-D-glucopyranoside (21)	[92]



Table 2. *Cont.*

Species	Plant Parts	Compound	Ref	
<b>Subgenus <i>Stachys</i></b>				
Section <i>Olisia</i>				
<i>S. spinosa</i> L.	Aerial parts	Chrysoeriol 7-O-[6'''-O-acetyl-alloxy]-(1→2)-glucoside (Stachyspinoside) (44)	[98]	
	Aerial parts	Chrysoeriol 7-O-[6''-O-acetyl-alloxy]-(1→2)-glucoside (Isostachyspinoside) (45)	[99]	
	Leaves #	Isoscutellarein 7-O-[6'''-O-acetyl]-β-D-allopyranosyl-(1→2)-β-D-glucopyranoside (15), 4'-Methyl-isoscutellarein 7-O-β-D-[6''-O-acetyl]-allopyranosyl-(1→2)-β-D-glucopyranoside (21)	[92]	
<i>S. tetragona</i> Boiss. & Hayek	Aerial parts	Isoscutellarein 7-O-[6'''-O-acetyl]-β-D-allopyranosyl-(1→2)-β-D-glucopyranoside (15), Isoscutellarein 7-O-[6''-O-acetyl]-β-D-alloxy-(1→2)-[6''-O-acetyl]-β-D-glucopyranoside (17)	[100]	
	Section <i>Swainsoniina</i>			
<i>S. anisochila</i> Vis. & Pantic	Leaves	Isoscutellarein 7-O-β-D- allopyranosyl-(1→2)-β-D-glucopyranoside (13), Isoscutellarein 7-O-[6''-O-acetyl]-β-D-allopyranosyl-(1→2)-β-D-glucopyranoside (15), Isoscutellarein 7-O-[6''-O-acetyl]-β-D-alloxy-(1→2)-[6''-O-acetyl]-β-D-glucopyranoside (17), 4'-Methyl-isoscutellarein-7-O-β-D-allopyranosyl-(1→2)-β-D-glucopyranoside (19), Hypolaetin 7-O-[6''-O-acetyl]-β-D-allopyranosyl-(1→2)-β-D-glucopyranoside (51), Hypolaetin 7-O-[6''-O-acetyl]-β-D-allopyranosyl-(1→2)-[6''-O-acetyl]-β-D-glucopyranoside (53), 4'-Methyl-hypolaetin-7-O-[6''-O-acetyl]-β-D-allopyranosyl-(1→2)-β-D-glucopyranoside (56), 4'-Methyl-hypolaetin 7-O-[6''-O-acetyl]-β-D-alloxy-(1→2)-[6''-O-acetyl]-β-D-glucopyranoside (58)	[101]	
		Leaves	Apigenin 7-O-(p-coumaroyl)-β-D-glucopyranoside (not determined)	[5]
		Aerial parts #	8-Hydroxyflavone-alloxyglucosides (not determined)	[75]
		Leaves #	Isoscutellarein 7-O-β-D-[6''-O-acetyl]-β-D-allopyranosyl-(1→2)-β-D-glucopyranoside (15), 4'-Methyl-isoscutellarein-7-O-β-D-[6''-O-acetyl]-β-D-allopyranosyl-(1→2)-β-D-glucopyranoside (21)	[92]
		Aerial parts	Apigenin (1), Apigenin 7-O-β-D-glucopyranoside (2), Apigenin 7-O-β-D-glucoside (2), Luteolin 7-O-β-D-glucopyranoside (37), Chrysoeriol (42), Chrysoeriol 7-O-β-D-glucopyranoside (43), Stachyspinoside (44)	[102]
<i>S. swainsonii</i> subsp. <i>argolica</i> (Boiss.) Phitos and Damboldt	Aerial parts	Apigenin (1), Luteolin 7-O-β-D-glucopyranoside (37), Chrysoeriol (42), Chrysoeriol-7-O-β-D-glucopyranoside (43), Chrysoeriol 7-(3''-E-p-coumaroyl)-β-D-glucopyranoside (46)	[102]	
	Aerial parts	Apigenin (1), Apigenin 7-O-β-D-glucopyranoside (2), Luteolin 7-O-β-D-glucopyranoside (37), Chrysoeriol-7-O-β-D-glucopyranoside (43), Stachyspinoside (44)	[102]	

Table 2. *Cont.*

Species	Plant Parts	Compound	Ref
<b>Subgenus <i>Stachys</i></b>			
Section Swainsomiana			
<i>S. swainsonii</i> subsp. <i>scymonica</i> (Boiss.) Phitos and Damboldt	Aerial parts	Apigenin (1), Apigenin 7-O- $\beta$ -D-glucopyranoside (2), Luteolin 7-O- $\beta$ -D-glucopyranoside (37), Chrysoeriol-7-O- $\beta$ -D-glucopyranoside (43), Stachyspinoside (44)	[102]
<i>S. ionica</i> Halácsy	Aerial parts	Apigenin (1), Apigenin 7-(6''-E- <i>p</i> -coumaroyl)- $\beta$ -D-glucopyranoside (6), Isoscutellarein 7-O-[6''-O-acetyl]- $\beta$ -D-allopyranosyl-(1 $\rightarrow$ 2)- $\beta$ -D-glucopyranoside (15), 4'-Methyl-isoscutellarein 7-O- $\beta$ -D-[6''-O-acetyl]- $\beta$ -D-allopyranosyl-(1 $\rightarrow$ 2)- $\beta$ -D-glucopyranoside (21)	[20]
Section <i>Stachys</i>			
<i>S. sieboldii</i> Miq. (= <i>S. affinis</i> Bunge)	Aerial parts	Isoscutellarein 7-O-[6'''-O-acetyl]- $\beta$ -D-allopyranosyl-(1 $\rightarrow$ 2)- $\beta$ -D-glucoside (15), 4'-Methyl-isoscutellarein 7-O-[6'''-O-acetyl]- $\beta$ -D-allopyranosyl-(1 $\rightarrow$ 2)- $\beta$ -D-glucoside (21)	[20]
<i>S. miathlesii</i> Noé	Aerial parts	Apigenin 7-(6''-E- <i>p</i> -coumaroyl)- $\beta$ -D-glucopyranoside (6), Isoscutellarein 7-O-[6'''-O-acetyl]- $\beta$ -D-allopyranosyl-(1 $\rightarrow$ 2)- $\beta$ -D-glucopyranoside (15)	[103]
<i>S. palustris</i> L.	Leaves #	5-(glycuroglucosyl)-7-methoxybaicalein (Palustrin) (63), 5-(glucuronosyl)-7-methoxybaicalein (Palustrinose) (64)	[104]
	Aerial parts #	Vicenin-2 (10), Apigenin 7-O- <i>p</i> -coumaroyl- $\beta$ -D-glucopyranoside (not determined)	[5]
<i>S. sylvatica</i> L.	Leaves #	8-Hydroxyflavone-allopyranosyl-glucosides (not determined), Chrysoeriol 7-O-acetylallopyranosylglucoside (not determined), Apigenin 7-O- <i>p</i> -coumaroyl- $\beta$ -D-glucopyranoside (not determined)	[75]
<i>S. plumosa</i> Griseb.	Leaves #	Apigenin-7-O- $\beta$ -D-glucoside (2), Luteolin 7-O- $\beta$ -D-glucoside (37), Chrysoeriol 7-O-acetyl-allopyranosyl-glucoside (not determined), Isoscutellarein 7-O-acetyl-allopyranosyl-glucoside (not determined), Apigenin 7-O- <i>p</i> -coumaroyl- $\beta$ -D-glucopyranoside (not determined)	[5]
Section <i>Zietenia</i>			
<i>S. larundatifolia</i> Vahl.	Aerial parts	Apigenin (1), Hydroxygenkwanin (Luteolin 7-Methyl ether) (35), Chrysoeriol (42)	[13]
<i>S. fibetica</i> Vatke	Roots	Apigenin 7-O- $\beta$ -D-glucoside (2)	[66]

Table 2. *Cont.*

Species	Plant Parts	Compound	Ref
<b>Subgenus <i>Betonica</i></b>			
Section <i>Betonica</i>			
<i>S. alopecuroides</i> (L.) Benth.	Aerial parts	<i>p</i> -coumaroyl-glucosides (not determined) # Isoscutellarein 7-O-glucoside (11a), Luteolin 7-O-glucuronide (36), Luteolin 7-O-glucoside (37), Chrysoeriol 7-O-glucoside (43), Hypolaetin 7-O-glucoside (49), Hypolaetin 7-O-glucuronide (49a), Selgin 7-O-glucoside (59), Tricin 7-O-glucuronide (60), Tricin 7-O-glucoside (61), Apigenin 7-O- <i>p</i> -coumaroyl glucopyranoside (not determined)	[75]
	Leaves #		[5]
<i>S. foliosa</i> Regel. (= <i>S. betoniciflora</i> Rupr.; <i>Betonica foliosa</i> Rupr.)		Four flavonoids (not determined)	[105]
<i>S. monieri</i> (Gouan) P.W. Ball. (= <i>S. officinalis</i> (L.) Trevis subsp. <i>officinalis</i> )	Aerial parts	<i>p</i> -coumaroyl-glucosides (not determined) #	[75]
<i>S. officinalis</i> (L.) Trevis (= <i>Betonica officinalis</i> L.)		Apigenin (1), 5, 6, 4'-trihydroxyflavone-7-O- $\beta$ -D-glucoside (30)	[20]
	Leaves #	Apigenin 8-C-glucoside (Vitexin) (9), Luteolin 7-O-glucuronide (36), Luteolin 6-C-glucoside (isoorientin) (38), Tricin 7-O-glucuronide (60), Tricin 7-O-glucoside (61), Tricetin 3',4',5'-trimethyl-7-O-glucoside (62), Apigenin 7-O- <i>p</i> -coumaroyl glucopyranoside (not determined)	[5]
	Aerial parts	<i>p</i> -coumaroyl-glucosides (not determined) #	[75]

Table 2. *Cont.*

Species	Plant Parts	Compound	Ref
<b>Subgenus <i>Betonica</i></b>			
Section <i>Macrostachya</i>			
<i>S. scardica</i> Griseb. (= <i>Betonica scardica</i> Griseb.)	Leaves #	Apigenin 8-C-glucoside (9), Luteolin 7-O-glucoside (37), Luteolin 6-C-glucoside (38), Hypolaetin 7-O-glucoside (49), Selgin 7-O-glucoside (59), Tricin 7-O-glucuronide (60), Tricin 7-O-glucoside (61), Tricetin 3',4',5'-trimethyl-7-O-glucoside (isolation) (62), Apigenin 7-O- <i>p</i> -coumaroyl glucopyranoside (not determined)	[5]

# identified compounds by means of HPLC, LC-MS, etc.

Table 3. Poly-methylated flavonoids from *Stachys* spp.

Species	Plant Parts	Compound	Ref
<b>Subgenus <i>Stachys</i></b>			
Section Ambleia			
<i>S. aegyptiaca</i> Pers.	Aerial parts	Xanthomicrol (69), Sideritiflavone (70), 5-Hydroxy-6,7,8,3',4'-pentamethoxyflavone (75), 5,4'-Dihydroxy-6,7,8,3'-tetramethoxyflavone (76), 5,3',4'-Trihydroxy-3,6,7,8-tetramethoxyflavone (82), Calycopterin (83), Chryso-splenetin (84), 5-Hydroxy-3,6,7,8,4'-pentamethoxyflavone (88), 5,4'-Dihydroxy-3,6,7,8,3'-pentamethoxyflavone (89)	[68]
	Aerial parts	5,7,3'-Trihydroxy-6,4'-dimethoxyflavone (67), 5,7,3'-Trihydroxy-6,8,4'-trimethoxyflavone (68)	[70]
	Aerial parts	Xanthomicrol (69), Eupatilin-7-methyl ether (73), Calycopterin (83), 5-Hydroxy-3,6,7,4'-tetramethoxy flavone (85), 5,8-Dihydroxy-3,6,7,4'-tetramethoxy flavone (86), 5-Hydroxy-auranetin (88), 4'-Hydroxy-3,5,7,3'- tetramethoxy flavone (90)	[106]
<i>S. schtschegleevii</i> Sosn. ex Grossh.	Stems	Cirsimaritin (66), Xanthomicrol (69)	[74]
Section Aucheriana			
<i>S. glutinosa</i> L.		Xanthomicrol (69), Sideritiflavone (70), 8-Methoxycirsilineol (71), Eupatilin (72a)	[107]
Section Candida			
<i>S. candida</i> Bory & Chaubard	Aerial parts	Xanthomicrol (69), Calycopterin (83)	[77,78]
<i>S. chrysantha</i> Boiss. and Heldr.	Aerial parts	Xanthomicrol (69), Calycopterin (83)	[77]
Section Swainsoniana			
<i>S. swainsonii</i> Benth. subsp. <i>swainsonii</i>	Aerial parts	Eupatorin (72), Penduletin (81), 5-Hydroxyauranetin (88)	[102]
<i>S. swainsonii</i> subsp. <i>argolica</i> (Boiss.) Phitos and Damboldt	Aerial parts	Xanthomicrol (69), Eupatorin (72), Salvigenin (74)	[102]
<i>S. swainsonii</i> subsp. <i>melangavica</i> D. Persson	Aerial parts	Eupatorin (72), 5-Hydroxyauranetin (88)	[102]
<i>S. swainsonii</i> subsp. <i>scyronica</i> (Boiss.) Phitos and Damboldt	Aerial parts	Eupatorin (72), Penduletin (81), 5-Hydroxyauranetin (88)	[102]
<i>S. ionica</i> Halácsy	Aerial parts	Xanthomicrol (69), Salvigenin (74), Chryso-splenetin (84), 5-Hydroxy-3,6,7,4'-tetramethoxyflavone (85), Casticin (87)	[20]
<i>S. lavandulifolia</i> Vahl.	Aerial parts	Velutin (Luteolin 7,3'-dimethyl ether) (65), Viscosine (5,7,4'-trihydroxy-3,6-dimethoxyflavone (78), Kumatakenin (Kaempferol 3,7-dimethyl ether) (79), Pachypodol (Quercetin 3,7,3'-trimethyl ether) (80), Penduletin (81), Chryso-splenetin (84),	[13]
<b>Subgenus <i>Betonica</i></b>			
Section <i>Betonica</i>			
<i>S. officinalis</i> (L.) Trevis = ( <i>Betonica officinalis</i> L.)		5,4'-Dihydroxy-7,3',5'-trimethoxyflavone (77)	[20]

**Table 4.** Flavonols from *Stachys* spp.

Species	Plant Parts	Compound	Ref
<b>Subgenus <i>Stachys</i></b>			
Section <i>Eriostomum</i>			
<i>S. cretica</i> subsp. <i>smyrnaea</i> Rech. f.	Aerial parts <sup>#</sup>	Kaempferol (91)	[81]
Section <i>Olisia</i>			
<i>S. tetragona</i> Boiss. & Hayek	Aerial parts	Kaempferol (91)	[100]
Section <i>Swainsoniana</i>			
<i>S. swainsonii</i> Benth. subsp. <i>swainsonii</i>	Aerial parts	Isorhamnetin (92)	[99]
<i>S. swainsonii</i> subsp. <i>argolica</i> (Boiss.) Phitos and Damboldt	Aerial parts	Isorhamnetin (92)	[99]
Section <i>Stachys</i>			
<i>S. palustris</i> L.	Leaves <sup>#</sup>	Quercetin-3-O-rutinoside (93), Isorhamnetin-3-O-rutinoside (94)	[5]

<sup>#</sup> identified compounds by means of HPLC, LC-MS, etc.

**Table 5.** Flavanones from *Stachys* spp.

Species	Plant Parts	Compound	Ref
<b>Subgenus <i>Stachys</i></b>			
Section <i>Ambleia</i>			
<i>S. aegyptiaca</i> Pers.	Aerial parts	Naringenin (96)	[69]
Section <i>Eriostomum</i>			
<i>S. cretica</i> subsp. <i>smyrnaea</i> Rech. f.	Aerial parts <sup>#</sup>	Hesperidin (97)	[81]
Section <i>Swainsoniana</i>			
<i>S. swainsonii</i> Benth. subsp. <i>swainsonii</i>	Aerial parts	Eriodictyol (95)	[102]
<i>S. swainsonii</i> subsp. <i>argolica</i> (Boiss.) Phitos and Damboldt	Aerial parts	Eriodictyol (95)	[102]
<i>S. swainsonii</i> subsp. <i>melangavica</i> D. Persson	Aerial parts	Eriodictyol (95)	[102]
<i>S. swainsonii</i> subsp. <i>scyronica</i> (Boiss.) Phitos and Damboldt	Aerial parts	Eriodictyol (95)	[102]

**Table 6.** Biflavonoid from *Stachys* spp.

Species	Plant Parts	Compound	Ref
<b>Subgenus <i>Stachys</i></b>			
Section <i>Ambleia</i>			
<i>S. aegyptiaca</i> Pers.	Aerial Parts	Diapigenin-7-O-(6''-trans,6''-cis- <i>p</i> , <i>p'</i> -dihydroxy- $\mu$ -truxinyl)glucoside (stachysetin) (98)	[69]
Section <i>Eriostomum</i>			
<i>S. lanata</i> Crantz. (= <i>S. germanica</i> L. subsp. <i>germanica</i> )	Aerial parts	Stachysetin (98)	[82]
Section <i>Candida</i>			
<i>S. iva</i> Griseb.	Flowering aerial parts	Stachysetin (98)	[56]

**Table 7.** Phenolic derivatives from *Stachys* spp.

Species	Plant Parts	Compound	Ref
<b>Subgenus <i>Stachys</i></b>			
Section <i>Candida</i>			
<i>S. candida</i> Bory & Chaubard	Aerial parts	Chlorogenic acid (103)	[78]
<i>S. iva</i> Griseb	Flowering aerial parts	Chlorogenic acid (103)	[56]
Section <i>Eriostomum</i>			
<i>S. cretica</i> subsp. <i>smyrnaea</i> Rech. f.	Aerial parts #	Chlorogenic acid (103)	[81]
<i>S. cretica</i> subsp. <i>vacillans</i> Rech. f.	Aerial parts #	Vanillic acid (100), Syringic acid (101), Chlorogenic acid (103)	[105]
<i>S. cretica</i> subsp. <i>mersinaea</i> (Boiss.) Rech. f.	Aerial parts #	Chlorogenic acid (103)	[108]
<i>S. lanata</i> Crantz. (= <i>S. germanica</i> L. subsp. <i>germanica</i> )	Roots	Chlorogenic acid (103)	[82]
<i>S. tmolea</i> Boiss	Aerial parts #	4-Hydroxybenzoic acid (99), Chlorogenic acid (103)	[85]
<i>S. thirkei</i> K. Koch	Aerial parts #	Chlorogenic acid (103)	[84]
<i>S. germanica</i> L. subsp. <i>salviifolia</i> (Ten.) Gams.	Aerial parts	Arbutin (107)	[109]
Section <i>Olisia</i>			
<i>S. atherocalyx</i> C. Koch.		Neochlorogenic acid (105), <i>p</i> -Coumaric acid (106), Caffeic acid (108)	[110]
<i>S. recta</i> L.	Aerial parts #	1-Caffeoylquinic acid (102), Chlorogenic acid (103), 4-Caffeoylquinic acid (104)	[14]
Section <i>Stachys</i>			
<i>S. palustris</i> L.		1-Caffeoylquinic acid (102), Chlorogenic acid (103), 4-Caffeoylquinic acid (104), Caffeic acid (108)	[104]
		Cryptochlorogenic acid (104), Neochlorogenic acid (105)	[23]
<b>Subgenus <i>Betonica</i></b>			
Section <i>Betonica</i>			
<i>S. officinalis</i> L. (= <i>Betonica officinalis</i> L.)	Leaves #	Chlorogenic acid (103)	[111]

# identified compounds by means of HPLC, LC-MS, etc.

**Table 8.** Acetophenone glycosides from *Stachys* spp.

Species	Plant Parts	Compound	Ref
<b>Subgenus <i>Stachys</i></b>			
Section <i>Eriostomum</i>			
<i>S. lanata</i> Crantz. (= <i>S. germanica</i> L. subsp. <i>germanica</i> )	Roots	Androsin (109), Neolloydosin (110), Glucoacetosyringone (111)	[82]

**Table 9.** Lignans from *Stachys* spp.

Species	Plant Parts	Compound	Ref
<b>Subgenus <i>Stachys</i></b>			
Section <i>Stachys</i>			
<i>S. mialhesii</i> Noé	Aerial Parts	(+)-Sesamin (112), (+)-Paulownin (113)	[103]
Section <i>Olisia</i>			
<i>S. tetragona</i> Boiss. & Heldr.	Aerial parts	(7S-8R)-Urolignoside (114)	[100]

Table 10. Phenylethanoid glycosides from *Stachyis* spp.

Species	Plant Parts	Compound	Ref
<b>Subgenus <i>Stachyis</i></b>			
Section <i>Ambleia</i>			
<i>S. schischgeleitii</i> Sosn. ex Crossh.	Stems	Acteoside (118), Betunyoside F (128)	[74]
Section <i>Candida</i>			
<i>S. candida</i> Bory & Chaubard	Aerial parts	Acteoside (118)	[78]
<i>S. ita</i> Griseb.	Flowering aerial parts	Acteoside (118), Leucoceptoside A (131), Lavandulifolioside (129)	[56]
Section <i>Eriostomum</i>			
<i>S. byzantina</i> K. Koch	Aerial parts	Verbasoside (118), 2'-O-Arabinosyl verbasoside (122), Aeschynanthoside C (133)	[33]
<i>S. cretica</i> L. subsp. <i>vacillans</i> Rech. f.	Aerial parts #	Verbasoside (118)	[112]
<i>S. germanica</i> L. subsp. <i>salvifolia</i> (Zen.) Gams	Aerial parts	Verbasoside (118)	[109]
	Aerial parts	Leonoside B (134), Martynoside (135)	[82]
<i>S. lanata</i> Crantz (= <i>S. germanica</i> L. subsp. <i>germanica</i> )	Roots	Rhodioloside (115), Verbasoside (116), Verbasoside (118), Isoacteoside (119), Darendoside B (120), Campneoside II (121), 2-Phenylethyl-D-xylopyranosyl-(1→6)-D-gluco-pyranoside (117), Campneoside I (136)	[82]
Section <i>Olisia</i>			
<i>S. tymphaea</i> Hausskn. (= <i>S. germanica</i> subsp. <i>tymphaea</i> (Hausskn.) R. Bhattacharjee)	Flowering aerial parts	Verbasoside (118), Stachyoside A (129)	[86]
<i>S. recta</i> L.	Aerial parts	Acteoside (118), Isoacteoside (119), β-OH-Acteoside (121), Betunyoside E (127), Campneoside I (136), Forsythoside B (137), β-OH-Forsythoside B methyl ether (138)	[14]
<i>S. tetragona</i> Boiss. & Heldr.	Aerial parts	Acteoside (118), Betonioside F (128), Leucoceptoside A (131), Stachyoside D (134), Forsythoside B (137), Lamio-phioside A (141)	[100]



Table 10. Cont.

Species	Plant Parts	Compound	Ref
<b>Subgenus <i>Stachys</i></b>			
Section <i>Stachys</i>			
<i>S. affinis</i> Bunge (= <i>S. sieboldii</i> Miq.)	Tubers	Acteoside (118), Leucosceptoside A (131), Martynoside (135)	[27]
	Whole plants	Stachyosides A (129), B (139), C (140) Acteoside (118), Campneoside II (121), Lavandulifolioside (129), Leonoside A (139)	[113] [114]
Section <i>Zietenia</i>			
<i>S. lavandulifolia</i> Vahl	Aerial parts	Acteoside (118), Lavandulifolioside (129)	[115]
	Aerial parts	Verbascoside (118), Lavandulifolioside A (129), Lavandulifolioside B (130), Leucosceptoside A (131)	[12]
	Aerial parts	Acteoside (118)	[116]
<b>Subgenus <i>Betonica</i></b>			
Section <i>Betonica</i>			
<i>S. macrantha</i> (C. Koch.) Steam (= <i>Betonica grandiflora</i> Willd.)	Aerial parts	Verbascoside (118), Leucosceptoside A (131), Martynoside (135), Lavandulifolioside (129)	[117]
	Aerial parts	Acteoside (118), Acteoside isomer (isoacteoside) (119), Campneoside II (121), Betoniosides A-F (123–128), Leucosceptoside B (132), Forsythoside B (137)	[118]
<i>S. alopecuroides</i> (L.) Benth subsp. <i>ditulsa</i> (Ten.) Grande	Flowering aerial parts	Verbascoside (118)	[119]
<b>Former <i>Stachys</i> species</b>			
<i>S. parviflora</i> Benth. (= <i>Ptilonidoschema parviflorum</i> (Benth.) Vved.)	Whole plant	Parvifloroside A (142), Parvifloroside B (143)	[120]

# identified compounds by means of HPLC, LC-MS, etc.

**Table 11.** Phenylpropanoid glucosides from *Stachys* spp.

Species	Plant Parts	Compound	Ref
<b>Subgenus <i>Stachys</i></b>			
Section Eriostomum			
<i>S. lanata</i> Crantz. (= <i>S. germanica</i> L. subsp. <i>germanica</i> )	Roots	Coniferin (144), Syringin (145)	[82]

**Table 12.** Iridoids from *Stachys* spp.

Species	Plant Parts	Compound	Ref
<b>Subgenus <i>Stachys</i></b>			
Section Ambleia			
<i>S. inflata</i> Benth.		Ajugol (146), Ajugoside (147),	[121]
Section Aucheriana			
<i>S. glutinosa</i> L.	Aerial parts	Harpagide (148), Acetylharpagide (150), Monomelittoside (165), Melittoside (166), Allobetonicoside (161), 5-Allosyloxy-aucubin (167)	[122]
Section Campanistrum			
<i>S. ocymastrum</i> (L.) Briq. (= <i>S. hirta</i> L.)	Leaves	6 $\beta$ -Acetoxypolamiide (172), 6 $\beta$ -Hydroxypolamiide (173), Ipolamiide (174), Ipolamiidoside (175), Lamiide (176)	[123]
Section Candida			
<i>S. iva</i> Griseb.	Flowering Aerial parts	Harpagide (148), 8-Acetylharpagide (150), 8- <i>Epi</i> -loganic acid (157), Gardoside (160), 8- <i>Epi</i> -loganin (159), Monomelittoside (165), Melittoside (166)	[56]
Section Corsica			
<i>S. corsica</i> Pers.		Harpagide (148), Acetylharpagide (150)	[79]
Section Eriostomum			
<i>S. alpina</i> L.	Stems, Leaves #	Ajugoside (147), Harpagide (148), Acetylharpagide (150), Harpagoside (154), Aucubin (164), Catalpol (163)	[124]
<i>S. balansae</i> Boiss. & Kotschy		Ajugol (146), Ajugoside (147)	[125]
<i>S. germanica</i> L.		Harpagide (148)	[125]
<i>S. germanica</i> L.	Leaf, Inflorescence #	Ajugoside (147), Harpagide (148), Acetylharpagide (150), Harpagoside (154), Aucubin (164), Catalpol (163)	[124]
<i>S. spectabilis</i> Choisy ex DC.		Ajugol (146), Ajugoside (147), Harpagide (148)	[125]
<i>S. byzantina</i> K. Koch.	Aerial parts #	Ajugoside (147), Harpagide (148), Acetylharpagide (150), Harpagoside (154), Catalpol (163), Aucubin (164)	[124]

Table 12. Cont.

Species	Plant Parts	Compound	Ref
<b>Subgenus <i>Stachys</i></b>			
Section <i>Eriostomum</i>			
<i>S. germanica</i> L. subsp. <i>salviifolia</i> (Zen.) Gams	Flowering Aerial parts	Harpagide (148)	[86]
	Aerial parts	Ajugol (146), Harpagide (148), 7-Hydroxyharpagide (149), 5-Alloxyloxy-aucubin (167)	[109]
<i>S. lanata</i> Crantz. (= <i>S. germanica</i> L. subsp. <i>germanica</i> )	Roots	Stachysosides E (168), G (170), H (171)	[82]
	Aerial parts	Stachysosides E (168), F (169)	[82]
<i>S. tymphaea</i> Hausskn. (= <i>S. germanica</i> subsp. <i>tymphaea</i> (Hausskn.) R. Bhattacharjee)	Aerial parts	Harpagide (148)	[86]
Section <i>Olisia</i>			
<i>S. angustifolia</i> M. Bieb.		Ajugoside (147), Acetylharpagide (150), Harpagide (148), Melittoside (166)	[92]
<i>S. annua</i> (L.) L.		Ajugoside (147), Acetylharpagide (150), Melittoside (166)	[92]
<i>S. atherocalyx</i> C. Koch.		Ajugol (146), Harpagide (148), Acetylharpagide (150), Melittoside (166)	[92, 125]
		Harpagide (148), Ajugol (146), Acetylharpagide (150), Melittoside (166)	[92]
<i>S. iberica</i> M. Bieb.		Ajugol (146), Ajugoside (147), Harpagide (148), Acetylharpagide (150)	[121]
<i>S. recta</i> L.	Leaves	Ajugol (146), Harpagide (148), Acetylharpagide (150), Melittoside (166)	[92]
	Aerial parts #	8-Acetylharpagide (150), Melittoside# (166)	[14]
<i>S. baldaccii</i> (Maly) Hand-Mazz (= <i>S. recta</i> L. subsp. <i>baldaccii</i> (K. Maly) Hayek)		Ajugol (146), Harpagide (148), Acetylharpagide (150), Melittoside (166)	[92]
<i>S. subcrenata</i> Vis. (= <i>S. recta</i> subsp. <i>subcrenata</i> )		Ajugol (146), Harpagide (148), Acetylharpagide (150), Melittoside (166)	[92]
<i>S. labiosa</i> Bertol.		Ajugol (146), Harpagide (148), Acetylharpagide (150), Melittoside (166)	[92]
<i>S. leucoglossa</i> Griseb.		Ajugol (146), Harpagide (148), Acetylharpagide (150), Melittoside (166)	[92]
<i>S. spinosa</i> L.	Aerial parts	Ajugol (146), Harpagide (148), 7-O-Acetyl-8- <i>epi</i> -loganic acid (158)	[98]
<i>S. tetragona</i> Boiss. & Heldr.		Ajugol (146), Ajugoside (147), Harpagide (148), Acetylharpagide (150), Melittoside (166)	[92]
	Aerial parts	8-Acetyl-harpagide (150), 5-O-Allopyranosyl-monomelittoside (167)	[100]

Table 12. Cont.

Species	Plant Parts	Compound	Ref
<b>Subgenus <i>Stachys</i></b>			
Section <i>Stachys</i>			
<i>S. affinis</i> Bunge (= <i>S. sieboldii</i> Miq.)	Tubers	Harpagide (148), Acetylharpagide (150), Melittoside (166), 5-Alloxyloxy-aucubin (167)	[27]
<i>S. palustris</i> L.	Aerial parts #	Ajugoside (147), Harpagide (148), Acetylharpagide (150), Harpagoside (154), Catalpol (163), Aucubin (164)	[124]
<i>S. sylvatica</i> L.	Aerial parts #	Ajugoside (147), Harpagide (148), Acetylharpagide (150), Harpagoside (154), Catalpol (163), Aucubin (164)	[124]
Section <i>Swainsoniana</i>			
<i>S. anisochila</i> Vis. & Pancic		Acetylharpagide (150), Melittoside (166)	[92]
<i>S. ionica</i> Halácsy		8- <i>epi</i> -loganic acid (157), Gardoside (160)	[20]
<i>S. menthifolia</i> Vis. (= <i>S. grandiflora</i> Host.)		Ajugol (146), Harpagide (148), Acetylharpagide (150), Melittoside (166)	[92]
	Aerial parts #	Ajugoside (147) Harpagide (148), Acetylharpagide (150), Harpagoside (154), Catalpol (163), Aucubin (164)	[124]
Section <i>Zietenia</i>			
<i>S. lavandulifolia</i> Vahl.		Ajugol (146), Ajugoside (147)	[125]
	Aerial parts	Melittoside (166), Monomelittoside (165), 5-O-Allopyranosyl-monomelittoside (167)	[12]
<b>Subgenus <i>Betonica</i></b>			
Section <i>Betonica</i>			
<i>S. alopecuros</i> (L.) Benth subsp. <i>divulsa</i> (Ten.) Grande	Flowering aerial parts	Harpagide (148), Acetylharpagide (150), 4'-O- $\beta$ -D-galactopyranosyl-teuhiroside (162)	[119]
<i>S. foliosa</i> Rupr. (= <i>S. betoniciflora</i> Rupr.; <i>Betonica foliosa</i> Rupr.)		Harpagide (148), Acetylharpagide (150)	[126]
<i>S. betonicaeflora</i> Rupr.		Harpagide (148), Acetylharpagide (150)	[126]
<i>S. macrantha</i> (C. Koch.) Stearn (= <i>Betonica grandiflora</i> Steph. ex Willd.)	Aerial parts	Ajugol (146), Ajugoside (147), Harpagide (148), 8-O-Acetyl-harpagide (150), Reptoside (153), Macranthoside [=8-O- (3,4-dimethoxy-cinnamoyl-harpagide)] (156), Allobetonicoside (161)	[117]
<i>S. officinalis</i> (L.) Trevis. (= <i>Betonica officinalis</i> L.)	Aerial parts	Acetylharpagide (150), Reptoside (153), 6-O-Acetylmioporoside (155), Allobetonicoside (161)	[127]
		Harpagide (148), Acetylharpagide (150)	[128]
	Aerial parts #	Ajugoside (147), Harpagide (148), Acetylharpagide (150), Harpagoside (154), Catalpol (163), Aucubin (164)	[124]

Table 12. Cont.

Species	Plant Parts	Compound	Ref
<b>Unknown Section</b>			
<i>S. grandidentata</i> Lindl. **	Aerial parts	Ajugol (146), Harpagide (148), Acetylharpagide (150), 5-Desoxy-harpagide (151), 5-Desoxy-8-acetyl-harpagide (152), Monomelittoside (165), Melittoside (166)	[129]

# identified compounds#identified compounds by means of HPLC, LC-MS, etc; \*\* endemic species of Chile.

Table 13. Diterpenes from *Stachys* spp.

Species	Plant Parts	Compound	Ref
<b>Subgenus <i>Stachys</i></b>			
Section Ambleia			
<i>S. aegyptiaca</i> Pers.	Aerial parts	Stachysolone (177), 11a,18-Dihydroxy- <i>ent</i> -kaur-16-ene (210)	[130]
		Stachysperoxide (189), Stachysolone (177), 7,13-Diacetyl-stachysolone (180)	[131]
	Aerial parts	Stachaegyptin A-C (190–192), Roseostachenone (184), Stachysolone (177), 7,13-Diacetyl-stachysolone (180)	[106]
	Aerial parts	Stachaegyptins D, E (193, 194)	[132]
	Aerial parts	Stachaegyptins A (190), F-H (195–197), Stachysperoxide (189)	[133]
<i>S. inflata</i> Benth.		Annuanone (181), Stachylone (182), Stachone (183)	[134]
Section Aucheriana			
<i>S. glutinosa</i> L.	Aerial parts	Roseostachenone (184), 3 $\alpha$ ,4 $\alpha$ -Epoxyroseostachenol (188)	[107]
Section Eriostomum			
<i>S. balansae</i> Boiss. & Kotschy		Annuanone (181), Stachylone (182)	[134]
<i>S. lanata</i> Crantz. (= <i>S. germanica</i> L. subsp. <i>germanica</i> )		<i>Ent</i> -3 $\alpha$ -acetoxy-kaur-16-en-19-oic acid (207), <i>Ent</i> -3 $\alpha$ ,19-dihydroxy-kaur-16-ene (208), <i>Ent</i> -3 $\alpha$ -hydroxy-kaur-16-en-19-oic acid (209)	[135]
Section Mucronata			
<i>S. mucronata</i> Sieb.	Aerial parts	Ribenone [=3 $\beta$ -hydroxy-13- <i>epi-ent</i> -manoyl oxide] (198), Ribenol [=3-keto-13- <i>epi-ent</i> -manoyl oxide] (199)	[57]
Section Olisia			
<i>S. annua</i> (L.) L.		Stachysolone (177)	[136,137]
		Annuanone (181), Stachylone (182), Stachone (183)	[138]

Table 13. Cont.

Species	Plant Parts	Compound	Ref
<b>Subgenus <i>Stachys</i></b>			
Section <i>Olisia</i>			
<i>S. atherocalyx</i> C. Koch.		Annuanone (181), Stachylone (182), Stachone (183)	[134]
<i>S. distans</i> Benth	Aerial parts	(+)-6-Deoxyandalusol (201)	[139]
<i>S. iberica</i> M. Bieb.		Annuanone (181), Stachylone (182), Stachone (183)	[134]
<i>S. recta</i> L.	Aerial parts	7,13-Diacetate stachysolone (180), 7-Acetate stachysolone (178), 13-Acetate stachysolone (179)	[140]
Section <i>Roseostachys</i>			
<i>S. rosea</i> Boiss.	Aerial parts	Roseostachenone (184), Roseostachone (185), 13- <i>epi</i> -sclareol (200), Roseostachenol (186), Roseotetrol (187)	[141]
Section <i>Stachys</i>			
<i>S. mialhesii</i> Noé	Aerial parts	Horminone (211)	[103]
<i>S. palustris</i> L.		Annuanone (181)	[134]
		Stachysic acid (204)	[142]
<i>S. sylvatica</i> L.		Annuanone (181), Stachylone (182), Stachone (183)	[134]
		Stachysic acid (204), 6 $\beta$ -Hydroxy- <i>ent</i> -kaur-16-ene (205), 6 $\beta$ ,18-Dihydroxy- <i>ent</i> -kaur-16-ene (206)	[142]
		Betolide (214)	[143]
Section <i>Swainsoniana</i>			
<i>S. ionica</i> Halácsy	Aerial parts	(+)-6-Deoxyandalusol (201)	[139]
<i>S. plumosa</i> Griseb.	Aerial parts	(+)-6-Deoxyandalusol (201), 13- <i>Epi</i> -jabugodiol (202), (+)-Plumosol (203)	[144]
Section <i>Zietenia</i>			
<i>S. lavandulifolia</i> Vahl.	Aerial parts	Stachysolone (177)	[116]
<b>Subgenus <i>Betonica</i></b>			
Section <i>Betonica</i>			
<i>S. officinalis</i> (L.) Trevis. (= <i>Betonica officinalis</i> L.)		Betolide (214)	[145]
		Betonicolide (215), Betonicosides A-D (216–219)	[145]
	Roots	Betolide (214)	[143]
<i>S. scardica</i> (Griseb.) Hayek (= <i>Betonica scardica</i> Griseb.)	Roots	Betolide (214)	[143]
<b>Former <i>Stachys</i> species</b>			
<i>S. parviflora</i> Benth. (= <i>Phlomidosema parviflorum</i> (Benth.) Vved.)	Whole plant	Stachyrosane 1 (212) Stachyrosane 2 (213)	[133]

**Table 14.** Triterpene derivatives, Phytosterols and Phytoecdysteroids from *Stachys* spp.

Species	Plant Parts	Compound	Ref
<b>Subgenus <i>Stachys</i></b>			
Section <i>Eriostomum</i>			
<i>S. byzantina</i> K. Koch	Aerial parts	Stigmasterol (220),	[17]
		$\beta$ -Sitosterol (221), Lawsaritol (223), Stigmastan-3,5-dien-7-one (224)	[35]
<i>S. hissarica</i> Regel	-	20-Hydroxyecdysone (239), Polipodin B (240), Integristeron A (241), 2-Desoxy-20-hydroxyecdysone (242), 2-Desoxyecdysone (243)	[67]
Section <i>Olisia</i>			
<i>S. annua</i> (L.) L.	Aerial parts	$\beta$ -Sitosterol (221), Ursolic acid (226)	[95]
<i>S. spinosa</i> L.	Aerial parts	Stigmasterol (220), $\beta$ -Sitosterol (221), Oleanolic acid (227), 12 $\alpha$ -Hydroxy-oleanolic lactone (228)	[99]
		Stigmasterol (220), $\beta$ -Sitosterol (221), Oleanolic acid (227),	[100]
Section <i>Stachys</i>			
<i>S. palustris</i> L.		$\beta$ -Sitosterol (221), $\alpha$ -amyrin (225)	[146]
<i>S. riederi</i> Cham.	Whole plant	Stachyssaponins I-VIII (231–238)	[147]
<b>Subgenus <i>Betonica</i></b>			
Section <i>Betonica</i>			
<i>S. alopecuroides</i> (L.) Benth subsp. <i>divulsa</i> (Ten.) Grande	Flowering aerial parts	3-O- $\beta$ -Sitosterol-glucoside (222)	[119]
<b>Former <i>Stachys</i> species</b>			
<i>S. parviflora</i> Benth. (= <i>Phlomidioschema parviflorum</i> Benth.) Vved.)	Aerial parts	Stachyssaponin A (229), Stachyssaponin B (230)	[63]

**Table 15.** Megastigmane derivatives from *Stachys* spp.

Species	Plant Parts	Compound	Ref
<b>Subgenus <i>Stachys</i></b>			
Section <i>Eriostomum</i>			
<i>S. byzantina</i> K. Koch.	Aerial parts	Byzantionoside A (244), Byzantionoside B (245), Icariside B2 (246), (6R, 9R)- and (6R, 9S)-3-oxo- $\alpha$ -ionol glucosides (247), Blumeol C glucoside (248)	[148]
		Vomifoliol (249), Dehydrovomifoliol (250)	[82]
<i>S. lanata</i> Crantz (= <i>S. germanica</i> L. subsp. <i>germanica</i> )	Aerial parts	Citroside A (251)	[82]
	Roots		

#### 4.1. Flavonoids

The genus *Stachys* consists a rich source of flavonoids. Accumulating studies have reported the several types of flavonoids occurring in *Stachys* spp., including flavones (Tables 2 and 16), poly-methylated flavones (Tables 3 and 17), flavonols (Tables 4 and 18), flavanones (Tables 5 and 19) and one biflavonoid (Tables 6 and 20).

Regarding the flavone derivatives (Tables 2 and 16), 18 flavone 7-O-acetylallosylglucosides were mentioned in the most species of subgenus *Stachys* (31 species). The flavone 7-O-glucosides were

also found in many species through the two subgenera. Marin et al. (2004) reported that tricetin 3',A',5'-trimethyl-7-O-glucoside (62) consists a chemotaxonomic marker for the subgenus *Betonica* [5]. Precisely, selgin 7-O-glucoside (59), tricrin 7-O-glucoside (61) and tricetin 3',A',5'-trimethyl-7-O-glucoside (62) were identified from the leaves of three species of the latter subgenus; *S. alopecurus* (section *Betonica*), *S. officinalis* (section *Betonica*) and *S. scardica* (section *Macrostachya*) [5]. Furthermore, derivatives of apigenin *p*-coumaroyl glucosides and chrysoeriol *p*-coumaroyl glucosides were reported in *Stachys* species, though some *p*-coumaroyl glucosides (not determined) were also identified [5,75]. To be mentioned that chrysoeriol 7-O-glucoside (43), chrysoeriol *p*-coumaroyl glucosides (46,47) and chrysoeriol 7-O-[6'''-O-acetyl-allosyl]-(1→2)-glucoside (stachyspinoside) (44) were mainly isolated from wild Greek taxa of the subgenus *Stachys* [3,77,98,99,102], apart from the Greek species *S. ionica* [20], *S. tetragona* [100] and the cultivated species *S. iva* [56]. Nazemiyeh et al. (2006) investigated the phytochemical profile of the stems of *S. schtschegleevii*, reporting four flavonoids, among them were also two *p*-coumaroyl derivatives of apigenin and chrysoeriol [74]. Moreover, flavone 7-O-mannosylglucosides were reported from the two species *S. atherocalyx* (section *Eriostomum*) and *S. spectabilis* (section *Olisia*) [72,89,90]. Few flavone C-glucosides were mentioned in the species *S. aegyptiaca* (subg. *Stachys*; sect. *Ambleia*), *S. officinalis* (subg. *Betonica*; sect. *Betonica*), and *S. scardica* (subg. *Betonica*; sect. *Macrostachya*) [5,68,104]. Zinchenko (1973) reported the existence of two derivatives of methoxybaicalein, namely palustrin (63) and palustrinoside (64), from the species *S. palustris* of subgenus *Stachys* (section *Stachys*) [104]. Notably, the subterranean organs of *S. annua* were investigated and the isolation of two flavone derivatives was reported, namely 4'-O-methyl-isoscutellarein (12) and 4'-O-methyl-isoscutellarein-7-O-(6'''-O-acetyl)allopyranosyl-(1→2)-glucopyranoside (21) [95].

Furthermore, our survey revealed the presence of poly-methylated flavones in the genus *Stachys* (Tables 3 and 17). Precisely, six species and four subspecies from subgenus *Stachys*, as well as one species from subgenus *Betonica*, are found to contain poly-methylated flavones. The most common representative was xanthomicrol (69) which was mentioned in seven *Stachys* species and subspecies of different sections from the subgenus *Stachys* [20,68,74,77,78,102,107]. In the stems of the species *S. schtschegleevii*, apart from xanthomicrol (69), was also found circimaritin (66) [74].

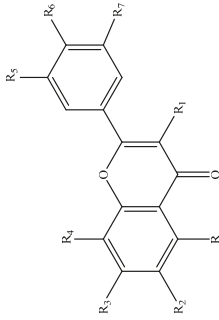
A few studies mentioned the existence of flavonols in *Stachys* spp. (Tables 4 and 18), mainly in species occurred in Greece. Afouxenidi and colleagues (2018) isolated kaempferol (91) from the *n*-butanol residue of the aerial parts of *S. tetragona* [100], which was also identified in the aerial parts of *S. cretica* subsp. *smyrnaea* [81]. Moreover, isorhamnetin (92) was isolated from the methanol extract of the aerial parts of *S. swainsonii* subsp. *swainsonii* and *S. swainsonii* subsp. *argolica* [102]. A study conducted by Marin et al. (2004) identified the presence of quercetin 3-O-rutinoside (93) and isorhamnetin 3-O-glucoside (94) from the aerial parts of *S. palustris* [5].

In addition, three flavanones were isolated from three species of the genus *Stachys* (Tables 5 and 19). Eriodictyol (95) was mentioned in *S. cretica* [108] and in one subspecies of *S. swainsonii* [102], while naringenin (96) was isolated from the aerial parts of the species *S. aegyptiaca* [104]. A flavanone rutinoside, known as hesperidin (97), was identified as one of the major compounds of the aerial parts of *S. cretica* subsp. *smyrnaea* [81].

Of great interest is the isolation of a rare diflavone ester of  $\mu$ -truxinic acid, namely stachysetin (98). It is well-known that diglycoside flavone esters of dicarboxylic acids are rare compounds in plant kingdom. Stachysetin was firstly isolated from the ethanol extract (70% v/v) of the aerial parts of *S. aegyptiaca* [69]. Then, Murata and co-workers (2008) reported it in the methanol residue (80% v/v) of the aerial parts of *S. lanata* [82]. In a current study carried out by Pritsas et al. (2020), stachysetin was isolated from the methanol: aqueous (5:1) extract from the flowering aerial parts of the cultivated *S. iva* (Tables 6 and 20) [56]. Up to now, there is no report of this secondary metabolite in the species of the subgenus *Betonica*. The presence of this rare natural compound in the sections *Ambleia*, *Eriostomum* and *Candida* of the subgenus *Stachys* might be considered as a chemotaxonomic marker among the two subgenera and of the genus *Stachys*.



Table 16. Chemical structures of flavones isolated from *Stachys* spp.



Name	R <sub>1</sub>	R <sub>2</sub>	R <sub>3</sub>	R <sub>4</sub>	R <sub>5</sub>	R <sub>6</sub>	R <sub>7</sub>
<b>R=OH</b>							
Apigenin (1)	H	H	OH	H	H	OH	H
Apigenin 7-O-β-D-glucoside (cosmoside) (2)	H	H	O-glc	H	H	OH	H
Apigenin 7-O-[6'''-O-acetyl]-β-D-allosyl-(1→2)-β-D-glucoside (3)	H	H	O-[6'''-acetyl]-allosyl-(1→2)-glc	H	H	OH	H
Apigenin 7-(3''-E-p-coumaroyl)-β-D-glucoside (4)	H	H	O-(3''-E-p-coumaroyl)-glc	H	H	OH	H
Apigenin 7-(3''-Z-p-coumaroyl)-β-D-glucoside (5)	H	H	O-(3''-Z-p-coumaroyl)-glc	H	H	OH	H
Apigenin 7-(6''-E-p-coumaroyl)-β-D-glucoside (6)	H	H	O-(6''-E-p-coumaroyl)-glc	H	H	OH	H
Apigenin 7-(6''-Z-p-coumaroyl)-β-D-glucoside (7)	H	H	O-(6''-Z-p-coumaroyl)-glc	H	H	OH	H
Apigenin 7-(3''',6''-p-dicoumaroyl)-β-D-glucoside (Anisofolin A) (8)	H	H	O-(3''',6''-p-dicoumaroyl)-glc	H	H	OH	H
Apigenin 8-C-glucoside (9)	H	H	OH	C-glc	H	OH	H
Apigenin 6,8-di-C-glucoside (Vicenin-2) (10)	H	C-glc	OH	C-glc	H	OH	H
Isoscutellarein (11)	H	H	OH	OH	H	OH	H
Isoscutellarein 7-O-glucoside (11a)	H	H	O-glc	OH	H	OH	H
4'-Methyl-isoscutellarein (12)	H	H	OH	OH	H	OCH <sub>3</sub>	H
Isoscutellarein 7-O-allosyl-(1→2)-glucoside (13)	H	H	O-allosyl-(1→2)-glc	OH	H	OH	H
3'-Hydroxy-isoscutellarein-7-O-[6'''-O-acetyl]-β-D-glucoside (14)	H	H	O-[6'''-O-acetyl]-glc	OH	OH	OH	H
Isoscutellarein 7-O-[6'''-O-acetyl]-β-D-allosyl-(1→2)-β-D-glucoside (15)	H	H	O-[6'''-O-acetyl]-allosyl-(1→2)-glc	OH	H	OH	H
Isoscutellarein 7-O-[6'''-O-acetyl]-β-D-glucoside (16)	H	H	O-[6'''-O-acetyl]-β-D-glucoside	OH	H	OH	H
Isoscutellarein 7-O-[6'''-O-acetyl]-β-D-allosyl-(1→2)-[6''-O-acetyl]-β-D-glucoside (17)	H	H	O-[6'''-O-acetyl]-allosyl-(1→2)-[6''-O-acetyl]-glc	OH	H	OH	H
Isoscutellarein 8-O-(6''-trans-p-coumaroyl)-β-D-glucoside (18)	H	H	OH	O-(6''-trans-p-coumaroyl)-glc	H	OH	H
4'-Methyl-isoscutellarein 7-O-β-D-allosyl-(1→2)-β-D-glucoside (19)	H	H	O-allosyl-(1→2)-glc	OH	H	OCH <sub>3</sub>	H

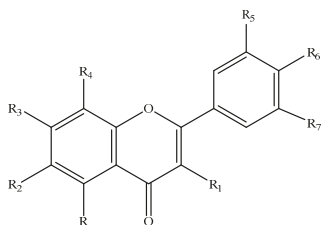
Table 16. Cont.

Name	R <sub>1</sub>	R <sub>2</sub>	R <sub>3</sub>	R <sub>4</sub>	R <sub>5</sub>	R <sub>6</sub>	R <sub>7</sub>
4'-Methyl- isoscutellarein 7-O-β-D-allosyl-(1→2)[6'-O-acetyl]-β-D-glucoside (20)	H	H	R=OH O-allosyl-(1→2)-[6'-O-acetyl]-glc	OH	H	OCH <sub>3</sub>	H
4'-Methyl- isoscutellarein 7-O-β-D-[6''-O-acetyl]-allosyl-(1→2)-β-D-glucoside (21)	H	H	O-[6''-O-acetyl]-allosyl-(1→2)-glc	OH	H	OCH <sub>3</sub>	H
4'-Methyl- isoscutellarein 7-O-[2''-O-acetyl]-β-D-allosyl-(1→2)-β-D-glucoside (22)	H	H	O-[2''-O-acetyl]-allosyl-(1→2)-glc	OH	H	OCH <sub>3</sub>	H
4'-Methyl- isoscutellarein 7-O-β-D-[4'''-O-acetyl]-allosyl-(1→2)-β-D-glucoside (mannoside) (23)	H	H	O-[4'''-O-acetyl]-allosyl-(1→2)-glc	OH	H	OCH <sub>3</sub>	H
4'-Methyl- isoscutellarein 7-O-[6'''-O-acetyl]-allosyl-(1→2)-[6''-O-acetyl]-glucoside (24)	H	H	O-[6'''-O-acetyl]-allosyl-(1→2)-[6''-O-acetyl]-glc	OH	H	OCH <sub>3</sub>	H
Isostachyflaside (25)	H	H	OH	OH	H	O-mannosyl-(1→2)-glc	H
Acetyl- isostachyflaside (26)	H	H	OH	OH	H	O-[acetyl]-mannosyl-(1→2)-glc	H
D-acetyl- isostachyflaside (27)	H	H	OH	OH	H	O-[diacetyl-mannosyl]- (1→2)-glc	H
Spectabiflaside (28)	H	H	O-mannosyl-(1→2)-glc	OH	OCH <sub>3</sub>	OH	H
Scutellarein (29)	H	OH	OH	H	H	OH	H
Scutellarein 7-O-β-D-glucoside[5,6,4'-trihydroxyflavone-7-O-β-D-glucoside] (30)	H	OH	O-glc	H	H	OH	H
Scutellarein 7-O-β-D-mannosyl-(1→2)-β-D-glucoside (stachyflaside) (31)	H	OH	O-mannosyl-(1→2)-glc	H	H	OH	H
7-O-β-D-glucopyranosyl-5,6-dihydroxy-4'-methoxyflavone (Stachamin A) (32)	H	OH	O-glc	H	H	OCH <sub>3</sub>	H
4'-Methoxy- scutellarein 7-[O-β-D-mannosyl-(1→2)-β-D-glucoside (stachaminoside B) (33)	H	OH	O-mannosyl-(1→2)-glc	H	H	OCH <sub>3</sub>	H
Luteolin (34)	H	H	OH	H	H	OH	H
Luteolin 7-methyl ether (35)	H	H	OCH <sub>3</sub>	H	H	OH	H
Luteolin 7-O-β-D-glucuronide (36)	H	H	O-glcA	H	H	OH	H
Luteolin 7-O-β-D-glucoside (37)	H	H	O-glc	H	H	OH	H
Luteolin 6-C-glucoside (isorientin) (38)	H	-C-glc	OH	H	H	OH	H
Luteolin 7-O-[6''-O-acetyl]-allosyl-(1→2)-glucoside (39)	H	H	O-[6''-O-acetyl]-allosyl-(1→2)-glc	H	H	OH	H
6,8-Di-C-β-D-glucopyranosyl luteolin (Lucerin-2) (40)	H	C-glc	OH	C-glc	OH	OH	H
3',4'-Dimethyl-luteolin-7-O-β-D-glucoside (41)	H	H	O-glc	H	OCH <sub>3</sub>	OCH <sub>3</sub>	H
Chrysoeriol (42)	H	H	OH	H	OCH <sub>3</sub>	OH	H
Chrysoeriol 7-O-β-D-glucoside (43)	H	H	O-glc	H	OCH <sub>3</sub>	OH	H

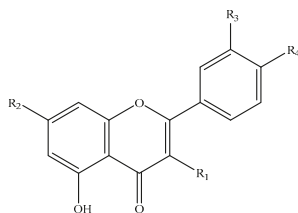
Table 16. Contd.

Name	R <sub>1</sub>	R <sub>2</sub>	R <sub>3</sub>	R <sub>4</sub>	R <sub>5</sub>	R <sub>6</sub>	R <sub>7</sub>
Chrysoeriol 7-O-[6''-O-acetyl]-β-D-allosyl-(1→2)-glucoside (Stachyspinoside) (44)	H	H	O-[6''-O-acetyl]-allosyl-(1→2)-glc	H	OCH <sub>3</sub>	OH	H
Chrysoeriol 7-O-[6''-O-acetyl]-β-D-allosyl-(1→2)-glucoside (Isostachyspinoside) (45)	H	H	O-[6''-O-acetyl]-allosyl-(1→2)-glc	H	OCH <sub>3</sub>	OH	H
Chrysoeriol 7-(3'-E-p-coumaroyl)-β-D-glucoside (46)	H	H	O-(3'-E-p-coumaroyl)-glc	H	OCH <sub>3</sub>	OH	H
Chrysoeriol 7-(6''-E-p-coumaroyl)-β-D-glucoside (47)	H	H	O-(6''-E-p-coumaroyl)-glc	H	OCH <sub>3</sub>	OH	H
Hypolaetin (48)	H	H	OH	OH	OH	OH	H
Hypolaetin-7-O-glucoside (49)	H	H	O-glc	OH	OH	OH	H
Hypolaetin-7-O-glucuronide (49a)	H	H	O-glcA	OH	OH	OH	H
Hypolaetin 7-O-allosyl-(1→2)-glucoside (50)	H	H	O-allosyl-(1→2)-glc	OH	OH	OH	H
Hypolaetin 7-O-[6''-O-acetyl]-β-D-allosyl-(1→2)-β-D-glucoside (51)	H	H	O-[6''-O-acetyl]-allosyl-(1→2)-glc	OH	OH	OH	H
Hypolaetin 7-O-[6''-O-acetyl]-allosyl-(1→2)-glucoside (52)	H	H	O-[6''-O-acetyl]-allosyl-(1→2)-glc	OH	OH	OH	H
Hypolaetin 7-O-[6''-O-acetyl]-allosyl-(1→2)-[6''-O-acetyl]-glucoside (53)	H	H	O-[6''-O-acetyl]-allosyl-(1→2)-[6''-O-acetyl]-glc	OH	OH	OH	H
Hypolaetin 7-O-[6''-O-acetyl]-allosyl-(1→2)-[3''-O-acetyl]-glucoside (54)	H	H	O-[6''-O-acetyl]-allosyl-(1→2)-[3''-O-acetyl]-glc	OH	OH	OH	H
4'-Methyl-hypolaetin-7-O-allosyl-(1→2)-glucoside (55)	H	H	O-allosyl-(1→2)-glc	OH	OH	OCH <sub>3</sub>	H
4'-Methyl-hypolaetin-7-O-[6''-O-acetyl]-β-D-allopyranosyl-(1→2)-β-D-glucopyranoside (56)	H	H	O-[6''-O-acetyl]-allosyl-(1→2)-glc	OH	OH	OCH <sub>3</sub>	H
4'-Methyl-hypolaetin-7-O-[6''-O-acetyl]-β-D-allopyranosyl-(1→2)-β-D-glucopyranoside (57)	H	H	O-[6''-O-acetyl]-allosyl-(1→2)-glc	OH	OH	OCH <sub>3</sub>	H
4-Methyl-hypolaetin-7-O-[6''-O-acetyl]-allosyl-(1→2)-[6''-O-acetyl]-glucoside (58)	H	H	O-[6''-O-acetyl]-allosyl-(1→2)-[6''-O-acetyl]-glc	OH	OH	OCH <sub>3</sub>	H
Selgin 7-O-glucoside (59)	H	H	O-glc	H	OCH <sub>3</sub>	OH	OH
Tricin 7-O-glucuronide (60)	H	H	O-glcA	H	OCH <sub>3</sub>	OH	OCH <sub>3</sub>
Tricin 7-O-glucoside (61)	H	H	O-glc	H	OCH <sub>3</sub>	OH	OCH <sub>3</sub>
Tricin 3',4',5'-trimethyl-7-O-glucoside (62)	H	H	O-glc	H	OCH <sub>3</sub>	OCH <sub>3</sub>	OCH <sub>3</sub>
Palustrin (63)	H	OH	R=O-glcA-glc (2→1)	H	H	H	H
Palustrinoside (64)	H	OH	R=O-glcA	H	H	H	H

glc: glucose, glcA: glucuronide.

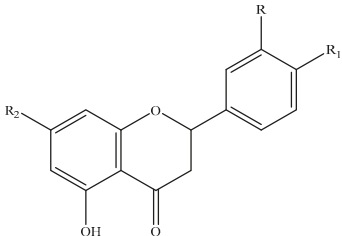
**Table 17.** Chemical structures of poly-methylated flavonoids from *Stachys* spp.

Name	R <sub>1</sub>	R <sub>2</sub>	R <sub>3</sub>	R <sub>4</sub>	R <sub>5</sub>	R <sub>6</sub>	R <sub>7</sub>
<b>R=OH</b>							
Velutin (luteolin 7,3'-dimethyl ether) (65)	H	H	OCH <sub>3</sub>	H	OCH <sub>3</sub>	OH	H
Cirsimaritin (66)	H	OCH <sub>3</sub>	OCH <sub>3</sub>	H	H	OH	H
5,7,3'-Trihydroxy-6,4'-dimethoxyflavone (67)	H	OCH <sub>3</sub>	OH	H	OH	OCH <sub>3</sub>	H
5,7,3'-Trihydroxy-6,8,4'-trimethoxyflavone (68)	H	OCH <sub>3</sub>	OH	OCH <sub>3</sub>	OH	OCH <sub>3</sub>	H
Xanthomicrol (69)	H	OCH <sub>3</sub>	OCH <sub>3</sub>	OCH <sub>3</sub>	H	OH	H
Sideritiflavone (70)	H	OCH <sub>3</sub>	OCH <sub>3</sub>	OCH <sub>3</sub>	OH	OH	H
8-Methoxycirsilineol (71)	H	OCH <sub>3</sub>	OCH <sub>3</sub>	OCH <sub>3</sub>	OCH <sub>3</sub>	OH	H
Eupatorin (72)	H	OCH <sub>3</sub>	OCH <sub>3</sub>	H	OH	OCH <sub>3</sub>	H
Eupatilin (72a)	H	OCH <sub>3</sub>	OH	H	OCH <sub>3</sub>	OCH <sub>3</sub>	H
Eupatilin-7-methyl ether (73)	H	OCH <sub>3</sub>	OCH <sub>3</sub>	H	OCH <sub>3</sub>	OCH <sub>3</sub>	H
Salvigenin (74)	H	OCH <sub>3</sub>	OCH <sub>3</sub>	H	H	OCH <sub>3</sub>	H
5-Hydroxy-6,7,8,3',4'-pentamethoxyflavone (75)	H	OCH <sub>3</sub>	OCH <sub>3</sub>	OCH <sub>3</sub>	OCH <sub>3</sub>	OCH <sub>3</sub>	H
5,4'-Dihydroxy-6,7,8,3'-tetramethoxyflavone (76)	H	OCH <sub>3</sub>	OCH <sub>3</sub>	OCH <sub>3</sub>	OCH <sub>3</sub>	OH	H
5,4'-Dihydroxy-7,3',5'-trimethoxyflavone (77)	H	H	OCH <sub>3</sub>	H	OCH <sub>3</sub>	OH	OCH <sub>3</sub>
Viscosine (5,7,4'-trihydroxy-3,6-dimethoxyflavone) (78)	OCH <sub>3</sub>	OCH <sub>3</sub>	OH	H	H	OH	H
Kumatakenin (kaempferol 3,7-dimethyl ether) (79)	OCH <sub>3</sub>	H	OCH <sub>3</sub>	H	H	OH	H
Pachypodol (quercetin 3,7,3'-trimethyl ether) (80)	OCH <sub>3</sub>	H	OCH <sub>3</sub>	H	OCH <sub>3</sub>	OH	H
Penduletin (81)	OCH <sub>3</sub>	OCH <sub>3</sub>	OCH <sub>3</sub>	H	H	OH	H
5,3',4'-Trihydroxy-3,6,7,8-tetramethoxyflavone (82)	OCH <sub>3</sub>	OCH <sub>3</sub>	OCH <sub>3</sub>	OCH <sub>3</sub>	OH	OH	H
Calycopterin (83)	OCH <sub>3</sub>	OCH <sub>3</sub>	OCH <sub>3</sub>	OCH <sub>3</sub>	H	OH	H
Chrysoplenetin (84)	OCH <sub>3</sub>	OCH <sub>3</sub>	OCH <sub>3</sub>	H	OCH <sub>3</sub>	OH	H
5-Hydroxy-3,6,7,4'-tetramethoxyflavone (85)	OCH <sub>3</sub>	OCH <sub>3</sub>	OCH <sub>3</sub>	H	H	OCH <sub>3</sub>	H
5,8-Dihydroxy-3,6,7,4'-tetramethoxyflavone (86)	OCH <sub>3</sub>	OCH <sub>3</sub>	OCH <sub>3</sub>	OH	H	OCH <sub>3</sub>	H
Casticin (87)	OCH <sub>3</sub>	OCH <sub>3</sub>	OCH <sub>3</sub>	H	OH	OCH <sub>3</sub>	H
5-Hydroxy-3,6,7,8,4'-pentamethoxyflavone (5-hydroxyauranetin) (88)	OCH <sub>3</sub>	OCH <sub>3</sub>	OCH <sub>3</sub>	OCH <sub>3</sub>	H	OCH <sub>3</sub>	H
5,4'-Dihydroxy-3,6,7,8,3'-pentamethoxyflavone (89)	OCH <sub>3</sub>	OCH <sub>3</sub>	OCH <sub>3</sub>	OCH <sub>3</sub>	OCH <sub>3</sub>	OH	H
<b>R=OCH<sub>3</sub></b>							
4'-Hydroxy-3,5,7,3'-tetramethoxyflavone (90)	OCH <sub>3</sub>	H	OCH <sub>3</sub>	H	OCH <sub>3</sub>	OH	H

**Table 18.** Chemical structures of flavonols from *Stachys* spp.

Name	R <sub>1</sub>	R <sub>2</sub>	R <sub>3</sub>	R <sub>4</sub>
Kaempferol (91)	OH	OH	H	OH
Isorhamnetin (92)	OH	OH	OCH <sub>3</sub>	OH
Quercetin 3-O-rutinoside (93)	O-rut	OH	OH	OH
Isorhamnetin 3-O-rutinoside (94)	O-rut	OH	OCH <sub>3</sub>	OH

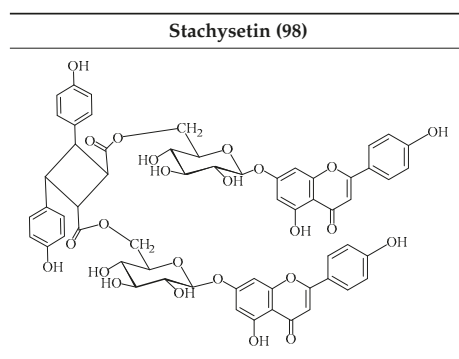
rut: rutinoside.

**Table 19.** Chemical structures of flavanones from *Stachys* spp.


The diagram shows the general chemical structure of a flavanone. It consists of a chromane ring system. The A-ring (left) has a hydroxyl group (OH) at the 5-position and a substituent R<sub>2</sub> at the 7-position. The C-ring (right) has a carbonyl group (C=O) at the 4-position and a substituent R at the 2-position. The B-ring (top right) is attached to the C-ring at the 3-position and has substituents R<sub>1</sub> at the 3' and 4' positions.

Name	R	R <sub>1</sub>	R <sub>2</sub>
Eriodictyol (95)	OH	OH	OH
Naringenin (96)	H	OH	OH
Hesperidin (97)	OH	OCH <sub>3</sub>	O-rut

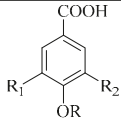
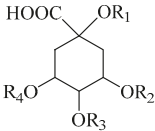
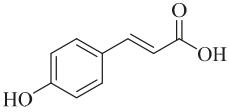
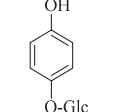
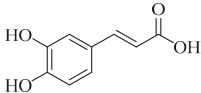
rut: rutinoside.

**Table 20.** Chemical structure of biflavonoid from *Stachys* spp.

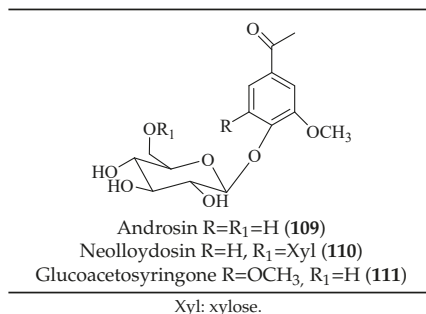
#### 4.2. Phenolic Derivatives; Acetophenone Derivatives

Regarding the phenolic derivatives of genus *Stachys* (Tables 7 and 21), mainly chlorogenic acid (103) was appeared in nine *Stachys* species; *S. candida* [78], *S. iva* [56], *S. cretica* (*S. cretica* subsp. *smyrnaea* [81], *S. cretica* subsp. *mersinaea* [108], *S. cretica* subsp. *vacillans* [112]), *S. lanata* [82], *S. tmolea* [85], *S. thirkei* [84], *S. recta* [14], *S. palustris* [104] and *S. officinalis* [111]. The isomers of chlorogenic acid (102, 104, 105) also reported in *S. atherocalyx* [110], *S. recta* [14] and *S. palustris* [23,104]. Caffeic (108) and *p*-coumaric (106) acids were found in two *Stachys* spp. [104,110]. Moreover, Kirkan (2019) identified vanillic (100) and syringic (101) acids from the aerial parts of *S. cretica* subsp. *vacillans* [112]. Though, 4-hydroxybenzoic acid (99) was reported from *S. tmolea* [85]. Arbutin (107) was also identified in the aerial parts of *S. germanica* subsp. *salviifolia* [109]. One study also reported the presence of acetophenone derivatives from the roots of *S. lanata*, namely androsin (109), neolloydosin (110) and glucoacetosyringone (111) (Tables 8 and 22) [82]. The isolation of the latter compounds might be attributed to the different investigated plant parts (roots).

**Table 21.** Chemical structures of phenolic derivatives from *Stachys* spp.

	4-Hydroxybenzoic acid R=H, R <sub>1</sub> =H, R <sub>2</sub> =H (99) Vanillic acid R=H, R <sub>1</sub> =H, R <sub>2</sub> =OCH <sub>3</sub> (100) Syringic acid R=H, R <sub>1</sub> =OCH <sub>3</sub> , R <sub>2</sub> =OCH <sub>3</sub> (101)	
	1-Caffeoylquinic acid R <sub>1</sub> =caffeoyl-, R <sub>2</sub> =R <sub>3</sub> =R <sub>4</sub> =H (102) 3-Caffeoylquinic acid (Chlorogenic acid) R <sub>1</sub> =H, R <sub>2</sub> =caffeoyl-, R <sub>3</sub> =R <sub>4</sub> =H (103) 4-Caffeoylquinic acid (cryptochlorogenic acid) R <sub>1</sub> =R <sub>2</sub> =H, R <sub>3</sub> =caffeoyl-, R <sub>4</sub> =H (104) 5-Caffeoylquinic acid (neochlorogenic acid) R <sub>1</sub> =R <sub>2</sub> =R <sub>3</sub> =H, R <sub>4</sub> =caffeoyl- (105)	
 <i>p</i> -Coumaric acid (106)	 Arbutin (107)	 Caffeic acid (108)

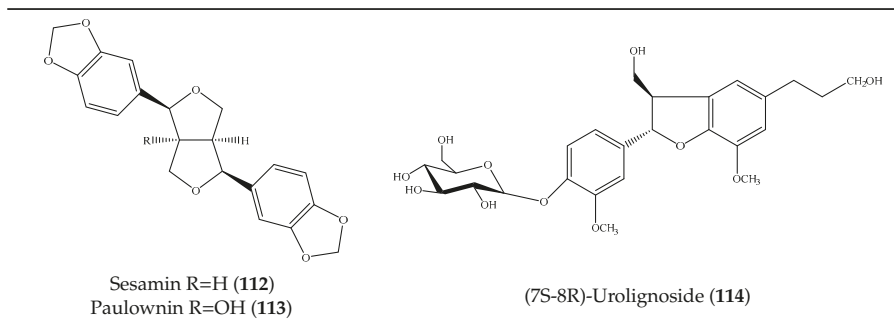
Glc: glucose.

**Table 22.** Chemical structures of acetophenone glycosides from *Stachys* spp.

Xyl: xylose.

#### 4.3. Lignans

Lignans are types of polyphenols with diverse structures. Although these bioactive compounds were presented in Lamiaceae family [149], a few studies reported their existence in plants of genus *Stachys*. Specifically, three lignans categorizing into two furanofuran-type derivatives (sesamin and paulownin) and one benzofuran-type lignan (urolignoside) were reported in two species of the subgenus *Stachys* (Tables 9 and 23). Lagoune et al. (2016) isolated sesamin (112) and paulownin (113) from the aerial parts of *S. mialhesii* [103], while urolignoside (114) was isolated from the aerial parts of *S. tetragona* [100]. Given that up to now there is no study reported the presence of lignans in the subgenus *Betonica*, the identification of lignans might be considered as a chemotaxonomic difference between the two subgenera *Stachys* and *Betonica*.

**Table 23.** Chemical structures of lignans from *Stachys* spp.

#### 4.4. Phenylethanoid Glycosides; Phenylpropanoid Glucosides

The present review unveiled 29 phenylethanoid glycosides in 17 *Stachys* species (Tables 10 and 24). Acteoside or verbascoside (118) was the most abundant found in 16 *Stachys* spp. of all sections through this survey. Additional phenylethanoid glycosides isolated and identified from this genus includes martynoside, leucosceptoside A and lavandulifoliosides. Lavandulifolioside A (or stachysoside A) (129) was firstly isolated from the methanol extract of the aerial parts of *S. lavandulifolia* in 1988 [115], while in 2011 Delazar et al. (2011) isolated lavandulifolioside B (130) from the same plant, for the first time [12]. Moreover, three phenylethanoid glycosides were reported from the aerial parts of *S. byzantina* (section *Eriostomum*), including verbascoside (118), 2'-O-arabinosyl verbascoside (122) and aeschynanthoside C (133) [35]. Among them, the first and the last compound has been isolated only from the specific species. A survey conducted by Murata and co-workers (2008) reported ten phenylethanoid glycosides from different plant parts [82]. In the aforementioned study, leonoside B (or stachysoside D) (134) and martynoside (135) were mentioned from the aerial parts of *S. lanata*, while from the roots of the specific species were reported eight phenylethanoid glycosides, namely rhodiolioside (115), verbascoside (116), 2-phenylethyl-D-xylopyranosyl-(1→6)-D-glucopyranoside (117), verbascoside (118), isoacteoside (119), darendoside B (120), campneoside II (121) and campneoside I (136). It is remarkable to point out that compounds 115, 117 and 120 haven't been reported in other *Stachys* species. This might be attributed to the fact that the plant material was roots. Another study carried out by Karioti et al. (2010) focused on the phenolic compounds from the aerial parts of *S. recta*, and reported many phenylethanoid glycosides from its aerial parts, including acteoside (118), isoacteoside (119), β-OH-acteoside (121), betunyoside E (127), campneoside I (136), forsythoside B (137), β-OH-forsythoside B methyl ether (138) [14]. Furthermore, lamiophloside A (141) was isolated with some other phenylethanoid glycosides from the aerial parts of *S. tetragona* [100]. Of great interest is that our survey revealed that this constituent is mentioned only in the specific species. Two rare phenylethanoid glycosides, parviflorosides A-B (142–143) were isolated from the whole plant of *S. parviflora* [120]. These two compounds are characterised by the presence of a third saccharide (rhamnose) linked to the proton H-2' of glucose, comparing to others common phenylethanoid glycosides where the connection of the third saccharide is in proton H-3' of glucose. Of great interest is that *S. parviflora* is now considered as the monotypic genus *Phlomidioschema* (only *P. parviflorum* (Benth.) Vved.) [2]. Furthermore, leonoside A (or stachysoside B) (139) was isolated with other three phenylethanoid glucosides from the whole plant of *S. riederi* [114]. To be mentioned that phenylethanoid glycosides were reported in both subgenera of genus *Stachys*.

Apart from phenylethanoid glucosides, Murata et al. (2008) mentioned two phenylpropanoid glucosides in the roots of *S. lanata* (subg. *Stachys*; sect. *Eriostomum*), coniferin (144) and syringin (145) (Tables 11 and 25) [82]. It is worth to mention that the isolation of phenylpropanoid glucosides only from the specific plant, might be assigned to the different studied plant material (roots).

Table 24. Chemical structures of phenylethanoid glycosides from *Stachys* spp.

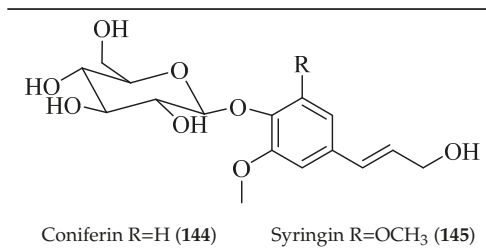
Name	Caffeic acid						Ferulic acid						
	R <sub>1</sub>	R <sub>2</sub>	R <sub>3</sub>	R <sub>4</sub>	R <sub>5</sub>	R <sub>6</sub>	R <sub>1</sub>	R <sub>2</sub>	R <sub>3</sub>	R <sub>4</sub>	R <sub>5</sub>	R <sub>6</sub>	R
Rhodiolide (Salidroside) (115)	H	H	H	H	H	OH	H	H	H	H	H	OH	H
Verbascoside (decaffeoyl-acteoside) (116)	H	H	Rha	H	H	OH	H	H	H	H	OH	OH	H
2-Phenylethyl-D-xylopyranosyl-(1 →6)-D-glucopyranoside (117)	Xyl	H	H	H	H	OH	H	H	H	H	H	H	H
Acteoside (Verbascoside) (118)	H	Caf	Rha	H	H	OH	H	H	H	H	OH	OH	H
Isoacteoside (119)	Caf	H	Rha	H	H	OH	H	H	H	H	OH	OH	H
Darendoside B (deacyl-martynoside) (120)	H	H	Rha	H	H	OH	H	H	H	H	OH	OCH <sub>3</sub>	H
β-OH-Acteoside (Campneoside II) (121)	H	Caf	Rha	H	H	OH	H	H	H	H	OH	OCH <sub>3</sub>	H
2'-O-Arabinosyl verbascoside (122)	H	Caf	Rha	H	H	OH	H	H	H	H	OH	OH	H
Betonyoside A (123)	H	Fer	Rha	H	H	OH	H	H	H	H	OH	OH	Ara
Betonyoside B/C (isomers) (124/125)	Fer	H	Rha	H	H	OH	H	H	H	H	OH	OH	H
Betonyoside D (126)	Api	Cis-fer	Rha	H	H	OH	H	H	H	H	OH	OCH <sub>3</sub>	H
Betonyoside E (127)	Api	Fer	Rha	H	H	OH	H	H	H	H	OH	OH	H
Betonyoside F (128)	H	Caf	Rha-Api	H	H	OH	H	H	H	H	OH	OH	H
Lavandulifolioside A (Stachyoside A) (129)	H	Caf	Rha-Ara	H	H	OH	H	H	H	H	OH	OH	H
Lavandulifolioside B (130)	H	4'-methyl-Fer	Rha-Ara	H	H	OH	H	H	H	H	OCH <sub>3</sub>	OH	H
Leucosceptoside A (131)	H	Fer	Rha	H	H	OH	H	H	H	H	OH	OH	H
Leucosceptoside B (132)	Api	Fer	Rha	H	H	OH	H	H	H	H	OCH <sub>3</sub>	OCH <sub>3</sub>	H
Aeschynanthoside C (133)	H	Fer	Xyl	H	H	OH	H	H	H	H	OH	OCH <sub>3</sub>	H
Leonoside B (Stachyoside D) (134)	H	Fer	Rha-Ara	H	H	OH	H	H	H	H	OH	OCH <sub>3</sub>	H
Martynoside (135)	H	Fer	Rha	H	H	OH	H	H	H	H	OH	OCH <sub>3</sub>	H
Campneoside I (136)	H	Caf	Rha	OCH <sub>3</sub>	H	OH	H	H	H	H	OH	OH	H



Table 24. *Cont.*

Name	R <sub>1</sub>	R <sub>2</sub>	R <sub>3</sub>	R <sub>4</sub>	R <sub>5</sub>	R <sub>6</sub>	R
Forsythoside B (137)	Api	Caf	Rha	H	OH	OH	H
β-OH-Forsythoside B methyl ether (138)	Api	Caf	Rha	OCH <sub>3</sub>	OH	OH	H
Leonoside A (Stachyoside B) (139)	H	Fer	Rha-Ara	H	OH	OH	H
* Stachyoside C (140)	H	Fer	Rha-Ara	H	OH	OH	H
Lamiophloside A (141)	Api	Fer	Rha	H	OCH <sub>3</sub>	OH	H
Parvifloroside A (142)	H	Caf	H	H	OH	OH	Rha
Parvifloroside B (143)	Caf	H	H	H	OH	OH	Rha

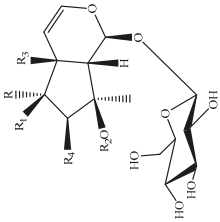
Caf: Caffeic acid, Fer: Ferulic acid, Api: Apioside, Rha: Rhamnoside, Ara: Arabinoside, Xyl: Xyloside, \*: might be synonym of Leonoside B.

**Table 25.** Chemical structures of phenylpropanoid glucosides from *Stachys* spp.

#### 4.5. Iridoids

Iridoids are among the major chemical compounds found in genus *Stachys*. According to Tundis et al. (2014), iridoids are considered as good chemotaxonomic markers of this genus [3]. Accumulating phytochemical studies have reported diverse types of iridoids [3]. The present review summarises all these studies, exemplifying 38 *Stachys* species which their iridoid cargo has been investigated (Tables 12 and 26). Harpagide (148; 31 species) and its acetyl derivative; 8 acetyl-harpagide (150; 28 species) are of common occurrence in genus *Stachys* and might be considered as characteristic iridoids of these plants. Furthermore, ajugol (146; 18 species), ajugoside (147; 18 species), melittoside (166; 17 species), monomelittoside (165; 4 species) and 5-alloxyloxy-aucubin or 5-O-allopyranosyl-monomelittoside (167; 4 species/1 subsp.) were also mentioned in various species. Allobetonoside (161) was firstly isolated from the aerial parts of *S. officinalis* [127] and then from the aerial parts of *S. glutinosa* [122] and of *S. macrantha* [117]. The latter study also mentioned the isolation of cinnamoyl-harpagide derivative, macranthoside (156), for the first time. To be mentioned that Jeker et al. (1989) also isolated 6-O-acetylmiporoside (155) from the aerial parts of *S. officinalis* [127]. In addition, two species revealed the presence of 8-*epi*-loganic acid (157), 8-*epi*-loganin (159) and gardoside (160) [20,56], as well as 7-O-acetyl-8-*epi*-loganic acid (158) was only mentioned from the aerial parts of *S. spinosa* [98]. Of note, Iannuzzi et al. (2019) isolated from the leaves of *S. ocymastrum* (syn. *S. hirta* L.) five iridoids which haven't been documented in other species, namely 6 $\beta$ -acetoxyipolamiide (172) 6 $\beta$ -hydroxyipolamiide (173), ipolamiide (174), ipolamiidoside (175) and lamiide (176) [123]. A study conducted by Háznagy-Radnai (2006) examined the phytochemical profiles of *Stachys* spp. growing in Hungary, reporting the iridoid content of ten taxa [124]. Murata and co-workers (2008) isolated five new esters of monomelittoside from the aerial parts and roots of *S. lanata* [82]. In particular, stachyosides E (168), G-H (170–171) were found in roots, while stachyosides E (168) and F (169) were discovered from the aerial parts of the specific species. It is important to be mentioned the detection of a new iridoid diglycoside, 4'-O- $\beta$ -D-galactopyranosyl-teuhircoside (162), which was isolated from the flowering aerial parts of *S. alopecuros* subsp. *divulsa* [119]. Muñoz et al. (2001) reported the presence of 5-desoxy-harpagide (151) and 5-desoxy-8-acetyl-harpagide (152) from the aerial parts of *S. grandidentata* [129]. Notably, this review unveiled some differences in iridoids among subgenera *Stachys* and *Betonica*. Firstly, it was observed that there is no report for the presence of monomelittoside or melittoside derivatives in the subgenus *Betonica*. Secondly, reptoside (153) was found in two species of subgenus *Betonica* (*S. macrantha* and *S. officinalis*) and not in the plants of subgenus *Stachys*.

Table 26. Chemical structures of iridoids from *Stachyis* spp.



Name	R	R <sub>1</sub>	R <sub>2</sub>	R <sub>3</sub>	R <sub>4</sub>
Ajugol (146)	H	OH	H	H	H
Ajugoside (147)	H	OH	Ac	H	H
Harpagide (148)	H	OH	H	OH	H
7-Hydroxyharpagide (149)	H	OH	H	OH	OH
8-Acetylharpagide (Acetylharpagide) (150)	H	OH	Ac	OH	H
5-Desoxyharpagide (151)	OH	OH	H	OH	H
5-Desoxy-8-acetylharpagide (152)	OH	OH	Ac	H	H
Reptoside (153)	H	H	Ac	OH	H
Harpagoside (154)	H	OH	Cinnamoyl-	OH	H
6-O-Acetylmioposide (155)	AcO	H	H	H	H
Macranthoside (156)	H	OH	3,4-dimethoxy cinnamoyl-	OH	H
8-Epi-loganic acid R=R'=H (157)					
7-O-Acetyl-8-epi-loganic acid R=Ac, R'=H (158)					
8-Epi-loganin R=H, R'=CH <sub>3</sub> (159)					

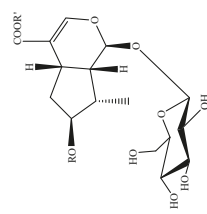


Table 26. *Cont.*

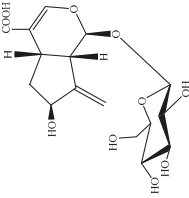
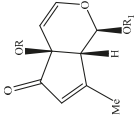
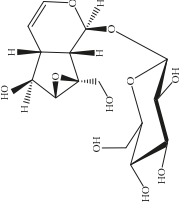
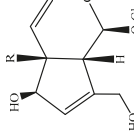
Name	R	R <sub>1</sub>	R <sub>2</sub>	R <sub>3</sub>	R <sub>4</sub>
			Gardoside (160)		
			Allobetonicoside R=Allose, R <sub>1</sub> =Glc (161) 4'-O-β-D-galactopyranosyl-teuhiroside R=H, R <sub>1</sub> =Glc-Gal (162)		
			Catalpol (163)		
			Aucubin R=H (164) Monomelittoside R=OH (165) Melittoside R=O-Glc (166) 5-O-Allopyranosyl-monomelittoside; 5-Alloxyloxy-aucubin R=O-Alo (167)		

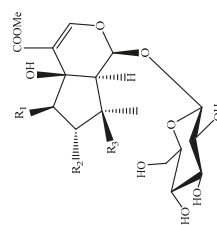
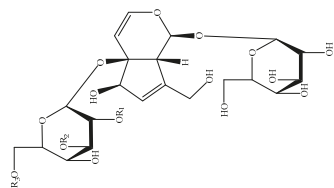
Table 26. Cont.

Name	R <sub>1</sub>	R <sub>2</sub>	R <sub>3</sub>
Stachyoside E (168)	H	<i>p</i> -( <i>E</i> )-coumaroyl-	H
Stachyoside F (169)	H	<i>p</i> -( <i>Z</i> )-coumaroyl-	H
Stachyoside G (170)	H	H	<i>p</i> -( <i>E</i> )-coumaroyl-
Stachyoside H (171)	<i>p</i> -( <i>E</i> )-coumaroyl-	H	H

Name	R <sub>1</sub>	R <sub>2</sub>	R <sub>3</sub>
6β-Acetoxyipolamiide (172)	OAc	H	OH
6β-Hydroxyipolamiide (173)	OH	H	OH
Ipolamiide (174)	H	H	OH
Ipolamiidoside (175)	H	H	OAc

Glc: Glucose, Gal: Galactose, Alo: Allose.



#### 4.6. Diterpenes

A landmark study for diterpenes of genus *Stachys* is the review article of Piozzi and Bruno (2011), including all the reported diterpenoids from roots and aerial parts of *Stachys* spp [21]. Up to now, several types of diterpenes have been mentioned, comprising types of *neo*-clerodane, labdane, rosane and *ent*-kaurene skeleton (Tables 13 and 27). The most common type is the *neo*-clerodane skeleton derivatives, as they were found in various species. *S. aegyptiaca* has thoroughly studied for its phytochemical profile. A study conducted by Hegazy et al. (2017) reported the discovery of three new *neo*-clerodane diterpenoids from the aerial parts of the aforementioned plant, namely stachaegyptins A-C (190–192) [106]. One year later, two new compounds were mentioned; stachaegyptins D-E (193–194) [131], while in a current work stachaegyptins F-H were isolated (195–197) [133]. Moreover, stachysperoxide (189) was isolated from the *S. aegyptiaca* [132]. These stachaegyptin derivatives and stachysperoxide reported only in the species *S. aegyptiaca* and might be a characteristic chemical compound of the specific plant of the section *Ambleia*. Derkach (1998) mentioned the compounds annuanone (*cis*-clerodane type) (181), stachylone (182) and stachone (183) in five species of the subgenus *Stachys*; *S. atherocalyx*, *S. inflata*, *S. iberica* and *S. sylvatica* [134]. Other *neo*-clerodane type diterpenes which were found in many species are roseostachenone (184), roseostachone (185), roseostachenol (186) and roseotetrol (187). Ruiu and co-workers (2015) explored the aerial parts of *S. glutinosa*, isolating roseostachenone and the new *neo*-clerodane diterpene, 3 $\alpha$ ,4 $\alpha$ -epoxyroseostachenol (188) [107]. Furthermore, labdane type derivatives were occurred in the genus *Stachys*. Fazio et al. (1994) investigated the aerial parts of *S. mucronata* and isolated three labdane skeleton compounds; ribenone (198), ribenol (199) and 13-*epi*-sclareol (200) [57]. The latter compound has also been found in *S. rosea* [141]. Paternostro et al. (2000) studied the aerial parts of *S. plumosa*, determining the following labdane type derivatives (+)-6-deoxyandalusol (201), 13-*epi*-jabugodiol (202) and (+)-plumosol (203) [144]. The compound (+)-6-deoxyandalusol were also found in *S. distans* and *S. ionica* [139]. Some *ent*-kaurene derivatives were reported in *S. aegyptiaca* [130], *S. lanata* [135] and *S. sylvatica* [142]. Moreover, one abietane diterpenoid, horminone (211), was isolated from the aerial parts of *S. mialhesii* [103]. It is noteworthy to be underlay the presence of two rare rosane type diterpenes in the aerial parts of *S. parviflora*, namely stachyrosanes 1 (212) and 2 (213) [134]. In addition, six diterpene lactone derivatives, i.e., betolide (214), betonicolide (215) and betonicosides A-D (216–219) were found in the species *S. officinalis* [143,145] and *S. scardica* [143] of the subgenus *Betonica*.

In the context of chemotaxonomic significance, it could be observed that species of subgenus *Stachys* product mainly *neo*-clerodane and labdane type derivatives, while the plants of subgenus *Betonica* biosynthesized diterpene lactone derivatives. Thus, the latter derivatives might be recognised as characteristic chemotaxonomic markers of subgenus *Betonica*. Another important chemotaxonomic point is reported by Piozzi et al. (2002), mentioning that (+)-6-deoxyandalusol has been determined only in three *Stachys* species of eastern part of the Mediterranean region [139].

Table 27. Diterpenes from *Stachys* spp.

Name	$R_1$	$R_2$
Stachysolone (177) 7-Monoacetyl-stachysolone (178) 13-Monoacetyl-stachysolone (179) 7,13-Diacetyl-stachysolone (180)	H Ac H Ac	H H Ac Ac
Annuanone (181)		
Stachylone (182)		
Stachone (183)		
Roseostachenone (184)		
Roseostachone (185)		
Roseostachenol (186)		
Roseotetrol (187)		
3 $\alpha$ ,4 $\alpha$ -Epoxyroseostachenol (188)		
Stachysperoxide (189)		

Table 27. Cont.

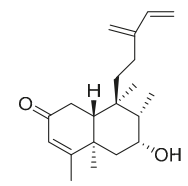
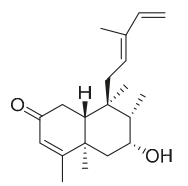
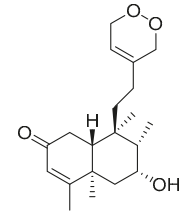
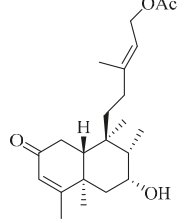
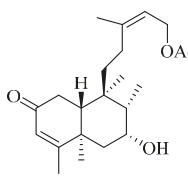
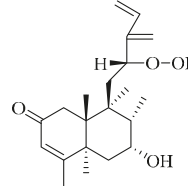
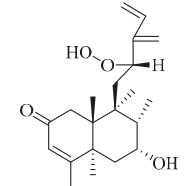
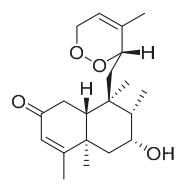
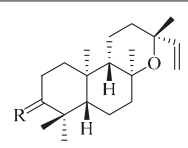
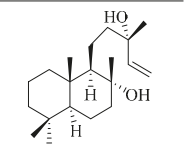
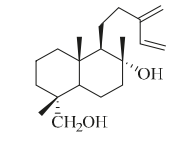
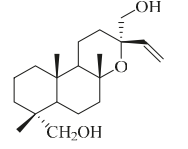
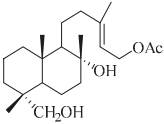
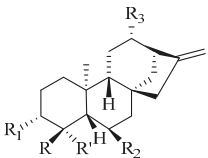
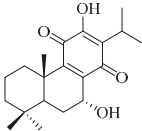
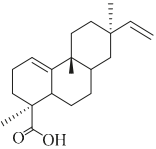
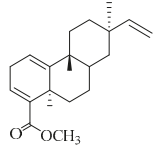
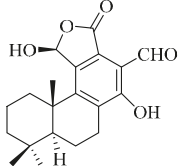
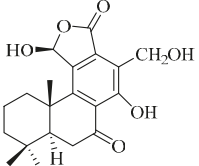
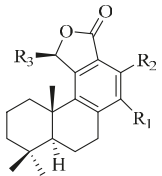
	
<p>Stachaegyptin A (190)</p>	<p>Stachaegyptin B (191)</p>
	
<p>Stachaegyptin C (192)</p>	<p>Stachaegyptin D (193)</p>
	
<p>Stachaegyptin E (194)</p>	<p>Stachaegyptin F (195)</p>
	
<p>Stachaegyptin G (196)</p>	<p>Stachaegyptin H (197)</p>
	
<p>Ribenone R=O (198) Ribenol R=αOH,βH(199)</p>	<p>13-Epi-sclareol (200)</p>
	
<p>(+)-6-Deoxyandalusol (201)</p>	<p>13-Epi-jabugodiol (202)</p>



Table 27. Cont.

						
(+)-Plumosol (203)						
						
<b>Name</b>	<b>R</b>	<b>R'</b>	<b>R<sub>1</sub></b>	<b>R<sub>2</sub></b>	<b>R<sub>3</sub></b>	
Stachysic acid (204)	COOH	CH <sub>3</sub>	H	OAc	H	
6β-hydroxy- <i>ent</i> -kaur-16-ene (205)	CH <sub>3</sub>	CH <sub>3</sub>	H	OH	H	
6β,18-dihydroxy- <i>ent</i> -kaur-16-ene (206)	CH <sub>2</sub> OH	CH <sub>3</sub>	H	OH	H	
<i>Ent</i> -3α-acetoxy-kaur-16-en-19-oic acid (207)	CH <sub>3</sub>	COOH	OAc	H	H	
3α,19-Dihydroxy- <i>ent</i> -kaur-16-ene (208)	CH <sub>3</sub>	CH <sub>2</sub> OH	OH	H	H	
<i>Ent</i> -3α-hydroxy-kaur-16-en-19-oic acid (209)	CH <sub>3</sub>	COOH	OH	H	H	
11a,18-Dihydroxy- <i>ent</i> -kaur-16-ene (210)	CH <sub>2</sub> OH	CH <sub>3</sub>	H	H	OH	
						
Horminone (211)						
						
Stachyrosane 1 (212)			Stachyrosane 2 (213)			
						
Betolide (214)			Betonicolide (215)			
	<b>Name</b>	<b>R<sub>1</sub></b>	<b>R<sub>2</sub></b>	<b>R<sub>3</sub></b>		
	Betonicoside A (216)	O-Glc	CH <sub>2</sub> OH	O-Glc		
	Betonicoside B (217)	O-Glc	CH <sub>2</sub> OH	OH		
	Betonicoside C (218)	OH	CH <sub>2</sub> OH	O-Glc		
	Betonicoside D (219)	OH	CH <sub>2</sub> O-Glc	OH		

Glc: Glucose.

#### 4.7. Triterpene Derivatives, Phytosterols and Phytoecdysteroids

Triterpene derivatives and phytosterols are major secondary metabolites of Lamiaceae family. In genus *Stachys*, five phytosterol derivatives (220–224) were found in *S. byzantina* [17,35], *S. annua* [95],

*S. spinosa* [99], *S. tetragona* [100], *S. palustris* [146] and *S. alopecurus* subsp. *divulsa* [119] (Tables 14 and 28). Furthermore, the triterpenoids; ursolic (226) and oleanolic (227) acids were only reported from the section *Olisia* (subg. *Stachys*) [95,99,100]. Kotsos et al. (2007) isolated an oleanolic lactone derivative (228) of the aerial parts of *S. spinosa* [99]. It is noteworthy to be mentioned the presence of saponin derivatives in genus *Stachys* (Tables 14 and 28). The first saponins isolated from this genus were from the water extract of the whole plant of *S. riederi*, including 8 stachyssaponins (I-VIII, 231–238) [147]. Afterwards, stachyssaponins A-B (229–230) were found from the methanol extract of the aerial parts of *S. parviflora* [63].

Few *Stachys* spp. include phytoecdysteroids (Tables 14 and 28). Ramazanov and co-workers (2016) isolated five phytoecdysteroids from *S. hissarica* [67], namely 20-hydroxyecdysone (239), polipodin B (240), integristeron A (241), 2-desoxy-20-hydroxyecdysone (242) and 2-desoxyecdysone (243).

**Table 28.** Triterpene derivatives, Phytosterols and Phytoecdysteroids from *Stachys* spp.

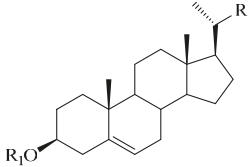
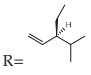
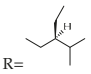
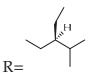
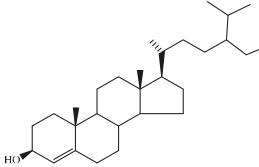
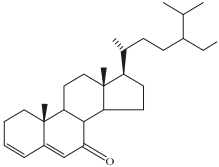
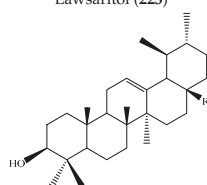
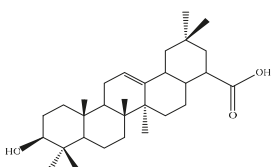
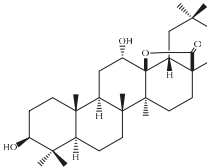
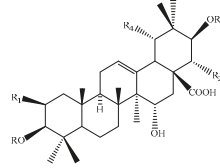
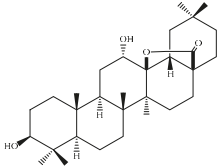
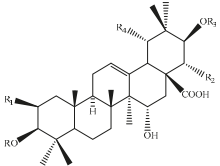
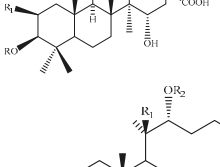
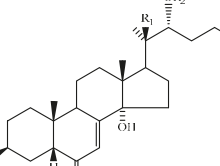
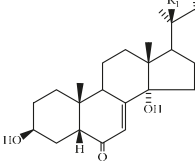
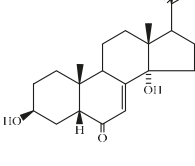
	Stigmasterol (220)		R <sub>1</sub> =H
	β-Sitosterol (221)		R <sub>1</sub> =H
	3-O-β-Sitosterol-glucoside (222)		R <sub>1</sub> =Glc
 <p>Lawsaritol (223)</p>	 <p>Stigmastan-3,5-dien-7-one (224)</p>		
 <p>α-Amyrin R=CH<sub>3</sub> (225) Ursolic acid R=COOH (226)</p>	 <p>Oleanolic acid (227)</p>		
 <p>12α-hydroxy-oleanolic lactone (228)</p>			
 <p>Stachyssaponin A (229) Stachyssaponin B (230)</p>	<p>R=Glc-Rha, R<sub>1</sub>=H, R<sub>2</sub>=Glc-Ara, R<sub>3</sub>=H, R<sub>4</sub>=OH R=Glc, R<sub>1</sub>=Ara, R<sub>2</sub>=H, R<sub>3</sub>=Glc, R<sub>4</sub>=H</p>		

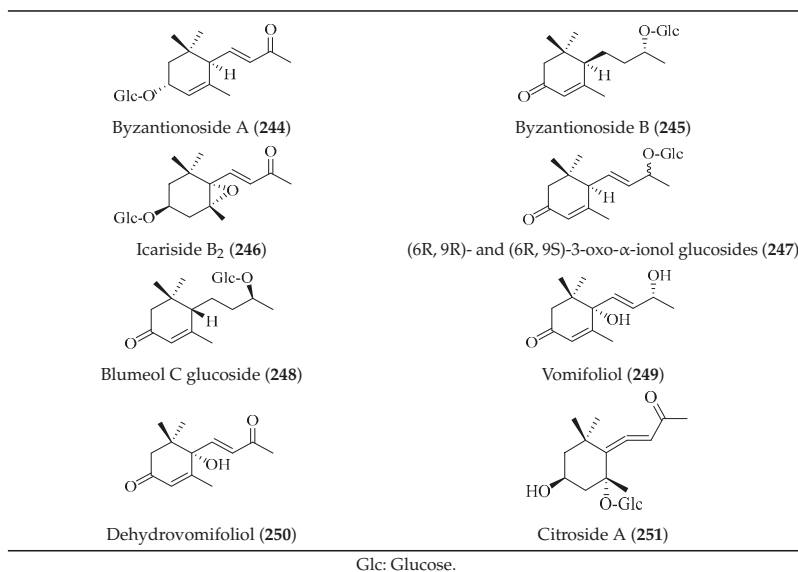
Table 28. Cont.

	Stachyssaponin I R=OGlc-Ara, R <sub>1</sub> =Ara (231) Stachyssaponin II R=OGlc-Ara, R <sub>1</sub> =Ara-Rha (232) Stachyssaponin III R=OGlc-Xyl, R <sub>1</sub> =Ara-Rha (233) Stachyssaponin IV R=OGlc-Ara, R <sub>1</sub> =Ara-Rha-Xyl (234) Stachyssaponin V R=OGlc-Ara, R <sub>1</sub> =Ara-Rha-Xyl- <sup>3</sup> Ac (235) Stachyssaponin VI R=OGlc-Ara, R <sub>1</sub> =Ara-Rha-Xyl- <sup>4</sup> Ac (236) Stachyssaponin VII R=OGlc-Ara, R <sub>1</sub> =Ara-Rha-( <sup>6</sup> Glc)-Xyl (237) Stachyssaponin VIII R=OGlc-Xyl, R <sub>1</sub> =Ara-Rha-Xyl (238)
	20-Hydroxyecdysone (239) R <sub>1</sub> =R <sub>2</sub> =R <sub>3</sub> =R <sub>5</sub> =H, R <sub>4</sub> =OH, R <sub>6</sub> =CH <sub>3</sub>
	Polipodin B (240) R <sub>1</sub> =R <sub>2</sub> =R <sub>5</sub> =H, R <sub>3</sub> =R <sub>4</sub> =OH, R <sub>6</sub> =CH <sub>3</sub>
	Integristeron A (241) R <sub>2</sub> =R <sub>3</sub> =R <sub>5</sub> =H, R <sub>1</sub> =R <sub>4</sub> =OH, R <sub>6</sub> =CH <sub>3</sub>
	2-Desoxy-20-hydroxyecdysone (242) R <sub>1</sub> =OH, R <sub>2</sub> =H
	2-Desoxyecdysone (243) R <sub>1</sub> =R <sub>2</sub> =H

Glc: Glucose, Xyl: Xylose, Rha: Rhamnose, Ara: Arabinose.

#### 4.8. Other Chemical Categories

Notable among the above-mentioned classes of compounds are the megastigmane derivatives from *Stachys* spp. (Tables 15 and 29). Takeda and colleagues (1997) isolated from the aerial parts of *S. byzantina* five bioactive compounds from this group, including byzantiosides A-B (244,245), icariside B2 (246), (6R, 9R)- and (6R, 9S)-3-oxo- $\alpha$ -ionol glucosides (247) and blumeol C glucoside (248) [148]. Furthermore, vomifoliol (249) and dehydrovomifoliol (250) were reported from the aerial parts of *S. lanata*, while citroside A (251) was isolated from the roots of this species [82]. This study also mentioned the presence of sugar ester (cistanoside F) from the roots of *S. lanata* [82]. At this point, we should note that few studies reported some oligosaccharides from *Stachys* spp. [3]. For instance, stachyose is a tetrasaccharide which consists one of the most common oligosaccharides in genus *Stachys* and shows beneficial effects for the gastrointestinal system as it can be directly consumed [3,23,119,150]. Precisely, the species *S. sieboldii* is a major source of this constituent [27,151,152]. Stachyose is an oligosaccharide, which can be directly consumed for the benefit of gastrointestinal system [150]. Furthermore, Yin and colleagues (2006) mentioned that the bitter taste of some *Stachys* species, such as *S. annua* and *S. balansae*, might be attributed to their bitter diterpene derivatives, like stachylone [22,151].

**Table 29.** Chemical structures of megastigmane derivatives from *Stachys* spp.

## 5. Pharmacological Activities

This section includes the most interesting pharmacological data of the last five years (from 2015 to 2020). Many studies exemplified the great antimicrobial, antioxidant and cytotoxic effects of the essential oils of these plants [3,15]. Tundis et al. (2014) described in detail the biological studies (in vitro and in vivo) of the essential oils, extracts and compounds [3]. Thus, in the present review, we focused on the current available pharmacological researches of the extracts and isolated compounds from *Stachys* spp. as they are presented in Table 30.

Table 30. Pharmacological activities of *Stachys* spp.

Species	Extract or Compound	Activity <sup>a</sup>	Ref
<i>S. aegyptiaca</i> Pers.	Stachysolone diacetate (180)	Cytotoxicity HepC2 cell line IC <sub>50</sub> : 59.5 µM	[132]
	Ethyl acetate fraction	Antioxidant DPPH IC <sub>50</sub> : 0.85 ± 0.04 µg/mL Superoxide radical scavenging activity: 38.63–61.41%	[28]
<i>S. affinis</i> Bunge (= <i>S. sieboldii</i> Miq.)	Ethanol	Cytotoxicity K562 cell line; SH-SY5Y cell line; Caco-2 cell line: n.a. Anti-ROS K562 cell line; SH-SY5Y cell line; Caco-2 cell line EC <sub>50</sub> : 0.0023 mg/mL; 0.05 mg/mL; 0.026 mg/mL	[27]
	Methanol	Antioxidant Phosphomolybdenum (mmol TEs/g extract): 1.49 ± 0.12 ABTS (mg TEs/g extract): 143.85 ± 0.47 Nitric oxide (mmol TEs/g extract): 1.84 ± 0.02 CUPRAC (mg TEs/g extract): 134.73 ± 10.37	
<i>S. byzantina</i> K. Koch.	Water	DPPH (mg TEs/g extract): 125.26 ± 1.47 Superoxide anion (mg TEs/g extract): 50.68 ± 2.05 FRAP (mg TEs/g extract): 98.73 ± 2.14 Chelating effect (mg EDTAs/g extract): 16.69 ± 0.96	[153]
	Ethyl acetate	Anti-Alzheimer's AChE inhibition (mg GALAEs/g extract): 2.08 ± 0.01 BChE inhibition (mg GALAEs/g extract): 4.09 ± 0.04 Anti-tyrosinase Tyrosinase inhibition (mg KAEs/g extract): 33.27 ± 0.54 Anti-diabetic α-Amylase inhibition (mmol ACEs/g extract): 0.31 ± 0.01 α-Glucosidase inhibition (mmol ACEs/g extract): 1.95 ± 0.20	

Table 30. *Cont.*

Species	Extract or Compound	Activity <sup>a</sup>	Ref
<i>S. cretica</i> L. subsp. <i>smyrneca</i> Rech. f.	Methanol	<b>Antioxidant</b>	
		Ferrous ion chelating (mg EDTAEs/g dp): 4.82 ± 0.04	
		Phosphomolybdenum (mg TEs/g dp): 71.94 ± 4.56	
		DPPH (mg TEs/g dp): 9.10 ± 0.04	
		ABTS (mg TEs/g dp): 17.36 ± 0.07	
	CUPRAC (mg TEs/g dp): 14.67 ± 0.02		
	FRAP (mg TEs/g dp): 12.98 ± 0.11	[81]	
	Methanol	<b>Anti-Alzheimer's</b>	ACHE inhibition (µg GALAEs/g dp): 343.78 ± 10.79
	Ethyl acetate	BChE inhibition (µg GALAEs/g dp): 167.68 ± 2.68	
	Ethyl acetate	<b>Anti-tyrosinase</b>	Tyrosinase inhibition (mg KAEs/g dp): 2.45 ± 0.05
Methanol	<b>Anti-diabetic</b>		
	α-Amylase inhibition (mg ACEs/g dp): 61.47 ± 0.05		
	α-Glucosidase inhibition (mg ACEs/g dp): 47.84 ± 0.78		
Water	<b>Antioxidant</b>		
	Phosphomolybdenum (mmol TEs/g extract): 2.17 ± 0.21		
	DPPH (mg TEs/g extract): 176.21 ± 2.52		
	ABTS (mg TEs/g extract): 292.67 ± 1.53		
	CUPRAC (mg TEs/g extract): 256.79 ± 2.02		
Methanol	FRAP (mg TEs/g extract): 236.44 ± 2.96		
	Ferrous ion chelating (mg EDTAEs/g extract): 18.57 ± 0.04	[108]	
	<b>Anti-Alzheimer's</b>		
Methanol	ACHE inhibition (mg GALAEs/g extract): 2.03 ± 0.15		
Ethyl acetate	BChE inhibition (mg GALAEs/g extract): 0.39 ± 0.01		
Ethyl acetate	<b>Anti-tyrosinase</b>		
	Tyrosinase inhibition (mg KAEs/g extract): 16.58 ± 0.31		
	<b>Anti-diabetic</b>		
Ethyl acetate	α-Amylase inhibition (mg ACEs/g extract): 396.50 ± 4.63		
Methanol	α-Glucosidase inhibition (mg ACEs/g extract): 734.47 ± 4.32		

Table 30. *Cont.*

Species	Extract or Compound	Activity <sup>a</sup>	Ref
<i>S. cretica</i> L. subsp. <i>vaccillans</i> Rech. f.	Methanol	<b>Antioxidant</b> (mg TE/g extract) DPPH: 191.47 ± 5.77 ABTS: 213.93 ± 21.83 CUPRAC: 579.23 ± 13.99 FRAP: 254.40 ± 8.58	[112]
	Water	Ferrous ion chelating (mg EDTAE/g extract): 68.72 ± 0.80	
<i>S. ehrenbergii</i> Boiss.	Methanol	<b>Anti-tyrosinase</b> Tyrosinase inhibition (mg KAE/g extract): 314.04 ± 2.05	
	Methanol	<b>Anti-diabetic</b> $\alpha$ -Amylase inhibition (mg ACE/g extract): 433.99 ± 5.10	
	Methanol	<b>Antioxidant</b> ABTS IC <sub>50</sub> : 52 ± 7.5 mg/mL <b>Cytotoxicity</b> A549 cell line IC <sub>50</sub> : 420 ± 104 $\mu$ g/mL	[154]
<i>S. glutinosa</i> L.	Dichloromethane; Xanthomicrol (69)	<b>Opioid Receptors binding affinity (in silico)</b> K <sub>i</sub> for MOR = 10.3 $\mu$ g/mL, K <sub>i</sub> for K <sub>1</sub> for MOR = 9.0 $\mu$ g/mL; K <sub>i</sub> for MOR = 0.83 $\mu$ M, K <sub>i</sub> for DOR = 3.6 $\mu$ M <b>Antinociceptive (in vivo)</b>	[107]
	Chloroform <i>n</i> -Butanol Chloroform <i>n</i> -Butanol	<b>Antioxidant</b> $\beta$ -carotene IC <sub>50</sub> : 2.30 ± 1.27 $\mu$ g/mL DPPH IC <sub>50</sub> : 2.91 ± 0.14 $\mu$ g/mL ABTS IC <sub>50</sub> : 7.29 ± 0.23 $\mu$ g/mL CUPRAC A <sub>0.50</sub> : 0.15 ± 0.05 $\mu$ g/mL Metal chelating assay: (%) of inhibition at 100 $\mu$ g/mL: 48.00 ± 1.71	[155]
<i>S. guyoniana</i> Noé ex Batt.	<i>n</i> -Butanol	<b>Anticholinesterase</b> AChE inhibition IC <sub>50</sub> : 5.78 ± 0.01 $\mu$ g/mL BChE inhibition IC <sub>50</sub> : 39.10 ± 1.41 $\mu$ g/mL	
	<i>n</i> -Butanol; Chloroform	<b>Antibacterial</b> MIC value: <i>S. aureus</i> 32 ± 0.90 $\mu$ g/mL, <i>E. aerogenes</i> 32 ± 0.70 $\mu$ g/mL; <i>E. coli</i> 64 ± 0.60 $\mu$ g/mL	
<i>S. hissarica</i> Regel	-	<b>Wound Healing (in vivo)</b>	[67]

Table 30. *Cont.*

Species	Extract or Compound	Activity <sup>a</sup>	Ref
<i>S. iberica</i> var. <i>densipilosa</i> R. Bhattacharjee	Ethyl acetate;	<b>Antioxidant</b> ABTS (mg TE <sub>s</sub> /g extract): 138.16 ± 0.49, Nitric oxide (mmol TE <sub>s</sub> /g extract): 1.81 ± 0.01, Superoxide anion (mg TE <sub>s</sub> /g extract): 41.31 ± 1.64, CUPRAC (mg TE <sub>s</sub> /g extract): 111.47 ± 4.67;	[153]
	Water	DPPH (mg TE <sub>s</sub> /g extract): 82.52 ± 1.62 FRAP (mg TE <sub>s</sub> /g extract): 89.15 ± 0.82 Chelating effect (mg EDTA <sub>s</sub> /g extract): 9.24 ± 0.87	
<i>S. ina</i> Griseb.	Ethyl acetate	<b>Anti-Alzheimer's</b> AChE inhibition (mg GALAE <sub>s</sub> /g extract): 2.16 ± 0.01 BChE inhibition (mg GALAE <sub>s</sub> /g extract): 4.20 ± 0.01 <b>Anti-tyrosinase</b> Tyrosinase inhibition (mg KAE <sub>s</sub> /g extract): 16.59 ± 0.33 <b>Anti-diabetic</b> α-Amylase inhibition (mmol ACE <sub>s</sub> /g extract): 0.34 ± 0.02 α-Glucosidase inhibition (mmol ACE <sub>s</sub> /g extract): 6.17 ± 0.51	[56]
	Stachysetin (98)	<b>Anti-diabetic (in silico)</b> Dipeptyl peptidase IV, peroxisome proliferator-active receptor gamma, aldose reductase, glycogen kinase, pancreatic alpha amylase precursor	
<i>S. mitalhesii</i> Noé	<i>n</i> -Butanol; Isoscutellarein-7-O-[6'''-O-acetyl]-β-D-allopyranosyl-(1→2)-β-D-glucoside (15)	<b>Antioxidant</b> DPPH IC <sub>50</sub> : 0.047 ± 0.0048 mg/mL; 0.066 ± 0.002 mg/mL	[103]
	<i>n</i> -Butanol	<b>Acute toxicity (in vitro)</b> Not toxic (10 g/kg of extract) <b>Antinociceptive (in vitro)</b> Inhibition of the writhing response induced by acetic acid (dose: 10,000; 5000 mg/kg) 77.11%, 58.22% <b>Antiinflammatory (in vitro)</b> Carrageenan-induced paw edema (dose: 5000 mg/kg) 52.03% <b>Ulcerogenic (in vitro)</b> n.a.	
<i>S. mucronata</i> Sieb.	<i>n</i> -Butanol fraction	<b>Anti-radical</b>	[156]



Table 30. *Cont.*

Species	Extract or Compound	Activity <sup>a</sup>	Ref
<i>S. laundifolia</i> Vahl.	Methanol Soxhlet extract; Arbutin (107), Ethanol; Arbutin (107), Methanol Soxhlet extract; Arbutin (107),	<b>Antioxidant</b> DPPH IC <sub>50</sub> : 25.0 ± 1.1 µg/mL; 62.5 ± 0.9 µg/mL, ABTS IC <sub>50</sub> : 19.9 µg/mL, 45.7 µg/mL, FRAP (µM Fe(II)/g): 44.5 ± 1.0; 12.2 ± 0.6,	[116]
	Methanol; Ethanol	β-carotene IC <sub>50</sub> : 29.3 µg/mL (30 min), 60.3 µg/mL (60 min); 33.0 µg/mL (30 min), 34.6 µg/mL (60 min)	
	Ethanol	<b>Anti-tyrosinase</b> Tyrosinase inhibition IC <sub>50</sub> : 33.4 ± 0.8 µg/mL	
	Hexane Dichloromethane	<b>Anti-Alzheimer's</b> AChE inhibition IC <sub>50</sub> : 13.7 ± 1.2 µg/mL BChE inhibition IC <sub>50</sub> : 143.9 µg/mL	
<i>S. officinalis</i> (L.) Trevis (= <i>Betonica officinalis</i> L.)	Chloroform	<b>Cytotoxicity</b> Brine Shrimp lethality test: 121.8 ± 5.6 µg/mL	[13]
	Apigenin (1); Chryso-splenetin (84)	MRC-5 cell line IC <sub>50</sub> : 35.67 µg/mL; MDA-MB-231 cell line IC <sub>50</sub> : 88.23 µg/mL, HT-29 cell line IC <sub>50</sub> : 116.50 µg/mL	
<i>S. ocymastrum</i> (L.) Briq. (= <i>S. hirta</i> L.)	Acetone Methanol	<b>Genotoxicity</b>	[157]
	6β-Acetoxyipolamiide (172); 6β-Hydroxyipolamiide (173); Ipolamiide (174); Ipolamiidoxide (175)	<b>Antiangiogenic (in vivo)</b>	
	Methanol	<b>Antioxidant</b> DPPH IC <sub>50</sub> : 76.87 ± 0.57 µg/mL BCB IC <sub>50</sub> : 188.47 ± 0.76 µg/mL <b>Cytotoxicity</b> A2780 cell line IC <sub>50</sub> : n.a HCT cell line IC <sub>50</sub> : n.a B16F10 cell line IC <sub>50</sub> : n.a <b>Antibacterial</b> MIC: <i>Bacillus cereus</i> 0.12 mg/mL	

Table 30. *Cont.*

Species	Extract or Compound	Activity <sup>a</sup>	Ref
<i>S. pilifera</i> Benth.	Terpenoid fraction	Cytotoxicity HT29 cell line IC <sub>50</sub> : 46.44 µg/mL	[45]
	70% Methanol Alkaloid fraction	Antiproliferative Caspase-8 increased 99% Caspase-9 increased 85.38%	
	70% Ethanol	Hepatoprotective ( <i>in vivo</i> )	[158]
	Hydroalcoholic	Antioxidant ( <i>in vivo</i> ) Hepatoprotective ( <i>in vivo</i> )	[159]
	Hydroalcoholic Water	Antioxidant ( <i>in vivo</i> ) Renoprotective ( <i>in vivo</i> ) Neuroprotective ( <i>in vivo</i> )	[19] [152]
<i>S. riederi</i> var. <i>japonica</i> (Miq.) H. Hara	80% Ethanol	Antioxidant/Cytoprotective UVA-irradiated human dermal fibroblasts (HDFs) Cytotoxicity HDFs: I.a./n.a.	[160]
<i>S. sieboldii</i> Miq. (= <i>S. affinis</i> Bunge)	<i>n</i> -Hexane fraction <i>n</i> -Hexane; 85% MeOH; <i>n</i> -BuOH; water fractions	Antioxidant ROS inhibition: 63% Increased GSH levels Inhibited oxidative DNA damage >90%	[29]
	(Root powder)	Anti-obesity ( <i>in vivo</i> ) Anti-dyslipidemic ( <i>in vivo</i> )	[161]
	20% Ethanol	Memory protective ( <i>in vivo</i> )	[162]
<i>S. sylvatica</i> L.	Hydroalcoholic	Polycystic ovary syndrome ( <i>in vivo</i> ) (500 mg/kg) (mIU/mL), FSH 5.95 ± 0.02 mIU/mL, LH 6.48 ± 0.09 mIU/mL, Estrogen 0.9 ± 0.07 mIU/mL, LH/FSH 6.48/5.59 mIU/mL.	[47]

Table 30. *Cont.*

Species	Extract or Compound	Activity <sup>a</sup>	Ref
<i>S. thirskii</i> K. Koch.	Methanol	<b>Antioxidant</b>	[84]
		$\beta$ -carotene IC <sub>50</sub> : 47.79 ± 0.59 µg/mL DPPH IC <sub>50</sub> : 49.31 ± 0.38 µg/mL ABTS IC <sub>50</sub> : 13.34 ± 0.02 µg/mL CUPRAC absorbance%: 1.88 ± 0.02	
	Acetone	<b>Anticholinesterase</b>	
		AChE inhibition IC <sub>50</sub> : 52.46 ± 1.26% BChE inhibition IC <sub>50</sub> : 75.04 ± 1.91%	
	Methanol	<b>Cytotoxicity</b>	
		A549 and L929 Fibroblast cells (100 mg/mL); n.a.	
	Acetone; Methanol	<b>Antimicrobial</b>	
		Inhibition zone diameter: <i>S. aureus</i> (10 mm), <i>S. pyogenes</i> (10 mm), <i>E. coli</i> (10 mm), <i>P. aeruginosa</i> (n.a.), <i>C. albicans</i> : n.a.; <i>S. aureus</i> (10 mm), <i>S. pyogenes</i> (10 mm), <i>E. coli</i> (10 mm), <i>P. aeruginosa</i> (n.a.), <i>C. albicans</i> : n.a.	
		MIC values: 250 ± 0.6 µg/mL, 300 ± 0.4 µg/mL, 250 ± 0.3 µg/mL, n.a., n.a.; 300 ± 0.1 µg/mL, 250 ± 0.2 µg/mL, 250 ± 0.4 µg/mL, n.a., n.a.	
<i>S. thmolen</i> Boiss.	Water	<b>Antioxidant</b>	[85]
		DPPH (mg TE/g dp): 50.88 ± 1.55 ABTS (mg TE/g dp): 44.39 ± 3.24 CUPRAC (mg TE/g dp): 87.57 ± 0.83 FRAP (mg TE/g dp): 51.80 ± 2.17	
		Phosphomolybdenum (mg TE/g dp): 40.58 ± 3.45 Ferrous ion chelating (mg EDTAES/g dp): 1.10 ± 0.03	

<sup>a</sup> Only the highest activity; n.a.:no activity; I.a.: low activity.

### 5.1. Antioxidant Activity/Cytoprotective

Tundis et al. (2015) evaluated five extracts (*n*-hexane, dichloromethane, methanol, methanol with Soxhlet apparatus and ethanol 70% extract) from the aerial parts of *S. lavandulifolia* for their antioxidant activity, using  $\beta$ -carotene bleaching test, 2,2'-azino-bis(3-ethylbenzothiazoline-6-sulphonic acid (ABTS), 1,1-Diphenyl-2-picrylhydrazyl (DPPH), and Ferric Reducing Antioxidant Power (FRAP) assays [116]. The most polar extracts, ethanol 70% and methanol extracts, showed the highest radical scavenging activity against ABTS radical (IC<sub>50</sub> values of 19.9 and 22.8  $\mu$ g/mL, respectively), whereas the methanol extract Soxhlet apparatus was the most active in the DPPH method (IC<sub>50</sub> of 25.0  $\mu$ g/mL). In the  $\beta$ -carotene bleaching test, the methanol and ethanol extract demonstrated the stronger activity after 30 min of incubation (IC<sub>50</sub> = 29.3 and 33.0  $\mu$ g/mL, respectively) and the IC<sub>50</sub> values were of 60.3 and 34.6  $\mu$ g/mL, respectively after 60 min of incubation. Moreover, they studied the antioxidant activity of bioactive secondary metabolites; arbutin (107), acteoside (118), monomelittoside (165), melittoside (166), 5-alloxyloxy-aucubin (167), and stachysolone (177), reporting that in both DPPH and ABTS assays the most active compounds was arbutin (107) with IC<sub>50</sub> values of 62.5 and 45.7  $\mu$ g/mL, respectively [116]. Another work investigated the antioxidant activity of three extracts of *S. guyoniana*, through  $\beta$ -carotene-linoleic acid, DPPH, ABTS, CUPric Reducing Antioxidant Capacity (CUPRAC) and metal chelating assays [155]. The chloroform extract had the highest antioxidant activity (IC<sub>50</sub> = 2.3  $\pm$  1.27  $\mu$ g/mL) in  $\beta$ -carotene-linoleic acid and in ABTS method (IC<sub>50</sub> = 7.29  $\pm$  0.23  $\mu$ g/mL). The *n*-butanol extract showed the better antioxidant capacity in DPPH test (IC<sub>50</sub> = 2.91  $\pm$  0.14  $\mu$ g/mL) compared to other extracts and to the reference compound  $\alpha$ -tocopherol (IC<sub>50</sub> = 7.31  $\pm$  0.17  $\mu$ g/mL), as well as it demonstrated highest activity in CUPRAC method (A<sub>0.50</sub> = 0.15  $\pm$  0.05  $\mu$ g/mL) and in metal chelating assay (inhibition at 100  $\mu$ g/mL: 48%). In addition, Laggoune et al. (2016) demonstrated the great antioxidant properties in vivo of *S. mialhesii* [103]. Particularly, the *n*-butanol extract of the specific plant showed IC<sub>50</sub> value of 0.047 mg/mL in DPPH assay, while the IC<sub>50</sub> value of the isolated compound isoscutellarein-7-O-[6'''-O-acetyl]- $\beta$ -D-allopyranosyl-(1 $\rightarrow$ 2)- $\beta$ -D-glucoside (15) was 0.066 mg/mL and the reference compound quercetin was 0.012 mg/mL. Notably, they also mentioned that the extract (up to 10 g/kg) did not show any toxicity in mice during 24 h after administration. In addition, the antioxidant activity of three subspecies of *S. cretica* (i.e., *S. cretica* subsp. *mersinaea*; *S. cretica* subsp. *smyrnaea*; *S. cretica* subsp. *vacillans*) were investigated in different works [81,108,112]. The antioxidant capacity of the methanol extract of *S. parviflora* was measured, exhibiting an IC<sub>50</sub> value of 76.87  $\pm$  0.57  $\mu$ g/mL (DPPH method) and of 188.47  $\pm$  0.76  $\mu$ g/mL ( $\beta$ -carotene bleaching test; BCB), while the standard compound, butylated hydroxytoluene (BHT), had stronger activity in both tests (DPPH test: IC<sub>50</sub> = 1.23  $\pm$  0.02  $\mu$ g/mL; BCB test: 34.31  $\pm$  0.40  $\mu$ g/mL) [64]. Guo et al. (2018) examined the antioxidant activity of five fractions from the 70% ethanol extract of tubers of *S. affinis* by DPPH assay and superoxide radical scavenging activity [28]. The ethyl acetate fraction showed extremely high antioxidant activity in DPPH method (IC<sub>50</sub> = 0.85  $\pm$  0.04  $\mu$ g/mL) with  $\alpha$ -tocopherol as positive control (IC<sub>50</sub> = 18.68  $\pm$  0.51  $\mu$ g/mL). They reported that this great antioxidant activity was attributed to the high content in phenolics and flavonoids of this fraction and confirmed the use of this plant as a natural antioxidant. Another work studied the antioxidant activity of the extracts and fractions of the same *Stachys* species on reactive oxygen species (ROS) production induced by H<sub>2</sub>O<sub>2</sub> in HT-1080 cells [29]. In particular, the *n*-hexane fraction decreased H<sub>2</sub>O<sub>2</sub>-induced ROS and oxidative stress-induced DNA damage, as well as it increased glutathione (GSH) production. The species *S. mucronata* demonstrated strong anti-radical activity due to the high content in polyphenols [156]. A recent study conducted by Aminfar et al. (2019) described a chemometric-based approach in order to classify *S. lanata* by Gas Chromatography-Mass Spectrometry (GC-MS) fingerprints and to correlate their chemical constituents with their antioxidant capacity [35]. They identified eight antioxidant markers which could also serve as volatile markers. In addition, Elfalleh and co-workers (2019) demonstrated the differences of the antioxidant properties of the extracts of *S. tmolea*, reporting that water extract exhibited highest activity than methanol extract, using DPPH, ABTS, CUPRAC, FRAP, phosphomolybdenum and ferrous ion chelating methods [85]. A survey

conducted by Hwang et al. (2019) demonstrated that the ethanol extract of *S. riederi* var. *japonica* exhibited antioxidant effects on ultraviolet A (UVA)-irradiated human dermal fibroblasts (HDFs), through suppression of ROS generation [160]. The antioxidant activity of the methanol extract of the Lebanese species *S. ehrenbergii* was measured by ABTS radical cation decolorization assay and the methanol extract showed an IC<sub>50</sub> value of 52 ± 7.5 mg/mL [154]. Furthermore, the chemical profile and some biological activities of three herbal teas in Anatolia were examined [84]. Among them, the methanol extract of *S. thirkei* showed strongest antioxidant capacity, through β-carotene (IC<sub>50</sub> = 47.79 ± 0.59 µg/mL), DPPH (IC<sub>50</sub> = 49.31 ± 0.38 µg/mL), ABTS (IC<sub>50</sub> = 13.34 ± 0.02 µg/mL) and CUPRAC (absorbance%: 1.88 ± 0.02 µg/mL) assays. Sadeghi et al. (2020) assessed the antioxidant properties of hydroalcoholic extract of *S. pilifera* on nephrotoxicity induced with cisplatin (CP) in vivo (in rats), showing that the specific extract restored the antioxidant capacity, as well as it had renoprotective activity [19].

### 5.2. Cytotoxicity and Antiproliferative Activity

Venditti et al., (2017) investigated the cytotoxic activity and the anti-reactive oxygen species activity of the ethanol extract from tubers of the Chinese artichock (*S. affinis*) [27]. Regarding the cytotoxicity, the specific extract didn't demonstrate any activity in K562, SH-SY5Y and Caco-2 cell lines, even at the highest concentrations (1.0 mg/mL). The cytotoxic activity of extracts and isolated flavonoids from the aerial parts of *S. lavandulifolia* were studied by Delnavazi et al. (2018) through the 3-(4,5-dimethylthiazol-2-yl)-2,5-diphenyltetrazolium bromide (MTT) assay [13]. The dichloromethane extract showed the highest cytotoxic activity in brine shrimp lethality test (BSLT) (LD<sub>50</sub> = 121.8 ± 5.6 µg/mL), while as a positive control was used podophyllotoxin (LD<sub>50</sub> = 3.1 ± 0.6 µg/mL). Afterwards, they explored the cytotoxic activity of isolated flavonoids in three cancer cell lines (MDA-MB-231, HT-29 and MRC-5), using as reference compound tamoxifen. All the nine isolated flavonoids moderated the cytotoxicity activated on the studied cell lines. However, chrysopterin (84) was reported as the most active compound in the first two cell lines. In MRC-5 cell line, apigenin (1) exhibited the greatest activity. It is remarkable to point out that the specific study also mentioned the selective activity against cancer cells, reporting that chrysopterin (84), kumatakenin (79) and viscosin (78) exhibited higher selective toxicity against MDA-MB-231 cell line than tamoxifen. At this point, we should underline that the great cytotoxic activity of these compounds is attributed to their substitutions with (poly)-methylated groups which increase this effect. Another study evaluated the methanol extract, the alkaloid and the terpenoid fractions of *S. pilifera* for their cytotoxic and antiproliferative activity in vitro (HT-29 cell line), indicating great results [45]. The terpenoid fraction was found to have the best cytotoxic activity compared to the other fractions and as reference compound was used cisplatin. Moreover, they investigated the antiproliferative activity, studying the effects on the activity of caspase-8 and caspase-9, Nuclear factor-κB (NF-κB) and Nitric Oxide (NO), reporting that the extract/fractions increased the activity of caspase-8/-9 and decreased NF-κB and subsequently NO level. Of note, they compared their results with previous data of cytotoxic activity in vitro of other *Stachys* species such as *S. acerosa*, *S. benthamiana*, *S. floridana*, *S. lavandulifolia*, *S. obtusirena*, *S. persica*, *S. pubescens* and *S. spectabilis*. Three isolated compounds from the extract (CH<sub>2</sub>Cl<sub>2</sub>:MeOH 1:1) of the aerial parts of *S. aegyptiaca* were investigated for the cytotoxic activity in HepG2 cell line, using MTT assay [132]. Precisely, the IC<sub>50</sub> values of stachaeptyin D (193), stachysolon monoacetate (178) and stachysolon diacetate (180) were 94.7, 63.4 and 59.5 µM, respectively, with stachysolon diacetate being the most active. In another study, the cytotoxic effect of the ethanol extract of *S. riederi* var. *japonica* on UVA-irradiated HDFs was evaluated at different concentrations for 48 h by MTT assay, showing no or little cytotoxicity [160]. Shakeri et al. (2019) mentioned that the methanol extract of *S. parviflora* demonstrated no cytotoxic activity toward the cancer cell lines, namely A2780, HCT, and B16F10 in all tested concentrations (>100 µg/mL) [64]. Moreover, the genotoxic activity of the extracts from four different plants were investigated by Slapšytė and colleagues (2019) [157]. They reported that all the plant extracts induced DNA damage, using

the comet assay, whereas the extract of *S. officinalis* induced the increase of sister chromatid exchange value. The methanol extract of the Lebanese species *S. ehrenbergii* was investigated for its antioxidant and cytotoxic activity [154]. The cytotoxicity was examined by MTT assay where the methanol extract showed the highest cytotoxicity ( $IC_{50} = 420 \pm 104 \mu\text{g/mL}$ ) at a concentration of 3000 mg/mL.

### 5.3. Polycystic Ovary Syndrome (PCOS)

In Iran, *S. sylvatica* is used for the treatment of women with polycystic ovary syndrome (PCOS). A current study carried out by Alizadeh et al. (2020) evaluated the hydroalcoholic extract of this plant in a rat model of PCOS [47]. It was observed that the extract at the dose of 500 mg/kg increased gonadotropins FSH and LH ( $5.95 \pm 0.02 \text{ mIU/mL}$ ;  $6.48 \pm 0.09 \text{ mIU/mL}$ ) and reduced the level of estrogen ( $0.9 \pm 0.07 \text{ mIU/mL}$ ) compared to the PCOS group (FSH level:  $1.69 \pm 0.08 \text{ mIU/mL}$ ; LH level:  $6.29 \pm 0.04 \text{ mIU/mL}$ ; estrogen level:  $1.42 \pm 0.05 \text{ mIU/mL}$ ), causing the ratio of LH/FSH to be close to 1:1 (6.48/5.59). According to the literature, this ratio LH/FSH is almost 1:1 in normal cases, while in PCOS women is higher e.g., 2:1 or 3:1. They also mentioned that these great results of the extract of *S. sylvatica* could be correlated to the flavonoid content of the plant. Previous studies showed that flavonoids could decrease the level of estrogen and could also act as GABA receptor agonists, regulating gonadotropins. Given that women with PCOS showed high concentrations of inflammation factors, they assumed that the extract could act as anti-inflammatory and antioxidant agent as flavonoids and iridoids demonstrated antioxidant and anti-inflammatory properties.

### 5.4. Anticholinesterase and Anti-Alzheimer's Activity/Neuroprotective Activity

The aqueous extract from the tubers of *S. sieboldii* ("chorogi") was studied in vivo in mice model for its neuroprotective potential [152]. Specifically, the study examined the effects of chorogi's extract on cerebral ischemia and scopolamine-induced memory impairment, using as positive control the extract of *Ginkgo biloba*, proving that *S. sieboldii* improves the learning and memory dysfunction correlated with ischemic brain injury. Another work examined the cholinesterase inhibitory activity of *S. lavandulifolia* extracts and isolated compounds [116]. Specifically, the most active extract against anticholinesterase (AChE) was the *n*-hexane extract with an  $IC_{50}$  value of  $13.7 \mu\text{g/mL}$ . However, the dichloromethane extract was the most effective against butyrylcholinesterase (BChE) ( $IC_{50} = 143.9 \mu\text{g/mL}$ ) where its major constituent, stachysolone (177), inhibited the activity of this enzyme with a percentage of inhibition of 50% at 0.06 mg/mL. Among the studied polar extracts, the methanol extract exhibited a selective inhibitory activity against AChE with an  $IC_{50}$  value of  $211.4 \mu\text{g/mL}$  and the isolated compounds, arbutin (107) and 5-alloxyloxy-aucubin (167), showed a percentage of inhibition of 50 and 23.1% at 0.06 mg/mL, respectively, against AChE. Notably, the other constituents of this species were inactive at the maximum concentration tested of 0.25 mg/mL. Ferhat et al. (2016) examined the AChE activity of *n*-butanol, the ethyl acetate and the chloroform extracts of the aerial parts of *S. guyoniana*, demonstrating that the *n*-butanol extract ( $IC_{50} = 5.78 \pm 0.01 \mu\text{g/mL}$ ) was a little less active than the used standard drug against Alzheimer's disease; galantamine ( $IC_{50} = 5.01 \pm 0.10 \mu\text{g/mL}$ ). Furthermore, they exhibited that this extract inhibited the BChE, having an  $IC_{50}$  value of  $39.1 \pm 1.41 \mu\text{g/mL}$  which was better than the standard ( $IC_{50} = 39.10 \pm 1.41 \mu\text{g/mL}$ ) [155]. Moreover, the anti-Alzheimer's activity of two subspecies of *S. cretica* (*S. cretica* subsp. *smyrnaea*; *S. cretica* subsp. *mersinaea*) were evaluated in different works [81,108]. In addition, the potential effects of 20% ethanol extract of *S. sieboldii* was evaluated against oxidative stress induced by  $\text{H}_2\text{O}_2$  in SK-N-SH cells and memory enhancement in ICR mice [162]. This study showed that the daily intake of the extract (dose: 500 mg/kg) through dietary supplementation produced memory enhancing effects in animals. Recently, Ertas and Yener (2020) reported that the acetone extract of *S. thirkei* demonstrated good activity against AChE and BChE with a percentage of inhibition of  $52.46 \pm 1.26\%$  and  $75.04 \pm 1.91\%$ , respectively [84].

### 5.5. Anti-tyrosinase Activity

The anti-tyrosinase activity of the ethanol and methanol Soxhlet apparatus extracts of the aerial parts of *S. lavandulifolia* exhibited the best activity with IC<sub>50</sub> values of 33.4 ± 0.8 and 42.8 ± 1.1 µg/mL [116]. They underlay that the specific extracts were characterized by the phenolic compounds, acteoside (118) and arbutin (107), which are recognised as tyrosinase inhibitors. Moreover, they evaluated the anti-tyrosinase activity of the isolated iridoids among which monomelittoside (165) and melittoside (166) showed IC<sub>50</sub> values of 119.6 ± 2.2 and 163.1 ± 3.1 µg/mL respectively, while 5-alloxyloxy-aucubin (167) inhibited the enzyme with a percentage of 22.4% at a concentration of 200 µg/mL. In addition, current works investigated the anti-tyrosinase activity of three subspecies of *S. cretica* (*S. cretica* subsp. *smyrnaea*; *S. cretica* subsp. *mersinaea*; *S. cretica* subsp. *vacillans*), reporting that the ethyl acetate extract was the most effective in the first two subspecies (2.45 mg KAEs/g; 16 mg KAEs/g, respectively) [81,108]. Though, the methanol extract of *S. cretica* subsp. *vacillans* had the higher activity against tyrosinase (314.04 ± 2.05 mg KAE/g extract) [112].

### 5.6. Anti-diabetic Activity

Bahadori et al. (2018) evaluated the anti-diabetic activity of the extracts of *S. cretica* subsp. *smyrnaea* [81]. Specifically, the methanol extract demonstrated strong anti-diabetic activity against α-amylase (61.4 mg ACEs/g dry plant) and α-glucosidase (47.8 mg ACEs/g dry plant), following by ethyl acetate extract. They assumed that the above good properties were attributed to the phenolic constituents of the methanol extract since the anti-glucosidase activity is associated with caffeic acid, *trans*-cinnamic acid, and vanillin, whereas the amylase inhibitory activity is related to kaempferol and *p*-hydroxybenzoic acid. A year later, the anti-diabetic activity of the extracts of *S. cretica* subsp. *mersinaea* was studied, reporting that the ethyl acetate extract had best activity against α-amylase (396.50 mg ACEs/g), while the methanol extract exerted strong activity against α-glucosidase (734 mg ACEs/g) [108]. Furthermore, the α-amylase inhibition of the methanol and water extract of *S. cretica* subsp. *vacillans* was evaluated, with the methanol extract exhibited stronger activity (433.99 ± 5.10 mg ACE/g extract) [112]. Currently, Pritsas et al. (2020) studied the anti-diabetic activity in silico of 17 isolated compounds from the cultivated *S. iva*, mentioning that stachysetin (98) interacted with five out of ten proteins implicated in diabetes [56]. This is the only study reported a pharmacological activity of this rare compound.

### 5.7. Antimicrobial Activity

Regarding the antibacterial activity, the *n*-butanol extract of *S. guyoniana* showed strong activity against *Staphylococcus aureus* (MIC = 32 ± 0.90 µg/mL) and *Enterobacter aerogenes* (MIC = 32 ± 0.70 µg/mL), while it was not active against *Pseudomonas aeruginosa* and *Morganella morganii* [155]. The ethyl acetate extract demonstrated the best inhibition against *Escherichia coli* (MIC = 64 ± 0.60 µg/mL), whereas it didn't show any activity against *P. aeruginosa* and *M. morganii*. Shakeri et al. (2019) reported the antimicrobial activity of the methanol extract of the aerial parts of *S. parviflora* which exerted the highest activity against the Gram-positive bacterium, *Bacillus cereus*, with a MIC of 0.12 mg/mL [64]. Furthermore, the antimicrobial activity of extracts of *S. thirkei* against different microorganisms were studied according to inhibition zone diameter and MIC value [84]. The acetone and methanol extract demonstrated good activity against *S. aureus*, *Streptococcus pyogenes* and *E. coli*. Intriguingly, *S. thirkei*'s extracts were not active against *P. aeruginosa* (Gram-negative bacterium) and *Candida albicans* (yeast).

### 5.8. Hepatoprotective

The hepatoprotective property of the ethanol extract of *S. pilifera* was studied in carbon tetrachloride (CCl<sub>4</sub>)-induced hepatotoxicity in rats and indicated that this extract could act as hepatoprotective agent [158]. They assumed that this property might be also related to the strong antioxidant activity of the species. Later, Mansourian et al. (2019) exhibited the hepatoprotective and antioxidant activity

of hydroalcoholic extract of *S. pilifera* on hepatotoxicity induced by acetaminophen (APAP) in male rats [159]. Precisely, the extract reduced hepatotoxicity by decreasing liver function markers/enzymes, aspartate aminotransferase (AST) and alanine aminotransferase (ALT) and protein carbonyl (PCO) compared to the APAP group. It also diminished the oxidative stress through inhibiting protein oxidation and inducing the activity of glutathione peroxidase (GPX) enzyme. So, they assumed that this great activity was attributed to the antioxidant activity of this plant.

### 5.9. Others

Ruii et al. (2015) investigated the phytochemical profile of the dichloromethane extract of *S. glutinosa* and studied the binding affinity to  $\mu$  and  $\delta$  opioid receptors (MOR and DOR) [107]. The extract showed an interesting binding affinity for MOR (Ki values of 10.3  $\mu\text{g/mL}$ ) and DOR (Ki values of 9.0  $\mu\text{g/mL}$ ), while xanthomicrol (69) demonstrated the strongest opioid binding affinity to both opioid receptors (Ki for MOR = 0.83  $\mu\text{M}$ , Ki for DOR = 3.6  $\mu\text{M}$ ) with the highest MOR selectivity with a ratio Ki (DOR)/Ki (MOR) = 4.4. Notably, they reported that the existence of a further hydroxy group at the 3' position like in sideritoflavone (70) reduced the binding affinity for MOR (Ki = 18.5  $\mu\text{M}$ ), whereas the replacement of this group with a methoxy moiety, as in 8-methoxycirsilineol (71), eliminated the affinity for MOR (Ki > 50  $\mu\text{M}$ ). Furthermore, they evaluated the antinociceptive activity of xanthomicrol in an animal model (in mice) of acute pain (tail-flick test). In another study, the *n*-butanol extract of *S. mialhesii* exhibited significant anti-inflammatory activity *in vivo*, reducing the weight of edema: 52.03% induced by carrageenan in the rat's paw, whereas indomethacin (dose: 5 mg/kg; decrease 83.36%) was used as a reference drug [103]. In the same study, the *n*-butanol extract exerted antinociceptive effect at dose-dependent manner. Ramazanov et al. (2016) evaluated the wound healing activity of the extract of *S. hissarica* on rats, showing that the extract improved the healing process of linear skin wounds at an oral dose of 10 mg/kg [67]. Of note, the wound healing activity of the extract was more effective than the known drug methyluracil (2,4-dioxo-6-methyl-1,2,3,4-tetrahydropyrimidine), especially in case of alloxan induced diabetic animals. A study carried out by Iannuzzi et al. (2019) studied the antiangiogenic activity in two *in vivo* models (zebrafish embryos and chick chorioallantoic membrane assays) of the isolated compounds of the leaf extract of *S. ocymastrum*. The isolated compounds with the best antiangiogenic activity in both assays were  $\beta$ -hydroxyipolamiide (173) and ipolamiide (174) [123]. Recently, Lee et al. (2020) studied the anti-obesity and anti-dyslipidemic property of the roots powder of *S. sieboldii* in rats, following a high-fat and high-cholesterol diet (HFC) [161]. This powder demonstrated the anti-adipogenic and lipid-lowering effects through enhancing lipid metabolism.

Taken together all the above pharmacological studies, we could observe that these findings confirmed most of the traditional medicinal uses of *Stachys* spp. However, the present review unveiled that there are still species pharmacologically uncharted.

## 6. Clinical Studies

Through our literature survey, four clinical studies for the species *S. lavandulifolia* were revealed. The first clinical study carried out by Rahzani et al. (2013) reported the effects of the aqueous extract of the specific plant (dose; infusion from 3 g aerial parts of plant, twice daily) on the oxidative stress in 26 healthy humans, underlying that the participants demonstrated a significant reduction in oxidative stress [163]. In parallel, another randomized clinical trial (33 women) examined the effects of *S. lavandulifolia* and medroxyprogesterone acetate (MPA) in abnormal uterine bleeding (AUB) in PCOS [164]. This study exemplified that the infusion of the aerial parts of wood betony (dose; 5 g of plant in 100 mL boiling water; duration 3 months) showed a reduction of AUB, recommending its consumption for the treatment of AUB related to PCOS. They also mentioned that this result might be attributed to the flavonoid content of the plant and mainly to apigenin. In addition, Monji et al. (2018) evaluated on a clinical trial the therapeutic effects of standardized formulation of *S. lavandulifolia* on primary dysmenorrhea, indicating that the standardized capsules of plant's extract could diminish



the menstrual pain, and might be recommended as an auxiliary therapy or an alternative remedy to nonsteroidal antiinflammatory drugs (NSAIDs) with fewer side effects in primary dysmenorrhea [165]. Recently, a double-blind randomized clinical study mentioned the analgesic activity of the herbal tea of *S. lavandulifolia* (10 g in 200 cc of boiling water) in 50 patients with migraine [166], showing the capability of this herbal tisane to decrease and also improve the pain intensity in these patients. In addition, Ashtiani et al. (2019) considered that the therapeutic properties of this plant associated with its rich phytochemical profile which include iridoids, flavonoids and phenylethanoid glucosides [166].

To sum up, the above clinical studies confirm the ethnomedicinal uses of *S. lavandulifolia* as a traditional medicine. Although these promising results, more clinical studies should be performed for obtaining data for diverse *Stachys* spp. As a future prospective, further studies should strengthen the research of bioavailability, dosage, toxicity and potential drug interactions in order to endorse the observed pharmacological activities of these plants.

## 7. Toxicity

*S. lavandulifolia* is popularly claimed as an abortifacient agent by Iranian women. The effect of its hydroalcoholic extract on fertility was investigated, revealing that the extract had a dose dependent abortifacient activity. Thus, its use during pregnancy may cause abortion and consequently, the plant should be considered as contraindicated or be used with caution [167]. In addition, the nephrotoxicity of the same extract was studied on male Wistar rats and a mild degeneration of renal tubular epithelial cell after one month was observed, while in the second month the histologic lesions were significantly more. However, further studies need to evaluate renal complications of this plant in human [168]. Moreover, the acute and subchronic toxicological evaluation of *S. lavandulifolia* aqueous extract in rats indicated that the high dose (2 g/kg) did not produce any symptoms of toxicity and there was no significant difference in body weights between the control and treatment groups of the animals [169].

## 8. Conclusions

In the present review, we attempted to describe in detail all the current knowledge and research advances of genus *Stachys*, focusing on pointing the significance of this genus as herbal supplement and medicine.

Taken together with all the analyzed studies in the current review, we categorized the used literature data into four categories according to their general characteristics; ethnobotanical (no of used studies: 48), phytochemical (no of used studies: 91), pharmacological (no of in vitro studies: 22, no of in vivo studies: 8 and 2 in silico study), clinical studies (no of used studies: 4) and reviews (no of used studies: 4). The general characteristics of the analyzed studies in the current review are showed in Table 31.

**Table 31.** General characteristics of the analyzed studies in the current review.

Type of Data	No of Studies *	Years of Publication
Ethnobotanical	48	since 1914
Phytochemical	91	since 1968
Pharmacological	22 (in vitro)	since 2015
	8 (in vivo)	
	2 (in silico)	
Clinical studies	4	since 2013
Reviews	4	since 1994

\* N.B. It could be found more than one type of data in the same article.

Several *Stachys* spp. have been used as traditional herbal medicines for thousands of years. Therefore, accumulating studies have been performed in order to explore the chemical compounds and the pharmacological properties of these species to validate their claimed ethnomedicinal properties. However, the present review data shows that there are still species phytochemically and pharmacologically unexplored. This comprehensive survey could serve as useful tool for scientists searching uncharted and interesting species to study, as well as it could be an informative guide for researchers aimed to identify leads for developing novel drugs. Although many pharmacological studies have demonstrated the great properties of these plants, only the clinical effects of one species have been investigated. As a result, further studies should be performed to validate the clinical efficiency of several *Stachys* spp. and if there is any potential toxicity. To be mentioned that there are still yet much to be done on the detailed documentation (safety and efficacy data) of genus *Stachys* in order to be developed an official monograph as a traditional use or well-established use plants.

**Author Contributions:** Conceptualization and supervision: H.S.; writing—original draft preparation: E.-M.T. & C.B.; writing—review and editing: all authors. All authors have read and agreed to the published version of the manuscript.

**Funding:** This research received no external funding.

**Conflicts of Interest:** The authors declare no conflict of interest.

## References

- Bhattacharjee, R. Taxonomic studies in *Stachys* II. A new infragenic classification of *Stachys* L. [1980]. *Notes R. Bot. Gard. Edinburgh* **2008**, *38*, 65–96.
- Salmaki, Y.; Heubl, G.; Weigend, M. Towards a new classification of tribe Stachydeae (Lamiaceae): Naming clades using molecular evidence. *Bot. J. Linn. Soc.* **2019**, *190*, 345–358. [[CrossRef](#)]
- Tundis, R.; Peruzzi, L.; Menichini, F. Phytochemical and biological studies of *Stachys* species in relation to chemotaxonomy: A review. *Phytochemistry* **2014**, *102*, 7–39. [[CrossRef](#)] [[PubMed](#)]
- Koeva-Todorovska, J. *The genus Stachys L. and the genus Betonica L. Flora of PR Bulgaria*; BAS Publishing House: Sofia, Bulgaria, 1979; Volume 9, pp. 388–416.
- Marin, P.; Grayer, R.; Grujic-Jovanovic, S.; Kite, G.; Veitch, N. Glycosides of tricetin methyl ethers as chemosystematic markers in *Stachys* subgenus *Betonica*. *Phytochemistry* **2004**, *65*, 1247–1253. [[CrossRef](#)]
- Strid, A.; Tan, K. *Mountain Flora of Greece. II*; Edinburgh University Press: Edinburgh, UK, 1991; Volume 2, pp. 97–107.
- Carnoy, A. *Dictionnaire Étymologique des Noms Grecs de Plantes*; Bibliothèque du Muséon: Louvain, Paris, 1959; p. 70.
- André, J. Lexique des termes de botanique en latin. In *Etudes et Commentaires*; Librairie, C., Ed.; Klincksieck: Paris, France, 1956; p. 79.
- Leonis, P. *Lexicon Phytologicon*; Librairie, C., Ed.; Athens, Greek, 1914; p. 912. (In Greek)
- Valiakos, E.; Marselos, M.; Sakellariadis, N.; Constantinidis, T.; Skaltsa, H. Ethnopharmacological approach to the herbal medicines of the “Antidotes” in Nikolaos Myrepsos’ *Dynameron*. *J. Ethnopharmacol.* **2015**, *163*, 68–82. [[CrossRef](#)]
- Camangi, F.; Stefani, A. Le piante nella magia e nella superstizione: Alcuni esempi di pratiche popolari in Toscana. *Riv. Preist. Etnogr. Stor. Nat.* **2003**, *1*, 1–5.
- Delazar, A.; Delnavazi, M.R.; Nahar, L.; Moghadam, S.B.; Mojarab, M.; Gupta, A.; Williams, A.S.; Rahman, M.M.; Sarker, S.D.; Mojarrab, M. Lavandulifolioside B: A new phenylethanoid glycoside from the aerial parts of *Stachys lavandulifolia* Vahl. *Nat. Prod. Res.* **2011**, *25*, 8–16. [[CrossRef](#)]
- Delnavazi, M.-R.; Saiyarsarai, P.; Jafari-Nodooshan, S.; Khanavi, M.; Tavakoli, S.; Hadavinia, H.; Yassa, N. Cytotoxic flavonoids from the aerial parts of *Stachys lavandulifolia* Vahl. *Pharm. Sci.* **2018**, *24*, 332–339. [[CrossRef](#)]
- Karioti, A.; Bolognesi, L.; Vincieri, F.F.; Bilia, A.R. Analysis of the constituents of aqueous preparations of *Stachys recta* by HPLC–DAD and HPLC–ESI-MS. *J. Pharm. Biomed. Anal.* **2010**, *53*, 15–23. [[CrossRef](#)]

15. Gören, A.C.; Piozzi, F.; Akçiçek, E.; Kılıç, T.; Çarıkcı, S.; Mozioglu, E.; Setzer, W.N. Essential oil composition of twenty-two *Stachys* species (mountain tea) and their biological activities. *Phytochem. Lett.* **2011**, *4*, 448–453. [CrossRef]
16. Öztürk, M.; Duru, M.E.; Aydoğmuş-Öztürk, F.; Harmandar, M.; Mahlıçlı, M.; Kolak, U.; Ulubelen, A. GC-MS analysis and antimicrobial activity of essential oil of *Stachys cretica* subsp. *smyrnaea*. *Nat. Prod. Commun.* **2009**, *4*, 109–114. [CrossRef] [PubMed]
17. Khanavi, M.; Sharifzadeh, M.; Hadjiakhoondi, A.; Shafiee, A. Phytochemical investigation and anti-inflammatory activity of aerial parts of *Stachys byzanthina* C. Koch. *J. Ethnopharmacol.* **2005**, *97*, 463–468. [CrossRef] [PubMed]
18. Jahani, R.; Khaledyan, D.; Jahani, A.; Jamshidi, E.; Kamalinejad, M.; Khoramjouy, M.; Faizi, M. Evaluation and comparison of the antidepressant-like activity of *Artemisia dracuncululus* and *Stachys lavandulifolia* ethanolic extracts: An in vivo study. *Res. Pharm. Sci.* **2019**, *14*, 544. [CrossRef] [PubMed]
19. Sadeghi, H.; Mansourian, M.; Kokhdan, E.P.; Salehpour, Z.; Sadati, I.; Abbaszadeh-Goudarzi, K.; Asfaram, A.; Doustimotlagh, A.H. Antioxidant and protective effect of *Stachys pilifera* Benth against nephrotoxicity induced by cisplatin in rats. *J. Food Biochem.* **2020**, *44*, e13190. [CrossRef] [PubMed]
20. Meremeti, A.; Karioti, A.; Skaltsa, H.; Heilmann, J.; Sticher, O. Secondary metabolites from *Stachys ionica*. *Biochem. Syst. Ecol.* **2004**, *32*, 139–151. [CrossRef]
21. Piozzi, F.; Bruno, M. Diterpenoids from roots and aerial parts of the genus *Stachys*. *Rec. Nat. Prod.* **2011**, *5*, 1–11.
22. Gören, A.C. Use of *Stachys* species (Mountain tea) as herbal tea and food. *Rec. Nat. Prod.* **2014**, *8*, 71–82.
23. Kartsev, V.G.; Stepanichenko, N.N.; Auelbekov, S.A. Chemical composition and pharmacological properties of plants of the genus *Stachys*. *Chem. Nat. Compd.* **1994**, *30*, 645–654. [CrossRef]
24. Plant List. 2013. Available online: <http://www.theplantlist.org/tp1.1/record/kew-195205> (accessed on 4 August 2020).
25. The Euro + Med Plantbase. The Information Resource for Euro-Mediterranean Plant Diversity. Available online: <http://www2.bgbm.org/EuroPlusMed/query.asp> (accessed on 4 August 2020).
26. International Plant Name Index (IPNI). Available online: <https://www.ipni.org/n/459647-1> (accessed on 4 August 2020).
27. Venditti, A.; Frezza, C.; Celona, D.; Bianco, A.; Serafini, M.; Cianfaglione, K.; Fiorini, D.; Ferraro, S.; Maggi, F.; Lizzi, A.R.; et al. Polar constituents, protection against reactive oxygen species, and nutritional value of Chinese artichoke (*Stachys affinis* Bunge). *Food Chem.* **2017**, *221*, 473–481. [CrossRef]
28. Guo, H.; Saravanakumar, K.; Wang, M.-H. Total phenolic, flavonoid contents and free radical scavenging capacity of extracts from tubers of *Stachys affinis*. *Biocatal. Agric. Biotechnol.* **2018**, *15*, 235–239. [CrossRef]
29. Lee, J.W.; Wu, W.; Lim, S.Y. Effect of extracts from *Stachys sieboldii* Miq. on cellular reactive oxygen species and glutathione production and genomic DNA oxidation. *Asian Pac. J. Trop. Biomed.* **2018**, *8*, 485. [CrossRef]
30. Huang, W.; Gao, X.; Zhang, Y.; Jin, C.; Wang, X. The complete chloroplast genome sequence of *Stachys sieboldii* Miquel. (Labiatae), a kind of vegetable crop and Chinese medicinal material plant. *Mitochondrial DNA Part B* **2020**, *5*, 1832–1833. [CrossRef]
31. Asghari, G.; Akbari, M.; Asadi-Samani, M. Phytochemical analysis of some plants from Lamiaceae family frequently used in folk medicine in Aligudarz region of Lorestan province. *Marmara Pharm. J.* **2017**, *21*, 506. [CrossRef]
32. Lotfipour, F.; Nazemiyeh, H.; Fathi-Azad, F.; Garaei, N.; Arami, S.; Talat, S.; Sadegpour, F.; Hasanpour, R. Evaluation of antibacterial activities of some medicinal plants from North-West Iran. *Iran. J. Basic Med. Sci.* **2008**, *11*, 80–85.
33. Asnaashari, S.; Delazar, A.; Alipour, S.; Nahar, L.; Williams, A.; Pasdaran, A.; Mojarab, M.; Azad, F.; Sarker, S.D. Chemical composition, free-radical-scavenging and insecticidal activities of the aerial parts of *Stachys byzantina*. *Arch. Biol. Sci.* **2010**, *62*, 653–662. [CrossRef]
34. Naghibi, F.; Mosaddegh, M.; Motamed, M.M.; Ghorbani, A. Labiatae family in folk medicine in Iran: From ethnobotany to pharmacology. *Iran. J. Pharm. Res.* **2005**, *2*, 63–79.
35. Aminfar, P.; Abtahi, M.; Parastar, H. Gas chromatographic fingerprint analysis of secondary metabolites of *Stachys lanata* (*Stachys byzantine* C. Koch) combined with antioxidant activity modelling using multivariate chemometric methods. *J. Chromatogr. A* **2019**, *1602*, 432–440. [CrossRef]

36. Maleki, N.; Garjani, A.; Nazemiyeh, H.; Nilfouroushan, N.; Sadat, A.E.; Allameh, Z.; Hasannia, N. Potent anti-inflammatory activities of hydroalcoholic extract from aerial parts of *Stachys inflata* on rats. *J. Ethnopharmacol.* **2001**, *75*, 213–218. [[CrossRef](#)]
37. Lazarević, J.; Palić, R.; Radulović, N.S.; Ristic, N.; Stojanovic, G. Chemical composition and screening of the antimicrobial and anti-oxidative activity of extracts of *Stachys* species. *J. Serb. Chem. Soc.* **2010**, *75*, 1347–1359. [[CrossRef](#)]
38. Amin, G. Popular medicinal plants of Iran, Iranian Research Institute of medicinal plants. *Tehran* **1991**, *80*, 1–66. (In Persian)
39. Rabbani, M.; Sajjadi, S.E.; Zarei, H. Anxiolytic effects of *Stachys lavandulifolia* Vahl on the elevated plus-maze model of anxiety in mice. *J. Ethnopharmacol.* **2003**, *89*, 271–276. [[CrossRef](#)] [[PubMed](#)]
40. Rabbani, M.; Sajjadi, S.-E.; Karimi-Firozjai, M.; Ghannadian, M. Bioactivity guided isolation of apigenin from *Stachys lavandulifolia* Vahl. in mice with anxiolytic effects. *J. Herbmed Pharmacol.* **2018**, *7*, 74–78. [[CrossRef](#)]
41. Hajhashemi, V.; Ghannadi, A.; Sedighifar, S. Analgesic and anti-inflammatory properties of the hydroalcoholic, polyphenolic and boiled extracts of *Stachys lavandulifolia*. *Res. Pharm. Sci.* **2007**, *2*, 92–98.
42. Arabsalehi, F.; Rahimmalek, M.; Ehtemam, M.H. Phytochemical and morphological variation of *Stachys lavandulifolia* Vahl. populations as affected by genotype × year interaction. *Ind. Crop. Prod.* **2018**, *112*, 342–352. [[CrossRef](#)]
43. Veisi, H.; Kazemi, S.; Mohammadi, P.; Safarimehr, P.; Hemmati, S. Catalytic reduction of 4-nitrophenol over Ag nanoparticles immobilized on *Stachys lavandulifolia* extract-modified multi walled carbon nanotubes. *Polyhedron* **2019**, *157*, 232–240. [[CrossRef](#)]
44. Fooladvand, Z.; Fazeli-nasab, B. Antibacterial activities of *Stachys lavandulifolia* Vahl. extract against eight bacteria. *J. Herb. Drugs* **2014**, *5*, 13–18.
45. Kokhdan, E.P.; Sadeghi, H.; Ghafoori, H.; Sadeghi, H.; Danaei, N.; Javadian, H.; Aghamaali, M.R. Cytotoxic effect of methanolic extract, alkaloid and terpenoid fractions of *Stachys pilifera* against HT-29 cell line. *Res. Pharm. Sci.* **2018**, *13*, 404–412. [[CrossRef](#)]
46. Maleki, F.; Valilou, M.M.S. Poulk plant (*Stachys schtschegleevii*) and its antibacterial specifications. *Asian J. Res. Bot.* **2019**, *2*, 1–13.
47. Alizadeh, F.; Ramezani, M.; Piravar, Z. Effects of *Stachys sylvatica* hydroalcoholic extract on the ovary and hypophysis-gonadal axis in a rat with polycystic ovary syndrome. *Middle East Fertil. Soc. J.* **2020**, *25*, 1–7. [[CrossRef](#)]
48. Polat, R.; Cakilcioglu, U.; Kaltalioglu, K.; Ulsan, M.D.; Türkmen, Z. An ethnobotanical study on medicinal plants in Espiye and its surrounding (Giresun-Turkey). *J. Ethnopharmacol.* **2015**, *163*, 1–11. [[CrossRef](#)]
49. Altundag, E.; Öztürk, M. Ethnomedical studies on the plant resources of east Anatolia, Turkey. *Procedia Soc. Behav. Sci.* **2011**, *19*, 756–777. [[CrossRef](#)]
50. Mükemre, M.; Behçet, L.; Çakılcioglu, U.; Cakilcioglu, U. Ethnobotanical study on medicinal plants in villages of Çatak (Van-Turkey). *J. Ethnopharmacol.* **2015**, *166*, 361–374. [[CrossRef](#)]
51. Lucchetti, L.; Zitti, S.; Taffetani, F. Ethnobotanical uses in the Ancona district (Marche region, Central Italy). *J. Ethnobiol. Ethnomed.* **2019**, *15*, 1–33. [[CrossRef](#)] [[PubMed](#)]
52. Venditti, A.; Bianco, A.; Quassinti, L.; Bramucci, M.; Lupidi, G.; Damiano, S.; Papa, F.; Vittori, S.; Bini, L.M.; Giuliani, C.; et al. Phytochemical analysis, biological activity, and secretory structures of *Stachys annua* (L.) L. subsp. *annua* (Lamiaceae) from Central Italy. *Chem. Biodivers.* **2015**, *12*, 1172–1183. [[PubMed](#)]
53. Cornara, L.; La Rocca, A.; Marsili, S.; Mariotti, M.G. Traditional uses of plants in the Eastern Riviera (Liguria, Italy). *J. Ethnopharmacol.* **2009**, *125*, 16–30. [[CrossRef](#)]
54. Cornara, L.; La Rocca, A.; Terrizzano, L.; Dente, F.; Mariotti, M.G. Ethnobotanical and phytomedical knowledge in the North-Western Ligurian Alps. *J. Ethnopharmacol.* **2014**, *155*, 463–484. [[CrossRef](#)]
55. Mulas, M. Traditional uses of labiatae in the mediterranean area. *Acta Hort.* **2006**, *723*, 25–32. [[CrossRef](#)]
56. Pritsas, A.; Tomou, E.-M.; Tsitsigianni, E.; Papaemmanouil, C.D.; Diamantis, D.A.; Chatzopoulou, P.; Tzakos, A.G.; Skaltsa, H. Valorisation of stachysetin from cultivated *Stachys iva* Griseb. as anti-diabetic agent: A multi-spectroscopic and molecular docking approach. *J. Biomol. Struct. Dyn.* **2020**, 1–15. [[CrossRef](#)]
57. Fazio, C.; Passannanti, S.; Paternostro, M.; Arnold, N. Diterpenoids from *Stachys mucronata*. *Planta Med.* **1994**, *60*, 499. [[CrossRef](#)]
58. Łuczaj, Ł.; Svanberg, I.; Köhler, P. Marsh woundwort, *Stachys palustris* L. (Lamiaceae): An overlooked food plant. *Genet. Resour. Crop. Evol.* **2011**, *58*, 783–793. [[CrossRef](#)]

59. Monigatti, M.; Bussmann, R.W.; Weckerle, C.S. Medicinal plant use in two Andean communities located at different altitudes in the Bolívar Province, Peru. *J. Ethnopharmacol.* **2013**, *145*, 450–464. [[CrossRef](#)] [[PubMed](#)]
60. Duarte, M.C.T.; Figueira, G.M.; Sartoratto, A.; Rehder, V.L.G.; Delarmelina, C. Anti-Candida activity of Brazilian medicinal plants. *J. Ethnopharmacol.* **2005**, *97*, 305–311. [[CrossRef](#)] [[PubMed](#)]
61. Gruenwald, J.; Brendler, T.; Jaenicke, T. *PDR for Herbal Medicines*; Medical Economics Company: Montvale, NJ, USA, 2000; p. 832.
62. Rustaiyan, A.; Masoudi, S.; Ameri, N.; Samiee, K.; Monfared, A. Volatile constituents of *Ballota aucheri* Boiss., *Stachys benthamiana* Boiss. and *Perovskia abrotanoides* Karel. Growing wild in Iran. *J. Essent. Oil Res.* **2006**, *18*, 218–221. [[CrossRef](#)]
63. Ahmad, V.U.; Arshad, S.; Bader, S.; Iqbal, S.; Khan, A.; Khan, S.S.; Hussain, J.; Tareen, R.B.; Ahmed, A. New terpenoids from *Stachys parviflora* Benth. *Magn. Reson. Chem.* **2008**, *46*, 986–989. [[CrossRef](#)]
64. Shakeri, A.; D’Urso, G.; Taghizadeh, S.F.; Piacente, S.; Norouzi, S.; Soheili, V.; Asili, J.; Salarbashi, D. LC-ESI/LTQOrbitrap/MS/MS and GC–MS profiling of *Stachys parviflora* L. and evaluation of its biological activities. *J. Pharm. Biomed. Anal.* **2019**, *168*, 209–216. [[CrossRef](#)] [[PubMed](#)]
65. Kepekçi, R.A.; Polat, S.; Çoşkun, G.; Celik, A.; Bozkurt, A.S.; Yumrutaş, Ö.; Pehlivan, M. Preliminary characterization of phenolic acid composition and hepatoprotective effect of *Stachys pumila*. *J. Food Biochem.* **2016**, *41*, 12286. [[CrossRef](#)]
66. Kumar, D.; Bhat, Z.A. Apigenin 7-glucoside from *Stachys tibetica* Vatke and its anxiolytic effect in rats. *Phytomedicine* **2014**, *21*, 1010–1014. [[CrossRef](#)]
67. Ramazanov, N.S.; Bobayev, I.D.; Yusupova, U.Y.; Aliyeva, N.K.; Egamova, F.R.; Yuldasheva, N.Y.; Syrov, V.N. Phytoecdysteroids-containing extract from *Stachys hissarica* plant and its wound-healing activity. *Nat. Prod. Res.* **2016**, *31*, 593–597. [[CrossRef](#)]
68. El-Ansari, M.A.; Abdalla, M.F.; Saleh, N.A.M.; Barron, D.; Le Quere, J.L. Flavonoid constituents of *Stachys aegyptiaca*. *Phytochemistry* **1991**, *30*, 1169–1173. [[CrossRef](#)]
69. El-Ansari, M.A.; Nawwar, M.A.; Saleh, N.A.M. Stachysetin, a diapiogenin-7-glucoside-p, p’-dihydroxy-truxinate from *Stachys aegyptiaca*. *Phytochemistry* **1995**, *40*, 1543–1548. [[CrossRef](#)]
70. El-Desoky, S.K.; Hawas, W.U.; Sharaf, M. A new flavone glycoside from *Stachys aegyptiaca*. *Chem. Nat. Compd.* **2007**, *43*, 542–543. [[CrossRef](#)]
71. Sharaf, M. Isoscutellarein 8-O-(6’’-trans-p-coumaroyl)-β-D-glucoside from *Stachys aegyptiaca*. *Fitoterapia* **1998**, *69*, 355–357.
72. Komissarenko, N.F.; Sheremet, I.P.; Derkach, A.I.; Pakaln, D.A. Stachyflaside from *Stachys inflata* and *St. atherocalyx*. *Chem. Nat. Compd.* **1976**, *12*, 88. [[CrossRef](#)]
73. Komissarenko, N.F.; Derkach, A.I.; Sheremet, I.P.; Kovalev, I.P.; Gordienko, V.G.; Pakaln, D.A. Flavonoids of *Stachys inflata*. *Chem. Nat. Compd.* **1978**, *14*, 445–446. [[CrossRef](#)]
74. Nazemiyeh, H.; Shoeb, M.; Movahhedini, N.; Kumarasamy, Y.; Talebpour, A.; Delazar, A.; Lutfun, N.; Sarker, S. Phenolic compounds and their glycosides from *Stachys schtscheglevii* (Lamiaceae). *Biochem. Syst. Ecol.* **2006**, *34*, 721–723. [[CrossRef](#)]
75. Tomás-Barberán, F.A.; Gil, M.I.; Ferreres, F.; Tomás-Lorente, F. Flavonoid p-coumaroylglucosides and 8-hydroxyflavone allosylglucosides in some Labiatae. *Phytochemistry* **1992**, *31*, 3097–3102. [[CrossRef](#)]
76. Lakhali, H.; Boudiar, T.; Kabouche, A.; Laggoun, S.; Kabouche, Z.; Topçu, G. Antioxidant activity and flavonoids of *Stachys ocymastrum*. *Chem. Nat. Compd.* **2011**, *46*, 964–965. [[CrossRef](#)]
77. Skaltsa, H.; Bermejo, P.; Lazari, D.; Silván, A.M.; Skaltsounis, A.-L.; Sanz, A.; Abad, M.J. Inhibition of prostaglandin E2 and leukotriene C4 in mouse peritoneal macrophages and thromboxane B2 production in human platelets by flavonoids from *Stachys chrysantha* and *Stachys candida*. *Biol. Pharm. Bull.* **2000**, *23*, 47–53. [[CrossRef](#)]
78. Michailidou, A.-M. Phytochemical study of *Stachys candida* Bory & Chaub. Master’s Thesis, National and Kapodistrian University of Athens, Athens, Greece, 2018.
79. Serrilli, A.; Ramunno, A.; Piccioni, F.; Serafini, M.; Ballero, M. Flavonoids and iridoids from *Stachys corsica*. *Nat. Prod. Res.* **2005**, *19*, 561–565. [[CrossRef](#)]
80. Demirtaş, I.; Gecibesler, I.H.; Yaglioglu, A.S.; Yaglioglu, A.S. Antiproliferative activities of isolated flavone glycosides and fatty acids from *Stachys byzantina*. *Phytochem. Lett.* **2013**, *6*, 209–214. [[CrossRef](#)]

81. Bahadori, M.B.; Kirkan, B.; Sarikurkcu, C. Phenolic ingredients and therapeutic potential of *Stachys cretica* subsp. *smyrnaea* for the management of oxidative stress, Alzheimer's disease, hyperglycemia, and melasma. *Ind. Crop. Prod.* **2019**, *127*, 82–87. [[CrossRef](#)]
82. Murata, T.; Endo, Y.; Miyase, T.; Yoshizaki, F. Iridoid glycoside constituents of *Stachys lanata*. *J. Nat. Prod.* **2008**, *71*, 1768–1770. [[CrossRef](#)]
83. Derkach, A.I.; Komissarenko, N.F.; Gordienko, V.G.; Sheremet, I.P.; Kovalev, I.P.; Pakaln, D.A. Flavonoids of *Stachys spectabilis*. *Chem. Nat. Compd.* **1980**, *16*, 128–130. [[CrossRef](#)]
84. Ertas, A.; Yener, I. A comprehensive study on chemical and biological profiles of three herbal teas in Anatolia: rosmarinic and chlorogenic acids. *S. Afr. J. Bot.* **2020**, *130*, 274–281. [[CrossRef](#)]
85. Elfalleh, W.; Kirkan, B.; Sarikurkcu, C. Antioxidant potential and phenolic composition of extracts from *Stachys tmolea*: An endemic plant from Turkey. *Ind. Crop. Prod.* **2019**, *127*, 212–216. [[CrossRef](#)]
86. Venditti, A.; Bianco, A.; Nicoletti, M.; Quassinti, L.; Bramucci, M.; Lupidi, G.; Vitali, L.A.; Papa, F.; Vittori, S.; Petrelli, D.; et al. Characterization of secondary metabolites, biological activity and glandular trichomes of *Stachys tymphaea* hausskn. from the Monti Sibillini National Park (Central Apennines, Italy). *Chem. Biodivers.* **2014**, *11*, 245–261. [[CrossRef](#)] [[PubMed](#)]
87. Sen, A.; Göğür, F.; Dogan, A.; Bitis, L. Two acylated isoscutellarein glucosides with anti-inflammatory and antioxidant activities isolated from endemic *Stachys subnuda* Montbret & Aucher ex Benth. *Acta Chim. Slov.* **2019**, *66*, 831–838. [[CrossRef](#)]
88. Kostyuchenko, O.I.; Komissarenko, N.F.; Zinchenko, T.V.; Derkach, A.I. Diacetylstachyflaside from *Stachys atherocalyx*. *Khim. Prir. Soedin.* **1981**, *3*, 389–390.
89. Kostyuchenko, O.I.; Komissarenko, N.F.; Kovalev, I.P.; Derkach, A.I.; Gordienko, V.G. Acetylspectabiflaside from *Stachys atherocalyx*. *Chem. Nat. Compd.* **1982**, *18*, 170–172. [[CrossRef](#)]
90. Kostyuchenko, O.I.; Komissarenko, N.F.; Zinchenko, T.V.; Derkach, A.I.; Gordienko, V.G. Diacetylisosstachyflaside and acetylisosstachyflaside from *Stachys atherocalyx*. *Chem. Nat. Compd.* **1982**, *18*, 235–236. [[CrossRef](#)]
91. Lenherr, A.; Lahloub, M.F.; Sticher, O. Three flavonoid glucosides containing acetylated allose from *Stachys recta*. *Phytochemistry* **1984**, *23*, 2343–2345. [[CrossRef](#)]
92. Lenherr, A.; Meier, B.; Sticher, O. Modern HPLC as a tool for chemotaxonomical investigations: Iridoid glucosides and acetylated flavonoids in the group of *Stachys recta*. *Planta Med.* **1984**, *50*, 403–409. [[CrossRef](#)] [[PubMed](#)]
93. Sheremet, I.P.; Komissarenko, N.F. Flavonoid glucosides of *Stachys annua*. *Khim. Prir. Soedin* **1971**, *5*, 583.
94. Movsumov, I.S.; Yusifova, D.Y.; Suleimanov, T.A.; Mahiou-Leddett, V.; Herbetette, G.; Baghdikian, B.; Ollivier, E.; Garayev, E.E.; Garayev, E.A. Biologically active compounds from chamaenerion angustifolium and *Stachys annua* growing in Azerbaidzhan. *Chem. Nat. Compd.* **2016**, *52*, 324–325. [[CrossRef](#)]
95. Movsumov, I.S.; Garayev, E.A.; Baghdikian, B.; Mabrouki, F.; Herbetette, G.; Ollivier, E.; Suleimanov, T.A.; Garayev, E.E. Flavonoids from *Stachys annua* growing in Azerbaijan. *Chem. Nat. Compd.* **2018**, *54*, 261–262. [[CrossRef](#)]
96. Delazar, A.; Celik, S.; Göktürk, R.S.; Unal, O.; Nahar, L.; Sarker, S.D. Two acylated flavonoid glucosides from *Stachys bombycina*, and their free radical scavenging activity. *Die Pharm.* **2005**, *60*, 878–880. [[CrossRef](#)]
97. Zinchenko, T.V. Flavonoids of *Stachys neglecta*. *Farm. Zhurnal* **1969**, *24*, 28804.
98. Kotsos, M.; Aligiannis, N.; Mitaku, S.; Skaltsounis, A.-L.; Charvala, C. Chemistry of plants from Crete: Stachyspinoside, a new flavonoid glycoside and iridoids from *Stachys spinosa*. *Nat. Prod. Lett.* **2001**, *15*, 377–386. [[CrossRef](#)]
99. Kotsos, M.P.; Aligiannis, N.; Mitakou, S. A new flavonoid diglycoside and triterpenoids from *Stachys spinosa* L. (Lamiaceae). *Biochem. Syst. Ecol.* **2007**, *35*, 381–385. [[CrossRef](#)]
100. Afouxenidi, A.; Milošević-Ifantis, T.; Skaltsa, H. Secondary metabolites from *Stachys tetragona* Boiss. & Heldr. ex Boiss. and their chemotaxonomic significance. *Biochem. Syst. Ecol.* **2018**, *81*, 83–85. [[CrossRef](#)]
101. Lenherr, A.; Mabry, T.J. Acetylated allose-containing flavonoid glucosides from *Stachys anisochila*. *Phytochemistry* **1987**, *26*, 1185–1188. [[CrossRef](#)]
102. Skaltsa, H.; Georgakopoulos, P.; Lazari, D.; Karioti, A.; Heilmann, J.; Sticher, O.; Constantinidis, T. Flavonoids as chemotaxonomic markers in the polymorphic *Stachys swainsonii* (Lamiaceae). *Biochem. Syst. Ecol.* **2007**, *35*, 317–320. [[CrossRef](#)]

103. Laggoune, S.; Zeghib, A.; Kabouche, A.; Kabouche, Z.; Maklad, Y.A.; Leon, F.; Brouard, I.; Bermejo, J.; Calliste, C.A.; Duroux, J.L. Components and antioxidant, anti-inflammatory, anti-ulcer and antinociceptive activities of the endemic species *Stachys mialhesii* de Noé. *Arab. J. Chem.* **2016**, *9*, S191–S197. [[CrossRef](#)]
104. Zinchenko, T.V. Phenolic compounds of *Stachys palustris*. *Chem. Nat. Compd.* **1973**, *6*, 261–262. [[CrossRef](#)]
105. Litvinenko, V.I.; Aronova, B.N. Phenolic compounds of *Betonica foliosa*. *Chem. Nat. Compd.* **1968**, *4*, 270. [[CrossRef](#)]
106. Hegazy, M.-E.F.; Hamed, A.R.; El-Kashoury, E.-S.A.; Shaheen, A.M.; Tawfik, W.A.; Paré, P.W.; Abdel-Sattar, E.A. Stachaegyptin A–C: Neo clerodane diterpenes from *Stachys aegyptiaca*. *Phytochem. Lett.* **2017**, *21*, 151–156. [[CrossRef](#)]
107. Ruiu, S.; Anzani, N.; Orruù, A.; Floris, C.; Caboni, P.; Alcaro, S.; Maccioni, E.; Distinto, S.; Cottiglia, F. Methoxyflavones from *Stachys glutinosa* with binding affinity to opioid receptors: *In Silico*, *in vitro*, and *in vivo* studies. *J. Nat. Prod.* **2015**, *78*, 69–76. [[CrossRef](#)]
108. Bahadori, M.B.; Kirkan, B.; Sarikurkcü, C.; Ceylan, O. Metabolite profiling and health benefits of *Stachys cretica* subsp. *mersinaca* as a medicinal food. *Ind. Crop. Prod.* **2019**, *131*, 85–89. [[CrossRef](#)]
109. Venditti, A.; Serrilli, A.; Di Cecco, M.; Ciaschetti, G.; Andrisano, T.; Bianco, A. Phytochemical composition of polar fraction of *Stachys germanica* L. subsp. *salviifolia* (Ten.) Gams, a typical plant of Majella National Park. *Nat. Prod. Res.* **2013**, *27*, 190–193. [[CrossRef](#)]
110. Litvinenko, V.I. *Some Questions of the Chemistry and Taxonomy of the Labiatae Family, the Plant Resources of the Ukraine, Their Isolation and Rational Use*; Naukova Dumka: Kiev, Ukraine, 1973; p. 128.
111. Šliumpaitė, I.; Venskutonis, P.; Murkovic, M.; Ragažinskienė, O. Antioxidant properties and phenolic composition of wood betony (*Betonica officinalis* L., syn. *Stachys officinalis* L.). *Ind. Crop. Prod.* **2013**, *50*, 715–722. [[CrossRef](#)]
112. Kirkan, B. Antioxidant potential, enzyme inhibition activity, and phenolic profile of extracts from *Stachys cretica* subsp. *vacillans*. *Ind. Crop. Prod.* **2019**, *140*, 111639. [[CrossRef](#)]
113. Nishimura, H.; Sasaki, H.; Inagaki, N.; Chin, M.; Mitsuhashi, H.; Masao, C.; Chen, Z. Nine phenethyl alcohol glycosides from *Stachys sieboldii*. *Phytochemistry* **1991**, *30*, 965–969. [[CrossRef](#)]
114. Ikeda, T.; Miyase, T.; Ueno, A. Phenylethanoid glycosides from *Stachys riederi*. *Nat. Med.* **1994**, *48*, 32–38. (In Japanese)
115. Başaran, A.A.; Calis, I.; Anklin, C.; Nishibe, S.; Sticher, O. Lavandulifolioside: A new phenylpropanoid glycoside from *Stachys lavandulifolia*. *Helv. Chim. Acta* **1988**, *71*, 1483–1490. [[CrossRef](#)]
116. Tundis, R.; Bonesi, M.; Pugliese, A.; Nadjafi, F.; Menichini, F.; Loizzo, M.R. Tyrosinase, Acetyl- and Butyryl-cholinesterase inhibitory activity of *Stachys lavandulifolia* Vahl (Lamiaceae) and its major constituents. *Rec. Nat. Prod.* **2015**, *9*, 81–93.
117. Çalis, I.; Basaran, A.; Saracoglu, C.; Sticher, O. Iridoid and phenylpropanoid glycosides from *Stachys macrantha*. *Phytochemistry* **1992**, *31*, 167–169. [[CrossRef](#)]
118. Miyase, T.; Yamamoto, R.; Ueno, A. Phenylethanoid glycosides from *Stachys officinalis*. *Phytochemistry* **1996**, *43*, 475–479. [[CrossRef](#)]
119. Venditti, A.; Bianco, A.; Nicoletti, M.; Quassinti, L.; Bramucci, M.; Lupidi, G.; Vitali, L.A.; Petrelli, D.; Papa, F.; Vittori, S.; et al. Phytochemical analysis, biological evaluation and 2 micromorphological study of *Stachys alopecuroides* (L.) Benth. subsp. *divulsa* (Ten.) Grande endemic to central Apennines, Italy. *Fitoterapia* **2013**, *90*, 94–103.
120. Ahmad, V.U.; Arshad, S.; Bader, S.; Ahmed, A.; Iqbal, S.; Tareen, R.B. New phenethyl alcohol glycosides from *Stachys parviflora*. *J. Asian Nat. Prod. Res.* **2006**, *8*, 105–111. [[CrossRef](#)]
121. Komissarenko, N.F.; Derkach, A.I.; Sheremet, I.P.; Pakaln, D.A. Iridoids of *Stachys inflata* and *St. iberica*. *Khim. Prir. Soedin.* **1979**, *1*, 99–100.
122. Serrilli, A.M.; Ramunno, A.; Piccioni, F.; Serafini, M.; Ballero, M.; Bianco, A. Monoterpenoids from *Stachys glutinosa* L. *Nat. Prod. Res.* **2006**, *20*, 648–652. [[CrossRef](#)] [[PubMed](#)]
123. Iannuzzi, A.M.; Camero, C.M.; D'ambola, M.; D'angelo, V.; Amira, S.; Bader, A.; Braca, A.; De Tommasi, N.; Germanò, M.P. Antiangiogenic Iridoids from *Stachys ocymastrum* and *Premna resinosa*. *Planta Med.* **2019**, *85*, 1034–1039. [[CrossRef](#)] [[PubMed](#)]
124. Háznagy-Radnai, E.; Czígö, S.; Janicsák, G.; Máthé, I. Iridoids of *Stachys* species growing in Hungary. *J. Planar Chromatogr. Mod. TLC* **2006**, *19*, 187–190. [[CrossRef](#)]

125. Derkach, A.I.; Komissarenko, N.F.; Pakaln, D.A. Iridoids from some *Stachys* L. species. *Rast Nye Resur.* **1987**, *23*, 92–95.
126. Litvinenko, V.I.; Aronova, B.N. Iridoids of *Betonica foliosa*. *Chem. Nat. Compd.* **1968**, *4*, 269–270. [[CrossRef](#)]
127. Jeker, M.; Sticher, O.; Calis, I.; Rüedi, P. Allobetonicoside and 6-O-Acetylmiosporoside: Two new iridoid glycosides from *Betonica officinalis* L. *Helv. Chim. Acta* **1989**, *72*, 1787–1791. [[CrossRef](#)]
128. Zinchenko, T.V. *Stachys* and *Betonica* iridoids. *Farm. Zhurnal* **1972**, *27*, 86–87.
129. Muñoz, O.; Peña, R.C.; Montenegro, G. Iridoids from *Stachys grandidentata*. *Z. Nat. C* **2001**, *56*, 902–903. [[CrossRef](#)]
130. Melek, F.R.; Radwan, A.S.; El-Ansari, M.A.; El-Gindi, O.D.; Hilal, S.H.; Genenah, A.A. Diterpenes from *Stachys aegyptiaca*. *Fitoterapia* **1992**, *63*, 276.
131. Mohamed, A.E.-H.H.; Mohamed, N.S. A new trans-neo clerodane diterpene from *Stachys aegyptiaca*. *Nat. Prod. Res.* **2013**, *28*, 30–34. [[CrossRef](#)]
132. Mohamed, T.A.; ElShamy, A.I.; Hamed, A.R.; Shams, K.A.; Hegazy, M.-E.F. Cytotoxic neo-clerodane diterpenes from *Stachys aegyptiaca*. *Phytochem. Lett.* **2018**, *28*, 32–36. [[CrossRef](#)]
133. Hussien, T.A.; Mahmoud, A.A.; Mohamed, N.S.E.-D.; Shahat, A.A.; El-Seedi, H.R.; Hegazy, M.-E.F. New rare ent-clerodane diterpene peroxides from Egyptian Mountain Tea (Qourtom) and its chemosystem as herbal remedies and phytonutrients agents. *Molecules* **2020**, *25*, 2172. [[CrossRef](#)] [[PubMed](#)]
134. Derkach, A.I. Biologically active substances of some species of the genus *Stachys* L. of the flora of the Ukraine. *Rastit. Nye Resur.* **1998**, *34*, 57–61.
135. Piozzi, F.; Savona, G.; Hanson, J.R. Kaurenoid diterpenes from *Stachys lanata*. *Phytochemistry* **1980**, *19*, 1237–1238. [[CrossRef](#)]
136. Orgiyani, T.M.; Popa, D.P. Diterpenoids from *Stachys annua*. *Khim. Prir. Soedin.* **1969**, *5*, 5–6. [[CrossRef](#)]
137. Popa, D.P.; Orgiyani, T.M. The stereochemistry of stachysolone. *Khim. Prir. Soedin.* **1972**, *8*, 717–719. [[CrossRef](#)]
138. Popa, D.P.; Orgiyani, T.M. Minor diterpenoids of *Stachys annua*. *Chem. Nat. Compd.* **1974**, *10*, 410. [[CrossRef](#)]
139. Piozzi, F.; Paternostro, M.; Servettaz, O.; Arnold, N. Occurrence of (+)-6-desoxyandalusol in *Stachys ionica* and *Stachys distans*. *Biochem. Syst. Ecol.* **2002**, *30*, 887–889. [[CrossRef](#)]
140. Adinolfi, M.; Barone, G.; Lanzetta, R.; Laonigro, G.; Mangoni, L.; Parrilli, M. Diterpenes from *Stachys recta*. *J. Nat. Prod.* **1984**, *47*, 541–543. [[CrossRef](#)]
141. Fazio, C.; Paternostro, M.P.; Passannanti, S.; Piozzi, F. Further neo-clerodane diterpenoids from *Stachys rosea*. *Phytochemistry* **1994**, *37*, 501–503. [[CrossRef](#)]
142. Popa, D.P.; Pasechnik, G.S. Structure of stachysic acid—A new diterpenoid of the kaurane series. *Chem. Nat. Compd.* **1974**, *10*, 454–457. [[CrossRef](#)]
143. Bankova, V.; Koeva-Todorovska, J.; Stambolijska, T.; Ignatova-Groceva, M.-D.; Todorova, D.; Popov, S. Polyphenols in *Stachys* and *Betonica* species (Lamiaceae). *Z. Nat. C* **1999**, *54*, 876–880. [[CrossRef](#)]
144. Paternostro, M.P.; Maggio, A.M.; Piozzi, F.; Servettaz, O. Lavdane diterpenes from *Stachys plumose*. *J. Nat. Prod.* **2000**, *63*, 1166–1167. [[CrossRef](#)] [[PubMed](#)]
145. Miyase, T.; Yamamoto, R.; Ueno, A. Betonicosides A–D and betonicolide, diterpenoids from the roots of *Stachys officinalis*. *Chem. Pharm. Bull.* **1996**, *44*, 1610–1613. [[CrossRef](#)]
146. Ross, S.A.; Zinchenko, T.V. Triterpenoids and steroids from *Stachys palustris*. *Farm. Zhurnal* **1975**, *30*, 91–92. [[PubMed](#)]
147. Yamamoto, R.; Miyase, T.; Ueno, A. Stachyssaponins I–VIII, new oleanane-type triterpene saponins from *Stachys riederi* CHAMISSO. *Chem. Pharm. Bull.* **1994**, *42*, 1291–1296. [[CrossRef](#)]
148. Takeda, Y.; Zhang, H.-J.; Masuda, T.; Honda, G.; Otsuka, H.; Sezik, E.; Yesilada, E.; Sun, H. Megastigmane glucosides from *Stachys byzantina*. *Phytochemistry* **1997**, *44*, 1335–1337. [[CrossRef](#)]
149. Rodríguez-García, C.; Sánchez-Quesada, C.; Toledo, E.; Delgado-Rodríguez, M.; Gaforio, J.J. Naturally lignan-rich foods: A dietary tool for health promotion? *Molecules* **2019**, *24*, 917. [[CrossRef](#)]
150. Sørensen, M.; Penn, M.; El Mowafi, A.; Storebakken, T.; Chunfang, C.; Øverland, M.; Krogdahl, Å. Effect of stachyose, raffinose and soya-saponins supplementation on nutrient digestibility, digestive enzymes, gut morphology and growth performance in Atlantic salmon (*Salmo salar*, L.). *Aquaculture* **2011**, *314*, 145–152. [[CrossRef](#)]



151. Yin, J.; Yang, G.; Wang, S.; Chen, Y. Purification and determination of stachyose in Chinese artichoke (*Stachys sieboldii* Miq.) by high-performance liquid chromatography with evaporative light scattering detection. *Talanta* **2006**, *70*, 208–212. [[CrossRef](#)]
152. Harada, S.; Tsujita, T.; Ono, A.; Miyagi, K.; Mori, T.; Tokuyama, S. *Stachys sieboldii* (Labiatae, Chorogi) protects against learning and memory dysfunction associated with ischemic brain injury. *J. Nutr. Sci. Vitaminol.* **2015**, *61*, 167–174. [[CrossRef](#)] [[PubMed](#)]
153. Sarikurkcu, C.; Kocak, M.S.; Uren, M.C.; Calapoglu, M.; Tepe, A.S. Potential sources for the management global health problems and oxidative stress: *Stachys byzantina* and *S. iberica* subsp. *iberica* var. *densipilosa*. *Eur. J. Integr. Med.* **2016**, *8*, 631–637. [[CrossRef](#)]
154. Abi-Rizk, A.; El Rayess, Y.; Iriti, M.; Tabet, E.; Mezher, R.; El Beyrouthy, M. Chemical composition, antitumor and antioxidant effects of four lebanese plants extracts on human pulmonary adenocarcinoma. *Nat. Prod. Res.* **2020**, 1–4. [[CrossRef](#)] [[PubMed](#)]
155. Ferhat, M.; Erol, E.; Beladjila, K.A.; Çetintaş, Y.; Duru, M.E.; Öztürk, M.; Kabouche, A.; Kabouche, Z. Antioxidant, anticholinesterase and antibacterial activities of *Stachys guyoniana* and *Mentha aquatica*. *Pharm. Biol.* **2016**, *55*, 324–329. [[CrossRef](#)] [[PubMed](#)]
156. Grigorakis, S.; Makris, D.P. Characterisation of polyphenol-containing extracts from *Stachys mucronata* and evaluation of their antiradical activity. *Medicines* **2018**, *5*, 14. [[CrossRef](#)]
157. Slapšytė, G.; Dedonytė, V.; Adomėnienė, A.; Lazutka, J.R.; Kazlauskaitė, J.; Ragažinskienė, O.; Venskutonis, P.R. Genotoxic properties of *Betonica officinalis*, *Gratiola officinalis*, *Vincetoxicum luteum* and *Vincetoxicum hirundinaria* extracts. *Food Chem. Toxicol.* **2019**, *134*, 110815. [[CrossRef](#)]
158. Kokhdan, E.P.; Ahmadi, K.; Sadeghi, H.; Sadeghi, H.; Dadgary, F.; Danaei, N.; Aghamaali, M.R. Hepatoprotective effect of *Stachys pilifera* ethanol extract in carbon tetrachloride-induced hepatotoxicity in rats. *Pharm. Biol.* **2017**, *55*, 1389–1393. [[CrossRef](#)]
159. Mansourian, M.; Mirzaei, A.; Azarmehr, N.; Vakilpour, H.; Kokhdan, E.P.; Doustimotlagh, A.H. Hepatoprotective and antioxidant activity of hydroalcoholic extract of *Stachys pilifera*. Benth on acetaminophen-induced liver toxicity in male rats. *Heliyon* **2019**, *5*, e03029. [[CrossRef](#)]
160. Hwang, J.Y.; Yadav, A.K.; Jang, B.C.; Kim, Y.C. Antioxidant and cytoprotective effects of *Stachys riederi* var. *japonica* ethanol extract on UVA-irradiated human dermal fibroblasts. *Int. J. Mol. Med.* **2019**, *43*, 1497–1504.
161. Lee, J.K.; Lee, J.; Kim, Y.-K.; Lee, Y.; Ha, J.-H. *Stachys sieboldii* Miq. root attenuates weight gain and dyslipidemia in rats on a high-fat and high-cholesterol diet. *Nutrients* **2020**, *12*, 2063. [[CrossRef](#)]
162. Ravichandran, V.A.; Kim, M.; Han, S.K.; Cha, Y. *Stachys sieboldii* extract supplementation attenuates memory deficits by modulating BDNF-CREB and its downstream molecules, in animal models of memory impairment. *Nutrients* **2018**, *10*, 917. [[CrossRef](#)]
163. Rahzani, K.; Malekirad, A.A.; Zeraatpishe, A.; Hosseini, N.; Seify, S.M.R.; Abdollahi, M. Anti-oxidative stress activity of *Stachys lavandulifolia* aqueous extract in human. *Cell J.* **2013**, *14*, 314–317. [[PubMed](#)]
164. Jalilian, N.; Modarresi, M.; Rezaei, M.; Ghaderi, L.; Bozorgmanesh, M. Phytotherapeutic management of polycystic ovary syndrome: Role of aerial parts of wood betony (*Stachys lavandulifolia*). *Phytother. Res.* **2013**, *27*, 1708–1713. [[CrossRef](#)] [[PubMed](#)]
165. Monji, F.; Hashemian, F.; Surmaghi, M.-H.S.; Mohammadyari, F.; Ghiyaei, S.; Soltanmohammadi, A. Therapeutic effects of standardized formulation of *Stachys lavandulifolia* Vahl on primary dysmenorrhea: A randomized, double-blind, crossover, placebo-controlled pilot study. *J. Altern. Complement. Med.* **2018**, *24*, 1092–1098. [[CrossRef](#)] [[PubMed](#)]
166. Ashtiani, A.R.; Jadidi, A.; Hezave, A.; Safarabadi, M.; Pour, S.A.; Ghassami, K.; Mohammadbeigi, A. An analgesic effect of *Stachys lavandulifolia* in patients with migraine: A double-blind randomised clinical trial study. *Adv. Hum. Biol.* **2019**, *9*, 76. [[CrossRef](#)]
167. Jafarzadeh, L.; Rafeiean-Kopaei, M.; Samani, R.A.; Asgari, A. The effect of hydroalcoholic extract of *Stachys lavandulifolia* Vahl on pregnant mice. *EXCLI J.* **2012**, *11*, 357–362.

168. Taghikhani, M.; Nasri, H.; Asgari, A.; Afrough, H.; Namjoo, A.; Ansari-Samani, R.; Shahinfard, N.; Rafieian-Kopaei, M. The renal toxicity of hydroalcoholic extract of *Stachys lavandulifolia* Vahl in Wistar rats. *Life Sci. J.* **2012**, *9*, 3025–3031.
169. Modarresi, M.; Hosseinzadeh, L.; Nematy, N.; Siavash-Haghighi, Z.; Ghanbari, K. Acute and subchronic toxicological evaluation of *Stachys lavandulifolia* aqueous extract in Wistar rats. *Res. Pharm. Sci.* **2015**, *9*, 165.



© 2020 by the authors. Licensee MDPI, Basel, Switzerland. This article is an open access article distributed under the terms and conditions of the Creative Commons Attribution (CC BY) license (<http://creativecommons.org/licenses/by/4.0/>).





Article

# Quantification of the Ability of Natural Products to Prevent Herpes Virus Infection

Kunihiko Fukuchi <sup>1</sup>, Hiroshi Sakagami <sup>2,\*</sup>, Yoshiaki Sugita <sup>3</sup>, Koichi Takao <sup>3</sup>, Daisuke Asai <sup>4,†</sup>, Shigemi Terakubo <sup>4</sup>, Hiromu Takemura <sup>4</sup>, Hirokazu Ohno <sup>5</sup>, Misaki Horiuchi <sup>6</sup>, Madoka Suguro <sup>6</sup>, Tomohiro Fujisawa <sup>6</sup>, Kazuki Toeda <sup>6</sup>, Hiroshi Oizumi <sup>6</sup>, Toshikazu Yasui <sup>7</sup> and Takaaki Oizumi <sup>6</sup>

<sup>1</sup> Graduate School of Health Sciences, Showa University, Hatanodai 1-5-8, Shinagawa, Tokyo 142-8555, Japan; kfukuchi@med.showa-u.ac.jp

<sup>2</sup> Research Institute of Odontology (M-RIO), Meikai University, Keyakidai 1-1, Sakado, Saitama 350-0283, Japan

<sup>3</sup> Department of Pharmaceutical Sciences, Faculty of Pharmacy and Pharmaceutical Sciences, Josai University, Keyakidai 1-1, Sakado, Saitama 350-0295, Japan; sugita@josai.ac.jp (Y.S.); ktakao@josai.ac.jp (K.T.)

<sup>4</sup> Department of Microbiology, St. Marianna University School of Medicine, Sugao 2-16-1, Miyamae, Kawasaki 216-8511, Japan; asai@marianna-u.ac.jp (D.A.); biseibutsu-001@marianna-u.ac.jp (S.T.); takeh@marianna-u.ac.jp (H.T.)

<sup>5</sup> Maruzen Pharmaceuticals Co., Ltd., Fukuyama, Hiroshima 729-3103, Japan; h-ohno@maruzenpcy.co.jp

<sup>6</sup> Daiwa Biological Research Institute Co., Ltd., Sakado 3-2-1, Takatsu-ku, Kawasaki, Kanagawa 213-0012, Japan; m\_horiuchi@daiwaseibutsu.co.jp (M.H.); m\_suguro@daiwaseibutsu.co.jp (M.S.); t\_fujisawa@daiwaseibutsu.co.jp (T.F.); k\_toeda@daiwaseibutsu.co.jp (K.T.); h\_oizumi@daiwaseibutsu.co.jp (H.O.); takaakio@daiwaseibutsu.co.jp (T.O.)

<sup>7</sup> Division of Oral Health, School of Dentistry, Meikai University, Keyakidai 1-1, Sakado, Saitama 350-0283, Japan; yasui@dent.meikai.ac.jp

\* Correspondence: sakagami@dent.meikai.ac.jp; Tel.: +81-049-279-2758

† Present Address: Laboratory of Microbiology, Showa Pharmaceutical University, 3-3165 Higashi-Tamagawagakuen, Machida, Tokyo 194-8543, Japan.

Received: 11 August 2020; Accepted: 30 September 2020; Published: 6 October 2020

**Abstract: Background:** Herpes simplex virus (HSV) is usually dormant and becomes apparent when body conditions decline. We investigated the anti-HSV activity of various natural and synthetic compounds for future clinical application. **Methods:** Mock- and HSV-infected Vero cells were treated for three days with various concentrations of samples. For short exposure, 100-fold concentrated virus were preincubated for 3 min with samples, diluted to normal multiplicity of infection (MOI), before the addition to the cells. Anti-HSV activity was evaluated by the chemotherapy index. **Results:** Alkaline extracts of the leaves of *Sasa* sp. (SE) and pine cone (PCE) showed higher anti-HSV activity than 20 Japanese traditional herb medicines (Kampo formulas), four popular polyphenols, and 119 chromone-related compounds. Exposure of HSV to SE or PCE for 3 min almost completely eliminated the infectivity of HSV, whereas much longer exposure time was required for Kakkonto, the most active Kampo formulae. Anti-HSV activity of PCE and Kakkonto could be detected only when they were dissolved by alkaline solution (pH 8.0), but not by neutral buffer (pH 7.4). Anti-HSV activity of SE and povidone iodine was stable if they were diluted with neutral buffer. **Conclusions:** The present study suggests the applicability of SE and PCE for treatment of oral HSV and possibly other viruses.

**Keywords:** Kampo formulae; alkaline extract of *Sasa* sp.; pine cone extract; povidone-iodine; HSV; HIV; loss of infectivity; solubilization method

## 1. Introduction

In the oral cavity, there are many viruses including norovirus, rabies, human papillomavirus, Epstein–Barr virus, herpes simplex viruses (HSVs), hepatitis C virus, and human immunodeficiency virus (HIV). Viral infections have been diagnosed using an oral sample (e.g., saliva mucosal transudate or an oral swab) based on the correlation of HIV anti-IgG/sIgA detection with saliva and serum samples [1]. Oral herpes viruses, HSV-1 and HSV-2, are very common and infectious, and debilitate patients, affect oral health, and have important psychological implications. The therapies currently used for the treatment of HSV infection are pharmacological, topical, systemic, or instrumental, occasionally with laser devices [2]. Many natural products have been investigated for their anti-HSV activity *in vitro* or *in vivo*. These include low molecular weight polyphenols [3–6], water-extracts [7–10] including Japanese traditional herb medicine (Kampo formulae) [11,12], and alkaline extracts [13] including a lignin-carbohydrate complex [14–17].

We have already reported the anti-HSV activity of five plant extracts, 13 tannin-related compounds determined by plaque assay [18], and the anti-HSV activity of eight licorice root extracts, 10 licorice flavonoids (including isoliquiritin apioside), five polymethoxyflavonoids (including triclin), and five polyphenols (including epigallocatechin gallate, chlorogenic acid, *p*-coumaric acid, curcumin, and resveratrol) determined by the 3-(4,5-dimethylthiazol-2-yl)-2,5-diphenyltetrazolium bromide (MTT) method [19]. Quantitative structure–activity relationship (QSAR) analysis of these 19 polyphenols and 1705 chemical descriptors demonstrated that their anti-HSV activity correlated well with six chemical descriptors that represent polarizability (MATS5p, GATS5p), ionization potential (GATS5i), number of ring systems (NRS), atomic number (J\_Dz(Z)) and mass (J\_Dz(m)) ( $r^2 = 0.684, 0.627, 0.624, 0.621, 0.619$ , and  $0.618$ , respectively,  $p < 0.0001$ ) [19]. However, most of lower molecular weight polyphenols showed very low anti-HSV-activity.

In the present study, we report the *in vitro* anti-HSV activity of 20 Kampo formulas and alkaline extracts of the leaves of *Sasa* sp. (SE) and pine cone combined with dextrin (PCE), representative polyphenols, and a total of 119 chromones, esters, and amides [20–26], synthesized from chromone (to search for new type of anti-HSV agents), a back-bone structure of flavonoids, together with positive control acyclovir [27], representative polyphenols (resveratrol, *p*-coumaric acid, and curcumin used as negative controls) [19] and povidone iodine (PVP-I), a popular gargle [28].

Since gargling time with mouth wash is usually a minute order, we investigated whether short exposure of HSV (1.5 or 3 min) is enough to inactivate HSV. Since PCE and the Kampo formula contain many acidic substances such as a lignin-carbohydrate complex and its degradation products, it is expected that an alkaline solution may be useful to extract the active substances in higher yield compared with the neutral buffer, although some elevation of degradation would be inevitable. Therefore, we also compared the anti-HSV activity and its stability using either an alkaline solution (1.39% NaHCO<sub>3</sub>, pH 8.0) or a neutral buffer [phosphate-buffered saline (PBS), pH 7.4].

## 2. Materials and Methods

### 2.1. Materials

The following chemicals and reagents were obtained from the indicated companies: Eagles minimum essential medium (MEM) (Gibco BRL, Grand Island, NY, USA); fetal bovine serum (FBS), 3-(4,5-dimethylthiazol-2-yl)-2,5-diphenyltetrazolium bromide (MTT), resveratrol, azidothymidine (AZT), 2',3'-dideoxycytidine (ddC) (Sigma-Aldrich Inc., St. Louis, MO, USA); dimethyl sulfoxide, dextran sulfate (DS) (5 kDa) (Wako Pure Chemical Ind., Ltd., Osaka, Japan); acyclovir, curcumin, trans *p*-coumaric acid (Tokyo Chemical Industry Co. Ltd., Tokyo, Japan); triclin (Carbosynth Ltd., Berkshire, UK); curdlan sulfate (79 kDa) (Ajinomoto Co., Inc., Tokyo, Japan); and PVP-I (Showa Seiyaku Co. Ltd., Tokyo, Japan). Twenty Kampo formula (Table 1) were provided by Tsumura & Co, Tokyo, Japan. Culture plastic dishes and plates (96-well) were purchased from Becton Dickinson Labware (Franklin Lakes, NJ, USA).

**Table 1.** Twenty Kampo formulas used in this study.

S1	Unkeito (TJ-106)	S11	Jumihaidokuto (TJ-6)
S2	Chotosan (TJ-47)	S12	Yokuininto (TJ-52)
S3	Hochuekkito (TJ-41)	S13	Shofusan (TJ-22)
S4	Hangebyakujutsutemmato (TJ-37)	S14	Hainosankyuto (TJ-122)
S5	Kakkonto (TJ-1)	S15	Jizusoippo (TJ-59)
S6	Shomakakkonto (TJ-101)	S16	Unseiin (TJ-57)
S7	Sokeikakketsuto (TJ-53)	S17	Rikkosan (TJ-110)
S8	Seijobofuto (TJ-58)	S18	Keigairengyoto (TJ-50)
S9	Yokukansan (TJ-54)	S19	Sansoninto (TJ-103)
S10	Orengedokuto (TJ-15)	S20	Kakkontokasenkyushin'1 (TJ-2)

## 2.2. Preparation of *Sasa sp.* (SE)

SE was prepared by iron ion substitution, alkaline extraction, and neutralization/desalting (Figure 1A). Lyophilization and measurement of the dry weight of SE showed that it contained  $58.2 \pm 0.96$  mg solid materials/mL [29]. The components of SE are shown in our previous review article [30].

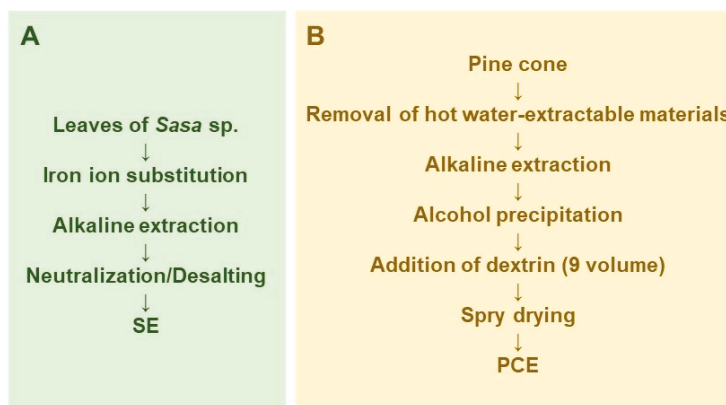


**Figure 1.** Scheme for large scale preparation of *Sasa sp.* (SE) (A) and pine cone extract (PCE) (B).

## 2.3. Preparation of Pine Cone Extract (PCE)

Pine cone extract was prepared by modification of the original method of preparation of the lignin-carbohydrate complex [31,32]. In brief, pine cone of *Pinus parviflora* Sieb et Zucc. was washed by hot water extract to remove contaminants and hot-water extractable materials, and then extracted with 0.15 N NaOH to obtain the lignin-carbohydrate complex. The lignin-carbohydrate complex was recovered by ethanol precipitation, and separated from salts and fat-soluble degradation products such as phenylpropanoids. Nine volumes of dextrin were added and spry dried to yield PCE (Figure 1B).

## 2.4. Preparation of Chromones, Esters, and Amides

Twenty four 2-azolychromone derivatives (E) were synthesized by the conjugated addition reaction of 3-iodochromone derivatives with various azoles [20]. Seventeen 3-benzylidenechromanone derivatives were synthesized by base-catalyzed condensation of the corresponding 4-chromanone with substituted benzaldehyde derivatives [21]. Fifteen chalcone derivatives were synthesized by base-catalyzed condensation of the corresponding acetophenones with various benzaldehyde derivatives [22]. Ten cinnamic acid phenethyl esters were synthesized by the condensation of cinnamic acid and its analogs such as caffeic acid, ferulic acid, and *p*-coumaric acid with the corresponding phenethyl alcohols [23]. Ten 3-flavene derivatives were synthesized by the reductive

intramolecular cycloaddition reaction of 2-hydroxychalcone derivatives [22]. Eleven piperic acid amides were synthesized by the condensation of the acid chloride of piperic acid with various amines. Piperic acid was prepared by alkaline hydrolysis of piperine [24]. Eighteen 2-styrylchromone derivatives were synthesized by base-catalyzed condensation of the corresponding 2-methylchromones with selected benzaldehyde derivatives [25]. Fourteen 3-styrylchromone derivatives were synthesized by Knoevenagel condensation of the corresponding 3-formylchromones with various phenylacetic acid derivatives [26]. All compounds were dissolved in DMSO at 40 mM and stored at  $-20\text{ }^{\circ}\text{C}$  before use.

### 2.5. Assay for Anti-Herpes Simplex Virus (HSV) Activity

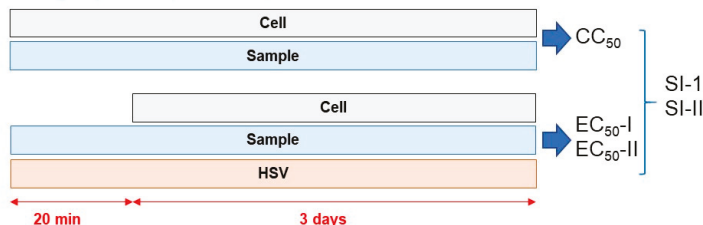
We dissolved the samples using the following three methods. (i) Method 1: Sample was dissolved at 1 mg/mL with culture medium (MEM + 10% FBS) and then sterilized by passing through a Millipore filter (pore size: 0.45  $\mu\text{m}$ ); (ii) Method 2: Sample was dissolved at 60 mg/mL with 1.39%  $\text{NaHCO}_3$  (pH 8.0) and then diluted to 3 mg/mL with medium and filtered; (iii) Method 3: Sample was dissolved at 100 mg/mL with phosphate-buffered saline (PBS, pH 7.4) or 1.39%  $\text{NaHCO}_3$ , vortexed, and shaken overnight at  $4\text{ }^{\circ}\text{C}$ . After centrifugation, the supernatant was collected and then filtered (Figure 2A).

#### A Sample preparation

Method 1	Method 2	Method 3
Sample (1 mg)	Sample (60 mg)	Sample (100 mg)
↓ Dissolved in 1 ml of medium	↓ Dissolved in 1 ml of 1.39% $\text{NaHCO}_3$	↓ Dissolved in 1 ml of PBS or 1.39% $\text{NaHCO}_3$
↓ Filtered	↓ diluted to 3 mg/ml with medium	↓ shaken overnight at $4^{\circ}\text{C}$
	↓ filtration	↓ Centrifugated Supernatant
		↓ filtration

#### B Treatment schedule

##### Long exposure (Method 2)



##### Short exposure (Method 3)

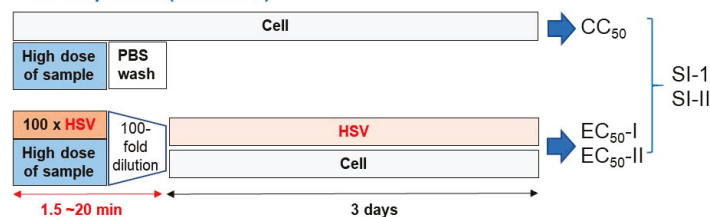


Figure 2. Experimental protocol. (A) Long treatment. (B) short treatment.

For the long treatment schedule (upper column in Figure 2B), Vero cells, isolated from the kidney of African green monkey (*Cercopithecus aethiops*) were infected with HSV-1 (multiplicity of infection (MOI) = 0.01). HSV-1 and test samples were mixed and stood for 20 min, and the mixture was then added to the adherent Vero cells. After incubation for three days, the relative viable cell number was determined by the MTT reagent.

For the short treatment schedule (lower column in Figure 2B), 100-fold concentrated HSV (MOI = 1) was mixed with samples and stood for 1.5, 3, or 20 min. Then, virus concentration was reduced to 1/100

(MOI = 0.01), added to the cells and incubated for three days. Mock-infected cells were first treated for 1.5, 3, or 20 min with the same concentrations of test samples without HSV, then the sample was removed by suction, washed once with PBS, and incubated for three days in the fresh culture medium. The viability of both HSV-infected and mock-infected cells was determined by the MTT method as described above.

From the dose-response curve, 50% cytotoxic concentration ( $CC_{50}$ ) in mock-infected cells, and the 50% effective concentration ( $EC_{50}$ ) in HSV-infected cells were determined.  $EC_{50}$ -I was defined as the concentration at which the viability was restored to the midpoint between that of HSV-infected cells and that of mock-infected cells.  $EC_{50}$ -II was defined as the concentration at which the viability was restored to 50% of that of the mock-infected cells. The anti-HSV activity was evaluated by the selectivity index (SI-I and SI-II), which was calculated using the following equation:  $SI-I = CC_{50}/EC_{50}$ -I;  $SI-II = CC_{50}/EC_{50}$ -II (Figure 3).

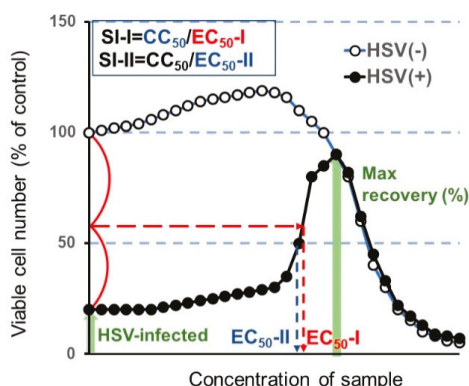


Figure 3. Calculation of anti-herpes simplex virus (HSV) activity.

## 2.6. Assay for Anti-Human Immunodeficiency Virus (HIV) Activity

Human T-cell leukemia virus I (HTLV-I)-bearing CD4-positive human T-cell line MT-4, established by Dr. Miyoshi [33], was cultured in RPMI-1640 medium supplemented with 10% FBS and infected with HIV-1<sub>III</sub>B at a multiplicity of infection (MOI) of 0.01. HIV- and mock-infected MT-4 cells ( $3 \times 10^4$  cells/96-microwell) were incubated for five days with different concentrations of extracts and the relative viable cell number was determined by the MTT assay. The concentration that reduced the viable cell number of the uninfected cells by 50% ( $CC_{50}$ ) and the concentration that increased the viable cell number of the HIV-infected cells to 50% of the control (mock-infected, untreated) cells ( $EC_{50}$ ) was determined from the dose-response curve with mock-infected and HIV-infected cells, respectively. The anti-HIV activity was evaluated by the selectivity index (SI), which was calculated using the following equation:  $SI = CC_{50}/EC_{50}$  [34,35]. Since the viable cell number of HIV-treated cell reached the baseline (zero), the  $EC_{50}$ -I and SI-I were nearly identical to  $EC_{50}$ -II and SI-II, respectively.

## 2.7. Statistical Treatment

Experimental values were expressed as the mean  $\pm$  standard deviation (SD). The statistical significance between the groups was assessed with analysis of variance (ANOVA) followed by Dunette's multiple comparison test. A  $p$  value less than 0.05 was considered significant.



### 3. Results

#### 3.1. Establishment of Assay Condition for Anti-HSV Activity

We have reported that the anti-HSV activity of most lower molecular weight polyphenols as assessed by SI value ( $CC_{50}/EC_{50}$ ) was very low ( $SI < 1$ ) when compared with the positive control (acyclovir and triclin) ( $SI > 27.3, 7.1$ ) [19]. We conducted the accurate determination of anti-HSV activity of natural products with low anti-HSV activity using two different plates: 96-well (for  $CC_{50}$  determination by the MTT method) and 6-well plates (for  $EC_{50}$  determination by plaque assay) may be difficult, especially for short exposure experiments that require quick medium change. Therefore, it was necessary to first investigate whether the infectivity of HSV-1 measured by the MTT method with the 96-well plate correlated with the plaque count of the 6-well plate under the light microscopy. We found that this was the case. With the dilution fold of the virus solution increased, the viable cell number was increased, reaching the plateau level where no plaque formation was observed (Figure 4A). We found that the virus titer of  $MOI = 0.01$  was much better than  $MOI = 0.1$  for the quantitative determination of the anti-HSV of acyclovir (ACV), one of the positive controls used in this study (Figure 4B). When we used  $MOI = 0.1$ , accurate evaluation of the viable cell number was difficult due to the presence of too much virus. Therefore, we used the fixed  $MOI = 0.01$  during the cell treatment period to maintain the viability of HSV-infected Vero cells at 20 ~ 40% (Figure 3). The selection of three days was the best incubation time for the determination of anti-HSV activity. We had to use 100-fold concentrated HSV solution ( $MOI = 1$ ) to treat the virus with extremely higher concentrated samples. We reduced the  $MOI$  100-fold during the days of cell culture ( $MOI = 0.01$ ).

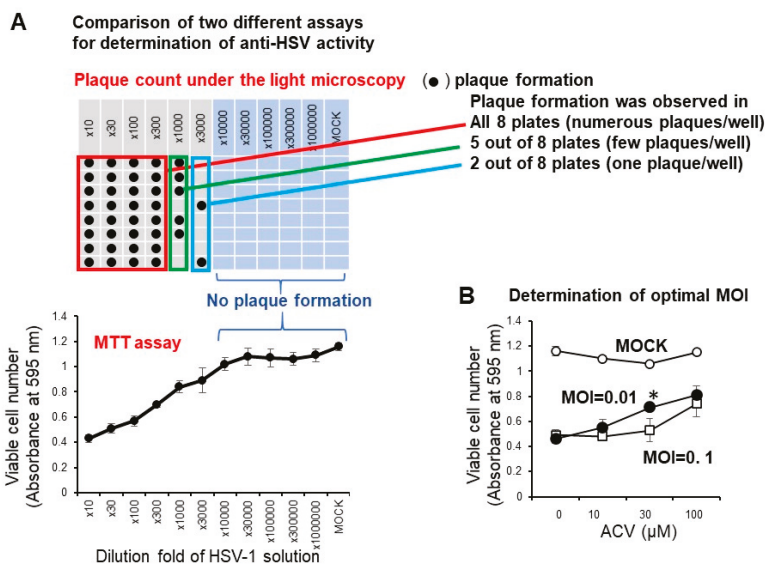


**Figure 4.** (A) Confirmation of correlation of optical density measurement with the MTT method and plaque counting. Vero cells (10,000 cells) were inoculated on a 96-microwell plate and incubated overnight at 37 °C. HSV-1 solution at the indicated dilution fold was then added. After incubation for three days, viable cell number (absorbance at 595 nm) was determined by the MTT method, and plaque formation was counted by light microscopy. (B) Effect of different MOI on the anti-HSV activity of ACV. Each value represented as mean  $\pm$  S.D. was determined (n = 3). Significant difference between  $MOI = 0.01$  and  $MOI = 0.1$  ( $p < 0.05$ ).

### 3.2. Anti-HSV Activity of Natural Products

#### 3.2.1. Hot-Water Extract (Kampo Formula) and Alkaline Extracts (SE, PCE)

It was important to first establish the method for dissolving the Kampo formulas. As a first step, we directly mixed 20 Kampo formulas with culture medium (MEM + 10% FBS), and then sterilized them by passing through a Millipore filter (Method 1 in Figure 2A). Both mock-infected and HSV-infected cells were incubated for three days without or with various concentrations of samples, and the viable cell number was determined by the MTT method. From the dose-response curve, we determined the 50% cytotoxic concentration (CC<sub>50</sub>) and 50% protective concentration (EC<sub>50-I</sub>, EC<sub>50-II</sub>) and maximum cell recovery (%) (MCR). The anti-HSV activity was assessed as the SI value (SI-I = CC<sub>50</sub>/EC<sub>50-I</sub> or SI-II = CC<sub>50</sub>/EC<sub>50-II</sub>) (Figure 3). It was unexpected that any Kampo formula, except for S19 (SI-I > 2.2; SI-II > 5.9) did not reduce the cytopathic effect of HSV infection (Supplementary Figure S1). We thought that the failure to detect anti-HSV activity may be due to the interaction of Kampo ingredients and medium components. Based on these data, we did not choose method I to solubilize the Kampo formula. We found that higher anti-HSV activity of Kampo formulas was recovered by dissolving them with 1.39% NaHCO<sub>3</sub> (pH 8.0) than with PBS (pH 7.4) (Supplementary Table S1, Supplementary Figure S2). Therefore, we dissolved all Kampo formula with 1.39% NaHCO<sub>3</sub> to make the initial concentration of 60 mg/mL, diluted with culture medium to make a 3 mg/mL solution, and sterilized by passing through a Millipore filter (Method 2 in Figure 2A).

Mock-infected and HSV-infected cells were incubated with increasing concentrations of samples and determined for viability (Figure 5). Among the 20 Kampo formulas (S1 ~ S20), Kakkonto (S5) showed the highest anti-HSV activity (SI-I > 5.2; SI-II > 5.4; MCR = 78%), followed by Yokukansan (S9) (SI-I > 1.0; SI-II > 1.6; MCR = 66%), Yokuininto (S12) (SI-II = 1.3; MCR = 52%) > Jumihaidokuto (S11) (SI-II = 1.1; MCR = 52%). However, their anti-HSV activity was much lower than that of the alkaline extract of *Sasa* sp. (SE) (Supplementary Table S2) (SI-I = 4.5; SI-II = 6.8; MCR = 90%), alkaline extract of pine cone of *Pinus parviflora* Sieb. et Zuc. (PCE) (SI-I = 13.1; SI-II = 14.7; MCR = 82%) and acyclovir (ACV) (SI-I > 23.1; SI-II > 27.3; MCR = 108%) (Table 2).

#### 3.2.2. Polyphenols and Chromone-Related Compounds

Among the four polyphenols, resveratrol (MCR = 20%), *p*-coumaric acid (MCR = 43%), and curcumin (MCR = 42%) showed little or no anti-HSV activity, whereas tricetin (SI-II = 7.1; MCR = 68%) showed weak anti-HSV activity (Figure 5, Table 2).

Among the 119 chromone-related compounds, only 2-(1*H*-pyrazol-1-yl)-4*H*-1-benzopyran-4-one (2a), 2-(1*H*-imidazol-1-yl)-6-methoxy-4*H*-1-benzopyran-4-one (3c), (3*E*)-2,3-dihydro-3-[(4-hydroxyphenyl)methylene]-7-methoxy-4*H*-1-benzopyran-4-one (14), (2*E*,4*E*)-5-(3,4-methylenedioxyphenyl)-2,4-pentadienoic acid (4-hydroxy-3-methoxyphenyl)methyl ester (2), 2-[(1*E*)-2-(4-fluorophenyl)ethenyl]-6-methoxy-4*H*-1-benzopyran-4-one (8), and 2-[(1*E*)-2-(3,4-dimethoxy)ethenyl]-6-methoxy-4*H*-1-benzopyran-4-one (12) showed weak anti-HSV activity (Figure 5). Chromone derivatives with higher antitumor activity (assessed with tumor-specificity determined by the ratio of mean CC<sub>50</sub> against four human oral squamous cell carcinoma cell lines (Ca9-22, HSC-2, HSC-3, HSC-4) to that for three normal oral cells such as human gingival fibroblasts, human periodontal ligament fibroblasts, and pulp cells (indicated by red color) showed no anti-HSV activity. Similarly, chromones with higher anti-HSV activity did not have higher antitumor activity (Supplementary Table S3).

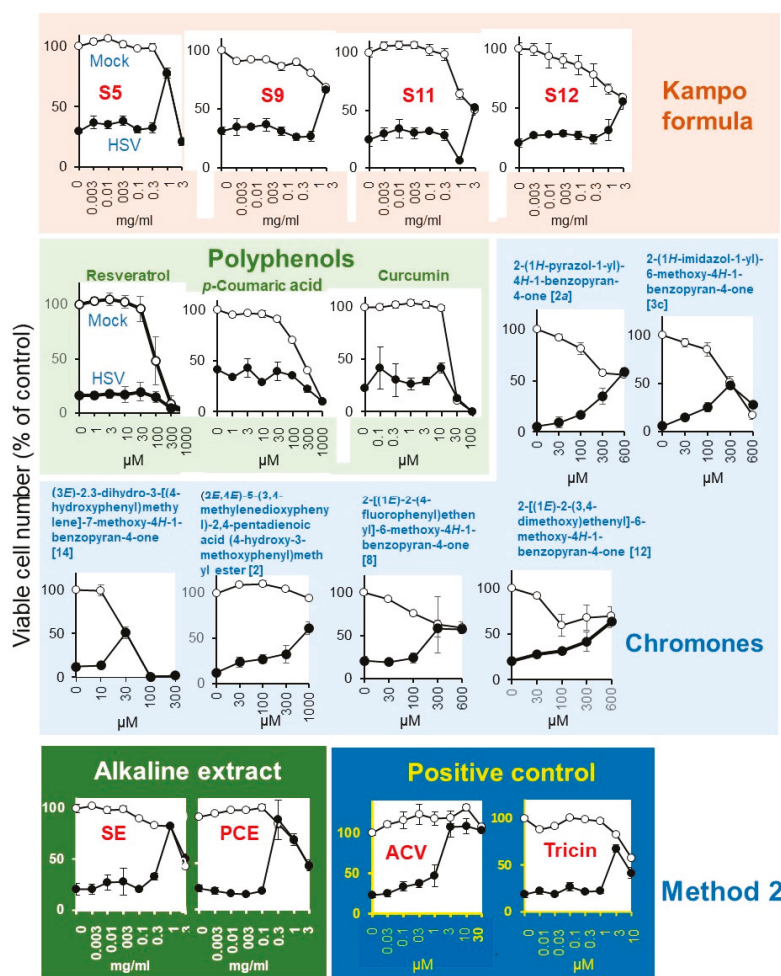


**Figure 5.** Anti-HSV activity of Kampo formulas, SE, PCE, and acyclovir (ACV). Mock-infected (○) and HSV-infected (●) cells were treated for three days and viable cell number [% of control (untreated, uninfected cells)] were determined. Each value is represented as mean ± S.D. (n = 3).

**Table 2.** Quantification of anti-HSV activity of Kampo formulas with reference compounds.

Test Sample	Viability of HSV-Infected Cells (%)	CC <sub>50</sub>	EC <sub>50-I</sub>	EC <sub>50-II</sub>	Anti-HSV Activity		Max. Cell Recovery (%)
					SI-I	SI-II	
Kampo formula (Supplementary Figure S2) (mg/mL)							
S1 Unkeito	27	>3.0	(-)	1	(-)	>3.0	51
S2 Chotosan	25	2.6	(-)	>3.0	(-)	<0.87	48
S3 Hochuekkito	25	>3.0	(-)	>3.0	(-)	><1.0	44
S4 Hangebyakujutsutemmato	26	1.35	(-)	>3.0	(-)	<0.45	41

Table 2. Cont.

Test Sample	Viability of HSV-Infected Cells (%)	CC <sub>50</sub>	EC <sub>50</sub> -I	EC <sub>50</sub> -II	Anti-HSV Activity		Max. Cell Recovery (%)
					SI-I	SI-II	
S5 Kakkonto	29	1.65	0.58	0.56	>5.2	>5.4	78
S6 Shomakakkonto	34	2.1	(-)	>3.0	(-)	<0.70	46
S7 Sokeikakketsuto	29	>3.0	(-)	>3.0	(-)	><1.0	46
S8 Seijobofuto	34	0.58	(-)	>3.0	(-)	<0.19	39
S9 Yokukansan	31	>3.0	2.9	1.9	>1.0	>1.6	66
S10 Orenge dokuto	22	0.76	(-)	>3.0	(-)	<0.25	30
S11 Jumihaidokuto	25	3	(-)	2.8	(-)	1.1	52
S12 Yokuininto	21	>3.0	(-)	2.4	(-)	1.3	55
S13 Shofusan	21	2.5	(-)	>3.0	(-)	<0.83	34
S14 Hainosankyuto	24	2.6	(-)	>3.0	(-)	<0.87	33
S15 Jizusoippo	23	1.3	(-)	>3.0	(-)	<0.43	33
S16 Unseiin	23	1.5	(-)	>3.0	(-)	<0.5	29
S17 Rikkosan	21	1.8	(-)	>3.0	(-)	<0.60	34
S18 Keigairengyoto	26	1.6	(-)	>3.0	(-)	<0.53	34
S19 Sansoninto	23	1.6	(-)	>3.0	(-)	<0.53	47
S20 Kakkontokasenyushin'I	32	2	(-)	>3.0	(-)	<0.67	45
Alkaline extracts (mg/mL)							
SE (Supplementary Table S1)	20	2.6	0.7	0.5	4.5	6.8	90
PCE	19	2	0.19	0.17	13.1	14.7	82
Polyphenols (μM)							
Resveratrol	16	18	(-)	>1000	(-)	<0.018	20
<i>p</i> -Coumaric acid	42	170	(-)	>1000	(-)	<0.17	43
Curcumin	22	16	(-)	>100	(-)	<0.16	42
Chromones (μM) (Supplementary Table S2)							
(2a) (Ref. 20)	9	>600	450	400	>1.3	>1.5	59
(3c) (Ref. 20)	9	310	NT	300	NT	1.0	50
(14) (Ref. 21)	11	31	NT	29	NT	1.1	51
(2) (Ref. 24)	11	>1000	820	640	>1.2	>1.6	61
(8) (Ref. 25)	23	86	ND	180	ND	>3.3	54
(12) (Ref. 25)	23	>600	ND	370	ND	>1.6	64
Positive controls (μM)							
ACV	23	>30	1.3	1.1	>23.1	>27.3	108
Tricin	18	10	(-)	1.4	(-)	7.1	68

Data were derived from Supplementary Figure S2 (for all 20 Kampo formula) and from Figure 4. (2a), 2-(1*H*-pyrazol-1-yl)-4*H*-1-benzopyran-4-one; (3c), 2-(1*H*-imidazol-1-yl)-6-methoxy-4*H*-1-benzopyran-4-one; (14), (3*E*)-2,3-dihydro-3-[(4-hydroxyphenyl)methylene]-7-methoxy-4*H*-1-benzopyran-4-one; (2), (2*E*,4*E*)-5-(3,4-methylenedioxyphenyl)-2,4-pentadienoic acid (4-hydroxy-3-methoxyphenyl)methyl ester; (8), 2-[(1*E*)-2-(4-fluorophenyl)ethenyl]-6-methoxy-4*H*-1-benzopyran-4-one; (12), 2-[(1*E*)-2-(3,4-dimethoxy) ethenyl]-6-methoxy-4*H*-1-benzopyran-4-one. Supplementary Tables S2 and S3 show the anti-HSV activity of SE (assayed 52 times) and a total of 119 chromone derivatives, esters, and amides.

### 3.3. Augmentation of Antiviral Potential of Alkaline Extracts by Reducing the Treatment Time

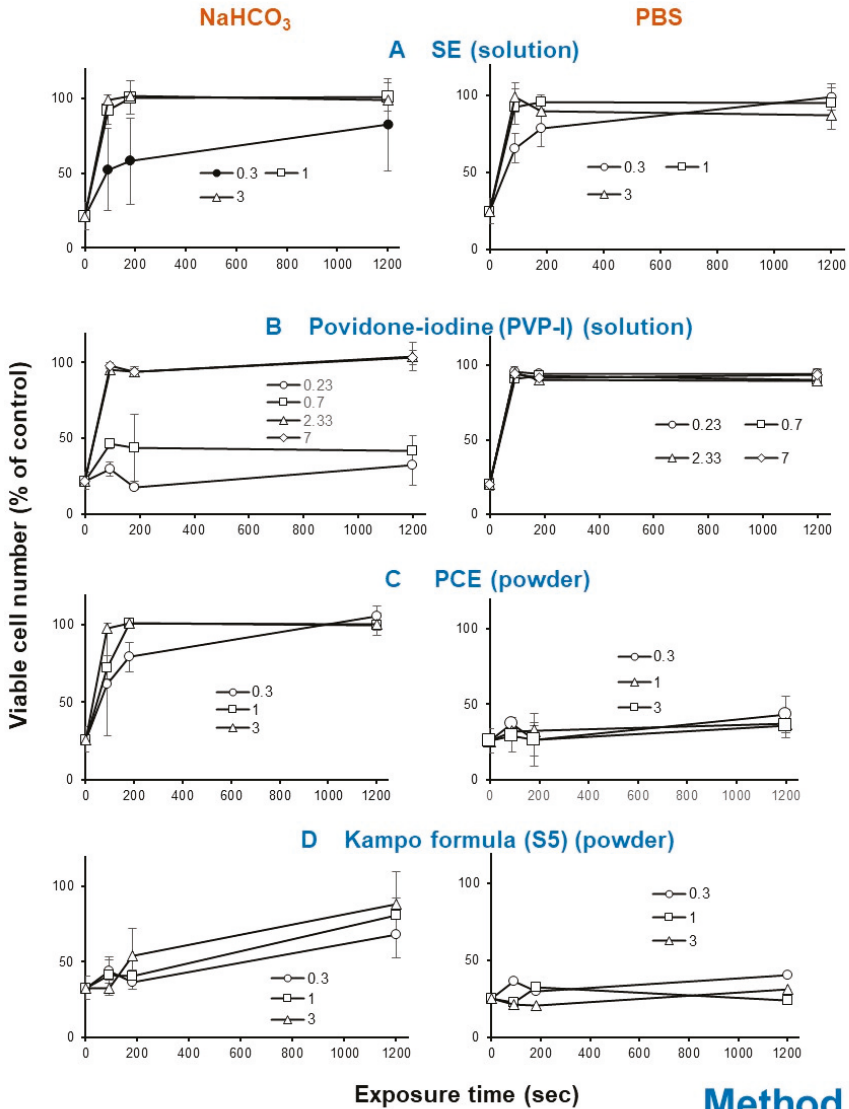
#### 3.3.1. Rapid HSV Inactivation by SE and PCE

Since SE and PCE showed approximately 10-fold higher anti-HSV activity (SI-II = 6.8, 14.7) than the twenty Kampo formulas (mean SI-II < 1.1), 6-fold higher than four polyphenols (mean SI-II = 1.9), and 6-fold higher than five of the most potent chromones (mean SI-II = 1.7) (Table 2), we next investigated whether short exposure of HSV to these samples could instantly reduce the infectivity.

Exposure of HSV with SE (A) (1 or 3 mg/mL), PCE (C) (1 or 3 mg/mL) as well as povidone iodine (B) (2.33 or 7 mg/mL) rapidly eliminated its infectivity within 3 min, whereas Kampo preparation (S5) (D) took 20 min to express HSV inactivation (Figure 6).

The HSV inactivation effect of SE was reproducibly diminished by dilution with 1.39% NaHCO<sub>3</sub> (pH 8.0), rather than (PBS, pH 7.4) in four independent experiments (compare left and right column in

Figure 6A). Povidone iodine showed similar instability under alkaline conditions (compare left and right column in Figure 6B). On the other hand, the anti-HSV activity of powders such as PCE and Kakkonto (S5) was enhanced more than 21.4 (=3/0.14) and 1.25-fold (=3/2.4), respectively, when they were first dissolved with 1.39% NaHCO<sub>3</sub> rather than PBS (Figure 6C,D).



### Method 3

**Figure 6.** Effect of short exposure of HSV to SE (means of four independent experiments) (A), povidone iodine (B), PCE (C) and Kakkonto (S5) (D). A 100-fold higher titer of HSV was exposed to these samples for 0, 1.5, 3, or 20 min, and then added to the cells after dilution of 100-fold. After incubation for three days, viable cells were determined. Each value represents mean ± S.D. (n = 3).

We next investigated the cytotoxicity (measured by CC<sub>50</sub>) and protective effect (measured by EC<sub>50</sub>) of short exposure (3 min) of SE (A, B), PCA (C, D) and PV-I (E, F) (Figure 7). From the dose-response

curve, we could calculate the SI values (Table 3). It is apparent that SE showed 2- to 3-fold higher anti-HSV activity when it was diluted with PBS (SI-I = 26.1, SI-II = 31.6) (B), rather than with NaHCO<sub>3</sub> (SI-I = 9.4, SI-II = 11.4) (A). On the other hand, PCE showed higher anti-HSV activity when it was dissolved by NaHCO<sub>3</sub> [SI-I > 222, SI-II > 322, MCR (maximum cell recovery) = 101.3%] (C), than by PBS (SI-I > 62.5, SI-II > 76.9, MCV = 26.8%) (D). However, we could not calculate the SI value of Kakkonto (S5) due to the lower protection effect. Povidone iodine (PVP-I) showed much lower anti-HSV activity, whenever diluted by NaHCO<sub>3</sub> (SI-I = 1.3, SI-II = 2.3) (E) or PBS (SI-I = 2.0, SI-II = 3.1) (F) (Figure 7).

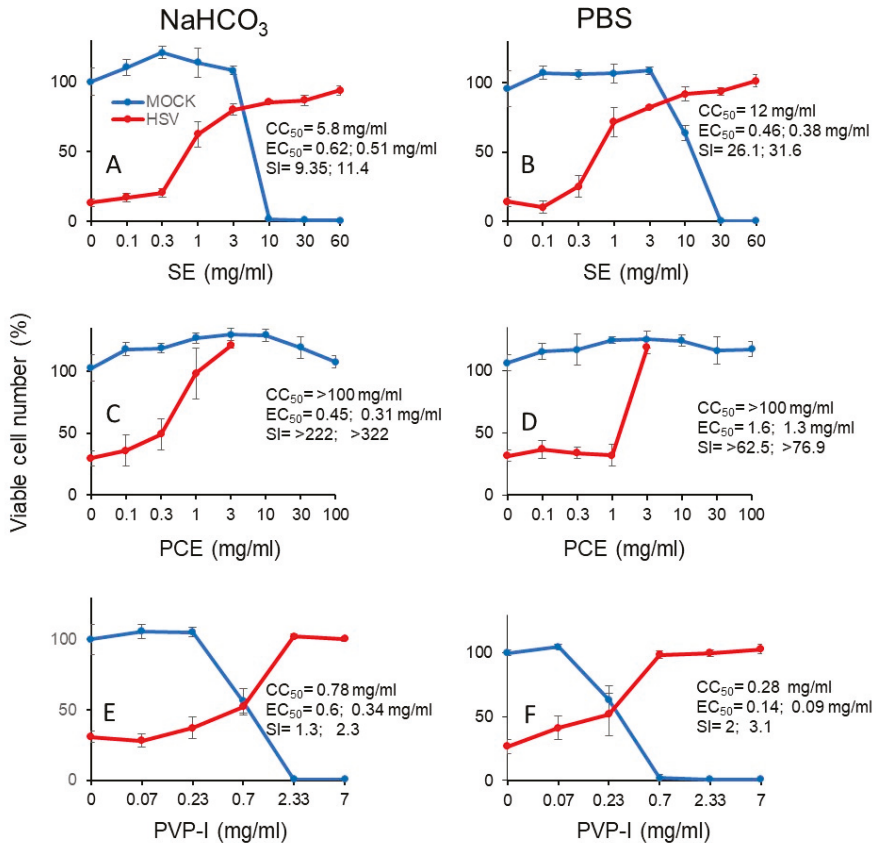


**Figure 7.** Dose-response curve of cytotoxicity and protective effect of short exposure (3 min) to SE (A, B), PCE (C,D), and PVP-I (E,F). Samples were dissolved and diluted either in 1.39% NaHCO<sub>3</sub> or PBS. HSV and Vero cells were preincubated for 3 min, and chased into fresh medium, and the viable cell number was determined. The indicated concentrations in the abscissa are the concentration at the time of contact to samples for 3 min. Each value is represented as mean ± S.D. (n = 3).

### 3.3.2. Rapid HIV Inactivation by SE

We investigated whether the short exposure with SE enhanced the anti-HIV activity. We found that exposure of HIV to SE for as little as 1 ~ 30 min quickly inactivated the virus (Figure 8A).

**Table 3.** Quantification of HSV inactivation by short exposure to SE and PCE.

	Exposure Time (min)		Viability of HSV-Infected Cells (%)	CC <sub>50</sub> (mg/mL)	EC <sub>50</sub> -I (mg/mL)	EC <sub>50</sub> -II (mg/mL)	Anti-HSV Activity		Max. Cell Recovery (%)
							SI-I	SI-II	
SE (solution)	3	NaHCO <sub>3</sub>	21.3	5.8	0.62	0.51	9.4	11.4	101.7
PCE (powder)	3	PBS	24.8	12.0	0.46	0.38	26.1	31.6	98.8
S5 (powder)	3	NaHCO <sub>3</sub>	25.9	>100	0.45	0.31	>222	>322	101.3
PVP-I (solution)	3	PBS	25.9	>100	1.6	1.3	>62.5	>76.9	26.8
	3	NaHCO <sub>3</sub>	32.7	>100	(-)	(-)	(-)	(-)	88.3
	3	PBS	25.0	>100	(-)	(-)	(-)	(-)	40.6
	3	NaHCO <sub>3</sub>	21.8	0.78	0.6	0.34	1.3	2.3	103.1
	3	PBS	20.2	0.28	0.14	0.09	2.0	3.1	94.3

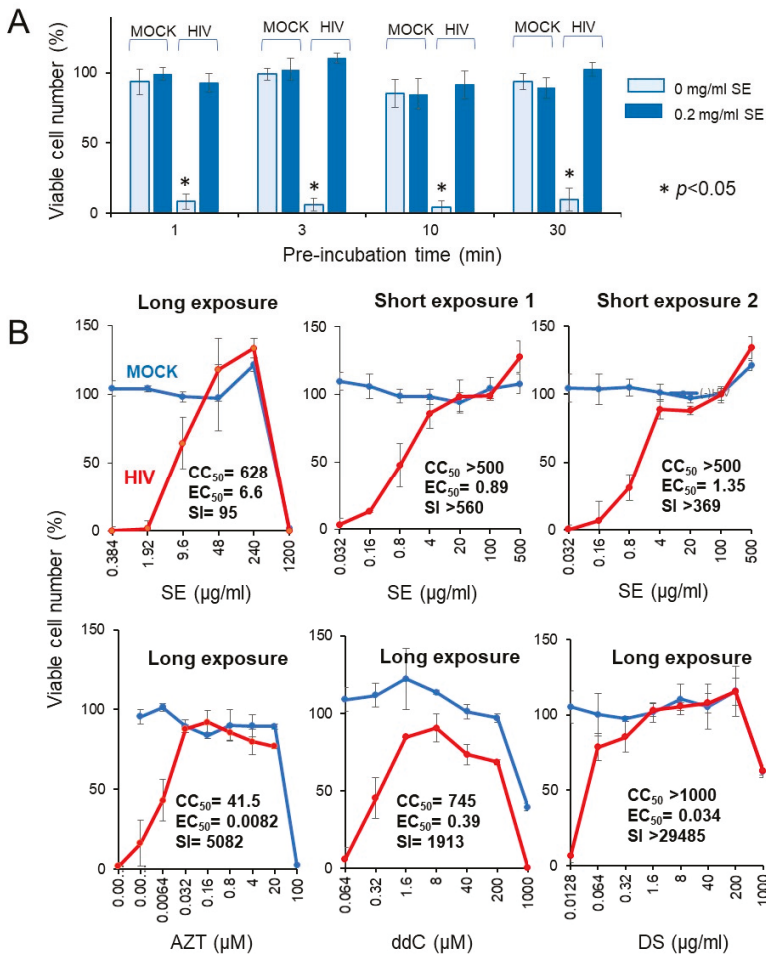


**Figure 8.** Rapid inactivation of HIV by SE. (A) Effect of preincubation time. A 20-fold higher titer of HIV (MOI = 0.2) was exposed to 0.2 mg/mL SE for 0, 1, 3, 10, or 30 min, and then added to the cells after dilution of 20-fold to make the final MOI = 0.01. After incubation for five days, viable cells were determined. Each value represented as the mean ± S.D. was determined (n = 3). HIV infection significantly reduced the viable cell number (*p* < 0.05). (B) Effect of long (five days) and short (10 min) exposure of HIV to SE, and popular anti-HIV agents on the cell viability. Each value represented as the mean ± S.D. was determined (n = 3).

Four popular anti-HIV agents (AZT, ddC, DS, CRDS, used as the positive controls) showed potent anti-HIV activity (SI = 5082, 1913 > 29,485, 4666), verifying this system for measuring the anti-HIV activity (lower panel in Figure 8B). Compared with regular long exposure (five days) (SI = 95), short exposure to SE more effectively inactivated the virus (SI > 560, >369), yielding more than a 4 ~ 6-fold increase (upper panel in Figure 8B). We repeated the same experiment with more wider dose ranges, and found that 10 min exposure of HIV with SE showed approximately 20-fold increase of anti-HIV activity (25.1 and 16.6-fold in two different assays) when compared with regular longer exposure (Table 4).

**Table 4.** Enhancement of anti-HIV activity of SE by shortening the treatment time.

	CC <sub>50</sub> (µg/mL)	EC <sub>50</sub> (µg/mL)	SI	n-Fold
SE (long exposure)	627.80	6.63	95	1
SE (short exposure 1)	>500	0.894	>560	>5.9
Repeat	1067	0.447	2388	25.1
SE (short exposure 2)	>500	1.35	>369	>3.9
Repeat	1067	0.677	1577	16.6
Positive controls				
AZT (µM)	41.49	0.00817	5082	
ddC (µM)	745.32	0.390	1913	
DS	>1000	0.0339	>29485	
CRDS	704.96	0.151	4666	

#### 4. Discussion

The present study demonstrated that the anti-HSV activity of the Kampo formula solely depended on the solubility. Kampo formulas are all powder, and therefore they have to be dissolved well and sterilized before treatment. We found that when they were directly dissolved with medium, no anti-HSV activity (Method 1) (Supplementary Table S1) and anti-HIV activity [36] were detected. On the other hand, when they were dissolved in alkaline solution such as 1.39% NaHCO<sub>3</sub> (pH 8), some anti-HSV activity was recovered (Method 2). However, when they were dissolved with neutral buffer such as PBS (pH 7.4), no anti-HSV activity was recovered. Using Method 3, contact with Kakkonto for 20 min reduced the infectivity of HSV, consistent with previous reports of the anti-HSV activity of Kakkonto [12]. We recently reported that most Kampo formulas including Kakkonto showed protection against cisplatin and amyloid-β-induced neurotoxicity [36].

We have previously separated various polysaccharide fractions of the pine cone of *Pinus parviflora* Sieb et Zucc by successive hot water and alkaline extractions. Hot water extract contains Fr. I (neutral), Fr. II (uronic acid-rich), and Fr. V (tightly bound to diethylaminoethyl cellulose (DEAE) cellulose chromatography). Alkaline extract contains Fr. VI (acid-precipitable), and Fr. VII, VIII, and IX (step-wise precipitated by increasing amounts of ethanol). All of these fractions contain glucose, mannose, galactose, and arabinose or fucose as the main component of polysaccharide. Chemical analysis (infrared spectroscopy (IR), nuclear magnetic resonance (NMR), thin layer chromatography (TLC)) identified Frs. V, VI, VII, VIII, and IX as a lignin-carbohydrate complex [31]. We found that only Frs. V, VI, VII, VIII, and IX showed potent anti-HIV activity whereas neutral and acidic polysaccharides (Frs. I and II) were inactive [32]. It is reasonable that PCE was richer in lignified material than the Kampo formula, and showed higher anti-HSV activity. Removal of dextrin from PCE power may further increase the specific activity of anti-HSV.

SE itself is an alkaline solution containing a lignin-carbohydrate complex and its degradation product such as *p*-coumaric acid, which has no anti-HSV activity. We found that dilution of SE with 1.39% NaHCO<sub>3</sub> reproducibly reduced the anti-HSV activity, possibly due to the degradation of the lignin-carbohydrate complex under alkaline condition. We reported diverse biological activity of SE (anti-inflammatory, antiviral, antibacterial, anti-UV, and anti-halitosis activity,



and synergism with acyclovir or vitamin C), some of which overlapped that of the lignin-carbohydrate complex [13,16,17,29,32,37–45] (Table 5).

**Table 5.** Diverse biological activity of SE and similarity with the lignin-carbohydrate complex.

Biological Activity	SE	Lignin–Carbohydrate Complex
Anti-inflammatory activity	[37,38]	[32]
Antiviral activity	[29]	[16,32]
Antibacterial activity	[29,39]	
Anti-UV activity	[40]	[41,42]
Synergism with acyclovir (Antiviral)	[13]	
Synergism with vitamin C (Anti-UV)	[43]	
Synergism with vitamin C (antitumor)		[44]
Anti-halitosis activity	[45]	

There are three commercially available products of alkaline extract of *Sasa* sp. (products A, B and C). SE (Product A) contains Fe (II)-chlorophyllin, whereas products B and C contain Cu (II)-chlorophyllin and less lignin-carbohydrate complex. Product C is supplemented with ginseng and pine (*Pinus densiflora*) leaf extracts. We found that SE (Product A) exhibited higher anti-HIV, anti-UV, and hydroxyl radical-scavenging activities compared to those of products B and C [46]. This finding further strengthens that major biological principles in SE may be the lignin-carbohydrate complex. The lignin-carbohydrate complex can be extracted by alkaline solution, but, once isolated by the alkaline solution, may be unstable under alkaline conditions [47–49], and gradually decompose into phenylpropanoid monomers and oligomers with little or no antiviral activity [50,51]. Based on these unique biological activities, we manufactured various medicines, cosmetics, toiletries, supplements, and foods using SE (Figure 9). If we could remove lower molecular weight degradation products that have essentially no antiviral activity, specific activity of SE may be further elevated. Considering that saliva is neutral with a pH of 7.2 ~ 7.3 [52] or 7.0 ~ 7.2 [53], SE may be stable in the oral cavity.

It was unexpected that lower molecular weight polyphenols such as resveratrol, curcumin, and *p*-coumaric acid had little or no anti-HSV activity. This may be due to their potent cytotoxicity against Vero cells. We have previously reported that tricetin, but not the other four polymethoxyflavonoids (3,3',4',5,6,7,8-heptamethoxyflavone, nobiletin, tangeretin, and sudachitin), showed potent anti-HSV activity, suggesting the importance of the 3D-structure of these polymethoxyflavonoids for expressing anti-HSV activity [19]. It remains to be investigated whether short-term exposure of HSV to a higher concentration of these polyphenols may inactivate HSV or not.

We recently found that many chromone derivatives, esters, and amides showed much higher cytotoxicity against human oral squamous cell carcinoma cell lines when compared with human normal mesenchymal oral cells (gingival fibroblast, periodontal ligament fibroblast, pulp cells). Their tumor-specificity exceeded that of the lower molecular weight polyphenols. Furthermore, they showed much less normal keratinocyte toxicity than conventional anticancer drugs. Our preliminary study demonstrated that some of them alleviated the HSV-induced cytopathic effects. However, there was no correlation between their tumor-specificity and anti-HSV activity (Supplementary Table S3).

Recently, povidone iodine has been broadcasted to improve the symptoms of corona virus-infected patients in TV ASAHI super-channel in Japan on August 5, 2020. However, many authorities of medical sciences have shown cautionary stance, since it may kill the good bacteria that protect the mouth and reduce thyroid function. The present study showed that it also rapidly reduced the infectivity of HSV. Further study of the safety of this gargle as an antiviral agent should be performed.

We have previously demonstrated that <sup>125</sup>I-labeled lignin-carbohydrate complex bound tightly to the influenza virus with sucrose gradient centrifugation [54]. The lignin-carbohydrate complex [55] and tannic acid [56] significantly inhibited the adsorption of <sup>3</sup>H-labeled HSV to Vero cells [18]. Anti-HSV activity of these substances was much greater when they were added during virus adsorption to

the cells rather than before and after adsorption [18,52]. These data suggest that the target of these substances may be virus or cell surface components. Since the lignin-carbohydrate complex significantly enhanced the expression of dectin-2 [53], possible interactions with the cell surface receptor should be investigated. Further study is necessary to identify the antiviral mechanisms of these substances.



**Figure 9.** Medicines, cosmetics, toiletries, supplements, and foods manufactured from SE. Right column: Yatsugatake mountain peak (top), factory of the Daiwa Biological Research Institute Co. Ltd., Chino, Nagano, Japan (middle), and the botanical garden in the “Sasa Rikyu (imperial villa)” (bottom).

## 5. Conclusions

The present study demonstrated for the first time that:

- Alkaline extracts of the leaves of *Sasa* sp. (SE) and pine cone extract (PCE) showed higher anti-HSV activity than 20 Japanese traditional herb medicines (Kampo formulas), resveratrol, *p*-coumaric acid, curcumin, tricrin, and 119 chromone-related compounds. This confirms our previous finding that the alkaline extract of tea and licorice root showed higher anti-HIV activity than the respective hot water extract [57,58].
- Exposure of HSV to SE or PCE for 3 min almost completely eliminated the infectivity of HSV, whereas a much longer exposure time was required for Kakkonto, the most active Kampo formulae.
- Anti-HSV activity of PCE and Kakkonto could be detected only when they were dissolved by an alkaline solution (pH 8.0), but not by neutral buffer (pH 7.4).
- Anti-HSV activity of SE and povidone iodine was unstable if they were diluted with alkaline solution.
- Anti-HSV activity of SE and PCE were one or two-orders higher than povidone iodide.
- Anti-HIV activity of SE was also enhanced when it was administered for a short period.
- The present study suggests the applicability of a short treatment of oral virus with SE and PCE.

**Supplementary Materials:** The following are available online at <http://www.mdpi.com/2305-6320/7/10/64/s1>, Figure S1: Method 1. Direct mixing of Kampo preparations with culture medium resulted in low recovery of anti-HSV activity, Figure S2: Method 2: Weak anti-HSV activity was detected in S5, S9, S11 and S12, Table S1: Higher anti-HSV activity of Kampo formulas was recovered by dissolving with 1.39% NaHCO<sub>3</sub> than with PBS, Table S2. Anti-HSV activity of SE from 52 experiments, Table S3. Anti-HSV activity of chromones, esters, and amides (119 compounds).

**Author Contributions:** Conceptualization, formal analysis, investigation and funding acquisition, K.F., H.S., Y.S., D.A., S.T. and K.T. (Koichi Takao); Methodology and resources, H.O. (Hiroshi Oizumi), M.H., M.S., T.F. and K.T. (Koichi Takao); Data curation, F.K., D.A., S.T., and H.S.; Writing—original draft preparation, H.S.; Writing—review and editing, F.K.; Supervision, H.S. and K.T. (Kazuki Toeda); Project administration, T.Y., K.T. (Kazuki Toeda), H.T., H.O. (Hirokazu Ohno), and T.O. All authors have read and agreed to the published version of the manuscript.

**Funding:** This research was funded by KAKENHI from the Japan Society for the Promotion of Science (JSPS) (No. 16K11519, No. 20K09885) (H.S.); the Showa University Graduate School Research Fund (K.F.); three Meikai University Miyata Research Fund B (H.S.); the Josai University Research Fund (Y.S., K.T.(Koichi Takao)); the Joint Research Fund of Meikai University; Daiwa Biological Co. Ltd.; and Maruzen Pharmaceuticals Co., Ltd. (H.S.).

**Acknowledgments:** The authors thank the Tsumura and Co. for providing the 20 Kampo formulas.

**Conflicts of Interest:** M.H., M.S., T.F., K.T. (Kazuki Toeda), H.O. and T.O. come from Daiwa Biological Research Institute Co., Ltd., Kanagawa, Japan. H.O. comes from Maruzen Pharmaceuticals Co., Ltd., Hiroshima, Japan. Corresponding authors (H.S.) received the financial support of research funds from Daiwa Biological Research Institute and Maruzen Pharmaceuticals. The authors confirm that such financial supports have not influenced the outcome of the experimental data. The other authors declare no conflict of interest.

## References

1. Corstjens, P.L.; Abrams, W.R.; Malamud, D. Saliva and viral infections. *Periodontol.* **2000** *2016*, *70*, 93–110. [[CrossRef](#)] [[PubMed](#)]
2. Crimi, S.; Fiorillo, L.; Bianchi, A.; D'Amico, C.; Amoroso, G.; Gorassini, F.; Mastroieni, R.; Marino, S.; Scoglio, C.; Catalano, F.; et al. Herpes virus, oral clinical signs and QoL: Systematic review of recent data. *Viruses* **2019**, *11*, 463. [[CrossRef](#)] [[PubMed](#)]
3. Annunziata, G.; Maisto, M.; Schisano, C.; Ciampaglia, R.; Narciso, V.; Tenore, G.C.; Novellino, E. Resveratrol as a novel anti-herpes simplex virus nutraceutical agent: An overview. *Viruses* **2018**, *10*, 473. [[CrossRef](#)] [[PubMed](#)]
4. de Oliveira, A.; Adams, S.D.; Lee, L.H.; Murray, S.R.; Hsu, S.D.; Hammond, J.R.; Dickinson, D.; Chen, P.; Chu, T.C. Inhibition of herpes simplex virus type 1 with the modified green tea polyphenol palmitoyl-epigallocatechin gallate. *Food Chem. Toxicol.* **2013**, *52*, 207–215. [[CrossRef](#)]
5. Xiang, Y.; Pei, Y.; Qu, C.; Lai, Z.; Ren, Z.; Yang, K.; Xiong, S.; Zhang, Y.; Yang, C.; Wang, D.; et al. In vitro anti-herpes simplex virus activity of 1,2,4,6-tetra-O-galloyl- $\beta$ -D-glucose from *Phyllanthus emblica* L. (Euphorbiaceae). *Phytother. Res.* **2011**, *25*, 975–982. [[CrossRef](#)]
6. de Oliveira, A.; Prince, D.; Lo, C.Y.; Lee, L.H.; Chu, T.C. Antiviral activity of theaflavin digallate against herpes simplex virus type 1. *Antivir. Res.* **2015**, *118*, 56–67. [[CrossRef](#)]
7. Ceole, L.F.; Companhia, M.V.P.; Sanches Lopes, S.M.; de Oliveira, A.J.B.; Gonçalves, R.A.C.; Dias Filho, B.P.; Nakamura, C.V.; Ueda-Nakamura, T. Anti-herpes activity of polysaccharide fractions from *Stevia rebaudiana* leaves. *Nat. Prod. Res.* **2020**, *34*, 1558–1562. [[CrossRef](#)]
8. Nawawi, A.; Nakamura, N.; Hattori, M.; Kurokawa, M.; Shiraki, K. Inhibitory effects of Indonesian medicinal plants on the infection of herpes simplex virus type 1. *Phytother. Res.* **1999**, *13*, 37–41. [[CrossRef](#)]
9. Schnitzler, P.; Nolkemper, S.; Stintzing, F.C.; Reichling, J. Comparative in vitro study on the anti-herpetic effect of phytochemically characterized aqueous and ethanolic extracts of *Salvia officinalis* grown at two different locations. *Phytomedicine* **2008**, *15*, 62–70. [[CrossRef](#)]
10. Zu, Y.; Fu, Y.; Wang, W.; Wu, N.; Liu, W.; Kong, Y.; Schiebel, H.M.; Schwarz, G.; Schnitzler, P.; Reichling, J. Comparative study on the antitherpetic activity of aqueous and ethanolic extracts derived from *Cajanus cajan* (L.) Millsp. *Complement. Med. Res.* **2010**, *17*, 15–20. [[CrossRef](#)]
11. Kido, T.; Mori, K.; Daikuhara, H.; Tsuchiya, H.; Ishige, A.; Sasaki, H. The protective effect of hochu-ekki-to (TJ-41), a Japanese herbal medicine, against HSV-1 infection in mitomycin C-treated mice. *Anticancer Res.* **2000**, *20*, 4109–4113. [[PubMed](#)]

12. Nagasaka, K.; Kurokawa, M.; Imakita, M.; Terasawa, K.; Shiraki, K. Efficacy of kakkon-to, a traditional herb medicine, in herpes simplex virus type 1 infection in mice. *J. Med. Virol.* **1995**, *46*, 28–34. [[CrossRef](#)] [[PubMed](#)]
13. Sakagami, H.; Fukuchi, K.; Kanamoto, T.; Terakubo, S.; Nakashima, H.; Natori, T.; Suguro-Kitajima, M.; Oizumi, H.; Yasui, T.; Oizumi, T. Synergism of Alkaline Extract of the Leaves of *Sasa senanensis* Rehder and Antiviral Agents. *In Vivo* **2016**, *30*, 421–426. [[PubMed](#)]
14. Gordts, S.C.; Féris, G.; D’Huys, T.; Petrova, M.I.; Lebeer, S.; Snoeck, R.; Andrei, G.; Schols, D. The Low-Cost Compound Lignosulfonic Acid (LA) Exhibits Broad-Spectrum Anti-HIV and Anti-HSV Activity and Has Potential for Microbicidal Applications. *PLoS ONE* **2015**, *10*, e0131219. [[CrossRef](#)]
15. Lopez, B.S.; Yamamoto, M.; Utsumi, K.; Aratsu, C.; Sakagami, H. A clinical pilot study of lignin—Ascorbic acid combination treatment of herpes simplex virus. *In Vivo* **2009**, *23*, 1011–1016. [[PubMed](#)]
16. Sakagami, H.; Kawazoe, Y.; Komatsu, N.; Simpson, A.; Nonoyama, M.; Konno, K.; Yoshida, T.; Kuroiwa, Y.; Tanuma, S. Antitumor, antiviral and immunopotentiating activities of pine cone extracts: Potential medicinal efficacy of natural and synthetic lignin-related materials (review). *Anticancer Res.* **1991**, *11*, 881–888. [[PubMed](#)]
17. Zhang, Y.; But, P.P.; Ooi, V.E.; Xu, H.X.; Delaney, G.D.; Lee, S.H.; Lee, S.F. Chemical properties, mode of action, and in vivo anti-herpes activities of a lignin-carbohydrate complex from *Prunella vulgaris*. *Antiviral Res.* **2007**, *75*, 242–249. [[CrossRef](#)]
18. Fukuchi, K.; Sakagami, H.; Okuda, T.; Hatano, T.; Tanuma, S.; Kitajima, K.; Inoue, Y.; Inoue, S.; Ichikawa, S.; Nonoyama, M.; et al. Inhibition of herpes simplex virus infection by tannins and related compounds. *Antiviral Res.* **1989**, *11*, 285–298. [[CrossRef](#)]
19. Fukuchi, K.; Okudaira, N.; Adachi, K.; Odai-Ide, R.; Watanabe, S.; Ohno, H.; Yamamoto, M.; Kanamoto, T.; Terakubo, S.; Nakashima, H.; et al. Antiviral and antitumor activity of licorice root extracts. *In Vivo* **2016**, *30*, 777–785. [[CrossRef](#)]
20. Takao, K.; Saito, T.; Chikuda, D.; Sugita, Y. 2-Azolychromone Derivatives as Potent and Selective Inhibitors of Monoamine Oxidases A and B. *Chem. Pharm. Bull.* **2016**, *64*, 1499–1504. [[CrossRef](#)]
21. Takao, K.; Yamashita, M.; Yashiro, A.; Sugita, Y. Synthesis and Biological Evaluation of 3-Benzylidene-4-chromanone Derivatives as Free Radical Scavengers and  $\alpha$ -Glucosidase Inhibitors. *Chem. Pharm. Bull.* **2016**, *64*, 1203–1207. [[CrossRef](#)] [[PubMed](#)]
22. Devakaram, R.; Black, D.S.; Andrews, K.T.; Fisher, G.M.; Davis, R.A.; Kumar, N. Synthesis and antimalarial evaluation of novel benzopyrano[4,3-b]benzopyran derivatives. *Bioorg. Med. Chem.* **2011**, *19*, 5199–5206. [[CrossRef](#)] [[PubMed](#)]
23. Takao, K.; Toda, K.; Saito, T.; Sugita, Y. Synthesis of Amide and Ester Derivatives of Cinnamic Acid and Its Analogs: Evaluation of Their Free Radical Scavenging and Monoamine Oxidase and Cholinesterase Inhibitory Activities. *Chem. Pharm. Bull.* **2017**, *65*, 1020–1027. [[CrossRef](#)] [[PubMed](#)]
24. Takao, K.; Miyashiro, T.; Sugita, Y. Synthesis and biological evaluation of piperic acid amides as free radical scavengers and  $\alpha$ -glucosidase inhibitors. *Chem. Pharm. Bull.* **2015**, *63*, 326–333. [[CrossRef](#)]
25. Takao, K.; Endo, S.; Nagai, J.; Kamauchi, H.; Takemura, Y.; Uesawa, Y.; Sugita, Y. 2-Styrylchromone derivatives as potent and selective monoamine oxidase B inhibitors. *Bioorg. Chem.* **2019**, *92*, 103285. [[CrossRef](#)]
26. Takao, K.; Ishikawa, R.; Sugita, Y. Synthesis and biological evaluation of 3-styrylchromone derivatives as free radical scavengers and  $\alpha$ -glucosidase inhibitors. *Chem. Pharm. Bull.* **2014**, *62*, 810–815. [[CrossRef](#)]
27. Elion, G.B. Mechanism of action and selectivity of acyclovir. *Am. J. Med.* **1982**, *73*, 7–13. [[CrossRef](#)]
28. Kawana, R.; Kitamura, T.; Nakagomi, O.; Matsumoto, I.; Arita, M.; Yoshihara, N.; Yanagi, K.; Yamada, A.; Morita, O.; Yoshida, Y.; et al. Inactivation of human viruses by povidone-iodine in comparison with other antiseptics. *Dermatology* **1997**, *195*, 29–35. [[CrossRef](#)]
29. Sakagami, H.; Amano, S.; Kikuchi, H.; Nakamura, Y.; Kuroshita, R.; Watanabe, S.; Satoh, K.; Hasegawa, H.; Nomura, A.; Kanamoto, T.; et al. Antiviral, antibacterial and vitamin C-synergized radical-scavenging activity of *Sasa senanensis* Rehder extract. *In Vivo* **2008**, *22*, 471–476.
30. Sakagami, H.; Matsuta, T.; Yasui, T.; Oguchi, K.; Kitajima, M.; Sugiura, T.; Oizumi, T.; Oizumi, T. Functional evaluation of *Sasa Makino* et *Shibata* leaf extract as group III OTC drug. In *Alternative Medicine*; Sakagami, H., Ed.; BoD—Books on Demand: Rijeka, Croatia, 2012; pp. 171–200.
31. Sakagami, H.; Ikeda, M.; Unten, S.; Takeda, K.; Murayama, J.; Hamada, A.; Kimura, K.; Komatsu, N.; Konno, K. Antitumor activity of polysaccharide fractions from pine cone extract of *Pinus parviflora* Sieb. et Zucc. *Anticancer Res.* **1987**, *7*, 1153–1159.

32. Sakagami, H.; Kushida, T.; Oizumi, T.; Nakashima, H.; Makino, T. Distribution of lignin-carbohydrate complex in plant kingdom and its functionality as alternative medicine. *Pharmacol. Ther.* **2010**, *128*, 91–105. [[CrossRef](#)] [[PubMed](#)]
33. Miyoshi, I.; Taguchi, H.; Kubonishi, I.; Yoshimoto, S.; Ohtsuki, Y.; Shiraiishi, Y.; Akagi, T. Type C virus-producing cell lines derived from adult T cell leukemia. *Gann Monogr. Cancer Res.* **1982**, *28*, 219–229.
34. Nakashima, H.; Masuda, M.; Murakami, T.; Koyanagi, Y.; Matsumoto, A.; Fujii, N.; Yamamoto, N. Anti-human immunodeficiency virus activity of a novel synthetic peptide, T22 ([Tyr-5,12, Lys-7]polyphemusin II): A possible inhibitor of virus-cell fusion. *Antimicrob. Agents Chemother.* **1992**, *36*, 1249–1255. [[CrossRef](#)]
35. Pauwels, R.; Balzarini, J.; Baba, M.; Snoeck, R.; Schols, D.; Herdewijn, P.; Desmyter, J.; De Clercq, E. Rapid and automated tetrazolium-based colorimetric assay for the detection of anti-HIV compounds. *J. Virol. Methods* **1988**, *20*, 309–321. [[CrossRef](#)]
36. Shi, H.; Fukuchi, K.; Asai, D.; Terakubo, S.; Takemura, H.; Sakagami, H. Quantification of antitumor, antiviral and neuroprotective activity of twenty Kampo preparations. *New Food Ind.* **2020**, *62*, 599–607.
37. Ono, M.; Kantoh, K.; Ueki, J.; Shimada, A.; Wakabayashi, H.; Matsuta, T.; Sakagami, H.; Kumada, H.; Hamada, N.; Kitajima, M.; et al. Quest for anti-inflammatory substances using IL-1 $\beta$ -stimulated gingival fibroblasts. *In Vivo* **2011**, *25*, 763–768. [[PubMed](#)]
38. Zhou, L.; Hashimoto, K.; Satoh, K.; Yokote, Y.; Kitajima, M.; Oizumi, T.; Oizumi, H.; Sakagami, H. Effect of Sasa senanensis Rehder extract on NO and PGE2 production by activated mouse macrophage-like RAW264.7 cells. *In Vivo* **2009**, *23*, 773–777.
39. Sakagami, H.; Amano, S.; Yasui, T.; Satoh, K.; Shioda, S.; Kanamoto, T.; Terakubo, S.; Nakashima, H.; Watanabe, K.; Sugiura, T.; et al. Biological interaction between Sasa senanensis Rehder leaf extract and toothpaste ingredients. *In Vivo* **2013**, *27*, 275–284.
40. Matsuta, T.; Sakagami, H.; Sugiura, T.; Kitajima, M.; Oizumi, H.; Oizumi, T. Structural characterization of anti-UV components from Sasa senanensis Rehder extract. *In Vivo* **2013**, *27*, 77–83.
41. Nanbu, T.; Shimada, J.; Kobayashi, M.; Hirano, K.; Koh, T.; Machino, M.; Ohno, H.; Yamamoto, M.; Sakagami, H. Anti-UV activity of lignin-carbohydrate complex and related compounds. *In Vivo* **2013**, *27*, 133–139.
42. Sakagami, H.; Sheng, H.; Okudaira, N.; Yasui, T.; Wakabayashi, H.; Jia, J.; Natori, T.; Suguro-Kitajima, M.; Oizumi, H.; Oizumi, T. Prominent Anti-UV Activity and Possible Cosmetic Potential of Lignin-carbohydrate Complex. *In Vivo* **2016**, *30*, 331–339. [[PubMed](#)]
43. Matsuta, T.; Sakagami, H.; Kitajima, M.; Oizumi, H.; Oizumi, T. Anti-UV Activity of Alkaline Extract of the Leaves of Sasa senanensis Rehder. *In Vivo* **2011**, *25*, 751–755. [[PubMed](#)]
44. Satoh, K.; Ida, Y.; Ishihara, M.; Sakagami, H. Interaction between sodium ascorbate and polyphenols. *Anticancer Res.* **1999**, *19*, 4177–4186. [[PubMed](#)]
45. Sakagami, H.; Sheng, H.; Ono, K.; Komine, Y.; Miyadai, T.; Terada, Y.; Nakada, D.; Tanaka, S.; Matsumoto, M.; Yasui, T.; et al. Anti-Halitosis Effect of Toothpaste Supplemented with Alkaline Extract of the Leaves of Sasa senanensis Rehder. *In Vivo* **2016**, *30*, 107–111. [[PubMed](#)]
46. Sakagami, H.; Iwamoto, S.; Matsuta, T.; Satoh, K.; Shimada, C.; Kanamoto, T.; Terakubo, S.; Nakashima, H.; Morita, Y.; Ohkubo, A.; et al. Comparative study of biological activity of three commercial products of Sasa senanensis Rehder leaf extract. *In Vivo* **2012**, *26*, 259–264.
47. Castro, R.C.A.; Ferreira, I.S.; Roberto, I.C.; Mussatto, S.I. Isolation and physicochemical characterization of different lignin streams generated during the second-generation ethanol production process. *Int. J. Biol. Macromol.* **2019**, *129*, 497–510. [[CrossRef](#)]
48. Miyamoto, T.; Yamamura, M.; Tobimatsu, Y.; Suzuki, S.; Kojima, M.; Takabe, K.; Terajima, Y.; Mihashi, A.; Kobayashi, Y.; Umezawa, T. A comparative study of the biomass properties of Erianthus and sugarcane: Lignocellulose structure, alkaline delignification rate, and enzymatic saccharification efficiency. *Biosci. Biotechnol. Biochem.* **2018**, *82*, 1143–1152. [[CrossRef](#)]
49. Srinivas, K.; de Carvalho Oliveira, F.; Teller, P.J.; Gonçalves, A.R.; Helms, G.L.; Ahring, B.K. Oxidative degradation of biorefinery lignin obtained after pretreatment of forest residues of Douglas Fir. *Bioresour. Technol.* **2016**, *221*, 394–404. [[CrossRef](#)]
50. Nakashima, H.; Murakami, T.; Yamamoto, N.; Naoe, T.; Kawazoe, Y.; Konno, K.; Sakagami, H. Lignified materials as medicinal resources. V. Anti-HIV (human immunodeficiency virus) activity of some synthetic lignins. *Chem. Pharm. Bull.* **1992**, *40*, 2102–2105. [[CrossRef](#)]

51. Sakagami, H.; Nagata, K.; Ishihama, A.; Oh-hara, T.; Kawazoe, Y. Anti-influenza virus activity of synthetically polymerized phenylpropenoids. *Biochem. Biophys. Res. Commun.* **1990**, *172*, 1267–1272. [[CrossRef](#)]
52. Belardinelli, P.A.; Morelato, R.A.; Benavidez, T.E.; Baruzzi, A.M.; López de Blanc, S.A. Effect of two mouthwashes on salivary ph. *Acta Odontol. Latinoam.* **2014**, *27*, 66–71. [[CrossRef](#)] [[PubMed](#)]
53. Gonçalves Ferreira, N.; Cerná, L.; Cedíková, M.; Bibková, K.; Mičanová, Z.; Ulčová-Gallová, Z. Some immunological properties of female saliva and its effect on sperm motility. *Cas. Lek. Cesk.* **2014**, *153*, 86–90. [[PubMed](#)]
54. Sakagami, H.; Takeda, M.; Kawazoe, Y.; Nagata, K.; Ishihama, A.; Ueda, M.; Yamazaki, S. Anti-influenza virus activity of a lignin fraction from cone of *Pinus parviflora* Sieb. et Zucc. *In Vivo* **1992**, *6*, 491–496. [[PubMed](#)]
55. Fukuchi, K.; Sakagami, H.; Ikeda, M.; Kawazoe, Y.; Oh-hara, T.; Konno, K.; Ichikawa, S.; Hata, N.; Kondo, H.; Nonoyama, M. Inhibition of herpes simplex virus infection by pine cone antitumor substances. *Anticancer Res.* **1989**, *9*, 313–318. [[PubMed](#)]
56. Kushida, T.; Makino, T.; Tomomura, M.; Tomomura, A.; Sakagami, H. Enhancement of dectin-2 gene expression by lignin-carbohydrate complex from *Lendinus edodes* extract (LEM) in mouse macrophage-like cell line. *Anticancer Res.* **2011**, *31*, 1241–1248. [[PubMed](#)]
57. Sakagami, H.; Ohkoshi, E.; Amano, S.; Satoh, K.; Kanamoto, T.; Terakubo, S.; Nakashima, H.; Sunaga, K.; Otsuki, T.; Ikeda, H.; et al. Efficient utilization of plant resources by alkaline extraction. *Altern. Integr. Med.* **2013**, *2*, 133. [[CrossRef](#)]
58. Ohno, H.; Miyoshi, S.; Araho, D.; Kanamoato, T.; Terakubo, S.; Nakashima, H.; Tsuda, T.; Sunaga, K.; Amano, S.; Ohkoshi, E.; et al. Efficient utilization of licorice root by alkaline extraction. *In Vivo* **2014**, *28*, 785–794. [[PubMed](#)]



© 2020 by the authors. Licensee MDPI, Basel, Switzerland. This article is an open access article distributed under the terms and conditions of the Creative Commons Attribution (CC BY) license (<http://creativecommons.org/licenses/by/4.0/>).





Review

# Development of Newly Synthesized Chromone Derivatives with High Tumor Specificity against Human Oral Squamous Cell Carcinoma

Yoshiaki Sugita <sup>1,\*</sup>, Koichi Takao <sup>1</sup>, Yoshihiro Uesawa <sup>2,\*</sup>, Junko Nagai <sup>2</sup>, Yosuke Iijima <sup>3</sup>, Motohiko Sano <sup>4</sup> and Hiroshi Sakagami <sup>5,\*</sup>

<sup>1</sup> Department of Pharmaceutical Sciences, Faculty of Pharmacy and Pharmaceutical Sciences, Josai University, Saitama 350-0295, Japan; ktakao@josai.ac.jp

<sup>2</sup> Department of Medical Molecular Informatics, Meiji Pharmaceutical University, Tokyo 204-858, Japan; nagai-j@my-pharm.ac.jp

<sup>3</sup> Department of Oral and Maxillofacial Surgery, Saitama Medical Center, Saitama Medical University, Kawagoe 350-8550, Japan; yoiijima@saitama-med.ac.jp

<sup>4</sup> Division of Applied Pharmaceutical Education and Research, Hoshi University, Tokyo 142-8501, Japan; m-sano@hoshi.ac.jp

<sup>5</sup> Meikai University Research Institute of Odontology (M-RIO), 1-1 Keyakidai, Sakado, Saitama 350-0283, Japan

\* Correspondence: sugita@josai.ac.jp (Y.S.); uesawa@my-pharm.ac.jp (Y.U.); sakagami@dent.meikai.ac.jp (H.S.); Tel.: +81-492-717-254 (Y.S.); +81-424-958-983 (Y.U.); +81-492-792-758 (H.S.)

Received: 3 August 2020; Accepted: 24 August 2020; Published: 26 August 2020

**Abstract:** Since many anticancer drugs show severe adverse effects such as mucositis, peripheral neurotoxicity, and extravasation, it was crucial to explore new compounds with much reduced adverse effects. Comprehensive investigation with human malignant and nonmalignant cells demonstrated that derivatives of chromone, back-bone structure of flavonoid, showed much higher tumor specificity as compared with three major polyphenols in the natural kingdom, such as lignin-carbohydrate complex, tannin, and flavonoid. A total 291 newly synthesized compounds of 17 groups (consisting of 12 chromones, 2 esters, and 3 amides) gave a wide range of the intensity of tumor specificity, possibly reflecting the fitness for the optimal 3D structure and electric state. Among them, 7-methoxy-3-[(1*E*)-2-phenylethenyl]-4*H*-1-benzopyran-4-one (compound **22**), which belongs to 3-styrylchromones, showed the highest tumor specificity. **22** induced subG1 and G2 + M cell population in human oral squamous cell carcinoma cell line, with much less keratinocyte toxicity as compared with doxorubicin and 5-FU. However, 12 active compounds selected did not necessarily induce apoptosis and mitotic arrest. This compound can be used as a lead compound to manufacture more active compound.

**Keywords:** chromone; tumor specificity; QSAR analysis; apoptosis; cell cycle analysis

## 1. Introduction

This review is composed of four parts. The first part reviews the adverse effect of chemotherapeutic agents. The second part introduces our life-work research of development of chromone derivatives that show comparable anticancer activity and lower keratinocyte toxicity, as compared with anticancer drug. The third part describes the serious problems of neurotoxicity in G2 + M blocker. The fourth part is the summary of our major findings and future direction of chromone research.



## 2. Adverse Effects of Anticancer Drugs

### 2.1. Oral Mucositis Associated with Anticancer Drug

Oral mucositis is one of the most frequent adverse events in cancer drug therapy and hematopoietic stem cell transplantation. Oral mucositis is reported to occur in 5–50% of patients receiving standard-dose chemotherapy and 68–98% of high-dose chemotherapy related to hematopoietic stem cell transplantation [1]. Oral mucositis not only lowers the patient's QOL due to pain but also lowers the oral intake, leads to undernutrition and dehydration, and deteriorates the general condition. It also serves as a gateway for bacterial invasion and may trigger systemic infection. Decreased doses and delayed schedules in chemotherapy lead to reduced efficacy and survival rates, but currently there are no established preventive or curative methods for oral mucositis, hindering smooth cancer treatment [2].

### 2.2. Neurotoxicity of Anticancer Drugs

Cancer drug therapy has contributed to the improvement of survival rate and QOL by the development of cytotoxic anticancer drugs and molecular targeted therapeutic agents, while the adverse effect of cancer drug therapy causes a decrease in QOL, sometimes causing the discontinuation of the drug therapy. Typical side effects include organ disorders such as bone marrow suppression, physical disorders such as nausea and vomiting, and neuropathy represented by paresthesia. Chemotherapy-induced peripheral neuropathy (CIPN) associated with an anticancer agent is not recovered quickly by a drug withdrawal like myelosuppression, and some disorders may remain for the lifetime. CIPN is a serious adverse event that interferes with the continuation of chemotherapy. It was reported that the incidence of CIPN was 68.1% within 1 month after chemotherapy, 60.0% after 3 months, and 30.0% after 6 months in a follow-up study of 4179 patients with colorectal cancer, breast cancer, gynecologic cancer, and multiple myeloma [3]. However, there are a few reports of preventive and therapeutic drugs for CIPN. Platinum, taxane, and vinca alkaloid are known as causative agents of CIPN. Different drugs have different mechanisms that cause peripheral neuropathy. For example, platinum-based cisplatin causes sensorineural deafness in the high range due to acoustic nerve damage. It has been reported that it is cumulative and that symptoms often continue for a long period of time after discontinuation of administration [4].

Oxaliplatin, a platinum drug, has acute and chronic symptoms. Acute symptoms are characterized by paresthesia around the extremities and around the lips and chronic symptoms may persist for months to years [5]. Carboplatin, a platinum drug, causes relatively few neurological symptoms when used at normal doses, and high doses may cause symptoms similar to cisplatin [6]. Paclitaxel, a taxane-based drug, mainly causes paresthesia of the extremities and is correlated with single dose and total dose [7]. Docetaxel, a taxane-based drug, causes sensory and motor disorders but is less frequent than paclitaxel [8]. Vincristine, a vinca alkaloid drug, causes sensory abnormalities in the fingers and movements within a few weeks after the start of treatment and often persists for a long time after the discontinuation of treatment [9]. CIPN pathological findings are classified into axonopathy, neuronopathy, and myelinopathy. Axonopathy is the most common disorder in CIPN. Neuronal cell body is relatively retained due to damage from thick and long axons. Clinically, glove and stocking type sensory deficits often begin at the extremities. Representative agents are microtubule inhibitors, vinca alkaloids, and taxanes. Neuronopathy is mainly cell bodies of lesions, mainly caused by cell death of dorsal root ganglion cells, and secondary damage to axons and myelin sheaths. Clinically, nerve cell bodies with short axons are also damaged, so sensory deficits occur not only on the extremities but also on the trunk and face. Representative agents are platinum agents such as oxaliplatin and cisplatin [10]. The frequency of mucositis and peripheral neuropathy of various anticancer agents was summarized from the interview form of the pharmaceutical company (Table 1).

**Table 1.** Incidence of oral mucositis and peripheral neuropathy induced by anticancer drugs.

Classification	Drugs	Reported Incidence (%)	
		Oral Mucositis	Peripheral Neuropathy
Vinca alkaloid	Vinorelbine (VNR)	15.2	12.2
	vinblastine (VBL)	0.4	2.2
	Vincristine (VCR)	0.1	25.5
Microtubule inhibitor	Eribulin (ERI)	39.5	24.7
Platinum	CDDP (cisplatin)	2.6	1.5
	L-OHP (oxaliplatin)	12.0	45.5
	CBDCA (carboplatin)	N.D.	N.D.
Taxane	DTX (docetaxel)	N.D.	N.D.
	PTX (paclitaxel)	18.2	55.0
	NabPTX (paclitaxel)	2.8	39.0
Antimetabolite	5-FU (fluorouracil)	6.7	0.2
	GEM (gemcitabine)	N.D.	N.D.
Topoisomerase inhibitor	IRT (irinotecan)	N.D.	N.D.
	ETP (etoposide)	N.D.	N.D.
Anthracycline	DOX (doxorubicin)	51.7	27.6
Molecular target drug	Rmab (ramucirumab)	54.3	N.D.
	Cmab (cetuximab)	>10.0	0.5~10.0
	Nmab (nivolumab)	1.0~5.0	3.1
Proteasome inhibitor	Bmib (bortezomib)	<5	28.3

N.D. no data reported.

### 2.3. Chemotherapy Extravasation

Systemic intravenous chemotherapy can cause multiple emergencies by local and systemic reactions. Drug extravasation is one of the most devastating complications in chemotherapy. Overall incidences of chemotherapy extravasation ranges from 0.01% to 6.5% [11–13], with reports of extravasation occurrence via central venous catheters ranging from 0.3% to 10.3% [14–17]. The exact incidence rate of extravasation varies greatly due to the general lack of reporting and absence of centralized registry of extravasation events. Therefore, no benchmark existed for the incidence of chemotherapy extravasations.

Extravasation is the accidental leakage of cytotoxic chemotherapy drugs that can cause severe tissue damage, tissue necrosis, blistering, or sloughing into the subcutaneous or subdermal tissue at the injection site [18,19]. Extravasated drugs are further classified into the three groups: vesicants, irritants, and nonvesicants/nonirritants, according to their potential for causing damage as (Table 2) [12,13,19,20].

Vesicant drugs have the capability to induce the formation of blisters and/or cause tissue destruction. Vesicant drugs may be subclassified into DNA-binding and non-DNA-binding compounds [20]. DNA-binding compounds are capable of producing more severe tissue damage and mainly include anthracyclines and alkylating agents. Non-DNA-binding compounds are mainly vinca alkaloids and taxanes.

Irritant drugs can cause pain at the injection site or along the vein, with or without an inflammatory reaction. Some of these agents have the potential to cause soft tissue ulcers only if a large amount of concentrated drug solution is inadvertently extravasated. Nonvesicant or nonirritant drugs, if extravasated, rarely produce acute reactions or tissue necrosis.

**Table 2.** Classification of chemotherapeutic drugs according to tissue damage after extravasation.

Type of Damages	Principal Categories	Drugs
<b>Vesicants</b>	<b>DNA-binding compounds</b>	
	Anthracyclines	Amrubicin; Daunorubicin; Doxorubicin; Epirubicin; Idarubicin; Mitoxantrone; Pirarubicin
	Alkylating agents	Bendamustine; Busulfan; Carmustine; Melphalan; Nimustine; Ranimustine; Streptozocin
	Antitumor antibiotic	Actinomycin D
	Other	Trabectedin
	<b>Non-DNA-binding compounds</b>	
	Taxanes	Docetaxel; Paclitaxel; Nab-paclitaxel
	Vinka alkaloids	Vinblastine; Vincristine; Vindesine; Vinorelbine
	<b>Others</b>	
	Antibody–drug conjugate	Gemtuzumab ozogamicin
	Antitumor antibiotic	Mitomycin C
	<b>Irritants</b>	Anthracyclines
Alkylating agents		Dacarbazine; Cyclophosphamide; Ifosfamide; Temozolomide
Antibody–drug conjugate		Trastuzumab emtansine
Antimetabolites		Azacitidine; Gemcitabine; Fluorouracil; Tegafur
Antitumor antibiotics		Bleomycin; Peplomycin
Platinum salts		Carboplatin; Cisplatin Oxaliplatin; Nedaplatin; Miriplatin
Proteasome inhibitor		Bortezomib
Taxane		Cabazitaxel
Topoisomerase I inhibitors		Irinotecan; Topotecan
Topoisomerase II inhibitor		Etoposide
Others		Arsenic Trioxide; Nelarabine; Picibanil; Porfimer; sodium
<b>Nonvesicants/ Nonirritants</b>		Antimetabolites
	Antibody–drug conjugates	Brentuximab vedotin; Ibritumomab tiuxetan
	Antineoplastic agents Hormonal	Degarelix; Fulvestrant; Goserelin; Leuprorelin
	Monoclonal antibodies	Alemtuzumab; Bevacizumab; Cetuximab; Ipilimumab; Mogamulizumab; Ofatumumab; Panitumumab; Pertuzumab; Ramucirumab; Rituximab; Trastuzumab
	Monoclonal antibodies (immune checkpoint inhibitors)	Atezolizumab; Avelumab; Durvalumab; Ipilimumab; Nivolumab; Pembrolizumab
	Others	BCG; Calcium folinate; Celmoleukin; Dexrazoxane; Eribulin; Interferon; L-asparaginase; Levofolinate; Octreotide; Pentostatin; Talaporfin sodium; Teceleukin

Tissue damage related to extravasation occurs by different mechanisms [3]. First, the drug is absorbed by local cells in the tissue and binds to critical structures, causing cell death. After the endocytolysis, surrounding cells can also die through the release of the drug from nearby dead cells. The repetitive nature of this process impairs healing and may result in progressive and chronic tissue injury. Second, the drug that does not bind to cellular DNA may metabolize and be cleared, limiting the degree of tissue injury [21]. However, the literature addressing extravasation is limited to animal studies, case reports, and small human studies. Classic randomized studies in humans for the treatment of extravasations are unthinkable because of ethical reasons. On the whole, the highest possible grade

of recommendation of each measure for extravasations would be low. Novel studies are clearly needed to elucidate the mechanism of chemotherapy extravasations.

### 3. Development of Newly Synthesized Chromone Derivatives with High Tumor Specificity, but Low Keratinocyte Toxicity

Our strategy to explore new compounds is composed with the following eight steps: search of natural products that shows the highest tumor specificity (Step 1); QSAR analysis of chromone-related compounds (Step 2); investigation of action mechanism (Step 3), identification of target molecules (Step 4), exploration of more activity compounds by prediction, synthesis, and confirmation (Step 5); check for adverse effects (Step 6); in vivo experiments with animals (Step 7); and clinical application (Step 8) (Figure 1).

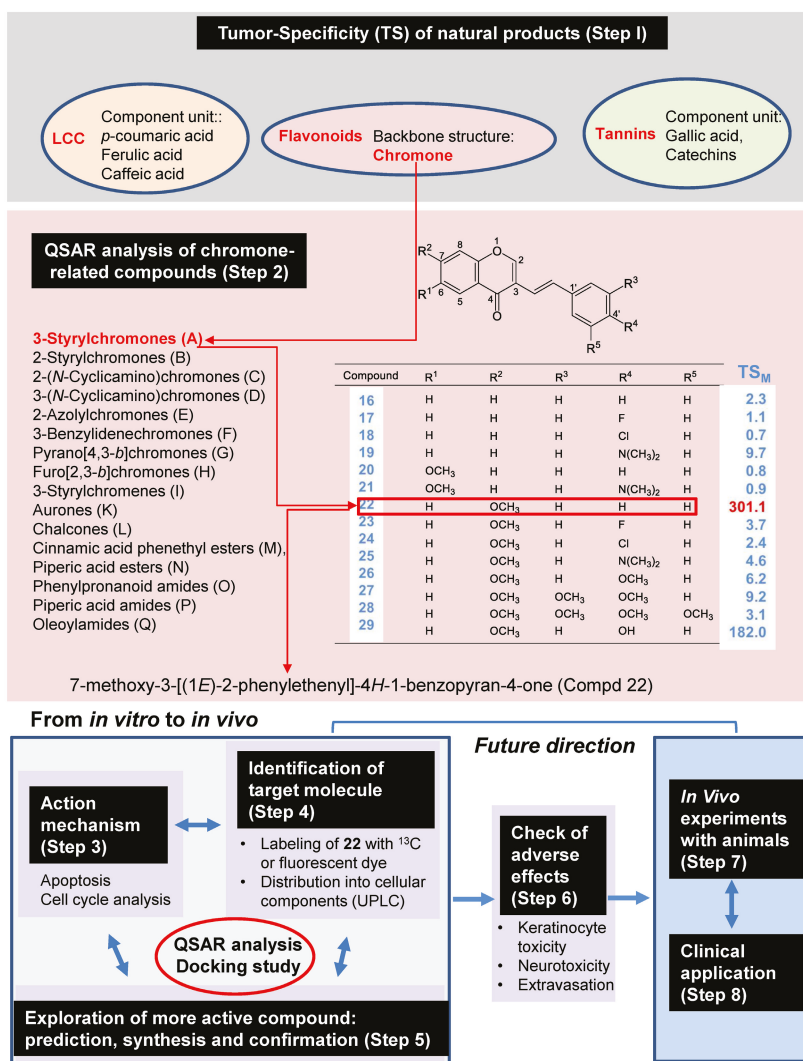


Figure 1. Strategy for exploring new anticancer drugs using chromone backbone structure.

### 3.1. Why We Focused on the Chromones

For the quantification of anticancer activity of text samples, it was necessary to establish the in vitro assay method (Figure 2) [22], using human malignant and nonmalignant cells: four human oral squamous cell carcinoma (OSCC) cell lines (Ca9-22, HSC-2, HSC-3, and HSC-4), three human normal oral mesenchymal cells (gingival fibroblast HGF, periodontal ligament fibroblast HPLF, and pulp cell HPC), and two human normal oral epithelial cells (human oral keratinocyte HOK and primary human gingival epithelial cells HGEP).

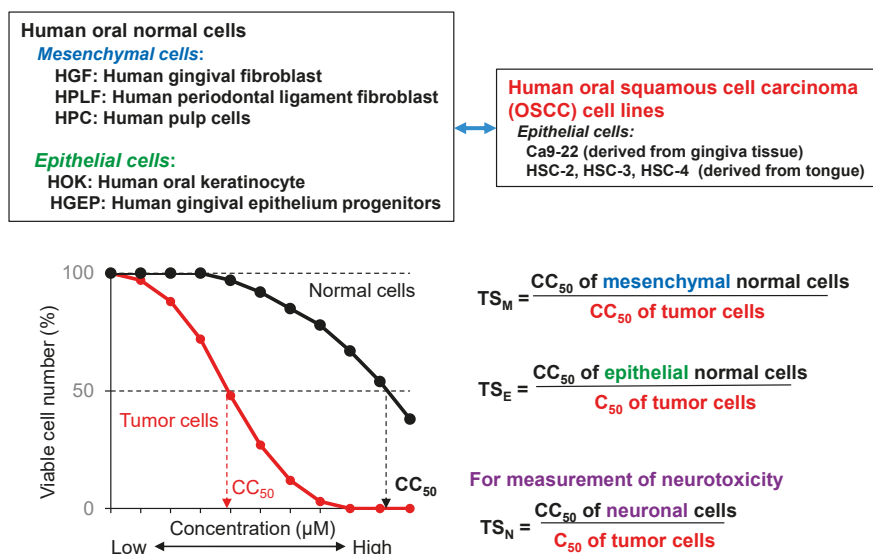


Figure 2. In vitro assay system for the measurement of tumor specificity.

Tumor specificity (TS) was defined as the ratio of the mean of CC<sub>50</sub> against normal cells to that against OSCC cells). When mesenchymal or epithelial cells were used, TS<sub>M</sub> and TS<sub>E</sub> could be obtained, respectively. TS<sub>E</sub> can be used as an index for neurotoxicity. (Figure 1). It would be the most ideal if we could use human epithelial cells as target cells. However, most of anticancer drugs show potent cytotoxicity against epithelial cells (as described later). Therefore, we used TS<sub>M</sub> value, rather than TS<sub>E</sub> at the first stage of random screening. Using this method, we found that three major polyphenols, i.e., lignin-carbohydrate complexes, tannins, and flavonoids, showed much lower TS<sub>M</sub> in comparison to popular chemotherapeutic antitumor drugs (Table 3). On the other hand, the derivatives of chromone, the backbone structure of various flavonoids such as flavonoid, flavone, flavanone, and isoflavone (Figure 3) showed much higher TS<sub>M</sub> than the majority of polyphenols [22]. These findings encouraged us to explore more active chromone derivatives.

Table 3. Tumor specificity (TS) of polyphenols.

Compound	Number of Compounds	Mean TS <sup>M</sup> (Range)
Lignin-carbohydrate complexes	4	2.7 (1.7~4.1) <sup>1</sup>
Flavones, flavonols	36	1.2 (0.3~3.2)
Flavonoids	31	3.2 (0.8~31.7)
Isoprenyl flavonoids	22	2.1 (1.6~3.0)
Tricin, morin, quercetin, kaempferol	4	1.5(1~2.2)
Isoliquiritigenin, datiscetin, galangin	3	2.0 (1~4)
Resveratrol, daidzein, genistein	3	2.1 (1.1~2.9)
Gallic acid, catechin, epigallocatechin gallate	3	2.1 (1.0~4.1)
Procyanidins	6	4.8 (1.0~7.4)
Hydrolyzable tannins (monomer)	7	1.5 (1.0~2.5)
Hydrolyzable tannins (oligomers)	3	1.4 (1.2~1.5)
Large circular ellagitannins	4	4.4 (2.3~8.2)
2-Styrylchromones	6	7.3 (1.1~17.4)
3-Styrylchromones	15	14.9 (1.6~69.0)
Anthracylines	4	181 (47~259)

<sup>1</sup> Cited from [22].

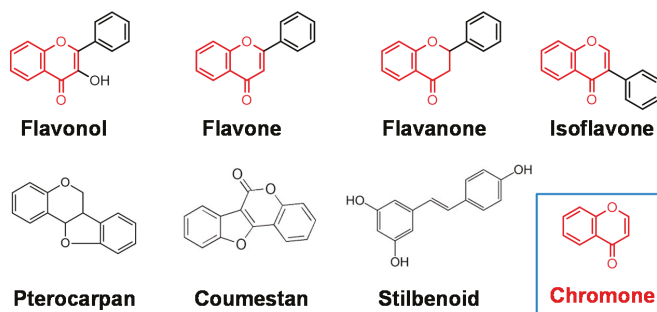


Figure 3. Chromone is a backbone structure of some flavonoids.

### 3.2. Synthesis of Chromones, Esters, and Amides

We have focused on the following three groups of compounds (Figure 4):

- **Chromone derivatives:**

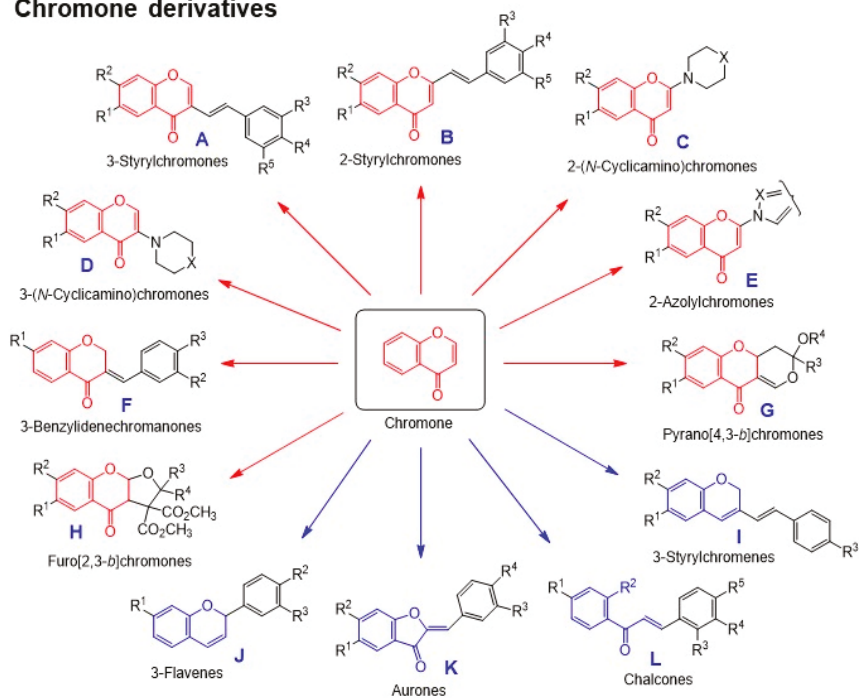
**having intact chromone ring:** 3-styrylchromones (A), 2-styrylchromones (B), 2-(*N*-cyclicamino)chromones (C), 3-(*N*-cyclicamino)chromones (D), 2-azolychromones (E), 3-benzylidenechromones (F), pyrano[4,3-*b*]chromones (G), furo[2,3-*b*]chromones (H).

**having chromen ring:** 3-styrylchromones (I) and 3-flavens (J) (unpublished).

**having cleaved chromone ring:** aurones (K) and chalcones (L).

- **Esters:** cinnamic acid phenethyl esters (M) and piperic acid esters (N).
- **Amides:** phenylpranonoid amides (O), piperic acid amides (P), and oleoylamides (Q) (Figure 4).

## Chromone derivatives



## Esters and amides

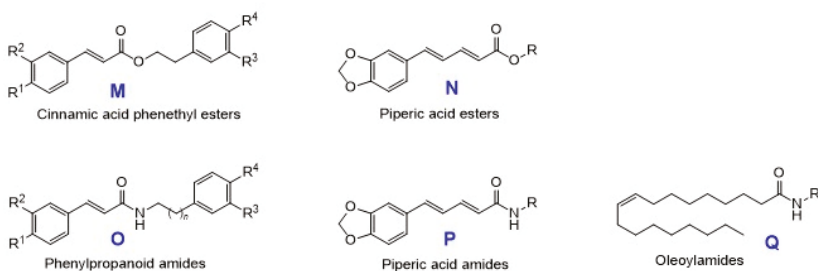


**Figure 4.** Structure of chromones (A–L), esters (M,N), and amides (O–Q).

As for chromone derivatives, 3-styrylchromones (A) were synthesized by Knoevenagel condensation of the corresponding 3-formylchromones with various phenylacetic acid derivatives [23] (Figure 5).

Here, 2-styrylchromones (B) were synthesized by base-catalyzed condensation of the corresponding 2-methylchromones with selected benzaldehyde derivatives [24].

Then, 2-(N-cyclicamino)chromones (C) were synthesized by the nucleophilic substitution reaction of 2-triazolychromone derivatives, derived from 3-iodochromones and triazole, with the cyclic secondary amines such as piperidine and piperazine derivatives [25].

Then, 3-(N-cyclicamino)chromones (D) were synthesized by the condensation of 2,3-epoxychromone derivatives with the cyclic secondary amines [25].

Then, 2-azolychromones (**E**) were synthesized by the conjugated addition reaction of 3-iodochromone derivatives with various azoles [26].

Next, 3-benzylidenechromones (**F**) were synthesized by base-catalyzed condensation of the corresponding 4-chromanone with substituted benzaldehyde derivatives [27].

Pyrano[4,3-*b*]chromones (**G**) were synthesized by the cycloaddition reaction of 3-formylchromones with selected enol ethers [28].

Furo[2,3-*b*]chromones (**H**) were synthesized by the ring expansion-cycloaddition reaction of methanochromanones with aldehydes or ketones [29].

Basically, 3-styrylchromenes (**I**) were synthesized by Horner-Wadsworth-Emmons reaction of the corresponding 2*H*-chromene-3-carbaldehydes with commercially available diethyl benzylphosphonate derivatives [30]. Additionally, 3-flavens (**J**) were synthesized by reductive intramolecular cycloaddition reaction of 2-hydroxychalcone derivatives [31]. Aurones (**K**) were synthesized by base-catalyzed condensation of 3(2*H*)-benzofuranones with selected benzaldehyde derivatives [32]. Chalcones (**L**) were synthesized by base-catalyzed condensation of the corresponding acetophenones with various benzaldehyde derivatives [31] (Figure 5).

As for esters and amides, cinnamic acid phenethyl esters (**M**) were synthesized by the condensation of cinnamic acid and its analogs, such as caffeic acid, ferulic acid, and *p*-coumaric acid, with the corresponding phenethyl alcohols. In addition, phenylpropanoid amides (**O**) were synthesized by the condensation of the corresponding cinnamic acid derivatives with various biogenic amines.

Piperic acid esters (**N**) were synthesized by the condensation of piperic acid with the corresponding alcohols. In addition, piperic acid amides (**P**) were synthesized by the condensation of the acid chloride of piperic acid with various amines. Piperic acid was prepared by alkaline hydrolysis of piperine.

Oleoylamides (**Q**) were synthesized by the condensation of oleoyl chloride, derived from oleic acid and oxalyl chloride, with the various corresponding biogenic amines (Figure 6).

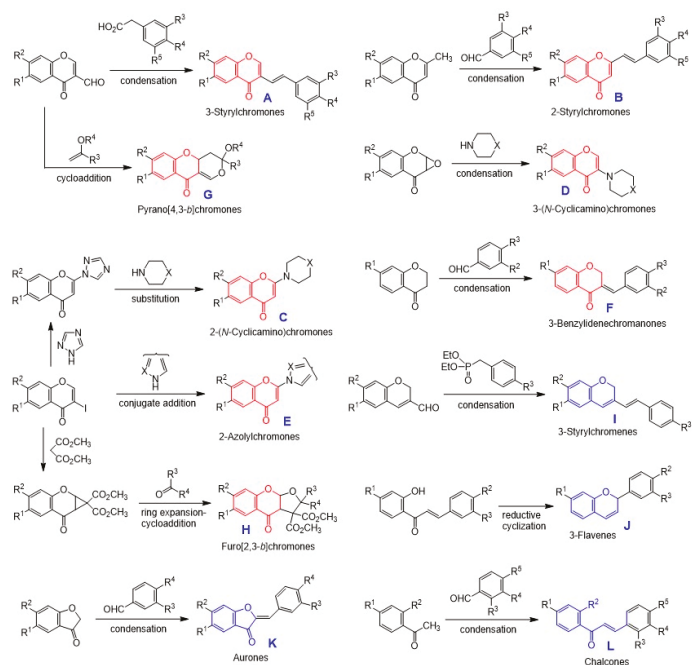


Figure 5. Synthesis of chromone derivatives.



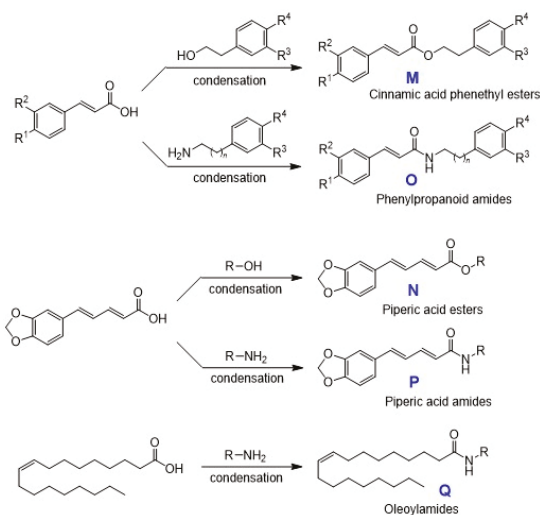


Figure 6. Synthesis of esters and amides.

### 3.3. Tumor Specificity of Chromones, Esters, and Amides

We investigated a total 291 compounds from 17 different groups (A~Q) of their cytotoxicity (assessed by  $CC_{50}$ ) against four human OSCC (Ca9-22, HSC-2, HSC-3, and HSC-4) and three human normal mesenchymal cells (HGF, HPLF, and HPC), and then their tumor specificity (assessed by  $TS_M$ , calculated as describe in Figure 2, and potency-selectivity expression (PSE)) [33–52]. PSE, that reflects both tumor specificity and cytotoxicity against tumor cells, was calculated by dividing the  $TS_M$  by  $CC_{50}$  for tumor cells, and then multiplying by 100. All these values are listed in Supplementary Table S1. This demonstrated that only limited numbers of compounds show higher tumor specificity, although their structures are very similar with each other. It is possible that such highly tumor-specific compounds show the optimal 3D structure, since the tumor specificity of chromone compounds shows the tight correlation with chemical descriptors that reflect the 3-D structure (Table 4) [33,35,37–53].

Table 4. Molecular shape is the key determinant of tumor specificity.

	Chemical Descriptors That Correlate with Tumor Specificity	Ref.
3-Styrylchromones (A)	Molecular shape, electrostatic interaction, charge	[33,35]
2-Styrylchromones (B)	Molecular shape and flatness	[37]
2-(N-Cyclicamino)chromones (C)	Molecular shape, 3D-structure	[38]
3-(N-Cyclicamino)chromones (D)	3D-structure, lipophilicity	[39]
2-Azolychromones (E)	3D/topological shape, size, polarizability, lipophilicity	[40,41]
3-Benzylidenechromones (F)	Molecular shape, size, polarization	[42]
Pyrano[4,3- <i>b</i> ]chromones (G)	3D structure, polarity, ionic potential, electric state	[43]
Furo[2,3- <i>b</i> ]chromones (H)	Molecular flexibility, density, size and shape, lipophilicity	[44]
3-Styrylchromenes (I)	Molecular shape and flatness	[45]
Aurones (K)	Molecular shape, size, polarizability	[46]
Chalcones (L)	Molecular shape and polarization	[47]
Cinnamic acid phenethyl esters (M)	Shape, size and ionization potential	[48]
Piperic acid esters (N)	Molecular shape, size, ionization potential, electronegativity	[49]
Phenylpropanoid amides (O)	Molecular size (surface area), electrostatic interaction	[50]
Piperic acid amides (P)	Molecular shape, electrostatic interaction	[51]
Oleoylamides (Q)	Molecular polarization and hydrophobicity	[52]

The most active compounds in each group are shown in Figure 7. Their cytotoxicity against human four OSCC cell lines, and three human normal oral mesenchymal (HGF, HPLF, and HPC),

two human epithelial cells (HOK and HGEP), and tumor specificity (TSM (determined with OSCC vs. human normal mesenchymal cells), TSE) (determined with OSCC vs. human normal epithelial cells) are shown in Table 5.

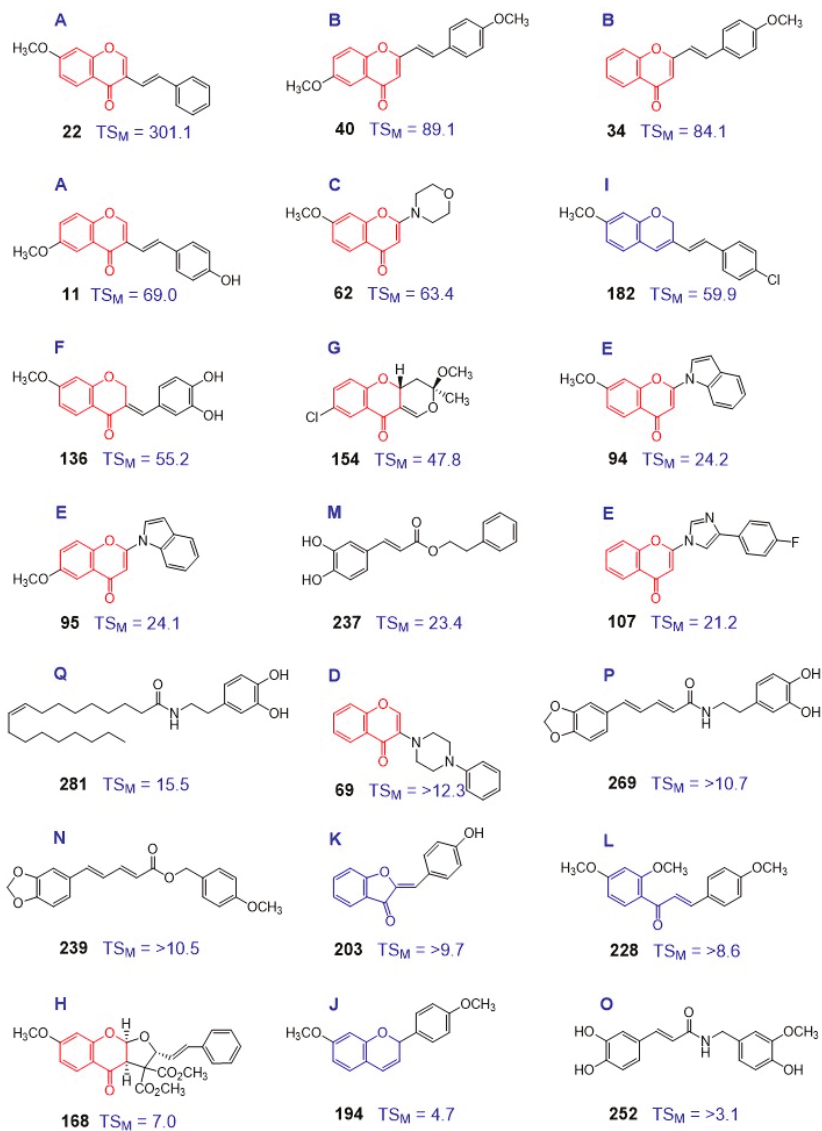


Figure 7. The most active compounds in each group, line-uped in the decreasing order of potency.

**Table 5.** Tumor specificity and keratinocyte toxicity of chromones and anticancer drugs.

Group	Compd.	CC <sub>50</sub> (μM)							Ref.
		Normal Oral Cells					TS <sub>M</sub>	TS <sub>E</sub>	
		Four OSCCs	Mesenchymal	Epithelial					
				(a)	(b)	HOK (c)	HGEP (d)	(b/a)	
3-Styrylchromones (A)	11	2.0	138	19.0	800	69.0	9.5	400.0	[33]
3-Styrylchromones (A)	22	0.6	182		400	301.1		662.1	[35]
2-Styrylchromones (B)	34	1.9	159		100	84.1		52.8	[37]
2-Styrylchromones (B)	40	3.8	336			89.1			
2-( <i>N</i> -Cyclicamino)chromones (C)	62	5.5	348	357.7		63.4	65.2		[38]
3-( <i>N</i> -Cyclicamino)chromones (D)	69	32.3	>397	400.0		>12.3	12.4		[39]
2-Azolychromones (E)	94	6.3	153			24.2			[40]
2-Azolychromones (E)	95	1.5	36			24.1			
2-Azolychromones (E)	107	18.4	389			21.2			[41]
3-Benzylidenechromones (F)	136	7.3	>400	3.8	3.3	55.2	0.5	0.5	[42]
Pyrano[4,3- <i>b</i> ]chromones (G)	154	5.0	240	20.3		47.8	4.1		[43]
Furo[2,3- <i>b</i> ]chromones (H)	168	37.2	261			7.0			[44]
3-Styrylchromones (I)	182	4.7	280			59.9			[45]
3-Flavens (J)	194	73.3	348			4.7			
Aurones (K)	203	41.4	>400			>9.7			[46]
Chalcones (L)	228	<4.4	38			>8.6			[47]
Cinnamic acid phenethyl esters (M)	237	8.5	199			23.4			[48]
Piperic acid esters (N)	239	37.9	>400			>10.5			[49]
Phenylpropanoid amides (O)	252	122.0	378			>3.1			[50]
Piperic acid amides (P)	269	75.0	>800			>10.7			[51]
Oleoylamides (Q)	281	0.6	9.7	2.5	0.4	15.5	4.0	0.6	[52]
DXR		0.1	9.7	0.1	0.027	121.8	1.5	0.3	[35, 39]
5-FU		61.8	1000.0	24.7	18.8	16.2	0.4	0.3	[35]

Further, 7-methoxy-3-[(1*E*)-2-phenylethenyl]-4*H*-1-benzopyran-4-one (compound **22**) showed the highest TS value (TS<sub>M</sub> = 301.1), followed by 2-[(1*E*)-2-(3,4-dimethoxy)ethenyl]-4*H*-1-benzopyran-4-one (compound **40**) (TS<sub>M</sub> = 89.1) > 2-[(1*E*)-2-(4-methoxyphenyl)ethenyl]-4*H*-1-benzopyran-4-one (compound **34**) (TS<sub>M</sub> = 84.1) > (E)-3-(4-Hydroxystyryl)-6-methoxy-4*H*-chromen-4-one (compound **11**) (TS<sub>M</sub> = 69.0) > 7-methoxy-2-(4-morpholinyl)-4*H*-1-benzopyran-4-one (compound **62**) (TS<sub>M</sub> = 63.4) > (E)-3-(4-cholorostyryl)-7-methoxy-2*H*-chromene (compound **182**) (TS<sub>M</sub> = 59.9) > (3*E*)-2,3-dihydro-3-[(3,4-dihydroxyphenyl)methylene]-7-methoxy-4*H*-1-benzopyran-4-one (TS<sub>M</sub> = 52.2) (compound **136**). It is noted that these compounds showed comparable TS values of doxorubicin (DXR) and much higher TS value than 5-FU. It was unexpected that DXR and 5-FU showed potent toxicity against human epithelial cells such as human oral keratinocyte (HOK) and human progenitor of human gingival epithelial cells (HGEP) (c/a and d/a in Table 5). We have reported previously that DXR induced apoptosis (characterized by the loss of cell surface microvilli, chromatin condensation, nuclear fragmentation, and caspase-3 activation) in these keratinocytes [54]. On the other hand, compounds **11**, **22**, **34**, **62**, and **69** showed much lower keratinocyte toxicity (Table 5).

### 3.4. Mechanism of Action

Compounds **11** and **22** in 3-styrylchromones (A), **34** and **40** in 2-styrylchromones (B), **95** in 2-azolychromones (E), **228** in chalcones (L), and **237** in cinnamic acid phenethyl esters (M) induced apoptosis [caspase-3 activation (assessed by western blot analysis) and subG1 cell accumulation (assessed by cell sorter analysis)] in human OSCC cell lines. On the other hand, compounds **62** in 2-(*N*-cyclicamino)chromones (C), **95** in 3-(*N*-cyclicamino)chromones (D), **107** in 2-azolychromones (E), **154** in pyrano[4,3-*b*]chromones (G), and **168** in furo[2,3-*b*]chromones (H) did not induce apoptosis (Table 6). Compounds **22**, **34**, **40**, and **107** also induced G2 + M cell accumulation, but only the first 3

compounds induced apoptosis. This indicated that the induction of G2 + M accumulation itself does not guarantee the induction of apoptosis.

**Table 6.** The most active compounds in each group do not necessarily induce apoptosis in human oral squamous cell carcinoma (OSCC) cell line.

Group	Compd.	Mechanism of Action	Ref.
3-Styrylchromones (A)	11	Mitochondrial vacuolization caspase-3 ↑	[34]
3-Styrylchromones (A)	22	subG1↑ G2 + M↑	[35]
2-Styrylchromones (B)	34, 40	subG1↑ G2 + M↑	[37]
2-(N-Cyclicamino)chromones (C)	62	No apoptosis cytotoxic	[38]
3-(N-Cyclicamino)chromones (D)	69	No apoptosis cytostatic	[39]
2-Azolychromones (E)	95	Caspase-3↑	
2-Azolychromones (E)	107	G2 + M phase cells↑ No apoptosis cytostatic	[41]
Pyrano[4,3- <i>b</i> ]chromones (G)	154	No apoptosis cytostatic	[43]
Furo[2,3- <i>b</i> ]chromones (H)	168	No apoptosis	[44]
Chalcones (L)	228	Caspase-3↑	[47]
Cinnamic acid phenethyl esters (M)	237	Caspase-3↑	[48]

### 3.5. Other Biological Actions of Chromones, Esters, and Amides

We searched other biological activities of chromones, esters, and amides (Supplementary Table S2). Table 7 listed up the most potent compounds that showed biological activity higher than positive controls. Compounds 10, 12, 15, 124, 136, 229, 231, 237, 258, and 261 scavenged the DPPH radical, more potently than ascorbic acid, a well-known antioxidant [23], suggesting its antioxidant action.

**Table 7.** Other biological activities of chromones, esters, and amides.

Group	Inhibition of	Compd. No	EC <sub>50</sub> or IC <sub>50</sub> (μM)		Ref.
			Compd.	Positive Control	
3-Styrylchromones (A)	DPPH radical α-glucosidase	10, 12, 15	17, 22, 23	23 (ascorbate)	[23]
		10, 14, 15, 18	16, 9, 10, 16	>100 (acarbose)	[23]
2-Styrylchromones (B)	MAO-B	38, 39	0.017, 0.024	0.22 (Pargyline)	[24]
2-Azolychromones (E)	MAO-B	87, 89	0.028, 0.019	0.22 (Pargyline)	[26]
3-Benzylidenechromones (F)	DPPH radical α-glucosidase	124, 136	13, 13	12 (ascorbate)	[27]
		131, 132, 136	15, 25, 28	900 (acarbose)	[27]
Pyrano[4,3- <i>b</i> ]chromones (G)	MAO-B	153	0.2	0.22 (Pargyline)	[28]
3-Styrylchromones (I)	MAO-B	173, 177, 181	0.010, 0.015, 0.016	0.22 (Pargyline)	[30]
Cinnamic acid phenethyl esters (M)	DPPH radical MAO-B BChE	229, 231, 237	18, 11, 18	23 (ascorbate)	[55]
		236	0.013,	0.22 (Pargyline)	[55]
		230, 235	4.9, 6.8	7.1 (Neostigmine)	[55]
Phenylpropanoid amides (O)	DPPH radical α-glucosidase	258, 261	8.7, 8.1	12 (ascorbate)	[55]
		266, 267	30, 29	900 (acarbose)	[56]

Compounds 10, 14, 15, 18, 131, 132, 136, 266, and 267 inhibited α-glucosidase (EC 3.2.1.20) that is responsible in breaking down starch and disaccharides to glucose, more potently than acarbose. This suggests their possible antihyperglycemic effect.

Compounds 10, 15, 124, and 136 show both α-glucosidase inhibitory and antioxidant actions, suggesting that they can be lead compounds for manufacturing as antidiabetic drugs.

Compounds 38, 39, 87, 89, 153, 173, 177, and 236 inhibited monoamine oxidase (MAO-B) more effectively than pargyline, an irreversible selective MAO-B inhibitor drug. This suggests their application to treat the Parkinson's disease and Alzheimer's disease [24,27,28,30,55]. Halogen-containing compounds show more potent inhibitory activity. All compounds showed higher MAO-B-specific inhibition than positive controls and, therefore, were not likely to exert adverse effects due to MAO-A inhibition. Furthermore, they show reversible inhibition and thus were much convenient for the sudden interruption of treatment, as compared with irreversible inhibitors.

Compounds **230** and **235** inhibited the butyrylcholinesterase (BChE) more potently than neostigmine, suggesting that they may serve as lead compounds for the development of novel BChE inhibitors and candidate lead compounds for the prevention or treatment of Alzheimer's disease [55].

We found that all compounds tested showed no anti-HIV activity ( $SI < 1$ ), in contrast to popular anti-HIV substances (dextran sulfate, curdlan sulfate, azidothymidine, 2',3'-dideoxycytidine, azidothymidine, and 2',3'-dideoxycytidine) ( $SI = 53\text{--}2512$ ) (Supplementary Table S3).

#### 4. Serious Problems of Neurotoxicity in G2 + M Blocker

We found that highly tumor-specific 3-styrylchromone derivatives [7-methoxy-3-[(1E)-2-phenylethenyl]-4H-1-benzopyran-4-one (compound **22**) and 3-[(1E)-2-(4-hydroxyphenyl)ethenyl]-7-methoxy-4H-1-benzopyran-4-one (compound **29**)] ( $TS_M = 301$  and  $182$ , respectively) (Supplementary Table S1) induced subG1 and G2 + M arrest [35]. We also have recently reported that several G2/M blockers such as taxanes paclitaxel (Taxol<sup>®</sup>, the first microtubule stabilizing agent [57]) and docetaxel, show very high  $TS_M$  values ( $>7267$  and  $>86,122$ , respectively) [58]. Marinho et al. reported recently that 4'-methoxy-2-styrylchromone induced mitotic arrest in human tumor (human Caucasian breast adenocarcinoma MCF-7 and human lung adenocarcinoma NCI-H460) cell lines, in a similar fashion to paclitaxel [59]. Soo et al. reported that cudraflavone C (Cud C), a naturally occurring flavonol, induced apoptosis (caspase activation) in colorectal cancer cells (CRC) and tumor-selective cytotoxicity by targeting the PI3K-AKT pathway [60].

However, many reports, including ours, demonstrated that microtubule-targeted agents have potent neurotoxicity, adversely affecting the quality of life of patients on a long-term basis [61–64]. Iijima et al. recently reported that carboplatin (CBDCA) was highly neurotoxic ( $TS_N = 0.11$  (3.2/27.9)), calculated using the data of Table 2 in Ref. [64]. It is urgent to investigate the neurotoxicity, extravasation as well as stomatitis of chromone derivatives, esters, and amides.

#### 5. Conclusions and Future Direction

We found that:

- (i) Chromone showed much higher tumor specificity as compared with three major polyphenols.
- (ii) A total 291 newly synthesized compounds of 17 groups (consisting of 12 chromones, 2 esters, and 3 amides) gave a wide range of the intensity of tumor specificity.
- (iii) Their tumor specificity is correlated with chemical descriptors that reflect 3D structure and electric state.
- (iv) 7-Methoxy-3-[(1E)-2-phenylethenyl]-4H-1-benzopyran-4-one (compound **22**), which belongs to 3-styrylchromones, showed the highest tumor specificity. Compound **22** induced subG1 and G2 + M cell population in human OSCC cell line, with much less keratinocyte toxicity as compared with doxorubicin and 5-FU. This compound can be used as a lead compound to manufacture more active compound.

It is crucial to identify the target molecules (Step 4 in Figure 1). To accomplish this, <sup>13</sup>C-labeled compound **22** will be prepared, using 2-hydroxyacetophenone derivatives and <sup>13</sup>C-dimethylformamide, or using <sup>13</sup>C-iodomethane as methylation agent, and then the differential incorporation of <sup>13</sup>C into malignant and nonmalignant cells will be investigated, with LC-MS. Compound **22**, labeled with fluorescence dye (Cy3, Cy5, Cy7), will be tested to detect the intracellular uptake and distribution into organelles, using confocal laser microscopy. Binding of cellular protein to and elution from chromone-attached beads may be useful to identify the binding proteins.

In order to explore more potent chromone derivatives, the following three steps will be repeated: (i) prediction by QSAR of the best fit substituents that yield the highest  $TS_M$  and TSE, (ii) synthesis of compounds introduced with such predicted substituents, and (iii) confirmation of antitumor potential (Step 5). However, it is important to eliminate the compounds that show potent keratinocyte toxicity,

neurotoxicity, and extravasation (Step 6), before animal experiment (Step 6) and clinical application (Step 7).

The present study demonstrated that only selected compounds that have the optimal 3D structure show the highest tumor specificity, whereas most of other analogs that have similar structure show much less tumor specificity (Supplementary Table S1). This suggests the presence of binding components or receptors for chromones. It remains to be investigated whether compounds **22** and **40** may interact with estrogen receptors, since these compounds have structural similarity with isoflavones (such as daidzein and genistein) and to some degree with tamoxifen, which have been used for the treatment of oral squamous cell carcinoma that express estrogen receptors [65–67]. In addition, it seems that the “para” like substitution is favorable, possibly because it mimics the structure of estrogen. It is highly probable that different groups of chromone-related compounds have different anticancer mechanisms depending on their structure (Table 6).

**Supplementary Materials:** The following are available online at <http://www.mdpi.com/2305-6320/7/9/50/s1>, Table S1: Tumor specificity of 291 compounds; Table S2: Radical scavenging and monoamine oxidase inhibitory and cholinesterase inhibitory activities of chromones, esters, and amides; Table S3: Test for anti-HIV activity of chromones, esters, and amides.

**Author Contributions:** Conceptualization was done by H.S., Y.U. and Y.S., Y.I., M.S. wrote the sections of adverse effects of anticancer drugs. Y.S. and K.T. wrote the section of chemical synthesis and drew the structures of chromones, esters, and amides and inhibitor assay. Y.U. and J.N. wrote the section of QSAR analysis. H.S. wrote the section of tumor specificity, apoptosis, and cell cycle assay and other parts of the text. All authors have read and agreed to the published version of the manuscript.

**Funding:** This research was funded by KAKENHI from the Japan Society for the Promotion of Science (JSPS): Sakagami H, 16K11519, and 20K09885.

**Acknowledgments:** We would like to thank Okudaira (Teikyo University School of Medicine) and Bando (Meikai University School of Dentistry) for technical support.

**Conflicts of Interest:** The authors declare no conflicts of interest.

## References

- Bellm, L.A.; Epstein, J.B.; Rose-Ped, A.; Martin, P.; Fuchs, H.J. Patient reports of complications of bone marrow transplantation. *Support. Care Cancer* **2000**, *8*, 33–39. [[CrossRef](#)] [[PubMed](#)]
- Vera-Llonch, M.; Oster, G.; Ford, C.M.; Lu, J.; Sonis, S. Oral mucositis and outcomes of allogeneic hematopoietic stem-cell transplantation in patients with hematologic malignancies. *Support. Care Cancer* **2007**, *15*, 491–496. [[CrossRef](#)] [[PubMed](#)]
- Serethy, M.; Currie, G.L.; Sena, E.S.; Ramnarine, S.; Grant, R.; MacLeod, M.R.; Colvin, L.A.; Fallon, M. Incidence, prevalence, and predictors of chemotherapy-induced peripheral neuropathy: A systematic review and meta-analysis. *Pain* **2014**, *155*, 2461–2470. [[CrossRef](#)] [[PubMed](#)]
- Mollman, J.E.; Hogan, W.M.; Glover, D.J.; McCluskey, L.F. Unusual presentation of cis-platinum neuropathy. *Neurology* **1988**, *38*, 488–490. [[CrossRef](#)] [[PubMed](#)]
- Argyriou, A.A.; Polychronopoulos, P.; Iconomou, G.; Chroni, E.; Kalofonos, H.P. A review on oxaliplatin-induced peripheral nerve damage. *Cancer Treat. Rev.* **2008**, *34*, 368–377. [[CrossRef](#)] [[PubMed](#)]
- Heinzlef, O.; Lotz, J.P.; Rouillet, E. Severe neuropathy after high dose carboplatin in three patients receiving multidrug chemotherapy. *J. Neurol. Neurosurg. Psychiatry* **1998**, *64*, 667–669. [[CrossRef](#)] [[PubMed](#)]
- Mielke, S.; Sparreboom, A.; Steinberg, S.M.; Gelderblom, H.; Unger, C.; Behringer, D.; Mross, K. Association of Paclitaxel pharmacokinetics with the development of peripheral neuropathy in patients with advanced cancer. *Clin. Cancer Res.* **2005**, *11*, 4843–4850. [[CrossRef](#)] [[PubMed](#)]
- Hilkens, P.H.; Verweij, J.; Stoter, G.; Vecht, C.J.; van Putten, W.L.; van den Bent, M.J. Peripheral neurotoxicity induced by docetaxel. *Neurology* **1996**, *46*, 104–108. [[CrossRef](#)] [[PubMed](#)]
- Legha, S.S. Vincristine neurotoxicity. Pathophysiology and management. *Med. Toxicol.* **1986**, *1*, 421–427. [[CrossRef](#)] [[PubMed](#)]
- Han, Y.; Smith, M.T. Pathobiology of cancer chemotherapy-induced peripheral neuropathy (CIPN). *Front. Pharm.* **2013**, *4*, 156. [[CrossRef](#)] [[PubMed](#)]

11. Bahrami, M.; Karimi, T.; Yadegarfar, G.; Norouzi, A. Assessing the Quality of Existing Clinical Practice Guidelines for Chemotherapy Drug Extravasation by Appraisal of Guidelines for Research and Evaluation II. *Iran. J. Nurs. Midwifery Res.* **2019**, *24*, 410–416. [[CrossRef](#)] [[PubMed](#)]
12. Boulanger, J.; Ducharme, A.; Dufour, A.; Fortier, S.; Almanric, K. Management of the extravasation of anti-neoplastic agents. *Support. Care Cancer* **2015**, *23*, 1459–1471. [[CrossRef](#)] [[PubMed](#)]
13. Ener, R.A.; Meglathery, S.B.; Styler, M. Extravasation of systemic hemato-oncological therapies. *Ann. Oncol.* **2004**, *15*, 858–862. [[CrossRef](#)] [[PubMed](#)]
14. Biffi, R.; Pozzi, S.; Agazzi, A.; Pace, U.; Floridi, A.; Cenciarelli, S.; Peveri, V.; Cocquio, A.; Andreoni, B.; Martinelli, G. Use of totally implantable central venous access ports for high-dose chemotherapy and peripheral blood stem cell transplantation: Results of a monocentre series of 376 patients. *Ann. Oncol.* **2004**, *15*, 296–300. [[CrossRef](#)] [[PubMed](#)]
15. Froiland, K. Extravasation injuries: Implications for WOC nursing. *J. Wound Ostomy Cont. Nurs.* **2007**, *34*, 299–302. [[CrossRef](#)] [[PubMed](#)]
16. Lemmers, N.W.; Gels, M.E.; Sleijfer, D.T.; Plukker, J.T.; van der Graaf, W.T.; de Langen, Z.J.; Droste, J.H.; Koops, H.S.; Hoekstra, H.J. Complications of venous access ports in 132 patients with disseminated testicular cancer treated with polychemotherapy. *J. Clin. Oncol.* **1996**, *14*, 2916–2922. [[CrossRef](#)] [[PubMed](#)]
17. Voog, E.; Campion, L.; du Rusquec, P.; Bourgeois, H.; Domont, J.; Denis, F.; Emmanuel, E.; Dupuis, O.; Ganem, G.; Lafont, C.; et al. Totally implantable venous access ports: A prospective long-term study of early and late complications in adult patients with cancer. *Support. Care Cancer* **2018**, *26*, 81–89. [[CrossRef](#)] [[PubMed](#)]
18. Harrold, K.; Gould, D.; Drey, N. The management of cytotoxic chemotherapy extravasation: A systematic review of the literature to evaluate the evidence underpinning contemporary practice. *Eur. J. Cancer Care* **2015**, *24*, 771–800. [[CrossRef](#)] [[PubMed](#)]
19. Kreidieh, F.Y.; Moukadem, H.A.; Saghir, N.S.E. Overview, prevention and management of chemotherapy extravasation. *World J. Clin. Oncol.* **2016**, *7*, 87–97. [[CrossRef](#)] [[PubMed](#)]
20. Fidalgo, J.A.P.; Fabregat, L.G.; Cervantes, A.; Margulies, A.; Vidall, C.; Roila, F. Management of chemotherapy extravasation: ESMO-EONS Clinical Practice Guidelines. *Ann. Oncol.* **2012**, *23*, 167–173. [[CrossRef](#)] [[PubMed](#)]
21. Boschi, R.; Rostagno, E. Extravasation of antineoplastic agents: Prevention and treatments. *Pediatric Rep.* **2012**, *4*, e28. [[CrossRef](#)] [[PubMed](#)]
22. Sakagami, H. Biological activities and possible dental application of three major groups of polyphenols. *J. Pharm. Sci.* **2014**, *126*, 92–106. [[CrossRef](#)] [[PubMed](#)]
23. Takao, K.; Ishikawa, R.; Sugita, Y. Synthesis and biological evaluation of 3-styrylchromone derivatives as free radical scavengers and  $\alpha$ -glucosidase inhibitors. *Chem. Pharm. Bull.* **2014**, *62*, 810–815. [[CrossRef](#)] [[PubMed](#)]
24. Takao, K.; Endo, S.; Nagai, J.; Kamauchi, H.; Takemura, Y.; Uesawa, Y.; Sugita, Y. 2-Styrylchromone derivatives as potent and selective monoamine oxidase B inhibitors. *Bioorg. Chem.* **2019**, *92*, 103285. [[CrossRef](#)] [[PubMed](#)]
25. Takao, K.; Sakatsume, T.; Kamauchi, H.; Sugita, Y. Syntheses and evaluation of 2- or 3-(N-cyclicamino) chromone derivatives as monoamine oxidase inhibitors. *Chem. Pharm. Bull.* **2020**, in press.
26. Takao, K.; Saito, T.; Chikuda, D.; Sugita, Y. 2-Azolychromone derivatives as potent and selective inhibitors of monoamine oxidases A and B. *Chem. Pharm. Bull.* **2016**, *64*, 1499–1504. [[CrossRef](#)] [[PubMed](#)]
27. Takao, K.; Yamashita, M.; Yashiro, A.; Sugita, Y. Synthesis and biological evaluation of 3-benzylidene-4-chromanone derivatives as free radical scavengers and  $\alpha$ -glucosidase inhibitors. *Chem. Pharm. Bull.* **2016**, *64*, 1203–1207. [[CrossRef](#)] [[PubMed](#)]
28. Takao, K.; Kubota, Y.; Kamauchi, H.; Sugita, Y. Synthesis and biological evaluation of pyrano[4,3-b][1]benzopyranone derivatives as monoamine oxidase and cholinesterase inhibitors. *Bioorg. Chem.* **2019**, *83*, 432–437. [[CrossRef](#)] [[PubMed](#)]
29. Sugita, Y.; Kawai, K.; Yokoe, I. Diastereoselective ring-expansion reaction of methanochromanone with aldehydes: Formation of trans-fused tetrahydrofuro[2,3-b][1]benzopyranones and their isomerization. *Heterocycles* **2001**, *55*, 135–144. [[CrossRef](#)]
30. Takao, K.; Yahagi, H.; Uesawa, U.; Sugita, Y. 3-(E)-Styryl-2H-chromene derivatives as potent and selective monoamine oxidase B inhibitors. *Bioorg. Chem.* **2018**, *77*, 436–442. [[CrossRef](#)] [[PubMed](#)]
31. Devakaram, R.; Black, D.S.; Andrews, K.T.; Fisher, G.M.; Davis, R.A.; Kumar, N. Synthesis and antimalarial evaluation of novel benzopyrano[4,3-b]benzopyran derivatives. *Bioorg. Med. Chem.* **2011**, *19*, 5199–5206. [[CrossRef](#)] [[PubMed](#)]

32. Okombi, S.; Rival, D.; Bonnet, S.; Mariotte, A.M.; Perrier, E.; Boumendjel, A. Discovery of benzylidenebenzofuran-3(2H)-one (aurone) as inhibitors of tyrosinase derived from human melanocytes. *J. Med. Chem.* **2006**, *49*, 329–333. [[CrossRef](#)] [[PubMed](#)]
33. Shimada, C.; Uesawa, Y.; Ishii-Nozawa, R.; Ishihara, M.; Kagaya, H.; Kanamoto, T.; Terakubo, S.; Nakashima, H.; Takao, K.; Sugita, Y.; et al. Quantitative structure-cytotoxicity relationship of 3-styrylchromones. *Anticancer Res.* **2014**, *34*, 5405–5411. [[PubMed](#)]
34. Sakagami, H.; Shimada, C.; Kanda, Y.; Amano, O.; Sugimoto, M.; Ota, S.; Soga, T.; Tomita, M.; Sato, A.; Tanuma, S.I.; et al. Effects of 3-styrylchromones on metabolic profiles and cell death in oral squamous cell carcinoma cells. *Toxicol. Rep.* **2015**, *2*, 1281–1290. [[CrossRef](#)] [[PubMed](#)]
35. Takao, K.; Hoshi, K.; Sakagami, H.; Shi, H.; Bandow, K.; Nagai, J.; Uesawa, Y.; Tomomura, A.; Tomomura, M.; Sugita, Y. Further Quantitative Structure-Cytotoxicity Relationship Analysis of 3-Styrylchromones. *Anticancer Res.* **2020**, *40*, 87–95. [[CrossRef](#)]
36. Momoi, K.; Sugita, Y.; Ishihara, M.; Satoh, K.; Kikuchi, H.; Hashimoto, K.; Yokoe, I.; Nishikawa, H.; Fujisawa, S.; Sakagami, H. Cytotoxic activity of styrylchromones against human tumor cell lines. *In Vivo* **2005**, *19*, 157–163. [[PubMed](#)]
37. Uesawa, Y.; Nagai, J.; Shi, H.; Sakagami, H.; Bandow, K.; Tomomura, A.; Tomomura, M.; Endo, S.; Takao, K.; Sugita, Y. Quantitative Structure-Cytotoxicity Relationship of 2-Styrylchromones. *Anticancer Res.* **2019**, *39*, 6489–6498. [[CrossRef](#)]
38. Shi, H.; Nagai, J.; Sakatsume, T.; Bandow, K.; Okudaira, N.; Sakagami, H.; Tomomura, M.; Tomomura, A.; Uesawa, Y.; Takao, K.; et al. Quantitative Structure-Cytotoxicity Relationship of 2-(N-cyclicamino)chromone Derivatives. *Anticancer Res.* **2018**, *38*, 3897–3906. [[CrossRef](#)]
39. Shi, H.; Nagai, J.; Sakatsume, T.; Bandow, K.; Okudaira, N.; Uesawa, Y.; Sakagami, H.; Tomomura, M.; Tomomura, A.; Takao, K.; et al. Quantitative Structure-Cytotoxicity Relationship of 3-(N-Cyclicamino)chromone Derivatives. *Anticancer Res.* **2018**, *38*, 4459–4467. [[CrossRef](#)]
40. Sakagami, H.; Okudaira, N.; Uesawa, Y.; Takao, K.; Kagaya, H.; Sugita, Y. Quantitative Structure-Cytotoxicity Relationship of 2-Azolychromones. *Anticancer Res.* **2018**, *38*, 763–770. [[CrossRef](#)]
41. Nagai, J.; Shi, H.; Sezaki, N.; Yoshida, N.; Bandow, K.; Uesawa, Y.; Sakagami, H.; Tomomura, M.; Tomomura, A.; Takao, K.; et al. Quantitative Structure-Cytotoxicity Relationship of 2-Arylazolychromones and 2-Triazolylchromones. *Anticancer Res.* **2019**, *39*, 6479–6488. [[CrossRef](#)] [[PubMed](#)]
42. Uesawa, Y.; Sakagami, H.; Kagaya, H.; Yamashita, M.; Takao, K.; Sugita, Y. Quantitative Structure-cytotoxicity Relationship of 3-Benzylidenechromanones. *Anticancer Res.* **2016**, *36*, 5803–5812. [[CrossRef](#)] [[PubMed](#)]
43. Nagai, J.; Shi, H.; Kubota, Y.; Bandow, K.; Okudaira, N.; Uesawa, Y.; Sakagami, H.; Tomomura, M.; Tomomura, A.; Takao, K.; et al. Quantitative Structure-Cytotoxicity Relationship of Pyrano[4,3-*b*]chromones. *Anticancer Res.* **2018**, *38*, 4449–4457. [[CrossRef](#)] [[PubMed](#)]
44. Uesawa, Y.; Sakagami, H.; Shi, H.; Hirose, M.; Takao, K.; Sugita, Y. Quantitative Structure-Cytotoxicity Relationship of Furo[2,3-*b*]chromones. *Anticancer Res.* **2018**, *38*, 3283–3290. [[CrossRef](#)] [[PubMed](#)]
45. Uesawa, Y.; Sakagami, H.; Ishihara, M.; Kagaya, H.; Kanamoto, T.; Terakubo, S.; Nakashima, H.; Yahagi, H.; Takao, K.; Sugita, Y. Quantitative Structure-Cytotoxicity Relationship of 3-Styryl-2H-chromenes. *Anticancer Res.* **2015**, *35*, 5299–5307. [[PubMed](#)]
46. Uesawa, Y.; Sakagami, H.; Ikezoe, N.; Takao, K.; Kagaya, H.; Sugita, Y. Quantitative Structure-Cytotoxicity Relationship of Aurones. *Anticancer Res.* **2017**, *37*, 6169–6176. [[CrossRef](#)]
47. Sakagami, H.; Masuda, Y.; Tomomura, M.; Yokose, S.; Uesawa, Y.; Ikezoe, N.; Asahara, D.; Takao, K.; Kanamoto, T.; Terakubo, S.; et al. Quantitative Structure-Cytotoxicity Relationship of Chalcones. *Anticancer Res.* **2017**, *37*, 1091–1098. [[CrossRef](#)]
48. Uesawa, Y.; Sakagami, H.; Okudaira, N.; Toda, K.; Takao, K.; Kagaya, H.; Sugita, Y. Quantitative Structure-Cytotoxicity Relationship of Cinnamic Acid Phenetyl Esters. *Anticancer Res.* **2018**, *38*, 817–823. [[CrossRef](#)]
49. Sakagami, H.; Uesawa, Y.; Masuda, Y.; Tomomura, M.; Yokose, S.; Miyashiro, T.; Murai, J.; Takao, K.; Kanamoto, T.; Terakubo, S.; et al. Quantitative Structure-Cytotoxicity Relationship of Newly Synthesized Piperic Acid Esters. *Anticancer Res.* **2017**, *37*, 6161–6168. [[CrossRef](#)]
50. Shimada, C.; Uesawa, Y.; Ishihara, M.; Kagaya, H.; Kanamoto, T.; Terakubo, S.; Nakashima, H.; Takao, K.; Saito, T.; Sugita, Y.; et al. Quantitative structure-cytotoxicity relationship of phenylpropanoid amides. *Anticancer Res.* **2014**, *34*, 3543–3548. [[PubMed](#)]



51. Shimada, C.; Uesawa, Y.; Ishihara, M.; Kagaya, H.; Kanamoto, T.; Terakubo, S.; Nakashima, H.; Takao, K.; Miyashiro, T.; Sugita, Y.; et al. Quantitative structure-cytotoxicity relationship of piperic acid amides. *Anticancer Res.* **2014**, *34*, 4877–4884. [[CrossRef](#)] [[PubMed](#)]
52. Sakagami, H.; Uesawa, Y.; Ishihara, M.; Kagaya, H.; Kanamoto, T.; Terakubo, S.; Nakashima, H.; Takao, K.; Sugita, Y. Quantitative Structure-Cytotoxicity Relationship of Oleoylamides. *Anticancer Res.* **2015**, *35*, 5341–5351. [[PubMed](#)]
53. Sakagami, H.; Watanabe, T.; Hoshino, T.; Suda, N.; Mori, K.; Yasui, T.; Yamauchi, N.; Kashiwagi, H.; Gomi, T.; Oizumi, T.; et al. Recent Progress of Basic Studies of Natural Products and Their Dental Application. *Medicines* **2018**, *6*, 4. [[CrossRef](#)] [[PubMed](#)]
54. Sakagami, H.; Okudaira, N.; Masuda, Y.; Amano, O.; Yokose, S.; Kanda, Y.; Suguro, M.; Natori, T.; Oizumi, H.; Oizumi, T. Induction of Apoptosis in Human Oral Keratinocyte by Doxorubicin. *Anticancer Res.* **2017**, *37*, 1023–1029. [[CrossRef](#)] [[PubMed](#)]
55. Takao, K.; Toda, K.; Saito, T.; Sugita, Y. Synthesis of amide and ester derivatives of cinnamic acid and its analogs: Evaluation of their free radical scavenging and monoamine oxidase and cholinesterase inhibitory activities. *Chem. Pharm. Bull.* **2017**, *65*, 1020–1027. [[CrossRef](#)] [[PubMed](#)]
56. Takao, K.; Miyashiro, T.; Sugita, Y. Synthesis and biological evaluation of piperic acid amides as free radical scavengers and  $\alpha$ -glucosidase inhibitors. *Chem. Pharm. Bull.* **2015**, *63*, 326–333. [[CrossRef](#)] [[PubMed](#)]
57. Yang, C.P.H.; Horwitz, S.B. Taxol<sup>®</sup>: The first microtubule stabilizing agent. *Int. J. Mol. Sci.* **2017**, *18*, 1733. [[CrossRef](#)] [[PubMed](#)]
58. Iijima, Y.; Bandow, K.; Sano, M.; Hino, S.; Kaneko, T.; Horie, N.; Sakagami, H. In vitro assessment of antitumor potential and combination Effect of classical and molecular-targeted anticancer drugs. *Anticancer Res.* **2019**, *39*, 6673–6684. [[CrossRef](#)] [[PubMed](#)]
59. Marinho, J.; Pedro, M.; Pinto, D.C.; Silva, A.M.; Cavaleiro, J.A.; Sunkel, C.E.; Nascimento, M.S. 4'-methoxy-2-styrylchromone a novel microtubule-stabilizing antimetabolic agent. *Biochem. Pharmacol.* **2008**, *75*, 826–835. [[CrossRef](#)]
60. Soo, H.C.; Chung, F.F.; Lim, K.H.; Yap, V.A.; Bradshaw, T.D.; Hii, L.W.; Tan, S.H.; See, S.J.; Tan, Y.F.; Leong, C.O.; et al. Cudraflavone C Induces Tumor-Specific Apoptosis in Colorectal Cancer Cells through Inhibition of the Phosphoinositide 3-Kinase (PI3K)-AKT Pathway. *PLoS ONE* **2017**, *12*, e0170551. [[CrossRef](#)]
61. Da Costa, R.; Passos, G.F.; Quintão, N.L.M.S.; Fernandes, E.; Maia, J.R.L.C.B.; Campos, M.M.; Calixto, J.B. Taxane-induced neurotoxicity: Pathophysiology and therapeutic perspectives. *Br. J. Pharmacol.* **2020**, *177*, 3127–3146. [[CrossRef](#)] [[PubMed](#)]
62. Pittman, S.K.; Gracias, N.G.; Fehrenbacher, J.C. Nerve growth factor alters microtubule targeting agent-induced neurotransmitter release but not MTA-induced neurite retraction in sensory neurons. *Exp. Neurol.* **2016**, *279*, 104–115. [[CrossRef](#)] [[PubMed](#)]
63. Rovini, A.; Savry, A.; Braguer, D.; Carré, M. Microtubule-targeted agents: When mitochondria become essential to chemotherapy. *Biochim. Biophys. Acta* **2011**, *1807*, 679–688. [[CrossRef](#)] [[PubMed](#)]
64. Iijima, Y.; Bandow, K.; Amano, S.; Sano, M.; Hino, S.; Kaneko, T.; Horie, N.; Sakagami, H. Protection of bortezomib-induced neurotoxicity by antioxidants. *Anticancer Res.* **2020**, *40*, 3685–3696. [[CrossRef](#)] [[PubMed](#)]
65. Johnson, T.L.; Lai, M.B.; Lai, J.C.; Bhushan, A. Inhibition of Cell Proliferation and MAP Kinase and Akt Pathways in Oral Squamous cell Carcinoma by Genistein and Biochanin, A. *Evid. Based Complement. Altern. Med.* **2010**, *7*, 351–358. [[CrossRef](#)] [[PubMed](#)]
66. Kim, M.J.; Lee, J.H.; Kim, Y.K.; Myoung, H.; Yun, P.Y. The role of tamoxifen in combination with cisplatin on oral squamous cell carcinoma cell lines. *Oral. Oncol.* **2008**, *44*, 94–99. [[CrossRef](#)] [[PubMed](#)]
67. Colella, G.; Izzo, G.; Carinci, F.; Campisi, G.; Muzio, L.L.; D'Amato, S.; Mazzotta, M.; Cannavale, R.; Ferrara, D.; Minucci, S. Expression of sexual hormones receptors in oral squamous cell carcinoma. *Int. J. Immunopathol. Pharm.* **2011**, *24*, 129–132. [[CrossRef](#)] [[PubMed](#)]



© 2020 by the authors. Licensee MDPI, Basel, Switzerland. This article is an open access article distributed under the terms and conditions of the Creative Commons Attribution (CC BY) license (<http://creativecommons.org/licenses/by/4.0/>).



Article

# Modulation of Th1/Th2 Cytokine Balance by Quercetin In Vitro

Yoshihito Tanaka <sup>1</sup>, Atsuko Furuta <sup>2</sup>, Kazuhito Asano <sup>3,\*</sup> and Hitome Kobayashi <sup>1</sup>

<sup>1</sup> Department of Otolaryngology, School of Medicine, Showa University, Tokyo 142-8555, Japan; ysh10tnk@gmail.com (Y.T.); hitomek@med.showa-u.ac.jp (H.K.)

<sup>2</sup> Department of Medical Education, School of Medicine, Showa University, Tokyo 142-8555, Japan; atsufuruichi2012@gmail.com

<sup>3</sup> School of Health Sciences, University of Human Arts and Sciences, Saitama 339-8555, Japan

\* Correspondence: asanok@med.showa-u.ac.jp; Tel.: +81-48-758-7111

Received: 29 June 2020; Accepted: 28 July 2020; Published: 30 July 2020

**Abstract:** **Background:** Allergic rhinitis (AR) is well known to be an IgE-mediated chronic inflammatory disease in the nasal wall, which is primarily mediated by Th2-type cytokines such as IL-4, IL-5, and IL-13. Although quercetin is also accepted to attenuate the development of allergic diseases such as AR, the influence of quercetin on Th2-type cytokine production is not well understood. The present study was designed to examine whether quercetin could attenuate the development of AR via the modulation of Th2-type cytokine production using an in vitro cell culture technique. **Methods:** Human peripheral-blood CD4<sup>+</sup> T cells ( $1 \times 10^6$  cells/mL) were cultured with 10.0 ng/mL IL-4 in the presence or absence of quercetin. The levels of IL-5, IL-13, and INF- $\gamma$  in 24 h culture supernatants were examined by ELISA. The influence of quercetin on the phosphorylation of transcription factors NF- $\kappa$ B and STAT6, and mRNA expression for cytokines were also examined by ELISA and RT-PCR, respectively. **Results:** Treatment of cells with quercetin at more than 5.0  $\mu$ M inhibited the production of IL-5 and IL-13 from CD4<sup>+</sup> T cells induced by IL-4 stimulation through the suppression of transcription factor activation and cytokine mRNA expression. On the other hand, quercetin at more than 5.0  $\mu$ M abrogated the inhibitory action of IL-4 on INF- $\gamma$  production from CD4<sup>+</sup> T cells in vitro. **Conclusions:** The immunomodulatory effects of quercetin, especially on cytokine production, may be responsible, in part, for the mode of therapeutic action of quercetin on allergic diseases, including AR.

**Keywords:** allergic rhinitis; quercetin; human CD4<sup>+</sup> T cells; Th1/Th2 cytokine balance; modulation; in vitro

## 1. Introduction

Allergic rhinitis (AR) is well accepted to be a chronic inflammatory IgE-mediated disorder of the nasal wall and is characterized by multiple symptoms such as sneezing, itching, and nasal congestion, among others [1,2]. AR is also accepted to be divided into two different phases of allergic reaction: an initial sensitization phase in which allergen exposure results in IgE formation, and subsequent clinical disease after repeated antigen exposure [3]. The clinical reaction is further subdivided into early- and late-phase responses [1,2]. The development of these responses is orchestrated by Th2-type helper T cells via the production of several types of cytokines and chemokines, which are responsible for the migration and activation of inflammatory cells [1,2].

Current therapeutic agents against AR are limited to antihistamines, antileukotriene, and nasal glucocorticoids that can mitigate allergic symptoms but fail to modulate the allergic reactions and bring adverse side effects such as throat irritation and dry mouth [2,4,5]. Consequently, it is desirable to develop safe and effective therapeutic agents for AR. Quercetin is well known to be one of the most

abundant dietary flavonoids, found in various vegetables such as onions, broccoli, tomatoes, etc. [6]. For many years, quercetin has been studied for its possible health benefits, and it has been revealed that quercetin attenuates oxidative stress responses through the suppression of free-radical generation [6,7]; increases in the production of thioredoxin [8] and glutathione [9,10]; quercetin–glutathione conjugate formation [11]; and upregulation of glutamate–cysteine ligases [11], which are important endogenous antioxidants [8–11]. In regard to allergic immune responses, quercetin has been reported to inhibit the production of both inflammatory cytokines and chemokines such as IL-5, eotaxin, and RANTES (regulated on activation normal T cell expressed and secreted) from eosinophils and mast cells after immunological stimulation *in vitro* and *in vivo* [12–15]. It has also been reported that quercetin inhibits the secretion of harmful chemical mediators, including histamine, leukotrienes, major basic protein, and eosinophil cationic protein from mast cells and eosinophils *in vitro* and *in vivo* [14,15]. Furthermore, the influence of quercetin on the production of T-cell cytokines was investigated using an asthmatic mouse model, and it was reported that quercetin could reduce the increased levels of IL-4, and increased IFN- $\gamma$  levels in bronchoalveolar lavage fluid after antigenic challenge via the modulation of T-box protein expressed in T cells (*T-bet*) and *GATA-3* gene expression, resulting in significant attenuation of all asthmatic reactions [16,17]. Although these reports strongly suggest that quercetin is a good candidate as a supplement for modulation of allergic diseases, including AR, the mechanisms of the therapeutic action of quercetin on allergic responses is not fully understood. There is much evidence that IL-4, one of the Th2-type T-cell cytokines, is a key player in immune modulation of allergic responses and plays essential roles in the development of pathological changes in allergic diseases [2,18]. Although it has been reported that quercetin can inhibit the ability of human peripheral-blood mononuclear cells to spontaneously produce IL-4, but not IFN- $\gamma$  *in vitro* via inhibition of cytokine mRNA expression [19], the precise mechanisms of quercetin' on cytokine production are not well understood. In the present study, therefore, we examined the influence of quercetin on IL-4-mediated immune responses by examining the secretion of cytokines from CD4<sup>+</sup> T cells *in vitro*.

## 2. Materials and Methods

### 2.1. Reagents

Quercetin was obtained from Sigma-Aldrich Co., Ltd. (St. Louis, MO, USA) as a preservative-free pure powder. It was dissolved in dimethyl sulfoxide at a concentration of 10.0 mM and was then diluted with RPMI-1640 medium (Sigma-Aldrich Co., Ltd.) supplemented with 10% heat-inactivated bovine serum (RPMI-FBS; Sigma-Aldrich Co., Ltd.) at appropriate concentrations for experiments. It was then sterilized by passing it through 0.2  $\mu$ m filters, and stored at 4 °C until use. Recombinant human IL-4 was purchased from R & D Systems, Inc. (Minneapolis, MN, USA) as a preservative-free pure powder. IL-4 was also dissolved in RPMI-FBS, sterilized with 0.2  $\mu$ m filters and stored at 4 °C until use. mRNA isolation kits were purchased from Milteny Biotec (Bergisch Gladbach, Germany). The reagents used for cDNA synthesis and the real-time reverse-transcription polymerase chain reaction (RT-PCR) kit were obtained from Invitrogen Corp. (Carlsbad, CA, USA) and Applied Biosystems (Foster City, CA, USA), respectively.

### 2.2. Preparation of CD4<sup>+</sup> T Cells

Heparinized human venous blood was obtained from five healthy subjects (all male, 41.0  $\pm$  10.1 years) after obtaining their written informed consent, which was approved by the Ethics Committee of Showa University (Approved No. 190613; Date of approval: 1 June 2019). Peripheral-blood mononuclear cells (PBMCs) were then obtained after centrifugation (1000 $\times$  *g* for 30 min) of blood with lymphocyte separation medium (Organon Technica, Durham, NJ, USA). CD4<sup>+</sup> T cells were purified from PBMCs using a magnetic cell separator (Milteny Biotec, Bergisch Gladbach, Germany) as described previously [20]. The cells were suspended in RPMI-FBS at a concentration of 1  $\times$  10<sup>6</sup> cells/mL.

The cell purity was more than 95%, as judged using a flow cytometer (FACScan; Becton Dickinson, San Jose, CA, USA).

### 2.3. Cell Culture

CD4<sup>+</sup> T cells ( $1 \times 10^6$  cells/mL) were introduced into each well of 24 well culture plates in triplicate, where each well contained 10.0 ng/mL of IL-4 and various concentrations of quercetin in a final volume of 2.0 mL [20]. The supernatants were collected 24 h later and stored at  $-40^\circ\text{C}$  until needed for assays for the levels of cytokines. To prepare cells for examining transcription factor activation and mRNA expression, CD4<sup>+</sup> T cells were cultured in a similar manner for 1 and 4 h, respectively [20]. In all experiments, quercetin treatment was started 1 h before IL-4 stimulation.

### 2.4. Assay for Cytokines

The levels of IL-5, IL-13, and IFN- $\gamma$  in culture supernatants were measured in duplicate with human cytokine ELISA kits (R & D) according to the manufacturer's instructions. The sensitivity of the ELISA kits for IL-5, IL-13, and IFN- $\gamma$  was 3.0 pg/mL, 32.0 pg/mL, and 8.0 pg/mL, respectively.

### 2.5. Assay for Transcription Factor Activities

NF- $\kappa\text{B}$  and STAT6 activity in cultured cells were examined using ELISA test kits (Active Mortif Co., Ltd., Carlsbad, Calif, USA) following the manufacturer's recommended procedures.

### 2.6. Assay for mRNA Expression

Poly A<sup>+</sup> mRNA was extracted from cells with oligo(dT)-coated magnetic micro beads (Milteny Biotec, Bergisch Gladbach, Germany). mRNA samples (1.0  $\mu\text{g}$ ) were reverse-transcribed to cDNA using a Superscript cDNA synthesis kit (Invitrogen Corp., Carlsbad, CA, USA). Polymerase chain reaction (PCR) was then conducted using a GeneAmp 5700 Sequence Detection System (Applied Biosystems, Forster City, CA, USA). The PCR mixture consisted of 2.0  $\mu\text{L}$  of sample cDNA solution (100 ng/ $\mu\text{L}$ ), 25.0  $\mu\text{L}$  of SYBR-Green Mastermix (Applied Biosystems), 0.3  $\mu\text{L}$  of both sense and antisense primers, and distilled water to give a final volume of 50.0  $\mu\text{L}$ . The reaction was conducted as follows: 4 min at  $94^\circ\text{C}$ , followed by 40 cycles of 4 min at  $95^\circ\text{C}$ , 1 min at  $60^\circ\text{C}$ , and 1 min at  $70^\circ\text{C}$  [20]. GAPDH was amplified as an internal control. mRNA levels for IL-5 and IL-13 were calculated by using the comparative parameter threshold cycle and normalized to GAPDH. The nucleotide sequences of the primers were as follows: for IL-5, 5'-GCTTCTGCATTGAGTTTGCTAGCT-3' (sense) and 5'-TGGCCGTCAATGTATTTCTTATTAAG-3' (antisense); for IL-13, 5'-CCACGGTCATTGCTCTCAGGCTGGACTG-3' (sense) and 5'-CCTTGTGCGGGCAGAATCCGCTCA-3' (antisense) [20]; and for GAPDH, 5'-TGCACCACCAACTGCTTAGC-3' (sense) and 5'-GGCATGGACTGTGGTCATGAG-3' (antisense) [7].

### 2.7. Statistical Analysis

Statistical analyses were performed with ANOVA followed by Dunnett's multiple-comparison test. Values of  $p < 0.05$  were considered statistically significant.

## 3. Results

### 3.1. Influence of Quercetin on the Production of T-Cell Cytokines

The first set of experiments was undertaken to examine whether quercetin could suppress the production of Th-2-type cytokines IL-5 and IL-13, by CD4<sup>+</sup> T cells after IL-4 stimulation. CD4<sup>+</sup> T cells ( $1 \times 10^6$  cells/mL) were cultured with 10.0 ng/mL IL-4 in the presence of 1.0 to 10.0  $\mu\text{M}$  quercetin for 24 h. The levels of IL-5 and IL-13 in culture supernatants were measured by ELISA. Treatment of cells with quercetin at lower than 2.5  $\mu\text{M}$  did not inhibit IL-5 production: IL-5 levels in experimental culture supernatants were similar (not significant) to those that received IL-4 stimulation alone (Figure 1a).

On the other hand, higher concentrations of quercetin (more than 5.0  $\mu\text{M}$ ) caused significant suppression of IL-5 production, which was increased by IL-4 stimulation (Figure 1a). We then examined the influence of quercetin on IL-13 production by  $\text{CD4}^+$  T cells after IL-4 stimulation. Quercetin suppressed IL-13 production as it did IL-5 production (Figure 1b). The minimum concentration of quercetin that caused significant suppression of IL-13 production was 5.0  $\mu\text{M}$  (Figure 1b). We finally examined the influence of quercetin on Th-1-type cytokine production using IFN- $\gamma$ . Stimulation of cells with IL-4 significantly decreased IFN- $\gamma$  levels in culture supernatants (Figure 2). Although addition of quercetin at less than 2.5  $\mu\text{M}$  did not inhibit the suppressive activity of IL-4 on IFN- $\gamma$  production, quercetin at more than 5.0  $\mu\text{M}$  suppressed the downregulation of IFN- $\gamma$  production induced by IL-4 stimulation (Figure 2).

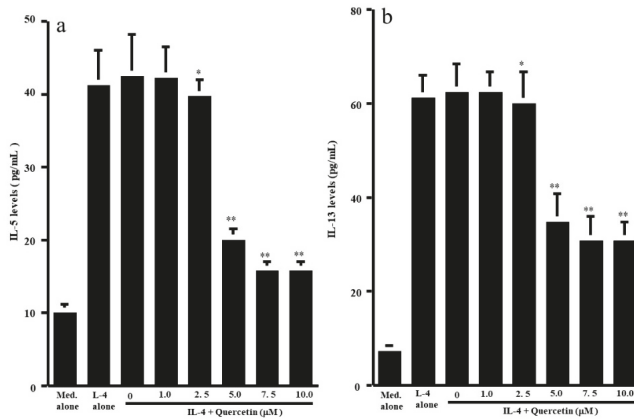


**Figure 1.** Influence of quercetin on Th2-type cytokine production from human peripheral-blood  $\text{CD4}^+$  T cells in vitro.  $\text{CD4}^+$  T cells ( $1 \times 10^6$  cells/mL) were stimulated with 10.0 ng/mL IL-4 in the presence of various concentrations of quercetin for 24 h. Cytokine levels in culture supernatants were examined by ELISA. The results were expressed as the mean pg/mL  $\pm$  SE of five subjects. (a): IL-5; (b): IL-13; \*  $p > 0.05$  versus IL-4 alone; \*\*  $p < 0.05$  versus IL-4 alone.

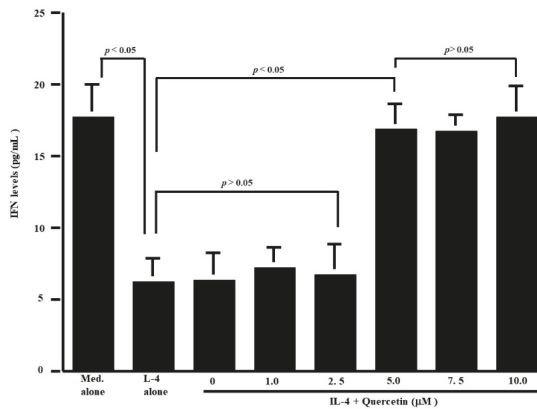


**Figure 2.** Influence of quercetin on interferon (IFN)- $\gamma$  production from human peripheral-blood  $\text{CD4}^+$  T cells in vitro.  $\text{CD4}^+$  T cells ( $1 \times 10^6$  cells/mL) were stimulated with 10.0 ng/mL IL-4 in the presence of various concentrations of quercetin for 24 h. IFN- $\gamma$  levels in culture supernatants were examined by ELISA. The results were expressed as the mean pg/mL  $\pm$  SE of five subjects.

3.2. Influence of Quercetin on Transcription Factor Activation and Cytokine mRNA Expression

The final set of experiments was carried out to examine the possible mechanisms by which quercetin could inhibit Th2-type cytokine production from CD4<sup>+</sup> T cells after IL-4 stimulation. CD4<sup>+</sup> T cells were stimulated with IL-4 in the presence of 1.0 to 10.0 μM quercetin. Activation of transcription factors NF-κB and STAT6 in 1 h cultured cells was examined by ELISA. As shown in Figure 3a, lower concentrations (1.0 and 2.5 μM) of quercetin did not affect NF-κB activation, which was increased by IL-4 stimulation. However, treatment of cells with higher concentrations (5.0 to 10.0 μM) of quercetin significantly inhibited IL-4-induced NF-κB activation. We then examined the influence of quercetin on STAT6 activation after IL-4 stimulation. The data presented in Figure 3b clearly showed that quercetin inhibited STAT6 activation, as was the case for NF-κB. The minimum concentration of quercetin that caused significant suppression was 5.0 μM. The final experiments in this section were performed to examine the influence of quercetin on Th2-type cytokine mRNA expression in 4 h cultured cells by real-time RT-PCR (Figure 4). Addition of quercetin at 2.5 μM did not suppress mRNA expression for either IL-5 or IL-13, but mRNA expression, which was increased by IL-4 stimulation, was significantly inhibited when cells were treated with quercetin at more than 5.0 μM.

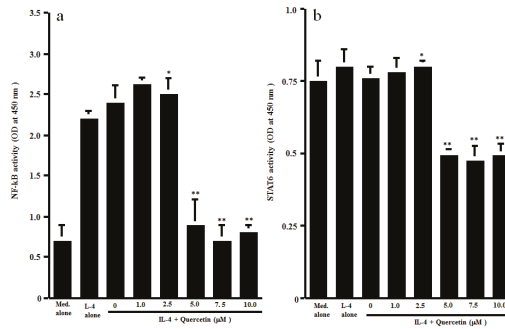


**Figure 3.** Influence of quercetin on transcription factor activation in CD4<sup>+</sup> T cells in vitro. CD4<sup>+</sup> T cells (1 × 10<sup>6</sup> cells/mL) were stimulated with 10.0 ng/mL IL-4 in the presence of various concentrations of quercetin for 1 h. Activation of transcription factors NF-κB (a) and STAT6 (b) was assessed by ELISA. The results were expressed as the mean OD at 450 nm ± SE of five subjects. \* *p* > 0.05 versus IL-4 alone; \*\* *p* < 0.05 versus IL-4 alone.

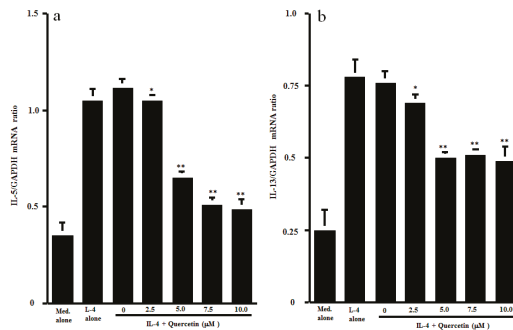


**Figure 4.** Influence of quercetin on mRNA expression for Th2-type cytokines in vitro. CD4<sup>+</sup> T cells (1 × 10<sup>6</sup> cells/mL) were stimulated with 10.0 ng/mL IL-4 in the presence of various concentrations of quercetin for 4 h. mRNA expression for IL-5 (a) and IL-13 (b) was examined by real-time RT-PCR. The results were expressed as the mean cytokine/GAPDH ± SE of five subjects. \* *p* > 0.05 versus IL-4 alone; \*\* *p* < 0.05 versus IL-4 alone.

#### 4. Discussion

Quercetin, a natural compound belonging to the flavonol subgroup, has been shown to favorably modify the clinical conditions of allergic diseases, including AR, through the inhibition of inflammatory cell (e.g., mast cells and eosinophils) activation [12–15]. It has also been reported that quercetin exerts suppressive effects on the production of neuropeptides, which are responsible for the development of AR symptoms [21]. Although it is established that Th2-type T cells play a key role in triggering the allergic inflammatory responses in AR [2,18], the influence of quercetin on Th2-type T-cell functions is not clearly defined. The present study, therefore, was undertaken to examine the influence of quercetin on Th2-type T-cell functions by examining Th2-type cytokine production.

The present results clearly showed that quercetin inhibited the ability of CD4<sup>+</sup> T cells to produce IL-5 and IL-13 after IL-4 stimulation through inhibition of the activation of transcription factors NF- $\kappa$ B and STAT6, and inhibition of cytokine mRNA expression. It is also showed that quercetin abrogated the suppressive activity of IL-4 on INF- $\gamma$  production by CD4<sup>+</sup> T cells. The minimum concentration of quercetin that caused significant modulation of cytokine production was 5.0  $\mu$ M. After oral administration of quercetin at 1200 mg, which is a standard recommended dosage, plasma levels of quercetin gradually increase and peak at 12  $\mu$ M [22,23], which is a much higher level than that which caused modulation of cytokine production by CD4<sup>+</sup> T cells after IL-4 stimulation *in vitro* in this study. From these reports, the findings of the present *in vitro* study may reflect the biological function of quercetin *in vivo*.

AR is well known to consist of type I hypersensitivity allergic responses in nasal membranes against several types of aeroallergens [1,2]. It is also accepted that type I allergic responses consist of two different phases [2,3]. The sensitization phase comprises IgE formation against specific allergens based on the Th2-type immune system. In the triggering phase, allergic symptoms are triggered by to secretion of several kinds of chemical mediators from mast cells and eosinophils after re-exposure to the same allergen [2,3]. These two phases are orchestrated by T cells, especially Th2-type helper T cells, through the secretion of several cytokines [1,2]. Among Th2-type cytokines, the first important cytokine is IL-4, which promotes the special production of IgE from resting B cells [2,18]. IL-3 and IL-5 are other important Th2-type cytokines, and have been shown to enhance the proliferation and differentiation of mast cells and eosinophils from their precursors [24]. IL-13 is a pleiotropic cytokine produced by activated Th2-type T cells [25]. It has a wide variety of effects on Th2-dominated inflammatory disorders, such as enhancement of IgE production and vascular cell adhesion molecule 1 expression, which increases the migration of inflammatory cells into the site of inflammation [26]. It has also been reported that IL-13 as well as IL-5 can activate and inhibit the apoptosis of eosinophils [25]. On the other hand, IFN- $\gamma$ , the principal Th1-type effector cytokine, initiates and maintains Th1-type immune responses, which dampen diseases promoted by Th2-type immune responses through the inhibition of Th2-type T-cell recruitment/differentiation, induction of apoptosis in eosinophils, and blockage of IgE isotype switch in B cells, among other actions [27]. From these reports, the present results strongly suggest that the beneficial immunomodulatory effects of quercetin may comprise, in part, the therapeutic mode of action of quercetin on allergic diseases, including AR.

Although the present results clearly showed a favorable modification of quercetin on IL-4-mediated Th1/Th2 cytokine balance, the precise mechanism(s) by which quercetin modulates cytokine balance after IL-4 stimulation is not fully understood. IL-4 exerts its biological functions by binding to a high-affinity receptor, IL-4 receptor  $\alpha$  chain (IL-4R $\alpha$ ), on the cell surface [28,29], and this complex then induces the activation of the tyrosine kinases, Janus kinase 1 and 3, which cause the phosphorylation of the transcription factor STAT6, which is essential for cytokine production from Th2-type T cells [28,29]. These reports may suggest that the immunomodulatory effect of quercetin on cytokine production is partially dependent on its suppressive activity on the STAT6 signal pathway. This speculation may be supported by the observation that treatment of CD4<sup>+</sup> cells with quercetin at more than 5.0  $\mu$ M inhibited STAT6 phosphorylation after IL-4 stimulation. In addition to IL-4R $\alpha$ , IL-4 binds with the common  $\gamma$  chain and induces phosphorylation of NF- $\kappa$ B, which is responsible for cytokine mRNA

expression [30,31]. From these reports, there is another possibility that quercetin inhibits the NF- $\kappa$ B signal pathway and results in suppression of Th2-type cytokine production from CD4<sup>+</sup> T cells after IL-4 stimulation. This speculation may be supported by the present observation showing the suppressive activity of quercetin at more than 5.0  $\mu$ M on NF- $\kappa$ B activation induced by IL-4 stimulation.

Activation of Janus kinase 1 and 3 and STAT6 phosphorylation require an increase in intracellular Ca<sup>2+</sup> levels [32]. Quercetin has been reported to be able to inhibit an increase in intracellular free Ca<sup>2+</sup> levels in human mast cells after inflammatory stimulation *in vitro* [33]. Quercetin has also been reported to inhibit the phosphorylation of several types of tyrosine kinases, which are responsible for transcription factor activation [34,35]. On the basis of these reports, quercetin might inhibit the phosphorylation of tyrosine kinases through the inhibition of an increase in Ca<sup>2+</sup> levels in CD4<sup>+</sup> cells after IL-4 stimulation, resulting in suppression of Th2-type cytokine production. Further experiments are required to clarify this point.

## 5. Conclusions

The present results strongly suggest that quercetin modulates IL-4-mediated immune responses, especially Th1/Th2 cytokine balance, and results in attenuation of the development of allergic immune responses.

**Author Contributions:** Cell culture, assays for cytokines and for mRNA expression: Y.T.; assay for transcription factor activation: A.F.; statistical analysis of the data and drawing figures: H.K.; conceptualization, study design, and manuscript writing: K.A. All authors have read and agreed to the published version of the manuscript.

**Funding:** This research received no external funding.

**Conflicts of Interest:** All the authors have no conflict of interest in this study.

## References

- Pawankar, R.; Mori, S.; Ozu, C.; Kimura, S. Overview on the pathomechanisms of allergic rhinitis. *Asia Pac. Allergy* **2011**, *1*, 157–167. [[CrossRef](#)] [[PubMed](#)]
- Ramirez-Jimenez, F.; Pavon-Romero, G.; Juarez-Martinez, L.L.; Teran, L.M. Allergic rhinitis. *J. Allergy Ther.* **2012**, *5*, 2–7.
- Kumazawa, T.; Takimoto, H.; Matsumoto, T.; Kawaguchi, S. Potential use of dietary natural products, especially polyphenols, for improving type-1 allergic symptoms. *Curr. Pharm. Des.* **2014**, *20*, 857–863. [[CrossRef](#)] [[PubMed](#)]
- Jung, D.; Lee, S.; Hong, S. Effects of acupuncture and moxibustion in a mouse model of allergic rhinitis. *Otolaryngol. Head Neck Surg.* **2011**, *146*, 19–25. [[CrossRef](#)]
- Jeong, K.T.; Kim, S.G.; Lee, J.; Park, Y.N.; Park, H.H.; Park, N.Y.; Kim, K.J.; Lee, H.; Lee, Y.J.; Lee, E. Anti-allergic effect of a Korean traditional medicine, Biyeom-Tang on mast cells and allergic rhinitis. *BMC Comp. Altern. Med.* **2014**, *14*, 1–10. [[CrossRef](#)]
- Mlcek, J.; Jurikova, T.; Skrovankova, S.; Sochor, J. Quercetin and its anti-allergic immune response. *Molecules* **2016**, *21*, 623. [[CrossRef](#)]
- Ebihara, N.; Asano, K.; Sunagawa, M. Suppressive activity of quercetin on nitric oxide production from nasal epithelial cells *in vitro*. *Evid. Based Complement. Alternat. Med.* **2018**. [[CrossRef](#)]
- Edo, Y.; Otaki, A.; Asano, K. Enhancement of thioredoxin production from nasal epithelial cells by quercetin *in vitro* and *in vivo*. *Medicines* **2018**, *5*, 124. [[CrossRef](#)]
- Abdelhalim, M.A.K.; Moussa, S.A.A.; Qaid, H.A.Y.; Ai-Ayed, M.S. Potential effects of different natural antioxidants on inflammatory damage and oxidative-mediated hepatotoxicity induced by gold nanoparticle. *Int. J. Nanomed.* **2018**, *13*, 7931–7938. [[CrossRef](#)]
- Guazelli, C.F.S.; Staurengo-Ferrari, L.; Zarpelon, A.; Pinho-Ribeiro, F.A.; Ruiz-Miyazaki, K.W.; Vicentini, F.T.M.C.; Vignoli, J.A.; Camilios-Neto, D.; Georgetti, S.R.; Baracat, M.M.; et al. Quercetin attenuates zymosan-induced arthritis in mice. *Biomed. Pharmacother.* **2018**, *102*, 175–184. [[CrossRef](#)]



11. Li, C.; Zhang, W.J.; Choi, J.; Frei, B. Quercetin affects glutathione levels and redox ratio in human aortic endothelial cells not through oxidation but formation and cellular export of quercetin-glutathione conjugates and upregulation of glutamate-cysteine ligase. *Redox Biol.* **2016**, *9*, 220–228. [[CrossRef](#)] [[PubMed](#)]
12. Sakai-Kashiwabara, M.; Abe, S.; Asano, K. Suppressive activity of quercetin on the production of eosinophil chemoattractants from eosinophils *in vitro*. *In Vivo* **2014**, *28*, 515–522.
13. Middleton, E. Effect of plant flavonoids on immune and inflammatory cell function. *Advances Exp. Med. Biol.* **1998**, *439*, 175–182.
14. Min, Y.D.; Choi, C.H.; Bark, H.; Son, H.Y.; Park, H.H.; Lee, S.; Park, J.W.; Park, E.K.; Shin, H.I.; Kim, S.H. Quercetin inhibits expression of inflammatory cytokines through attenuation of NF- $\kappa$ B and p38 MAPK in HMC-1 human mast cell line. *Inflamm. Res.* **2007**, *56*, 210–215. [[CrossRef](#)] [[PubMed](#)]
15. Sakai-Kashiwabara, M.; Asano, K. Inhibitory action of quercetin on eosinophil activation *in vitro*. *Evid. Based Complement. Alternat. Med.* **2013**, *2013*. [[CrossRef](#)] [[PubMed](#)]
16. Park, H.J.; Lee, C.M.; Jung, I.D.; Lee, J.S.; Jeong, Y.I.; Chang, J.H.; Chun, S.H.; Kim, M.J.; Choi, I.W.; Ahn, S.C.; et al. Quercetin regulates Th1/Th2 balance in a murine model of asthma. *Int. Immunopharmac.* **2009**, *9*, 261–267. [[CrossRef](#)]
17. Jafarinaia, M.; Hosseini, M.S.; Kasiri, N.; Fazel, N.; Fathi, F.; Hakemi, M.G.; Eskandari, N. Quercetin with the potential effect on allergic diseases. *Allergy Asthma Clin. Immunol.* **2020**, *16*, 1–11. [[CrossRef](#)]
18. Wynn, T.A. Type 2 cytokines: Mechanisms and therapeutic strategies. *Nat. Rev.* **2015**, *15*, 271–282. [[CrossRef](#)]
19. Nair, M.P.N.; Kandaswami, C.; Mahajan, S.; Chadha, K.C.; Chawda, R.; Nair, H.; Kumar, N.; Nair, R.E.; Schwartz, S.A. The flavonoid, quercetin, differentially regulated Th-1(IFN $\gamma$ ) and Th-2 (IL-4) cytokine gene expression by normal peripheral blood mononuclear cells. *Biochem. Biophys. Acta* **2002**, *1593*, 29–36. [[CrossRef](#)]
20. Kanai, K.; Asano, K.; Watanabe, S.; Kyo, Y.; Suzaki, H. Epinastine hydrochloride antagonism against interleukin-4-mediated T cell cytokine imbalance *in vitro*. *Int. Arch. Allergy Immunol.* **2006**, *140*, 43–52. [[CrossRef](#)]
21. Kashiwabara, M.; Kazuhito Asano, K.; Mizuyoshi, T.; Kobayashi, H. Suppression of neuropeptide production by quercetin in allergic rhinitis model rats. *BMC Complement. Alternat. Med.* **2016**, *16*, 132. [[CrossRef](#)] [[PubMed](#)]
22. Hollman, P.C.; vd Gaag, M.; Mengelers, M.J.; van Trijp, J.M.; de Vries, J.H.; Katan, M.B. Absorption and disposition kinetics of the dietary antioxidant quercetin in man. *Free Rad. Biol. Med.* **1996**, *21*, 703–707. [[CrossRef](#)]
23. Wadsworth, T.L.; Koop, D.R. Effects of *Ginkgo biloba* extract (EGb 761) and quercetin on lipopolysaccharide-induced release of nitric oxide. *Chem. Biol. Interact.* **2001**, *137*, 43–58. [[CrossRef](#)]
24. Kimura, M.; Okafuji, I.; Yoshida, T. Theophyllin suppresses IL-5 and IL-13 production, and lymphocyte proliferation upon stimulation with house dust mite in asthmatic children. *Int. Arch. Allergy Immunol.* **2003**, *131*, 189–194. [[CrossRef](#)] [[PubMed](#)]
25. De Vries, J.E. The role of IL-13 and its receptor in allergy and inflammatory responses. *J. Allergy Clin. Immunol.* **1998**, *102*, 165–169. [[CrossRef](#)]
26. Bochner, B.S.; Klunk, D.A.; Sterbinsky, S.A.; Coffman, R.L.; Schleimer, R.P. IL-13 selectively induces vascular cell adhesion molecule-1 expression in human endothelial cells. *J. Immunol.* **1995**, *154*, 799–803.
27. Teixeira, L.K.; Fonseca, B.P.F.; Barboza, B.A.; Viola, J.P.B. The role of interferon- $\gamma$  on immune and allergic responses. *Mem. Inst. Oswaldo Cruz* **2005**, *100*, 137–144. [[CrossRef](#)]
28. Junntila, I.S. Tuning the cytokine responses: An update on interleukin (IL)-4 and IL-13 receptor complexes. *Front. Immunol.* **2018**, *9*, 888. [[CrossRef](#)]
29. Sastre, J.; Davila, I. Dupilumab: A new paradigm for treatment of allergic diseases. *J. Investig. Allergol. Clin. Immunol.* **2018**, *28*, 139–150. [[CrossRef](#)]
30. Duran, A.; Rodriguez, A.; Martin, P.; Serrano, M.; Flores, J.M.; Leitges, M.; Diaz-Meco, M.T.; Moscat, J. Crosstalk between PKC $\zeta$  and IL-4/STAT6 pathway during T-cell-mediated hepatitis. *EMBO J.* **2004**, *23*, 4595–4605. [[CrossRef](#)]
31. Thieu, V.T.; Nguyen, E.T.; McCarthy, B.P.; Bruns, H.A.; Kapur, R.; Chang, C.H.; Kaplan, M.H. IL-4-stimulated NF- $\kappa$ B activity is required for STAT6 DNA binding. *J. Leukoc. Biol.* **2007**, *82*, 370–379. [[CrossRef](#)] [[PubMed](#)]

32. Chiba, Y.; Todoroki, M.; Nishida, Y.; Tanabe, M.; Misawa, M. A novel STAT6 inhibitor AS1517499 ameliorates antigen-induced bronchial hypercontractility in mice. *Am. J. Respir. Cell Mol. Biol.* **2009**, *41*, 516–524. [[CrossRef](#)]
33. Kim, S.H.; Choi, C.H.; Kim, S.Y.; Eun, J.S.; Shin, T.Y. Antiallergic effect of *Artemisia iwayomogi* on mast cell-mediated allergy model. *Exp. Biol. Med.* **2005**, *230*, 82–88. [[CrossRef](#)]
34. Shoskes, D.A.; Zeitlin, S.I.; Shahed, A.; Raifer, J. Quercetin in men with category III chronic prostatitis: A preliminary prospective, double-blind, placebo-controlled trial. *Urology* **1999**, *54*, 960–963. [[CrossRef](#)]
35. Chen, J.C.; Ho, F.M.; Chao, P.D.L.; Chen, C.P.; Jeng, K.C.; Hsu, H.B.; Lee, S.T.; Wu, W.T.; Lin, W.W. Inhibition of iNOS gene expression by quercetin is mediated by the inhibition of I $\kappa$ B kinase, nuclear factor-kappa B and STAT1, and depends on hemoxygenase-1 induction in mouse BV-2 microglia. *Eur. J. Pharmacol.* **2005**, *521*, 9–20. [[CrossRef](#)]



© 2020 by the authors. Licensee MDPI, Basel, Switzerland. This article is an open access article distributed under the terms and conditions of the Creative Commons Attribution (CC BY) license (<http://creativecommons.org/licenses/by/4.0/>).





Article

# Preventive Effect of the Japanese Traditional Herbal Medicine Boiogito on Posttraumatic Osteoarthritis in Rats

Jun Oike <sup>1,2</sup>, Takayuki Okumo <sup>1,2,\*</sup>, Hideshi Ikemoto <sup>1</sup>, Yusuke Kunieda <sup>1,2</sup>, Shingo Nakai <sup>3</sup>, Haruka Takemura <sup>1,2</sup>, Hiroshi Takagi <sup>2</sup>, Koji Kanzaki <sup>2</sup> and Masataka Sunagawa <sup>1</sup>

<sup>1</sup> Department of Physiology, School of Medicine, Showa University, 1-5-8 Hatanodai, Shinagawa-ku, Tokyo 142-8555, Japan; jun0724@med.showa-u.ac.jp (J.O.); h\_ikemoto@med.showa-u.ac.jp (H.I.); situation2@med.showa-u.ac.jp (Y.K.); yawatuki@icloud.com (H.T.); suna@med.showa-u.ac.jp (M.S.)

<sup>2</sup> Department of Orthopedic Surgery, Showa University Fujigaoka Hospital, 1-30 Fujigaoka, Aoba-ku, Yokohama City, Kanagawa 227-8501, Japan; htakagi@med.showa-u.ac.jp (H.T.); kkanzaki@med.showa-u.ac.jp (K.K.)

<sup>3</sup> Department of Judo Seifuku and Health Sciences, Faculty of Health Promotional Sciences, Tokoha University, 1230 Miyakoda-cho, Kita-ku, Hamamatsu City, Shizuoka 431-2102, Japan; nakai4n5@gmail.com

\* Correspondence: tokumo@med.showa-u.ac.jp; Tel.: +81-3-3784-8110

Received: 28 October 2020; Accepted: 3 December 2020; Published: 4 December 2020

**Abstract:** **Background:** Considering the anti-inflammatory properties of the Japanese traditional Kampo medicine Boiogito (BO), we aimed to investigate the therapeutic effect of BO to prevent the development of knee osteoarthritis (KOA) in rats with surgically induced KOA. **Methods:** Destabilization of the medial meniscus (DMM) was performed to induce osteoarthritis in the right knees of 12-week-old Wistar rats under general anesthesia. The rats were orally administered 3% BO in standard powder chow for 4 weeks after surgery (controls:  $n = 6$ ; sham group:  $n = 6$ ; DMM group:  $n = 5$ ; DMM + BO group:  $n = 5$ ). During this period, the rotarod test was performed to monitor locomotive function. After 4 weeks, histological assessment was performed on the right knee. **Results:** Oral administration of BO improved locomotive function in the rotarod test. Walking time on postoperative days 1, 14, or later was significantly longer in the DMM + BO group than in the DMM group. Histologically, the DMM group showed significant progression of KOA, which, in the DMM + BO group, was strongly suppressed, as assessed by the Osteoarthritis Research Society International score. **Conclusions:** Our results showed that oral administration of BO had a clinically preventive effect on early stage posttraumatic KOA.

**Keywords:** boiogito; knee osteoarthritis; rat

## 1. Introduction

The number of osteoarthritis (OA) patients is >300 million worldwide. OA can affect any joint of the body, such as the hip, spine, hand, and especially, the knee [1]. Knee osteoarthritis (KOA) is characterized by the gradual progression of functional disorders, such as restricted range of motion due to degenerative changes in the knee joints, often with pain and swelling, and KOA impairs the daily life activities of patients [2,3]. Moreover, the pathophysiology of KOA is characterized not only by abnormal articular cartilage but also by synovitis, osteophyte synthesis, excessive turnover of subchondral bone, and periarticular soft tissue contracture, which all lead to malfunction of the affected joint [4]. Although the etiology of KOA is not fully understood, obesity, age, metabolic syndrome, and knee injury are considered to be risk factors [5,6], and posttraumatic KOA accounts for 12% of all cases. Knee injury is apparently the main factor for development of KOA in younger people [7].

Currently, KOA can be treated surgically and non-surgically. In non-surgical treatments, oral or topical administration of non-steroidal anti-inflammatory drugs (NSAIDs) or oral selective cyclooxygenase-2 (COX-2) inhibitors, intra-articular injection of hyaluronic acid, land-based exercise, dietary weight management with physical exercise, and mind–body exercise (such as Tai Chi and Yoga) have been recommended as effective strategies for KOA patients [8]. Surgical treatments, such as total/uni-compartmental knee arthroplasty (or osteotomy around the knee), are generally considered when non-surgical approaches have failed to control several clinical symptoms of KOA. Since posttraumatic joint instability due to meniscal tear or anterior cruciate ligament (ACL) rupture can cause destruction of the articular cartilage [9], orthopedic surgery aims to achieve meniscal repair or ACL reconstruction. These operative procedures can delay KOA progression; however, they cannot completely prevent the devastation of articular cartilage, even after ACL reconstruction [10]. In fact, KOA degenerative changes tend to be worse when they coexist with meniscal tear due to ACL rupture [11]. Although various kinds of biochemical mediators, such as interleukin-1 $\beta$  (IL-1 $\beta$ ), tumor necrotic factor- $\alpha$  (TNF- $\alpha$ ), nitric oxide (NO), and proteolytic enzymes, reportedly can have important roles in the progression of posttraumatic KOA [9], there are no effective preventive treatments for the pathological changes caused by KOA.

Several compelling reports and a review article on pharmaceutical treatment for KOA by using herbs or flavonoids have been published [12–14]. Some plant extracts, such as rosehip and curcumin, have shown therapeutic roles for OA by suppressing inflammatory mediators, including IL-1 $\beta$ , TNF- $\alpha$ , and NO; proteolytic enzymes, such as matrix metalloproteases; and/or a disintegrin and metalloproteinase with thrombospondin motifs. Choi et al. [15] reported the preventive effect of SKI 306X, a mixture of three herbs, against collagenase-induced arthritis in rabbits. Interestingly, SKI 306X potentially can inhibit proteoglycan degradation, unlike dexamethasone or NSAIDs.

Boiogito (BO), a traditional Japanese herbal medicine (Kampo) composed of six medicinal plants, may also be a potent medication for preventing osteoarthritis. BO is effective for the symptoms of chronic fatigue or hyperhidrosis, as well as leg edema or painful arthritis, and its use for these indications has been approved by the Japanese Ministry of Health, Labour, and Welfare. Some clinical studies have suggested that BO potentially can alleviate inflammation and hydrarthrosis in KOA [16,17]. Majima et al. [16] studied the effects of BO on KOA and joint effusion. Oral administration of BO improved functional capacity while stair climbing, and significantly reduced joint effusion without severe adverse effects. Although BO could have some therapeutic effects for KOA, there is no evidence that BO suppresses KOA progression, especially when evaluating locomotive dysfunction and structural destruction, such as articular cartilage devastation. If a preventive effect against KOA can be demonstrated, BO may become a therapeutic option for early stage KOA. The study's aim was to evaluate the disease modifying effect of BO on osteoarthritis in a rat model of surgically induced KOA.

## 2. Materials and Methods

### 2.1. Animals

Male Wistar rats at 12 weeks old, average weight 300–350 g, were purchased from Nippon Bio-Supp. Center (Tokyo, Japan). All rats were fed standard powdered rodent chow (CE-2; CLEA Japan, Tokyo, Japan) and water ad libitum before and after the surgical procedure. The animals were housed two to three per cage in an animal room with a controlled environment (12-h light/dark cycle, temperature 20–25 °C, and humidity 50–60%). The experimental protocols (Figure 1) were approved by the Institutional Ethics Committee for Care and Use of Animals of Showa University (certificate number: 09056, date of approval: 1 April 2019).

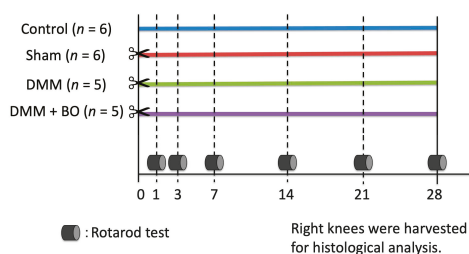


**Figure 1.** Experimental protocol of the present study. Destabilization of the medial meniscus (DMM) and the sham surgery were performed on the right knee on day 0 (⇐). Boiogito (BO) was mixed in the chow at a concentration of 3%. The rotarod test was performed prior to and 1, 3, 7, 14, 21, and 28 days after the DMM surgery. The rats were sacrificed, and their right knees were harvested for histological analysis on day 28.

## 2.2. Drug Administration

The dry powdered extract of BO was supplied by Tsumura & Co. (TJ-20; Tokyo, Japan) and contained a dry extract of the mixed drug substances consisting of *Sinomenium* stem 5.0 g, *Astragalus* root 5.0 g, *Atractylodes lancea* rhizome 3.0 g, Jujube 3.0 g, *Glycyrrhiza* 1.5 g, and Ginger 1.0 g. These herbs were mixed and extracted with purified water at 95.1 °C for 1 h, and the soluble extract was then separated from the insoluble residue and dried by removing water under reduced pressure. The dry powdered extract of BO was mixed with powdered chow at a concentration of 3% and fed to the BO-treated rats. The rats not treated with BO were fed powdered chow only. The concentration of BO was chosen on the basis of the effective doses recommended by a previous report [18].

## 2.3. Surgery

Destabilization of the medial meniscus (DMM) was adopted as a KOA-inducing model [19]. We divided rats into four groups: control, sham, DMM, and DMM + BO-treated groups. DMM and sham surgeries were performed on the right knee fixed in a flexed position under isoflurane (Fujifilm Wako Pure Chemical Corp., Osaka, Japan) inhalation general anesthesia. A skin incision was made in the midline of the right knee to expose the quadriceps muscle and patellar tendon. The medial edges of the patella tendon and medial joint capsule were separated (Figure 2A), and then, the patella was dislocated from the lateral femoral condyle (Figure 2B). The medial meniscotibial ligament (MMTL) was then able to be observed. The MMTL was transected, and the medial meniscotibial joint capsule was horizontally cut in the DMM and DMM + BO groups (Figure 2C) to induce meniscal extrusion out of the bone contact area between the femur and tibia (Figure 2D). No cutting procedure was performed in the sham group. Finally, the medial joint capsule and patella tendon were sutured with 6-0 Vicryl® (Ethicon Inc., Somerville, NJ, USA), and the subcutaneous layer was sutured with 5-0 Vicryl®.

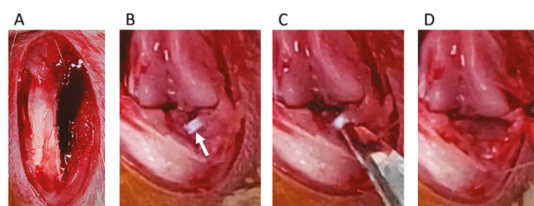


**Figure 2.** Surgical procedure of destabilization of the medial meniscus (DMM). (A) The medial edge of the patella tendon and the medial joint capsule are separated. (B) The medial meniscotibial ligament (MMTL) is detected. White arrow indicates the MMTL. (C) The MMTL is transected, and the medial meniscotibial joint capsule is horizontally cut. (D) Meniscal extrusion is confirmed.

#### 2.4. Meniscus Extrusion Ratio

To assess the validity of the DMM operation, the degree of extrusion of the medial meniscus was evaluated. The animals were intraperitoneally anesthetized with pentobarbital sodium (50 µg/kg; Somnopentyl, Kyoritsu Seiyaku, Tokyo, Japan) and intracardially perfused with phosphate-buffered saline at pH 7.4 until all the blood had been removed from the system. After perfusion with 4% paraformaldehyde in 0.1 M phosphate-buffered saline, only the right leg was amputated because the contralateral side of the knee joint may not yet have an osteoarthritic change [20]. Then, the right knee joint was fixed with 4% paraformaldehyde for 3 days and decalcified with a 20% EDTA solution for 21 days. Then, the knee joint was cut in a coronal shape amid and along the medial collateral ligament fiber, and the degree of meniscal lateral deviation out of the outer edge of the femoral condyle was measured by using a Stemi 305 stereomicroscope (Carl Zeiss, Oberkochen, Germany) (Figure 3A). This measurement was performed three times in each sample, and the average of these three was finally defined as the meniscus extrusion (ME) ratio, which is the length of the extruded meniscus/the length of the medial meniscus  $\times 100$  (%) [21] (Figure 3B). Specimens with  $<20\%$  of the ME ratio in the DMM and DMM + BO groups were excluded from this study because they were considered to indicate failure of the DMM surgery.

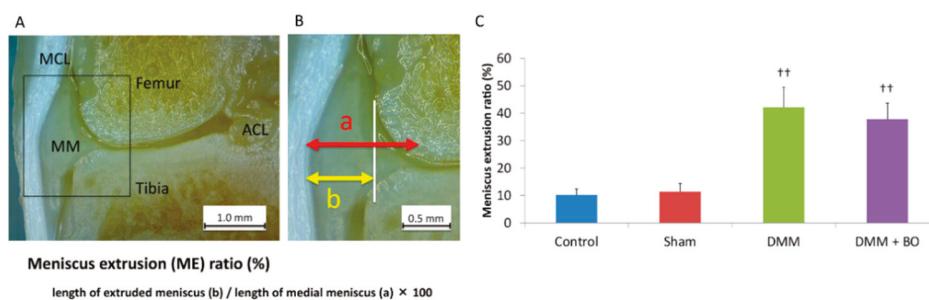


**Figure 3.** Meniscus extrusion (ME) ratio. (A) Coronal view of the medial tibiofemoral compartment. The medial collateral ligament and tibial footprint of the anterior cruciate ligament is confirmed. MCL—medial collateral ligament; ACL—anterior cruciate ligament; MM—medial meniscus. (B) Definition of ME ratio. White vertical line indicates the medial edge of the femoral condyle. (C) ME ratio; quantitation of the extruded meniscus. Bars show the mean  $\pm$  SD ( $n = 6$  in the control and sham groups,  $n = 5$  in the DMM and DMM + BO groups). The stars indicate a significant difference from the control group by the Tukey–Kramer test ( $^{**} p < 0.01$  vs. Control).

#### 2.5. Rotarod Test

The rotarod test easily validates the effects of drugs, brain disorders, and disease on rodent motor coordination and fatigue tolerance [22,23]. The test was performed by a third person who was not engaged in the surgery and did not know the grouping. The influences on locomotive performance were assessed prior to and 1, 3, 7, 14, 21, and 28 days after the DMM surgery by using an automated accelerating rotarod apparatus (LE8305), with a lane width of 75 mm and rod diameter of 60 mm (Panlab Harvard Apparatus, Barcelona, Spain) (Figure 1). The rats were forced to make forward walking movements to circumvent falling. The rat was trained 5 min per day for 2 days to stay on the drum. The rotarod was accelerated 5–40 rpm over 30 s. The time that rats remained on the rotarod was recorded. All values were averaged over three consecutive measurements. The cutoff time was set at 45 s.

## 2.6. Histological Analysis

After measuring the ME ratio with a stereomicroscope, decalcified knees were embedded in paraffin, and specimen preparation and tissue staining were performed following the recommendations of the Osteoarthritis Research Society International (OARSI) [24]. All sections were sliced 4- $\mu$ m thick every 200  $\mu$ m from the center of the medial collateral ligament. The sections were visualized by using an Olympus BX 53 microscope (Olympus, Tokyo, Japan) after toluidine blue staining was performed. At least three tissue sections were prepared from each specimen. Histological assessment was determined following the OARSI scoring system [24]. The slides were evaluated by two independent histologists. Cartilage degeneration was evaluated on a scale of 0–15 points, subchondral bone destruction was evaluated on a scale of 0–5 points, osteophyte formation was evaluated on a scale of 0–4 points, and the total score ranged from 0–24 points, in which a lower score indicated less joint degeneration. The average value of the three slices with the poorest scores was taken as the OARSI score of each knee.

## 2.7. Statistical Analysis

Data are represented as the mean  $\pm$  SD of multiple repeats of the same experiment for the data of ME ratio and rotarod test, and median and interquartile range for the histological analysis (control,  $n = 6$ ; sham,  $n = 6$ ; DMM,  $n = 5$ ; DMM + BO,  $n = 5$ ). Statistical analysis was performed by using one-way analysis of variance and the Tukey–Kramer method in JMP<sup>®</sup> Pro version 14.0 software (SAS Inc., Cary, NC, USA).  $p$  values  $< 0.05$  were taken as indicating statistically significant differences.

## 3. Results

### 3.1. Meniscus Extrusion Ratio

To assess the validity of the DMM operation, the degree of extrusion of the medial meniscus was evaluated 4 weeks after the operation (Figure 3A,B). The ME ratios were  $10.2 \pm 2.3\%$  in the control group,  $11.4 \pm 3.0\%$  in the sham group,  $42.2 \pm 7.3\%$  in the DMM group, and  $37.8 \pm 5.8\%$  in the DMM + BO group (Figure 3C). The differences were not significant between the control and sham groups. However, the ME ratios were significantly higher in the DMM and DMM + BO groups than in the control and sham groups, but the differences between the DMM and DMM + BO groups were not significant. These findings strongly suggested that meniscal extrusion and displacement of the medial meniscus out of the femoral condyle occurred with DMM surgery.

### 3.2. Rotarod Test

Rotarod performances were assessed prior to and 1, 3, 7, 14, 21, and 28 days after the DMM surgery (Figure 4). In the acute phase (on days 1 and 3), although walking time on the rotarod apparatus was slightly improved in the control group, there was no significant difference. The latencies to fall off the rotarod apparatus (walking time) were significantly lower in the DMM group than in the control group ( $p < 0.01$ ). However, the decreases were inhibited in the DMM + BO group, especially significant on day 1 ( $p < 0.05$ ). In the chronic phase (on days 14, 21, and 28), the latencies were significantly lower in the DMM group than in the control and sham groups ( $p < 0.01$ ). Those decreases were significantly inhibited in the DMM + BO group (on day 14;  $p < 0.01$ , on days 21 and 28;  $p < 0.05$ ). Furthermore, walking time on day 28 in the DMM + BO group had no significant difference than that in the control group.



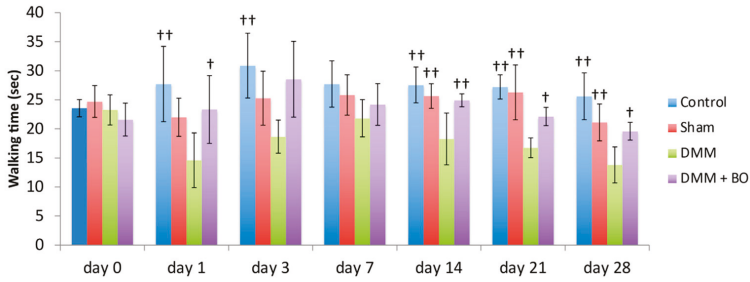


**Figure 4.** Locomotive functional test with the rotarod test. The stars indicate a significant difference from the DMM group by the Tukey–Kramer test (<sup>†</sup>  $p < 0.05$ , <sup>††</sup>  $p < 0.01$  vs. DMM).

3.3. Histological Analysis

Histological assessment was determined by OARSI score 4 weeks after the operation [23]. Although cartilage degeneration was significantly greater in the DMM group than in the control and sham groups, the degeneration observed in the DMM group was alleviated in the DMM + BO group (Figure 5A). The OARSI cartilage scores were 0.0 points (0.0–0.25) in the control group, 0.33 points (0.08–0.58) in the sham group, 2.67 points (2.25–3.00) in the DMM group, and 0.67 points (0.33–2.33) in the DMM + BO group. There was no significant difference in the OARSI cartilage scores between the control and sham groups. The OARSI cartilage score was significantly higher in the DMM group than in the control and sham groups ( $p < 0.01$ ) but was significantly lower in the DMM + BO group than in the DMM group ( $p < 0.05$ ) (Figure 5B). The total OARSI scores, including the cartilage score, osteophyte formation score, and subchondral bone damage score, were 0.0 points (0.0–0.25) in the control group, 0.33 points (0.08–0.58) in the sham group, 5.00 points (3.00–5.25) in the DMM group, and 0.67 points (0.33–4.33) in the DMM + BO group. As in the cartilage score results, there were no significant differences between the control, sham, and DMM + BO groups; however, the total OARSI score was significantly higher in the DMM group than in the other groups (vs. control and sham;  $p < 0.01$ , vs. DMM + BO;  $p < 0.05$ ) (Figure 5C).

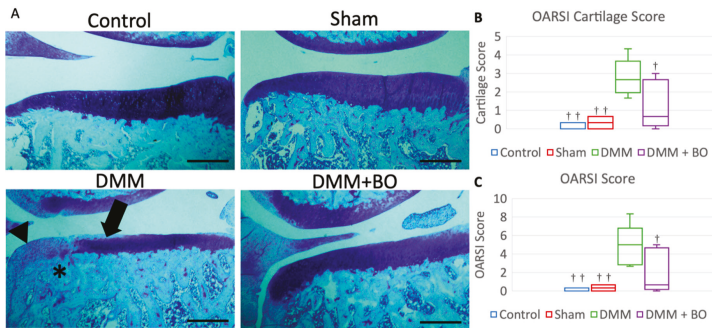


**Figure 5.** Histological analysis of the medial tibial cartilage. (A) Representative images of coronal sections of the medial tibial plateau stained with toluidine blue. Magnification: \* 40. Scale bars = 500  $\mu$ m. Arrow ( $\blackrightarrow$ ) indicates degeneration of the extracellular matrix in articular cartilage. Asterisk (\*) indicates subchondral bone damage. Arrowhead ( $\blacktriangleright$ ) indicates osteophyte synthesis. (B) OARSI cartilage score. (C) Total OARSI score. Boxplots denote median values and interquartile ranges. Vertical bars show ranges ( $n = 6$  in the control and sham groups,  $n = 5$  in the DMM and DMM + BO groups). The marks indicate a significant difference from the DMM group by the Tukey–Kramer test (<sup>†</sup>  $p < 0.05$ , <sup>††</sup>  $p < 0.01$  vs. DMM).

#### 4. Discussion

Although the pathological mechanism of KOA has not been fully elucidated, KOA is a disease involving articular cartilage but also synovium, subchondral bone, and periarticular soft tissue [25]. Inflammation of synovium is associated with alterations in the adjacent cartilage. Catabolic and pro-inflammatory mediators, such as cytokines, NO, and prostaglandin E2, produced by the inflamed synovial membrane, lead to excessive production of proteolytic enzymes associated with cartilage degradation [26]. Current strategies for treatment of KOA are aimed at relieving clinical symptoms, such as pain or swelling of the knee joint and disability of walking, and delaying the progression of KOA, such as cartilage degradation, osteophyte synthesis, or subchondral bone destruction [27,28].

Considering the latency to fall off the rotating drum in the rotarod test in this study, administration of BO improved walking ability in the DMM rat model. Although the rotarod test can detect general locomotive function in experimental rodent models [29], it can also reflect, at least in part, pain-related locomotive dysfunction derived from surgical invasion, especially within a few days after surgery. In the present study, walking time on the rotarod apparatus was improved by administration of BO not only on days 14–28 (chronic phase) but also a few days after the operation (acute phase) (Figure 4). Among the crude drugs of BO, *Astragalus* root [30], *Atractylodes lancea* rhizome [31], Jujube [32], *Glycyrrhiza* [33], and Ginger [34] have been reported to have analgesic actions in various kinds of animal models of pain. BO can potentially relieve acute postoperative pain.

Meniscus extrusion is one of the factors for progression for KOA. In humans, medial meniscus posterior root tear reportedly contributes to meniscus extrusion, possibly because of extensive mechanical loading of the articular cartilage and subchondral bone [35]. The DMM rat was established to develop KOA by transection of the MMTL, which induces medial meniscus extrusion. We confirmed that the anterior part of the medial meniscus was completely dislocated from the femoral condyle in rats with DMM surgery (Figure 3). In the present study, the patellar tendon and medial joint capsule were split in the sham group, but KOA did not occur as evaluated by OARSI score. Surgical invasion did not evidently induce osteoarthritic change in the knee joint. Therefore, it is considered that the biomechanical disorder caused by meniscus extrusion strongly influences the development of KOA in the DMM group. Surprisingly, BO inhibited progressive destructive damage of the knee joint, although meniscus extrusion was observed as well in the DMM group. To the best of our knowledge, this is the first report in which BO has been shown to have a preventive effect on posttraumatic KOA.

There has been some basic research suggesting that BO could have a therapeutic effect against KOA, especially on joint fluid retention and the inflammatory response in KOA. Fujitsuka et al. [36] showed that BO inhibited IL-1 $\beta$  secretion due to synovitis in an ACL-transected rat KOA model. Indomethacin, an NSAID, also has been shown to decrease IL-1 $\beta$  in the synovial fluid but failed to inhibit joint fluid retention in the rats' knee joints. These results are similar to those in the clinical study mentioned above [16]. Takenaga et al. [37] reported a suppressive effect of BO extract on MMP-13 production in rats with adjuvant-induced arthritis as well as an inhibitory effect on the secretion of IL-1 $\beta$  and MMP-13 in cultured chondrocytes. These findings suggest that BO could inhibit the secretion of pro-inflammatory cytokines, decrease excessive joint effusion, and stimulate proper irrigation of the knee joint with joint fluid. Further study is needed to elaborate on the morphopathogenetic and therapeutic mechanism of BO in the DMM-induced KOA model to prove the link between tissue and clinical changes in the rats.

As mentioned above, BO is composed of six crude drugs and contains various kinds of chemical components, but it is not clear which components contribute to the preventive effect against KOA progression. Previous studies have investigated some potential components for alleviating the development of KOA. *Sinomenium* stem, a principal crude drug of BO, has been shown to have anti-inflammatory activity [38]. In animal models of adjuvant and collagen-induced arthritis, *Sinomenium* stem improved symptoms and decreased the expressions of pro-inflammatory cytokines, such as IL-1 $\beta$  and TNF- $\alpha$  [39]. *Astragalus* root also has been shown to have anti-inflammatory activity by decreasing the pro-inflammatory cytokine, TNF- $\alpha$ , although in a rat autoimmune myocarditis

model and mouse diabetic model [40,41]. Given those findings, a synergistic effect by combining the anti-inflammatory activity of *Sinomenium* stem and *Astragalus* root may provide the characteristic therapeutic effect of BO against early stage KOA. This ideal combination of chemical components in BO can be applied clinically, such as in the perioperative period for meniscal tears and ACL ruptures, to improve excessive joint effusion and prevent the progression of KOA. Further investigation is needed.

Several limitations of our study need to be considered. First, as mentioned above, we have to elucidate the therapeutic mechanism to prove drug efficacy. We are performing subsequent studies such as immunohistochemical staining and the gene expression of proteins related to cartilage metabolism, including collagen type II and matrix metalloproteinase (MMP)-13. However, the results from this study would be a proposal of a new strategy for posttraumatic KOA. Second, in this study, we estimated the effect for 4 weeks after surgery to assess a preventive effect on the early stage of posttraumatic KOA. However, we need to verify the efficacy longitudinally. When the disease state lasts long, the contralateral side must also be influenced [20]. Therefore, in the future, we will follow the long-term changes of both knees.

## 5. Conclusions

In conclusion, oral administration of BO was found to have some therapeutic effect on preventing clinical osteoarthritic changes in a posttraumatic KOA-inducing rat model. BO potentially could be applied in various clinical situations, such as for perioperative administration to relieve pain, and prevent the future progression of KOA.

**Author Contributions:** Conceptualization: J.O. and T.O.; methodology: T.O., H.I., and S.N.; validation: T.O.; formal analysis: J.O.; investigation: J.O., T.O., Y.K., and H.T. (Haruka Takemura); data curation: T.O. and H.I.; resources: H.I.; writing—original draft: J.O.; writing—review and editing: T.O. and M.S.; visualization: J.O.; supervision: H.T. (Hiroshi Takagi), K.K., and M.S.; project administration: M.S.; funding acquisition: O.T. All authors have read and agreed to the published version of the manuscript.

**Funding:** This work was supported by the Showa University Research Fund.

**Acknowledgments:** The authors are grateful to Tsumura & Co. for generously providing BO.

**Conflicts of Interest:** The authors declare no conflict of interest. The funders had no role in the design of the study; in the collection, analyses, or interpretation of data; in the writing of the manuscript, or in the decision to publish the results.

## References

1. Kloppenburg, M.; Berenbaum, F. Osteoarthritis years in review 2019: Epidemiology and therapy. *Osteoarthr. Cartil.* **2020**, *28*, 242–248. [[CrossRef](#)] [[PubMed](#)]
2. Chijimatsu, R.; Kunugiza, Y.; Taniyama, Y.; Nakamura, N.; Tomita, T.; Yoshikawa, H. Expression and pathological effects of periostin in human osteoarthritis cartilage. *BMC Musculoskelet. Disord.* **2015**, *16*, 215–226. [[CrossRef](#)] [[PubMed](#)]
3. Loeser, R.F.; Goldring, S.R.; Scanzello, C.R.; Goldring, M.B. Osteoarthritis: A disease of the joint as an organ. *Arthritis Rheum.* **2012**, *64*, 1697–1707. [[CrossRef](#)] [[PubMed](#)]
4. Yu, S.P.C.; Hunter, D.J. Emerging drugs for the treatment of knee osteoarthritis. *Expert Opin. Emerg. Drugs* **2015**, *20*, 361–378. [[CrossRef](#)] [[PubMed](#)]
5. Zhang, Y.; Jordan, J.M. Epidemiology of osteoarthritis. *Clin. Geriatr. Med.* **2010**, *26*, 355–369. [[CrossRef](#)]
6. Vina, E.R.; Kwok, C.K. Epidemiology of osteoarthritis: Literature update. *Curr. Opin. Rheumatol.* **2018**, *30*, 160–167. [[CrossRef](#)] [[PubMed](#)]
7. Brown, T.D.; Johnston, R.C.; Saltzman, C.L.; Marsh, J.L.; Buckwalter, J.A. Posttraumatic osteoarthritis: A first estimate of incidence, prevalence, and burden of disease. *J. Orthop. Trauma* **2006**, *20*, 739–744. [[CrossRef](#)]
8. Bannuru, R.R.; Osani, M.C.; Vaysbrot, E.E.; Arden, N.K.; Bennell, K.; Bierma-Zeinstra, S.M.A.; Kraus, V.B.; Lohmander, L.S.; Abott, J.H.; Bhandari, M.; et al. OARSI guidelines for the non-surgical management of osteoarthritis. *Osteoarthr. Cartil.* **2019**, *27*, 1578–1589. [[CrossRef](#)]

9. Hong, L.; Chen, C.; Shiyi, C. Posttraumatic knee osteoarthritis following anterior cruciate ligament injury: Potential biochemical mediators of degenerative alteration and specific biochemical markers. *Biomed. Rep.* **2015**, *3*, 147–151. [[CrossRef](#)]
10. Hiranaka, T.; Furumatsu, T.; Kamatsuki, Y. Posttraumatic cartilage degradation progresses following anterior cruciate ligament reconstruction: A second-look arthroscopic evaluation. *J. Orthop. Sci.* **2019**, *24*, 1058–1063. [[CrossRef](#)]
11. Hiranaka, T.; Furumatsu, T.; Kamatsuki, Y. Early chondral damage following meniscus repairs with anterior cruciate ligament reconstruction. *Asia Pac. J. Sports Med. Arthrosc. Rehabil. Technol.* **2020**, *20*, 1–5. [[CrossRef](#)]
12. Mobasheri, A. Intersection of inflammation and herbal medicine in the treatment of osteoarthritis. *Curr. Rheumatol. Rep.* **2012**, *14*, 604–616. [[CrossRef](#)]
13. Christensen, R.; Bartels, E.M.; Altman, R.D.; Astrup, A.; Bliddal, H. Does the hip powder of *Rosa canina* (rosehip) reduce pain in osteoarthritis patients? A meta-analysis of randomized controlled trials. *Osteoarthr. Cartil.* **2008**, *16*, 965–972. [[CrossRef](#)] [[PubMed](#)]
14. Schulze-Tanzil, G.; Mobasheri, A.; Sendzik, J.; John, T.; Shakibaei, M. Effects of curcumin (diferuloylmethane) on nuclear factor kappaB signaling in interleukin-1beta-stimulated chondrocytes. *Ann. N. Y. Acad. Sci.* **2004**, *1030*, 578–586. [[CrossRef](#)] [[PubMed](#)]
15. Choi, J.H.; Kim, D.Y.; Yoon, J.H.; Youn, H.Y.; Yi, J.B.; Rhee, H.I.; Ryu, K.H.; Jung, K.; Han, C.-K.; Kwak, W.-J.; et al. Effects of SKI 306X, a new herbal agent, on proteoglycan degradation in cartilage explant culture and collagenase-induced rabbit osteoarthritis model. *Osteoarthr. Cartil.* **2002**, *10*, 471–478. [[CrossRef](#)] [[PubMed](#)]
16. Majima, T.; Inoue, M.; Kasahara, Y.; Onodera, T.; Takahashi, D.; Minami, A. Effect of the Japanese herbal medicine, Boiogito, on the osteoarthritis of the knee with joint effusion. *Sports Med. Arthrosc. Rehabil. Ther. Technol.* **2012**, *4*, 3. [[CrossRef](#)] [[PubMed](#)]
17. Yasui, H. Effects of stephania and astragalus decoction on osteoarthritis of the knee. *J. Kampō. Acupunct. Integr. Med.* **2006**, *1*, 8–13.
18. Shimada, T.; Takase, T.; Kosugi, M.; Aburada, M. Preventive effect of boiogito on metabolic disorders in the TSOD mouse, a model of spontaneous obese type II diabetes mellitus. *Evid. Based Complement. Alternat. Med.* **2011**, *2011*, 931073. [[CrossRef](#)]
19. Glasson, S.S.; Blanchet, T.J.; Morris, E.A. The surgical destabilization of the medial meniscus (DMM) model of osteoarthritis in the 129/SvEv mouse. *Osteoarthr. Cartil.* **2007**, *15*, 1061–1069. [[CrossRef](#)]
20. Gardiner, M.D.; Vincent, T.L.; Driscoll, C.; Burleigh, A.; Bou-Gharios, G.; Saklatvala, J.; Nagase, H.; Chanalaris, A. Transcriptional analysis of micro-dissected articular cartilage in post-traumatic murine osteoarthritis. *Osteoarthr. Cartil.* **2015**, *23*, 616–628. [[CrossRef](#)]
21. Ozeki, N.; Muneta, T.; Kawabata, K.; Koga, H.; Nakagawa, Y.; Saito, R.; Udo, M.; Yanagisawa, K.; Ohara, T.; Mochizuki, T.; et al. Centralization of extruded medial meniscus delays cartilage degeneration in rats. *J. Orthop. Sci.* **2017**, *3*, 542–548. [[CrossRef](#)] [[PubMed](#)]
22. Osmon, K.J.; Vyas, M.; Woodley, E.; Thompson, P.; Walia, J.S. Battery of behavioral tests assessing general locomotion, muscular strength, and coordination in mice. *J. Vis. Exp.* **2018**, *131*, e55491. [[CrossRef](#)]
23. Shiotsuki, H.; Yoshimi, K.; Shimo, Y.; Funayama, M.; Takamatsu, Y.; Ikeda, K.; Takahashi, R.; Kitazawa, S.; Hattori, N. A rotarod test for evaluation of motor skill learning. *J. Neurosci. Methods* **2010**, *189*, 180–185. [[CrossRef](#)] [[PubMed](#)]
24. Gerwin, N.; Bendele, A.M.; Glasson, S.; Carlson, C.S. The OARSI histopathology initiative recommendations for histological assessments of osteoarthritis in the rat. *Osteoarthr. Cartil.* **2010**, *18*, S24–S34. [[CrossRef](#)] [[PubMed](#)]
25. Goldring, M.B.; Goldring, S.R. Osteoarthritis. *J. Cell Physiol.* **2007**, *213*, 626–634. [[CrossRef](#)] [[PubMed](#)]
26. Sellam, J.; Berenbaum, F. The role of synovitis in pathophysiology and clinical symptoms of osteoarthritis. *Nat. Rev. Rheumatol.* **2010**, *6*, 625–635. [[CrossRef](#)]
27. Gallagher, B.; Tjoumakaris, F.P.; Harwood, M.; Good, R.P.; Ciccotti, M.G.; Freedman, K.B. Chondroprotection and the prevention of osteoarthritis progression on the knee. A systematic review of treatment agents. *Am. J. Sports Med.* **2014**, *43*, 734–744. [[CrossRef](#)]
28. Veronesi, F.; Fini, M.; Giavaresi, G.; Ongaro, A.; Mattei, M.; Pellati, A.; Setti, S.; Tschon, M. Experimentally induced cartilage degeneration treated by pulsed electromagnetic field stimulation; an in vitro study on bovine cartilage. *BMC Musculoskelet. Disord.* **2015**, *16*, 308. [[CrossRef](#)]

29. Terada, T.; Hara, K.; Haranishi, Y.; Sata, T. Antinociceptive effect of intrathecal administration of taurine in rat models of neuropathic pain. *Can. J. Anesth.* **2011**, *58*, 630–637. [[CrossRef](#)]
30. Yu, J.; Zhang, Y.; Sun, S.; Shen, J.; Qiu, J.; Yin, X.; Yin, H.; Jiang, S. Inhibitory effects of astragaloside IV on diabetic peripheral neuropathy in rats. *Can. J. Physiol. Pharmacol.* **2006**, *84*, 579–587. [[CrossRef](#)]
31. Chen, L.-G.; Jan, Y.-S.; Tsai, P.-W.; Norimoto, H.; Michihara, S.; Murayama, C.; Wang, C.-C. Anti-inflammatory and antinociceptive constituents of *Atractylodes japonica* Koidzumii. *J. Agric. Food Chem.* **2016**, *64*, 2254–2262. [[CrossRef](#)] [[PubMed](#)]
32. Boakye-Gyasi, E.; Henneh, I.T.; Abotsi, W.K.M.; Ameyaw, E.O.; Woode, E. Hydro-ethanolic leaf extract of *Ziziphus abyssinica* Hochst Ex A. Rich (Rhamnaceae) exhibits anti-nociceptive effects in murine models. *BMC Complement. Altern. Med.* **2017**, *17*, 231. [[CrossRef](#)] [[PubMed](#)]
33. Zhang, M.-T.; Wang, B.; Jia, Y.-N.; Liu, N.; Ma, P.-S.; Gong, S.-S.; Niu, Y.; Sun, T.; Li, Y.-X.; Yu, J.-Q. Neuroprotective effect of liquiritin against neuropathic pain induced by chronic constriction injury of the sciatic nerve in mice. *Biomed. Pharmacother.* **2017**, *95*, 186–198. [[CrossRef](#)]
34. Montserrat-de la Paz, S.; Garcia-Gimenez, M.D.; Quilez, A.M.; De la Puerta, R.; Fernandez-Arche, A. Ginger rhizome enhances the anti-inflammatory and anti-nociceptive effects of paracetamol in an experimental mouse model of fibromyalgia. *Inflammopharmacology* **2018**, *26*, 1093–1101. [[CrossRef](#)] [[PubMed](#)]
35. Allaire, R.; Muriuki, M.; Gilbertson, L.; Harner, C.D. Biomechanical consequences of a tear of the posterior root of the medial meniscus: Similar to total meniscectomy. *J. Bone Jt. Surg. Am.* **2008**, *90*, 1922–1931. [[CrossRef](#)]
36. Fujitsukam, N.; Tamai, M.; Tsuchiya, K. Boiogito, a Kampo medicine, improves hydrarthrosis in a rat model of knee osteoarthritis. *BMC Complement. Altern. Med.* **2015**, *15*, 451. [[CrossRef](#)]
37. Takenagam, M.; Niimi, J.; Hamaguchi, A.; Asano, T.; Tsuchiya, R.; Ohta, Y.; Yudoe, K.; Inoue, H. Protective effect of boiogito extract with glucosamine HCL against adjuvant-induced arthritis in rats. *Tradit. Kampo. Med.* **2018**, *5*, 38–44. [[CrossRef](#)]
38. Wang, Q.; Li, X.-K. Immunosuppressive and anti-inflammatory activities of sinomenine. *Int. Immunopharmacol.* **2011**, *11*, 373–376. [[CrossRef](#)]
39. Liu, L.; Buchner, E.; Beitz, D.; Schmidt-Weber, C.B.; Kaever, V.; Emmrich, F.; Kinne, R.W. Amelioration of rat experimental arthritides by treatment with the alkaloid sinomenine. *Int. J. Immunopharmacol.* **1996**, *18*, 529–543. [[CrossRef](#)]
40. Zhao, P.; Su, G.; Xiao, X.; Hao, E.; Zhu, X.; Ren, J. Chinese medicinal herb *Radix Astragali* suppresses cardiac contractile dysfunction and inflammation in a rat model of autoimmune myocarditis. *Toxicol. Lett.* **2008**, *182*, 29–35. [[CrossRef](#)]
41. Hoom, R.L.C.; Wong, J.Y.L.; Qiao, C.F.; Xu, A.; Xu, H.X.; Lam, K.S.L. The effective fraction isolated from *Radix Astragali* alleviates glucose intolerance, insulin resistance and hypertriglyceridemia in db/db diabetic mice through its anti-inflammatory activity. *Nutr. Metab.* **2010**, *7*, 67–79. [[CrossRef](#)]

**Publisher's Note:** MDPI stays neutral with regard to jurisdictional claims in published maps and institutional affiliations.



© 2020 by the authors. Licensee MDPI, Basel, Switzerland. This article is an open access article distributed under the terms and conditions of the Creative Commons Attribution (CC BY) license (<http://creativecommons.org/licenses/by/4.0/>).



Article

# Analgesic Efficacy of a Combination of Fentanyl and a Japanese Herbal Medicine “Yokukansan” in Rats with Acute Inflammatory Pain

Yuko Akanuma <sup>1,2</sup>, Mami Kato <sup>1</sup>, Yasunori Takayama <sup>1</sup>, Hideshi Ikemoto <sup>1</sup>, Naoki Adachi <sup>1</sup>, Yusuke Ohashi <sup>1,3</sup>, Wakako Yogi <sup>1,4</sup>, Takayuki Okumo <sup>1</sup>, Mana Tsukada <sup>1</sup> and Masataka Sunagawa <sup>1,\*</sup>

- <sup>1</sup> Department of Physiology, School of Medicine, Showa University, Tokyo 142-8555, Japan; yukoaka@med.showa-u.ac.jp (Y.A.); jt.kato0513@med.showa-u.ac.jp (M.K.); ytakayama@med.showa-u.ac.jp (Y.T.); h\_ikemoto@med.showa-u.ac.jp (H.I.); nadachi@med.showa-u.ac.jp (N.A.); denta1986@gmail.com (Y.O.); wkkyg0613@cmed.showa-u.ac.jp (W.Y.); tokumo@med.showa-u.ac.jp (T.O.); m-tsukada@med.showa-u.ac.jp (M.T.)
  - <sup>2</sup> Department of Anesthesiology, St. Luke's International Hospital, Tokyo 104-8560, Japan
  - <sup>3</sup> Department of Palliative Medicine, Showa University Yokohama Northern Hospital, Kanagawa 224-8503, Japan
  - <sup>4</sup> Pharmaceutical Department, Showa University Hospital, Tokyo 142-8666, Japan
- \* Correspondence: suna@med.showa-u.ac.jp; Tel.: +81-3-3784-8110

Received: 12 November 2020; Accepted: 15 December 2020; Published: 17 December 2020

**Abstract: Background:** Fentanyl can induce acute opioid tolerance and postoperative hyperalgesia when administered at a single high dose; thus, this study examined the analgesic efficacy of a combination of fentanyl and *Yokukansan* (YKS). **Methods:** Rats were divided into control, formalin-injected (FOR), YKS-treated+FOR (YKS), fentanyl-treated+FOR (FEN), and YKS+FEN+FOR (YKS+FEN) groups. Acute pain was induced via subcutaneous injection of formalin into the paw. The time engaged in pain-related behavior was measured. **Results:** In the early (0–10 min) and intermediate (10–20 min) phases, pain-related behavior in the YKS+FEN group was significantly inhibited compared with the FOR group. In the late phase (20–60 min), pain-related behavior in the FEN group was the longest and significantly increased compared with the YKS group. We explored the influence on the extracellular signal-regulated kinase (ERK) pathway in the spinal cord, and YKS suppressed the phosphorylated ERK expression, which may be related to the analgesic effect of YKS in the late phase. **Conclusions:** These findings suggest that YKS could reduce the use of fentanyl and combined use of YKS and fentanyl is considered clinically useful.

**Keywords:** *Yokukansan*; fentanyl; transient receptor potential ankyrin 1 (TRPA1) channel; phosphorylated extracellular signal-regulated kinase (pERK); whole-cell patch-clamp recording; herbal medicine

## 1. Introduction

Fentanyl and remifentanyl are potent ultra-short-acting  $\mu$ -opioid receptor agonists widely used for pain management in the perioperative period [1]. However, their use is limited because they can induce acute opioid tolerance and a post-treatment state of heightened pain sensitivity, known as opioid-induced hyperalgesia (OIH), when administered at a single high dose [2–5]. Development of OIH causes several problems, including delayed recovery after surgery, higher consumption of analgesics, and side effects associated with their administration. Remifentanyl-induced hyperalgesia (RIH) has been extensively investigated [6–11]. There is some evidence that glutamate release and N-methyl-D-aspartate (NMDA) receptor activation may be important in the development of RIH [9–11]. In addition, remifentanyl infusion downregulates  $\mu$ -opioid receptors [12]. Moreover, glial activation is

involved in RIH. Microglia and astrocytes are activated by chronic opioid use, and their inhibition seems to reduce RIH [6,13]. Some clinical [14–17] and basic studies [18–22] reported that high-dose fentanyl use may also cause hyperalgesia. Xuerong et al. [14] conducted a randomized controlled trial on 90 women undergoing total abdominal hysterectomy. Patients in the control group who were administered bupivacaine requested significantly less morphine postoperatively compared with patients treated with fentanyl. However, the combined use of ketamine, an NMDA receptor antagonist, and fentanyl significantly decreased the need for postoperative morphine administration. Richeb é et al. [18] reported a similar phenomenon in fentanyl-treated rats. These results suggest that NMDA receptor activation is involved in the development of fentanyl-induced hyperalgesia (FIH).

*Yokukansan* (YKS) is a Japanese traditional herbal (Kampo) medicine that comprises seven herbs (Table 1). YKS is officially approved as an ethical pharmaceutical by the Japanese Ministry of Health, Labor, and Welfare. The three-dimensional high-performance liquid chromatography (3D-HPLC) profile chart of YKS was provided by Tsumura & Co. (Figure 1). YKS is administered to patients with symptoms, such as emotional irritability, neurosis, and insomnia, and to infants who suffer from night crying and convulsions [23,24]. Recently, it has been reported that YKS is effective against pain disorders, including headache, post-herpetic neuralgia, fibromyalgia, phantom-limb pain, and trigeminal neuralgia [25–28]. Studies have demonstrated antinociceptive effects of YKS in animal models with chronic neuropathic and inflammatory pain [29–32]. We previously reported that pre-administration of YKS attenuated the development of antinociceptive morphine tolerance and that suppression of glial cell activation may be one mechanism underlying this phenomenon [33,34]. YKS is also known to have an ameliorative effect on glutamate clearance in astrocytes and an antagonistic action at the NMDA receptor [35–37]. As mentioned above, NMDA receptor activation may be involved in FIH development [14,18]. Thus, we hypothesized that YKS might inhibit FIH development.

**Table 1.** The component galenicals of *Yokukansan* (YKS).

<i>Uncariae cum Uncis ramulus</i>	3.0 g
<i>Cnidii rhizoma</i>	3.0 g
<i>Bupleuri radix</i>	2.0 g
<i>Atractylodis Lanceae rhizoma</i>	4.0 g
<i>Poria</i>	4.0 g
<i>Angelicae radix</i>	3.0 g
<i>Glycyrrhizae radix</i>	1.5 g

Weights indicate relative amounts mixed.

In the present study, we first evaluated the effect of combined treatment with YKS and fentanyl using the well-established inflammatory pain model induced by formalin injection [38]. The injection of formalin into the plantar surface of rodent paws induces acute nociceptive responses, such as lifting, licking, and flinching of the paw, which are biphasic. In the initial period of about 10 min (phase I), behavioral responses occur due to activated primary afferent nerve terminals and are mediated by activation of the transient receptor potential ankyrin 1 (TRPA1) channel [39,40]. Thus, we performed whole-cell patch-clamp recording in HEK293T cells expressing human TRPA1 to assess the influence of YKS or fentanyl on the TRPA1 channel. Phase II (10–60 min) reflects central sensitization of neurons in the dorsal horn and peripheral sensitization of nociceptors by the formalin-induced inflammatory response [41]. Accordingly, the expression of phosphorylated extracellular signal-regulated kinase (pERK) in the spinal dorsal horn was analyzed by immunofluorescent staining. ERK is an important molecule in pain signaling and a potential novel target for pain treatment [42].

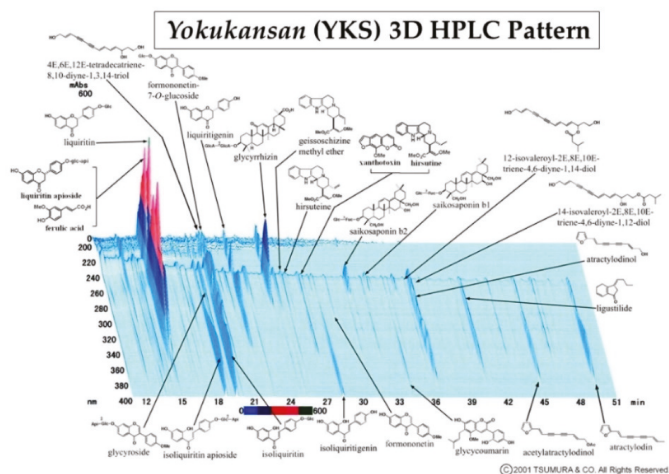


**Figure 1.** Three-dimensional high-performance liquid chromatography (3D-HPLC) profile chart of the major chemical compounds in *Yokukansan* (YKS).

## 2. Materials and Methods

### 2.1. Animals

Experiments were performed using 7–8-week-old male Wistar rats (Nippon Bio-Supp. Center, Tokyo, Japan). Animals were housed two to three per cage (W 24 × L 40 × H 20 cm) under a 12 h light/dark cycle in our animal facility at 25 °C ± 2 °C and 55% ± 5% humidity. Food (CLEA Japan, CE-2, Tokyo, Japan) and water were provided ad libitum. The experiments were performed in accordance with the guidelines of the Committee of Animal Care and Welfare of Showa University. All experimental procedures were approved by the Committee of Animal Care and Welfare of Showa University (certificate number: 07064, date of approval: 1 April 2017). Effort was made to minimize the number of animals used and their suffering.

### 2.2. Administration of Drugs

Dry powdered extracts of YKS (Lot No. 2110054010) used in the present study were supplied by Tsumura & Co. (Tokyo, Japan). The seven herbs comprising YKS (Table 1) were mixed and extracted with purified water at 95.1 °C for 1 h; the soluble extract was separated from insoluble waste and concentrated by removing water under reduced pressure. YKS was mixed with powdered rodent chow (CE-2: CLEA Japan) at a concentration of 3% and fed to YKS-treated rats for 7 days prior to the test. This dose was chosen on the basis of effective doses of YKS in our previous study [33]. Previous studies have indicated that pre-administration of YKS may inhibit development of antinociceptive tolerance to morphine [33,34,43]. Thus, in this study, YKS administration was started 7 days before fentanyl injection. Rats that were not treated with YKS were fed powdered chow only.

Fentanyl (0.08 µg/kg) (Daiichisankyo, Tokyo, Japan) was injected intraperitoneally 10 min before pain induction using a 27 G hypodermic needle. This dose was determined by performing a preliminary experiment according to a previous study [38]. Rats not treated with fentanyl were intraperitoneally administered saline.



### 2.3. Assessment of Analgesia

The analgesic effects of fentanyl and YKS were examined using the formalin test and immunofluorescence staining of pERK. Subcutaneous injections of formalin have been widely used as an animal model of acute inflammatory pain [38–40].

#### 2.3.1. Formalin Test

Rats were randomly divided into five groups as follows: control ( $n = 7$ ), formalin-injected (FOR;  $n = 7$ ), YKS-treated + FOR (YKS;  $n = 9$ ), fentanyl-treated + FOR (FEN;  $n = 9$ ), and YKS + FEN + FOR (YKS + FEN;  $n = 9$ ). The experimental protocol is shown in Table 2. Animals were housed individually in wire observation cages and habituated for 30 min. Ten minutes prior to the formalin test, animals were injected intraperitoneally with fentanyl or saline and returned to individual housing. Acute inflammatory pain was induced via an intraplantar injection of formalin (5%, 50  $\mu$ L, Polysciences, Warrington, PA, US) into the right paw using a 30 G hypodermic needle. Rats in the control group were administered saline instead of formalin. Immediately after the injection, animals were returned to individual housing again, and the total time spent engaged in pain-related behavior was measured for the first 10 min (early phase), between 10 and 20 min (intermediate phase), and between 20 and 60 min (late phase) following the intraplantar injection of formalin or saline. Pain-related behavior was defined as paw shaking, licking, and lifting from the ground.

**Table 2.** The experimental protocol.

Groups	Days 1–7	Day 8		
		10 min before Test	Formalin Test	
control	Powdered chow	Saline (i.p.)	Saline (50 $\mu$ L; s.c.)	
FOR	Powdered chow	Saline (i.p.)	Formalin (5%, 50 $\mu$ L; s.c.)	
YKS	Powdered chow mixed with YKS (3%)	Saline (i.p.)	Formalin (5%, 50 $\mu$ L; s.c.)	
FEN	Powdered chow	Fentanyl (0.08 $\mu$ g/kg; i.p.)	Formalin (5%, 50 $\mu$ L; s.c.)	
YKS+FEN	Powdered chow mixed with YKS (3%)	Fentanyl (0.08 $\mu$ g/kg; i.p.)	Formalin (5%, 50 $\mu$ L; s.c.)	

Groups are as follows: control, formalin-injected (FOR), YKS-treated + FOR (YKS), fentanyl-treated + FOR (FEN), and YKS + FEN + FOR (YKS + FEN). YKS was mixed with powdered rodent chow at a concentration of 3% and fed to YKS-treated rats for 7 days prior to the test. YKS, *Yokukansan*; i.p., intraperitoneal injection; s.c., subcutaneous injection.

#### 2.3.2. Immunofluorescent Staining

The appearance of pERK in the dorsal horn was investigated using immunofluorescent staining. Rats were randomly divided into the same five groups ( $n = 4$  in each group) and administered the same drugs as the formalin test. Forty-five minutes after formalin injection, rats were intraperitoneally anesthetized with pentobarbital sodium (50  $\mu$ g/kg; Somnopentyl, Kyoritsu Seiyaku, Tokyo, Japan) and intracardially perfused with phosphate-buffered saline at pH 7.4 until all the blood had been removed from the system. After perfusion with 4% paraformaldehyde in 0.1 M phosphate-buffered saline, fifth lumbar spinal cord (L5) samples were harvested. Tissue specimens were immersed in 20% sucrose solution for 48 h and subsequently embedded in optimum cutting temperature compound (Tissue-Tek OCT, Sakura Finetek, Torrance, CA, USA), frozen, and cut into 15  $\mu$ m sections using a cryostat (CM3050S, Leica Biosystems, Nussloch, Germany). Sections were incubated overnight at 4  $^{\circ}$ C with rabbit anti-pERK antibody (1:500, #4370, Cell Signaling Technology, Danvers, MA, USA). Sections were then incubated for 2 h with fluorophore-tagged secondary antibody (donkey anti-rabbit Alexa Fluor 555, 1:1000, #A31572, Thermo Fisher Scientific, Waltham, MA, USA). Nuclei were counterstained with DAPI (4',6-diamidino-2-phenylindole, 1:1000, Thermo Fisher Scientific). Samples were imaged using a confocal laser scanning fluorescence microscope (FV1000D, Olympus, Tokyo, Japan), and cell co-localization of pERK and DAPI in the same area of laminae I–II were counted as pERK(+) cells by a

third person who was not engaged in the staining process. The mean value was calculated using five sequential sections from each rat.

#### 2.4. Cell Culture

HEK293T cells were cultured in Dulbecco's modified Eagle's medium (high glucose) with L-glutamine and phenol red (FUJIFILM Wako Pure Chemical, Osaka, Japan) containing 10% fetal bovine serum (#G121-6, JR Scientific, Woodland, CA, USA), penicillin/streptomycin (FUJIFILM Wako Pure Chemical), and GlutaMax (Gibco, Massachusetts, NY, USA) at 37 °C in humidified air containing 5% CO<sub>2</sub>. Cells were transfected with human TRPA1 cDNA (a generous gift from Dr. Yasuo Mori, Kyoto University) and 0.01 µg DsRed-express 2 vector (Takara Bio, Shiga, Japan) using Lipofectamine 3000 (Invitrogen, Waltham, CA, USA). Cells were replaced on cover slips after a 3 h incubation period and used 24–36 h after transfection.

#### 2.5. Whole-Cell Patch-Clamp Recording

Transfected cells were identified by the red fluorescence signal excited by an LED illuminator, X-Cite XYLIS (Excelitas, Waltham, MA, USA). The bath solution contained 140 mM NaCl, 5 mM KCl, 2 mM CaCl<sub>2</sub>, 2 mM MgCl<sub>2</sub>, 10 mM glucose, and 10 mM HEPES (pH adjusted to 7.4 with NaOH). Pipette solution contained 140 mM CsCl, 5 mM 1.2-bis(o-aminophenoxy)ethane -N,N,N',N'-tetraacetic acid (BAPTA), and 10 mM HEPES (pH adjusted to 7.4 with CsOH). Cells were treated with formalin (0.003%), FEN (10 µM), and YKS (1 mg/mL). YKS was decocted in standard bath solution at 60 °C for 15 min, and the supernatant after centrifugation (3000 rpm, 25 °C, 10 min) was used for the experiment. The TRPA1 currents were recorded in voltage-clamp mode using a Multiclamp 700B amplifier (Molecular Devices, California, USA), filtered at 1 kHz with a low-pass filter, and digitized with a Digidata 1550 B digitizer (Molecular Devices, San Jose, CA, USA). Data were acquired with pCLAMP 11 (Molecular Devices, California, USA). Pipette resistances were 3 ± 1 MΩ. The holding potential was −60 mV, and ramp pulses from −100 mV to +100 mV were applied for 300 ms every 5 s.

#### 2.6. Statistical Analysis

Experimental data are presented as mean ± standard deviation. Statistical analyses were performed using one-way analysis of variance with Tukey's test or the Tukey–Kramer post hoc test for comparisons (SPSS 24, IBM Japan, Tokyo, Japan). The *p*-value < 0.05 were considered statistically significant.

### 3. Results

#### 3.1. Formalin Test

The analgesic effects of fentanyl and YKS were examined using the formalin test. The dose of fentanyl (0.08 µg/kg) was determined according to a previous study using the same experimental system. It is reported that 0.04 µg/kg of fentanyl has no effect on formalin-induced pain and 0.16 µg/kg significantly inhibits it [38]. We then performed a preliminary confirmation test using the doses of 0.04, 0.08, and 0.16 µg/kg, and the dose (0.08 µg/kg) that provided a moderate non-significant analgesic effect for the first 20 min was used because we would not be able to evaluate the effect of the drug combination if the dose (≥0.16 µg/kg) that provides significant analgesic effect was administered. With the formalin test, the effects are generally evaluated in two phases: phase I (0–10 min) and phase II (10–60 min). In the present study, we divided the total evaluation time into three phases: the early phase (0–10 min), the intermediate phase (10–20 min), and the late phase (20–60 min), because the effect of a single intraperitoneal administration of fentanyl lasts for approximately 30 min and administration was performed 10 min before pain induction.

In the early and intermediate phases, the duration of pain-related behavior was significantly increased according to the formalin injection; however, the increase was significantly inhibited in the

YKS+FEN group (early phase,  $p < 0.01$ ; intermediate phase,  $p < 0.05$ ), but no significant effect was recognized in the YKS and FEN groups (Figure 2).

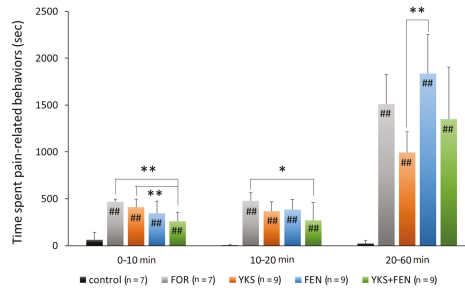


**Figure 2.** Duration of pain-related behavior with the formalin test. The combination of *Yokukansan* (YKS) and fentanyl (FEN) significantly inhibited pain-related behavior during the early phase (0–10 min after formalin injection) and the intermediate phase (10–20 min). The duration in the YKS group was significantly shorter compared with the FEN group during the late phase. FOR, formalin-injected group; YKS, YKS-treated+FOR group; FEN, fentanyl-treated+FOR group; YKS+FEN, YKS+FEN+FOR group. Mean  $\pm$  SD. ##  $p < 0.01$  (vs. control), \*  $p < 0.05$ , \*\*  $p < 0.01$  (Tukey–Kramer test).

In the late phase, that is, after having lost the effects of fentanyl, the duration of pain-related behavior in the FEN group ( $1835.8 \pm 415.4$  s) was the longest and significantly increased compared with the YKS group ( $995.1 \pm 220.3$  s) ( $p < 0.01$ ) (Figure 2).

### 3.2. Immunofluorescent Staining of pERK(+) Cells

The appearance of pERK in the late phase, 45 min after injection of formalin, was investigated to evaluate central sensitization. As a result, a similar tendency was observed with the formalin test in the late phase. Representative pictures are shown in Figure 3a. The number of pERK(+) cells in the FOR ( $5.96 \pm 1.86$  cells), FEN ( $6.83 \pm 1.49$  cells), and YKS+FEN ( $4.88 \pm 1.42$  cells) groups was significantly increased compared with the control group ( $0.83 \pm 0.53$  cells) ( $p < 0.01$ ); however, the number of pERK(+) cells in the YKS group ( $3.19 \pm 0.44$  cells) was significantly lower ( $p < 0.05$  vs. FOR,  $p < 0.01$  vs. FEN) (Figure 3b).

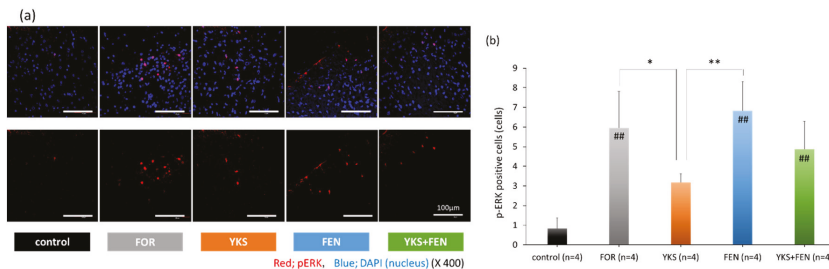


**Figure 3.** Immunofluorescent staining of pERK(+) cells. (a) Appearance of pERK in the dorsal horn. The upper row includes pERK and nuclei, and the lower row includes only pERK. Red, pERK; blue, DAPI (nuclei). (b) The number of pERK(+) cells in the FOR, FEN, and YKS+FEN groups was significantly increased compared with the control group ( $p < 0.01$ ); however, the number of pERK(+) cells in the YKS group was significantly lower ( $p < 0.05$  vs. FOR,  $p < 0.01$  vs. FEN). FOR, formalin-injected group; YKS, YKS-treated+FOR group; FEN, fentanyl-treated+FOR group; YKS+FEN, YKS+FEN+FOR group. Mean  $\pm$  SD. ##  $p < 0.01$  (vs. control), \*  $p < 0.05$ , \*\*  $p < 0.01$  (Tukey’s test).

### 3.3. Whole-Cell Patch-Clamp Recording of TRPA1 Currents

The TRPA1 channel is involved in formalin-induced pain sensation [39,40]. To investigate the pharmacological effects of fentanyl and YKS on TRPA1, we performed whole-cell patch-clamp recording in HEK293T cells expressing human TRPA1 and DsRed (Figure 4). TRPA1 was activated by 0.003% formalin, approximately the half maximal effective concentration according to a previous report [39]. First, we applied YKS and fentanyl, YKS, or fentanyl alone to check whether these medicines directly activated TRPA1. In these cells, exposure to YKS or fentanyl did not evoke a change in basal currents (Figure 4a,b) while the concomitant application of fentanyl and YKS slightly induced the current (Figure 4c). Subsequent addition of formalin activated TRPA1 and evoked a current with two phases, slow and rapid. However, the formalin-induced currents were observed in all experimental conditions. Thus, TRPA1 could be not inhibited by both fentanyl and YKS.

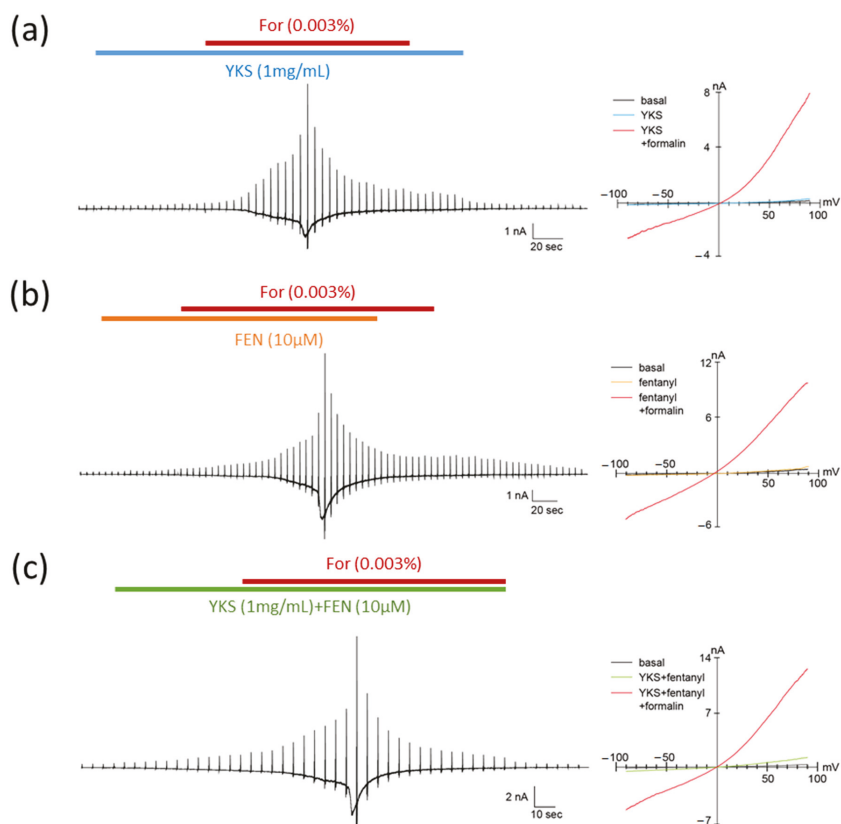


**Figure 4.** Pharmacological effects of formalin, fentanyl, and *Yokukansan* on TRPA1. Typical traces (left) and current–voltage relationships (right) of formalin-induced TRPA1 currents in HEK293T cells expressing human TRPA1. The concentrations of formalin (For), fentanyl (FEN), and *Yokukansan* (YKS) were 0.003%, 10 µM, and 1 mg/mL, respectively. YKS (a) or FEN (b), and YKS and FEN (c) were pretreated for 1 min before the concomitant administration of formalin. TRPA1 was not inhibited by both fentanyl and YKS. The holding potential was  $-60$  mV, and ramp pulses ( $-100$  to  $+100$  mV, 300 ms) were applied every 5 s.

#### 4. Discussion

Administration of fentanyl at a single high dose (e.g.,  $\geq 0.16$   $\mu\text{g}/\text{kg}$ ; i.p. [38]) can inhibit pain induced by formalin; however, it may induce acute opioid tolerance and hyperalgesia [14–22]. We hypothesized that if the dose of fentanyl could be reduced, the risks may be mitigated. The present study examined the analgesic effect of a combination of fentanyl and YKS using a rat model of acute inflammatory pain. The effect of a single intraperitoneal administration of fentanyl lasted for approximately 20 min following formalin injection. In the early (0–10 min) and intermediate (1–20 min) phases, the combination of fentanyl and YKS significantly inhibited the time spent engaged in pain-related behavior, though the administration of fentanyl alone did not work effectively (Figure 2).

In the late phase (20–60 min); that is, after the effect of fentanyl had subsided, the duration of pain-related behavior in the YKS group was significantly decreased compared with the FEN group ( $p < 0.01$ ). Moreover, that in the YKS group tended to be reduced compared with the FOR group ( $p = 0.061$ ). However, when a strong analgesic effect is necessary, such as during the perioperative period, the use of opioid analgesics cannot be avoided. Although there was no significant difference ( $p = 0.057$ ), that in the YKS+FEN group was shorter than the FEN group, and therefore combined use of YKS and fentanyl is thought to be clinically useful.

To elucidate its mechanism of action, we investigated the expression of pERK in the dorsal horn of the spinal cord. Moreover, we investigated the influence of YKS and fentanyl on TRPA1 in vitro. TRPA1, a calcium-permeable non-selective cation channel, is activated by various chemicals, including irritant exogenous ligands and endogenous ligands produced by inflammation [44]. TRPA1 expression in the nociceptive primary sensory nerve is related to the reception of noxious stimuli and signal transduction to the secondary sensory nerve, and activation of TRPA1 induces hyperalgesia [44]. Pain in phase I (0–10 min) of the formalin test is mediated by the activation of TRPA1, and is attenuated by TRPA1-selective antagonists [39,40]. Therefore, the influence of YKS and fentanyl on TRPA1 was investigated. According to the patch-clamp recording, both YKS and fentanyl had no antagonistic activity on TRPA1 (Figure 4). One report suggested that morphine activates TRPA1 [45], and influences of opioids on TRPA1 may be different depending on the type of opioid. In this study, we could not reveal the mechanism of analgesic efficacy of the combination of fentanyl and YKS in the early (0–10 min) and intermediate (10–20 min) phases. We previously reported that the administration of YKS increased the secretion of oxytocin in rats with acute psychological stress [46], and Gamal-Eltrabily et al. [47] reported the injection of oxytocin inhibited formalin-induced pain. Including this, further studies concerning the action mechanism are needed.

Mitogen-activated protein kinase (MAPK) pathways play an important role in nociceptive and neuropathic pain [42,48]. In phase II of the biphasic pain response caused by formalin, the ERK pathway was activated in the central nucleus, which may be involved in nociceptive plasticity [49]. U0126, a specific inhibitor of the ERK pathway, suppressed persistent pain induced by formalin [50]. Moreover, pERK(+) neurons in the spinal cord were increased following remifentanyl infusion [51]. Thus, we explored the influence on the ERK pathway as the mechanism underlying the therapeutic effect of YKS. Our results show that YKS suppressed pERK expression, which may be related to the analgesic effect of YKS in the late phase. The anti-inflammatory action of saikosaponin A isolated from *Bupleuri radix* [52], the anti-inflammatory and anti-tumorigenic effects of total flavonoids from *Glycyrrhizae radix* [53], and the neuroprotective effects of liquiritigenin isolated from *Glycyrrhizae radix* [54] are exerted by inhibition of the ERK pathway. In the future, we will examine whether these components inhibit the ERK pathway in the present experimental system.

OIH, including RIH and FIH, is thought to be a complex physiological response involving glial cell activity [6,13], neuroinflammation [55], opioid receptor desensitization [12], and NMDA receptor activation [9–11,18]. YKS has an ameliorative effect on glutamate clearance in astrocytes and an antagonistic action at the NMDA receptor [35–37]. Additionally, we previously reported that administration of YKS attenuated the development of antinociceptive morphine tolerance, and that suppression of glial cell activation in the spinal cord and mesencephalon may be one mechanism underlying this phenomenon [33,34]. These

mechanisms are also thought to contribute to the preventative effect of YKS on the development of FIH. In this study, obvious FIH was not observed in the late phase, possibly because the dose of fentanyl was low; thus, further studies should be conducted using higher doses of fentanyl.

With respect to the analgesic effect of YKS, almost all clinical and basic studies investigated chronic pain [25–32], and no studies have investigated acute pain. The results from this study suggest that combination use with opioid analgesics might contribute to a reduction in opioid dose and prevention of paradoxical reactions following opioid use; however, YKS alone cannot be expected to provide a sufficient analgesic effect against acute inflammatory pain.

## 5. Conclusions

Fentanyl may induce acute opioid tolerance and postoperative hyperalgesia when administered at a single high dose. In this study, although fentanyl, the dose of which (0.08 µg/kg) cannot provide a significant analgesic effect, was used, combined use of YKS and fentanyl could significantly inhibit pain in the early and intermediate phases of the formalin test. Our findings suggest that YKS could reduce the use of fentanyl and the combined use considered clinically useful.

**Author Contributions:** Conceptualization and methodology, Y.T. and M.S.; investigation, Y.A., Y.T., M.K., H.I., N.A., Y.O., W.Y., T.O., M.T., and M.S.; resources, N.A. and Y.T.; data curation, Y.A., M.K., Y.T., and M.S.; formal analysis, Y.A., Y.T., and M.S.; writing—original draft preparation, Y.A.; writing—review and editing, Y.T. and M.S.; visualization, Y.A. and M.S.; supervision and project administration, M.S. All authors have read and agreed to the published version of the manuscript.

**Funding:** This research received no external funding.

**Acknowledgments:** The authors wish to thank Tsumura & Co. (Tokyo, Japan) for generously providing *Yokukansan* (TJ-54) and Enago for English language review. The authors also thank Yasuo Mori (Kyoto University, Japan) for providing human TRPA1 cDNA.

**Conflicts of Interest:** The authors declare no conflict of interest.

## References

1. Jowkar, S.; Khosravi, M.B.; Sahmeddini, M.A.; Eghbal, M.H.; Samadi, K. Preconditioning effect of remifentanyl versus fentanyl in prevalence of early graft dysfunction in patients after liver transplant: A randomized clinical trial. *Exp. Clin. Transplant.* **2020**, *18*, 598–604. [[CrossRef](#)] [[PubMed](#)]
2. Fletcher, D.; Martinez, V. Opioid-induced hyperalgesia in patients after surgery: A systematic review and a meta-analysis. *Br. J. Anaesth.* **2014**, *112*, 991–1004. [[CrossRef](#)] [[PubMed](#)]
3. Yu, E.H.; Tran, D.H.; Lam, S.W.; Irwin, M.G. Remifentanyl tolerance and hyperalgesia: Short-term gain, long-term pain? *Anaesthesia* **2016**, *71*, 1347–1362. [[CrossRef](#)] [[PubMed](#)]
4. Chia, Y.Y.; Liu, K.; Wang, J.J.; Kuo, M.C.; Ho, S.T. Intraoperative high dose fentanyl induces postoperative fentanyl tolerance. *Can. J. Anaesth.* **1999**, *46*, 872–877. [[CrossRef](#)]
5. Rupniewska-Ladyko, A.; Malec-Milewska, M.A. High dose of fentanyl may accelerate the onset of acute postoperative pain. *Anesthesiol. Pain Med.* **2019**, *9*, e94498. [[CrossRef](#)] [[PubMed](#)]
6. Hong, H.K.; Ma, Y.; Xie, H. TRPV1 and spinal astrocyte activation contribute to remifentanyl-induced hyperalgesia in rats. *Neuroreport* **2019**, *30*, 1095–1101. [[CrossRef](#)] [[PubMed](#)]
7. Deng, L.; Zhang, L.; Zhao, H.; Song, F.; Chen, G.; Zhu, H. The role of p38MAPK activation in spinal dorsal horn in remifentanyl-induced postoperative hyperalgesia in rats. *Neurol. Res.* **2016**, *38*, 929–936. [[CrossRef](#)]
8. Lv, C.C.; Xia, M.L.; Shu, S.J.; Chen, F.; Jiang, L.S. Attenuation of remifentanyl-induced hyperalgesia by betulinic acid associates with inhibiting oxidative stress and inflammation in spinal dorsal horn. *Pharmacology* **2018**, *102*, 300–306. [[CrossRef](#)]
9. Li, T.; Wang, H.; Wang, J.; Chen, Y.; Yang, C.; Zhao, M.; Wang, G.; Yang, Z. Annexin 1 inhibits remifentanyl-induced hyperalgesia and NMDA receptor phosphorylation via regulating spinal CXCL12/CXCR4 in rats. *Neurosci. Res.* **2019**, *144*, 48–55. [[CrossRef](#)]
10. Lu, A.; Lei, H.; Li, L.; Lai, L.; Liang, W.; Xu, S. Role of mitochondrial Ca<sup>2+</sup> uniporter in remifentanyl-induced postoperative allodynia. *Eur. J. Neurosci.* **2018**, *47*, 305–313. [[CrossRef](#)]

11. Li, S.; Zeng, J.; Wan, X.; Yao, Y.; Zhao, N.; Yu, Y.; Yu, C.; Xia, Z. Enhancement of spinal dorsal horn neuron NMDA receptor phosphorylation as the mechanism of remifentanil induced hyperalgesia: Roles of PKC and CaMKII. *Mol. Pain* **2017**, *13*, 1–33. [[CrossRef](#)] [[PubMed](#)]
12. Lu, C.; Shi, L.; Zhang, J.; Kong, M.; Liu, Y.; Zhou, Y.; Xu, L.; He, J.; Ma, Z.; Gu, X. Neuron-restrictive silencer factor in periaqueductal gray contributes to remifentanil-induced postoperative hyperalgesia via repression of the mu-opioid receptor. *J. Neurol. Sci.* **2015**, *352*, 48–52. [[CrossRef](#)]
13. Ye, L.; Xiao, L.; Yang, S.Y.; Duan, J.J.; Chen, Y.; Cui, Y.; Chen, Y. Cathepsin S in the spinal microglia contributes to remifentanil-induced hyperalgesia in rats. *Neuroscience* **2017**, *344*, 265–275. [[CrossRef](#)] [[PubMed](#)]
14. Xuerong, Y.; Yuguang, H.; Xia, J.; Hailan, W. Ketamine and lornoxicam for preventing a fentanyl-induced increase in postoperative morphine requirement. *Anesth. Analg.* **2008**, *107*, 2032–2037. [[CrossRef](#)] [[PubMed](#)]
15. Cooper, D.W.; Lindsay, S.L.; Ryall, D.M.; Kokri, M.S.; Eldabe, S.S.; Lear, G.A. Does intrathecal fentanyl produce acute cross-tolerance to i.v. morphine? *Br. J. Anaesth.* **1997**, *78*, 311–313. [[CrossRef](#)] [[PubMed](#)]
16. Carvalho, B.; Drover, D.R.; Ginosar, Y.; Cohen, S.E.; Riley, E.T. Intrathecal fentanyl added to bupivacaine and morphine for cesarean delivery may induce a subtle acute opioid tolerance. *Int. J. Obstet. Anesth.* **2012**, *21*, 29–34. [[CrossRef](#)]
17. Yildirim, V.; Doganci, S.; Cinar, S.; Eskin, M.B.; Ozkan, G.; Eksert, S.; Ince, M.E.; Dogrul, A. Acute high dose-fentanyl exposure produces hyperalgesia and tactile allodynia after coronary artery bypass surgery. *Eur. Rev. Med. Pharmacol. Sci.* **2014**, *18*, 3425–3434.
18. Richebé, P.; Rivat, C.; Laulin, J.P.; Maurette, P.; Simonnet, G. Ketamine improves the management of exaggerated postoperative pain observed in perioperative fentanyl-treated rats. *Anesthesiology* **2005**, *102*, 421–428. [[CrossRef](#)]
19. Li, Q.B.; Chang, L.; Ye, F.; Luo, Q.H.; Tao, Y.X.; Shu, H.H. Role of spinal cyclooxygenase-2 and prostaglandin E2 in fentanyl-induced hyperalgesia in rats. *Br. J. Anaesth.* **2018**, *120*, 827–835. [[CrossRef](#)]
20. Chang, L.; Ye, F.; Luo, Q.; Tao, Y.; Shu, H. Increased hyperalgesia and proinflammatory cytokines in the spinal cord and dorsal root ganglion after surgery and/or fentanyl administration in rats. *Anesth. Analg.* **2018**, *126*, 289–297. [[CrossRef](#)]
21. Li, Z.; Yin, P.; Chen, J.; Jin, S.; Liu, J.; Luo, F. CaMKII $\alpha$  may modulate fentanyl-induced hyperalgesia via a CeLC-PAG-RVM-spinal cord descending facilitative pain pathway in rats. *PLoS ONE* **2017**, *12*, e0177412. [[CrossRef](#)] [[PubMed](#)]
22. Wei, X.; Wei, W. Role of gabapentin in preventing fentanyl- and morphine-withdrawal-induced hyperalgesia in rats. *J. Anesth.* **2012**, *26*, 236–241. [[CrossRef](#)] [[PubMed](#)]
23. Caires, S.; Steenkamp, V. Use of Yokukansan (TJ-54) in the treatment of neurological disorders: A review. *Phytother. Res.* **2010**, *24*, 1265–1270. [[CrossRef](#)] [[PubMed](#)]
24. Ikarashi, Y.; Mizoguchi, K. Neuropharmacological efficacy of the traditional Japanese Kampo medicine yokukansan and its active ingredients. *Pharmacol. Ther.* **2016**, *166*, 84–95. [[CrossRef](#)]
25. Nakamura, Y.; Tajima, K.; Kawagoe, I.; Kanai, M.; Mitsuhata, H. Efficacy of traditional herbal medicine, Yokukansan on patients with neuropathic pain. *Masui. Jpn. J. Anesthesiol.* **2009**, *58*, 1248–1255. (In Japanese, English Abstract)
26. Yamaguchi, K. Traditional Japanese herbal medicines for treatment of odontopathy. *Front. Pharmacol.* **2015**, *6*, 176. [[CrossRef](#)]
27. Sugasawa, Y. Effect of Yokukansan, Japanese Herbal Medicine, on Phantom-limb pain. *Middle East J. Anaesthesiol.* **2016**, *23*, 499–500.
28. Akiyama, H.; Hasegawa, Y. Effectiveness of the traditional Japanese Kampo medicine Yokukansan for chronic migraine: A case report. *Medicine (Baltimore)* **2019**, *98*, e17000. [[CrossRef](#)]
29. Suzuki, Y.; Mitsuhata, H.; Yuzurihara, M.; Kase, Y. Antiallodynic effect of herbal medicine yokukansan on peripheral neuropathy in rats with chronic constriction injury. *Evid. Based Complement. Altern. Med.* **2012**, *2012*, 953459. [[CrossRef](#)]
30. Ebisawa, S.; Andoh, T.; Shimada, Y.; Kuraishi, Y. Yokukansan improves mechanical allodynia through the regulation of interleukin-6 expression in the spinal cord in mice with neuropathic pain. *Evid. Based Complement. Altern. Med.* **2015**, *2015*, 870687. [[CrossRef](#)]
31. Suga, H.; Sunagawa, M.; Ikemoto, H.; Nakanishi, T.; Fujiwara, A.; Okada, M. The analgesic and anti-stress effects of a Kampo medicine (Yokukansan) in rats with chronic constriction injury—A comparative study with kamishoyosan. *J. Integr. Med. Ther.* **2015**, *2*, 5. [[CrossRef](#)]

32. Honda, Y.; Sunagawa, M.; Yoneyama, S.; Ikemoto, H.; Nakanishi, T.; Iwanami, H.; Hisamitsu, T. Analgesic and anti-stress effects of Yokukansan in rats with adjuvant arthritis. *Kampo Med.* **2013**, *64*, 78–85. [[CrossRef](#)]
33. Takemoto, M.; Sunagawa, M.; Okada, M.; Ikemoto, H.; Suga, H.; Katayama, A.; Otake, H.; Hisamitsu, T. Yokukansan, a Kampo medicine, prevents the development of morphine tolerance through the inhibition of spinal glial cell activation in rats. *Integr. Med. Res.* **2016**, *5*, 41–47. [[CrossRef](#)]
34. Katayama, A.; Kanada, Y.; Tsukada, M.; Akanuma, Y.; Takemura, H.; Ono, T.; Suga, H.; Mera, H.; Hisamitsu, T.; Sunagawa, M. Yokukansan (Kampo medicinal formula) prevents the development of morphine tolerance by inhibiting the secretion of orexin A. *Integr. Med. Res.* **2018**, *7*, 141–148. [[CrossRef](#)] [[PubMed](#)]
35. Kawakami, Z.; Ikarashi, Y.; Kase, Y. Isoliquiritigenin is a novel NMDA receptor antagonist in kampo medicine yokukansan. *Cell Mol. Neurobiol.* **2011**, *31*, 1203–1212. [[CrossRef](#)]
36. Kawakami, Z.; Omiya, Y.; Mizoguchi, K. Comparison of the effects of Yokukansan and Yokukansankachimpihange on glutamate uptake by cultured astrocytes and glutamate-induced excitotoxicity in cultured PC12 cells. *Evid. Based Complement. Altern. Med.* **2019**, *2019*, 9139536. [[CrossRef](#)]
37. Takeda, A.; Itoh, H.; Tamano, H.; Yuzurihara, M.; Oku, N. Suppressive effect of Yokukansan on excessive release of glutamate and aspartate in the hippocampus of zinc-deficient rats. *Nutr. Neurosci.* **2008**, *11*, 41–46. [[CrossRef](#)]
38. Vissers, K.C.; Geenen, F.; Biermans, R.; Meert, T.F. Pharmacological correlation between the formalin test and the neuropathic pain behavior in different species with chronic constriction injury. *Pharmacol. Biochem. Behav.* **2006**, *84*, 479–486. [[CrossRef](#)]
39. McNamara, C.R.; Mandel-Brehm, J.; Bautista, D.M.; Siemens, J.; Deranian, K.L.; Zhao, M.; Hayward, N.J.; Chong, J.A.; Julius, D.; Moran, M.M.; et al. TRPA1 mediates formalin-induced pain. *Proc. Natl. Acad. Sci. USA* **2007**, *104*, 13525–13530. [[CrossRef](#)]
40. Sałat, K.; Filipek, B. Antinociceptive activity of transient receptor potential channel TRPV1, TRPA1, and TRPM8 antagonists in neurogenic and neuropathic pain models in mice. *J. Zhejiang Univ. Sci. B* **2015**, *16*, 167–178. [[CrossRef](#)]
41. Latremoliere, A.; Woolf, C.J. Central sensitization: A generator of pain hypersensitivity by central neural plasticity. *J. Pain* **2009**, *10*, 895–926. [[CrossRef](#)] [[PubMed](#)]
42. Ji, R.R.; Gereau, R.W., IV; Malcangio, M.; Strichartz, G.R. MAP kinase and pain. *Brain Res. Rev.* **2009**, *60*, 135–148. [[CrossRef](#)] [[PubMed](#)]
43. Nakagawa, T.; Nagayasu, K.; Nishitani, N.; Shirakawa, H.; Sekiguchi, K.; Ikarashi, Y.; Kase, Y.; Kaneko, S. Yokukansan inhibits morphine tolerance and physical dependence in mice: The role of  $\alpha_2$  A-adrenoceptor. *Neuroscience* **2012**, *227*, 336–349. [[CrossRef](#)] [[PubMed](#)]
44. Takayama, Y.; Derouiche, S.; Maruyama, K.; Tominaga, M. Emerging perspectives on pain management by modulation of TRP channels and ANO1. *Int. J. Mol. Sci.* **2019**, *20*, 3411. [[CrossRef](#)]
45. Forster, A.B.; Reeh, P.W.; Messlinger, K.; Fischer, M.J. High concentrations of morphine sensitize and activate mouse dorsal root ganglia via TRPV1 and TRPA1 receptors. *Mol. Pain* **2009**, *5*, 17. [[CrossRef](#)]
46. Kanada, Y.; Katayama, A.; Ikemoto, H.; Takahashi, K.; Tsukada, M.; Nakamura, A.; Ishino, S.; Hisamitsu, T.; Sunagawa, M. Inhibitory effect of the Kampo medicinal formula Yokukansan on acute stress-induced defecation in rats. *Neuropsychiatr. Dis. Treat.* **2018**, *14*, 937–944. [[CrossRef](#)]
47. Gamal-Eltrabily, M.; Espinosa de Los Monteros-Zúñiga, A.; Manzano-García, A.; Martínez-Lorenzana, G.; Condés-Lara, M.; González-Hernández, A. The Rostral Agranular Insular Cortex, a New Site of Oxytocin to Induce Antinociception. *J. Neurosci.* **2020**, *40*, 5669–5680. [[CrossRef](#)]
48. Zhuang, Z.Y.; Gerner, P.; Woolf, C.J.; Ji, R.R. ERK is sequentially activated in neurons, microglia, and astrocytes by spinal nerve ligation and contributes to mechanical allodynia in this neuropathic pain model. *Pain* **2005**, *114*, 149–159. [[CrossRef](#)]
49. Karim, F.; Wang, C.C.; Gereau, R.W., IV. Metabotropic glutamate receptor subtypes 1 and 5 are activators of extracellular signal-regulated kinase signaling required for inflammatory pain in mice. *J. Neurosci.* **2001**, *21*, 3771–3779. [[CrossRef](#)]
50. Tsuda, M.; Ishii, S.; Masuda, T.; Hasegawa, S.; Nakamura, K.; Nagata, K.; Yamashita, T.; Furue, H.; Tozaki-Saitoh, H.; Yoshimura, M.; et al. Reduced pain behaviors and extracellular signal-related protein kinase activation in primary sensory neurons by peripheral tissue injury in mice lacking platelet-activating factor receptor. *J. Neurochem.* **2007**, *102*, 1658–1668. [[CrossRef](#)]



51. Ma, Y.; Bao, Y.; Wang, S.; Li, T.; Chang, X.; Yang, G.; Meng, X. Anti-inflammation effects and potential mechanism of saikosaponins by regulating nicotinate and nicotinamide metabolism and arachidonic acid metabolism. *Inflammation* **2016**, *39*, 1453–1461. [[CrossRef](#)] [[PubMed](#)]
52. Zhu, J.; Luo, C.; Wang, P.; He, Q.; Zhou, J.; Peng, H. Saikosaponin A mediates the inflammatory response by inhibiting the MAPK and NF- $\kappa$ B pathways in LPS-stimulated RAW 264.7 cells. *Exp. Ther. Med.* **2013**, *5*, 1345–1350. [[CrossRef](#)]
53. Jiang, Y.X.; Dai, Y.Y.; Pan, Y.F.; Wu, X.M.; Yang, Y.; Bian, K.; Zhang, D.D. Total flavonoids from radix glycyrrhiza exert anti-inflammatory and antitumorigenic effects by inactivating iNOS signaling pathways. *Evid. Based Complement. Altern. Med.* **2018**, *2018*, 6714282. [[CrossRef](#)] [[PubMed](#)]
54. Yang, E.J.; Park, G.H.; Song, K.S. Neuroprotective effects of liquiritigenin isolated from licorice roots on glutamate-induced apoptosis in hippocampal neuronal cells. *Neurotoxicology* **2013**, *39*, 114–123. [[CrossRef](#)] [[PubMed](#)]
55. Roeckel, L.A.; Le Coz, G.M.; Gavériaux-Ruff, C.; Simonin, F. Opioid-induced hyperalgesia: Cellular and molecular mechanisms. *Neuroscience* **2016**, *338*, 160–182. [[CrossRef](#)] [[PubMed](#)]

**Publisher's Note:** MDPI stays neutral with regard to jurisdictional claims in published maps and institutional affiliations.



© 2020 by the authors. Licensee MDPI, Basel, Switzerland. This article is an open access article distributed under the terms and conditions of the Creative Commons Attribution (CC BY) license (<http://creativecommons.org/licenses/by/4.0/>).

Review

# PARP Inhibitors in Biliary Tract Cancer: A New Kid on the Block?

Angela Dalia Ricci <sup>1,†</sup>, Alessandro Rizzo <sup>1,\*†</sup>, Chiara Bonucci <sup>1</sup>, Nastassja Tober <sup>1</sup>,  
Andrea Palloni <sup>1</sup>, Veronica Mollica <sup>1</sup>, Ilaria Maggio <sup>1</sup>, Marzia Deserti <sup>2</sup>, Simona Tavolari <sup>2</sup>  
and Giovanni Brandi <sup>1</sup>

<sup>1</sup> Department of Experimental, Diagnostic and Specialty Medicine, S.Orsola-Malpighi Hospital, University of Bologna, 40128 Bologna, Italy; dalia.ricci@gmail.com (A.D.R.); chiarabonucci1@gmail.com (C.B.); nastassja@cheapnet.it (N.T.); andrepalloni@gmail.com (A.P.); veronica.mollica7@gmail.com (V.M.); ila.mag88@gmail.com (I.M.); giovanni.brandi@unibo.it (G.B.)

<sup>2</sup> Center of Applied Biomedical Research, S. Orsola-Malpighi University Hospital, 40128 Bologna, Italy; marzia.deserti@gmail.com (M.D.); simona.tavolari@unibo.it (S.T.)

\* Correspondence: rizzo.alessandro179@gmail.com

† These authors contributed equally to this study.

Received: 26 July 2020; Accepted: 29 August 2020; Published: 31 August 2020

**Abstract:** Poly adenosine diphosphate-ribose polymerase inhibitors (PARPi) represent an effective therapeutic strategy for cancer patients harboring germline and somatic aberrations in DNA damage repair (DDR) genes. *BRCA1/2* mutations occur at 1–7% across biliary tract cancers (BTCs), but a broader spectrum of DDR gene alterations is reported in 28.9–63.5% of newly diagnosed BTC patients. The open question is whether alterations in genes that are well established to have a role in DDR could be considered as emerging predictive biomarkers of response to platinum compounds and PARPi. Currently, data regarding PARPi in BTC patients harboring BRCA and DDR mutations are sparse and anecdotal; nevertheless, a variety of clinical trials are testing PARPi as monotherapy or in combination with other anticancer agents. In this review, we provide a comprehensive overview regarding the genetic landscape of DDR pathway deficiency, state of the art and future therapeutic implications of PARPi in BTC, looking at combination strategies with immune-checkpoint inhibitors and other anticancer agents in order to improve survival and quality of life in BTC patients.

**Keywords:** biliary tract cancer; cholangiocarcinoma; PARP; BRCA; olaparib; rucaparib; liver cancer

## 1. Introduction

Biliary tract cancers (BTCs) are a relatively rare group of malignancies arising from different anatomical locations of the biliary tree and including intrahepatic cholangiocarcinoma (iCCA), extrahepatic cholangiocarcinoma (eCCA), gallbladder cancer (GBC), and ampulla of Vater cancer (AVC) (Figure 1) [1,2].

BTC represents the second most frequent primary liver cancer after hepatocellular carcinoma (HCC), accounting for about 3% of all gastrointestinal tumors [3,4]. The incidence of BTC has increased in both western and eastern countries in the past two decades, concurrently with the rising incidence of iCCA, probably related to changes in tumor classification and better disease recognition [5]. Despite recent advances in the management of localized and metastatic disease, the prognosis of BTC patients remains dismal since the majority of cases are often diagnosed when unresectable or metastatic and the 5-year survival for patients with distant disease is about 5% [6]. To date, radical surgery is the only curative treatment option for BTC, but unfortunately, these malignancies are frequently asymptomatic in early stages, and approximately 40% of the patients considered resectable at the moment of diagnosis are found to be unresectable during exploratory laparotomy [7,8]. Systemic chemotherapy is the backbone

of palliative treatment for BTC patients, with the combination of cisplatin plus gemcitabine representing the current standard of care in the front-line setting, following the results of the ABC-02 trial [9]. Although this phase III trial showed a survival advantage for cisplatin–gemcitabine over gemcitabine monotherapy, nearly all BTC patients develop progressive disease during first-line treatment, with a median overall survival (OS) of less than a year [10]. Thus, improving outcomes in patients affected by advanced/metastatic BTC represents an urgent need.

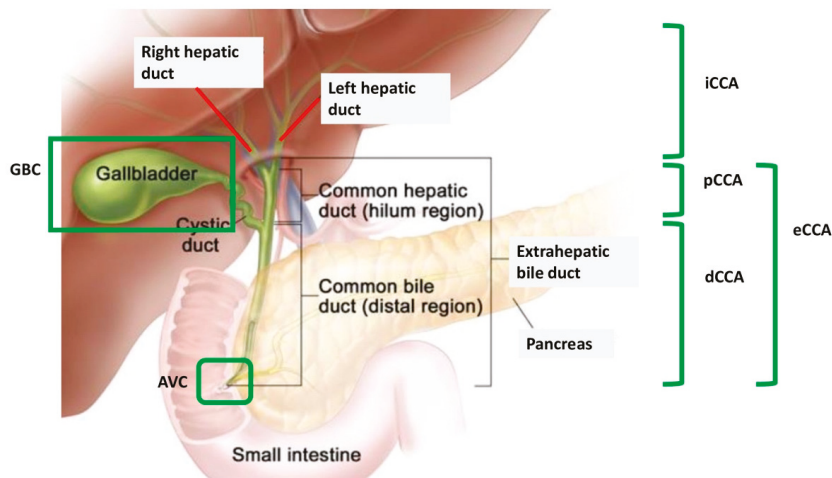


**Figure 1.** Anatomical subvariants of biliary tract cancer. AVC: ampulla of Vater cancer; dCCA: distal cholangiocarcinoma; eCCA: extrahepatic cholangiocarcinoma; GBC: gallbladder cancer; iCCA: intrahepatic cholangiocarcinoma; pCCA: perihilar cholangiocarcinoma.

In recent years, an unprecedented amount of genomic studies has begun to unveil the complex molecular landscape of BTC, shedding new light on novel therapeutic opportunities of this poor-prognosis malignancy and opening the era of tailor-made oncology in BTC [11]. In fact, the emergence of novel therapies is modifying previous treatment algorithms for BTC—especially in iCCA, where targeting isocitrate dehydrogenase (IDH) mutations and fibroblast growth factor receptor (FGFR) fusions is entering in clinical practice [12]. Comprehensive sequencing studies of BTC showed that nearly 40% of patients harbor a potentially targetable genetic alteration, emphasizing the genomic complexity of the disease, with several reports that have been focused on cell-cycle dysregulation, DNA damage repair (DDR) pathway deficiency, and genomic instability [13].

*BRCA1/2* are the most well-studied DDR genes, and their prevalence fluctuates from 1% to 7% in patients affected by BTC [13], with *BRCA2* suggested to be more frequent in GBC [14]. Although these mutations generally correlate with poor response to standard treatments, previous reports about BTC suggested a role for platinum salts and poly (ADP-ribose) polymerase-inhibitors (PARPi) as successful therapeutic options in somatic and/or germline *BRCA* mutations (*BRCAm*) carriers [15]. Evidence from phase III clinical trials has led to PARPi approval in breast and ovarian cancers, and the use of PARPi is going to be extended also to prostate and pancreatic cancer [16–18]. In fact, from the first launch of the PARPi olaparib in 2014, recent years have seen the FDA approval of other PARPi, including niraparib, rucaparib, and talazoparib in distinct settings [16,19]. More specifically, niraparib can be actually used as maintenance therapy in recurrent platinum-sensitive epithelial ovarian cancer following the results of the PRIMA/ENGOT-OV26/GOG-3012 trial [16]. In this randomized phase III trial, median progression-free survival (PFS) was significantly longer in the niraparib arm compared to that in the placebo group (21.9 versus 10.4 months) in patients affected by advanced ovarian cancer experiencing response to platinum-based chemotherapy. Similarly, many other PARPi have also

entered clinical practice, as in the case of breast cancer where the OlympiAD and the EMBRACA trials have opened the doors of a new world, inaugurating the “PARPi Era” in HER2-negative *BRCAm* metastatic breast cancer [20,21]. According to OlympiAD—comparing olaparib monotherapy with single-agent chemotherapy of the physician’s choice (capecitabine, eribulin, or vinorelbine)—olaparib treatment provided a significant benefit in terms of PFS, with risk of disease progression or death 42% lower with olaparib single-agent than with chemotherapy [20]. With a study design similar to OlympiAD, the randomized phase III EMBRACA trial compared talazoparib versus standard single-agent chemotherapy of the physician’s choice (capecitabine, eribulin, gemcitabine, or vinorelbine) in advanced breast cancer patients with germline *BRCAm*, observing that talazoparib provided a statistically significant benefit in terms of PFS (8.6 versus 5.6 months; Hazard Ratio 0.54; 95% CI, 0.41–0.71,  $p < 0.001$ ) [21]. Moreover, PARPi have shown an overall manageable safety profile, with hematological toxicity—mainly anemia—representing the most frequent adverse event [20,21]. In fact, incidence of grade 3–4 anemia has been reported to be around 19% in subjects receiving olaparib or rucaparib, 25% in niraparib, and 23% in patients treated with talazoparib [22] while neutropenia and thrombocytopenia ranges from 10% to 27%; thus, a strict monitoring on blood cell counts should be conducted in patients receiving these treatments [22].

As previously stated, previous experiences in ovarian and breast cancer have paved the way toward a number of trials testing PARPi in several tumors, with PARPi that are currently under active evaluation also in BRCA-mutated biliary malignancies [8–10]. However, a larger spectrum of genes that compromise DDR pathway has been reported to occur in up to 28.9% of patients with newly diagnosed BTC, and to date, the optimal therapeutic strategy in BTC tumors harboring Homologous Recombination Deficiency (HRD) alterations is yet to be defined [23].

In this review, we provide a comprehensive overview regarding the genetic landscape of DDR pathway deficiency, the emerging therapeutic role of PARPi in BTC, and current perspectives and possible future therapeutic implications of DDR alterations across BTC.

## 2. HRD, the Role of PARP in DDR and Synthetic Lethality

DNA damage and DNA repair, or lack thereof, have central importance in the induction of mutations. Additionally, since mutations drive the onset of nearly all malignancies, in physiological conditions, cells activate to defend themselves through a series of molecular pathways, the DDR, in order to handle genotoxic damage usually arising as single-strand breaks (SSBs) or double-strand breaks (DSBs) (Figure 2) [24].

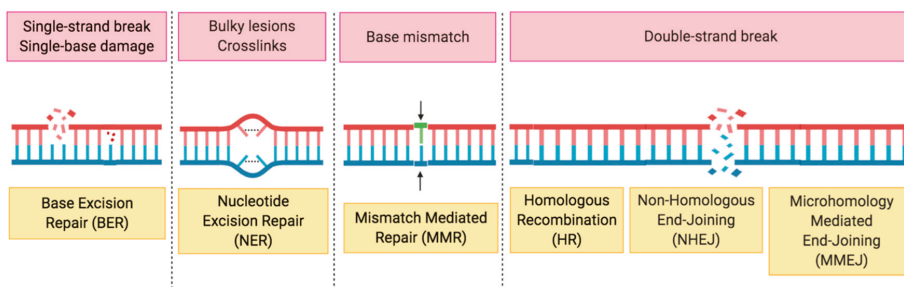


**Figure 2.** Overview of DNA repair mechanisms. BER: base excision repair; HR: homologous recombination; MMEJ: microhomology mediated end-joining; MMR: mismatch mediated repair; NER: nucleotide excision repair; NHEJ: non-homologous end-joining.

Critical pathways able to fix DSBs are homologous recombination repair (HRR)—a form of DNA repair using homologous DNA sequences—microhomology mediated end-joining (MMEJ), and non-homologous end-joining (NHEJ), which conversely often leads to genetic material loss,

thus resulting in genetic alterations [25,26]. Conversely, SSBs are mainly repaired by mechanisms such as base excision repair (BER), nucleotide excision repair (NER), or mismatch mediated repair (MMR) (Figure 2) [27,28]. Key elements in the DDR are the PARP enzymes, having an important role in SSBs repair and also taking part in HRR and NHEJ [29].

PARP (poly (ADP-ribose) polymerase) is a family of enzymes, including PARP1, PARP2, and PARP3 [30]. Interestingly, PARP1 is responsible for almost 80–90% of DDR activity, and in terms of structure, PARP1 presents a DNA binding domain at the N-terminus, with three zinc-finger-related domains able to recognize sites of damaged sequences [31]; moreover, PARP1 has a catalytic domain encompassing two subdomains: a helical domain and an ADP-ribosyltransferase catalytic transferring the ADP-ribose from NAD<sup>+</sup> to protein residues, generating poly(ADP-ribose) chains (PAR) [32,33]. In fact, PARP1 and PARP2 are DNA damage sensors and signal transducers, able to synthesize branched PAR chains on target proteins through a process termed PARylation [34]. When PARP1 binds DNA, the catalytic function of PARP1 is activated following several allosteric modifications, leading to PARylation and recruitment of DNA repair effectors, including XRCC1 [35].

*BRCA1* and *BRCA2* are fundamental genes involved in HRR [36] and since they are critical in the process of DSBs repair, *BRCA1/2* germline mutations are associated with higher risk of carcinogenesis due to a mutational event on the other allele [37]. The same occurs when other genes essential for HRR are mutated, resulting in HRD [38–40].

PARPi are oral small-molecule inhibitors of PARP1, PARP2, and PARP3, whose action is based on synthetic lethality, a well-known concept proposed nearly a century ago [41,42]. As schematically represented in Figure 3, according to synthetic lethality the concurrent alteration of two different genes results in cell death while the alteration of a single gene does not. In the specific case of cancer treatment, with gene *A* representing a tumor suppressor gene or an oncogene, gene *B* could represent a candidate therapeutic target which may be used in order to target cells with *A* dysfunction.

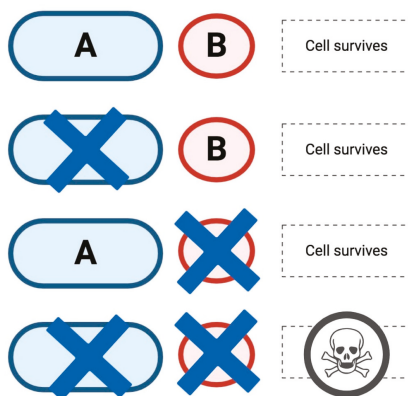


**Figure 3.** Schematic figure representing synthetic lethality. As outlined, the simultaneous alteration of gene *A* and gene *B* results in cell death while the alteration of either gene does not. When the concept of synthetic lethality is applied to poly adenosine diphosphate-ribose polymerase inhibitors (PARPi) treatment, gene *B* represents a candidate therapeutic target used to target cells with gene *A* dysfunctions.

The inhibition of PARP causes the persistence of SSBs, resulting in DSBs [43,44]. More specifically, there are two main mechanisms of action of PARPi, both responsible for their antitumoral effect. First, PARPi inhibit catalytic activity of the enzyme by avoiding both PARylation of the repair site and autoPARylation [45]. The second and even more significant mechanism is represented by PARP trapping activity; in fact, PARPi trap PARP at its DNA binding site preventing repair processes, resulting in cell death by mitotic catastrophe [46,47]. Moreover, the inhibition of this pathway

can force cells to use alternative damage repair systems, namely non-homologous recombination processes [48,49], which are more error-prone and can result in large-scale genomic rearrangements, and finally, in apoptotic cell death [50].

### 3. DDR Deficiency and *BRCAm* in BTC

The role of DDR alterations is still widely unknown in BTC and only few data about their clinical impact are currently available [51]. However, germline or somatic *BRCAm* are being increasingly reported due to the possibility to identify a distinct subgroup of carriers that may benefit from a personalized treatment strategy [52,53]. Curiously, *BRCAm* in BTC have been observed more frequently as somatic rather than as germline mutations [54].

The prevalence of DDR defects in BTC has been described in a range between 28.9% and 63.5%, and unfortunately, this range of frequencies depends on current lack of consensus regarding methods for testing and defining DDR alterations in BTC [54,55]. The recent evolution of sequencing technologies and the use of comprehensive gene sequencing panels has resulted in improved ability to detect variations in DDR genes, beyond *BRCA1/2* [56]. Nevertheless, two major limitations of these methods are represented by the unclear functional role of variants of unknown significance in DDR genes and the inability to identify epigenetic silencing of the same genes [57]. Moreover, the main open question is whether defects in genes that are well established to have a role in DDR could be considered as predictive biomarkers of response to platinum compounds and PARPi [58].

Another issue concerns how many germline and somatic pathogenic variants should be tested in order to identify “BRCAness” phenotypes [59]. A panel of 17 germline and somatic DDR gene alterations (*ATM*, *BAP1*, *BARD1*, *BLM*, *BRCA1*, *BRCA2*, *BRIPI*, *CHEK2*, *FAM175A*, *FANCA*, *FANCC*, *NBN*, *PALB2*, *RAD50*, *RAD51*, *RAD51C*, and *RTEL1*) in addition to *BRCAm* has been recently proposed in order to evaluate a correlation with genomic instability in patients affected by pancreatic ductal adenocarcinoma (PDAC), thereby excluding potential emerging DDR genes such as *ARID1A*, *ATR*, *ATRX*, *CHEK1*, *RAD51L1*, and *RAD51L3* [60]. Notably, mutations in *ARID1A* have been reported in up to 14% of cholangiocarcinomas (CCAs) [61], and interestingly, *ARID1A*—a chromatin remodeler of the SWI/SNF (Switch/Sucrose Non-Fermentable) family—probably contributes to recruiting and stabilizing the SWI/SNF complex at DSBs, thus regulating the DNA damage checkpoint [62,63]. Moreover, evidence from in vivo and in vitro studies suggested that *ARID1A* deficiency may sensitize cancer cells to PARPi [57]. Another gene involved in HR mechanisms is *BAP1*, a tumor suppressor gene and a deubiquitinase promoting DNA DSBs repair [64]. Yu and colleagues suggested that BAP1-deficient cells were sensitive to ionizing radiation and other agents that induce DNA DSBs [65], and additionally, *BAP1* mutant CCAs are likely to have poorer prognosis and a predisposition to bone metastasis development [66].

Patients with *BRCAm* are predisposed for BTC, as *BRCA1/2* alterations have been associated with early onset BTC [51–54]. More specifically, data from the early 2000s by the Breast Cancer Linkage Consortium (BCLC) suggested that *BRCA2*-carriers had higher relative risk (RR) of developing BTC than patients affected by infection with liver parasites, hepatitis C virus, and hepatitis B virus (RR 4.97, 95% confidence interval (CI) 1.50–16.52) [67].

Importantly, defective DNA repair enhances tumor heterogeneity and promotes tumor progression [68]. Hence, *BRCAm* generally correlate with poor response to standard treatments, although notable responses to platinum-based treatment or PARPi have been reported [69]. In 2017, Golan and colleagues published a retrospective analysis of 18 patients with confirmed *BRCAm* CCA [15]. Interestingly, the 44% of patients (8 of 18) had personal or family history of *BRCA*-associated malignancy (breast, ovarian, prostate, and pancreatic cancer) [15]. Overall, clinical germline testing for BTC risk is currently not recommended in clinical practice and more efforts are needed to better identify high-risk groups that might benefit from screening, further exploring, and eventually confirming the potential predictive and prognostic value of DDR gene alterations.

#### 4. PARPi in BTC

Available data regarding PARPi in BTC patients harboring *BRCAM* and DDR mutations are sparse and anecdotal, with OS ranging from 11 to 65 months and sporadic cases of sustained response to PARPi, which have been reported [15,70–72]. As previously stated, although based on a small number of subjects, the multicenter retrospective study by Golan and colleagues suggested some clinical features of patients affected by BTC with germline and/or somatic *BRCAM* [15]. The study included 18 patients, 5 with germline *BRCAM* and 13 with somatic mutations; interestingly, 13 patients were treated with platinum-based chemotherapy and 4 with PARPi. In terms of survival, BTC patients with stage I–stage II presented a median OS of 40.3 months (95% CI, 6.73–108.15) and of 25 months in stage III–stage IV BTC [15]. According to the results of this study, the presence of *BRCAM* appeared to carry a more favorable prognosis since patients experienced a prolonged survival compared to historical data regarding BTC [15]. In a recent report by Chae et al., DDR gene mutations were observed in 55 out of 88 (63.5%) patients receiving first-line platinum-based chemotherapy for advanced BTC, with DDR gene mutations associated with longer OS (21.0 vs. 13.3 months,  $p = 0.009$ ) and PFS (6.9 vs. 5.7 months,  $p = 0.013$ ) after treatment with platinum salts [52]. This association between platinum sensitivity and DDR gene mutations has been widely described in other malignancies, including ovarian and breast cancer [73–75]. Platinum salts such as carboplatin and cisplatin exert their cytotoxic effects through distinct cellular mechanisms [76]; more specifically, after entrance into cells, platinum salts react with DNA generating monoadducts, inter- and intraDNA strand cross-links, and are able to cause SSBs and DSBs [77]. Consequently, DNA replication and transcription are blocked by this structural distortion, resulting in cell cycle arrest, cell apoptosis, and necrosis [78]. In physiological conditions, DNA lesions caused by platinum salts are properly repaired by DDR mechanisms; therefore, since platinum salts are DNA cross-linking agents, it is readily apparent that these compounds are more likely to be effective in *BRCAM* malignancies [79]. For example, higher rates of pathological complete response have been observed in *BRCAM*, triple negative breast cancer patients treated with neoadjuvant platinum salts compared to wild-type subjects [80]. Similarly, the randomized *TNT* trial highlighted a notable response rate and PFS benefit in metastatic *BRCAM* breast cancer patients receiving carboplatin compared to those receiving docetaxel [81]. This topic is particularly important if we look at BTC, where platinum-based chemotherapy represents the mainstay of palliative treatment following the results of the landmark ABC-02 trial and the more recent ABC-06 study [9,82,83].

To date, there is no evidence in literature regarding the efficacy of PARPi in BTC patients harboring DDR gene alterations, with the exception of a recent case report demonstrating a clinical benefit with olaparib monotherapy in a patient affected by gallbladder cancer with an Ataxia telangiectasia mutated (*ATM*)-inactivating mutation [84]. Following several trials assessing PARPi in breast cancer and ovarian cancer, recent studies have tested the role of PARPi in patients affected by HRD gastrointestinal malignancies, with the pivotal POLO trial, which has provided important data in this setting [71]. In fact, this randomized phase III trial has suggested a novel option for precision oncology in PDAC by evaluating the PARPi olaparib (300 mg twice daily) as maintenance in PDAC patients with *BRCAM* and whose disease had not progressed during first-line platinum-based chemotherapy [71]. Among the 154 enrolled patients, PFS was significantly longer in the olaparib maintenance arm compared to that in the placebo group, with 7.4 versus 3.8 months (Hazard Ratio 0.95; 95% CI 0.35–0.82,  $p = 0.004$ ). Meanwhile, in analogy to previous reports in other solid malignancies, olaparib maintenance treatment has presented an acceptable and manageable safety profile, without a significant impact on quality of life [85]. More recently, a recent randomized phase II trial showed impressive response rates (75% and 64%, respectively) and survival in *BRCAM* PDAC patients receiving platinum-based chemotherapy plus the PARPi veliparib or platinum-based chemotherapy alone as front-line treatment [86].

Considering the anatomical and histological analogies with PDAC, and in an attempt to translate this experience, multiple clinical trials are now evaluating the potential role of PARPi in metastatic BTC. We reviewed MEDLINE/PubMed and ClinicalTrial.gov for published or ongoing clinical trials evaluating the efficacy of PARPi in BTC until 20th July 2020. The medical subject heading terms used for

PubMed search were ((olaparib[Title]) OR (veliparib[Title]) OR (rucaparib[Title]) OR (niraparib[Title]) OR (talazoparib[Title]) OR (PARP[Title])) AND ((biliary[Title]) OR (cholangiocarcinoma[Title]) OR (gallbladder[Title])). The medical subject headings terms used for the search in [ClinicalTrials.gov](https://clinicaltrials.gov) were (“Recruiting or not yet recruiting” as status), (“biliary tract cancer”, “biliary tract neoplasm”, “cholangiocarcinoma”, “gallbladder cancer”, “Ampulla cancer” as condition/disease) and (“PARP”, “olaparib”, “veliparib”, “niraparib”, “rucaparib”, or “talazoparib” as other terms). Table 1 summarizes ongoing trials on PARPi in BTC registered on [clinicaltrials.gov](https://clinicaltrials.gov).

**Table 1.** Current ongoing trials involving PARP inhibitors in biliary tract cancer (BTC) registered on [clinicaltrials.gov](https://clinicaltrials.gov).

Clinical Trial	Design	Cohort	Agent(s)	DDR Defect Screenings	Primary Endpoint
NCT03212274	Phase II, single arm	Refractory, metastatic CCA with <i>IDH1</i> or <i>IDH2</i> mutation	Olaparib	no	ORR
NCT03207347 (UF-STO-ETI-001)	Phase II, non-randomized	CCA after prior standard systemic treatment	Niraparib	yes *	ORR
NCT03991832	Phase II, non-randomized	<i>IDH</i> -mutated BTC after no more than 2 previous treatments	Olaparib + durvalumab	no	ORR, DCR
NCT03878095	Phase II, single arm	CCA or other <i>IDH</i> -mutated solid tumors after prior standard treatment	Olaparib + ceralasertib	no	ORR
NCT03639935	Phase II, single arm	BTC after prior standard systemic treatment	Rucaparib + nivolumab	no	Proportion of patients alive and without radiological or clinical progression at 4 months
NCT04042831	Phase II, single arm	BTC with somatic/germline mutations in DDR genes after platinum-based chemotherapy	Olaparib	yes **	ORR
NCT03337087	Phase I-II, single arm	Metastatic BTC after no more than 1 line of prior therapy in the metastatic setting	Nal-IRI and 5-FU with rucaparib	yes, only for phase II ( <i>HRD</i> or <i>BRCA1</i> or <i>BRCA2</i> or <i>PALB2</i> )	dose limiting toxicities, ORR
NCT04171700	Phase II, single arm	Unresectable, locally advanced, or metastatic solid tumor after first-line treatment (including ampullary cancer)	Rucaparib	yes ***	ORR

CCA: cholangiocarcinoma; DCR: disease control rate; DDR: DNA damage repair; 5-FU: 5-fluorouracil; HRD: homologous recombination deficiency; IDH: isocitrate dehydrogenase; Nal-IRI: nanoliposomal irinotecan; ORR: overall response rate; \* somatic/germline mutation of *ARID1A*, *ATM*, *ATR*, *BACH1* [*BRIPI1*, *BAP1*, *BARD1*, *BLM*, *CHEK1*, *CHEK2*, *CDK2*, *CDK4*, *ERCC*, *FAM175A*, *FEN1*, *IDH1*, *IDH2*, *MRE11A*, *NBN* [*NBS1*], *PALB2*, *POLD1*, *PRKDC* [*DNA-PK*], *PTEN*, *RAD50*, *RAD51*, *RAD52*, *RAD54*, *RPA1*, *SLX4*, *WRN*, or *XRCC*; \*\* somatic/germline mutation of *ATM*, *ATR*, *CHEK2*, *BRCA1*, *BRCA2*, *PALB2*, *PTEN*, *FANCA*, *NBN*, *EMSY*, *MRE11*, *ARID1A*; \*\*\* deleterious mutation of *BRCA1*, *BRCA2*, *PALB2*, *RAD51C*, *RAD51D*, *BARD1*, *BRIPI1*, *FANCA*, *NBN*, *RAD51*, or *RAD51B*.



## 5. Future Directions

With the aim to provide novel effective combinations, several ongoing clinical trials are evaluating PARPi in combination with other agents, including cytotoxic chemotherapy, immune-checkpoint inhibitors (ICIs), and tyrosine kinase inhibitors (Table 1) [87].

Early preclinical reports have suggested that PARP1 is implicated in *STAT3* (Signal Transduced and Activator of Transcription 3) dephosphorylation, thus resulting in a reduced transcriptional activity of *STAT3* and lower PD-L1 expression [88]. Conversely, inhibiting PARP would clearly result in higher PD-L1 transcription in cancer cells and Programmed death-ligand 1 (PD-L1) expression [88]. These preliminary findings have paved the way toward a number of studies assessing ICIs combined with PARPi in several malignancies since PARP inhibition has been suggested to increase tumor mutational burden, augmenting DNA damage processes and upregulating PD-L1 expression. The combination of PARPi with PD-1 inhibitors highlighted interesting response rates and a manageable safety profile in early reports evaluating this therapeutic strategy [89]. In a phase I trial assessing the PARPi pamiparib with the PD-1 inhibitor tislelizumab in 25 patients affected by advanced solid tumors, a response rate of 25% was observed, with two complete responses (4%) and eight partial responses (16%) [89]. Interestingly, this study included highly pretreated patients, with 14 out of 25 harboring a germline or somatic *BRCA1/2* mutation. More recently, the report by Spizzo and colleagues on 1292 tumor samples of BTC patients suggested a potential association between *BRCAm* and ICIs response, with tumor mismatch repair, microsatellite instability status, and PD-L1 overexpression associated with *BRCAm* [54].

Another interesting strategy is based on angiogenesis. In fact, hypoxia decelerates the downregulation of DNA repair processes, which in turn may result in genomic instability [90,91]. Therefore, the combination of PARPi and anti-angiogenic agents could enhance synthetic lethality, as witnessed in other solid malignancies such as ovarian cancer [92]. Unfortunately, acquired resistance to PARPi is a major issue in patients receiving these molecules, for which several potential mechanisms have been suggested, including the inactivation of the DNA repair proteins 53BP1 or REV7 [93,94]. Thus, novel drug combinations and treatment strategies able to overcome or at least delay the emergence of resistant clones are required [95]. PI3k/Akt, MAPK, and other mitogen signaling pathways have been related to reduction in *HR* repair, and consequently, have been associated with secondary resistance to PARPi [96]. As in the case of ICIs, preclinical and early clinical reports have suggested a possible synergistic activity provided by the combination of PI3k and MEK inhibitors plus PARPi [97,98], and further data are awaited.

Lastly, another strategy could be based on targeting IDH, a therapeutic option that is entering into clinical practice, with *IDH1* and *IDH2* mutations occurring in about 20% of iCCA patients [99,100]. Interestingly, *IDH1* action relies on the conversion of isocitrate to alfa-ketoglutarate; in case of *IDH* mutations, alfa-ketoglutarate is transformed by *IDH1* into 2-hydroxyglutarate (2-HG), which plays a role in tumor progression [101,102]. Since preclinical reports have detected alterations in the *HR* pathway and an increased PARPi sensitivity in *IDH1*-mutated malignancies, the strategy of combining PARPi with IDH-targeted treatments is under evaluation in the subgroup of BTC patients harboring IDH mutations (Table 1) [103,104].

## 6. Conclusions

Unfortunately, patients with advanced/metastatic BTC have a dismal prognosis and few therapeutic options, and therefore, there is an urgent need for novel treatment strategies in this setting. If PARPi have shown meaningful activity in several solid tumors, further efforts are needed to define the role of these novel agents in BTC. A key point would certainly be the identification of which patients are most likely to benefit from PARPi monotherapy or combinations. In fact, combination strategies of PARPi with ICIs and other anticancer treatments are being tested and the results of these investigations are awaited, with the hope to increase the number of medical options and to improve survival and quality of life in BTC patients.

**Author Contributions:** Conceptualization, A.D.R. and A.R.; methodology, A.D.R. and A.R.; writing—original draft preparation, A.D.R., A.R., C.B., and N.T.; writing—review and editing, A.D.R., A.R., C.B., and N.T.; visualization, A.P., V.M., I.M., M.D., S.T., and G.B.; supervision, S.T. and G.B.; project administration, A.D.R., A.R., and G.B. All authors have read and agreed to the published version of the manuscript.

**Funding:** This research received no external funding.

**Conflicts of Interest:** The authors declare no conflict of interest.

## References

1. Razumilava, N.; Gores, G.J. Cholangiocarcinoma. *Lancet* **2014**, *383*, 2168–2179. [[CrossRef](#)]
2. Forner, A.; Vidili, G.; Rengo, M.; Bujanda, L.; Ponz-Sarvisé, M.; Lamarca, M. Clinical Presentation, Diagnosis and Staging of Cholangiocarcinoma. *Liver Int.* **2019**, *39*, 98–107. [[CrossRef](#)] [[PubMed](#)]
3. Khan, S.A.; Davidson, B.R.; Goldin, R.D.; Heaton, N.; Karani, J.; Pereira, S.P.; Rosenberg, W.M.C.; Tait, P.; Taylor-Robinson, S.D.; Thillainayagam, A.V.; et al. Guidelines for the Diagnosis and Treatment of Cholangiocarcinoma: An Update. *Gut* **2012**, *61*, 1657–1669. [[CrossRef](#)] [[PubMed](#)]
4. Charbel, H.; Al-Kawas, F.H. Cholangiocarcinoma: Epidemiology, risk factors, pathogenesis, and diagnosis. *Curr. Gastroenterol. Rep.* **2011**, *13*, 182–187. [[CrossRef](#)] [[PubMed](#)]
5. Saha, S.K.; Zhu, A.X.; Fuchs, C.S.; Brooks, G.A. Forty-year trends in cholangiocarcinoma incidence in the US: Intrahepatic disease on the rise. *Oncologist* **2016**, *21*, 594–599. [[CrossRef](#)]
6. Alsaleh, M.; Leftley, Z.; Barbera, T.A.; Sithithaworn, P.; Khuntikeo, N.; Loilome, W.; Yongvanit, P.; Cox, I.J.; Chamadol, N.; Syms, R.R.A.; et al. Cholangiocarcinoma: A Guide for the Nonspecialist. *Int. J. Gen. Med.* **2019**, *12*, 13–23. [[CrossRef](#)]
7. Brandi, G.; Rizzo, A.; Dall’Olio, F.G.; Felicani, C.; Ercolani, G.; Cescon, M.; Frega, G.; Tavolari, S.; Palloni, A.; De Lorenzo, S.; et al. Percutaneous radiofrequency ablation in intrahepatic cholangiocarcinoma: A retrospective single-center experience. *Int. J. Hyperther.* **2020**, *37*, 479–485. [[CrossRef](#)]
8. Rizvi, S.; Khan, S.A.; Hallemeier, C.L.; Kelley, R.K.; Gores, G.J. Cholangiocarcinoma - evolving concepts and therapeutic strategies. *Nat. Rev. Clin. Oncol.* **2018**, *15*, 95–111. [[CrossRef](#)]
9. Valle, J.W.; Furuse, J.; Jitlal, M.; Baere, S.; Mizuno, N.; Wasan, H.; Bridgewater, J.; Okusaka, T. Cisplatin and Gemcitabine for Advanced Biliary Tract Cancer: A Meta-Analysis of Two Randomised Trials. *Ann. Oncol.* **2014**, *25*, 391–398. [[CrossRef](#)]
10. Rizzo, A.; Ricci, A.D.; Tober, N.; Nigro, M.C.; Mosca, M.; Palloni, A.; Abbati, F.; Frega, G.; De Lorenzo, S.; Tavolari, S.; et al. Second-line Treatment in Advanced Biliary Tract Cancer: Today and Tomorrow. *Anticancer Res.* **2020**, *40*, 3013–3030. [[CrossRef](#)] [[PubMed](#)]
11. Jusakul, A.; Cutcutache, I.; Yong, C.H.; Lim, J.Q.; Huang, M.N.; Padmanabhan, N.; Nellore, V.; Kongpetch, S.; Ng, A.W.T.; Ng, L.M.; et al. Whole-Genome and Epigenomic Landscapes of Etiologically Distinct Subtypes of Cholangiocarcinoma. *Cancer Discov.* **2017**, *7*, 1116–1135. [[CrossRef](#)] [[PubMed](#)]
12. Ou, S.; Li, J.; Zhou, H.; Frech, C.; Jiang, X.; Chu, J.S.; Zhao, X.; Li, Y.; Li, Q.; Wang, H.; et al. Mutational Landscape of Intrahepatic Cholangiocarcinoma. *Nat. Commun.* **2014**, *5*, 5596.
13. Rizzo, A.; Frega, G.; Ricci, A.D.; Palloni, A.; Abbati, F.; De Lorenzo, S.; Deserti, M.; Tavolari, S.; Brandi, G. Anti-EGFR Monoclonal Antibodies in Advanced Biliary Tract Cancer: A Systematic Review and Meta-analysis. *In Vivo* **2020**, *34*, 479–488. [[CrossRef](#)] [[PubMed](#)]
14. Jain, A.; Kwong, L.N.; Javle, M. Genomic Profiling of Biliary Tract Cancers and Implications for Clinical Practice. *Curr. Treat. Options Oncol.* **2016**, *17*, 58. [[CrossRef](#)]
15. Golan, T.; Raites-Gurevich, M.; Kelley, R.K.; Bocobo, A.G.; Borgida, A.; Shroff, R.T.; Holter, S.; Gallinger, S.; Ahn, D.H.; Aderka, D.; et al. Overall Survival and Clinical Characteristics of BRCA-Associated Cholangiocarcinoma: A Multicenter Retrospective Study. *Oncologist* **2017**, *22*, 804–810. [[CrossRef](#)]
16. González-Martín, A.; Pothuri, B.; Vergote, I.; Christensen, R.D.; Graybill, W.; Mirza, M.R.; McCormick, C.; Lorusso, D.; Hoskins, P.; Freyer, G.; et al. Niraparib in Patients with Newly Diagnosed Advanced Ovarian Cancer. *N. Engl. J. Med.* **2019**, *381*, 2391–2402. [[CrossRef](#)] [[PubMed](#)]
17. Paschalis, A.; de Bono, J. Prostate Cancer 2020: “The Times They Are a’Changing”. *Cancer Cell* **2020**, *38*, 25–27. [[CrossRef](#)]

18. Moore, K.; Colombo, N.; Scambia, G.; Kim, B.-G.; Oaknin, A.; Friedlander, M.; Lisyanskaya, A.; Floquet, A.; Leary, A.; Sonke, G.S.; et al. Maintenance Olaparib in Patients with Newly Diagnosed Advanced Ovarian Cancer. *N. Engl. J. Med.* **2018**, *379*, 2495–2505. [[CrossRef](#)]
19. Patel, M.; Nowsheen, S.; Maraboyina, S.; Xia, F. The role of poly(ADP-ribose) polymerase inhibitors in the treatment of cancer and methods to overcome resistance: A review. *Cell Biosci.* **2020**, *10*, 35. [[CrossRef](#)]
20. Robson, M.; Im, S.-A.; Senkus, E.; Xu, B.; Domchek, S.M.; Masuda, N.; Delaloge, S.; Li, W.; Tung, N.; Armstrong, A.; et al. Olaparib for Metastatic Breast Cancer in Patients with a Germline BRCA. Mutation. *N. Engl. J. Med.* **2017**, *377*, 523–533. [[CrossRef](#)]
21. Litton, J.K.; Rugo, H.S.; Ettl, J.; Hurvitz, S.A.; Gonçalves, A.; Lee, K.-H.; Fehrenbacher, L.; Yerushalmi, R.; Mina, L.A.; Martin, M.; et al. Talazoparib in Patients with Advanced Breast Cancer and a Germline BRCA Mutation. *N. Engl. J. Med.* **2018**, *379*, 753–763. [[CrossRef](#)] [[PubMed](#)]
22. Peyraud, F.; Italiano, A. Combined PARP Inhibition and Immune Checkpoint Therapy in Solid Tumors. *Cancers* **2020**, *12*, 1502. [[CrossRef](#)]
23. Marks, E.L.; Yee, N.S. Molecular genetics and targeted therapeutics in biliary tract carcinoma. *World J. Gastroenterol.* **2016**, *22*, 1335–1347. [[CrossRef](#)] [[PubMed](#)]
24. Cerrato, A.; Morra, F.; Celetti, A. Use of poly ADP-ribose polymerase [PARP] inhibitors in cancer cells bearing DDR defects: The rationale for their inclusion in the clinic. *J. Exp. Clin. Cancer Res.* **2016**, *35*, 179. [[CrossRef](#)] [[PubMed](#)]
25. Rabenau, K.; Hofstatter, E. DNA Damage Repair and the Emerging Role of Poly(ADP-ribose) Polymerase Inhibition in Cancer Therapeutics. *Clin. Ther.* **2016**, *38*, 1577–1588. [[CrossRef](#)]
26. Min, A.; Im, S.A. PARP Inhibitors as Therapeutics: Beyond Modulation of PARylation. *Cancers* **2020**, *12*, 394. [[CrossRef](#)]
27. Garje, R.; Vaddepally, R.K.; Zakharia, Y. PARP Inhibitors in Prostate and Urothelial Cancers. *Front. Oncol.* **2020**, *10*, 114. [[CrossRef](#)]
28. De Vos, M.; Schreiber, V.; Dantzer, F. The diverse roles and clinical relevance of PARPs in DNA damage repair: Current state of the art. *Biochem. Pharmacol.* **2012**, *84*, 137–146. [[CrossRef](#)]
29. Beck, C.; Robert, I.; Reina-San-Martin, B.; Schreiber, V.; Dantzer, F. Poly(ADP-ribose) polymerases in double-strand break repair: Focus on PARP1, PARP2 and PARP3. *Exp. Cell Res.* **2014**, *329*, 18–25. [[CrossRef](#)]
30. Bai, P. Biology of Poly(ADP-Ribose) Polymerases: The Factotums of Cell Maintenance. *Mol. Cell* **2015**, *58*, 947–958. [[CrossRef](#)]
31. Xie, S.; Mortusewicz, O.; Ma, H.T.; Herr, P.; Poon, R.Y.C.; Helleday, T.; Qian, C. Timeless Interacts with PARP-1 to Promote Homologous Recombination Repair. *Mol. Cell* **2015**, *60*, 163–176. [[CrossRef](#)] [[PubMed](#)]
32. Luscher, B.; Butepage, M.; Ecker, L.; Krieg, S.; Verheugd, P.; Shilton, B.H. ADP-Ribosylation, a Multifaceted Posttranslational Modification Involved in the Control of Cell Physiology in Health and Disease. *Chem. Rev.* **2018**, *118*, 1092–1136. [[CrossRef](#)] [[PubMed](#)]
33. Noordermeer, S.M.; van Attikum, H. PARP Inhibitor Resistance: A Tug-of-War in BRCA-Mutated Cells. *Trends Cell Biol.* **2019**, *29*, 820–834. [[CrossRef](#)]
34. Hottiger, M.O.; Hassa, P.O.; Luscher, B.; Schuler, H.; Koch-Nolte, F. Toward a unified nomenclature for mammalian ADP-ribosyltransferases. *Trends Biochem. Sci.* **2010**, *35*, 208–219. [[CrossRef](#)] [[PubMed](#)]
35. Altmeyer, M.; Messner, S.; Hassa, P.O.; Fey, M.; Hottiger, M.O. Molecular mechanism of poly(ADP-ribose)ylation by PARP1 and identification of lysine residues as ADP-ribose acceptor sites. *Nucleic Acids Res.* **2009**, *37*, 3723–3738. [[CrossRef](#)]
36. Daniels, C.M.; Ong, S.E.; Leung, A.K. Phosphoproteomic approach to characterize protein mono and poly(ADP-ribose)ylation sites from cells. *J. Proteome Res.* **2014**, *13*, 3510–3522. [[CrossRef](#)]
37. Palazzo, L.; Leidecker, O.; Prokhorova, E.; Dauben, H.; Matic, I.; Ahel, I. Serine is the major residue for ADP-riboseylation upon DNA damage. *Elife* **2018**, *7*. [[CrossRef](#)]
38. Leidecker, O.; Bonfiglio, J.J.; Colby, T.; Zhang, Q.; Atanassov, I.; Zaja, R.; Palazzo, L.; Stockum, A.; Ahel, I.; Matic, I. Serine is a new target residue for endogenous ADP-riboseylation on histones. *Nat. Chem. Biol.* **2016**, *12*, 998–1000. [[CrossRef](#)]
39. Leslie Pedrioli, D.M.; Leutert, M.; Bilan, V.; Nowak, K.; Gunasekera, K.; Ferrari, E.; Imhof, R.; Malmstrom, L.; Hottiger, M.O. Comprehensive ADP-ribosylome analysis identifies tyrosine as an ADP-ribose acceptor site. *EMBO Rep.* **2018**, *19*, e45310. [[CrossRef](#)]

40. Martello, R.; Leutert, M.; Jungmichel, S.; Bilan, V.; Larsen, S.C.; Young, C.; Hottiger, M.O.; Nielsen, M.L. Proteome-wide identification of the endogenous ADP-ribosylome of mammalian cells and tissue. *Nat. Commun.* **2016**, *7*, 12917. [[CrossRef](#)]
41. Bitler, B.G.; Watson, Z.L.; Wheeler, L.J.; Behbakht, K. PARP inhibitors: Clinical utility and possibilities of overcoming resistance. *Gynecol. Oncol.* **2017**, *147*, 695–704. [[CrossRef](#)] [[PubMed](#)]
42. Taylor, K.N.; Eskander, R.N. PARP Inhibitors in Epithelial Ovarian Cancer. *Recent Pat. Anticancer Drug Discov.* **2018**, *13*, 145–158. [[CrossRef](#)] [[PubMed](#)]
43. Alvarez-Gonzalez, R.; Jacobson, M.K. Characterization of polymers of adenosine diphosphate ribose generated in vitro and in vivo. *Biochemistry* **1987**, *26*, 3218–3224. [[CrossRef](#)] [[PubMed](#)]
44. Alemasova, E.E.; Lavrik, O.I. Poly(ADP-ribosyl)ation by PARP1: Reaction mechanism and regulatory proteins. *Nucleic Acids Res.* **2019**, *47*, 3811–3827. [[CrossRef](#)] [[PubMed](#)]
45. Kamaletdinova, T.; Fanaei-Kahrani, Z.; Wang, Z.Q. The Enigmatic Function of PARP1: From PARylation Activity to PAR Readers. *Cells* **2019**, *8*, 1625. [[CrossRef](#)]
46. Ray Chaudhuri, A.; Nussenzweig, A. The multifaceted roles of PARP1 in DNA repair and chromatin remodelling. *Nat. Rev. Mol. Cell. Biol.* **2017**, *18*, 610–621. [[CrossRef](#)]
47. Kunze, F.A.; Hottiger, M.O. Regulating Immunity via ADP-Ribosylation: Therapeutic Implications and Beyond. *Trends Immunol.* **2019**, *40*, 159–173. [[CrossRef](#)]
48. Hanzlikova, H.; Caldecott, K.W. Perspectives on PARPs in S Phase. *Trends Genet.* **2019**, *35*, 412–422. [[CrossRef](#)]
49. Azarm, K.; Smith, S. Nuclear PARPs and genome integrity. *Genes Dev.* **2020**, *34*, 285–301. [[CrossRef](#)]
50. Hanzlikova, H.; Kalasova, I.; Demin, A.A.; Pennicott, L.E.; Cihlarova, Z.; Caldecott, K.W. The Importance of Poly(ADP-Ribose) Polymerase as a Sensor of Unligated Okazaki Fragments during DNA Replication. *Mol. Cell* **2018**, *71*, 319–331. [[CrossRef](#)]
51. Heeke, A.L.; Pishvaian, M.J.; Lynce, F.; Xiu, J.; Brody, J.R.; Chen, W.J.; Baker, T.M.; Marshall, J.L.; Isaacs, C. Prevalence of Homologous Recombination-Related Gene Mutations Across Multiple Cancer Types. *JCO Precis. Oncol.* **2018**, *2*, 1–13. [[CrossRef](#)] [[PubMed](#)]
52. Chae, H.; Kim, D.; Yoo, C.; Kim, K.P.; Jeong, J.H.; Chang, H.M.; Lee, S.S.; Park, D.H.; Song, T.J.; Hwang, S.; et al. Therapeutic relevance of targeted sequencing in management of patients with advanced biliary tract cancer: DNA damage repair gene mutations as a predictive biomarker. *Eur. J. Cancer* **2019**, *120*, 31–39. [[CrossRef](#)] [[PubMed](#)]
53. Ahn, D.H.; Bekaii-Saab, T. Biliary tract cancer and genomic alterations in homologous recombinant deficiency: Exploiting synthetic lethality with PARP inhibitors. *Chin. Clin. Oncol.* **2020**, *9*, 1–6. [[CrossRef](#)] [[PubMed](#)]
54. Spizzo, G.; Puccini, A.; Xiu, J.; Goldberg, R.M.; Grothey, A.; Shields, A.F.; Arora, S.P.; Khushmann, M.; Salem, M.E.; Battaglin, F.; et al. Molecular profile of BRCA-mutated biliary tract cancers. *ESMO Open* **2020**, *5*, e000682. [[CrossRef](#)]
55. Saeed, A.; Park, R.; Al-Jumayli, M.; Al-Rajabi, R.; Sun, W. Biologics, Immunotherapy, and Future Directions in the Treatment of Advanced Cholangiocarcinoma. *Clin. Colorectal. Cancer* **2019**, *18*, 81–90. [[CrossRef](#)]
56. Jenner, Z.B.; Sood, A.K.; Coleman, R.L. Evaluation of rucaparib and companion diagnostics in the PARP inhibitor landscape for recurrent ovarian cancer therapy. *Future Oncol.* **2016**, *12*, 1439–1456. [[CrossRef](#)]
57. Knijnenburg, T.A.; Wang, L.; Zimmermann, M.T.; Chambwe, N.; Gao, G.F.; Cherniack, A.D.; Fan, H.; Shen, H.; Way, G.P.; Greene, C.S.; et al. Genomic and Molecular Landscape of DNA Damage Repair Deficiency across The Cancer Genome Atlas. *Cell Rep.* **2018**, *23*, 239–254. [[CrossRef](#)]
58. Pellegrino, B.; Mateo, J.; Serra, V.; Balmana, J. Controversies in oncology: Are genomic tests quantifying homologous recombination repair deficiency (HRD) useful for treatment decision making? *ESMO Open* **2019**, *4*, 1–5. [[CrossRef](#)]
59. Lord, C.J.; Ashworth, A. BRCAness revisited. *Nat. Rev. Cancer* **2016**, *16*, 110–120. [[CrossRef](#)]
60. Park, W.; Chen, J.; Chou, J.F.; Varghese, A.M.; Yu, K.H.; Wong, W.; Capanu, M.; Balachandran, V.; McIntyre, C.A.; Dika, I.E.; et al. Genomic Methods Identify Homologous Recombination Deficiency in Pancreas Adenocarcinoma and Optimize Treatment Selection. *Clin. Cancer Res.* **2020**, *26*, 3239–3248. [[CrossRef](#)]
61. Moeini, A.; Sia, D.; Bardeesy, N.; Mazzaferro, V.; Llovet, J.M. Molecular Pathogenesis and Targeted Therapies for Intrahepatic Cholangiocarcinoma. *Clin. Cancer Res.* **2016**, *22*, 291–300. [[CrossRef](#)] [[PubMed](#)]

62. Shen, J.; Peng, Y.; Wei, L.; Zhang, W.; Yang, L.; Lan, L.; Kapoor, P.; Ju, Z.; Mo, Q.; Shih, I.M.; et al. ARID1A Deficiency Impairs the DNA Damage Checkpoint and Sensitizes Cells to PARP Inhibitors. *Cancer Discov.* **2015**, *5*, 752–767. [[CrossRef](#)] [[PubMed](#)]
63. Wilson, B.G.; Roberts, C.W.M. SWI/SNF nucleosome remodellers and cancer. *Nat. Rev. Cancer* **2011**, *11*, 481–492. [[CrossRef](#)] [[PubMed](#)]
64. Lamarca, A.; Barriuso, J.; McNamara, M.G.; Valle, J.W. Biliary Tract Cancer: State of the Art and potential role of DNA Damage Repair. *Cancer Treat. Rev.* **2018**, *70*, 168–177. [[CrossRef](#)]
65. Yu, H.; Pak, H.; Hammond-Martel, I.; Ghran, M.; Rodrigue, A.; Daou, S.; Barbour, H.; Corbeil, L.; Hebert, J.; Drobetsky, E.; et al. Tumor suppressor and deubiquitinase BAP1 promotes DNA double-strand break repair. *Proc. Natl. Acad. Sci. USA.* **2014**, *111*, 285–290. [[CrossRef](#)]
66. Adeva, J.; Sangro, B.; Salati, M.; Edeline, J.; La Casta, A.; Bittoni, A.; Berardi, R.; Bruix, J.; Valle, J.W. Medical treatment for cholangiocarcinoma. *Liver Int.* **2019**, *39*, 123–142. [[CrossRef](#)]
67. Easton, D. Cancer risks in BRCA2 mutation carriers: The breast cancer linkage consortium. *J. Natl. Cancer Inst.* **1999**, *91*, 1310–1316.
68. Kiwerska, K.; Szyfter, K. DNA repair in cancer initiation, progression, and therapy—a double-edged sword. *J. Appl. Genet.* **2019**, *60*, 329–334. [[CrossRef](#)]
69. Sharma, M.B.; Carus, A.; Sunde, L.; Hamilton-Dutoit, S.; Ladekarl, M. BRCA-associated pancreatico-biliary neoplasms: Four cases illustrating the emerging clinical impact of genotyping. *Acta Oncol.* **2016**, *55*, 377–381. [[CrossRef](#)]
70. Xie, Y.; Jiang, Y.; Yang, X.B.; Wang, A.Q.; Zheng, Y.C.; Wan, X.S.; Sang, X.T.; Wang, K.; Zhang, D.D.; Xu, J.J.; et al. Response of BRCA1-mutated gallbladder cancer to olaparib: A case report. *World J. Gastroenterol.* **2016**, *22*, 10254–10259. [[CrossRef](#)]
71. Golan, T.; Hammel, P.; Reni, M.; Van Cutsem, E.; Macarulla, T.; Hall, M.J.; Park, J.O.; Hochhauser, D.; Arnold, D.; Oh, D.Y.; et al. Maintenance Olaparib for Germline BRCA -Mutated Metastatic Pancreatic Cancer. *N. Engl. J. Med.* **2019**, *381*, 317–327. [[CrossRef](#)] [[PubMed](#)]
72. Fehling, S.C.; Miller, A.L.; Garcia, P.L.; Vance, R.B.; Yoon, K.J. The combination of BET and PARP inhibitors is synergistic in models of cholangiocarcinoma. *Cancer Lett.* **2020**, *468*, 48–58. [[CrossRef](#)] [[PubMed](#)]
73. Caramelo, O.; Silva, C.; Caramelo, F.; Frutuoso, C.; Almeida-Santos, T. The effect of neoadjuvant platinum-based chemotherapy in BRCA mutated triple negative breast cancers -systematic review and meta-analysis. *Hered. Cancer Clin. Pract.* **2019**, *17*, 11. [[CrossRef](#)] [[PubMed](#)]
74. Pignata, S.; Cecere, S.; Du Bois, A.; Harter, P.; Heitz, F. Treatment of recurrent ovarian cancer. *Ann. Oncol.* **2017**, *28*, viii51–viii56. [[CrossRef](#)] [[PubMed](#)]
75. Kowalewski, A.; Szyłberg, Ł.; Saganek, M.; Napiontek, W.; Antosik, P.; Grzanka, D. Emerging strategies in BRCA-positive pancreatic cancer. *J. Cancer Res. Clin. Oncol.* **2018**, *144*, 1503–1507. [[CrossRef](#)] [[PubMed](#)]
76. Go, R.S.; Adjei, A.A. Review of the Comparative Pharmacology and Clinical Activity of Cisplatin and Carboplatin. *J. Clin. Oncol.* **1999**, *17*, 409–422. [[CrossRef](#)]
77. Tutt, A.N.J.; Lord, C.J.; McCabe, N.; Farmer, H.; Turner, N.; Martin, N.M.; Jackson, S.P.; Smith, G.C.; Ashworth, A. Exploiting the DNA Repair Defect in BRCA Mutant Cells in the Design of New Therapeutic Strategies for Cancer. *Cold Spring Harb. Symp. Quant. Biol.* **2005**, *70*, 139–148. [[CrossRef](#)]
78. Byrski, T.; Gronwald, J.; Huzarski, T.; Dent, R.A.; Zuziak, D.; Wiśniowski, R.; Marczyk, E.; Blecharz, P.; Szurek, O.; Cybulski, C.; et al. Neoadjuvant therapy with cisplatin in BRCA1-positive breast cancer patients. *Hered. Cancer Clin. Pract.* **2011**, *9*, A4. [[CrossRef](#)]
79. Silver, D.P.; Richardson, A.L.; Eklund, A.C.; Wang, Z.C.; Szallasi, Z.; Li, Q.; Juul, N.; Leong, C.O.; Calogrias, D.; Buraimoh, A.; et al. Efficacy of Neoadjuvant Cisplatin in Triple-Negative Breast Cancer. *J. Clin. Oncol.* **2010**, *28*, 1145–1153. [[CrossRef](#)]
80. Byrski, T.; Huzarski, T.; Dent, R.; Marczyk, E.; Jasiowka, M.; Gronwald, J.; Jakubowicz, J.; Cybulski, C.; Wisniowski, R.; Godlewski, D.; et al. Pathologic complete response to neoadjuvant cisplatin in BRCA1-positive breast cancer patients. *Breast Cancer Res. Treat.* **2014**, *147*, 401–405. [[CrossRef](#)]
81. Tutt, A.; Tovey, H.; Cheang, M.C.U.; Kernaghan, S.; Kilburn, L.; Gazinska, P.; Owen, J.; Abraham, J.; Barrett, S.; Barrett-Lee, P.; et al. Carboplatin in BRCA1/2-mutated and triple-negative breast cancer BRCAness subgroups: The TNT Trial. *Nat. Med.* **2018**, *24*, 628–637. [[CrossRef](#)] [[PubMed](#)]
82. Martinez, F.J.; Shroff, R.T. Biliary tract cancers: Systemic therapy for advanced disease. *Chin. Clin. Oncol.* **2020**, *9*, 5. [[CrossRef](#)] [[PubMed](#)]

83. Lamarca, A.; Barriuso, J.; McNamara, M.G.; Valle, J.W. Molecular targeted therapies: Ready for “prime time” in biliary tract cancer. *J. Hepatol.* **2020**, *73*, 170–185. [[CrossRef](#)] [[PubMed](#)]
84. Zhang, W.; Shi, J.; Li, R.; Han, Z.; Li, L.; Li, G.; Yang, B.; Yin, Q.; Wang, Y.; Ke, Y.; et al. Effectiveness of Olaparib Treatment in a Patient with Gallbladder Cancer with an ATM-Inactivating Mutation. *Oncologist* **2020**, *25*, 375–379. [[CrossRef](#)]
85. Ricci, A.D.; Rizzo, A.; Novelli, M.; Tavolari, S.; Palloni, A.; Tober, N.; Abbati, F.; Mollica, V.; De Lorenzo, S.; Turchetti, D.; et al. Specific Toxicity of Maintenance Olaparib Versus Placebo in Advanced Malignancies: A Systematic Review and Meta-analysis. *Anticancer Res.* **2020**, *40*, 597–608. [[CrossRef](#)]
86. O’Reilly, E.M.; Lee, J.W.; Zalupski, M.; Capanu, M.; Park, J.; Golan, T.; Tahover, E.; Lowery, M.A.; Chou, J.F.; Sahai, V.; et al. Randomized, Multicenter, Phase II Trial of Gemcitabine and Cisplatin With or Without Veliparib in Patients With Pancreas Adenocarcinoma and a Germline *BRCA/PALB2* Mutation. *J. Clin. Oncol.* **2020**, *13*, 1378–1388. [[CrossRef](#)]
87. Chong, D.Q.; Zhu, A.X. The landscape of targeted therapies for cholangiocarcinoma: Current status and emerging targets. *Oncotarget* **2016**, *7*, 46750–46767. [[CrossRef](#)]
88. Ding, L.; Chen, X.; Xu, X.; Qian, Y.; Liang, G.; Yao, F.; Yao, Z.; Wu, H.; Zhang, J.; He, Q.; et al. PARP1 Suppresses the Transcription of PD-L1 by Poly(ADP-Ribosyl)ating STAT3. *Cancer Immunol. Res.* **2019**, *7*, 136–149. [[CrossRef](#)]
89. Friedlander, M.; Meniawy, T.; Markman, B.; Mileshkin, L.R.; Harnett, P.; Millward, M.; Lundy, J.; Freimund, A.E.; Norris, C.; Wu, J.; et al. A phase 1b study of the anti-PD-1 monoclonal antibody BGB-A317 (A317) in combination with the PARP inhibitor BGB-290 (290) in advanced solid tumors. *J. Clin. Oncol.* **2018**, *36*. [[CrossRef](#)]
90. Hasvold, G.; Lund-Andersen, C.; Lando, M.; Patzke, S.; Hauge, S.; Suo, Z.; Lyng, H.; Syljuasen, R.G. Hypoxia-induced alterations of G2 checkpoint regulators. *Mol. Oncol.* **2016**, *10*, 764–773. [[CrossRef](#)]
91. Daly, C.S.; Flemban, A.; Shafei, M.; Conway, M.E.; Qualtrough, D.; Dean, S.J. Hypoxia modulates the stem cell population and induces EMT in the MCF-10A breast epithelial cell line. *Oncol. Rep.* **2018**, *39*, 483–490. [[CrossRef](#)] [[PubMed](#)]
92. Haddad, F.G.; Karam, E.; Moujaess, E.; Kourie, H.R. Poly-(ADP-ribose) polymerase inhibitors: Paradigm shift in the first-line treatment of newly diagnosed advanced ovarian cancer. *Pharmacogenomics* **2020**, *21*, 721–727. [[CrossRef](#)] [[PubMed](#)]
93. D’Andrea, A.D. Mechanisms of PARP inhibitor sensitivity and resistance. *DNA Repair* **2018**, *71*, 172–176. [[CrossRef](#)] [[PubMed](#)]
94. Jiang, X.; Li, X.; Li, W.; Bai, H.; Zhang, Z. PARP inhibitors in ovarian cancer: Sensitivity prediction and resistance mechanisms. *J. Cell. Mol. Med.* **2019**, *23*, 2303–2313. [[CrossRef](#)]
95. Wang, D.; Wang, M.; Jiang, N.; Zhang, Y.; Bian, X.; Wang, X.; Roberts, T.M.; Zhao, J.J.; Liu, P.; Cheng, H. Effective use of PI3K inhibitor BKM120 and PARP inhibitor Olaparib to treat PIK3CA mutant ovarian cancer. *Oncotarget* **2016**, *7*, 13153–13166. [[CrossRef](#)]
96. Sun, C.; Fang, Y.; Yin, J.; Chen, J.; Ju, Z.; Zhang, D.; Chen, X.; Vellano, C.P.; Jeong, K.J.; Ng, P.K.S.; et al. Rational combination therapy with PARP and MEK inhibitors capitalizes on therapeutic liabilities in RAS mutant cancers. *Sci. Transl. Med.* **2017**, *9*, eal5148. [[CrossRef](#)]
97. Schmitz, K.J.; Lang, H.; Wohlschlaeger, J.; Sotiropoulos, G.C.; Reis, H.; Schmid, K.W.; Baba, H.A. AKT and ERK1/2 signaling in intrahepatic cholangiocarcinoma. *World J. Gastroenterol.* **2007**, *13*, 6470–6477. [[CrossRef](#)]
98. Chung, J.Y.; Hong, S.M.; Choi, B.Y.; Cho, H.; Yu, E.; Hewitt, S.M. The expression of phospho-AKT, phospho-mTOR, and PTEN in extrahepatic cholangiocarcinoma. *Clin. Cancer Res.* **2009**, *15*, 660–667. [[CrossRef](#)]
99. Borger, D.R.; Tanabe, K.K.; Fan, K.C.; Lopez, H.U.; Fantin, V.R.; Straley, K.S.; Schenkein, D.P.; Hezel, A.F.; Ancukiewicz, M.; Liebman, H.M.; et al. Frequent mutation of isocitrate dehydrogenase (IDH)1 and IDH2 in cholangiocarcinoma identified through broad-based tumor genotyping. *Oncologist* **2012**, *17*, 72–79. [[CrossRef](#)]
100. Kipp, B.R.; Voss, J.S.; Kerr, S.E.; Fritcher, E.G.B.; Graham, R.P.; Zhang, L.; Highsmith, W.E.; Zhang, J.; Roberts, L.R.; Gores, G.J.; et al. Isocitrate dehydrogenase 1 and 2 mutations in cholangiocarcinoma. *Hum. Pathol.* **2012**, *43*, 1552–1558. [[CrossRef](#)]
101. Wang, P.; Dong, Q.; Zhang, C.; Kuan, P.F.; Liu, Y.; Jeck, W.R.; Andersen, J.B.; Jiang, W.; Savich, G.L.; Tan, T.X.; et al. Mutations in isocitrate dehydrogenase 1 and 2 occur frequently in intrahepatic cholangiocarcinomas and share hypermethylation targets with glioblastomas. *Oncogene* **2013**, *32*, 3091–3100. [[CrossRef](#)] [[PubMed](#)]

102. Saha, S.K.; Parachoniak, C.A.; Ghanta, K.S.; Fitamant, J.F.; Ross, K.N.; Najem, M.S.; Gurumurthy, S.; Akbay, E.A.; Sia, D.; Cornella, H.; et al. Mutant IDH inhibits HNF-4alpha to block hepatocyte differentiation and promote biliary cancer. *Nature* **2014**, *513*, 110–114. [CrossRef] [PubMed]
103. IDH-Mutant Tumors Vulnerable to PARP Inhibition. Available online: <https://cancerdiscovery.aacrjournals.org/content/7/4/OF4> (accessed on 30 August 2020).
104. Sulkowski, P.L.; Corso, C.D.; Robinson, N.D.; Scanlon, S.E.; Purshouse, K.R.; Bai, H.; Liu, Y.; Sundaram, R.K.; Hegan, D.C.; Fons, N.; et al. 2-Hydroxyglutarate produced by neomorphic IDH mutations suppresses homologous recombination and induces PARP inhibitor sensitivity. *Sci. Transl. Med.* **2017**, *9*. [CrossRef] [PubMed]



© 2020 by the authors. Licensee MDPI, Basel, Switzerland. This article is an open access article distributed under the terms and conditions of the Creative Commons Attribution (CC BY) license (<http://creativecommons.org/licenses/by/4.0/>).

Review

# Minimising Blood Stream Infection: Developing New Materials for Intravascular Catheters

Charnete Casimero, Todd Ruddock, Catherine Hegarty, Robert Barber, Amy Devine and James Davis \*

School of Engineering, Ulster University, Jordanstown BT37 0QB, Northern Ireland, UK; casimero-c@ulster.ac.uk (C.C.); ruddock-t1@ulster.ac.uk (T.R.); hegarty-c19@ulster.ac.uk (C.H.); barber-r@ulster.ac.uk (R.B.); devine-a14@ulster.ac.uk (A.D.)

\* Correspondence: james.davis@ulster.ac.uk; Tel.: +44-(0)289-0366-407

Received: 30 July 2020; Accepted: 24 August 2020; Published: 26 August 2020

**Abstract:** Catheter related blood stream infection is an ever present hazard for those patients requiring venous access and particularly for those requiring long term medication. The implementation of more rigorous care bundles and greater adherence to aseptic techniques have yielded substantial reductions in infection rates but the latter is still far from acceptable and continues to place a heavy burden on patients and healthcare providers. While advances in engineering design and the arrival of functional materials hold considerable promise for the development of a new generation of catheters, many challenges remain. The aim of this review is to identify the issues that presently impact catheter performance and provide a critical evaluation of the design considerations that are emerging in the pursuit of these new catheter systems.

**Keywords:** intravascular catheter; CRBSI; biofilm; CVC; antimicrobial; antifouling

## 1. Introduction

Intravascular catheters are ubiquitous in contemporary care and it has been estimated that 30–80% of hospital patients will have a peripheral venous catheter (PVC) in place at some point during their stay [1–3]. While PVCs are by far the most commonplace, a wide range of catheter designs are employed to aid the delivery of life saving fluids and differ in terms of anticipated use. In contrast to the short-lived PVCs, central venous catheters (CVC) are designed for main vein access and mid to long-term (months/years) applications such as: the delivery of chemotherapy drugs, nutritional fluids and for haemodialysis. Used across every hospital unit as well as for outpatient management, CVCs are some of the most common indwelling medical devices of modern times with approximately 5 million catheters inserted annually in the US (cf. 330 million PVCs) [4,5]. While such devices provide ease of access to the vascular highways of the body, it must also be recognised that they can also serve as an entry point for life threatening infection [6]. It has been estimated that CVCs are some 64 times more likely to result in a catheter related blood stream infection (CRBSI) than other intravascular access devices [7].

Patients in intensive care units (ICUs) across the US are exposed to an estimated 15 million (catheter) days of CVC usage each year [8] from which up to 8% result in CRBSI [5,9]. CRBSI-induced sepsis accounts for 25% of annual haemodialysis patient mortality [10]. The US Centre for Disease Control and Prevention (CDC) estimates that a total of 250,000 blood stream infections are diagnosed each year [11] of which 80,000–120,000 are catheter-related [8,12]. While rates of attributable mortality vary from 12% to 25% for nosocomial CRBSIs [11,13,14], a meta-analysis concluded that an average of 3% of CRBSIs result in death [8]. Further complications can also arise such as intravascular thrombosis and endocarditis leading to myocardial infarction or stroke [15]. It is of little surprise that the consequences of CRBSI results in a considerable economic burden on both the healthcare provider



and patient. The attributable cost per infection in the US varies considerably based on infection type and healthcare factors, costs are reported to range from USD 3700 to USD 56,000 per patient, with an upper estimate of USD 2.3 billion spent on CRBSIs arising from CVC use annually [8,16].

The combined morbidity, mortality and economic burden posed by CRBSIs, is an ever present concern among clinicians and has prompted much effort in the search for more effective frontline procedures (i.e., aseptic technique education and prophylactic antimicrobial lock systems) [17–19], but there has also been radical rethinks of the design and the development of new catheter components, materials and smart sensing solutions. There has been substantial progress in these areas in recent years but, despite concerted efforts in education and the implementation of care bundles, bacterial contamination and the resulting CRBSI remains problematic. As such, there are considerable opportunities for recent advances in materials and sensing technologies to complement improved clinical practice in providing a more integrated solution. The provision of materials that minimise the adherence of bacteria to the intraluminal space, provide antimicrobial action, and sensors that can proactively monitor the condition of the line herald a new generation of smart catheter systems that aim to eliminate infection or provide early warning diagnostics. The aim of this review is to provide a critical evaluation of the design considerations that are emerging in the pursuit of these new catheter systems. While the focus here is on CVCs, it should be recognised that bacterial contamination is commonplace and much of the discussion here should be transferrable to a range of devices.

## 2. Catheter Components

There are a variety of CVC subsets available, the most common of which are: non-tunnelled, tunnelled, peripherally inserted central catheters (PICC) and totally implantable venous access ports (TIVAPs) [20]. The main components of a central venous catheter and the implanted venous access ports are highlighted in Figure 1A,B, respectively. In the case of CVCs, these are typically inserted through the jugular, subclavian or femoral veins to either the superior vena cava, right atrium or inferior vena cava of the heart [20,21].

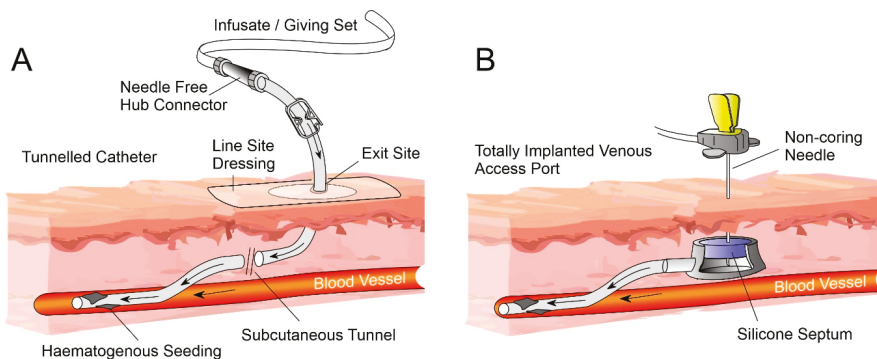


**Figure 1.** (A) Tunnelled central venous catheter and associated components. (B) Totally implantable venous access port.

Selection of the catheter system is invariably based on patient-specific factors such as: purpose, anticipated lifetime and the frequency with which the catheter will need to be accessed. It can be anticipated that the longer the catheter is in place, the greater the risk of infection. It is of little surprise therefore that tunnelled CVCs and TIVAPs which are intended for long term use (typically months to years) dominate the CRBSI literature. While TIVAPs are primarily designed for periodic/infrequent applications (i.e., haemodialysis) [22], tunnelled CVCs are generally targeted at those interventions where regular administration of fluids, medication, parenteral nutrition or the aspiration of blood is required. As such, the frequency with which the needle free connector (NFC) is manipulated

can be particularly problematic with the majority of the infections arising as a consequence of its contamination [23,24].

A multitude of NFCs are available commercially but most share common design features relating to the access port. In almost all cases, access to the catheter is activated through the insertion of a male Luer connector (from a fluid giving set or syringe) which causes the deformation of a silicone septum and therein provides access to the catheter line [25–27]. Three of the more common approaches are highlighted in Figure 2. While they differ in terms of internal mechanism, most rely on a split septum design which, when disconnected, acts as a physical barrier to the entry of bacteria. Solid sealed silicone surfaces (BD Max Zero™) are also available and, while these potentially reduce the surface crevices through which bacteria can adhere, they still rely on the Luer activated displacement/compression of the silicone cap within the device to enable fluid flow to or from the line.

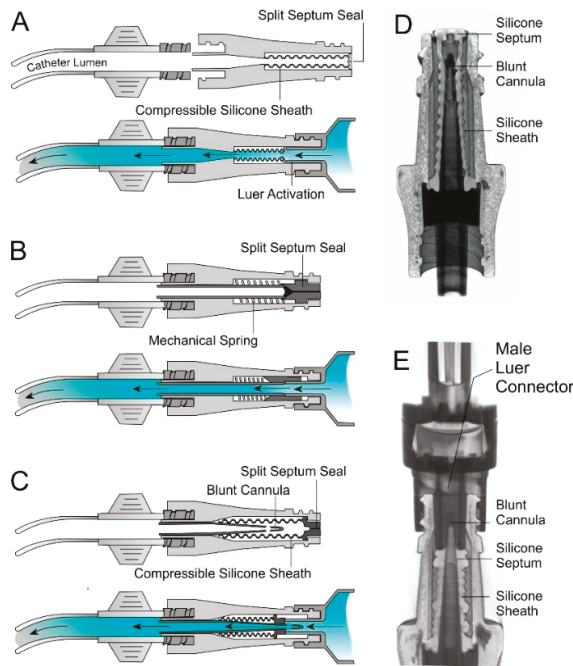


**Figure 2.** Needle free connectors based on (A) simple split septum, (B) mechanical spring compression and (C) blunt cannula. Computerised tomography scans of the internal components of an intensive care unit (ICU) Medical Clave™ connector before (D) and after connection to a giving set with a Luer connector (E).

A variety of engineering features have been implemented in recent years as a means of improving the performance of such devices in terms of haemocompatibility and in reducing the potential for CRBSI. The presence of blood within the fluid pathway of an NFC can result in haemolysis of the red blood cells which increases the risk of a fibrin clot leading to occlusion and ultimately prevents fluid transfer. Moreover, it provides a pool of nutrients that can promote the growth of bacteria [25]. Body movements (muscle flexing, respiration, coughing etc.) and clamping of the catheter can all induce changes in the mechanical and physiological pressure within the catheter that can serve to push blood along the line [28,29]. It has been estimated that even the smallest blood reflux (4–30 mL) can result in fibrin activation and occlude the inner pathways of the NFC [25]. Removing blood from the NFC is a critical concern and there has been an increasing shift from opaque NFC structures to more transparent

polymers that can enable visual inspection of the internal working of the hub. The movement of blood within the catheter and its propensity to travel (reflux) to the needle free hub upon the insertion and disconnection of the external Luer is however dependent on the design of the NFC hub [25,26].

It is of little surprise therefore that understanding the operation of these systems can be a major factor in minimising the risk of infection. Depending on the displacement of blood upon insertion/disconnection, hubs are generally classified as: negative, neutral, positive and anti-reflux. A summary of the various designs and their mechanism is provided in Table 1.

**Table 1.** Classification of needle free connector hubs in terms of fluid displacement.

Action	Negative	Neutral	Positive	Anti-Reflux
Disconnection	Blood refluxes into catheter	Blood refluxes into catheter	Fluid moves towards patient	Fluid restricted by diaphragm
Connection	Fluid moves toward patient	Fluid moves toward patient	Blood refluxes into catheter	Fluid restricted by diaphragm
Clamping sequence	Clamp before disconnection	No specified clamping	Clamp after disconnection	No specified clamping
Commercial Examples	BD Smartsite BD Q-Syte Baxter Interlink ICU Medical Clave*	ICU Medical Microclave Clear Baxter One-Link RyMed Invision Nexus NIS-6P	Braun Ultrasite BD MaxPlus Braun Caresite	ICU Medical Neutron Nexus TKO-5 Nexus TKO-6P

It can be seen from Table 1 that in the case of negative and positive displacement systems, there is a recommended clamping procedure associated with the use of these systems to prevent the inadvertent reflux of blood. There is, however, an assumption that the clinical staff (or the patient in the case of known as home parenteral nutrition (HPN)) are aware of the mode through which a particular NFC operates. Hadaway (2011), in a survey of healthcare workers, found that of 554 responses, some 25% were unaware of whether the NFC used in the CVC line they were managing was positive, negative or neutral [30]. Moreover, 47% were unsure as to the correct approach to the flushing and clamping procedures associated with a particular NFC with the situation being compounded by the presence of multiple NFC brand variants in use within a given institution [27,30,31]. The early introduction of NFCs was characterised by an increase in CRBSI and a lack of appropriate training in device operation has often been cited as a contributing factor. This has been corroborated in instances where an institution has switched NFC brands and recorded an increase in CRBSI rates only to find the latter returned to previously lower levels when resuming use of their original NFC system [31]. While improvements in the physical design of NFCs will undoubtedly aid approaches to the prevention of CRBSI, the continuing prevalence of the latter however highlights that there is much still to be done.

### 3. Pathogens, Colonisation, Biofilms and Infection

In general, catheter related infection occurs mainly through two mechanisms—migration of adventitious skin pathogens (i.e., *S. aureus*) along the external surfaces of the polymer tubing through the cutaneous tract to the blood stream (extraluminal) and, as noted in the previous section, ingress via the needle free connector hub (intraluminal) [24]. In either case, upon contact with the blood, the microbes interact with fibrin to yield an adherent biofilm which promotes microbial colonisation and furthers the spread of the organisms. Extraluminal contamination has historically been more common in short term intravascular devices (peripheral venous/arterial catheters and non-cuffed/non-tunnelled CVCs) and typically arises through issues encountered during insertion/implantation [24].

Breaching the skin barrier to enable the insertion of a medical device inevitably provides an opportunity for skin flora or adventitious contaminants from the healthcare environment to gain access to the underlying tissues and from there sets a foundation for subsequent infection. Such issues are not restricted to intravascular access devices but have become increasingly common with

cardiovascular implantable electronic devices (CEID) such as pacemakers, cardioverter–defibrillators, cardiac resynchronisation devices etc. This is compounded by the increasing longevity of the patient cohorts where the number of surgical interventions (revisions, extractions and upgrades) have increased substantially year on year [32,33]. As the prime risk occurs at the time of insertion, it is of little surprise that repeated surgical replacement of a CVC (or the CEID) increases the risk of infection. The implementation of catheter care initiatives during the insertion of CVCs (such as the Keystone Central Line Bundle [34] and Epic3 guidelines [19]) have however led to significant improvements in outcomes and, in the US, has led to reductions in insertion related infections [23,25,35].

In contrast, contamination of the NFC and internal lumen tends to occur post-operatively as a consequence of failures in the aseptic manipulation of the connecting hub prior to the administration of fluids or aspiration of blood. Intraluminal colonisation tends to be predominant in those devices intended for longer term function such as cuffed Hickman and Broviac type catheters, cuffed haemodialysis CVCs, TIVAPs, and PICC systems [36]. It is of little surprise that the increased duration of placement and frequency with which such lines are accessed will also increase the risk of CRBSI where there will be more opportunities for the intraluminal migration of planktonic (free-swimming) bacteria arising from a contaminated hub to the bloodstream [7,24]. Examination of the microbial contamination of NFCs after periods of non-use found that colony forming units (CFU) varied from 15 to 1000 CFU which, if improperly disinfected, would be sufficient to induce colonisation of the catheter and result in bacteraemia [31,37,38]. Potential trouble spots in the use of the NFC, in terms of disinfection, relate to the point where the sterile Luer connector or syringe contacts the surfaces of the NFC—mainly the septum, side threads and side surfaces (between septum and NFC structure) [23]. The presence of grooves/gaps either in the core design between septum seal and housing (as highlighted in Figure 3 for the Clave™ NFC), or as a result of repeated use (i.e., abrasion or other physical damage) can all influence the ease with which disinfection can be achieved [26,27,30,39].

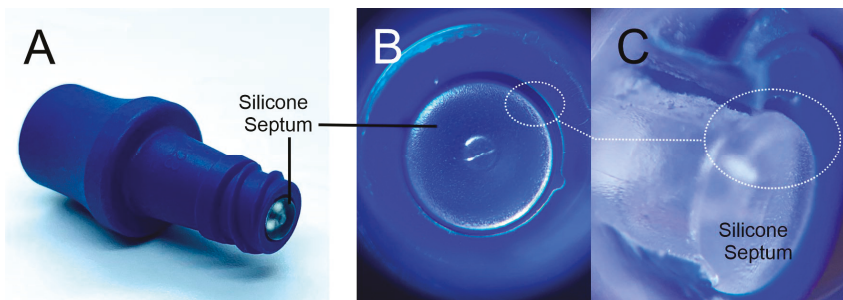


**Figure 3.** ICU Medical Clave™ needle free connector (A). Optical image of the septum (B) and cut through section (C) highlighting gaps in the structure.

While the majority of CRBSI are known to originate from issues in aseptic manipulation, two other sources of infection also need to be considered which are effectively independent of any attempt at external decontamination of the catheter or the NFC. Contamination of the fluid to be infused will effectively bypass any aseptic precautions employed during administration and offers microbes unimpeded access to the bloodstream [40]. Fortunately, such occurrences are exceedingly rare. Haematogenous seeding occurs when pathogens already present in the bloodstream as a consequence of local infection (i.e., pneumonia) encounter the foreign extraluminal surface and then subsequently colonise it (indicated in Figure 1A). Though it must also be recognised that a contaminated catheter can also serve as a potential seeding source for the contamination of other intravascular devices [41]. The pathogens most commonly cultured from infected CVCs are listed in Table 2. *Staphylococcus aureus* and coagulase-negative staphylococci (typically *S. epidermidis*) are the two pathogens most frequently isolated in CRBSI cases, with *S. aureus* responsible for between 10% and 25% of infections [42,43].

**Table 2.** Catheter related blood stream infection (CRBSI) associated pathogens [42].

Pathogen	Prevalence
Coagulase-negative staphylococci (i.e., <i>S. epidermidis</i> )	20.9%
<i>Staphylococcus aureus</i>	18.1%
<i>Escherichia coli</i>	7.4%
<i>Klebsiella pneumoniae</i> / <i>Klebsiella oxytoca</i>	9.4%
<i>Enterococcus faecalis</i>	9.1%

The introduction of bacteria to the lumen of the catheter line will inevitably result in the formation of a biofilm (largely polysaccharide in nature) which serves as a foundation for the sustained growth of the microbes and ultimately as a latent infective source [44,45]. The film itself is an extracellular 3D network that protects the emerging communities through serving as a physical barrier against the body's intrinsic immune response (phagocytes) and limits the diffusion of antibiotics. These protective qualities can be particularly problematic when attempting to salvage a catheter (rather than its direct replacement) where the presence of any surviving bacteria within the biofilm can lead to a resumption of the infection [45]. As such, conventional antimicrobial therapies require concentrations some 100–1000 times greater than the normal minimum inhibitory concentrations (MIC) to be applied and the dosage maintained over longer durations in order to eradicate the biofilm [46]. A more worrisome issue is that in aiding bacterial reproduction, the biofilm can aid the alteration of bacterial gene expression, leading to mutations and modifications in the physiology of the pathogenic antigens, limiting immune and drug response and contributing to antimicrobial resistant species [47,48].

Extra and endoluminal colonisation rates are dependent on the interaction between physiological properties of the pathogen and the surface characteristics (i.e., hydrophobicity/hydrophilicity) of the catheter [49]. The initial adhesion of pathogens is improved by the initial formation of a conditioning film (comprised of platelets and plasma proteins such as albumin, fibrinogen, and fibronectin) that binds to the luminal surfaces [50]. Pathogens will more readily adhere to this film than to the bare catheter material itself [49] and, once attached, to the luminal surface, will rapidly establish a biofilm. It is of little surprise that there have been extensive efforts to modify the surface of the polymers used in the production of both the catheters and NFCs such that the initial deposition of the conditioning film is impeded.

## 4. Current Practice

### 4.1. Disinfection

Alcohol/antimicrobial wipes are widely employed as the primary anti-infective measure in the management of catheter lines and decontamination of NFCs. Alcohol wipes (typically 70% isopropyl alcohol (IPA)) are the most commonly applied measure and their biocide activity relies on their ability to dehydrate the bacterial cell—both during the application and as the alcohol evaporates [51,52]. While the use of the alcohol alone can be effective, its veracity can be greatly enhanced by the presence of an appropriate antimicrobial agent (chlorhexidine or povidone iodine) where the disinfection mixture exploits the immediacy of the alcohol and sustained action of the antimicrobial agent [23,30,53–56].

Alcohol disinfection is not however fool proof and will always be subject to human factors (time allocated to the procedure, friction applied etc.) and device designs (ability to penetrate the device crevices) and there remains a contentious debate as to whether complete removal of bacteria from NFCs is in fact possible [52,57–60]. Menyhay and Maki (2008) in an in vitro study of 30 NFCs contaminated with *E. faecalis* and then subsequently disinfected with 70% IPA, found that 67% of the NFCs continued to transmit microbial contaminants (440–25,000 CFU) [52]. The time allocated to disinfection appears to be a significant factor with studies by Kaler and Chin [52] finding that 15 and 60 s cleaning cycles with

70% IPA eliminated all organisms whereas studies by Smith et al. (2012), Simmons et al. (2011) and Rupp et al. (2012) highlighted that short to moderate cleansing (3–15 s), while decreasing bacterial load, were less effective at total decontamination [57–59]. There is nevertheless considerable variability and contrasting results, as befits the nature of human intervention involving “scrubbing the hub”. The UK EPIC3 report on the evidence-based evaluations of an expert panel have recommended that NFCs be disinfected with 70% alcoholic chlorhexidine with the application of friction pre and post access [19].

#### 4.2. Education and Aseptic Techniques

Training at the core of the management of CVCs—from implantation to the day to day care of the line but the reliance on human compliance and adherence to the main tenets of aseptic manipulation can be an inherently variable phenomenon [61–64]. While the introduction of care bundles has led to significant gains, it must also be noted that improved compliance rates are seldom universal. A recent study by Jeong et al. (2013) revealed compliance rates were only 37% after the intervention [63] and a recent meta-analysis by Ista et al. (2016) highlighted that total compliance is essentially unattainable [18].

While the significance of disinfection of the NFC prior to accessing the catheter has long been recognised, it is surprising that it remains a common point of failure [23,30,64]. Patients with long term CVCs undergoing total parenteral nutrition (TPN) are trained to administer their nutrition at home, or have it administered at home on their behalf, known as home parenteral nutrition (HPN). In a study conducted by Bond et al. (2018), 16% of HPN patients contracted at least one CRBSI, accounting for 0.31 CRBSI per 1000 catheter days [65]. Out of these 16%, the rate of CRBSI per 1000 catheter days was 0.27 when HPN was administered by a trained home care nurse, compared to 0.342 and 0.320 when self-administered or administered by a non-medical carer (such as a family member), respectively. It is noteworthy that although there are gains in having a trained caregiver—the benefits are only marginally better than having the patient manage the line. There is little doubt that more attention is required for training in aseptic access and maintenance [66].

#### 4.3. Catheter Locks

A second line of defence in preventing bacterial ingress rests on the use of catheter locks. The latter is typically used where the catheter is not being used and the line is flushed with saline. This has the primary purpose of removing blood from the line such that occlusion and bacterial growth are minimised (discussed in Section 2) [26,27,30,67]. While the use of a saline flush is standard, other components can also be introduced and perform a variety of roles: anti-occlusion (heparin), antibiotic (vancomycin, gentamicin) and antimicrobial (citrate, ethanol and taurolidine) [68–70]. Vancomycin and gentamicin are generally reserved for therapeutic measures once a CRBSI has been diagnosed [22,46,71–73]. In contrast, heparin, citrate and, increasingly, taurolidine are used prophylactically [9,74–76]. There is no standard recommendation as to the use of catheter locks and their over-arching function is to maintain the integrity of the line. An extensive literature based on their application and investigations of their efficacy has emerged in recent years but a detailed discussion of their individual use is beyond the scope of the present study and the reader is directed to more comprehensive reviews [68–70].

#### 4.4. Barrier Caps

In most cases, the silicone septum is the main physical barrier preventing the entry of microorganisms to the catheter lumen. Disinfection, while widely recognised as critical, still falls foul of issues relating to adherence and on the vagaries of the person performing the cleansing process [23,25,27]. Passive NFC caps have come more to the fore in recent years through providing a passive means of continuous disinfection whilst the catheter is not in use [77–84]. A number of different approaches have been taken in the design of the disinfectant barrier cap and their mode of operation is summarised in Figure 4. The simplest approach is the incorporation of a foam/gauze insert soaked with 70% IPA (i.e., 3M Curoc™, SwabCap®, Site-Scrub®) or one that contains an antimicrobial (povidone iodine or alcoholic chlorhexidine) which is threaded onto the Luer connector when the

line is not in use. As the foam pad contacts the silicone septum, the twisting of the cap provides a modicum of friction which can aid in the removal of the bacteria. Menyhay et al. (2008) have reported on a refinement of the basic design whereby a two-part system is employed with the antimicrobial contained within a capsule (Figure 4A) [52]. As the cap is threaded onto the Luer, the capsule is forced into contact with a spike at the top of the cap which pierces the capsule releasing the antimicrobial into the foam. The core advantage of this and similar systems are that their application is relatively independent of the NFC manufacturer and simply require a Luer connector. An alternative design has been proposed by Buchmann et al. (2009) whereby the cap encapsulates the entire terminal end of the NFC including the thread (Figure 4B) and, in contrast to the simple insert cap highlighted in Figure 4A, is intended to remain attached during flush procedures [85]. Mariyaselvam et al. (2015) reported that contamination of syringe tips is an often overlooked factor in the development of CRBSI and hence retention of the antimicrobial foam as a secondary septum could aid in the decontamination of the tips prior to entering the NFC [86].

In both designs, the barrier cap does not interact directly with the catheter lumen but aims to disinfect the silicone septum and surrounding area and are intended for applications where the frequency of access may be high. ClearGuard®, in contrast to the previous designs, relies upon a chlorhexidine impregnated rod that is inserted directly into the end of catheter lumen in place of the NFC connector (Figure 4C). The chlorhexidine diffuses into the intraluminal space and has been shown to be highly effective at reducing CRBSI risk within haemodialysis patients—a cohort that has hitherto been characterised with high rates of infection [82].

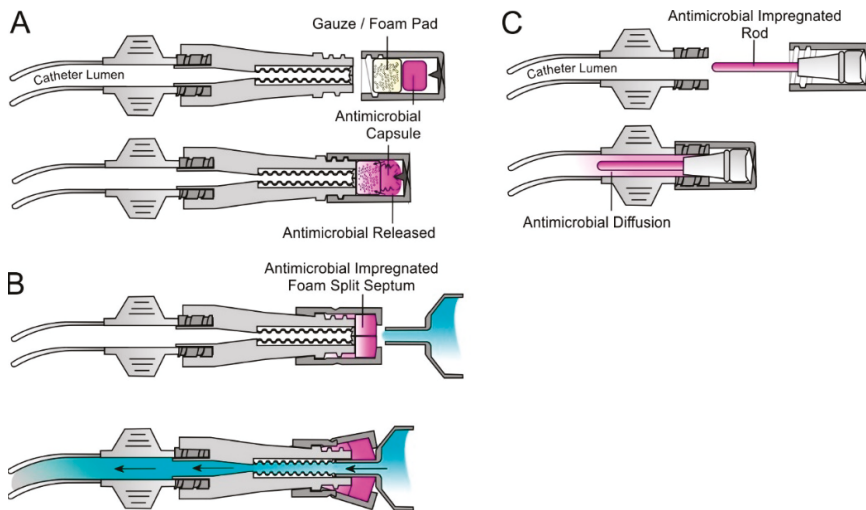


**Figure 4.** Needle free connector barrier caps based on simple foam insert (A), an encapsulating split septum (B) and the Clearguard® terminal cap (C).

### 5. Catheter Designs and Antimicrobial Mechanisms

The provision of training programmes to educate clinicians and patients in the maintenance of vascular access lines is a critical frontline response that can dramatically lower the risk of CRBSI but, as noted earlier in Section 4.2, achieving 100% compliance and prevention is unlikely. The provision of antibacterial caps is another advance which has demonstrated considerable gains but, as with conventional aseptic practice, there remains a human element in their successful application as well as several contentious cost issues that can be a barrier to their widespread adoption. The development of materials resistant to antimicrobial colonisation has long been regarded as a means through which to counter the potential lapses in practice and where elimination of the propensity to form a biofilm is

the principal goal. The majority of the research efforts targeted at this problem are generally directed towards materials that possess antimicrobial and/or antifouling properties and a summary of the various strategies are highlighted in Figure 5.

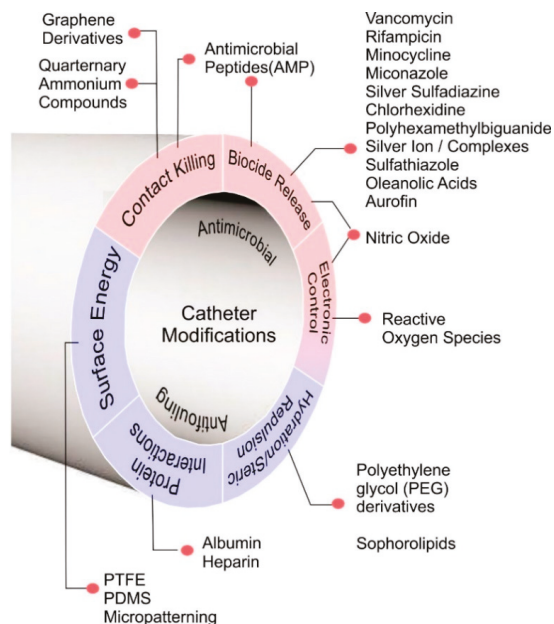


**Figure 5.** Material approaches to counter bacterial colonisation of central venous catheters.

Tunnelled CVCs, non-tunnelled CVCs and PICC-lines are typically made of polyurethane (PU) or silicone materials, with tunnelled CVC cuffs composed of polyethylene terephthalate (PET) [87]. The preference for PU stems from the versatility with which the physical and chemical properties of the material can be manipulated through judicious choice of the monomers [88–90]. In general, PU is prepared from the reaction of hydroxyl and isocyanate groups to yield the carbamate linkage (the urethane) and, with a large array of commercially available polyols and polyisocyanates bearing a range of chemical functionalities from which to choose [89,90], it is of little surprise that the properties of the polymer can be tuned to particular applications. The polymer properties can be critical in influencing the processability of the material and its resulting mechanical performance and biocompatibility [88,91–93]. Critically, the ability to alter the chemical functionality allows for modifications to the hydrophilicity/hydrophobicity of the surface and, through the presence of reactive chemical side chains, provides the ability to further tailor the catheter interface with antimicrobial/antifouling features [88,93–101].

### 5.1. Biocide Release

The antimicrobial systems employed on both the extra and endoluminal surfaces aim to kill the bacteria (or at the very least inhibit further growth) and a number of different mechanisms have been evaluated. Drug eluting materials in which the biocidal agent is released passively into the lumen represent the most common approach (as listed in Figure 5) and cover a wide variety of chemical species [95,102–110]. Incorporation within the catheter can be achieved through simple adsorption of the active agent but, more recent strategies have involved electrostatic interactions with surfactants and polyelectrolyte systems to yield more coherent and stable coatings. Thermally stable biocides such as silver ions/complexes can be melt processed along with the polymer used in the



production of the catheter such that the antimicrobial is homogeneously distributed throughout the material. Alternatively, exposing the catheter surfaces to a suitable solvent can induce swelling of the polymer and impregnation/incorporation of the biocide at low temperature. Some of the commercial antimicrobial catheter systems and their characteristics are compared in Table 3.

**Table 3.** Commercial catheter incorporating antimicrobial/antifouling features.

Manufacturer	Product	Antimicrobial Agent	Mode of Action
Kimal	Altius® ProActiv+	Polyhexamethylene biguanide (PHMB)	Contact
Teleflex	ARROWg+ard®	Chlorhexidine and silver sulfadiazine	Eluting
	Chlorag+ard®	Chlorhexidine only	
Cook Medical	Spectrum®	Minocycline & Rifampin	Eluting
B. Braun	Certofix®	Polyhexamethylene biguanide (PHMB)	Contact
Edward Lifesciences	Vantex CVC Oligon	Silver ions	Contact
	AMC Thromboshield	Benzalkonium chloride with heparin coating	

The efficacy of employing antimicrobial catheters has been widely studied for most of the systems outlined in Table 3 or their equivalent, and there is a substantial body of the literature which has found marked improvements over the use of unmodified catheters. There have also been numerous reports that have found little benefit. It must be noted that there are a large number of factors involved in the maintenance of CVCs (as noted in earlier sections) which can make comparisons between the different systems and between coated/uncoated challenging. Nevertheless, a number of systematic reviews have conducted meta analyses of the available literature and there is substantive evidence that the implementation of catheters coated/impregnated with chlorhexidine/silver sulfadiazine and antibiotics (5-fluorouracil, vancomycin, benzalkonium chloride, teicoplanin, miconazole/rifampicin, minocycline, and minocycline/rifampicin) were associated with lower incidences of catheter colonization and had the greatest potential to reduce the incidence of CRBSIs per 1000 catheter days. In contrast, the efficacy of silver impregnated systems is much more contentious and, in many cases, fail to yield statistically significant results.

The Healthcare Infection Control Practices Advisory Committee (HICPAC) recommend the use of a CVC impregnated with chlorhexidine-silver sulfadiazine (CSS) or minocycline-rifampicin (MR) in patients with at least five consecutive days of catheterisation [111]. A recent systematic survey by Lai et al. (2016) found that the most effective system within this class of material was the rifampicin but it must be noted that such studies were of limited duration and their efficacy in CVCs destined for long term placement is questionable [112]. As such, most of the commercial systems highlighted in Table 3 recommend a maximum dwell time. A core issue is the limited repository of the drug within the polymer or coating such that release does not simply terminate after a given time period but results in sub lethal doses being administered which can facilitate the development of antimicrobial resistance.

Putting the issue of dwell time aside, the release of antibiotic moieties (i.e., rifampicin) have a long history but the increasing threat of bacterial resistance has driven considerable effort to examine alternative antimicrobial agents. Various antimicrobial peptides [100,108,113–115], guanidine derivatives (i.e., poly hexamethyl biguanide, polyarginines) [103,104], quaternary ammonium compounds [96,98], nitric oxide precursors [105,106,116,117], silver [118–120] and a host of other small molecules/metal ions or nanoparticles [107,110,118,121–124] with possible biocidal activity have all been investigated as potential modifiers for use in catheters and, while these invariably impact bacterial colonisation, they have yet to make the leap to commercial exploitation and/or substantive clinical trials.

## 5.2. Contact Kill Systems

Contact killing of bacteria, in contrast to passive elution, relies on the immobilisation of the antimicrobial at the catheter surface and, as such, sets out to present a lethal barrier to the microbes attempting to colonise the catheter surfaces [96,98,100,104,114,115,119,125,126]. Grafting through plasma processes, polymerisation of a biocide functionalised monomer, covalent linkage (i.e., click chemistry) onto side chains or the deposition of insoluble layers are common techniques through which the catheter interface can be functionalised. Quaternary ammonium compounds (QACs), guanidine derivatives, antimicrobial peptides (AMPs) and, more recently, graphene/graphene oxide [125] systems have all been evaluated as contact killing agents. In terms of QAC and AMPs, their cationic functionality and ability to disrupt the phospholipid bilayer are the main weapons through which they attack the integrity of microbial cell wall/membrane. The mechanisms through which graphene and its various analogues work are more contentious though there is evidence to suggest that the edge planes of graphene platelets directly exert a membrane disruption effect. The in situ generation of reactive oxygen species (ROS) through redox cycling of quinoid functionalities in graphene oxide has also been shown to be a potential cytotoxic pathway [125].

As the active agents are immobilised at the surface of the catheter, the biocidal activity is, at least in a model system, capable of being maintained indefinitely. Unfortunately, the need for direct contact between the agent and the bacteria can also be a significant limitation. The deposition of conditioning films or macromolecular debris (i.e., from dead bacteria or non-specific binding of proteins) along the lumen can negate the antimicrobial effects through preventing these killing interactions. Although the contact killing approach, like the drug elution systems, appears to offer only short-term activity, it should be noted that, unlike the latter, the underpinning mechanism has no impact on emerging antimicrobial resistance. Applied in isolation, the contact approach is clearly limited by fouling but, if the latter were removed, then it could be envisaged that long term effectiveness could be achieved.

## 5.3. Surface Hydration/Hydrophilicity

Prevention of fouling has been the second main route through which to avoid biofilm formation and minimise the risk of both CRBSI [97,99,114,127] and catheter related thrombotic complications [128–131]. The latter can be categorised into four types: mural thrombosis, ball-valve-thrombosis, intraluminal thrombotic occlusion and, the most common cause, pericatheter sheath [128–131]. In short, the presence of the fibrin sleeve is due to catheter insertion causing local venous injury, leading to the deposition of fibrin on the catheter surface and subsequent intraluminal growth of endothelial and smooth muscles within hours after CVC insertion [130]. This in turn could lead to blood flow reduction which further increases the risk of endoluminal cellular attachment and thus thrombus formation [129,130]. Further movement of the catheter within the vein causes endothelial erosions which prompt the formation of mural thrombosis within the catheter lumen [128,130]. On the other hand, a thrombus on the catheter tip could lead to ball-valve thrombosis where infusion can still occur, but fluid aspiration is impeded [128,130].

As indicated in Figure 5, a number of strategies aim to prevent fouling. Historically, the modulation of hydration and steric interactions were among the first approaches and typically exploit polyethylene glycol (PEG) derivatives tethered at the polymer–solution interface [99]. The rationale here is to control the hydrophilicity of the polymer interface to create a tightly bound water layer. This alters the thermodynamics of adhesion through making it both physically and energetically less favourable for the adsorption of proteins. While PEG derivatives have dominated the early literature, alternative systems incorporating zwitterionic moieties (i.e., polysulfobetaine) have been used in PICC lines and shown to reduce the adhesion of bacteria and the onset of thrombosis [132]. Instead of hydrogen bonding, zwitterionic based coatings use electrostatic interactions to create the hydration layer [131,133]. Roth et al. (2020) demonstrated the use of branched polyethyleneimine (PEI) modified polyurethane as a means of reducing the coefficient of friction and haemolysis ratio providing a material with considerable antithrombogenic properties [131]. The intrinsic inertness of silicone-based catheter

materials can be problematic, but plasma treatment can enable the introduction of more reactive surface functionalities onto which antifouling coatings can be anchored. This was adopted by Blanco et al. (2014) who demonstrated the use of a laccase/phenolic/sulfobetaine mixture to yield a zwitterionic film tethered to a plasma aminated silicone substrate [133]. The system, although initially targeting urinary catheters, demonstrated considerable antifouling capabilities which could however be translated to intravascular systems. The novelty of the biocatalytic film formation is clear but it could be argued that the complexity of the approach would be a detractor from more widespread adoption.

It is clear that the adaptation and incorporation of the antifouling film systems could have a significant impact on mortality as it has been estimated that some 20% to 40% catheters develop pericatheter thrombus or fibrin sheath [134]. The latter predisposes the patient to infection and increases the risk of thrombosis [135,136] and, if detachment occurs, the possibility of potentially fatal thromboembolism [137].

#### 5.4. Protein Layer Interactions

The use of a protein coat to prevent the adhesion of other proteins can appear counter intuitive but such interactions are typified by the precoating of catheter surfaces with albumin (a relatively benign protein). This approach has been shown to markedly reduce the deposition of proteins that would otherwise adhere and contribute to biofilm formation [138,139]. The effectiveness of such an approach is however relatively short term as prolonged contact with blood eventually leads to the removal of the albumin. The use of heparin as a catheter lock is well established where it is employed to prevent thrombus and occlusion of the line [67–70,84]; catheter surfaces coated with the molecule have also exhibited marked resistance to non-specific protein fouling [92,119,140]. Several conflicting mechanisms for this action have been suggested (electrostatic repulsion, protein specific interactions, inhibition of bacterial adhesions etc.) but much remains to be done in order to elucidate whether they act in concert or if one predominates. The use of heparin coatings, as with its inclusion in lock solutions, can also give rise to concerns over sensitivity [141–143].

#### 5.5. Surface Energy

The ideal solution would be to have the catheter composed of a material that minimises adhesion without the complexities of extensive surface modification. The adoption of materials possessing low surface energy has been proffered as one route through which to tackle biofilm formation and is typified by hydrophobic fluoropolymers (PTFE) and silicones (PDMS) [139,144–146]. Despite possessing very low surface energy (<25 mN/m), their effectiveness at preventing the non-specific adhesion of proteins is contentious with a number of investigations offering conflicting evidence. Where such polymers have found success, it has been suggested that passivation by albumin is the main factor in hindering cell attachment rather than the intrinsic low energy properties of the polymer substrate [139,144]. The exploitation of hydrophobicity in anti-adhesion contexts may however require a more nuanced application and there have been some notable advances through manipulating the surface topography [97,147]. Increasing surface roughness or the introduction of specific patterning inspired by biological materials (i.e., Sharklet), have shown to provide superhydrophobic coatings that are effective against *E. coli* and *S. aureus* [97]. The translation of the technology to catheter systems to prevent extra and intra luminal colonisation may be more challenging and, at present, such approaches remain speculative.

#### 5.6. Smart/Electronic Materials

The majority of materials research aimed at combatting CRBSIs tend to focus on the modification of catheter surfaces and, while many of the strategies have shown to be effective in the short term, almost all succumb to fouling with increased dwell time and a loss of activity. Advances in electronics have seen some interest in the development of “smart” materials that can detect the presence of a

biofilm or, upon activation by an appropriate stimulus, release a biocidal agent into the lumen. Such research is still in its infancy but could herald a wholly new avenue for tackling CRBSI.

Li et al. (2014) were among the first to consider the introduction of sensors within the catheter line as a means of detecting the presence of bacteria [148]. Their approach relied upon the use of carbon fibre filaments (possessing the dimensional properties necessary for insertion with a typical catheter lumen) serving as electrodes which could measure changes in the pH of the intraluminal space as a consequence of bacterial growth. This was based on examining the change in the voltammetric response of uric acid (present within the blood) with changes in pH. An alternative approach by Davis et al. (2013) took the system further through the use of polymer modified electrodes in which pH dependent redox polymers based on plumbagin were used to indirectly measure pH and removed the dependence on the endogenous urate [149]. This was followed by Casimero et al. (2018) with a poly(flavin) system, again exploiting the redox transition of the immobilised flavin to gauge pH changes caused by bacterial growth [150]. These reagentless sensors, while capable of measuring pH within complex bacterial environments, also possessed the advantageous attribute of being capable of catalysing the electroreduction of oxygen resulting in the generation of biocidal reactive oxygen species (ROS) [149]. The core mechanism of the polymer modified electrodes relies upon the pH dependence of quinoid redox interconversions and, in this respect, they could be considered analogous to some of the more recent investigations employing graphene oxide where similar transitions are associated with ROS. The main difference here being that the amount of ROS generated via the poly(plumbagin) could be controlled through manipulation of the electrode potential. Such work was however purely proof of concept and there is no supplementary data on their effectiveness in reducing/preventing bacterial colonisation [149].

Paredes et al. (2014) proposed a novel technique for in-line diagnosis of bloodstream infections through impedimetric biosensing [151]. The system incorporates an interdigitated microelectrode biosensor (IDM), wireless electronics and antenna to detect infection and then trigger an external alarm. Colonisation and subsequent biofilm growth on the IDM alters the capacitance, which is compared to a threshold generated using laboratory-based impedance spectroscopy, providing a preventative warning at the earliest signs of colonisation. The use of a label-free IDM provides the system with a lifetime of over 11 months, requiring only a 50 mAh coin-cell battery. A critical issue here, however, is an assumption that material on the surface of the electrode is a biofilm, when it could be the adsorption of macromolecular components intrinsic to blood. There is little doubt that the introduction of diagnostic systems that can inform the clinician (or patients self-administering their line) of the presence of contaminated NFCs could aid in the management of the CVC and optimise the use of hygiene care bundles.

The smart approach, as indicated previously, is not necessarily limited to diagnostics but can also be harnessed to yield an “on demand” antimicrobial action. In addition to the generation of ROS, reactive nitrogen species (RNS) have also been considered and several reports have targeted the selective release of nitric oxide (NO) as the principal weapon through which to prevent bacterial colonisation [105,106,116,117]. Such work builds on the fact that NO is a chemical transmitter which has a multitude of biochemical roles but, in this context, its status as a key player in minimising platelet adhesion whilst also acting as a broad spectrum antimicrobial is of greatest value. Numerous studies have investigated the use of NO donor molecules (i.e., diazoniumdiolates and S-nitrosothiols) immobilised at catheter surfaces [105,106]. In such cases, the mode of action following the passive release mechanism (through trans-nitrosation of other molecules within the matrix and/or homolytic cleavage) is common to conventional antimicrobial elution systems. Goudie et al. (2019) recently demonstrated the covalent linkage of N-acetyl penicillamine onto silicone catheters in which the thiol could be further functionalised to serve as a NO donor [106]. The use of branch (and hyper branched) methacrylate linkers as indicated in Figure 6A enables a greater density of NO to be stored at the interface with the polymeric network found to retain its anti-fouling properties even after the NO biocides have been delivered.

Mihu et al. (2017) have sought to take a different approach through the thermal reaction between nitrite and glucose during a sol–gel process [152]. This results in the in situ generation of NO and its subsequent entrapment with the sol–gel nanoparticle matrix. In contrast to the previous investigations involving donor molecules, NO is released directly from the nanoparticles. This has been shown to afford activity against bacteria with MRSA cellular growth decreased by 40% following incubation with 2.5 mg/mL NO-np, and by 50% at concentrations greater than 5 mg/mL. The viability of staphylococcal biofilms also reduced by 51.8% under the latter conditions. Furthermore, MRSA growth was seen to be reduced by 50% after 8 h of normal exposure (no incubation) with 2.5 mg/mL NO-np, remaining at these reduced levels after 24 h. The latter results indicate a similar level of success to antibiotic locks, with comparable dwell times. Impregnation of nitric oxide-releasing nanoparticles could prove to be a potential alternative to prophylactic locking, removing reliance on antibiotics and providing a broader effective range; but further research into their in vivo effects are required.

The electrochemical generation of NO represents a new stage in the evolution of active catheters and various reports have examined its electrocatalytic generation from nitrite [116,117]. A variety of copper complexes have been investigated as potential redox cyclers (indicated in Figure 6B). Both the copper complex and nitrite ion must be supplied to the system in order to facilitate the electrogeneration of NO as neither will be present in the IV fluids being delivered. This stands in marked contrast to the plumbagin (or graphene oxide) system where the catalyst can be immobilised at the electrode and the principal feedstock is oxygen which is already endogenous to both the blood and IV fluids being administered. In order to counter this, the authors have suggested the use of a dual lumen CVC in which one lumen is dedicated to the NO generation with the other for the IV fluid transfer. This separates the potentially harmful catalyst and nitrite from direct contact with the vascular system and relies upon the diffusion of electrogenerated NO across the silicone membrane separating the two fluid lines as indicated in Figure 6B. This is a much more complex arrangement from both procedural and instrumental perspectives. However, the availability of a large reservoir of the nitrite feedstock could counter the issues of depletion and fouling that is common to most of the conventional antimicrobial/anti-adhesion approaches and prove to be effective on long CVC dwell times.

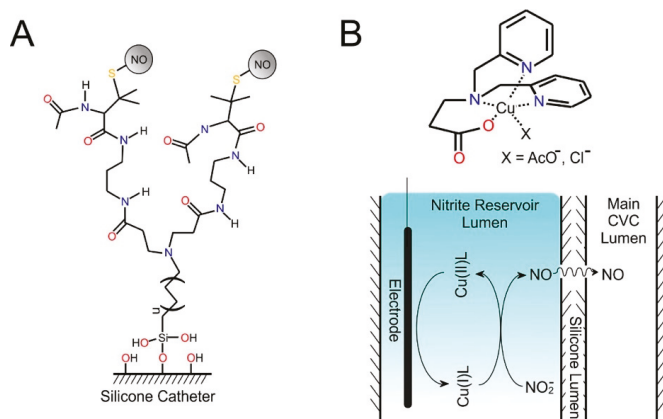


**Figure 6.** (A) Hyperbranched methacrylate-penicillamine based nitric oxide (NO) donors. (B) Dual lumen electrocatalytic release of nitric oxide using copper complexes.

## 6. Conclusions

Catheter-related bloodstream infections have proven to be one of the most common nosocomial infections in the modern healthcare setting. For a condition that seems almost extraneous, they have a considerable impact on patient quality of life, up to the point of mortality, and pose a serious and

undue economic burden on patients and health services. While there have been advances in each of the discussed areas, from improved aseptic techniques, new antibiotics and alternative lock therapies, these revolutions do not negate the core issues: aseptic techniques are only as reliable as the compliance of the user, systemic antibiotics are successful if you catch the symptoms early and the efficacy of antibiotic lock therapy is still up for debate.

Current practices for CRBSI diagnosis, prevention and management rely too much on therapeutic techniques, effectively waiting for patient quality of life to deteriorate before any action is taken. While there have been advances in catheter-sparing and prophylactic techniques, with the new guidelines promoting the use of impregnated catheters, and the improved variety, efficacy and range (outside of antibiotics) of antimicrobial locks looking promising, the impact on patient quality of life, cost and mortality is still too significant to declare these practices as viable solutions. There still remains a pressing need to develop a long-term solution for the proactive monitoring of catheters, a solution that will detect infection earlier or prevent it altogether.

**Author Contributions:** Conceptualization, C.C., T.R., J.D.; methodology, T.R.; formal analysis, R.B., A.D., C.H.; investigation, T.R.; writing—original draft preparation, T.R., C.C.; writing—review, editing and supervision, J.D. All authors have read and agreed to the published version of the manuscript.

**Funding:** This research was funded by the Department for the Economy Northern Ireland, Kimal PLC and Abbott Diabetes Care PLC., European Union's INTERREG VA Programme, managed by the Special EU Programmes Body (SEUPB).

**Conflicts of Interest:** Charnete Casimero is presently engaged on Cooperative Award in Science and Technology (CAST) PhD studentship cofounded by the Department for the Economy (DfE) Northern Ireland and Kimal PLC. Robert Barber is similarly engaged on Cooperative Award in Science and Technology (CAST) PhD studentship cofounded by the Department for the Economy (DfE) Northern Ireland and Abbott Diabetes Care PLC.

## References

1. Ripa, M.; Morata, L.; Rodriguez-Nunez, O.; Cardozo, C.; Puerta-Alcalde, P.; Hernandez-Meneses, M.; Ambrosioni, J.; Linares, L.; Bodro, M.; Valcárcel, A.; et al. Short-Term Peripheral Venous Catheter-Related Bloodstream Infections: Evidence for Increasing Prevalence of Gram-Negative Microorganisms from a 25-Year Prospective. *Antimicrob. Agents Chemother.* **2018**, *62*, 1–11. [[CrossRef](#)] [[PubMed](#)]
2. Lim, S.; Gangoli, G.; Adams, E.; Hyde, R.; Broder, M.S.; Chang, E.; Reddy, S.R.; Tarbox, M.H.; Bentley, T.; Ovington, L.; et al. Increased Clinical and Economic Burden Associated with Peripheral Intravenous Catheter-Related Complications: Analysis of a US Hospital Discharge Database. *Inquiry* **2019**, *56*. [[CrossRef](#)] [[PubMed](#)]
3. Sato, A.; Nakamura, I.; Fujita, H.; Tsukimori, A.; Kobayashi, T.; Fukushima, S.; Fujii, T.; Matsumoto, T. Peripheral venous catheter-related bloodstream infection is associated with severe complications and potential death: A retrospective observational study. *BMC Infect. Dis.* **2017**, *17*, 1–6. [[CrossRef](#)]
4. Zhang, L.; Cao, S.; Marsh, N.; Ray-Barruel, G.; Flynn, J.; Larsen, E.; Rickard, C.M. Infection risks associated with peripheral vascular catheters. *J. Infect. Prev.* **2016**, *17*, 207–213. [[CrossRef](#)] [[PubMed](#)]
5. Frasca, D.; Dahyot-Fizelier, C.; Mimos, O. Prevention of central venous catheter-related infection in the intensive care unit. *Crit. Care* **2010**, *14*, 212. [[CrossRef](#)]
6. Bouza, E. Intravascular catheter-related infections: A growth problem, the search for better solutions. *Clin. Microbiol. Infect.* **2002**, *8*, 255. [[CrossRef](#)]
7. Gahlöt, R.; Nigam, C.; Kumar, V.; Yadav, G.; Anupurba, S. Catheter-related bloodstream infections. *Int. J. Crit. Illn. Inj. Sci.* **2014**, *4*, 162–167. [[CrossRef](#)]
8. Mermel, L.A. Prevention of Intravascular Catheter-Related Infections. *Ann. Intern. Med.* **2000**, *132*, 391. [[CrossRef](#)]
9. McGrath, E.; Du, W.; Rajpurkar, M. Preemptive Ethanol Lock Therapy in Pediatric Hematology/Oncology Patients with Catheter-Associated Bloodstream Infection: Impact on Length of Stay, Cost, and Catheter Salvage. *Clin. Pediatr. (Phila)* **2018**, *57*, 285–293. [[CrossRef](#)]
10. Labriola, L. Antibiotic locks for the treatment of catheter-related blood stream infection: Still more hope than data. *Semin. Dial.* **2019**, *32*, 402–405. [[CrossRef](#)]

11. Maki, D.G.; Kluger, D.M.; Crnich, C.J. The risk of bloodstream infection in adults with different intravascular devices: A systematic review of 200 published prospective studies. *Mayo Clin. Proc.* **2006**, *81*, 1159–1171. [[CrossRef](#)] [[PubMed](#)]
12. Bouza, E.; Burillo, A.; Muñoz, P. Catheter-related infections: Diagnosis and intravascular treatment. *Clin. Microbiol. Infect.* **2002**, *8*, 265–274. [[CrossRef](#)] [[PubMed](#)]
13. Dimick, J.B.; Pelz, R.K.; Consunji, R.; Swoboda, S.M.; Hendrix, C.W.; Lipsett, P.A. Increased Resource Use Associated with Catheter-Related Bloodstream Infection in the Surgical Intensive Care Unit. *Arch. Surg.* **2001**, *136*, 229–234. [[CrossRef](#)]
14. Saliba, P.; Hornero, A.; Cuervo, G.; Grau, I.; Jimenez, E.; García, D.; Tubau, F.; Martínez-Sánchez, J.M.; Carratalà, J.; Pujol, M. Mortality risk factors among non-ICU patients with nosocomial vascular catheter-related bloodstream infections: A prospective cohort study. *J. Hosp. Infect.* **2018**, *99*, 48–54. [[CrossRef](#)] [[PubMed](#)]
15. Wolf, J.; Curtis, N.; Worth, L.J.; Flynn, P.M. Central Line-associated Bloodstream Infection in Children. *Pediatr. Infect. Dis. J.* **2013**, *32*, 905–910. [[CrossRef](#)] [[PubMed](#)]
16. O’Grady, N.P.; Alexander, M.; Dellinger, E.P.; Gerberding, J.L.; Heard, S.O.; Maki, D.G.; Masur, H.; McCormick, R.D.; Mermel, L.A.; Pearson, M.L.; et al. Guidelines for the Prevention of Intravascular Catheter-Related Infections. *Clin. Infect. Dis.* **2002**, *35*, 1281–1307. [[CrossRef](#)]
17. Helder, O.K.; Kornelisse, R.F.; Reiss, I.K.M.; Ista, E. Disinfection practices in intravenous drug administration. *Am. J. Infect. Control* **2016**, *44*, 721–723. [[CrossRef](#)]
18. Ista, E.; van der Hoven, B.; Kornelisse, R.F.; van der Starre, C.; Vos, M.C.; Boersma, E.; Helder, O.K. Effectiveness of insertion and maintenance bundles to prevent central-line-associated bloodstream infections in critically ill patients of all ages: A systematic review and meta-analysis. *Lancet Infect. Dis.* **2016**, *16*, 724–734. [[CrossRef](#)]
19. Loveday, H.P.; Wilson, J.A.; Pratt, R.J.; Golsorkhi, M.; Tingle, A.; Bak, A.; Browne, J.; Prieto, J.; Wilcox, M. Epic3: National evidence-based guidelines for preventing healthcare-associated infections in nhs hospitals in england. *J. Hosp. Infect.* **2014**, *86*, S1–S70. [[CrossRef](#)]
20. Smith, R.N.; Nolan, J.P. Central venous catheters. *BMJ* **2013**, *347*, f6570. [[CrossRef](#)]
21. Wells, S. Venous access in oncology and haematology patients: Part two. *Nurs. Stand.* **2008**, *23*, 35–42. [[CrossRef](#)] [[PubMed](#)]
22. Pinelli, F.; Cecero, E.; Degl’Innocenti, D.; Selmi, V.; Giua, R.; Villa, G.; Chelazzi, C.; Romagnoli, S.; Pittiruti, M. Infection of totally implantable venous access devices: A review of the literature. *J. Vasc. Access* **2018**, *19*, 230–242. [[CrossRef](#)]
23. Moureau, N.L.; Flynn, J. Disinfection of Needleless Connector Hubs: Clinical Evidence Systematic Review. *Nurs. Res. Pract.* **2015**, *2015*, 1–20. [[CrossRef](#)] [[PubMed](#)]
24. Mermel, L.A. What is the predominant source of intravascular catheter infections? *Clin. Infect. Dis.* **2011**, *52*, 211–212. [[CrossRef](#)] [[PubMed](#)]
25. Hull, G.J.; Moureau, N.L.; Sengupta, S. Quantitative assessment of reflux in commercially available needle-free IV connectors. *J. Vasc. Access* **2018**, *19*, 12–22. [[CrossRef](#)] [[PubMed](#)]
26. Hadaway, L.; Richardson, D. Needleless connectors: A primer on terminology. *J. Infus. Nurs.* **2010**, *33*, 22–31. [[CrossRef](#)] [[PubMed](#)]
27. Hadaway, L. Needleless connectors for IV catheters. *Am. J. Nurs.* **2012**, *112*, 32–44. [[CrossRef](#)] [[PubMed](#)]
28. Jacobs, B.R.; Schilling, S.; Doellman, D.; Hutchinson, N.; Rickey, M.; Nelson, S. Central Venous Catheter Occlusion: A Prospective, Controlled Trial Examining the Impact of a Positive-Pressure Valve Device. *J. Parenter. Enter. Nutr.* **2004**, *28*, 113–118. [[CrossRef](#)] [[PubMed](#)]
29. Schilling, S.; Doellman, D.; Hutchinson NJacobs, B.R. The impact of needleless connector device design on central venous catheter occlusion in children: A prospective, controlled trial. *J. Parenter. Enter. Nutr.* **2006**, *30*, 85–90. [[CrossRef](#)]
30. Hadaway, L. Needleless connectors: Improving practice, reducing risks. *JAVA-J. Assoc. Vasc. Access* **2011**, *16*, 20–24. [[CrossRef](#)]
31. Jarvis, W.R.; Murphy, C.; Hall, K.K.; Fogle, P.J.; Karchmer, T.B.; Harrington, G.; Salgado, C.; Giannetta, E.T.; Cameron, C.; Sherertz, R.J. Health Care-Associated Bloodstream Infections Associated with Negative- or Positive-Pressure or Displacement Mechanical Valve Needleless Connectors. *Clin. Infect. Dis.* **2009**, *49*, 1821–1827. [[CrossRef](#)] [[PubMed](#)]

32. Tarakji, K.G.; Ellis, C.R.; Defaye, P.; Kennergren, C. Cardiac implantable electronic device infection in patients at risk. *Arrhythmia Electrophysiol. Rev.* **2016**, *5*, 65–71. [[CrossRef](#)] [[PubMed](#)]
33. Bongiorno, M.G.; Tascini, C.; Tagliaferri, E.; Cori, A.D.; Soldati, E.; Leonildi, A.; Zucchelli, G.; Ciullo, I.; Menichetti, F. Microbiology of cardiac implantable electronic device infections. *Europace* **2012**, *14*, 1334–1339. [[CrossRef](#)] [[PubMed](#)]
34. Pronovost, P. Interventions to decrease catheter-related bloodstream infections in the ICU: The Keystone Intensive Care Unit Project. *Am. J. Infect. Control* **2008**, *36*, S171.e1–S171.e5. [[CrossRef](#)]
35. Drews, F.A.; Bakdash, J.Z.; Gleed, J.R. Improving central line maintenance to reduce central line-associated bloodstream infections. *Am. J. Infect. Control* **2017**, *45*, 1224–1230. [[CrossRef](#)]
36. Crnich, C.J.; Maki, D.G.G. The Promise of Novel Technology for the Prevention of Intravascular Device-Related Bloodstream Infection. II. Long-Term Devices. *Clin. Infect. Dis.* **2002**, *34*, 1362–1368. [[CrossRef](#)]
37. Chernecky, C.; Waller, J. Comparative evaluation of five needleless intravenous connectors. *J. Adv. Nurs.* **2011**, *67*, 1601–1613. [[CrossRef](#)]
38. Menyhay, S.; Maki, D. Disinfection of Needleless Catheter Connectors and Access Ports with Alcohol May Not Prevent Microbial Entry: The Promise of a Novel Antiseptic-Barrier Cap. *Infect. Control Hosp. Epidemiol.* **2006**, *27*, 23–27. [[CrossRef](#)]
39. Rupp, M.E.; Sholtz, L.A.; Jourdan, D.R.; Marion, N.D.; Tyner, L.K.; Fey, P.D.; Iwen, P.C.; Anderson, J.R. Outbreak of Bloodstream Infection Temporally Associated with the Use of an Intravascular Needleless Valve. *Clin. Infect. Dis.* **2007**, *44*, 1408–1414. [[CrossRef](#)]
40. Macias, A.E.; Huertas, M.; Ponce de Leon, S.; Munoz, J.M.; Chavez, A.R.; Sifuentes-Osornio, J.; Romero, C.; Bobadilla, M. Contamination of intravenous fluids: A continuing cause of hospital bacteremia. *Am. J. Infect. Control* **2010**, *38*, 217–221. [[CrossRef](#)]
41. Fowler, V.G.; Justice, A.; Moore, C.; Benjamin, D.K.; Woods, C.W.; Campbell, S.; Reller, L.B.; Corey, G.R.; Day, N.P.J.; Peacock, S.J. Risk Factors for Hematogenous Complications of Intravascular Catheter-Associated Staphylococcus aureus Bacteremia. *Clin. Infect. Dis.* **2005**, *40*, 695–703. [[CrossRef](#)] [[PubMed](#)]
42. Lake, J.G.; Weiner, L.M.; Milstone, A.M.; Saiman, L.; Magill, S.S.; See, I. Pathogen distribution and antimicrobial resistance among pediatric healthcare-associated infections reported to the National Healthcare Safety Network, 2011–2014. *Infect. Control Hosp. Epidemiol.* **2018**, *39*, 1–11. [[CrossRef](#)] [[PubMed](#)]
43. Alby-Laurent, F.; Lambe, C.; Ferroni, A.; Salvi, N.; Lebeaux, D.; Le Gouëz, M.; Castelle, M.; Moulin, F.; Nassif, X.; Lortholary, O.; et al. Salvage strategy for long-term central venous catheter-associated Staphylococcus aureus infections in children. *Front. Pediatr.* **2019**, *6*, 427. [[CrossRef](#)] [[PubMed](#)]
44. Veerachamy, S.; Yarlagadda, T.; Manivasagam, G.; Yarlagadda, P.K. Bacterial adherence and biofilm formation on medical implants: A review. *Proc. Inst. Mech. Eng. Part H J. Eng. Med.* **2014**, *228*, 1083–1099. [[CrossRef](#)] [[PubMed](#)]
45. Oliveira, W.F.; Silva, P.M.S.; Silva, R.C.S.; Silva, G.M.M.; Machado, G.; Coelho, L.C.B.B.; Correia, M.T.S. Staphylococcus aureus and Staphylococcus epidermidis infections on implants. *J. Hosp. Infect.* **2018**, *98*, 111–117. [[CrossRef](#)]
46. Zanwar, S.; Jain, P.; Gokarn, A.; Devadas, S.K.; Punatar, S.; Khurana, S.; Bonda, A.; Pruthy, R.; Bhat, V.; Qureshi, S.; et al. Antibiotic lock therapy for salvage of tunneled central venous catheters with catheter colonization and catheter-related bloodstream infection. *Transpl. Infect. Dis.* **2019**, *21*, 1–6. [[CrossRef](#)]
47. Kostakioti, M.; Hadjifrangiskou, M.; Hultgren, S.J. Bacterial biofilms: Development, dispersal, and therapeutic strategies in the dawn of the postantibiotic era. *Cold Spring Harb. Perspect. Med.* **2013**, *3*, a010306. [[CrossRef](#)]
48. Pérez-Zárate, P.; Aragón-Piña, A.; Soria-Guerra, R.E.; González-Amaro, A.M.; Pérez-Urizar, J.; Pérez-González, L.F.; Martínez-Gutierrez, F. Risk factors and biofilm detection on central venous catheters of patients attended at tertiary hospital. *Micron* **2015**, *78*, 33–39. [[CrossRef](#)]
49. Gominet, M.; Compain, F.; Beloin, C.; Lebeaux, D. Central venous catheters and biofilms: Where do we stand in 2017? *Apmis* **2017**, *125*, 365–375. [[CrossRef](#)]
50. Murga, R.; Miller, J.M.; Donlan, R.M. Biofilm formation by gram-negative bacteria on central venous catheter connectors: Effect of conditioning films in a laboratory model. *J. Clin. Microbiol.* **2001**, *39*, 2294–2297. [[CrossRef](#)]



51. Devries, M.; Mancos, P.S.; Valentine, M.J. Reducing bloodstream infection risk in central and peripheral intravenous lines: Initial data on passive intravenous connector disinfection. *JAVA-J. Assoc. Vasc. Access* **2014**, *19*, 87–93. [[CrossRef](#)]
52. Menyhay, S.Z.; Maki, D.G. Preventing central venous catheter-associated bloodstream infections: Development of an antiseptic barrier cap for needleless connectors. *Am. J. Infect. Control* **2008**, *36*, S174.e1–S174.e5. [[CrossRef](#)]
53. Soothill, J.S.; Bravery, K.; Ho, A.; Macqueen, S.; Collins, J.; Lock, P. A fall in bloodstream infections followed a change to 2% chlorhexidine in 70% isopropanol for catheter connection antiseptics: A pediatric single center before/after study on a hemopoietic stem cell transplant ward. *Am. J. Infect. Control* **2009**, *37*, 626–630. [[CrossRef](#)] [[PubMed](#)]
54. Macias, J.H.; Arreguin, V.; Munoz, J.M.; Alvarez, J.A.; Mosqueda, J.L.; Macias, A.E. Chlorhexidine is a better antiseptic than povidone iodine and sodium hypochlorite because of its substantive effect. *Am. J. Infect. Control* **2013**, *41*, 634–637. [[CrossRef](#)]
55. Kaler, W.; Chinn, R. Successful Disinfection of Needleless Access Ports: A Matter of Time and Friction. *J. Assoc. Vasc. Access* **2007**, *12*, 140–142. [[CrossRef](#)]
56. Mazher, M.A.; Kallen, A.; Edwards, J.R.; Donlan, R.M. An In Vitro evaluation of disinfection protocols used for needleless connectors of central venous catheters. *Lett. Appl. Microbiol.* **2013**, *57*, 282–287. [[CrossRef](#)] [[PubMed](#)]
57. Smith, J.; Irwin, G.; Viney, M.; Watkins, L.; Morris, S.; Kirksey, K.; Brown, A. Optimal Disinfection Times for Needleless Intravenous Connectors. *J. Assoc. Vasc. Access* **2012**, *17*, 137–143. [[CrossRef](#)]
58. Simmons, S.; Bryson, C.; Porter, S. “Scrub the hub”: Cleaning duration and reduction in bacterial load on central venous catheters. *Crit. Care Nurs. Q.* **2011**, *34*, 31–35. [[CrossRef](#)]
59. Rupp, M.E.; Yu, S.; Huerta, T.; Cavalieri, R.J.; Alter, R.; Fey, P.D.; Van Schooneveld, T.; Anderson, J.R. Adequate Disinfection of a Split-Septum Needleless Intravascular Connector with a 5-Second Alcohol Scrub. *Infect. Control Hosp. Epidemiol.* **2012**, *33*, 661–665. [[CrossRef](#)]
60. Caspari, L.; Epstein, E.; Blackman, A.; Jin, L.; Kaufman, D.A. Human factors related to time-dependent infection control measures: “Scrub the hub” for venous catheters and feeding tubes. *Am. J. Infect. Control* **2017**, *45*, 648–651. [[CrossRef](#)]
61. Sannoh, S.; Clones, B.; Munoz, J.; Montecalvo, M.; Parvez, B. A multimodal approach to central venous catheter hub care can decrease catheter-related bloodstream infection. *Am. J. Infect. Control* **2010**, *38*, 424–429. [[CrossRef](#)]
62. Young, E.M.; Commiskey, M.L.; Wilson, S.J. Translating evidence into practice to prevent central venous catheter-associated bloodstream infections: A systems-based intervention. *Am. J. Infect. Control* **2006**, *34*, 503–506. [[CrossRef](#)] [[PubMed](#)]
63. Jeong, I.S.; Park, S.M.; Lee, J.M.; Song, J.Y.; Lee, S.J. Effect of central line bundle on central line-associated bloodstream infections in intensive care units. *Am. J. Infect. Control* **2013**, *41*, 710–716. [[CrossRef](#)] [[PubMed](#)]
64. Hadaway, L. Intermittent Intravenous Administration Sets: Survey of Current Practices. *J. Assoc. Vasc. Access.* **2007**, *12*, 143–147. [[CrossRef](#)]
65. Bond, A.; Teubner, A.; Taylor, M.; Cawley, C.; Abraham, A.; Dibb, M.; Chadwick, P.R.; Soop, M.; Carlson, G.; Lal, S. Assessing the impact of quality improvement measures on catheter related blood stream infections and catheter salvage: Experience from a national intestinal failure unit. *Clin. Nutr.* **2018**, *37*, 2097–2101. [[CrossRef](#)]
66. Davis, J. Central-Line-Associated Bloodstream Infection: Comprehensive, Data-Driven Prevention. Pennsylvania Patient Saf Auth. *Patient Saf. Advis.* **2011**, *8*, 100–104.
67. Goossens, G.A. Flushing and Locking of Venous Catheters: Available Evidence and Evidence Deficit. *Nurs. Res. Pract.* **2015**, *2015*, 1–12. [[CrossRef](#)]
68. Norris, L.A.B.; Kablaoui, F.; Brilhart, M.K.; Bookstaver, P.B. Systematic review of antimicrobial lock therapy for prevention of central-line-associated bloodstream infections in adult and pediatric cancer patients. *Int. J. Antimicrob. Agents* **2017**, *50*, 308–317. [[CrossRef](#)]
69. Dang, F.P.; Li, H.J.; Wang, R.J.; Wu, Q.; Chen, H.; Ren, J.J.; Tian, J.H. Comparative efficacy of various antimicrobial lock solutions for preventing catheter-related bloodstream infections: A network meta-analysis of 9099 patients from 52 randomized controlled trials. *Int. J. Infect. Dis.* **2019**, *87*, 154–165. [[CrossRef](#)]

70. Vassallo, M.; Dunais, B.; Roger, P.M. Antimicrobial lock therapy in central-line associated bloodstream infections: A systematic review. *Infection* **2015**, *43*, 389–398. [[CrossRef](#)]
71. Krishnasami, Z.; Carlton, D.; Bimbo, L.; Taylor, M.E.; Balkovetz, D.F.; Barker, J.; Allon, M. Management of hemodialysis catheter-related bacteremia with an adjunctive antibiotic lock solution. *Kidney Int.* **2002**, *61*, 1136–1142. [[CrossRef](#)] [[PubMed](#)]
72. Basas, J.; Palau, M.; Ratia, C.; del Pozo, J.L.; Martín-Gomez, M.T.; Gomis, X.; Torrents, E.; Almirante, B.; Gavaldà, J. High-Dose Daptomycin is Effective as an Antibiotic Lock Therapy in a Rabbit Model of Staphylococcus epidermidis Catheter-Related Infection. *Antimicrob. Agents Chemother.* **2018**, *62*, 1–4. [[CrossRef](#)] [[PubMed](#)]
73. Carratalà, J. The antibiotic-lock technique for therapy of “highly needed” infected catheters. *Clin. Microbiol. Infect.* **2002**, *8*, 282–289. [[CrossRef](#)] [[PubMed](#)]
74. Zhang, P.; Lei, J.H.; Su, X.J.; Wang, X.H. Ethanol locks for the prevention of catheter-related bloodstream infection: A meta-analysis of randomized control trials. *BMC Anesthesiol.* **2018**, *18*, 1–15. [[CrossRef](#)] [[PubMed](#)]
75. Arechabala, M.C.; Catoni, M.I.; Claro, J.C.; Rojas, N.P.; Rubio, M.E.; Calvo, M.A.; Letelier, L.M. Antimicrobial lock solutions for preventing catheter-related infections in haemodialysis. *Cochrane Database Syst. Rev.* **2018**, *2018*. [[CrossRef](#)]
76. Gudiol, C.; Nicolae, S.; Royo-Cebrecos, C.; Aguilar-Guisado, M.; Montero, I.; Martín-Gandul, C.; Perayre, M.; Berbel, D.; Encuentra, M.; Arnan, M.; et al. Administration of taurolidine-citrate lock solution for prevention of central venous catheter infection in adult neutropenic haematological patients: A randomised, double-blinded, placebo-controlled trial (TAURCAT). *Trials* **2018**, *19*, 1–10. [[CrossRef](#)]
77. Oto, J.; Imanaka, H.; Konno, M.; Nakataki, E.; Nishimura, M. A prospective clinical trial on prevention of catheter contamination using the hub protection cap for needleless injection device. *Am. J. Infect. Control* **2011**, *39*, 309–313. [[CrossRef](#)]
78. Voor In 't Holt, A.F.; Helder, O.K.; Vos, M.C.; Schafthuisen, L.; Sülz, S.; van den Hoogen, A.; Ista, E. Antiseptic barrier cap effective in reducing central line-associated bloodstream infections: A systematic review and meta-analysis. *Int. J. Nurs. Stud.* **2017**, *69*, 34–40. [[CrossRef](#)]
79. Sweet, M.A.; Cumpston, A.; Briggs, F.; Craig, M.; Hamadani, M. Impact of alcohol-impregnated port protectors and needleless neutral pressure connectors on central line-associated bloodstream infections and contamination of blood cultures in an inpatient oncology unit. *Am. J. Infect. Control* **2012**, *40*, 931–934. [[CrossRef](#)]
80. Hankins, R.; Majorant, O.D.; Rupp, M.E.; Cavalieri, R.J.; Fey, P.D.; Lyden, E.; Cawcutt, K.A. Microbial colonization of intravascular catheter connectors in hospitalized patients. *Am. J. Infect. Control* **2019**, *47*, 1489–1492. [[CrossRef](#)]
81. Kamboj, M.; Blair, R.; Bell, N.; Son, C.; Huang, Y.T.; Dowling, M.; Lipitz-Snyderman, A.; Eagan, J.; Sepkowitz, K. Use of disinfection cap to reduce central-line—Associated bloodstream infection and blood culture contamination among hematology—Oncology patients. *Infect. Control Hosp. Epidemiol.* **2015**, *36*, 1401–1408. [[CrossRef](#)] [[PubMed](#)]
82. Brunelli, S.M.; Van Wyck, D.B.; Njord, L.; Ziebol, R.J.; Lynch, L.E.; Killion, D.P. Cluster-randomized trial of devices to prevent catheter-related bloodstream infection. *J. Am. Soc. Nephrol.* **2018**, *29*, 1336–1343. [[CrossRef](#)] [[PubMed](#)]
83. Nicolás, F.G.; Casariego, G.J.N.; Romero, M.M.V.; García, J.G.; Diaz, R.R.; Perez, J.A.P. Reducing the degree of colonisation of venous access catheters by continuous passive disinfection. *Eur. J. Hosp. Pharm.* **2016**, *23*, 131–133. [[CrossRef](#)] [[PubMed](#)]
84. Golestaneh, L.; Mokrzycki, M.H. Prevention of hemodialysis catheter infections: Ointments, dressings, locks, and catheter hub devices. *Hemodial. Int.* **2018**, *22*, S75–S82. [[CrossRef](#)]
85. Buchman, A.L.; Spapperi, J.; Leopold, P. A new central venous catheter cap: Decreased microbial growth and risk for catheter-related bloodstream infection. *J. Vasc. Access* **2009**, *10*, 11–21. [[CrossRef](#)]
86. Mariyaselvam, M.; Hodges, E.; Richardson, J.; Steel, A.; Moondi, P.; Young, P. The coated antiseptic tip (CAT) syringe. *J. Med. Eng. Technol.* **2015**, *39*, 259–263. [[CrossRef](#)]
87. Wildgruber, M.; Lueg, C.; Borgmeyer, S.; Karimov, I.; Braun, U.; Kiechle, M.; Meier, R.; Koehler, M.; Ettl, J.; Berger, H. Polyurethane versus silicone catheters for central venous port devices implanted at the forearm. *Eur. J. Cancer* **2016**, *59*, 113–124. [[CrossRef](#)]

88. Yuh, J.; Yi, T.; Fen, M.; Talsma, H.; Hennink, W.E. Polyurethane-based drug delivery systems. *Int. J. Pharm.* **2013**, *450*, 145–162. [[CrossRef](#)]
89. Thomas, S.; Datta, J.; Haponiuk, J.; Reghunadhan, A. *Polyurethane Polymers: Composites and Nanocomposites*; Elsevier: Amsterdam, The Netherlands, 2017.
90. Akindoyo, J.; Beg, M.; Ghazali, S.; Islam, M.; Jeyaratnam, N.; Yuvaraj, A. Polyurethane types, synthesis and applications—A review. *RSC Adv.* **2016**, *6*, 114453–114482. [[CrossRef](#)]
91. Ishihara, K.; Liu, Y.; Inoue, Y. *Advances in Polyurethane Biomaterials*; Woodhead Publishing: Cambridge, UK, 2016.
92. Mathew, E.; Domínguez-Robles, J.; Larrañeta, E.; Lamprou, D.A. Fused deposition modelling as a potential tool for antimicrobial dialysis catheters manufacturing: New trends vs. conventional approaches. *Coatings* **2019**, *9*, 515. [[CrossRef](#)]
93. Viola, G.M.; Rosenblatt, J.; Raad, I.I. Drug eluting antimicrobial vascular catheters: Progress and promise. *Adv. Drug. Deliv. Rev.* **2017**, *112*, 35–47. [[CrossRef](#)] [[PubMed](#)]
94. Villani, M.; Consonni, R.; Canetti, M.; Bertoglio, F.; Iervese, S.; Bruni, G.; Visai, L.; Iannace, S.; Bertini, F. Polyurethane-Based Composites: Effects of Antibacterial Fillers on the Physical-Mechanical Behavior of Thermoplastic Polyurethanes. *Polymers* **2020**, *12*, 362. [[CrossRef](#)] [[PubMed](#)]
95. Barde, M.; Davis, M.; Rangari, S.; Mendis, H.C.; De La Fuente, L.; Auad, M.L. Development of antimicrobial-loaded polyurethane films for drug-eluting catheters. *J. Appl. Polym. Sci.* **2018**, *135*, 1–8. [[CrossRef](#)]
96. Zander, Z.K.; Chen, P.; Hsu, Y.H.; Dreger, N.Z.; Savariau, L.; McRoy, W.C.; Cerchiari, A.E.; Chambers, S.D.; Barton, H.A.; Becker, M.L. Post-fabrication QAC-functionalized thermoplastic polyurethane for contact-killing catheter applications. *Biomaterials* **2018**, *178*, 339–350. [[CrossRef](#)]
97. May, R.M.; Magin, C.M.; Mann, E.E.; Drinkler, M.C.; Fraser, J.C.; Siedlecki, C.A.; Brennan, A.B.; Reddy, S.T. An engineered micropattern to reduce bacterial colonization, platelet adhesion and fibrin sheath formation for improved biocompatibility of central venous catheters. *Clin. Transl. Med.* **2015**, *4*, 9–16. [[CrossRef](#)]
98. Peng, C.; Vishwakarma, A.; Li, Z.; Miyoshi, T.; Barton, H.A.; Joy, A. Modification of a conventional polyurethane composition provides significant anti-biofilm activity against: *Escherichia coli*. *Polym. Chem.* **2018**, *9*, 3195–3198. [[CrossRef](#)]
99. Francolini, I.; Silvestro, I.; Di Lisio, V.; Martinelli, A.; Piozzi, A. Synthesis, characterization, and bacterial fouling-resistance properties of polyethylene glycol-grafted polyurethane elastomers. *Int. J. Mol. Sci.* **2019**, *20*, 1001. [[CrossRef](#)]
100. Yu, H.; Liu, L.; Li, X.; Zhou, R.; Yan, S.; Li, C.; Luan, S.; Yin, J.; Shi, H. Fabrication of polylysine based antibacterial coating for catheters by facile electrostatic interaction. *Chem. Eng. J.* **2019**, *360*, 1030–1041. [[CrossRef](#)]
101. Lozeau, L.D.; Alexander, T.E.; Camesano, T.A. Surface-Tethered Antimicrobial Peptides: An Invention to Create Effective Antimicrobial Coatings. *Technol. Innov.* **2019**, *20*, 441–454. [[CrossRef](#)]
102. McCoy, C.P.; Irwin, N.J.; Donnelly, L.; Jones, D.S.; Hardy, J.G.; Carson, L. Anti-Adherent Biomaterials for Prevention of Catheter Biofouling. *Int. J. Pharm.* **2018**, *535*, 420–427. [[CrossRef](#)]
103. Machuca, J.; Lopez-Rojas, R.; Fernandez-Cuenca, F.; Pascual, A. Comparative activity of a polyhexanide–betaine solution against biofilms produced by multidrug-resistant bacteria belonging to high-risk clones. *J. Hosp. Infect.* **2019**, *103*, e92–e96. [[CrossRef](#)] [[PubMed](#)]
104. Yu, H.; Liu, L.; Yang, H.; Zhou, R.; Che, C.; Li, X.; Li, C.; Luan, S.; Yin, J.; Shi, H. Water-Insoluble Polymeric Guanidine Derivative and Application in the Preparation of Antibacterial Coating of Catheter. *ACS Appl. Mater. Interfaces* **2018**, *10*, 39257–39267. [[CrossRef](#)] [[PubMed](#)]
105. Pant, J.; Goudie, M.J.; Chaji, S.M.; Johnson, B.W.; Handa, H. Nitric oxide releasing vascular catheters for eradicating bacterial infection. *J. Biomed. Mater. Res. Part B Appl. Biomater.* **2018**, *106*, 2849–2857. [[CrossRef](#)] [[PubMed](#)]
106. Goudie, M.J.; Singha, P.; Hopkins, S.P.; Brisbois, E.J.; Handa, H. Active Release of an Antimicrobial and Antiplatelet Agent from a Nonfouling Surface Modification. *ACS Appl. Mater. Interfaces* **2019**, *11*, 4523–4530. [[CrossRef](#)] [[PubMed](#)]
107. Sajeevan, S.E.; Chatterjee, M.; Paul, V.; Baranwal, G.; Kumar, V.A.; Bose, C.; Banerji, A.; Nair, B.G.; Prasanth, B.P.; Biswas, R. Impregnation of catheters with anacardic acid from cashew nut shell prevents *Staphylococcus aureus* biofilm development. *J. Appl. Microbiol.* **2018**, *125*, 1286–1295. [[CrossRef](#)]

108. Lim, K.; Saravanan, R.; Chong, K.K.L.; Goh, S.H.M.; Chua, R.R.Y.; Tambyah, P.A.; Chang, M.W.; Kline, K.A.; Leong, S.S.J. Anhydrous polymer-based coating with sustainable controlled release functionality for facile, efficacious impregnation, and delivery of antimicrobial peptides. *Biotechnol. Bioeng.* **2018**, *115*, 2000–2012. [[CrossRef](#)]
109. Bayston, R.; Ashraf, W.; Pelegrin, I.; Fowkes, K.; Bienemann, A.S.; Singleton, W.G.B.; Scott, I.S. An external ventricular drainage catheter impregnated with rifampicin, trimethoprim and triclosan, with extended activity against MDR Gram-negative bacteria: An in vitro and in vivo study. *J. Antimicrob. Chemother.* **2019**, *74*, 2959–2964. [[CrossRef](#)]
110. Liu, H.; Shukla, S.; Vera-González, N.; Tharmalingam, N.; Mylonakis, E.; Fuchs, B.B.; Shukla, A. Auranofin Releasing Antibacterial and Antibiofilm Polyurethane Intravascular Catheter Coatings. *Front. Cell Infect. Microbiol.* **2019**, *9*, 37. [[CrossRef](#)]
111. O’Grady, N.P.; Alexander, M.; Burns, L.A.; Dellinger, E.P.; Garland, J.; Heard, S.O.; Lipsett, P.A.; Masur, H.; Mermel, L.A.; Pearson, M.L.; et al. *Prevention Strategies*; BSI Guidelines Library Infection Control CDC n.d.: Atlanta, GA, USA, 2011.
112. Lai, N.M.; Chaiyakunapruk, N.; Lai, N.A.; O’Riordan, E.; Pau, W.S.C.; Saint, S. Catheter impregnation, coating or bonding for reducing central venous catheter-related infections in adults. *Cochrane Database Syst. Rev.* **2016**, 2016. [[CrossRef](#)]
113. Narayana, J.L.; Mishra, B.; Lushnikova, T.; Golla, R.M.; Wang, G. Modulation of antimicrobial potency of human cathelicidin peptides against the ESKAPE pathogens and in vivo efficacy in a murine catheter-associated biofilm model. *Biochim. Biophys. Acta Biomembr.* **2019**, *1861*, 1592–1602. [[CrossRef](#)]
114. Zhang, X.Y.; Zhao, Y.Q.; Zhang, Y.; Wang, A.; Ding, X.; Li, Y.; Duan, S.; Ding, X.; Xu, F.J. Antimicrobial Peptide-Conjugated Hierarchical Antifouling Polymer Brushes for Functionalized Catheter Surfaces. *Biomacromolecules* **2019**, *20*, 4171–4179. [[CrossRef](#)] [[PubMed](#)]
115. Mauro, N.; Schillaci, D.; Varvarà, P.; Cusimano, M.G.; Geraci, D.M.; Giuffrè, M.; Cavallaro, G.; Maida, C.M.; Giammona, G. Branched High Molecular Weight Glycopolypeptide with Broad-Spectrum Antimicrobial Activity for the Treatment of Biofilm Related Infections. *ACS Appl. Mater. Interfaces* **2018**, *10*, 318–331. [[CrossRef](#)] [[PubMed](#)]
116. Konopińska, K.K.; Schmidt, N.J.; Hunt, A.P.; Lehnert, N.; Wu, J.; Xi, C.; Meyerhoff, M.E. Comparison of Copper(II)-Ligand Complexes as Mediators for Preparing Electrochemically Modulated Nitric Oxide-Releasing Catheters. *ACS Appl. Mater. Interfaces* **2018**, *10*, 25047–25055. [[CrossRef](#)] [[PubMed](#)]
117. Hunt, A.P.; Batka, A.E.; Hosseinzadeh, M.; Gregory, J.D.; Haque, H.K.; Ren, H.; Meyerhoff, M.R.; Lehnert, N. Nitric Oxide Generation on Demand for Biomedical Applications via Electrocatalytic Nitrite Reduction by Copper BMPA- And BEPA-Carboxylate Complexes. *ACS Catal.* **2019**, *9*, 7746–7758. [[CrossRef](#)]
118. Maharubin, S.; Nayak, C.; Phatak, O.; Kurhade, A.; Singh, M.; Zhou, Y.; Tan, G. Polyvinylchloride coated with silver nanoparticles and zinc oxide nanowires for antimicrobial applications. *Mater. Lett.* **2019**, *249*, 108–111. [[CrossRef](#)]
119. Stevens, K.N.J.; Croes, S.; Boersma, R.S.; Stobberingh, E.E.; van der Marel, C.; van der Veen, F.H.; Knetsch, M.L.W.; Koole, L.H. Hydrophilic surface coatings with embedded biocidal silver nanoparticles and sodium heparin for central venous catheters. *Biomaterials* **2011**, *32*, 1264–1269. [[CrossRef](#)]
120. Lotlikar, S.R.; Galloway, E.; Grant, T.; Popis, S.; Whited, M.; Guragain, M.; Rogers, R.; Hamilton, S.; Gerasimchuk, N.G.; Patrauchan, M.A. Polymeric composites with silver (I) cyanoximates inhibit biofilm formation of gram-positive and gram-negative bacteria. *Polymers* **2019**, *11*, 1018. [[CrossRef](#)]
121. Redfern, J.; Geerts, L.; Seo, J.W.; Verran, J.; Tosheva, L.; Wee, L.H. Toxicity and Antimicrobial Properties of ZnO@ZIF-8 Embedded Silicone against Planktonic and Biofilm Catheter-Associated Pathogens. *ACS Appl. Nano Mater.* **2018**, *1*, 1657–1665. [[CrossRef](#)]
122. Balne, P.K.; Harini, S.; Dhand, C.; Dwivedi, N.; Chalasani, M.L.S.; Verma, N.K.; Barathi, V.A.; Beuerman, R.; Agrawal, R.; Lakshminarayanan, R. Surface characteristics and antimicrobial properties of modified catheter surfaces by polypyrogallol and metal ions. *Mater. Sci. Eng. C* **2018**, *90*, 673–684. [[CrossRef](#)]
123. Kumar, S.; Thakur, J.; Yadav, K.; Mitra, M.; Pal, S.; Ray, A.; Gupta, S.; Medatwal, N.; Gupta, R.; Mishra, D.; et al. Cholic Acid-Derived Amphiphile which Combats Gram-Positive Bacteria-Mediated Infections via Disintegration of Lipid Clusters. *ACS Biomater. Sci. Eng.* **2019**, *5*, 4764–4775. [[CrossRef](#)]
124. Blanco-Cabra, N.; Vega-Granados, K.; Moya-Andérico, L.; Vukomanovic, M.; Parra, A.; Álvarez De Cienfuegos, L.; Torrents, E. Novel Oleanolic and Maslinic Acid Derivatives as a Promising Treatment against

- Bacterial Biofilm in Nosocomial Infections: An in Vitro and in Vivo Study. *ACS Infect. Dis.* **2019**, *5*, 1581–1589. [[CrossRef](#)] [[PubMed](#)]
125. Gomes, R.N.; Borges, I.; Pereira, A.T.; Maia, A.F.; Pestana, M.; Magalhães, F.D.; Pinto, A.M.; Gonçalves, I.C. Antimicrobial graphene nanoplatelets coatings for silicone catheters. *Carbon N. Y.* **2018**, *139*, 635–647. [[CrossRef](#)]
  126. Hadjesfandiari, N.; Yu, K.; Mei, Y.; Kizhakkedathu, J.N. Polymer brush-based approaches for the development of infection-resistant surfaces. *J. Mater. Chem. B* **2014**, *2*, 4968–4978. [[CrossRef](#)] [[PubMed](#)]
  127. Valotteau, C.; Baccile, N.; Humblot, V.; Roelants, S.; Soetaert, W.; Stevens, C.V.; Dufrière, Y.F. Nanoscale antiadhesion properties of sophorolipid-coated surfaces against pathogenic bacteria. *Nanoscale Horiz.* **2019**, *4*, 975–982. [[CrossRef](#)]
  128. Baumann Kreuziger, L.; Jaffray, J.; Carrier, M. Epidemiology, diagnosis, prevention and treatment of catheter-related thrombosis in children and adults. *Thromb. Res.* **2017**, *157*, 64–71. [[CrossRef](#)]
  129. Baskin, J.L.; Pui, C.H.; Reiss, U.; Wilimas, J.A.; Metzger, M.L.; Ribeiro, R.C.; Howard, S.C. Management of occlusion and thrombosis associated with long-term indwelling central venous catheters. *Lancet* **2009**, *374*, 159–169. [[CrossRef](#)]
  130. Geerts, W. Central venous catheter-related thrombosis. *Hematology* **2014**, *2014*, 306–311. [[CrossRef](#)]
  131. Roth, Y.; Lewitus, D.Y. The grafting of multifunctional antithrombogenic chemical networks on polyurethane intravascular catheters. *Polymers* **2020**, *12*, 1131. [[CrossRef](#)]
  132. Smith, R.S.; Zhang, Z.; Bouchard, M.; Li, J.; Lapp, H.S.; Brotske, G.R.; Lucchnio, D.L.; Weaver, D.; Roth, L.A.; Coury, A.; et al. Vascular Catheters with a Nonleaching Poly-Sulfobetaine Surface Modification Reduce Thrombus Formation and Microbial Attachment. *Sci. Transl. Med.* **2012**, *4*. [[CrossRef](#)]
  133. Diaz Blanco, C.; Ortner, A.; Dimitrov, R.; Navarro, A.; Mendoza, E.; Tzanov, T. Building an antifouling zwitterionic coating on urinary catheters using an enzymatically triggered bottom-up approach. *ACS Appl. Mater. Interfaces* **2014**, *6*, 11385–11393. [[CrossRef](#)]
  134. Alomari, A.I.; Falk, A. The Natural History of Tunneled Hemodialysis Catheters Removed or Exchanged: A Single-Institution Experience. *J. Vasc. Interv. Radiol.* **2007**, *18*, 227–235. [[CrossRef](#)] [[PubMed](#)]
  135. Van Rooden, C.J.; Schippers, E.F.; Barge, R.M.Y.; Rosendaal, F.R.; Guiot, H.F.L.; Van Der Meer, F.J.M.; Meinders, E.; Huisman, M.V. Infectious complications of central venous catheters increase the risk of catheter-related thrombosis in hematology patients: A prospective study. *J. Clin. Oncol.* **2005**, *23*, 2655–2660. [[CrossRef](#)]
  136. Mehall, J.R.; Saltzman, D.A.; Jackson, R.J.; Smith, S.D. Fibrin sheath enhances central venous catheter infection. *Crit. Care Med.* **2002**, *30*, 908–912. [[CrossRef](#)] [[PubMed](#)]
  137. Gorbet, M.B.; Sefton, M.V. Biomaterial-associated thrombosis: Roles of coagulation factors, complement, platelets and leukocytes. *Biomaterials* **2004**, *25*, 5681–5703. [[CrossRef](#)] [[PubMed](#)]
  138. Wallace, A.; Albadawi, H.; Patel, N.; Khademhosseini, A.; Zhang, Y.S.; Naidu, S.; Knuttinen, G.; Oklu, R. Anti-fouling strategies for central venous catheters. *Cardiovasc. Diagn. Ther.* **2017**, *7*, S246–S257. [[CrossRef](#)]
  139. Zander, Z.K.; Becker, M.L. Antimicrobial and Antifouling Strategies for Polymeric Medical Devices. *ACS Macro Lett.* **2018**, *7*, 16–25. [[CrossRef](#)]
  140. Ps, S.; Shah, N. Heparin-bonded catheters for prolonging the patency of central venous catheters in children (Review) summary of findings for the main comparison. *Cochrane Database Syst. Rev.* **2014**, 3–5. [[CrossRef](#)]
  141. Falk, A. The Role of Surface Coatings on Central Venous and Hemodialysis Catheters. *Buyers Guid* **2009**, *2009*, 51–53.
  142. Arepally, G.M. Clinical platelet disorders heparin-induced thrombocytopenia. *Blood* **2017**, *129*, 2864–2872. [[CrossRef](#)]
  143. Chong, B. Heparin-induced thrombocytopenia. *J. Thromb. Haemost.* **2003**, *1*, 1471–1478. [[CrossRef](#)]
  144. Zhang, H.; Chiao, M. Anti-fouling coatings of poly(dimethylsiloxane) devices for biological and biomedical applications. *J. Med. Biol. Eng.* **2015**, *35*, 143–155. [[CrossRef](#)] [[PubMed](#)]
  145. Falde, E.J.; Yohe, S.T.; Colson, Y.L.; Grinstaff, M.W. Superhydrophobic materials for biomedical applications. *Biomaterials* **2016**, *104*, 87–103. [[CrossRef](#)]
  146. Geyer, F.; D'Acunzi, M.; Sharifi-Aghili, A.; Saal, A.; Gao, N.; Kaltbeitzel, A.; Sloot, T.F.; Berger, R.; Butt, H.J.; Vollmer, D. When and how self-cleaning of superhydrophobic surfaces works. *Sci. Adv.* **2020**, *6*, 1–12. [[CrossRef](#)] [[PubMed](#)]

147. Wen, G.; Guo, Z.; Liu, W. Biomimetic polymeric superhydrophobic surfaces and nanostructures: From fabrication to applications. *Nanoscale* **2017**, *9*, 3338–3366. [[CrossRef](#)]
148. Li, M.; Phair, J.; Cardosi, M.F.M.F.; Davis, J. Nanostructuring carbon fibre probes for use in central venous catheters. *Anal. Chim. Acta* **2014**, *812*, 1–5. [[CrossRef](#)]
149. Davis, J.; Molina, M.T.; Leach, C.P.; Cardosi, M.F. Plasma-polyplumbagin-modified microfiber probes: A functional material approach to monitoring vascular access line contamination. *ACS Appl. Mater. Interfaces* **2013**, *5*, 9367–9371. [[CrossRef](#)] [[PubMed](#)]
150. Casimero, C.; McConville, A.; Fearon, J.J.; Lawrence, C.L.; Taylor, C.M.; Smith, R.B.; Davis, J. Sensor systems for bacterial reactors: A new flavin-phenol composite film for the in situ voltammetric measurement of pH. *Anal. Chim. Acta* **2018**, *1027*, 1–8. [[CrossRef](#)] [[PubMed](#)]
151. Paredes, J.; Alonso-Arce, M.; Schmidt, C.; Valderas, D.; Sedano, B.; Legarda, J.; Arizti, F.; Gómez, E.; Aguinaga, A.; Del Pozo, J.L.; et al. Smart central venous port for early detection of bacterial biofilm related infections. *Biomed. Microdevices* **2014**, *16*, 365–374. [[CrossRef](#)] [[PubMed](#)]
152. Mihu, M.M.R.M.; Cabral, V.; Patabhi, R.; Tar, M.M.T.M.; Davies, K.K.P.K.; Friedman, A.J.A.; Martinez, L.R.; Nosanchuk, J.D. Sustained nitric oxide-releasing nanoparticles interfere with methicillin-resistant staphylococcus aureus adhesion and biofilm formation in a rat central venous catheter model. *Antimicrob. Agents Chemother.* **2017**, *61*. [[CrossRef](#)] [[PubMed](#)]



© 2020 by the authors. Licensee MDPI, Basel, Switzerland. This article is an open access article distributed under the terms and conditions of the Creative Commons Attribution (CC BY) license (<http://creativecommons.org/licenses/by/4.0/>).



Review

# Genetic Alterations in Renal Cancers: Identification of The Mechanisms Underlying Cancer Initiation and Progression and of Therapeutic Targets

Ugo Testa \*, Elvira Pelosi and Germana Castelli

Department of Oncology, Istituto Superiore di Sanità, Vaile Regina Elena 299, 00161 Rome, Italy; elvira.pelosi@iss.it (E.P.); germana.castelli@iss.it (G.C.)

\* Correspondence: ugo.testa@iss.it

Received: 22 June 2020; Accepted: 24 July 2020; Published: 29 July 2020

**Abstract:** Renal cell cancer (RCC) involves three most recurrent sporadic types: clear-cell RCC (70–75%, CCRCC), papillary RCC (10–15%, PRCC), and chromophobe RCC (5%, CHRCC). Hereditary cases account for about 5% of all cases of RCC and are caused by germline pathogenic variants. Herein, we review how a better understanding of the molecular biology of RCCs has driven the inception of new diagnostic and therapeutic approaches. Genomic research has identified relevant genetic alterations associated with each RCC subtype. Molecular studies have clearly shown that CCRCC is universally initiated by Von Hippel Lindau (VHL) gene dysregulation, followed by different types of additional genetic events involving epigenetic regulatory genes, dictating disease progression, aggressiveness, and differential response to treatments. The understanding of the molecular mechanisms that underlie the development and progression of RCC has considerably expanded treatment options; genomic data might guide treatment options by enabling patients to be matched with therapeutics that specifically target the genetic alterations present in their tumors. These new targeted treatments have led to a moderate improvement of the survival of metastatic RCC patients. Ongoing studies based on the combination of immunotherapeutic agents (immune check inhibitors) with VEGF inhibitors are expected to further improve the survival of these patients.

**Keywords:** renal cell cancer; genomic landscape; targeted therapy; tumor evolution; tumor heterogeneity

## 1. Introduction

Renal cell cancer (RCC) accounts for about 4% of all adult tumors. In the United States there are approximately 74,000 new cases, 5% of all tumors in male and 3% in female and almost 15,000 deaths from RCCs each year, 3.2% of all cancer deaths in male and 1.7% of all cancer deaths in female [1]. It was estimated a probability of 2.2% in male and 1.2% in female of developing a kidney cancer from birth to death [1]. In the European Community, RCC accounts for approximately 84,000 cases each year and 35,000 deaths, as estimated in 2002 [2]. RCC incidence and mortality were evaluated in the United States during the last two decades showing that: The incidence of this tumor type initially increased by 2.4% per year but later became stable since 2008; the incidence of clear cell subtype continued to increase; RCC-related mortality declined since 2001, but mortality of RCC with metastases starts to decrease only from 2012 [3]. Men are more affected than women. The highest incidence rates of RCC were observed in Eastern Europe and North America, while its mortality rates were highest in European countries [4]. Kidney cancer incidence was positively correlated with human development index and gross domestic product [4].

RCC is a complex disease entity with different histological subtypes, characterized by distinct clinical and pathophysiological features; three main histological subtypes have been identified: clear cell RCC (CCRCC), papillary RCC (PRCC), and chromophobe RCC (CHRCC). In addition, there are



some less frequent subtypes, such as transitional cell carcinoma, nephroblastoma or Wilms' tumor, collecting duct RCC, medullary RCC, tubulocystic RCC oncocytoma, and RCC associated with MiTF family translocation [5]. The most common type of RCC is CCRCC, responsible for about 75% of cases; PRCC is subdivided according to histological criteria into type I PRCC (basophilic) and type II PRCC (eosinophilic) accounting for about 15% of all RCCs; CHRCC, accounting for about 5% of RCC cases.

Hereditary cases are responsible for about 5% of all cases of RCC [5]. Many autosomal dominant hereditary RCC syndromes have been reported and included those in which germline pathogenic mutations at the level of *VHL*, *MET*, *FH*, *SDH A/B/C/D*, *FLCN*, *TSC1/TSC2*, *BAP1*, *CDC73*, and *MiTF* are involved [6]. *FH* and *BAP1* germline RCCs are associated with more aggressive disease [6]. Familial RCCs occurred earlier as age of onset (mean ages 37–39 years) compared to sporadic RCCs (63–64 years) [7]. Inherited RCC syndromes are thought to account for 5% of all cases [7].

Genomic research has identified relevant alterations associated with each RCC subtype, as it will be discussed below.

## 2. Hereditary RCCs

The prevalence of germline mutations in known predisposition genes and other genes associated with cancer development was explored in 254 patients with advanced RCC; about 16% carried pathogenic or seemingly pathogenic germline variants at the level of 17 different cancer-predisposition genes: 5.5% of these patients carried mutations at the level of RCC-associated genes, such as *FH*, *BAP1*, *VHL*, *MET*, *SDHA*, and *SDHB*; 10.5% of these patients carried mutations in genes not clearly associated with RCC, including the *CHEK2* gene [8]. For the genes not traditionally associated with RCC, only the *CHEK2* gene was mutated more frequently among RCC patients, compared to the general population [7]. A typical disease-associated feature of germline-associated RCCs was the early onset and multifocal disease at diagnosis [7]. The main features of hereditary RCCs are reported in Table 1.

**Table 1.** Hereditary RCC syndromes, associated molecular alterations, and clinical manifestations.

Syndrome	Gene (chromosome)	Protein	Clinical Manifestations	Histology
Von Hippel-Lindau Syndrome	VHL (3p25)	pVHL	CCRCC, Pheochromocytoma, pancreatic endocrine tumors, CNS, and retinal hemangioblastomas	CCRCC Clear cell papillary
Hereditary Papillary RCC (HPRCC)	MET (7q31)	MET	Type 1 papillary RCC	Papillary type 1
Cowden Syndrome	PTEN (10q23.31)	Phosphatase and tensin homolog	Dermatological lesions, breast cancer, thyroid cancer, endometrial cancer	Papillary Chromophobe CCRCC
BAP1 Hereditary Syndrome	BAP1 (3p21)	BRCA1-associated protein-1	Uveal and cutaneous, melanoma, malignant mesothelioma, and/or lung adenocarcinoma	Undefined

Table 1. Cont.

Syndrome	Gene (chromosome)	Protein	Clinical Manifestations	Histology
Hereditary paraganglioma-pheochromocytoma syndromes	SDHA (5p15.33) SDHB (1p36.1-p35) SDHC (1q23.3) SDHD (11q23.1)	Succinate dehydrogenase	Bilateral and extra-adrenal pheochromocytoma, paraganglioma, RCC, and other malignancies	SDH-deficient RCC (solid nests or tubular architecture with variable cysts; vacuolated cells with eosinophilic cytoplasm)
Hereditary leiomyomatosis and renal cell carcinoma (HLRCC)	FH (1q42.1)	Fumarate hydratase	RCC, leiomyomas of skin and uterus (leiomyosarcoma), malignant pheochromocytoma/paraganglioma	HLRCC-associated RCC papillary type 2
Birt-Hogg-Dubé (BHD) Syndrome	FLCN (17p11.2)	Folliculin	RCC (hybrid oncocytic and other types), fibrofolliculomas, pulmonary cysts	Chromophobe Oncocytoma Hybrid CCRCC
MITF-associated susceptibility to melanoma and RCC syndrome	MITF (3p14.1)	Microphthalmia-associated transcription factor	Melanoma, pancreatic cancer, and/or pheochromocytoma	Undefined

### 3. Von Hippel-Lindau Disease

VHL disease is an autosomal dominantly inherited familial neoplastic condition with an incidence of approximately 1/30,000–1/36,000 live births and is caused by constitutional mutations at the level of the *VHL* tumor suppressor gene [8]. Germline *VHL* gene mutations predispose affected subjects to the development of benign and malignant tumors located at the central nervous system and visceral organs. Typical clinical characteristics are represented by hemangioblastomas of the brain, spinal cord, and retina; renal cysts and renal cell carcinoma; pheochromocytoma, pancreatic cysts, and neuroendocrine tumors; endolymphatic sac tumors; and ependymal and broad ligament cysts. Particularly, according to genotype-phenotype correlations VHL disease is classified into two subtypes, type 1 and 2 distinguished on the basis of the presence or not of pheochromocytoma: type 1 is associated with a very low risk of pheochromocytoma; while type 2 is associated with high risk of pheochromocytoma and is subdivided into type 2A (low risk of RCC), 2B (high risk of RCC), and 2C (only pheochromocytomas) [9]. The genotype correlates with the type of tumor risk observed in VHL syndrome: truncating or missense mutations are associated with type 1 and missense mutations with type 2 [10]. Recent studies have explored the relationship between genotype and phenotype in VHL syndrome: G239T mutation was linked with VHL type 2B, associated with renal cell carcinoma, pheochromocytoma, and cerebellar hemangioma; A232T mutation was related to VHL type I, associated with renal cell carcinoma alone; G500A mutation was associated with VHL type II, characterized by pheochromocytoma and cerebellar, retina and spinal cord hemangioblastoma; A293G mutation was associated with pheochromocytoma and thus with type IIC VHL [11]. The role of different types of germline *VHL* mutations classified as missense or truncating mutations and two subgroups of missense mutations subdivided according to mutations affecting the HIF- $\alpha$  binding site (HM) and mutations not affecting the HIF- $\alpha$  binding site (nHM) was also investigated [12]. In fact, the  $\beta$ -domain of the VHL protein comprises several  $\beta$ -sheets and binds HIF- $\alpha$  through residues 65–117. The results of this study showed that: (i) Missense mutations are associated with an increased risk of pheochromocytoma,

but a lower risk of renal cancer than truncating mutations; among missense mutations, HM mutations conferred a higher risk than nHM mutations of developing renal cancer [12]. At prognostic level, nHM mutations were associated with a better overall survival than HM and truncating mutations [12].

In individuals with VHL syndrome the lifetime risk of developing CCRCC is over 70%, with an average age of 40–45 years, about two decades earlier than the age of presentation of sporadic RCC [13]. Patients with VHL disease and asymptomatic family members carriers of the VHL mutation are annually screened for asymptomatic tumors and starting from the age of 16 years are controlled for RCC by magnetic resonance imaging, thus these patients undergo RCC removal when the tumor mass reaches 3 cm of diameter [13].

An increased level of genetic homogeneity was observed among clear-cell RCC (CCRCCs) with germline *VHL* mutations, compared to sporadic CCRCCs; this greater homogeneity reflects the smaller number of copy number alterations occurring in VHL syndrome-associated CCRCCs [14]. Both in CCRCC with germline *VHL* mutation and in sporadic CCRCC, the most relevant copy number alterations occurred at the level of 3p deletion involving the *VHL* gene, p9 deletion involving *CDKN2A* and *CDKN2B* genes, and of 8q amplification involving the *MYC* gene amplification [14].

At macroscopic level, kidneys display multiple specific and solid lesions, the majority being of low-grade. Several studies have explored the evolution at clonal level of RCCs developing in individuals with germline *VHL* mutations. The genomic analysis on multi-focal RCCs developing in an individual with germline *VHL* mutation showed that tumors arising in this multifocal context are clonally independent and harbor distinct secondary events, such as loss of chromosome 3p; despite this heterogeneity, the genetic alterations converge upon PI3K-AKT-mTOR signaling pathway; the tumors display only a minimal intratumoral heterogeneity [15]. These observations suggested the development of RCC from germline *VHL* mutation, follow the evolutionary principles of complementary contingency and convergence [15]. The analysis of 40 different RCC tumor foci derived from six patients with VHL syndrome confirmed that tumor foci are clonally independent [16]. The pattern of nucleotide substitution and the number and type of copy number alterations follow an individual pattern, thus suggesting that the genetic background and the environment plays a significant role in the types of secondary genetic alterations occurring during the development of RCCs with germline *VHL* mutations [16].

Studies based on the analysis of early renal cancers derived from nephrectomies performed in VHL disease patients provided evidence that biallelic inactivation of *VHL* is observed in preneoplastic renal lesions, in association with HIF activation [17]. It is important to note that in Von Hippel-Lindau disease only one of the two *VHL* alleles carries a germline mutation; therefore, in these patients, the inactivation of the second allele is one of the first events during renal cancer development. Biallelic *VHL* inactivation is also required for the development of sporadic renal cancer, but requires a longer time than in VHL disease since the two *VHL* alleles must be inactivated [18]. Sporadic CCRCC displays loss of the short arm of chromosome 3 (observed in  $\geq 90\%$  of patients), with a deletion region encompassing four tumor suppressor genes that are also frequent targets for inactivating point mutations on the other chromosomal allele: *VHL* (with point mutations in 60–70% of cases and epigenetic silencing in about 5–10% of patients), *PBRM1* (40%), *BAP1* (10%), and *SETD2* (10%). In CCRCC developing in patients with VHL disease, one allele is mutated via germline mutation, whereas the other allele is lost by 3p chromosome loss. Both in sporadic and VHL-hereditary CCRCC the most common cause of 3p loss is a chromotripsis event leading also to concurrent 5q chromosome gain [18]. In VHL disease, one allele is altered through germline mutations and this explains the high penetrance and the accelerated RCC development observed in these patients [18].

The retrospective study analysis of the natural history of RCC developing in VHL disease showed that: (i) The mean age of onset was 38.8 years, with a mean initial tumor size of 3.1 cm; (ii) the mean tumor growth rate was 0.49 cm/year; (iii) some factors, such as later age of onset, larger initial tumor size, missense mutation, mutations located at the level of exon 3, were associated with faster tumor

growth; (iv) bilateral tumors, large initial tumors, fast tumor growth, and presence of metastases are high-risk factors for poor prognosis in germline VHL-related RCCs [19].

#### 4. Hereditary Papillary Renal Carcinoma Type I

Hereditary papillary renal carcinoma is an autosomal dominant syndrome with a predisposition to the development of bilateral and multifocal type I papillary renal cell cancer. Germline mutations located at the level of the tyrosine kinase domain of the hepatocyte growth factor receptor, *c-Met*, are responsible for hereditary papillary renal cell cancer (HPRCC) type I, a very rare form of familial kidney cancer [20]. The mutants *c-Met* observed in these patients in suitable cellular and animal models display enhanced and dysregulated kinase activity and induce cell transformation and tumorigenicity [20]. A fundamental study by Schmidt and coworkers in 1997 led to the identification of missense mutations located in the tyrosine kinase domain of the *MET* gene in the germline of affected members of HPRCC families, as well as in a subset of sporadic PRCCs [21]. The same authors in a study on PRCCs identified 13% of cases with *c-MET* mutations: half of these patients were found to harbor germline *c-MET* and the rest only somatic *c-MET* mutations [22]. Interestingly, these patients, including those with germline *c-MET* mutations do not have a history of familial disease related to HPRCC [22]. *MET* mutations cause constitutive activation of the cytoplasmic domain of the receptor, stimulate cell growth, and represent the main pathogenetic event in the development of HPRCC. Direct DNA diagnosis in HPRCC is based on the identification of mutations at the level of *MET* exons 15–21, encoding the cytoplasmic domain of the receptor.

HPRCC is characterized by multiple, bilateral neoplasms which are hypovascular; the disease is usually indolent and diagnosed at radiological examination [23]. Papillary renal neoplasms from both patients with hereditary or somatic *c-MET* mutations share the same histologic features typical of chromophil basophilic type I PRCC, including macrophages and psammoma bodies; a papillary and/or tubulopapillary architecture is observed in all these tumors; clear cells were commonly detected in variable proportions in all *c-MET*-mutated PRCCs [23].

In addition to *c-MET* mutations, other genetic abnormalities are commonly observed in HPRCCs: trisomies of chromosomes 7 and 17 are common in HPRCCs [24]; trisomy 7 harboring non-random duplication of the mutant *c-MET* proto-oncogene seems to play a significant role in the development of multiple renal tumors [25,26]; multifocal bilateral renal tumors of hereditary PRCC develop as different clones in the renal parenchyma [25]. Interestingly, a case of a family with HPRCC was reported with a novel germline missense mutation of *c-MET* with a histological pattern consisting in multiple adenomas and papillary renal cell carcinomas with focal clear cells and a mixture of type I and type II pattern [27].

Interestingly, for the treatment of patients with advanced disease, the use of *c-MET* inhibitors was explored. Thus, foretinib, a pan-kinase inhibitor of *MET*, *VEGFR2*, *RON*, and *AXL*, was evaluated in patients with PRCC, showing 50% of partial responses among patients with HPRCC and 20% in PRCC patients with somatic *c-MET* mutations [28].

#### 5. Germline PTEN Mutation Cowden Syndrome

Cowden syndrome, or *PTEN* hamartoma tumor syndrome, is a rare (estimated incidence of 1 in 200,000 individuals) cancer syndrome, inherited in an autosomal dominant pattern, with a penetrance up to 90% in the second decade. The majority of patients with this syndrome were found to have germline mutations in *PTEN* [29]. These patients develop multiple hamartomas and are at increased risk for breast, endometrial, thyroid, and kidney cancers. RCC in Cowden syndrome is predominantly of the papillary and chromophobe type, beginning around 40–50 years. Mester and coworkers analyzed a cohort of patients with Cowden syndrome and RCC and estimated that these patients had a >30 fold increased risk of developing renal cancer [30].

Shuch et al. reported the study of 24 patients with Cowden syndrome and observed the development of RCC in 4 of these patients: three with solitary tumors, two with papillary type I

histology and one with clear cell histology; one patient with bilateral, synchronous chromophobe tumors [31].

A recent study reported an atypical presentation of Cowden syndrome in a subject with heterozygous mutation C1003T in the *PTEN* gene, who developed four primary onset carcinomas (one melanoma, two CCRCC, and a follicular variant of papillary thyroid carcinoma). Interestingly, the analysis of family's genetic background identified deleterious variants in two candidate modifier genes: *CECAM1* and *MIB2*; *CECAM1* is a tumor suppressor gene which presents loss of expression in RCC [32].

## 6. Hereditary BAP1 Tumor Syndrome

The BRCA1-associated protein1 (BAP1) syndrome is a tumor predisposition syndrome dependent on the presence of germline pathogenic variants at the level of the tumor suppressor gene *BAP1* that predisposes to the development of various types of tumors including uveal melanoma, mesothelioma, cutaneous melanoma, and RCC [33]. The first null variants were described in patients with uveal melanoma [34] and melanocytic tumors [35]. Subsequent studies have reported patients developing RCCs [36,37]. However, the incidence of RCC in these patients is less frequent than that of melanoma and mesothelioma [33]. The median age of RCC development in these patients is around 50 years [33]. The three most frequently observed missense mutations in these patients are H94R, L100P, and T173C [33]. Popova et al. identified in a family prone to RCC a germline mutation of *BAP1* gene (277A>G; Thr93Ala); furthermore, these authors screened 11 families that included individuals carrying germline deleterious *BAP1* mutations and 6 of these families presented with RCC-affected individuals [36]. Farley et al. reported a family with a *BAP1* germline variant (41T>A; L14H), disrupting a highly conserved residue in the catalytic domain: 22% of the individuals of this family display RCC, mostly multifocal and of the clear cell type [37].

The evaluation of the growth rates of a cohort of 292 patients with genetically defined renal tumors and showed that BAP1-deficient tumors are those growing at the fastest rates [38].

## 7. Succinate Dehydrogenase (SDH) and Fumarate Hydratase (FH)-Deficient Renal Cell Carcinoma

SDH, member of the Krebs cycle and electron transport chain, is a mitochondrial enzyme complex composed of four subunits (SDHA, SDHB, SDHC, and SDHD). Germline mutations of the genes encoding the SDH subunits result in hereditary syndromes associated with the development of paraganglioma-pheochromocytoma, gastrointestinal stromal tumors, and RCC [39].

FH deficiency is a rare autosomal recessive hereditary syndrome, resulting in the homozygote condition, in a severe defect of cellular metabolism, associated with progressive encephalopathy and, in the heterozygote condition, in the predisposition to develop an early-onset kidney cancer syndrome [40].

Most of the renal tumors developing in individuals with SDH deficiency, particularly those associated with germline *SDHB* mutations, exhibit a distinctive morphology consisting in tumors composed by cuboidal cells with bubbly eosinophilic cytoplasm, arranged in solid nests or in tubules surrounding central spaces [41].

Gill et al. have reported SDH-deficient renal carcinomas from 27 patients and estimated that 0.05%–0.2% of all carcinomas are SDH deficient; 94% of these tumors displayed the typical morphology of SDH-deficient renal cancers; all the patients performing a genetic evaluation displayed germline *SDHB* mutations (only in one patient *SDHA* mutations were detected); a part of these patients had a metastatic disease, associated with high-grade nuclear atypia or coagulative necrosis [42]. Williamson et al. reported the characterization of 11 SDH-deficient RCC and observed the common presence of intratumoral mast cells; the majority of patients with *SDHB* gene mutations exhibited also loss of the second allele [43]. These studies have supported the existence of a unique subtype of renal cell

carcinoma, characterized by SDH deficiency [43]. In line with these studies, SDH-deficient renal cell carcinoma was accepted as a specific tumor type in the World Health Organization Classification [5].

In some rare patients, *SDH* mutations may co-occur with *Xp11* translocation RCC, characterized by *TFE3* chromosomal translocations involving break points in the *TFE3* gene; renal cell carcinomas with translocations make part of *MiT* family translocation renal cell carcinoma and are composed by eosinophilic cells, with cytoplasmic inclusions and prominent nucleoli [44].

Gupta et al. have recently reported the results of a screening of *SDHA/B* deficiency in a group of 1009 renal cell neoplasms: SDH-deficient renal cell cancers were detected only in the cases originally classified as oncocytomas (1.1% of these tumors) [45].

Ajamir et al. have performed a systematic review of all the main studies reporting SDH-mutant renal cell carcinoma [46]. The most commonly mutated gene was *SDHB* (with 137G>A being the most frequent mutation) and less frequently *SDHC* (380A>G being the most frequent mutation) and *SDHA* [46]. Rare cases of SDH-deficient renal cell cancers are related to alterations of the *SDHA* gene: Yakirevich et al. reported a case of SDH-deficiency RCC, characterized by homozygous deletion of the *SDHA* gene (9 of the *SDHA* gene exons were deleted): at immunohistochemical level, the expression of both *SDHA* and *SDHB* was lost [47].

The characterization of an *SDHB*-deficient RCC cell line isolated from young patient carrying the *SDHB*<sup>R46Q</sup> mutation was used as a tool to elucidate the alterations of metabolism caused by SDH deficiency [48]. *SDHA* catalyzes the oxidation of succinate to fumarate with the reduction of FAD<sup>+</sup> to FADH<sub>2</sub>; three iron-sulfur (Fe-S) clusters present in *SDHB* improve the transfer of electrons from FADH<sub>2</sub> to ubiquinone, bound by SDH through the *SDHC* and *SDHD* subunits. The SDH function and molecular organization require two conserved L(I)YR motifs present in *SDHB*; the *SDHB*<sup>R46Q</sup> mutation impairs one of these two L(I)YR motifs, by changing IYR to IYQ and thus determining an incapacity of *SDHB* to incorporate Fe-S cluster, with its consequent instability [49]. *SDHB*-deficient renal tumor cells displayed a marked change in their energetic metabolism with a shift to aerobic glycolysis and marked decrease of oxidation phosphorylation, with very low entry of glucose into TCA cycle metabolites. As a consequence of *SDHB* degradation, *SDHB*-mutant cells displayed markedly decreased oxygen consumption, increased succinate levels, and pronounced use of glutamine as the main source of TCA cycle metabolites via reductive carboxylation (reduction of glutamine-derived  $\alpha$ -ketoglutarate into citrate) [48]. The metabolic changes determine also an increase of HIF-1 $\alpha$ , but not HIF-2 $\alpha$  levels, and a marked DNA cycle island methylator phenotype [48]. Through the study of *SDHB*-ablated kidney mouse cells it was shown that lack of SDH activity induces the commitment of the cells to consume extracellular pyruvate, inducing Warburg-like bioenergetic features; pyruvate carboxylation shifts glucose-derived carbons into aspartate biosynthesis and, through this mechanism, sustains tumor cell growth [50].

SDH inactivation leads to a massive accumulation of succinate, acting as an oncometabolite. Succinate levels, assessed on tumor biopsies are a high specific biomarker of SDH-mutated tumors. Succinate can be detected in vivo by magnetic resonance spectroscopy (MRS). A pulsed proton magnetic resonance spectroscopy (1)H-MRS sequence was developed, optimized, and applied to imaging of patients with paraganglioma: a succinate peak was detected at 2.44 ppm in all paraganglioma patients carrying an *SDHx* gene mutation, but not in patients exempt of *SDHx* mutation [51]. Potential suitable applications of this technique include non-invasive diagnosis and disease stratification, extended also to monitoring of tumor response to anticancer treatments [52].

Succinate accumulated in individuals with germline *SDHx* mutations acts as an oncometabolite and is responsible at a large extent for the oncogenic effect mediated by SDH mutational deficiency [53–55]. Thus, succinate deregulates the HIF pathway through a direct inhibition of prolyl hydroxylases (PHDs), targeting HIF for degradation [56]. The stabilization of HIF1 $\alpha$  and HIF2 $\alpha$  causes an upregulation of downstream HIF targets, such as VEGF and GLUT1 [57] and the consequent generation of hypoxic and highly vascularized phenotypes [58]. In addition to the induction of a pseudohypoxic phenotype, succinate exerts other biological activities involved in its protumorigenic effects: (i) epigenetic

dyregulation due to direct inhibition of histone lysine demethylases (KDM) and TET2, with consequent hypermethylation phenotypes and alteration of the expression of multiple genes involved in the control of cell proliferation and differentiation [59]; (ii) activation of succinate receptor (SUCNR1) with consequent activation of angiogenic proteins; (iii) post-translational protein modification through a process of succinylation; (iv) dependency on pyruvate carboxylase to funnel pyruvate into the truncated TCA cycle for biosynthesis of aspartate [54].

A recent study discovered a potential vulnerability of hereditary SDH-deficient RCCs related to a peculiar sensitivity to synthetic-lethal targeting poly(ADP)-ribose polymerase (PARP) inhibitors [60]. This peculiar sensitivity is due to the capacity of succinate to suppress the homologous recombination (HR) DNA-repair pathway required for the reparation of DNA double-strand breaks and for maintenance of genome integrity [60].

Germline mutations in *FH* predispose to dominantly inherited uterine fibroids, skin leiomyomata, and aggressive papillary renal cancer; according to these observations, it was proposed that *FH* acts as a tumor suppressor [61]. For the frequent occurrence of cutaneous and uterine leiomyomas this hereditary syndrome is also known as hereditary leiomyomatosis and renal cell carcinoma (HLRCC). *FH*-deficient renal cell cancers can occur also sporadically: thus Pan et al. have investigated 13 patients with *FH*-deficient renal cancers and observed absent expression in 12/13 cases, germline *FH* mutations in seven cases, and somatic mutations of *FH* gene in the remaining four cases [62].

Linehan and coworkers reported a comprehensive characterization of papillary RCCs; in this context, they identified a subset of papillary type 2 RCCs, characterized by increased DNA methylation at the level of loci unmethylated in corresponding normal cells (CIMP, CpG Island Methylator Phenotype) [63]. These tumors correspond to 5.6% of all PRCCs and were characterized by: (i) Universal methylation of *CDKN2A* promoter, and germline or somatic mutations of *FH* (4 patients displayed germline *FH* mutations and one showed somatic *FH* mutations); low *FH* mRNA expression, associated with increased expression of genes associated with cell-cycle progression and response to hypoxia [63]. Chen and coworkers have performed an extensive molecular analysis of 62 cases of RCC with unclassified histology and observed *FH* deficiency in 6% of these tumors [64]. These four cases were *FH*-negative and 2SC-positive at immunohistochemical level and in 3/4 cases harbored germline *FH* mutations and in 1/4 somatic *FH* mutations [64].

Germline *FH* mutations are observed in about 90% of families with HLRCC [65]. The remaining cases, apparently negative for *FH* mutations, could lack point mutation for several different reasons, including the presence of inactivating mutations in noncoding gene regions (promoter or enhancer) or deletion of the *FH* gene. In cases positive for *FH* mutations, the most frequent mutations located along the entire length of the coding region were represented by missense and frameshifts, and more rarely, by non-sense and splice site mutations [65]. In a large series of HLRCC patients, 68 different germline mutations of the *FHG* gene were identified: 18 truncating or frameshift mutations, 37 missense mutations, 9 splice-site, and 4 large deletions [66].

Vocke et al. have explored the occurrence of *FH* gene mutations in a group of patients with phenotypic manifestations consistent with HLRCC reporting in the 13 families explored, 11 complete *FH* gene deletions, and 2 partial *FH* gene deletion; kidney cancer was diagnosed in 32% of these patients and in 54% of families possessing either complete or partial *FH* deletions [67]. These observations clearly indicate that *FH* gene deletions, as well as gene mutations are associated with the development of RCCs [67].

The histologic growth patterns of *FH*-deficient tumors are heterogeneous: the large majority of these cases exhibited multiple histologic growth patterns, with papillary being the most frequent histotype (52%), followed by solid (21%), cribriform/sieve-like (14%), sarcomatoid (3%), tubular (3%), cystic (3%), and low-grade oncocytic (3%) [68]. Forde et al. showed that the histopathologic features of 18 cases of *FH*-deficient RCCs were variable, with 7/18 CCRCC, 9/18 PRCC (6/18 type 2 PRCC), 1 collecting duct cancer, 1 with oncocytic cystic morphology [69]. Median age of RCC onset was 44 years [69]. Pan et al. reported the clinicopathologic features of 13 cases of *FH*-deficient RCCs and

subdivided these tumors according to the features of nuclei: The presence of typical big nuclei with or without eosinophilic nucleoli (observed in 11/13 case) were associated with disease progression or death; the presence of low-grade nuclei and eosinophilic cytoplasm (observed in 11/13 cases) showed no disease progression [62]. Furuya et al. recently reported the clinicopathological and molecular features of 13 Japanese patients with hereditary FH-deficient renal cell carcinomas: most tumors had type 2 papillary architecture or tubulocystic pattern or both; at immunohistochemical level, 10 tumors were positive for PD-L1; somatic mutation analysis showed loss of heterozygosity of *FH* in 10 tumors [70].

In HLRCC subjects the most frequent age of RCC development is 40–50 years. In a minority of FH-deficient patients RCC development occurs in patients aged younger than 20 years; a significant proportion of these young patients exhibited a metastatic disease [71].

FH deficiency in RCC determines a marked alteration of energetic metabolism. *FH* gene encodes for the TCA cycle gene fumarate hydratase, responsible for the bidirectional conversion of fumarate and L-malate. HLRCC-related RCCs display a marked FH deficiency in these cells, one allele is germline mutated and the other allele is somatically lost. The FH deficiency in kidney cancer cells determines a marked metabolic remodeling, with changes at the level of glucose and glutamine metabolism and of mitochondrial respiration. Particularly, FH-deficient cancer cells undergo a Warburg metabolic shift characterized by aerobic glycolysis and reduced oxidative phosphorylation [72–75]. Isotope tracer studies in FH-deficient renal cancer cells showed that the contribution of glucose-derived carbon to TCA cycle is very limited, whereas glutamine-derived carbon enters the TCA cycle through reductive carboxylation of  $\alpha$ -ketoglutarate [72–75].

The glycolytic shift induced by fumarate deficiency induced several consequences at the level of the AMP-activated pathway (AMPK): (i) AMPK levels were decreased with consequent lowered expression of the iron transported DNMT1; (ii) in turn, reduced DNMT1 levels induced a condition of cytosolic iron deficiency, activating the iron regulatory proteins, IRP1 and IRP2, and increasing the expression of HIF-1 $\alpha$ ; (iii) activation of AMPK or silencing of HIF-1 $\alpha$  decreases the invasive properties of FH-deficient renal cancer cells [76].

Fumarate promotes tumorigenesis through various mechanisms: (i) by reversibly inhibiting dioxygenase involved in epigenetic signaling: fumarate inhibits TET-mediated demethylation of a DNA region involved in the regulation of the antimetastatic miRNA cluster 6 *miR-200ba249*, inducing the expression of transcription factors involved in the activation of epithelial-to-mesenchymal (EMT) [77]; fumarate is a competitive inhibitor of 2-oxoglutarate-dependent prolyl hydroxylase domain: containing proteins (PHD) that hydroxylate HIF and this inhibition lead to HIF stabilization [78] by inducing post-translational protein modification through succinylation due to the peculiar capacity of fumarate to interact with specific cysteine residues [79,80].

Several potentially important targets of succination have been identified in FH-deficient renal cancer cells: (i) Fumarate induces succination of key components of the iron-sulfur cluster biogenesis family of proteins, inducing defects in the biogenesis of iron-sulfur clusters that affect the function of the complex I of respiratory chain [81]; (ii) succinate targets the protein Kelch-like ECH-associated protein-1 (KEAP1), abrogating its repressive effects on the transcription factor NRF2 and thus resulting in upregulation of NRF2-dependent genes involved in the regulation of key antioxidant pathway mediating the capacity of cells to adapt to oxidative stress [82,83]. In line with these findings, NRF2 as well as downstream NRF2 target genes are upregulated in FH-deficient renal cancers [82,83].

Interestingly, somatic mutations in *NRF2*, *CUL3*, and *SIRT1*, rarely observed in PRCC2, are responsible for driving the NRF2 activation phenotype in these tumors [84]. In addition to these effects on KEAP1, fumarate can react with the sulfur atom of glutathione to generate succinated glutathione, thus inhibiting the function of glutathione and resulting in increased oxidative stress in FH-deficient RCCs [85,86].

Kulkarni et al. have recently reported the results of a study based on the use of chemoproteomic probes to explore the spectrum of occupancy of fumarate-reactive cysteines and identified an



FH-sensitive cysteine in SMARCC1, a member of the SWI-SNF ((Switch/Sucrose Non Fermentable) ATP-dependent chromatin remodeling complexes [87].

Interestingly, a proteasomal inhibitor, marizomib, disrupts glucose and glutamine metabolism in HLRCC cells via inhibition of glycolysis and lowered expression of glutaminases, thus restricting nutrients and the cells' antioxidant response capacity, supporting a potential use of proteasome inhibitors in HLRCC [88].

## 8. Birt-Hogg-Dubé (BHD) Syndrome

BHD syndrome is an autosomal dominant inherited disease that predisposes at-risk individuals to develop benign cutaneous fibrofolliculomas, pulmonary cysts, spontaneous pneumothoraces, and increased risk for renal cancer. Renal tumors that develop in the context of BHD syndrome are heterogenous and are frequently bilateral with various histologies. Through the study of numerous families inheriting the mutated gene responsible for BHD syndrome it is estimated an increased risk of developing RCC for BHD-affected family members of about 7-fold in comparison with unaffected individuals [89]. Various histologic types of RCC are associated with DHB syndrome, including hybrid oncocytic tumor (50%) with histological features of both chromophobe RCC and renal oncocytoma; chromophobe RCC (35%); CCRCC (9%); renal oncocytoma (5%) [90,91]. A peculiar histologic finding of these tumors is represented by the presence of so-called "oncocytosis" defined as a pathological condition in which renal parenchyma is diffusely involved by numerous oncocytic nodules [92]. These foci of oncocytic cells have been suggested to represent the precursor lesions of BHD-associated tumors [90,91]. A recent study performed on clinicopathologic information on 220 families with BHD syndrome confirmed the consistent histologic heterogeneity of BHD-associated kidney tumors, with 43% of the chromophobe subtype and 34% of the hybrid oncocytic/chromophobe subtype; 64% of the patients with renal cancer had multiple lesions at the time of genetic diagnosis [93].

In 2002, genetic linkage studies in BHD families allowed the localization of the gene responsible for BHD syndrome at the level of chromosome 17p11, and the identification of this gene as the folliculin (*FLCN*) gene [94,95]. Various mutations (over 150) spanning the entire *FLCN* region were observed at the level of the *FLCN* gene, including insertion/deletion, nonsense, missense and splice-site mutations, and partial deletions [96]. The majority of *FLCN* mutations identified in the germline of BHD patients are frameshift mutations (insertion/deletion), nonsense mutations that are predicted to truncate and to inactivate the *FLCN* protein [96].

*FLCN* behaves as a classical tumor suppressor gene. These conclusions were supported by a study carried out by Vocke and coworkers on 77 renal tumors derived from 12 patients with germline *FLCN* mutations to identify somatic mutations in the second copy of BHD, showing *FLCN* somatic mutations in 53% of cases and loss-of-heterozygosity at the *BHD* locus in 17% of cases [97]. These findings strongly support the view that *FLCN* gene acts as a tumor suppressor of renal tumorigenesis and both copies of the gene need to be altered for renal cancer development [97].

The study of some germline missense mutations in the folliculin gene, such as *H255Y* and *K508R*, observed in BHD patients with renal carcinomas has directly supported their pathogenic role: the *FLCN H255Y* mutant protein displayed a loss of its tumor suppressive function inducing kidney cell proliferation and the clinical manifestations of BHD, the *FLCN K508R* mutant protein exerted a dominant negative effect on the function of *WT FLCN* in the regulation of kidney cell proliferation [98].

Some studies explored the cytogenetic features of these tumors. BHD-associated RCCs, either of chromophobe or of hybrid oncocytic/chromophobe subtype are characterized by a disomic pattern on FISH analysis using probes targeting the centromeric regions of chromosomes 2, 6, and 17, whereas sporadic chromophobe RCCs very frequently displayed a monosomic pattern [99]. Hasumi et al. performed a detailed analysis of the molecular characteristics observed in 29 BHD-associated kidney cancers from 15 BHD patients [100]. All patients displayed *FLCN* germline mutations; somatic *FLCN* mutations were observed in 25 out of the 29 kidney tumors: 20 tumors displayed frameshift/nonsense mutations or loss of heterozygosity at the level of the allele not affected by the

germline mutation [100]. Copy number variation in BHD-associated kidney cancer was usually low and was lower in chromophobe and in HOCT histological subtypes than CCRCC and PRCC subtypes; interestingly, in CCRCC subtypes no loss of chromosome 3p was observed, a condition usually found in sporadic CCRCC [100]. The number of somatic variants was similar in the various histological subtypes of BHD-associated kidney tumors; the frequency of gene mutations was usually low in these tumors, with variants in chromatin remodeling genes being frequently observed (59% of cases); furthermore, variants in genes associated with the mitochondrial pathway, lipid metabolism, and glycolytic pathway were observed in 28%, 24%, and 7% of cases, respectively [100]. Therefore, this study clearly showed that BHD-related renal cancer lacks the mutations in driver genes, such as *TP53*, *CDKN2A*, *RB1*, *PTEN*, and *mTOR*, typically observed in CHRCC. It is of interest to note that at molecular level BHD-related hybrid oncocytic/chromophobe tumors can be differentiated from the sporadic counterpart of these tumors in that these last tumors have copy number losses in chromosomes 1 and XY, but lacks recurrent mutations [101].

The understanding of the molecular mechanisms underlying the BHD syndrome requires the elucidation of the function of *FLCN* gene. The protein folliculin is involved in numerous biological processes, such as membrane trafficking, energy and nutrient homeostasis, and lysosomal biogenesis, and the mutations affecting this protein generate different phenotypes, in relation with their cellular context. *FLCN* forms molecular complexes with two large proteins, called folliculin interacting protein 1 (FNIP1) and folliculin interacting protein 2 (FNIP2) [102–104]. Structural studies have clarified the molecular mechanism induced by *FLCN* through interaction with FNIP1 and FNIP2: both *FLCN* and FNIP proteins contain a longin and are differentially expressed in normal versus neoplastic cells (DENN) domain, which are protein folds that have been implicated in the regulation of small GTPases and membrane trafficking [105,106].

Functional studies show that *FLCN* regulates both the Rag and Rab GTPases depending on nutrient-availability, which are respectively involved in the mTORC1 pathway and lysosomal positioning. Thus, functional studies have shown that *FNIP1* and *FNIP2* act as tumor suppressors since mice deficient in *FNIP1* and *FNIP2* tumors display tumors developing at the level of several organs [107]. Importantly, *FNIP1* and *FNIP2* were essential also for the tumor suppressive function of *FLCN* at the level of kidney tissue, thus supporting the view that the development of kidney tumors in BHD patients may be due to the loss of essential *FLCN*-FNIP interactions [107].

Functional studies support a major role for *FLCN*-FNIP complex in the regulation of both the Rag and Rab GTPase families, which in turn modulate the mTORC1 signaling pathway and lysosomal distribution, respectively, in a manner dependent upon amino acid availability. mTORC1 is a central, key regulator of cellular metabolism, ensuring cell growth only under suitable conditions [108]. Studies in mice with the kidney-targeted *FLCN* inactivation develop polycystic kidneys and cystic tumors, exhibiting activation of mTORC1 [109–111]. Homozygous deletion of *FLCN* in mice resulted in early embryonic lethality; *FLCN* heterozygous knockout (*FLCN*<sup>+/-</sup>) mice appeared normal at birth, but developed kidney cysts and solid tumors, as they aged, of different histologic types (oncocytic hybrid, oncocytoma, and clear cell carcinoma with concomitant loss of heterozygosity of *FLCN*); these tumors displayed increased mTORC1 and TORC2 activity [112]. The investigation of other mouse models further supported a role for *FLCN* as a positive regulator of TORC1 and provided evidence that inappropriate mTORC1 levels can be associated with renal cancerogenesis [113,114]. Interestingly, the tumorigenic potential of *FLCN*-deficient renal cancer cells is inhibited by sirolimus, a mTOR inhibitor [115].

Recent studies support a functional role for the *FLCN*-FNIP complex as a GTPase activating protein involved in the fine modulation of Rag GTPase are nucleotide binding and transmission of the nutrient status to mTORC1 [116]. It was proposed that the GTPase activating properties of the *FLCN*-FNIP complex occurs downstream of GATAR1 protein complex and together orchestrate a unique molecular regulation: when amino acid levels are low, the GTPase activating protein activity of

GATOR1 promotes the GDP-Rag A7B condition and the FLCN-FNIP complex is recruited at the level of lysosomes to drive the GTPase activating properties toward Rag C/D [117,118].

FNIP1 and FNIP2 were also identified as proteins capable to interact also with AMPK, although FLCN does not seem to be essential for FNIP-AMPK interaction [102–104]. AMPK is a heterotrimeric kinase whose activation increases ATP production through stimulation of catabolic pathways, concomitantly with the inhibition of anabolic pathways that consume ATP, in a way antagonistic to mTORC1 activity. Furthermore, various studies have shown that FLCN deficiency triggers AMPK activation [119–121]; furthermore, *FNIP1* mutations are associated with high AMPK activity [122].

Finally, FLCN deficiency exerts also important effects at the level of energetic metabolism, with a consistent metabolic change in favor of aerobic glycolysis. Thus, Yan et al. reported a “Warburg effect” metabolic transformation in FLCN-deficient embryonic fibroblasts, with increased glucose uptake, lactate production, and extracellular acidification, associated with HIF transcriptional activity and enhanced expression of HIF-dependent genes [120]. The increase in metabolic activity was associated in FLCN-deficient fibroblasts with an increased mitochondrial mass and respiration [120]. This effect elicited by FLCN deficiency on mitochondrial mass is remarkable and seems to be associated with an enhanced expression and activity of PGC1 $\alpha$  (peroxisome proliferation-activated receptor gamma coactivator 1-alpha), a transcriptional regulator of genes involved in mitochondrial biosynthesis [123]. PGC1 $\alpha$  levels were found to be elevated in FLCN-deficient renal cancers [124]. Furthermore, BHD-related tumors were characterized by up-regulation of mitochondrial gene expression [124]. The study of FLCN-deficient mice clearly showed the existence of a condition of chronic AMPK activation, which in turn, induces the expression and activation of PGC1 $\alpha$  [125].

### 9. Familial MITF Microphthalmia-Associated Transcription Factor

Subjects carrying a germline pathogenic variant of *MITF* have a more than five-fold increased risk of developing melanoma and renal cancer, as compared to the individuals not bearing these variants. The molecular characterization of these *MITF* oncogenic variants showed a mutation at the level of codon 318 (E318K), located at the level of a small-ubiquitin-like modifier (SUMO) consensus site ( $\psi$ KXE), determining a strong impairment of SUMOylation of MITF [126]. The E318K mutation increased the binding to the HIF1 $\alpha$  promoter and increased its transcriptional activity [126]. However, the *MITF* E318K mutation does not seem to be involved in sporadic RCC: in fact, in a screening based on the analysis of 403 sporadic RCCs only one *MITF* E318K mutation was detected [127].

### 10. Chromophobe Renal Cancer

CHRCC is the second most common form of non-CCRCC after papillary RCC and displays a frequency corresponding to 5–10% of all RCCs. The main molecular features of CCRCC are reported in Table 2. The analysis of the genomic alterations observed in CHRCC supports that this tumor subtype originates from distal convoluted tubules, compared with other kidney cancers, including CCRCC with more origin from proximal tubules [128].

The main symptoms of patients with CHRCC at presentation are represented by flank pain and hematuria. CHRCCs are usually solitary tumors that can reach a big size (up to 25 cm in diameter). At microscopic level, these tumors are usually arranged in solid sheets, with tumor parenchyma intersected by fibrous septa and blood vessels. Two cellular elements usually compose these tumors: one, chromophobe cells, being represented by large polygonal cells with abundant, chromophobe cytoplasm and the other one represented by smaller cells, with a small eosinophilic cytoplasm. It was described a variant of chromophobe RCC described as eosinophilic variant of CHRCC and characterized by the whole composition by intensively eosinophilic cells; two types of cellular elements have been described in these tumors: type 1 cells, small with moderately granular cytoplasm and type 2 cells, with abundant eosinophilic cytoplasm denser at the periphery [129]. The genetic abnormality most frequently observed in CHRCC is represented by the loss of one copy of the entire chromosomes 1, 2, 6, 10, 13, 17, and 21 (observed in about 86% of cases) and losses of several other chromosomes

(observed in about 12–58 of cases) [130]. These chromosome abnormalities have been observed both in the classic and in the eosinophilic variants of CHRCC, although loss of chromosomes 2 and 6 was less frequent in eosinophilic than in classic variant of CHRCC [131]. It is important to note that about 50% of CHRCCs display loss of all chromosomes and about 10% display no loss of any chromosome [131]. The chromosome losses were not observed in oncocytomas [131]. A recent study, through cumulative analysis of various database containing data on chromosome number alterations in CHRCC, reached the conclusion that losses of chromosomes 1, 2, 6, 10, 13, and 17 were significantly more frequent among classic CHRCC compared to eosinophilic CHRCC, thus suggesting that classic CHRCCs are characterized by higher chromosomal instability [132]. In addition to these typical chromosomal losses, CHRCCs display also copy number gains that were detected in chromosomes 4, 7, 11, 12, 14q, and 18q [133].

**Table 2.** Molecular abnormalities of main sporadic renal cell cancers (RCCs).

RCC Subtype	Somatic Mutations or Alterations	Copy Number Variations or Translocations	Prognostic Implications of Genomic Alterations
CCRCC	Mutations in <i>VHL</i> , <i>PBM1</i> , <i>SETD2</i> , <i>BAP1</i> , <i>KDM5C</i> , <i>TERT promoter</i> , <i>MTOR</i>	Loss of chromosomes 3p, 14q, 9p, 6q, 8p, 15q Gain of chromosome 5q	<i>VHL</i> : no association <i>PBM1</i> : greater survival/no benefit <i>BAP1</i> , <i>SETD2</i> , <i>CDKN2A</i> , <i>TP53</i> : reduced survival <i>PDH</i> genes, Ribose sugar metabolism genes: reduced survival
PRCC, type I	Mutations in <i>MET</i> , <i>NRF2</i> , <i>CUL3</i>	Gains of chromosomes 3, 7, 16, 17	<i>CDKN2A</i> , <i>PBM1</i> , <i>TP53</i> : reduced survival <i>DKK1/SFRP1</i> : unmethylation: reduced survival
PRCC, type II	Mutations in <i>CDKN2A</i> , <i>CDKN2B</i> , <i>TERT</i> , <i>NF2</i> , <i>FH</i> , <i>MET</i> , <i>SETD2</i>	Gains of chromosomes 7, 16, 17, 5q Loss of chromosomes: 3p, 14q, 22q Translocation of <i>TFE3</i>	<i>CDKN2A</i> , <i>TP53</i> : reduced survival <i>DKK1/SFRP1</i> : unmethylation: reduced survival
CHRCC	Mutations in <i>TP53</i> , <i>PTEN</i>	Loss of chromosomes 1, 2, 6, 10, 13, 17, 21	<i>PTEN</i> , <i>CDKN2A</i> : reduced survival <i>DKK1/SFRP1</i> : unmethylation: reduced survival Metabolically divergent tumors: highly reduced survival
RMC	Mutations in <i>SMARCB1</i>	Amplification of <i>ABL</i>	Unknown
TCRCC	Mutations in <i>ABL1</i> , <i>PDGFRA</i>	Gains of chromosomes: 7, 17	Unknown
Wilms Nephroblastoma	Mutations in <i>TP53</i> , <i>AMER1</i> , <i>CTNBN1</i> , <i>WT1</i> , <i>DROSHA</i> , <i>DGGR8</i> , <i>DICER1</i> , <i>SIX1/SIX2</i> , <i>SMARCA-4</i> , <i>MLTT1</i>	Loss of chromosomes 1p, 16q, 1q, 17p, 4q, 14q, 11q, 11p15.	<i>TP53</i> , <i>SIX1/SIX2</i> , <i>DROSHA/DGGR8</i> : reduced survival Loss of chromosomes 1p, 1q, 11p15, and 16q: reduced survival

About 2% of CHRCC display sarcomatoid features; these tumors were explored for their chromosomal abnormalities, showing some remarkable differences compared to the rest of CHRCC:

sarcomatoid CHRCCs frequently display multiple gains (polysomy) of chromosomes 1, 2, 6, 10, and 17; distant metastases show the same chromosome abnormalities, usually chromosome losses found in the primary tumors [134].

The analysis of gene copy number by next generation sequencing showed the occurrence of multiple abnormalities in CHRCC; this analysis showed that the two most frequent deletions involved the tumor suppressor genes *RB1* and *ERBB4* [135]. Fluorescence in situ hybridization showed hemizygous deletion of *RB1* in 52% of cases and of *ERBB4* in 33% of cases; in total, 70% of CHRCC display either hemizygous deletion of *RB1* or *ERBB4* [135].

Davis and coworkers in the context of TCGA studies have performed a comprehensive characterization of 66 primary CHRCC using diverse molecular platforms, including whole-genome sequencing and mtDNA analysis [128]. The results of this study showed: (i) The typical and frequent chromosome losses described in other studies, observed in all cases corresponding to the classic variant and in about 53% of cases corresponding to the eosinophilic variant; (ii) *TP53* (32% of cases) and *PTEN* (9% of cases) were the only two genes frequently mutated in these tumors, while mutations of other cancer-relevant genes (such as *MTOR*, *NRAS*) were found at lower frequencies; (iii) the gene expression profile showed a high index of mRNA expression correlation for CHRCC with distal regions of the nephron; (iv) the analysis of mitochondrial DNA showed mutations at the level of genes involved in respiration and oxidative phosphorylation; (v) whole genome sequencing analysis showed the occurrence of kataegis (a mutational phenomenon involving highly localized substitution mutations, C > T or C > G), occurring at the level of some chromosome regions involved in rearrangements, involving also rearrangements occurring within the *TERT* promoter gene region (observed in 12% of cases) and associated with elevated *TERT* expression [128].

Durinck et al. have reported a study of extensive characterization of the genomic alterations observed in non-clear RCC subtypes, including CHRCC (36 classic and 12 eosinophilic). In CHRCC, the frequently mutated genes were: *TP53* (21.3%); *PTEN* and *KIAA 1731* (6.4% of cases); *FAAH2*, *PDHB*, *PDXD1*, *ZNF 765*, *PRKAG2*, *ARID1A*, and *ABHD3* (4.3% of cases) [136]. Some of these mutations may play a relevant role in the pathogenesis of CHRCC. Thus, the *PDHB* gene encodes the E1 $\beta$  subunit of the pyruvate dehydrogenase complex (PDHc), catalyzing the conversion of pyruvate to acetyl-CoA, thus providing a link between glycolysis and the TCA cycle; the two mutations observed in CHRCC are reminiscent of those observed in a neurological condition associated with germline mutations of this gene and causing lactic acidosis [136]. *PRKAG2* encodes one of the three  $\gamma$  subunits of AMPK, a key sensor of cellular metabolism; the mutations of this gene, observed at the level of the inhibitory pseudosubstrate sequence within AMPK  $\gamma$  subunit, may lead to constitutive AMPK activation [136]. Furthermore, gene expression analysis led to the identification of five genes, *ADAP1*, *SDCBP2*, *HOOK2*, *BAIAP3*, and *SPINT1* markedly expressed in CHRCCs and that clearly differentiated these tumors from oncocytomas [136].

Ricketts et al. reported a comprehensive analysis of different subtypes of RCCs, including 81 cases of CHRCC [137]. Some recurrent mutations have a prognostic impact in CHRCC patients: *PTEN* mutations correlated with decreased survival; *CDKN2A* alterations (including loss of the region of chromosome 9p encoding *CDKN2A* and promoter hypermethylation) correlated with a decreased survival [137]. About 20% of CHRCCs displayed a hypermethylation DNA profile and these tumors were associated with a higher tumor grade and with a poor outcome [137]. The metabolic gene expression profile showed that: expression of the Krebs cycle and the electron transport chain genes was high in CHRCC, in association with increased expression of the pyruvate dehydrogenase complex activation genes; expression of AMPK was increased in CHRCC; a small subgroup of CHRCCs displayed a peculiar metabolic profile with low expression of the Krebs cycle and electron transport chain genes, lower expression of the *AMPK* pathway genes, and increased expression of the genes in ribose synthesis pathway, and was associated with a particularly poor prognosis [137].

Although CHRCC is a relatively indolent tumor, 5–10% of patients may develop metastases and metastatic tumors may possess peculiar molecular properties compared to those not generating

metastases. This analysis provided evidence that metastatic CHRCC, at variance with non-metastatic CHRCCs that are hyperdiploid (with a ploidy estimated above 2); importantly, these hyperdiploid metastatic CHRCC maintained their typical CHRCC-7 set- chromosomes loss [138]. This hyperdiploid pattern is due to either loss of the CHRCC-7 set-chromosomes, associated with duplication of the remaining genome or duplication of multiple chromosomes excluding the CHRCC-7 set-chromosomes: this condition was defined as imbalanced chromosome duplication (ICD) [138]. The comparative analysis of metastatic and non-metastatic CHRCC showed among metastatic tumors increased frequencies of *TP53* mutations, *PTEN* mutations, and ICD (observed at frequency of 55%, 27%, and 43%, respectively) compared with those observed in nonmetastatic CHRCC (25%, 7%, and 10%, respectively) [138]. Phylogenetic studies of paired-primary-metastatic samples allowed to propose a tumor progression process, involving the nearly universal loss of CHRCC-7 set-chromosomes as the only driver event in the pathogenesis of CHRCC, followed by *TP53* mutations that were detected in 82% of metastatic samples and then by ICD and *PTEN* mutations that were detected in 82% of metastatic samples and then by ICD and *PTEN* mutation, occurring in a mutually exclusive manner [138].

Initial studies have shown that the membrane receptor KIUT is overexpressed in CHRCC (83% of cases positive), whereas it was not expressed in other RCCs [139].

CHRCC is usually associated with a favorable prognosis. Przybycin and coworkers in a retrospective study in 200 CHRCC patients have shown that: 2.5% of cases displayed metastases at presentation; disease-specific events, including recurrence, metastasis, and death due to disease were observed in additional 4% of patients; 2% of patients had tumors with sarcomatoid features [140]. 5-year and 10-year disease-specific events occurred in 3.7% and 6.4% of patients, respectively [140]. Therefore, these observations showed a significant association of outcomes with tumor size; small-vessel invasion, sarcomatoid features, and microscopic necrosis, whereas T stage showed a statistically non-significant association [140]. A large multicenter study involving the analysis of 291 patients with CHRCC diagnosis confirmed the good prognosis of CHRCC patients, with only 1.3% of these patients presenting distant metastases at diagnosis and a 5-year and 10-year cancer-specific survival of 93% and 88.9%, respectively [141]. Only patients with locally advanced disease at diagnosis or with metastatic cancers, as well as those with sarcomatoid differentiation have a poor prognosis [141].

Because of the rarity of this condition, only few studies have specifically explored the outcomes of metastatic CHRCC patients. The analysis of a very large cohort of 4970 metastatic RCC patients treated with targeted therapy showed that only 2.2% of these patients displayed metastatic CHRCC and the large majority (97.8%) pertains to CCRCC [142]. Metastatic CHRCC exhibited a similar overall survival compared to patients with CCRCC (23.8 months vs. 22.4 months) [142]. Ged and coworkers have analyzed the outcomes of metastatic CHRCC according to the presence or not of sarcomatoid features [143]. In a group of 109 metastatic CHRCC patients, these authors observed that 29 of them exhibited sarcomatoid differentiation; patients with sarcomatoid features showed a shorter time to metastatic recurrence than those with non-sarcomatoid differentiation (2.7 months vs. 48.8 months); a similar observation was made for time to treatment failure (1.8 months vs. 8.0 months). Finally and importantly, median overall survival was clearly inferior for patients with sarcomatoid differentiation compared to those without this differentiation properties (7.5 months vs. 38 months) [143]. Recently, Casuscelli et al. have reported a survey on a very large cohort of 496 CHRCC patients diagnosed and surgically treated at Memorial Sloan Kettering Cancer Center [144]. This study definitely confirmed the findings observed in previous studies, showing that: at 10 years, the relapse-free survival was 91.7% and the overall survival 82.1% for CHRCC patients, compared to 79.4% and 63.6% for CCRCC patients; patients with CHRCC displayed less frequently sarcomatoid differentiation compared to CCRCC patients (1.2% vs. 4%); larger tumor size, sarcomatoid differentiation, and higher tumor-stage are significantly associated with adverse RFS and OS in CCRCCs [144].

## 11. Papillary Renal Carcinoma

PRCCs make up about 15% of RCCs, are heterogeneous, and characterized by the presence of papillae in the tumor; these tumors are commonly subdivided into two subtypes based on staining features: subtype 1 basophilic, type 2 eosinophilic [145]. Particularly, type 1 PRCCs display papillae lined by a single layer of cells with scanty basophilic cytoplasm and low nuclear grade; type 2 PRCCs show papillae lined by pseudostratified layers of cells with more abundant eosinophilic cytoplasm and low nuclear grade [145]. About 15% of PRCCs cannot be classified as type 1 or type 2 subtypes and are grouped in an unclassified group.

Type 1 and type 2 PRCCs have distinct molecular pathways and clinical behavior. Type 2 tumors were larger, more common in patients younger than age 40, and more frequently stages 3 or 4 than were type 1 tumors [146].

In 2016 TCGA provided the first detailed, comprehensive molecular analysis of PRCCs [147]. The study of copy number alterations displayed the existence of three main tumor subgroups: (i) One subgroup is predominantly composed of type 1 and lower-grade tumors and is characterized by multiple chromosomal gains involving the very frequent gain of chromosomes 7 and 17 and the less frequent gain of chromosomes 2, 3, 12, 16, and 20; (ii) the other two subgroups are predominantly composed by type 2 tumors and one of these two subgroups is characterized by a limited number of copy alterations, whereas the other one is characterized by extensive aneuploidy, with numerous chromosomal losses, including frequent loss of chromosome 9p and is associated with poor survival [147]. The higher frequency of the number of DNA gains per tumor at the level of chromosomes 7 and 17 in type 1 than in type 2 PRCCs was previously reported by Jiang and coworkers [148].

Whole exome sequencing performed in 157 PRCCs identified several somatic mutations, occurring with a significant frequency, at the level of tumor-related genes, such as *MET*, *SETD2*, *NF2*, *KDM6A*, *SMARCB1*, *FAT1*, *BAP1*, *PBRM1*, *STAG2*, *NFE2L2*, and *TP53* [63,147]. Assignment of these genes to their biochemical pathways showed that: SWI/SNF complex (*SMARCB1* and *PBRM1*) was altered in 20% of type 1 and 27% of type 2 PRCCs; chromatin modifier pathways (*SETD2*, *KDM6A*, and *BAP1*) was altered in 35% of type 1 and 38% of type 2 PRCCs; the Hippo pathway (*NF2*) was altered in 3% of type 1 and 10% of type 2 PRCCs [63,147]. However, some genetic alterations are specific to types of PRCCs: (1) *MET* mutations are much more frequent in type 1 than type 2 PRCCs (17% vs. 1.6%, respectively) and were observed in 11% of unclassified PRCCs; levels of *MET* mRNA and *MET* protein phosphorylation were higher in type 1 than type 2 tumors. (2) 8% type 2 PRCCs displayed 9p21 chromosomal focal loss with loss of *CDKN2A* locus; other type 2 PRCCs exhibited *CDKN2A* mutations or promoter hypermethylation, resulting in a total of 13% of tumors with *CDKN2A* alterations; *CDKN2A* loss was associated with low overall survival. (3) Type 2 PRCCs are associated with mutations in chromatin-modifying genes *SETD2* (19.4%), *BAP1* (10.4%), and *PBRM1* (11.9%) which are frequently mutated in CCRCCs; mutations of *BAP1* and *PBRM1* were mutually exclusive, whereas *SETD2* mutations co-occurred with *PBRM1* mutations in most cases. (4) Another feature of type 2 PRCCs consists in the increased expression of NRF2-associated response element (ARE) pathway; these findings were in line with other studies showing increased activation of the NRF2-ARE pathway in type 2 PRCCs and mutations in NRF2-ARE pathway genes *NFE2L2*, *CUL3*, *KEAP1*, and *SRT1* [82,84,149,150]. (5) A CpG island methylator phenotype (CIMP) was observed in a subgroup of type 2 PRCCs characterized by mutations of *FH* gene and poor survival [63,147].

Finally, from this study it emerges that unclassified PRCCs display molecular properties hybrid between type 1 and type 2 PRCCs; the frequency of chromosomal 7 gain in these tumors is intermediate (26%) between type 1 (85%) and type 2 (18%) [63,147].

Durinck et al. in their study of molecular characterization of non-clear RCCs reported a detailed analysis of *MET* mutations occurring in PRCCs; particularly, they observed *MET* mutations in 15% of the PRCC samples: all these mutations, with just a single exception, affected the kinase domain of *MET*, all displaying elevated phosphorylation, suggesting their constitutive activation [136].

A large data set of 169 patients with advanced PRCC was published by Pal et al., basically corroborating the data reported in the TCGA study [151]. Particularly, in patients with type 1 PRCC the most commonly altered genes were *MET* (33%), *TERT* (30%), *CDKN2A/B* (18%), and *EGFR* (8%); in patients with type 2 PRCC the most recurrent gene mutations were *CDKN2A/B* (18%), *TERT* (18%), *NF2* (13%), *FH* (13%), and *MET* (7%) [151]. Remarkable differences from TCGA data involve higher frequencies of *MET*, *NF2*, and *CDKN2A/B* [151].

In 2018, TCGA network refined the molecular analysis of PRCCs, showing that: at the level of single gene mutations, in PRCCs *TP53* and *PBRM1* mutations correlated with decreased survival; *CDKN2A* mutation, hypermethylation, or deletion was found in 5% of type 1 PRCC, 18.6% of type 2 PRCC, 100% of CIMP-PRCC, and was associated with decreased survival; at the level of DNA methylation analysis, increased hypermethylation was associated with higher-stage disease in both type 1 and type 2 PRCCs and with decreased survival: among the hypermethylated genes, there were WNT pathway regulatory genes *SFRP1* and *DKK1*, whose hypermethylation was associated with poor survival; at the level of metabolic gene expression features, type 2 PRCCs displayed a more elevated expression of Krebs cycle genes compared to type 1 PRCC; concerning the immune signature analysis, both in whole population of PRCC and in type 2 PRCC, the high expression of a high T helper 2 (Th2) was associated with a reduced survival [137].

Two studies have reported the characterization of PRCCs by whole-genome sequencing. Li and coworkers using this approach discovered mutations at the level of an intron of *MET* gene, connected to an oncogenically relevant splicing event; furthermore, in other cases a methylation dysregulation on nearby, leading to a cryptic promoter activation of the *MET* gene was identified [152]. Furthermore, it was identified the recurrent mutation of the long noncoding RNA *NEAT1* and these mutations are associated with increased *NEAT1* expression and negative outcome [152]. Zhu and coworkers have explored the intratumoral heterogeneity and clonal evolution of PRCC integrating whole-genome sequencing and DNA methylation data [153]. Through the analysis of 29 patients at the level of various tumor regions (center and periphery of each tumor) the authors reached the important conclusion that, at variance with previous studies in CCRCC, in PRCC driver gene mutations and most arm-level somatic copy number alterations are clonal [153].

The main treatments used for RCC patients are based on clinical studies involving a limited participation from patients with PRCC; therefore, it is not surprising that conventional therapies are usually less for non-CCRCC compared to CCRCC. Thus, PRCCs are less responsive to conventional therapy used in RCC compared with CCRCCs, both at the level of PFS and OS, as supported by the analysis of large cohorts of patients [154,155]. The same difference in therapeutic response applies to VEGF inhibitors, such as sunitinib by showing shorter PFS in metastatic PRCC compared to metastatic CCRCC. However, sunitinib treatment in metastatic PRCC induced a slightly better PFS compared to the mTOR inhibitor everolimus and this gives support to the choice of the guidelines from the National Comprehensive Cancer Network and the European Society for Medical Oncology both recommending sunitinib as first line therapy in metastatic non-CCRCC.

Various agents targeting *MET*, such as crizotinib, savotinib, cabozantinib, foretinib, and tivantinib have been explored in clinical trials involving PRCC patients [156].

Among the studies carried out with *MET* inhibitors promising are those with cabozantinib and savolitinib. Two retrospective studies have shown therapeutic activity of cabozantinib in PRCC patients [157,158]. In fact, both these studies showed an objective response rate in metastatic PRCC patients treated with cabozantinib ranging from 14% to 27%, with a mean overall survival of 11 months in one of these studies [157,158]. Recently, the results of the SAVOIR phase 3 randomized clinical trial, comparing the efficacy of savolitinib to sunitinib in patients with *MET*-driven PRCC were published: in this study, a PFS of 7.0 months for savolitinib and of 5.6 months for sunitinib was observed, with significantly fewer adverse events reported in the savolitinib arm compared to the sunitinib arm [159]. These results suggest that savolitinib shows an encouraging efficacy compared to sunitinib.



Finally, another recent clinical study explored the association of a MET inhibitor (savolitinib) with a PD-L1 inhibitor (durvalumab). The first results observed in the PRCC cohort of the phase I/II CALYPSO clinical trial were recently presented at the ASCO Meeting [160]. In a population of PRCC patients with metastatic PRCC either treatment-naïve or VEGFR TKI-resistant, an OS at 12 months of 52%, not showing significant differences among PD-L1 positive, MET positive, and PD-L1/MET negative patients, was reported [160]. Some patients displayed durable responses [160].

## 12. Genetic Alterations of CCRCC

The most frequent and typical genetic alteration of CCRCC is represented by biallelic inactivation on the *VHL* gene determined by allelic deletion or loss of heterogeneity on chromosome 3p (observed in >90% of cases) [161], together with gene mutation (observed in about 50% of cases) [162,163] or promoter hypermethylation (observed in 5–10% of cases) [164]. Other frequent genetic alterations are represented by mutations in genes involved in chromatin modification, such as *PBRM1* [165], *SETD2* [166], *KDM5C* [166], *KDM6A* [166], and *BAP1* [167,168].

Sato and coworkers reported the first comprehensive, integrated molecular analysis of CCRCC [169]. Four (*VHL*, *PBRM1*, *SETD2*, and *BAP1*) of the five mutated genes in CCRCC are all located at the level of the 3p chromosomal region involved in LOH; 98% of the CRCC cases displaying LOH at 3p showed the remaining *VHL* allele altered by somatic mutation or promoter methylation [169]. Almost all cases exhibiting *PBRM1*, *SETD2*, and *BAP1* mutations occurred in CCRCC cases displaying *VHL* inactivation. Importantly, *SETD2* and *BAP1* mutations displayed lower allelic burdens than coexisting *VHL* mutations, suggesting that these mutations are acquired at later times during tumor development [169]. *PBRM1* mutations had no significant impact on overall survival, whereas *BAP1* mutations, mutually exclusive with *PBRM1* mutations, were associated with a shorter overall survival; finally, *SETD2* mutations displayed a high relapse rate [169]. Interestingly, 5% of CCRCC patients displayed *TCEB1* mutations, not associated with *VHL* gene alterations, but constantly associated with loss of chromosome 8; *TCEB1* encodes a protein involved in the formation of the RNA polymerase II elongation factor complex but also involved in the VHL complex formation [169]. In line with this finding, *TCEB1*-mutated tumors displayed increased HIF-1 $\alpha$  protein expression, as well as tumors with *VHL* loss [169]. Therefore, CCRCC with *VHL* loss or with *TCEB1* mutations accounts for 95.4% of the cases. Other genes recurrently mutated in CCRCC included *TET2*, *KEAP1*, and *MTOR*: *TET2* mutations and deletions occurred in 16% of cases; mutually exclusive mutations in *KEAP1*, *NRF2*, and *CUL3* occurred in 6.6% of cases; *MTOR* mutations were observed in 5.7% of cases [169].

A parallel study by TCGA reported the comprehensive molecular analysis of 417 samples of CRCC [170]. Most of the results reported in this analysis are in line with those reported by Sato et al. [169] and here are discussed the results of this study not analyzed in the other study. At the level of copy number the most recurrent event was loss of chromosome 3p observed in 91% of cases; 17q chromosome loss, associated with loss of *HIF1A* and with a more aggressive disease, was observed in 45% of samples; gains of 5q were frequently observed (67% of cases); several focal amplifications involved genes relevant at oncogenic level, such as *PRKCI*, *MDS1*, *EVII*, *MDM4*, *MYC*, *JAK2*; focally deleted regions involved the tumor suppressor gene *CDKN2A* and *PTEN* [170]. Importantly, Sato et al. reported among the CNAs the loss of 8p with or without loss of 8q (20% of cases), an abnormality frequently associated with *TCEB1* mutations [169]. Integrative data analysis showed that the most frequently mutated network involved *VHL* and numerous interacting partners, leading to activation of the transcription factor program mediated by HIF1A/ARNT; the second most mutated network included *PBRM1*, *ARID1A*, and *SMARCA4*, key genes at the level of chromatin remodeling complex; the mutations of the chromatin regulators *PBRM1*, *STD2*, and *BAP1* induce different patterns of altered gene expression in the context of a background caused by *VHL* loss; mutually exclusive alterations targeting multiple complexes of the PI3K/AKT/MTOR pathway occur in about 28% of the cases and suggest a potential therapeutic targeting [170]. In their evaluation of the main signaling pathways, Sato et al. evaluated all genetic alterations occurring in CCRCC-inducing activation of PI3K signaling and estimated a frequency of

76% of cases exhibiting PI3K activation; furthermore, they reported also the frequent (40%) activation of p53 signaling [169].

Finally, the TCGA study reported clear evidence about a metabolic gene expression pattern associated with aggressive disease, related to downregulation of genes the pentose phosphate pathway and the glutamine transporter genes and increased acetyl-CoA carboxylase protein levels [170].

The focal amplifications occurring at the level of chromosome 5q were explored in greater detail in subsequent studies. Copy number gains of chromosome 5q occurring in CCRCC drive overexpression of the gene *SQSTM1*; the p62 SQSTM1 protein is involved in activation of NRF2, and through this mechanism, in promotion of resistance to redox stress and in stimulation of renal cancer cell growth in vitro and in vivo [171]. A study based on multi-region whole-genome sequencing of 30 CCRCCs in the context of the TRACERx study showed that the gain of the chromosome arm 5q, together with the loss of chromosome arm 3p occur at the same time during CCRCC development: the concomitant occurrence of these two chromosomal abnormalities may be mediated by an unbalanced translocation event occurring between chromosomes 3 and 5 that involves chromotripsis [18,172]. This event was proposed as the initiating event for CCRCCs [18,172].

Ricketts et al. refined the analysis of molecular abnormalities of CCRCC performed by TCGA and showed that in these tumors: *TP53* and *BAP1* mutations and *CDKN2A* alterations were associated with decreased survival; at mRNA expression level an increased expression of the vasculature development signature, due to the activation of the VHL/HIF pathway, increased the immune response signature compared to other RCC types and increased ribose metabolism pathway, associated with poor survival [136].

Few studies have investigated the genomic landscape of metastases compared to primary tumors in CCRCC. At histological level, metastatic CCRCC tumors display pathological features similar to those of primary tumors from which they derive [173]. At gene expression level, the paired analysis of primary and metastatic CCRCC displayed an enrichment in metastatic tumors of the expression of genes involved in the formation of extracellular matrix [174]. De Velasco and coworkers have reported the analysis of a large cohort of metastatic CCRCCs, and through the analysis of matched metastases and primary tumors reached the conclusion that CCRCC primary tumors and metastases display a highly comparable distribution of common genetic alterations [175]. This finding supports the view that there is no single gene driving the metastatic disease or that changes at expression protein or epigenetic level are responsible for the development of metastatic properties of CCRCCs [175].

The study of tumor heterogeneity provided more information in the understanding of the molecular mechanisms involved in CCRCC evolution. In this context, fundamental were two studies by Gerlinger and coworkers reporting the analysis of 10 CCRCC patients (7 with metastatic disease) by exome sequencing on multiple regions of the same tumor and performing a comparison with a mutational spectrum across all regions [176,177]. The results of these two studies provided some fundamental data about intratumor heterogeneity of CCRCC: only a small fraction of genetic alterations display a clonal distribution, such as VHL loss and chromosome arm 3p loss, whereas other genes recurrently mutated such as *SETD2* and *BAP1* have a subclonal pattern of distribution within the tumor [176,177]. It is of interest to note that the multi-region sequencing allowed the identification of a higher frequency of gene mutations and copy number alterations than by single tumor sampling [176,177]. Thus, according to these data it is possible to infer that the TCGA data obtained on single tumor sampling could underestimate the frequency of some driver mutations such as *BAP1* and *TP53* [176,177].

These initial observations have been expanded through the multiregional analysis of 100 primary CCRCC and 38 cases of metastases; these two additional studies strongly supported the view that the intertumor heterogeneity and the pattern of intratumor heterogeneity influence the tumor evolution and metastasis development [178,179] (Table 3). Particularly, variations in the number, timing, and order of driver events are major determinants of disease evolution and metastatic potential. In tumors in which VHL is the only driver event, metastatic evolution is rare, whereas cases with multiple drivers are associated with metastatic development; the sequence and the intratumor distribution of these

additional drivers, either clonal (present in all tumor cells) or subclonal (present in only a part of tumor cells) is a key determinant of tumor evolution, thus if the driver events in addition to VHL loss occur clonally the metastatic spread is slower [178]. Thus, CCRCC characterized by low chromosomal complexity and low intratumor heterogeneity evolves following a linear pathway with VHL as sole mutation; CCRCC evolving through a branched pathway acquires early PBRM1 mutation and subsequent subclonal driver alterations slowly evolves to a oligometastatic potential; CCRCC evolving through a punctuated pathway results from the development of tumors characterized by the presence of multiple driver genetic alterations occurring clonally (punctuated evolution) and evolves more rapidly to metastatic potential [178] (Table 3). These studies showed also that losses of chromosomes 9p and 14q are events of fundamental importance for metastatic evolution of CCRCC: these two chromosomal abnormalities are enriched in all metastases and are therefore drivers of metastatic progression and higher overall mortality [179].

**Table 3.** Evolutionary patterns of clear-cell RCC (CCRCCs) that are associated with the development of different metastatic potentials. Tumors that follow a linear pattern of evolution have a limited intratumor heterogeneity (ITH), a low genomic instability index (GII), few mutations in addition to VHL and a low fraction of their genome affected by copy number alterations (SCNAs), and display a low metastatic potential. The branched pattern of tumor progression implies high ITH and GII, the progressive acquisition of additional mutations after VHL loss, with early acquisition of PBRM1 mutations and then subclonal acquisition of additional genetic alterations (SETD2 mutations, PI3K-AKT-mTOR pathway mutations, etc.), associated with a slow metastatic development. The punctuated pattern is characterized by high GII and low ITH, early chromosome 9p and 14q loss, acquisition of multiple driver mutations, including BAP1 mutations and rapid acquisition of a metastatic potential.

Evolution Pattern	Early Events	Primary Tumor	Genomic Characterization	Metastatic Potential
Linear	Chr 3p loss VHL inactivation Initial clonal expansion	3p loss → VHL	Low GII Low ITH	Non-Metastatic
Branched	Chr 3p loss VHL inactivation Initial clonal expansion	3p loss → VHL → PBRM1 → SETD2 → PI3K → SCNAs	High GII High ITH	Slow Progression
Punctuated	Chr 3p loss VHL inactivation Initial clonal expansion	3p loss → VHL → BAP1, PBMRA, SCNAs 9p loss 14q loss	High GII Low ITH	Rapid Progression

Huang and coworkers have analyzed the clonal architectures of 473 CCRCC patients and showed that the evolution patterns of CCRCC have consistent inter-patient heterogeneity, with del(3p) being considered as the common earliest molecular event, followed by three most recurrent patterns of clonal evolution dictated by different molecular events: (i) VHL and PBRM1 mutations; (ii) del(14q); (iii) amp(7), del(1p), del(6q), amp(7q), del(3q) [180]. The analysis of these patients allowed to identify three prognostic subtypes of CCRCC with different clonal architectures and immune infiltrates: patients with a long-life expectancy are enriched with VHL, but depleted of BAP1 mutations, and have high levels of Th17 and CD8+T lymphocytes, while patients with a short survival are characterized by high burden of CNAs (frequent del(14q)), high levels of Tregs and Th2 cells [180].

Recently, Clark and coworkers reported an integrated proteogenomic characterization of CCRCC; in this study, 110 treatment-naïve CCRCCs were explored by wide genome sequencing and by epigenomic, transcriptomic, proteomic, and phosphoproteomic analyses. At arm level, 3p loss (93%) was the most frequent CNA, followed by 5q gain (54%), chromosome 14q loss (42%), chromosome 7 gain (34%), and chromosome 9 loss (21%); furthermore, about 13% of tumors displayed extensive copy number variations along all chromosomes, thus indicating a high degree of genomic instability [181]. This analysis showed also that 61% of CCRCC cases displayed one or more translocations, mainly involving the chromosome 3p locus and chromosome 5 (20%) [181]. This study confirmed the data on the frequency of most recurrence gene mutations and provided evidence that all the genetic alterations, including *VHL*, *PBRM1*, *BAP1*, *KDM5C*, and *SETD2* are related to genetic events resulting in reduced expression of both mRNA and protein, thus indicating loss-of-function and supporting the classification of these genes as tumor suppressors [181]. The proteomic analysis allowed to better characterize the metabolic shift occurring in CCRCC tumors, illustrated at protein level by upregulation of glycolysis and downregulation of the Krebs cycle and electron transport chain (OXPHOS), associated with the Warburg effect; the downregulation of the Krebs cycle and the majority of OXPHOS proteins were not observed at mRNA level [181]. This analysis of proteo-metabolic profile allowed also to identify late-stage tumors upregulating OXPHOS pathway relative to early stage tumors, a finding that may be related to dysregulation of HIF-1  $\alpha$  caused by 14q loss; similar observations were previously reported by Hakimi et al. through analysis of the metabolic profiling of CCRC [182]. The proteomic analysis allowed the subdivision of CCRCC into three groups: CCRCC1 associated with higher tumor grade and stage and characterized by elevated adaptive immune response, N-linked glycosylation, OXPHOS protein expression and fatty acid metabolism and high frequency of BAP1 mutations and CIMP+ status; CCRCC2 and CCRCC3 were associated with lower tumor grade and stage: tumors in CCRCC2 were associated with tumor immunity, whereas tumors in CCRCC3 with glycolysis, mTOR signaling, and hypoxia and display higher frequency of PBRM1 mutations [181].

Over the past years, the therapy for patients with advanced/metastatic CCRCC has considerably evolved and new therapeutic options are now available for these patients, including targeted agents such as those targeting the VEGF pathway (mainly represented by VEGFR-directed tyrosine kinase inhibitors, TKIs) or targeting mTOR (such as everolimus) or immunotherapy based on immune checkpoint inhibitors and combination treatment strategies [183]. Molecular studies have contributed to define the subpopulations of CCRCC patients more responsive to these treatments and to define the mechanisms of primary or acquired resistance to these therapies.

Thus, several retrospective studies have analyzed the prognostic impact of chromatin-modifying gene alterations in CCRCC. *PBRM1*, the gene most frequently altered after *VHL*, seems to play a different role in localized and advanced disease, constituting a poor prognostic factor in localized disease and a good prognostic factor in advanced disease [184]. Retrospective studies on metastatic CCRCC patients indicate that *PBRM1* loss is associated with improved outcomes in patients treated with either VEGFR TKIs or mTOR inhibitors, whereas *BAP1* and *TP53* mutations were associated with unfavorable cancer-specific outcomes [185].

A part of patients with advanced CCRCC respond to treatment with immune check blockage and some of these responses are durable. Immune check inhibitors (ICI) have become a key therapeutic strategy to stimulate the immune anti-cancer response; across various solid tumor malignancies, response to PD-1 or PD-L1 blockade was associated with some tumor-intrinsic (high tumor antigen burden, high neoantigen load) or microenvironmental features (PD-L1 expression, T lymphocyte infiltration). McDermott and coworkers have analyzed the CCRCC patients enrolled in the context of IMmotion150 clinical trial, a randomized phase II study of atezolizumab (anti-PD-L1) alone or in combination with bevacizumab (anti-VEGF) versus sunitinib (multi TKI) [186]. Exploratory biomarker analyses failed to show that tumor mutation burden and neoantigen load display any significant association with PFS; angiogenesis, T-effector/IFN-gamma response, and myeloid inflammatory gene expression signatures were strongly and differentially associated with PFS [186]. 62% of these patients

displayed VHL mutations and 44% *PBRM1* mutations; angiogenesis-related gene expression signature was higher in VHL-mutated and *PBRM1*-mutated CCRCCs; within treatment evaluation showed that *PBRM1* mutations were associated with improved PFS in the sunitinib arm; in the *PBRM1*-mutated patients atezolizumab+bevacizumab showed improved PFS compared to atezolizumab alone [186]. Whole genome sequencing studies performed in 35 metastatic CCRCC patients undergoing treatment with an anti-PD-1 blocking agent showed that clinical benefit to this treatment was significantly associated with mutations in the *PBRM1* gene [187]. These findings were confirmed in independent validation cohorts of CCRCC patients treated with PD-1 or PD-L1 blockade therapy [188].

The analysis of 592 tumors derived from patients with advanced CCRCC enrolled in clinical trials based on the treatment with PD-1 confirmed that conventional genomic and immunological markers were not associated with clinical response, but some genomic abnormalities associated with response or resistance to PD-1 blockade [189].

### 13. Genetic Abnormalities of Renal Medullary Carcinoma (RMC)

RMC is a rare aggressive subtype of renal cancer that mainly affects young adults with sickle cell trait. This condition was initially described by Davis et al. in 1995, reporting a series of cases of aggressive kidney cancers occurring in young individuals (15–30 years) with sickle cell trait; most of these patients presented with advanced disease and poor survival [190]. Beyond the strong clinical association with sickle disease trait, the underlying biology of this rare cancer is poorly understood. Loss of *SMARCB1* (also known as *INI1*) is a key diagnostic feature of these tumors: Calderaro et al. reported the loss of *SMARCB1* expression by immunohistochemistry by 6/6 RMC patients; in two cases explored by FISH analysis, loss of one *SMARCB1* allele was observed [191].

The mechanisms underlying *SMARCB1* protein loss in RMC were explored by more recent studies. Thus, in 2016 Calderaro et al. reported novel balanced translocations disrupting *SMARCB1* in 4 of 5 cases studied; all these 4 cases occurred in patients with sickle cell trait or disease, whereas the remaining case displayed a homozygous deletion of *SMARCB1* and presented in a patient with normal hemoglobin [192]. Total of 36 patients with RMC were reported by Carlo et al.; 33 of these patients were explored for tissue expression by immunohistochemistry and 100% of them displayed *SMARCB1* loss; 10 patients were explored by FISH analysis and 2 of them displayed biallelic *SMARCB1* loss; 6 patients were explored by NGS and none of them displayed *SMARCB1* gene mutations [193]. More recently, Jia et al. reported the molecular characterization of 20 RMC patients: all cases displayed protein loss; 55% showed concurrent hemizygous loss and translocation of *SMARCB1*, 30% with homozygous loss of *SMARCB1*, and 15% without structural or copy number alterations of *SMARCB1* despite protein loss; targeted sequencing provided evidence about the existence of a pathogenic somatic mutation in 1 of the 3 cases that were negative by FISH [194]. Tumors pertaining to the three subsets associated with different FISH findings displayed comparable clinicopathologic features; the only peculiarity was related to the cases with homozygous *SMARCB1* deletion being associated with the solid growth pattern, whereas tumor-bearing *SMARCB1* translocations were more associated with reticular/cribriform growth [194].

Hong et al. have developed patient-derived RMC models based on loss-of-function fusion events in one *SMARCB1* allele and loss of the other allele; through functional experiments, it was shown that RMC requires the loss of *SMARCB1* for survival [195]. Using loss-of-function genetic screens and small-molecule screen, it was found that the ubiquitin-proteasome system was essential in RMC: proteasome inhibitors caused G2/M arrest of RMC cells caused by cyclin B1 accumulation and cell apoptosis [195]. These observations support clinical trials based on the use of proteasome inhibitors for the treatment of RMC patients [195].

### 14. Genetic Alterations of Tubulocystic Renal Carcinoma (TCRCC)

In 1997 MacLennan et al. reported the existence of renal cancers that microscopically consisted of well-defined cystic lesions lined by hobnail-shaped cells with low mitotic activity and with a low

propensity for recurrence and metastasis [196]. These tumors were classified as low-grade collecting duct carcinoma; immunohistochemical markers suggested a collecting duct origin for these tumors [196]. Subsequent studies have supported the idea that low-grade collecting duct carcinoma and TCRCC are synonymous of the same clinicopathologic entity. The microscopic appearance was characterized by the presence of variable-sized cystically dilated tubules lined by a single layer of epithelium [197]. Immunohistochemistry and ultrastructural analysis supported features of proximal convoluted tubules and distal nephron; gene expression profiling supported a unique molecular signature, different from other RCC types [197].

Recent studies support the existence of TCRCC as a rare peculiar subtype of RCC. In fact, Lawrie et al. performed miRNA expression analysis and targeted next-generation sequencing mutational profiling on 13 cases of TCRCC: the expression profile of some miRs, such as *miR-155* and *miR-34a*, that were downregulated was clearly different from that observed in PRCC; the gene sequencing showed recurrent mutations of *ABL1* and *PDGFRA* genes, both genes being only rarely mutated in other RCC types [198]. More recently, Sarungbam et al. performed a molecular characterization of 10 cases of pure TCRCC by targeted next-generation sequencing and FISH analysis for X and Y chromosomes: all these carcinomas displayed combined losses at chromosomes 9 and gains at chromosome 17, and loss of chromosome Y; none of these tumors displayed mutational profiles typical of other RCCs; recurrent mutations in chromatin-modifying genes, *KMT2C* and *KDM5C*, were detected in about 25% of tumors; non *ABL1* and *PDGFRA* mutations were detected [199]. Thus, TCRCC demonstrates genomic features distinct from other subtypes of RCC.

## 15. Wilms Nephroblastoma

Wilms tumor (WT) is largely the most frequent kidney tumor in children (80–90% of the cases). These tumors contain three different histological components: A mesenchymal component resembling primitive fetal mesenchyme; an epithelial component resembling fetal renal tubules and glomeruli; a blastomatous component made by clusters of blast cells that contributed to the definition of these tumors as nephroblastoma. The histopathological features of WTs may be variable and usually the presence of all these histological components is a favorable determinant; unfavorable elements are represented by diffuse anaplasia and the predominance of the blastomatous component.

Initial studies have shown genetic abnormalities of *WT1* gene, Wnt-activating mutations of *CTNNB1* and *WTX*, abnormalities of *11p15* copy number, and methylation [200]. Subsequent genetic studies of large cohorts of WT patients have identified new mutations: recurrent mutations of the miRNA-processing gene *DROSHA* (observed in about 12% of cases) and non-recurrent mutations in other genes of this pathway (*DICER1*, *DGCR8*, *XPO5*, and *TARBP2*), associated with the downregulation of miRNA expression in a subset of WTs [201]. Recurrent mutations at the level of the homeodomain of *SIX1* and *SIX2* genes involved in the control of renal development, particularly frequent in WTs with blastemal histology (18% of cases), as well as *DROSHA* mutations (18% of cases) [202]; mutations of *MYCN*, *SMARCA4*, and *ARID1A* [203].

The most recurrent gene mutations occurring in high-risk subgroups of WT patients subdivided into those exhibiting a favorable histology (FHWT) that subsequently relapsed and those with diffuse anaplasia (DAWT) were defined: recurrent *DROSHA*, *DGCR8*, and *SIX1/2* homeodomain genes were observed in FHWT [204]; recurrent *TP53* alterations are observed in DAWT, with 48% of cases showing *TP53* mutations, 11% copy loss without mutation: patients with stage III/IV DAWTs had lower relapse and death rates than those with *TP53* abnormalities [205]. Another study showed the frequent occurrence of insertion/deletion *MLTT1* (a gene known to be involved in transcriptional elongation during early development) mutations, associated with altered binding to acetylated histone tails: these tumors show an increase in *MYC* gene expression and *HOX* genes dysregulation [206].

The Children Oncology Group and Target initiative published in 2017 a fundamental study reporting a genome-wide sequencing, mRNA and miRNA expression analyses, DNA copy number, and DNA methylation analyses in 117 WTs, followed by targeted sequencing of 651 WTs [207].

In addition to genes previously found to be mutated in WTs (*WT1*, *CTNNB1*, *AMER1*, *DROSHA*, *DGCR8*, *XPO5*, *DICER1*, *SIX1*, *SIX2*, *MLLT1*, *MYCN*, and *TP53*), this study discovered as frequently mutated in WTs also *BCOR*, *BCORL1*, *NONO*, *MAX*, *COL6A3*, *ASXL1*, *MAP3K4*, and *ARID1A* genes [207]. *TP53* was the most frequently mutated gene in the discovery set, enriched in DAWT histology; importantly, mutations in *TP53* were significantly associated with DAWT histology (56/118 DAWT and 9/533 FHWT); frequently, *TP53* mutations display a lower allelic fraction, consistent with the role of *TP53* as a secondary mutation in WTs [207]. *CTNNB1* was the most frequently mutated gene with global frequency of 13.5%; *CTNNB1* mutations were much more frequent among FHWT (16%) than among DWAT (1.7%); analysis of co-occurrence mutations showed a significant co-occurrence of *CTNNB1* mutations *WT1* (about 39% of tumors with *CTNNB1* mutations also had *WT1* mutations and about 74% of tumors with *WT1* mutations also had *CTNNB1* mutations) [207]. A significant co-occurrence was also observed between *DROSHA* and *SIX1/SIX2* mutations (15% of tumors with *DROSHA* mutations also had mutations in *SIX1* or *SIX2*, and 23% tumors with *SIX1* or *SIX2* mutations also had *DROSHA* mutations) [207].

At the level of CNAs, WTs are characterized by gains and losses of entire chromosomes or chromosomal arms, such as gains of *1q*, *6*, and *12* and loss of *4q*, *16q*, *17p*, *14*, *11*, and *22*; gain of *1q* was shown in about 48% of cases; gain of *1q* was not concurrent with any recurrent mutation, suggesting a possible role as a secondary event; amplification of *2p24* including *MYCN* locus, was found in 11.5% of FHWTs and 25.5% DAWTs; loss of *17p* correlated with *TP53* mutations, as well as loss of *4q* and *14q* [207]. Gain of chromosomal segments containing *6q16*, the location of *LIN28B*, was observed in 25.5% of cases and was related to the gain of whole chromosome 6 [207]. Chromosomal loss at *9q22* caused recurrent loss of *MIRLET7A* gene family: *MIRLET7A1* (5%), *MIRLET7A2* (18%), *MIRLET7A3* (21%) [207]. Gene expression analysis allowed the stratification of FHWT into six clusters: cluster 1 was characterized by *LIN28B* gain, *MIRLET7A* loss, *1q* gain, *WT1* loss, and absence of the most recurrent gene mutations; cluster 2 is characterized by frequent *DROSHA*, *DGCR8*, *SIX1*, and *SIX2* mutations, *11p15* methylation; cluster 3 is characterized by frequent *MLLT1*, *WT1*, *CTNNB1*, and *WTX* mutations, *WT1* and *WTX* loss, and *MYCN* amplification; cluster 4 is characterized by recurrent *WT1*, *CTNNB1*, and *WTX* mutations and *11p15* methylation; cluster 5 is characterized by the expression of genes involved in oxidative phosphorylation; cluster 6 is characterized by the absence of recurrent mutations, frequent *WT1* loss, and *Let7a* loss [207].

This study showed that WTs: (i) Derive from the cooperation of multiple genetic events; (ii) display different genetic alterations, associated with differential gene expression profiles; (iii) have multiple driver genes, the majority being altered in <5% of tumors; (iv) display mutations at the level of genes with common functions, mainly represented by genes involved in early renal development or epigenetic regulation [207].

Recurrent hot spot mutations have been found in ENL YEATS domain in WTs [208]. ENL protein is a reader of histone acetylation through its YEATS domain. Using human and mouse cellular models, evidence was provided that ENL mutants induce gene expression changes that promote a premalignant condition and in nephrogenesis models induce the formation of undifferentiated cellular structures resembling those observed in WTs [208]. At mechanistic level, these ENL mutations exhibit a function similar to their normal counterpart, occupying similar target genomic loci, but with a clearly increased occupancy, leading to a pronounced increase in the recruitment and activity of transcription elongation machinery, thus enforcing the rate and the level of gene transcription of these target genes [208].

Wilms tumors are characterized by persistent embryonic kidney tissues and arrested cellular differentiation. WTs often evolve from pre-cancerous clonal expansions [209]. To discover potential precursors of WTs, Coorens et al. used somatic mutations to infer the phylogenetic relationship that may occur between kidney tumors and corresponding normal tissues (blood) [209]. To perform this analysis, these investigators initially investigated some children with unilateral WTs and sampled tumor, blood and normal kidney tissue specimens from the same individuals: in two of the three cases analyzed, mosaic mutations in normal kidneys that were present in the corresponding tumor, but absent

from blood were observed [209]. Several features of these mutations observed in normal kidney tissue suggest that they can be defined as clonal expansions [209]. Importantly, the study of additional 23 cases of WTs showed evidence of clonal nephrogenesis in 53% of cases with unilateral disease and 100% of those with bilateral disease [209]. These observations suggested that clonal expansions in histologically normal kidney tissue as an atypical outcome of renal tissue development, antedating WT development; a direct phylogenetic link between clonal expansions, H19 hypermethylation, and the formation of cancer, thus supporting the view that these clonal expansions are an epigenetic progenitor of cancer; however, at variance with precursors of adult cancer, clonal nephrogenesis generated histological and functionally normal kidney tissue [209].

## 16. RCCs with Sarcomatoid (sRCC) Features

sRCC is a very aggressive form of RCC, characterized at histological level by the presence of a cellular component that has lost the epithelial features and has acquired mesenchymal features with spindle cells, high cellularity and cellular atypia; sarcomatoid features are observed in 5–10% of CCRCC and CHRCC and in 2–3% of PRCC [210–212].

sRCC is not a distinct RCC subtype, but represents a shift in the epithelial differentiation to mesenchymal differentiation in the context of pre-existing RCC; this conclusion is supported by two lines of observations: both an epithelial and a mesenchymal component is present in these tumors; both the epithelial and sarcomatoid components share the large majority of gene mutations, copy number alterations, and X-chromosome inactivation patterns [213]. In spite of these similarities of the epithelial and mesenchymal components suggesting a common origin, several remarkable differences exist between these two components strongly suggesting the evolution of sarcomatoid elements from carcinomatous elements by acquisition of additional genetic abnormalities: (i) Increased burden of cancer driver mutations and CNAs in sarcomatoid elements; (ii) existence of some sarcomatoid-specific mutations, such as *TP53*, *ARID1A*, and *BAP1* mutations [214] and TGF $\beta$  regulator *RELN* and *PTEN* mutations [215]; (iii) several genes involved in epithelial-to-mesenchymal transition display an increased expression in the mesenchymal component compared to the epithelial tumor components [212]; (iv) sarcomatoid components of these tumors displayed increased Aurora kinase-1 expression, supporting a potential role for increased mTOR activation as a driver of mesenchymal shift [216].

Malouf et al. reported the mutational analysis of 26 sRCCs and showed that *TP53* (42%), *VHL* (35%), *CDKN2A* (27%), *NF2* (19%) were the most frequently altered genes [217]. In a more recent report, these authors performed a detailed analysis of targeted sequencing of sRCCs, including also paired sequencing of epithelial and mesenchymal components isolated by microdissection. The most recurrent mutations in these patients involved *VHL* (72%), chromatin remodeling genes *SETD2* (40%), *PBMR1* (34%) and *BAP1* (26%), *TERT* promoter (18%), *PTEN* (14%), *TSC2* (12%), and Hippo pathway members *NF2* (10%) and *FAT1* (10%) [218]. The most altered pathways involved *VHL* (72%), chromatin remodeling genes (72%), MTOR pathway (50%), DNA repair (30%), and the Hippo pathway (20%) [218]. It is of interest to note that concerning the chromatin remodeling genes, in addition to *SETD2*, *PBMR1*, and *BAP1* mutations, were observed also mutations of *ARID1A* and *ARID1B* genes and of several genes acting as epigenetic regulators [218]. In 23 patients the genomic profiles of paired epithelial and mesenchymal components were compared, showing that: *SETD2* and *TERT* alterations markedly differed between the two components; one tumor harbored *NF2* and *CDKN2A* mutations exclusively in the mesenchymal component; two tumors harbored *TP53* mutations exclusively in the mesenchymal component [218]. Hippo pathway alterations were clearly more frequent in sRCC compared to non-sRCC [218]. Hippo-mutant sRCCs showed YAP/TAZ upregulation, thus showing that Hippo pathway is activated in these tumors; furthermore, Hippo pathway inhibition or restoration of normal *NF2* expression inhibited the proliferation and invasiveness of sRCC [218].

Ito and coworkers reported a detailed analysis on CNAs occurring in 17 sRCCs, showing that these tumors are associated with a high rate of chromosomal abnormalities involving losses



of 9q, 15q, 18p/q, and 22q and gains of 1q and 8q occurring at significantly higher frequencies compared to the corresponding non-sarcomatoid RCCs [219]. Among sRCC patients, those with >9 chromosomal abnormalities showed significantly worse overall survival than those with <9 copy number alterations [219].

In addition to sRCCs that are among the most aggressive RCCs, a high proportion of aggressive RCCs is observed at the level of the group of RCCs with unclassified histology (uRCC); these tumors are poorly characterized at molecular level. Chen et al. [64] reported the extensive molecular characterization of 62 primary high-grade uRCCs: sequencing analysis showed recurrent mutations at the level of 29 genes, the most frequent being *NF2* (18%), *SETD2* (18%), *BAP1* (13%), *KMT2C* (10%), *MTOR* (8%), *PTEN* (7%), and *TSC1* (7%); integrated molecular analyses showed the existence of a subset (26% of uRCCs) characterized by *NF2* loss, dysregulated Hippo-YAP pathway and poor survival and of another subset (21% of uRCCs), characterized by recurrent mutations of *MTOR*, *TSC1*, *TSC2*, or *PTEN*, hyperactive MT OR signaling and a better clinical outcome [64]. The frequent *NF2* abnormalities and the consequent dysregulation of the Hippo pathway represent a common feature of both sRCC and uRCC and support the targeting of this pathway for the therapy of a subset of these aggressive RCCs [220].

sRCCs are often metastatic and show a poor response to current therapeutic approaches. However, recent studies suggest that these tumors could be sensitive to immunotherapy treatments based on immune check inhibitors. Several studies have shown that PD-L1 expression is increased in sRCCs: importantly, PD-L1 expression is increased at the level of the sarcomatoid and not at the level of the epithelial component of these tumors [221,222]. Data from tumors of patients enrolled in clinical trials involving treatment with immune check inhibitors confirmed high levels of PD-L1 expression in sRCC of clear-cell type, with ≥50% of patients exhibiting a PD-L1 expression ≥1% of tumor [223] or microenvironment immune-infiltrating cells [224]. In a part of these patients elevated PD-L1 expression seems to be related to a molecular mechanism dependent upon *9p24.1* amplifications [225]. Ongoing clinical trials support the immunogenic potential of sRCCs both at the level of gene expression profile and at the level of response to treatment with immune check inhibitors combined with VEGF inhibitors [226].

## 17. Conclusions

RCC is among the top ten most commonly diagnosed cancers worldwide, accounting for 5% and 3% of all adult malignancies in men and women, respectively and representing the 7th most common cancer in men and the 10th most common cancer in women. Approximately, 2–3% of all RCCs are hereditary and several autosomal dominant syndromes have been identified, each with a distinct genetic basis and phenotype, the most common one being VHL disease. CCRCC is the most frequent RCC, accounting for about 70–75% of all cases and for the majority of renal cancer-caused deaths, followed by PRCC and CHRCC. Site of origin within the nephron is a major determinant in this classification in three major subtypes.

These various types of RCC have been defined on the basis of their histological appearance, the presence of distinct driver mutations, varying clinical course, and different responses to therapy. Extensive genomic, epigenomic, and transcriptomic profiling studies support that the different types of RCC are different diseases each different from the other. Integrated, multi-platform analysis of RCCs showed that these tumors can be subdivided into nine molecular-based RCC subtypes: (i) Three different subtypes were predominantly CCRCC cases and were designated CC-e.1, CCe.2, and CC-e.3, characterized by individual molecular features and by intermediate, better, and worse prognosis, respectively; (ii) four different subtypes of predominantly PRCC cases, P-e.1a, P-e.1b, P-e.1.2, and P-CIMP-e; (iii) one subtype of predominantly CHRCC [227]. These different subtypes can be further subdivided according to differences in patient survival or at the level of alterations of specific biochemical pathways, such as hypoxia, metabolism, Hippo pathway, MAP kinase, PI3K-AKT, NRF2-ARE, mTOR, and immune checkpoint [227].

These studies have allowed fundamental progresses in our understanding of the molecular mechanisms involving RCC development. Thus, molecular studies in CCRCC have defined the dysregulation of the *VHL* gene as an almost universal initial, founding event, followed by different types of additional genetic events involving *PBRM1*, *KDM5C*, *SETD2*, or *BAP1* that differentially dictate disease progression and aggressiveness [178,179]. CCRCC tumors with *PBRM1* mutations respond to targeted therapy differently than tumors with *BAP1* mutations [228]. These studies have strongly supported the utility of molecular studies, in addition to histological studies, to stratify CCRCC patients and to identify new potential therapeutic targets.

CCRCC is the prototype of a cancer resistant to conventional chemotherapy and radiotherapy and there is consistent hope that a better understanding of the molecular pathogenesis of RCC could contribute to the definition of more efficacious treatments. The discovery of abnormalities of several pathways has led to the approval of six different types of drugs for the treatment of metastatic RCC: inhibitors of VEGFR, mTORC1, c-MET, and FGFR; cytokines; anti-PD1/PDL1 immune checkpoint inhibitors [229]. These treatments have led to an improvement of metastatic RCC patients; however, in most of cases, the responses to these agents have been limited [229].

In the past two decades there has been a consistent improvement in the number of RCC therapies, characterized by a first period related to the development of targeted approaches based on the identification of targetable altered pathways, followed by a second period related to the development of immune-oncological therapies based on the stimulation of host immune system to promote an efficient immunological anti-tumor response; finally, the ongoing third period based on combination therapies that could improve survival in metastatic RCC [230].

RCC patients with localized stage I to III disease are treated with surgical resection; about one-third of these patients eventually recur; furthermore, 15% of RCC patients present with locally advanced or metastatic RCC, for which surgery is a noncurative treatment. For this last type of patients, over the past decade the standard of care has undergone significant changes and is currently in a state of continuous revisions. Anti-angiogenic inhibitors were the first targeted therapies approved for RCC treatment. The rationale for their use was related to the very frequent *VHL* alterations observed in RCCs and responsible for activation of hypoxia signaling pathway in these tumors [230]. Thus, sorafenib was approved by FDA in 2005 and was followed by other VEGFR small molecular TKIs, such as pazopanib and axitinib [230]. Early studies have suggested a sensitivity of a small subset of RCC patients to immunotherapy-based approaches using IL2 or IFN- $\alpha$ . The development of a more modern era of anticancer immunotherapy was based on the use of anti-CTLA4 and anti-PD-1/PD-L1 checkpoint inhibitors. These inhibitors have the capacity to block the inhibitory effects on the immune anticancer response existing in various tumors, including RCC. Many trials have examined the effect of immunotherapy alone or in combination with antiangiogenic TKIs and were shown to be superior to the existing standard of care [230].

Currently, sunitinib, pazopanib, nivolumab plus ipilimumab, pembrolizumab plus axitinib, avelumab plus axitinib are considered first-line treatments. Two recent clinical trials based on combination therapy strongly support the great potentialities of this approach to improve the survival of mRCC patients. Thus, the KEYNOTE-426 trial evaluated in first-line mRCC patients the safety and efficacy of pembrolizumab (anti-PD1) plus axitinib (VEGF inhibitor) versus sunitinib: patients treated with pembrolizumab plus axitinib had increased 12-month overall survival at 90%, compared to sunitinib at 78%; at 15.1 months, the progression-free survival was longer for pembrolizumab plus axitinib compared to sunitinib; the rate of adverse events was slightly higher in the pembrolizumab plus axitinib arm than in the sunitinib arm [231]. The overall survival, progression-free survival, and overall response rate were not significantly influenced by tumor PD-L1 expression and by patient risk stratification [231]. The updated results of this trial were presented at the last ASCO Meeting, showing that 74% of the patients were alive from the pembrolizumab plus axitinib arm at 24 months, compared to 66% in the sunitinib arm; the median overall survival was 35.7 months for patients treated with sunitinib and not reached for those treated with pembrolizumab plus axitinib;

the progression-free survival was 15.4 months versus 11.1 months; the overall response rate was 60.2% with pembrolizumab plus axitinib and 40% with sunitinib; the median duration of response was 23.5 months with pembrolizumab plus axitinib versus 15.9 months with sunitinib [232]. The analysis of treated patients stratified according to the tumor risk category showed that the benefit in terms of overall survival, progression-free survival, and overall response rate related to pembrolizumab plus axitinib therapy was limited to intermediate- and high-risk mRCC patients [232].

Another combination therapy study was the JAVELIN Renal 101 trial comparing axitinib plus avelumab, an anti-PDL1 antibody, with sunitinib in first-line metastatic RCCs: the treatment with axitinib plus avelumab increased the median PFS compared to sunitinib (13.8 months vs. 8.4 months); tumor PD-L1 positivity did not modify progression-free survival or the overall response rate; the safety profile was comparable in the two arms of treatment [233]. A recent update of this study confirmed the improvement of progression-free survival in the axitinib plus avelumab arm compared to sunitinib arm; overall survival data were still immature for evaluation [234].

Very recent studies further supported the rationale to therapeutically target pathways altered in RCCs. Thus, a very recent study presented at the last Genitourinary Cancer Symposium reported promising results of a phase I/II study involving the study of MK-6482, a HIF2- $\alpha$  inhibitor [235]. The very frequent VHL loss in CCRCC determines HIF accumulation and activation, and through this mechanism, stimulates blood vessels formation in RCCs. This study involved 55 patients with advanced RCCs who had an average of 3 prior lines of therapies; after a median follow-up of 13 months, the overall response rate was 24%; 74.5% of patients had stable disease, with a disease control rate of 80%; median PFS for whole population was 11.0 months; for favorable, intermediate, and poor risk RCC patients the PFS was 16.5, 11, and 6.9 months, respectively [235].

A report by Jonesch et al. showed the preliminary results of a phase II study (NCT 03401788) involving the treatment of 61 patients with germline VHL mutant, localized/nonmetastatic CCRCC, common lesions outside the kidney (non-RCC tumors such as hemangioblastomas (80%) and pancreatic lesions (50%)); about 28% of the patients displayed objective responses and about 87% of patients showed decrease in the size of target lesions [236].

The current, updated ESMO guidelines for treatment of advanced/metastatic RCC indicate that: the combination of pembrolizumab and axitinib should be considered as a front-line therapeutic option for patients with advanced disease, irrespective of prognostic groups and of the PD-L1 biomarker status; the combination nivolumab and ipilimumab should be considered in patients with intermediate/poor risk status; VEGF-targeted therapy is recommended for those patients where pembrolizumab/axitinib or nivolumab/ipilimumab are not available or contraindicated.

Given the heterogeneity of RCCs and the variability of their response to immunotherapy-based combination treatments, it will be of fundamental importance to acquire a better understanding of the genetic and epigenetic features of RCC patients who respond to these treatments.

**Author Contributions:** G.C., E.P. and U.T. have equally contributed to this manuscript, through search of bibliography, reading and interpretation of manuscripts, and preparation of the present manuscript. Particularly, U.T. mostly contributed to conceptualization, analysis of literature data and supervision; G.C. mostly contributed to writing-original draft preparation; E.P. mostly contributed to writing-review and editing and preparation of Tables. All authors have read and agreed to the published version of the manuscript.

**Funding:** This research received no external funding.

**Acknowledgments:** We are grateful to the library of the Istituto Superiore di Sanità Rome to have access to the reading of a large number of biomedical journals.

**Conflicts of Interest:** The authors declare no conflict of interest.

## References

1. Siegel, R.L.; Miller, K.D.; Jemal, A. Cancer statistics. *CA Cancer J. Clin.* **2019**, *69*, 7. [CrossRef]
2. Ferlay, J.; Steliarova-Foucher, E.; Leortet-Tieulent, J. Cancer incidence and mortality patterns in Europe: Estimates for 40 countries in 2012. *Eur. J. Cancer* **2013**, *49*, 1374. [CrossRef] [PubMed]

3. Saad, A.M.; Gad, M.M.; Al-Husseine, M.J.; Ruhban, M.I.; Sonbol, M.B.; Ho, T.H. Trends in renal cell carcinoma incidence and mortality in the United States in the last two decades: A SEER study. *Clin. Genitourin. Cancer* **2019**, *17*, 46–57. [[CrossRef](#)] [[PubMed](#)]
4. Wong, M.C.S.; Goggins, W.B.; Yip, B.H.K.; Fung, F.D.H.; Leung, C.; Fang, Y.; Wong, S.Y.S.; Ng, C.F. Incidence and mortality of kidney cancer: Temporal patterns and global trends in 39 countries. *Sci. Rep.* **2017**, *7*, 15698. [[CrossRef](#)] [[PubMed](#)]
5. Moch, H.; Cubilla, A.L.; Humphrey, P.A.; Reuter, V.E.; Ulbright, T.M. The 2016 WHO classification of tumours of the urinary system and male genital organs—Part A: Renal, penile and testicular tumours. *Eur. Urol.* **2016**, *70*, 93–105. [[CrossRef](#)]
6. Carlo, M.I.; Hakimi, A.A.; Stewart, G.D.; Bratslavsky, G.; Brugoroles, J.; Chen, Y.B.; Linehan, W.M.; Maher, E.R.; Merino, M.J.; Offit, K.; et al. Familial kidney cancer: Implications of new syndromes and molecular insights. *Eur. Urol.* **2019**, *76*, 754–764. [[CrossRef](#)]
7. Shuch, B.; Vourganti, S.; Ricketts, C.J.; Middletoth, L.; Peterson, J.; Merino, M.J.; Metwalli, A.R.; Svrinivasan, R.; Linehan, W.M. Defining early-onset kidney cancer: Implications for germline and somatic mutation testing and clinical management. *J. Clin. Oncol.* **2013**, *32*, 431–437. [[CrossRef](#)]
8. Carlo, M.I.; Mukherjee, S.; Mandelker, D.; Vijai, J.; Kemel, Y.; Zhang, L.; Krezcec, A.; Patil, S.; Cayan-birsoy, O.; Huang, K.C.; et al. Prevalence of germline mutations in cancer susceptibility genes in patients with advanced renal cell carcinoma. *JAMA Oncol.* **2018**, *4*, 1228–1235. [[CrossRef](#)]
9. Varshney, N.; Kebede, A.A.; Owusu-Dapaah, H.; Lather, J.; Kaushik, M.; Bullar, J.S. A review of Von Hippel-Lindau syndrome. *J. Kidney Cancer VHL* **2017**, *4*, 20–29. [[CrossRef](#)]
10. Gossage, L.; Essen, T.; Maher, E.R. VHL, the story of a tumor suppressor gene. *Nat. Rev. Cancer* **2015**, *15*, 55–64. [[CrossRef](#)]
11. Liu, Q.; Yuan, G.; Tong, D.; Liu, G.; Yi, Y.; Zhang, J.; Zhang, Y.; Wang, L.; Wang, L.; Zhang, D.; et al. Novel genotype-phenotype correlations in five Chinese families with von Hippel-Lindau disease. *Endocr. Connect.* **2018**, *7*, 870–878. [[CrossRef](#)] [[PubMed](#)]
12. Liu, S.J.; Wang, J.Y.; Peng, S.H.; Li, T.; Ning, X.H.; Hong, B.A.; Liu, J.Y.; Wu, P.J.; Zhou, B.W.; Zhou, J.C.; et al. Genotype and phenotype correlation in von Hippel-Lindau disease based on alteration of the HIF- $\alpha$  binding site in VHL protein. *Genet. Med.* **2018**, *20*, 1266–1274. [[CrossRef](#)] [[PubMed](#)]
13. Maher, E.R. Hereditary renal cell carcinoma syndromes: Diagnosis, surveillance and management. *World J. Urol.* **2018**, *36*, 1891–1898. [[CrossRef](#)] [[PubMed](#)]
14. Beroukhi, R.; Brunet, J.P.; Di Napoli, A.; Mertz, K.D.; Seeley, A.; Pires, M.M.; Linhart, D.; Warrell, R.A.; Moch, H.; Rubin, M.A.; et al. Patterns of gene expression and copy-number alterations in von-Hippel Lindau disease-associated and sporadic clear cell carcinoma of the kidney. *Cancer Res.* **2009**, *69*, 4674–4681. [[CrossRef](#)]
15. Fisher, R.; Horsewell, S.; Rowan, A.; Salm, M.P.; De Bruin, E.C.; Gulati, S.; Mc Granahan, N.; Stares, M.; Gerlinger, M.; Varela, I.; et al. Developtment of synchronous VHL syndrome tumors reveals contingencies and constraints ti tumor evolution. *Genome Biol.* **2014**, *15*, 433. [[CrossRef](#)]
16. Fei, S.S.; Mitchell, A.D.; Heskett, M.B.; Vocke, C.D.; Ricketts, C.J.; Peto, M.; Whang, N.J.; Sonmez, K.; Linehan, W.M.; Spellman, P.T. Patient-specific factors influence somatic variation patterns in von Hippel-Lindau disease renal tumors. *Nat. Commun.* **2016**, *7*, 11588. [[CrossRef](#)]
17. Mandriota, S.J.; Turner, K.J.; Davies, D.R.; Murray, P.G.; Morgan, N.V.; Sowter, H.M.; Wykoff, C.C.; Maher, E.R.; Harris, A.L.; Ratcliffe, P.J.; et al. HIG identifies early lesions in VHL kidneys: Evidence for site-specific tumor suppressor function in the nephron. *Cancer Cell* **2002**, *1*, 459–468. [[CrossRef](#)]
18. Mitchell, T.J.; Turajilic, S.; Rowan, A.; Nicol, D.; Farmery, J.; O'Brien, T.; Martincorena, I.; Tarpey, P.; Angelopoulos, N.; Yates, L.R.; et al. Timing and landmark events in the evolution of clear cell cancer: TRACERx renal. *Cell* **2018**, *173*, 611–623. [[CrossRef](#)]
19. Peng, X.; Chen, J.; Wang, J.; Peng, S.; Liu, S.; Ma, K.; Zhou, J.; Hong, B.; Zhou, B.; Zhang, J.; et al. Natural history of tumors in von Hippel-Lindau disease: A large retrospective study of Chinese patients. *J. Med. Genet.* **2019**, *56*, 380–387. [[CrossRef](#)]
20. Dharmawardana, P.G.; Giubellino, A.; Bottaro, D.P. Hereditary papillary renal carcinoma type I. *Curr. Mol. Med.* **2004**, *4*, 855–868. [[CrossRef](#)]

21. Schmidt, L.; Duh, F.M.; Chen, F.; Kishida, T.; Glenn, G.; Choyke, P.; Scherer, S.W.; Zhuang, Z.; Lubensky, I.; Dean, M.; et al. Germline and somatic mutations in the tyrosine kinase domain of the MET proto-oncogene in papillary renal carcinomas. *Nat. Genet.* **1997**, *16*, 68–73. [[CrossRef](#)] [[PubMed](#)]
22. Schmidt, L.; Junker, K.; Nakaigawa, N.; Kinjerski, T.; Wierich, G.; Miller, M.; Lubensky, I.; Neumann, H.P.H.; Brauch, H.; Decker, J.; et al. Novel mutations of the MET proto-oncogene in papillary renal carcinomas. *Oncogene* **1999**, *18*, 2343–2350. [[CrossRef](#)]
23. Lubensky, I.A.; Schmidt, L.; Zhuang, Z.; Meirich, G.; Pack, S.; Zambreno, N.; Walther, M.C.M.; Choyke, P.; Linehan, W.M.; Zbar, B. Hereditary and sporadic papillary renal carcinomas with c-met mutations share a distinct morphological phenotype. *Am. J. Pathol.* **1999**, *155*, 517–526. [[CrossRef](#)]
24. Bentz, M.; Bergerheim, U.S.R.; Li, C.; Joos, S.; Werner, C.A.; Baudis, M.; Gnarra, T.; Merino, M.; Zbar, B.; Linehan, W.M.; et al. Chromosome imbalances in papillary renal cell carcinoma and first cytogenetic data of familial cases analyzed by comparative genomic hybridization. *Cytogenet. Cell Genet.* **1996**, *75*, 17–21. [[CrossRef](#)] [[PubMed](#)]
25. Zhuang, Z.; Park, W.S.; Pack, S.; Schmidt, L.; Vortmeyer, A.O.; Pak, E.; Pham, T.; Weil, R.J.; Candidus, S.; Lubensky, I.A.; et al. Trisomy 7-harboring non-random duplication of the mutant MET allele in hereditary papillary renal carcinomas. *Nat. Genet.* **1998**, *17*, 66–69. [[CrossRef](#)] [[PubMed](#)]
26. Fischer, J.; Palmedo, G.; Von Knobloch, R.; Bugert, P.; Prayer-Galetti, T.; Pagano, F.; Kovacs, G. Duplication and overexpression of the mutant allele of the MET proto-oncogene in multiple hereditary papillary renal cell tumors. *Oncogene* **1998**, *17*, 733–739. [[CrossRef](#)] [[PubMed](#)]
27. Wadt, K.A.; Gerdes, A.M.; Hansen, T.V.; Toft, B.G.; Fziis-Hausen, L.; Andersen, M.K. Novel germline c-MET mutation in a family with hereditary papillary renal carcinoma. *Fam. Cancer* **2012**, *11*, 535–537. [[CrossRef](#)] [[PubMed](#)]
28. Choueiri, T.K.; Vaishimpayan, U.; Rosenberg, J.E.; Logan, T.F.; Harszatarik, A.L.; Bukowski, R.M.; Rini, B.I.; Srinival, S.; Skin, M.N.; Adams, L.M.; et al. Phase II and biomarker study of the dual MET/VEGFR2 inhibitor Foretinib in patients with papillary renal cell carcinoma. *J. Clin. Oncol.* **2013**, *31*, 181–186. [[CrossRef](#)]
29. Lynch, E.D.; Ostermayer, E.A.; Lee, M.K. Inherited mutations in PTEN that are associated with breast cancer, Cowden disease, and juvenile polyposis. *Am. J. Hum. Genet.* **1997**, *61*, 1254. [[CrossRef](#)]
30. Mester, J.L.; Zhou, M.; Prescott, N. Papillary renal cell carcinoma is associated with PTEN hamartoma tumor syndrome. *Urology* **2012**, *79*, 1187. [[CrossRef](#)]
31. Shugh, B.; Ricketts, C.J.; Vocke, C.D.; Komiya, T.; Middleton, L.A.; Kauffman, E.C.; Merino, M.J.; Metwalli, A.R.; Dennis, P.; Linehan, W.M. Germline PTEN mutation Cowden syndrome: An under-appreciated form of hereditary kidney cancer. *J. Urol.* **2013**, *190*, 1990–1998. [[CrossRef](#)]
32. Cavallé, M.; Ponelle-Chachuat, F.; Urhammer, N.; Viala, S.; Gay-Balille, M.; Privat, M.; Bidet, Y.; Bignon, J.Y. Early onset multiple primary tumors in atypical presentation of Cowden syndrome identified by whole-exome-sequencing. *Front. Genet.* **2018**, *9*, 353. [[CrossRef](#)]
33. Walpole, S.; Pritchard, A.L.; Cebulla, C.M.; Pilorski, R.; Stautberg, M.; Davidorf, F.H.; De la Fouchardiere, A.; Cabaret, O.; Golamrd, L.; Stoppa-Lyonnet, D.; et al. Comprehensive study of the clinical phenotype of germline BAP1 variant-carrying families worldwide. *J. Natl. Cancer Inst.* **2018**, *110*, 1328–1341. [[CrossRef](#)]
34. Testa, J.R.; Cheung, M.; Pei, J.; Below, J.E.; Tan, Y.; Sementino, E.; Cox, N.J.; Dogan, A.U.; Pass, H.L.; Testa, J.R.; et al. Germline BAP1 mutations predispose to malignant mesotheliomas. *Nat. Genet.* **2011**, *43*, 1022–1025. [[CrossRef](#)] [[PubMed](#)]
35. Wiesner, T.; Obenaus, A.C.; Murali, R.; Fried, I.; Griewank, K.G.; Ulz, P.; Windpassinger, C.; Wackernagel, W.; Loy, S.; Wolf, I.; et al. Germline mutations in BAP1 predispose to melanocytic tumors. *Nat. Genet.* **2011**, *43*, 1018–1021. [[CrossRef](#)] [[PubMed](#)]
36. Popova, T.; Hebert, L.; Jaquemin, V.; Gad, S.; Caux-Moncoutier, V.; Dubois-d’Enghien, C.; Richadeau, B.; Renaudin, X.; Sellers, J.; Nicolas, A.; et al. Germline BAP1 mutations predispose to renal cell carcinomas. *Am. J. Hum. Genet.* **2013**, *92*, 974–980. [[CrossRef](#)]
37. Farley, M.N.; Schmidt, L.S.; Mester, J.L.; Pena-Llopis, S.; Pavia-Jimenez, A.; Christie, A.; Vocke, C.D.; Ricketts, C.J.; Peterson, J.; Middleton, L. A novel germline mutation in Bap1 predisposes to familial clear-cell renal cell carcinoma. *Mol. Cancer Res.* **2013**, *11*, 1061–1071. [[CrossRef](#)] [[PubMed](#)]
38. Ball, M.W.; An, J.Y.; Gomella, P.T.; Gautam, R.; Ricketts, C.J.; Vocke, C.D.; Schmidt, L.S.; Merino, M.J.; Srinivisan, R.; Malayeri, A.A.; et al. Growth rates of genetically defined renal tumors: Implications for active surveillance and intervention. *J. Clin. Oncol.* **2020**, *38*, 1146–1153. [[CrossRef](#)] [[PubMed](#)]

39. AL-Rasheed, M.R.H.; Tarjan, G. Succinate dehydrogenase complex: An updated review. *Arch. Pathol. Lab. Med.* **2018**, *142*, 1564–1570. [[CrossRef](#)] [[PubMed](#)]
40. Chan, M.; Barnocoat, A.; Mumtaz, F.; Aitchinson, M.; Side, L.; Brittain, H.; Bates, A.; Gale, D.P. Cascade fumarate hydratase mutation screening allows early detection of kidney tumour: A case report. *BMC Med. Genet.* **2017**, *18*, 79. [[CrossRef](#)]
41. Gill, A.J.; Pachter, N.S.; Chou, A.; Young, B.; Clarkson, A.S.; Tucker, K.M.; Winship, I.M.; Early, P.; Benn, D.E.; Robinson, B.G.; et al. Renal tumors associated with with germline SDHB mutation show distinctive morphology. *Am. J. Surg. Pathol.* **2011**, *35*, 1578–1585. [[CrossRef](#)] [[PubMed](#)]
42. Gill, A.J.; Hes, O.; Papathomas, T.; Sedivcova, M.; Tan, P.H.; Agaimy, A.; Andresen, P.A.; Kedziora, A.; Clarkson, A.; Toon, C.W.; et al. Succinate dehydrogenase (SDH)-deficient renal carcinoma: A morphologically distinct entity. A clinicopathologic series of 36 tumors from 27 patients. *Am. J. Surg. Pathol.* **2014**, *38*, 1588–1602. [[CrossRef](#)] [[PubMed](#)]
43. Williamson, S.R.; Eble, J.N.; Amin, M.B.; Gupta, N.S.; Smith, S.G.; Sholl, L.M.; Montironi, R.; Hirsch, M.S.; Hornick, J.L. Succinate dehydrogenase-deficient renal cell carcinoma: Detailed characterization of 11 tumors defining a unique subtype of renal cell carcinoma. *Mod. Pathol.* **2015**, *28*, 80–94. [[CrossRef](#)] [[PubMed](#)]
44. Caliò, A.; Grignon, D.J.; Stohr, B.A.; Williamson, S.R.; Eble, J.N.; Cheng, L. Renal cell carcinoma with TFE3 translocation and succinate dehydrogenase B mutation. *Mod. Pathol.* **2017**, *30*, 407–415. [[CrossRef](#)] [[PubMed](#)]
45. Gupta, S.; Swanson, A.A.; Chen, Y.B.; Lopez, T.; Milosevic, D.; Kipp, B.R.; Leibovich, B.C.; Thompson, R.H.; Herrera-Hernandez, L.; Cheville, J.C.; et al. Incidence of succinate dehydrogenase and fumarate hydratase-deficient renal cell carcinoma based on immunohistochemical screening with SDHA/SDHB and FH/2SC. *Hum. Pathol.* **2019**, *91*, 114–122. [[CrossRef](#)]
46. Ajhamir, S.M.K.; Haeshmat, R.; Ebrahimi, M.; Katabchi, S.E.; Dizaji, S.P.; Khatami, F. The impact of succinate dehydrogenase gene (SDH) mutations in renal cell carcinoma (RCC): A systematic review. *OncoTarg. Ther.* **2019**, *12*, 7929–7940. [[CrossRef](#)]
47. Hakirevich, E.; Ali, S.M.; Mega, A.; McMahon, C.; Brodsky, A.S.; Ross, J.S.; Allen, J.; Elvin, J.A.; Resnick, M.B. A novel SDHA-deficient renal cell carcinoma revealed by comprehensive genomic profiling. *Am. J. Surg. Pathol.* **2015**, *39*, 858–863. [[CrossRef](#)]
48. Saxena, N.; Maio, N.; Crooks, D.R.; Ricketts, C.J.; Yang, Y.; Wei, M.H.; Fan, T.; Lane, A.N.; Soubier, C.; Singh, A.; et al. SDHB-deficient cancers: The role of mutations that impair iron sulfur cluster delivery. *J. Natl. Cancer Inst.* **2016**, *108*, djv287. [[CrossRef](#)]
49. Maio, N.; Singh, A.; Uhrigshardt, H.; Saxena, N.; Tong, W.H.; Rouault, T.A. Chaperone binding to LYR motifs confers specificity of iron sulfur cluster delivery. *Cell Metab.* **2014**, *19*, 445–457. [[CrossRef](#)]
50. Cardaci, S.; Zheng, L.; MacKay, G.; Van den Broek, N.; MacKenzie, E.D.; Nixon, C.; Stevenson, D.; Tumanov, S.; Bulusu, V.; Kamphorst, J.J.; et al. Pyruvate carboxylation enables growth of SDH-deficient cells by supporting aspartate biosynthesis. *Nat. Cell Biol.* **2015**, *17*, 1317–1326. [[CrossRef](#)]
51. Lussey-Lepoutre, C.; Bellucci, A.; Morin, A.; Buffet, A.; Amar, L.; Janin, M.; Ottolenghi, C.; Zinzindohoué, F.; Autret, G.; Burnichon, N.; et al. In vivo detection of succinate by magnetic resonance spectroscopy as a hallmark of SDHx mutations in paraganglioma. *Clin. Cancer Res.* **2016**, *22*, 1120–1129. [[CrossRef](#)] [[PubMed](#)]
52. Casey, R.T.; McLean, M.A.; Madhu, B.; Challis, R.G.; Ten Hoopen, R.; Roberts, T.; Clark, G.R.; Pittfield, D.; Simpson, H.L.; Bulusu, V.R.; et al. Translating in vivo metabolomic analysis of succinate dehydrogenase deficient tumors into clinical utility. *JCO Precis. Oncol.* **2018**, *2*, 1–12. [[CrossRef](#)]
53. Yang, M.; Soga, T.; Pollard, P.J. Oncometabolites: Linking altered metabolism with cancer. *J. Clin. Investig.* **2013**, *123*, 3652–3658. [[CrossRef](#)] [[PubMed](#)]
54. Yong, C.; Stewart, G.D.; Frezza, C. Oncometabolites in renal cancer. *Nat. Rev. Nephrol.* **2019**, in press. [[CrossRef](#)]
55. Martinez-Reyes, I.; Chandel, N.S. Mitochondrial TCA cycle metabolites control physiology and disease. *Nat. Commun.* **2020**, *11*, 102. [[CrossRef](#)] [[PubMed](#)]
56. Selak, M.A.; Amour, B.M.; MacKenzie, E.D.; Boulahbel, H.; Watson, D.G.; Mansfield, K.D.; Pan, Y.; Simon, M.C.; Thompson, C.B.; Gottlieb, E. Succinate links TCA cycle dysfunction to oncogenesis by inhibiting HIF- $\alpha$  prolyl hydroxylase. *Cancer Cell* **2005**, *7*, 77–85. [[CrossRef](#)] [[PubMed](#)]
57. Pollard, P.J.; Briere, J.J.; Alam, N.A.; Barwell, J.; Barclay, E.; Wortham, N.C.; Hunt, T.; Mitchell, M.; Olpin, S.; Moat, S.J.; et al. Accumulation of Krebs cycle intermediates and over-expression of HIF1 $\alpha$  in tumours which result from germline FH and SDH mutations. *Hum. Mol. Genet.* **2005**, *14*, 2231–2239. [[CrossRef](#)]

58. Pollard, P.; Wotham, N.; Barclay, E.; Alam, A.; Elia, G.; Manek, S.; Poulson, R.; Tomlinson, I. Evidence of increased microvessel density and activation of the hypoxia pathway in tumours from the hereditary leiomyomatosis and renal cell cancer syndrome. *J. Pathol.* **2005**, *205*, 41–49. [[CrossRef](#)] [[PubMed](#)]
59. Letouzé, E.; Martinelli, C.; Lorient, C.; Burnichon, N.; Abemili, N.; Ottolenghi, C.; Janin, M.; Menara, M.; Nguyen, A.T.; Benit, P.; et al. SDH mutations establish a hypermethylator phenotype in paraganglioma. *Cancer Cell* **2013**, *23*, 739–752. [[CrossRef](#)] [[PubMed](#)]
60. Sulkowski, P.L.; Sundaram, R.K.; Oeck, S.; Corso, C.D.; Liu, Y.; Noorbakhsh, S.; Niger, M.; Boeke, M.; Ueno, D.; Kalathil, A.N.; et al. Krebs-cycle-deficient hereditary cancer syndromes are defined by defects in homologous-recombination DNA repair. *Nat. Genet.* **2018**, *50*, 1086–1092. [[CrossRef](#)]
61. Tomlinson, I.P.; Alam, N.A.; Rowan, A.J.; Barclay, E.; Jaeger, E.E.; Kelsell, D.; Laigh, I.; Groman, P.; Lamlum, H.; Rahman, S.; et al. Germline mutations in FH predispose to dominantly inherited uterine fibroids, skin leiomyomata and papillary renal cancer. *Nat. Genet.* **2002**, *30*, 406–410. [[PubMed](#)]
62. Pan, X.; Zhang, M.; Yao, J.; Zeng, H.; Nie, L.; Gong, J.; Chen, X.; Xu, M.; Zhou, Q.; Chen, N. Fumarate hydratase-deficient renal cell carcinoma: A clinicopathological and molecular study of 13 cases. *J. Clin. Pathol.* **2019**, *72*, 748–754. [[CrossRef](#)] [[PubMed](#)]
63. Cancer Genome Atlas Research Network; Linehan, W.M.; Spellman, P.T.; Ricketts, C.J.; Creighton, C.J.; Fei, S.S.; Davis, C.; Wheeler, D.A.; Murray, B.A.; Schmidt, L.; et al. Comprehensive molecular characterization of papillary renal-cell carcinoma. *N. Engl. J. Med.* **2016**, *374*, 135–145.
64. Chen, Y.B.; Xu, J.; Skanderup, J.; Dong, Y.; Brannon, A.R.; Wang, L.; Wan, H.H.; Wang, P.J.; Nanjangud, G.J.; Jungbluth, A.A.; et al. Molecular analysis of aggressive renal cell carcinoma with unclassified histology reveals distinct subsets. *Nat. Commun.* **2016**, *7*, 13131. [[CrossRef](#)]
65. Wei, M.H.; Toure, O.; Glenn, G.M.; Pithukpakorn, M.; Neckers, L.; Stolle, C.; Choyke, P.; Grubb, R.; Middleton, L.; Turner, M.L.; et al. Novel mutations in FH and expansion of the spectrum of phenotypes expressed in families with hereditary leiomyomatosis and renal cell cancer. *J. Med. Genet.* **2006**, *43*, 18–27. [[CrossRef](#)]
66. Muller, M.; Ferlicot, S.; Guillaud-Bataille, M.; Le Teuff, G.; Genestie, C.; Deveaux, S.; Slama, A.; Poulahon, N.; Escudier, B.; Albiges, L.; et al. Reassessing the clinical spectrum associated with hereditary leiomyomatosis and renal cell carcinoma syndrome in French FH mutation carriers. *Clin. Genet.* **2017**, *92*, 606–615. [[CrossRef](#)]
67. Vocke, C.D.; Ricketts, C.J.; Merino, M.J.; Srinivasan, R.; Metwalli, A.R.; Middleton, L.A.; Peterson, J.; Yang, Y.; Linehan, W.M. Comprehensive genomic and phenotypic characterization of germline FH deletion in hereditary leiomyomatosis and renal cell carcinoma. *Genes Chromosom. Cancer* **2017**, *56*, 484–492. [[CrossRef](#)]
68. Lau, H.D.; Chan, E.; Fan, A.C.; Kunder, C.A.; Williamson, C.R.; Zhou, M.; Idrees, M.T.; MacLean, F.M.; Gill, A.J.; Cao, C.S. A clinicopathologic and molecular analysis of fumarate hydratase-deficient renal cell carcinoma in 32 patients. *Am. J. Surg. Pathol.* **2020**, *44*, 98–110. [[CrossRef](#)]
69. Forde, C.; Lim, D.; Alwan, Y.; Burghel, G.; Butland, L.; Cleaver, R.; Dixit, A.; Evans, D.G.; Hnason, H.; Lalloo, F.; et al. Hereditary leiomyomatosis and renal cell cancer: Clinical, molecular, and screening features in a cohort of 185 affected individuals. *Eur. Urol. Oncol.* **2020**, in press. [[CrossRef](#)]
70. Furuya, M.; Iribe, Y.; Nagashima, Y.; Kambe, N.; Ohe, C.; Kinoshita, H.; Sato, C.; Kishida, T.; Okubo, Y.; Nakamura, K.; et al. Clinicopathologic and molecular features of hereditary leiomyomatosis and renal cell cancer-associated renal cell carcinomas. *J. Clin. Pathol.* **2020**, in press. [[CrossRef](#)]
71. Hol, J.A.; Jongmans, M.C.J.; Littooij, A.S.; De Krjger, R.R.; Kuiper, R.P.; Van Harsseel, J.J.T.; Mensenkamp, A.; Simons, M.; Tytgat, G.A.M.; Van Den Heuvel-Eibrink, M.M.; et al. Renal cell carcinoma in young FH mutation carriers: Case series and review of the literature. *Fam. Cancer* **2020**, *19*, 55–63. [[CrossRef](#)] [[PubMed](#)]
72. Yang, Y.; Valera, V.A.; Padilla-Nash, H.M.; Sourbier, C.; Vocke, C.D.; Vira, M.A.; Abu-Asab, M.S.; Bratslavsky, G.; Tsokos, M.; Merino, M.J.; et al. UOK 262 cell line, fumarate hydratase deficient (FH-/FH.) hereditary leiomyomatosis renal cell carcinoma: In vitro and in vivo model of an aberrant energy metabolic pathway in human cancer. *Cancer Genet. Cytogenet.* **2010**, *196*, 45–55. [[CrossRef](#)] [[PubMed](#)]
73. Mullen, A.R.; Wheaton, W.W.; Jin, E.S.; Chen, P.H.; Sullivan, L.B.; Cheng, T.; Yang, Y.; Linehan, W.M.; Chandel, N.S.; DeBernardinis, R.J.; et al. Reductive carboxylation supports growth in tumor cells with defective mitochondria. *Nature* **2011**, *481*, 385–388. [[CrossRef](#)] [[PubMed](#)]
74. Yang, Y.; Valera, V.; Sourbier, C.; Vocke, C.D.; Wei, M.; Pike, L.; Huang, Y.; Merino, M.A.; Bratslavsky, G.; Wu, M.; et al. A novel fumarate hydratase-deficient HLRCC kidney cancer cell line, UOK268: A model of the Warburg effect in cancer. *Cancer Genet.* **2012**, *205*, 377–390. [[CrossRef](#)]

75. Yang, Y.; Lane, A.N.; Ricketts, C.J.; Sourbier, C.; Wei, M.H.; Shuch, B.; Pike, L.; Wu, M.; Rouault, T.A.; Boros, L.G.; et al. Metabolic reprogramming for producing energy and reducing power in fumarate hydratase null cells from hereditary leiomyomatosis renal cell carcinoma. *PLoS ONE* **2013**, *8*, e72179. [[CrossRef](#)]
76. Tong, W.H.; Sourbier, C.; Kovtunovych, G.; Geong, S.Y.; Vira, M.; Ghosh, M.; Romero, V.V.; Sougrat, R.; Vaultont, S.; Viollet, B.; et al. The glycolytic shift in fumarate-hydratase-deficient kidney cancer lowers AMPK levels, increases anabolic propensities and lowers cellular iron levels. *Cancer Cell* **2011**, *20*, 315–327. [[CrossRef](#)]
77. Sciacovelli, M.; Gonçalves, E.; Johnson, T.I.; Zecchini, V.R.; Henriques da Costa, A.S.; Gaude, E.; Drubbel, A.V.; Theobald, S.J.; Abbo, S.; Tran, M.; et al. Fumarate is an epigenetic modifier that elicits epithelial-to-mesenchymal transition. *Nature* **2016**, *537*, 544–547. [[CrossRef](#)]
78. Mackenzie, E.D.; Selak, M.A.; Tennant, D.A.; Payne, L.J.; Crosby, S.; Frederiksen, C.M.; Watson, D.G.; Gottlieb, E. Cell-permeating alpha-ketoglutarate derivatives alleviate pseudohypoxia in succinate-dehydrogenase-deficient cells. *Mol. Cell Biol.* **2007**, *27*, 3282–3289. [[CrossRef](#)]
79. Alderson, N.L.; Wang, Y.; Blatnik, M.; Frizzell, N.; Walla, M.D.; Lyons, T.J.; Alt, N.; Carson, J.A.; Nagai, R.; Thorpe, S.R.; et al. S-(2-succinyl) cysteine: A novel chemical modification of tissue proteins by a Krebs cycle intermediate. *Arch. Biochem. Biophys.* **2006**, *450*, 1–8. [[CrossRef](#)] [[PubMed](#)]
80. Bardella, C.; El-Bahrawy, M.; Frizzell, N.; Adam, J.; Ternette, N.; Hatipoglu, E.; Howarth, K.; O’Flaherty, L.; Roberts, I.; Turner, G.; et al. Aberrant succination of proteins in fumarate hydratase-deficient mice and HLRCC patients is a robust biomarker of mutation status. *J. Pathol.* **2011**, *225*, 4–11. [[CrossRef](#)]
81. Tyrakis, P.A.; Yurkovich, M.E.; Sciacovelli, M.; Papachristou, E.K.; Bridges, H.R.; Gaude, E.; Schreiner, A.; D’Santos, C.; Hirst, J.; Hernandez-Fernaund, J.; et al. Fumarate hydratase loss causes combined respiratory chain defects. *Cell Rep.* **2017**, *21*, 1036–1047. [[CrossRef](#)]
82. Ooi, A.; Wong, J.C.; Petillo, D.; Roossien, D.; Perrier-Trudova, V.; Whitten, D.; Wong Hui Min, B.; Tan, M.H.; Zhang, Z.; Yang, X.J.; et al. An antioxidant response phenotype shared between hereditary and sporadic type 2 papillary renal cell carcinoma. *Cancer Cell* **2011**, *20*, 511–523. [[CrossRef](#)] [[PubMed](#)]
83. Adam, J.; Hapitoglu, E.; O’Fallherty, L.; Ternette, N.; Sahgal, N.; Lockstone, H.; Baban, D.; Nye, E.; Stamp, G.W.; Wolhuter, K.; et al. Renal cyst formation in Fh1-deficient mice is independent of the Hif/Phd pathway: Roles for fumarate in KEAP1 succination and Nrf2 signaling. *Cancer Cell* **2011**, *20*, 524–537. [[CrossRef](#)]
84. Ooi, A.; Dykema, K.; Ansari, A.; Petillo, D.; Snider, J.; Kahnoski, R.; Anema, J.; Craig, D.; Carpten, J.; Teh, B.T.; et al. CUL3 and NRF2 mutations confer an NRF2 activation phenotype in a sporadic form of papillary renal cell carcinoma. *Cancer Res.* **2013**, *73*, 2044–2051. [[CrossRef](#)]
85. Sullivan, L.B.; Martinez-Garcia, E.; Nguyen, H.; Mullen, A.R.; Dufour, E.; Sudarshan, S. The protonometabolite fumarate binds glutathione to amplify ROS-dependent signaling. *Mol. Cell* **2013**, *51*, 236–248. [[CrossRef](#)] [[PubMed](#)]
86. Zheng, L.; Cardaci, S.; Jerby, L.; MacKenzie, E.D.; Sciacovelli, M.; Johnson, T.I. Fumarate induces redox-dependent senescence by modifying glutathione metabolism. *Nat. Commun.* **2015**, *6*, 6001. [[CrossRef](#)]
87. Kulkarni, R.A.; Bak, D.W.; Wei, D.; Bergholtz, S.E.; Briney, C.A.; Shrimps, J.H.; Alpsy, A.; Thorpe, A.L.; Bavari, A.E.; Crooks, D.R.; et al. A chemoproteomic portrait of the oncometabolite fumarate. *Nat. Chem. Biol.* **2019**, *15*, 391–400. [[CrossRef](#)] [[PubMed](#)]
88. Sourbier, C.; Ricketts, C.J.; Liao, P.J.; Matsumoto, S.; Wei, D.; Lang, M.; Railkar, R.; Yang, Y.; Wei, M.H.; Agarwal, P.; et al. Proteasome inhibition disrupts the metabolism of fumarate hydratase-deficient tumors by downregulating p62 and c-Myc. *Sci. Rep.* **2019**, *9*, 18409. [[CrossRef](#)] [[PubMed](#)]
89. Zbar, B.; Alvord, W.G.; Glenn, G.; Turner, M.; Pavlovich, C.P.; Schmidt, L.; Walther, M.C.; Choyke, P.; Weirich, G.; Hewitt, S.M.; et al. Risk of renal and colonic neoplasms and spontaneous pneumothorax in the Birt-Hogg-Dubé syndrome. *Cancer Epidemiol. Biomark. Prev.* **2002**, *11*, 393–400.
90. Pavlovich, C.P.; Walther, M.C.; Eyer, R.A.; Hewitt, S.M.; Zbar, B.; Linehan, M.; Merino, M.J. Renal tumors in the Birt-Hogg-Dubé syndrome. *Am. J. Surg. Pathol.* **2002**, *26*, 1542–1552. [[CrossRef](#)]
91. Schmidt, L.S.; Linehan, W.M. Molecular genetics and clinical features of Birt-Hogg-Dubé-syndrome. *Nat. Rev. Urol.* **2015**, *12*, 558–569. [[CrossRef](#)] [[PubMed](#)]
92. Adami, A.; Lowrance, W.T.; Yee, D.S.; Chong, K.T.; Bernstein, M.; Tickoo, S.K.; Coleman, J.A.; Russo, P. Renal oncocytosis: Management and clinical outcomes. *J. Urol.* **2011**, *185*, 795–801. [[CrossRef](#)] [[PubMed](#)]
93. Furuya, M.; Hasumi, H.; Yao, M.; Nagashima, Y. Birt-Hogg-Dubé syndrome-associated renal cell carcinoma: Histopathological features and diagnostic conundrum. *Cancer Sci.* **2019**, *111*, 15–22. [[CrossRef](#)] [[PubMed](#)]



94. Schmidt, L.S.; Warren, M.B.; Nickerson, M.L.; Weirich, G.; Matrasova, V.; Toro, J.R.; Turner, M.L.; Duray, P.; Merino, M.; Hewitt, S.; et al. Birt-Hogg-Dubé syndrome, a genodermatosis associated with spontaneous pneumothorax and kidney neoplasia, maps to chromosome 17p11.2. *Am. J. Hum. Genet.* **2001**, *69*, 876–882. [[CrossRef](#)] [[PubMed](#)]
95. Nickerson, M.L.; Warren, B.; Toro, J.R.; Matrosova, V.; Glenn, G.; Turner, M.L.; Duray, P.; Merino, M.; Choyke, P.; Pavlovich, C.P.; et al. Mutations in a novel gene lead to kidney tumors, lung wall defects, and benign tumors of the hair follicle in patients with the Birt-Hogg-Dubé syndrome. *Cancer Cell* **2002**, *2*, 157–164. [[CrossRef](#)]
96. Schmidt, L.S.; Linehan, W.M. FLCN: The causative gene for Birt-Hogg-Dubé syndrome. *Gene* **2018**, *640*, 28–42. [[CrossRef](#)]
97. Vocke, C.D.; Yang, Y.; Pavlovich, C.P.; Schmidt, L.S.; Nickerson, M.L.; Torres-Cabala, C.A.; Merino, M.J.; Walther, M.M.; Zbar, B.; Linehan, W.M.; et al. High frequency of somatic frameshift BHD gene mutations in Birt-Hogg-Dubé-associated renal tumors. *J. Natl. Cancer Inst.* **2005**, *97*, 931–935. [[CrossRef](#)]
98. Hasumi, H.; Hasumi, Y.; Baba, M.; Nishi, H.; Furuya, M.; Vocke, C.D.; Lang, M.; Irie, N.; Esumi, C.; Merino, M.J.; et al. H255Y and K580R missense mutations in tumour suppressor folliculin (FLCN) promote kidney cell proliferation. *Hum. Mol. Genet.* **2017**, *26*, 354–366.
99. Kato, I.; Iribe, Y.; Nagashima, Y.; Kuroda, N.; Tanaka, R.; Nakatani, Y.; Hasumi, H.; Yao, M.; Furuya, M. Fluorescent and chromogenic in situ hybridization of CEN17q as a potent useful diagnostic marker for Birt-Hogg-Dubé syndrome-associated chromophobe renal cell carcinomas. *Hum. Pathol.* **2016**, *52*, 74–82. [[CrossRef](#)]
100. Hasumi, H.; Furuya, M.; Tatsuno, K.; Yamamoto, S.; Baba, M.; Hasumi, Y.; Isono, Y.; Suzuki, K.; Jikuya, R.; Otake, S.; et al. BHD-associated kidney cancer exhibits unique molecular characteristics and a wide variety of variants in chromatin remodeling genes. *Hum. Mol. Genet.* **2018**, *27*, 2712–2724. [[CrossRef](#)]
101. Ruiz-Cordero, R.; Rao, P.; Li, L.; Qi, Y.; Atherton, D.; Peng, B.; Singh, R.R.; Kim, T.B.; Kawakami, F.; Routbort, M.J.; et al. Hybrid oncocytic/chromophobe renal tumors are molecularly distinct from oncocytoma and chromophobe renal cell carcinoma. *Mod. Pathol.* **2019**, *32*, 1698–1707. [[CrossRef](#)] [[PubMed](#)]
102. Baba, M.; Hong, S.B.; Sharma, N.; Warren, M.B.; Nickerson, M.L.; Iawamatsu, A. Folliculin encoded by the BHD gene interacts with a binding protein, FNIP1, and AMPK, and is involved in AMPK and mTOR signaling. *Proc. Natl. Acad. Sci. USA* **2006**, *103*, 15552–15557. [[CrossRef](#)] [[PubMed](#)]
103. Hasumi, H.; Baba, M.; Hong, S.B.; Hasumi, Y.; Huang, Y.; Yao, M. Identification and characterization of a novel folliculin-interacting protein FNIP2. *Gene* **2008**, *415*, 60–67. [[CrossRef](#)] [[PubMed](#)]
104. Takagi, Y.; Kobayashi, T.; Shiono, M.; Wang, L.; Piao, X.; Sun, G. Interaction of folliculin (Birt-Hogge-Dubé gene product) with a novel Fnip1-like (PnipL/Fnip2) protein. *Oncogene* **2008**, *27*, 5339–5347. [[CrossRef](#)] [[PubMed](#)]
105. Lawrence, R.E.; Fromm, S.A.; Fu, Y.; Yokom, A.L.; Kim, D.J.; Thelen, A.M. Structural mechanism of a rag GTPase activation checkpoint by the lysosomal folliculin complex. *Science* **2019**, *366*, 971–977. [[CrossRef](#)] [[PubMed](#)]
106. Shen, K.; Rogala, K.R.; Chou, H.T.; Huang, R.K.; Yu, Z.; Sabatini, D.M. Cryo-EM structure of the human FLCN-FNIP2-Rag-regulator complex. *Cell* **2019**, *179*, 1319–1329. [[CrossRef](#)]
107. Hasumi, H.; Baba, M.; Hasumi, Y.; Lang, M.; Huang, Y.; Oh, H.F.; Matsuo, M.; Merino, M.J.; Yao, M.; Ito, Y.; et al. Folliculin-interacting proteins Fnip1 and Pnip2 play critical roles in kidney tumor suppression in cooperation with Flcn. *Proc. Natl. Acad. Sci. USA* **2015**, *112*, E1624–E1631. [[CrossRef](#)]
108. Rabanal-Ruiz, Y.; Korolchuk, V.I. mTORC1 and nutrient homeostasis: The central role of the lysosome. *Int. J. Mol. Sci.* **2018**, *19*, 818. [[CrossRef](#)]
109. Baba, M.; Furihata, M.; Hong, S.B.; Tessarollo, L.; Haines, D.C.; Southon, E. Kidney-targeted Birt-Hogg-Dubé gene inactivation in a mouse model: Erk1/2 and Akt-mTOR activation, cell hyperproliferation, and polycystic kidneys. *J. Natl. Cancer Inst.* **2008**, *100*, 40–54. [[CrossRef](#)]
110. Chen, J.; Futami, K.; Petillo, D.; Peng, J.; Wang, P.; Knol, J. Deficiency of FLCN in mouse kidney led to development of polycystic kidneys and renal neoplasia. *PLoS ONE* **2008**, *3*, e3581. [[CrossRef](#)]
111. Chen, J.; Huang, D.; Rubera, I.; Futami, K.; Wang, P.; Zickert, P. Disruption of tubular Flcn expression as a mouse model for renal tumor induction. *Kidney Int.* **2015**, *88*, 1057–1069. [[CrossRef](#)] [[PubMed](#)]

112. Hasumi, Y.; Baba, M.; Ajima, R.; Hasumi, H.; Valera, V.A.; Klein, M.E.; Haines, D.C.; Merino, M.J.; Hong, S.B.; Yamaguchi, T.P.; et al. Homozygous loss of BHD causes early embryonic lethality and kidney tumor development with activation of mTORC1 and mTORC2. *Proc. Natl. Acad. Sci. USA* **2009**, *106*, 18722–18727. [[CrossRef](#)] [[PubMed](#)]
113. Hartman, T.R.; Klein-Szanto, A.; Al-Saleem, T.; Cash, T.P.; Simon, M.C.; Henske, E.P. The role of the Birt-Hogg-Dubé protein in mTOR activation and renal tumorigenesis. *Oncogene* **2009**, *28*, 1594–1604. [[CrossRef](#)]
114. Hudon, V.; Sabourin, S.; Dydensborg, A.B.; Kottuis, V.; Ghazi, A.; Paquet, M.; Crosby, K.; Pomerleau, V.; Ueatani, N.; Pause, A. Renal tumour suppressor function of the Birt-Hogg-Dubé syndrome gene product folliculin. *J. Med. Genet.* **2010**, *47*, 182–189. [[CrossRef](#)] [[PubMed](#)]
115. Wu, M.; Si, S.; Li, Y.; Schoen, S.; Xiao, G.Q.; Li, X.; Teh, B.T.; Wu, G.; Chen, J. Plcn-deficient renal cells are tumorigenic and sensitive to mTOR suppression. *Oncotarget* **2015**, *6*, 32761–32773. [[CrossRef](#)]
116. De Martin Garrido, N.; Aylett, C. Nutrient signaling and lysosome positioning crosstalk through a multifunctional protein folliculin. *Front. Cell Dev. Biol.* **2020**, *8*, 108. [[CrossRef](#)]
117. Shen, K.; Huang, R.K.; Brignole, E.J.; Kondon, K.J.; Valenstein, M.L.; Chantranupong, L. Architecture of the human GATOR1 and GATOR1-Rag GTPases complexes. *Nature* **2018**, *556*, 64–69. [[CrossRef](#)]
118. Meng, J.; Ferguson, S.M. GATOR1-dependent recruitment of FLCN-FNIP to lysosomes coordinates rag GTPase heterodimer nucleotide status in response to amino acids. *J. Cell. Biol.* **2017**, *217*, 2765–2776. [[CrossRef](#)]
119. Possik, E.; Jalali, S.; Nouet, Y.; Yan, M.; Gingras, M.C.; Schmeisser, K. Folliculin regulates AMPK-dependent autophagy and metabolic stress survival. *PLoS Genet.* **2014**, *10*, e1004273. [[CrossRef](#)]
120. Yan, M.; Gingras, M.C.; Dunlop, E.A.; Nouet, Y.; Dupuy, F.; Jalali, J.A. The tumor suppressor folliculin regulates AMPK metabolic transformation. *J. Clin. Investig.* **2014**, *124*, 2640–2650. [[CrossRef](#)]
121. El-Houjeiri, L.; Possik, E.; Vijayaraghavan, T.; Paquette, M.; Martina, J.A.; Kazan, J.M. The transcription factors TFEB and TFE3 link the FLCN-AMPK signaling axis to innate immune response and pathogen resistance. *Cell Rep.* **2019**, *26*, 3613–3628. [[CrossRef](#)] [[PubMed](#)]
122. Siggs, O.M.; Stockenhuber, A.; Deobagkar-Lele, M.; Bull, K.R.; Crockford, T.L.; Kingston, B.L.; Crawford, G.; Anzilotti, C.; Steeples, V.; Ghaffari, S.; et al. Mutation of FNIP1 is associated with B-cell deficiency, cardiomyopathy, and elevated AMPK activity. *Proc. Natl. Acad. Sci. USA* **2016**, *113*, E3706–E3715. [[CrossRef](#)]
123. Hasumi, H.; Baba, M.; Hasumi, Y.; Huang, Y.; Oh, H.; Hughes, R.M.; Klein, M.E.; Takikita, S.; Nagashima, K.; Schmidt, L.S.; et al. Regulation of mitochondrial oxidative metabolism by tumor suppressor FLCN. *J. Natl. Cancer Inst.* **2012**, *104*, 1750–1764. [[CrossRef](#)] [[PubMed](#)]
124. Klomp, J.A.; Petillo, D.; Niemi, N.M.; Dykema, K.J.; Chen, J.; Yang, X.J.; Saaf, A.; Zickert, P.; Aly, M.; Bewrgerheim, U.; et al. Birt-Hogg-Dubé renal tumors are genetically distinct from other renal neoplasias and are associated with up-regulation of mitochondrial gene expression. *BMC Med. Genom.* **2010**, *3*, 59. [[CrossRef](#)] [[PubMed](#)]
125. Yan, M.; Sudet-Walsh, E.; Manteghi, S.; Dufour, C.R.; Walker, B.; Baba, M.; St.Pierre, J.; Giguère, V.; Pause, A. Chronic AMPK activation via loss of FLCN induces functional beige adipose through PGC-1 $\alpha$ /ERR $\alpha$ . *Genes Dev.* **2016**, *30*, 1034–1046. [[CrossRef](#)] [[PubMed](#)]
126. Bertolotto, C.; Lesuer, F.; Giuliano, S.; Strub, T.; De Lichy, M.; Bille, K.; Dessen, P.; D’Haver, B.; Mohamdi, H.; Remenieras, A.; et al. A SUMOylation-defective MITF germline mutation predisposes to melanoma and renal carcinoma. *Nature* **2011**, *480*, 94–98. [[CrossRef](#)]
127. Stoehr, C.G.; Walter, B.; Denzinger, S.; Ghiorzo, P.; Sturm, R.A.; Hinze, R.; Moch, H.; Junker, K.; Hartmann, A.; Stoehr, R. The microphthalmia-associated transcription factor p.E318K mutation does not play a major role in sporadic renal cell tumors from Caucasian patients. *Pathobiology* **2016**, *85*, 165–169. [[CrossRef](#)]
128. Davis, C.F.; Ricketts, C.J.; Wang, M.; Yang, L.; Cherniack, A.D.; Shen, H.; Buhay, C.; Kang, H.; Kim, S.C.; Fahey, C.C.; et al. The somatic genomic landscape of chromophobe renal cell carcinoma. *Cancer Cell* **2014**, *26*, 319–330. [[CrossRef](#)]
129. Martignoni, G.; Pea, M.; Chilosi, M.; Brunelli, M.; Scarpa, A.; Colato, C.; Tardanico, R.; Zamboni, G.; Bonetti, F. Parvalbumin is constantly expressed in chromophobe renal carcinoma. *Mod. Pathol.* **2001**, *14*, 760–767. [[CrossRef](#)]

130. Speicher, M.R.; Schoell, B.; Du Manoir, S.; Schrock, E.; Ried, T.; Cremer, T.; Storkel, S.; Kovacs, A.; Kovacs, G. Specific loss of chromosomes 1, 2, 6, 10, 13, 17 and 21 in chromophobe renal cell carcinomas revealed by comparative genomic hybridization. *Am. J. Pathol.* **1994**, *145*, 356–364.
131. Brunelli, M.; Eble, J.N.; Zhang, S.; Martignoni, G.; Delahunt, B.; Cheng, L. Eosinophilic and classic chromophobe renal cell carcinomas have similar frequent losses of multiple chromosomes from among chromosomes 1, 2, 6, 10, and 17, and this pattern of genetic abnormality is not present in renal oncocytoma. *Mod. Pathol.* **2005**, *18*, 161–169. [[CrossRef](#)] [[PubMed](#)]
132. Ohashi, R.; Schraml, P.; Angori, S.; Batavia, A.A.; Rupp, N.J.; Ohe, C.; Otsuki, Y.; Kawasaki, T.; Kobayashi, H.; Kobayashi, K.; et al. Classic chromophobe renal cell carcinoma incur a larger number of chromosomal losses than seen in the eosinophilic subtype. *Cancers* **2019**, *11*, 1492. [[CrossRef](#)] [[PubMed](#)]
133. Tam, M.H.; Wong, C.F.; Tan, H.L.; Yang, X.J.; Ditlev, J.; Matsuda, D.; Khoo, S.K.; Sugimura, J.; Fujioka, T.; Furge, K.A.; et al. Genomic expression and single-nucleotide polymorphism discriminates chromophobe renal cell carcinoma and oncocytoma. *BMC Cancer* **2010**, *10*, 196.
134. Brunelli, M.; Gobbo, S.; Cossu-Rocca, P.; Cheng, L.; Hse, O.; Delahunt, B.; Pea, M.; Bonetti, F.; Mina, M.M.; Ficarra, V.; et al. Chromosomal gains in the sarcomatoid transformation of chromophobe renal cell carcinoma. *Mod. Pathol.* **2007**, *20*, 303–309. [[CrossRef](#)] [[PubMed](#)]
135. Liu, Q.; Cornejo, K.M.; Cheng, L.; Hutchinson, L.; Wang, M.; Zhang, S.; Tomaszewicz, K.; Cosar, E.F.; Woda, B.A.; Jiang, Z. Next-generation sequencing to detect deletion of RB1 and ERBB4 genes in chromophobe renal cell carcinoma. A potential role in distinguishing chromophobe renal cell carcinoma from renal oncocytoma. *Am. J. Pathol.* **2018**, *188*, 846–851. [[CrossRef](#)] [[PubMed](#)]
136. Durinck, S.; Stawiski, E.W.; Pavia-Jimenez, A.; Modrusan, Z.; Kapur, P.; Jaiswal, B.S.; Zhang, N.; Tofessi-Tcheuyap, V.; Nguyen, T.T.; Pabujia, K.B.; et al. Spectrum of diverse genomic alterations define non-clear cell renal carcinoma subtypes. *Nat. Genet.* **2015**, *47*, 13–21. [[CrossRef](#)]
137. Ricketts, C.J.; De Cubas, A.A.; Fan, H.; Smith, C.C.; Lang, M.; Reznik, E.; Bowlby, R.; Gibb, E.A.; Akbani, R.; Berookhim, R.; et al. The cancer genome atlas comprehensive molecular characterization of renal carcinoma. *Cell Rep.* **2018**, *23*, 313–326. [[CrossRef](#)]
138. Casuscelli, J.; Weinhold, N.; Gundem, G.; Wung, L.; Zaboar, E.C.; Drill, E.; Wang, P.I.; Nanjangud, G.J.; Redzematovic, A.; Nargund, A.M.; et al. Genomic landscape and evolution of metastatic chromophobe and renal cell carcinoma. *JCI Insight* **2017**, *2*, e92688. [[CrossRef](#)]
139. Pan, C.C.; Chen, P.C.H.; Chiang, H. Overexpression of KIT (CD117) in chromophobe renal cell carcinoma and renal oncocytoma. *Am. J. Clin. Pathol.* **2004**, *121*, 878–883. [[CrossRef](#)]
140. Przybycin, C.G.; Cronin, A.M.; Darvishian, F.; Gopalan, A.; Li-Ahmadie, H.A.; Fine, S.W.; Chen, Y.B.; Bernstein, M.; Russo, P.; Reuter, V.E.; et al. Chromophobe renal cell carcinoma: A clinicopathologic study of 203 tumors in 200 patients with primary resection at a single institution. *Am. J. Surg. Pathol.* **2011**, *35*, 962–970. [[CrossRef](#)]
141. Volpe, A.; Novara, G.; Antonelli, A.; Bertini, R.; Billia, M.; Carmignani, G.; Cunico, S.C.; Longo, N.; Martignoni, G.; Minervini, A.; et al. Chromophobe renal cell carcinoma (RCC): Oncological outcomes and prognostic factors in a large multicentre series. *BJU Int.* **2012**, *110*, 76–83. [[CrossRef](#)] [[PubMed](#)]
142. Yip, S.M.; Ruiz Morales, J.M.; Donskov, F.; Fracon, A.; Basso, U.; Rini, B.I.; Lee, J.L.; Bjarnason, J.A.; Sim, H.W.; Beuselinck, B.; et al. Outcomes of metastatic chromophobe renal cell carcinoma (chrRCC) in the targeted therapy era: Results from the international metastatic renal cell cancer database consortium (IMDC). *Kidney Cancer* **2017**, *1*, 41–47. [[CrossRef](#)] [[PubMed](#)]
143. Ged, Y.; Chen, Y.B.; Knezevic, A.; Casuscelli, J.; Redzematovic, A.; DiNatale, R.G.; Carlo, M.I.; Lee, C.H.; Feldman, D.R.; Patil, S.; et al. Metastatic chromophobe renal cell carcinoma: Presence or absence of sarcomatoid differentiation determines clinical course and treatment outcomes. *Clin. Genitourin. Cancer* **2019**, *17*, e678–e688. [[CrossRef](#)] [[PubMed](#)]
144. Casuscelli, J.; Becerra, M.F.; Seier, K.; Menley, B.J.; Benfants, N.; Redzematovic, A.; Stief, C.G.; Hsieh, J.J.; Tichoo, S.K.; Reuter, V.E.; et al. Chromophobe renal cell carcinoma: Results from a large institution series. *Clin. Genitourin. Cancer* **2019**, *17*, 373–379. [[CrossRef](#)]
145. Hsieh, J.J.; Purdue, M.P.; Signoretti, S.; Swanton, C.; Albiges, L.; Schmidinger, M.; Heng, D.Y.; Larkin, J.; Ficarra, V. Renal cell carcinoma. *Nat. Rev. Dis. Primers* **2017**, *3*, 17009. [[CrossRef](#)]
146. Delahunt, B.; Eble, J.N. Papillary renal cell carcinoma: A clinicopathologic and immunohistochemical study of 105 tumors. *Mod. Pathol.* **1997**, *10*, 537–544.

147. Lee, B.H. Commentary on: “Comprehensive molecular characterization of papillary renal-cell carcinoma.” Cancer genome atlas research network.: N Eng J Med 2016 Jan 374(2): 135–142. *Urol. Oncol.* **2017**, *35*, 578–579. [[CrossRef](#)]
148. Jiang, F.; Richter, J.; Schraml, P.; Budendorf, L.; Gasser, T.; Sauter, G.; Mihatsch, M.J.; Moch, H. Chromosomal imbalances in papillary renal cell carcinoma: Genetic differences between histological subtypes. *Am. J. Pathol.* **1998**, *153*, 1467–1473. [[CrossRef](#)]
149. Akhtar, M.; Al-Bozom, I.A.; Al Hussain, T. Papillary renal cell carcinoma (PRCC): An update. *Adv. Anat. Pathol.* **2019**, *26*, 124–132. [[CrossRef](#)]
150. Ooi, A. Advances in hereditary leiomyomatosis and renal cell carcinoma (HLRCC) research. *Semin. Cancer Biol.* **2020**, *61*, 158–166. [[CrossRef](#)]
151. Pal, S.K.; Ali, S.M.; Yakirevich, E.; Geynisman, D.M.; Karam, J.A.; Elvin, J.A.; Frampton, G.M.; Huang, X.; Lin, D.I.; Rosenzweig, M.; et al. Characterization of clinical cases of advanced papillary renal cell carcinoma via comprehensive genomic profiling. *Eur. Oncol.* **2018**, *73*, 71–78. [[CrossRef](#)] [[PubMed](#)]
152. Li, S.; Such, B.M.; Gerstein, M.B. Whole-genome analysis of papillary kidney cancer finds significant noncoding alterations. *PLoS Genet.* **2017**, *13*, e1006685. [[CrossRef](#)] [[PubMed](#)]
153. Zhu, B.; Poeta, M.L.; Costantini, M.; Zhang, T.; Shi, J.; Sentinelli, S.; Zhao, W.; Pompeo, V.; Cardelli, M.; Alexandrov, B.S.; et al. The genomic and epigenomic evolutionary history of papillary renal cell carcinomas. *BioRxiv* **2020**, in press. [[CrossRef](#)] [[PubMed](#)]
154. Vera-Badillo, F.E.; Templeton, A.J.; Duran, I.; Ocana, A.; De Gouveia, P.; Aneja, P.; Knox, J.J.; Tannock, I.F.; Escudier, B.; Amir, E. Systemic therapy for non-clear cell renal cell carcinomas: A systematic review and meta-analysis. *Eur. Urol.* **2015**, *67*, 740–749. [[CrossRef](#)] [[PubMed](#)]
155. Wells, J.C.; Donskov, F.; Fraccon, A.P.; Pasini, F.; Bjarnason, G.A.; Beuselinck, B.; Knox, J.J.; Rha, S.Y.; Agarwal, N.; Bowman, I.A.; et al. Characterizing the outcomes of metastatic papillary renal cell carcinoma. *Cancer Med.* **2017**, *6*, 902–909. [[CrossRef](#)]
156. Rhoades Smith, K.E.; Bilen, M.A. A review of papillary renal cell carcinoma and MET inhibitors. *Kidney Cancer J.* **2019**, *3*, 151–161. [[CrossRef](#)]
157. Campbell, M.T.; Bilen, M.A.; Shah, A.Y.; Lerule, E.; Jouasch, E.; Venka, A.M.; Aetinmakas, E.; Duran, C.; Msaouel, P.; Tannir, N.M. Cabozantinib for the treatment of patients with metastatic non-clear renal cell carcinoma: A retrospective analysis. *Eur. J. Cancer* **2018**, *104*, 188–194. [[CrossRef](#)]
158. Chanza, N.M.; Xie, W.; Bilen, M.A.; Dzimitrowicz, H.; Burkert, J.; Geynisman, D.M.; Balakrishnan, A.; Bowman, I.A.; Jain, R.; Stadler, W.; et al. Cabozantinib in advanced non-clear-cell renal cell carcinoma: A multicentre, retrospective, cohort study. *Lancet Oncol.* **2019**, *20*, 581–590. [[CrossRef](#)]
159. Choueiri, T.K.; Heng, D.; Lee, J.L.; Cancel, M.; Verheijen, R.B.; Mellemegaard, A.; Ottesen, L.H.; Frigault, M.M.; L’Hernault, A.; Sziogyarto, Z.; et al. Efficacy of savolitinib vs sunitinib in patients with MET-driven papillary renal cell carcinoma: The SAVOIR phase 3 randomized clinical trial. *JAMA Oncol.* **2020**, in press. [[CrossRef](#)]
160. Powles, T.; Larkin, J.; Patel, P.; Perez-Valderrama, B.; Rodriguez-Vida, A.; Glen, H.; Thistlethwaite, F.; Ralph, C.; Srinivasan, G.; Mendez-Vidal, M.J.; et al. A phase II study investigating the safety and efficacy of savolitinib and durvalumab in metastatic papillary renal cancer (CALYPSO). *J. Clin. Oncol.* **2019**, *37*, 545. [[CrossRef](#)]
161. Gnarr, J.R.; Tory, K.; Weng, Y.; Schmidt, L.; Wei, M.H.; Li, H.; Latif, F.; Liu, S.; Chen, F.; Duh, F.M.; et al. Mutations of the VHL tumour suppressor gene in renal carcinoma. *Nat. Genet.* **1994**, *7*, 85–90. [[CrossRef](#)] [[PubMed](#)]
162. Gallou, C.; Joly, D.; Méjean, A.; Staroz, F.; Martin, N.; Tarlet, G.; Orfanelli, M.T.; Bouvier, R.; Droz, D.; Chréien, C.; et al. Mutations of the VHL gene in sporadic renal cell carcinoma: Definition of a risk factor for VHL patients to develop an RCC. *Hum. Mutat.* **1999**, *13*, 464–475. [[CrossRef](#)]
163. Schraml, P.; Struckman, K.; Hatz, F.; Sonnet, S.; Kully, C.; Gasser, T.; Sauter, G.; Mihatsch, M.J.; Moch, H. VHL mutations and their correlation with tumour cell proliferation, microvessel density, and patient prognosis in clear cell renal cell carcinoma. *J. Pathol.* **2002**, *196*, 186–193. [[CrossRef](#)] [[PubMed](#)]
164. Herman, J.G.; Latif, F.; Weng, Y.; Lerman, M.I.; Zbar, B.; Liu, S.; Samod, D.; Duan, D.S.; Gnarr, J.R.; Linehan, W.M.; et al. Silencing of the VHL tumor-suppressor gene by DNA methylation in renal carcinoma. *Proc. Natl. Acad. Sci. USA* **1994**, *91*, 9700–9704. [[CrossRef](#)]

165. Varela, I.; Tarpey, P.; Raine, K.; Huang, D.; Ong, C.K.; Stephens, P.; Davies, H.; Jones, D.; Lin, M.L.; Teague, J.; et al. Exome sequencing identifies frequent mutation of the SWI/SNF complex gene PBRM1 in renal carcinoma. *Nature* **2011**, *469*, 539–542. [[CrossRef](#)]
166. Dalglish, G.L.; Furge, K.; Greenman, C.; Chen, L.; Bignell, G.; Butler, A.; Davies, H.; Edlins, S.; Hardy, C.; Latimer, C.; et al. Systematic sequencing of renal carcinoma reveals inactivation of histone modifying genes. *Nature* **2000**, *463*, 360–363. [[CrossRef](#)]
167. Pena-Lopis, S.; Vega-Rubin-de-Celis, S.; Liao, A.; Leng, N.; Pavia-Jimenez, A.; Wang, S.; Yamasaki, T.; Zhrebker, L.; Sivanand, S.; Spence, P.; et al. BAP1 loss defines a new class of renal cell carcinoma. *Nat. Genet.* **2012**, *44*, 751–759. [[CrossRef](#)]
168. Guo, G.; Gui, Y.; Gao, S.; Tang, A.; Hu, X.; Huang, Y.; Jia, W.; Li, Z.; He, M.; Sun, L.; et al. Frequent mutations of genes encoding ubiquitin-mediated proteolysis pathway components in clear cell renal cell carcinoma. *Nat. Genet.* **2011**, *44*, 17–19. [[CrossRef](#)]
169. Sato, Y.; Yoshizato, T.; Shiraiishi, Y.; Maekawa, S.; Okuno, Y.; Kamura, T.; Shimamura, T.; Sato-Otsubo, A.; Nagae, G.; Suzuki, H.; et al. Integrated molecular analysis of clear-cell renal cell carcinoma. *Nat. Genet.* **2013**, *45*, 860–867. [[CrossRef](#)]
170. The Cancer Genome Atlas Research Network. Comprehensive molecular characterization of clear cell renal cell carcinoma. *Nature* **2013**, *499*, 43–48. [[CrossRef](#)]
171. Li, L.; Shen, C.; Nakamura, E.; Ando, K.; Signoretti, S.; Beroukhim, R.; Cowley, G.S.; Lizotte, P.; Liberzon, E.; Bair, S.; et al. SQSTM1 is a pathogenic target of 5q copy number gains in kidney cancer. *Cancer Cell* **2013**, *24*, 738–750. [[CrossRef](#)] [[PubMed](#)]
172. Tippu, Z.; Au, L.; Turajilic, S. Evolution of renal cell carcinoma. *Eur. Urol. Focus* **2020**, *29*, S2405–S4569. [[CrossRef](#)] [[PubMed](#)]
173. Psutka, S.P.; Cheville, J.C.; Costello, B.A.; Stewart-Merrill, S.B.; Lohse, C.M.; Leibovich, B.C.; Boorjian, S.A.; Thompson, R.H. Concordance of pathologic features between metastatic sites and the primary tumor in surgically resected metastatic renal cell carcinoma. *Urology* **2016**, *96*, 106–113. [[CrossRef](#)] [[PubMed](#)]
174. Ho, T.H.; Parasramka, M. Differential gene expression of matched primary renal clear cell carcinoma and metastases reveals upregulation of extracellular matrix genes. *Annals of Oncology* **2017**, *28*, 604–610. [[CrossRef](#)]
175. De Velasco, G.; Wankowicz, S.A.; Madison, R.; Ali, S.M.; Norton, C.; Duquette, A.; Ross, J.S.; Bossé, D.; Lalani, A.K.; Miller, V.A.; et al. Targeted genomic landscape of metastases compared to primary tumours in clear cell metastatic renal cell carcinoma. *Br. J. Cancer* **2018**, *118*, 1238–1242. [[CrossRef](#)]
176. Gerlinger, M.; Rowan, A.J.; Horswell, S.; Larkin, J.; Endesfelder, D.; Gronroos, E.; Matthews, N.; Stewart, A.; Tarpey, P.; Varela, I.; et al. Intratumor heterogeneity and branched evolution revealed by multiregion sequencing. *N. Engl. J. Med.* **2012**, *366*, 883–892. [[CrossRef](#)]
177. Gerlinger, M.; Horswell, S.; Larkin, J.; Rowan, A.J.; Salm, M.P.; Varela, I.; Fisher, R.; McGranahan, N.; Matthews, N. Genomic architecture and evolution of clear cell renal cell carcinomas defined by multiregion sequencing. *Nat. Genet.* **2014**, *46*, 225–233. [[CrossRef](#)]
178. Turajilic, S.; Xu, H.; Litchfield, K.; Rowan, A.; Horswell, S.; Chambers, T.; O'Brien, T.; Lopez, J.I.; Watkins, T.; Nicol, D.; et al. Deterministic evolutionary trajectories influence primary tumor growth: TRACERx renal. *Cell* **2018**, *173*, 595–610. [[CrossRef](#)]
179. Turajilic, S.; Xu, H.; Litchfield, K.; Rowan, A.; Chambers, T.; Lopez, J.I.; Nicol, D.; O'Brien, T.; Larkin, J.; Horswell, S.; et al. Tracking cancer evolution reveals constrained routes to metastases: TRACERx renal. *Cell* **2018**, *173*, 581–594.
180. Huang, Y.; Wang, J.; Jia, P.; Li, X.; Pei, G.; Wang, C.; Fang, X.; Zhao, Z.; Cai, Z.; Yi, X.; et al. Clonal architectures predict clinical outcome in clear cell renal cell carcinoma. *Nat. Commun.* **2019**, *10*, 1245. [[CrossRef](#)]
181. Clark, D.J.; Dhaansekaran, S.M.; Petralia, F.; Pan, J.; Song, X.; Hu, Y.; Da Veiga Leprevost, F.; Reva, B.; Lih, T.S.; Chang, H.Y. Integrated proteogenomic characterization of clear cell renal cell carcinoma. *Cell* **2019**, *179*, 964–983. [[CrossRef](#)] [[PubMed](#)]
182. Hakimi, A.A.; Reznik, E.; Lee, C.H.; Creighton, C.J.; Brannon, A.R.; Luna, A.; Aksoy, B.A.; Liu, E.M.; Shen, R.; Lee, W.; et al. An integrated metabolic atlas of clear cell renal carcinoma. *Cancer Cell* **2016**, *29*, 104–116. [[CrossRef](#)] [[PubMed](#)]
183. Kotecha, R.R.; Motzer, R.J.; Voss, M.H. Towards individualized therapy for metastatic renal cell carcinoma. *Nat. Rev. Clin. Oncol.* **2019**, *16*, 621–633. [[CrossRef](#)]

184. Carill-Ajuria, L.; Santos, M.; Roldán-Romero, J.M.; Rodríguez-Antona, C.; De Velasco, G. Prognostic and predictive value of PBRM1 in clear cell renal cell carcinoma. *Cancers* **2020**, *12*, 16. [[CrossRef](#)] [[PubMed](#)]
185. Voss, M.H.; Reising, A.; Cheng, Y.; Patel, P.; Marker, M.; Kuo, F.; Chan, T.A.; Choueiri, T.K.; Hsieh, J.J.; Hakimi, A.A.; et al. Genomically annotated risk model for advanced renal-cell carcinoma: A retrospective cohort study. *Lancet Oncol.* **2018**, *19*, 1688–1698. [[CrossRef](#)]
186. McDermott, D.F.; Huseni, M.A.; Atkins, M.B.; Motzer, R.J.; Rini, B.I.; Escudier, B.; Fong, L.; Joseph, R.W.; Pai, S.K.; Reeves, J.A.; et al. Clinical activity and molecular correlates of response to atezolizumab alone or in combination with bevacizumab versus sunitinib in renal cell carcinoma. *Nat. Med.* **2018**, *24*, 749–757. [[CrossRef](#)]
187. Miao, D.; Margolis, C.A.; Gao, W.; Voss, M.H.; Li, W.; Martini, D.J.; Norton, C.; Bossé, D.; Wancowicz, S.M.; Cullen, D.; et al. Genomic correlates of response to immune checkpoint therapies in clear cell renal cell carcinoma. *Science* **2018**, *359*, 801–806. [[CrossRef](#)]
188. Braun, D.A.; Ishii, Y.; Van Allen, E.M.; Wu, C.J.; Shukla, S.A.; Choueiri, T.K. Clinical validation of PBRM1 alterations as a marker of immune check inhibitor response in renal cell carcinoma. *JAMA Oncol.* **2019**, *5*, 1631–1633. [[CrossRef](#)]
189. Braun, D.A.; Hou, Y.; Bakouni, Z.; Ficial, M.; Sant’Angelo, M.; Forman, J.; Ross-MacDonald, P.; Berger, A.C.; Jegede, O.A.; Elagina, L.; et al. Interplay of somatic alterations and immune infiltration modulates response to PD-1 blockade in advanced clear cell renal cell carcinoma. *Nat. Med.* **2020**, in press. [[CrossRef](#)]
190. Davis, C.J.; Mostofi, F.K.; Sesterhenn, I.A. Renal medullary carcinoma. The seventh sickle cell nephropathy. *Am. J. Surg. Pathol.* **1995**, *19*, 1–11. [[CrossRef](#)]
191. Calderaro, J.; Moorch, J.; Pierron, G.; Pedentour, F.; Grison, C.; Maillé, P.; Sayeux, P.; De la Taille, A.; Coutourier, J.; Viellefond, A.; et al. SMARCB1/INI1 inactivation in renal medullary carcinoma. *Histopathology* **2012**, *61*, 428–435. [[CrossRef](#)] [[PubMed](#)]
192. Calderaro, J.; Maslah-Planchon, J.; Richer, W.; Maillot, L.M.; Mansuy, L.; Bastien, C.; De la Taille, A.; BouSSION, H.; Carpy, C.; Jourdain, A.; et al. Balanced translocations disrupting SMARCB1 are hallmark recurrent genetic alterations in renal medullary carcinomas. *Eur. Urol.* **2016**, *69*, 1055–1061. [[CrossRef](#)] [[PubMed](#)]
193. Carlo, M.I.; Chaim, J.; Patil, S.; Kemel, Y.; Schram, A.M.; Woo, K.; Coskey, D.; Nanjangud, G.J.; Voss, M.H.; Feldman, D.R.; et al. Genomic characterization of renal medullary carcinoma and treatment outcomes. *Clin. Genitourin. Cancer* **2017**, *15*, e987–e994. [[CrossRef](#)] [[PubMed](#)]
194. Jia, L.; Carlo, M.I.; Khan, H.; Nanjangud, G.J.; Rana, S.; Cimera, R.; Zhang, Y.; Ari Hakimi, A.; Verma, A.K.; Al-Ahmadie, H.A.; et al. Distinctive mechanisms underlie the loss of SMARCB1 protein expression in renal medullary carcinoma: Morphologic and molecular analysis of 20 cases. *Mod. Pathol.* **2019**, *32*, 1329–1343. [[CrossRef](#)] [[PubMed](#)]
195. Hong, A.L.; Tseng, Y.Y.; Wala, J.A.; Kim, W.J.; Kynnap, B.D.; Doshi, M.B.; Kugener, G.; Sandoval, G.J.; Howard, T.P.; Li, J.; et al. Renal medullary carcinomas depend upon SMARCB1 loss and are sensitive to proteasome inhibition. *Elife* **2019**, *8*, e44161. [[CrossRef](#)]
196. Mac Lennan, G.T.; Farrow, G.M.; Bostwick, D.G. Low-grade collecting duct carcinoma of the kidney: Report of 13 cases of low-grade mucinous tubulocystic renal carcinoma of possible collecting duct origin. *Urology* **1997**, *50*, 679–684. [[CrossRef](#)]
197. Amin, M.B.; MacLennan, G.T.; Gupta, R.; Grignon, D.; Paraf, F.; Viellefond, A.; Paner, G.P.; Stovsky, M.; Young, A.N.; Srigley, J.R.; et al. Tubulocystic carcinoma of the kidney: Clinicopathologic analysis of 31 cases of a distinctive rare subtype of renal cell carcinoma. *Am. J. Surg. Pathol.* **2009**, *33*, 384–392. [[CrossRef](#)]
198. Lawrie, C.H.; Armesto, M.; Fernandez-Mercado, M.; Arestin, M.; Manterola, L.; Giocoechea, I.; Larrea, E.; Caffarel, M.M.; Araujo, A.M.; Sole, C.; et al. Noncoding RNA expression and targeted next-generation sequencing distinguish tubulocystic renal cell carcinoma (TC-RCC) from other renal neoplasms. *J. Mol. Diagn.* **2018**, *20*, 34–45. [[CrossRef](#)]
199. Sarungbam, J.; Mehra, R.; Tomlins, S.A.; Smith, S.C.; Jayakumar, G.; Al-Ahmadie, H.; Gopalan, A.; Sirintrapun, S.J.; Fine, S.W.; Zhang, Y.; et al. Tubulocystic renal cell carcinoma: A distinct clinicopathologic entity with a characteristic genomic profile. *Mod. Pathol.* **2019**, *32*, 701–709. [[CrossRef](#)]

200. Gadd, S.; Huff, V.; Huang, C.C.; Ruteshouser, E.C.; Dome, J.S.; Grundy, P.E.; Breslow, N.; Jenniong, L.; Green, D.M.; Beckwith, J.B.; et al. Clinically relevant subsets identified by gene expression patterns support a revised ontogenic model of Wilms tumor: A children’s oncology group study. *Neoplasia* **2012**, *14*, 742–756. [[CrossRef](#)]
201. Torrezan, G.T.; Ferreira, E.N.; Nakahata, A.M.; Barros, B.; Castro, M.; Correa, B.R.; Krepischi, A.C.; Olivieri, E.; Cunha, I.W.; Tabori, U.; et al. Recurrent mutation in DROSHA induces microRNA profile changes in Wilms tumour. *Nat. Commun.* **2014**, *5*, 4039. [[CrossRef](#)] [[PubMed](#)]
202. Weigert, J.; IOshaque, N.; Vardapour, R.; Georg, C.; Gu, Z.; Bieg, M.; Ziegler, B.; Bausenwein, S.; Nourkami, N.; Ludwig, N.; et al. Mutations in SIX1/2 pathway and the DROSHA/DGCR8 miRNA microprocessor complex underlie high-risk blastemal type Wilms tumors. *Cancer Cell* **2015**, *27*, 298–311. [[CrossRef](#)] [[PubMed](#)]
203. Rakheja, D.; Chen, K.S.; Liu, Y.; Shukla, A.A.; Schmid, V.; Chang, T.C.; Khokhar, S.; Wickiser, J.E.; Karandikar, N.J.; Malter, J.S.; et al. Somatic mutations in DROSHA and DICER1 impair microRNA biogenesis through distinct mechanisms in Wilms tumours. *Nat. Commun.* **2014**, *2*, 4802. [[CrossRef](#)] [[PubMed](#)]
204. Walz, A.L.; Ooms, A.; Gadd, S.; Gerhard, D.S.; Smith, M.A.; Auvil, J.; Meerzaman, D.; Chen, Q.R.; Hsu, C.H.; Yan, C.; et al. Recurrent DGCR8, DROSHA, and SIX homeodomain mutations in favorable histology Wilms tumors. *Cancer Cell* **2015**, *27*, 286–297. [[CrossRef](#)]
205. Ooms, A.A.; Gadd, S.; Gerhard, D.S.; Smith, M.A.; Auvil, J.; Meerzaman, D.; Chen, Q.R.; Hsu, C.H.; Yan, C.; Nguyen, C.; et al. Significance of TP53 mutation in Wilms tumors with diffuse anaplasia: A report from the children’s oncology group. *Clin. Cancer Res.* **2016**, *22*, 5582–5591. [[CrossRef](#)]
206. Perlman, E.J.; Gadd, S.; Arold, S.T.; Radhakrishnan, A.; Gerhard, D.S.; Jenning, L.; Huff, V.; Auvil, J.; Davidsen, T.M.; Dome, J.S.; et al. MLLT1 YEATS domain mutations in clinically distinctive favourable histology Wilms tumours. *Nat. Commun.* **2015**, *6*, 10013. [[CrossRef](#)]
207. Gadd, S.; Huff, V.; Walz, A.L.; Ooms, A.; Armstrong, A.E.; Gerhard, D.S.; Smith, M.A.; Auvil, J.; Meerzaman, D.; Chen, Q.R.; et al. Children Oncology Group and TARGET initiative exploring the genetic landscape of Wilms Tumors. *Nat. Genet.* **2017**, *49*, 1487–1494. [[CrossRef](#)]
208. Wan, L.; Chong, S.; Xuan, F.; Liang, A.; Cui, X.; Gates, L.; Carroll, T.S.; Li, Y.; Feng, L.; Chen, G.; et al. Impaired cell fate through gain-of-function mutations in a chromatin reader. *Nature* **2020**, *577*, 121–126. [[CrossRef](#)]
209. Coorens, T.; Treger, T.D.; Al-Saadi, R.; Moore, L.; Tran, M.; Mitchell, T.J.; Tugnait, S.; Thevanesan, C.; Young, M.D.; Oliver, T.; et al. Embryonal precursors of Wilms tumor. *Science* **2019**, *366*, 1247–1251. [[CrossRef](#)]
210. Jones, T.D.; Eble, J.N.; Wang, M.; MacLennan, G.T.; Jain, S.; Cheng, I. Clonal divergence and genetic heterogeneity in clear cell renal cell carcinomas with sarcomatoid transformation. *Cancer* **2005**, *104*, 1195–1203. [[CrossRef](#)]
211. Chevillet, J.C.; Lohse, C.M.; Zincke, H.; Weaver, A.L.; Leibovich, B.C.; Franck, I.; Blute, M.L. Sarcomatoid renal cell carcinoma: An examination of underlying histologic subtype and an analysis of associations with patient outcome. *Am. J. Surg. Pathol.* **2004**, *28*, 435–441. [[CrossRef](#)] [[PubMed](#)]
212. De Peralta-Venturina, M.; Moch, H.; Amin, M.; Tamboli, P.; Hallemariam, S.; Mihatsch, M.; Javidan, J.; Stricker, H.; Ro, J.Y.; Amin, M.B. Sarcomatoid differentiation in renal cell carcinoma: A study of 101 cases. *Am. J. Surg. Pathol.* **2001**, *25*, 275–284. [[CrossRef](#)] [[PubMed](#)]
213. Sircar, K.; Yoop, S.Y.; Majewski, T.; Wani, K.; Patel, L.R.; Voicu, H.; Torres-Garcia, W.; Verhaak, R.G.W.; Tannir, N.; Karam, J.A.; et al. Biphasic components of sarcomatoid clear cell renal cell carcinomas are molecularly similar to each other, but distinct from, non-sarcomatoid renal carcinomas. *J. Pathol. Clin. Res.* **2015**, *1*, 212–224. [[CrossRef](#)] [[PubMed](#)]
214. Bi, M.; Zhao, S.; Said, J.W.; Merino, M.J.; Adeniran, A.J.; Xie, Z.; Nawaf, C.B.; Choi, J.; Belldegrun, A.S.; Pantuck, A.J.; et al. Genomic characterization of sarcomatoid transformation in clear cell renal cell carcinoma. *Proc. Natl. Acad. Sci. USA* **2016**, *113*, 2170–2175. [[CrossRef](#)] [[PubMed](#)]
215. Wang, Z.; Kim, T.B.; Peng, B.; Karam, J.A.; Creighton, C.J.; Joon, A.Y.; Kawakami, F.; Trevisan, P.; Jonash, E.; Chow, C.W.; et al. Sarcomatoid renal cell carcinoma has a distinct molecular pathogenesis, driver mutation profile and transcriptional landscape. *Clin. Cancer Res.* **2017**, *23*, 6686–6696. [[CrossRef](#)]
216. Pal, S.K.; He, M.; Tong, T.; Wu, H.; Liu, X.; Lau, C.; Wang, J.H.; Warden, C.; Wu, X.; Signoretti, S.; et al. RNA-seq reveals aurora kinase-driven mTOR pathway activation in patients with sarcomatoid metastatic renal cell carcinoma. *Mol. Cancer Res.* **2015**, *13*, 130–137. [[CrossRef](#)]

217. Malouf, G.G.; Ali, S.M.; Wang, K.; Balasubramanian, S.; Ross, J.S.; Miller, V.A.; Stephens, P.J.; Khayat, D.; Pal, S.K.; Su, X.; et al. Genomic characterization of renal cell carcinoma with sarcomatoid dedifferentiation pinpoints recurrent genomic alterations. *Eur. Urol.* **2016**, *70*, 348–357. [[CrossRef](#)]
218. Malouf, G.G.; Filippot, R.; Dong, Y.; Dinatale, R.G.; Chen, Y.B.; Su, X.; Comperat, E.; Rouporet, M.; Mano, R.; Blum, K.A.; et al. Molecular characterization of sarcomatoid clear cell renal cell carcinoma unveils new candidate oncogenic drivers. *Sci. Rep.* **2020**, *10*, 701. [[CrossRef](#)]
219. Ito, T.; Pei, J.; Dulaimi, E.; Menges, C.; Abbosh, P.H.; Smaldone, M.C.; Chen, D.Y.; Greenberg, R.E.; Kutikov, A.; Viterbo, R.; et al. Genomic copy number alterations in renal cell carcinoma with sarcomatoid features. *J. Urol.* **2016**, *195*, 852–858. [[CrossRef](#)]
220. White, S.M.; Avantaggiato, M.L.; Nemazanyy, I.; Di Poto, C.; Yang, Y.; Pende, M.; Gibney, G.; Ransom, H.; Field, J.; Atkins, M.B.; et al. YAP/TAZ inhibition induces metabolic and signaling rewiring resulting in targetable vulnerabilities in NF2-deficient tumor cells. *Dev. Cell* **2019**, *49*, 425–443. [[CrossRef](#)]
221. Kawakami, F.; Sircar, K.; Rodriguez-Canales, J.; Fellman, B.L.; Urbauer, D.L.; Tamboli, P.; Tannir, N.M.; Jonasch, E.; Wistuba, L.L.; Woodid, C.G.; et al. Programmed cell death ligand 1 and tumor-infiltrating lymphocyte status in patients with renal cell carcinoma and sarcomatoid dedifferentiation. *Cancer* **2017**, *123*, 4823–4831. [[CrossRef](#)] [[PubMed](#)]
222. Joseph, R.W.; Millis, S.Z.; Carballido, E.M.; Bryant, D.; Gatalica, Z.; Reddy, S.; Bryce, A.H.; Vogelzang, N.J.; Stanton, M.L.; Castle, E.P.; et al. PD-1 and PD-L1 expression in renal cell carcinoma with sarcomatoid differentiation. *Cancer Immunol. Res.* **2015**, *3*, 1303–1307. [[CrossRef](#)] [[PubMed](#)]
223. Flippot, R.; McGregor, B.A.; Flaifel, A.; Gray, K.P.; Signoretti, S.; Steinharter, J.A.; Van Allen, E.M.; Walsh, M.K.; Gundy, K.; Wei, X.X.; et al. Atezolizumab plus bevacizumab in non-clear cell renal cell carcinoma (NccRCC) and clear cell renal cell carcinoma with sarcomatoid differentiation (ccRCCsd): Updated results of activity and predictive biomarkers from a phase II study. *J. Clin. Oncol.* **2019**, *3*, 4583. [[CrossRef](#)]
224. Rini, B.I.; Motzer, R.J.; Powles, T.; McDermott, D.F.; Escudier, B.; Donskov, F.; Hawkins, R.E.; Bracarda, S.; Bedke, J.; De Giorgi, U.; et al. Atezolizumab (atezo) + bevacizumab (bev) versus sunitinib (sun) in pts with untreated metastatic renal cell carcinoma (mRCC) and sarcomatoid histology: IMmotion151 subgroup analysis. *J. Clin. Oncol.* **2019**, *37*, 4512. [[CrossRef](#)]
225. Gupta, S.; Cheville, J.C.; Jungbluth, A.A.; Zhang, Y.; Zhang, L.; Chen, Y.B.; Tickoo, S.K.; Fine, S.W.; Gopalan, A.; Al-Ahmadie, H.A.; et al. JAK2/PD-L1/PD-L2 (9p24.1) amplifications in renal cell carcinomas with sarcomatoid transformation: Implications for clinical management. *Mod. Pathol.* **2019**, *32*, 1344–1358. [[CrossRef](#)] [[PubMed](#)]
226. Rini, B.I.; Powles, T.; Atkins, M.B.; Escudier, B.; McDermott, D.F.; Suarez, C.; Bracarda, S.; Stadler, W.M.; Donskov, F.; Lee, J.L.; et al. Atezolizumab plus bevacizumab versus sunitinib in patients with previously untreated metastatic renal cell carcinoma (IMmotion151): A multicenter, open-label, phase 3, randomized controlled trial. *Lancet* **2019**, *393*, 2404–2415. [[CrossRef](#)]
227. Chen, F.; Zhang, Y.; Senbabaoglu, Y.; Ciriello, G.; Yang, L.; Reznik, E.; Shuch, B.; Micevic, G.; De Velasco, N.; Shinbrot, E.; et al. Multilevel genomics-based taxonomy of renal cell carcinoma. *Cell Rep.* **2016**, *14*, 2476–2489. [[CrossRef](#)]
228. Poehlman, W.L.; Hsieh, J.J.; Feltus, F.A. Linking binary gene relationships to drivers of renal cell carcinoma reveals convergent function in alternate tumor progression paths. *Sci. Rep.* **2019**, *9*, 2899. [[CrossRef](#)]
229. Hsieh, J.J.; Le, V.; Cao, D.; Cheng, E.H.; Creighton, C.J. Genomic classifications of renal cell carcinoma: A critical step towards the future application of personalized kidney cancer care with pan-omics precision. *J. Pathol.* **2018**, *244*, 525–537. [[CrossRef](#)]
230. Huang, J.J.; Hsieh, J.J. The therapeutic landscape of renal cell carcinoma: From the dark age to the golden age. *Semin. Nephrol.* **2020**, *40*, 28–41. [[CrossRef](#)]
231. Rini, B.I.; Plimack, E.R.; Stus, V.; Gafanov, R.; Hawkins, R.; Nosov, D.; Pouliot, F.; Alekseev, B.; Soulieres, D.; Melichar, B.; et al. Pembrolizumab plus axitinib versus sunitinib for advanced renal-cell carcinoma. *N. Engl. J. Med.* **2019**, *380*, 1116–1127. [[CrossRef](#)] [[PubMed](#)]
232. Plimack, E.R.; Rini, B.I.; Stus, V.; Gafanov, R.; Waddell, T.; Nosov, D.; Pouliot, F.; Soulieres, D.; Meichar, B.; Vynnychenko, I.; et al. Pembrolizumab plus axitinib as first-line therapy for advanced renal cell carcinoma (RCC): Updated analysis of KEYNOTE-426. *J. Clin. Oncol.* **2020**, *38*, 5001. [[CrossRef](#)]



233. Motzer, R.J.; Penkov, K.; Haanen, J.; Rini, B.I.; Albiges, L.; Campbell, M.T.; Venugopal, B.; Kollmannsberger, C.; Negrier, S.; Uemura, M.; et al. Avelumab plus axitinib versus sunitinib for advanced renal-cell carcinoma. *N. Engl. J. Med.* **2019**, *380*, 1103–1115. [[CrossRef](#)] [[PubMed](#)]
234. Choueiri, T.K.; Motzer, R.J.; Rini, B.I.; Haanen, J.; Campbell, M.T.; Vengogal, B.; Kollmannsberger, C.; Grais-Mescom, G.; Uemura, M.; Lee, J.L.; et al. Updated efficacy results from the JAVELIN Renal 101 trial: First-line avelumab plus axitinib versus sunitinib in patients with advanced renal cell carcinoma. *Ann. Oncol.* **2020**; in press.
235. Choueiri, T.K.; Plimack, E.R.; Bauer, T.M.; Merchan, J.R.; Papadopoulos, K.; McDermott, D.F.; Michaelson, D.; Appleman, L.J.; Zojwalle, N.; Jonasch, E. Phase I/II study of the oral HIF-2 $\alpha$  inhibitor MK-6482 in patients with advanced clear cell renal cell carcinoma (RCC). *J. Clin. Oncol.* **2020**, *38*, 611. [[CrossRef](#)]
236. Jonasch, E.; Donskov, F.; Iliopoulos, O.; Rathmell, W.K.; Narayan, V.; Maughan, B.L.; Oudard, S.; Else, T.; Marouchie, J.K.; Walsh, S.J.; et al. Phase II study of the oral HIF-2 $\alpha$  inhibitor MK-6482 for von Hippel-Lindau disease-associated renal cell carcinoma. *J. Clin. Oncol.* **2020**, *38*, 5003. [[CrossRef](#)]



© 2020 by the authors. Licensee MDPI, Basel, Switzerland. This article is an open access article distributed under the terms and conditions of the Creative Commons Attribution (CC BY) license (<http://creativecommons.org/licenses/by/4.0/>).



Case Report

# Recurrent Superior Vena Cava Syndrome in a Patient with Sarcoidosis and Pancreatic Adenocarcinoma: A Case Report and Literature Review

Ganesh Shenoy <sup>1</sup>, Yunsung Kim <sup>1</sup>, Kyra Newmaster <sup>1</sup>, Kathryn L. McGillen <sup>2</sup>,  
Francesca Ruggiero <sup>3</sup> and Nelson S. Yee <sup>4,\*</sup>

<sup>1</sup> Penn State College of Medicine Medical Scientist Training Program, Hershey, PA 17033, USA; gshenoy@pennstatehealth.psu.edu (G.S.); ykim3@pennstatehealth.psu.edu (Y.K.); knewmaster@pennstatehealth.psu.edu (K.N.)

<sup>2</sup> Department of Radiology, Penn State Health Milton S. Hershey Medical Center, Hershey, PA 17033, USA; kmcgillen@pennstatehealth.psu.edu

<sup>3</sup> Department of Pathology, Penn State Health Milton S. Hershey Medical Center, Hershey, PA 17033, USA; fruggiero@pennstatehealth.psu.edu

<sup>4</sup> Division of Hematology-Oncology, Department of Medicine, Penn State Health Milton S. Hershey Medical Center, Next-Generation Therapies Program, Penn State Cancer Institute, The Pennsylvania State University College of Medicine, Hershey, PA 17033, USA

\* Correspondence: nyee@pennstatehealth.psu.edu; Tel.: +1-717-531-8678

Received: 31 July 2020; Accepted: 1 September 2020; Published: 4 September 2020

**Abstract:** **Background:** Superior vena cava (SVC) syndrome may result from extravascular compression or intravascular obstruction such as thrombosis. Recurrent venous thrombosis is typically associated with a hypercoagulable state such as malignancy, and inheritable or acquired coagulopathy. Sarcoidosis is a derangement of the immune system, and it has been associated with malignant diseases and hypercoagulation. The association of pancreatic cancer and sarcoidosis with SVC syndrome has not been reported previously. Here, we present a case of recurrent venous thrombosis causing SVC syndrome in a patient with pancreatic ductal adenocarcinoma and underlying thoracic sarcoidosis. **Methods:** The patient's electronic health record was retrospectively analyzed. **Results:** A 66-year-old woman with pancreatic adenocarcinoma was treated with neoadjuvant chemotherapy followed by Whipple procedure, before developing tumor recurrence in the liver. Her treatment course was complicated with repeated incidents of venous thrombosis in the presence of a central venous catheter leading to recurrent SVC syndrome, which resolved with anti-coagulation. **Conclusions:** This case raises a plausible inter-relationship between sarcoidosis, pancreatic cancer, and hypercoagulable state. We suggest that patients with multiple risk factors for developing venous thrombosis should be carefully monitored for any thrombotic event, and they may benefit from prophylactic anti-coagulation.

**Keywords:** pancreatic adenocarcinoma; pancreatic cancer; sarcoidosis; superior vena cava syndrome; venous thrombosis

## 1. Introduction

Superior vena cava (SVC) syndrome is a medical emergency that comprises a group of symptoms caused by obstruction of the SVC. Characteristic symptoms of SVC syndrome include edema of the face, neck, upper-body and extremities that are often accompanied by dyspnea. The buildup of pressure proximal to the SVC obstruction results in the distension of veins on the neck and chest and dilation of collateral vessels that return blood to the heart [1,2]. An estimated 60 to 85% of cases of SVC syndrome are thought to be due to malignancy, with lung cancer and non-Hodgkin lymphoma being the most

commonly cited cancers associated with the syndrome [2]. As a result of their location, cancers of the lungs and mediastinum can compress the SVC from mass effect or invade into the lumen of the SVC resulting in its obstruction. Several cases of SVC syndrome have been reported as a rare manifestation of sarcoidosis, in which the thoracic granuloma causes compression of the SVC [3–7].

The other cases of SVC syndrome, particularly in acute settings, have been attributed to thrombosis, resulting in intraluminal obstruction of the SVC. Thrombotic etiology of SVC syndrome has been recently reported to be on the rise due to an increased usage of intravascular devices, which are known to increase the risk of thrombotic events [1,2]. Spontaneous thrombosis of the SVC has also been reported in patients with hypercoagulable states or malignancies as a paraneoplastic manifestation [8–12]. While sarcoidosis has been associated with hypercoagulation [13], SVC syndrome caused by venous thrombosis in the setting of sarcoidosis, cancer, and a venous catheter has not been reported previously.

Here, we present the case of a patient with a history of thoracic sarcoidosis, who developed pancreatic adenocarcinoma and whose treatment course with systemic chemotherapy was complicated with multiple thrombotic events leading to SVC syndrome. This represents the first reported case in which recurrent SVC syndrome caused by venous thrombosis may be attributed to multiple predisposing factors that concurrently exist in the individual patient.

## 2. Materials and Methods

This is a retrospective review of the electronic health record, images, and histopathology at our institution. We have obtained the written informed consent of the patient's spouse since the patient is deceased. The Human Subjects Protection Office of the Penn State Health Milton S. Hershey Medical Center determined that this case report does not meet the definition of human subject research as defined in 45 CFR 46.102 (d) and/or (f); Institutional Review Board (IRB) review and approval is not required. Review of the literature on the associations among sarcoidosis, malignancy, hypercoagulability, and SVC syndrome was conducted.

## 3. Case Presentation

A 66-year-old Caucasian woman presented with acholic stool and dark, tea-colored urine accompanied with a feeling of discomfort in the posterior thoracic region. She reported an unintentional weight loss of 15 pounds over 5 months. Her past medical history included thoracic sarcoidosis previously treated with steroid medication by her primary care physician, non-insulin dependent diabetes mellitus, hyperlipidemia, hypertension, gastroesophageal reflux disease, and allergic rhinitis. She denied any history of smoking cigarettes or consuming alcohol. Her family history was notable for a brother with lung cancer and prior asbestos exposure; otherwise, she did not have any known family history of pancreatic cancer, sarcoidosis, or thrombotic disorder. Her home medications included azelastine spray pump, diclofenac sodium, glipizide, lisinopril, loratadine, magnesium oxide, metformin, omeprazole, and simvastatin.

Upon physical examination, the patient appeared in no acute distress and had a pleasant mood. Blood pressure was 188/93, heart rate 105 beats per minutes. Sclera were slightly icteric, and skin mildly jaundiced. Lungs were clear to auscultation. A soft systolic murmur was appreciated in her right upper chest. Bowel sounds were normal, the abdomen was soft and non-tender, and no hepatosplenomegaly or mass was palpated. There was no peripheral edema, with an unremarkable remaining physical examination.

The laboratory results were notable for elevated total bilirubin 3.2 mg/dL (normal 0–1.2 mg/dL), aspartate aminotransferase 278 U/L (normal 0–32 U/L), alanine aminotransferase 320 U/L (normal 0–33 U/L), and alkaline phosphatase 424 U/L (normal 35–115 U/L). Glucose was found to be elevated at 307 mg/dL (normal 70–100 mg/dL). An intravenous (IV) contrast-enhanced CT scan of the chest, abdomen and pelvis showed a mass in the pancreatic head. In the chest, calcified nodules in the lungs and calcified mediastinal lymph nodes were present, representing non-specific sequela of a prior granulomatous process and consistent with the known history of sarcoidosis (Figure 1). Endoscopic

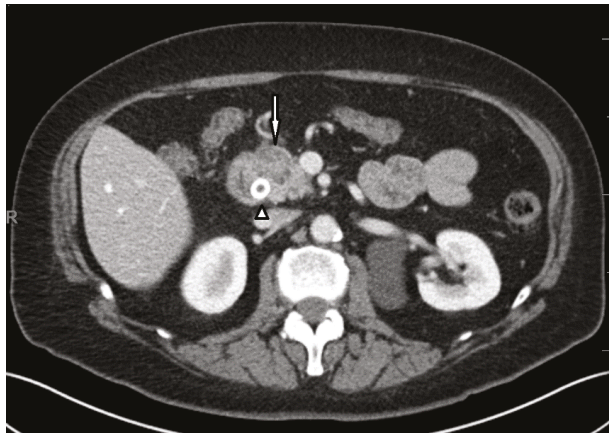
retrograde cholangiopancreatography (ERCP) was performed for the pancreatic mass, and it showed a high-grade, malignant-appearing stricture. She underwent a biliary sphincterotomy and placement of a metal biliary stent in the common bile duct. Endoscopic ultrasonography showed a hypoechoic mass measuring 29.5 × 24.5 mm in the pancreatic head with invasion into the portal vein and proximal portion of the duodenum along with peri-pancreatic lymphadenopathy. Fine-needle aspiration of the pancreatic mass revealed malignant cells consistent with pancreatic ductal adenocarcinoma.

Considering her uncontrolled diabetes mellitus, high serum level of CA 19-9 (4511 U/mL; normal 0–36 U/mL), and vascular involvement by the pancreatic mass, it was decided that the patient would receive neoadjuvant chemotherapy and then be re-evaluated for surgical resection of tumor. A double-lumen MediPort was placed in the right internal jugular vein, with the catheter ending at the junction between SVC and right atrium. She started to receive neoadjuvant chemotherapy with oxaliplatin, irinotecan, leucovorin, and 5-fluorouracil (FOLFIRINOX).

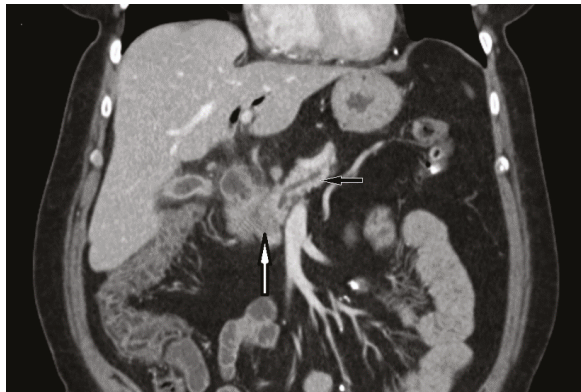
One week following the initiation of the first cycle of chemotherapy, the patient presented with a non-neutropenic fever (102 °F). Diagnostic evaluation with labs, cultures, urinalysis, and a chest x-ray was unremarkable, and the fever was resolved with acetaminophen. However, approximately two weeks later, she again presented to the Emergency Department (ED) with non-neutropenic fever (102.2 °F). Blood cultures grew *Klebsiella pneumoniae*, and the urine culture was positive for >100,000 colonies of Group B streptococci. The patient was treated with a course of piperacillin and tazobactam and subsequently discharged with levofloxacin and metronidazole.

Approximately three months after starting chemotherapy, she presented to the ED with new symptoms of dyspnea, facial edema, flushing of the neck, and fatigue. Physical examination was remarkable for peri-orbital and facial edema, plethora of the upper chest and neck, distention of superficial veins in the neck, and edema in the bilateral upper extremities. An IV contrast-enhanced CT scan of the chest showed a thrombus around the port catheter involving the SVC (Figure 2), while a CT scan of the neck showed no thrombosis in the internal jugular veins. Venous duplex imaging showed acute, non-occlusive thrombosis in the bilateral cephalic veins (Figure 3). These physical and radiological findings were consistent with SVC syndrome. Blood tests for hypercoagulation were not conducted. Vascular surgery was consulted and determined that no acute surgery was required as the thrombus was non-occlusive. The patient was initially anti-coagulated using IV bolus and infusion of heparin to achieve therapeutic activated partial thromboplastin time (aPTT, 60–80 s). As her edema improved, she was subsequently treated with enoxaparin (1 mg/kg) 80 mg subcutaneously every 12 h and discharged with instructions to continue this anti-coagulation regimen.

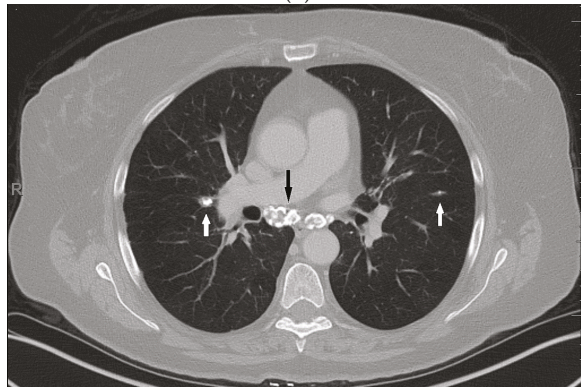
Twenty-three days later, the patient again presented to the ED, now with abdominal pain and non-bloody emesis. She was found to have a fever (102 °F) and hypotension, the latter of which improved with 2 L of normal saline. An IV contrast-enhanced CT scan of the abdomen showed fat stranding near the common bile duct stent and features of cholangitis. Blood cultures were positive for *Enterobacter cloacae*. The patient was treated with cefepime, metronidazole, and vancomycin and enoxaparin was temporarily discontinued in preparation for endoscopy. ERCP showed worsening biliary tract obstruction caused by a mass in the lower third of the main duct, and a new biliary stent was placed in the common bile duct. Transthoracic echocardiogram showed no evidence of endocarditis. Surveillance blood cultures were negative, and she was discharged to home with levofloxacin, metronidazole, and instructions to continue enoxaparin 80 mg subcutaneously every 12 h for anti-coagulation.



(a)



(b)



(c)

**Figure 1.** Axial (a) and coronal (b) intravenous contrast-enhanced CT scans of the chest, abdomen, and pelvis at initial presentation show a 3.1 × 2.1 cm hypo-enhancing mass in the head of the pancreas (white arrows) with mild upstream pancreatic ductal dilatation and parenchymal atrophy (black arrow). The dilated biliary tree has been decompressed via a metal common bile duct stent (white arrow head); (c) Images through the chest on lung windows show calcified mediastinal lymph nodes (black arrow) and calcified pulmonary nodules (white arrows)—non-specific sequela of prior granulomatous process, including sarcoid.

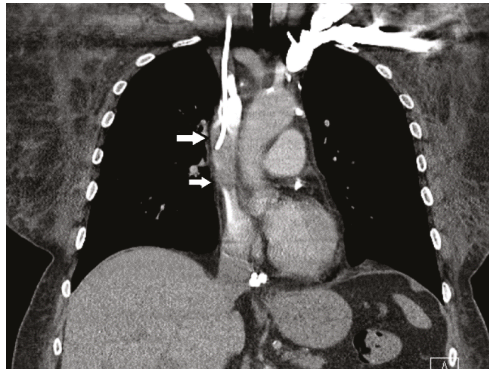


**Figure 2.** An IV contrast-enhanced CT scan of the chest timed to evaluate the superior vena cava shows a thrombus along the port catheter (white arrows) involving up to half of the lumen, shown on coronal reconstruction. There is a small amount of the thrombus within the right atrium (not shown).

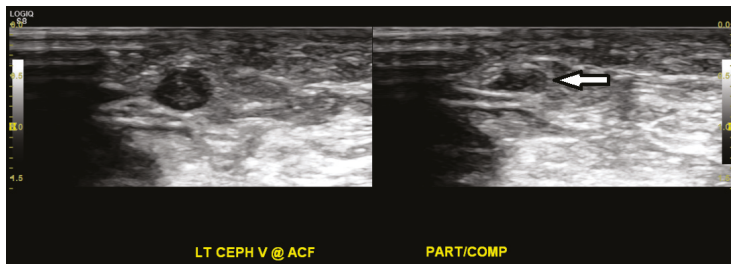
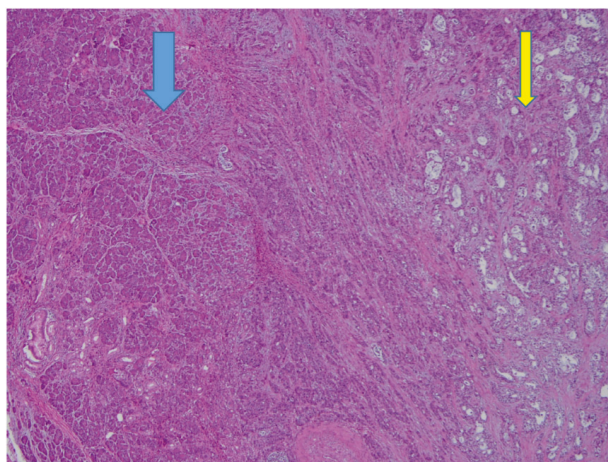


**Figure 3.** Ultrasound venous duplex imaging of the bilateral upper extremities shows echogenic, non-compressible material in the left cephalic vein, representing acute, non-occlusive thrombosis (white arrow), and also in the right cephalic vein in the distal arm (not shown).

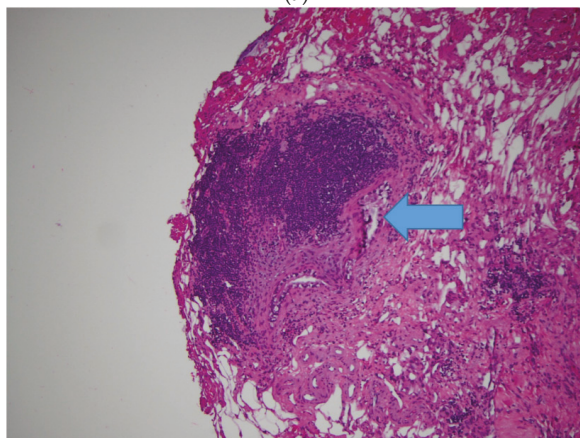
Upon completion of five cycles of FOLFIRINOX, the CA 19-9 level had reduced to 342.2 U/mL. Restaging CT scans with IV contrast showed that the known primary pancreatic lesion and the previously identified thrombus around the port catheter involving the SVC were no longer visualized. Treatment with enoxaparin was discontinued and the patient underwent pancreaticoduodenectomy (Whipple resection). Pathology of the surgical specimen revealed ductal adenocarcinoma in the pancreatic head and two lymph nodes (Figure 4). A double-lumen peripherally inserted central catheter (PICC) was placed in the left basilic vein with the final tip position in the SVC for total parenteral nutrition due to oral intolerance of diet. Three weeks later, she presented to the ED with edema and pain in the right upper extremity. Venous duplex ultrasound imaging of the right upper extremity did not reveal any deep or superficial vein thrombus.

One month following Whipple resection, the patient started receiving adjuvant chemotherapy using gemcitabine and capecitabine. Two and a half weeks later, she presented to the ED with peri-orbital edema, a distended superficial vein on the left side of the neck, as well as edema in the face, neck, and bilateral upper extremities. The serum levels of both D-dimer (2.56  $\mu\text{g/mL}$ ; normal  $< 0.54 \mu\text{g/mL}$ ) and fibrinogen (443 mg/dL; normal 208–435  $\mu\text{g/mL}$ ) were elevated, and these findings are consistent with a thrombotic state. Venous duplex ultrasound imaging showed acute, partially occlusive thrombus in the left subclavian vein and the left basilic vein surrounding an indwelling venous catheter (Figure 5). A CT scan of the neck, chest, abdomen, and pelvis with IV contrast showed a thrombus along the left-sided PICC in the left brachiocephalic vein, a small thrombus in the lower SVC, and new hypodense lesions in the liver (Figure 6). The physical examination and radiological findings were consistent with recurrent SVC syndrome, the PICC was subsequently

removed, and the patient was treated with IV bolus and infusion of heparin. Upon improvement of the edema, her anti-coagulation was converted to enoxaparin (1 mg/kg) 70 mg subcutaneously every 12 h with instructions to continue this regimen for prophylaxis.



(a)



(b)

**Figure 4.** Pancreaticoduodenectomy (Whipple resection) and partial pancreatectomy. (a) Pancreas, 40×, hematoxylin and eosin (H&E) stain. The blue arrow indicates normal pancreatic parenchyma; the yellow arrow indicates moderately differentiated adenocarcinoma, characterized by infiltrating glands. (b) Lymph node, 100×, H&E stain. Lymph node with metastatic adenocarcinoma (blue arrow indicates metastasis).

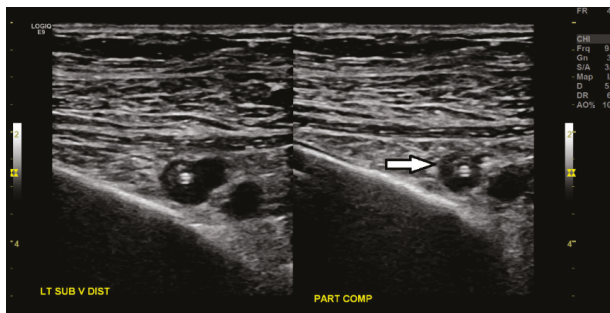
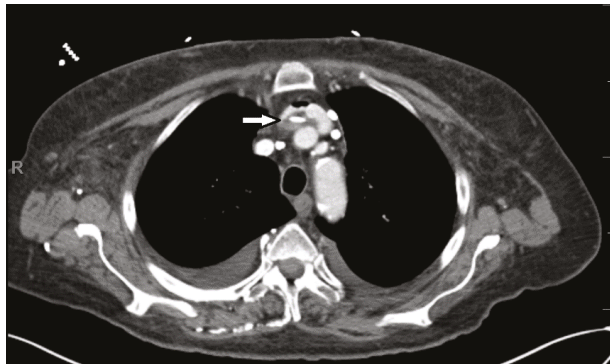
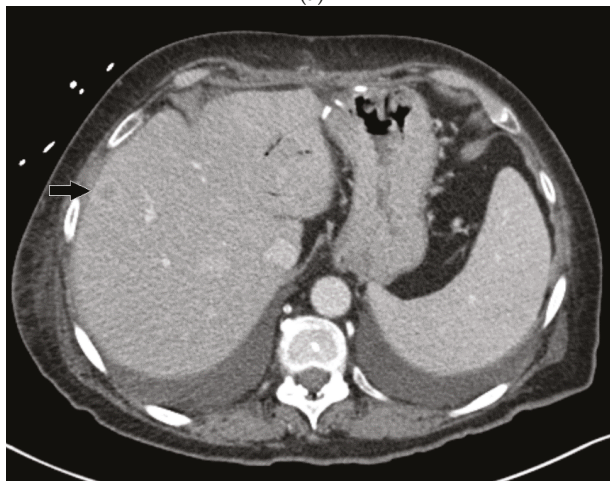


**Figure 5.** Ultrasound venous duplex imaging of the bilateral upper extremities shows an acute, partially occlusive deep-vein thrombus within the left subclavian vein along an indwelling venous catheter (white arrow).



(a)



(b)

**Figure 6.** IV contrast-enhanced CT scan of the neck, chest, abdomen, and pelvis shows (a) a left-sided catheter with surrounding hypodense thrombus in the left brachiocephalic vein (white arrow), and small thrombus in the lower superior vena cava (SVC) at the SVC/atrial junction (not shown). Trace amount of iatrogenic air is also present immediately anterior to the clot in the brachiocephalic vein. (b) New hypo-enhancing liver lesions are also present (the black arrow denotes one of them).



CT-guided biopsy of the hepatic lesion revealed malignant cells consistent with metastatic pancreatic ductal adenocarcinoma. Molecular profiling of the biopsied liver lesion was notable for a pathogenic mutation G12V in exon 2 of the *KRAS* gene (by Caris Life Sciences™). Furthermore, the CA 19-9 level began to trend upward (1256 U/mL). Considering disease progression with tumor metastasis, the patient started to receive palliative chemotherapy using nanoparticle albumin-bound (nab) paclitaxel and gemcitabine. Following three 28-day cycles of nab-paclitaxel and gemcitabine, an IV contrast-enhanced CT scan showed a decrease in the size of some of the hepatic lesions, but also the presence of new lesions. Additionally, CA 19-9 levels were trending upward, suggesting tumor progression, and nab-paclitaxel and gemcitabine were discontinued.

A palliative chemotherapeutic regimen consisting of liposomal irinotecan, leucovorin, and 5-fluorouracil was initiated. Following four 14-day cycles, CA 19-9 levels (>9000 U/mL) continued to rise, suggesting continued tumor progression. Chemotherapy was discontinued and the patient opted to pursue hospice care. She expired 18 days after discontinuation of chemotherapy. The timeline of the clinical events is illustrated in Figure 7.

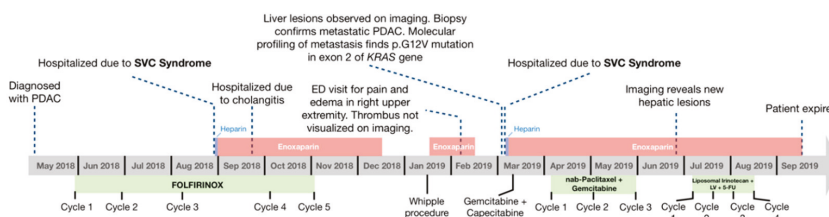


**Figure 7.** Timeline of major events during the course of the patient's treatment for pancreatic ductal adenocarcinoma (PDAC). Complications and notable findings on imaging are listed above the timeline, while the patient's chemotherapy regimens are indicated below.

#### 4. Discussion

In this case presentation, a patient with a history of thoracic sarcoidosis was diagnosed with pancreatic adenocarcinoma, who developed recurrent venous thrombosis causing SVC syndrome in the presence of indwelling venous catheters. Previous studies have suggested that sarcoidosis is associated with a hypercoagulable state and malignant diseases, including pancreatic adenocarcinoma [14–17]. This case report adds to the rare association of pancreatic adenocarcinoma with sarcoidosis. Moreover, to our knowledge, this represents the first reported case of SVC syndrome caused by venous thrombosis as a paraneoplastic manifestation of pancreatic cancer (Table 1). Since this patient has a diagnosis of pancreatic adenocarcinoma, which is known to be associated with a thrombotic state, a diagnostic evaluation for thrombophilia is not indicated.

While patients with cancer have increased thrombotic risk [18], most do not develop repeated and significantly symptomatic clots even in the presence of chronic indwelling lines. In agreement with this, the locations of multiple episodes of thrombosis in this patient do not always correlate with those of the venous catheters. The occurrence of repeated episodes of SVC syndrome in this patient can be related to the presence of multiple known risk factors of venous thrombosis. These include her underlying sarcoidosis, pancreatic adenocarcinoma, and systemic cytotoxic chemotherapy. While the exact pathogenic mechanism of sarcoidosis is unclear, this case report may help shed new light into the inter-relationship of sarcoidosis, pancreatic cancer, and venous thrombosis.

**Table 1.** SVC syndrome caused by intravascular thrombosis in association with malignancy.

Malignant disease	Age	Sex	Clinical Presentation of SVC Syndrome	Diagnosis of SVC Syndrome	Management	Reference
Pancreatic Adenocarcinoma	64	Female	Dyspnea, facial edema, flushing of neck, fatigue	Physical exam and IV contrast enhanced CT	IV heparin followed by enoxaparin	This Report
Soft Tissue Sarcoma	46	Female	Dyspnea, right arm pain, dysphagia	Spiral chest CT with contrast	Enoxaparin	[8]
Bronchogenic Carcinoma	55	Male	Dyspnea, edema of face, neck, and chest	Physical exam and Doppler ultrasonography	Low molecular weight heparin	[9]
Prostate Carcinoma	60	Male	Facial edema	Physical exam, contrast enhanced CT and MRI	Warfarin	[10]
Renal Cell Carcinoma	54	Male	Edema of face and neck	CT and MRI	IV Heparin	[11]
Ovarian Papillary Carcinoma	62	Female	Telangiectasias on face and anterior trunk	Thoracic CT	Acenocoumarol	[12]

Numerous studies have examined the link between sarcoidosis and the development of cancers [13,19–22]. A systematic meta-analysis of 16 observational studies found that the relative-risk of sarcoidosis patients developing any cancer was 1.19 (95% CI 1.07–1.32). The most common cancer sites were the skin, followed by hematopoietic organs, upper-digestive organs, kidney, liver, and colorectum [23]. The results of a cohort study by Søggaard, et al. indicated that patients with sarcoidosis have a 20% increased risk of being diagnosed with cancer 3 to 10 years following the initial diagnosis of sarcoidosis [24]. These studies suggest that sarcoidosis is indeed a risk factor for the development of cancer. An incidental diagnosis of pancreatic cancer in this reported patient with underlying sarcoidosis cannot be excluded. Further evidence will be needed to demonstrate or support a relationship between pancreatic cancer and sarcoidosis. Whether the aberrant immune system or other pathogenic factors of sarcoidosis contribute to its association with cancer, including pancreatic cancer, remains to be determined.

Venous thrombosis and SVC syndrome have also been reported as rare manifestations of sarcoidosis. SVC syndrome has been shown to result from the direct compression of SVC by sarcoidosis-associated granuloma or lymphadenopathy [4,5,7,25]. While the exact mechanism behind the increased risk of thrombosis in patients with sarcoidosis is unknown, a few mechanisms have been proposed [26]. Firstly, the local inflammatory profile of sarcoid lesions is hypothesized to alter factors associated with coagulability [27]. A correlation between the location of sarcoid lesions and the location of thrombus formation has been reported [28]. These anatomic relationships suggest that local inflammation produced by sarcoid lesions modifies the surrounding environment into a hypercoagulable state [26]. Secondly, sarcoid lesions may alter the surrounding hemodynamics, predisposing to clot formation. Disruption in laminar flow is a well-characterized risk factor for thrombus formation [29]. Lastly, patients with sarcoidosis may suffer from complications associated with chronic steroid therapy (osteoporosis, obesity, pulmonary hypertension, etc.) that result in impaired mobility [30]—a known risk factor for the development of deep-vein thrombosis.

## 5. Conclusions

In this case report, a patient with underlying thoracic sarcoidosis was diagnosed with pancreatic adenocarcinoma; she received cytotoxic systemic chemotherapy and developed recurrent venous thrombosis causing SVC syndrome in the presence of an indwelling venous catheter. This study provides further support for an inter-relationship among sarcoidosis, hypercoagulation, and cancer. Caution about venous thrombosis should be raised in cancer patients with additional risk factors such as sarcoidosis, and prophylactic anti-coagulation for those individuals may be warranted.

**Author Contributions:** Conceptualization, N.S.Y.; methodology, G.S., Y.K., K.N., K.L.M., F.R., and N.S.Y.; formal analysis, G.S., K.L.M., F.R., and N.S.Y.; data curation, G.S., K.L.M., F.R., and N.S.Y.; writing—original draft preparation, G.S., K.L.M., and N.S.Y.; writing—review and editing, G.S., Y.K., K.N., K.L.M., F.R., and N.S.Y.; supervision, N.S.Y. All authors have read and agreed to the published version of the manuscript.

**Funding:** This research received no external funding.

**Conflicts of Interest:** The authors declare no conflict of interest.

## References

1. Cheng, S. Superior vena cava syndrome. *Cardiol. Rev.* **2009**, *17*, 16–23. [[CrossRef](#)]
2. Khan, U.A.; Shanholtz, C.B.; McCurdy, M.T. Oncologic mechanical emergencies. *Hematol. Clin.* **2017**, *31*, 927–940. [[CrossRef](#)] [[PubMed](#)]
3. Morgans, W.E.; Al-Jilahawi, A.N.; Mbatha, P.B. Superior vena caval obstruction caused by sarcoidosis. *Thorax* **1980**, *35*, 397–398. [[CrossRef](#)] [[PubMed](#)]
4. Radke, J.R.; Kaplan, H.; Conway, W.A. The significance of superior vena cava syndrome developing in a patient with sarcoidosis. *Radiology* **1980**, *134*, 311–312. [[CrossRef](#)] [[PubMed](#)]
5. Brandstetter, R.; Hansen, D.; Jarowski, C.; King, T.; Barletta, A. Superior vena cava syndrome as the initial clinical manifestation of sarcoidosis. *Heart Lung J. Crit. Care* **1981**, *10*, 101–104.
6. Case Records of the Massachusetts General Hospital. Weekly clinicopathological exercises. Case 11-1984. Long-standing sarcoidosis with the recent onset of the superior-vena-cava syndrome. *N. Engl. J. Med.* **1984**, *310*, 708–716. [[CrossRef](#)]
7. McPherson, J.G., III; Yeoh, C.B. Rare manifestations of sarcoidosis. *J. Natl. Med. Assoc.* **1993**, *85*, 869–872.
8. Ghorbani, H.; Vakili Sadeghi, M.; Hejazian, T.; Sharbatdaran, M. Superior vena cava syndrome as a paraneoplastic manifestation of soft tissue sarcoma. *Hematol. Transfus. Cell Ther.* **2018**, *40*, 75–78. [[CrossRef](#)]
9. Santra, A.; Nandi, S.; Mondal, S.; Chakraborty, S. Superior vena cava syndrome due to thrombosis: A rare paraneoplastic presentation of bronchogenic carcinoma. *Iran. J. Med. Sci.* **2016**, *41*, 354–358.
10. Takeda, T.; Saitoh, M.; Takeda, S. Superior Vena Cava Syndrome Caused by an Intravascular Thrombosis Due to Underlying Prostate Carcinoma. *Intern. Med.* **2008**, *47*, 2007–2010. [[CrossRef](#)]
11. May, M.; Seehafer, M.; Helke, C.; Uberruck, T.; Gunia, S.; Hoschke, B. V.-cava-superior-syndrom mit beidseitiger jugularis- und subklaviavenenthrombose. *Der Urol. A* **2003**, *42*, 1374–1377. [[CrossRef](#)] [[PubMed](#)]
12. Padovani, M.; Tillie-Leblond, I.; Vennin, P.; Demarcq, G.; Wallaert, B. Paraneoplastic superior vena cava thrombosis disclosing an ovarian tumor. *Rev. Mal. Respir.* **1996**, *13*, 598–600. [[PubMed](#)]
13. Ungprasert, P.; Crowson, C.S.; Matteson, E.L. Risk of malignancy among patients with sarcoidosis: A population-based cohort study. *Arthritis Care Res.* **2017**, *69*, 46–50. [[CrossRef](#)]
14. Maradona Hidalgo, J.A.; Alvarez Alvarez, C.; Fernández Rippe, M.L.; Suárez García, E.; Soler Sánchez, T. Sarcoidosis, pancreatic adenocarcinoma and granulomas of undetermined origin in a patient with xeroderma pigmentosum. *Rev. Clin. Esp.* **1983**, *168*, 357–360. [[PubMed](#)]
15. Mao, J.T.; Fisnbein, M.C. Metastatic pancreatic cancer masquerading as pulmonary sarcoidosis. *Am. J. Med.* **2000**, *109*, 598–599. [[CrossRef](#)]
16. Goto, T.; Toyama, H.; Asari, S.; Terai, S.; Mukubou, H.; Shirakawa, S.; Nanno, Y.; Mizumoto, T.; Kinoshita, H.; Tanaka, M.; et al. A case of pancreatic cancer with multiple lymph node swelling caused by sarcoidosis. *Gan Kagaku Ryoho.* **2017**, *44*, 1886–1888.
17. Gupta, K.; Hassan, T.; Rizwan, S.; Hans, B.; Jawale, R.; Desilets, D. Hepatic sarcoidosis complicated with pancreatic adenocarcinoma. *Case Rep. Hepatol.* **2019**, *2019*, 1–4. [[CrossRef](#)]
18. Fernandes, C.J.; Morinaga, L.T.K.; Alves, J.L.; Castro, M.A.; Calderaro, D.; Jardim, C.V.P.; Souza, R. Cancer-associated thrombosis: The when, how and why. *Eur. Respir. Rev.* **2019**, *28*, 180119. [[CrossRef](#)]
19. Rømer, F.K.; Hommelgaard, P.; Schou, G. Sarcoidosis and cancer revisited: A long-term follow-up study of 555 Danish sarcoidosis patients. *Eur. Respir. J.* **1998**, *12*, 906–912. [[CrossRef](#)]
20. Askling, J.; Grunewald, J.; Eklund, A.; Hillerdal, G.; Ekbo, A. Increased risk for cancer following sarcoidosis. *Am. J. Respir. Crit. Care Med.* **1999**, *160*, 1668–1672. [[CrossRef](#)]
21. Ji, J.; Shu, X.; Li, X.; Sundquist, K.; Sundquist, J.; Hemminki, K. Cancer risk in hospitalized sarcoidosis patients: A follow-up study in Sweden. *Ann. Oncol.* **2009**, *20*, 1121–1126. [[CrossRef](#)] [[PubMed](#)]

22. Le Jeune, I.; Gribbin, J.; West, J.; Smith, C.; Cullinan, P.; Hubbard, R. The incidence of cancer in patients with idiopathic pulmonary fibrosis and sarcoidosis in the UK. *Respir. Med.* **2007**, *101*, 2534–2540. [[CrossRef](#)]
23. Arkema, E.V.; Cozier, Y.C. Epidemiology of sarcoidosis: Current findings and future directions. *Ther. Adv. Chronic Dis.* **2018**, *9*, 227–240. [[CrossRef](#)] [[PubMed](#)]
24. Søgaard, K.K.; Sværke, C.; Thomsen, R.W.; Nørgaard, M. Sarcoidosis and subsequent cancer risk: A Danish nationwide cohort study. *Eur. Respir. J.* **2015**, *45*, 269. [[CrossRef](#)]
25. Gordonson, J.; Trachtenberg, S.; Sargent, E.N. Superior vena cava obstruction due to sarcoidosis. *Chest* **1973**, *63*, 292–293. [[CrossRef](#)] [[PubMed](#)]
26. Bonifazi, M.; Bravi, F.; Gasparini, S.; La Vecchia, C.; Gabrielli, A.; Wells, A.U.; Renzoni, E.A. Sarcoidosis and cancer risk: Systematic review and meta-analysis of observational studies. *Chest* **2015**, *147*, 778–791. [[CrossRef](#)] [[PubMed](#)]
27. Geremek, A.G.; Tomkowski, W.; Geremek, M.; Puścińska, E.; Małek, G.; Nowiński, A.; Bednarek, M.; Śliwiński, P. Sarcoidosis as a risk factor for venous thromboembolism. *Sarcoidosis Vasc. Diffus. Lung Dis. Off. J. WASOG* **2017**, *34*, 170–178. [[CrossRef](#)]
28. Goljan-Geremek, A.; Geremek, M.; Puscinska, E.; Sliwinski, P. Venous thromboembolism and sarcoidosis: Co-incidence or coexistence? *Cent. J. Immunol.* **2015**, *40*, 477–480. [[CrossRef](#)]
29. Hathcock, J.J. Flow effects on coagulation and thrombosis. *Arterioscler. Thromb. Vasc. Biol.* **2006**, *26*, 1729–1737. [[CrossRef](#)]
30. Gerke, A.K. Morbidity and mortality in sarcoidosis. *Curr. Opin. Pulm. Med.* **2014**, *20*, 472–478. [[CrossRef](#)]



© 2020 by the authors. Licensee MDPI, Basel, Switzerland. This article is an open access article distributed under the terms and conditions of the Creative Commons Attribution (CC BY) license (<http://creativecommons.org/licenses/by/4.0/>).





Review

# Oral Manifestations of Inflammatory Bowel Disease and the Role of Non-Invasive Surrogate Markers of Disease Activity

Davide Giuseppe Ribaldone <sup>1,\*</sup>, Selvaggia Brigo <sup>2</sup>, Michela Mangia <sup>1</sup>, Giorgio Maria Saracco <sup>1</sup>, Marco Astegiano <sup>3</sup> and Rinaldo Pellicano <sup>3</sup>

<sup>1</sup> Department of Medical Sciences, University of Turin, 10126 Turin, Italy; mickela.89.mm@gmail.com (M.M.); giorgiomaria.saracco@unito.it (G.M.S.)

<sup>2</sup> Bow Lane Dental Group, St George's Hospital, Bupa Dental Care, London SW17 0QT, UK; selvy.brigo@gmail.com

<sup>3</sup> Unit of Gastroenterology, Molinette Hospital, 10126 Turin, Italy; marcoastegiano58@gmail.com (M.A.); rinaldo\_pellican@hotmail.com (R.P.)

\* Correspondence: davidegiuseppe.ribaldone@unito.it

Received: 11 May 2020; Accepted: 15 June 2020; Published: 16 June 2020

**Abstract:** Inflammatory bowel disease (IBD), which includes Crohn's disease (CD) and ulcerative colitis (UC), can be associated with several extra-intestinal manifestations requiring a multidisciplinary management both in terms of work-up and therapy. Oral lesions are common in patients with IBD, with a prevalence ranging from 5% to 50%. These can represent an oral location of IBD as well as a side-effect of drugs used to treat the intestinal disease. Oral manifestations, occurring in patients with IBD, can be divided in nonmalignant, specific, and non-specific ones, and malignant lesions. While there is undoubtedly a need to search for an IBD in patients with oral lesions associated with intestinal symptoms, the work-up of those with an exclusive oral lesion should be personalized. Fecal calprotectin is a non-invasive marker of intestinal inflammation and may be used to select which patients need to undergo endoscopic examination, thereby avoiding unnecessary investigations. The pharmacological armamentarium to treat oral lesions associated with IBD includes topical or systemic corticosteroids, immunosuppressive agents, and biologic drugs.

**Keywords:** inflammatory bowel disease; Crohn's disease; ulcerative colitis; extra-intestinal manifestations; orofacial granulomatosis; tag-like lesions; cobblestoning; mucogingivitis; lip swelling; aphthous stomatitis

---

## 1. Introduction

Inflammatory bowel disease (IBD) comprises chronic heterogeneous disorders of unknown etiology, resulting from multifactorial environmental precipitants in genetically susceptible individuals [1]. IBD are distinguished in two main phenotypes, Crohn's disease (CD) and ulcerative colitis (UC), characterized by inflammation of the intestinal mucosa [2]. While UC affects the rectum and a variable extent of the colon, CD can involve any location of the gastrointestinal (GI) tract, from the oral cavity to the anus. Furthermore, up to 36% of patients with IBD may have extra-intestinal manifestations (EIM) [3–5] which can affect almost any organ of the body (eyes, joints, liver, pancreas, skin, blood, and mouth) [6,7].

The pathogenesis of IBD and EIM remain to be elucidated. Common genetic background (IBD1 gene [8], MHC allele HLADRB1\*0103 [9], ABCB1 gene [10]) between the two conditions may be the predisposing cause, but the detailed mechanisms remain unknown, especially because the environmental triggers responsible for disease onset have not been elucidated. In fact, although many factors (such as infectious agents, diet, drugs, smoking) have been investigated, a precise causal agent, or a cluster of agents, has not been identified. In the last few years, a role of GI microbiota in the

pathogenesis of IBD has been proposed [11]. The human GI microbiota consists of a wide variety of bacteria, viruses, fungi and other single-celled organisms. Although bacteria belong to four phyla (Firmicutes, Bacteroidetes, Proteobacteria, and Actinobacteria) the majority are from either Firmicutes or Bacteroidetes [12]. It remains to be clarified, in IBD patients, if there is a decrease in microbial diversity as a consequence of intestinal changes, or if this could play a role in the pathogenesis of these diseases. Because of the potential wide spectrum of involvement and of the genetic commonalities, it has been hypothesized that IBD represents a systemic disease with a predominantly intestinal manifestation [13].

## 2. Oral Lesions in Patients with IBD

The first cases of oral IBD manifestations were described in 1969 in two patients with CD [14]. In the last 50 years, the prevalence of oral lesions in patients with IBD has been reported to range from 5% to 50%, according to heterogeneous studies [15,16]. This wide range could be due to various reasons: first, the heterogeneity of the studies, including patients of different ages, ethnicities, and genetic backgrounds; second, the authors' level of experience; third, the variability in the definition of lesions. The latter, in fact, could be a specific IBD lesion, but could also have iatrogenic origin, due to the drugs used to treat IBD.

The prevalence of oral manifestations is higher in males and in children [16]. The higher incidence of upper GI tract involvement in children with CD, compared to adults, could explain the higher prevalence of oral lesions in pediatric CD [17]. Although oral lesions are generally more prevalent in CD (20–50%) [18] than in UC (8%) patients, in some studies a significant difference was not observed [19]. Moreover, in adult CD patients, the prevalence rate of oral manifestations is higher in those with upper GI tract involvement and perianal disease [20].

Oral manifestations can occur either concomitantly with intestinal symptoms or before the presentation of IBD. In 60% of these patients, oral lesions may be the primary presenting sign, preceding GI manifestations [21,22]. Although the oral mucosa lesions and oral symptoms can be more severe during disease activity period, the correlation is not universal, and up to 30% of affected patients continue to suffer active oral manifestations (especially in the pediatric age group) despite remission of IBD [23]. Oral IBD manifestations can be divided into specific and not-specific lesions (Table 1), according to the presence of granulomas noted on the histopathology examinations [19,24]. It should be highlighted that some of these lesions can be considered an oral location of IBD while others are the result of nutritional deficiencies secondary to intestinal malabsorption.

**Table 1.** Specific oral lesions in patients with inflammatory bowel disease (IBD).

Lesion	Location	Features
Cobblestoning	Posterior buccal mucosa	Fissured swollen mucosa with corrugation and hyperplastic
Indurated tag-like lesions	Labial and buccal vestibules; retromolar region	Hyperplastic edge firm or boggy
Mucogingivitis	Whole gingiva	Gingiva edematous, granular and hyperplastic
Others:		
Lip swelling with vertical fissures	Lips, tongue, buccal sulci, face	
Deep linear ulceration		
Edema of the face		

For IBD, and for its oral manifestations, the pathogenesis remains unclear. Parallel to what has been reported on the potential role of microbiota in the pathogenesis of IBD and its oral location, it has been proposed that dysbiosis (term that means imbalance within the bacterial community) of salivary microbiota (with relative abundance of *Streptococcus*, *Prevotella*, *Haemophilus*, and *Veillonella*) may play a crucial role [25].

### 3. Specific Oral Lesions

Specific oral lesions are less common than non-specific ones. The main feature of specific lesions is the presence of non-caseous granulomas, observed only in patients with CD (CD with concomitant orofacial granulomatosis) [26]. Granulomas consist of a core of activated macrophages, some of which merge to form giant cells, surrounded by lymphocytes and fibrotic tissue. Granulomas are found in only 24–61% of patients with CD, whereas in those with orofacial granulomatosis, granuloma formation in the oral lesions occurs in 70–100% of cases, irrespective of coexisting CD. It has been reported that CD with concomitant orofacial granulomatosis is frequently associated with perianal lesions; furthermore, children with CD and concomitant orofacial granulomatosis show a more extensive disease phenotype and proximal GI tract involvement than CD patients with intestinal inflammation only [27].

The differential diagnosis should consider that granulomatous oral lesions can also occur in other diseases, including orofacial granulomatosis, sarcoidosis, mycobacterial infection, and foreign-body reactions.

The specific oral lesions include indurated tag-like lesions, cobblestoning, mucogingivitis, lip swelling with vertical fissures, and deep linear ulcerations (Table 1).

#### 3.1. Clinical Characteristics

In cobblestoning, fissured swollen buccal mucosa with corrugation and hyperplastic appearance of the mucosa resemble a “cobblestone”. These lesions are usually detected in the posterior buccal mucosa and consist of mucosal-colored papules that produce firm plaques on the buccal mucosa and palate. In addition, indurated polypoid fringe-like lesions can be observed in the vestibule and in the retromolar region. Such lesions may cause pain and make speaking and eating difficult [28].

Mucosal tags and deep linear ulcerations (lip and tongue fissures) have hyperplastic edges, which can be firm or boggy to palpation. Attached gingiva and alveolar mucosa can become granulated, swollen, and hyperplastic with or without ulcerations. These lesions are mostly present in the labial and buccal vestibules and in retromolar regions.

In the setting of specific lesions, edema of the face, of one or both lips, and of the buccal mucosa has been described. The lips are the most commonly affected, and they are usually painless, tender, and firm to palpation [29]. Painful vertical fissures can occur in numerous patients with swollen lips; many microorganisms can be isolated in lip fissures [30].

Mucogingivitis can be present. The gingiva appears edematous, granular, and hyperplastic in CD, with or without ulcerations. The whole gingiva up to the mucogingival line might be involved [31].

A rare manifestation of CD could be represented by autoimmune changes of the minor salivary glands and dry mouth [32]. Chronic inflammatory processes near the parotid duct result in partial to total duct obstruction and cause dilated ducts and cyst formation, which can lead to the formation of cutaneous fistulas. All these changes can also lead to a reduction in saliva production and dry mouth [33].

Other specific manifestations include granulomatous cheilitis, macrocheilia, and palatal ulcer. In case of granulomatous cheilitis the main change is a chronic granulomatous inflammation, with edema and lumpy swelling of the lips.

#### 3.2. Diagnosis

The differential diagnosis of specific oral lesions includes syndromes presenting with multiple mucosal swellings, such as multiple hamartoma syndrome (Cowden disease), multiple endocrine neoplasia (MEN) 2B/III, neurofibromatosis, and idiopathic orofacial granulomatosis.

In the case of histologically confirmed oral granulomatous, the differential diagnosis includes foreign body reaction, allergic reaction to benzoate or cinnamon, and idiopathic orofacial granulomatosis. Systemic conditions associated with granulomatous inflammation include deep fungal infections, mycobacterial infections, sarcoidosis, and tertiary syphilis.



#### 4. Non-Specific Oral Lesions

Non-specific oral lesions (Table 2) occur more frequently than specific lesions, so differential diagnosis can be difficult. These lesions may occur as result of chronic inflammation, malnutrition and malabsorption syndrome, or as a side effect of pharmacological treatment.

**Table 2.** Non-specific oral lesions in patients with IBD.

Lesion	Location	Features
Aphthous stomatitis	Anywhere in the oral cavity	Shallow round ulcerations with central fibrinous exudate surrounded by an erythematous border
Pyostomatitis vegetans	Labial gingiva, buccal and labial mucosa; less common: tongue, soft and hard palate	Erythematous and thickened oral mucosa with multiple pustules and superficial erosions
Angular cheilitis	Corner of the oral cavity	Erythema at the corners of the mouth with or without painful fissures and sores
Others:		
Glossitis		
Periodontitis and dental caries	Oral mucosa, gingiva, tongue, teeth, periodontal tissue,	
Perioral dermatitis	alveolar bone, perioral skin, palate,	
Recurrent buccal abscesses	lips, lymph nodes, salivary glands	
Submandibular lymphadenopathy		
Salivary duct fistula		

Patients with IBD and EIM may suffer from recurrent aphthous stomatitis more often than others; these lesions may occur in up to 10% of patients with UC and up to 20–30% of patients with CD [34]. Aphthae are shallow, round ulcerations with central fibrinous exudate surrounded by an erythematous border (“halo”). Aphthous stomatitis are not specific for IBD and may be observed in several other disorders including celiac sprue, human immunodeficiency virus (HIV)/acquired immune deficiency syndrome, autoimmune rheumatic disease (lupus, Bechet’s disease and Reiter’s syndrome), infections (herpes virus, cytomegalovirus), autoimmune bullous diseases, and common aphthae seen in the normal population.

Angular cheilitis is characterized by erythema at the corners of the mouth with or without painful fissures and sores. It can be a consequence of anemia or fungal and bacterial infections [35].

Pyostomatitis vegetans (PV) is a rare, benign, chronic, mucocutaneous ulcerative disorder, considered the oral equivalent of pyodermitis vegetans of the skin [36]. There is a frequent association between PV and IBD; it occurs in patients with UC more commonly than in those with CD and, in the former, is considered a specific marker of disease activity [37]. PV is characterized by erythematous and thickened oral mucosa with multiple pustules and superficial erosions. Multiple white or yellow pustules may rupture, and form folded, fissured appearances resembling a “snail-track”. The most affected areas are the labial gingiva, buccal and labial mucosa, and soft and hard palate. PV may present with oral ulcers (with possibly oral malodor). The differential diagnosis includes autoimmune pemphigoid diseases and infections [38]. The diagnosis of PV is based on the result of biopsy specimen obtained from the affected area. Microscopic sections show intraepithelial clefting and acantholysis. Within the spinous layer, the accumulation of eosinophils (intraepithelial abscesses) are also seen. The underlying connective tissue demonstrates the infiltration of mixed inflammatory cells [39]. Some authors have suggested that PV belongs to the spectrum of neutrophilic dermatoses or even represents an oral form of pyoderma gangrenosum [40].

In patients with IBD, caries and periodontal disease occur with a higher prevalence than in those without IBD. This is supported by the results of a meta-analysis, reporting that the risk of periodontitis is significantly increased in IBD compared to the control group and that it is more pronounced in UC than in

CD [41]. In addition, the severity and extent of periodontitis is greater in IBD patients when compared to healthy controls [42], probably in association with the high expression of interleukin (IL)-18 in the serum of IBD patients with periodontitis [43]. The pathogenesis of periodontal disease, similar to that of IBD, involves local pathogens and the host immune-inflammatory response, and is influenced by genetic and environmental factors [44]. The increase in dental caries risk is thought to be associated to dietary habits, changes in saliva and microbiological conditions of the oral cavity, and deficient intestinal absorption of food substances. The malabsorption of vitamin D, which is common in IBD patients [45], may possibly be related to the complex multifactorial etiopathology of dental caries [46].

Other non-specific oral manifestations of IBD include stomatitis, glossitis, odynophagia and dysphagia, perioral dermatitis, diffuse pustules and non-specific gingivitis, lichenoid reactions, candidiasis, gingival hyperplasia, papillomatosis of the oral mucosa, pemphigus vegetans, persistent submandibular lymphadenopathy, recurrent buccal abscesses, and metallic dysgeusia [47].

## 5. Malignant Oral Manifestations

It is well-known that oral cancer is linked to several risk factors such as alcohol consumption, tobacco smoking, the male gender, and an age over 40 [48]. Furthermore, patients undergoing organ transplantation, especially in case of prolonged immunosuppression and those with HIV infection have an increased risk of developing oral cancer [49].

Oral cancer has a poor prognosis, with a 5-year survival <50%, higher for lip and lower for tongue and gingiva. Precancerous lesions are oral lichen planus, leukoplakia, erythroplakia, and erythroleukoplakia. In patients with IBD, oral cancerous and precancerous lesions have been reported. In particular, a higher risk of oral cavity tumors, especially of the tongue, has been reported in IBD patients compared to controls; furthermore, female have a higher risk than males. Based on the published literature, it is evident that patients with IBD are at high risk for developing these lesions, a phenomenon amplified by the increasing human papillomavirus (HPV) prevalence [50] reported in this population. The role of immunosuppression, considering that all the drugs used to treat IBD could be in theory involved in carcinogenic processes, remains to be defined.

## 6. Diagnosis of IBD in Patients with Oral Manifestation

When an oral manifestation occurs, the presence of IBD should be suspected, even in absence of GI symptoms. Because oral lesions can precede the onset of IBD, a cooperation between specialists in oral medicine and gastroenterologists is required in order to allow an early diagnosis.

The diagnosis of IBD requires evaluation and a combination of clinical, laboratory, radiological, endoscopic, and pathological data [1]. Currently, an endoscopic examination with a colonoscopy and multiple biopsies is the gold standard to confirm IBD diagnosis. This procedure defines the extent and severity of mucosal involvement and allows biopsies collection for histological examination. Colonoscopy also enables the assessment of suspected stenosis in the distal ileum. However, it is considered an invasive and expensive procedure [51]. Imaging techniques for the diagnosis of suspected IBD include ultrasonography (US), computed tomography (CT) scanning, and magnetic resonance imaging (MRI) [52]. US is an accurate diagnostic tool to detect suspected CD and to evaluate disease activity (sensitivity 84%, specificity 92%); it is a widely available and non-invasive technique, but its accuracy is lower for the disease proximal to the terminal ileum [53]. MRI is a technique with a high accuracy for diagnosis and assessment of extension and activity of the disease (sensitivity 93%, specificity 90%); it is less dependent on the examiner's experience and disease location compared to US [54]. CT and MRI have similar accuracy in evaluating the extent and activity of a disease. The three techniques detect fistulas, abscesses, and stenosis with high accuracy (sensitivity and specificity >0.80), although US may give false positive results for abscesses. US or MRI should be preferred over CT, particularly in young patients, due to its lack of radiation [53–55].

Blood tests include the “traditional” non-specific parameters of inflammation (i.e., erythrocyte sedimentation rate and C-reactive protein), and serologic markers of CD. Currently, among the

latter, anti-neutrophil cytoplasmic antibodies (ANCA) and anti-Saccharomyces cerevisiae antibodies (ASCA) are the most used for diagnosis as well as for prognostic stratification of CD patients. ANCA are autoantibodies whose antigen targets are found mostly in azurophilic granules of neutrophils. In particular, in patients with inflammatory vasculitides, the major ANCA antigen targets are the proteinase-3, cytoplasmic granular with accentuation between nuclear lobes (cANCA), while in those with IBD, the target is the myeloperoxidase, which is a fine, homogenous, diffuse rim-like staining of perinuclear cytoplasm (pANCA) [56]. Positive p-ANCA are more common among UC patients, with a frequency of 40–80% in this cohort [57]. ASCA are antibodies directly against carbohydrate epitopes of phosphopeptidomannan, a 200 kDa glycoprotein of Saccharomyces cerevisiae cell wall, and have been specifically associated with CD, with 40%–60% sensitivity and 80%–90% specificity [58,59]. Recent studies reported the identification and preliminary evaluation of three new anti-glycan antibodies, called anti-laminaribioside carbohydrate antibodies (ALCA), anti-chitobioside carbohydrate antibodies (ACCA), and anti-mannobioside carbohydrate antibodies (AMCA). Some authors have assessed the accuracy of these tests showing that ASCA and ALCA antibody titers were significantly higher in CD patients than in controls. Moreover, significantly higher ACCA levels in patients with CD than in those affected by other GI diseases, were found; however, when comparing CD patients with healthy controls, a difference was not observed. Specificity and positive predictive value were always good candidates to confirm the association between considered markers (except ACCA) and CD [60,61]. The antimicrobial antibodies anti-I2 (CD related protein from *Pseudomonas fluorescens*), anti-Cbir 1 (flagellin-like antigen), and anti-OmpC (*Escherichia coli* outer membrane porin C) seem to be associated with CD but the role and utility of these additional markers have yet to be determined [62].

The direct assay on feces for inflammatory markers has the potential to improve the accuracy of the serologic tests. Among candidate markers, fecal calprotectin has been investigated with promising results in terms of accuracy in distinguishing patients with an inflammatory disease compared to those without [63]. Calprotectin is a 36 kDa calcium- and zinc-binding protein found in blood cells and plasma; it accounts for about 60% of the cytosol in neutrophils [64], which are one of the major players in intestinal inflammation but also in monocytes and macrophages [65]. Calprotectin is not actively secreted from the neutrophils, but it is released following cell death or cell disruption [66]. The amount of fecal calprotectin is strongly correlated to the migration of neutrophils cells through the gut wall and its increase is proportional to the severity of inflammation. High levels of fecal calprotectin have been associated with IBD [67]. Moreover, calprotectin is fairly unaffected by therapy and enzymatic degradation and its level is stable outside the body at room temperature for up to 7 days, so it is a useful component for reliable enzyme-linked immunosorbent assay (ELISA) testing [68]. Based on a literature study, a fecal calprotectin of >200 µg/g permits the detection of CD in 50% of suspected cases. On the contrary, when it is <100 µg/g, further tests should be ruled out because the possibility of finding an inflammatory disease is low [69].

Fecal lactoferrin is an iron-binding glycoprotein of activated neutrophils. The fecal levels of lactoferrin are found to be strongly elevated in IBD patients as well as in those affected by infectious colitis. In patients with suspected CD, fecal lactoferrin has a sensitivity and specificity of 82% and 93%, respectively. However, the dosage of fecal lactoferrin seems to be less effective than that of calprotectin for the differential diagnosis between IBD and irritable bowel syndrome [70].

Granuloma on biopsy examination is the histological hallmark of both orofacial granulomatosis and oral CD. Orofacial granulomatosis is a complex condition characterized microscopically by a non-caseating granulomatous inflammation and macroscopically by chronic swelling of the lips, oral ulcers, and hyperplastic gingivitis, with no evidence of bowel and systemic involvement [71]. The differential diagnosis between these conditions, as well as from other disorders that can manifest with granulomas, requires clinical, invasive, and non-invasive approaches. Two key-points should be highlighted. First, it is known that the presence of oral granulomas could represent a manifestation of a silent intestinal CD. Previous studies have shown that half of the patients with these oral lesions had inflammatory involvement of mucosa, discovered on ileo-colonoscopy, in absence of specific GI

symptoms. Histological abnormalities in intestinal mucosal samples are more likely to be found in case of an early onset of oral granulomatosis or in the presence of more severe oral inflammation [72]. Second, it is unknown if the presence of oral granulomas could be the early manifestation of a future CD of the GI tract [73]. In fact, the evolution of these lesions over time remains undetermined. Therefore, in absence of intestinal manifestations of CD, the diagnosis of isolated oral lesions may be difficult to ascribe to CD [74]. Some authors suggested that patients with orofacial granulomas should undergo a non-invasive test such as fecal calprotectin and eventually an endoscopic examination in the presence of GI symptoms for a differential diagnosis between an early oral manifestation of CD and orofacial granulomatosis [75].

As reported above, since there is no clear or expected pattern of intestinal IBD presenting with oral manifestations, the diagnostic algorithm should be personalized.

Regarding the non-invasive approach, while it would seem easy to support an oral location of IBD in the presence of intestinal manifestations, in subjects without abdominal complaints, there are no data concordant with the possibility that non-specific parameters of inflammation can help to diagnose an oral IBD manifestation. A different consideration must be made for serologic markers of IBD and fecal calprotectin. Both, as above reported, are the expression of intestinal inflammation. Hence, these could be useful in contributing to the detection of silent forms of concurrent intestinal IBD in patients with suspected oral IBD. If intestinal IBD-like abnormalities are found, then this will support the diagnosis of concomitant oral location of IBD. Obviously, in the clinical setting, it is difficult (on both ethic and economic bases) to propose an endoscopic or an imaging approach in patients with exclusive oral granulomatosis, without a family history of intestinal disease. Only non-invasive biomarkers, due to their low costs and lack of radiation, are the most appropriate medical investigations to screen patients with suspected IBD.

## 7. Treatment of Oral Manifestations in Patients with IBD

The goals of treatment in IBD patients are to induce and maintain clinical and, when possible, endoscopic remission. Furthermore, the prevention of complications must be another main objective.

The first-line therapeutic management of IBD should consider the severity, location, and behavior of the disease, as well as the presence of EIM. Subsequently, the assessment of response to previous treatments and the precedent side effects due to prescribed drugs should be considered. The therapeutic approach for IBD includes a standard treatment, with aminosalicylates, corticosteroids, immunosuppressive and immunomodulator agents (thiopurines, methotrexate and cyclosporin), and antibiotics. In the last few decades, the advent of biologic drugs, especially for patients resistant to or depending from standard treatment (in particular corticosteroids), has permitted a revolutionization of the natural history of IBD (Figure 1).

The most diffuse approach in the clinical setting is based on a sequential strategy. This includes the initial use of aminosalicylates patients with mild diseases, and that of corticosteroids in patients with moderate to severe symptoms or in those who failed to respond to aminosalicylates. For maintenance therapy, after clinical remission has been obtained, immunomodulators (thiopurines) are used. Patients who failed steroid-induction or maintenance therapy with a thiopurine should be treated with a biologic drug.

Overall, in most patients, clinical remission of IBD is associated to healing of oral manifestations. When this does not occur, the treatment of oral manifestations mirrors the treatments utilized in the gastroenterological setting. The pharmacological armamentarium includes topical or systemic corticosteroids, immunosuppressive agents, and biologic (mainly anti-Tumor necrosis factor (TNF)- $\alpha$ ) drugs. Topical treatment includes intralesional injections, mouthwashes, and ointments. This approach generally starts with corticosteroid ointments and/or mouthwashes and nonsteroidal anti-inflammatory pastes. In the case of non-response, an intralesional injection of corticosteroids is prescribed. If the patient's symptoms do not improve, a systemic approach with corticosteroids is required [15]. In severe cases, for example of fistulising oral CD or difficult-to-treat aphthous stomatitis, treatment with biologic drugs has obtained satisfactory results [50].

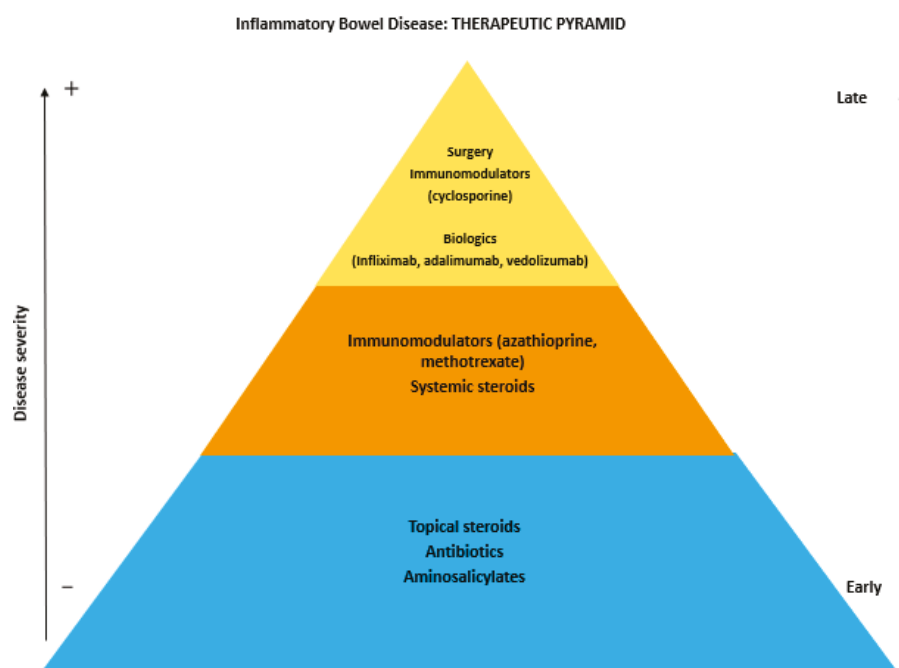


**Figure 1.** The therapeutic pyramid of inflammatory bowel disease.

## 8. Conclusions

In conclusion, while it is recommended to proceed with non-invasive investigations aiming to exclude IBD, in patients with oral granulomatosis and intestinal manifestations, the approach for subjects with only the former remains unclear and the diagnostic strategy should be personalized. Fecal calprotectin can be considered a noninvasive reliable marker of intestinal inflammation and may be used to improve the appropriate use of endoscopic examination in patients suffering from abdominal complaints, thereby avoiding unnecessary investigations. However, a diagnostic strategy with fecal calprotectin monitoring over time, in association to clinical follow-up, should be considered before endoscopy indication, highlighting that some organic intestinal diseases require an endoscopic approach and cannot be detected only by fecal calprotectin.

**Author Contributions:** Conceptualization, R.P., D.G.R., S.B. and M.A.; methodology, R.P. and D.G.R.; software, D.G.R.; validation, G.M.S., S.B. and M.A.; formal analysis, D.G.R.; investigation, D.G.R. and R.P.; resources, G.M.S.; data curation, D.G.R.; writing—original draft preparation, D.G.R.; writing—review and editing, R.P., S.B. and M.M.; visualization, M.M.; supervision, M.A. and G.M.S.; project administration, R.P. All authors have read and agreed to the published version of the manuscript.

**Funding:** This research received no external funding.

**Conflicts of Interest:** The authors declare no conflict of interest.

## References

1. Abraham, C.; Cho, J.H. Inflammatory bowel disease. *N. Engl. J. Med.* **2009**, *361*, 2066–2078. [[CrossRef](#)]
2. Sands, B.E. From symptom to diagnosis: Clinical distinctions among various forms of intestinal inflammation. *Gastroenterology* **2004**, *126*, 1518–1532. [[CrossRef](#)] [[PubMed](#)]
3. Bernstein, C.N.; Blanchard, J.F.; Rawsthorne, P.; Yu, N. The Prevalence of Extraintestinal Diseases in Inflammatory Bowel Disease: A Population-Based Study. *Am. J. Gastroenterol.* **2001**, *96*, 1116–1122. [[CrossRef](#)] [[PubMed](#)]

4. Ribaldone, D.G.; Pellicano, R.; Actis, G.C. The gut and the Inflammatory Bowel Diseases inside-out: The extra-intestinal manifestations. *Minerva Gastroenterol. Dietol.* **2019**. [[CrossRef](#)]
5. Su, C.G.; Judge, T.A.; Lichtenstein, G.R. Extraintestinal manifestations of inflammatory bowel disease. *Gastroenterol. Clin. North Am.* **2002**, *31*, 307–327. [[CrossRef](#)]
6. Adriani, A.; Pantaleoni, S.; Luchino, M.; Ribaldone, D.G.; Reggiani, S.; Sapone, N.; Sguazzini, C.; Isaia, G.; Pellicano, R.; Astegiano, M. Osteopenia and osteoporosis in patients with new diagnosis of inflammatory bowel disease. *Panminerva Med.* **2014**, *56*, 145–149. [[PubMed](#)]
7. Colia, R.; D’Onofrio, F.; Cantatore, F.P. Ulcerative colitis and systemic lupus erythematosus. *Minerva Med.* **2013**, *104*, 579–581.
8. Hugot, J.-P.; Chamaillard, M.; Zouali, H.; Lesage, S.; Cézard, J.-P.; Belaiche, J.; Almer, S.; Tysk, C.; O’Morain, C.A.; Gassull, M.; et al. Association of NOD2 leucine-rich repeat variants with susceptibility to Crohn’s disease. *Nature* **2001**, *411*, 599–603. [[CrossRef](#)]
9. Silverberg, M.S.; Mirea, L.; Bull, S.B.; Murphy, J.E.; Steinhart, A.H.; Greenberg, G.R.; McLeod, R.S.; Cohen, Z.; Wade, J.A.; Siminovitch, K.A. A population- and family-based study of Canadian families reveals association of HLA DRB1\*0103 with colonic involvement in inflammatory bowel disease. *Inflamm. Bowel Dis.* **2003**, *9*, 1–9. [[CrossRef](#)]
10. Langmann, T.; Moehle, C.; Mauerer, R.; Scharl, M.; Liebisch, G.; Zahn, A.; Stremmel, W.; Schmitz, G. Loss of detoxification in inflammatory bowel disease: Dysregulation of pregnane X receptor target genes. *Gastroenterology* **2004**, *127*, 26–40. [[CrossRef](#)]
11. Caviglia, G.P.; Rosso, C.; Stalla, F.; Rizzo, M.; Massano, A.; Abate, M.L.; Olivero, A.; Armandi, A.; Vanni, E.; Younes, R.; et al. On-Treatment Decrease of Serum Interleukin-6 as a Predictor of Clinical Response to Biologic Therapy in Patients with Inflammatory Bowel Diseases. *J. Clin. Med.* **2020**, *9*, 800. [[CrossRef](#)] [[PubMed](#)]
12. Mari, A.; Abu Baker, F.; Mahamid, M.; Sbeit, W.; Khoury, T. The Evolving Role of Gut Microbiota in the Management of Irritable Bowel Syndrome: An Overview of the Current Knowledge. *J. Clin. Med.* **2020**, *9*, 685. [[CrossRef](#)] [[PubMed](#)]
13. Ardizzone, S.; Puttini, P.S.; Cassinotti, A.; Porro, G.B. Extraintestinal manifestations of inflammatory bowel disease. *Dig. Liver Dis.* **2008**, *40*, S253–S259. [[CrossRef](#)]
14. Dudeney, T.P. Crohn’s disease of the mouth. *Proc. R. Soc. Med.* **1969**, *62*, 1237. [[CrossRef](#)] [[PubMed](#)]
15. Katsanos, K.H.; Torres, J.; Roda, G.; Brygo, A.; Delaporte, E.; Colombel, J.F. Review article: Non-malignant oral manifestations in inflammatory bowel diseases. *Aliment. Pharmacol. Ther.* **2015**, *42*, 40–60. [[CrossRef](#)]
16. Pittock, S.; Drumm, B.; Fleming, P.; McDermott, M.; Imrie, C.; Flint, S.; Bourke, B. The oral cavity in Crohn’s disease. *J. Pediatr.* **2001**, *138*, 767–771. [[CrossRef](#)]
17. Lenaerts, C.; Roy, C.C.; Vaillancourt, M.; Weber, A.M.; Morin, C.L.; Seidman, E. High incidence of upper gastrointestinal tract involvement in children with Crohn disease. *Pediatrics* **1989**. [[CrossRef](#)]
18. Dupuy, A.; Cosnes, J.; Revuz, J.; Delchier, J.C.; Gendre, J.P.; Cosnes, A. Oral Crohn disease: Clinical characteristics and long-term follow-up of 9 cases. *Arch. Dermatol.* **1999**. [[CrossRef](#)]
19. Lauritano, D.; Boccalari, E.; Di Stasio, D.; Della Vella, F.; Carinci, F.; Lucchese, A.; Petruzzi, M. Prevalence of oral lesions and correlation with intestinal symptoms of inflammatory bowel disease: A systematic review. *Diagnostics* **2019**, *9*, 77. [[CrossRef](#)]
20. Harty, S.; Fleming, P.; Rowland, M.; Crushell, E.; McDermott, M.; Drumm, B.; Bourke, B. A prospective study of the oral manifestations of Crohn’s disease. *Clin. Gastroenterol. Hepatol.* **2005**. [[CrossRef](#)]
21. Vasovic, M.; Gajovic, N.; Brajkovic, D.; Jovanovic, M.; Zdravkovaic, N.; Kanjevac, T. The relationship between the immune system and oral manifestations of inflammatory bowel disease: A review. *Cent. Eur. J. Immunol.* **2016**, *41*, 302–310. [[CrossRef](#)] [[PubMed](#)]
22. Rehberger, A.; Püspök, A.; Stallmeister, T.; Jurecka, W.; Wolff, K. Crohn’s disease masquerading as aphthous ulcers. *Eur. J. Dermatol.* **1998**, *8*, 274–276. [[PubMed](#)]
23. Laranjeira, N.; Fonseca, J.; Meira, T.; Freitas, J.; Valido, S.; Leitão, J. Oral mucosa lesions and oral symptoms in inflammatory bowel disease patients. *Arq. Gastroenterol.* **2015**, *52*, 105–110. [[CrossRef](#)] [[PubMed](#)]
24. Lourenco, S.V.; Hussein, T.P.; Bologna, S.B.; Sipahi, A.M.; Nico, M.M. Oral manifestations of inflammatory bowel disease: A review based on the observation of six cases. *J. Eur. Acad. Dermatol. Venereol.* **2010**, *24*, 204–207. [[CrossRef](#)]

25. Said, H.S.; Suda, W.; Nakagome, S.; Chinen, H.; Oshima, K.; Kim, S.; Kimura, R.; Iraha, A.; Ishida, H.; Fujita, J.; et al. Dysbiosis of salivary microbiota in inflammatory bowel disease and its association with oral immunological biomarkers. *DNA Res.* **2014**, *21*, 15–25. [[CrossRef](#)]
26. Muhvić-Urek, M.; Tomac-Stojmenović, M.; Mijandrušić-Sinčić, B. Oral pathology in inflammatory bowel disease. *World J. Gastroenterol.* **2016**, *22*, 5655–5667. [[CrossRef](#)]
27. Gale, G.; Sigurdsson, G.V.; Östman, S.; Malmborg, P.; Högkil, K.; Hasséus, B.; Jontell, M.; Saalman, R. Does Crohn's Disease with Concomitant Orofacial Granulomatosis Represent a Distinctive Disease Subtype? *Inflamm. Bowel Dis.* **2016**, *22*, 1071–1077. [[CrossRef](#)]
28. Halme, L.; Meurman, J.H.; Laine, P.; von Smitten, K.; Syrjänen, S.; Lindqvist, C.; Strand-Pettinen, I. Oral findings in patients with active or inactive Crohn's disease. *Oral Surg. Oral Med. Oral Pathol.* **1993**. [[CrossRef](#)]
29. Fatahzadeh, M.; Schwartz, R.A.; Kapila, R.; Rochford, C. Orofacial Crohn's disease: An oral enigma. *Acta Dermatovenerol. Croat.* **2009**, *17*, 289–300.
30. Gibson, J.; Wray, D.; Bagg, J. Oral staphylococcal mucositis: A new clinical entity in or ofacial granulomatosis and Crohn's disease. *Oral Surg. Oral Med. Oral Pathol. Oral Radiol. Endod.* **2000**. [[CrossRef](#)]
31. Nagpal, S.; Acharya, A.B.; Thakur, S.L. Periodontal disease and anemias associated with Crohn's disease. A case report. *N. Y. State Dent. J.* **2012**, *78*, 47–50.
32. Turchi, R.M.; Soriano, H.; Rodgers, G.L. Tb or not Tb: Crohn's disease presenting with tonsillar granulomas. *Otolaryngol. Head Neck Surg.* **2006**, *134*, 528–530. [[CrossRef](#)] [[PubMed](#)]
33. Katz, J.; Shenkman, A.; Stavropoulos, F.; Melzer, E. Oral signs and symptoms in relation to disease activity and site of involvement in patients with inflammatory bowel disease. *Oral Dis.* **2003**. [[CrossRef](#)] [[PubMed](#)]
34. Trikudanathan, G.; Venkatesh, P.G.K.; Navaneethan, U. Diagnosis and therapeutic management of extra-intestinal manifestations of inflammatory bowel disease. *Drugs* **2012**, *72*, 2333–2349. [[CrossRef](#)] [[PubMed](#)]
35. Rogers, R.S.; Bekic, M. Diseases of the lips. *Semin. Cutan. Med. Surg.* **1997**, *16*, 328–336. [[CrossRef](#)]
36. Mijandrusic-Sincic, B.; Licul, V.; Gorup, L.; Brnčić, N.; Glažar, I.; Lučin, K. Pyostomatitis vegetans associated with inflammatory bowel disease—Report of two cases. *Coll. Antropol.* **2010**, *34*, 279–282.
37. Atarbashi-Moghadam, S.; Lotfi, A.; Atarbashi-Moghadam, F. Pyostomatitis Vegetans: A Clue for Diagnosis of Silent Crohn's Disease. *J. Clin. Diagn. Res.* **2016**, *10*, ZD12–ZD13. [[CrossRef](#)]
38. Correll, R.W.; Wescott, W.B.; Jensen, J.L. Recurring, painful oral ulcers. *J. Am. Dent. Assoc.* **1981**. [[CrossRef](#)]
39. Femiano, F.; Lanza, A.; Buonaiuti, C.; Perillo, L.; Dell'Ermo, A.; Cirillo, N. Pyostomatitis vegetans: A review of the literature. *Med. Oral Patol. Oral Cir. Bucal* **2009**, *14*, E114–E117.
40. Markopoulos, A.K.; Antoniadis, D.Z.; Gaga, E. Pyostomatitis Vegetans as an Oral Manifestation of Ulcerative Colitis: Report of Two Cases. *Oral Surg. Oral Med. Oral Pathol. Oral Radiol. Endodontol.* **2005**. [[CrossRef](#)]
41. Papageorgiou, S.N.; Hagner, M.; Nogueira, A.V.B.; Franke, A.; Jäger, A.; Deschner, J. Inflammatory bowel disease and oral health: Systematic review and a meta-analysis. *J. Clin. Periodontol.* **2017**, *44*, 382–393. [[CrossRef](#)] [[PubMed](#)]
42. Habashneh, R.A.; Khader, Y.S.; Alhumouz, M.K.; Jadallah, K.; Ajlouni, Y. The association between inflammatory bowel disease and periodontitis among Jordanians: A case-control study. *J. Periodont. Res.* **2012**, *47*, 293–298. [[CrossRef](#)] [[PubMed](#)]
43. Figueredo, C.M.; Brito, F.; Barros, F.C.; Menegat, J.S.B.; Pedreira, R.R.; Fischer, R.G.; Gustafsson, A. Expression of cytokines in the gingival crevicular fluid and serum from patients with inflammatory bowel disease and untreated chronic periodontitis. *J. Periodont. Res.* **2011**, *46*, 141–146. [[CrossRef](#)] [[PubMed](#)]
44. Lira-Junior, R.; Figueredo, C.M. Periodontal and inflammatory bowel diseases: Is there evidence of complex pathogenic interactions? *World J. Gastroenterol.* **2016**, *22*, 7963–7972. [[CrossRef](#)]
45. Kabbani, T.A.; Koutroubakis, I.E.; Schoen, R.E.; Ramos-Rivers, C.; Shah, N.; Swoger, J.; Regueiro, M.; Barrie, A.; Schwartz, M.; Hashash, J.G.; et al. Association of Vitamin D level with clinical status in inflammatory bowel disease: A 5-year longitudinal study. *Am. J. Gastroenterol.* **2016**. [[CrossRef](#)]
46. Schroth, R.J.; Rabbani, R.; Loewen, G.; Moffatt, M.E. Vitamin D and Dental Caries in Children. *J. Dent. Res.* **2016**. [[CrossRef](#)]
47. Rowland, M.; Fleming, P.; Bourke, B. Looking in the mouth for Crohn's disease. *Inflamm. Bowel Dis.* **2010**, *16*, 332–337. [[CrossRef](#)]
48. Campisi, G.; Giovannelli, L. Controversies surrounding human papilloma virus infection, head & neck vs oral cancer, implications for prophylaxis and treatment. *Head Neck Oncol.* **2009**, *1*, 8. [[CrossRef](#)]
49. Vial, T.; Descotes, J. Immunosuppressive drugs and cancer. *Toxicology* **2003**, *185*, 229–240. [[CrossRef](#)]

50. Katsanos, K.H.; Roda, G.; Brygo, A.; Delaporte, E.; Colombel, J.F. Oral cancer and oral precancerous lesions in inflammatory bowel diseases: A systematic review. *J. Crohn's Colitis* **2015**, *9*, 1043–1052. [[CrossRef](#)]
51. Mowat, C.; Cole, A.; Windsor, A.; Ahmad, T.; Arnott, I.; Driscoll, R.; Mitton, S.; Orchard, T.; Rutter, M.; Younge, L.; et al. Guidelines for the management of inflammatory bowel disease in adults. *Gut* **2011**, *60*, 571–607. [[CrossRef](#)] [[PubMed](#)]
52. Cammarota, T.; Ribaldone, D.G.; Resegotti, A.; Repici, A.; Danese, S.; Fiorino, G.; Sarno, A.; Robotti, D.; Debani, P.; Bonenti, G.; et al. Role of bowel ultrasound as a predictor of surgical recurrence of Crohn's disease. *Scand. J. Gastroenterol.* **2013**, *48*. [[CrossRef](#)] [[PubMed](#)]
53. Sarno, A.; Varello, S.; Debani, P.; Bonenti, G.; Robotti, D. Intestinal ultrasonography in adults with Crohn's disease: A 2020 update. *Minerva Gastroenterol. Dietol.* **2019**, *65*, 335–345. [[CrossRef](#)]
54. Gatti, M.; Allois, L.; Carisio, A.; Dianzani, C.; Garcia Martinez, M.; Ruggirello, I.; Varello, S.; Darvizeh, F.; Faletti, R. Magnetic resonance enterography. *Minerva Gastroenterol. Dietol.* **2019**, *65*, 319–334. [[CrossRef](#)] [[PubMed](#)]
55. Panés, J.; Bouzas, R.; Chaparro, M.; García-Sánchez, V.; Gisbert, J.P.; Martínez de Guereñu, B.; Mendoza, J.L.; Paredes, J.M.; Quiroga, S.; Ripollés, T.; et al. Systematic review: The use of ultrasonography, computed tomography and magnetic resonance imaging for the diagnosis, assessment of activity and abdominal complications of Crohn's disease. *Aliment. Pharmacol. Ther.* **2011**, *34*, 125–145. [[CrossRef](#)]
56. Kallenberg, C.G.M.; Heeringa, P.; Stegeman, C.A. Mechanisms of disease: Pathogenesis and treatment of ANCA-associated vasculitides. *Nat. Clin. Pract. Rheumatol.* **2006**, *2*, 661–670. [[CrossRef](#)]
57. Papp, M.; Norman, G.L.; Altorjay, I.; Lakatos, P.L. Utility of serological markers in inflammatory bowel diseases: gadget or magic? *World J. Gastroenterol.* **2007**, *13*, 2028–2036. [[CrossRef](#)]
58. Gao, X.; Hu, P.; He, Y.; Liao, S.; Peng, S.; Chen, M. Diagnostic role of anti-saccharomyces cerevisiae and antineutrophil cytoplasmic autoantibodies in inflammatory bowel disease. *Zhonghua Nei Ke Za Zhi* **2005**, *44*, 428–430. [[CrossRef](#)]
59. Sandborn, W.J.; Loftus, E.V.; Colombel, J.F.; Fleming, K.A.; Seibold, F.; Homburger, H.A.; Sendid, B.; Chapman, R.W.; Tremaine, W.J.; Kaul, D.K.; et al. Evaluation of serologic disease markers in a population-based cohort of patients with ulcerative colitis and Crohn's disease. *Inflamm. Bowel Dis.* **2001**, *7*, 192–201. [[CrossRef](#)]
60. Simondi, D.; Mengozzi, G.; Betteto, S.; Bonardi, R.; Ghignone, R.P.; Fagoonee, S.; Pellicano, R.; Sguazzini, C.; Pagni, R.; Rizzetto, M.; et al. Antiglycan antibodies as serological markers in the differential diagnosis of inflammatory bowel disease. *Inflamm. Bowel Dis.* **2008**, *14*, 645–651. [[CrossRef](#)]
61. Malickova, K.; Lakatos, P.L.; Bortlik, M.; Komarek, V.; Janatkova, I.; Lukas, M. Anticarbohydrate antibodies as markers of inflammatory bowel disease in a Central European cohort. *Eur. J. Gastroenterol. Hepatol.* **2010**. [[CrossRef](#)] [[PubMed](#)]
62. Amcoff, K.; Joossens, M.; Pierik, M.J.; Jonkers, D.; Bohr, J.; Joossens, S.; Romberg-Camps, M.; Nyhlin, N.; Wickbom, A.; Rutgeerts, P.J.; et al. Concordance in Anti-OmpC and Anti-I2 Indicate the Influence of Genetic Predisposition: Results of a European Study of Twins with Crohn's Disease. *J. Crohns. Colitis* **2016**, *10*, 695–702. [[CrossRef](#)] [[PubMed](#)]
63. Caviglia, G.P.; Ribaldone, D.G.; Rosso, C.; Saracco, G.M.; Astegiano, M.; Pellicano, R. Fecal calprotectin: Beyond intestinal organic diseases. *Panminerva Med.* **2018**, *60*, 29–34. [[CrossRef](#)] [[PubMed](#)]
64. Berntzen, H.B.; Fagerhol, M.K. L1, a major granulocyte protein: Antigenic properties of its subunits. *Scand. J. Clin. Lab. Investig.* **1988**, *48*, 647–652. [[CrossRef](#)]
65. Foell, D.; Wittkowski, H.; Roth, J. Monitoring disease activity by stool analyses: From occult blood to molecular markers of intestinal inflammation and damage. *Gut* **2009**, *58*, 859–868. [[CrossRef](#)]
66. Voganatsi, A.; Panyutich, A.; Miyasaki, K.T.; Murthy, R.K. Mechanism of extracellular release of human neutrophil calprotectin complex. *J. Leukoc. Biol.* **2001**. [[CrossRef](#)]
67. Burri, E.; Beglinger, C. Faecal calprotectin in the diagnosis of inflammatory bowel disease. *Biochem. Med.* **2011**, 245–253. [[CrossRef](#)]
68. Sydora, M.J.; Sydora, B.C.; Fedorak, R.N. Validation of a point-of-care desk top device to quantitate fecal calprotectin and distinguish inflammatory bowel disease from irritable bowel syndrome. *J. Crohns. Colitis* **2012**, *6*, 207–214. [[CrossRef](#)]
69. Koulaouzidis, A.; Douglas, S.; Rogers, M.A.; Arnott, I.D.; Plevris, J.N. Fecal calprotectin: A selection tool for small bowel capsule endoscopy in suspected IBD with prior negative bi-directional endoscopy. *Scand. J. Gastroenterol.* **2011**, *46*, 561–566. [[CrossRef](#)]



70. Wright, E.K. Calprotectin or Lactoferrin: Do They Help. *Dig. Dis.* **2016**, *34*, 98–104. [[CrossRef](#)]
71. Ojha, J.; Cohen, D.M.; Islam, N.M.; Stewart, C.M.; Katz, J.; Bhattacharyya, I. Gingival involvement in Crohn disease. *J. Am. Dent. Assoc.* **2007**. [[CrossRef](#)] [[PubMed](#)]
72. Zbar, A.P.; Ben-Horin, S.; Beer-Gabel, M.; Eliakim, R. Oral Crohn's disease: Is it a separable disease from orofacial granulomatosis? A review. *J. Crohns. Colitis* **2012**, *6*, 135–142. [[CrossRef](#)] [[PubMed](#)]
73. Bishop, R.P.; Brewster, A.C.; Antonioli, D.A. Crohn's disease of the mouth. *Gastroenterology* **1972**, *62*, 302–306. [[CrossRef](#)]
74. Bradley, P.J.; Ferlito, A.; Devaney, K.O.; Rinaldo, A. Crohn's disease manifesting in the head and neck. *Acta Otolaryngol.* **2004**, *124*, 237–241. [[CrossRef](#)]
75. Khouri, J.M.; Bohane, T.D.; Day, A.S. Is orofacial granulomatosis in children a feature of Crohn's disease? *Acta Paediatr. Int. J. Paediatr.* **2005**. [[CrossRef](#)]



© 2020 by the authors. Licensee MDPI, Basel, Switzerland. This article is an open access article distributed under the terms and conditions of the Creative Commons Attribution (CC BY) license (<http://creativecommons.org/licenses/by/4.0/>).

Case Report

# Contrast-Enhanced Ultrasonography for Screening and Diagnosis of Hepatocellular Carcinoma: A Case Series and Review of the Literature

Kathryn L. McGillen <sup>1,\*</sup>, Syeda Zaidi <sup>2</sup>, Amer Ahmed <sup>3</sup>, Shantell Harter <sup>1</sup> and Nelson S. Yee <sup>4,\*</sup>

<sup>1</sup> Department of Radiology, Penn State Health Milton S. Hershey Medical Center, Hershey, PA 17033, USA; sharter@pennstatehealth.psu.edu

<sup>2</sup> Stritch School of Medicine, Loyola University Chicago, 2160 S 1st Ave, Maywood, IL 60531, USA; szaidi2@luc.edu

<sup>3</sup> Chicago College of Osteopathic Medicine, Midwestern University, 555 31st St, Downers Grove, IL 60515, USA; aahmed77@midwestern.edu

<sup>4</sup> Division of Hematology-Oncology, Department of Medicine, Penn State Health Milton S. Hershey Medical Center, Next-Generation Therapies Program, Penn State Cancer Institute, Hershey, PA 17033, USA

\* Correspondence: kmcgillen@pennstatehealth.psu.edu (K.L.M.); nyee@pennstatehealth.psu.edu (N.S.Y.); Tel.: +1-717-531-6881 (K.L.M.); +1-717-531-8678 (N.S.Y.)

Received: 30 July 2020; Accepted: 22 August 2020; Published: 27 August 2020

**Abstract: Background:** Contrast-enhanced ultrasound (CEUS) is a safe and noninvasive imaging technique that can characterize and evaluate liver lesions, and has been approved for this use in the United States since 2016. CEUS has been shown to be similar in accuracy to computed tomography (CT) and magnetic resonance imaging (MRI) for noninvasive diagnosis of hepatocellular carcinoma (HCC) and offers several advantages in certain patient populations who have contraindications for CT or MRI. However, CEUS has inherent limitations and has not been widely employed for evaluation of HCC. **Methods:** We present three retrospective cases of liver lesions in patients with cirrhosis, who underwent screening for HCC using concurrent, well-timed CT and CEUS. **Results:** In these cases, the liver lesions were better visualized and then diagnosed as malignancy via CEUS, whereas the lesions were best appreciated on CT only in retrospect. **Conclusions:** In some cirrhotic patients, a focal lesion may be more easily identifiable via CEUS than on CT and thus accurately characterized, suggesting an important and complementary role of CEUS with CT or MRI. Further studies are indicated to support the use of CEUS for the diagnosis and characterization of liver lesions in screening patients at risk for developing HCC.

**Keywords:** contrast-enhanced ultrasound; hepatocellular carcinoma; LI-RADS; chronic liver disease

## 1. Introduction

Hepatocellular carcinoma (HCC) is the most common primary liver tumor and the fourth most common cause of cancer-related mortality worldwide [1]. Chronic hepatic injury and liver cirrhosis are known to pose an increased risk for development of HCC over time [2]. Major risk factors for chronic hepatic injury include alcoholism, infection with hepatitis B or C virus, and nonalcoholic fatty liver disease [1]. Nonmodifiable risk factors include autoimmune hepatitis, Wilson's disease, hereditary hemochromatosis, primary biliary cirrhosis, and alpha 1-antitrypsin deficiency [3]. The American Association for the Study of Liver Diseases (AASLD) and European Association for the Study of the Liver (EASL) guidelines recommend surveillance in patients at high risk for developing HCC. The goal is to detect HCC early when it is amenable to curative therapy such as liver transplantation or surgical resection, and to reduce mortality [4]. Otherwise, palliative liver-directed therapy, such as chemoembolization, radiofrequency ablation, and stereotactic

body radiation therapy, is an option for treatment [5–7]. However, for patients with advanced or metastatic HCC, palliative systemic treatment is the only therapeutic option, and the associated survival benefit is limited [8–10].

HCC is commonly diagnosed by imaging studies including multiphase computed tomography (CT) or magnetic resonance imaging (MRI) scans with and without intravenous (IV) contrast. These are considered the gold standard imaging modalities for noninvasive diagnosis of HCC [11]. However, there are various limitations of CT and MRI scans for patients with HCC. For CT scans, contrast-related allergy, respiratory motion, renal impairment, and cumulative radiation doses, especially in young patients, are factors of concern. For MRI scans, respiratory motion, certain cardiac pacemakers or metal in the body, significant ascites, and claustrophobia may limit its utility for patients. Ultrasonography (US) is often used for screening, sometimes nearly exclusively, other times alternating with CT or MRI, the choice of which may depend upon the individual patient's risk factors, clinician's preference, and health insurance approval of advanced imaging. If a lesion is found on screening US, further characterization of the lesion with a contrast-enhanced examination is required. In recent years, contrast-enhanced ultrasonography (CEUS) has been utilized for diagnostic imaging evaluation of HCC in the United States, with a meta-analysis showing a sensitivity of 85% and specificity of 91% [12]. CEUS may provide unique advantages that complement conventional CT and MRI scans in patients at risk for HCC.

CEUS is an imaging modality that has been approved for use in the characterization of liver lesions in the United States since 2016. It utilizes the standard US techniques of grayscale and color Doppler, with the addition of an US-specific intravenous contrast agent. By enhancing the organs and targeted lesions, the contrast agent yields additional diagnostic information. Several brands are approved by the Food and Drug Administration in the United States, and they utilize similar microbubble technology. Of the agents approved, contrast with a sulfur hexafluoride core (Lumason<sup>®</sup>, Bracco Diagnostics Inc., Monroe Township, NJ, USA) is widely used in the United States, Europe, and China [13] and at our own institution. CEUS has several unique features in comparison with CT or MRI with contrast. The contrast agent used with US is made of microbubbles that are smaller than a red blood cell, so that they do not cross the endothelium but instead remain in the intravascular space [13,14]. The microbubbles burst after several minutes of imaging, with byproducts exhaled through the pulmonary system [13]. This is unlike the contrast agents used with CT or MRI scans, which diffuse into the parenchyma and are excreted through the kidneys (and sometimes biliary system) and therefore can be affected by poor hepatic and renal function. Because of this, CEUS agents are safe to use in patients with poor renal function. Additionally, because of their limited duration in the bloodstream, patients can be dosed several times in the same setting, as opposed to CT or MRI, for which a wait time of hours or even a day may be necessary to perform a second injection and repeat imaging. This allows evaluation of multiple lesions using CEUS in one setting, and more importantly, re-evaluation of a single lesion, if necessary.

For characterization of individual lesions within the liver, CEUS has been proven to have accuracy similar to that of CT or MRI [15]. The American College of Radiology (ACR) created the Liver Reporting and Data System (LI-RADS) for noninvasive imaging diagnosis of HCC in patients at risk for its development. ACR released LI-RADS criteria for both routine US and CEUS, with the latter utilizing the same numbering system as CT and MRI for noninvasively diagnosing HCC [16]. This diagnostic algorithm categorizes imaging findings, lesion size, and enhancement patterns on a scale of 1 to 5 [17]. LI-RADS 1–3 lesions range from benign to intermediate, while LI-RADS 4 and 5 lesions are likely and almost definitively HCC, respectively [18], and they can be diagnosed via imaging criteria alone. An additional category, LI-RADS M, denotes the presence of a malignant liver lesion, but this is not specific for HCC [19,20]. In at-risk patients, screening programs to detect early HCC, while it is treatable, are most often conducted with multiphase CT or MRI, but may be performed with US, although it is less sensitive [15]. If a suspicious area is identified on US, the patient will need to return and have a CT or MRI for further characterization, requiring two visits and creating additional medical

bills. Within our practice, insurance companies have increasingly denied pre-authorization for the gold standard four-phase CT or MRI for screening of HCC. An alternative solution is to screen patients with CEUS. Moreover, as mentioned above, some patients have poor renal function or history of allergic reaction to contrast agents used with CT or MRI, and may be precluded from safe use of these tests. CEUS, therefore, has an important potential role in this population in particular.

While CEUS and CT/MRI share similar fundamental imaging diagnostic criteria via LI-RADS, there are still notable differences with regard to image acquisition, contrast material, and visualization [17]. Here, we present three patients who were undergoing routine screening for HCC due to chronic liver disease and found to have lesions present on grayscale ultrasound, and then proceeded immediately to CEUS. In this case series, we compare the visibility of liver lesions using CEUS against the gold standard four-phase CT. We present evidence that demonstrates the accuracy of CEUS for identifying malignancy in at-risk cirrhotic patients, suggesting an important and complementary role of CEUS with CT or MRI.

## 2. Materials and Methods

This is a retrospective review examining the electronic medical records and images at our 548-bed semirural institution, which is also a liver transplant center, as well as the pertinent literature about CEUS in HCC diagnosis. All CEUS were performed on a Siemens S2000 with 2.5 mL of Lumason<sup>®</sup> IV contrast. All CT scans were performed on a 64-slice scanner utilizing 150 mL of Omnipaque<sup>™</sup> 350 IV contrast unless otherwise stated—each scan consisted of noncontrast, late arterial phase (bolus-triggered), portal venous, and 3 min delayed phase imaging. None of our patients had MRI performed for liver imaging. We have obtained the written informed consent of patients. The Human Subjects Protection Office of the Penn State Health Milton S. Hershey Medical Center determined that this case study does not meet the definition of human subject research as defined in 45 CFR 46.102(d) and/or (f); Institutional Review Board (IRB) review and approval is not required.

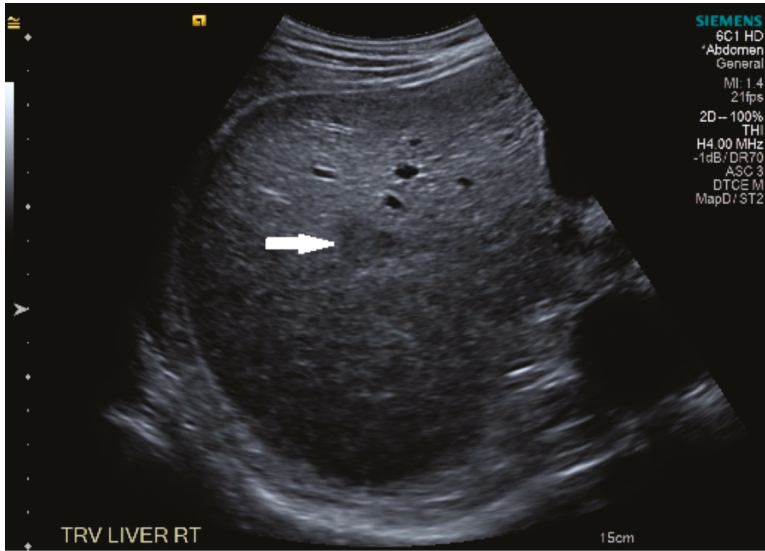
## 3. Case Presentation

### 3.1. Case 1

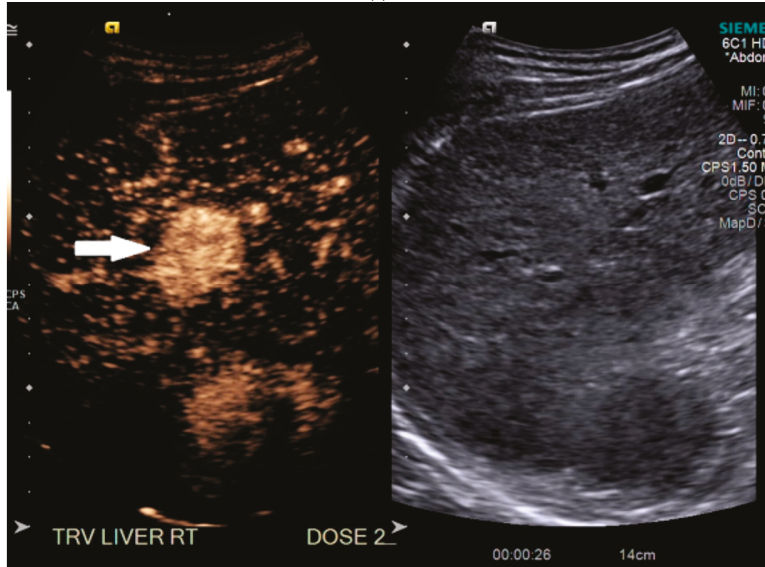
A 62-year-old Caucasian man with advanced hepatic fibrosis secondary to hepatitis C viral infection was scheduled for a four-phase CT to screen for HCC, but was denied insurance pre-approval for the imaging study. He was diagnosed with hepatitis C viral infection a decade earlier, which was subsequently treated and cleared with interferon and ribavirin. Cirrhosis was confirmed via biopsy at that time, and stage III fibrosis diagnosed via biopsy four years later. At the time of his screening request, he had no additional medical problems or sequela of advanced liver disease. His physical exam was essentially normal—including vital signs and for stigmata of chronic liver disease. His alpha-fetoprotein (AFP) was 3.0 ng/mL with normal liver function tests, albumin, and platelets.

Routine US showed a heterogeneous, coarsened liver parenchyma with a suspected 2.2 cm hypochoic structure in the right lobe on a background of geographic hepatic steatosis (Figure 1). Contrast was then administered intravenously with targeted imaging of the lesion to determine if it was focal fatty sparing or tumor. The lesion markedly enhanced (Supplementary Video S1) and began washout rapidly, and on delayed imaging, showed intense washout. It was deemed a LI-RADS M because of its early enhancement and for its marked washout (Figure 1). Given the LI-RADS M designation and for treatment planning, a four-phase CT was then approved by his health insurance company. Despite its size, the lesion was poorly visualized on the well-timed late arterial phase (Figure 2). It was equally subtle on the portal venous and 3 min phases. Knowing where the lesion was on CEUS allowed the radiologist to confirm the findings on CT, where it was deemed a LI-RADS 5 lesion. However, without the pre-existing knowledge of its presence in that location, the lesion was initially missed. The late arterial phase on the CT was bolus-triggered, which resulted in scanning occurring at 35 s post injection. Interestingly, on the CEUS, the lesion was already washing out and

was iso-intense to liver by 35 s. This may explain why it was poorly seen on CT despite its intense, avid enhancement on US.



(a)



(b)

Figure 1. Cont.

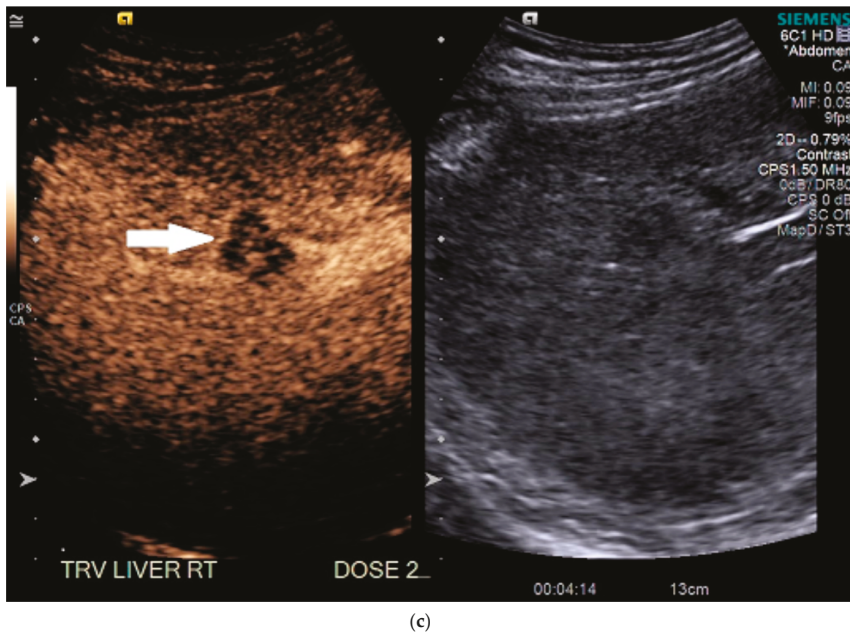


**Figure 1.** Patient 1 ultrasound images, with liver lesion denoted by white arrow: (a) grayscale images showing the hypoechoic lesion. Post contrast administration ultrasound in arterial phase with matched low-mechanical-index B-mode grayscale on the right and subtraction-type post contrast images on the left (b) and delayed phase (c) of the lesion, which shows marked washout. Liver Reporting and Data System (LI-RADS M).

Given the LI-RADS 5 designation on CT, the lesion was not biopsied prior to treatment, as may be indicated by an initial LI-RADS M diagnosis. Instead, it was treated as HCC with several transcatheter arterial chemoembolizations (TACEs). Despite two treatments with TACE, persistent and progression of tumor was identified on follow-up CTs over the next 8 months.

### 3.2. Case 2

A 63-year-old Caucasian man with hepatic cirrhosis presented for screening US. He had been diagnosed with viral hepatitis C-induced cirrhosis and achieved a sustained virologic response after treatment with Vosevi. He had a well-compensated cirrhosis, with grade 1 esophageal varices and portal hypertensive gastropathy. Just prior to his US, he was asymptomatic. His physical examination was significant for hypertension, elevated body mass index (BMI) of 38, but with no physical signs of chronic liver disease. His albumin was low (3.3 gm/dL), as was his total protein (6.1 gm/dL). Liver function tests were normal except for an elevated total and direct bilirubin (4.4 and 0.8 mg/dL, respectively). His AFP level was normal at 5.7 ng/mL, and his hepatitis C viral load was undetectable.



**Figure 2.** Patient 1 CT images using liver windows to highlight the subtle lesion easily seen on contrast-enhanced ultrasound (CEUS) (white arrow): (a) late arterial phase axial contrast-enhanced CT; (b) 3 min delayed phase.

On grayscale US, a subtle 1.2 cm hypoechoic focal area was identified on a background of echogenic, heterogeneous liver echotexture (Figure 3). This area was targeted with contrast, which showed avid arterial-phase enhancement, and rapid, but mild washout (Figure 3). This was also designated LI-RADS

M due to the early washout. CT was performed to confirm the finding and initially, the lesion was not identified by the radiologist, despite a diagnostic late arterial phase. On closer inspection with the US finding in mind, subtle enhancement and washout on the CT was seen and considered LI-RADS 4 (Figure 4), and due to this designation and its small size, a shorter interval follow-up was performed at 3 months rather than 6 months.

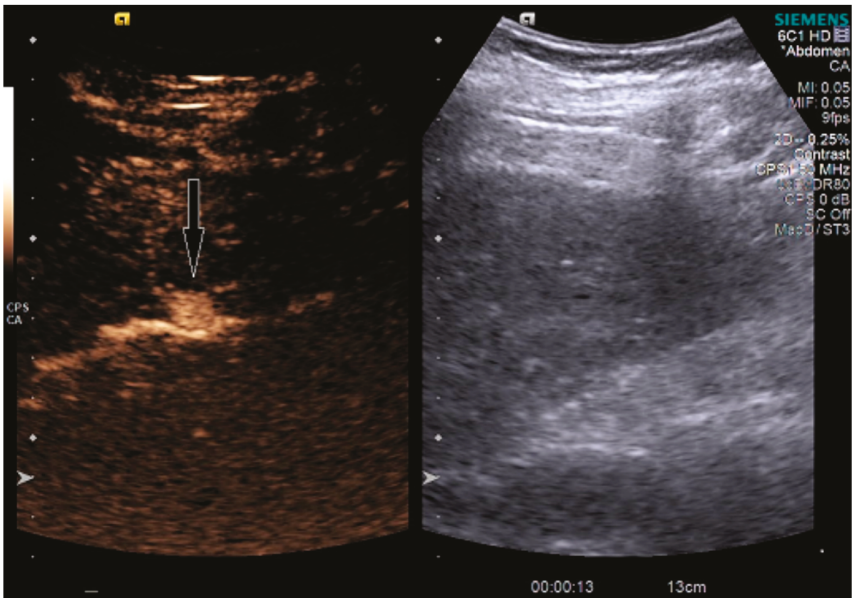
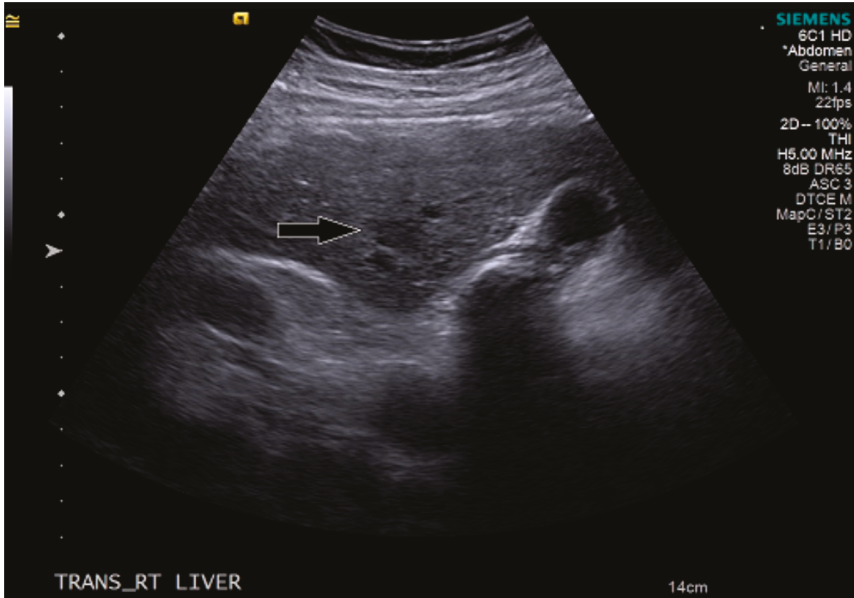
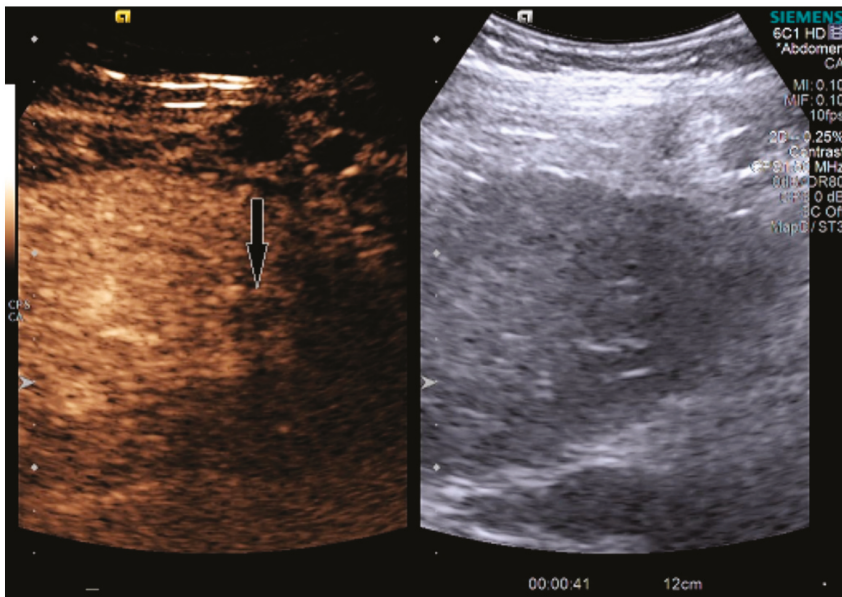


Figure 3. Cont.





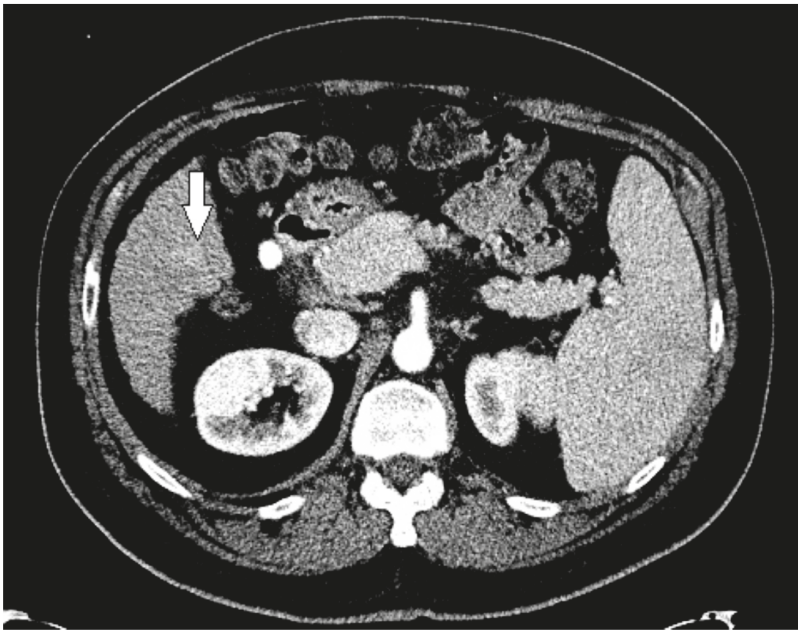
(c)

**Figure 3.** Patient 2 ultrasound images, with liver lesion denoted by black arrow: (a) grayscale images showing the hypoechoic lesion. Post contrast administration ultrasound in arterial phase (b) and early washout (c) of the lesion, LI-RADS M.

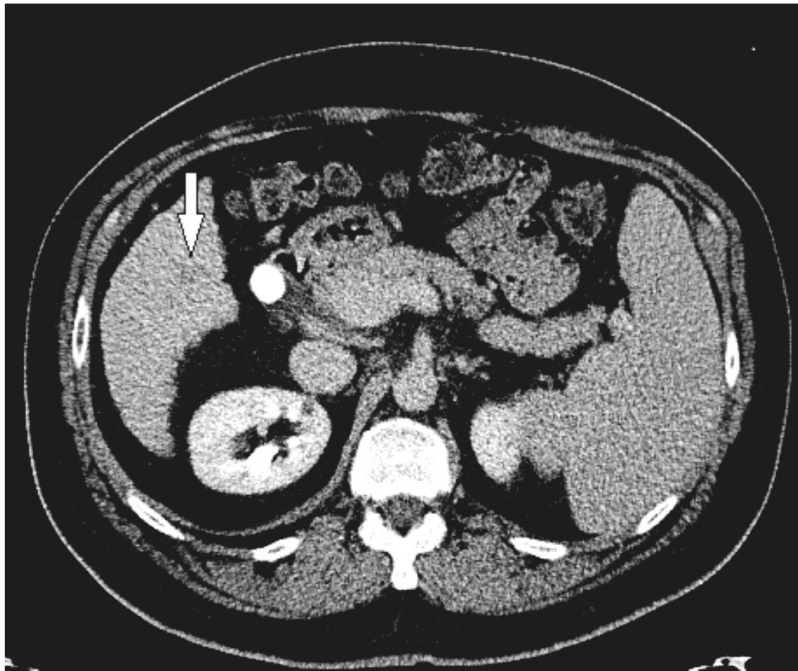
The patient indeed followed up with an additional four-phase CT 3 months later, and the lesion had grown and was then clearly evident (Figure 4). It was upgraded to a LI-RADS 5, and the patient proceeded to treatment with a successful TACE. However, follow-up CTs over the next 6 months demonstrated development of new LI-RADS 5 lesions, which were subsequently treated with an additional TACE.

### 3.3. Case 3

A 59-year-old Caucasian man with hepatic cirrhosis secondary to alcoholism presented to the hospital with acutely worsening hepatic decompensation and acute on chronic renal dysfunction. He presented through the emergency department with worsening confusion and abdominal distention. He had a history of hepatic encephalopathy, moderate antral erosive gastritis, and ascites. At the time of admission, his physical examination was remarkable for scleral icterus, and fluid wave present in the abdomen. He was awake and oriented to person and place. Laboratory values were notable for an elevated, baseline international normalized ratio (INR) of prothrombin time (2.4), mildly elevated potassium (5.3 mmol/L), elevated creatinine (3.27 mg/dL, up from baseline of 2.3), platelets of 101,000/ $\mu$ L, and elevated liver function tests (alanine aminotransferase 57 unit/L, total bilirubin 10.3 mg/dL, alkaline phosphatase 185 unit/L) and ammonia elevated at 64  $\mu$ mol/L. A four-phase CT had been performed 2 months earlier and interpreted as negative for HCC. US was performed to detect any HCC during acute evaluation for liver transplantation, in order to ensure the patient remained within transplant criteria.



(a)



(b)

**Figure 4.** Patient 2 CT images using liver windows to highlight the lesion seen on CEUS (white arrow): (a) late arterial phase axial contrast-enhanced CT; (b) 3 min delayed phase.

On grayscale imaging, a 2.9 cm hypoechoic lesion at the dome of the right lobe on a background of heterogeneous liver parenchyma was identified (Figure 5). Due to his acute on chronic renal failure, CEUS was then performed, which showed subtle enhancement of the lesion, above background enhancement of the adjacent liver at the same depth. At or greater than 10 cm depth is most often the limit of penetration in standard CEUS software packages [13], but can be extended in the presence of ascites, as in our case. Subtle washout was identified on delayed imaging, and the lesion was deemed LI-RADS 5 (Figure 5).

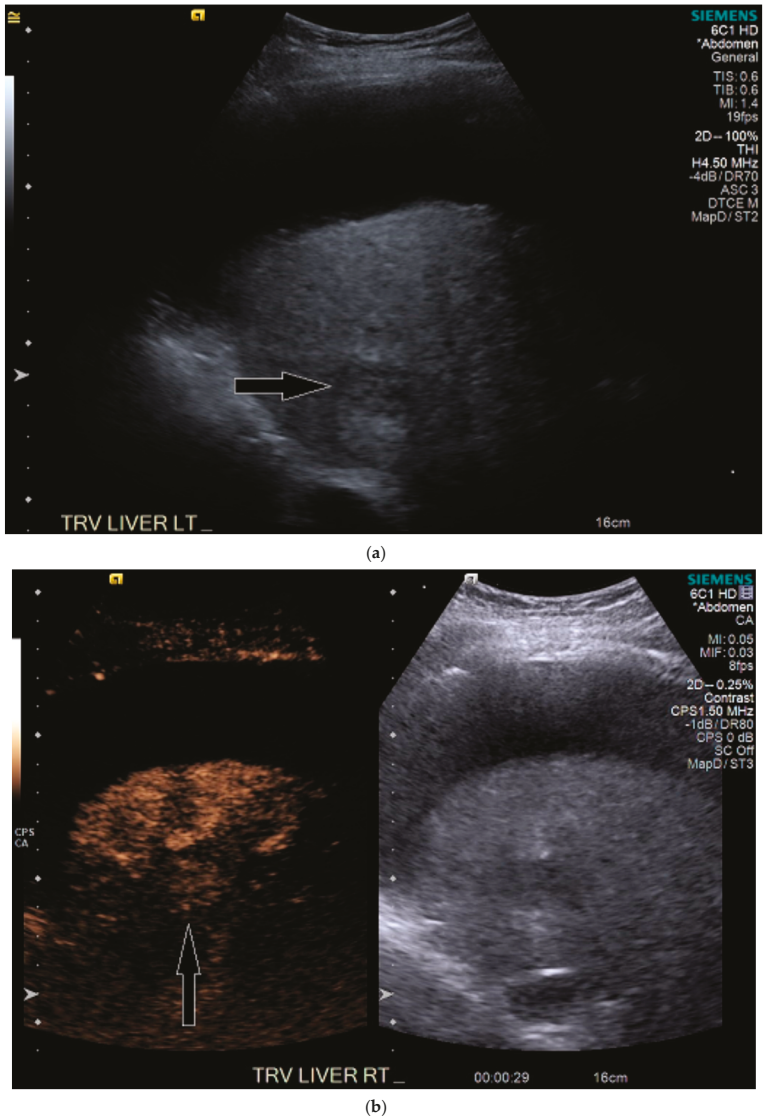
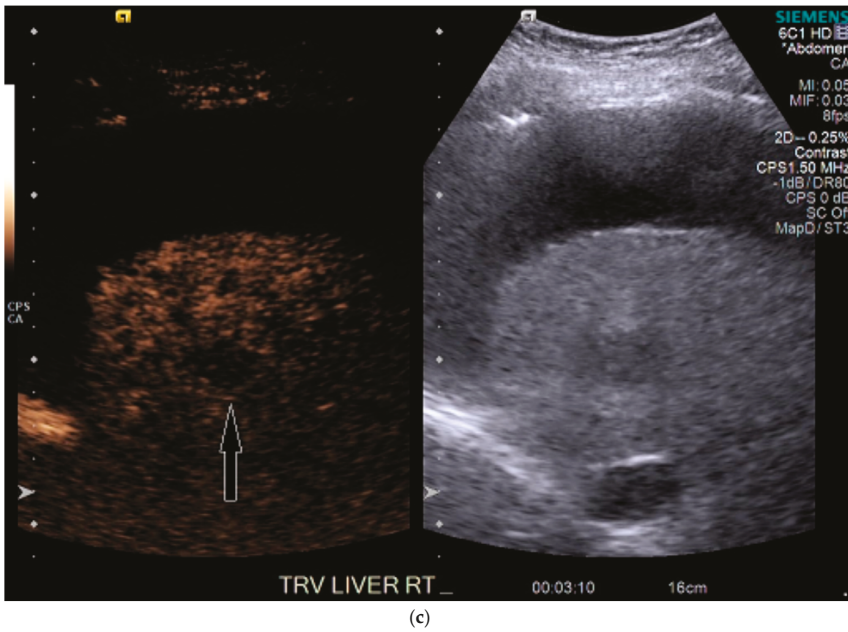
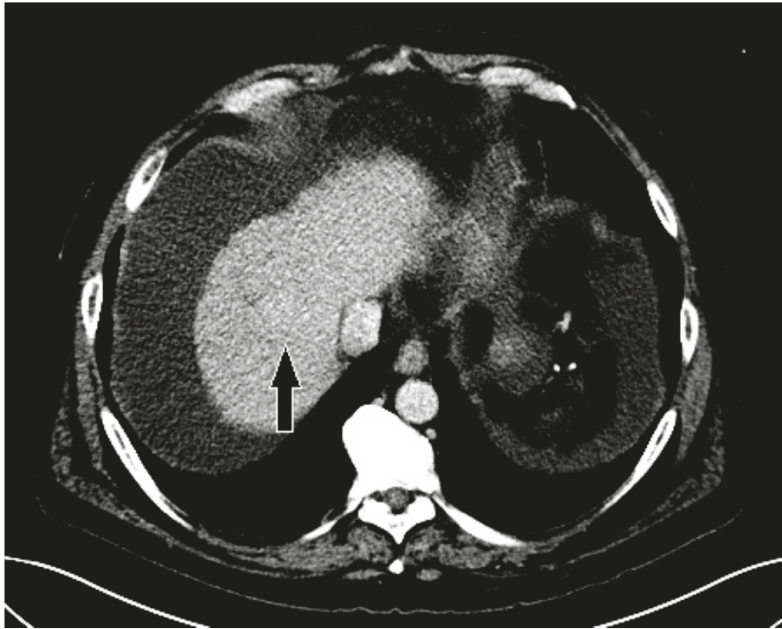


Figure 5. Cont.



**Figure 5.** Patient 3 ultrasound images, ascites is present with lesion denoted by white arrow: (a) grayscale images showing the hypochoic lesion. Post contrast administration ultrasound in arterial phase shows subtle enhancement compared with liver parenchyma at the same level (b) and delayed phase mild washout (c) of the lesion, LI-RADS 5.

His liver function continued to decline during his stay, and within two weeks he received a deceased donor liver transplantation. HCC within the explanted liver was confirmed by histopathological examination, corresponding to the findings on CEUS. Upon review of the prior CT, for which a reduced contrast bolus (75 mL Omnipaque™ 350) was given due to his chronic renal disease, the tumor was subtle but faintly visible with the knowledge of its location based on the findings on CEUS (Figure 6).



(a)



(b)

**Figure 6.** Patient 3 CT images using liver windows to highlight the subtle enhancement and washout of the lesion seen on CEUS (white arrow): (a) late arterial phase axial contrast-enhanced CT; (b) 3 min delayed phase.

#### 4. Discussion

With CEUS, patients at risk for HCC do not necessarily need to return for a second visit to get a CT or MRI when screening ultrasound identifies a focal abnormality—the lesion can be characterized at the time of the initial study. As of the 2017 edition of LI-RADS for CEUS [20], the United Network for Organ Sharing does not officially recognize CEUS, therefore while it can be used for transplant candidates, the patient will need a multiphase CT or MRI or biopsy to receive exception points for HCC. This is not a factor for patients who do not qualify for transplantation or are already at the top of the list. In our geographic area, MRI is not as commonly performed as CT for screening of HCC. Health insurance companies have increasingly denied screening CT, and so many of our patients are being monitored with US. However, even with characterization via CEUS, CT or MRI may still be performed subsequently for several reasons. In a practice just starting a CEUS program, it is useful to clinicians and radiologists to confirm that the diagnosis is correct via gold standard, noninvasive means. If a large lesion is confirmed as HCC, CT may still be required for staging purposes or for mapping arterial anatomy prior to TACE or transplant, however less phases may be required, resulting in decreased radiation. If the US is limited in visualizing the entire liver, CT or MRI may be appropriate to identify any additional lesions prior to treatment or transplant.

In the three presented cases, CEUS readily and accurately identified malignant lesions in each patient, as compared with their CT counterparts. For the first two cases, the patients had subsequent well-timed four-phase CTs, with very subtle lesions that may not have been detected without prior knowledge of the US findings. We postulate that this may have occurred in these cases, both of which were LI-RADS M, because the lesions enhanced so rapidly—likely earlier than the diagnostic late arterial phase CT—and then quickly became isoechoic, about the time the CT arterial bolus would have begun scanning (confirmed in our first patient). LI-RADS M lesions per ACR are diagnostic for a malignancy but are not specific to HCC [17,18]. HCC classically enhances in the arterial phase, and it has a late, but mild washout, which necessitates the timing for the CT phases, but in CEUS, continuous scanning can be performed. Those in the “M” category have rapid (less than 60 s) and/or marked washout on delayed images [20]. It is currently unknown how many “M” lesions represent HCC in at-risk patients diagnosed via CEUS, versus intrahepatic cholangiocarcinoma or mixed HCC–cholangiocarcinoma subtypes. However, it has been shown that LI-RADS M lesions on CT and MRI are HCC approximately one-third of the time [18]. It is unclear if this will hold true for CEUS, as it may identify “M” lesions at smaller sizes and earlier than CT, and thus if biopsied, could have a different, earlier tumor biology. In our first case, despite its appearance on CEUS, the tumor did not respond well to TACE. As a multiphase CT LI-RADS 5 designation is considered noninvasively diagnostic of HCC, a tissue biopsy would not be necessary. It is feasible that it could have represented a tumor that was not as responsive to TACE, and biopsy should be considered when CEUS and CT present discordant diagnoses of malignancy.

In our experience, CEUS identifies more “M” lesions than CT. In fact, both of our presented first and second cases were considered LI-RADS 4 or 5 by CT, despite the CEUS designation. Additional research into this area is needed—both in terms of histopathology of “M” lesions on CEUS in patients at risk for HCC, as well as if “M” lesions are more apparent and presenting earlier on CEUS than they are on well-timed CT. It is possible that MRI may have clearly identified both lesions when CT did not, as it does not rely solely on post contrast imaging. In the case of our second patient, a very small lesion may still be obscured via MRI if the patient is not able to consistently breath-hold, which is not usually an issue in CEUS.

In our third case, the lesion was not seen on the prior CT. This may have been due to location, and a lower dose of intravenous contrast that was used due to the patient’s impaired renal function. Interestingly, this lesion was well seen with CEUS, despite its challenging location at the dome, which can be a blind spot in US. We postulate that the ascites may have aided the CEUS exam—even though it increased the depth of the lesion, the ascites created a window to view the lesion, even with patient breathing, both of which would have negatively impacted on MRI.

HCC is the most common primary liver tumor [1], and imaging is a necessary component in screening patients at high risk of developing HCC with the current noninvasive gold standards of multiphase CT or MRI. The use of CEUS offers an alternative and reliable modality to diagnose HCC. CEUS is less expensive, it does not involve radiation, does not affect the kidneys, and it allows for multiple doses in one setting. In a meta-analysis, CEUS has been shown to have a sensitivity of 85% and specificity of 91% in diagnosing HCC [12]. Quai et al., has shown increased sensitivity when CEUS is used in conjunction with CT (97%) as compared with CT only (71–74%) in patients at risk for malignancy secondary to cirrhosis [21]. Our case series supports this finding, although it argues that, at least in some cases, CEUS may be more predictive than CT and if discordant LI-RADS results occur, a tie-breaker should be considered, such as biopsy if amenable, or MRI.

The ACR has created the LI-RADS criteria for noninvasive imaging diagnosis of HCC in patients at risk for its development. Recent articles have reviewed approaches to diagnosing HCC with CEUS [20,22,23]. Additional societies worldwide also have guidelines for noninvasive diagnosis of HCC, including European Federation of Societies for Ultrasound in Medicine and Biology (EFSUMB), World Federation for Ultrasound in Medicine and Biology (WFUMB), and Erlanger Synopsis of Contrast-Enhanced Ultrasound for Liver Lesion Assessment in Patients at risk (ESLAP), with studies comparing and contrasting them with LI-RADS. Schellhass et al. recently completed a multicenter study comparing prospective diagnosis at the time of CEUS with retrospective categorizing lesions via ESLAP and LIRADS guidelines [24]. This re-demonstrated accuracy of CEUS for noninvasive diagnosis of HCC and intrahepatic cholangiocarcinoma in cirrhotic patients and found that real-time diagnosis and ESLAP had highest sensitivities, while LIRADS had superior sensitivity. Negative predictive value of LIRADS was inferior, with positive predictive value similarly high among all three diagnostic categories [24]

Within LI-RADS guidance, there is an additional category for malignant lesion that is not specific for HCC- LI-RADS M [18,19]. CEUS can provide crucial information that can be used to differentiate HCC from intrahepatic cholangiocarcinoma (ICC), by demonstrating differences in their enhancement patterns [23]. As discussed, HCC classically shows arterial hyperenhancement and delayed, mild contrast washout in the late phase [22]. In contrast, ICC shows peripheral arterial contrast enhancement with early contrast washout of the vascularized parts of the lesion in the portal-venous and late phase [23,25]. This may allow for key differentiation between two malignancies and further argues for the usefulness of CEUS as a diagnostic modality. However, it is unclear how common a mixed subtype ICC/HCC is in cirrhotic patients or its enhancement patterns, and biopsy may still be necessary.

Small liver nodules can be a challenge to diagnose in these patients regardless of modality used, and this is no different in CEUS. A recent study by Huang et al. has shown that when CEUS is used for lesions less than 2 cm, that LI-RADS has a high specificity for HCC. It did also note that LI-RADS had lower sensitivity than when guidelines from EFSUMB and WFUMB were utilized [26]. It may be a challenge to accurately determine the LI-RADS categorization of lesions less than 1 cm via morphology due to their small size and this may be more dependent upon the patients' sonographic characteristics (such as obesity, steatosis, location of the lesion). Regardless, sub-centimeter lesions do not reach noninvasive imaging criteria for HCC diagnosis in LI-RADS, the most they can reach is intermediate (LI-RADS 3) or "probably" HCC (LI-RADS 4) when utilizing CEUS, CT, or MRI. As this does not earn potential transplant patient exception points, nor exclude them from transplant, many institutions will continue to observe these small lesions with shorter interval follow-ups, and treat them when they are larger and definitively declare themselves if growth is observed [16,20].

Adenomas are liver lesions that are rarely seen in cirrhotics, but do in general have a transformation risk to HCC of 5-10%, with risk factors of male sex, glycogen storage disease, anabolic steroid use, and beta-catenin adenoma subtype [27,28]. On imaging, adenomas can show enhancement features that overlap with HCC, and unfortunately there are not yet definitive noninvasive diagnostic characteristics of the highest-risk subtype of beta-catenin on imaging [28]. While different subtypes of adenomas have

differing transformation risks, differentiating imaging characteristics are not necessarily dependable, and biopsy may be required to determine the subtype and therefore the transformation risk, or if transformation has already occurred. On CEUS, there is significant overlap of adenoma with HCC in their enhancement patterns [15,22] but there may be differentiation by very early features in how the lesion enhances [15]. It is important to note that CEUS may show washout in adenomas, when MRI does not, which may be attributable to the contrast characteristics—CEUS contrast agents remain intravascular, whereas MRI agents diffuse into the interstitium [28]. Diagnosis in these patients depends upon patient characteristics and cirrhotic risks, consideration of multimodality imaging, and ultimately may depend upon biopsy.

CEUS does have inherent limitations, many of which are shared with routine US. Accuracy depends on the operator with room for variability in interpretation and diagnosis [24]. CEUS also performs similarly to grayscale US where significant adiposity or advanced hepatic steatosis can cause limited visibility [13]. Furthermore, it may not detect very deep lesions (classically dome and central/medial lesions) that are greater than 10 cm from the probe and therefore cannot be characterized via CEUS. However, newer contrast software programs are available that can image significantly greater depths to overcome this limitation. CEUS can target several lesions during a visit and can distinguish portal vein bland versus tumor thrombus [29]. However, screening the whole liver in terms of convenience and cost-effectiveness can prove difficult, as repeated injections of the contrast agent are needed to examine all of the level segments [30]. Moreover, CEUS cannot stage a patient, and single-phase CT may be needed in patients who are at risk for distant HCC metastasis, which would reduce their overall radiation dose.

Future directions with CEUS include continuing studies on accuracy, particularly LIRADS M lesion pathology as these may be a more common finding on CEUS than diagnosed with CT in the cirrhotic population due to continual imaging, as opposed to limited timepoints post contrast in CT. Additional studies have looked at quantitative enhancement patterns and perfusion analysis in HCC [31] by looking at time intensity curves, peak enhancement, and area under the curve to differentiate lesions. However, in the United States, not all US contrast software packages currently have this capability. Molecular ultrasound imaging is another emerging field within CEUS, using targeted contrast agents. In the future, this could be in use for diagnosing specific lesions and for targeted therapeutics delivery [32,33].

## 5. Conclusions

Accumulating evidence has demonstrated the important role of CEUS in diagnosing tumors of the liver, and that CEUS can offer certain advantages over or in conjunction with CT in specific patient populations. These include patients with contraindications to CT or MRI due to renal dysfunction, contrast-related allergy, inability to breath-hold without anesthesia, MRI noncompatible pacemaker, and so forth. Our case series shows that, in some cases, the tumors may be visible earlier via CEUS than CT, when both studies are optimized, and when results are discrepant between LIRADS M and LIRADS 5 lesions, biopsy or an alternate tie-breaking imaging modality should strongly be considered. CEUS is an important imaging modality that is complementary to CT for detecting and diagnosing tumors in liver such as HCC and should be incorporated into HCC screening imaging paradigms. Future studies are indicated to evaluate the utility of CEUS for early detection of the subtypes of tumors, and to examine the value of CEUS for monitoring the therapeutic response of HCC.

**Supplementary Materials:** The following are available online at <http://www.mdpi.com/2305-6320/7/9/51/s1>. Video S1: Patient with dynamic arterial phase ultrasound imaging of the liver lesion via after Lumason® injection. Dynamic ultrasound imaging of the right lobe of the liver after contrast administration in Patient 1, during active patient breathing with sweeps through the area of concern. The lesion is seen to enhance above background liver at time stamp 0:24 s and has started to washout by the end of the 60 s clip. Sweeps include images of the right kidney posterior to the liver, and patency of the portal vein.

**Author Contributions:** Conceptualization, K.L.M. and N.S.Y.; methodology, K.L.M. and N.S.Y.; formal analysis, K.L.M.; data curation, K.L.M, S.H.; writing—original draft preparation, K.L.M., S.Z., A.A., and N.S.Y.;



writing—review and editing, K.L.M., S.Z., A.A., S.H, and N.S.Y. All authors have read and agreed to the published version of the manuscript.

**Funding:** This research received no external funding.

**Conflicts of Interest:** The authors declare no conflict of interest.

## References

1. El-Serag, H.B.; Rudolph, K.L. Hepatocellular carcinoma: Epidemiology and molecular carcinogenesis. *Gastroenterology* **2007**, *132*, 2557–2576. [[CrossRef](#)] [[PubMed](#)]
2. Janevska, D.; Chaloska-Ivanova, V.; Janevski, V. Hepatocellular carcinoma: Risk factors, diagnosis and treatment. *Open Access Maced. J. Med. Sci.* **2015**, *3*, 732–736. [[CrossRef](#)] [[PubMed](#)]
3. Heidelbaugh, J.J.; Bruderly, M. Cirrhosis and chronic liver failure: Part I. Diagnosis and evaluation. *Am. Fam. Physician* **2006**, *74*, 756–762. [[PubMed](#)]
4. Singal, A.G.; Pillai, A.; Tiro, J. Early detection, curative treatment, and survival rates for hepatocellular carcinoma surveillance in patients with cirrhosis: A meta-analysis. *PLoS Med.* **2014**, *11*, e1001624. [[CrossRef](#)]
5. Schaub, S.K.; Hartvigson, P.E.; Lock, M.I.; Høyer, M.; Brunner, T.B.; Cardenes, H.R.; Dawson, L.A.; Kim, E.Y.; Mayr, N.A.; Lo, S.S.; et al. Stereotactic body radiation therapy for hepatocellular carcinoma: Current trends and controversies. *Technol. Cancer Res. Treat.* **2018**, *17*, 1533033818790217. [[CrossRef](#)]
6. Shetty, S.K.; Rosen, M.P.; Raptopoulos, V.; Goldberg, S.N. Cost-effectiveness of percutaneous radiofrequency ablation for malignant hepatic neoplasms. *J Vasc. Interv. Radiol.* **2001**, *12*, 823–833. [[CrossRef](#)]
7. Vogl, T.J.; Naguib, N.N.; Nour-Eldin, N.E.; Rao, P.; Emami, A.H.; Zangos, S.; Nabil, M.; Abdelkader, A. Review on transarterial chemoembolization in hepatocellular carcinoma: Palliative, combined, neoadjuvant, bridging, and symptomatic indications. *Eur. J. Radiol.* **2009**, *72*, 505–516. [[CrossRef](#)]
8. Marks, E.I.; Yee, N.S. Molecular genetics and targeted therapy in hepatocellular carcinoma. *Curr. Cancer Drug Targets* **2016**, *16*, 53–70. [[CrossRef](#)]
9. Posadas, K.; Ankola, A.; Zang, Z.; Yee, N.S. Tumor molecular profiling for an individualized approach to the treatment of hepatocellular carcinoma: A patient case study. *Biomedicines* **2018**, *6*, 46. [[CrossRef](#)]
10. Yee, N.S. Update in systemic and targeted therapies in gastrointestinal oncology. *Biomedicines* **2018**, *6*, 34. [[CrossRef](#)]
11. Marrero, J.A.; Kulik, L.M.; Sirlin, C.B.; Zhu, A.X.; Finn, R.S.; Abecassis, M.M.; Roberts, L.R.; Heimbach, J.K. Diagnosis, staging, and management of hepatocellular carcinoma: 2018 practice guidance by the American association for the study of liver diseases. *Hepatology* **2018**, *68*, 723–750. [[CrossRef](#)] [[PubMed](#)]
12. Zhang, J.; Yu, Y.; Li, Y.; Wei, L. Diagnostic value of contrast-enhanced ultrasound in hepatocellular carcinoma: A meta-analysis with evidence from 1998 to 2016. *Oncotarget* **2017**, *8*, 75418–75426. [[CrossRef](#)]
13. Pang, E.H.T.; Chan, A.; Ho, S.G.; Harris, A.C. Contrast-Enhanced ultrasound of the liver: Optimizing technique and clinical applications. *AJR Am. J. Roentgenol.* **2018**, *210*, 320–332. [[CrossRef](#)] [[PubMed](#)]
14. Quaia, E. Microbubble ultrasound contrast agents: An update. *Eur. Radiol.* **2007**, *17*, 1995–2008. [[CrossRef](#)] [[PubMed](#)]
15. Burrowes, D.P.; Medellin, A.; Harris, A.C.; Milot, L.; Wilson, S.R. Contrast-enhanced US approach to the diagnosis of focal liver masses. *Radiographics* **2017**, *37*, 1388–1400. [[CrossRef](#)] [[PubMed](#)]
16. American College of Radiology. Liver Reporting & Data System (LI-RADS). 2020. Available online: <https://www.acr.org/Clinical-Resources/Reporting-and-Data-Systems/LI-RADS>. (accessed on 30 June 2020).
17. Kim, T.K.; Noh, S.Y.; Wilson, S.R.; Kono, Y.; Piscaglia, F.; Jang, H.J.; Lyshchik, A.; Dietrich, C.F.; Willmann, J.K.; Vezeridis, A.; et al. Contrast-enhanced ultrasound (CEUS) liver imaging reporting and data system (LI-RADS) 2017—A review of important differences compared to the CT/MRI system. *Clin. Mol. Hepatol.* **2017**, *23*, 280–289. [[CrossRef](#)]
18. Van der Pol, C.B.; Lim, C.S.; Sirlin, C.B.; McGrath, T.A.; Salameh, J.P.; Bashir, M.R.; Tang, A.; Singal, A.G.; Costa, A.F.; Fowler, K.; et al. Accuracy of the liver imaging reporting and data system in computed tomography and magnetic resonance image analysis of hepatocellular carcinoma or overall Malignancy-A systematic review. *Gastroenterology* **2019**, *156*, 976–986. [[CrossRef](#)]
19. Schima, W.; Heiken, J. LI-RADS v2017 for liver nodules: How we read and report. *Cancer Imaging* **2018**, *18*, 14. [[CrossRef](#)]

20. American College of Radiology. CEUS LI-RADS® v2017 CORE. Available online: <https://www.acr.org/-/media/ACR/Files/RADS/LI-RADS/CEUS-LI-RADS-2017-Core.pdf> (accessed on 30 June 2020).
21. Quaia, E.; Alaimo, V.; Baratella, E.; Medeot, A.; Midiri, M.; Cova, M.A. The added diagnostic value of 64-row multidetector CT combined with contrast-enhanced US in the evaluation of hepatocellular nodule vascularity: Implications in the diagnosis of malignancy in patients with liver cirrhosis. *Eur. Radiol.* **2009**, *19*, 651–663. [CrossRef]
22. Burrowes, D.P.; Kono, Y.; Medellin, A.; Wilson, S.R. *RadioGraphics* Update: Contrast-enhanced US approach to the diagnosis of focal liver masses. *Radiographics* **2020**, *40*, E16–E20. [CrossRef]
23. Wang, D.C.; Jang, H.J.; Kim, T.K. Characterization of indeterminate liver lesions on CT and MRI With contrast-enhanced ultrasound: What is the evidence? *AJR Am. J. Roentgenol.* **2020**, *214*, 1295–1304. [CrossRef] [PubMed]
24. Schellhaas, B.; Bernatik, T.; Bohle, W.; Borowitzka, F.; Chang, J.; Dietrich, C.; Dirks, K.; Donoval, R.; Drube, K.; Friedrich-Rust, M.; et al. Contrast-Enhanced ultrasound algorithms (CEUS-LIRADS/ESCALAP) for the noninvasive diagnosis of hepatocellular carcinoma—A prospective multicenter DEGUM study. *Ultraschall Med.* **2020**. [CrossRef]
25. Wildner, D.; Bernatik, T.; Greis, C.; Seitz, K.; Neurath, M.; Strobel, D. CEUS in hepatocellular carcinoma and intrahepatic cholangiocellular carcinoma in 320 patients—Early or late washout matters: A subanalysis of the DEGUM multicenter trial. *Ultraschall Med.* **2015**, *36*, 132–139. [CrossRef] [PubMed]
26. Huang, J.; Li, J.; Lu, Q.; Luo, Y.; Lin, L.; Shi, Y.; Li, T.; Liu, J.; Lyshchik, A. Diagnostic accuracy of CEUS LI-RADS for the characterization of liver nodules 20 mm or smaller in patients at risk for hepatocellular carcinoma. *Radiology* **2020**, *294*, 329–339. [CrossRef]
27. Gordic, S.; Thung, S.N.; Roayaie, S.; Wagner, M.; Taouli, B. Hepatic adenomatosis in liver cirrhosis. *Eur. J. Radiol. Open.* **2017**, *4*, 115–117. [CrossRef]
28. Katabathina, V.S.; Menias, C.O.; Shanbhogue, A.K.; Jagirdar, J.; Paspulati, R.M.; Prasad, S.R. Genetics and imaging of hepatocellular adenomas: 2011 update. *Radiographics* **2011**, *31*, 1529–1543. [CrossRef]
29. Tarantino, L.; Ambrosino, P.; Di Minno, M.N. Contrast-enhanced ultrasound in differentiating malignant from benign portal vein thrombosis in hepatocellular carcinoma. *World J. Gastroenterol.* **2015**, *21*, 9457–9460. [CrossRef]
30. Jang, J.Y.; Kim, M.Y.; Jeong, S.W.; Kim, T.; Kim, S.; Lee, S.; Suk, K.; Park, S.; Woo, H.; Kim, S.G.; et al. Current consensus and guidelines of contrast enhanced ultrasound for the characterization of focal liver lesions. *Clin. Mol. Hepatol.* **2013**, *19*, 1–16. [CrossRef]
31. Schaible, J.; Stroszczyński, C.; Beyer, L.P.; Jung, E.M. Quantitative perfusion analysis of hepatocellular carcinoma using dynamic contrast enhanced ultrasound (CEUS) to determine tumor microvascularization. *Clin. Hemorheol. Microcirc.* **2019**, *73*, 95–104. [CrossRef]
32. Hackl, C.; Schacherer, D.; Anders, M.; Wiedemann, L.M.; Mohr, A.; Schlitt, H.J.; Stroszczyński, C.; Tranquart, F.; Jung, E.M. Improved detection of preclinical colorectal liver metastases by high resolution ultrasound including molecular ultrasound imaging using the targeted contrast agent BR55. *Ultraschall Med.* **2016**, *37*, 290–296. [CrossRef]
33. Unnikrishnan, S.; Klibanov, A.L. Microbubbles as ultrasound contrast agents for molecular imaging: Preparation and application. *AJR Am. J. Roentgenol.* **2012**, *199*, 292–299. [CrossRef] [PubMed]



© 2020 by the authors. Licensee MDPI, Basel, Switzerland. This article is an open access article distributed under the terms and conditions of the Creative Commons Attribution (CC BY) license (<http://creativecommons.org/licenses/by/4.0/>).



Review

# Worldwide Use of RUCAM for Causality Assessment in 81,856 Idiosyncratic DILI and 14,029 HILI Cases Published 1993–Mid 2020: A Comprehensive Analysis

Rolf Teschke <sup>1,\*</sup> and Gaby Danan <sup>2</sup>

<sup>1</sup> Department of Internal Medicine II, Division of Gastroenterology and Hepatology, Klinikum Hanau, D-63450 Hanau, Teaching Hospital of the Medical Faculty of the Goethe University, D-60590 Frankfurt/Main, Germany

<sup>2</sup> Pharmacovigilance Consultancy, F-75020 Paris, France; gaby.danan@gmail.com

\* Correspondence: rolf.teschke@gmx.de

Received: 19 August 2020; Accepted: 25 September 2020; Published: 29 September 2020

**Abstract:** **Background:** A large number of idiosyncratic drug induced liver injury (iDILI) and herb induced liver injury (HILI) cases of variable quality has been published but some are a matter of concern if the cases were not evaluated for causality using a robust causality assessment method (CAM) such as RUCAM (Roussel Uclaf Causality Assessment Method) as diagnostic algorithm. The purpose of this analysis was to evaluate the worldwide use of RUCAM in iDILI and HILI cases. **Methods:** The PubMed database (1993–30 June 2020) was searched for articles by using the following key terms: Roussel Uclaf Causality Assessment Method; RUCAM; Idiosyncratic drug induced liver injury; iDILI; Herb induced liver injury; HILI. **Results:** Considering reports published worldwide since 1993, our analysis showed the use of RUCAM for causality assessment in 95,885 cases of liver injury including 81,856 cases of idiosyncratic DILI and 14,029 cases of HILI. Among the top countries providing RUCAM based DILI cases were, in decreasing order, China, the US, Germany, Korea, and Italy, with China, Korea, Germany, India, and the US as the top countries for HILI. **Conclusions:** Since 1993 RUCAM is certainly the most widely used method to assess causality in iDILI and HILI. This should encourage practitioner, experts, and regulatory agencies to use it in order to reinforce their diagnosis and to take sound decisions.

**Keywords:** RUCAM; Roussel Uclaf Causality Assessment Method; diagnostic algorithm; iDILI; iDrug induced liver injury; DILI; HILI; herb induced liver injury

## 1. Introduction

Idiosyncratic drug induced liver injury (DILI), in short also termed iDILI, and herb induced liver injury (HILI) are complex diseases and received much attention in recent years [1–9]. The present scientometric study comprehensively analyzed the global knowledge base and specific emerging topics of DILI derived from 1995 publications in 79 countries and regions, with an impressive annual growth of reports between 2010 and 2019 and almost 340 studies published in 2020 [1]. In parallel, more and more publications on DILI and HILI cases refer to RUCAM (Roussel Uclaf Causality Assessment Method) for causality assessment [10–13]. The original RUCAM was first published in 1993 [14] and updated in 2016 [15] with additional information on its use and perspectives [16,17], which is now the preferred version to be used in future cases of DILI and HILI [15]. It is widely recognized that causality assessment in DILI and HILI is a multifaceted approach [7–9,15], a real medical challenge, for which a diagnostic quantitative algorithm such as RUCAM is an easy tool for case evaluation [10–18] to solve complex conditions [18].

The RUCAM algorithm is a structured, standardized, transparent, liver specific and quantitative diagnostic clinical scale based on key elements of liver injury, which are individually scored and

provide a score for five-degree causality grading from unrelated up to highly probable causality levels [15]. Since key elements are specifically described and scored, assessments are objective with little risk of subjectivity [15–17] commonly observed if the approach to assess causality lacks scored key elements [19]. RUCAM can help expand our knowledge by enlarging population analysis with prospective and scored causality assessment, allowing for harmonized interpretation of data across populations [20]. In this context, RUCAM should be viewed as a cornerstone approach assessing causality of liver injury cases [15–17,21], because robust diagnostic biomarkers are rarely available due to misconducted studies as outlined by EMA (European Medicines Agency: Formerly London, UK, now Amsterdam, Netherlands) [21].

In this review article, current conditions of DILI and HILI cases assessed worldwide using RUCAM were critically analyzed. For the first time, the focus is on reports published from 1993 to mid 2020 and the discussion of their potential use to describe specific features of DILI and HILI cases.

## 2. Literature Search and Source

The PubMed database (1993–30 June 2020) was searched for articles by using the following key terms: Roussel Uclaf Causality Assessment Method; RUCAM; Idiosyncratic drug induced liver injury (iDILI); Herb induced liver injury (HILI). Key terms were used alone or in combination. Limited to the English language, publications from each search terms were analyzed for suitability of this review article. The electronic search was completed on 30 June 2020 and supplemented by a manual literature search, using also the large private archive of the authors when the publication was not yet referenced in PubMed. The final compilation consisted of original papers including individual case reports and case series, consensus reports, and review articles with the most relevant publications included in the reference list of this review.

## 3. Definitions

RUCAM is presented as an algorithm that requires a few criteria allowing for a final quantitative evaluation. In particular, establishing RUCAM based criteria of liver test thresholds and liver injury patterns was revolutionary at the time of first publication issued from an international consensus meeting of experts, without the requirement of a liver biopsy [14] with same principles preserved in the updated RUCAM [15].

### 3.1. RUCAM Based Liver Injury

#### 3.1.1. Liver Test Thresholds

A liver injury caused by exogenous compounds such as drugs and herbs is defined by specific threshold values established for the liver tests (LTs) alanine aminotransferase (ALT) and alkaline phosphatase (ALP), with current serum activities considered as relevant for  $ALT \geq 5 \times ULN$  (upper limit of normal) and  $ALP \geq 2 \times ULN$  [15] provided that ALP is of hepatic origin. The original RUCAM was the first causality assessment method (CAM) ever considering threshold criteria although initially with lower values for ALT [15] as compared to currently used criteria [16]. Of note, serum bilirubin is not part of the diagnostic RUCAM algorithm that uses ALT or ALP as diagnostic liver test. In this context, conjugated bilirubin is a sign of the severity of the liver injury.

#### 3.1.2. Liver Injury Pattern

RUCAM was also the first CAM proposing different patterns of liver injury based on LTs [14] and are included also in the updated RUCAM [15]. To determine the liver injury pattern, the ratio R is to be calculated using the multiple of the ULN of serum ALT divided by the multiple of the ULN of serum ALP, provided the ALP increase is of hepatic origin. For causality assessment purposes, two types of liver injury are defined (independently from histological findings): first a hepatocellular injury with  $R > 5$ , and second, a cholestatic/mixed liver injury with  $R \leq 5$ .

### 3.2. Idiosyncratic Versus Intrinsic Liver Injury

Liver injury is either idiosyncratic, due to the interaction between the exogenous synthetic chemical or phytochemical and a susceptible individual with some genetic factor(s), or it is intrinsic due to chemical overdose [11–13]. In the present analysis, idiosyncratic injury is considered, as opposed to intrinsic liver injury most commonly observed with overdosed drugs such as acetaminophen [22].

## 4. Worldwide Publications of DILI

The current scientometric report from China on knowledge mapping confirmed the high worldwide interest in DILI publications and identified a total of 1995 DILI studies published between 2010 and 2019, although information on the applied method of causality assessment was not provided and will need further clarification [1]. This Chinese analysis on the top 10 countries involved in DILI research listed the US, China, Japan, Germany, UK, Spain, France, the Netherlands, Sweden, and Canada. In addition, many interesting details on DILI were comprehensively discussed with focus on definition, incidence rate, clinical characteristics, etiology or pathogenesis such as the character of the innate immune system, the regulation of cell-death pathways, susceptible HLA (Human Leukocyte Antigen) identification, or criteria and methods of causality assessment, all topics were considered as the knowledge base for DILI research [1].

## 5. Worldwide Publications of RUCAM Based Idiosyncratic DILI

The worldwide impact of DILI can best be quantified by using liver injury cases assessed for causality with a robust method that allows for establishing causality gradings for each implicated drug and to exclude alternative causes unrelated to drug administration.

### 5.1. Countries and Regions

In the current analysis, authors from 31 countries worldwide reported on cases of idiosyncratic DILI caused by multiple drugs published from 1993 up to mid 2020 and applied in all cases RUCAM to assess causality (Table 1) [23–180]. Such a table with a comprehensive list of publications over a long period has never been reported before and will facilitate the search for RUCAM based DILI cases caused by individual drugs, considering that databases such as LiverTox may have problems providing real DILI cases [10,74].

### 5.2. Hospital and Other Sources

RUCAM based DILI cases were mostly published by authors from university hospitals and their affiliated teaching hospitals known for their high reputation (Table 1). Among these were a broad range of departments, which in most cases include departments of Hepatology and Gastroenterology, ensuring careful clinical evaluation of patients with suspected DILI and associated causality assessment for the offending drug(s). To a lesser degree, other departments were contributors, for instance, Pharmacology, or Pharmacy and Pharmaceutical sciences [170].

**Table 1.** Worldwide countries with a selection of published DILI cases assessed for causality using RUCAM.

Country/ DILI Cases, <i>n</i>	First Author/Year	DILI Cases, <i>n</i>	Drugs	Comments on RUCAM Based DILI Cases
<b>Argentina</b> <i>n</i> = 625	Bessone, 2016 [23]	197	Various drugs	DILI caused by a variety of drugs, not allowing individual description of features
	Bessone, 2019 [24]	114	Various drugs	Individual drugs not available for DILI feature characterization
	Colaci, 2019 [25]	311	Various drugs	DILI features for single drugs were not presented
<b>Australia</b> <i>n</i> = 106	García, 2019 [26]	3	Methotrexate	Feature details provided for DILI by methotrexate
	Lin, 2014 [27]	47	Various volatile anaesthetics	DILI by anaesthetics without individual features of isoflurane, desflurane, or sevoflurane
	Ahmed, 2015 [28]	1	Ipilimumab	Detailed features of the DILI case
<b>Bahrain</b> <i>n</i> = 25	Laube, 2019 [29]	1	Atorvastatin	Good feature presentation of this DILI case
	Worland, 2020 [30]	57	Infliximab	Feature presentation of DILI by the drug
	Sridharan, 2020 [31]	25	Various antiepileptic drugs	No feature details provided of DILI due to individual drugs
<b>Brazil</b> <i>n</i> = 4	Becker, 2019 [32]	4	Various drugs	Features of DILI caused by some drugs
	Yan, 2006 [33]	2	Rofecoxib	Two well described case features of DILI caused by rofecoxib
	Nhean, 2019 [34]	2	Dolutegravir	Careful described features of DILI
<b>Canada</b> <i>n</i> = 4	Hou, 2012 [35]	300	Various drugs	No feature details available for DILI by individual drugs
	Lv, 2012 [36]	89	Various drugs	Specific features of DILI by individual drugs were not presented
	Hao, 2014 [37]	140	Anti-Tuberculotics	Lacking specific DILI features of any drug
<b>China</b> <i>n</i> = 35,825	Ou, 2015 [38]	231	Various drugs	No feature specifics of DILI are available for individual drugs
	Zhu, 2015 [39]	39	Various drugs	Specific features of DILI caused by individual drugs were not provided
	Lu, 2016 [40]	513	Various drugs	Missing specific features of DILI caused by individual drugs
	Yang, 2016 [41]	124	Various drugs	Feature specifics of DILI caused by individual drugs were not provided
	Zhu, 2016 [42]	870	Various drugs	No specific features of DILI by individual drugs were presented
	Naqiong, 2017 [43]	157	Various statins	Cohort consisted of patients with DILI caused by atorvastatin, simvastatin, and rosuvastatin, but specific features were not provided for individual statins
	Li, 2018 [44]	1	Iguratomod	Detailed feature description of DILI
	Song, 2018 [45]	1	Posaconazole	Careful feature presentation of DILI by this drug

Table 1. *Cont.*

Country/ DILI Cases, <i>n</i>	First Author/Year	DILI Cases, <i>n</i>	Drugs	Comments on RUCAM Based DILI Cases
<b>China</b> <i>n</i> = 35,825	Tao, 2018, [46]	290	Anti-Tuberculoitics	Cohort included patients with DILI caused by isoniazid, rifampin, pyrazinamide, ethambutol, and streptomycin, but specific features were not presented for individual drugs
	Liao, 2019 [47]	1	Cefepime	Well described features of DILI by this drug
	Shen, 2019 [48]	18,956	Various drugs	Cohort comprized patients with DILI, but special DILI features related to individual drugs were not published.
	Xing, 2019 [49]	133	Various drugs	No specific feature presentation of DILI by individual drugs
	Ma, 2020 [50]	1	Fenofibrate	Specific feature of DILI by this drug presented
	Tao, 2020 [51]	146	Anti-Tuberculoitics	Lacking feature data of DILI caused by individual drugs
	Wang, 2020 [52]	155	Anti-Tuberculoitics	Cohort included patients with DILI due to not further identified anti-TB regimens, hence attributing specific DILI features to individual drugs was not possible
<b>Colombia</b> <i>n</i> = 19	Yang, 2020 [53]	13,678	Various drugs	No feature details of DILI by individual drugs
	Ríos, 2013 [54]	1	Albendazole	Detailed feature description of DILI caused by albendazole
	Cano-Paniagua, 2019 [55]	18	Various drugs	Perfect feature description of DILI by drugs in this excellent prospective epidemiology study using the updated RUCAM for causality assessment
	Alhaddad, 2020 [56]	75	Various drugs	Feature details of DILI by individual drugs incompletely provided
<b>Egypt</b> <i>n</i> = 75	Bénichou, 1993 [57]	94	Various drugs	No detailed feature description of DILI by the drugs
	Arotcarena, 2004 [58]	1	Pioglitazone	Feature description of the case
	Moch, 2012 [59]	18	Etofexine	Detailed features of DILI due to etofexine treatment
	Carrier, 2013 [60]	1	Methyl-prednisolone	Features of DILI well described for the drug
	Ripault, 2013 [61]	1	Crizotinib	Good feature details provided for DILI by this drug
<b>France</b> <i>n</i> = 170	Dumontier, 2017 [62]	5	Methyl-prednisolone	Careful feature description of DILI caused by the drug
	Meunier, 2018 [63]	50	Nimesulide	No feature description of DILI by this drug



Table 1. *Cont.*

Country/ DILI Cases, <i>n</i>	First Author/Year	DILI Cases, <i>n</i>	Drugs	Comments on RUCAM Based DILI Cases
Germany <i>n</i> = 10,907	Stammshulte, 2012 [64]	37	Flupirtine	Carefully presented features of DILI caused by flupirtine
	Douros, 2014 [65]	7	Flupirtine	Comprehensive feature presentation of DILI due to flupirtine
	Douros, 2014 [66]	198	Various drugs	Cohort of patients with DILI associated with the use of various drugs, but special features of DILI by individual drugs were not provided
	Buechter, 2018 [67]	15	Various drugs	No detailed feature presentation of DILI caused by individual drugs
	Dragoi, 2018 [68]	16	Diclofenac	Cohort of DILI patients with presentation of limited specific DILI features
	Teschke, 2018 [69]	7278	Various drugs	Cohort of DILI patients without feature specification for individual drugs
	Teschke, 2018 [70]	3312	Various drugs	Cohort of DILI cases not providing special features of DILI by individual drugs
	Weber, 2019 [71]	44	Various drugs	No specific features of DILI caused by individual drugs provided
	Björnsson, 2012 [72]	73	Statins	Specific feature details provided of DILI by statins
	Björnsson, 2013 [73]	72	Various drugs	Cohort of DILI cases without providing typical features of DILI by single drugs
Iceland <i>n</i> = 367	Björnsson, 2016 [74]	222	Various drugs	The two assessed cohorts provided no typical features of DILI caused by the evaluated drugs
	Harugeri, 2009 [75]	1	Montelukast	Good feature presentation of a patient with DILI caused by montelukast
	Devarbhavi, 2010 [76]	313	Various drugs	No feature description of DILI due to individual drugs
	Rathi, 2017 [77]	82	Various drugs	Cohort of DILI cases but features of DILI by individual drugs were not presented
	Taneja, 2017 [78]	2	Etodolac	Detailed feature presentation of DILI
	Das, 2018 [79]	24	Various drugs	Cohort with limited feature description of few patients with DILI caused by drugs assessed for causality by RUCAM or other CAMs
	Dutta, 2020 [80]	1	Haloperidol	Perfect presented feature details of DILI caused by this drug
	Kulkarni, 2020 [81]	1	Vitamin A	Perfect feature details of this DILI case
	Gluck, 2011 [82]	1	Amiodarone	Careful feature description of a patient with DILI caused by a single drug
	Israel <i>n</i> = 1			

Table 1. *Cont.*

Country/ DILI Cases, <i>n</i>	First Author/Year	DILI Cases, <i>n</i>	Drugs	Comments on RUCAM Based DILI Cases
<b>Italy</b> <i>n</i> = 1562	Rigato, 2007 [83]	1	Flavoxate	Good feature presentation of a patient with DILI caused by flavoxate
	Licata, 2010 [84]	46	Various drugs including Nimesulide	Feature description of patients with DILI by nimesulide but no description for DILI by other drugs
	Abenavoli, 2013 [85]	1	Cyproterone acetate	Detailed feature description of a patient with DILI
	Ferrajolo, 2017 [86]	938	Various antibiotics	Combined feature presentation of all antibiotics causing DILI in paediatric patients
	Licata, 2017 [87]	185	Various drugs	Epidemiology study, hence no feature description of patients with DILI by any drug
	Giacomelli, 2018 [88]	362	Nevirapine	Detailed feature description of DILI by nevirapine observed in all patients
	Licata, 2018 [89]	28	Rivaroxaban	Perfect feature description of this DILI cohort
	Lovero, 2018 [90]	1	Ustekinumab	Careful feature description of DILI caused by this drug
	Masumoto, 2003 [91]	85	Various drugs	No detailed feature description of DILI caused by drugs
	Hanatani, 2014 [92]	182	Various drugs	Detailed features of DILI by individual drugs not provided
	Nijjima, 2017 [93]	1	Ipragliflozin	Provided case features of DILI
	<b>Japan</b> <i>n</i> = 939	Ji, 2017 [94]	1	Methimazole
Aiso, 2019 [95]		270	Various drugs	Global feature description of DILI by all drugs
Kishimoto, 2019 [96]		1	Clonazepam	Detailed feature of DILI by this drug
Hiraki, 2019 [97]		1	Tegafur-Uracil	Good feature presentation of DILI caused by the drug
Kakisaki, 2019 [98]		398	Various drugs	Perfect feature description of the cohort
Choi, 2008 [99]		1	Albendazole	Detailed feature description of DILI by albendazole in a case report of a single patient
<b>Korea</b> <i>n</i> = 6528	Suk, 2012 [100]	101	Various drugs	Lacking detailed feature description of DILI by individual drugs
	Son, 2015 [101]	1	Various drugs	No specific feature description of DILI due to comedication
	Woo, 2016 [102]	1	Various comedicated drugs	Lacking specific feature description of DILI due to comedication
	Byeon, 2019 [103]	6391	Various drugs	Missing specific feature of DILI caused by individual drugs
	Kwon, 2019 [104]	33	Nimesulide	Detailed feature description of DILI caused by nimesulide, using a prospective study design in this perfect analysis

Table 1. *Cont.*

Country/ DILI Cases, <i>n</i>	First Author/Year	DILI Cases, <i>n</i>	Drugs	Comments on RUCAM Based DILI Cases
<b>Malaysia</b> <i>n</i> = 1	Thalha, 2018 [105]	1	Kombiglyze	Perfect feature description of DILI caused by the combination of metformin and saxagliptin
<b>Mexico</b> <i>n</i> = 1	Lammel-Lindemann, 2018 [106]	1	Candesartan	Well described features of DILI by this drug
<b>Morocco</b> <i>n</i> = 1	Essaid, 2010 [107]	1	Tadalafil	Feature description of DILI due to the drug
<b>Pakistan</b> <i>n</i> = 264	Abid, 2020 [108]	264	Various drugs	No specific feature details presented for DILI caused by individual drugs
<b>Portugal</b> <i>n</i> = 53	Costa-Moreira, 2020 [109]	53	Various drugs	Specific feature details of DILI caused by individual drugs were not provided
<b>Saudi Arabia</b> <i>n</i> = 1	Alqinawi, 2020 [110]	1	Menotropin	Perfect feature details of DILI by this specific drug
<b>Serbia</b> <i>n</i> = 99	Mijikovic, 2010 [111] Mijikovic, 2011 [112]	80 19	Various drugs Various drugs	No detailed feature description of DILI by individual drugs Lacking detailed feature presentation of DILI caused by individual drugs
<b>Singapore</b> <i>n</i> = 14	Wai, 2006 [113]	14	Various drugs	Limited feature description of DILI
	Rodriguez, 1996 [114]	35	Various drugs	No feature details of DILI cases provided for individual drugs
	Andrade, 2005 [115]	461	Various drugs	Limited feature description of DILI case details
	Andrade, 2006 [116]	28	Various drugs	Partial feature description of DILI by few drugs
	Garcia-Cortés, 2008 [117]	225	Various drugs	Limited feature description of DILI by few drug groups
<b>Spain</b> <i>n</i> = 1181	Lucena, 2011 [118]	78	Amoxicillin Clavulanate	Careful feature description of DILI by the drug combination
	Lucena, 2011 [119]	9	Various drugs	Feature description of DILI caused by individual drugs
	Robles-Diaz, 2015 [120]	25	Anabolic and androgenetic steroids	Limited feature description of DILI
	Tong, 2015 [121]	1	Methylphenidate	Careful evaluation of feature details provided for this DILI case
	Medina-Calitz, 2016 [122]	298	Various drugs	No specific feature description for DILI by any drug
	López-Riera, 2018 [123]	17	Various drugs	Lack of specific feature presentation of DILI by any drug

Table 1. *Cont.*

Country/ DILI Cases, <i>n</i>	First Author/Year	DILI Cases, <i>n</i>	Drugs	Comments on RUCAM Based DILI Cases
<b>Spain</b> <i>n</i> = 1181	Machlab, 2019 [124]	1	Apixabam	Careful feature description of the DILI case caused by the drug
	Zoubek, 2019 [125]	3	Methyl-prednisolone	Perfect feature presentation of DILI
	Björnsson, 2005 [126]	784	Various drugs	Detailed feature description of DILI by few drugs
<b>Sweden</b> <i>n</i> = 1508	De Valle, 2006 [127]	77	Various drugs	Limited feature description of DILI by a few drugs
	Björnsson, 2007 [128]	77	Various drugs	Lacking substantial feature description of DILI caused by few drugs
	Björnsson, 2007 [129]	570	Various drugs	Feature details of DILI presented
	Goossens, 2013 [130]	1	Ibandronate	Detailed description of immune DILI features by ibandronate, a bisphosphonate
	Russmann, 2014 [131]	14	Rivaroxaban	Perfect individual feature presentation of each DILI case
<b>Switzerland</b> <i>n</i> = 68	Scalfaro, 2017 [132]	49	Sacubitril Valsartan	No feature details of DILI caused by the drugs
	Schneider, 2017 [133]	1	Zoledronic acid	Feature details provided for DILI by this drug
	Terzioli Beretta-Piccoli, 2018 [134]	1	Atovaquon/Proguanil	Detailed feature description of DILI
	Visentin, 2018 [135]	2	NSAID Amoxicillin/Clavulanate	Lack of feature details of DILI by individual drugs
	Treeratsrutsak, 2010 [136]	80	Various antibiotics	No feature details provided for DILI caused by individual drugs in the context of this epidemiology study
<b>Thailand</b> <i>n</i> = 509	Sobhonsidsuk, 2016 [137]	383	Various drugs	Missing feature details of DILI caused by individual drugs
	Chayanupatkul, 2020 [138]	46	Various drugs	Feature details of DILI due to individual drugs not provided
	Duzenli, 2019 [139]	1	Phenprobamate	Detailed feature description of DILI by this drug
	Hussaini, 2007 [140]	43	Various antibiotics	No feature details of DILI caused by individual drugs
	Daly, 2009 [141]	51	Flucloxacillin	Excellent feature details presented for DILI cases

Table 1. *Cont.*

Country/ DILI Cases, <i>n</i>	First Author/Year	DILI Cases, <i>n</i>	Drugs	Comments on RUCAM Based DILI Cases
Turkey <i>n</i> = 1	Spraggs, 2011 [142]	61	Lapatinib	Excellent feature description of DILI case
	Islam, 2014 [143]	1	Anastrozole	Feature presentation of a patient with DILI due to anastrozole
United Kingdom <i>n</i> = 263	Dyson, 2016 [144]	1	Sofosbuvir	Features of DILI by this drug provided
	Abbara, 2017 [145]	105	Various anti-Tuberculoitics	Feature presentation of all DILI cases due to various anti-tuberculosis drugs
	Vliegenthart, 2017 [146]	1	Nitrofurantoin	Feature description of DILI by the drug
	Fontana, 2005 [147]	2	Amoxicillin, Amoxicillin/Clavulanate	Well described features of DILI caused by the drugs
Lee, 2005 [148]	6448	Ximelagatran	Perfect presentation of DILI features	
Stojanovski, 2007 [149]	1	Atomoxetine	Good DILI case feature presentation	
Lammert, 2008 [150]	598	Various drugs	No feature presentation of DILI by individual drugs	
Singla, 2010 [151]	1	Cephalexin	DILI features of a single case	
Nabha, 2012 [152]	1	Etravirine	Presentation of DILI feature	
Sprague, 2012 [153]	1	Varenicline	Careful DILI feature description	
Markova, 2013 [154]	56	Bosentan	Some global feature description	
Marumoto, 2013 [155]	4	NSAID	Limited feature details of DILI cases	
Bohm, 2014 [156]	1	Deptomycin	DILI feature description in this case	
Cheetham, 2014 [157]	11,109	Various drugs	No specific feature presentation of any drug under consideration	
Lim, 2014 [158]	1	Various drugs	No presentation of specific features of DILI by 4 drugs used concomitantly or sequentially	
Russo, 2014 [159]	22	Statins	No individual feature description for DILI caused by various statins	
Veluswamy, 2014 [160]	1	Polamidomide	Feature presentation of DILI	
Baig, 2015 [161]	1	Rivaroxaban	Good feature description of this DILI case	
Hammerstrom, 2015 [162]	1	Amblopidipine	Feature presentation of DILI caused by this drug	
Stinc, 2015 [163]	2	Simeprevir	Detailed feature presentation of the DILI cases	

United States  
*n* = 20,311

Table 1. *Cont.*

Country/ DILI Cases, #	First Author/Year	DILI Cases, #	Drugs	Comments on RUCAM Based DILI Cases
	Tang, 2015 [164]	1	Bupropion, doxycycline	Complex feature presentation of DILI due to comedication
	Unger, 2016 [165]	1	Ciprofloxacin	Detailed feature description of DILI by this single drug
	Gharia, 2017 [166]	1	Letrozole	Perfect feature presentation of DILI
	Nicoletti, 2017 [167]	339	Various drugs	No specific feature details of DILI caused by individual drugs
	Gayam, 2018 [168]	3	Various drugs	Feature details of DILI by the drugs
	Hayashi, 2018 [169]	493	Various drugs	Lacking specific feature details of DILI by individual drugs
	Patel, 2018 [170]	1	Everolimus	Specific features described for DILI by this drug
	Shamberg, 2018 [171]	34	Various drugs	No specific features of DILI caused by individual drugs presented
	Cirulli, 2019 [172]	268	Various drugs	Feature details of DILI by individual drugs not provided
	Nicoletti, 2019 [173]	197	Flucloxacillin	Specific feature details of DILI by flucloxacillin were not provided
	Sandritter, 2019 [174]	1	Various drugs	No feature description of DILI by individual drugs
	Shumar, 2019 [175]	1	Memantine	Detailed feature description of DILI by this drug
	Tsung, 2019 [176]	70	Pembrolizumab	Features described in detail for DILI caused by this drug
	Xie, 2019 [177]	1	Anastrozole	Feature details of DILI presented
	Ghabril, 2020 [178]	551	Various drugs	No feature details of DILI by individual drugs
	Mullins, 2020 [179]	99	Micafungin	Feature details presented of DILI by this drug

United States  
# = 20,311

Abbreviations: CAMs, Causality Assessment Methods; DILI, Drug induced liver injury; NSAID, Non-steroidal anti-inflammatory drug; RUCAM, Rousset Uclaf Causality Assessment Method.

In addition to hospitals, other sources provided RUCAM based DILI cases (Table 1). Among these were National Institutes of Health from Japan [92] and the US [165], consortia from Spain [115,141], the adverse drug reactions advisory committee (ADRAC) from Sweden [126], regulatory pharmacovigilance and pharmacoepidemiology centers from France [58,59] and Italy [86], drug commission of medical association from Germany [64], committee for drug induced liver injury from China [42]; also, drug reaction reporting database from Spain [65], regulatory agency from Spain [114] health insurance from the US [157], and drug safety departments of drug companies from France [57], Sweden [148], and Switzerland [132]. Some of these played an eminent role in promoting the use of RUCAM in prospective studies, particularly those from Spain [115], Sweden [126], and the US with France and Sweden [148].

### 5.3. Top Ranking Countries

Among the top 10 countries were in decreasing order China, the US, Germany, Korea, Italy, Sweden, Spain, Japan, Argentina, and Thailand, whereby the top 5 countries provided most of the DILI cases (Table 2). Authors from these 5 countries contributed together 75,133 DILI cases out of a total 81,856 worldwide DILI cases, corresponding to 91.8%. On the lower part of the list ranked the 6 countries Israel, Malaysia, Mexico, Morocco, Saudi Arabia, and Turkey, authors from these low ranking countries provided each one single DILI case assessed for causality using RUCAM, corresponding to 6 cases altogether out of a total of 81,856 DILI cases. Authors from the remaining 20 countries with a ranking from 6 down to 25 contributed 6,723 DILI cases out of overall 81,856 cases corresponding to 8.2%. In essence, RUCAM based DILI cases were mostly published in English language journals, raising the question how DILI cases were assessed and published by the other countries in local journals in languages other than English. Currently, overall 81,856 cases of idiosyncratic DILI assessed for causality by RUCAM have been retrieved via PubMed, all published 1993–June 2020 (Table 1) [23–180].

### 5.4. Annual Growth Trends of RUCAM Based DILI Case Publications

Analyses of growth trends provided additional information after identification of a total 1995 DILI studies, published between 2010 and 2019 but not stratified for causality assessment using RUCAM [1]. In the frame of the present analysis, only publications of idiosyncratic DILI cases were included if they had been assessed for causality using RUCAM, providing a more homogenous series with established DILI diagnoses.

#### 5.4.1. Published Annual RUCAM Based DILI Cases

Considering the period from 1993 to 2019, annually published cases of RUCAM based idiosyncratic DILI ranged between 0 and 27,224 in 2019, but data of 2020 were not included because case counting stopped by end of June in this particular year (Figure 1). Three phases of trends appeared with respect to published RUCAM based DILI cases: (1) phase 1 with clinical field testing from 1996 to 2004 (2) phase 2 with promotion from 2005 to 2013, and (3) phase 3 of worldwide use from 2014 to 2019.

Phase 1 started after the launch of RUCAM in 1993 [16,47] and the analysis of 94 DILI cases [47], the number of subsequent annual published DILI cases remained small until 2004, reaching 121 cases (Figure 1). This was the period of initial testing the RUCAM algorithm under clinical field conditions with interesting early information provided by 3 reports [58,91,114]. The first report came from Spain, was published in 1996, analyzed a major study cohort of DILI due to amoxicillin and clavulanate, and described their typical clinical features, with Rodríguez as first author and Zimmerman as senior author [114] who actually was involved as an expert from the US in the international consensus meetings [14] but did not promote RUCAM in DILI evaluations in his own country. Of interest was also the retrospective design of this analysis, suggesting that this particular study approach is feasible [114] although a prospective approach is recommended [15]. The second report was from Japan with Japanese patients, published in 2003 by Masumoto et al. [91]. This study favored RUCAM over other CAMs, provided evidence that the performance of the lymphocyte transformation test was poor in line

with previous reports, and the RUCAM criteria were viewed as useful for diagnosing DILI in Japanese patients. The third publication came from France, reported in 2004 on details of a patient with DILI by pioglitazone, and showed the feasibility of a good case report to be assessed by RUCAM, evaluated by Arotcarena et al. [58]. All three reports were hallmarks of the first phase of RUCAM based DILI case series devoted to clinical field evaluation that ended in 2004 (Figure 1).

**Table 2.** Top ranking of countries providing DILI cases assessed for causality by RUCAM.

Top Ranking Countries	Cases, <i>n</i>	References
1. China	35,825	[35–53]
2. United States	20,311	[147–179]
3. Germany	10,907	[64–71]
4. Korea	6528	[99–104]
5. Italy	1562	[83–90]
6. Sweden	1508	[126–129]
7. Spain	1181	[114–125]
8. Japan	939	[91–98]
9. Argentina	625	[23–26]
10. Thailand	509	[136–138]
11. India	424	[75–81]
12. Iceland	367	[72–74]
13. Pakistan	264	[108]
14. UK	263	[140–146]
15. France	170	[57–63]
16. Australia	106	[27–30]
17. Serbia	99	[111,112]
18. Egypt	75	[56]
19. Switzerland	68	[130–135]
20. Portugal	53	[109]
21. Bahrain	25	[31]
22. Colombia	19	[54]
23. Singapore	14	[113]
24. Brazil	4	[32]
25. Canada	4	[33,34]
26. Israel	1	[82]
27. Malaysia	1	[105]
28. Mexico	1	[106]
29. Morocco	1	[107]
30. Saudi Arabia	1	[110]
31. Turkey	1	[139]

Abbreviations: DILI, Drug induced liver injury; RUCAM, Roussel Uclaf Causality Assessment Method.

Phase 2 started in 2005 with overall 7695 annually published RUCAM based DILI cases (Figure 1) [115,126,147,148]. Among these were 461 cases provided by Andrade et al. from Spain retrieved from a prospective study involving various drugs [115], additional 784 cases from Sweden were published by Björnsson and Olsson retrieved from a prospective study of DILI by various drugs [126], whereas from the US 2 case reports of DILI by amoxicillin and clavulanate were presented by Fontana et al. [147] as well as a large cohort of DILI caused by ximelagatran occurred in clinical trials was published by Lee et al. [148]. These 4 studies promoted the usefulness of RUCAM evaluating DILI cases [115,126,147,148] by preferring a prospective study design [115,126], evaluating single DILI case reports [147], and correctly assessing suspected DILI cases in clinical trials [148]. Whereas RUCAM had already a firm place among DILI experts in Europe, it seems that experts in the US became more familiar with the use and practicability of RUCAM.

Phase 3 is characterized by the worldwide use of RUCAM for DILI started in 2014 with 11,525 DILI cases (Figure 1), mostly attributed to one study with 11,109 DILI cases provided by Cheetham et al. [157]. Starting in 2015, there was a continuous rise of published RUCAM based DILI cases (Figure 1), likely



driven also by the updated RUCAM available online 2015 and published in 2016 [15]. With 27,224 published DILI cases, the maximum level on an annual base was achieved in 2019 (Figure 1). Until end of June 2020, additional 15,153 published DILI cases were counted but not included in Figure 1, corresponding already to more than half of the cases counted in 2019 and representing a good base for 2020 and further years.

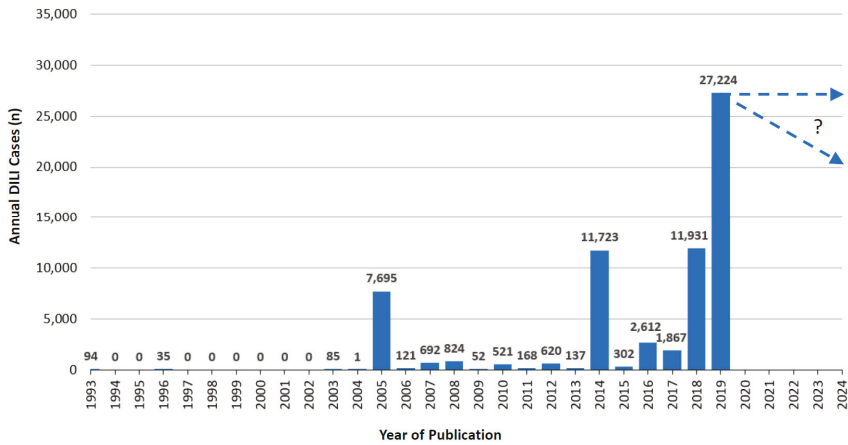


Figure 1. Annual cases of DILI assessed for causality by RUCAM and published since 1993.

5.4.2. Annual RUCAM Based DILI Publications and Growth Trend

Over the years starting from 1993, when RUCAM was launched [14,57], and until 2019 an upward trend of annual RUCAM based DILI publications can be observed with some dips in between (Figure 2). In 2019, 26 publications were counted, and 15 publications from January 2020 until end of June 2020 that were not included in the listing (Figure 2). Overall 158 publications with RUCAM based DILI cases were counted from 1993 until mid 2020 (Table 1).

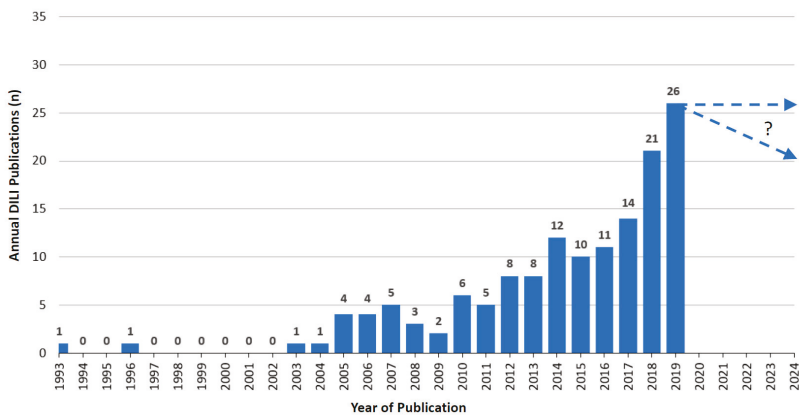


Figure 2. Annual publications of DILI cases assessed for causality by RUCAM as reported since 1993.

5.5. Specificities of DILI Case Evaluation

Large study cohorts of RUCAM based DILI cases accumulated many different drugs and provided as expected a global information of the DILI cases due to various drugs without a detailed description

of clinical features drug by drug (Table 1). Consequently, typical clinical features of a DILI by a single drug cannot be obtained from large cohorts as opposed to single DILI case reports or case series that included DILI cases due to a single drug (Table 1). In general, studies with a single DILI case or a few cases are more informative because they provide an exhaustive past medical history with clinical details required for a sound case evaluation. In search for typical DILI features by specific drugs, therefore, assistance may be provided by the drug listing (Table 1). In addition, details can be retrieved via the internet, using the search terms drug induced liver injury and the name of the suspected drug, combined with RUCAM or the updated RUCAM.

### 5.6. Worldwide Top Ranking of Drugs Causing DILI

There is concern how best to establish a top ranking of drugs most commonly implicated in DILI [70,74]. A recent study presented a list with top ranking drugs out of overall 3312 DILI cases evaluated by RUCAM (Table 3) [70]. The RUCAM based DILI cases were retrieved from 15 reports by six national databases of DILI registries and three large medical centers worldwide, which provided the DILI cases under consideration. Contributing countries and regions were in alphabetical order China, Germany, Latin America, Iceland, India, Singapore, Spain, Sweden, and the US. It was found that the databases of national registries and large medical centers are the best sources of drugs implicated in DILI cases. There is also the note that presently DILI cases of the LiverTox database are less suitable for clinical or regulatory purposes as presented on its website because many suspected DILI cases were derived from published cases of poor quality, lacking a robust CAM such as RUCAM [70,74]. Consequently, the majority of LiverTox based cases of assumed DILI could previously not be classified as real DILI [74]. To overcome these diagnostic shortcomings, LiverTox attempted a top ranking of drugs by counting the published DILI cases for each individual drug [74]. It was assumed that the degree of causality probability increases with the number of published DILI reports: the higher the case number the higher the probability. This special approach explains the variability of the top listing presented by liverTox [74] as compared to RUCAM based cohorts [70].

**Table 3.** Worldwide top ranking of drugs causing DILI cases with causality assessment by RUCAM.

Drug	RUCAM Based DILI Cases (n)
1. Amoxicillin-clavulanate	333
2. Fluclxacillin	130
3. Atorvastatin	50
4. Disulfiram	48
5. Diclofenac	46
6. Simvastatin	41
7. Carbamazepine	38
8. Ibuprofen	37
9. Erythromycin	27
10. Anabolic steroids	26
11. Phenytoin	22
12. Sulfamethoxazole/Trimethoprim	21
13. Isoniazid	19
14. Ticlopidine	19
15. Azathioprine/6-Mercaptopurine	17
16. Contraceptives	17
17. Flutamide	17
18. Halothane	15
19. Nimesulide	13
20. Valproate	13

Table 3. Cont.

Drug	RUCAM Based DILI Cases (n)
21. Chlorpromazine	11
22. Nitrofurantoin	11
23. Methotrexate	8
24. Rifampicin	7
25. Sulfazalazine	7
26. Pyrazinamide	6
27. Gold salts	5
28. Sulindac	5
29. Amiodarone	4
30. Interferon beta	3
31. Propylthiouracil	2
32. Allopurinol	1
33. Hydralazine	1
34. Infliximab	1
35. Interferon alpha/Peginterferon	1
36. Ketaconazole	1
37. Busulfan	0
38. Dantrolene	0
39. Didanosine	0
40. Efavirenz	0
41. Floxuridine	0
42. Methyldopa	0
43. Minocycline	0
44. Telithromycin	0
45. Nevirapine	0
46. Quinidine	0
47. Sulfonamides	0
48. Thioguanine	0

Substantially modified from a previous report [70], which provides references for each implicated drug.

## 6. Worldwide Publications of HILI Cases Assessed for Causality Using RUCAM

Highlights of liver injury cases have been reported not only for DILI but with increasing frequency also for HILI cases questionable due to lack of a robust CAM [7–9]. The problems associated with HILI are specifically addressed in the current analysis, which considers for the first time worldwide HILI cases using RUCAM as a robust algorithm for assessing causality.

### 6.1. Countries and Regions

Authors from many countries around the world reported on cases of HILI in connection with the consumption of various herbs, all published since 1993 (Table 4) [29,37,38,42,48,100–103,113,115–118, 181–255]. Specifically considered were patients, who experienced HILI with established causality using RUCAM. Such a table with a comprehensive list of publications over a long period of time will help the search for RUCAM based HILI cases caused by specific herbs or herbal products containing a mixture of several herbs. This list is unique as compared to databases that may have problems providing real HILI cases not confounded by alternative causes or lack of a robust causality assessment.

Table 4. Worldwide countries with a selection of published HILI cases assessed for causality using RUCAM.

Country/ HILI Cases, n	First Author/ Year	HILI Cases, n	Herbal Products	Comments on RUCAM Based HILI Cases
Australia n = 2	Smith, 2016 [181]	1	<i>Garcinia Cambogia</i>	Careful feature detail description of HILI by this herb
	Laube, 2019 [29]	1	Ginseng	Feature presentation of this single HILI case
Austria n = 2	Stadlbauer, 2005 [182]	2	Various herbs contained in Tahitian NONI juice	Features described for these HILI cases
Brazil n = 1	Barcelos, 2019 [183]	1	<i>Senecio brasiliensis</i>	Complete feature description of HSOS caused by this herb
	Yuen, 2006 [184]	7	Various herbs	No specific feature description of HILI by individual herbs
	Cheung, 2009 [185]	3	<i>Psoralea corylifolia</i>	Well described features of HILI cases
	Chau, 2011 [186]	27	Various herbs	Lacking feature presentation of HILI by individual herbs
	Lin, 2011 [187]	1	<i>Gynura segetum</i>	Perfect feature presentation of HSOS
	Gao, 2012 [188]	5	<i>Gynura segetum</i>	Excellent feature description of HSOS
	Lai, 2012 [189]	74	Various herbs <i>Polygonum multiflorum</i>	Missing feature presentation of HILI by individual herbs
	Dong, 2014 [190]	18	Various herbs	Good feature presentation of HILI
	Hao, 2014 [37]	8	PA containing herbs	Lacking feature presentation of HILI by individual herbs
	Gao, 2015 [191]	23	Various herbs	Perfect feature presentation of HSOS cases
China n = 10,914	Ou, 2015 [38]	130	<i>Polygonum multiflorum</i>	No feature description of HILI caused by the herb
	Wang, 2015 [192]	40	<i>Polygonum multiflorum</i>	Comprehensive feature description of HILI cases
	Zhu, 2015 [193]	158	<i>Polygonum multiflorum</i>	Detailed feature presentation of HILI cases
	Zhang, 2016 [194]	54	Various herbs	No feature details described of HILI by individual herbs
	Zhu, 2016 [42]	866	Various herbs	Missing feature details of HILI caused by individual herbs
	Li, 2017 [195]	1	<i>Polygonum multiflorum</i>	Excellent description of feature details provided for HILI case
	Chow, 2019 [196]	1552	Various herbs	No feature presentation of HILI by individual herbs but excellent listings
	Jing, 2019 [197]	145	<i>Polygonum multiflorum</i>	Missing feature presentation of HILI caused by individual herbs
	Li, 2019 [198]	1	<i>Psoralea corylifolia</i>	Perfect feature presentation of HILI
	Ni, 2019 [199]	331	<i>Polygonum multiflorum</i>	Feature description of HILI cases

Table 4. Cont.

Country/ HILI Cases, n	First Author/ Year	HILI Cases, n	Herbal Products	Comments on RUCAM Based HILI Cases
China n = 10/914	Shen, 2019 [48]	6971	Variou herbs	No feature details presented for HILI by individual herbs
	Tan, 2019 [200]	3	<i>Sweetenia macrophylla</i>	Perfect presentation of feature details for these HILI cases
	Zhu, 2019 [201]	488	Variou herbs	Lacking feature details of HILI caused by individual herbs
	Gao, 2020 [202]	1	<i>Psoralea</i>	Feature description of this HILI case
	Xia, 2020 [203]	7	<i>Sweetenia macrophylla</i> , syn skyfruit	Careful description of HILI features
Colombia n = 1	Cárdenas, 2006 [204]	1	<i>Polygonum multiflorum</i>	Features well described for this HILI case
France n = 10	Parlati, 2017 [205]	10	<i>Aloe vera</i>	Excellent feature presentation of the HILI cases
	Teschke, 2009 [206]	1	Ayurveda herbs	Complete feature presentation of the HILI case
Germany n = 170	Teschke, 2011 [207]	22	<i>Chelidonium majus</i> syn. Greater Celandine	Complete feature description provided for HILI cases
	Teschke, 2012 [208]	21	<i>Chelidonium majus</i> syn. Greater Celandine	Thorough features presented of HILI cases
	Douros, 2015 [209]	10	Variou herbs	No detailed features reported of HILI caused by individual herbs
	Teschke, 2015 [210]	12	<i>Camellia sinensis</i> , syn. Green tea, or Lu Cha	Feature details presented of HILI cases
	Melchart, 2017 [211]	26	Herbal TCMs	Well described features of HILI caused by individual TCM herbs
	Diener, 2018 [212]	10	<i>Petasites hybridus</i>	Provided features of HILI by this herb
	Anderson, 2019 [213]	48	<i>Petasites hybridus</i>	Description of HILI features
	Gerhardt, 2019 [214]	1	<i>Chelidonium majus</i> , syn. Greater Celandine	HILI features described
	Teschke, 2019 [215]	19	<i>Camellia sinensis</i>	Careful feature presentation of HILI cases
	Philips, 2018 [216]	94	Ayurvedic and other herbs	Features not individually described for HILI by various herbs
India n = 117	Philips, 2019 [217]	17	Variou herbs	No detailed features presented for HILI cases by individual herbs

Table 4. Contd.

Country/ HILI Cases, n	First Author/ Year	HILI Cases, n	Herbal Products	Comments on RUCAM Based HILI Cases
Italy n = 77	Lapi, 2010 [218]	1	<i>Serenoa repens</i>	Detailed feature presentation of HILI
	Mazzanti, 2015 [219]	19	<i>Camellia sinensis</i> , syn. green tea	Careful feature description of HILI cases
	Sáez-González, 2016 [220]	1	<i>Chelidonium majus</i>	Feature details of the HILI case
	Mazzanti, 2017 [221]	55	<i>Red yeast rice</i>	Thorough feature presentation of HILI
	Osborne, 2019 [222]	1	<i>Mitragyna speciosa</i> , syn. Kraton	Individual feature details not provided for the HILI case
	Tsuda, 2010 [223]	1	Saireito	Perfect feature details presented for the HILI case
	Hisamochi, 2013 [224]	2	<i>Agaricus blazei Murill</i>	Excellent presentation of HILI features
	Ahn, 2004 [225]	64	Various herbs	Missing feature presentation of HILI by individual herbs
	Seo, 2006 [226]	17	Various herbs	No individual feature description of HILI by specific herbs
	Kang, 2008 [227]	66	Various herbs	Lacking feature details of HILI by individual herbs
Japan n = 3	Sohn, 2008 [228]	24	Various herbs	Feature details of HILI by individual herbs not provided
	Kang, 2009 [229]	1	<i>Corydalis spiciosa</i>	Perfect feature details provided for this single HILI
	Kim, 2009 [230]	2	Arrowroot, syn. ge Gen	Excellent presentation of features for these HILI cases
	Bae, 2010 [231]	1	<i>Polygonum multiflorum</i>	Careful feature details presented for this HILI case
	Yang, 2010 [232]	3	<i>Aloe vera</i> or <i>arborescens</i>	Thorough description of features of these HILI cases
	Jung, 2011 [233]	25	<i>Polygonum</i>	Excellent feature presentation of the HILI cases
	Kim, 2012 [234]	1	<i>multiflorum</i>	Perfect feature description for this HILI case
	Suk, 2012 [100]	149	<i>Hovenia dulcis</i> , syn. Juguju	No feature description of HILI caused by individual herbs
	Lee, 2015 [235]	27	Various herbs	Lacking feature details of HILI caused by individual herbs
	Lee, 2015 [236]	97	Various herbs	Feature details of HILI cases caused by individual herbs were not provided
Korea n = 2507	Woo, 2015 [102]	5	Various herbs	No feature details presented for HILI by individual herbs
	Cho, 2017 [237]	6	Various herbs	Missing feature details of HILI cases by individual herbs
	Byeon, 2019 [103]	2019	Various herbs	No detailed feature description of HILI by individual herbs

Table 4. *Cont.*

Country/ HILI Cases, <i>n</i>	First Author/ Year	HILI Cases, <i>n</i>	Herbal Products	Comments on RUCAM Based HILI Cases	
Singapore <i>n</i> = 25	Wai, 2006 [113]	15	Various herbs	No detailed features presented for HILI cases by individual herbs	
	Teo, 2016 [238]	10	Various herbs	Missing feature details of HILI cases	
South Africa <i>n</i> = 47	Awortwe, 2018 [239]	47	Various herbs	Features were not provided for cases of HILI caused by individual herbs	
	Andrade, 2005 [115]	9	Various herbs	No feature details of HILI by individual herbs	
	Jimenez-Saenz, 2006 [240]	1	<i>Camellia sinensis</i>	Feature details presented for this HILI case	
Spain <i>n</i> = 46	García-Cortés, 2008 [241]	13	Various herbs	Lacking feature details of HILI caused by individual herbs	
	García-Cortés, 2008 [117]	5	Various herbs	Specific feature details of HILI by individual herbs not provided	
	Medina-Caliz, 2018 [242]	18	<i>Camellia sinensis</i> and other herbs	No specific feature details provided for HILI	
Sweden <i>n</i> = 5	Björnsson, 2007 [243]	5	<i>Camellia sinensis</i>	Feature details provided for HILI cases	
Switzerland <i>n</i> = 1	Ruperti-Repilado, 2019 [244]	1	<i>Artemisia annua</i>	Careful feature presentation of this HILI case	
Turkey <i>n</i> = 1	Yilmaz, 2015 [245]	1	Lesser Celandine, syn. Pilewort	Excellent feature presentation of the HILI case	
	Papafraqkakis, 2016 [246]	1	Chinese skullcap plus Black catechu	Perfect feature presentation of this HILI case	
United States <i>n</i> = 100	Dalai, 2017 [247]	1	Ayurvedic herb	Specific case features described	
	Kesavarapu, 2017 [248]	1	Yogi Detox tea with multiple herbs	Individual specific features not provided for this HILI case caused specifically by a single herb	
	Kothadia, 2018 [249]	19	<i>Garcinia Cambogia</i>	Careful feature presentation of HILI cases	
	Surapaneni, 2018 [250]	19	<i>Camellia sinensis</i>	Feature details provided for the HILI case	
	Imam, 2019 [251]	1	Curcumin	Thorough feature description of the HILI case	
	Yousaf, 2019 [252]	9	<i>Garcinia Cambogia</i>	Excellent feature description of the HILI case	
	Oketch-Rabah, 2020 [253]	29	<i>Camellia sinensis</i> extract	Perfect feature presentation of HILI by this herb	
	Schimmel, 2020 [254]	20	<i>Mitragyna speciosa</i> , syn. Kraton	Feature details provided for HILI cases	

Abbreviations: DILI, Drug induced liver injury; HILI, Herb induced liver injury; HSOS, Hepatic sinusoidal obstruction syndrome; RUCAM, Roussel Uclaf Causality Assessment Method, TCM, Traditional Chinese Medicines; USP, United States Pharmacopeia; WHO, World Health Organizations.

## 6.2. Hospital and Other Sources

Most RUCAM based HILI cases were provided by authors from university hospitals and their affiliated teaching hospitals with their departments of Hepatology and Gastroenterology, Medicine or Internal Medicine (Table 3). Rare contributors were other departments like those with focus on Emergency Medicine [255], Clinical Pharmacology and Toxicology in Berlin [209], Pharmacology and Toxicology in Hannover [213], Pharmacy in Singapore [238], Physiology and Pharmacology in Rome [219,221], Anatomical, Histological, Forensic and Orthopedic Sciences in Rome [222], Pediatrics in Seoul [234], and among the contributors were even the Neurology and Headache Center in Essen [212] and Spine and Joint Research Institute in Seoul [235].

Other sources providing RUCAM based HILI cases include the Chinese Academy of Medical Sciences in Beijing [195], School of Chinese Materia Medica in Beijing [199,202], Competence Centre for Complementary Medicine and Naturopathy in Munich [211], Biomedical Research and Innovation Platform South African Medical Research Council in Tygerberg [239], United States Pharmacopeia in Rockville [254], and Center of Pharmacovigilance of Florence [218].

## 6.3. Top Ranking Countries

Among the countries presenting RUCAM based HILI cases were on top in descending order China and Korea, followed by Germany, India and the US, whereby the top 5 countries provided most of the HILI cases (Table 5). Authors from these 5 countries contributed together 13,808 HILI cases out of a total 14,029 worldwide HILI cases, corresponding to 98.4%. On the lower part of the list ranked the 4 countries Brazil, Colombia, Switzerland, and Turkey, authors from these low ranking countries provided each one HILI case assessed for causality using RUCAM, corresponding to 4 cases altogether out of a total of 14,029 HILI cases. Authors from the remaining 20 countries with a ranking from 6 down to 14 contributed 217 HILI cases out of overall 14,029 cases corresponding to almost 1.6%.

**Table 5.** Top ranking of countries providing HILI cases assessed for causality by RUCAM.

Top Ranking Countries	Cases, <i>n</i>	References
1. China	10,914	[37,38,42,48,184–203]
2. Korea	2507	[100–103,225–237]
3. Germany	170	[206–215]
4. India	117	[216,217]
5. US	100	[247–255]
6. Italy	77	[218–222]
7. South Africa	47	[239]
8. Spain	46	[115,117,240–242]
9. Singapore	25	[113,238]
10. France	10	[205]
11. Sweden	5	[244]
12. Japan	3	[223,224]
13. Australia	2	[29,181]
14. Austria	2	[182]
15. Brazil	1	[183]
16. Colombia	1	[204]
17. Switzerland	1	[245]
18. Turkey	1	[246]

Abbreviations: HILI, Herb induced liver injury; RUCAM, Roussel Uclaf Causality Assessment Method.

### 6.3.1. Published Annual RUCAM Based HILI Cases

From 1993 to 2019, published annual cases of RUCAM based HILI ranged between 0 and 11,609 in 2019, while 57 HILI cases of 2020 were not included because case counting stopped by end of June in this particular year (Figure 3). Three phases of trends appeared with respect to published RUCAM



based HILI cases: (1) phase 1 with lack of any clinical field testing from 1993 to 2003, (2) phase 2 with slow promotion from 2004 to 2016, and (3) phase 3 of worldwide use from 2017 to 2019.

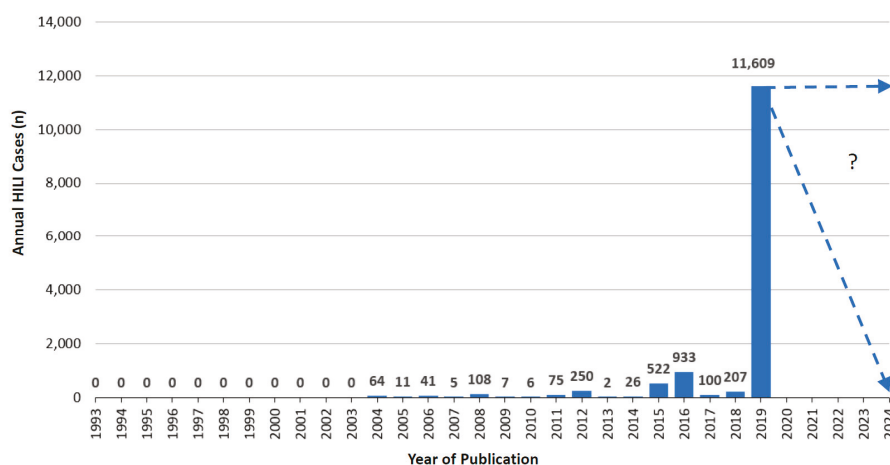


**Figure 3.** Annual cases of HILI cases assessed for causality by RUCAM and published since 1993.

Phase 1 started after the launch of RUCAM in 1993 [16,47] but without a single published HILI case until 2003 (Figure 3). The lack of published RUCAM based HILI cases during this period might be due to the fact that the value of RUCAM was not yet sufficiently known or to uncertainties whether herbs have the potential to cause liver injury. In addition, the term of herb induced liver injury or its acronym HILI was unknown at that time and therefore not in common use.

During the subsequent phase 2, the number of annual published HILI cases remained small with cases ranging from 2 to 933, considering the years from 2004 until 2016 (Figure 3). In 2008, there were 108 HILI cases, with 18 Spanish cases published by García-Cortés et al. [117,241] and 90 Korean cases published by Kang et al. [227] and Sohn et al. [228]. During 2016, there was a sharp increase with 933 HILI cases, mostly attributed to 866 cases from China published by Zhu et al. [42]. As a reminder and outlined recently, herb induced liver injury with HILI as its acronym was first introduced and proposed as a specific term in the scientific literature only in 2011 [12]. This may explain retarded publications on HILI cases (Figure 3).

Phase 3 started with low HILI case numbers in 2017 and 2018 (Figure 3), considering that the updated RUCAM applicable also to HILI cases was published only in 2016 [15]. With 11,609 the largest HILI case number was published in 2019 (Figure 3) as a consequence of the ongoing worldwide use of RUCAM for assessing causality in suspected HILI cases (Table 4). In particular, contributing countries were in alphabetical order Australia [29], Brazil [183], China [48,196–201], Germany [213–215], India [217], Italy [222], Korea [103], Spain [115,117,240–242], Switzerland [244], and the US [245–254]. Most of the 11,619 HILI cases published in 2019 were from China [48,196] and Korea [103], with 6971 cases published by Shen et al. [48], 2019 cases reported by Byeon et al. [103], and 1552 cases provided by Chow et al. [196]. However, until mid 2020 only 57 HILI cases were published (Table 4) [202,203,253,254], suggesting for the whole year 2020 at best 100 cases (Figure 3).

### 6.3.2. Annual RUCAM Based HILI Publications and Growth Trend

Over the years starting from 1993, when RUCAM was launched [14,57] and until 2019, an upward trend of annual RUCAM based HILI publications can be observed with some dips in between (Figure 4). In 2019, 18 publications were counted and 4 publications until end of June 2020 that were not included (Figure 4). For the whole year 2020, therefore, at best perhaps 8 publications can be anticipated

(Figure 4). These figures show that a total of 85 publications with RUCAM based HILI cases were reported from 1993 until mid 2020 (Table 2).

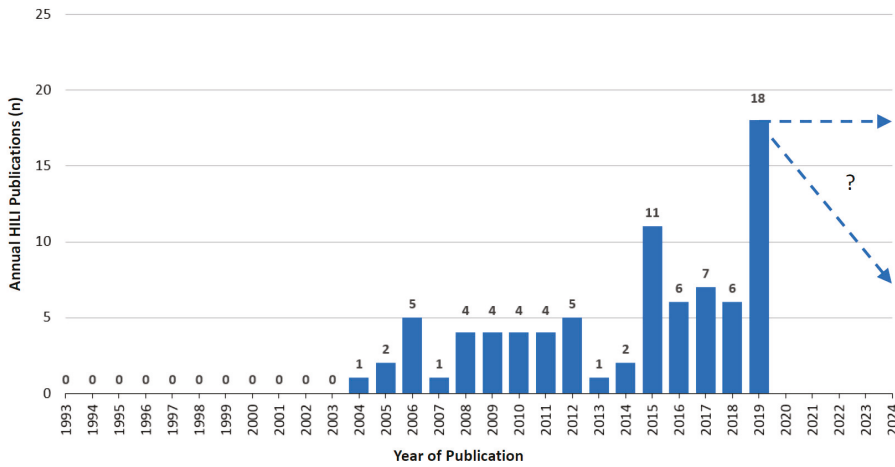


**Figure 4.** Annual publications of HILI cases assessed for causality by RUCAM as reported since 1993.

#### 6.4. Specificities of HILI Cases

Large study cohorts of RUCAM based HILI cases accumulate many different herbs and provide as expected a global information of many HILI cases without a detailed description of clinical features for specific herbs (Table 4). Consequently, studies with a single or a few HILI cases have many advantages because they focus on a single herb or herbal product causing the liver injury and usually provide an exhaustive past medical history with clinical details required for a sound case evaluation. For interested physicians, regulators, and manufacturers, this listing provides individual cases with herbs causing HILI.

#### 7. Utility of RUCAM

The utility of RUCAM has been confirmed in many liver injury cases of DILI (Table 1) and HILI (Table 4) published from countries and regions around the world, as outlined in various reports [5,11,15–18] and briefly summarized (Table 6). In short, the high qualification of RUCAM as an objective diagnostic algorithm to assess causality in liver injury cases of DILI and HILI is the clue of its increasing use (Figures 1–4). RUCAM is smoothly applied by clinicians or regulators and obviously without problems (Tables 1 and 4). The worldwide use allows data comparison among different countries, a unique condition for multifaceted diseases as DILI and HILI are. RUCAM is also applied in epidemiology studies. Finally and most importantly, each individual DILI and HILI case report contain important details of liver injury cases that may be helpful for physicians in care of patients with suspected DILI and HILI.

**Table 6.** Characteristics of RUCAM.

<b>RUCAM Specificities</b>	
<b>Basic features</b>	
•	Validated method (gold standard) based on cases with positive reexposure test results, providing thereby a robust CAM
•	Worldwide use with 46,266 DILI cases assessed by RUCAM published 2014–2019, outperforming thereby any other CAM in term of number of cases published
•	Assesses causality in DILI and HILI cases validly and reproducibly
•	A typical intelligent diagnostic algorithm in line with artificial intelligence (AI) concepts
•	A diagnostic algorithm for objective, robust causality assessment
•	Assessment is user friendly, cost effective with results available in time and without needing expert rounds that often provide subjective and fragile, arbitrary opinions based on own experience
•	Transparency of case data and clear result presentation
•	Suitable for reevaluation by peers and any of other interested parties such as national regulatory agencies international registries, and pharma companies
•	Mandatory application for DILI cases if to be used for establishing new robust diagnostic biomarkers
•	High causality gradings with complete data
•	With prospective case data collection best results are obtainable
<b>Clearly defined and scored key elements</b>	
•	Time frame of latency period
•	Time frame of dechallenge
•	Recurrent ALT or ALP increase
•	Risk factors
•	Individual comedications
•	Exclusion of alternative causes
•	Markers of HAV, HBV, HCV, HEV
•	Markers of CMV, EBV, HSV, VZV
•	Cardiac hepatopathy and other alternative causes
•	Liver and biliary tract imaging
•	Doppler sonography of liver vessels
•	Prior known hepatotoxicity of drug or herb
•	Unintentional reexposure
<b>Other important specificities</b>	
•	Laboratory based hepatotoxicity criteria
•	Laboratory based liver injury pattern
•	Hepatotoxicity specific method
•	Structured, liver related method
•	Quantitative, liver related method, based on scored key elements

Abbreviations: AI: Artificial Intelligence; ALT: Alanine aminotransferase; ALP: Alkaline phosphatase; CAM: Causality assessment method; CMV: Cytomegalovirus; DILI: Drug induced liver injury; EBV: Epstein Barr virus; HAV: Hepatitis A virus; HBV: Hepatitis B virus; HCV: Hepatitis C virus; HEV: Hepatitis E virus; HILI: herb induced liver injury; HSV: Herpes simplex virus; RUCAM: Roussel Uclaf Causality Assessment Method; VZV: Varicella zoster virus.

## 8. Other CAMs

Apart from the objective diagnostic RUCAM algorithm, a few non-RUCAM based CAMs are known, critically discussed elsewhere in detail [5,15]. In short, they are less accurate than RUCAM, not quantitative as not based on specific elements to be scored individually, not specific for liver injury cases, not structured, not validated, or based on individual arbitrary subjective opinions. In fact, other CAMs are still caught up in the pre-RUCAM and pre-AI era [18] and thereby neglecting the use of diagnostic algorithms such as the original RUCAM [14] or the now preferred updated version [18].

## 9. Limitation of the Analysis

The current analysis is based on published data of DILI and HILI reports in English, or at least an abstract in English, rather than on unpublished data contained in the original data sets that were not available to the authors of the analysis for re-analysis. Although most of the published DILI and HILI cases provide excellent data, some authors forgot presenting RUCAM based causality gradings or included cases with a possible causality grading in their final evaluations of cases together with a probable or highly probable causality level. Nevertheless, a broad range of different causality gradings was commonly provided in most published cases, respective references allow for detailed information. As being outside the scope of this article, causality gradings for individual reports were not provided (Tables 1 and 5), but some details of 46,266 DILI cases assessed by RUCAM were published earlier [11]. Problematic are study cohorts with inclusion of both DILI and HILI cases, unless both groups were separately evaluated [48]. As expected, not all of the patients were commonly confirmed as being DILI by RUCAM scoring, but the number of published cases remained accurate. For instance, special conditions are evident in the randomized clinical trial of ximelagatran [148]. In this prospective, report, hepatic findings were analyzed in all suspected cases with regard to causal relationship to ximelagatran by using RUCAM, considered as the most reliable tool to assess causality [148]. Applying RUCAM based on ALT thresholds only is insufficient since 92% of the ximelagatran group did not meet this criterion missing then a final robust causality grading, as opposed to 8% of the study group receiving partially high causality gradings. This study reaffirms the utility of RUCAM to identify cases with real DILI cases in cohorts under real world conditions.

## 10. Outlook

The perspectives using the updated RUCAM in future DILI and HILI cases are favorable because many authors including those from the US become more familiar with RUCAM and are ready to use this diagnostic algorithm (Tables 1–4), in line with principles of Artificial Intelligence to solve difficult processes [18]. Moreover, as in the US and many other countries RUCAM was successfully used to assess causality in cases of DILI, there is no need to invent another instrument specifically designed for drug development [255]. The issue of overlooked alternative causes remains a clinical problem and was described already in 1999 by Aithal et al. [256] and guided by RUCAM subsequently confirmed [69,257].

Future DILI and HILI studies should adhere on a prospective study design as strongly recommended in the RUCAM updated in 2016 because a retrospective approach may create concern on the validity of the published results due to incomplete information [15]. Neglecting this recommendation and using instead a retrospective design could be problematic [48]. In addition, attempts to lift RUCAM based causality gradings from possible to probable must be resisted [48]. Discouraged is in particular the use of a non-RUCAM based CAM in addition to RUCAM, because such a combination causes uncertainty due to disputable results of causality gradings. It is not recommended to mix in the same cohort patients with DILI or HILI [48] because this situation will complicate a separate evaluation of DILI or HILI features. However, it is clear that in individual cases RUCAM allows for a distinction between a drug and a medicinal herb when causality gradings are different.

## 11. Conclusions

The current analysis showed a favorable run of the RUCAM algorithm globally used since its launch in 1993, considering the annually published DILI and HILI cases. Overall 95,885 liver injury cases were published using RUCAM for causality assessment, namely 81,856 iDILI cases and 14,029 HILI cases. The global use of RUCAM assessing causality in cases of DILI and HILI helps compare study results among various countries and facilitates description of typical clinical features, best derived from case reports or small case series. RUCAM solves complex conditions as an algorithm in line with principles of Artificial Intelligence. Top ranking countries providing RUCAM based DILI cases were China, the United States, Germany, Korea, and Italy, whereas most RUCAM based HILI cases were published by authors from China, Korea, Germany, India, and the United States. In term of number of cases published, there is no other causality assessment method that could outperform RUCAM evaluating DILI and HILI cases. This should encourage all the stakeholders involved in DILI and HILI to systematically use RUCAM in order to reinforce their diagnosis and take the right decisions for the benefit of the patients.

**Author Contributions:** Conceptualization and methodology, R.T. and G.D.; formal analysis and draft preparation, R.T.; review and editing, G.D. All authors have read and agreed to the published version of the manuscript.

**Funding:** This research received no external funding.

**Acknowledgments:** The authors are grateful to Sabine Veltens for her professional providing of the figures.

**Conflicts of Interest:** The authors declared that they have no conflict of interests regarding this invited article.

## References

- Ke, L.; Lu, C.; Shen, R.; Lu, T.; Ma, B.; Hua, Y. Knowledge mapping of drug-induced liver injury: A scientometric investigation (2010–2019). *Front. Pharmacol.* **2020**, in press. [CrossRef]
- Utrecht, J. Mechanistic studies of idiosyncratic DILI: Clinical implications. *Front. Pharmacol.* **2019**, *10*, 837, In: Special issue: Clinical drug induced liver injury: Current diagnostic and mechanistic challenges, guest editors: Rolf Teschke, Gaby Danan & James H. Lewis. [CrossRef]
- Teschke, R.; Utrecht, J. Mechanism of idiosyncratic drug induced liver injury (DILI): Unresolved basic issues. *Ann. Transl. Med.* **2020**. In special issue: Unresolved basic issues in hepatology, guest editors Ralf Weiskirchen & Wolfgang Stremmel. [CrossRef]
- Chen, M.; Will, Y. *Drug-Induced Liver Toxicity*; Series: Methods in Pharmacology and Toxicology; James, K., David, C., Eds.; Springer Protocols, Springer Nature: Berlin, Germany, 2018.
- Teschke, R.; Danan, G. Causality assessment methods in drug-induced liver injury. In *Drug-Induced Liver Toxicity*; Series: Methods in Pharmacology and Toxicology; James, K., David, C.C., Minjun, C., Yvonne, W., Eds.; Springer Nature: Berlin, Germany, 2018; Chapter 27; pp. 555–594. [CrossRef]
- Teschke, R.; Danan, G.; Lewis, J.H. Special issue: Clinical drug induced liver injury: Current diagnostic and mechanistic challenges, guest editors: Rolf Teschke, Gaby Danan & James H. Lewis. *Front. Pharmacol.* **2019**. Available online: <https://www.frontiersin.org/research-topics/9104/clinical-drug-induced-liver-injury-current-diagnostic-and-mechanistic-challenges> (accessed on 30 June 2020).
- Sarges, P.; Steinberg, J.M.; Lewis, J.H. Drug-induced liver injury: Highlights from a review of the 2015 literature. *Drug Saf.* **2016**, *39*, 561–575. [CrossRef] [PubMed]
- Shahbaz, O.; Mahajan, S.; Lewis, J.H. Highlights of drug- and herb-induced liver injury in the literature from 2016, How best to translate new information into clinical practice? *Exp. Opin. Drug Metab. Toxicol.* **2017**, *13*, 935–951. [CrossRef]
- Real, M.; Barnhill, M.S.; Higley, C.; Rosenberg, J.; Lewis, J.H. Drug-induced liver injury: Highlights of the recent literature. *Drug Saf.* **2019**, *42*, 365–387. [CrossRef]
- Rosenberg, J.J.; Higley, C.; Lewis, J.H. Selected highlights from the recent literature of newly reported herbal and dietary supplement-induced liver injury. *Adv. Res. Gastroenterol. Hepatol.* **2020**, *15*, 555904. [CrossRef]
- Teschke, R. Idiosyncratic DILI: Analysis of 46, 266 cases assessed for causality by RUCAM and published from 2014 to early 2019. In: Special issue: Clinical drug induced liver injury: Current diagnostic and mechanistic challenges. Guest editors: Rolf Teschke, Gaby Danan & James H. Lewis. *Front. Pharmacol.* **2019**, *10*, 730. [CrossRef]

12. Teschke, R.; Zhu, Y.; Jing, J. Herb induced liver injury (HILI) in the Asian region and current role of RUCAM for causality assessment in 11, 160 published cases: Analysis and outlook. *J. Clin. Transl. Hepatol.* **2020**, *8*, 1–15.
13. Teschke, R.; Eickhoff, A.; Schulze, J.; Danan, G. Herb-induced liver injury (HILI) with 12,068 worldwide cases published with causality assessments by Roussel Uclaf Causality Assessment Method (RUCAM): An overview. *Transl. Gastroenterol. Hepatol.* **2020**, in press. [[CrossRef](#)]
14. Danan, G.; Bénichou, C. Causality assessment of adverse reactions to drugs—I. A novel method based on the conclusions of international consensus meetings: Application to drug-induced liver injuries. *J. Clin. Epidemiol.* **1993**, *46*, 1323–1330. [[CrossRef](#)]
15. Danan, G.; Teschke, R. RUCAM in drug and herb induced liver injury: The update. *Int. J. Mol. Sci.* **2016**, *17*, 14. [[CrossRef](#)]
16. Danan, G.; Teschke, R. Drug-induced liver injury: Why is the Roussel Uclaf Causality Assessment Method (RUCAM) still used 25 years after its launch? *Drug Saf.* **2018**, *41*, 735–743. [[CrossRef](#)]
17. Danan, G.; Teschke, R. Roussel Uclaf Causality Assessment Method for drug-induced liver injury: Present and Future. In: Special issue “Clinical drug induced liver injury: Current diagnostic and mechanistic challenges”, guest editors: Rolf Teschke, Gaby Danan & James H. Lewis. *Front. Pharmacol.* **2019**, *10*, 853. [[CrossRef](#)]
18. Teschke, R. Editorial. DILI, HILI, RUCAM algorithm, and AI, the Artificial Intelligence: Provocative issues, progress, and proposals. *Arch. Gastroenterol. Res.* **2020**, *1*, 4–11.
19. Hayashi, P.H. Drug-Induced Liver Injury Network causality assessment: Criteria and experience in the United States. *Int. J. Mol. Sci.* **2016**, *17*, 201. [[CrossRef](#)]
20. Teschke, R.; Andrade, R.J. Drug-induced liver injury: Expanding our knowledge by enlarging population analysis with prospective and scoring causality assessment. *Gastroenterology* **2015**, *148*, 1271–1273. [[CrossRef](#)]
21. Teschke, R.; Eickhoff, A.; Brown, A.C.; Neuman, M.G.; Schulze, J. Diagnostic biomarkers in liver injury by drugs, herbs, and alcohol: Tricky dilemma after EMA correctly and officially retracted Letter of Support. *Int. J. Mol. Sci.* **2020**, *21*, 212. [[CrossRef](#)]
22. Teschke, R. Acetaminophen syn. paracetamol: Acute liver injury and acute on chronic liver failure with case analysis and causality assessment using RUCAM. In *Liver Failure: Acute and Acute on Chronic*; Nikolaos, T., Ed.; Springer Nature: Cham, Switzerland, 2020.
23. Bessone, F.; Hernandez, N.; Lucena, M.I.; Andrade, R.J. The Latin American DILI registry experience: A successful ongoing collaborative strategic initiative. *Int. J. Mol. Sci.* **2016**, *17*, 313. [[CrossRef](#)]
24. Bessone, F.; Hernandez, N.; Mendizabal, M.; Sanchez, A.; Parana, R.; Arrese, M.; Tagle, M.; Giralda, M.; Lizarzabal, M.; Carrera, E.; et al. When the creation of a consortium provides useful answers: Experience of The Latin American DILI Network (LATINDILIN). *Clin. Liver Dis.* **2019**, *13*, 51–57. [[CrossRef](#)] [[PubMed](#)]
25. Colaci, C.S.; Mendizaba, M.; Bessone, F. Idiosyncratic drug-induced acute liver failure: A challenging and distressing scenario. *Curr. Drug Saf.* **2019**, *14*, 94–101. [[CrossRef](#)] [[PubMed](#)]
26. García, D.S.; Saturansky, E.I.; Poncino, D.; Martínez-Artola, Y.; Rosenberg, S.; Abritta, G.; Ascimani-Peña, C.; Cravero, A. Hepatic toxicity by methotrexate with weekly single doses associated with folic acid in rheumatoid and psoriatic arthritis. What is its real frequency? *Ann. Hepatol.* **2019**, *18*, 765–769. [[CrossRef](#)]
27. Lin, J.; Moore, D.; Hockey, B.; Di Lerna, R.; Gorelik, A.; Liew, D.; Nicoll, A. Drug-induced hepatotoxicity: Incidence of abnormal liver function tests consistent with volatile anaesthetic hepatitis in trauma patients. *Liver Int.* **2014**, *34*, 576–586. [[CrossRef](#)] [[PubMed](#)]
28. Ahmed, T.; Pandey, R.; Shah, R.; Black, J. Resolution of ipilimumab induced severe hepatotoxicity with triple immunosuppressants therapy. *BMJ Case Rep.* **2015**, *2015*, bcr2014208102. [[CrossRef](#)]
29. Laube, R.; Liu, K. An unwanted complement: Rare case of potential liver injury induced by an interaction between ginseng and atorvastatin. *Br. J. Clin. Pharm.* **2019**, *85*, 1612–1613. [[CrossRef](#)]
30. Worland, T.; Chin, K.L.; van Langenberg, D.; Garg, M.; Nicoll, A. Retrospective study of idiosyncratic drug-induced liver injury from infliximab in an inflammatory bowel disease cohort: The IDLE study. *Ann. Gastroenterol.* **2020**, *33*, 162–169. [[CrossRef](#)]
31. Sridharan, K.; Al Daylami, A.; Ajjawi, R.; Al Ajoos, H.A.M. Drug-induced liver injury in critically ill children taking antiepileptic drugs: A retrospective study. *Curr. Ther. Res.* **2020**, in press.
32. Becker, M.W.; Muller Lunardelli, M.J.; Valle Tovo, C. Drug and herb-induced liver injury: A critical review of Brazilian cases with proposals for the improvement of causality assessment using RUCAM. *Ann. Hepatol.* **2019**, *18*, 742–750. [[CrossRef](#)]

33. Yan, B.; Leung, Y.; Urbanski, S.J.; Myers, R.P. Rofecoxib-induced hepatotoxicity: A forgotten complication of the coxibs. *Can. J. Gastroenterol.* **2006**, *20*, 351–355. [[CrossRef](#)]
34. Nhean, S.; Yoong, D.; Wong, D.K.; Gough, K.; Tseng, A.L. Probable hepatotoxicity with dolutegravir: Report of two cases and review of the literature. *Aids* **2019**, *33*, 1261–1263. [[CrossRef](#)] [[PubMed](#)]
35. Hou, F.Q.; Zeng, Z.; Wang, G.Q. Hospital admissions for drug-induced liver injury: Clinical features, therapy, and outcomes. *Cell Biochem. Biophys.* **2012**, *64*, 77–83. [[CrossRef](#)]
36. Lv, X.; Tang, S.; Xia, Y.; Zhang, Y.; Wu, S.; Yang, Z.; Li, X.; Tu, D.; Chen, Y.; Deng, P.; et al. NAT2 genetic polymorphisms and anti-tuberculosis drug-induced hepatotoxicity in Chinese community population. *Ann. Hepatol.* **2012**, *11*, 700–707. [[CrossRef](#)]
37. Hao, K.; Yu, Y.; He, C.; Wang, M.; Wang, S.; Li, X. RUCAM scale-based diagnosis, clinical features and prognosis of 140 cases of drug-induced liver injury. *Chin. J. Hepatol.* **2014**, *22*, 938–941. (Abstract in English, Article in Chinese). [[CrossRef](#)]
38. Ou, P.; Chen, Y.; Li, B.; Zhang, M.; Liu, X.; Li, F.; Li, Y.; Chen, C.; Mao, Y.; Chen, J. Causes, clinical features and outcomes of drug-induced liver injury in hospitalized patients in a Chinese tertiary care hospital. *SpringerPlus* **2015**, *4*, 802. [[CrossRef](#)]
39. Zhu, Y.; Li, Y.G.; Wang, J.B.; Liu, S.H.; Wang, L.F.; Zhao, Y.L.; Bai, Y.F.; Wang, Z.X.; Li, J.Y.; Xiao, X.H. Causes, features, and outcomes of drug-induced liver injury in 69 children from China. *Gut Liver* **2015**, *9*, 525–533. [[CrossRef](#)]
40. Lu, R.J.; Zhang, Y.; Tang, F.L.; Zheng, Z.W.; Fan, Z.D.; Zhu, S.M.; Qian, X.F.; Liu, N.N. Clinical characteristics of drug-induced liver injury and related risk factors. *Exp. Med.* **2016**, *12*, 2606–2616. [[CrossRef](#)]
41. Yang, J.; Yu, Y.L.; Jin, Y.; Zhang, Y.; Zheng, C.Q. Clinical characteristics of drug-induced liver injury and primary biliary cirrhosis. *World J. Gastroenterol.* **2016**, *22*, 7579–7586. [[CrossRef](#)]
42. Zhu, Y.; Niu, M.; Chen, J.; Zou, Z.S.; Ma, Z.J.; Liu, S.H.; Wang, R.L.; He, T.T.; Song, H.B.; Wang, Z.X.; et al. Comparison between Chinese herbal medicine and Western medicine-induced liver injury of 1985 patients. *J. Gastroenterol. Hepatol.* **2016**, *31*, 1476–1482. [[CrossRef](#)]
43. Naiqiong, W.; Liansheng, W.; Zhanying, H.; Yuanlin, G.; Chenggang, Z.; Ying, G.; Qian, D.; Dongchen, L.; Yanjun, Z.; Jianjun, L. A multicenter and randomized controlled trial of Bicyclol in the treatment of statin-induced liver injury. *Med. Sci. Monit.* **2017**, *23*, 5760–5766. [[CrossRef](#)]
44. Li, X.L.; Liu, X.; Song, Y.; Hong, R.T.; Shi, H. Suspected drug-induced liver injury associated with iguratimod: A case report and review of the literature. *BMC Gastroenterol.* **2018**, *18*, 130. [[CrossRef](#)] [[PubMed](#)]
45. Song, Z.W.; Panx, Y.C.; Huang, Z.C.; Liu, W.X.; Zhao, R.S.; Jing, H.M.; Dong, F. Posaconazole-associated severe hyperbilirubinemia in acute myeloid leukemia following chemotherapy: A case report. *World J. Clin. Cases* **2018**, *6*, 1206–1209. [[CrossRef](#)] [[PubMed](#)]
46. Tao, B.; Chen, S.; Lin, G.; Yang, M.; Lu, L.; He, X.; Pan, H.; Tang, S. Genetic polymorphisms of *UGT 1A1* and susceptibility to anti-tuberculosis drug-induced liver injury: A RUCAM-based case-control study. *Int. J. Immunopathol. Pharm.* **2018**, *32*, 1–6. [[CrossRef](#)]
47. Liao, P.F.; Wu, Y.K.; Huang, K.L.; Chen, H.Y. A rare case of cefepime-induced cholestatic liver injury. *Tzu Chi Med. J.* **2019**, *31*, 124–128.
48. Shen, T.; Liu, Y.; Shang, J.; Xie, Q.; Li, J.; Yan, M.; Xu, J.; Niu, J.; Liu, J.; Watkins, P.B.; et al. Incidence and etiology of drug-induced liver injury in Mainland China. *Gastroenterology* **2019**, *156*, 2230–2241. [[CrossRef](#)]
49. Xing, M.; Zhai, L.; Li, J.; Li, Q.; Gao, M.; Wen, J.; Xu, Z. Assessment of cholestasis in drug-induced liver injury by different methods. *Medicine* **2019**, *98*, e14399. [[CrossRef](#)]
50. Ma, S.; Liu, S.; Wang, Q.; Chen, L.; Yang, P.; Sun, H. Fenofibrate-induced hepatotoxicity: A case with a special feature that is different from those in the LiverTox database. *J. Clin. Pharm.* **2020**, *45*, 204–207. [[CrossRef](#)]
51. Tao, B.; Yang, M.; Chen, H.; Pan, H.; Liu, W.; Yi, H.; Tang, S. Association of ABO blood group and antituberculosis drug-induced liver injury: A case-control study from a Chinese Han population. *J. Clin. Pharm.* **2020**. [[CrossRef](#)]
52. Wang, S.; Shangguan, Y.; Ding, C.; Li, P.; Ji, Z.; Shao, J.; Fang, H.; Yang, M.; Shi, P.; Wu, J.; et al. Risk factors for acute liver failure among inpatients with anti-tuberculosis drug-induced liver injury. *J. Int. Med. Res.* **2020**, *48*. [[CrossRef](#)]

53. Yang, H.; Guo, D.; Xu, Y.; Zhu, M.; Yao, C.; Chen, C.; Jia, W. Comparison of different liver test thresholds for drug-induced liver injury: Updated RUCAM versus other methods. In: Special issue: Clinical drug induced liver injury: Current diagnostic and mechanistic challenges, guest editors Rolf Teschke, Gaby Danan, James H. Lewis. *Front. Pharmacol.* **2019**, *10*, 816. [[CrossRef](#)]
54. Ríos, D.; Restrepo, J.C. Abendazole-induced liver injury: A case report. *Colomb. Med.* **2013**, *44*, 118–120. [[CrossRef](#)] [[PubMed](#)]
55. Cano-Paniagua, A.; Amariles, P.; Angulo, N. Epidemiology of drug-induced liver injury in a university hospital from Colombia: Updated RUCAM being used for prospective causality assessment. *Ann. Hepatol.* **2019**, *18*, 501–507. [[CrossRef](#)] [[PubMed](#)]
56. Alhaddad, O.; Elsabaawy, M.; Abdelsameea, E.; Abdalla, A.; Shabaan, A.; Ehsan, N.; Elrefaey, A.; Elsabaawy, D.; Salama, M. Presentations, causes and outcomes of drug-induced liver injury in Egypt. *Sci. Rep.* **2020**, *10*, 5124. [[CrossRef](#)] [[PubMed](#)]
57. Bénichou, C.; Danan, G.; Flahault, A. Causality assessment of adverse reactions to drugs—II. An original model for validation of drug causality assessment methods: Case reports with positive rechallenge. *J. Clin. Epidemiol.* **1993**, *46*, 1331–1336.
58. Arotcarena, R.; Bigué, J.P.; Etcharry, F.; Pariente, A. Pioglitazone-induced acute severe hepatitis. *Gastroenterol. Clin. Biol.* **2004**, *28*, 609–618. (In French)
59. Moch, C.; Rocher, F.; Lainé, P.; Lacotte, J.; Biour, M.; Gouraud, A.; Bernard, N.; Descotes, J.; Vial, T. Etifoxine-induced acute hepatitis: A case series. *Clin. Res. Hepatol. Gastroenterol.* **2012**, *36*, e85–e88. [[CrossRef](#)]
60. Carrier, P.; Godet, B.; Crepin, S.; Magy, L.; Debette-Gratien, M.; Pillegand, B.; Jacques, J.; Sautereau, D.; Vidal, E.; Labrousse, F.; et al. Acute liver toxicity due to methylprednisolone: Consider this diagnosis in the context of autoimmunity. *Clin. Res. Hepatol. Gastroenterol.* **2013**, *37*, 100–104. [[CrossRef](#)]
61. Ripault, M.P.; Pinzani, V.; Fayolle, V.; Pageaux, G.P.; Larrey, D. Crizotinib-induced acute hepatitis: First case with relaps after reintroduction with reduced dose. *Clin. Res. Hepatol. Gastroenterol.* **2013**, *37*, e21–e23. [[CrossRef](#)]
62. Dumortier, J.; Cottin, J.; Lavie, C.; Guillaud, O.; Hervieu, V.; Chambon-Augoyard, C.; Scoazec, J.Y.; Vukusic, S.; Vital, T. Methylprednisolone liver toxicity: A new case and a French regional pharmacovigilance survey. *Clin. Res. Hepatol. Gastroenterol.* **2017**, *41*, 497–501. [[CrossRef](#)]
63. Meunier, L.; Larrey, D. Recent advances in hepatotoxicity of non steroidal anti-inflammatory drugs. *Ann. Hepatol.* **2018**, *17*, 187–191. [[CrossRef](#)]
64. Stammshulte, T.; Treichel, U.; Pacht, H.; Gundert-Remy, U. Cases of Liver Failure in Association with Flupirtine in the German Spontaneous Reporting System. Available online: <http://www.akdae.de/Kommission/Organisation/Aufgaben/Publikationen/PDF/Stammshulte2012.pdf> (accessed on 30 June 2020).
65. Douros, A.; Bronder, E.; Andersohn, F.; Klimpel, A.; Thomae, M.; Orzechowski, H.D.; Kreutz, R.; Garbe, E. Flupirtine-induced liver injury—Seven cases from the Berlin Case-control Surveillance Study and review of the German spontaneous adverse drug reaction reporting database. *Eur. J. Clin. Pharm.* **2014**, *70*, 453–459. [[CrossRef](#)] [[PubMed](#)]
66. Douros, A.; Bronder, E.; Andersohn, F.; Klimpel, A.; Thomae, M.; Sarganas, G.; Kreutz, R.; Garbe, E. Drug-induced liver injury: Results from the hospital-based Berlin Case-Control Surveillance Study. *Br. J. Clin. Pharm.* **2014**, *79*, 988–999. [[CrossRef](#)] [[PubMed](#)]
67. Buechter, M.; Manka, P.; Heinemann, F.M.; Lindemann, M.; Baba, H.A.; Schlattjan, M.; Canbay, A.; Gerken, G.; Kahraman, A. Potential triggering factors of acute liver failure as a first manifestation of autoimmune hepatitis—a single center experience of 52 adult patients. *World J. Gastroenterol.* **2018**, *24*, 1410–1418. [[CrossRef](#)]
68. Dragoi, D.; Benesic, A.; Pichler, G.; Kulak, N.A.; Bartsch, H.S.; Gerbes, A.L. Proteomics analysis of monocyte-derived hepatocyte-like cells identifies integrin beta 3 as a specific biomarker for drug-induced liver injury by diclofenac. *Front. Pharmacol.* **2018**, *9*, 699. [[CrossRef](#)] [[PubMed](#)]
69. Teschke, R.; Danan, G. Review: Drug induced liver injury with analysis of alternative causes as confounding variables. *Br. J. Clin. Pharm.* **2018**, *84*, 1467–1477. [[CrossRef](#)]
70. Teschke, R. Review. Top-ranking drugs out of 3312 drug-induced liver injury cases evaluated by the Roussel Uclaf Causality Assessment Method. *Expert Opin. Drug Metab. Toxicol.* **2018**, *14*, 1169–1187. [[CrossRef](#)]
71. Weber, S.; Benesic, A.; Rotter, I.; Gerbes, A.L. Early ALT response to corticosteroid treatment distinguishes idiosyncratic drug-induced liver injury from autoimmune hepatitis. *Liver Int.* **2019**, *39*, 1906–1917. [[CrossRef](#)]



72. Björnsson, E.; Jacobsen, E.I.; Kalaitzakis, E. Hepatotoxicity associated with statins: Reports of idiosyncratic liver injury post-marketing. *J. Hepatol.* **2012**, *56*, 374–380. [[CrossRef](#)]
73. Björnsson, E.S.; Bergmann, O.M.; Björnsson, H.K.; Kvaran, R.B.; Olafsson, S. Incidence, presentation and outcomes in patients with drug-induced liver injury in the general population of Iceland. *Gastroenterology* **2013**, *144*, 1419–1425. [[CrossRef](#)]
74. Björnsson, E.S.; Hoofnagle, J.H. Categorization of drugs implicated in causing liver injury: Critical assessment based on published case reports. *Hepatology* **2016**, *63*, 590–603. [[CrossRef](#)]
75. Harugeri, A.; Parthasarathi, G.; Sharma, J.; D'Souza, G.A.; Ramesh, M. Montelukast induced acute hepatocellular injury. *J. Postgrad. Med.* **2009**, *55*, 141–142.
76. Devarbhavi, H.; Dierkhising, R.; Kremers, W.K.; Sandeep, M.S.; Karanth, D.; Adarsh, C.K. Single center experience with drug-induced liver injury from India: Causes, outcome, prognosis, and predictors of mortality. *Am. J. Gastroenterol.* **2010**, *105*, 2396–2404. [[CrossRef](#)] [[PubMed](#)]
77. Rathi, C.; Pipaliya, N.; Patel, R.; Ingle, M.; Phadke, A.; Sawant, P. Drug induced liver injury at a tertiary hospital in India: Etiology, clinical features and predictors of mortality. *Ann. Hepatol.* **2017**, *16*, 442–450. [[CrossRef](#)]
78. Taneja, S.; Kumar, P.; Rathi, S.; Duseja, A.; Singh, V.; Dhiman, R.K.; Chawla, Y.K. Acute liver failure due to Etodolac, a selective cyclooxygenase-2 (COX-2) inhibitor non-steroidal anti-inflammatory drug established by RUCAM-based causality assessment. *Ann. Hepatol.* **2017**, *16*, 818–821. [[CrossRef](#)] [[PubMed](#)]
79. Das, S.; Behera, S.K.; Xavier, A.S.; Velupula, S.; Dkhar, S.A.; Selvarajan, S. Agreement among different scales for causality assessment in drug-induced liver injury. *Clin. Drug Investig.* **2018**, *38*, 211–218. [[CrossRef](#)] [[PubMed](#)]
80. Dutta, S.K.; Chakravarty, P.J.; Borah, A.J. Haloperidol induced hepatotoxicity: A case report. *Ann. Clin. Case Rep.* **2020**, *5*, 1827.
81. Kulkarni, A.V.; Kumar, P.; Talukdar, R.; Rao, N. Steroids as rescue therapy for vitamin A-induced acute liver failure. *BMJ Case Rep. CP* **2020**, *13*, e233902. [[CrossRef](#)] [[PubMed](#)]
82. Gluck, N.; Fried, M.; Porat, R. Acute amiodarone liver toxicity likely due to ischemic hepatitis. *Isr. Med. Assoc. J.* **2011**, *13*, 748–752.
83. Rigato, I.; Cravatari, M.; Avellini, C.; Ponte, E.; Crocè, S.L.; Tiribelli, C. Drug-induced acute cholestatic liver damage in a patient with mutation of UGT1A1. *Nat. Clin. Pr. Gastroenterol. Hepatol.* **2007**, *4*, 43–408. [[CrossRef](#)]
84. Licata, A.; Calvaruso, V.; Capello, M.; Craxi, A.; Almasio, P.L. Clinical course and outcomes of drug-induced liver injury: Nimesulide as the first implicated medication. *Dig. Liver Dis.* **2010**, *42*, 143–148. [[CrossRef](#)]
85. Abenavoli, L.; Milic, N.; Beaugrand, M. Severe hepatitis by cyproterone acetate: Role of corticosteroids. A case report. *Ann. Hepatol.* **2013**, *1*, 152–155. [[CrossRef](#)]
86. Ferrajolo, C.; Verhamme, K.M.; Trifirò, G.; W't Jong, G.; Picelli, G.; Giaquinto, C.; Mazzaglia, G.; Stricker, B.H.; Rossi, F.; Capuano, A.; et al. Antibiotic-induced liver injury in paediatric outpatients: A case-control study in primary care databases. *Drug Saf.* **2017**, *40*, 305–315. [[CrossRef](#)] [[PubMed](#)]
87. Licata, A.; Minissale, M.G.; Calvaruso, V.; Craxi, A. A focus on epidemiology of drug-induced liver injury; analysis of a prospective cohort. *Eur. Rev. Pharm. Sci.* **2017**, *21*, 112–121.
88. Giacomelli, A.; Rusconi, S.; Falvella, F.S.; Oreni, M.L.; Cattaneo, D.; Cozzi, V.; Renisi, G.; Monge, E.; Cheli, S.; Clementi, E.; et al. Clinical and genetic determinants of nevirapine plasma through concentration. *SAGE Open Med.* **2018**, *6*. [[CrossRef](#)] [[PubMed](#)]
89. Licata, A.; Puccia, F.; Lombardo, V.; Serruto, A.; Minissale, M.G.; Morreale, I.; Giannitrapani, L.; Soresi, M.; Montalto, G.; Almasio, P.L. Rivaroxaban-induced hepatotoxicity: Review of the literature and report of new cases. *Eur. J. Gastroenterol. Hepatol.* **2018**, *30*, 226–232. [[CrossRef](#)] [[PubMed](#)]
90. Lovero, R.; Losurdo, G.; Mastromauro, M.; Castellana, N.M.; Mongelli, A.; Gentile, A.; Di Leo, A.; Principi, M. A case of severe transaminase elevation following a single Ustekinumab dose with remission after drug withdrawal. *Curr. Drug Saf.* **2018**, *13*, 221–223. [[CrossRef](#)] [[PubMed](#)]
91. Masumoto, T.; Horiike, N.; Abe, M.; Kumaki, T.; Matsubara, H.; Fazole Akbar, S.M.; Michitaka, K.; Hyodo, I.; Onji, M. Diagnosis of drug-induced liver injury in Japanese patients by criteria of the Consensus Meetings in Europe. *Hepatol. Res.* **2003**, *25*, 1–7. [[CrossRef](#)]

92. Hanatani, T.; Sai, K.; Tohkin, M.; Segawa, K.; Kimura, M.; Hori, K.; Kawakami, J.; Saito, Y. A detection algorithm for drug-induced liver injury in medical information databases using the Japanese diagnostic scale and its comparison with the Council for International Organizations of Medical Sciences/the Roussel Uclaf Causality Assessment Method scale. *Pharm. Drug Saf.* **2014**, *23*, 984–988. [[CrossRef](#)]
93. Nijijima, K.; Nijijima, Y.; Okada, S.; Yamada, M. Drug-induced liver injury caused by Ipragliflozin administration with causality established by a positive lymphocyte transformation test (LTT) and the Roussel Uclaf Causality Assessment Method (RUCAM): A case report. *Ann. Hepatol.* **2017**, *16*, 308–311. [[CrossRef](#)]
94. Ji, H.; Yue, F.; Song, J.; Zhou, X. A rare case of methimazole-induced cholestatic jaundice in an elderly man of Asian ethnicity with hyperthyroidism: A case report. *Medicine* **2017**, *96*, e9093. [[CrossRef](#)]
95. Aiso, M.; Takikawa, H.; Tsuji, K.; Kagawa, T.; Watanabe, M.; Tanaka, A.; Sato, K.; Sakisaka, S.; Hiasa, Y.; Takei, Y.; et al. Analysis of 307 cases with drug-induced liver injury between 2010 and 2018 in Japan. *Hepatol. Res.* **2019**, *49*, 105–110. [[CrossRef](#)] [[PubMed](#)]
96. Kishimoto, M.; Adachi, M.; Takahashi, K.; Washizaki, K. Clonazepam-induced liver dysfunction, severe hyperlipidaemia, and hyperglycaemic crisis: A case report. *SAGE Open Med. Cases Rep.* **2019**, *7*, 1–5. [[CrossRef](#)] [[PubMed](#)]
97. Hiraki, M.; Tanaka, T.; Koga, F.; Saito, A.; Oza, N.; Ikeda, O.; Manabe, T.; Miyoshi, A.; Kitahara, K.; Sato, S.; et al. An unusual case of acute liver failure caused by adjuvant oral Tegafur-Uracil with folinate therapy for colon cancer patient: A case report. *J. Gastrointest. Cancer* **2020**, *51*, 296–299. [[CrossRef](#)]
98. Kakisaka, K.; Suzuki, Y.; Jinnouchi, Y.; Kanazawa, J.; Sasaki, T.; Yonezawa, T.; Yoshida, Y.; Kuroda, H.; Takikawa, Y. Unfavorable prognosis of patients with acute liver injury due to drug-induced liver injury and acute exacerbation of hepatitis B virus infection. *Hepatol. Res.* **2019**, *49*, 1286–1293. [[CrossRef](#)] [[PubMed](#)]
99. Choi, G.Y.; Yang, H.W.; Cho, S.H.; Kang, D.W.; Go, H.; Lee, W.C.; Lee, Y.J.; Jung, S.H.; Kim, A.N.; Cha, S.W. Acute drug-induced hepatitis caused by albendazole. *J. Korean Med. Sci.* **2008**, *23*, 903–905. [[CrossRef](#)] [[PubMed](#)]
100. Suk, K.T.; Kim, D.J.; Kim, C.H.; Park, S.H.; Yoon, J.H.; Kim, Y.S.; Baik, G.H.; Kim, J.B.; Kweon, Y.O.; Kim, B.L.; et al. A prospective nationwide study of drug-induced liver injury in Korea. *Am. J. Gastroenterol.* **2012**, *107*, 1380–1387. [[CrossRef](#)]
101. Son, C.G. Drug-induced liver injury by Western medication. *J. Int. Korean Med.* **2015**, *36*, 69–75.
102. Woo, H.J.; Kim, H.Y.; Choi, E.S.; Cho, Y.; Kim, Y.; Lee, J.H.; Jang, E. Drug-induced liver injury: A 2-year retrospective study of 1169 hospitalized patients in a single medical center. *Phytomedicine* **2015**, *22*, 1201–1205. [[CrossRef](#)] [[PubMed](#)]
103. Byeon, J.H.; Kil, J.H.; Ahn, Y.C.; Son, C.S. Systematic review of published data on herb induced liver injury. *J. EthnoPharmacol.* **2019**, *233*, 190–196. [[CrossRef](#)] [[PubMed](#)]
104. Kwon, J.; Kim, S.; Yoo, H.; Lee, E. Nimesulide-induced hepatotoxicity: A systemic review and meta-analysis. *PLoS ONE* **2019**, *14*, e0209264. [[CrossRef](#)] [[PubMed](#)]
105. Thalha, A.M.; Mahadeva, S.; Tan, A.T.B.; Mun, K.S. Kombiglyze (metformin and saxagliptin)-induced hepatotoxicity in a patient with non-alcoholic fatty liver disease. *JGH Open* **2018**, *2*, 242–245. [[CrossRef](#)] [[PubMed](#)]
106. Lammel-Lindemann, J.A.; Clores-Villalba, E.; Martagón, A.J.; DeObeso-Gonzalez, E.; Puente-Gallegos, F. Non-cholestatic acute hepatitis following Candesartan administration. *Br. J. Clin. Pharm.* **2018**, *84*, 204–207. [[CrossRef](#)] [[PubMed](#)]
107. Essaid, A.; Timraz, A. Cholestatic acute hepatitis induced by tadalafil (Cialis®). *Gastroenterol. Clin. Biol.* **2010**, *34*, e1–e2. (In French) [[CrossRef](#)] [[PubMed](#)]
108. Abid, A.; Subhani, F.; Kayani, F.; Awan, S.; Abid, S. Drug induced liver injury is associated with high mortality-A study from a tertiary care hospital in Pakistan. *PLoS ONE* **2020**, *15*, e0231398. [[CrossRef](#)]
109. Costa-Moreira, P.; Gaspar, R.; Pereira, P.; Lopes, S.; Canao, P.; Lopes, J.; Carneiro, F.; Macedo, G. Role of liver biopsy in the era of clinical prediction scores for “drug-induced liver injury” (DILI): Experience of a tertiary referral hospital. *Virchows Arch.* **2020**. [[CrossRef](#)]
110. Alqrinawi, S.H.; Akbar, N.; AlFaddag, H.; Akbar, S.; Akbar, L.; Butt, S.A.; Aljawad, M. Menotrophin induced autoimmune hepatitis. *Case Rep. Gastrointest. Med.* **2019**. [[CrossRef](#)]

111. Miljkovic, M.M.; Dobric, S.; Dragojevic-Simic, V. Consistency between causality assessments obtained with two scales and their agreement with clinical judgments in hepatotoxicity. *Pharm. Drug Saf.* **2011**, *20*, 272–285. [[CrossRef](#)]
112. Miljkovic, M.M.; Dobric, S.; Dragojevic-Simic, V. Accuracy and reproducibility of two scales in causality assessment of unexpected hepatotoxicity. *J. Clin. Pharm.* **2012**, *37*, 196–203. [[CrossRef](#)]
113. Wai, C.T. Presentation of drug-induced liver injury in Singapore. *Singap. Med. J.* **2006**, *47*, 116–120.
114. Rodríguez, L.A.; Stricker, B.H.; Zimmerman, H.J. Risk of acute liver injury associated with the combination of amoxicillin and clavulanic acid. *Arch. Int. Med.* **1996**, *156*, 1327–1332. [[CrossRef](#)]
115. Andrade, R.J.; Lucena, M.I.; Fernández, M.C.; Pelaez, G.; Pachkoria, K.; García-Ruiz, E.; García-Muñoz, B.; Gonzalez-Grande, R.; Pizarro, A.; Durán, J.A.; et al. Spanish Group for the Study of Drug-induced Liver Disease. Drug-induced liver injury: An analysis of 461 incidences submitted to the Spanish registry over a 10-year period. *Gastroenterology* **2005**, *129*, 512–521. [[CrossRef](#)]
116. Andrade, R.J.; Lucena, M.I.; Kaplowitz, N.; García-Muñoz, B.; Borraz, Y.; Pachkoria, K.; García-Cortés, M.; Fernández, M.C.; Pelaez, G.; Rodrigo, L.; et al. Outcome of acute idiosyncratic drug-induced liver injury: Long term follow-up in a hepatotoxicity registry. *Hepatology* **2006**, *44*, 1581–1588. [[CrossRef](#)] [[PubMed](#)]
117. García-Cortés, M.; Lucena, M.I.; Pachkoria, K.; Borraz, Y.; Hidalgo, R.; Andrade, R.J. Evaluation of Naranjo Adverse Drug Reactions Probability Scale in causality assessment of drug-induced liver injury. *Aliment. Pharm.* **2008**, *27*, 780–789. [[CrossRef](#)] [[PubMed](#)]
118. Lucena, M.I.; Molokhia, M.; Shen, Y.; Urban, T.J.; Aithal, G.P.; Andrade, R.J.; Day, C.P.; Ruiz-Cabello, F.; Donaldson, P.T.; Stephens, C.; et al. Susceptibility to amoxicillin-clavulanate-induced liver injury is influenced by multiple HLA class I and II alleles. *Gastroenterology* **2011**, *141*, 338–347. [[CrossRef](#)]
119. Lucena, M.I.; Kaplowitz, N.; Hallal, H.; Castiella, A.; Garcia-Bengochea, M.; Otazua, P.; Berenguer, M.; Fernandez, M.C.; Planas, R.; Andrade, R.J. Recurrent drug-induced liver injury (DILI) with different drugs in the Spanish Registry: The dilemma of the relationship to autoimmune hepatitis. *J. Hepatol.* **2011**, *55*, 820–827. [[CrossRef](#)] [[PubMed](#)]
120. Robles-Diaz, M.; Gonzalez-Jimenez, A.; Medina-Caliz, I.; Stephens, C.; García-Cortes, M.; García-Muñoz, B.; Ortega-Alonso, A.; Blanco-Reina, E.; Gonzalez-Grande, R.; Jimenez-Perez, M.; et al. on behalf of the Spanish DILI Registry and the SLatinDILI Network. Distinct phenotype of hepatotoxicity associated with illicit use of anabolic androgenic steroids. *Aliment. Pharm.* **2015**, *41*, 116–125. [[CrossRef](#)]
121. Tong, H.Y.; Díaz, C.; Collantes, E.; Medrano, N.; Borobia, A.M.; Jara, P.; Ramírez, E. Liver transplant in a patient under methylphenidate therapy: A case report and review of the literature. *Case Rep. Pediatr.* **2015**, *2015*, 437298. [[CrossRef](#)]
122. Medina-Caliz, I.; Robles-Diaz, M.; Garcia-Muñoz, B.; Stephens, C.; Ortega-Alonso, A.; Garcia-Cortes, M.; González-Jimenez, A.; Sanabria-Cabrera, J.A.; Moreno, I.; Fernandez, M.C.; et al. Spanish DILI registry. Definition and risk factors for chronicity following acute idiosyncratic drug-induced liver injury. *J. Hepatol.* **2016**, *65*, 532–542. [[CrossRef](#)]
123. López-Riera, M.; Conde, I.; Quitas, G.; Pedrola, L.; Zaragoza, Á.; Perez-Rojas, J.; Saledo, M.; Benlloch, S.; Castell, J.V.; Jover, R. Non-invasive prediction of NAFLD severity: A comprehensive, independent validation of previously postulated serum microRNA biomarkers. *Sci. Rep.* **2018**, *8*, 10606. [[CrossRef](#)]
124. Machlab, S.; Mireia, M.; Vergara, M.; Escoda, M.R.; Casas, M. Apixaban-induced liver injury. *Rev. Esp. Enferm. Dig.* **2019**, *111*, 161–163. [[CrossRef](#)]
125. Zoubek, M.E.; Pinazo-Bandera, J.; Ortega-Alonso, A.; Hernández, N.; Crespo, J.; Contreras, F.; Medina-Cáliz, I.; Sanabria-Cabrera, J.; Sanjuan-Jiménez, R.; González-Jiménez, A.; et al. Liver injury after methylprednisolone pulses: A disputable cause of hepatotoxicity. A case series and literature review. *United Eur. Gastroenterol. J.* **2019**, *7*, 825–837. [[CrossRef](#)] [[PubMed](#)]
126. Björnsson, E.; Olsson, R. Outcome and prognostic markers in severe drug-induced liver disease. *Hepatology* **2005**, *42*, 481–489. [[CrossRef](#)] [[PubMed](#)]
127. De Valle, M.B.; Klinteberg, A.V.; Alem, N.; Olsson, R.; Björnsson, E. Drug-induced liver injury in a Swedish University hospital out-patient hepatology clinic. *Aliment. Pharm.* **2006**, *24*, 1187–1195. [[CrossRef](#)] [[PubMed](#)]
128. Björnsson, E.; Kalaitzakis, E.; Klinteberg, V.A.V.; Alem, E.; Olsson, R. Long-term follow-up of patients with mild to moderate drug-induced liver injury. *Aliment. Pharm.* **2007**, *26*, 79–85. [[CrossRef](#)]
129. Björnsson, E.S. Epidemiology and risk factors for idiosyncratic drug-induced liver injury. *Semin Liver Dis.* **2014**, *34*, 115–122. [[CrossRef](#)]

130. Goossens, N.; Spahr, L.; Rubbia-Brandt, L. Severe immune-mediated drug-induced liver injury linked to ibandronate: A case report. *J. Hepatol.* **2013**, *59*, 1139–1142. [[CrossRef](#)]
131. Russmann, S.; Niedrig, D.F.; Budmiger, M.; Schmidt, C.; Stieger, B.; Hürlimann, S.; Kullak-Ublick, G.A. Rivaroxaban postmarketing risk of liver injury. *J. Hepatol.* **2014**, *61*, 293–300. [[CrossRef](#)]
132. Scalfaro, E.; Streefkerk, H.J.; Merz, M.; Meier, C.; Lewis, D. Preliminary results of a novel algorithmic method aiming to support initial causality assessment of routine pharmacovigilance case reports for medication-induced liver injury: The PV-RUCAM. *Drug Saf.* **2017**, *40*, 715–727. [[CrossRef](#)]
133. Schneider, J.S.; Montani, M.; Stickel, F. Drug-induced autoimmune hepatitis following treatment with Zoledronic acid. *Case Rep. Gastroenterol.* **2017**, *11*, 440–445. [[CrossRef](#)]
134. Terziroli Beretta-Piccoli, B.; Mieli-Vergani, G.; Bertoli, R.; Mazzucchelli, L.; Nofziger, C.; Paulmichl, M.; Vergani, D. Atovaquone/proguanil-induced autoimmune-like hepatitis. *Hepatol. Commun.* **2017**, *1*, 293–298. [[CrossRef](#)]
135. Visentin, M.; Lenggenhager, D.; Gai, Z.; Kullak-Ublick, G.A. Drug-induced bile duct injury. *BBA Mol. Basis Dis.* **2018**, *1864*, 1498–1506. [[CrossRef](#)]
136. Treeprasertsuk, S.; Huntrakul, J.; Ridditid, W.; Kullavanijaya, P.; Björnsson, E.S. The predictors of complications in patients with drug-induced liver injury caused by antimicrobial agents. *Aliment. Pharm.* **2010**, *11*, 1200–1207.
137. Sobhonslidsuk, A.; Poovorawan, K.; Soonthornworasiri, N.; Pangnum, W.; Phaosawasdi, K. The incidence, presentation, outcomes, risk of mortality and economic data of drug-induced liver injury from a national database in Thailand: A population-base study. *BMC Gastroenterol.* **2016**, *16*, 135. [[CrossRef](#)] [[PubMed](#)]
138. Chayanupatkul, M.; Schiano, T.D. Acute liver failure secondary to drug-induced liver injury. *Clin. Liver Dis.* **2020**, *24*, 75–87. [[CrossRef](#)] [[PubMed](#)]
139. Duzenli, T.; Tanoglu, A.; Akyol, T.; Kara, M.; Yazgan, Y. Drug-induced liver injury caused by Phenprobamate: Strong probability due to repeated toxicity. *Eur. J. HepatoGastroenterol.* **2019**, *9*, 49–51. [[CrossRef](#)]
140. Hussaini, S.H.; O'Brien, C.S.; Despott, E.J.; Dalton, H.R. Antibiotic therapy: A major cause of drug-induced jaundice in southwest England. *Eur. J. Gastroenterol. Hepatol.* **2007**, *19*, 15–20. [[CrossRef](#)] [[PubMed](#)]
141. Daly, A.K.; Donaldson, P.T.; Bhatnagar, P.; Shen, Y.; Pe'er, I.; Floratos, A.; Daly, M.J.; Goldstein, D.B.; John, S.; Nelson, M.R.; et al. HLA-B\*5701 genotype is a major determinant of drug-induced liver injury due to flucloxacillin. *Nat. Genet.* **2009**, *41*, 816–819.
142. Spraggs, C.F.; Budde, L.R.; Briley, L.P.; Bing, N.; Cox, C.J.; King, K.S.; Whittaker, J.C.; Mooser, V.E.; Preston, A.J.; Stein, S.H.; et al. HLA-DQA1\*02, 01 is a major risk factor for Lapatinib-induced hepatotoxicity in women with advanced breast cancer. *J. Clin. Oncol.* **2011**, *29*, 667–673. [[CrossRef](#)]
143. Islam, M.; Wright, G.; Tanner, P.; Lucas, R. A case of anastrozole-related drug-induced autoimmune hepatitis. *Clin. J. Gastroenterol.* **2014**, *7*, 414–417. [[CrossRef](#)]
144. Dyson, J.K.; Hutchinson, J.; Harrison, L.; Rotimi, O.; Tiniakos, D.; Foster, G.R.; Aldersley, M.A.; McPherson, S. Liver toxicity associated with sofosbuvir, an NS5A inhibitor and ribavirin use. *J. Hepatol.* **2016**, *64*, 234–238. [[CrossRef](#)]
145. Abbara, A.; Chitty, S.; Roe, J.K.; Ghani, R.; Collin, S.M.; Ritchie, A.; Kon, O.M.; Dzvova, J.; Davidson, H.; Edwards, T.E.; et al. Drug-induced liver injury from antituberculous treatment: A retrospective study from a large TB centre in the UK. *BMC Infect. Dis.* **2017**, *17*, 231. [[CrossRef](#)] [[PubMed](#)]
146. Vliegenthart, A.D.B.; Berends, C.; Potter, C.M.J.; Kersaudy-Kerhoas, M.; Dear, J.W. MicroRNA-122 can be measured in capillary blood which facilitates point-of-care testing for drug-induced liver injury. *Br. J. Clin. Pharm.* **2017**, *83*, 2027–2033. [[CrossRef](#)] [[PubMed](#)]
147. Fontana, R.J.; Shakil, O.; Greenson, J.K.; Boyd, I.; Lee, W.M. Acute liver failure due to amoxicillin and amoxicillin/clavulanate. *Dig. Dis. Sci.* **2005**, *10*, 1785–1790. [[CrossRef](#)]
148. Lee, W.M.; Larrey, D.; Olsson, R.; Lewis, J.H.; Keisu, M.; Auclert, L.; Sheth, S. Hepatic findings in long-term clinical trials of ximelagatran. *Drug Saf.* **2005**, *28*, 351–370. [[CrossRef](#)] [[PubMed](#)]
149. Stojanovski, S.D.; Casavant, M.J.; Mousa, H.M.; Baker, P.; Nahata, M.C. Atomoxetine-induced hepatitis in a child. *Clin. Toxicol.* **2007**, *45*, 51–55. [[CrossRef](#)]
150. Lammert, C.; Einarsson, S.; Saha, C.; Niklasson, A.; Björnsson, E.; Chalasani, N. Relationship between daily dose of oral medications and idiosyncratic drug-induced liver injury: Search for signals. *J. Hepatol.* **2008**, *47*, 2003–2009. [[CrossRef](#)]
151. Singla, A.; Hammad, H.T.; Hammoud, G.M. Uncommon cause of acute drug-induced liver injury following mammoplasty. *Gastroenterol. Res.* **2010**, *3*, 171–172. [[CrossRef](#)]

152. Nabha, L.; Balba, G.P.; Tuanzon, C.; Kumar, P.N. Etravirine induced severe hypersensitivity reaction and fulminant hepatitis: A case report and review of the literature. *J. Aids Clin. Res.* **2012**, *3*, 005. [[CrossRef](#)]
153. Sprague, D.; Bamha, K. Drug-induced liver injury due to varenicline. *BMC Gastroenterol.* **2012**, *12*, 65. [[CrossRef](#)]
154. Markova, S.M.; De Marco, T.; Bendjilali, N.; Kobashigawa, E.A.; Mefford, J.; Sodhi, J.; Le, H.; Zhang, C.; Halladay, J.; Rettie, A.E.; et al. Association of CYP2C9\*2 with bosentan-induced liver injury. *Clin. Pharm.* **2013**, *94*, 678–686. [[CrossRef](#)]
155. Marumoto, A.; Roytman, M.M.; Tsai, N.C.S. Trial and error: Investigational drug induced liver injury, a case series report. *Hawaii J. Med. Public Health* **2013**, *72*, 30–33. [[PubMed](#)]
156. Bohm, N.; Bohm, N.; Makowski, C.; Machado, M.; Davie, A.; Seabrook, N.; Wheless, L.; Beville, B.; Clark, B.; Kyle, T.R., III. Case report and cohort analysis of drug-induced liver injury associated with daptomycin. *Antimicrob. Agents Chemother.* **2014**, *58*, 4902–4903. [[CrossRef](#)] [[PubMed](#)]
157. Cheetham, T.C.; Lee, J.; Hunt, C.M.; Niu, F.; Reisinger, S.; Murray, R.; Powell, G.; Papay, J. An automated causality assessment algorithm to detect drug-induced liver injury in electronic medical record data. *Pharm. Drug Saf.* **2014**, *23*, 601–608. [[CrossRef](#)]
158. Lim, R.; Choundry, H.; Conner, K.; Karnsakul, W. A challenge for diagnosing acute liver injury with concomitant/sequential exposure to multiple drugs: Can causality assessment scales be utilized to identify the offending drug? *Case Rep. Pediatr.* **2014**, *2014*, 156389. [[CrossRef](#)] [[PubMed](#)]
159. Russo, M.W.; Hoofnagle, J.H.; Gu, J.; Fontana, R.J.; Barnhart, H.; Kleiner, D.E.; Chalasani, N.; Bonkovsky, H.L. Spectrum of statin hepatotoxicity: Experience of the drug-induced liver injury network. *Hepatology* **2014**, *60*, 679–686. [[CrossRef](#)] [[PubMed](#)]
160. Veluswamy, R.R.; Ward, S.C.; Yum, K.; Abramovitz, R.B.; Isola, L.M.; Jagannath, S.; Parekh, S. Adverse drug reaction: Pomalidomide-induced liver injury. *Lancet* **2014**, *383*, 2125–2126. [[CrossRef](#)]
161. Baig, M.; Wool, K.J.; Halalnych, J.H.; Sarmad, R.A. Acute liver failure after initiation of rivaroxaban: A case report and review of the literature. *N. Am. J. Med. Sci.* **2015**, *7*, 407–410. [[CrossRef](#)]
162. Hammerstrom, A.E. Possible Amlodipine-induced hepatotoxicity after stem cell transplant. *Ann. Pharm.* **2015**, *49*, 135–139. [[CrossRef](#)]
163. Stine, J.G.; Intagliata, N.; Sha, N.L.; Argo, C.K.; Caldwell, S.H.; Lewis, J.H.; Northup, P.G. Hepatic decompensation likely attributable to Simeprevir in patients with advanced cirrhosis. *Dig. Dis. Sci.* **2015**, *60*, 1031–1035. [[CrossRef](#)]
164. Tang, D.M.; Koh, C.; Twaddell, W.S.; von Roseninge, E.C.; Han, H. Acute hepatocellular drug-induced liver injury from bupropion and doxycycline. *ACG Case Rep. J.* **2015**, *3*, 66–68. [[CrossRef](#)]
165. Unger, C.; Al-Jashaami, L. Ciprofloxacin exposure leading to fatal hepatotoxicity: An unusual correlation. *Am. J. Case Rep.* **2016**, *17*, 676–681. [[CrossRef](#)]
166. Gharia, B.; Seegobin, K.; Maharaj, S.; Marji, N.; Deutch, A.; Zuberi, L. Letrozole-induced hepatitis with autoimmune features: A rare adverse drug reaction with review of the relevant literature. *Oxf. Med. Case Rep.* **2017**, *2017*, omx074. [[CrossRef](#)]
167. Nicoletti, P.; Aithal, G.P.; Björnsson, E.S.; Andrade, R.J.; Sawle, A.; Arrese, M.; Barnhart, H.X.; Bondon-Guitton, E.; Hayashi, P.H.; Bessone, F.; et al. International Drug-Induced Liver Injury Consortium, Drug-Induced Liver Injury Network Investigators, and International Serious Adverse Events Consortium. Association of liver injury from specific drugs or group of drugs with polymorphisms in HLA and other genes in a Genome-wide Association Study. *Gastroenterology* **2017**, *152*, 1078–1089.
168. Gayam, V.; Khalid, M.; Shrestha, B.; Rajib Hossain, M.; Dahal, S.; Garlapati Gill, P.A.; Kumar Mandal, A.; Sangha, R. Drug-Induced Liver Injury: An institutional case series and review of literature. *J. Investig. Med. High Impact Case Rep.* **2018**, *6*, 1–7. [[CrossRef](#)] [[PubMed](#)]
169. Hayashi, P.H.; Björnsson, E.S. Long-term outcomes after drug-induced liver injury. *Curr. Hepatol. Rep.* **2018**, *17*, 292–299. [[CrossRef](#)] [[PubMed](#)]
170. Patel, S.; Mendler, M.H.; Valasek, M.A.; Tsunoda, S.M. Drug-induced liver injury associated with the use of Everolimus in a liver transplantant patient. *Case Rep. Transpl.* **2018**. [[CrossRef](#)]
171. Shamberg, L.; Vaziri, H. Hepatotoxicity of inflammatory bowel disease medications. *J. Clin. Gastroenterol.* **2018**, *52*, 674–684. [[CrossRef](#)] [[PubMed](#)]

172. Cirulli, E.T.; Nicoletti, P.; Abramson, K.; Andrade, R.J.; Bjornsson, E.S.; Chalasani, N.; Fontana, R.J.; Hallberg, P.; Li, Y.J.; Lucena, M.L.; et al. Drug-Induced Liver Injury Network (DILIN) investigators; International DILI consortium (iDILIC). A missense variant in PTPN22 is a risk factor for drug-induced liver injury. *Gastroenterology* **2019**, *56*, 1707–1716. [[CrossRef](#)] [[PubMed](#)]
173. Nicoletti, P.; Aithal, G.P.; Chamberlain, T.C.; Coulthard, S.; Alshabeeb, M.; Grove, J.I.; Andrade, R.J.; Björnsson, E.; Dillon, J.F.; Hallberg, P.; et al. International Drug-Induced Liver Injury Consortium (iDILIC). Drug-induced liver injury due to Flucloxacillin: Relevance of multiple human leukocyte antigen alleles. *Clin. Pharm.* **2019**, *106*, 245–253. [[CrossRef](#)]
174. Sandritter, T.L.; Goldman, J.L.; Habiger, C.J.; Daniel, J.F.; Lowry, J.; Fisher, R.T. An electronic medical records-based approach to identify idiosyncratic drug-induced liver injury in children. *Sci. Rep.* **2019**, *9*, 18090. [[CrossRef](#)]
175. Shumar, J.; Ordway, S.; Junga, Z.; Sadowski, B.; Torres, D. Memantine-induced liver injury with probable causality as assessed using the Roussel Uclaf Causality Assessment Method (RUCAM). *ACG Case Rep. J.* **2019**, *6*, e00184. [[CrossRef](#)]
176. Tsung, I.; Dolan, R.; Lao, C.D.; Fecher, L.; Riggensbach, K.; Yeboah-Korang, A.; Fontana, R.J. Liver injury is most commonly due to hepatic metastases rather than drug hepatotoxicity during pembrolizumab immunotherapy. *Aliment. Pharm.* **2019**, *50*, 800–808. [[CrossRef](#)] [[PubMed](#)]
177. Xie, C.; Abdullah, H.; Abdallah, M.; Quist, E.; Niazi, M. Anastrozole-induced liver injury after a prolonged latency: A very rare complication of a commonly prescribed medication. *BMJ Case Rep.* **2019**, *12*, e231741. [[CrossRef](#)] [[PubMed](#)]
178. Ghabril, M.; Gu, J.; Yoder, L.; Corbitto, L.; Dakhoul, L.; Ringel, A.; Beyer, C.D.; Vuppalachni, R.; Barnhart, H.; Hayashi, P.H.; et al. Significant medical comorbidities are associated with lower causality scores in patients presenting with suspected drug-induced liver injury. *Clin. Transl. Gastroenterol.* **2020**, *11*, e00141. [[CrossRef](#)]
179. Meher Shahi, S.; Mantri, N.; Kumar, A.; Danial, S.; Harish, P. Enoxaparin-induced liver injury. *Case Rep. Gastroenterol.* **2020**, *14*, 315–319. [[CrossRef](#)] [[PubMed](#)]
180. Mullins, C.; Beaulac, K.; Sylvia, L. Drug-induced liver injury (DILI) with Micafungin: The importance of causality assessment. *Ann. Pharm.* **2020**, *54*, 526–532. [[CrossRef](#)] [[PubMed](#)]
181. Smith, R.J.; Bertilone, C.; Robertson, A.G. Fulminant liver failure and transplantation after use of dietary supplements. *Med. J. Aust.* **2016**, *204*, 30–32. [[CrossRef](#)] [[PubMed](#)]
182. Stadlbauer, V.; Fickert, P.; Lackner, C.; Schmerlaib, J.; Krisper, P.; Trauner, M.; Stauber, E.R. Hepatotoxicity of NONI juice: Report of two cases. *World J. Gastroenterol.* **2005**, *11*, 4758–4760. [[CrossRef](#)] [[PubMed](#)]
183. Barcelos, S.T.A.; Dall’Oglio, V.M.; de Araujo, A.; Schmidt Cerski, C.T. Sinusoidal obstruction syndrome secondary the intake of *Senecio brasiliensis*: A case report. *Ann. Hepatol.* **2019**, in press. [[CrossRef](#)]
184. Yuen, M.F.; Tam, S.; Fung, J.; Wong, D.K.H.; Wong, B.C.Y.; Lai, C.L. Traditional Chinese Medicine causing hepatotoxicity in patients with chronic hepatitis B infection: A 1-year prospective study. *Aliment. Pharm.* **2006**, *24*, 1179–1186. [[CrossRef](#)]
185. Cheung, W.I.; Tse, M.L.; Ngan, T.; Lin, J.; Lee, W.K.; Poon, W.T.; Mak, T.W.; Leung, V.K.S.; Chau, T.N. Liver injury associated with the use of Fructus Psoraleae (Bol-gol-zhee or Bu-gu-zhi) and its related proprietary medicine. *Clin. Toxicol.* **2009**, *47*, 683–685. [[CrossRef](#)] [[PubMed](#)]
186. Chau, T.N.; Cheung, W.I.; Ngan, T.; Lin, J.; Lee, K.W.S.; Poon, W.T.; Leung, V.K.S.; Mak, T.; Tse, M.L.; the Hong Kong Herb-Induced Liver Injury Network (HK-HILIN). Causality assessment of herb-induced liver injury using multidisciplinary approach and the Roussel Uclaf Causality Assessment Method (RUCAM). *Clin. Toxicol.* **2011**, *49*, 34–39. [[CrossRef](#)] [[PubMed](#)]
187. Lin, G.; Wang, J.Y.; Li, N.; Li, M.; Gao, H.; Ji, Y.; Zhang, F.; Wang, H.; Zhou, Y.; Ye, Y.; et al. Hepatic sinusoidal obstruction syndrome associated with consumption of *Gynura segetum*. *J. Hepatol.* **2011**, *54*, 666–673. [[CrossRef](#)]
188. Gao, H.; Li, N.; Wang, J.Y.; Zhang, S.C.; Lin, D. Definitive diagnosis of hepatic sinusoidal obstruction syndrome induced by pyrrolizidine alkaloids. *J. Dig. Dis.* **2012**, *13*, 33–39. [[CrossRef](#)]
189. Lai, R.T.; Wang, H.; Gui, H.L.; Ye, M.Z.; Dai, W.J.; Xiang, X.; Zhao, G.D.; Wang, W.J.; Xie, Q. Clinical and pathological features in 138 cases of drug-induced liver injury. *Zhonghua Gan Zang Bing Za Zhi Zhonghua Ganzangbing Zazhi Chin. J. Hepatol.* **2012**, *20*, 185–189. [[CrossRef](#)]
190. Dong, H.; Slain, D.; Cheng, J.; Ma, W.; Liang, W. Eighteen cases of liver injury following ingestion of *Polygonum multiflorum*. *Complement. Med.* **2014**, *22*, 70–74. [[CrossRef](#)] [[PubMed](#)]

191. Gao, H.; Ruan, J.Q.; Chen, J.; Li, N.; Ke, C.Q.; Ye, Y.; Lin, G.; Wang, J.Y. Blood pyrrole-protein adducts as diagnostic and prognostic index in pyrrolizidine alkaloid-hepatic sinusoidal obstruction syndrome. *Drug Des. Dev.* **2015**, *9*, 4861–4868. [[CrossRef](#)] [[PubMed](#)]
192. Wang, J.; Ma, Z.; Niu, M.; Li, N.; Meng, Y.; Li, Q.; Qin, L.; Teng, G.; Cao, J.; Li, B.; et al. Evidence chain-based causality identification in herb-induced liver injury: Exemplification of a well-known liver-restorative herb *Polygonum multiflorum*. *Front. Med.* **2015**, *9*, 457–467. [[CrossRef](#)]
193. Zhu, Y.; Liu, S.H.; Wang, J.B.; Song, H.B.; Li, Y.G.; He, T.T.; Ma, X.; Wang, Z.X.; Wang, L.P.; Zhou, K.; et al. Clinical analysis of drug-induced liver injury caused by *Polygonum multiflorum* and its preparations. *Zhongguo Zhong Xi Yi Jie He Za Zhi* **2015**, *35*, 1442–1447, (Abstract in English, Article in Chinese).
194. Zhang, P.; Ye, Y.; Yang, X.; Jiao, Y. Systematic review on Chinese herbal medicine induced liver injury. *Evid.-Based Complement. Altern. Med.* **2016**. [[CrossRef](#)]
195. Li, C.Y.; He, Q.; Gao, D.; Li, R.Y.; Zhu, Y.; Li, H.F.; Feng, W.W.; Yang, M.H.; Xiao, X.H.; Wang, J.B. Idiosyncratic drug-induced liver injury linked to *Polygonum multiflorum*: A case study by pharmacognosy. *Chin. Integr. Med.* **2017**, *23*, 625–630. [[CrossRef](#)] [[PubMed](#)]
196. Chow, H.C.; So, T.H.; Choi, H.C.W.; Lam, K.O. Medicine herbs-induced liver injury from an oncological perspective with RUCAM. *Integr. Cancer* **2019**, *18*, 1–13.
197. Jing, J.; Wang, R.L.; Zhao, X.Y.; Zhu, Y.; Niu, M.; Wang, L.F.; Song, X.A.; He, T.T.; Sun, Y.Q.; Xu, W.-T.; et al. Association between the concurrence of pre-existing chronic liver disease and worse prognosis in patients with an herb-*Polygonum multiflorum* thumbeduced liver injury: A case-control study from a specialised liver disease center in China. *BMJ Open* **2019**, *9*, e023567. [[CrossRef](#)] [[PubMed](#)]
198. Li, A.; Gao, M.; Zhao, N.; Li, P.; Zhu, J.; Li, W. Acute liver failure associated with *Fructus Psoraleae*: A case report and literature review. *BMC Complement. Altern. Med.* **2019**, *19*, 84. [[CrossRef](#)]
199. Ni, J.; Liu, Y.; Wang, W.; Sun, M.; Ma, B.; Pang, L.; Du, Y.; Dong, X.; Yin, X. *Polygonum multiflorum*-induced liver injury: Clinical characteristics, risk factors, material basis, action mechanism and current challenges. *Front. Pharmacol.* **2019**, *10*, 1467.
200. Tan, Y.; Chen, H.; Zhou, X.; Sun, L. RUCAM-based assessment of liver injury by xian-tian-guo (*Swietenia macrophylla*) seeds, a plant used for treatment of hypertension and diabetes. *Ann. Hepatol.* **2019**, *18*, 403–407. [[CrossRef](#)]
201. Zhu, Y.; Niu, M.; Wang, J.B.; Wang, R.L.; Li, J.Y.; Ma, Y.; Zhao, Y.L.; Zhang, Y.F.; He, T.T.; Yu, S.M.; et al. Predictors of poor outcomes in 488 patients with herb-induced liver injury. *Turk. J. Gastroenterol.* **2019**, *30*, 47–58. [[CrossRef](#)]
202. Gao, Y.; Wang, Z.; Tang, J.; Liu, X.; Shi, W.; Qin, N.; Wang, X.; Pang, Y.; Li, R.; Zhang, Y.; et al. New incompatible pair of TCM: *Epimedii Folium* combined with *Psoraleae Fructus* induces idiosyncratic hepatotoxicity under immunological stress conditions. *Front. Med.* **2020**, *28*. [[CrossRef](#)]
203. Xia, C.; Liu, Y.; Yao, H.; Zhu, W.; Ding, J.; Jin, J. Causality assessment of skyfruit-induced liver injury using the updated RUCAM: A case report and review of the literature. *J. Int. Med. Res.* **2020**, *48*, 300060520917569. [[CrossRef](#)]
204. Cárdenas, A.; Restrepo, J.C.; Sierra, F.; Correa, G. Acute hepatitis due to shen-min: A herbal product derived from *Polygonum multiflorum*. *J. Clin. Gastroenterol.* **2006**, *40*, 629–632. [[CrossRef](#)]
205. Parlati, L.; Voican, C.S.; Perlemuter, K.; Perlemuter, G. Aloe vera-induced acute liver injury: A case report and literature review. *Clin. Res. Hepatol. Gastroenterol.* **2017**, *41*, e39–e42. [[CrossRef](#)]
206. Teschke, R.; Bahre, R. Severe hepatotoxicity by Indian Ayurvedic herbal products: A structured causality assessment. *Ann. Hepatol.* **2009**, *8*, 258–266. [[CrossRef](#)]
207. Teschke, R.; Glass, X.; Schulze, J. Herbal hepatotoxicity by Greater Celandine (*Chelidonium majus*): Causality assessment of 22 spontaneous reports. *Regul. Toxicol. Pharm.* **2011**, *61*, 282–291. [[CrossRef](#)] [[PubMed](#)]
208. Teschke, R.; Glass, X.; Schulze, J.; Eickhoff, A. Suspected Greater Celandine hepatotoxicity: Liver specific causality evaluation of published case reports from Europe. *Eur. J. Gastroenterol. Hepatol.* **2012**, *24*, 270–280. [[CrossRef](#)]
209. Douros, A.; Bronder, E.; Andersohn, F.; Klimpel, A.; Kreutz, R.; Garbe, E.; Bolbrinker, J. Herb-induced liver injury in the Berlin Case-Control Surveillance Study. *Int. J. Mol. Sci.* **2016**, *17*, 114. [[CrossRef](#)]
210. Teschke, R.; Zhang, L.; Long, H.; Schwarzenboeck, A.; Schmidt-Taenzer, W.; Genthner, A.; Wolff, A.; Frenzel, C.; Schulze, J.; Eickhoff, A. Traditional Chinese Medicine and herbal hepatotoxicity: A tabular compilation of reported cases. *Ann. Hepatol.* **2015**, *14*, 7–19. [[CrossRef](#)]

211. Melchart, D.; Hager, S.; Albrecht, S.; Dai, J.; Weidenhammer, W.; Teschke, R. Herbal Traditional Chinese Medicine and suspected liver injury: A prospective study. *World J. Hepatol.* **2017**, *18*, 1141–1157. [[CrossRef](#)]
212. Diener, H.C.; Freitag, F.G.; Danesch, U. Safety profile of a special butterbur extract from *Petasites hybridus* in migraine prevention with emphasis on the liver. *Ceph. Rep.* **2018**, *1*, 1–8. [[CrossRef](#)]
213. Anderson, N.; Borlak, J. Hepatobiliary events in migraine therapy with herbs—The case of Petadolex, a *Petasites hybridus* extract. *J. Clin. Med.* **2019**, *8*, 652. [[CrossRef](#)]
214. Gerhardt, F.; Benesic, A.; Tillmann, H.L.; Rademacher, S.; Wittekind, C.; Gerbes, A.L.; Henker, R.; Berg, T.; Maidhof, H.; Trauer, H.; et al. Iberogast-induced acute liver failure-reexposure and in vitro assay support causality. *Am. J. Gastroenterol.* **2019**, *114*, 1358–1359. [[CrossRef](#)]
215. Teschke, R.; Xuan, T.D. Suspected herb induced liver injury by green tea extracts: Critical review and case analysis applying RUCAM for causality assessment. *Jpn. J. Gastroenterol. Hepatol.* **2019**, *1*, 1–16.
216. Philips, C.A.; Paramaguru, R.; Joy, A.K.; Anthony, K.L.; Augustine, P. Clinical outcomes, histopathological patterns, and chemical analysis of Ayurveda and herbal medicine associated with severe liver injury—A single-center experience from southern India. *Indian J. Gastroenterol.* **2018**, *37*, 9–17. [[CrossRef](#)]
217. Philips, C.A.; Augustine, P.; Rajesh, S.; Kumar, P.; Madhu, D. Complementary and alternative medicine-related drug-induced liver injury in Asia. *J. Clin. Transl. Hepatol.* **2019**, *7*, 263. [[CrossRef](#)] [[PubMed](#)]
218. Lapi, F.; Gallo, E.; Giocalliere, E.; Vietri, M.; Baronti, R.; Pieraccini, G.; Tafi, A.; Menniti-Ippolito, F.; Mugelli, A.; Firenzuoli, F.; et al. Acute liver damage due to *Serenoa repens*: A case report. *Br. J. Clin. Pharm.* **2010**, *69*, 558–560. [[CrossRef](#)] [[PubMed](#)]
219. Mazzanti, G.; Di Soto, A.; Vitalone, A. Hepatotoxicity of green tea: An update. *Arch. Toxicol.* **2015**, *89*, 1175–1191. [[CrossRef](#)] [[PubMed](#)]
220. Sáez-González, E.; Conde, I.; Díaz-Jaime, F.C.; Benlloch, S.; Prieto, M.; Berenguer, M. Iberogast-induced severe hepatotoxicity leading to liver transplantation. *Am. J. Gastroenterol.* **2016**, *111*, 1364–1365. [[CrossRef](#)] [[PubMed](#)]
221. Mazzanti, G.; Moro, P.A.; Raschi, E.; Da Cas, R.; Menniti-Ippolito, F. Adverse reactions to dietary supplements containing red yeast rice: Assessment of cases from the Italian surveillance system: Safety of red yeast rice dietary supplements. *Br. J. Clin. Pharm.* **2017**, *83*, 894–908. [[CrossRef](#)]
222. Osborne, C.S.; Overstreet, A.N.; Rockey, D.C.; Shreiner, A.D. Drug-induced liver injury caused by Kratom use as an alternative pain treatment amid an ongoing opioid epidemic. *J. Investig. Med. High Impact Case Rep.* **2019**, *7*. [[CrossRef](#)]
223. Tsuda, T.; Yashiro, S.; Gamo, Y.; Watanabe, K.; Hoshino, T.; Oikawa, T.; Hanawa, T. Discrepancy between clinical course and drug-induced lymphocyte stimulation tests in a case of Saireito-induced liver injury accompanied by Sjögren syndrome. *J. Altern. Complement. Med.* **2010**, *16*, 501–505. [[CrossRef](#)]
224. Hisamochi, A.; Kage, M.; Arinaga, T.; Ide, T.; Miyajima, I.; Ogata, K.; Kuwhara, T.; Koga, Y.; Kumashiro, R.; Sata, M. Drug-induced liver injury associated with *Agaricus blazei* Murill which is very similar to autoimmune hepatitis. *Clin. J. Gastroenterol.* **2013**, *6*, 139–144. [[CrossRef](#)]
225. Ahn, B.M. Herbal preparation-induced liver injury. *Korean J. Gastroenterol.* **2004**, *44*, 113–125. [[PubMed](#)]
226. Seo, J.C.; Jeon, W.J.; Park, S.S.; Kim, S.H.; Lee, K.M.; Chae, H.B.; Park, S.M.; Youn, S.J. Clinical experience of 48 acute toxic hepatitis patients. *Korean J. Hepatol.* **2006**, *12*, 74–81, (Abstract in English, Article in Korean).
227. Kang, S.H.; Kim, J.I.; Jeong, K.H.; Ko, K.H.; Ko, P.G.; Hwang, S.W.; Kim, E.M.; Kim, S.H.; Lee, H.Y.; Lee, B.S. Clinical characteristics of 159 cases of acute toxic hepatitis. *Korean J. Hepatol.* **2008**, *14*, 483–492, (Abstract in English, Article in Korean). [[CrossRef](#)]
228. Sohn, C.H.; Cha, M.I.; Oh, B.J.; Yeo, W.H.; Lee, J.H.; Kim, W.; Lim, K.S. Liver transplantation for acute toxic hepatitis due to herbal medicines and preparations. *J. Korean Soc. Clin. Toxicol.* **2008**, *6*, 110–116. (Abstract in English, Article in Korean).
229. Kang, H.S.; Choi, H.S.; Yun, T.J.; Lee, K.G.; Seo, Y.S.; Yeon, J.E.; Byun, K.S.; Um, H.S.; Kim, C.D.; Ryu, H.S. A case of acute cholestatic hepatitis induced by *Corydalis speciosa* Max. *Korean Hepatol.* **2009**, *15*, 517–523, (Abstract in English, article in Korean). [[CrossRef](#)] [[PubMed](#)]
230. Kim, S.Y.; Yim, H.J.; Ahn, J.H.; Kim, J.H.; Kim, J.N.; Yoon, I.; Kim, D.I.; Lee, H.S.; Lee, S.W.; Choi, J.H. Two cases of toxic hepatitis caused by arrowroot juice. *Korean J. Hepatol.* **2009**, *15*, 504–509. (Abstract in English, Article in Korean). [[CrossRef](#)]



231. Bae, S.H.; Kim, D.H.; Bae, Y.S.; Lee, K.J.; Kim, D.W.; Yoon, J.B.; Hong, J.H.; Kim, S.H. Toxic hepatitis associated with *Polygoni multiflori*. *Korean J. Hepatol.* **2010**, *16*, 182–186. (Abstract in English, Article in Korean). [\[CrossRef\]](#)
232. Yang, H.; Kim, D.J.; Kim, Y.M.; Kim, B.H.; Sohn, K.M.; Choi, M.J.; Choi, Y.H. Aloe-induced toxic hepatitis. *J. Korean Med. Sci.* **2010**, *25*, 492–495. [\[CrossRef\]](#) [\[PubMed\]](#)
233. Jung, K.A.; Min, H.J.; Yoo, S.S.; Kim, H.J.; Choi, S.N.; Ha, C.Y.; Kim, H.J.; Kim, T.H.; Jung, W.T.; Lee, O.J. Drug-induced liver injury: Twenty five cases of acute hepatitis following ingestion of *Polygonum multiflorum* Thun. *Gut Liver* **2011**, *5*, 493–499. [\[CrossRef\]](#)
234. Kim, Y.J.; Ryu, S.L.; Shim, J.W.; Kim, D.S.; Shim, J.Y.; Park, M.S.; Jung, H.L. A pediatric case of toxic hepatitis induced by *Hovenia dulcis*. *Pediatr. Gastroenterol. Hepatol. Nutr.* **2012**, *15*, 111–116. [\[CrossRef\]](#)
235. Lee, J.; Shin, J.S.; Kim, M.R.; Byon, J.H.; Lee, S.Y.; Shin, Y.S.; Kim, H.; Park, K.B.; Shin, B.C.; Lee, M.S.; et al. Liver enzyme abnormalities in taking traditional herbal medicine in Korea: A retrospective large sample cohort study of musculoskeletal disorder patients. *J. Ethnopharmacol.* **2015**, *169*, 407–412. [\[CrossRef\]](#) [\[PubMed\]](#)
236. Lee, W.J.; Kim, H.W.; Lee, H.Y.; Son, C.G. Systematic review on herb-induced liver injury in Korea. *Food Chem. Toxicol.* **2015**, *84*, 47–54. [\[CrossRef\]](#) [\[PubMed\]](#)
237. Cho, J.H.; Oh, D.S.; Hong, S.H.; Ko, H.; Lee, N.H.; Park, S.E.; Han, C.W.; Kim, S.M.; Kim, Y.C.; Kim, K.S. A nationwide study of the incidence rate of herb-induced liver injury in Korea. *Arch. Toxicol.* **2017**, *91*, 4009–4015. [\[CrossRef\]](#) [\[PubMed\]](#)
238. Teo, D.C.H.; Ng, P.S.L.; Tan, S.H.; Lim, A.T.; Toh, D.S.L.; Chan, S.Y.; Cheong, H.H. Drug-induced liver injury associated with Complementary and Alternative Medicine: A review of adverse event reports in an Asian community from 2009 to 2014. *BMC Complement. Altern. Med.* **2016**, *16*, 192. [\[CrossRef\]](#)
239. Awortwe, C.; Makiwane, M.; Reuter, H.; Muller, C.; Louw, J.; Rosenkranz, B. Critical evaluation of causality assessment of herb-drug interactions in patients. *Br. J. Clin. Pharm.* **2018**, *84*, 679–693. [\[CrossRef\]](#)
240. Jimenez-Saenz, M.; Martinez-Sanchez, C. Acute hepatitis associated with the use of green tea infusions. *J. Hepatol.* **2006**, *44*, 616–617. [\[CrossRef\]](#)
241. García-Cortés, M.; Borraz, Y.; Lucena, M.I.; Paláez, G.; Salmerón, J.; Diago, M.; Martínez-Sierra, J.M.; Navarro, J.M.; Planas, M.J.; Bruguera, M.; et al. Liver injury induced by “natural remedies”: An analysis of cases submitted to the Spanish Liver Toxicity Registry. *Rev. Esp. Enferm. Dig.* **2008**, *100*, 688–695.
242. Medina-Caliz, I.; Garcia-Cortes, M.; Gonzalez-Jimenez, A.; Cabello, M.R.; Robles-Diaz, M.; Sanabria-Cabrera, J.; Sanjuan-Jimenez, R.; Ortega-Alonso, A.; Garcia-Munoz, B.; Moreno, I.; et al. Herbal and dietary supplement-induced liver injuries in the Spanish DILI Registry. *Clin. Gastroenterol. Hepatol.* **2018**, *16*, 1495–1502. [\[CrossRef\]](#)
243. Björnsson, E.; Olsen, R. Serious adverse liver reactions associated with herbal weight-loss supplements. *J. Hepatol.* **2007**, *47*, 295–302. [\[CrossRef\]](#)
244. Ruperti-Repilado, F.J.; Haefliger, S.; Rehm, S.; Zweier, M.; Rentsch, K.M.; Blum, J.; Jetter, A.; Heim, M.; Leuppi-Taegtmeyer, A.; Terracciano, L.; et al. Danger of herbal tea: A case of acute cholestatic hepatitis due to *Artemisia annua* tea. *Front. Med.* **2019**, *6*, 221. [\[CrossRef\]](#)
245. Yilmaz, B.; Yilmaz, B.; Aktaş, B.; Unlu, O.; Roach, E.C. Lesser celandine (pilewort) induced acute toxic liver injury: The first case report worldwide. *World J. Hepatol.* **2015**, *7*, 285–288. [\[CrossRef\]](#)
246. Papafragkakis, C.; Ona, M.A.; Reddy, M.; Anand, S. Acute hepatitis after ingestion of a preparation of Chinese Skullcap and Black Catechu for joint pains. *Case Rep. Hepatol.* **2016**. [\[CrossRef\]](#)
247. Dalal, K.K.; Holdbrook, T.; Peikin, S.R. Ayurvedic drug induced liver injury. *World J. Hepatol.* **2017**, *9*, 1205–1209. [\[CrossRef\]](#) [\[PubMed\]](#)
248. Kesavarapu, K.; Kang, M.; Shin, J.J.; Rothstein, K. Yogi Detox Tea: A potential cause of acute liver failure. *Case Rep. Gastrointest. Med.* **2017**, *2017*, 3540756. [\[CrossRef\]](#) [\[PubMed\]](#)
249. Kothadia, J.P.; Kaminski, M.; Samant, H.; Olivera-Martinez, M. Hepatotoxicity associated with use of the weight loss supplement *Garcinia cambogia*: A case report and review of the literature. *Case Rep. Hepatol.* **2018**, *2018*, 6483605. [\[CrossRef\]](#) [\[PubMed\]](#)
250. Surapaneni, B.K.; Le, M.; Jakobovits, J.; Vinayek, R.; Dutta, S. A case of acute severe hepatotoxicity and mild constriction of common bile duct associated with ingestion of green tea extract: A clinical challenge. *Clin. Med. Insights Gastroenterol.* **2018**, *11*, 1–4. [\[CrossRef\]](#)
251. Imam, Z.; Khasawneh, M.; Jomaa, D.; Iftikhar, H.; Sayedahmad, Z. Drug induced liver injury attributed to a curcumin supplement. *Case Rep. Gastrointest. Med.* **2019**, *2019*, 6029403. [\[CrossRef\]](#) [\[PubMed\]](#)

252. Yousaf, M.N.; Chaudhary, F.S.; Hodanazari, S.M.; Sittambalam, C.D. Hepatotoxicity associated with with *Garcinia cambogia*: A case report. *World J. Hepatol.* **2019**, *11*, 735–742. [[CrossRef](#)]
253. Oketch-Rabah, H.A.; Roe, A.L.; Rider, C.V.; Bonkovsky, H.L.; Giancaspro, G.I.; Navarro, V.; Paine, M.F.; Betz, J.M.; Marles, R.J.; Casper, S.; et al. United States Pharmacopeia (USP) comprehensive review of the hepatotoxicity of green tea extracts. *Toxicol. Rep.* **2020**, *7*, 386–402. [[CrossRef](#)]
254. Schimmel, J.; Dart, R.C. Kratom (*Mitrogyna speciosa*) Liver Injury: A Comprehensive Review. *Drugs* **2020**. [[CrossRef](#)] [[PubMed](#)]
255. Le Louet, H. Drug-Induced Liver Injury (DILI): Current Status and Future Directions for Drug Development and the Post-Marketing Setting. Available online: [https://cioms.ch/wp-content/uploads/2020/06/CIOMS\\_DILI\\_Web\\_16Jun2020.pdf](https://cioms.ch/wp-content/uploads/2020/06/CIOMS_DILI_Web_16Jun2020.pdf) (accessed on 30 June 2020).
256. Aithal, G.P.; Rawlins, M.D.; Day, C.P. Accuracy of hepatic adverse drug reaction reporting in one English health region. *Br. Med. J.* **1999**, *319*, 154. [[CrossRef](#)] [[PubMed](#)]
257. Teschke, R.; Frenzel, C.; Wolff, A.; Eickhoff, A.; Schulze, J. Drug induced liver injury: Accuracy of diagnosis in published reports. *Ann. Hepatol.* **2014**, *13*, 248–255. [[CrossRef](#)]



© 2020 by the authors. Licensee MDPI, Basel, Switzerland. This article is an open access article distributed under the terms and conditions of the Creative Commons Attribution (CC BY) license (<http://creativecommons.org/licenses/by/4.0/>).





Article

# Comorbidities Associated with Granuloma Annulare: A Cross-Sectional, Case-Control Study

Erik Almazan <sup>1</sup>, Youkyung S. Roh <sup>1</sup>, Micah Belzberg <sup>2</sup>, Caroline X. Qin <sup>1</sup>, Kyle Williams <sup>1</sup>, Justin Choi <sup>1</sup>, Nishadh Sutaria <sup>1</sup>, Benjamin Kaffenberger <sup>3</sup>, Yevgeniy R. Semenov <sup>4</sup>, Jihad Alhariri <sup>2,\*</sup>,<sup>†</sup> and Shawn G. Kwatra <sup>2,\*</sup>,<sup>†</sup>

<sup>1</sup> The Johns Hopkins University School of Medicine, Baltimore, MD 21205, USA; erikalmazan@jhmi.edu (E.A.); sophieroh@jhmi.edu (Y.S.R.); cqin8@jhmi.edu (C.X.Q.); kwill223@jhmi.edu (K.W.); jchoi222@uic.edu (J.C.); Nishadh.Sutaria@tufts.edu (N.S.)

<sup>2</sup> Department of Dermatology, Johns Hopkins Hospital, Baltimore, MD 21287, USA; mbelzbe@jhu.edu

<sup>3</sup> Division of Dermatology, Ohio State University, Columbus, OH 43215, USA;

Benjamin.Kaffenberger@osumc.edu

<sup>4</sup> Department of Dermatology, Massachusetts General Hospital, Boston, MA 02114, USA;

YSEMENOV@mgh.harvard.edu

\* Correspondence: jalhari1@jhmi.edu (J.A.); skwatra1@jhmi.edu (S.G.K.)

† Indicates Co-Senior Author.

Received: 5 August 2020; Accepted: 27 August 2020; Published: 28 August 2020

**Abstract: Background:** Granuloma annulare (GA) is a cutaneous granulomatous disorder of unknown etiology. There are conflicting data on the association between GA and multiple systemic conditions. As a result, we aimed to clarify the reported associations between GA and systemic conditions. **Methods:** A retrospective, cross-sectional, case-control study was performed in which the medical records of biopsy-confirmed GA patients  $\geq 18$  years of age, who presented to the Johns Hopkins Hospital System between 1 January 2009 and 1 June 2019, were reviewed. GA patients were compared to controls matched for age, race, and sex. **Results:** After adjusting for confounders, GA patients ( $n = 82$ ) had higher odds of concurrent type II diabetes (odds ratio (OR) = 5.27; 95% confidence interval (CI), 1.73–16.07;  $p < 0.01$ ), non-migraine headache (OR = 8.70; 95% CI, 1.61–46.88;  $p = 0.01$ ), and a positive smoking history (OR = 1.93; 95% CI, 1.10–3.38;  $p = 0.02$ ) compared to controls ( $n = 164$ ). Among GA patients, women were more likely to have ophthalmic conditions ( $p = 0.04$ ), and men were more likely to have cardiovascular disease ( $p < 0.01$ ) and type II diabetes ( $p = 0.05$ ). No differences in systemic condition associations were observed among GA subtypes. **Conclusions:** Our results support the reported association between GA and type II diabetes. Furthermore, our findings indicate that GA may be associated with cigarette smoking and non-migraine headache disorders.

**Keywords:** granuloma annulare; granulomatous disorders of the skin; inflammatory skin conditions; medical dermatology

## 1. Introduction

Granuloma annulare (GA) is a granulomatous cutaneous disorder of unknown etiology with an estimated prevalence of 0.1–0.4% [1]. Clinically, GA has various presentations, including localized, generalized, subcutaneous, patch, or perforating subtypes [1–4]. Due to this variation in clinical presentation, characteristic histological findings are critical for diagnosis [2,4]. Given the unknown etiology of GA, studies have focused on uncovering its association with systemic conditions [2].

Systemic diseases proposed to have an association with GA include diabetes mellitus [1,5,6], dyslipidemia [7], hypothyroidism [8], and various malignancies [2]. However, results from the current literature have been conflicting, as several reports have also found no association between

GA and diabetes mellitus [9], thyroid function [1], or dyslipidemia [5]. Additionally, reports on GA's association with malignancy have largely been confined to case reports or studies with small sample sizes, which make an association difficult to ascertain [2]. Therefore, we performed a retrospective cross-sectional, case-control study of patients with clinically diagnosed and biopsy-confirmed GA to clarify the conflicting evidence of associations between GA and systemic conditions.

## 2. Materials and Methods

### 2.1. Study Design

Patients with GA were identified through a review of medical records at the Johns Hopkins Health System (JHHS), mainly comprised of tertiary-care, academic medical centers. A search was performed for patients with an ICD-10 (International Statistical Classification of Diseases and Related Health Problems, Tenth Revision) code L92.0 who received outpatient care between 1 January 2009 and 1 June 2019. Patients with incomplete medical records were excluded. The GA patient study cohort included patients 18 years or older with both a documented clinical presentation and biopsy consistent with GA, including histological evidence of lymphohistiocytic inflammation, mucin deposition, and collagen degradation. All clinical and histopathologic evaluations were performed by board-certified dermatologists and dermatopathologists at JHHS, respectively. Patients with incomplete medical records, lack of biopsy-confirmed GA, or foreign body reactions at the time of diagnosis were excluded. Patients with GA were matched to controls in a 1:2 ratio by age ( $\pm 3$  years), race, and sex. Controls presented to JHHS as outpatients for regularly scheduled skin exams or for benign, localized chief complaints. The study was found exempt by the JHHS institutional review board, and patient consent was waived as only de-identified data were used.

### 2.2. Data Collection

Histopathological reports and medical records of patients with GA were reviewed. Patient characteristics and comorbidities present on the date of GA diagnosis by pathology were manually extracted from medical records.

### 2.3. Definition of Smoking History and Comorbidities

Smoking history was defined as self-reported cigarette smoking at the time of GA diagnosis or a previous history of smoking, regardless of amount. Comorbidities were any diseases that were ongoing problems at the time of GA diagnosis. Cardiovascular disease included active problems such as atherosclerosis, arrhythmias, cardiomyopathies, and cardiac infections. A history of myocardial infarction, heart failure, and stroke was included even if they were past medical events, insofar as the sequelae of those events were deemed significant enough to be considered active problems in the patient medical record. Liver disease encompassed viral liver infections, non-alcoholic steatohepatitis, hepatic steatosis, autoimmune liver disease, and hereditary liver diseases. Ophthalmic conditions included retinal degeneration, vitreous degeneration, inflammatory conditions of the eye proper or the optic nerve, closed-angle glaucoma, open-angle glaucoma, cataracts, and myopia.

### 2.4. Statistical Analysis

Continuous variables were presented as mean  $\pm$  standard deviation (SD), and categorical variables were analyzed as proportions. Means were compared between cohorts using Student's *t*-test, while proportions were compared using the chi-squared or Fisher's exact test, as appropriate. Logistic regression results were expressed using odds ratios with 95% confidence intervals. Analyses were conducted with Stata/SE, v. 15.1 (StataCorp LLC, College Station, TX, USA). Univariable analyses were performed to compare patient characteristics between the GA cohort and controls. Logistic regression was used to adjust for potential confounding variables in our comparisons. A *p*-value  $< 0.05$  (two-tailed) was considered significant in all analyses.

### 3. Results

Patient billing codes and pathology reports identified 471 patients with an ICD-10 L92.0 code who were seen at JHHS from January 2009 to June 2019. A total of 82 patients (17.4%) met the inclusion criteria and were included in the retrospective chart review. Table 1 displays patient demographics and clinical characteristics. On average, both cohorts were aged  $58 \pm 16$  years, predominately female, and of non-Hispanic white race. In regard to smoking, a greater proportion of GA patients had a history of smoking or were active smokers at the time of their diagnosis ( $p = 0.03$ ). Type II diabetes mellitus ( $p < 0.01$ ), liver disease ( $p = 0.04$ ), and non-migraine headache ( $p = 0.02$ ) were present more frequently in patients with GA compared to patients without GA. The prevalence of clinically diagnosed dyslipidemia ( $p = 0.41$ ), hypothyroidism ( $p = 0.63$ ), and solid organ malignancy ( $p = 0.76$ ) did not significantly differ between the study groups.

**Table 1.** Demographic and clinical characteristics of granuloma annulare (GA) patients.

Demographic and Clinical Characteristics	GA ( $n = 82$ )	Control ( $n = 164$ )	$p$ -Value
Age (years), mean $\pm$ SD	$58 \pm 16$	$58 \pm 16$	0.99
Sex, n (%)			
Male	22 (27)	44 (27)	1.00
Female	60 (73)	120 (73)	
Race/Ethnicity, n (%)			
Non-Hispanic White	70 (85)	140 (85)	
Black	6 (7)	12 (7)	1.00
Asian	4 (5)	8 (5)	
Other	2 (2)	4 (2)	
Smoking History, n (%)	39 (48)	54 (33)	0.03
Comorbidities, n (%)			
Solid Organ Malignancy	3 (4)	8 (5)	0.76
HIV Positive Antibody	0 (0)	1 (1)	1.00
Ophthalmic Condition	26 (32)	56 (34)	0.70
Cardiovascular Disease	11 (13)	22 (13)	1.00
Unspecified Osteoarthritis	10 (12)	14 (9)	0.36
Depressive Disorder	6 (7)	15 (9)	0.63
Anxiety Disorder	6 (7)	12 (7)	1.00
Systemic Lupus Erythematosus	2 (2)	0 (0)	0.11
Type II Diabetes Mellitus	12 (15)	5 (3)	<0.01
Liver Disease	5 (6)	2 (1)	0.04
Dyslipidemia	24 (29)	40 (24)	0.41
Hypothyroidism	8 (10)	13 (8)	0.63
Essential Hypertension	21 (26)	44 (27)	0.84
Migraine	6 (7)	8 (5)	0.44
Non-Migraine Headache	6 (7)	2 (1)	0.02

Logistic regression was performed to address for potential confounding variables. A smoking history was associated with higher odds of GA (odds ratio (OR) = 1.93; 95% confidence interval (CI), 1.10–3.38;  $p = 0.02$ ) after accounting for age, race, and sex. Patients with type II diabetes ( $p < 0.01$ ), but not liver disease, also had higher odds of concurrent GA after accounting for age, race, sex, and smoking (Table 2). Non-migraine headache remained associated with GA after including age, race, sex, smoking history, cardiovascular disease, and essential hypertension in the logistic regression model (OR = 8.70; 95% CI, 1.61–46.88;  $p = 0.01$ ).

**Table 2.** Logistic regression for comorbidities and granuloma annulare (GA) controlling for age, race, sex, and smoking.

Comorbidities (Yes/No)	Odds Ratio	95% Confidence Intervals	p-Value
Solid Organ Malignancy	0.64	0.16–2.59	0.53
HIV Positive Antibody	-	-	-
Ophthalmic Condition	0.84	0.46–1.53	0.57
Cardiovascular Disease	0.89	0.37–2.14	0.80
Unspecified Osteoarthritis	1.46	0.59–3.59	0.41
Depressive Disorder	0.68	0.25–1.87	0.46
Anxiety Disorder	0.91	0.32–2.60	0.86
Systemic Lupus Erythematosus	-	-	-
Type II Diabetes Mellitus	5.27	1.73–16.07	<0.01
Liver Disease	4.41	0.81–23.96	0.09
Dyslipidemia	1.24	0.66–2.34	0.50
Hypothyroidism	1.24	0.48–3.19	0.65
Essential Hypertension	0.84	0.44–1.62	0.61
Migraine	1.48	0.48–4.55	0.50
Non-Migraine Headache	7.55	1.45–39.30	0.02

A sub-analysis of patients with GA was performed, examining variation by sex (Table 3). Among GA patients, females were more likely than males to present with ophthalmic conditions ( $p = 0.04$ ), while males were more likely than females to have concurrent cardiovascular disease ( $p < 0.01$ ) and type II diabetes ( $p = 0.05$ ). Further analysis by GA subtype, generalized or localized GA (Table 4), demonstrated that patients with localized GA were younger than patients with generalized GA ( $p < 0.01$ ). Differences were not observed in comorbidities or smoking history by GA subtype.

**Table 3.** Demographic and clinical characteristics of granuloma annulare (GA) patients by sex.

Demographic and Clinical Characteristics	Female (n = 60)	Male (n = 22)	p-Value
Age (years), mean $\pm$ SD	57 $\pm$ 14	60 $\pm$ 19	0.50
Smoking History, n (%)	27 (45)	12 (55)	0.44
Comorbidities, n (%)			
Solid Organ Malignancy	2 (3)	1(5)	1.00
Ophthalmic Condition	23 (38)	3 (14)	0.04
Cardiovascular Disease	2 (3)	9 (41)	<0.01
Unspecified Osteoarthritis	6 (10)	4 (18)	0.45
Depressive Disorder	4 (7)	2 (9)	0.66
Anxiety Disorder	5 (8)	1 (5)	1.00
Systemic Lupus Erythematosus	2 (3)	0 (0)	1.00
Type II Diabetes Mellitus	6 (10)	6 (27)	0.05
Liver Disease	5 (8)	0 (0)	0.32
Dyslipidemia	16 (27)	8 (36)	0.42
Hypothyroidism	6 (10)	2 (9)	1.00
Essential Hypertension	13 (22)	8 (36)	0.25
Migraine	4 (7)	2 (9)	0.66
Non-Migraine Headache	6 (10)	0 (0)	0.18

**Table 4.** Demographic and clinical characteristics of granuloma annulare (GA) patients by subtype.

Demographic and Clinical Characteristics	Generalized (n = 47)	Localized (n = 35)	p-Value
Age (years), mean ± SD	63 ± 15	52 ± 14	<0.01
Smoking History, n (%)	23 (49)	16 (46)	0.77
Comorbidities, n (%)			
Solid Organ Malignancy	2 (4)	1(3)	1.00
Ophthalmic Condition	16 (34)	10 (29)	0.60
Cardiovascular Disease	5 (11)	6 (17)	0.39
Unspecified Osteoarthritis	6 (13)	4 (12)	1.00
Depressive Disorder	4 (9)	2 (6)	1.00
Anxiety Disorder	3 (6)	3 (9)	1.00
Systemic Lupus Erythematosus	1 (2)	1 (3)	1.00
Type II Diabetes Mellitus	6 (13)	6 (17)	0.58
Liver Disease	4 (9)	1 (3)	0.39
Dyslipidemia	14 (30)	10 (29)	0.90
Hypothyroidism	6 (13)	2 (6)	0.46
Essential Hypertension	11 (23)	10 (29)	0.60
Migraine	3 (6)	3 (9)	1.00
Non-Migraine Headache	3 (6)	3 (9)	1.00

#### 4. Discussion

The results of our study investigating systemic disease associations with GA support previously published reports of an association between GA and type II diabetes. Additionally, our results align with previous studies which found no associations between GA and dyslipidemia [5], hypothyroidism [1], or malignancy [10,11]. However, we observed a significantly increased prevalence of a smoking history and non-migraine headaches among GA patients. An association between GA and a positive smoking history has not previously been reported, while associations with non-migraine headaches have not been reported outside of case reports.

Type II diabetes mellitus and dyslipidemia are two metabolic disorders that have been reported to be associated with GA. In 2009, a retrospective, multicenter study in Korea found a higher prevalence of diabetes mellitus in generalized GA patients compared to the general Korean population [6]. This observation was corroborated by similar findings in a retrospective analysis in which 44 GA patients in Taiwan were compared to the general Taiwanese population [5], as well as another study that found increased levels of fasting blood sugar in 28 Iranian GA patients compared to healthy controls [1]. However, another study using psoriasis patients as internal controls instead of national data failed to find a statistically significant association between GA and type II diabetes [9]. Studies exploring the relationship between GA and dyslipidemia have similarly observed conflicting results. A case-control study found significant associations between GA and dyslipidemia as well as increased levels of low-density lipoprotein, triglyceride, and total cholesterol [7]. However, these findings were not replicated in a more recent retrospective analysis in 2016 [5]. Our study found an association between type II diabetes and GA but did not observe a significant association between GA and dyslipidemia.

Hypothyroidism and solid organ malignancy are other systemic conditions with inconsistent reports on their associations with GA. A retrospective correlation study of 100 GA patients by Dabski and Winkelmann found 13 patients to have a thyroid disorder (in descending frequency: hypothyroidism, Grave's disease, thyroiditis, thyroid adenoma) [12]. However, whether GA is truly associated with hypothyroidism is unclear. For example, while one small case-control study failed to demonstrate a significant difference in thyroid hormone levels between GA patients and healthy controls [1], another case-control study of similar sample size did, in fact, report an association between localized GA and autoimmune thyroiditis, specifically in adult women [8]. In the latter, the authors suggested a common immunogenetic pathophysiology potentially underlying the two conditions, as well as other systemic, GA-like, granulomatous conditions that lie on a spectrum [8]. Our study did not show that



GA is associated with hypothyroidism. Collectively, these findings indicate that the current literature cannot definitely support or deny any association between GA and hypothyroidism. Additional large-scale, controlled studies are necessary to determine whether a true association between GA and hypothyroidism exists.

The question of whether or not malignancy is associated with GA is also debated. Multiple case reports have demonstrated GA occurring concurrently with various malignancies, which has led to speculation about a potential relationship [2]. While the exact etiology of GA is unknown, several studies have supported the hypothesis that the pathogenesis of GA involves a T-cell mediated response [13]. As a corollary, it has also been hypothesized that GA, in certain settings, may be a cutaneous manifestation of a chronic immune response to an underlying malignancy [14]. However, despite the seemingly high occurrence of GA in cases of malignancy, a meta-analysis of multiple case reports and correlation studies has not supported an association—with the caveat that clinically atypical GA in elderly individuals warrants investigation for an underlying malignancy that can histologically mimic GA [10]. A more recent review article by Hawryluk et al. echoed such conclusions, as well as cautioning against misdiagnoses, since other granulomatous dermatoses could in fact implicate malignancy [15]. Furthermore, a recent case-control study failed to find any association between malignancy and generalized GA [11]. Likewise, our study did not show that GA was associated with solid organ malignancy, thereby corroborating the results of the current literature on the topic.

The results of our study not only help to clarify previously reported associations between GA and certain systemic diseases but also reveal previously unrecognized relationships. For instance, we demonstrate increased prevalence of a smoking history in patients with GA. Even though the mechanism is unclear, smoking has been previously implicated in complications of sarcoidosis, another granulomatous disease [16]. Specifically, cigarette smoking has been shown to predict the development of ocular sarcoidosis in sarcoidosis patients. Smoking is thought to trigger systemic increases in cytokines, such as IL-6, IL-1 $\beta$ , and TNF- $\alpha$ , which are critical in the formation of granulomas [16]. As sarcoidosis and GA are both granulomatous diseases, it is possible that similar mechanisms may underlie the association between smoking and GA.

GA's association with non-migraine headache has not been previously supported by a well-defined study. Our results showed that patients who received a diagnosis for GA were more likely to have non-migraine headache. Due to the lack of specific documentation in the medical record, it was not possible to identify the source of these non-migraine headaches. However, this finding is interesting due to reports of GA occurring simultaneously with giant cell arteritis (GCA), a particular cause of headaches. These conditions have been reported to occur together, and resolve with the same medications [17,18]. The presence of giant cells, granulomas, vascular deposition of IgM and C3, CD4 T-cell involvement [17], and an increased expression of HLA-B15 [18] in both GA and GCA lends credence to the possibility of a shared pathophysiologic mechanism. Despite the limitations of our study, it is possible that our non-migraine headache classification could have served as a proxy for a headache of a vascular origin. These findings encourage further inquiry to elucidate whether a relationship exists between specific headache disorders and GA, as well as their respective mechanisms.

Finally, our study found certain differences in the associations of systemic conditions with GA when stratified by sex. Females were more likely to present with a concurrent ophthalmic condition, while males were more likely to present with cardiovascular disease and type II diabetes. Given our sample size, it is difficult to determine whether these differences are generalizable. However, sex differences may be important to consider in future studies aiming to determine how GA presents in different patient populations.

This study had several limitations. Firstly, this was a retrospective study at an academic, tertiary-care medical center system, which may limit the generalizability of our results. Additionally, there was incomplete information in the medical record, which limited the conclusions that we could draw from our analyses. Important lab values and body mass indexes were difficult to obtain near the time of GA diagnosis. These values may have been confounding variables in our assessment of GA

and comorbidities. Furthermore, the lack of detail in the medical record on the source of documented headaches did not allow for the assessment of whether or not GA was associated with a particular type of headache disorder. Lastly, our study was also limited by its sample size and study design. The limited GA cohort size affected the associations that could be made and parts of our cross-sectional study design do not allow us to determine causality.

A range of systemic conditions have been suggested to be associated with GA. Our study contributes to this literature by uncovering meaningful associations between GA and type II diabetes, a history of cigarette smoking, and non-migraine headache. In contrast to prior studies, no associations were detected between GA and dyslipidemia, hypothyroidism, and malignancy. These results contribute to the growing body of literature on GA and suggest further avenues for investigation.

**Author Contributions:** Conceptualization, J.A. and S.G.K.; Formal analysis, E.A. and C.X.Q.; Investigation, E.A.; Methodology, E.A., M.B., B.K., Y.R.S., J.A. and S.G.K.; Project administration, S.G.K.; Resources, M.B.; Supervision, M.B., J.A. and S.G.K.; Validation, M.B., B.K., Y.R.S., J.A. and S.G.K.; Visualization, C.X.Q. and S.G.K.; Writing—original draft, E.A.; Writing—review and editing, E.A., Y.S.R., M.B., C.X.Q., K.W., J.C., N.S., B.K., Y.R.S., J.A. and S.G.K. All authors have read and agreed to the published version of the manuscript.

**Funding:** This research received no external funding.

**Conflicts of Interest:** The authors declare no conflict of interest.

## References

- Alirezaei, P.; Farshchian, M. Granuloma annulare: Relationship to diabetes mellitus, thyroid disorders and tuberculin skin test. *Clin. Cosmet. Investig. Dermatol.* **2017**, *10*, 141–145. [[CrossRef](#)] [[PubMed](#)]
- Thornsberry, L.A.; English, J.C. Etiology, diagnosis, and therapeutic management of granuloma annulare: An update. *Am. J. Clin. Dermatol.* **2013**, *14*, 279–290. [[CrossRef](#)] [[PubMed](#)]
- Schmieder, S.J.; Schmieder, G.J. Granuloma annulare. In *Treasure Island (FL)*; StatPearls: Treasure Island, FL, USA, 2020.
- Wang, J.; Khachemoune, A. Granuloma annulare: A focused review of therapeutic options. *Am. J. Clin. Dermatol.* **2018**, *19*, 333–344. [[CrossRef](#)] [[PubMed](#)]
- Cheng, Y.-W.; Tsai, W.-C.; Chuang, F.-C.; Chern, E.; Lee, C.-H.; Sung, C.-H.; Ho, J.-C. A retrospective analysis of 44 patients with granuloma annulare during an 11-year period from a tertiary medical center in south Taiwan. *Dermatol. Sin.* **2016**, *34*, 121–125. [[CrossRef](#)]
- Yun, J.H.; Lee, J.Y.; Kim, M.K.; Seo, Y.J.; Kim, M.H.; Cho, K.H.; Kim, M.B.; Lee, W.S.; Lee, K.H.; Kim, Y.C.; et al. Clinical and pathological features of generalized granuloma annulare with their correlation: A retrospective multicenter study in Korea. *Ann. Dermatol.* **2009**, *21*, 113–119. [[CrossRef](#)] [[PubMed](#)]
- Wu, W.; Robinson-Bostom, L.; Kokkotou, E.; Jung, H.-Y.; Kroumpouzou, G. Dyslipidemia in granuloma annulare: A case-control study. *Arch. Dermatol.* **2012**, *148*, 1131–1136. [[CrossRef](#)] [[PubMed](#)]
- Vazquez-Lopez, F.; Pereiro, M.; Haces, J.; López, M.; Sánchez, T.; Coto, T.; Oliva, N.; Toribio, J. Localized granuloma annulare and autoimmune thyroiditis in adult women: A case-control study. *J. Am. Acad. Dermatol.* **2003**, *48*, 517–520. [[CrossRef](#)] [[PubMed](#)]
- Nebesio, C.L.; Lewis, C.; Chuang, T.Y. Lack of an association between granuloma annulare and type 2 diabetes mellitus. *Br. J. Dermatol.* **2002**, *146*, 122–124. [[CrossRef](#)] [[PubMed](#)]
- Li, A.; Hogan, D.J.; Sanusi, I.D.; Smoller, B.R. Granuloma annulare and malignant neoplasms. *Am. J. Dermatopathol.* **2003**, *25*, 113–116. [[CrossRef](#)] [[PubMed](#)]
- Gabaldón, V.H.; Haro-González-Vico, V. Lack of an association between generalized granuloma annulare and malignancy: A case-control study. *J. Am. Acad. Dermatol.* **2019**, *80*, 1799–1800. [[CrossRef](#)] [[PubMed](#)]
- Dabski, K.; Winkelmann, R.K. Generalized granuloma annulare: Clinical and laboratory findings in 100 patients. *J. Am. Acad. Dermatol.* **1989**, *20*, 39–47. [[CrossRef](#)]
- Mempel, P.D.M.; Musette, P.; Flageul, B.; Schnopp, C.; Remling, R.; Gachelin, G.; Kourilsky, P.; Ring, J.; Abeck, D. T-cell receptor repertoire and cytokine pattern in granuloma annulare: Defining a particular type of cutaneous granulomatous inflammation. *J. Invest. Dermatol.* **2002**, *118*, 957–966. [[CrossRef](#)] [[PubMed](#)]
- Bassi, A.; Scarfi, F.; Galeone, M.; Arunachalam, M.; Difonzo, E. Generalized granuloma annulare and non-Hodgkin's lymphoma. *Acta Derm. Venereol.* **2013**, *93*, 484–485. [[CrossRef](#)] [[PubMed](#)]

15. Hawryluk, E.B.; Izikson, L.; English, J.C. Non-infectious granulomatous diseases of the skin and their associated systemic diseases. *Am. J. Clin. Dermatol.* **2010**, *11*, 171–181. [[CrossRef](#)] [[PubMed](#)]
16. Janot, A.C.; Huscher, D.; Walker, M.; Grewal, H.K.; Yu, M.; Lammi, M.R.; Saketkoo, L.A.; Grewal, H.K. Cigarette smoking and male sex are independent and age concomitant risk factors for the development of ocular sarcoidosis in a New Orleans sarcoidosis population. *Sarcoidosis Vasc. Diffus. Lung Dis.* **2015**, *32*, 138–143.
17. Fukai, K.; Ishii, M.; Kobayashi, H.; Someda, Y.; Hamada, T.; Tsujino, S. Generalized granuloma annulare in a patient with temporal arteritis—Are these conditions associated? *Clin. Exp. Dermatol.* **1990**, *15*, 70–72. [[CrossRef](#)] [[PubMed](#)]
18. Torisu, Y.; Horai, Y.; Michitsuji, T.; Kawahara, C.; Mori, T.; Iwanaga, N.; Izumi, Y.; Kawakami, A. Giant cell arteritis with generalized granuloma annulare. *Intern. Med.* **2019**, *58*, 1173–1177. [[CrossRef](#)]



© 2020 by the authors. Licensee MDPI, Basel, Switzerland. This article is an open access article distributed under the terms and conditions of the Creative Commons Attribution (CC BY) license (<http://creativecommons.org/licenses/by/4.0/>).

Review

# Effects of Diaphragmatic Breathing on Health: A Narrative Review

Hidetaka Hamasaki

Hamasaki Clinic, 2-21-4 Nishida, Kagoshima, Kagoshima 890-0046, Japan; h-hamasaki@umin.ac.jp; Tel.: +81-099-2503535; Fax.: +81-099-250-1470

Received: 30 August 2020; Accepted: 13 October 2020; Published: 15 October 2020

**Abstract: Background:** Breathing is an essential part of life. Diaphragmatic breathing (DB) is slow and deep breathing that affects the brain and the cardiovascular, respiratory, and gastrointestinal systems through the modulation of autonomic nervous functions. However, the effects of DB on human health need to be further investigated. **Methods:** The author conducted a PubMed search regarding the current evidence of the effect of DB on health. **Results:** This review consists of a total of 10 systematic reviews and 15 randomized controlled trials (RCTs). DB appears to be effective for improving the exercise capacity and respiratory function in patients with chronic obstructive pulmonary disease (COPD). Although the effect of DB on the quality of life (QoL) of patients with asthma needs to be investigated, it may also help in reducing stress; treating eating disorders, chronic functional constipation, hypertension, migraine, and anxiety; and improving the QoL of patients with cancer and gastroesophageal reflux disease (GERD) and the cardiorespiratory fitness of patients with heart failure. **Conclusions:** Based on this narrative review, the exact usefulness of DB in clinical practice is unclear due to the poor quality of studies. However, it may be a feasible and practical treatment method for various disorders.

**Keywords:** diaphragmatic breathing; abdominal breathing; breathing exercise; systematic review; randomized controlled trial; respiratory function

## 1. Introduction

Breathing is an essential part of life. The diaphragm is one of the major respiratory muscles, and its function is vital for proper respiration. At the end of 19th century, Sewall and Pollard [1] firstly investigated the relationship between the movement of diaphragm and chest during respiration. The diaphragm also contributes to vocalization and swallowing, as well as respiration. Its dysfunction is associated with various disorders, such as respiratory insufficiency, exercise intolerance, sleep disturbance, and potential mortality [2,3]. The diaphragm has multiple physiological roles. The phrenic nerve that innervates the functions of the diaphragm has a connection with the vagus nerve, which can affect the whole body system [4]. Diaphragmatic motion in breathing directly and indirectly affects the sympathetic and parasympathetic nervous systems and also influences motor nerve activities and brain mass [5]. The diaphragm also controls the postural stability, defecation, micturition, and parturition by modulating intra-abdominal pressure. Furthermore, its function is associated with metabolic balance [6] and cardiovascular and intraperitoneal lymphatic systems [3].

As diaphragmatic (abdominal) breathing (DB) is a slow and deep breathing method, it should not be considered as just a breathing control [7]. Since time out of mind, traditional martial arts such as tai chi and yoga utilize DB in their practice. DB is defined as breathing in slowly and deeply through the nose using the diaphragm with a minimum movement of the chest in a supine position with one hand placed on the chest and the other on the belly [8]. During breathing, practitioners should be careful that chest remains as still as possible and stomach moves against the hand focusing

on contracting the diaphragm. Generally, DB practitioners inhale and exhale for approximately six seconds, respectively. DB is a fundamental procedure during meditation practices in individuals who engage in yoga and traditional martial arts such as tai chi. Recently, a systematic review has reported that mind–body exercise (yoga/tai chi) can reduce stress in individuals under high stress or negative emotions by modulating the sympathetic–vagal balance [9]. Martarelli et al. [10] showed that DB increased the antioxidant activity and reduced the oxidative stress after exercise in athletes. DB has a potential to be a non-pharmacological treatment for patients with stress disorder as well as chronic respiratory disease. Although a number of studies have investigated the efficacy of breathing exercises in treating chronic obstructive pulmonary disease (COPD) [11–29], asthma [30–35], postoperative pulmonary function [36–40], and cardiorespiratory performance in post-Fontan patients [41], the effect of DB on other disorders, for example, cancer, heart failure, and anxiety, still needs to be further investigated. As a martial arts practitioner, the author uses DB in daily mind–body exercises (Figure 1) and feels the necessity to assess whether DB has a favorable impact on the overall health. This review aims to summarize the current evidence of the impact of DB on diseases as described above as well as respiratory function and to discuss its future perspective.

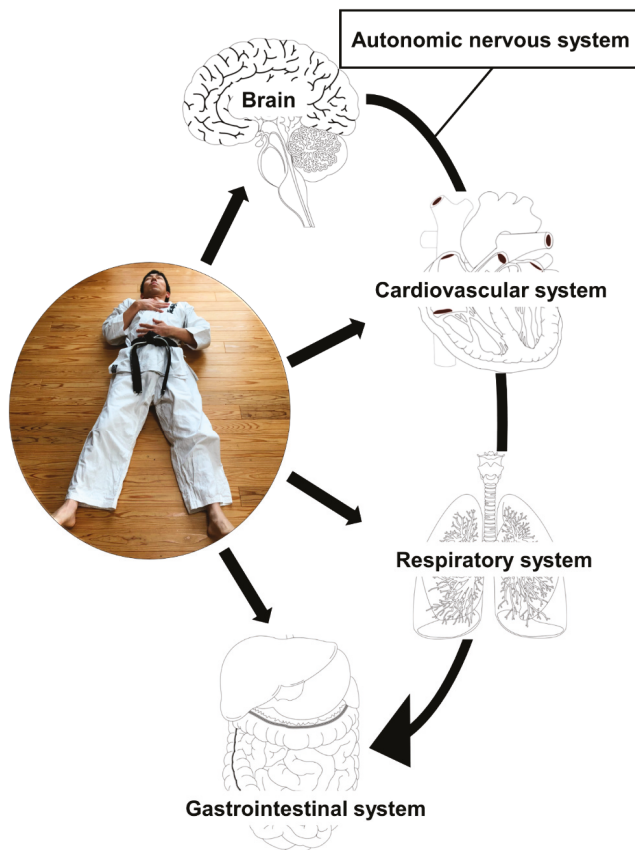


**Figure 1.** Breathing in slowly and deeply through the nose with a minimum movement of the chest in a supine position with one hand placed on the chest and the other on the belly. Diaphragmatic breathing has an impact on the brain and cardiovascular, respiratory, and gastrointestinal systems through the modulation of the autonomic nervous function.

## 2. Methods

This is a narrative review searching the current evidence on the effect of DB on human health. The author searched the literature on DB using PubMed and Cochrane Library from its inception to May 2020. The search terms (MeSH) were “diaphragmatic,” “breathing exercise,” “systematic review,” and “randomized controlled trial (RCT).” First, the author conducted a search in the systematic reviews, which yielded 19 published articles. Second, the author searched in the RCTs, and this yielded 98 articles. Crossover trials and RCTs already assessed in previous systematic reviews were excluded from this review. The titles and abstracts of the identified articles were reviewed to determine their relevance. Overall, a total of 10 systematic reviews and 15 RCTs were included.

## 3. Results

### 3.1. Systematic Reviews

COPD is the most well-studied disease on which DB has a significant effect. In 2012, the Cochrane Airway Group reported the efficacy of breathing exercises in treating COPD [42]. In this study, 16 RCTs involving 1233 subjects were included with a mean age of 51–73 years and mean forced expiratory volume in 1 s (FEV<sub>1</sub>) of 30–51%, which suggested that the study subjects had moderate-to-severe COPD. Of these, 13 studies were included in the meta-analysis. Primary outcomes were dyspnea, quality of life (QoL), and exercise capacity. Breathing exercises, such as yoga with pranayama timed breathing, pursed-lip breathing, and DB, effectively improved the six-minute walk distance. However, no effects on dyspnea and QoL were observed. Although only two studies [25,43] were included in this systematic review, the four-week supervised DB training improved the six-minute walk distance (mean difference (MD), 34.7 m; 95% confidence interval (CI), 4.1–65.3) [25]. On the other hand, another study reported that DB had an unfavorable effect on dyspnea [43]. Recently, Ubolnuar et al. [44] have also assessed 19 RCTs investigating the efficacy of breathing exercises in patients with any severity stage of COPD. The types of breathing exercise include DB, pursed-lip breathing, just relaxation and slow breathing, ventilatory feedback training, and singing. Overall, the breathing exercises improved the respiratory function such as respiratory rate (RR), tidal volume (V<sub>T</sub>), respiratory time, and QoL of COPD patients. In particular, DB significantly improved the RR (MD, −1.09; 95% CI, −2.19 to 0.00), although the quality of evidence is low [14,29]. However, the QoL measured using the St. George’s Respiratory Questionnaire and dyspnea did not differ between the DB and control groups. Furthermore, these results indicate that, although breathing exercises including DB are promising to improve the exercise capacity and respiratory function, their effects on clinical symptoms and QoL are inconsistent due to the severity stage of COPD.

The Cochrane Airway Group reevaluated the efficacy of breathing exercises in adults with asthma in 2020 [45]. Nine studies were added to the previous systematic review published in 2013, and a total of 22 RCTs were included in this systematic review and meta-analysis. Unfortunately, since only one RCT met the inclusion criteria [46], the effect of DB on QoL and asthma symptoms was inconclusive. However, breathing exercises such as yogic breathing and the Buteyko breathing technique had positive effects on QoL and asthma symptoms. Moreover, breathing exercises improved the QoL measured using the Asthma Quality of Life Questionnaire at three months (MD, 0.42; 95% CI, 0.17–0.68) and at six months (odds ratio, 1.34; 95% CI, 0.17–0.68) compared with no active control. Furthermore, hyperventilation symptoms and FEV<sub>1.0%</sub> were predicted to be improved by breathing exercises.

Prem et al. [47] investigated the effect of DB on the QoL of patients with asthma. Only three RCTs assessing the effect of DB on asthma were included [30–32]. The intervention used in the study by Thomas et al. [31] was DB plus nasal breathing exercise. In addition, the interventions as controls were asthma education [30,31] and conventional asthma medication [32]. This systematic review did not perform a meta-analysis. However, DB improved the QoL measured using the Asthma Quality of Life Questionnaire; specifically, the questionnaire score was improved: 0.79 [30] and 1.12 [31]. Moreover, the scores of the Asthma Control Test (from 18 ± 2.5 to 22 ± 3.3) and end-tidal CO<sub>2</sub> (by 4 mmHg)

were improved in the study by Grammatopoulou et al. [32]. The authors suggested that DB improved the QoL of patients with asthma based on the reduction in hyperventilation, which physiologically improved the respiratory function.

The effect of breathing exercise in children with asthma was systematically reviewed in 2016 [48]. Only three studies [33–35] were eligible for this systematic review. The primary outcomes were QoL, asthma symptoms, and adverse events. None of these studies evaluated the single effect of DB, and the breathing exercise programs consisted of DB, lateral costal breathing [33], pursed-lip breathing [35], and endurance exercise [34]. A heterogeneity in the asthma severity of patients among the studies was observed. The difference in the primary outcomes could not be found in the comparisons between the intervention and control groups. Lima et al. [35] reported that the peak expiratory flow (PEF) was improved after the intervention, but based on the meta-analysis, no clear evidence could confirm that DB improved the respiratory function. Moreover, it was inconclusive that DB had a benefit or risk in children with asthma.

Dysfunctional breathing is associated with poor asthma control in children [49, 50]. Barker et al. [51] assessed the effect of breathing exercises in children with dysfunctional/hyperventilation syndrome. However, no eligible studies were found for this systematic review. This lack of evidence is due to the insufficient number of well-designed RCTs conducted in children. On the other hand, Jones et al. [52] evaluated the effect of breathing exercises in adults with dysfunctional/hyperventilation syndrome. Since only a single RCT [53] met the inclusion criteria, this systematic review could not provide a reliable conclusion regarding the effect of DB on dysfunctional breathing. The included study enrolled 45 patients with hyperventilation syndrome and divided them into three groups (relaxation therapy, relaxation therapy and DB, and control) of 15 patients each. As the frequency and severity of hyperventilation attacks were significantly reduced in the DB group compared with the control group, no detailed data and statistical analysis were presented in this study [53]. Therefore, the effect of DB on dysfunctional breathing is still unclear.

A systematic review with meta-analysis examined (1) the generalizability, consistency, volume, and quality of the evidence for breathing control; and (2) the effect of breathing control on various clinical outcomes [54]. This systematic review included a total of 20 studies: 2 RCTs [55,56], 3 non-RCTs [57–59], and 15 quasi-experimental studies [14,60–73]. The study participants were also heterogeneous; 80% of the studies recruited patients with chronic respiratory disease, such as COPD, and 20% of the studies included patients with other conditions (e.g., post-surgery, chronic progressive multiple sclerosis) and asymptomatic individuals. DB was required to be the single intervention used in all studies. DB had beneficial effects on abdominal excursion (MD, 1.36; 95% CI, 0.42–2.31), diaphragm excursion (MD, 1.39; 95% CI, 1.00–1.77), short-term changes in respiratory function, RR (MD, −0.84; 95% CI, −1.09 to 0.60),  $V_T$  (MD, 0.98; 95% CI, 0.71–1.25), gas exchange, arterial oxygen saturation (MD, 0.63; 95% CI, 0.25–1.02), and percutaneous oxygen (MD, 1.48; 95% CI, 0.85–2.11). On the other hand, DB had a negative impact on the work of breathing (MD, 1.06; 95% CI, 0.52–1.60) and dyspnea (MD, 1.47; 95% CI, 0.88–2.05) in patients with severe respiratory disease. DB had no significant effects on ventilation, long-term change in respiratory function, vital capacity (VC), forced vital capacity (FVC), expiratory flow rate, FEV<sub>1</sub>, respiratory muscle strength, oxygen consumption, respiratory muscle efficiency, ventilation distribution, and 12-min walk test. On the other hand, DB was effective in the short-term improvement of respiratory function, but it did not have a beneficial effect on the long-term physiological outcomes and energy cost of breathing. Interestingly, DB could negatively affect the respiratory symptoms of patients with severe respiratory disease and may not be applicable to all kinds of respiratory disease. However, the generalizability and quality of evidence is not high as this systematic review included only two RCTs and the heterogeneity of the characteristics of study subjects and the intervention methods used among the studies was large.

Grams et al. [74] examined the effects of breathing exercises on the prevention of postoperative pulmonary complications and recovery of pulmonary function in patients who had upper abdominal surgery. A total of six RCTs or quasi-RCTs were included in this systematic review [36–40,75], four of

which were conducted in Brazil. The meta-analysis showed that the maximal expiratory pressure and maximal inspiratory pressure increased by 12.8 (95% CI, 7.6–18.1) and 5.6 (95% CI, 0.6–10.5) mmH<sub>2</sub>O, respectively, on Day 1 postop [38–40]. However, DB was observed to have no significant effects on respiratory function including FVC, FEV, and FEV<sub>1</sub>. This systematic review indicates that breathing exercises, which mainly consist of DB, improve the respiratory muscle strength of patients after upper abdominal surgery. However, the included studies investigated the effect of DB on Day 1–5 postop, and the respiratory functions of the study subjects at baseline were heterogeneous. Therefore, the findings of this systematic review are limited to a specific circumstance and the generalizability is low.

Recently, Hopper et al. [76] reported that DB might have reduced the physiological and psychological stress, although the meta-analysis could not be performed due to the methodological heterogeneity and outcome measures. One RCT [77] and quasi-experimental studies [78,79] were included in this qualitative analysis. Ma et al. [77] reported that DB reduced the RR and salivary cortisol levels in an RCT, suggesting that DB has a favorable effect on stress. Two experimental studies also showed that DB was effective for improving the blood pressure control [78] and stress measured using the Depression Anxiety Stress Scale-21 [79]. However, more well-designed RCTs with an appropriate sample size are needed to conclude whether DB is beneficial for reducing stress.

Table 1 summarizes the results of these systematic reviews.

**Table 1.** Systematic reviews and meta-analyses assessing the effects of diaphragmatic breathing on various disorders.

Authors, Year	Subjects	Included Studies	Primary Outcomes	Results
Holland et al., 2012 [42]	COPD	16 RCTs	Dyspnea, exercise capacity, and health-related quality of life	Dyspnea↑ 6-min walk distance↑
Ubolnuar et al., 2019 [44]	COPD	19 RCTs	Ventilation, exercise capacity, dyspnea, and quality of life	Respiratory rate↓ Quality of life→
Santino et al., 2020 [45]	Asthma	22 RCTs	Quality of life	Unknown due to insufficient data
Prem et al., 2013 [47]	Asthma	3 RCTs	Quality of life	Quality of life↑? (meta-analysis was not performed)
Macêdo et al., 2016 [48]	Asthma (children)	3 RCTs	Quality of life, asthma symptoms, and adverse effects	Unknown due to insufficient data
Barker et al., 2013 [51]	Dysfunctional/hyperventilation syndrome (children)	No eligible studies	Quality of life	Unknown
Jones et al., 2013 [52]	Dysfunctional/hyperventilation syndrome (adults)	1 RCT	Quality of life and adverse effects	Unknown due to insufficient data



Table 1. Cont.

Authors, Year	Subjects	Included Studies	Primary Outcomes	Results
Lewis et al., 2007 [54]	Chronic respiratory disease, post-surgical, or asymptomatic individuals	2 RCTs, 3 non-RCTs, and 15 quasi-experimental studies	Short-term clinical outcomes (not specified)	Abdominal excursion↑, diaphragm excursion↑, respiratory rate↓, tidal volume↑, arterial oxygen saturation↑, percutaneous oxygen↑, Work of breathing↑, dyspnea↑
Grams et al., 2012 [74]	Post upper abdominal surgery	6 RCTs or quasi-RCTs	Respiratory function and postoperative complications	Respiratory muscle strength↑, Respiratory function→
Hopper et al., 2019 [76]		1 RCT and 2 quasi-experimental studies	Stress	Stress↓ (meta-analysis was not performed)

COPD, chronic obstructive pulmonary disease; RCT, randomized controlled trial; ↑, increase; →, no change; ↓, decrease.

### 3.2. Randomized Controlled Trials

#### 3.2.1. COPD and Asthma

It is apparent that previous studies investigating the effects of DB have been conducted in patients with COPD. The author has identified a recent RCT that was not included in previous systematic reviews. Yekefallah et al. [80] compared the effect of the breathing exercise involving DB and pursed-lip breathing and upper limb exercise on exercise capacity measured through a six-minute walking test in patients with COPD. Seventy-five patients with moderate-to-severe COPD were recruited and divided into three groups: upper limb exercise group ( $n = 25$ ), breathing exercise group ( $n = 25$ ), and control group ( $n = 25$ ). Participants in the breathing exercise group performed DB and pursed-lip breathing for one minute, respectively, with a one-minute rest between these exercises. They were asked to do these exercises four times a day for four weeks. On the other hand, participants in the upper limb exercise group performed upper limb strengthening exercises using dumbbells for 20 min per session, thrice a week, for four weeks. Moreover, all participants completed the study. The mean walking distance significantly increased in the breathing exercise group (from  $355.3 \pm 47.9$  m to  $376.9 \pm 37$  m) and in the upper limb exercise group (from  $389.8 \pm 5.8$  m to  $409.5 \pm 29.8$  m) during the study, whereas the control group did not show any significant change. Although both the upper limb exercise and DB plus pursed-lip breathing were effective in increasing the walking distance, a post hoc analysis revealed that the walking distance of the upper limb exercise group was longer than that of the breathing exercise group. This study indicates that the upper limb strengthening exercise is more effective for improving the exercise capacity of COPD patients than DB training.

The respiratory function and abdominal and thoracic kinematics changes due to DB training in patients with moderate persistent asthma were evaluated, although the intervention might be a respiratory muscle training rather than a simple DB training [81]. Eighty-eight inactive patients with asthma aged between 18 and 34 were enrolled in this RCT. The study participants were categorized into aerobic exercise ( $n = 22$ ), DB ( $n = 22$ ), aerobic exercise combined with DB ( $n = 22$ ), and control ( $n = 22$ ) groups. The participants in the intervention groups performed the training program thrice a week

for eight weeks. The DB training in this study was unique. The participants in the DB group breathed using a tube to maximize their inspiration and expiration, and a 2.5 kg weight (Week 1–4) or a 5 kg weight (Week 5–8) was put on their abdominal cavity. Moreover, they completed three sets of 5–10 repetitions using one second of inspiration and two seconds of expiration, three sets of 10–15 repetitions using two seconds of inspiration and four seconds of expiration, and three sets of 15–20 repetitions using three seconds of inspiration and six seconds of inspiration. The participants in the aerobic exercise group walked and/or jogged for 30 min at the intensity of 60% of the age-predicted maximum heart rate. After the eight-week intervention, the DB training improved the FVC (from  $3.01 \pm 0.58$  L to  $3.52 \pm 0.74$  L), FEV<sub>1</sub> (from  $2.85 \pm 0.57$  L to  $3.22 \pm 0.63$  L), FEV<sub>1</sub>/FVC ratio (from  $94.86 \pm 4.94\%$  to  $90.64 \pm 6.67\%$ ), PEF (from  $7.10 \pm 1.57$  L to  $7.68 \pm 1.26$  L), and inspiratory VC, but the forced expiratory flow (FEF) rate, maximum voluntary ventilation (MVV), and V<sub>T</sub> did not change. On the other hand, aerobic exercise improved the FVC (from  $2.77 \pm 0.48$  to  $3.11 \pm 0.71$  L), FEV<sub>1</sub> (from  $2.72 \pm 0.53$  to  $2.97 \pm 0.65$  L), PEF (from  $7.15 \pm 1.45$  L to  $7.57 \pm 1.47$  L), MVV (from  $103.65 \pm 27.86$  L/min to  $128.97 \pm 27.56$  L/min), and inspiratory VC, but the FEV<sub>1</sub>/FVC ratio, FEF, and V<sub>T</sub> did not change. Aerobic exercise combined with DB more effectively improved the FVC (from  $2.87 \pm 0.67$  L to  $3.68 \pm 0.82$  L) and FEV<sub>1</sub> (from  $2.70 \pm 0.67$  L to  $3.30 \pm 0.70$  L) than aerobic exercise alone, but DB and aerobic exercise were equally effective in the improvement of FVC and FEV<sub>1</sub>. Aerobic exercise, DB, and DB combined with aerobic exercise improved the chest circumferences during inspiration, but no significant improvement was observed during the rest and expiration phases. Interestingly, DB improved the resting, inspiratory, and expiratory abdominal circumferences at the height of the midpoint between the umbilicus and the xiphoid process, but aerobic exercise did not change the resting circumference.

### 3.2.2. Cancer

Campbell et al. [82] investigated the efficacy of relaxation techniques in treating the eating problems of cancer patients who have a prognosis of at least six months and have nutritional problems such as weight loss. The relaxation technique includes DB, autosuggestion, relaxing of muscles, and image control. The changes in weight and performance status measured using the Karnofsky Performance Status Scale during the study period were assessed. Twenty-two patients with cancer were randomly assigned to the intervention ( $n = 12$ ) and control groups ( $n = 10$ ), respectively. After performing the relaxation training for six weeks, 75% of the patients gained weight within 10% of one's ideal weight. Performance status was improved in 33% of the patients after the eight-week intervention. Moreover, relaxation training using DB may support the treatment of eating problems in patients with cancer.

Shahirai et al. [83] evaluated the effect of DB, muscle relaxation, and body image on the QoL of older patients with breast or prostate cancer. Fifty patients were recruited and categorized into the intervention ( $n = 25$ ) and control ( $n = 25$ ) groups. The functional QoL score was immediately improved after the intervention (from 31.6 to 60.5 points) and six weeks after the intervention (from 31.6 to 66 points), whereas no significant changes were observed in the control group. Furthermore, the mean score of the general domain of QoL was also immediately increased after the intervention (from 36.33 to 64.33 points) and six weeks after the intervention (from 36.33 to 52.33 points). On the other hand, it was decreased in the control group during the study period. These studies applied the use of concurrent techniques, but not DB techniques, and the outcome measures were mortality and survival period. Thus, whether DB is useful for cancer treatment or not is inconclusive. However, relaxation and DB techniques may be a cost-effective and convenient method for improving the general condition of patients with cancer.

### 3.2.3. Other Diseases

Silva and Motta [84] investigated the effect of DB, abdominal muscle training, and massage on pediatric patients with chronic functional constipation. Seventy-two patients aged 4–18 were categorized into the physiotherapy plus medication ( $n = 36$ ) and the medication using only laxatives

( $n = 36$ ) groups. The physiotherapy consisted of DB, isometric training of the abdominal muscles to increase intra-abdominal pressure, and slow circular clockwise abdominal massage. After the six-week intervention, the defecation frequency was significantly higher in the physiotherapy group than the medication-only group. Furthermore, DB may increase intra-abdominal pressure and stimulate the parasympathetic activity, which increases the colonic motility and improves the defecation frequency.

Wang et al. [85] investigated the effect of DB on blood pressure in prehypertensive patients. Twenty-six postmenopausal women aged 45–60 were enrolled and categorized into the intervention and control groups. Twenty-two participants (intervention group,  $n = 12$ ; control group,  $n = 10$ ) completed the study. The intervention group was treated with DB combined with the frontal electromyographic biofeedback-assisted relaxation training, whereas the control group only performed DB techniques. All participants performed 10 sessions of treatment once every 3 days. After the training, in the intervention group, systolic and diastolic blood pressures were decreased by 8.4 and 3.9 mmHg, respectively. Single DB also significantly decreased the systolic blood pressure by 4.3 mmHg, but no changes in the diastolic blood pressure were observed. DB combined with the biofeedback training was more effective in lowering the blood pressure than DB alone. In addition, the RR interval increased during the training in the intervention group, whereas no change was observed in the control group. The standard deviation of the normal-normal intervals significantly increased in both groups. Although DB alone was effective in lowering the blood pressure and improving the heart rate variability, the biofeedback training seemed to strengthen its effect through inhibiting sympathetic activity and improving vagal tone [86].

Seo and colleagues [87] examined the effect of DB on dyspnea and physical activity of patients with heart failure. Thirty-six patients were enrolled in this study and were categorized into the home-based DB retraining ( $n = 18$ ) and control ( $n = 18$ ) groups. A total of 29 patients (intervention group,  $n = 13$ ; control group,  $n = 16$ ) completed the study, and 27 patients (intervention group,  $n = 12$ ; control group,  $n = 15$ ) who continued the home-based DB retraining were followed up for five months. After the eight-week intervention, the DB group showed little improvement in dyspnea. The functional status in the DB and control groups increased by 10.5% and 4.4%, respectively, but declined by 2.2% in the control group in the five-month follow-up. On the other hand, the average daily activity measured by a triaxial accelerometer, ActiGraph, significantly increased by 14% in the DB group and decreased by 6% in the control group. No adverse effects were reported. Moreover, DB was a feasible treatment option for patients with heart failure. Daily physical activity can be increased due to the improvement of dyspnea through regular DB exercise, which may lead to maintaining or improving the cardiorespiratory fitness of patients with heart failure. Furthermore, the results of the studies by Wang et al. [85] and Seo et al. [87] indicate that DB has beneficial effects on cardiovascular health.

Subbeyaz and colleagues [88] conducted an interesting RCT that compared the efficacy of DB and pursed-lip breathing in inspiratory muscle training for improving the cardiopulmonary functions of patients with subacute stroke. Forty-five inpatients with stroke were recruited and categorized into the breathing retraining ( $n = 15$ ), inspiratory muscle training ( $n = 15$ ), and control ( $n = 15$ ) groups. The breathing training program consisted of 15 min of DB combined with pursed-lip breathing, 5 min of air-shifting techniques, and 10 min of voluntary isocapnic hyperpnea. The participants received daily training, six times a week, for six weeks. No significant changes in VC, FVC, FEV<sub>1</sub>, FEF<sub>25–75%</sub>, and MVV from baseline in the DB group were observed, but the PEF of the DB intervention group improved as compared with both the inspiratory training and control groups. In contrast, inspiratory muscle training significantly improved VC, FVC, FEV<sub>1</sub>, FEF<sub>25–75%</sub>, and MVV as compared with controls. Interestingly, DB increased both the maximum inspiratory and expiratory pressures, but inspiratory muscle training did not increase the maximum expiratory pressure. In contrast to DB, inspiratory muscle training improved the exertional dyspnea and functional status based on the Barthel Index and Functional Ambulation Category scores. The general health, pain, vitality, and emotional role domains of the SF-36 improved in the DB group from baseline as compared with the control group. The short-term inspiratory muscle training effectively improved the respiratory function and exercise

capacity of patients with stroke, but DB was also effective in improving the PEF, inspiratory and expiratory pressures, and QoL. Considering that inspiratory muscle training requires the appropriate medical equipment, DB is a more feasible treatment option for improving the cardiopulmonary function of inpatients with stroke.

Eherer and colleagues [89] assessed the effect of the four-week DB training on the QoL, pH-metry, and on-demand proton pump inhibitor usage of patients with nonerosive gastroesophageal reflux disease (GERD). Nineteen patients were enrolled in this RCT and were categorized into the training ( $n = 10$ ) and control ( $n = 9$ ) groups. The training group engaged in daily DB practice for at least 30 min. After the four-week DB training, the time with a pH < 4.0 in the training group decreased from  $9.1\% \pm 1.3\%$  to  $4.7\% \pm 0.9\%$ , and the QoL scores measured using the GERD Health-Related Quality of Life Scale also improved from  $13.4 \pm 1.98$  to  $10.8 \pm 1.86$ , but no changes in the control group were observed. Furthermore, after the nine-month follow-up, patients who continued the DB techniques showed an improvement in their QoL scores (from  $15.2 \pm 2.2$  to  $9.7 \pm 1.6$ ) and proton pump inhibitor usage (from  $98 \pm 34$  mg/week to  $25 \pm 12$  mg/week). Furthermore, DB as a non-pharmacological intervention was observed to reduce the proton pump inhibitor usage and improve the long-term QoL of patients with GERD.

In 2005, an interesting RCT was conducted in India [90]. Migraine is a common but hard-to-treat disease. Kaushik et al. investigated whether biofeedback-assisted DB could treat migraine. This study enrolled 192 patients who were then categorized into biofeedback ( $n = 96$ ) and control ( $n = 96$ ) groups. Moreover, 24 (25%) patients in the biofeedback group were excluded. The control group received 80 mg/day of propranolol, whereas the biofeedback group was subjected to DB and relaxation with electromyogram and temperature feedback for six months. Biofeedback-assisted DB was effective in 66.66% of the patients. In both groups, the severity, frequency, number of vomiting episodes, and duration of attacks were decreased. One year after the intervention, the resurgence of migraine was observed in 9.37% of the participants in the biofeedback group, which was significantly lower than that of the propranolol group (38.54%). Differences in the resurgence rate between the groups were observed ( $p < 0.001$ ). In the propranolol group, adverse effects such as fatigue and nausea were observed in 13.54% of the patients, whereas the side effects were only observed in 5.2% of the patients in the biofeedback group. The authors recommended that biofeedback-assisted DB and relaxation techniques should be used as a treatment for migraine.

A systematic review has shown that DB may be useful for stress management [76]. Chen et al. [91] evaluated the effectiveness of DB training program on anxiety. Anxiety is associated with respiratory symptoms such as dyspnea, shallow respiratory breathing, hyperventilation, and chest tightness [92], as well as cardiovascular symptoms such as tachycardia and palpitations [92,93]. The authors hypothesized that relaxation and DB techniques could reduce anxiety. Forty-six individuals who had anxiety for at least a month were recruited, but only 30 participants (DB group,  $n = 15$ ; control group,  $n = 15$ ) completed the eight-week study. The DB group practiced DB at least twice a day and 10 exercises per session. The anxiety scores measured using the Beck Anxiety Inventory declined from baseline ( $19.13 \pm 7.52$ ) to week 4 ( $12.67 \pm 7.09$ ) and also from week 4 to week 8 ( $5.33 \pm 4.52$ ). Moreover, after the eight-week DB training, the peripheral temperature increased from  $33.26^\circ\text{C} \pm 1.49^\circ\text{C}$  to  $34.77^\circ\text{C} \pm 1.01^\circ\text{C}$ , heart rate decreased from  $85.52 \pm 8.0$  to  $72.45 \pm 5.57$  beats/min, and breathing rate decreased from  $16.24 \pm 2.27$  to  $12.59 \pm 2.40$  breaths/min, whereas no significant changes in the control group were observed. Furthermore, DB is effective to reduce anxiety, which leads to favorable changes in physiological indicators.

Table 2 summarizes the results of these RCTs.

**Table 2.** Randomized controlled trials assessing the effects of diaphragmatic breathing on various disorders.

Authors, Year	Subjects	Intervention Study Duration	Results
Yekefallah et al., 2019 [80]	75 patients with COPD	Breathing exercise (DB and pursed-lip breathing) and upper limb exercise One month	6-min walking distance↑
Shaw and Shaw, 2011 [81]	88 patients with asthma	DB, aerobic exercise, and aerobic exercise plus DB 8 weeks	FVC↑, FEV <sub>1</sub> ↑, FEV <sub>1</sub> /FVC ratio↓, PEF↑, FEF rate→, MVV→, V <sub>T</sub> →
Campbell et al., 1984 [82]	22 patients with cancer (except breast cancer)	Relaxation technique including DB 6 weeks	Desirable weight gain Improvement in Performance Status
Shahirai et al., 2017 [83]	50 elderly patients with breast or prostate cancer	Muscle relaxation, guided imagery, and DB 6 weeks	Quality of life↑
Silva and Motta, 2013 [84]	72 pediatric patients with chronic functional constipation	Isometric training of the abdominal muscle, DB, and abdominal massage 6 weeks	Defecation frequency↑ Fecal incontinence→
Wang et al., 2010 [85]	22 postmenopausal women with prehypertention	DB and DB with frontal electromyographic biofeedback training	Systolic blood pressure↓
Seo et al., 2016 [87]	29 patients with heart failure	Home-based DB retraining 8 weeks	Dyspnea↓ Daily physical activity↑ Functional status↑
Sutbeyaz et al., 2010 [88]	45 inpatients with subacute stroke	DB combined with pursed-lip breathing and inspiratory muscle training 6 weeks	PEF ↑, VC→, FVC→, FEV <sub>1</sub> →, FEF <sub>25–75%</sub> →, MVV→
Eherer et al., 2012 [89]	19 patients with non-erosive gastroesophageal reflux disease	DB 4 weeks	Time with a pH < 4.0↓ Quality of life↑
Kaushik et al., 2005 [90]	167 patients with migraine	DB with biofeedback and 80 mg/day of propranolol 6 months	Resurgence of migraine↓
Chen et al., 2017 [91]	30 patients with anxiety	DB 8 weeks	Anxiety score↓, peripheral temperature↑, heart rate↓, breathing rate↓

COPD, chronic obstructive pulmonary disease; DB, diaphragmatic breathing; VC, vital capacity; FVC, forced vital capacity; FEV<sub>1</sub>, forced expiratory volume in 1 s; PEF, peak expiratory flow; FEF, forced expiratory flow; MVV, maximum voluntary ventilation; V<sub>T</sub>, tidal volume; ↑, increase; →, no change; ↓, decrease.

### 3.2.4. Healthy Individuals

The effects of DB on healthy individuals have been also investigated. An experimental study was conducted to investigate whether DB had an impact on motion sickness in a virtual reality environment [94]. Healthy individuals were screened for motion sickness susceptibility. A total of 60 motion sickness susceptible subjects were randomly categorized into the DB ( $n = 31$ ) and control ( $n =$

29) groups. The participants wore 3D goggles and experienced motion sickness in a virtual reality space (10-min fluctuating view of a stormy sea). During the virtual reality experience, the respiration rate was significantly lower ( $11.38 \pm 3.49$  breaths/min vs.  $16.21 \pm 2.77$  breaths/min) and the heart rate variability (respiratory sinus arrhythmia) was significantly higher ( $7.46\% \pm 1.05\%$  vs.  $6.38\% \pm 0.86\%$ ) in the DB group compared with the control group. In addition, the self-reported motion sickness rating ( $1.37 \pm 0.44$  vs.  $1.78 \pm 0.63$ ) and the motion sickness assessment questionnaire score ( $2.1 \pm 0.91$  vs.  $2.85 \pm 1.72$ ) were significantly lower in the DB group than those in the control group. In the DB group, a positive correlation between the respiration rate and motion sickness rating and negative relationships of the heart rate variability with respiration rate and motion sickness rating were observed. Therefore, these findings suggested that DB increased the parasympathetic nervous system activity, decreased the respiration rate, and improved the motion sickness symptoms.

Gimenez et al. [95] compared the effectiveness of comprehensive directed breathing retraining with DB on male smokers who had exertional dyspnea but normal spirometry. Twenty-four active male smokers aged 33–60 were enrolled and categorized into the experimental (comprehensive directed breathing retraining) and control (DB) groups. Both groups performed 60 min of DB, 30 min of walking, and conditioning exercises for 5 days a week for 4 weeks. The participants were asked to continue DB at home, walking, and exercises twice daily for at most 30 min. The experimental group was educated about the anatomy and physiology of respiration, enhanced their awareness on abnormal breathing patterns, shown the ventilator rhythm on a spirogram, and watched a DB instructional film. The measurement of physiologic parameters was performed at rest and at 40-W exercise for 10 min. In the experimental group, 34 of 44 lung function parameters, such as dyspnea index, ventilation capacity, FEV<sub>1</sub>, PEF, VO<sub>2</sub>, VCO<sub>2rest</sub>, and PaO<sub>2</sub>, were improved. The single DB intervention did not effectively improve the exertional dyspnea and lung function. Moreover, the authors referred to an unfavorable effect of DB that previous studies on patients with COPD had shown: the possibility that DB worsened the chest wall motion, reduced the efficiency of ventilation, and increased the respiratory workload [64,96,97].

Han and Kim [98] investigated the effect of DB combined with upper extremity exercise on the lung function of young healthy individuals. Forty male adults were recruited and categorized into the experimental (DB with upper extremity exercise;  $n = 20$ ) and control (only DB;  $n = 20$ ) groups. Both groups performed 10 min of warm-up exercise, 5 min of DB, and 10 min of cool-down exercise. Additionally, the experimental group performed breathing exercises with 25 min of dynamic upper extremity exercise using an elastic band with 40% resistance for one repetition maximum, whereas the control group performed 25 min of regular breathing exercise. Both groups performed the exercise session thrice a week for four weeks. After the four-week training, FVC significantly increased in both experimental and control groups. FEV<sub>1</sub> and PEF did not change in both groups. However, FEV<sub>1</sub> increased by 0.05 L in the experimental group, whereas it decreased by 0.02 L in the control group. This study indicates that DB is effective in improving FVC, but the upper extremity exercise may have an additional effect on obstructive ventilatory disturbance.

Bahensky et al. [99] investigated how DB based on yoga affects the efficiency of breathing in adolescent endurance runners. This study included 37 runners who performed endurance training at least six times a week. The intervention group ( $n = 21$ ) engaged in DB exercise for at least 10 min per session, at least 5 times a week, for 4 months. The V<sub>T</sub> and breathing frequency were measured at two and four months after the intervention started. A spiroergometry test was performed using a bicycle ergometer at the point of subjective exhaustion. In the intervention group, V<sub>T</sub> significantly increased from  $2.02 \pm 0.43$  L at baseline to  $2.11 \pm 0.43$  L after the two-month intervention and to  $2.25 \pm 0.51$  L after the four-month intervention, whereas no changes in the control group were observed. Moreover, the breathing frequency significantly increased from  $59.0 \pm 8.6$  breaths/min at baseline to  $55.6 \pm 9.5$  breaths/min after the two-month intervention and to  $52.2 \pm 9.2$  breaths/min after the four-month intervention, whereas no changes in the control group were observed. The DB training for four months

effectively increased the  $V_T$  by 10.96% and decreased the breathing frequency by 11.47%. DB may improve the endurance capacity of the respiratory muscles in healthy adolescents.

Previous studies have shown that DB has no significant impacts on aerobic capacity in healthy individuals. Respiratory muscle trainings also appear to have no beneficial effects on  $VO_{2max}$  in healthy non-smokers [100] and athletes [101].

#### 4. Discussion

DB has various physiological effects in humans. The diaphragm is the major respiratory muscle. As the movement of the diaphragm has a positive correlation with the lung volume [102], using the diaphragm consciously during respiration increases the lung capacity. DB facilitates slow respiration, but if RR decreases, hypercapnia and the activation of chemoreceptors would be induced to increase RR to maintain the respiratory homeostasis [103]. DB that controlled RR at six breaths/min reduces the chemoreflex response to hypoxia and hypercapnia compared with normal breathing [104]. Decreased RR increases the  $V_T$ , which improves the efficiency of ventilation for oxygen [105] through alveolar recruitment and distention, improving the alveolar ventilation due to reduced alveolar dead space and increasing the arterial oxygen saturation [103]. Therefore, DB has a potential to improve the blood oxygen levels.

RR also affects the heart rate, systemic blood pressure, and circulating blood volume. Generally, inspiration decreases the intrathoracic pressure and increases the pressure gap between the right heart and the systemic circulation, which increases the venous return to the right heart. On the other hand, the pulmonary venous return decreases and the blood volume in the left heart is reduced. As a result, the cardiac output increases due to the increase of blood volume in the right heart. This physiological action is reversed in expiration [103]. Heart rate increases during inspiration and decreases during expiration while arterial blood pressure is lowered [106]. DB enhances the fluctuations in blood pressure and heart rate [103] via slow breathing [107] and diaphragm excursions, therefore improving the baroreflex sensitivity, heart rate variability, and blood pressure oscillations [103,108].

Breathing has a close relationship with autonomic nervous system function. The phrenic nerve that controls the movement of the diaphragm is connected to the vagus (parasympathetic) nerve [4]. Decreasing the RR by DB activates the parasympathetic nervous activity while suppressing the sympathetic nervous activity [11]. Chang et al. [109] reported that slow breathing with eight breaths/min makes the balance of the parasympathetic nervous activity dominant. Autonomic dysfunction, for example, a reduction in heart rate variability, is associated with an increased risk of cardiovascular mortality and morbidity [110]. Hyperactive sympathetic nervous activity and hypoactive parasympathetic nervous activity can be regulated by DB, which will improve the cardiovascular health. In addition, yoga practice tends to tune the brain toward a parasympathetically driven mode and positive states [111]. Jerath et al. [112] indicated that breathing stimulated the vagal activation of gamma-aminobutyric acid pathways in the brain, and reduced stress and anxiety. Furthermore, DB appears to have a favorable effect on the cardiovascular system and brain through the improvement of the autonomic balance.

Although the current evidence regarding the effects of DB on human health is accumulating, several limitations should be considered to conclude its efficacy in clinical practice. Firstly, the DB technique among the studies has not been standardized. The inspiratory and expiratory phase times ranged from 4 to 8 s, respectively, and the practitioners performed DB in various postures such as supine position, semi-recumbent position, or seated position. Moreover, the optimal RR and posture for achieving physiological benefits are still unknown. Secondly, the effect of DB may differ depending on the severity of the diseases. For instance, DB could be harmful for dyspnea in patients with severe COPD. Therefore, future studies should investigate whether the effects of DB differ according to the severity of diseases. Thirdly, considerable heterogeneity among studies was observed, such as the characteristics of the study subjects, intervention frequency and duration, and controls. Furthermore, previous systematic reviews assessed in this study have different criteria of inclusion. For

example, several studies that did not investigate the single effect of DB were included in a systematic review (e.g. Thomas et al. [31]). Fourthly, systematic reviews included a wide range of studies from the 1950s to 2010s. Studies that were performed 50 years ago have important information; however, recent studies may be more important because statistical methods and quality of data advances with the times. Such heterogeneity might cause the findings of this review to be inconclusive. Finally, the primary outcomes of systematic reviews are usually clinical symptoms, QoL, respiratory function, and exercise capacity, and no studies have evaluated the effect of DB on hard endpoints, such as the development of respiratory failure, cardiovascular disease, and mortality. Most of the studies have short study periods (e.g., 4–6 weeks). Thus, the long-term effect of DB should be clarified in the future. Despite these limitations, DB has the potential to improve various kinds of disease. Moreover, no serious adverse effects have also been reported in the RCTs. Recently, a number of studies have shown that physical rehabilitation improves exercise capacity in transplant recipients and candidates [113,114]. DB could also be safe and feasible in the post-transplant management due to its non-invasive technique.

## 5. Conclusions

Previous systematic reviews and meta-analyses have shown that DB is effective for improving the exercise capacity and RR in patients with COPD. On the other hand, DB could deteriorate dyspnea in severe COPD patients. Moreover, the effect of DB on the QoL of patients with asthma still needs to be investigated further. DB may also be beneficial for reducing both physiological and psychological stress and could improve the respiratory function and respiratory muscle strength, but more firm evidence will be needed in the future. In addition, DB may help in treating eating disorders, chronic functional constipation, hypertension, migraine, and anxiety, as well as the QoL of patients with cancer and GERD and the cardiorespiratory fitness of patients with heart failure. Furthermore, DB could be a feasible and practical technique for patients with such disorders. Although further studies are needed to clarify the effects of DB on human health, DB can support clinical practice.

**Funding:** This research received no external funding.

**Conflicts of Interest:** The author declares no conflict of interest.

## References

1. Sewall, H.; Pollard, M.E. On the Relations of Diaphragmatic and Costal Respiration, with particular reference to Phonation. *J. Physiol.* **1890**, *11*, 159–264. [[CrossRef](#)]
2. Fogarty, M.J.; Mantilla, C.B.; Sieck, G.C. Breathing: Motor control of diaphragm muscle. *Physiology* **2018**, *33*, 113–126. [[CrossRef](#)]
3. Ricoy, J.; Rodríguez-Núñez, N.; Álvarez-Dobaño, J.M.; Toubes, M.E.; Riveiro, V.; Valdés, L. Diaphragmatic dysfunction. *Pulmonology* **2019**, *25*, 223–235. [[CrossRef](#)]
4. Kocjan, J.; Adamek, M.; Gzik-Zroska, B.; Czyżewski, D.; Rydel, M. Network of breathing. Multifunctional role of the diaphragm: A review. *Adv. Respir. Med.* **2017**, *85*, 224–232. [[CrossRef](#)]
5. Bordoni, B.; Purgol, S.; Bizzarri, A.; Modica, M.; Morabito, B. The Influence of Breathing on the Central Nervous System. *Cureus* **2018**, *10*, e2724. [[CrossRef](#)]
6. Bordoni, B.; Zanier, E. The continuity of the body: Hypothesis of treatment of the five diaphragms. *J. Altern. Complement. Med.* **2015**, *21*, 237–242. [[CrossRef](#)]
7. Bruton, A.; Garrod, R.; Thomas, M. Respiratory physiotherapy: Towards a clearer definition of terminology. *Physiotherapy* **2011**, *97*, 345–349. [[CrossRef](#)]
8. Rama, S.; Ballentine, R.; Hymes, A. *Science of Breath: A Practical Guide*; Himalayan Institute Press: Honesdale, PA, USA, 1998; pp. 26–44.
9. Zou, L.; Sasaki, J.E.; Wei, G.X.; Huang, T.; Yeung, A.S.; Neto, O.B.; Chen, K.W.; Hui, S.S. Effects of Mind-Body Exercises (Tai Chi/Yoga) on Heart Rate Variability Parameters and Perceived Stress: A Systematic Review with Meta-Analysis of Randomized Controlled Trials. *J. Clin. Med.* **2018**, *7*, 404. [[CrossRef](#)]
10. Martarelli, D.; Cocchioni, M.; Scuri, S.; Pompei, P. Diaphragmatic breathing reduces exercise-induced oxidative stress. *Evid. Based Complement. Altern. Med.* **2011**, *2011*, 932430. [[CrossRef](#)]



11. Ambrosino, N.; Paggiaro, P.L.; Macchi, M.; Filieri, M.; Toma, G.; Lombardi, F.A.; Del Cesta, F.; Parlanti, A.; Loi, A.M.; Baschieri, L. A study of short-term effect of rehabilitative therapy in chronic obstructive pulmonary disease. *Respiration* **1981**, *41*, 40–44. [[CrossRef](#)]
12. Tiep, B.L.; Burns, M.; Kao, D.; Madison, R.; Herrera, J. Pursed lips breathing training using ear oximetry. *Chest* **1986**, *90*, 218–221. [[CrossRef](#)]
13. Collins, E.G.; Fehr, L.; Bammert, C.; O’Connell, S.; Laghi, F.; Hanson, K.; Hagarty, E.; Langbein, W.E. Effect of ventilation-feedback training on endurance and perceived breathlessness during constant work-rate leg-cycle exercise in patients with COPD. *J. Rehabil. Res. Dev.* **2003**, *40*, 35–44. [[CrossRef](#)] [[PubMed](#)]
14. Jones, A.Y.; Dean, E.; Chow, C.C. Comparison of the oxygen cost of breathing exercises and spontaneous breathing in patients with stable chronic obstructive pulmonary disease. *Phys. Ther.* **2003**, *83*, 424–431. [[CrossRef](#)]
15. Garrod, R.; Dallimore, K.; Cook, J.; Davies, V.; Quade, K. An evaluation of the acute impact of pursed lips breathing on walking distance in nonspontaneous pursed lips breathing chronic obstructive pulmonary disease patients. *Chron. Respir. Dis.* **2005**, *2*, 67–72. [[CrossRef](#)]
16. Spahija, J.; de Marchie, M.; Grassino, A. Effects of imposed pursed-lips breathing on respiratory mechanics and dyspnea at rest and during exercise in COPD. *Chest* **2005**, *128*, 640–650. [[CrossRef](#)]
17. Nield, M.A.; Soo Hoo, G.W.; Roper, J.M.; Santiago, S. Efficacy of pursed-lips breathing: A breathing pattern retraining strategy for dyspnea reduction. *J. Cardiopulm. Rehabil. Prev.* **2007**, *27*, 237–244. [[CrossRef](#)]
18. Collins, E.G.; Langbein, W.E.; Fehr, L.; O’Connell, S.; Jelinek, C.; Hagarty, E.; Edwards, L.; Reda, D.; Tobin, M.J.; Laghi, F. Can ventilation-feedback training augment exercise tolerance in patients with chronic obstructive pulmonary disease? *Am. J. Respir. Crit. Care Med.* **2008**, *177*, 844–852. [[CrossRef](#)]
19. Faager, G.; Ståhle, A.; Larsen, F.F. Influence of spontaneous pursed lips breathing on walking endurance and oxygen saturation in patients with moderate to severe chronic obstructive pulmonary disease. *Clin. Rehabil.* **2008**, *22*, 675–683. [[CrossRef](#)]
20. Bonilha, A.G.; Onofre, F.; Vieira, M.L.; Prado, M.Y.; Martinez, J.A. Effects of singing classes on pulmonary function and quality of life of COPD patients. *Int. J. Chron. Obstruct. Pulmon. Dis.* **2009**, *4*, 1–8.
21. Lord, V.M.; Cave, P.; Hume, V.J.; Flude, E.J.; Evans, A.; Kelly, J.L.; Polkey, M.I.; Hopkinson, N.S. Singing teaching as a therapy for chronic respiratory disease—A randomised controlled trial and qualitative evaluation. *BMC Pulm. Med.* **2010**, *10*, 41. [[CrossRef](#)]
22. Lin, W.C.; Yuan, S.C.; Chien, J.Y.; Weng, S.C.; Chou, M.C.; Kuo, H.W. The effects of respiratory training for chronic obstructive pulmonary disease patients: A randomised clinical trial. *J. Clin. Nurs.* **2012**, *21*, 2870–2878. [[CrossRef](#)] [[PubMed](#)]
23. Lord, V.M.; Hume, V.J.; Kelly, J.L.; Cave, P.; Silver, J.; Waldman, M.; White, C.; Smith, C.; Tanner, R.; Sanchez, M.; et al. Singing classes for chronic obstructive pulmonary disease: A randomized controlled trial. *BMC Pulm. Med.* **2012**, *12*, 69. [[CrossRef](#)]
24. van Gestel, A.J.; Kohler, M.; Steier, J.; Teschler, S.; Russi, E.W.; Teschler, H. The effects of controlled breathing during pulmonary rehabilitation in patients with COPD. *Respiration* **2012**, *83*, 115–124. [[CrossRef](#)]
25. Yamaguti, W.P.; Claudino, R.C.; Neto, A.P.; Chammas, M.C.; Gomes, A.C.; Salge, J.M.; Moriya, H.T.; Cukier, A.; Carvalho, C.R. Diaphragmatic breathing training program improves abdominal motion during natural breathing in patients with chronic obstructive pulmonary disease: A randomized controlled trial. *Arch. Phys. Med. Rehabil.* **2012**, *93*, 571–577. [[CrossRef](#)]
26. Bhatt, S.P.; Luqman-Arafath, T.K.; Gupta, A.K.; Mohan, A.; Stoltzfus, J.C.; Dey, T.; Nanda, S.; Guleria, R. Volitional pursed lips breathing in patients with stable chronic obstructive pulmonary disease improves exercise capacity. *Chron. Respir. Dis.* **2013**, *10*, 5–10. [[CrossRef](#)]
27. de Araujo, C.L.; Karloh, M.; Dos Reis, C.M.; Palú, M.; Mayer, A.F. Pursed-lips breathing reduces dynamic hyperinflation induced by activities of daily living test in patients with chronic obstructive pulmonary disease: A randomized cross-over study. *J. Rehabil. Med.* **2015**, *47*, 957–962.
28. Cabral, L.F.; D’Elia, T.C.; Marins, D.S.; Zin, W.A.; Guimarães, F.S. Pursed lip breathing improves exercise tolerance in COPD: A randomized crossover study. *Eur. J. Phys. Rehabil. Med.* **2015**, *51*, 79–88.
29. Borge, C.R.; Mengshoel, A.M.; Omenaas, E.; Moum, T.; Ekman, I.; Lein, M.P.; Mack, U.; Wahl, A.K. Effects of guided deep breathing on breathlessness and the breathing pattern in chronic obstructive pulmonary disease: A double-blind randomized control study. *Patient Educ. Couns.* **2015**, *98*, 182–190. [[CrossRef](#)]

30. Thomas, M.; McKinley, R.K.; Freeman, E.; Foy, C.; Prodder, P.; Price, D. Breathing retraining for dysfunctional breathing in asthma: A randomised controlled trial. *Thorax* **2003**, *58*, 110–115. [[CrossRef](#)] [[PubMed](#)]
31. Thomas, M.; McKinley, R.K.; Mellor, S.; Watkin, G.; Holloway, E.; Scullion, J.; Shaw, D.E.; Wardlaw, A.; Price, D.; Pavord, I. Breathing exercises for asthma: A randomised controlled trial. *Thorax* **2009**, *64*, 55–61. [[CrossRef](#)] [[PubMed](#)]
32. Grammatopoulou, E.P.; Skordilis, E.K.; Stavrou, N.; Myrianthefs, P.; Katrteroliotis, K.; Baltopoulos, G.; Koutsouki, D. The effect of physiotherapy-based breathing retraining on asthma control. *J. Asthma* **2011**, *48*, 593–601. [[CrossRef](#)] [[PubMed](#)]
33. Asher, M.I.; Douglas, C.; Airy, M.; Andrews, D.; Trenholme, A. Effects of chest physical therapy on lung function in children recovering from acute severe asthma. *Pediatr. Pulmonol.* **1990**, *9*, 146–151. [[CrossRef](#)] [[PubMed](#)]
34. Bingöl, G.K.; Yilmaz, M.; Sur, S.; Ufuk, D.A.; Sarpel, T.; Güneter, S.K. The effects of daily pulmonary rehabilitation program at home on childhood asthma. *Allergol. Immunopathol.* **2000**, *28*, 12–14.
35. Lima, E.V.N.C.L.; Lima, W.L.; Nobre, A.; dos Santos, A.M.; Brito, L.M.O.; do Rosário da Silva Ramos Costa, M. Inspiratory muscle training and respiratory exercises in children with asthma. *J. Bras. Pneumol.* **2008**, *34*, 552–558. [[CrossRef](#)]
36. Manzano, R.M.; Carvalho, C.R.; Saraiva-Romanholo, B.M.; Vieira, J.E. Chest physiotherapy during immediate postoperative period among patients undergoing upper abdominal surgery: Randomized clinical trial. *Sao Paulo Med. J.* **2008**, *126*, 269–273. [[CrossRef](#)]
37. Roukema, J.A.; Carol, E.J.; Prins, J.G. The prevention of pulmonary complications after upper abdominal surgery in patients with noncompromised pulmonary status. *Arch. Surg.* **1988**, *123*, 30–34. [[CrossRef](#)]
38. Ribeiro, S.; Gastaldi, A.C.; Fernandes, C. The effect of respiratory kinesiotherapy in patients undergoing upper abdominal surgery. *Einstein* **2008**, *6*, 166–169.
39. Gastaldi, A.C.; Magalhães, C.M.B.; Baraúna, M.A.; Silva, E.M.C.; Souza, H.C.D. Benefícios da cinesioterapia respiratória no pós-operatório de colecistectomia laparoscópica. *Rev. Bras. Fisioter.* **2008**, *12*, 100–106. [[CrossRef](#)]
40. Forgiarini, L.A., Jr.; Carvalho, A.T.; Ferreira, T.S.; Monteiro, M.B.; Bosco, A.D.; Gonçalves, M.P.; Dias, A.S. Atendimento fisioterapêutico no pós-operatório imediato de pacientes submetidos à cirurgia abdominal. *J. Bras. Pneumol.* **2009**, *35*, 445–459. [[CrossRef](#)]
41. Ali, L.A.; Pingitore, A.; Piaggi, P.; Brucini, F.; Passera, M.; Marotta, M.; Cadoni, A.; Passino, C.; Catapano, G.; Festa, P. Respiratory Training Late After Fontan Intervention: Impact on Cardiorespiratory Performance. *Pediatr. Cardiol.* **2018**, *39*, 695–704. [[CrossRef](#)]
42. Holland, A.E.; Hill, C.J.; Jones, A.Y.; McDonald, C.F. Breathing exercises for chronic obstructive pulmonary disease. *Cochrane Database Syst. Rev.* **2012**, *10*, CD008250. [[CrossRef](#)] [[PubMed](#)]
43. Lausin, G.; Gouilly, P. Étude des effets de la ventilation dirigée abdomino-diaphragmatique (Vdad) chez des patients BPCO de stade I et II: Study of the effects of controlled abdominodiaphragmatic ventilation in patients with level I and II COPD. *Kinésithér. Revue* **2009**, *9*, 29–38. [[CrossRef](#)]
44. Ubolnuar, N.; Tantisuwat, A.; Thaveeratitham, P.; Lertmaharit, S.; Kruapanich, C.; Mathiyakom, W. Effects of Breathing Exercises in Patients with Chronic Obstructive Pulmonary Disease: Systematic Review and Meta-Analysis. *Ann. Rehabil. Med.* **2019**, *43*, 509–523. [[CrossRef](#)] [[PubMed](#)]
45. Santino, T.A.; Chaves, G.S.; Freitas, D.A.; Fregonezi, G.A.; Mendonça, K.M. Breathing exercises for adults with asthma. *Cochrane Database Syst. Rev.* **2020**, *3*, CD001277. [[CrossRef](#)]
46. Girodo, M.; Ekstrand, K.A.; Metivier, G.J. Deep diaphragmatic breathing: Rehabilitation exercises for the asthmatic patient. *Arch. Phys. Med. Rehabil.* **1992**, *73*, 717–720.
47. Prem, V.; Sahoo, R.C.; Adhikari, P. Effect of diaphragmatic breathing exercise on quality of life in subjects with asthma: A systematic review. *Physiother. Theory Pract.* **2013**, *29*, 271–277. [[CrossRef](#)]
48. Macêdo, T.M.; Freitas, D.A.; Chaves, G.S.; Holloway, E.A.; Mendonça, K.M. Breathing exercises for children with asthma. *Cochrane Database Syst. Rev.* **2016**, *4*, CD011017. [[CrossRef](#)] [[PubMed](#)]
49. Thomas, M.; McKinley, R.K.; Freeman, E.; Foy, C. Prevalence of dysfunctional breathing in patients treated for asthma in primary care: Cross sectional survey. *BMJ* **2001**, *322*, 1098–1100. [[CrossRef](#)]

50. Gridina, I.; Bidat, E.; Chevallier, B.; Stheneur, C. Prevalence of chronic hyperventilation syndrome in children and teenagers. *Arch. Pediatr. Organe Off. Soc. Fr. Pediatr.* **2013**, *20*, 265–268. [[CrossRef](#)]
51. Barker, N.J.; Jones, M.; O'Connell, N.E.; Everard, M.L. Breathing exercises for dysfunctional breathing/hyperventilation syndrome in children. *Cochrane Database Syst. Rev.* **2013**, *12*, CD010376.
52. Jones, M.; Harvey, A.; Marston, L.; O'Connell, N.E. Breathing exercises for dysfunctional breathing/hyperventilation syndrome in adults. *Cochrane Database Syst. Rev.* **2013**, *5*, CD009041. [[CrossRef](#)] [[PubMed](#)]
53. Lindeboom, I.; Vlaander-van der Giessen, G. Hyperventilation and therapy [Hyperventilatie en therapie]. *Ned. Tijdschr. Voor Fysiother.* **1980**, *90*, 18–21.
54. Lewis, L.K.; Williams, M.T.; Olds, T. Short-term effects on outcomes related to the mechanism of intervention and physiological outcomes but insufficient evidence of clinical benefits for breathing control: A systematic review. *Aust. J. Physiother.* **2007**, *53*, 219–227. [[CrossRef](#)]
55. Mcneill, R.S.; Mckenzie, J.M. An assessment of the value of breathing exercises in chronic bronchitis and asthma. *Thorax* **1955**, *10*, 250–252. [[CrossRef](#)]
56. Wiens, M.E.; Reimer, M.A.; Guyn, H.L. Music therapy as a treatment method for improving respiratory muscle strength in patients with advanced multiple sclerosis: A pilot study. *Rehabil. Nurs.* **1999**, *24*, 74–80. [[CrossRef](#)]
57. Sackner, M.A.; Silva, G.; Banks, J.M.; Watson, D.D.; Smoak, W.M. Distribution of ventilation during diaphragmatic breathing in obstructive lung disease. *Am. Rev. Respir. Dis.* **1974**, *109*, 331–337.
58. Brach, B.B.; Chao, R.P.; Sgroi, V.L.; Minh, V.D.; Ashburn, W.L.; Moser, K.M. 133Xenon washout patterns during diaphragmatic breathing. Studies in normal subjects and patients with chronic obstructive pulmonary disease. *Chest* **1977**, *71*, 735–739. [[CrossRef](#)]
59. Sackner, M.A.; Gonzalez, H.F.; Jenouri, G.; Rodriguez, M. Effects of abdominal and thoracic breathing on breathing pattern components in normal subjects and in patients with chronic obstructive pulmonary disease. *Am. Rev. Respir. Dis.* **1984**, *130*, 584–587.
60. Becklake, M.R.; McGregor, M.; Goldman, H.I.; Braudo, J.L. A study of the effects of physiotherapy in chronic hypertrophic emphysema using lung function tests. *Dis. Chest* **1954**, *26*, 180–191. [[CrossRef](#)]
61. Blaney, F.; Sawyer, T. Sonographic measurement of diaphragmatic motion after upper abdominal surgery: A comparison of three breathing manoeuvres. *Physiother. Theo. Pract.* **1997**, *13*, 207–215. [[CrossRef](#)]
62. Campbell, E.J.; Friend, J. Action of breathing exercises in pulmonary emphysema. *Lancet* **1955**, *265*, 325–329. [[CrossRef](#)]
63. Chuter, T.A.; Weissman, C.; Mathews, D.M.; Starker, P.M. Diaphragmatic breathing maneuvers and movement of the diaphragm after cholecystectomy. *Chest* **1990**, *97*, 1110–1114. [[CrossRef](#)]
64. Gosselink, R.A.; Wagenaar, R.C.; Rijswijk, H.; Sargeant, A.J.; Decramer, M.L. Diaphragmatic breathing reduces efficiency of breathing in patients with chronic obstructive pulmonary disease. *Am. J. Respir. Crit. Care Med.* **1995**, *151*, 1136–1142. [[PubMed](#)]
65. Grimby, G.; Oxhøj, H.; Bake, B. Effects of abdominal breathing on distribution of ventilation in obstructive lung disease. *Clin. Sci. Mol. Med.* **1975**, *48*, 193–199. [[CrossRef](#)]
66. Ito, M.; Kakizaki, F.; Tsuzura, Y.; Yamada, M. Immediate effect of respiratory muscle stretch gymnastics and diaphragmatic breathing on respiratory pattern. Respiratory Muscle Conditioning Group. *Intern. Med.* **1999**, *38*, 126–132. [[CrossRef](#)] [[PubMed](#)]
67. Mckinley, H.; Gersten, J.W.; Speck, L. Pressure-volume relationships in emphysema patients before and after breathing exercises. *Arch. Phys. Med. Rehabil.* **1961**, *42*, 513–517.
68. Miller, W.F. A physiologic evaluation of the effects of diaphragmatic breathing training in patients with chronic pulmonary emphysema. *Am. J. Med.* **1954**, *17*, 471–477. [[CrossRef](#)]
69. Shearer, M.O.; Banks, J.M.; Silva, G.; Sackner, M.A. Lung ventilation during diaphragmatic breathing. *Phys. Ther.* **1972**, *52*, 139–148. [[CrossRef](#)]
70. Sinclair, J.D. The effect of breathing exercises in pulmonary emphysema. *Thorax* **1955**, *10*, 246–249. [[CrossRef](#)]
71. Vitacca, M.; Clini, E.; Bianchi, L.; Ambrosino, N. Acute effects of deep diaphragmatic breathing in COPD patients with chronic respiratory insufficiency. *Eur. Respir. J.* **1998**, *11*, 408–415. [[CrossRef](#)]

72. Williams, I.P.; Smith, C.M.; McGavin, C.R. Diaphragmatic breathing training and walking performance in chronic airways obstruction. *Br. J. Dis. Chest* **1982**, *76*, 164–166. [[CrossRef](#)]
73. Willeput, R.; Vachadeuz, J.P.; Lenders, D.; Nys, A.; Knoops, T.; Sergysels, R. Thoracoabdominal motion during chest physiotherapy in patients affected by chronic obstructive lung disease. *Respiration* **1983**, *44*, 204–214. [[CrossRef](#)] [[PubMed](#)]
74. Grams, S.T.; Ono, L.M.; Noronha, M.A.; Schivinski, C.I.; Paulin, E. Breathing exercises in upper abdominal surgery: A systematic review and meta-analysis. *Rev. Bras. Fisioter.* **2012**, *16*, 345–353. [[CrossRef](#)] [[PubMed](#)]
75. Hallböök, T.; Lindblad, B.; Lindroth, B.; Wolff, T. Prophylaxis against pulmonary complications in patients undergoing gall-bladder surgery. A comparison between early mobilization, physiotherapy with and without bronchodilatation. *Ann. Chir. Gynaecol.* **1984**, *73*, 55–58. [[PubMed](#)]
76. Hopper, S.I.; Murray, S.L.; Ferrara, L.R.; Singleton, J.K. Effectiveness of diaphragmatic breathing for reducing physiological and psychological stress in adults: A quantitative systematic review. *JBI Database Syst. Rev. Implement. Rep.* **2019**, *17*, 1855–1876. [[CrossRef](#)] [[PubMed](#)]
77. Ma, X.; Yue, Z.Q.; Gong, Z.Q.; Zhang, H.; Duan, N.Y.; Shi, Y.T.; Wei, G.X.; Li, Y.F. The Effect of Diaphragmatic Breathing on Attention, Negative Affect and Stress in Healthy Adults. *Front. Psychol.* **2017**, *8*, 874. [[CrossRef](#)] [[PubMed](#)]
78. Joshi, A.; Kiran, R.; Singla, H.K.; Sah, A.N. Stress management through regulation of blood pressure among college students. *Work* **2016**, *54*, 745–752. [[CrossRef](#)]
79. Sundram, B.M.; Dahlui, M.; Chinna, K. “Taking my breath away by keeping stress at bay”—An employee assistance program in the automotive assembly plant. *Iran. J. Public Health* **2014**, *43*, 263–272.
80. Yekefallah, L.; Zohal, M.A.; Keshavarzsarkar, O.; Barikani, A.; Gheraati, M. Comparing the effects of upper limb and breathing exercises on six-minute walking distance among patients with chronic obstructive pulmonary disease: A three-group randomized controlled clinical trial. *Adv. Respir. Med.* **2019**, *87*, 77–82. [[CrossRef](#)]
81. Shaw, B.S.; Shaw, I. Pulmonary function and abdominal and thoracic kinematic changes following aerobic and inspiratory resistive diaphragmatic breathing training in asthmatics. *Lung* **2011**, *189*, 131–139. [[CrossRef](#)]
82. Campbell, D.F.; Dixon, J.K.; Sanderford, L.D.; Denicola, M.A. Relaxation: Its effect on the nutritional status and performance status of clients with cancer. *J. Am. Diet. Assoc.* **1984**, *84*, 201–204.
83. Shahriari, M.; Dehghan, M.; Pahlavanzadeh, S.; Hazini, A. Effects of progressive muscle relaxation, guided imagery and deep diaphragmatic breathing on quality of life in elderly with breast or prostate cancer. *J. Educ. Health Promot.* **2017**, *6*, 1.
84. Silva, C.A.; Motta, M.E. The use of abdominal muscle training, breathing exercises and abdominal massage to treat paediatric chronic functional constipation. *Colorectal. Dis.* **2013**, *15*, e250–e255. [[CrossRef](#)]
85. Wang, S.Z.; Li, S.; Xu, X.Y.; Lin, G.P.; Shao, L.; Zhao, Y.; Wang, T.H. Effect of slow abdominal breathing combined with biofeedback on blood pressure and heart rate variability in prehypertension. *J. Altern. Complement. Med.* **2010**, *16*, 1039–1045. [[CrossRef](#)]
86. Nolan, R.P.; Kamath, M.V.; Floras, J.S.; Stanley, J.; Pang, C.; Picton, P.; Young, Q.R. Heart rate variability biofeedback as a behavioral neurocardiac intervention to enhance vagal heart rate control. *Am. Heart J.* **2005**, *149*, 1137. [[CrossRef](#)]
87. Seo, Y.; Yates, B.; LaFramboise, L.; Pozehl, B.; Norman, J.F.; Hertzog, M. A Home-Based Diaphragmatic Breathing Retraining in Rural Patients with Heart Failure. *West. J. Nurs. Res.* **2016**, *38*, 270–291. [[CrossRef](#)]
88. Sutbeyaz, S.T.; Koseoglu, F.; Inan, L.; Coskun, O. Respiratory muscle training improves cardiopulmonary function and exercise tolerance in subjects with subacute stroke: A randomized controlled trial. *Clin. Rehabil.* **2010**, *24*, 240–250. [[CrossRef](#)] [[PubMed](#)]
89. Eherer, A.J.; Netolitzky, F.; Högenauer, C.; Pusching, G.; Hinterleitner, T.A.; Scheidl, S.; Kraxner, W.; Krejs, G.J.; Hoffmann, K.M. Positive effect of abdominal breathing exercise on gastroesophageal reflux disease: A randomized, controlled study. *Am. J. Gastroenterol.* **2012**, *107*, 372–378. [[CrossRef](#)]
90. Kaushik, R.; Kaushik, R.M.; Mahajan, S.K.; Rajesh, V. Biofeedback assisted diaphragmatic breathing and systematic relaxation versus propranolol in long term prophylaxis of migraine. *Complement. Ther. Med.* **2005**, *13*, 165–174. [[CrossRef](#)]

91. Chen, Y.F.; Huang, X.Y.; Chien, C.H.; Cheng, J.F. The Effectiveness of Diaphragmatic Breathing Relaxation Training for Reducing Anxiety. *Perspect. Psychiatr. Care* **2017**, *53*, 329–336. [[CrossRef](#)]
92. Kavan, M.G.; Elsasser, G.; Barone, E.J. Generalized anxiety disorder: Practical assessment and management. *Am. Fam Physician* **2009**, *79*, 785–791. [[PubMed](#)]
93. Liu, C.J.; Tu, G.Y.; Lin, S.L.; Yeh, C.C. Comparisons of different breathing ratios of slow breathing among outpatients with anxiety disorders. *J. Med. Health* **2014**, *3*, 57–66.
94. Russell, M.E.; Hoffman, B.; Stromberg, S.; Carlson, C.R. Use of controlled diaphragmatic breathing for the management of motion sickness in a virtual reality environment. *Appl. Psychophysiol. Biofeedback* **2014**, *39*, 269–277. [[CrossRef](#)] [[PubMed](#)]
95. Gimenez, M.; Servera, E.; Abril, E.; Saavedra, P.; Darias, M.; Gomez, A.; Hannhart, B. Comprehensive directed breathing retraining improves exertional dyspnea for men with spirometry within normal limits. *Am. J. Phys. Med. Rehabil.* **2010**, *89*, 90–98. [[CrossRef](#)] [[PubMed](#)]
96. Cahalin, L.P.; Braga, M.; Matsuo, Y.; Hernandez, E.D. Efficacy of diaphragmatic breathing in persons with chronic obstructive pulmonary disease: A review of the literature. *J. Cardiopulm. Rehabil.* **2002**, *22*, 7–21. [[CrossRef](#)] [[PubMed](#)]
97. Dechman, G.; Wilson, C.R. Evidence underlying cardiopulmonary physical therapy in stable COPD. *Cardiopulmonary Phys. Ther. J.* **2002**, *13*, 20–22. [[CrossRef](#)]
98. Han, J.W.; Kim, Y.M. Effect of breathing exercises combined with dynamic upper extremity exercises on the pulmonary function of young adults. *J. Back Musculoskelet. Rehabil.* **2018**, *31*, 405–409. [[CrossRef](#)]
99. Bahenský, P.; Malátová, R.; Bunc, V. Changed dynamic ventilation parameters as a result of a breathing exercise intervention program. *J. Sports Med. Phys. Fit.* **2019**, *59*, 1369–1375. [[CrossRef](#)] [[PubMed](#)]
100. Sperlich, B.; Fricke, H.; de Marées, M.; Linville, J.W.; Mester, J. Does respiratory muscle training increase physical performance? *Mil. Med.* **2009**, *174*, 977–982. [[CrossRef](#)]
101. Riganas, C.S.; Vrabas, I.S.; Christoulas, K.; Mandroukas, K. Specific inspiratory muscle training does not improve performance or VO<sub>2</sub>max levels in well trained rowers. *J. Sports Med. Phys. Fit.* **2008**, *48*, 285–292.
102. Kolar, P.; Neuwirth, J.; Sanda, J.; Suchanek, V.; Svata, Z.; Volejnik, J.; Pivec, M. Analysis of diaphragm movement during tidal breathing and during its activation while breath holding using MRI synchronized with spirometry. *Physiol. Res.* **2009**, *58*, 383–392.
103. Russo, M.A.; Santarelli, D.M.; O'Rourke, D. The physiological effects of slow breathing in the healthy human. *Breathe* **2017**, *13*, 298–309. [[CrossRef](#)]
104. Bernardi, L.; Gabutti, A.; Porta, C.; Spicuzza, L. Slow breathing reduces chemoreflex response to hypoxia and hypercapnia, and increases baroreflex sensitivity. *J. Hypertens.* **2001**, *19*, 2221–2229. [[CrossRef](#)]
105. Bilo, G.; Revera, M.; Bussotti, M.; Bonacina, D.; Styczkiewicz, K.; Caldara, G.; Giglio, A.; Faini, A.; Giuliano, A.; Lombardi, C.; et al. Effects of slow deep breathing at high altitude on oxygen saturation, pulmonary and systemic hemodynamics. *PLoS ONE* **2012**, *7*, e49074. [[CrossRef](#)]
106. Billman, G.E. Heart rate variability—A historical perspective. *Front. Physiol.* **2011**, *2*, 86. [[CrossRef](#)] [[PubMed](#)]
107. Dick, T.E.; Mims, J.R.; Hsieh, Y.H.; Morris, K.F.; Wehrwein, E.A. Increased cardio-respiratory coupling evoked by slow deep breathing can persist in normal humans. *Respir. Physiol. Neurobiol.* **2014**, *204*, 99–111. [[CrossRef](#)]
108. Lee, J.S.; Lee, M.S.; Lee, J.Y.; Cornélissen, G.; Otsuka, K.; Halberg, F. Effects of diaphragmatic breathing on ambulatory blood pressure and heart rate. *Biomed. Pharmacother.* **2003**, *57* (Suppl. S1), 87s–91s. [[CrossRef](#)]
109. Chang, Q.; Liu, R.; Shen, Z. Effects of slow breathing rate on blood pressure and heart rate variabilities. *Int. J. Cardiol.* **2013**, *169*, e6–e8. [[CrossRef](#)] [[PubMed](#)]
110. Thayer, J.F.; Yamamoto, S.S.; Brosschot, J.F. The relationship of autonomic imbalance, heart rate variability and cardiovascular disease risk factors. *Int. J. Cardiol.* **2010**, *141*, 122–131. [[CrossRef](#)]
111. Villemure, C.; Čeko, M.; Cotton, V.A.; Bushnell, M.C. Neuroprotective effects of yoga practice: Age-, experience-, and frequency-dependent plasticity. *Front. Hum. Neurosci.* **2015**, *9*, 281. [[CrossRef](#)]
112. Jerath, R.; Crawford, M.W.; Barnes, V.A.; Harden, K. Self-regulation of breathing as a primary treatment for anxiety. *Appl. Psychophysiol. Biofeedback* **2015**, *40*, 107–115. [[CrossRef](#)] [[PubMed](#)]

113. Roi, G.S.; Mosconi, G.; Totti, V.; Angelini, M.L.; Brugin, E.; Sarto, P.; Merlo, L.; Sgarzi, S.; Stancari, M.; Todeschini, P.; et al. Renal function and physical fitness after 12-mo supervised training in kidney transplant recipients. *World J. Transplant.* **2018**, *8*, 13–22. [[CrossRef](#)] [[PubMed](#)]
114. Wickerson, L.; Rozenberg, D.; Janaudis-Ferreira, T.; Deliva, R.; Lo, V.; Beauchamp, G.; Helm, D.; Gottesman, C.; Mendes, P.; Vieira, L.; et al. Physical rehabilitation for lung transplant candidates and recipients: An evidence-informed clinical approach. *World J. Transplant.* **2016**, *6*, 517–531. [[CrossRef](#)] [[PubMed](#)]

**Publisher's Note:** MDPI stays neutral with regard to jurisdictional claims in published maps and institutional affiliations.



© 2020 by the author. Licensee MDPI, Basel, Switzerland. This article is an open access article distributed under the terms and conditions of the Creative Commons Attribution (CC BY) license (<http://creativecommons.org/licenses/by/4.0/>).





Review

# The Effects of Tai Chi and Qigong on Immune Responses: A Systematic Review and Meta-Analysis

Byeongsang Oh <sup>1,2,3,\*</sup>, Kyeore Bae <sup>1,4</sup>, Gillian Lamoury <sup>1,2,3</sup>, Thomas Eade <sup>1,2,3</sup>, Frances Boyle <sup>2,3</sup>, Brian Corless <sup>1</sup>, Stephen Clarke <sup>1,3</sup>, Albert Yeung <sup>5</sup>, David Rosenthal <sup>5</sup>, Lidia Schapira <sup>6</sup> and Michael Back <sup>1,2,3</sup>

<sup>1</sup> Northern Sydney Cancer Centre, Royal North Shore Hospital, St Leonards NSW 2065 Australia;

kyeorebae@gmail.com (K.B.); Gillian.Lamoury@health.nsw.gov.au (G.L.);

Thomas.Eade@health.nsw.gov.au (T.E.); bcorless@shoalhaven.net.au (B.C.);

stephen.clarke@sydney.edu.au (S.C.); michael.back@health.nsw.gov.au (M.B.)

<sup>2</sup> The Mater Hospital, North Sydney NSW 2060, Australia; franb@bigpond.net.au

<sup>3</sup> Sydney Medical School, University of Sydney, Sydney NSW 2060, Australia

<sup>4</sup> Center for Immunity and Pain, Kwanghye Hospital, Seoul 06174, Korea

<sup>5</sup> Harvard Medical School, Boston, MA 02115, USA; AYEUNG@mgh.harvard.edu (A.Y.);

drose@huhs.harvard.edu (D.R.)

<sup>6</sup> Stanford University School of Medicine, Stanford, CA 94305, USA; schapira@stanford.edu

\* Correspondence: byeong.oh@sydney.edu.au

Received: 21 June 2020; Accepted: 28 June 2020; Published: 30 June 2020

**Abstract: Background:** Effective preventative health interventions are essential to maintain well-being among healthcare professionals and the public, especially during times of health crises. Several studies have suggested that Tai Chi and Qigong (TQ) have positive impacts on the immune system and its response to inflammation. The aim of this review is to evaluate the current evidence of the effects of TQ on these parameters. **Methods:** Electronic searches were conducted on databases (Medline, PubMed, Embase and ScienceDirect). Searches were performed using the following keywords: “Tai Chi or Qigong” and “immune system, immune function, immunity, Immun\*, inflammation and cytokines”. Studies published as full-text randomized controlled trials (RCTs) in English were included. Estimates of change in the levels of immune cells and inflammatory biomarkers were pooled using a random-effects meta-analysis where randomised comparisons were available for TQ versus active controls and TQ versus non-active controls. **Results:** Nineteen RCTs were selected for review with a total of 1686 participants and a range of 32 to 252 participants within the studies. Overall, a random-effects meta-analysis found that, compared with control conditions, TQ has a significant small effect of increasing the levels of immune cells (SMD, 0.28; 95% CI, 0.13 to 0.43,  $p = 0.00$ ),  $I^2 = 45\%$ , but not a significant effect on reducing the levels of inflammation (SMD,  $-0.15$ ; 95% CI,  $-0.39$  to  $0.09$ ,  $p = 0.21$ ),  $I^2 = 85\%$ , as measured by the systemic inflammation biomarker C-reactive protein (CRP) and cell mediated biomarker cytokines. This difference in results is due to the bidirectional regulation of cytokines. An overall risk of bias assessment found three RCTs with a low risk of bias, six RCTs with some concerns of bias, and ten RCTs with a high risk of bias. **Conclusions:** Current evidence indicates that practising TQ has a physiologic impact on immune system functioning and inflammatory responses. Rigorous studies are needed to guide clinical guidelines and harness the power of TQ to promote health and wellbeing.

**Keywords:** Tai Chi; qigong; immune system; immunity; inflammation

## 1. Introduction

The effectiveness of the human immune system to prevent disease and aid recovery is critical [1]. Inflammation is an adaptive biological response of the immune system that can be triggered by several



factors, such as pathogens, damaged cells and toxic compounds [2,3]. In response to infection, immune cells produce pro-inflammatory cytokines [4] and suppress anti-inflammatory genes [5] as key elements of the pathogenic defense process. In the current COVID-19 pandemic, humanity is facing one of its greatest public health challenges with more physical and psychological demands placed on the immune system and a greater need for evidence-based healthy lifestyle interventions, such as increased physical activity, to support and maintain the integrity of immune functions [6]. Several studies have reported that older people with comorbid conditions are more likely to have more severe symptoms and a higher risk of mortality from COVID-19 infection compared to children or younger adults [7–9]. Older adults with chronic disease and diminished immune responses have been found to have an increased risk of infection [10].

Supporting this view, a recent case study demonstrated that robust immune responses were observed during clinical recovery from the COVID-19 virus in a middle aged healthy adult [11,12]. Other studies also reported that the total number of NK and CD8<sup>+</sup> T cells had decreased significantly in patients with SARS-CoV 2 infection [13] as a result of T cell infection by SARS-CoV 2 [14,15].

Recently, several studies have demonstrated that physical activity and meditation play a pivotal role in regulating inflammation and supporting immune function [16–19]. Consequently, general recommendations for a healthy lifestyle, including physical activities and meditation, have been made worldwide to help prevent disease, enhance immune function and improve global health and well-being [17,19]. Emerging evidence indicates that there are substantial benefits for practising Tai Chi and Qigong (TQ) for health and well-being. TQ, also known as moving meditation, is a classical mind-body exercise originating in China and has been utilised as a preventative health intervention for many centuries. TQ is the most common form of physical exercise among adults in China [20]. The 2012 US National Health Interview Survey (NHIS) data suggested that more than 7 million adults in the US practised TQ and its popularity is growing globally [21–23]. Reasons given for practicing TQ were to optimize overall health and well-being, prevent disease and prevent the progression of medical conditions [20,21]. Respondents who practice TQ indicated that the positive outcomes of practice were reduced levels of stress (83%) and improved overall health and well-being (74%) [21]. Recently, a number of systematic reviews and meta-analyses have demonstrated the positive impact of TQ on physical conditions such as arthritis [24], cancer [25], diabetes [26], falls prevention [27], fibromyalgia [28], osteoarthritis [29], chronic pain [24,30] and cognitive function [31]. Evidence also supports the psychological benefits of TQ, particularly for symptoms of anxiety and depression [32]. Furthermore, several descriptive reviews have examined the beneficial effects of mind-body interventions, i.e., TQ, yoga and meditation on immune function and immune system-related inflammatory biomarkers [33,34]. Another recent study conducted with healthy women demonstrated that TQ can change gene expression associated with inflammation (HSF1, HSPA1A, IL6, IL10, CCL2 and NF-kB mRNA) [35]. Although a number of studies have reviewed the effects of TQ on physical and psychological wellbeing [36,37], few studies have explored the effects of TQ on immunoregulatory responses. The aim of the current review is to assess the effects of TQ on immune function and immune system-related inflammatory biomarkers.

## 2. Methods

A systematic review and meta-analysis was conducted following the 2018 Preferred Reporting Items for Systematic Reviews and Meta-analyses (PRISMA) guidelines [38] for systematic reviews and meta-analyses. Electronic searches were conducted on four English databases (Medline, PubMed, Embase and ScienceDirect) from inception through to April 2020. Searches were performed using the following keywords: “Tai Chi or Qigong” and “immune system, immune function, immunity, Immun\*, inflammation and cytokines”. Additional searches were performed in Google Scholar. Eligibility criteria were: full-text studies published in English, RCTs with the primary outcome of immune response, sample size ( $n \geq 30$ ), and a TQ intervention period of at least four weeks. Interventions using qigong (QG) or emitting qi therapy by a qi master were excluded. Purely meditational techniques, such as Zen meditation, were excluded. Two reviewers (KB and BO) screened the titles and abstracts

and reviewed them for eligibility after reading the full-text. Additionally, searches were conducted for other potential studies by screening references in the identified studies.

### *2.1. Data Analysis*

Outcomes at the initial post-intervention assessment were summarised and compared by TQ intervention arms. Estimates of intervention effects on immune responses (change of immune cells and inflammatory biomarkers) were extracted and compared for randomised arms [intervention, active control (exercise or health education) or non-active control (usual care/daily activities/wait-list)]. A random-effects meta-analysis was used to compute pooled estimates allowing for variation.

Effect sizes were estimated from the difference between study group means divided by variances pooled from both treatment and control groups. Where necessary, known equations were used to calculate the effect sizes from the reported data [39,40]. Standardised mean differences (SMD, Hedge's  $g$ ) and 95% confidence intervals (CIs) were calculated.  $I^2$  was calculated to assess heterogeneity [40]. The outcomes of immune system and inflammatory-related biomarkers were reported in Table 1, and Figures 2–6. A negative SMD value indicated a greater decrease in biomarkers.

Table 1. Study characteristics of the 19 randomized clinical trials.

Author/Years/Reference	Population	Sample Size (% Female)	Mean Age (Range)	Intervention Duration, Type	Intervention Frequency, Style	Control Condition	Results
Yon et al. [41] 2019 China	Older adults with chronic pain	N = 40 (43%) TC (n = 19) CG (n = 21)	74 (65–87)	12 weeks; TC	60 min, 2 times/week, 8-form Yang style	Light physical exercise	↑ ↓ NS CRP NS IL-6 NS TNF-α
Sungkarat et al. [42] 2018 Thailand	Older adults with mild cognitive impairment	N = 56 (86%) TC (n = 29) CG (n = 27)	68	6 months; TC	50 min, 3 times/week, TC in-class for 9 sessions (3 times per week for 3 weeks) plus practice at home 3 times a week with video, 10 forms TC	Health Education	NS TNF-α NS IL-10
Liu et al. [43] 2017 Hong Kong	Women with breast cancer	N = 158 (100%) QG (n = 50) CG (n = 51)	51 (21–80)	24 weeks; QG	60 min session, 2 times/week for 24 weeks, Guolin-Qigong	Stretching exercise	NS IL-2 NS IFN-γ ↑ TNF-α (95% CI, 0.48–3.41, <i>p</i> < 0.03)
Vera et al. [44] 2016 Spain	College students	N = 43 (79%) QQ (n = 23) CG (n = 18)	(18–21)	4 weeks; QG	25–30 min, 3 times/week In total 20 qigong sessions, Taoist QG	Daily activities	↑ Number of B lymphocytes ( <i>p</i> = 0.006) ↑ % of B lymphocytes ( <i>p</i> = 0.006) ↓ % NK ( <i>p</i> = 0.05) NS Number of NK NS Neutrophils, NS Monocytes, NS Eosinophils,
Robins et al. [45] 2016 USA	Women with high risk of cardiovascular disease	N = 96 (100%) TC (n = 47) CG (n = 49)	43 (35–50)	8 weeks; TC	60 min, 1/week, TC (short form)	Wait-list control	↓ TNF-α ( <i>p</i> < 0.002) ↓ IFN-γ ( <i>p</i> < 0.002) ↓ IL 8 ( <i>p</i> < 0.026) ↓ IL-4 ( <i>p</i> < 0.001) Result not reported (IL-1β, IL-2, IL-10, IL-12, IL-6, GCSE, CRP)
Campo et al. [46] 2015 USA	Older female cancer survivors	N = 63 (100%) TC (n = 29) CG (n = 25)	67	12 weeks; TC	60 min, 3 times/week, TC (19 movements)	Health education	NS IL-6 NS IL-12 NS TNF-α NS IL-4 NS IL-10

Table 1. *Cont.*

Author/Years/Reference	Population	Sample Size (% Female)	Mean Age (Range)	Intervention Duration, Type	Intervention Frequency, Style	Control Condition	Results
Irwin et al. [47,48] 2015 and 2014 USA	Older adults with insomnia	N = 123 (73%) TC (n = 48) CBT (n = 50) CG (n = 25)	65 (55–85)	16 weeks; TC	120 min, 1/week, TC	Health education, CBT	<p>↓ CRP (n = 0.06)</p> <p>↓ % monocytes producing IL-6 (p &lt; 0.01)</p> <p>↓ % monocytes producing TNF-α (p &lt; 0.01)</p> <p>↓ % monocytes co-producing TNF-α and IL-6 (p &lt; 0.01) at different time points</p> <p>↓ Pro-inflammatory gene expression (NF-κB, IRF+, AP-1) (month 4, p &lt; 0.001).</p>
Liu et al. [49] 2015 Wang et al. [50] 2013 Zhang et al. [51] 2013 China	Lung cancer survivors	N = 32 (50%) TC (n = 16) CG (n = 16)	61	16-weeks; TC	60 min, 3 times/week, Yang style 24-form	Daily activities	<p>↑ NKT cells (p &lt; 0.05)</p> <p>↑ % NKT cells (p &lt; 0.05)</p> <p>NS NK cells</p> <p>NS % NK cells</p> <p>NS DC 123c cells</p> <p>% of DC 123c cells</p> <p>↑ DC11c cells (p &lt; 0.01)</p> <p>NS % DC11c cells</p> <p>T lymphocyte cells (T1) and (T2)</p> <p>↑ T1/T2 ratio (p &lt; 0.01)</p> <p>↑ Tc1/Tc2 ratios (p &lt; 0.01)</p> <p>NS TH1/TH2 ratio</p> <p>↓ T2 (p &lt; 0.001)</p> <p>↓ Tc2 (p &lt; 0.003)</p> <p>↑ Th2 (p &lt; 0.025)</p> <p>↓ CD55 (p &lt; 0.05)</p> <p>NS T-helper/T-suppressor (CD4<sup>+</sup>/CD8<sup>+</sup> ratio)</p> <p>NS CD59 expression</p>
Irwin et al. [52] 2014 USA	Breast cancer survivors with insomnia	N = 90 (100%) TC (n = 45) CG (n = 45)	59 (42–83)	12 weeks; TC	120 min, 1/week, TC	CBT	<p>NS CRP</p> <p>↓ % monocytes producing IL-6 (p = 0.07)</p> <p>↓ % monocytes producing TNF-α (p &lt; 0.05)</p> <p>↓ % monocytes coproducing TNF-α and IL-6 (p &lt; 0.02)</p> <p>↓ Proinflammatory mediators (NF-κB) (p = 0.001)</p>

Table 1. *Contd.*

Author/Years/Reference	Population	Sample Size (% Female)	Mean Age (Range)	Intervention Duration, Type	Intervention Frequency, Style	Control Condition	Results
Liu et al. [53] 2012 China	Healthy middle-aged and older women	N = 60 TC (n = 30) CG (n = 30)	54 (50–65)	6 months; TC (24 forms and 42 Sword forms)	60 min, 4 times/week TC (24 forms and 42 Sword forms)	Daily activities	↑ % of CD4+ T lymphocytes ( $p < 0.05$ ) NS CD3 NS CD8+ ↑ CD4+CD8+ ratio ( $p < 0.05$ ) ↑ % of NK cell ( $p < 0.05$ ) ↑ % of NKT cells ( $p < 0.05$ ) ↑ TNF- $\gamma$ ( $p < 0.05$ )
Irwin et al. [54,55] 2007 and 2012 USA	Healthy older adults with history of varicella	N = 112 (61%) TC (n = 59) CG (n = 53)	70 (59–86)	16 weeks; TC	40 min, 3 times/week for a total of 120 min, TC with 20 movements	Health education	↑ % of CD123+ DCs ( $p < 0.01$ ) ↑ % of CD11c+ DCs ( $p < 0.01$ ) ↑ Levels of VZV-CMI ( $p < 0.05$ ) NS IL-6 ( $p = 0.06$ ) NS IL-18 NS CRP NS sIL-1RA NS sIL-6R NS sICAM,
Oh et al. [56,57] 2012 and 2012 Australia	Cancer survivors	N = 162 (57%) TC (n = 79) CG (n = 83)	60 (31–86)	10 weeks; QG	90 min, 2 times/week + individual practice recommended for 30 min per day, Medical QG	Usual Care	↓ CRP ( $p < 0.044$ )
Lavretsky et al. [58] 2011 USA	Older adults with major depression	N = 73 (62%) TC (n = 36) CG (n = 37)	71	10 weeks; TC	120 min, 1 times/week TC Chih	Health education	↓ CRP ( $p < 0.05$ )
Wang et al. [59] 2011, China	Healthy sedentary female college students	N = 60 (100%) TC (n = 30) CG (n = 30)	19	12 weeks; TC	45 min, 5 times/week; TC 24 standardized movements	Daily activities	NS IgG NS IgA NS IgM NS (CD3, CD4+, CD8+) NS IFN- $\gamma$ NS IL-4 NS IL-12
Chen et al. [60] 2010 Taiwan	Adults with diagnosis of Type II diabetes and BMI 30–35	N = 104 (43%) TC (n = 56) CG (n = 48)	58	12 weeks; TC	60 min, 3 times/week; Chen-style 99-form	Conventional aerobic exercise	↓ CRP ( $p < 0.014$ )

Table 1. *Cont.*

Author/Years/Reference	Population	Sample Size (% Female)	Mean Age (Range)	Intervention Duration, Type	Intervention Frequency, Style	Control Condition	Results
Manzanaque et al. [61] 2009 Spain	Healthy college students	N = 39 (87%) QG (n = 21) CG (n = 18)	18–21	4 weeks; QG	30 min, 3 times/week; Ba Duan Jin Qg	Daily activities	↑ ↓ NS TNF-α NS IFN-γ
McCain et al. [62] 2008 USA	Adults with diagnosis of HIV	N = 252 (40%) TC (n = 62) RLXN (n = 65) SPRT (n = 68) CG (n = 57)	42	10 weeks; TC	90 min, 1 time/week; Focused short form TC training with 8 movements	Wait-list control	NS CD4+, CD8+, and CD57+ T lymphocytes; NS NK cytotoxicity NS Lymphocyte proliferation NS TNF-α NS IFN-γ NS IL-2 NS IL-4 NS IL-6 NS IL-10
Chen et al. [63] 2006 Taiwan	Healthy middle-aged women with BMD T scores ≥ -2.5	N = 87 (100%) QG (n = 44) CG (n = 43)	45 (35–60)	12 weeks; QG	3 times/week; Ba Duan Jin Qg 8 sections	Daily activities	↓ IL-6 (p < 0.001)
Irwin et al. [64] 2003 USA	Healthy older adults with history of varicella	N = 36 (72%) TC (n = 18) CG (n = 18)	70	15 weeks; TC	45 min, 3 times/week for a total of 45 sessions; TC with 20 standardized movements	Wait-list control (maintenance of routine activities)	↑ Levels of VZV-CMI (p < 0.05)

Abbreviations: IL-2: interleukin-2, IFN-γ: interferon-γ, TNF-α: tumor necrosis factor-α, CRP: C-reactive protein, IL-1: interleukin-1, IL-4: interleukin-4, IL-6: interleukin-6, IL-10: interleukin-10, IL-18: interleukin-18, sIL-1RA: soluble IL-1 receptor antagonist, sIL-6R: soluble IL-6 receptor, sICAM: soluble intercellular adhesion molecule, VZV-RFC: varicella zoster virus responder cell frequency, IgG: Immunoglobulin G, IgM: Immunoglobulin M, NK: natural killer cell; NKT: natural killer T cell; DC: Dendritic cells, CRP-C-reactive protein, IL-1ra: interleukin 1 receptor antagonist, RLXN: relaxation training, SPRT: spiritual growth groups, CBT: Cognitive Behavioural Therapy, GLQG: Guolin Qigong, TC: Tai Chi, QG: Qigong, TG: Tai Chi and Qigong, CG: Control group, NS: Not significant, ↑: increase, ↓: decrease.

## 2.2. Quality Assessment of Original Papers

Risk of Bias (RoB) Assessment: To adequately assess RoB of the included RCTs, two reviewers independently assessed the RoB using the Cochrane Collaboration’s tool for assessing RoB version 2 (RoB 2) [65]. The Cochrane Collaboration tool RoB2 consists of six domains: “randomization process”, “deviations from intended interventions”, “missing outcome data”, “measurement of the outcome”, “selection of the reported result”, and “overall bias”. Any disagreement between the two reviewers was resolved through discussion.

## 3. Results

A total of 969 studies were initially identified and screened in this literature search. After an in-depth evaluation of screening titles and abstracts, 53 articles remained for assessment of eligibility to be included in the review. Nineteen studies were included in the review (Figure 1). Seventeen studies were included in the meta-analyses.

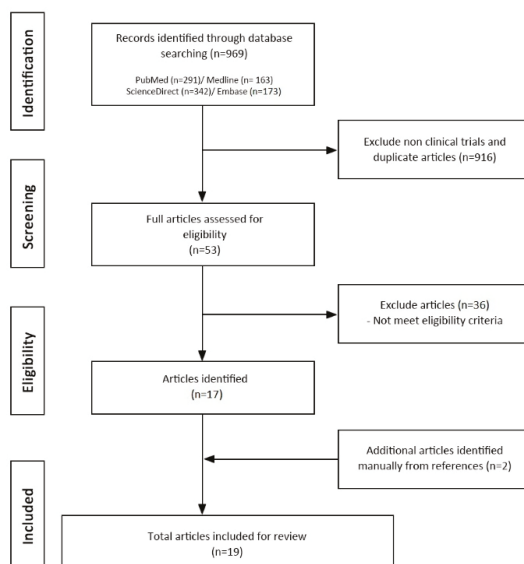


Figure 1. Flow chart.

### 3.1. Characteristics of Clinical Studies and Quality of Evidence

In the nineteen RCTs [Tai Chi (n = 14) and Qigong (n = 5)], there were a total of 1686 participants with an age range 18 to 87 years, and a sample size range of 32 to 252 participants within the studies, of which 775 were in the intervention groups and 911 in the control groups (Table 1). Studies were conducted across several countries viz. USA (n = 8), China (n = 4), Taiwan (n = 2), Australia (n = 1), Spain (n = 2), and one each were from Hong Kong and Thailand. Participants in the studies were categorised as cancer survivors (n = 5), older adults with a history of varicella (n = 2), healthy college students (n = 3), healthy older adults (n = 2), and a further seven studies with older adults with chronic neck pain (n = 1), mild cognitive impairment (n = 1), cardiovascular disease, (n = 1), diabetes (n = 1), insomnia (n = 1), HIV (n = 1), and depression (n = 1). Seventeen studies were designed with two arms while one study was conducted with three arms (TC vs. CBT vs. Health education) and one with four arms (TC vs. relaxation vs. spiritual growth vs. wait-list), respectively. In the control group conditions, physical exercise (n = 3), health education (n = 4) and/or CBT (n = 2), wait-list group (n = 2), and usual care and daily activities (n = 9) were used. The TQ intervention period varied from 4 weeks to

6 months and included periods of 4 weeks (n = 2), 8 weeks (n = 1), 10 weeks (n = 3), 12 weeks (n = 6), 15 weeks (n = 1), 16 weeks (n = 3) and 6 months (n = 3). The number of intervention sessions ranged from one to five times per week, with session frequencies of once per week (n = 5), two sessions per week (n = 3), three sessions per week (n = 9), and one study each with four sessions per week and five sessions per week, respectively. The majority of studies used an intervention time of 60 min (n = 7), whereas other intervention times comprised 30 to 50 min (n = 6), 90 min (n = 2), 120 min (n = 3) and 1 study did not report an intervention time.

### 3.2. Outcomes on the Immune System and Inflammation Associated Biomarkers

The effects of TQ interventions on the selected immune system outcomes and inflammatory biomarkers are reported in Figures 2–6. Meta-analysis data are presented as SMD (95% CI) unless otherwise stated.

#### 3.3. Outcomes on the Immune System

Overall, a random-effects meta-analysis found that TQ had a significant small effect of increasing the levels of immune cells (SMD, 0.28; 95% CI, 0.13 to 0.43,  $p < 0.01$ ,  $I^2 = 45\%$ ) (Figure 2).

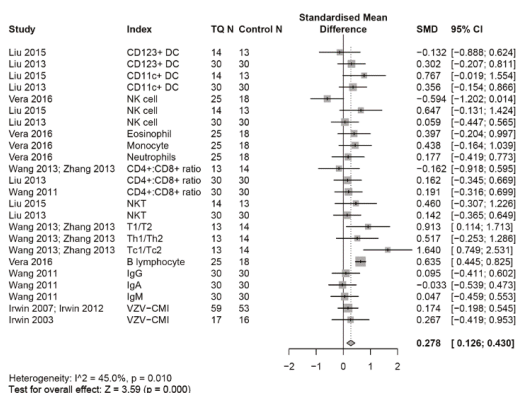


Figure 2. Forest plot for random-effects meta-analysis of the effects of TQ on the immune system.

#### 3.4. Effects on the Innate Immune System

Overall, a random-effects meta-analysis found that TQ had a small effect of increasing the levels of innate immune cells compared with controls (SMD, 0.22; 95% CI, -0.00 to 0.45,  $p = 0.05$ ,  $I^2 = 27\%$ ), with no significant heterogeneity across the studies (Figure 3A).

##### 3.4.1. NK Cells

A meta-analysis performed with three studies showed that there were no significant effects for the levels of NK cells (SMD, 0.00; 95% CI, -0.64 to 0.64,  $p = 0.99$ ,  $I^2 = 68\%$ ), (Figure 3B). Despite two studies reporting positive trends on NK cells, one study showed significant decreases in NK cells which may offset the effect size.

##### 3.4.2. Dendritic Cells (DCs)

There were significant small effects on DCs (SMD, 0.32; 95% CI, 0.02 to 0.62,  $p = 0.04$ ) in favour of TQ compared to control groups (Figure 3C).



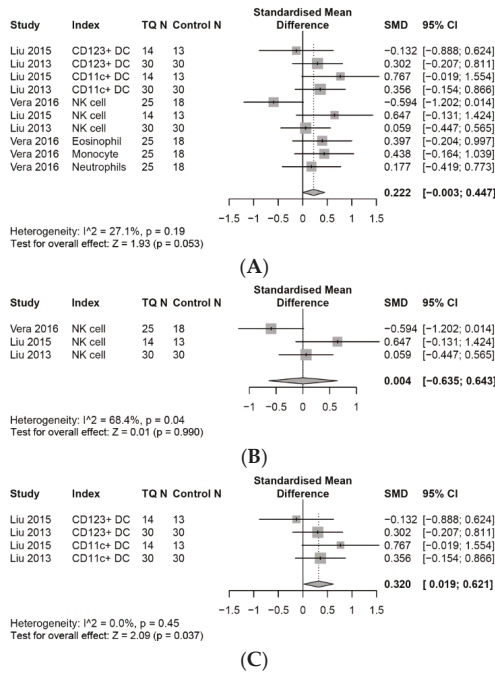


**Figure 3.** Forest plot for random-effects meta-analysis of the effects of TQ on the innate immune system. (A): The effects on the innate immune system, (B): the effects on the NK cells, (C): the effects on the DCs.

3.5. Other Innate Immune Cells

A meta-analysis of one study which examined innate immune cells showed that TQ had a small effect of increasing the levels of eosinophils (SMD, 0.40; 95% CI, -0.20 to 1.00), monocytes (SMD, 0.44; 95% CI, -0.16 to 1.04), and a marginally small effect on neutrophils (SMD, 0.18; 95% CI, -0.42 to 0.77), compared with daily activities.

3.6. Effects on the Adaptive Immune System

3.6.1. Adaptive Immune Cells

Overall, a random-effects meta-analysis found that TQ had a small effect of increasing the levels of adaptive immune cells compared with controls (SMD, 0.31; 95% CI, 0.11 to 0.51,  $p = 0.01$ ),  $I^2 = 52\%$ , with low to moderate heterogeneity across studies (Figure 4A–D).

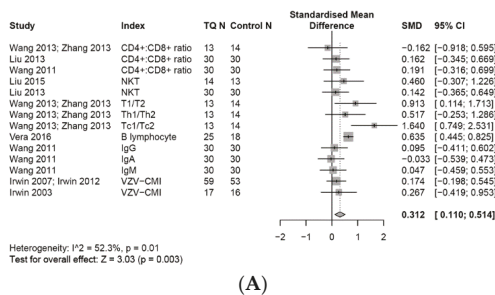


**Figure 4.** Cont.

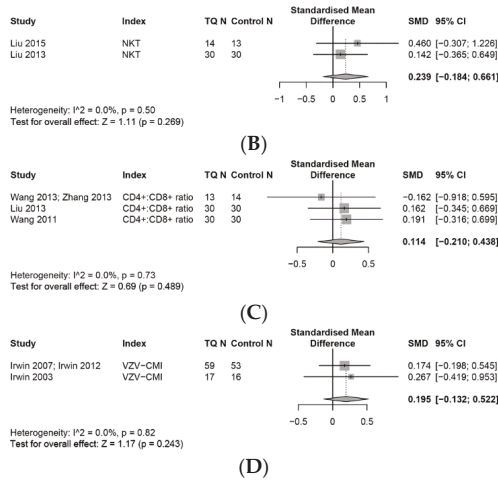


**Figure 4.** Forest plot for random-effects meta-analysis of the effects of TQ on the adaptive immune system. (A): The effects on the adaptive immune system, (B): the effects on the NKT cells, (C): the effects on the CD4+/CD8+ ratio, (D): the effects on the VZV-cell-mediated immunity.

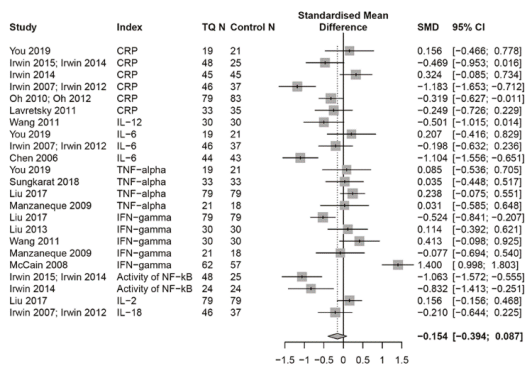
### 3.6.2. T Cell Associated Adaptive Immune Cells

A meta-analysis showed that TQ had a small but non-significant effect of increasing levels of NKT cells (SMD 0.24, 95% CI, -0.18 to 0.66,  $p = 0.27$ ), a moderate effect on the Th1/Th2 ratio (SMD, 0.52; 95% CI, -0.25 to 1.29), and a significant large effect on the Tc1/Tc2 ratio (SMD, 1.64; 95% CI, 0.75 to 2.53), compared with daily activities. Also, there was a small non-significant effect on the CD4+/CD8+ ratio (SMD, 0.11, 95% CI: -0.21 to 0.44,  $p = 0.49$ ).

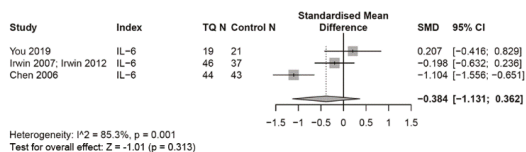
Other adaptive immune cell responses associated with the biomarker B lymphocytes showed a significant moderate effect for TQ increasing the proportion of B lymphocytes (SMD, 0.64; 95% CI, 0.45 to 0.83), but there were negligible effects for immunoglobulin antibodies IgA (SMD, -0.03; 95% CI, -0.54 to 0.47), IgG (SMD, 0.10; 95% CI, -0.41 to 0.60), and IgM (SMD, 0.05; 95% CI, -0.46 to 0.55), when compared with a health education control group. (Figure 4A–C). For VZV-cell-mediated immunity, two RCTs measured VZV responder cell frequency (VZV-RCF) compared with daily activity and health education controls. A meta-analysis found that TQ had a small effect (SMD, 0.20; 95% CI, -0.13 to 0.52),  $I^2 = 0\%$ , of elevating VZV-RCF (Figure 4D).

### 3.7. Effects on the Inflammation Response

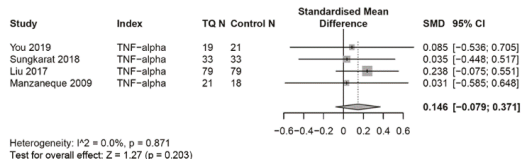
Overall, a random-effects meta-analysis indicated that TQ had no significant effects on responses to inflammation (SMD, -0.15; 95% CI, -0.39 to 0.09,  $p = 0.21$ ,  $I^2 = 85\%$ ), as measured by the systemic inflammation biomarker CRP, the cell mediated biomarker cytokines (IL1 $\beta$ , IL2, IL4, IL6, IL10, IL12, IL18, TNF- $\alpha$ , INF- $\gamma$ , GCSF) and NF- $\kappa$ B, compared with controls, due to several bidirectional cytokine responses. However, sub-group analyses showed TQ had positive trend on levels of CRP, IL6 and NF- $\kappa$ B, separately (Figure 5A–E).



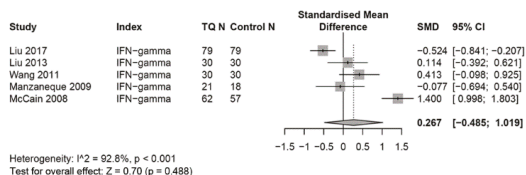
(A)



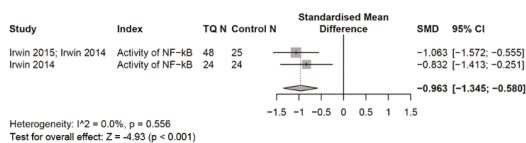
(B)



(C)



(D)



(E)

**Figure 5.** Forest plot for random-effects meta-analysis of the effects of TQ on the inflammation response. (A): The effects on the inflammation response, (B): the effects on the levels of IL6, (C): the effects on the levels of TNF- $\alpha$ , (D): the effects on the levels of IFN- $\gamma$ , (E): the effects on the activity of NF- $\kappa$ B.

### 3.7.1. CRP

A meta-analysis conducted with six studies suggested that TQ had a small effect of reducing CRP compared with control groups (SMD,  $-0.30$ ; 95% CI,  $-0.70$  to  $0.11$ ,  $p = 0.16$ ,  $I^2 = 80\%$ ). Furthermore, a subgroup analysis (Figure 6A,B) of the effect of TQ on CRP, with different control conditions (TQ vs. health education control, TQ vs. exercise control, TQ vs. inactive control, TQ vs. CBT), showed that studies that compared TQ with “health education” resulted in a moderate effect (SMD  $-0.64$ , 95% CI,  $-1.19$  to  $-0.08$ ,  $I^2 = 76\%$ ), of reducing CRP, and with “inactive (usual care)” resulted in a small effect (SMD,  $-0.32$ ; 95% CI,  $-0.63$  to  $-0.01$ ) of reducing CRP. In contrast, a study that compared TQ with an “exercise” group, demonstrated non-significant effects (SMD,  $0.16$ ; 95% CI,  $-0.47$  to  $0.78$ ), and another study comparing TQ with “Cognitive Behavioural Therapy (CBT)” showed a small effect of increasing CRP (SMD,  $0.32$ ; 95% CI,  $-0.09$  to  $0.73$ ).

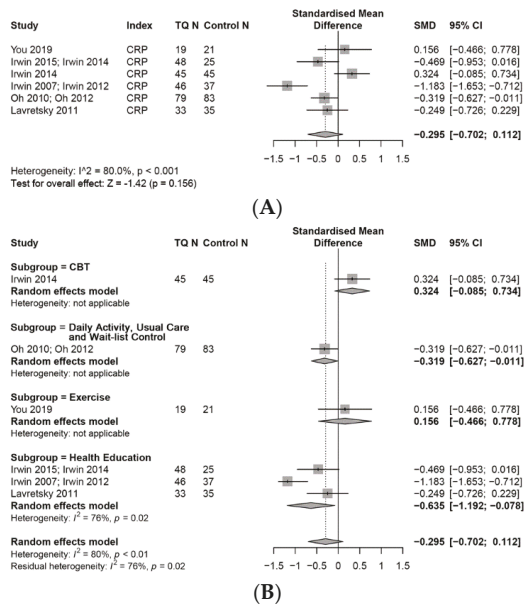


**Figure 6.** Forest plot for random-effects meta-analysis of the effects of TQ on levels of CRP. (A): The effects on the levels of CRP, (B): subgroup analysis of CRP based on control interventions.

### 3.7.2. IL-6

A meta-analysis of three studies suggested that, compared to controls, TQ had a small effect of reducing the levels of IL-6 (SMD,  $-0.38$ ; 95% CI,  $-0.13$  to  $0.36$ ,  $I^2 = 85\%$ ). Of these three studies, one study showed that TQ increased the levels of IL-6, while another two studies showed reduced IL-6 levels following a TQ intervention.

### 3.7.3. TNF- $\alpha$

A meta-analysis of four RCTs found that TQ had a negligible effect on levels of TNF- $\alpha$  compared with controls (SMD,  $0.15$ ; 95% CI,  $-0.08$  to  $0.37$ ,  $I^2 = 0\%$ ).

### 3.7.4. INF- $\gamma$

A meta-analysis of five RCTs showed that TQ had a small effect of increasing the level of INF- $\gamma$  (SMD,  $0.27$ ; 95% CI,  $-0.49$  to  $1.02$ ,  $I^2 = 93\%$ ). This result may have been influenced by considerable heterogeneity.

### 3.7.5. Effects on Other Pro-Inflammatory Biomarkers

A meta-analysis conducted on one study showed a non-significant effect of TQ on levels of IL-2 (SMD, 0.16; 95% CI, -0.16 to 0.47) when compared with controls, whereas another study showed a small effect of TQ on levels of IL-18 (SMD, -0.21; 95% CI, -0.64 to 0.23), and a third study showed a moderate effect for TQ on IL-12 (SMD, -0.50; 95% CI, -1.02 to 0.01). Another meta-analysis found larger effects in favour to TQ on levels of NF-κB (SMD, -0.96; 95% CI, -1.35 to -0.58).

### 3.8. Effects on Anti-Inflammatory Biomarkers

#### IL-4

A meta-analysis conducted on two studies suggests that TQ had no significant effect on levels of IL-4 (SMD, 0.03; 95% CI, -0.33 to 0.39,  $I^2 = 0%$ ), when compared with controls (data not presented).

### 3.9. Assessment of Risk of Bias

A RoB assessment was conducted with a revised tool (RoB 2) [65], to examine randomization process, deviations from intended interventions, missing outcome data, measurement of the outcome, selection of the reported result, and overall bias. In an overall assessment of bias, three RCTs were assessed as having a low RoB, six RCTs with some RoB concerns and ten RCTs with high RoB. In the domain of “measurement of the outcome” all of the reviewed RCTs have low RoB, whereas in domain of “missing outcome data” the majority of reviewed studies displayed high RoB. Individual scores for RoB are presented in Figure 7.

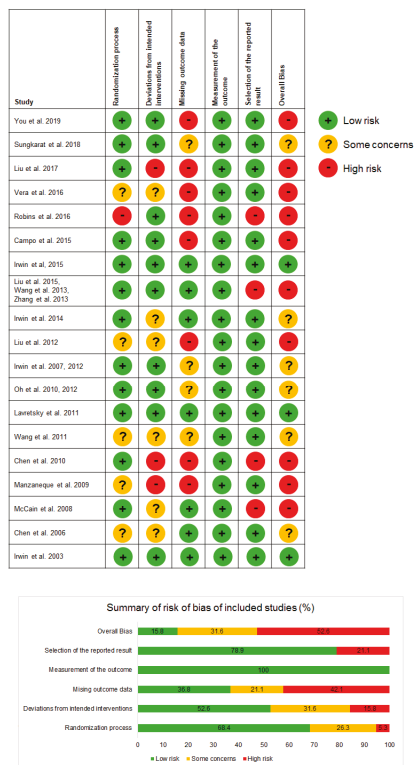


Figure 7. Risk of bias assessment.

#### 4. Discussion

In this systematic review and meta-analysis of nineteen RCTs that examined the effects of TQ on the immune system and inflammation, we found that TQ is capable of modulating immune system functioning and inflammatory biomarker responses. An important finding of the current review was that a minimum of 4 weeks practice of TQ enables participants to enhance their immune system functioning by stimulating innate and adaptive immune cell responses and regulating biomarkers associated with inflammation. In addition, we found two studies that showed that practising TQ for more than 12 weeks can alter gene expression, as demonstrated in NF- $\kappa$ B signal pathways.

Our findings are comparable with similar studies that assessed the effect of mind-body therapies using mixed interventions including meditation, Yoga and TQ [33,66]. Prior reviews that examined the effect of TQ on immunity and inflammation have reported no strong evidence of a favorable effect of TQ on inflammation [67] and the immune system [68] and insufficient evidence to support the clinical application of TQ to reduce infection [68,69]. These earlier reviews included fewer RCTs, and non-RCT studies, and a less comprehensive literature search which limits the conclusions made.

Another important aspect of the present review is that, to the best of our knowledge, this is the first comprehensive systematic review specifically evaluating the effects of TQ on the immune system and inflammatory biomarker responses. In order to assess the effect of TQ on the immune system and inflammation, immune related cell types were categorized into two groups, viz. innate immune cells and adaptive immune cells, and inflammatory biomarkers into three groups, viz. the systemic inflammatory biomarker CRP, cytokines and gene expression associated with pro-inflammatory processes. Of the nineteen reviewed RCTs, four studies measured innate immune cells (eosinophils, monocytes, neutrophils, NK and dendritic cells), six studies measured adaptive immune cells (T cells, NKT, and B cells), and four studies measured both. Overall, a random-effects meta-analysis found that TQ had a significant small effect of increasing the levels of immune cells (SMD, 0.28; 95% CI, 0.13 to 0.43,  $p < 0.01$ ,  $I^2 = 45\%$ ), compared to controls. The effect of TQ on inflammation is measured commonly by levels of the inflammatory biomarkers CRP, IL6 and TNF- $\alpha$ . In general, the levels of CRP decreased following a TQ intervention. Of the eight studies measuring CRP, four studies reported that TQ significantly decreased levels of CRP compared to controls, whereas three studies conducted with older adults with symptoms of chronic ill-health (pain, insomnia and older adults with history of varicella) showed no differences between the intervention and control groups (Table 1). Considering that CRP is a commonly used diagnostic marker of systemic inflammation, non-significant changes in levels of CRP may be associated with the progression of the chronic disease in these older participants. Given these mixed results, further investigation of this aspect, with a homogeneous study population, is warranted. In addition to CRP, cell mediated inflammatory cytokines (IL6, TNF- $\alpha$ ) were also found to demonstrate an overall trend of reduced levels following the TQ intervention. However, for inflammatory cytokines (IL2, IL4, IL6, IL10, IL12, TNF- $\alpha$ , INF- $\gamma$ ) both downregulation and upregulation of cytokine responses were observed across the studies.

These bidirectional results for inflammatory cytokines are consistent with the results of recent studies that examined cytokine levels following mind-body therapies [33,66] and exercise [70] interventions, that also included TQ. Several studies have suggested that increases in inflammatory cytokines are not only in response to immune system activation or infection, but also can occur when immune cells are stimulated to activate cytotoxicity [71,72]. For example, a review paper on pro-inflammatory and anti-inflammatory processes in patients with multiple myeloma, examined the effects of locally produced cytokines, as a primary immune response, and found that efficacious tumour immunosurveillance due to tumour-specific CD4<sup>+</sup> T cells was consistently related to increased local concentrations of both proinflammatory (IL-6, IL-1 $\alpha$ , and IL-1 $\beta$ ) and Th1-associated cytokines (IL-2, IL-12, and IFN- $\gamma$ ) [71]. It was concluded that the influence of cytokines on the immune system occurs as parallel processes and that changes in one specific cytokine can be balanced by others within the cytokine system, leading to a modulation of the immune response. In light of the current findings of a bidirectional response of inflammatory cytokines, additional clinical trials with a homogeneous

study population will help to better understand the directional nature of the relationship between inflammation and immunity. Despite these mixed results in outcomes for inflammatory responses, as measured by levels of CRP, cytokines, and NF- $\kappa$ B, overall, there were trends towards reduced levels of inflammation compared with control conditions.

Several limitations were identified in the current study. Firstly, caution is required in interpreting the overall random effect size on immune cells (SMD, 0.28; 95% CI, 0.13 to 0.43) and inflammation responses (SMD,  $-0.15$ ; 95% CI,  $-0.39$  to 0.09). Studies included in this review measured changes in a range of immune system and inflammatory biomarkers, rather than changes in a single identical biomarker in each study, thus confounding assumptions for independent variables associated with confidence intervals and heterogeneity in the meta-analysis.

Secondly, the demographic profile of participants in the original studies included in this review were heterogeneous in respect of age, ranging from 18 to 89 years, and health status viz. from healthy to various symptoms of medical conditions, which limit the generalizability of our findings. Furthermore, the TQ interventions that were examined were heterogeneous in respect of duration (from 4 weeks to 6 months), frequency (one to five times per week) and type of TQ intervention. Considering the heterogeneity of these studies, future investigations into the modulatory effects on immune responses of different types of TQ interventions and their dosage levels will be worthwhile. For example, one study was conducted with a TQ intervention duration of 4 weeks and a frequency of three sessions per week, whereas the duration of other studies varied from 4 weeks to 24 weeks with frequencies ranging from one session to five sessions per week. However, at present there is no standardised protocol to inform healthcare professionals and the general public on the minimum dosage levels of TQ required to modulate immune responses [73]. Finally, the current review did not investigate the physiological mechanisms underlying the effects of TQ on immune responses, despite previous studies attempting to explain these potential mechanisms in mind-body medicine and psychoneuroimmunology models [33]. Given the complexity of TQ as a movement-based mind-body therapy, compared with other mind-body therapies that have less movement components, investigating these underlying TQ mechanisms will provide important insights into future clinical applications. Moreover, some recent RCTs comparing TQ with exercise or CBT have suggested that there were no significant differences in outcomes between the intervention groups, indicating that TQ may be equivalent to conventional exercise or CBT interventions. However, more studies with robust study designs and adequate statistical power are required. Considering that the immune system is vital for protection from external pathogens, including bacterial and viral pathogens often occurring in the natural environment, the evidence supporting TQ for a healthier immune system, can have important implications for promoting TQ programs for health and well-being. Recommending TQ programs for people with low immunity, particularly those receiving treatment that induces immune suppression and older adults with chronic diseases, could have a beneficial effect of strengthening immune function. More clinical outcome studies are required to examine TQ as a stand-alone or adjunctive intervention for these patients and its effects on comparative rates of recovery. For the general public, TQ offers a preventative health measure that can strengthen the immune system and assist overall health and well-being.

In conclusion, despite several limitations, the current review of RCTs indicates that practising TQ can have a positive impact on immune system functioning and inflammatory processes. Given the vital role of the immune system, and in particular the influence of cytokines, in the current viral pandemic, preventative public health strategies to improve immune functioning in the general public, and those with medical conditions, are needed. However, while the promotion of TQ to the general public and healthcare professionals as a preventative health intervention for strengthening the immune system is recommended, further robust studies to develop clinical practice guidelines for using TQ with vulnerable populations is warranted.

**Author Contributions:** All authors cooperated on developing the concept design and preparing the manuscript. B.O. and K.B. had full access to the study data and take responsibility for the integrity and accuracy of data analysis. Statistical analysis and interpretation of data: K.B., B.C., B.O. Drafting of the manuscript: K.B., B.O. and

B.C. Critical revision of the manuscript for important intellectual content: B.O., K.B., G.L., T.E., F.B., B.C., S.C., A.Y., D.R., L.S., M.B. All authors have read and agreed to the published version of the manuscript.

**Funding:** This research received no external funding.

**Conflicts of Interest:** The authors declare that the research was conducted in the absence of any commercial or financial relationships that could be construed as a potential conflict of interest.

## References

1. Bennett, J.M.; Reeves, G.; Billman, G.E.; Sturmburg, J.P. Inflammation-Nature's way to efficiently respond to all types of challenges: Implications for understanding and managing "the epidemic" of chronic Diseases. *Front. Med.* **2018**, *5*, 316. [[CrossRef](#)] [[PubMed](#)]
2. Chen, L.; Deng, H.; Cui, H.; Fang, J.; Zuo, Z.; Deng, J.; Li, Y.; Wang, X.; Zhao, L. Inflammatory responses and inflammation-associated diseases in organs. *Oncotarget* **2017**, *9*, 7204–7218. [[CrossRef](#)] [[PubMed](#)]
3. Kritas, S.K.; Ronconi, G.; Caraffa, A.L.; Gallenga, C.E.; Ross, R.; Conti, P. Mast cells contribute to coronavirus-induced inflammation: New anti-inflammatory strategy. *J. Biol. Regul. Homeost Agents* **2020**, *34*, 10–23812.
4. Zhang, W.; Zhao, Y.; Zhang, F.; Wang, Q.; Li, T.; Liu, Z.; Wang, J.; Qin, Y.; Zhang, X.; Yan, X.; et al. The use of anti-inflammatory drugs in the treatment of people with severe coronavirus disease 2019 (COVID-19): The Perspectives of clinical immunologists from China. *Clin. Immunol.* **2020**, *214*, 108393. [[CrossRef](#)]
5. Dantzer, R.; O'Connor, J.C.; Freund, G.G.; Johnson, R.W.; Kelley, K.W. From inflammation to sickness and depression: When the immune system subjugates the brain. *Nat. Rev. Neurosci.* **2008**, *9*, 46–56. [[CrossRef](#)]
6. Jakobsson, J.; Malm, C.; Furberg, M.; Ekelund, U.; Svensson, M. Physical Activity During the Coronavirus (COVID-19) Pandemic: Prevention of a decline in metabolic and immunological functions. *Front. Sports Act. Living* **2020**, *2*, 57. [[CrossRef](#)]
7. Hong, K.S.; Lee, K.H.; Chung, J.H.; Shin, K.-C.; Choi, E.Y.; Jin, H.J.; Jang, J.G.; Lee, W.; Ahn, J.H. Clinical features and outcomes of 98 patients hospitalized with SARS-CoV-2 infection in Daegu, South Korea: A brief descriptive study. *Yonsei Med. J.* **2020**, *61*, 431–437. [[CrossRef](#)]
8. Liu, K.; Chen, Y.; Lin, R.; Han, K. Clinical features of COVID-19 in elderly patients: A comparison with young and middle-aged patients. *J. Infect.* **2020**, *80*, e14–e18. [[CrossRef](#)]
9. Richardson, S.; Hirsch, J.S.; Narasimhan, M.; Crawford, J.M.; McGinn, T.; Davidson, K.W.; The Northwell COVID-19 Research Consortium. Presenting characteristics, comorbidities, and outcomes among 5700 patients hospitalized with COVID-19 in the New York City area. *JAMA* **2020**, *323*, 2052–2059. [[CrossRef](#)]
10. Keilich, S.R.; Bartley, J.M.; Haynes, L. Diminished immune responses with aging predispose older adults to common and uncommon influenza complications. *Cell. Immunol.* **2019**, *345*, 103992. [[CrossRef](#)]
11. Thevarajan, I.; Nguyen, T.H.O.; Koutsakos, M.; Druce, J.; Caly, L.; Sandt, C.E.v.d.; Jia, X.; Nicholson, S.; Catton, M.; Cowie, B.; et al. Breadth of concomitant immune responses prior to patient recovery: A case report of non-severe COVID-19. *Nat. Med.* **2020**, *26*, 453–455. [[CrossRef](#)] [[PubMed](#)]
12. Nikolich-Zugich, J.; Knox, K.S.; Rios, C.T.; Natt, B.; Bhattacharya, D.; Fain, M.J. SARS-CoV-2 and COVID-19 in older adults: What we may expect regarding pathogenesis, immune responses, and outcomes. *GeroScience* **2020**, *42*, 505–514. [[CrossRef](#)] [[PubMed](#)]
13. Zheng, M.; Gao, Y.; Wang, G.; Song, G.; Liu, S.; Sun, D.; Xu, Y.; Tian, Z. Functional exhaustion of antiviral lymphocytes in COVID-19 patients. *Cell. Mol. Immunol.* **2020**, *17*, 533–535. [[CrossRef](#)]
14. Wang, X.; Xu, W.; Hu, G.; Xia, S.; Sun, Z.; Liu, Z.; Xie, Y.; Zhang, R.; Jiang, S.; Lu, L. SARS-CoV-2 infects T lymphocytes through its spike protein-mediated membrane fusion. *Cell. Mol. Immunol.* **2020**, *7*, 1–3. [[CrossRef](#)]
15. di Mauro, G.; Cristina, S.; Concetta, R.; Francesco, R.; Annalisa, C. SARS-Cov-2 infection: Response of human immune system and possible implications for the rapid test and treatment. *Int. Immunopharmacol.* **2020**, *84*, 106519. [[CrossRef](#)]
16. Febbraio, M.A. Health benefits of exercise—More than meets the eye! *Nat. Rev. Endocrinol.* **2017**, *13*, 72–74. [[CrossRef](#)] [[PubMed](#)]
17. Black, D.S.; Slavich, G.M. Mindfulness meditation and the immune system: A systematic review of randomized controlled trials. *Ann. N. Y. Acad. Sci.* **2016**, *1373*, 13–24. [[CrossRef](#)]



18. Nieman, D.C.; Wentz, L.M. The compelling link between physical activity and the body's defense system. *J. Sport Health Sci.* **2019**, *8*, 201–217. [[CrossRef](#)]
19. Sellami, M.; Gasmi, M.; Denham, J.; Hayes, L.D.; Stratton, D.; Padulo, J.; Bragazzi, N. Effects of acute and chronic exercise on immunological parameters in the elderly aged: Can physical activity counteract the effects of aging? *Front. Immunol.* **2018**, *9*, 2187. [[CrossRef](#)]
20. Birdee, G.S.; Cai, H.; Xiang, Y.-B.; Yang, G.; Li, H.; Gao, Y.; Zheng, W.; Shu, X.O. T'ai chi as exercise among middle-aged and elderly Chinese in urban China. *J. Altern. Complement. Med. (N. Y.)* **2013**, *19*, 550–557. [[CrossRef](#)]
21. Lauche, R.; Wayne, P.M.; Dobos, G.; Cramer, H. Prevalence, patterns, and predictors of T'ai Chi and Qigong use in the United States: Results of a nationally representative survey. *J. Altern. Complement. Med.* **2016**, *22*, 336–342. [[CrossRef](#)] [[PubMed](#)]
22. Guo, Y.; Qiu, P.; Liu, T. Tai Ji Quan: An overview of its history, health benefits, and cultural value. *J. Sport Health Sci.* **2014**, *3*, 3–8. [[CrossRef](#)]
23. Lan, C.; Chen, S.-Y.; Lai, J.-S.; Wong, A.M.-K. Tai Chi Chuan in medicine and health promotion. *Evid. Based Complementary Altern. Med.* **2013**, *2013*, 502131. [[CrossRef](#)] [[PubMed](#)]
24. Wang, C.; Schmid, C.H.; Iversen, M.D.; Harvey, W.F.; Fielding, R.A.; Driban, J.B.; Price, L.L.; Wong, J.B.; Reid, K.F.; Rones, R.; et al. Comparative Effectiveness of Tai Chi Versus Physical Therapy for Knee Osteoarthritis: A Randomized Trial. *Ann. Intern. Med.* **2016**, *165*, 77–86. [[CrossRef](#)] [[PubMed](#)]
25. Luo, X.-C.; Liu, J.; Fu, J.; Yin, H.Y.; Shen, L.; Liu, M.-L.; Lan, L.; Ying, J.; Qiao, X.-L.; Tang, C.-Z.; et al. Effect of Tai Chi Chuan in breast cancer patients: A systematic review and meta-analysis. *Front. Oncol.* **2020**, *10*, 607. [[CrossRef](#)] [[PubMed](#)]
26. Zhou, Z.; Zhou, R.; Li, K.; Zhu, Y.; Zhang, Z.; Luo, Y.; Luan, R. Effects of tai chi on physiology, balance and quality of life in patients with type 2 diabetes: A systematic review and meta-analysis. *J. Rehabil. Med.* **2019**, *51*, 405–417. [[CrossRef](#)]
27. Liu, H.-H.; Yeh, N.-C.; Wu, Y.-F.; Yang, Y.-R.; Wang, R.-Y.; Cheng, F.-Y. Effects of Tai Chi exercise on reducing falls and improving balance performance in parkinson's disease: A meta-analysis. *Parkinson's Dis.* **2019**, *2019*, 9626934. [[CrossRef](#)]
28. Cheng, C.-A.; Chiu, Y.-W.; Wu, D.; Kuan, Y.-C.; Chen, S.-N.; Tam, K.-W. Effectiveness of Tai Chi on fibromyalgia patients: A meta-analysis of randomized controlled trials. *Complement. Ther. Med.* **2019**, *46*, 1–8. [[CrossRef](#)]
29. Kolasinski, S.L.; Neogi, T.; Hochberg, M.C.; Oatis, C.; Guyatt, G.; Block, J.; Callahan, L.; Copenhaver, C.; Dodge, C.; Felson, D.; et al. 2019 American College of Rheumatology/Arthritis Foundation guideline for the management of osteoarthritis of the hand, hip, and knee. *Arthritis Rheumatol.* **2020**, *72*, 220–233. [[CrossRef](#)]
30. Kong, L.J.; Lauche, R.; Klose, P.; Bu, J.H.; Yang, X.C.; Guo, C.Q.; Dobos, G.; Cheng, Y.W. Tai Chi for Chronic pain conditions: A systematic review and meta-analysis of randomized controlled trials. *Sci. Rep.* **2016**, *6*, 25325. [[CrossRef](#)]
31. Yang, J.; Zhang, L.; Tang, Q.; Wang, F.; Li, Y.; Peng, H.; Wang, S. Tai Chi is effective in delaying cognitive decline in older adults with mild cognitive impairment: Evidence from a systematic review and meta-analysis. *Evid. Based Complementary Altern. Med.* **2020**, *2020*, 3620534. [[CrossRef](#)]
32. So, W.W.Y.; Cai, S.; Yau, S.Y.; Tsang, H.W.H. The neurophysiological and psychological mechanisms of Qigong as a treatment for depression: A systematic review and meta-analysis. *Front. Psychiatry* **2019**, *10*, 820. [[CrossRef](#)] [[PubMed](#)]
33. Bower, J.E.; Irwin, M.R. Mind-body therapies and control of inflammatory biology: A descriptive review. *Brain Behav. Immun.* **2016**, *51*, 1–11. [[CrossRef](#)] [[PubMed](#)]
34. Bottaccioli, A.G.; Bottaccioli, F.; Carosella, A.; Cofini, V.; Muzi, P.; Bologna, M. Psychoneuroendocrinology-based meditation (PNEIMED) training reduces salivary cortisol under basal and stressful conditions in healthy university students: Results of a randomized controlled study. *EXPLORE* **2020**, *16*, 189–198. [[CrossRef](#)] [[PubMed](#)]
35. Pótróla, P.; Wilk-Franczuk, M.; Wilczyński, J.; Nowak-Starz, G.; Góral-Pótróla, J.; Chruściński, G.; Bonisławska, I.; Pedrycz, A.; Żychowska, M. Anti-inflammatory effect on genes expression after four days of Qigong training in peripheral mononuclear blood cells in healthy women. *Ann. Agric. Environ. Med.* **2018**, *25*, 329–333. [[CrossRef](#)] [[PubMed](#)]
36. Klein, P.J.; Baumgarden, J.; Schneider, R. Qigong and Tai Chi as Therapeutic Exercise: Survey of Systematic Reviews and Meta-Analyses Addressing Physical Health Conditions. *Altern. Ther. Health Med.* **2019**, *25*, 48–53.

37. Lauche, R.; Peng, W.; Ferguson, C.; Cramer, H.; Frawley, J.; Adams, J.; Sibbritt, D. Efficacy of Tai Chi and qigong for the prevention of stroke and stroke risk factors: A systematic review with meta-analysis. *Medicine* **2017**, *96*, e8517. [[CrossRef](#)]
38. McInnes, M.D.F.; Moher, D.; Thombs, B.D.; McGrath, T.A.; Bossuyt, P.M.; The PRISMA-DTA Group. Preferred reporting items for a systematic review and meta-analysis of diagnostic test accuracy studies: The PRISMA-DTA statement. *Jama* **2018**, *319*, 388–396. [[CrossRef](#)]
39. Wan, X.; Wang, W.; Liu, J.; Tong, T. Estimating the sample mean and standard deviation from the sample size, median, range and/or interquartile range. *BMC Med. Res. Methodol.* **2014**, *14*, 135. [[CrossRef](#)]
40. Higgins, J.P. Cochrane Handbook for Systematic Reviews of Interventions Version 6.0 (Updated July 2019). Cochrane. 2019. Available online: [www.training.cochrane.org/handbook](http://www.training.cochrane.org/handbook) (accessed on 18 May 2020).
41. You, T.; Ogawa, E.F.; Thapa, S.; Cai, Y.; Yeh, G.Y.; Wayne, P.M.; Shi, L.; Leveille, S.G. Effects of Tai Chi on beta endorphin and inflammatory markers in older adults with chronic pain: An exploratory study. *Aging Clin. Exp. Res.* **2019**, *20*, 20. [[CrossRef](#)]
42. Sungkarat, S.; Boripuntakul, S.; Kumfu, S.; Lord, S.R.; Chattipakorn, N. Tai Chi improves cognition and plasma BDNF in Older adults with mild cognitive impairment: A randomized controlled trial. *Neurorehabilit. Neural Repair* **2018**, *32*, 142–149. [[CrossRef](#)]
43. Liu, P.; You, J.; Loo, W.T.Y.; Sun, Y.; He, Y.; Sit, H.; Jia, L.; Wong, M.; Xia, Z.; Zheng, X.; et al. The efficacy of Guolin-Qigong on the body-mind health of Chinese women with breast cancer: A randomized controlled trial. *Qual. Life Res.* **2017**, *26*, 2321–2331. [[CrossRef](#)] [[PubMed](#)]
44. Vera, F.M.; Manzanegue, J.M.; Rodríguez, F.M.; Bendayan, R.; Fernandez, N.; Alonso, A. Acute effects on the counts of innate and adaptive immune response cells after 1 month of Taoist Qigong Practice. *Int. J. Behav. Med.* **2016**, *23*, 198–203. [[CrossRef](#)] [[PubMed](#)]
45. Robins, J.L.; Elswick, R.K.; Sturgill, J., Jr.; McCain, N.L. The Effects of Tai Chi on Cardiovascular Risk in Women. *Am. J. Health Promot.* **2016**, *30*, 613–622. [[CrossRef](#)]
46. Campo, R.A.; Light, K.C.; O'Connor, K.; Nakamura, Y.; Lipschitz, D.; LaStayo, P.C.; Pappas, L.M.; Boucher, K.M.; Irwin, M.R.; Hill, H.R.; et al. Blood pressure, salivary cortisol, and inflammatory cytokine outcomes in senior female cancer survivors enrolled in a tai chi chih randomized controlled trial. *J. Cancer Surviv. Res. Pract.* **2015**, *9*, 115–125. [[CrossRef](#)] [[PubMed](#)]
47. Irwin, M.R.; Olmstead, R.; Breen, E.C.; Witarama, T.; Carrillo, C.; Sadeghi, N.; Arevalo, J.M.G.; Ma, J.; Nicassio, P.; Bootzin, R.; et al. Cognitive behavioral therapy and Tai Chi reverse cellular and genomic markers of inflammation in late-life Insomnia: A randomized controlled trial. *Biol. Psychiatry* **2015**, *78*, 721–729. [[CrossRef](#)]
48. Irwin, M.R.; Olmstead, R.; Carrillo, C.; Sadeghi, N.; Breen, E.C.; Witarama, T.; Yokomizo, M.; Lavretsky, H.; Carroll, J.E.; Motivala, S.J.; et al. Cognitive behavioral therapy vs. Tai Chi for late life insomnia and inflammatory risk: A randomized controlled comparative efficacy trial. *Sleep* **2014**, *37*, 1543–1552. [[CrossRef](#)] [[PubMed](#)]
49. Liu, J.; Chen, P.; Wang, R.; Yuan, Y.; Wang, X.; Li, C. Effect of Tai Chi on mononuclear cell functions in patients with non-small cell lung cancer. *BMC Complementary Altern. Med.* **2015**, *15*, 3. [[CrossRef](#)] [[PubMed](#)]
50. Wang, R.; Liu, J.; Chen, P.; Yu, D. Regular Tai Chi exercise decreases the percentage of type 2 cytokine-producing cells in postsurgical non-small cell lung cancer survivors. *Cancer Nurs.* **2013**, *36*, E27–E34. [[CrossRef](#)] [[PubMed](#)]
51. Zhang, Y.-J.; Wang, R.; Chen, P.-J.; Yu, D.-H. Effects of Tai Chi Chuan training on cellular immunity in post-surgical non-small cell lung cancer survivors: A randomized pilot trial. *J. Sport Health Sci.* **2013**, *2*, 104–108. [[CrossRef](#)]
52. Irwin, M.R.; Olmstead, R.; Breen, E.C.; Witarama, T.; Carrillo, C.; Sadeghi, N.; Arevalo, J.M.G.; Ma, J.; Nicassio, P.; Ganz, P.A.; et al. Tai Chi, cellular inflammation, and transcriptome dynamics in breast cancer survivors with insomnia: A randomized controlled trial. *JNCI Monogr.* **2014**, *2014*, 295–301. [[CrossRef](#)] [[PubMed](#)]
53. Liu, J.; Chen, P.; Wang, R.; Yuan, Y.; Li, C. Effect of Tai Chi exercise on immune function in middle-aged and elderly women. *J. Sports Med. Doping Stud.* **2012**, *2*, 1–7. [[CrossRef](#)]

54. Irwin, M.R.; Olmstead, R.; Oxman, M.N. Augmenting immune responses to varicella zoster virus in older adults: A randomized, controlled trial of Tai Chi. *J. Am. Geriatr. Soc.* **2007**, *55*, 511–517. [[CrossRef](#)]
55. Irwin, M.R.; Olmstead, R. Mitigating cellular inflammation in older adults: A randomized controlled trial of Tai Chi Chih. *Am. J. Geriatr. Psychiatry Off. J. Am. Assoc. Geriatr. Psychiatry* **2012**, *20*, 764–772. [[CrossRef](#)] [[PubMed](#)]
56. Oh, B.; Butow, P.; Mullan, B.; Clarke, S.; Beale, P.; Pavlakis, N.; Kothe, E.; Lam, L.; Rosenthal, D. Impact of medical Qigong on quality of life, fatigue, mood and inflammation in cancer patients: A randomized controlled trial. *Ann. Oncol.* **2010**, *21*, 608–614. [[CrossRef](#)] [[PubMed](#)]
57. Oh, B.; Butow, P.N.; Mullan, B.A.; Clarke, S.J.; Beale, P.J.; Pavlakis, N.; Lee, M.S.; Rosenthal, D.S.; Larkey, L.; Vardy, J. Effect of medical Qigong on cognitive function, quality of life, and a biomarker of inflammation in cancer patients: A randomized controlled trial. *Supportive Care Cancer* **2012**, *20*, 1235–1242. [[CrossRef](#)] [[PubMed](#)]
58. Lavretsky, H.; Alstein, L.L.; Olmstead, R.E.; Ercoli, L.M.; Riparetti-Brown, M.; Cyr, N.S.; Irwin, M.R. Complementary use of tai chi chih augments escitalopram treatment of geriatric depression: A randomized controlled trial. *Am. J. Geriatr. Psychiatry Off. J. Am. Assoc. Geriatr. Psychiatry* **2011**, *19*, 839–850. [[CrossRef](#)]
59. Wang, M.Y.; An, L.G. Effects of 12-Week’s Tai Chi Chuan practice on the immune function of female college students who lack physical exercise. *Biol. Sport* **2011**, *28*, 45–49. [[CrossRef](#)]
60. Chen, S.-C.; Ueng, K.-C.; Lee, S.-H.; Sun, K.-T.; Lee, M.-C. Effect of T’ai Chi Exercise on biochemical profiles and oxidative stress indicators in obese patients with type 2 diabetes. *J. Altern. Complement. Med.* **2010**, *16*, 1153–1159. [[CrossRef](#)]
61. Manzanque, J.M.; Vera, F.M.; Rodriguez, F.M.; Garcia, G.J.; Leyva, L.; Blanca, M.J. Serum Cytokines, mood and sleep after a Qigong program: Is Qigong an effective psychobiological tool? *J. Health Psychol.* **2009**, *14*, 60–67. [[CrossRef](#)]
62. McCain, N.L.; Gray, D.P.; Elswick, R.K.; Robins, J.W.; Tuck, I.; Walter, J.M.; Rausch, S.M.; Ketchum, J.M. A randomized clinical trial of alternative stress management interventions in persons with HIV infection. *J. Consult. Clin. Psychol.* **2008**, *76*, 431–441. [[CrossRef](#)]
63. Chen, H.-H.; Yeh, M.-L.; Lee, F.-Y. The Effects of baduanjin Qigong in the prevention of bone loss for middle-aged women. *Am. J. Chin. Med.* **2006**, *34*, 741–747. [[CrossRef](#)]
64. Irwin, M.R.; Pike, J.L.; Cole, J.C.; Oxman, M.N. Effects of a behavioral intervention, Tai Chi Chih, on Varicella-Zoster virus specific immunity and health functioning in older adults. *Psychosom. Med.* **2003**, *65*, 824–830. [[CrossRef](#)] [[PubMed](#)]
65. Sterne, J.A.C.; Savović, J.; Page, M.J.; Elbers, R.G.; Blencowe, N.S.; Boutron, I.; Cates, C.J.; Cheng, H.-Y.; Corbett, M.S.; Eldridge, S.M.; et al. RoB 2: A revised tool for assessing risk of bias in randomised trials. *BMJ* **2019**, *366*, l4898. [[CrossRef](#)] [[PubMed](#)]
66. Morgan, N.; Irwin, M.R.; Chung, M.; Wang, C. The effects of mind-body therapies on the immune system: Meta-Analysis. *PLoS ONE* **2014**, *9*, e100903. [[CrossRef](#)]
67. You, T.; Ogawa, E.F. Effects of T’ai Chi on chronic systemic inflammation. *J. Altern. Complement. Med.* **2019**, *25*, 656–658. [[CrossRef](#)]
68. Wang, C.-W.; Ng, S.-M.; Ho, R.-T.H.; Ziea, E.T.C.; Wong, V.C.W.; Chan, C.L.W. The effect of qigong exercise on immunity and infections: A systematic review of controlled trials. *Am. J. Chin. Med.* **2012**, *40*, 1143–1156. [[CrossRef](#)] [[PubMed](#)]
69. Ho, R.T.H.; Wang, C.-W.; Ng, S.-M.; Ho, A.H.Y.; Ziea, E.T.C.; Wong, V.T.; Chan, C.L.W. The effect of T’ai Chi exercise on immunity and infections: A systematic review of controlled trials. *J. Altern. Complement. Med.* **2013**, *19*, 389–396. [[CrossRef](#)]
70. Khosravi, N.; Stoner, L.; Farajivafa, V.; Hanson, E.D. Exercise training, circulating cytokine levels and immune function in cancer survivors: A meta-analysis. *Brain. Behav. Immun.* **2019**, *81*, 92–104. [[CrossRef](#)]
71. Ben-Sasson, S.Z.; Hu-Li, J.; Quiel, J.; Cauchetaux, S.; Ratner, M.; Shapira, I.; Dinarello, C.A.; Paul, W.E. IL-1 acts directly on CD4 T cells to enhance their antigen-driven expansion and differentiation. *Proc. Natl. Acad. Sci. USA* **2009**, *106*, 7119. [[CrossRef](#)]

72. Musolino, C.; Allegra, A.; Innao, V.; Allegra, A.G.; Pioggia, G.; Gangemi, S. Inflammatory and anti-inflammatory equilibrium, proliferative and antiproliferative balance: The role of cytokines in multiple myeloma. *Mediat. Inflamm.* **2017**, *2017*, 1852517. [[CrossRef](#)] [[PubMed](#)]
73. Zhou, S.; Zhang, Y.; Kong, Z.; Loprinzi, P.D.; Hu, Y.; Ye, J.; Liu, S.; Yu, J.J.; Zou, L. The effects of Tai Chi on markers of atherosclerosis, lower-limb physical function, and cognitive ability in adults aged over 60: A randomized controlled trial. *Int. J. Environ. Res. Public Health* **2019**, *16*, 753. [[CrossRef](#)] [[PubMed](#)]



© 2020 by the authors. Licensee MDPI, Basel, Switzerland. This article is an open access article distributed under the terms and conditions of the Creative Commons Attribution (CC BY) license (<http://creativecommons.org/licenses/by/4.0/>).





Protocol

# Auricular Acupuncture for Preoperative Anxiety—Protocol of Systematic Review and Meta-Analysis of Randomized Controlled Trials

Joanna Dietzel <sup>1</sup>, Mike Cummings <sup>2</sup>, Kevin Hua <sup>1</sup>, Klaus Hahnenkamp <sup>3</sup>, Benno Brinkhaus <sup>1</sup> and Taras I. Usichenko <sup>3,4,\*</sup>

<sup>1</sup> Institute of Social Medicine, Epidemiology and Health Economics, Charité University Medicine, 10117 Berlin, Germany; Joanna.dietzel@charite.de (J.D.); Kevin.Hua@charite.de (K.H.); benno.brinkhaus@charite.de (B.B.)

<sup>2</sup> British Medical Acupuncture Society, London WC1N 3HR, UK; Mike.Cummings@btinternet.com

<sup>3</sup> Department of Anesthesiology, University Medicine of Greifswald, 17475 Greifswald, Germany; klaus.hahnenkamp@med.uni-greifswald.de

<sup>4</sup> Department of Anesthesia, McMaster University, Hamilton, ON L8S 4K1, Canada

\* Correspondence: usichent@mcmaster.ca or taras.usichenko@med.uni-greifswald.de; Tel.: +49-(0)-383486-5893

Received: 31 October 2020; Accepted: 24 November 2020; Published: 26 November 2020

**Abstract:** *Background:* Preoperative anxiety causes profound psychological and physiological reactions that may lead to a worse postoperative recovery, higher intensity of acute and persistent postsurgical pain and impaired quality of life in the postoperative period. Previous randomized controlled trials (RCTs) suggest that auricular acupuncture (AA) is safe and effective in the treatment of preoperative anxiety; however there is a lack of systematic evidence on this topic. Therefore, this protocol was developed following the PRISMA guidelines to adequately evaluate the existing literature regarding the value of AA for the reduction in anxiety in patients in a preoperative setting, compared to other forms of acupuncture, pharmacological, or no control interventions and measured with questionnaires regarding anxiety and fear. *Methods:* The following databases will be searched: MEDLINE (PubMed), EMBASE, Cochrane Central Register of Controlled Trials (CENTRAL), ISI Web of Science, and Scopus Database. RCTs will be included if an abstract is available in English. Data collection and analysis will be conducted by two reviewers independently. Quality and risk assessment of included studies will be done using the Cochrane 5.1.0 handbook criteria and meta-analysis of effectiveness and symptom scores will be conducted using the statistical software RevMan V.5.3. *Conclusions:* This systematic review will evaluate the efficacy and safety of AA for preoperative anxiety. Since all data used in this systematic review and meta-analysis have been published, this review does not require ethical approval. The results may be published in a peer-reviewed journal or be presented in relevant conferences. Registration number: PROSPERO ID CRD42020.

**Keywords:** auricular acupuncture; preoperative anxiety; protocol; randomized controlled trials; systematic review; meta-analysis

## 1. Introduction

Preoperative anxiety is the most frequent burden affecting patients before various surgical procedures [1]. Facing the prospect of surgery and hospitalization, patients experience fear, anxiety, uncertainty, loss of control and decreased self-esteem [2]. More than 90% of adult patients scheduled for elective surgery developed preoperative anxiety, and 40.5% reported severe anxiety [3]. Although the preoperative anxiety is a kind of situational anxiety, which terminates itself when the underlying condition (surgery) is over, it causes a profound psychological and physiological response via the

release of stress-hormones, that may be associated with a worse postoperative recovery, higher intensity of acute and persistent postsurgical pain and greater anesthetic requirement as well as impaired quality of life in the postoperative period [4–8].

A large variety of approaches is used to treat preoperative anxiety including both psychological and pharmacological interventions; however, none of them seem to be ideal in providing effective, safe and low-cost therapy [9–11].

Auricular stimulation (including acupuncture and comparable techniques such as electroacupuncture and acupressure) is a method of complementary medicine, based on stimulation of cranial nerves. It has already been used to treat situational anxiety in experimental and clinical conditions [12]. In several randomised controlled trials (RCTs) evaluating a treatment of preoperative anxiety, auricular stimulation was superior to an array of control procedures, including placebo and sham interventions, and equally effective like premedication with benzodiazepines in patients scheduled for surgery under general anesthesia [13–17]. Moreover, this method was associated with fewer side effects compared with benzodiazepines, as well as a diminished physical stress reaction such as a reduced response of the autonomic nervous system [12,16,17].

The potential mechanism of auricular stimulation is attributed to the neuroanatomical conditions of external auricle. It is presumed that auricular stimulation exerts its anxiolytic effects via the involvement of cranial nerves [18], which leads to the modulation of the brain areas involved in the stress response, including the limbic system, locus coeruleus and hypothalamus [19–21].

Although the majority of RCTs on auricular stimulation for preoperative anxiety were in favor of this technique, these clinical investigations demonstrated a heterogeneity in regard to surgical procedures, control conditions and effect size, thus making it difficult to draw any definitive recommendations. It seems possible that auricular stimulation might serve as an effective replacement for insufficient conventional pharmacological premedication [9,22], thus more accurate estimation of the efficacy and safety of this complementary medicine intervention is needed. Therefore, this planned systematic review, including a meta-analysis of RCTs, will be performed to evaluate the effect size of auricular stimulation on preoperative anxiety applied alone or in addition to standard care in comparison with various control conditions. Data on the efficacy and safety of treatment will be calculated and summarized. The review will also try to identify the factors that may influence the effects of this intervention.

## 2. Materials and Methods

### 2.1. Eligibility Criteria for Including Studies in the Review

#### 2.1.1. Types of Studies

Only randomized controlled trials (RCTs) in European languages will be included. Results from quasi RCT will be discussed if little evidence is available, but they will not be part of the analysis. The funding source will be registered. Case reports, case-series, non-randomized case-control studies and retrospective data will not be included in the analysis.

#### 2.1.2. Types of Participants

No restrictions on study populations will be made, as long as they are described as patients undergoing surgical procedures, including all medical interventions requiring intra-procedural sedation or analgesia. There will be no restrictions regarding the age, gender or ethnicity of participants.

#### 2.1.3. Types of Interventions/Comparators

This review will include all studies, comparing auricular stimulation or related interventions (auricular acupuncture, auricular acupressure, auricular electroacupuncture, etc.) alone or in addition to routine care with a variety of control conditions, such as: sham acupuncture, sham acupressure,

placebo, routine care, various cognitive-behavioral therapies (CBTs) such as relaxation techniques, music therapy, hypnosis, etc.

#### 2.1.4. Types of Outcome Measures

The primary outcome of this review will be the intensity of preoperative anxiety, measured using patient-reported psychophysical anxiety scales, such as the State Trait Anxiety Inventory (STAI), Anxiety Visual Analogue Scale-100 (VAS-100), the Amsterdam Preoperative Anxiety and Information Scale (APAIS), Self-Rating Anxiety Scale (SAS), extensively described elsewhere [23]. Since anxiety leads to the release of stress-hormones (i.e., vasoactive) the impact on physiological parameters will be collected and evaluated, being a surrogate parameter for pain and anxiety. Secondary outcomes will therefore include physiological parameters describing the response of the autonomic nervous system (e.g., heart rate, blood pressure, respiratory rate, sweating reaction); the preoperative requirement of anxiolytic medication; the intraoperative requirement of anesthetic and analgesic medication; the intensity of postoperative pain; the postoperative requirement for analgesic medication, the quality of blinding and patient-satisfaction with the treatment of preoperative anxiety.

#### 2.1.5. Safety of Intervention

Adverse events and serious adverse events reporting will be analyzed, including events such as pain, inflammation and infection at the sites of auricular stimulation, and vasovagal reactions during the auricular interventions.

### 2.2. Search Methods for Identification of Studies

The search will be done across the following electronic databases and registries, from their inception until June 2020: MEDLINE (PubMed), EMBASE, Cochrane Central Register of Controlled Trials (CENTRAL), ISI Web of Science, Scopus Database. The search terms will include: auricular, acupuncture, acupressure, preoperative anxiety, randomized clinical trials (Table 1).

**Table 1.** Search strategy used in MEDLINE database.

N	Search Item [Title/Abstract]
1	Randomized controlled trial
2	Controlled clinical trial
3	Randomized
4	Randomly
5	Trial
6	OR #1-6
7	Anxiety
8	Fear
9	Preoperative
11	Surgical
12	Intervention
14	Anesthesia
15	OR #7-14
16	Auricular acupuncture
17	Auricular
18	Ear
19	Acupressure
20	Electro-acupuncture
21	OR #16-20

This search strategy will be modified as required for other electronic databases.



2.3. Data Extraction and Management

2.3.1. Study Identification

Two researchers will screen the titles and abstracts of articles found in the search, and discard trials that are not eligible. They will independently assess whether the trials meet the inclusion criteria, with disagreements to be resolved by discussion with a third researcher following objective criteria. When articles contain insufficient information to make a decision about eligibility, one of the researchers will attempt to contact the authors of the original reports to obtain further details via email. The details of data search and management are given as Figure 1. A new database for each of the two researchers will be set up to organize the data of the literature search.

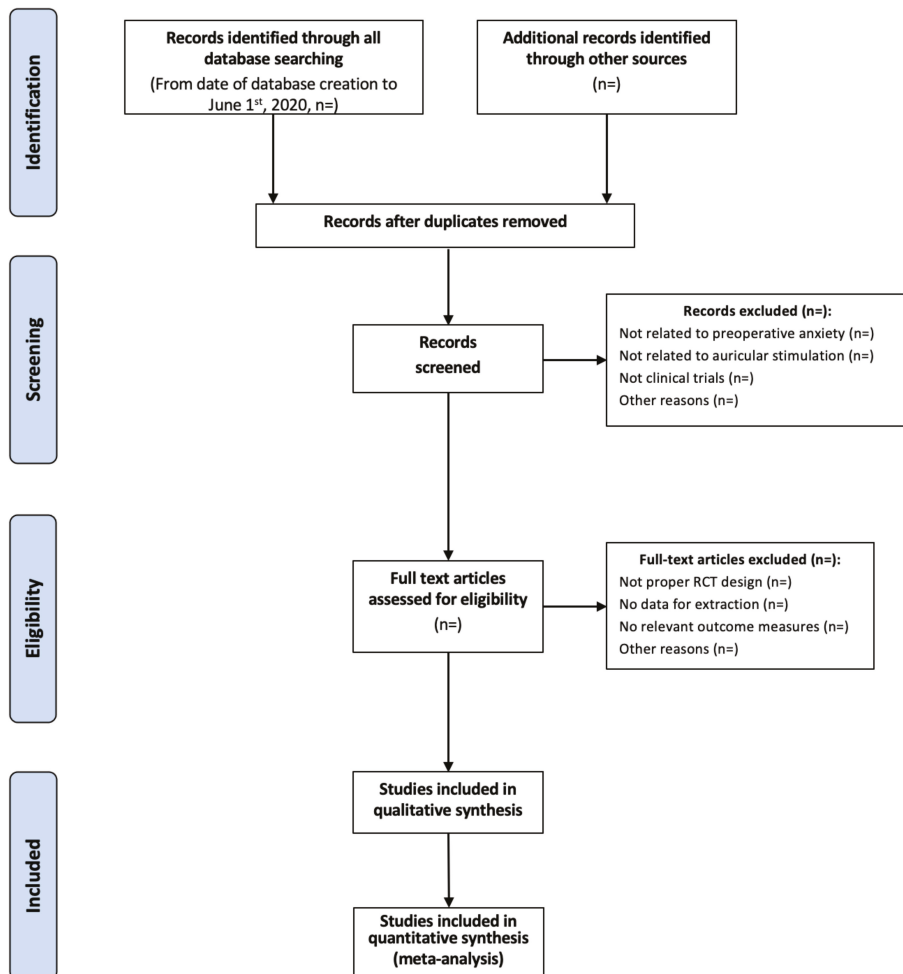


Figure 1. Flow diagram of details of data search and management.

### 2.3.2. Data Extraction

Following the selection for inclusion, two researchers will independently extract data according to the standardized form designed by the review group (Table 2). A third researcher will check for accuracy and enter data into Review Manager software (RevMan 5.3. 2011).

**Table 2.** Content of data extraction.

N	Categories	Items Extracted
1	General information	Author, year of publication, title, journal (title, volume, pages), country, language of publication
2	Research method	Random allocation, allocation concealment, blinding, baseline level
3	Participants	Total sample size, number in experimental group, number in control group, gender, age, ethnicity, type of surgery, setting
4	Intervention	Type of intervention (auricular acupuncture, auricular acupressure, auricular electro-acupuncture, etc.), selection of auricular sites/auricular acupuncture points, selected for stimulation, type of device/needles, used for auricular stimulation, length of auricular stimulation, type of control condition
5	Outcome parameter	Levels of preoperative anxiety (taken using questionnaires and psychophysical scales), physiological parameters (heart rate, blood pressure, respiratory rate, sweating reaction, etc.), preoperative requirement of anxiolytic medication, intraoperative requirement of anaesthetic and analgesic medication, the intensity of postoperative pain, postoperative requirement of analgesic medication, patient satisfaction with the treatment of preoperative anxiety, safety and side effects of intervention and type of control condition

### 2.3.3. Assessment of Risk of Bias in Included Studies

Two researchers will assess all included trials for risk of bias, blind to each other's assessments. Random sequence generation, allocation concealment, blinding of participants and personnel, incomplete outcome data, selective reporting and other potential sources of bias will be evaluated regarding low, high and unclear risk of bias according to Cochrane Collaboration assessment tool. Any disagreements will be resolved by discussion or by involving a third researcher to adjudicate.

### 2.3.4. Measures of Treatment Effects

Since all outcome measures of this review represent continuous data, they will be presented as mean differences with 95% confidence intervals (CI), or as standardized mean differences (SMD).

### 2.3.5. Dealing with Missing Data

All outcomes will be analyzed on an intention-to-treat basis. Corresponding authors from the trials with incomplete or insufficient data will be contacted via email to complete the data. Trials with greater than 20% of the data missing will be excluded from the analysis.

#### 2.3.6. Assessment of Heterogeneity

Statistical heterogeneity will be assessed in each meta-analysis using the  $T^2$ ,  $I^2$  and  $\text{Chi}^2$  statistics calculated by RevMan software. Heterogeneity will be regarded as substantial if  $T^2$  is greater than zero and either  $I^2$  is greater than 50% or there is a low P value (less than 0.10) in the  $\text{Chi}^2$  test for heterogeneity.

#### 2.3.7. Assessment of Reporting Biases

If the meta-analysis includes more than 10 investigations, reporting biases will be studied using a funnel plot with asymmetry testing.

### 2.4. Data Synthesis

Statistical analysis will be carried out using the RevMan software. Fixed-effect meta-analysis for combining data including primary outcome (anxiety scales) will be performed to estimate the treatment effect using SMD and 95% CI. In case of substantial clinical or statistical heterogeneity, a random-effects (RE) meta-analysis will be done to yield an overall summary. If RE analyses are necessary, their results will be presented as the average treatment effect with its 95% confidence interval, and the estimates of  $T^2$  and  $I^2$ .

#### 2.4.1. Subgroup Analysis and Investigation of Heterogeneity

To assess potential heterogeneity, subgroup analyses will be performed including the following comparisons: adult versus pediatric patients; female versus male patients; emergency surgery versus elective surgery; inpatient versus outpatient surgery, as well as auricular acupuncture or auricular acupressure versus auricular acupuncture or acupressure plus other treatments (if applicable). The differences between subgroups will be assessed by interaction tests for fixed-effect inverse variance meta-analyses. For fixed-effect meta-analyses and RE using methods other than inverse variance, the comparison of subgroups' confidence intervals will be used: non-overlapping confidence intervals indicate a statistically significant difference in the treatment effect between the subgroups.

#### 2.4.2. Sensitivity Analysis

Where subgroup analysis fails to explain the heterogeneity, data analysis using the RE model will be used. A priori sensitivity analyses on results will be done to look at the possible contribution of differences in methodological quality, comparing trials with a low risk of bias to all trials.

#### 2.4.3. Quality of Outcome Evidence

The quality of outcome evidence will be summarized using the Grading of Recommendations Assessment, Development and Evaluation (GRADE) approach. Each grade of evidence will be rated as: high, moderate, low or very low.

## 3. Discussion

Although almost 50% of adult patients scheduled for elective surgery suffer from preoperative anxiety [3], there is no ideal method to treat this kind of situational anxiety in clinical conditions so far. Pharmacological premedication is convenient in preoperative setting, however it seems to be less effective than previously suggested, if compared with placebo in trials with rigorous designs [9,22]. Psychological (cognitive-behavioral) approaches seem to be effective and lack dangerous side effects, however they are too time-consuming in their execution and thus are seldom used in routine clinical practice [24].

An array of data suggest that auricular stimulation might become such an effective, safe and easy-to-perform treatment for preoperative anxiety in adults scheduled for elective surgery and painful procedures with sedation [12–17]. Despite these promising results from clinical trials on the treatment of preoperative anxiety using auricular stimulation supported by neurophysiological explanation of its potential mechanisms [25], the systematic evaluation of the evidence for the treatment of anxiety using auricular acupuncture is not available.

This review and meta-analysis will fill this gap, analyzing the RCTs based on this protocol, which was designed according to the PRISMA statement (Supplementary Materials). The review will calculate and summarise the data on the efficacy and safety of auricular stimulation in the treatment of preoperative anxiety in adult patients scheduled for elective surgery.

The results of this systematic review may be biased, since only the trials described in European languages will be considered, excluding the full format papers in native languages from the countries of the Far East, where auricular stimulation is widely used in traditional medicine [26]. Furthermore, the trials using transauricular vagal nerve stimulation (TaVNS) are considered to be beyond the scope of this review, despite the number of such trials growing rapidly in last two decades [27].

In summary, this systematic review will evaluate the existing evidence on the treatment of preoperative anxiety using auricular acupuncture and related procedures. The scheduled meta-analysis will estimate the effect of auricular stimulation on several perioperative parameters that are known to be influenced by preoperative anxiety. The results of this review will provide the basis for a better understanding of auricular acupuncture in the treatment of perioperative anxiety and will yield the evidence for the implementation of this method in clinical practice.

#### Investigation Status

The data search is being performed for the present systematic review.

**Supplementary Materials:** The following are available online at <http://www.mdpi.com/2305-6320/7/12/73/s1>, PRISMA-P 2015 Checklist. Supplementary material: PRISMA-P (Preferred Reporting Items for Systematic review and Meta-Analysis Protocols) 2015 checklist: recommended items to address in a systematic review protocol.

**Author Contributions:** Data collection: J.D., K.H. (Kevin Hua), T.I.U. Formal analysis: M.C. Supervision: M.C., K.H. (Klaus Hahnenkamp). Writing—original draft: J.D., T.I.U., B.B. Writing—review & editing: J.D., T.I.U., M.C. All authors have read and agreed to the published version of the manuscript.

**Funding:** This research received no external funding.

**Conflicts of Interest:** The authors declare no conflict of interest.

#### References

1. Walker, E.M.K.; Bell, M.; Cook, T.M.; Grocott, M.P.W.; Moonesinghe, S.R. Patient reported outcome of adult perioperative anaesthesia in the United Kingdom: A cross-sectional observational study. *Br. J. Anaesth.* **2016**, *117*, 758–766. [[CrossRef](#)] [[PubMed](#)]
2. Breemhaar, B.; van den Borne, H.W.; Mullen, P.D. Inadequacies of surgical patient education. *Patient Educ. Couns.* **1996**, *28*, 31–36. [[CrossRef](#)]
3. Eberhart, L.; Aust, H.; Schuster, M.; Sturm, T.; Gehling, M.; Euteneuer, F.; Rüscher, D. Preoperative anxiety in adults—A cross-sectional study on specific fears and risk factors. *BMC Psychiatry* **2020**, *20*, 140. [[CrossRef](#)] [[PubMed](#)]
4. Maranets, I.; Kain, Z.N. Preoperative anxiety and intraoperative anesthetic requirements. *Anesth. Analg.* **1999**, *89*, 1346–1351.
5. Kain, Z.N.; Sevarino, F.; Alexander, G.M.; Pincus, S.; Mayes, L.C. Preoperative anxiety and postoperative pain in women undergoing hysterectomy. A repeated-measures design. *J. Psychosom. Res.* **2000**, *49*, 417–422. [[CrossRef](#)]

6. Scott, A. Managing anxiety in ICU patients: The role of preoperative information provision. *Nurs. Crit. Care* **2004**, *9*, 72–79. [[CrossRef](#)] [[PubMed](#)]
7. Theunissen, M.; Peters, M.L.; Bruce, J.; Gramke, H.F.; Marcus, M.A. Preoperative anxiety and catastrophizing: A systematic review and meta-analysis of the association with chronic postsurgical pain. *Clin. J. Pain* **2012**, *28*, 819–841. [[CrossRef](#)] [[PubMed](#)]
8. Ali, A.; Altun, D.; Oguz, B.H.; Ilhan, M.; Demircan, F.; Koltka, K. The effect of preoperative anxiety on postoperative analgesia and anesthesia recovery in patients undergoing laparoscopic cholecystectomy. *J. Anesth.* **2014**, *28*, 222–227. [[CrossRef](#)]
9. Maurice-Szamburski, A.; Auquier, P.; Viarre-Oreal, V.; Cuvillon, P.; Carles, M.; Ripart, J.; Honore, S.; Triglia, T.; Loundou, A.; Leone, M.; et al. Effect of sedative premedication on patient experience after general anesthesia: A randomized clinical trial. *JAMA* **2015**, *313*, 916–925. [[CrossRef](#)]
10. Powell, R.; Scott, N.W.; Manyande, A.; Bruce, J.; Vögele, C.; Byrne-Davis, L.M.; Unsworth, M.; Osmer, C.; Johnston, M. Psychological preparation and postoperative outcomes for adults undergoing surgery under general anaesthesia. *Cochrane Database Syst. Rev.* **2016**, *5*, CD008646. [[CrossRef](#)]
11. Kim, J.; Chiesa, N.; Raazi, M.; Wright, K.D. A systematic review of technology-based preoperative preparation interventions for child and parent anxiety. *Can. J. Anaesth.* **2019**, *66*, 966–986. [[CrossRef](#)]
12. Pilkington, K.; Kirkwood, G.; Rampes, H.; Cummings, M.; Richardson, J. Acupuncture for anxiety and anxiety disorders—A systematic literature review. *Acupunct. Med.* **2007**, *25*, 1–10. [[CrossRef](#)] [[PubMed](#)]
13. Wang, S.M.; Maranets, I.; Weinberg, M.E.; Caldwell-Andrews, A.A.; Kain, Z.N. Parental auricular acupuncture as an adjunct for parental presence during induction of anesthesia. *Anesthesiology* **2004**, *100*, 1399–1404. [[CrossRef](#)] [[PubMed](#)]
14. Michalek-Sauberer, A.; Gusenleitner, E.; Gleiss, A.; Tepper, G.; Deusch, E. Auricular acupuncture effectively reduces state anxiety before dental treatment—A randomised controlled trial. *Clin. Oral Investig.* **2012**, *16*, 1517–1522. [[CrossRef](#)] [[PubMed](#)]
15. Luo, L.; Dai, Q.; Mo, Y.; Yan, Y.; Qian, M.; Zhuang, X.; Huang, L.; Wang, J. The effect of auricular acupressure on preoperative anxiety in patients undergoing gynecological surgery. *Int. J. Clin. Exp. Med.* **2016**, *9*, 4065–4070.
16. Lewis, G.B.H.; Litt, M. An alternative approach to premedication: Comparing diazepam with auriculotherapy and a relaxation method. *Am. J. Acupunct.* **1987**, *15*, 205–211.
17. Karst, M.; Winterhalter, M.; Münte, S.; Francki, B.; Hondronikos, A.; Eckardt, A.; Hoy, L.; Buhck, H.; Bernateck, M.; Fink, M. Auricular acupuncture for dental anxiety: A randomized controlled trial. *Anesth. Analg.* **2007**, *104*, 295–300. [[CrossRef](#)]
18. Peuker, E.T.; Filler, T.J. The nerve supply of the human auricle. *Clin. Anat.* **2002**, *15*, 35–37. [[CrossRef](#)]
19. Frangos, E.; Ellrich, J.; Komisaruk, B.R. Non-invasive Access to the Vagus Nerve Central Projections via Electrical Stimulation of the External Ear: fMRI Evidence in Humans. *Brain Stimul.* **2015**, *8*, 624–636. [[CrossRef](#)]
20. Chen, J.; Barrett, D.W.; He, Y.; Gonzalez-Lima, F. Anxiolytic-like behavioural effects of head electroacupuncture in rats susceptible to stress. *Acupunct. Med.* **2016**, *34*, 235–240. [[CrossRef](#)]
21. Qu, F.; Zhang, D.; Chen, L.T.; Wang, F.F.; Pan, J.X.; Zhu, Y.M.; Ma, C.M.; Huang, Y.T.; Ye, X.Q.; Sun, S.J.; et al. Auricular acupressure reduces anxiety levels and improves outcomes of in vitro fertilization: A prospective, randomized and controlled study. *Sci. Rep.* **2014**, *4*, 5028. [[CrossRef](#)] [[PubMed](#)]
22. Walker, K.J.; Smith, A.F. Premedication for anxiety in adult day surgery. *Cochrane Database Syst. Rev.* **2009**, *4*, CD002192. [[CrossRef](#)] [[PubMed](#)]
23. Zemla, A.J.; Nowicka-Sauer, K.; Jarmoszewicz, K.; Wera, K.; Batkiewicz, S.; Pietrzykowska, M. Measures of preoperative anxiety. *Anaesthesiol. Intensive Ther.* **2019**, *51*, 64–69. [[CrossRef](#)]
24. Wilson, C.J.; Mitchelson, A.J.; Tzeng, T.H.; El-Othmani, M.M.; Saleh, J.; Vasdev, S.; LaMontagne, H.J.; Saleh, K.J. Caring for the surgically anxious patient: A review of the interventions and a guide to optimizing surgical outcomes. *Am. J. Surg.* **2016**, *212*, 151–159. [[CrossRef](#)] [[PubMed](#)]
25. Usichenko, T.; Hacker, H.; Lotze, M. Transcutaneous auricular vagal nerve stimulation (taVNS) might be a mechanism behind the analgesic effects of auricular acupuncture. *Brain Stimul.* **2017**, *10*, 1042–1044. [[CrossRef](#)] [[PubMed](#)]

26. Kim, Y.S.; Jun, H.; Chae, Y.; Park, H.J.; Kim, B.H.; Chang, I.M.; Kang, S.K.; Lee, H.J. The practice of Korean medicine: An overview of clinical trials in acupuncture. *Evid. Based Complement Alternat. Med.* **2005**, *2*, 325–352. [[CrossRef](#)]
27. Carreno, F.R.; Frazer, A. The Allure of Transcutaneous Vagus Nerve Stimulation as a Novel Therapeutic Modality. *Biol. Psychiatry* **2016**, *79*, 260–261. [[CrossRef](#)]

**Publisher's Note:** MDPI stays neutral with regard to jurisdictional claims in published maps and institutional affiliations.



© 2020 by the authors. Licensee MDPI, Basel, Switzerland. This article is an open access article distributed under the terms and conditions of the Creative Commons Attribution (CC BY) license (<http://creativecommons.org/licenses/by/4.0/>).





Concept Paper

# e-Health: A Future Solution for Optimized Management of Elderly Patients. GER-e-TEC™ Project

Abrar-Ahmad Zulfiqar <sup>1,\*</sup>, Noël Lorenzo-Villalba <sup>1</sup>, Oumair-Ahmad Zulfiqar <sup>2</sup>,  
Mohamed Hajjam <sup>3</sup>, Quentin Courbon <sup>3</sup>, Lucie Esteouille <sup>3</sup>, Bernard Geny <sup>4,5</sup>, Samy Talha <sup>4,5</sup>,  
Dominique Letourneau <sup>6</sup>, Jawad Hajjam <sup>7</sup>, Sylvie Erve <sup>7</sup>, Amir Hajjam El Hassani <sup>8</sup> and  
Emmanuel Andres <sup>1</sup>

- <sup>1</sup> Diabètes et Maladies Métaboliques, Service de Médecine Interne, Hôpitaux Universitaires de Strasbourg, 67000 Strasbourg, France; noellorenzo@gmail.com (N.L.-V.); emmanuel.andres@chru-strasbourg.fr (E.A.)
  - <sup>2</sup> Engineer Department, Neoma Business School, 51100 Reims, France; oumair.zulfiqar.19@neoma-bs.com
  - <sup>3</sup> Predimed Technology, 67300 Schiltigheim, France; mohamed.hajjam@predimed-technology.com (M.H.); quentin.courbon@predimed-technology.com (Q.C.); esteouillelucie@gmail.com (L.E.)
  - <sup>4</sup> Service de Physiologie et Laboratoire d'Explorations Fonctionnelles, Hôpitaux Universitaires de Strasbourg, 67000 Strasbourg, France; bernard.geny@chru-strasbourg.fr (B.G.); samy.talha@chru-strasbourg.fr (S.T.)
  - <sup>5</sup> Equipe de recherche EA 3072 "Mitochondrie, Stress oxydant et Protection musculaire", Faculté de Médecine de Strasbourg, Université de Strasbourg, 67000 Strasbourg, France
  - <sup>6</sup> Fondation de l'Avenir pour la Recherche Médicale Appliquée, 75015 Paris, France; dominique.letourneau@u-pec.fr
  - <sup>7</sup> Centre d'Expertise des TIC pour l'autonomie (CenTich) et Mutualité Française Anjou-Mayenne (MFAM)–Angers, 49000 Angers, France; jawad.hajjam@centich.fr (J.H.); sylvie.erve@centich.fr (S.E.)
  - <sup>8</sup> Laboratoire IRTES-SeT, Université de Technologie de Belfort-Montbéliard (UTBM), Belfort-Montbéliard, 90000 Belfort, France; amir.hajjam@utbm.fr
- \* Correspondence: abzulfiqar@gmail.com; Tel.: +336-27-10-24-93

Received: 9 June 2020; Accepted: 21 July 2020; Published: 23 July 2020

**Abstract: Background:** Elderly residents in nursing homes have multiple comorbidities (including cognitive and psycho-behavioral pathologies, malnutrition, heart failure, diabetes, chronic obstructive pulmonary disease, and renal failure) and use multiple medications. **Methods:** The GER-e-TEC project aims to provide these fragile and complex patients with telemedicine tools, more specifically telemonitoring, backed by a well-defined and personalized protocol. **Results:** Medically, this implies the need for regular monitoring and a high level of medical and multidisciplinary expertise for the healthcare team. The tools use non-invasive communicating sensors and artificial intelligence techniques, allowing daily monitoring with the ability to detect any abnormal changes in the patient's condition early. **Conclusions:** The GER-e-TEC project specifically considers the challenges of aging residents and significant challenges in nursing homes, with the main geriatric syndromes (falls, malnutrition, cognitive-behavioral disorders, and iatrogenic conditions).

**Keywords:** telemedicine; remote monitoring; GER-e-TEC; elderly patient; artificial intelligence; geriatric syndromes; detection of the precursory signs of decompensation of geriatric syndromes

## 1. Introduction

Life expectancy continues to rise worldwide, approaching or exceeding 85 years for women and 80 years for men in Europe [1]. In 2060, one-third of the French population will be over 60, with 5 million over 85 compared to 1.4 million today. This epidemiological trend will require more healthcare expenditures and a rebalance of public finances.



At the end of 2015, the number of persons in nursing homes reached 728,000 in France according to the Survey of Establishments for Elderly People (EHPA) implemented by the Directory of Research, Evaluation, and Statistics Studies (DRESS) [2]. Older people enter nursing homes later in their lives, and when they do, they are most often dependent, as shown in the study carried out in 2011 by Morley. In that study, the proportion of residents classified from 4 to 1 in the Iso-Resource Group (GIR) represented 91% of cases [3].

Today, residents in nursing homes have multiple comorbidities (such as heart failure, diabetes, chronic obstructive pulmonary disease (COPD), and renal failure) and are on multiple medications. From the medical perspective, this implies the need for regular monitoring and a high level of medical expertise. In addition, people aged 75 and older often have a certain level of fragility, determined by a reduction in functional reserve of vital organs with age, with geriatric syndromes which are specific to the age group (malnutrition, sedentary lifestyle).

According to the results of a national analysis carried out by the National Agency for the Evaluation and Quality of Social and Medico-Social Establishments and Services (ANESM) in 2015, one out of every two residents in nursing homes are admitted to a hospital each year for an average hospital stay of three weeks. Moreover, these hospitalizations are frequently preceded by an emergency department admission [4]. Thus, visits to the emergency room are frequent for residents in nursing homes, with one in four patients subsequently admitted at least once per year and one in ten residents admitted at least twice per year [5]. According to France's national High Committee for the Future of Health Insurance (HCAAM), hospitalizations of this population represent an expenditure of 1.7 billion euros per year for health insurance [6].

Urgent hospitalizations for residents in nursing homes could be preventable in up to 67% of cases [7]. High rates could be reduced by improving decision-making procedures. Among the causes of preventable hospitalizations is the lack of medical availability or lack of communication between paramedics and healthcare physicians [8].

Telemedicine, particularly telemonitoring, has been shown to be effective in the management of chronic pathologies such as heart failure. For example, the MyPredi remote monitoring platform, formerly known as E-care, has been tested for monitoring chronic diseases, both in hospitals and at home. The system makes it possible to combine the data collected daily with the operator's clinical knowledge of the patient using artificial intelligence tools for personalized and predictive monitoring. These systems are particularly suited for monitoring patients in nursing homes and their geriatric risks. As a result, the GER-e-TEC program was created and will be detailed in the present article.

## 2. Some Examples of Remote Monitoring Programs in Elderly Individuals

According to the French Public Health Code, telemedicine is defined as a form of remote medical practice using information and communication technologies. It connects different networks with a patient and one or more health professionals, and if necessary, other professionals providing care to the patient. Telemedicine, and specifically telemonitoring, has shown its effectiveness in the follow-up of chronic diseases such as heart failure and hypertension [9]. Monitoring patients with chronic pathologies using telemedicine systems is one way of optimizing the cost of care for these patients. Telesurveillance aims to give autonomy at home to people suffering from various pathologies and handicaps which would normally compel them to hospitalization or placement in specialized institutions: patients suffering from certain chronic diseases, disabled, but also dependent elderly people [10].

The telemonitoring objectives are ambitious: improvement in morbidity and mortality, reduction in rehospitalizations, and improvement in the quality of life and in medico-economic costs. Remote monitoring is a medical procedure that results from the transmission and interpretation by a doctor of a clinical, radiological, or biological indicator, collected by the patient or by a health professional [11]. The interpretation of the data can lead to the decision of early medical intervention. The data are analyzed by a doctor, who could delegate management to another health professional

from a task validated by the Regional Agency of Health. Management decisions are based on a written protocol for monitoring the indicator that has been validated by the attending physician or a designated responsible physician. This system, therefore, allows the attending physician to know whether the patient is stable and warn about the possible destabilization of the indicator, which could be immediately corrected to prevent complications leading to hospitalization. The advantages of medical telemonitoring include an accumulated prevention of conditions posing a risk of acute decompensation of chronic pathology with consequently a better quality of life, a reduction in rehospitalizations and their economic cost, better medical follow-up, and better commitment and compliance of the patient to the management of diseases with, consequently, better therapeutic compliance [12].

The digitized selected indicators are available to health professionals for medical interpretation through different methods (via different internet media and communication channels, such as web-based, mobile apps, and direct sensor connection to the internet/cloud application). This must be the location of the patient's primary medical file so that a change in a clinical indicator is noted and the prescription registered. These actions must be traced and can be recorded in the shared medical file. The transfer of these indicators must be secured. Integrating telemonitoring into the care of a patient with a chronic disease can help prevent complications and unscheduled hospitalizations.

All the benefits described above strongly support the deployment of telemonitoring and teleconsultation in the elderly, and in particular, in dependent patients. In the area of heart failure, the rate of hospital referrals for patients over the age of 70 has increased by 30% in the past ten years [12]. In Quebec, remote monitoring of patients with heart failure at home has reduced the rate of hospitalization by more than 60% [12].

EPI-MEDIC [13] is a European project implemented in France, Italy, and Sweden. It has allowed for the development of a personal ECG monitor (PEM) for the early detection of cardiac ischemia and arrhythmia. A clinical study was conducted with 794 patients, in which healthcare professionals performed 1372 PEM ECGs. In addition, 188 patients in self-care situations performed 1287 ECGs with their PEMs. The EPI-MEDIC system generates different levels of alerts and transmits these alerts with the patient's ECG results and personal electronic medical record to healthcare providers by way of a mobile phone. In severe cases, the alerts are automatically sent to the nearest emergency call center. Clinical trials have shown that the EPI-MEDIC solution can save lives and is invaluable for prehospital triage.

Developed in England, TeleHealth [14] is a remote monitoring platform that monitors a patient's vital signs and activity. It is designed for elderly people who live alone and suffer from chronic diseases (congestive heart failure and chronic obstructive pulmonary disease). A primary study was conducted with 36 participants for a duration of up to one year, depending on the patient. Each day, the patients measured their vital signs (blood pressure and weight for CHF, oxygen saturation level for COPD) with sensors, as well as their activity (passive infrared motion sensor and/or a chair or bed sensor). An algorithm is used to process the data and sends an alert in case of an abnormality. Measurements and alerts are sent to the platform wirelessly and can be consulted online by both the patient and the physician. TeleHealth allows for improved prevention and faster medical interventions, and consequently, an overall increase in patient wellbeing

Two other projects were conducted for the remote monitoring of heart failure: the Doctor/Patient Health Interactive Platform [15] and SEDIC [16] studies. The SEDIC study showed a significant decrease in cardiovascular mortality, and the results of the first mentioned study are underway.

The COMPAS [17] and ECOST [18] studies focused on pacemaker monitoring. These studies demonstrated the safety and benefit of cardiac telemonitoring in randomized studies of 538 and 433 patients, respectively. The COMPAS study showed a 56% reduction in follow-up consultations and a reduction in hospitalizations for atrial arrhythmia or stroke. The ECOST study showed that telemonitoring of implantable defibrillators can have a positive medical-economic impact, including a reduction in inappropriate shocks due to early regulations and a reduction in hospitalizations related to these shocks.

Dary et al. conducted a study on the telemonitoring of atrial fibrillation. In total, 200 patients were enrolled at the start of the study: 45% male and 55% female, with an average age of 67 years; 16% of the enrolled patients were over the age of 80; 35% had a history of treated arrhythmias. For the 200 patients enrolled in the study, 63 had a known arrhythmia and 137 patients were in sinus rhythm at the outset. Of the latter group, 61 (45%) maintained a normal pattern, 43 (22%) had a detected atrial fibrillation, and 33 (16%) had episodes of tachycardia. For the 63 patients in arrhythmia, 24 had their rhythm monitored and 39 had their heart rate monitored. In total, for 33% of this study's patients, telemonitoring improved the diagnosis and treatment of atrial fibrillation, allowing their treatment to be adapted according to rhythm, rate, and conduction time [19].

In 2003, Goldberg et al. [20] published the WHARF study, which included the largest randomized multicenter sample and compared the value of telemonitoring aftercare to that of in-person aftercare. After six months, there was no significant difference in the rate or time frame of hospital readmissions ( $p = 0.28$ ), but there was a reduction in mortality rates ( $p < 0.003$ ). The Tele-HF study (Telemonitoring to Improve Heart Failure Outcomes) [21] included patients who had presented with decompensated heart failure in the last 30 days. The average age was 61. There was no notable difference between the two groups based on the criteria of mortality rate and hospitalization for any cause, nor on the secondary criteria of death, hospital readmission, and length of hospital stay.

Other projects have focused on medical telemonitoring. Minutolo et al., used a decision support system for remote monitoring of people with heart failure [22]. The program is based on systems grouping the data related to the patient: posture, cardiac sensor, physical activities, and alerts.

The SETAM study (Strategy of Early Detection and Active Management of Supraventricular Arrhythmia with Telecardiology) was a randomized study of telemedicine in rhythmology, looking at two groups of patients with pacemakers. It showed that telemedicine promoted the early detection of events, with a 66% reduction in hospitalizations related to atrial arrhythmias, and the prevention of strokes. The study showed that telecardiology allowed for earlier diagnosis and treatment of patients with atrial arrhythmias, and a reduction in the atrial fibrillation burden after nine months of monitoring in patients in sinus rhythm upon enrollment, with a score of CHA<sub>2</sub>DS<sub>2</sub>-VASc  $\geq 2$ . In total, 595 patients were enrolled in 57 general hospitals (CHGs) in France, for an average period of 12.8  $\pm$  3.3 months and an average age of 79  $\pm$  8 years [23].

Many studies have been conducted in the field of activity monitoring for the elderly, in particular to prevent the risk of falls. The majority of the devices are designed for home care, but they are also suitable for monitoring in nursing homes.

One such device was developed by Gerhome [24], which seeks to help elderly people to continue to live at home. Sensors are placed in various parts of the home and communicate wirelessly (by radio frequency) with a computer center. These sensors include ambient sensors (temperature, humidity, and luminosity), volumetric sensors, occupancy sensors (bed, armchair), water sensors, electricity sensors, door sensors, and image sensors.

An experiment conducted in a nursing home in Antibes highlighted the effectiveness of activity detection devices in nursing homes. For example, if a resident gets up during the night, an alert is sent to the night nurse who can subsequently take all the necessary precautions for a potential fall. RESPECT [25] has developed an innovative telehealth device, a smart insole that communicates wirelessly and measures activity and energy levels autonomously. The insole helps with physical activity and the monitoring of frailty indicators, in particular those related to walking. It measures weight, the number of strides, total distance, and the average walking speed. Its battery life is 7 to 13 months. Several tests have demonstrated the accuracy of the technology of smart insoles. AphyCare Technologies has developed an alert bracelet called Séréo'Z [26] to address the risk of falling. Séréo'Z is a multi-sensor ambulatory monitoring system that is worn on the wrist. It collects and processes physiological and activity data (breathing rate, heart rate, skin temperature) and detects falls. The data are transmitted via a secure radio link to a remote transmitter connected to a telephone socket in the

home. Alerts are sent to a remote assistance center. A similar bracelet, Vivago [27], has been developed in Finland.

In France, the Limoges University Hospital began the Icare project [28]. Unique to Europe, this pilot research project assesses the effectiveness of home medical telemonitoring for elderly people with chronic diseases. The aim is to prevent the loss of autonomy of elderly individuals at home and to show that remote monitoring of chronic diseases in elderly patients avoids decompensation (disruption of balance) and unscheduled hospitalizations. The study is being conducted over a 12-month period with 500 elderly volunteers. Some patients will utilize remote monitoring using biometric sensors installed in their homes. These sensors (not worn) monitor vital parameters, such as blood pressure, blood sugar, weight, blood oxygen saturation, or temperature. A box transmits these data daily and securely to the attending physician and the private nurse, who usually follow the patient simultaneously, but also to the expert geriatrician in the University Hospital.

The study by Edirippulige et al. suggested that the quality of “medical evidence” for telemedicine is low, but this should be considered carefully since there is only one randomized study [29]. In addition, most of the studies are observational and qualitative. They mainly result from surveys and interviews (patients and healthcare personnel). The study showed that there is evidence of the feasibility and satisfaction of stakeholders in the use of telemedicine in long-term care facilities in several clinical specialties and especially, geriatrics [29]. With respect to costs, this study highlighted the following observations: (i) the costs related to the medical coordination of patients followed up by telemedicine decreases when there are more than 850 uses per year; (ii) for dermatology, remote expertise makes telemedicine profitable; (iii) for geriatrics, it is especially the geriatric assessment and patient education which appear to be the most profitable.

However, in all situations, telemedicine seems likely to help optimize the care and cost to patients treated by avoiding certain emergencies and repetitive hospitalizations [30].

### 3. MyPredi: A Platform for Early Detection and Reporting of Risk Situations

The MyPredi remote monitoring platform, formerly known as the E-care project, selected within the framework of the Investments for the Future call for projects known as “Health and autonomy in the living environment thanks to digital technology”, has the initial main objective of optimizing the follow-up of patients with heart failure by detecting the warning signs of cardiac decompensation through a telemedicine system that combines motivation and education tools [31]. The project will, in theory, make it possible to decrease the number of rehospitalizations, reduce the length of hospitalization, and improve the quality of life of these patients.

It helps the medical professionals by automating the processing of information from sensors by the automatic generation of alerts, in order to detect early indicators of cardiac decompensation [32]. This analysis is adapted to the phenotype of each patient (personalized medicine). The platform also allows the sharing of heterogeneous knowledge to integrate the information necessary for monitoring any medical condition (predictive medicine).

Early detection of cardiac decompensation involves integrating data from sensors: weight, blood pressure, heart rate, oxygen saturation, patient ergonomics, and questionnaires asking the patient about the symptoms of cardiac decompensation (edema, dyspnea, habitual fatigue), as well as the addition of dietary monitoring. All these consolidated elements, along with the patient profile [12], allow detection of cardiac anomalies with the goal of preventing situations at risk of cardiac decompensation (preventive medicine).

The MyPredi platform uses a system to define a controlled vocabulary (diseases, drugs, symptoms, etc.) and to model the concepts related to the monitoring of heart failure [32]. The effectiveness of the system for diagnostic purposes implies that operational semantics are included, semantics which specify how the knowledge modeled in the system will be processed and automatically produce further knowledge. The reasoning part is based on an inference engine where the rules are either introduced by medical experts or from generated data, then, validated by medical experts.

As shown in Figure 1, the MyPredi platform includes a patient module and a server module. The first is installed in the patient's residence, making it possible to collect and integrate data from different types of non-invasive medical sensors [32] or exchanges in the form of questions and answers. All of the functionalities are embedded in a mobile device, such as a tablet, in order to allow greater patient autonomy. The server module centralizes the data from the patient module and the interpreters. The two modules communicate securely with each other according to standards used in healthcare informatics including Health Level 7 (HL7 V2.6 associated to IHE DEC PCD-01 (patient care device)) and Integrating the Healthcare Enterprise (IHE) protocols.

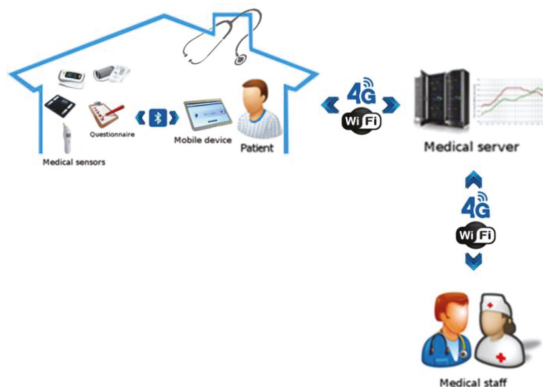


**Figure 1.** Remote monitoring according to the MyPredi platform. (Source: PrediMed, Schiltigheim, France).

#### 4. The Patient Module

This module, installed in the patient's house, includes several sensors (devices, also called Agents) and a receiver (Aggregation Manager) for collecting data from physiological sensors (thermometer, oximeter, blood pressure monitor, scale, etc.) as well as exchanges in the form of questions and answers. The receiver (computer, touch pad, or smartphone) sends the data to the server via the internet. In the MyPredi platform, touch pads are used with an ergonomic application that allows the patient or their relatives to submit their measurements for advice and to communicate directly with their doctor.

#### 5. The Server Module

The server receives data from all patient modules and manages authentication and communications security, as well as data consistency. These are stored to preserve the privacy of patients. The server uses systems and an intelligent component to detect risk situations and warn caregivers.

A service portal is used to allow users, depending on their role (patient, caregiver, relatives, etc.), to access and follow the evolution of vital signs as well as the general condition of the patient or even to enter medical information and consult transmitted alerts.

The MyPredi platform was initially tested in a 20-bed Internal Medicine unit receiving patients from emergency facilities as part of a care system for patients with heart failure (HF) at the University Hospitals of Strasbourg [33]. In this study, 180 patients were included and 1500 measurements were made. The patient population profile included in this study was elderly patients, multiple medical diagnoses in more than 90% of the cases, and loss of autonomy in 25%. Healthcare professionals used the E-care platform daily. This experiment made it possible to validate the technological choices, to consolidate the system, and to test the robustness of the platform. An analysis shows the relevance of the alerts generated (indicators of deterioration of the patient's heart condition).

The MyPredi platform allows automated, non-invasive generation of alerts related to the detection of situations at risk of cardiac decompensation, subsequently preventing hospitalization. Currently,

an upgraded telemonitoring platform has been deployed in the homes of patients with heart failure in the Bas-Rhin as part of the PRADO INCADO project (project funded by ARS of Alsace) [33] (Figure 2).

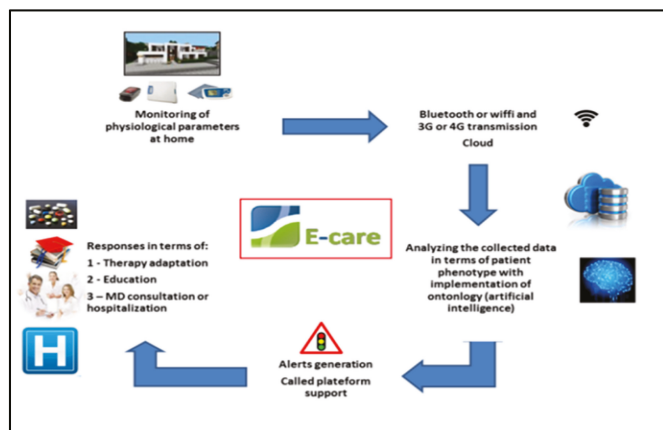


Figure 2. Structure of telemedical platform developed in the E-care project. (Source: PrediMed, Schiltigheim, France).

## 6. Development of the MyPredi Platform

The MyPredi platform integrates the monitoring of other chronic diseases including diabetes, hypertension, and COPD [34]. The MyPredi platform is an evolutive platform with original architecture and proven functionalities to manage patients with chronic pathologies who require long-term follow-up. It consists of a patient module, with a tablet and sensors, and a server module, which receives and processes the data collected from the various patient modules. The server module combines semantic web and artificial intelligence technologies (AI). An inference engine is used to monitor the patient’s health and to detect any abnormal situation [12]. We propose a medical telemonitoring platform with an open and flexible architecture, offering the ability to build predictive models of risk situations.

In the detection of anomalies, we use an expert system based on inference rules built with medical experts. These rules are generic and evolve with the new knowledge generated by deep learning algorithms on the data collected and the evolution of the patient’s condition. All alerts detected by the system are forwarded to the nursing staff responsible for monitoring the patient.

In the future, the MyPredi platform should gradually be enriched with other communicating sensors such as the ECG and electronic stethoscope, integrating the signal processing tools that will enable better detection of situations of risk [34,35]. Other communicating sensors could also be considered, such as an electronic spirometer, in order to complete the platform and extend its interest in other chronic diseases, such as asthma, COPD, and chronic renal failure [36,37].

## 7. Geriatrics and e-Technology: GER-e-TEC Project

We have implemented the GER-e-TEC project incorporating all the information mentioned above. The aim of the project is to study the contribution of telesurveillance to residents in nursing homes of Strasbourg University Hospitals through a structured and a protocolized medical follow-up to avoid acute decompensations and complications of geriatric conditions. The project relies on partners who work together, a multidisciplinary team consistent with the requirements in terms of medical, scientific, and structural skills.

7.1. Objective

The objective of our work is to develop a codified preventive approach for the management of the main geriatric risks in nursing homes using a personalized remote monitoring platform of residents, in order to avoid factors leading to acute decompensation in the elderly.

The collection of information by the platform allows not only personalized monitoring, but also a better understanding of the patient, providing a particularly effective tool for information transmission between the medical staff (doctors, nurses) in nursing homes. This data collection will also permit the identification of markers subsequently used to improve the early detection of decompensation, thus, improving the monitoring of patients and hopefully reducing the number of hospitalizations. This work creates a resident liaison file.

7.2. Main Developments and Functions

The platform used helps caregivers by automating the processing of sensor information, questions, and questionnaires in order to detect and report medical risk situations early. MyPredi will provide personalized care for the main geriatric risks to avoid the occurrence of acute factors leading to decompensation in elderly patients. The information collected will be supplemented by codified therapeutic care, according to international recommendations in nursing homes.

This platform provides all paramedical and medical health professionals with information on the resident’s geriatric data. This information will be updated regularly, including anthropometric, nutritional, cognitive, and iatrogenic data. Together, the data will provide a real-time complete picture integrated into an electronic platform, creating a standardized gerontological assessment based on simple and rapid measures. Geriatric risks include the risks of falling, constipation, dehydration, confusion, iatrogenic, malnutrition, heart failure, diabetes, infections, and bedsores (Figure 3).

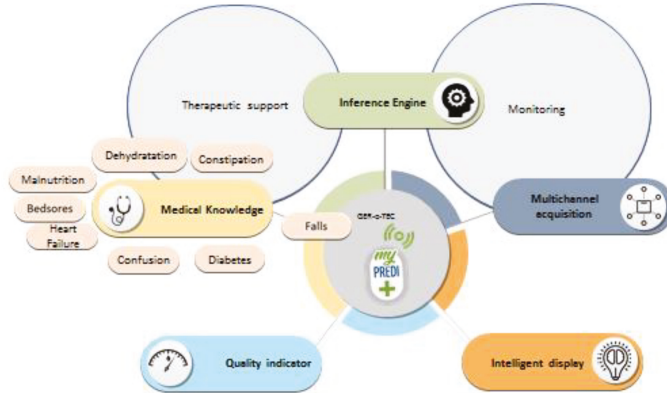


Figure 3. GER-e-TEC project. (Source: PrediMed, Schiltigheim, France).

The platform uses an intelligent algorithm to process data and generate alerts based on medical knowledge of the diseases treated, as modeled by ontologies. The general principle adopted by this platform is the anticipation of decompensation through the detection of warning signs that lead, ultimately, to hospitalization. A series of measures and questionnaires will be integrated into the platform for adaptive and personalized monitoring of the patient’s state of health in nursing homes. This study benefited from the support of CENTICH (National Expertise Center for Information and Communication Technologies for Autonomy).

7.3. Expected Results and Prospects

The improvements and perspectives of this project will be, in the medium-term:

To decrease the number of preventable hospitalizations by implementing the platform in nursing homes;

To ensure continuity and regularity in the follow-up of patients, particularly in those with complex chronic diseases;

To improve the quality of life of nursing home patients through better follow-up;

To take into consideration the residents' needs and expectations;

To improve access to hospital care facilities, reducing the use of emergency services, medical care, inappropriate hospitalization, and transport; to promote safe medical practices, sharing, and optimization of knowledge in order to safely improve information exchange among health professionals to better articulate the different healthcare levels.

#### 7.4. Project Stages

The three stages of the project are:

To deploy the system at the residents' bedside in nursing homes;

To validate the solution and develop it with healthcare professionals;

To validate the alerts.

The phasing of the GER-e-TEC project involves two stages:

Phase 1: this corresponds to the implementation and validation of technological processes in an Internal Medicine–Geriatrics department at Strasbourg University Hospitals in the period June 2019–November 2019 (preliminary study (evidence concept));

Phase 2: this aims at generalizing the telemonitoring of elderly patients in nursing homes related to Strasbourg University Hospitals as the referral medical facility (study itself).

#### 7.5. Methodology

Using a tablet and connected sensors (Figure 4), the patient's vital signs are measured daily: blood pressure, heart rate, weight, oxygen saturation, capillary glucose, temperature, and physical activity. The technical characteristics of the sensors are detailed in Table 1. The entire device of the MyPredi platform is ISO13485 medical certified with CE marking.



**Figure 4.** Devices used within the framework of the MyPredi platform. (Source: PrediMed, Schiltigheim, France).



**Table 1.** Technical characteristics of the MyPredi platform sensors.

Sensors	Characteristics
Balance	A&D Medical, Model: UC-352BLE Bluetooth: 4.0
Sphygmomanometer	A&D Medical Model: UA-651BLE Bluetooth 4.0
Pulse oximeter	Jumper Model: JPD-500F Bluetooth: 4.0
Pedometer	Ecare Fit No model Bluetooth 4.0
Glucometer	FORA Advanced pro GD40 Model: TD-4272H/GD40h Bluetooth 4.0
Thermometer	Jumper Model JPD-FR302 Bluetooth 4.0

The vital signs are automatically sent to the MyPredi platform. Questionnaires are also integrated in order to be regularly updated by the medical and paramedical team. This includes the main gerontological risks and disorders such as constipation (frequency of daily bowel movements), hydration (quantification of daily fluid intake), iatrogenic risk, heart failure, quality of sleep (neurological, psycho-behavioral), and level of bed rest (bedsores/physical activity).

Figure 5 illustrates the dashboard of geriatric risks available on the tablet of caregivers in charge of nursing home residents.



**Figure 5.** Description of the MyPredi gerontological risk dashboard. (Source: PrediMed, Schiltigheim, France).

In the event of a consequent variation in vital signs (Figure 6), an alert is sent to the MyPredi platform.

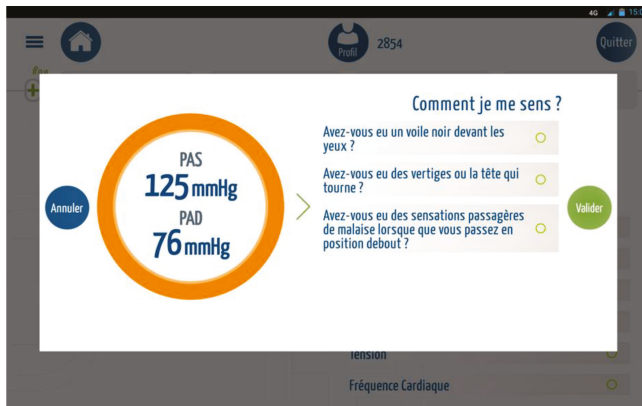


(a)



(b)

Figure 6. Cont.



(c)



(d)



(e)

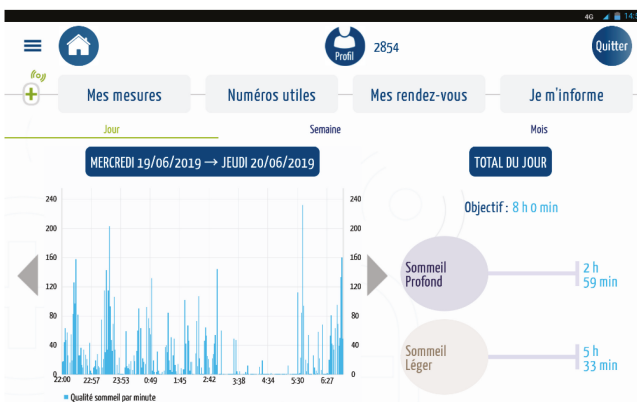
Figure 6. Cont.



(f)



(g)



(h)

Figure 6. Cont.

Statuts : lc-dia\_ger  
 Réalisé par : N/R  
 Titre : Questionnaire Medecin Hebdo IC-DIA\_GER  
 Date : 12/11/2019 11:42:20  
 Date début de saisie : 12/11/2019 11:42:21  
 Date fin de saisie : 12/11/2019 11:42:27  
 Commentaire : N/R



Question	Réponse(s)	Date de saisie
Est-ce que le patient a des oedèmes ?	non	12/11/2019 11:42:22
Est-ce que le patient a des problèmes de dyspnée ?	non	12/11/2019 11:42:23
Est-ce que le patient tousse ?	non	12/11/2019 11:42:25
Est-ce que le patient fait de l'orthopnée ?	non	12/11/2019 11:42:26

Précédent **1** Suivant

(i)

Statuts : lc-dia\_ger  
 Réalisé par : N/R  
 Titre : Alitement  
 Date : 14/11/2019 09:10:22  
 Date début de saisie : 14/11/2019 09:10:23  
 Date fin de saisie : 14/11/2019 09:10:25  
 Commentaire : N/R



Question	Réponse(s)	Date de saisie
L'alitement du (ou de la) patient(e) dure-t-il plus de 50 pour cent de la journée ?	Non	14/11/2019 09:10:24

Précédent **1** Suivant

(j)

**Questionnaire - Iatrogénie-Anticoagulants**

Date : \* 07/08/2019 21:25      Commentaire :

Question	Réponse(s)
Prise d'anticoagulants ?	Oui
Aspirine à forte dose ?	
Antibiotiques ? ( fluoroquinolones, macrolides, cyclines, cotrimoxazole, certaines céphalosporines)	
Antiagrégants plaquettaires ?	
Antifongiques oraux ?	
AINS pyrazolés ?	
Prothèse valvulaire ?	

(k)

Figure 6. Cont.

Statuts : **lc-dia\_ger**  
 Réalisé par : **N/R**  
 Titre : **Selles du jour**  
 Date : **12/11/2019 20:32:24**  
 Date début de saisie : **12/11/2019 20:32:25**  
 Date fin de saisie : **12/11/2019 20:32:32**  
 Commentaire : **N/R**



Question	Réponse(s)	Date de saisie
Nombre de selles ce matin ?	0	12/11/2019 20:32:28
Nombre de selles cet après-midi ?	0	12/11/2019 20:32:31

Précédent **1** Suivant

(l)

**Indicateurs**

**Score de douleur EYS**

**0.0**  
(score)

14/11/2019 09:10:04

**Sexe :** Femme  
**Age :** 84  
**NIP (IPP) :** 644543  
**Statut :** lc-dia\_ger

**Glycémie**

	Matin avant petit déjeuner	Matin après petit déjeuner	Après-midi avant déjeuner	Après-midi après déjeuner	Soirée avant dîner	Soirée après dîner	Nuit au coucher
lundi 23/03/2020							
mardi 24/03/2020							
mercredi 25/03/2020							
jeudi 26/03/2020							
vendredi 27/03/2020							
samedi 28/03/2020							
dimanche 29/03/2020							

Moyenne du taux de glycémie: -- -- -- -- -- --

Précédent Suivant

■ Taux de glycémie ■ Insuline lente ■ Insuline rapide

**Calendrier**

Mar 2020


Lu	Ma	Me	Je	Ve	Sa	Di
						1
2	3	4	5	6	7	8
9	10	11	12	13	14	15
16	17	18	19	20	21	22
23	24	25	26	27	28	29
30	31					

**Note Médical**

Aucune note médicale n'a été trouvée. Consulter

(m)

Statuts : **lc-dia\_ger**  
 Réalisé par : **N/R**  
 Titre : **Volume hydrique**  
 Date : **13/11/2019 20:29:17**  
 Date début de saisie : **13/11/2019 20:29:18**  
 Date fin de saisie : **13/11/2019 20:29:23**  
 Commentaire : **N/R**



Question	Réponse(s)	Date de saisie
Volume hydrique journalier ?	1100	13/11/2019 20:29:22

Précédent **1** Suivant

(n)

**Figure 6.** Measurements: (a) heart rate/oxygen saturation, (b) heart rate/oxygen saturation, (c) Illustration measure blood pressure, (d) blood pressure, (e) body temperature, (f) weight, (g) physical activity, (h) sleep quality, (i) heart failure questionnaire, (j) sleeping questionnaire, (k) anticoagulants questionnaire, (l) stools, (m) capillary glucose table, and (n) hydration questionnaire. (Source: PrediMed, Schiltigheim, France).

## 8. Discussion

With the GER-e-TEC project, we can now offer medical teams and paramedics a remote monitoring device that optimizes the management of patients with geriatric syndromes and their accompanying conditions. This remote monitoring system will allow monitored patients to record their daily physiological data (weight, oxygen saturation, blood pressure, heart rate, blood sugar) and complete questionnaires on the state of their health. The data will be automatically sent to our MyPredi platform, which is designed to predict situations that are at risk of deteriorating.

A coordination unit will then be able to monitor the patient remotely, providing comprehensive and personalized treatment of the areas of concern detected by the platform and helping the patient with their therapy.

Patients monitored remotely:

- Physiological data analyzed daily;
- Help with therapy-related questions;
- Remote consultations.

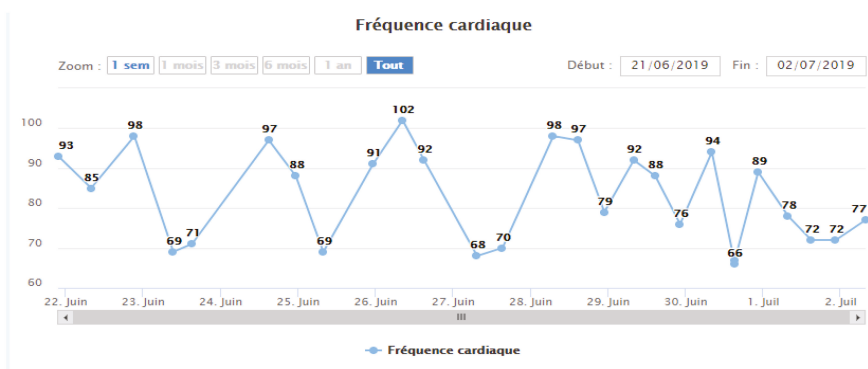
Coordination unit:

- Processing of alerts;
- Help with therapy;
- Coordination of doctors and patients;
- Sending of reports to doctors on the health status of their patients;
- Monitoring of patient compliance.

Medical team:

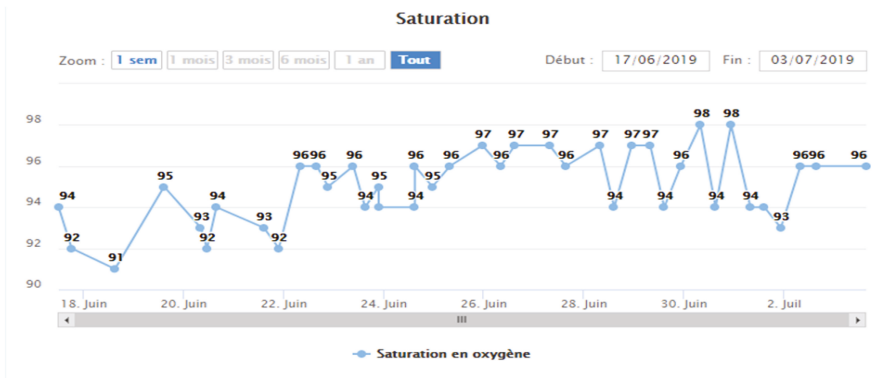
- Medical advice if needed.

The GER-e-TEC project was tested on a patient (Figure 7) who, after providing written consent, was monitored daily by a team of healthcare professionals. The patient was given a pedometer to monitor his sleep and activity. The goal was to test the ergonomics and functionality of the remote monitoring platform on a daily basis before using it in the study.

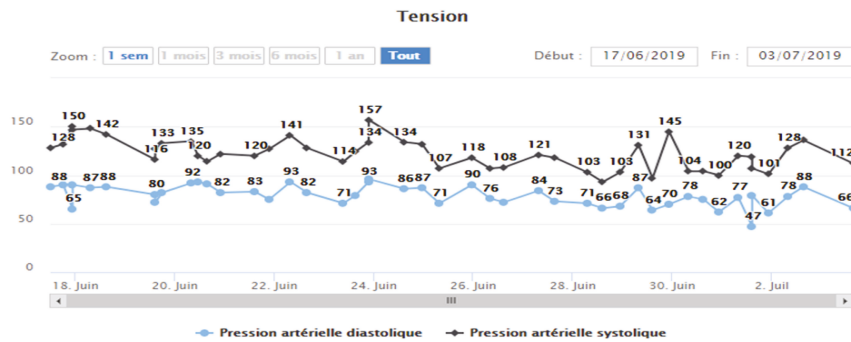


(a)

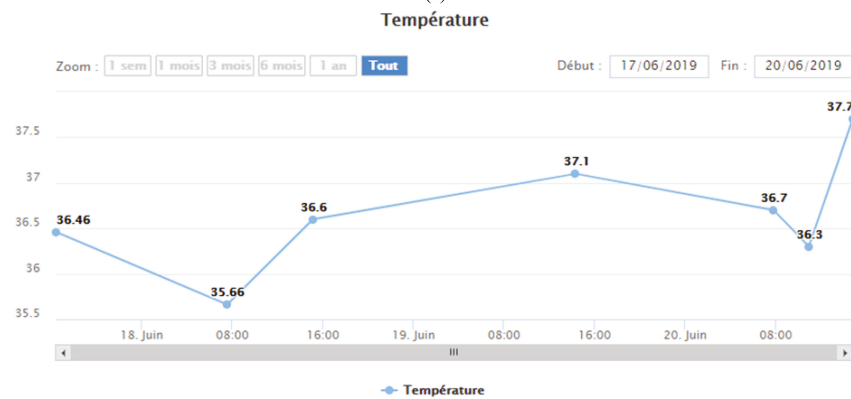
Figure 7. Cont.



(b)



(c)



(d)

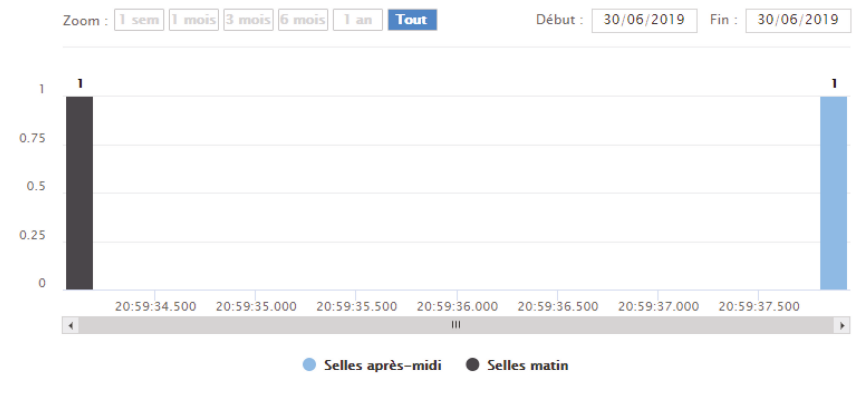
Figure 7. Cont.





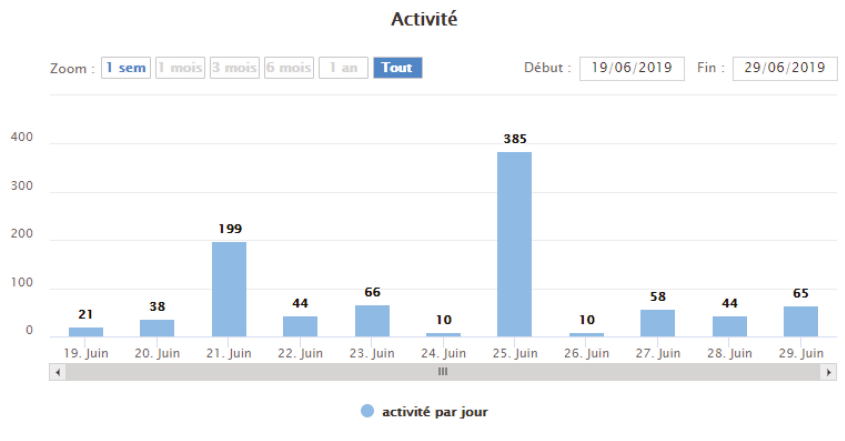
(e)

### Selles



(f)

Figure 7. Cont.



(g)



(h)

Figure 7. Cont.

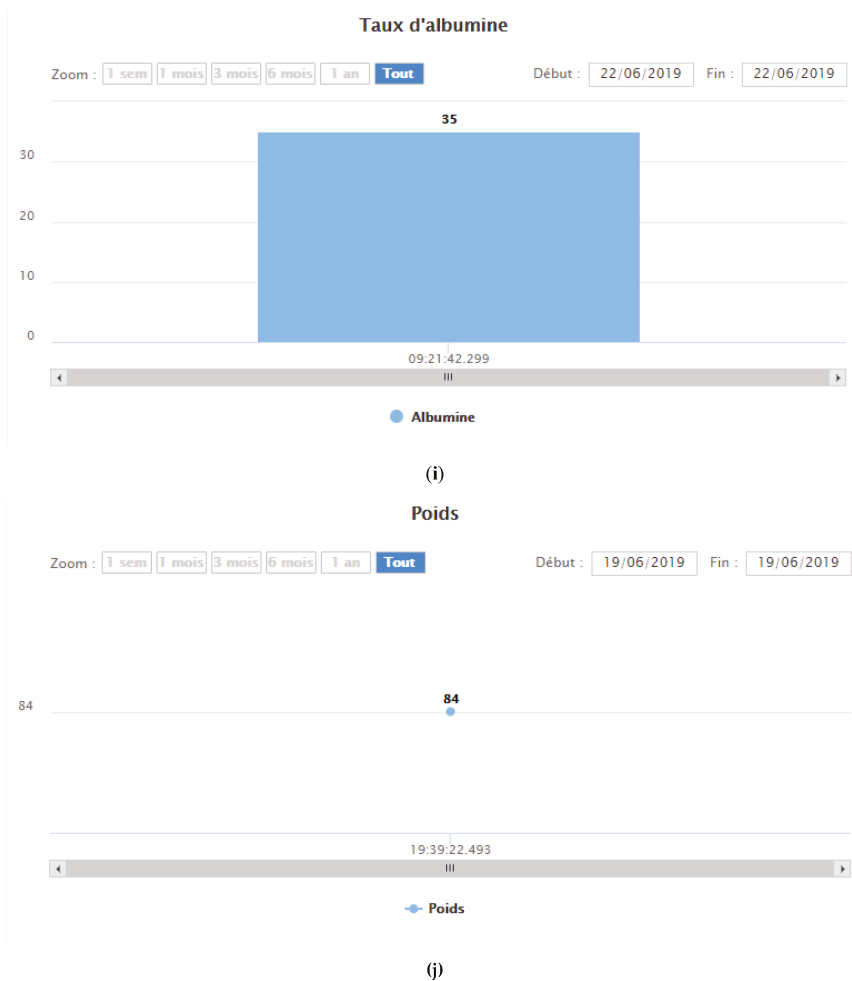
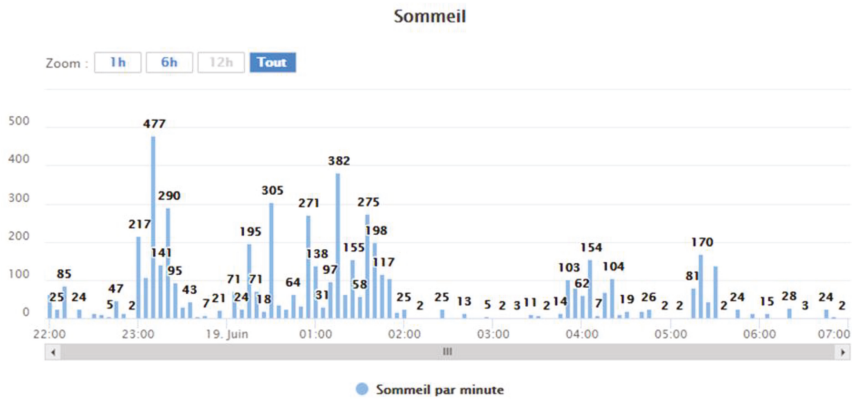


Figure 7. Cont.



(k)

**Figure 7.** Daily monitoring measurements: (a) heart rate, (b) oxygen saturation, (c) blood pressure, (d) body temperature, (e) hydratation state, (f) Stools, (g,h) daily physical activity surveillance, (i,j) nutritional surveillance, (k) sleeping surveillance. (Source: PrediMed, Schiltigheim, France).

By monitoring the patient’s geriatric health indicators and hemodynamic data, the remote monitoring system was able to issue alerts (Figure 8) with varying degrees of severity (low to critical).

Faible	21/06/2019 22:04:41	Risque de constipation de niveau 1	●	
Faible	21/06/2019 22:01:35	Temps immobilisation trop long: IAJ =7<50%	●	
Critique	23/06/2019 21:35:04	PAS = 157 mmHg	●	

**Figure 8.** Alerts: faible/weak constipation risk (level 1), faible/weak inappropriate physical activity, and critique/critical systolic blood pressure = 157 mmHg. (Source: PrediMed, Schiltigheim, France).

This remote monitoring system can generate automated, non-intrusive alerts in the event of high-risk situations.

The feedback from healthcare professionals who used the MyPredi platform daily was positive. Surveys completed by nurses, nurses’ aides, doctors, and the patient found the satisfaction rate to be upwards of 90%. Thanks to the comments and suggestions from those who participated in the test, we have been able to make improvements to the platform interface both on the app and the web. The test helped us validate our choice of technology, as well as consolidate and assess the durability of the monitoring system. This proof of concept allowed us to test the remote monitoring system, evaluate its ergonomics, and analyze its use by the hospital care team.

The system will now be tested over the course of three months in an 18-bed medical unit at a University Hospital of Strasbourg. Between 100 and 110 patients will participate in the study using remote monitoring. This study will make it possible to consolidate the technological and ergonomic aspects of the system, and thanks to its daily use by doctors and nurses, allow for the MyPredi platform technology to be validated before the system is used in nursing homes (GER-IA project). The results of the study will be published upon completion.

## 9. Conclusions

Remote monitoring in nursing homes is a major issue in light of the current COVID-19 health crisis and the repeated (yet avoidable) hospitalizations required for the elderly. The goal of our “GER-e-TEC” project is to identify the early warning signs of (1) an exacerbation of geriatric problems

(falls, constipation, dehydration, confusion, iatrogenesis, infections, bedsores, malnutrition), and (2) an exacerbation of accompanying syndromes (heart failure, diabetes, hypertension), and to provide for the early treatment of these conditions.

The initial phase of our project will consist of implementing and validating our technological processes in a Department of Internal and Geriatric Medicine at a University Hospital in Strasbourg (preliminary study (proof of concept)). This phase will involve around 110 elderly hospitalized patients and will allow us to validate our medical, technological, and ergonomic choices with elderly patients, healthcare professionals, and patient associations. In addition, our platform will provide healthcare professionals and paramedics with regularly updated geriatric information on each patient, i.e., their anthropometric, nutritional, cognitive, and iatrogenic data, and present a comprehensive digital overview of a standardized geriatric assessment that is both quick and easy to complete.

Once validated, this platform will be expanded to the nursing homes of the University Hospitals of Strasbourg.

**Author Contributions:** Conceptualization, A.-A.Z. and E.A.; methodology, A.-A.Z., N.L.-V., E.A.; software, O.-A.Z.; validation, A.-A.Z., N.L.-V., E.A., M.H., Q.C., L.E., J.H., S.E., A.H.E.H.; formal analysis, A.-A.Z.; investigation, A.-A.Z.; resources, A.-A.Z., N.L.-V., E.A., M.H., Q.C., L.E., J.H., S.E., D.L., A.H.E.H.; data curation, A.-A.Z., N.L.-V., E.A.; writing—original draft preparation, A.-A.Z., N.L.-V., E.A., M.H., A.H.E.H.; writing—review and editing, A.-A.Z., N.L.-V., E.A., M.H., Q.C., L.E., J.H., S.E., A.H.E.H.; visualization, A.-A.Z., N.L.-V., E.A., M.H., Q.C., L.E., J.H., S.E., A.H.E.H.; supervision, A.-A.Z., N.L.-V., E.A., M.H., Q.C., L.E., B.G., S.T., J.H., S.E., A.H.E.H.; project administration, A.-A.Z., N.L.-V., E.A., M.H., Q.C., L.E., J.H., S.E., A.H.E.H.; funding acquisition, A.-A.Z., N.L.-V., E.A., M.H., Q.C., L.E., J.H., S.E., A.H.E.H. All authors have read and agreed to the published version of the manuscript.

**Funding:** This research received no external funding.

**Conflicts of Interest:** The authors declare no conflict of interest except Mohamed HAJJAM who is CEO of PREDIMED

## References

1. OCDE. *Panorama de la Santé 2015: Les Indicateurs de L'OCDE*; Editions OCDE: Paris, France, 2015. [CrossRef]
2. DREES. *728000 Résidents en Etablissements D'hébergements Pour Personnes Agées en 2015. Premiers Résultats de L'enquête EHPA 2015*; DREES: Paris, France, 2017.
3. Morley, J.E.; Rolland, Y.; Tolson, D.; Vellas, B. The time has come to enhance nursing home care. *Arch. Gerontol. Geriatr.* **2011**, *53*, 1–2. [CrossRef] [PubMed]
4. HAS-ANESM. *Comment Réduire les Hospitalisations non Programmées des Résidents des EHPAD ? Note méthodologique et de Synthèse Documentaire. Points clés Organisation des Parcours*; HAS/ANESM: Paris, France, 2015; 97p.
5. Salles, N. Télé médecine en EHPAD. Les clés pour se lancer. *Partag. d'expérience* **2017**, *168*, 13–89.
6. Haut Comité Pour L'avenir de L'assurance-Maladie (HCAAM) Assurance-Maladie et Perte D'autonomie; Rapport 23 Juin 2011. Available online: [https://www.securite-sociale.fr/files/live/sites/SSFR/files/medias/HCAAM/2011/RAPPORT/HCAAM-2011-JUIN-RAPPORT-ASSURANCE\\_MALADIE\\_ET\\_PERTE\\_D-AUTONOMIE.pdf](https://www.securite-sociale.fr/files/live/sites/SSFR/files/medias/HCAAM/2011/RAPPORT/HCAAM-2011-JUIN-RAPPORT-ASSURANCE_MALADIE_ET_PERTE_D-AUTONOMIE.pdf) (accessed on 15 May 2020).
7. Le Fur-Musquer, É.; Delamarre-Damier, F.; Sonnic, A.; Berrut, G. Existe-t-il des facteurs prédictifs de l'hospitalisation non programmée de résidents d'EHPAD. *Geriatr. Psychol. Neuropsychiatr. Vieil.* **2012**, *10*, 137–142. [PubMed]
8. Young, Y.; Barhydt, N.R.; Broderick, S.; Colello, A.D.; Hannan, E.L. Factors associated with potentially preventable hospitalization in nursing home residents in New York state: A survey of directors of nursing. *J. Am. Geriatr. Soc.* **2010**, *58*, 901–907. [CrossRef] [PubMed]
9. Martínez-González, N.A.; Berchtold, P.; Ullman, K.; Busato, A.; Egger, M. Integrated care programmes for adults with chronic conditions: A meta-review. *Int. J. Qual. Health Care* **2014**, *26*, 561–570. [CrossRef]
10. Barralon, P. *Classification et Fusion de Données Actimétriques Pour la Télésurveillance Médicale. (Projet de thèse)*. Bachelor's Thesis, Université Joseph Fourier, Grenoble, France, 2005.

11. La télésanté: Un nouvel atout au service de notre bien-être. Un plan quinquennal éco-responsable pour le déploiement de la télésanté en France. 2009. (Ministerial document reported to Madame Roselyne Bachelot-Narquin, Health Minister by Monsieur Pierre Lasbordes, Essonne deputy). Available online: <https://solidarites-sante.gouv.fr/ministere/documentation-et-publications-officielles/rapports/sante/article/la-telesante-un-nouvel-atout-au-service-de-notre-bien-etre#> (accessed on 15 May 2020).
12. Ahmed Benyahia, A.; Hajjam, A.; Talha, S.; Hajjam, M.; Andrès, E.; Hilaire, V. E-care: Évolution ontologique et amélioration des connaissances pour le suivi des insuffisants cardiaques. *Med. Ther.* **2014**, *20*, 79–86.
13. Rubel, P.; Fayn, J.; Nollo, G.; Assanelli, D.; Li, B.; Restier, L.; Adami, S.; Arod, S.; Atoui, H.; Ohlsson, M.; et al. Toward personal eHealth in cardiology. Results from the EPI-MEDICS telemedicine project. *J. Electrocardiol.* **2005**, *38*, 100–106. [[CrossRef](#)]
14. Gokalp, H.; de Folter, J.; Verma, V.; Fursse, J.; Jones, R.; Clarke, M. Integrated Telehealth and Telecare for Monitoring Frail Elderly with Chronic Disease. *Telemed. e-Health* **2018**, *24*, 940–957. [[CrossRef](#)]
15. Jourdain, P.; Desnos, M.; Jullière, Y. Establishment of an Interactive Patient Health Platform (PIMPS) Based on Home-Based Selfmeasurement of a Bi-Omarter in Chronic Ambulatory Heart Failure. Presented at the 6th European Congress of ANTEL, Paris, France, 15 November 2013.
16. Biannic, C.; Coutance, G.; Calus, J.; Belin, A.; Loiselet, P.; Michel, L. Educational home follow-up by telemedicine in cases of cardiac insufficiency. Randomised, multicentric study from the Basse-Normandie region. Preliminary results. *Eur. Telemed. Res.* **2012**, *1*, 40–48. [[CrossRef](#)]
17. Mabo, P.; Victor, F.; Bazin, P.; Ahres, S.; Babuty, D.; Costa, A.D.; Binet, D.; Daubert, J.-C. A randomized trial of long-term remote monitoring of pacemaker recipients (the COMPAS trial). *Eur. Heart J.* **2012**, *33*, 1105–1111. [[CrossRef](#)]
18. Guédon-Moreau, L.; Lacroix, D.; Sadoul, N.; Clémenty, J.; Kouakam, C.; Hermida, J.S.; Aliot, E.; Boursier, M.; Bizeau, O.; Kacet, S.; et al. A randomized study of remote follow-up of implantable cardioverter defibrillators: Safety and efficacy report of the ECOST trial. *Eur. Heart J.* **2013**, *34*, 605–614. [[CrossRef](#)] [[PubMed](#)]
19. Dary, P. Telemonitoring of atrial fibrillation: Feasibility study and results on 200 patients. *Eur. Res. Telemed.* **2013**, *2*, 113–120. [[CrossRef](#)]
20. Goldberg, L.R.; Piette, J.D.; Walsh, M.N.; Frank, T.A.; Jaski, B.E.; Smith, A.L.; Rodriguez, R.; Mancini, D.M.; Hopton, L.A.; Orav, E.J.; et al. Randomized trial of a daily electronic home monitoring system in patients with advanced heart failure: The Weight Monitoring in Heart Failure (WHARF) trial. *Am. Heart J.* **2003**, *146*, 705–712. [[CrossRef](#)]
21. Chaudhry, S.I.; Barton, B.; Mattera, J.; Spertus, J.; Krumholz, H.M. Randomized trial of telemonitoring to improve heart failure outcomes (Tele-HF): Study design. *J. Card. Fail.* **2007**, *13*, 709–714. [[CrossRef](#)] [[PubMed](#)]
22. Minutolo, A.; Sannino, G.; Esposito, M.; De Pietro, G. A Rule-Based mHealth System for Cardiac Monitoring. In Proceedings of the 2010 IEEE EMBS Conference on Biomedical Engineering & Sciences, Kuala Lumpur, Malaysia, 1 November 2010; pp. 1021–1034.
23. Amara, W.; Montagnier, C.; Cheggour, S.; Boursier, M.; Gully, C.; Barnay, C.; Georger, F.; Deplagne, A.; Fromentin, S.; Mlotek, M.; et al. Early detection and treatment of atrial arrhythmias alleviates the arrhythmic burden in paced patients: The SETAM study. *Pacing Clin. Electrophysiol.* **2017**, *40*, 527–536. [[CrossRef](#)] [[PubMed](#)]
24. Anfosso, A.; Rebaudo, S. Gérontologies et contrôle de l’environnement au service du maintien à domicile: Le projet GERHOME. *Gérontologie et société* **2011**, *34/136*, 119–131. [[CrossRef](#)]
25. Charlon, Y. Conception de dispositifs électroniques portés pour le suivi de l’état de santé des personnes âgées. Micro et nanotechnologies/Microélectronique. Université de Toulouse III, 2014. French. Available online: <https://tel.archives-ouvertes.fr/tel-01079731> (accessed on 23 April 2020).
26. Cosquer, P.; Guézou, T. Système séreo’z développé par la société aphyca technologies. *Gérontologie et Société* **2005**, *28/113*, 83–88. [[CrossRef](#)]
27. Grönholm, K. The Vivago watch: A telecare solution for cost-efficient care. *Gerontechnology* **2009**. [[CrossRef](#)]
28. Projet Icare. Available online: <http://www.revue-hospitaliere.fr/Actualites/Telesurveillance-a-domicile-des-personnes-agees-Projet-Icare> (accessed on 23 April 2020).
29. Edirippulige, S.; Martin-Khan, M.; Beattie, E.; Smith, A.C.; Gray, L.C. A systematic review of telemedicine services for residents in long-term care facilities. *J. Telemed. Telecare* **2013**, *19*, 1–8. [[CrossRef](#)]
30. Talha, S.; Andrès, E. Place de la télé-médecine et projet e-Care. In *Workshop e-Care: Ingénierie des Connaissances et Traitement du Signal pour la Télé-médecine*; Université de Haute Alsace: Mulhouse, France, 2014.

31. Projet E-CARE. Available online: <http://www.projet-e-care.fr/> (accessed on 23 April 2020).
32. Andrès, E.; Talha, S.; Benyahia, A.; Keller, O.; Hajjam, M.; Moukadem, A.; Dieterlen, A.; Hajjam, J.; Euvé, S.; Hajjam, A. Expérimentation d'une plateforme de détection automatisée des situations à risque de décompensation cardiaque (plateforme ECARE) dans une unité de médecine interne. *Rev. Med. Interne* **2016**, *37*, 587–593. [CrossRef]
33. Ahmed Benyahia, A.; Hajjam, A.; Andrès, E.; Hajjam, M.; Hilaire, V. Including other system in E-Care telemonitoring platform. *Stud. Health Technol. Inform.* **2013**, *190*, 115–117. [PubMed]
34. Ahmed Benyahia, A.; Moukadem, A.; Dieterlen, A.; Hajjam, A.; Talha, S.; Andrès, E. Adding ontologies based on PCG analysis in E-care project. *Int. J. Eng. Innov. Technol.* **2013**, *5*, 2277–3754.
35. Elasri, H.; Sekkaki, A.; Hajjam, A.; Benmimoune, L.; Talha, S.; Andrès, E. Ontologies et intégration des connaissances pour un suivi polypathologique. *Med. Ther.* **2014**, *20*, 67–78.
36. Andrès, E.; Hajjam, A. Advances and innovations in the field of auscultation. *Health Technol.* **2012**, *2*, 5–16. [CrossRef]
37. Andrès, E.; Reichert, S.; Gass, R.; Brandt, C. A French national research project to the creation of an auscultation's school: The ASAP project. *Eur. J. Intern. Med.* **2009**, *20*, 323–327. [CrossRef]



© 2020 by the authors. Licensee MDPI, Basel, Switzerland. This article is an open access article distributed under the terms and conditions of the Creative Commons Attribution (CC BY) license (<http://creativecommons.org/licenses/by/4.0/>).

MDPI  
St. Alban-Anlage 66  
4052 Basel  
Switzerland  
Tel. +41 61 683 77 34  
Fax +41 61 302 89 18  
[www.mdpi.com](http://www.mdpi.com)

*Medicines* Editorial Office  
E-mail: [medicines@mdpi.com](mailto:medicines@mdpi.com)  
[www.mdpi.com/journal/medicines](http://www.mdpi.com/journal/medicines)







MDPI  
St. Alban-Anlage 66  
4052 Basel  
Switzerland

Tel: +41 61 683 77 34  
Fax: +41 61 302 89 18

[www.mdpi.com](http://www.mdpi.com)



ISBN 978-3-0365-3686-6